TRANSPORTATION RESEARCH RECORD 950

Second Bridge Engineering Conference

Volume 1

Conducted by the Transportation Research Board, National Research Council, and the Federal Highway Administration, U.S. Department of Transportation, September 24-26, 1984

TRB
TRANSPORTATION RESEARCH BOARD
NATIONAL RESEARCH COUNCIL
WASHINGTON, D.C. 1984

Transportation Research Record 950
Price $18.00
Edited for TRB by Naomi Kassabian, Scott Herman, Elizabeth W. Kaplan, and Jane Starkey

modes
1 highway transportation
3 rail transportation

subject areas
22 hydrology and hydraulics
25 structures design and performance
33 construction
34 general materials
40 maintenance

Transportation Research Board publications are available by ordering directly from TRB. They may also be obtained on a regular basis through organizational or individual affiliation with TRB; affiliates or library subscribers are eligible for substantial discounts. For further information, write to the Transportation Research Board, National Academy of Sciences, 2101 Constitution Avenue, N.W., Washington, D.C. 20418.

Printed in the United States of America

Library of Congress Cataloging in Publication Data
National Research Council. Transportation Research Board.
Bridge Engineering Conference (2nd: 1984: Minneapolis, Minn.)
Second Bridge Engineering Conference.
(Transportation research record; 950)
1. Bridges–Congresses. I. National Research Council (U.S.). Transportation Research Board. II. United States. Federal Highway Administration. III. Title. IV. Series.
TE7.H5 no. 950 380.5 s 84–14831
ISBN 0-309-03659-3 [624'.2] ISSN 0361-1981

Sponsorship of the Papers in This Transportation Research Record

GROUP 2–DESIGN AND CONSTRUCTION OF TRANSPORTATION FACILITIES
Robert C. Deen, University of Kentucky, chairman

Planning Committee for the Second Bridge Engineering Conference
John M. Hanson, Wiss, Janney, Elstner & Associates, chairman
James W. Baldwin, Jr., Robert M. Barnoff, Keith V. Benthin, Roland H. Berger, Bernard E. Butler, Robert C. Cassano, James D. Cooper, Robert N. Kamp, Jimmy D. Lee, Albert D.M. Lewis, Clellon L. Loveall, Frank D. Sears, Arunprakash M. Shirole, and A. Mainard Wacker

General Design Section
Samuel V. Fox, Texas State Department of Highways, chairman

Committee on Hydrology, Hydraulics and Water Quality
A. Mainard Wacker, Wyoming Highway Department, chairman
J. Sterling Jones, Federal Highway Administration, secretary
James E. Alleman, John J. Bailey, Jr., Harry H. Barnes, Jr., Darwin L. Christensen, Earl C. Cochran, Jr., Stanley R. Davis, Robert M. Engler, Samuel V. Fox, Benjamin M. Givens, Jr., John L. Grace, Jr., Richard B. Howell, William T. Jack, Jr., Kenneth D. Kerri, Floyd J. Laumann, Walter F. Megahan, Marshall E. Moss, Robert E. Rallison, Everett V. Richardson, Robert F. Shattuck, Michael D. Smith, Michael B. Sonnen, Charles Whittle, Henry B. Wyche, Jr.

Structures Section
John M. Hanson, Wiss, Janney, Elstner & Associates, chairman

Committee on General Structures
Clellon Lewis Loveall, Tennessee Department of Transportation, chairman
John M. Kulicki, Modjeski & Masters, secretary
John J. Ahlskog, Dan S. Bechly, Neal H. Bettigole, Edwin G. Burdette, Martin P. Burke, Jr., Jack H. Emanuel, Dah Fwu Fine, Richard S. Fountain, Frederick Gottemoeller, J. Leroy Hulsey, Walter J. Jestings, Robert N. Kamp, Heinz P. Koretzky, Celal N. Kostem, Wendell B. Lawing, Richard M. McClure, Gordon R. Pennington, David R. Schelling, Arunprakash M. Shirole, Marcello H. Soto, Robert F. Victor, Stanley W. Woods

Committee on Steel Bridges
Frank D. Sears, Federal Highway Administration, chairman
Chris S.C. Yiu, Pavlo Engineering Company, secretary
Pedro Albrecht, Dan S. Bechly, Chester F. Comstock, J. Hartley Daniels, David A. Dock, Jackson L. Durkee, Nicholas M. Engelman, John W. Fisher, Karl H. Frank, Louis A. Garrido, Wayne Henneberger, Robert B. Jarvis, B.F. Kotalik, Richard W. Lautensleger, Albert D.M. Lewis, Abba G. Lichtenstein, Joseph M. McCabe, Jr., Roy L. Mion, W.H. Munse, Robert H. Scanlan, Frederick H. Sterbenz, Carl E. Thunman, Jr., Carl C. Ulstrup

Committee on Concrete Bridges
Robert C. Cassano, California Department of Transportation, chairman
T. Alberdi, Jr., Craig A. Ballinger, W. Gene Corley, C.S. Gloyd, John M. Hanson, James J. Hill, Ti Huang, Cornie L. Hulsbos, Roy A. Imbsen, Hubert Janssen, Heinz P. Koretzky, H.G. Kriegel, John M. Kulicki, R. Shankar Nair, Edward G. Nawy, Walter Podolny, Jr., Adrianus Vankampen, Julius F.J. Volgyi, Jr., Donald J. Ward, W. Jack Wilkes

Committee on Dynamics and Field Testing of Bridges
James W. Baldwin, Jr., University of Missouri-Columbia, chairman
Charles F. Galambos, Federal Highway Administration, secretary
Baidar Bakht, Furman W. Barton, David B. Beal, Harold R. Bosch, John L. Burdick, William G. Byers, Gene R. Cudney, Bruce M. Douglas, Ismail A.S. Elkholy, Hota V.S. Gangarao, David William Goodpasture, Roy A. Imbsen, F. Wayne Klaiber, Celal N. Kostem, Robert H. Lee, Fred Moses, M. Noyszewski, Gajanan M. Sabnis, R. Varadarajan, William H. Walker, Kenneth R. White

Construction Section
Garland W. Steele, West Virginia Department of Highways, chairman

Committee on Construction of Bridges and Structures
Robert M. Barnoff, Pennsylvania State University, chairman
Mrinmay Biswas, John K. Bright, John F. Cain, David A. Dock, Jackson L. Durkee, Thomas H. Ellis, George A. Harper, Marvin H. Hilton, Frank J. Kempf, Andrew Lally, John P. Rutter, Michael M. Sprinkel, Man-Chung Tang, J.R. Wilder, Thomas G. Williamson, Kenneth C. Wilson

Committee on Fabrication and Inspection of Metal Structures
Robert N. Kamp, Byrd, Tallamy, MacDonald & Lewis, chairman
William G. Byers, Hubert F. Crick, Moss V. Davis, A.J. Dunn, Jackson L. Durkee, Nicholas M. Engelman, Philip F. Frandina, Karl H. Frank, G.A. Gix, Carl Hartbower, Kenneth F. Hurst, Frank J. Kempf, Michael Lauriente, Anthony Leone, Eric F. Nordlin, Jack P. Shedd, William F. Via, Jr., John P. Weisner

GROUP 3–OPERATION AND MAINTENANCE OF TRANSPORTATION FACILITIES
D.E. Orne, Michigan Department of Transportation, chairman

Committee on Structures Maintenance
Jimmy D. Lee, North Carolina Department of Transportation, chairman
Robert N. Kamp, Byrd, Tallamy, MacDonald & Lewis, secretary
John J. Ahlskog, Robert M. Barnoff, Roland H. Berger, Alfred G. Bishara, William G. Byers, A.J. Dunn, Ian J. Dussek, Nicholas M. Engelman, Ray W. James, Eldon D. Klein, Robert H. Krier, David G. Manning, Wallace T. McKeel, Jr., Richard J. Posthauer, Jack W. Roberts, George P. Romack, Steven J. Shecter, Arunprakash M. Shirole, Charles V. Slavis, Lloyd M. Smith, Marilyn H. Tobey, Robert G. Tracy, Alden L. West

Lawrence F. Spaine, Adrian G. Clary, William G. Gunderman, and Neil F. Hawks, Transportation Research Board staff

Sponsorship is indicated by a footnote at the end of each report. The organizational units, officers, and members are as of December 31, 1983.

Notice: The Transportation Research Board does not endorse products or manufacturers. Trade and manufacturers' names appear in this Record because they are considered essential to its object.

Contents

Authors of the Papers in This Record

Alison, Gordon A., Aluminum Association, 818 Connecticut Avenue, N.W., Washington, D.C. 20006
Bakht, Baidar, Research and Development Branch, Ministry of Transportation and Communications, 1201 Wilson Avenue, Downsview, Ontario M3M 1J8, Canada
Bales, Fred B., Virginia Department of Highways and Transportation, 1401 East Broad Street, Richmond, Va. 23219
Barnoff, Robert M., Department of Civil Engineering, Pennsylvania State University, University Park, Pa. 16802
Batla, Fahim A., Department of Civil Engineering, North Dakota State University, Fargo, N.Dak. 58105
Beckman, Richard D., Howard, Needles, Tammen and Bergendoff, 330 Passaic Avenue, Fairfield, N.J. 07006
Billing, J.R., Research and Development Branch, Ontario Ministry of Transportation and Communications, Downsview, Ontario M3M 1J8, Canada
Biswas, Mrinmay, Civil and Environmental Engineering Department, Duke University, Durham, N.C. 27706
Brungraber, Robert J., Department of Civil Engineering, Bucknell University, Lewisburg, Pa. 17837
Cady, Philip D., Department of Civil Engineering, Pennsylvania State University, University Park, Pa. 16802
Christian, George A., New York State Department of Transportation, 1220 Washington Avenue, Albany, N.Y. 12232
Cole, Alexander P., New York State Department of Transportation, 1220 Washington Avenue, Albany, N.Y. 12232
Dorton, Roger A., Research and Development Branch, Ministry of Transportation and Communications, 1201 Wilson Avenue, Downsview, Ontario M3M 1J8, Canada
Fazio, A.E., 408 North Manioa Road, Haverstown, Pa. 19083
Fazio, R.N., New Jersey Transit Corporation, 11 Midtown Road, Carle Place, N.Y. 11514
Freeh, William S., Howard, Needles, Tammen and Bergendoff, One Erieview Plaza, Cleveland, Ohio 44114
Geschwindner, Louis F., Jr., Department of Architectural Engineering, Pennsylvania State University, University Park, Pa. 16802
Ghosn, Michel, Department of Civil Engineering, Case Western Reserve University, Cleveland, Ohio 44106
Goto, Yuji, Laboratory of Nihon Doro Kodan, 1-4-1 Tadao, Machida City, Tokyo, Japan
Green, R., Department of Civil Engineering, University of Waterloo, Waterloo, Ontario N2L 3G1, Canada
Grey, John, New Mexico State Highway Department, P.O. Box 1149, Santa Fe, N. Mex. 87504-1149
Grossman, George, New Mexico State Highway Department, P.O. Box 1149, Santa Fe, N. Mex. 87504-1149
Hand, Terry D., United States Military Academy, West Point, N.Y. 10996
Hill, J.J., Minnesota Department of Transportation, Transportation Building, St. Paul, Minn. 55155
Imbsen, Roy A., Engineering Computer Corporation, 3217 Ramos Circle, Sacramento, Calif. 95827
Jaeger, Leslie G., Technical University of Nova Scotia, Halifax, Nova Scotia B3J 2X4, Canada
Kato, Takeaki, Laboratory of Nihon Doro Kodan, 1-4-1 Tadao, Machida City, Tokyo, Japan
Kim, Jai B., Department of Civil Engineering, Bucknell University, Lewisburg, Pa. 17837
Kostem, Celal N., Fritz Engineering Laboratory, No. 13, Lehigh University, Bethlehem, Pa. 18015
Lea, J., Engineering Computer Corporation, 3217 Ramos Circle, Sacramento, Calif. 95827
Mancarti, Guy D., Office of Structures Design, California Department of Transportation, 1120 N Street, Sacramento, Calif. 95814
Matsumoto, T., Kobe Construction Division, Hansin Expressway Public Corporation, 1, 16-ban, Shinko-cho, Chuo-ku, Kobe, 650, Japan
McCarthy, William C., Civil Engineering Department, New Mexico State University, Las Cruces, N. Mex. 88003
McClure, Richard M., Department of Civil Engineering, Pennsylvania State University, University Park, Pa. 16802
Merz, H. William, Jr., I.A. Construction Corporation, P.O. Box 8, Concordville, Pa. 19331
Miller, David O., Minnesota Department of Transportation, 2055 North Lilac Drive, Golden Valley, Minn. 55422
Moses, Fred, Department of Civil Engineering, Case Western Reserve University, Cleveland, Ohio 44106
Motomura, S., Kobe Construction Division, Hansin Expressway Public Corporation, 1, 16-ban, Shinko-cho, Chuo-ku, Kobe, 650, Japan
Nagle, Gordon, Schuylkill Products, Inc., P.O. Box 55, Cressona, Pa. 17929
Noel, James S., Texas Transportation Institute, Texas A&M University, College Station, Tex. 77843

Norton, Paul G., Gannett Fleming Transportation Engineers, Inc., P.O. Box 1963, Harrisburg, Pa. 17105-1963
Nutt, Richard V., Engineering Computer Corporation, 3217 Ramos Circle, Sacramento, Calif. 95827
Osegueda, Roberto A., Texas Transportation Institute, Texas A&M University, College Station, Tex. 77843
Pathak, Divakar V., Bechtel Associates Power Corporation, P.O. Box 1000, Ann Arbor, Mich. 48106
Peng, Shih C., Public Works Canada, Sir Charles Tupper Building, Riverside Drive, Ottawa, Ontario K1A 0M2, Canada
Pluemer, Gunther, Viaduct GMBH, Postfach 1568, 7050 Waiblingen, Federal Republic of Germany
Reisnour, Patrick R., Department of Civil Engineering, North Dakota State University, Fargo, N.Dak. 58105
Shirole, A.M., Department of Public Works, 203 City Hall, Minneapolis, Minn. 55415
Snyder, Richard E., Bridge Weighing Systems, Inc., 4423 Emery Industrial Parkway, Warrensville Heights, Ohio 44128
Sprinkel, Michael M., Virginia Highway and Transportation Research Council, Box 3817, University Station, Charlottesville, Va. 22903-0817
Suarez, Mario G., Schupack Suarez Engineers, Inc., 225 Wilson Avenue, South Norwalk, Conn. 06854
Taylor, R.J., Ontario Ministry of Transportation and Communications, 1201 Wilson Avenue, Downsview, Ontario M3M 1J8, Canada
Walsh, H., Ontario Ministry of Natural Resources, Sudbury, Ontario P3E 5P9, Canada
West, Harry H., Department of Civil Engineering, Pennsylvania State University, University Park, Pa. 16802
Weyers, Richard E., Lafayette College, Easton, Pa. 18042
Woods, Stanley W., Wisconsin Department of Transportation, P.O. Box 7916, Madison, Wis. 53707

Preface

The most recent national bridge inventory of deficient bridges conducted by the Federal Highway Administration, U.S. Department of Transportation, indicates a continuous increase in the total number of bridges that are being classified as structurally deficient or functionally obsolete. Approximately 27,000 bridges in the federal-aid highway system alone are considered structurally deficient along with more than 123,000 bridges in the remainder of the system. The problem faced by railroad and transit agencies is just as severe. More than half of the one million bridges in the United States are more than 50 years old.

The problem is widely recognized, and increasing federal, state, and operating-agency appropriations are being made available for bridge construction, maintenance, and rehabilitation. Finding a solution to the rapid and continuous deterioration in existing bridge systems demands the best efforts of professional employees of state, federal, and local governments; private transportation agencies; consulting engineering firms; industry; planners; scientists; engineers; and other interested groups.

With an annual investment of billions of dollars in fixed transportation systems and the concomitant decision to protect the investment during an inflationary period has come a realization that the results of research and development and modern management methods must be applied to optimize the limited funds. Incremental savings that result from technical and administrative decisions will result in substantial long-term savings to owners and users.

The Second Bridge Engineering Conference was organized to facilitate an interchange of information on all aspects of planning, design, construction, repair, rehabilitation, replacement, and maintenance of vehicular bridges with specific emphasis on problems and solutions of interest to bridge engineers and administrators of highway, railroad, and transit agencies. The papers in these two volumes were prepared in advance and presented at the conference held September 24-26, 1984, in Minneapolis, Minnesota. Several of the papers are not included in the program because of limitations of time and space.

Organization and direction of the conference are the responsibility of the Planning Committee, whose members are listed on the reverse side of the title page. Technical reviews of papers were conducted by the several committees also listed on the same page.

The Bridge Engineering Conference was partly funded by the Federal Highway Administration. Financial contributions were also received from several contracting companies and suppliers in Minnesota.

The following organizations cooperated to make the conference possible:

COSPONSOR

Federal Highway Administration

COOPERATING AGENCIES

Associated General Contractors of America
American Railway Engineering Association
American Road and Transportation Builders Association
International Road Federation
Minnesota Department of Transportation
Minnesota Chapter, American Public Works Association
National Association of County Engineers

Feasibility of Computer-Aided Drafting

GEORGE A. CHRISTIAN and ALEXANDER P. COLE

ABSTRACT

Studies made by the New York State Department of Transportation to justify implementation of a computer-aided drafting (CAD) system for structural drafting are described. A demonstration project using existing available equipment during off-shift hours was organized to evaluate operations for this application and provide drawing productivity data. Observations, productivity results, and recommendations for a full-scale drafting operation are presented. The project results were the basis for an analysis to quantify potential cost savings and to recommend a CAD system configuration. The assumptions, methodology, and results of the cost analysis are outlined. The findings led to the conclusion that CAD is well justified from a cost standpoint provided minimum work-load and system utilization requirements are met.

The background studies and investigations made by the New York State Department of Transportation (NYSDOT) for the purpose of implementing computer-aided drafting (CAD) within the department's Structures Division are summarized. The Structures Division is a centralized operation responsible for all bridge design and design management activities for the department. At the time of the study the division was producing in-house contract documents including about 1,800 contract drawings for about 75 bridges a year. The principal activity of the implementation study was a demonstration project that was used to develop a capability in CAD for bridge structures and to provide data for a subsequent cost-benefit analysis.

CAD DEMONSTRATION PROJECT

Organization and Implementation

NYSDOT was in the unique position of having an in-house interactive graphics (IG) system purchased through a federal highway safety grant for the purpose of creating a statewide computer-based map for storing accident information (CLASS Project). As a result of the availability of graphics terminal time during the second and third daily operating shifts, a demonstration project was initiated in the summer of 1981 to evaluate the benefits of computer graphics in the Structures Division. That division investigated CAD by using nine staff members for drafting and engineering support work. Many different types of contract drawings were produced for several bridge projects. The results proved conclusively that computer graphics has not only a place in NYSDOT but a potential for increasing drafting productivity many times over.

The project was staffed with personnel from the division's Structures Design Systems Unit, the Bridge Design Section, and the Preliminary Plans Unit. Planning, scheduling, software development, and project management were the responsibility of the Structures Design Systems Unit. The CAD technicians were volunteers selected from the Bridge Design Section and Preliminary Plans Unit. The plotter operators and system manager were personnel assigned to the department's Computer Services Bureau and the CLASS Project and thus were already involved with the IG system.

Some of the major criteria in selecting the volunteer CAD drafting technicians for this project were as follows:

1. No more than one person would be selected from a single design squad;
2. Personnel selected would do the work assigned to them by their respective design units;
3. All volunteers would have permanent drafting titles, not engineering titles; and
4. All volunteers had to agree to work full time on either the second or third shift.

The project began with a CAD operator-training program for all project members. Each member was given about 3 hr per week of hands-on training from July through September 1981. Each person trained about 30 to 40 hr before becoming proficient enough in the IG system to start productive assignments.

By the end of this initial training period, the CAD technicians were proficient enough to start creating modules (cells) to be used repeatedly for many different drawings. By October 1981 about 60 cells had been stored and were available for use. Cell types include the standard contract drawing sheet with titles, the standard north arrow, and all standard prestressed-concrete shapes. During this time some user-friendly programs were written by Structures Design Systems Unit personnel by using standard software packages available on the IG system. The software development has progressed to the point that to date about 200 cells have been developed and about 25 user-friendly programs are in use.

A major portion of the initial work for this project was convincing some of the design unit supervisors that they would not be losing a skilled drafting technician but gaining a much more productive CAD technician. Most of the skepticism of the design supervisors was due to lack of knowledge of the capabilities of computer drafting, especially not knowing what the final product would look like. Demonstrations of the system and examples of typical computer-produced details were important in convincing design personnel of the merits of computer drafting.

Overall supervision for the structures drafting project was the responsibility of the project managers. In addition one or more persons on each shift were designated as a shift supervisor or assistant shift supervisor. All volunteer computer-drafting technicians were highly enthusiastic and self-motivated, so personnel supervision was minimal. Direct technical supervision was possible only during periods when the CAD shifts overlapped with the prime shift, when the computer-drafting technicians could receive instruction from the project managers or the design unit supervisors for whom they were detailing. A key ingredient in meeting production goals throughout this project was the technical expertise of the drafting technicians. Each was highly experienced and proficient in the detailing practices of the Structures Division and thus needed almost no ongoing technical supervision.

In addition, they were able to learn how to handle computer operations problems with little difficulty, largely because of the assistance provided by the CLASS Project staff.

Project Operations

This project started as a demonstration project but quickly progressed into a production-mode operation for the Structures Division. After a few months of full-time operation, the individual design units could not keep their designated volunteers busy, and the project managers decided to seek work from design squads that had no one involved in the CAD operation. This decision gave the project many more different types of drawings than originally planned. At this time 95 percent of the types of drawings found in a set of contract plans have been produced by the project, including preliminary plans, earthwork drawings, estimate tables, abutment and pier drawings, steel and concrete superstructure framing plans and sections, beam details, and tables.

The scheduling of work was and is important and critical and requires coordination among management, the design engineer, and the CAD technician. To use the equipment most efficiently, enough work has to be available so that each operator has been assigned at least two or three drawings at any one time. By soliciting work from all the design squads in the office, this was accomplished.

The pool concept is the best means of providing a continued, steady work flow to CAD so as to maximize productive use of the equipment. By providing a large pool of possible work, some selectivity can be used in assignments, and this was done during the demonstration project. For example, work scheduling was sometimes concentrated on projects with tight completion schedules. Drawings that could be produced quickly were sometimes emphasized and sought out from as many design squads as possible. Furthermore, the pool concept allowed for some specialization of drawing types among the computer-drafting technicians.

The pool operation also provides a work environment that helps maximize productive use of the equipment. When all CAD technicians are working together, they can freely exchange ideas on operating techniques. To become proficient on an IG terminal, one must find the most efficient of a number of possible ways to perform a given operation. The pool operation provides a means to learn from each other's experiences and greatly speeds the learning process. Having the CAD technican in a separate location also eliminates outside distractions and interference from those not involved with the work. Also, supervision is easier with a pool, because all members are performing similar tasks in a well-defined work space.

To monitor production, a reporting procedure was initiated to allow the CAD technicians to record the time it took them to complete a drawing. This same procedure was also provided for the manual-drafting technicians. As of April 1982, 94 logs of drawings produced on the IG system and 173 logs of drawings done manually were on file.

Observations

Working on a second or third shift and being removed from the design engineers except for an hour or two daily was a major change for the CAD technicians and required some adjustments, mainly by the design engineers. Design computations required quicker checking, and messages as to what details were required had to be clearly stated.

The major communication problem due to shift work occurred between the Preliminary Bridge Plans Unit and their CAD technician. Creation of preliminary bridge plans is somewhat of an iterative graphic design process, requiring a high degree of interaction between the engineer and the detailer. Graphical alternatives of fitting a bridge plan to a site often require immediate review by the supervising engineer. Also, it is difficult to have all the final layout information available from all outside sources before a plan is begun, which means that data are received or revised on an ongoing and sometimes unpredictable basis. For these reasons, continual contact between detailer and engineer is desirable, whether the bridge preliminary is done manually or by computer.

Despite these solely shift-related problems, computer-aided preliminary-plan creation showed great potential. In a fully integrated operation, the bridge site and survey plan would be passed electronically from a highway design file, thus eliminating the need for recreating these data by tracing and digitizing. Layout alternatives can be viewed and modified instantly on a graphics terminal. Finally, certain parts of the preliminary-plan drawings are extremely standardized, which means that they can be produced by using standard graphics cells or application programs much more quickly than by manual means.

Although the IG system was not purchased as a drafting system, it handled this task well. The software was flexible enough to meet drafting needs without difficulty. The programming features that it provided are a tremendously productive asset, and strong programming capabilities should be specified when a new system is acquired. It also had the capacity to handle the large workload of this project with little difficulty.

Problems were encountered only when the drafting operation was running simultaneously with the CLASS data-base system during the second and third shifts. When this happened, which was often, the system would degrade and some long response times for drafting operations would result. At its worst this condition would result in reducing the productive drafting time on a shift by 50 percent. For computer drafting to be fully effective, it must operate on a separate dedicated system free from data-base or other large program operations.

The plotting process was the bottleneck in the demonstration project. The flatbed plotter provided for the CLASS Project was too precise and slow for bridge drafting needs, and the time and effort required for final ink-on-Mylar drawings resulted in a slow turnaround time. There were no delays in submissions because of plotting, but if production increased, delays occurred. Normally a drawing was plotted three times during its production life. The first two plots were ballpoint pen on vellum, the first being an initial-check plot and the second being used for advance detail plans as well as a final check plot. The average ballpoint plots required about 1 hr to complete on the flatbed plotter, which is too long a time for this type of plot.

The final plot, with liquid ink on Mylar, required 1.5 to 2 hr on the average and could not be run unattended. The liquid-ink plotting required constant attention by the plotter operator to minimize variations in line thickness due to dust accumulation on the pens and to watch for skipping of the pen. Also, the pen points used with liquid ink tended to wear out after only three or four plots, so close attention to pen supplies and costs was required. As an alternative, a photographic print was made from a ballpoint plot on high-quality vellum, and it turned out well. The final product is of good, consistent quality and is competitive with

ink on Mylar when all costs are compared. It is also a much more reliable way to produce a large number of plots.

This experience has shown that a high-speed plotter of contract-plan size is an essential part of a CAD system. A likely choice would be an electrostatic plotter of sufficient quality for all check and advance plots, and it should be on line to the graphics system. Such plotters are available and they are precise enough to produce final plots if desired; the current flatbed plotter could still be used for final plots only.

From previous experiences cited by other state agencies using CAD, it became apparent that checking of computer-produced drawings is sometimes more precise than needed. Checking appeared to be necessary at the beginning of the project, but the checkers were convinced that the drawings were as good as or better than those drawn with manual methods. It was found that prints from the plotter are faster and easier to check when colors are used to represent different line weights. Although it was not monitored, review time is expected to be reduced substantially as graphics operations increase. Use of repetitive drawings and precise dimensioning eliminates much of the human error.

Results

During the first 6 months of the project, about 84 drawings were produced for 19 bridge projects, including 11 of the 15 to 16 types of drawings found in a typical bridge project document. This number exceeded initial estimates because of the ability of the operators to pick up the technique and the quantity of work available from the design squads.

Uniformity of lines and lettering and accuracy of line position in the drawings could not be faulted. The lettering was made to conform with the Leroy lettering style used in the manual operation. The line weights were selected based on the experience of the drafting technicians working on the project and were set to match line weights for manual drafting as closely as possible.

The productivity ratio determined from the demonstration project data is summarized graphically in Figure 1. Average productivity ratios for each 2-week pay period for the duration of the demonstration project were computed and used to determine the plotted cumulative average productivity. Also plotted is the rolling average for the 10-day pay period, which better indicates the ratios being attained after the initial learning period. Both curves show the learning-curve effect and if extended would eventually converge on a steady-state productivity ratio. The ratio attained at the end of 9 months is shown to be 2.3:1.

It is projected that an overall average productivity ratio between 2.5:1 to 3.0:1 is achievable. The project value of 2.3:1 was attained under conditions that were far from ideal, namely, with an old system that was overtaxed between mapping with data-base and mapping with bridge drafting demands. It was also attained in 9 months of operation at less than full time. Other states, such as Michigan, have documented average productivity ratios for structural drafting of 3:1; 10:1 has been achieved on some types of bridge drawings. Based on this information, a 2.75:1 average ratio is a reasonable and attainable goal and was assumed for a new system implementation.

COST-BENEFIT ANALYSIS

In order to demonstrate the potential cost benefits of implementing a computer-drafting system for the Structures Division, the following cost analysis was made. This study compared the average costs of producing a drawing by manual versus computer-aided methods and was used to determine a CAD system capacity that would best fit production needs and optimize cost savings.

The basic cost and production equations used for this analysis are outlined as follows:

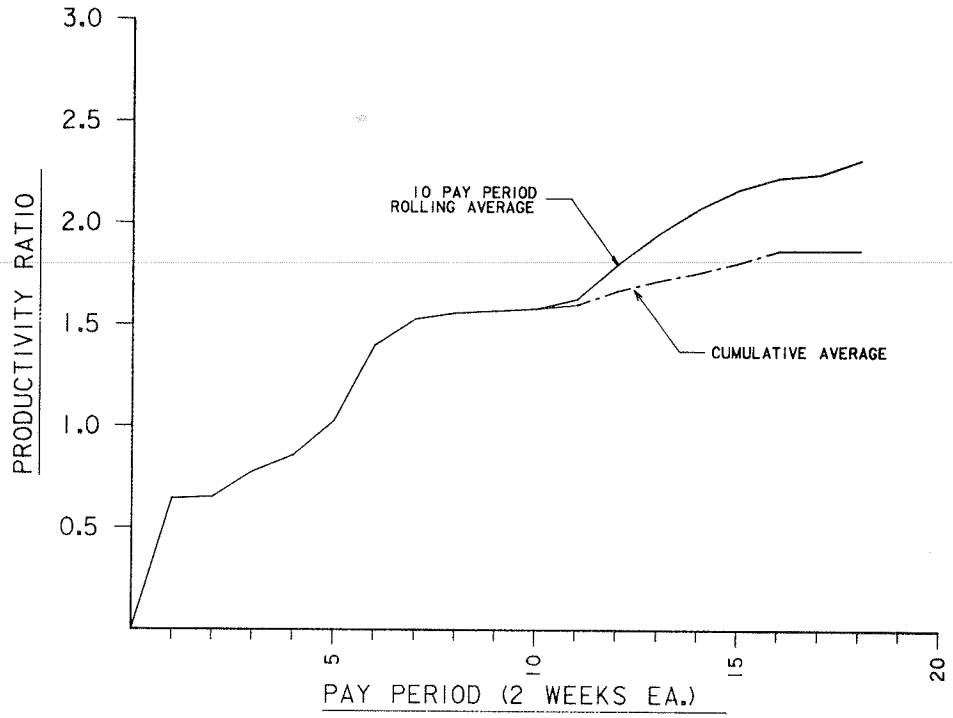

FIGURE 1 Structural drafting productivity in the CAD demonstration project.

Drawing output for computer drafting

$$ND = WYEAR * NT * TUF * (PR/MDR) \quad (1)$$

Manual drafting

$$MDC = MDR * MSCOST \quad (2)$$

Computer drafting

$$GDC = [GSCOST * (MDR/PR)] + (AEQ + ADMIN)/ND \quad (3)$$

where

ND = number of drawings,
MDR = average manual-drafting rate (hours per drawing),
MDC = cost per manual drawing ($/hr),
MSCOST = direct manual-drafting salary cost + fringe benefits ($/hr),
GDC = cost per computer drawing ($/hr),
GSCOST = direct computer-drafting salary cost + fringe benefits ($/hr),
WYEAR = standard work year (hr),
AEQ = annual cost of computer-drafting equipment including maintenance ($),
ADMIN = annual administrative and overhead personnel cost for computer-drafting system ($),
NT = number of work stations (terminals),
TUF = terminal use factor, and
PR = productivity ratio (manual hours per drawing divided by CAD hours per drawing).

The cost equation for computer drafting consists of two parts. The first is the direct cost per drawing of the graphics operator. The second is the cost per drawing of the added expenses of equipment and administrative salaries. These fixed administrative and equipment costs are divided by the number of drawings produced to give their contribution to the cost per drawing. Personnel costs and production rates for manual drafting were determined from department accounting records for a 2-year period and verified by the drawing production monitoring procedure established during the demonstration project. Salary plus fringe benefit costs were included. Equipment costs were based on manufacturer's averages for systems of comparable size. The dollar values used were all present-value (1982) amounts and capital costs of equipment amortized over a 5-year period. The standard work year was assumed to be 2,000 hr per person.

For computer drafting to be cost effective, the PR and TUF must be sufficient to offset the added personnel, equipment, and administrative costs charged to each computer-produced drawing. The PR, or ratio of production time savings per drawing by using graphics over manual methods, directly influences the direct manpower charges. Furthermore, it has an effect on the equipment and administrative costs per drawing, because higher productivity allows for more drawing units to be produced to offset these fixed charges.

TUF measures the amount of time a computer-graphics work station is being used for drawing production and will influence the equipment and overhead charges per drawing. A TUF of 1.0 would mean that the terminal is being used for production for a full 2,000-hr work shift per year. Multiple work shifts can increase TUF to 3.0 (for three 2,000-hr shifts). Full production use per shift is not practical because of equipment down time, operator leave time, and system support tasks requiring terminal use. Based on a combination of employee attendance records, CAD equipment performance records, and information obtained from other agencies using CAD, a 75 percent terminal use per work shift was believed to be reasonable.

Figure 2 shows the necessary combinations of TUF and PR for three IG system configurations that will result in equal CAD manual-drafting costs. Any combination of TUF and PR that falls above these curves will result in a cost-benefit ratio in favor of CAD. This graph indicates that the PRs necessary to make a one-shift operation cost effective are higher than those that can reasonably be expected to be an attainable average for most structural drafting. A one-shift operation could possibly be cost justified if the drawings assigned to computer drafting were limited to those types that demonstrate PRs greater than 4:1, but this would seriously limit the available CAD workload.

Multiple shifts with the terminal use provided will permit achievable PRs as an average for all structural drawings. PRs in the range of 2.5:1 to 3:1 have been shown to be practical, and such values will result in a positive cost-benefit ratio with multiple shifts.

Figure 3 shows CAD costs computed per drawing for various scenarios of number of work stations, work shifts, and PRs. These plotted costs are compared with the average cost of manual drafting. The graph indicates positive benefits of multiple shifts, although increasing from two to three shifts provides less of a decrease in drawing cost than increasing from one to two shifts. Figure 3 also shows the strong influence of the productivity value on cost per drawing for each system and use configuration.

Although maximizing system size and terminal use reduces drawing cost, the configuration chosen must be compatible with the total drawing output of the Structures Division of 1,800 drawings per year. When a target number of drawings for computer drafting is chosen, the following criteria must be considered:

1. The number must be great enough to provide a positive cost-benefit ratio;
2. The number must be well within the 1,800-drawing annual office output to provide a steady flow of work; and
3. The number must provide for a combination of computer drafting plus manual work that is compatible with the entire bridge design engineering work force; if cost savings are to be attained by staff reductions, the number must allow for a manageable rate of attrition to occur while production is being met.

Cumulative costs of drawing production with four-, five-, six-, or eight-terminal systems versus the number of drawings produced are plotted in Figure 4. The cumulative cost of manual drafting is also plotted for comparison. In this graph it is indicated that, in this case, it takes a minimum of about 650 drawings to fully offset the increased costs of computer drafting when compared with manual methods. This minimum is readily attainable from the total division annual workload of 1,800 drawings.

It is also indicated in Figure 4 that system size in terms of number of terminals has little effect on the cumulative drafting cost. The CAD system configuration used for this study was assumed to consist of a series of CAD work stations driven by a central processing unit (CPU), and the cost of one work station compared with the overall cost of the CPU, peripherals, and plotter was found to be small. Therefore the equipment cost approaches a fixed cost regardless of the number of terminals,

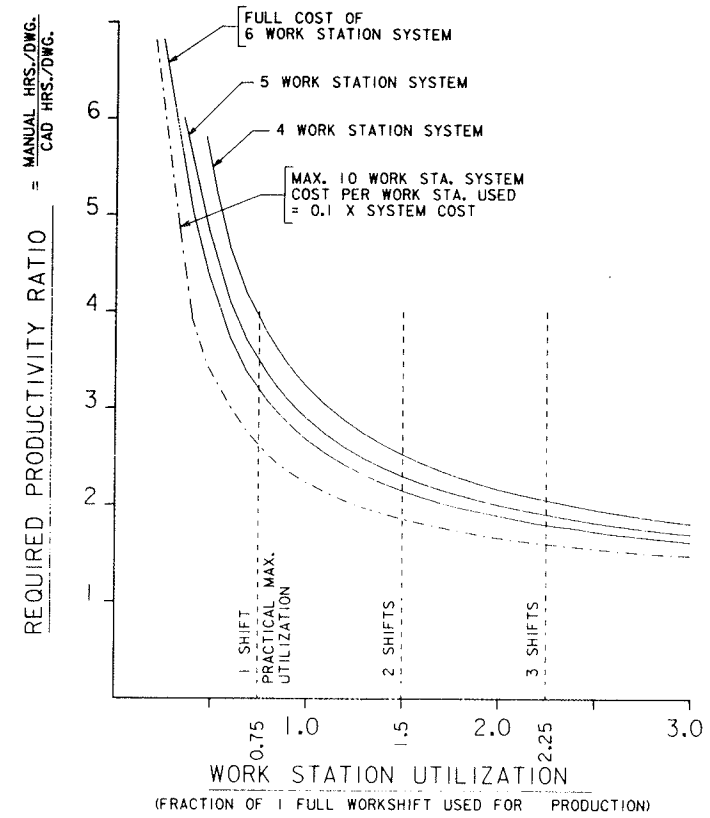

FIGURE 2 Use analysis: equal production cost per drawing for CAD versus manual drafting.

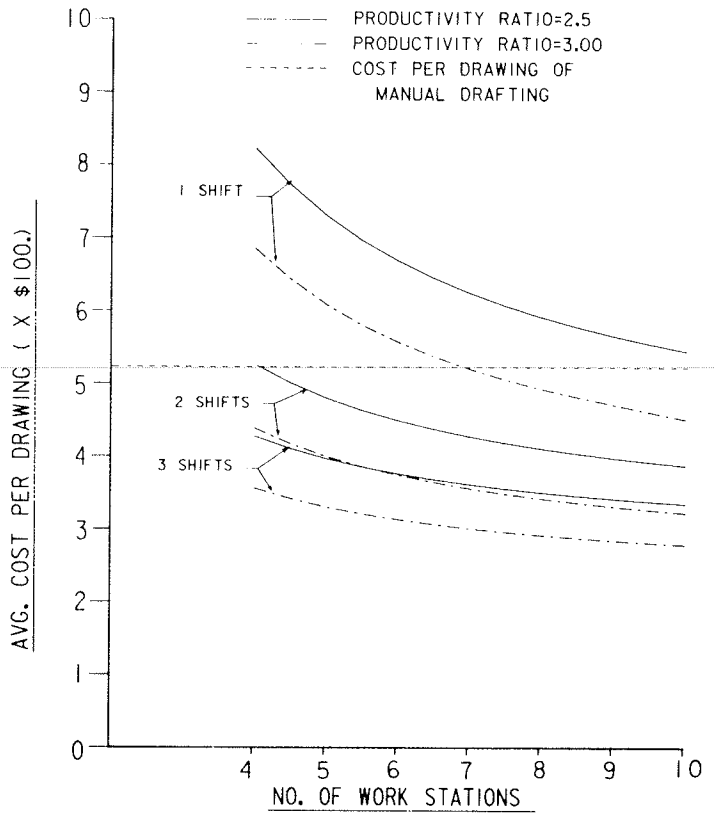

FIGURE 3 Cost per drawing of computer drafting.

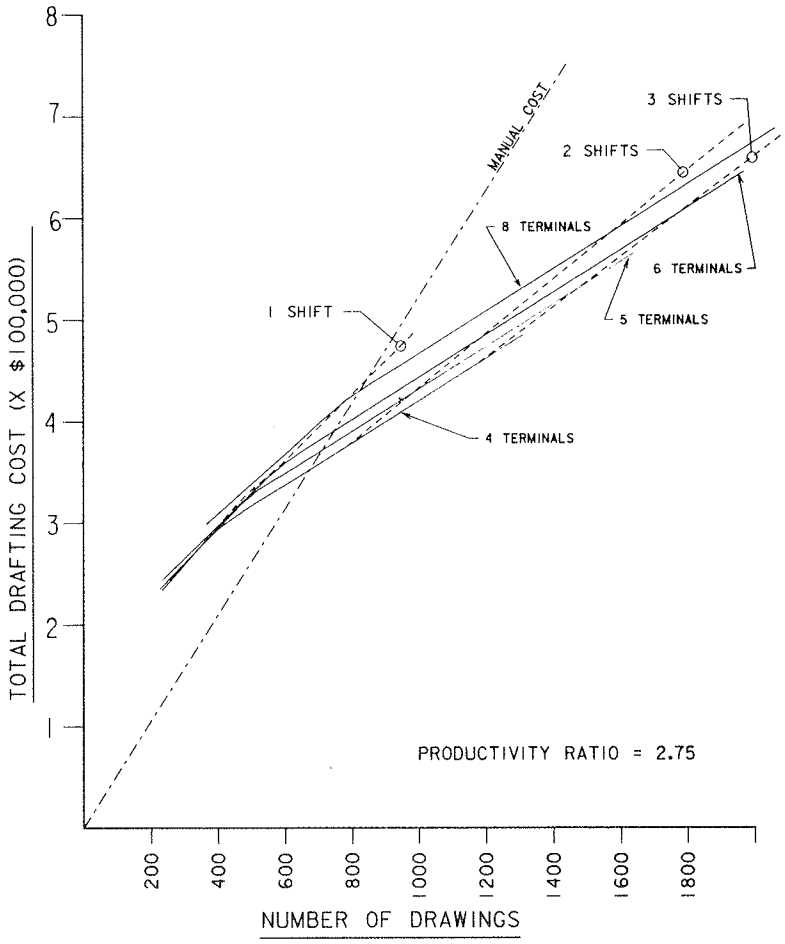

FIGURE 4 Cumulative costs of computer drafting.

and the total computer-drafting cost is nearly a linear function of the numbers of drawings produced. Moreover, cumulative savings over manual drafting increase almost linearly as production increases. Choosing a system for structural drafting becomes a question of deciding on a target number of drawings to be assigned to computer drafting and choosing a system size and terminal use (i.e., number of shifts) that provides the capability for that number.

To implement a full-scale computer-drafting operation for this application, an annual target of about 1,000 drawings was recommended. This is well above the 650-drawing minimum shown necessary for cost effectiveness and will result in a net annual production savings exceeding $100,000. It is also a little more than one-half the total division output of 1,800 drawings, thus providing a larger pool of drawings, which will help smooth the computer-drafting work flow yet allow for some selectivity in drawing types most suited to computer drafting. This distribution of work load also provides for a large enough manual-drafting work load so that a balanced work force can be maintained. In addition to detailing, technicians will be needed for estimating, review work, and other assignments, and they must provide a pool of expertise for vacancies in the computer-drafting work force.

Figure 4 shows that a 1,000-drawing capability is theoretically possible with four terminals on three shifts or five or six terminals on two shifts. It was recommended that a two-shift operation be used to meet this production goal. It was believed that two shifts would be easier to implement initially from a personnel standpoint and allow for more production flexibility than three shifts. A third shift could be implemented at a later date if production demand warranted it or it could be used as an overtime shift. Because two shifts alone are cost effective, any use of a third is cost free from an equipment standpoint. Finally, a five- or six-terminal three-shift operation results in drawing capacity levels too near the available 1,800 limit to be efficient. Four terminals and three shifts fit production needs but allow for no use flexibility or immediate expansion of applications.

The final question was the number of terminals. It was recommended that a six-terminal system be acquired initially. Full production of five terminals on two shifts falls close to the production goal. Adding a sixth terminal provides for nearly a 200-drawing capability increase over five terminals at little added cost and provides a slight excess capacity with full use. Even if the sixth terminal is not fully used for production, its cost is easily carried by the benefits derived from a 1,000-drawing work load. The sixth terminal will provide a little added flexibility for production and development work as well as an equipment backup. Future developmental work is essential to introduce new CAD applications, and this recommended work-shift and equipment proposal will provide the additional terminal time necessary to developmental work in new applications for the department.

Cost Savings

System costs must be justified by providing real

dollar savings to the department. These are attained through increased productivity, that is, decreasing the number of man hours to perform a given task (e.g., structural drafting). Increased productivity provides two options for real dollar savings:

1. Savings in personal service costs through decreasing the work force or
2. Savings in expenditures to outside consultants by using the increased capacity to do more work in house.

Whichever option is used to produce savings, it must be assured that a balance in production capacity is maintained between the drafting and engineering phases of the work. Because the CAD system is to improve productivity in drafting only, the total bridge design staffing pattern must be adjusted to balance engineering and drafting needs.

In computing savings in personnel made possible by the CAD system, it was assumed that the current in-house work load of ±1,800 drawings would remain constant. Staff savings will be made by reducing the drafting work force to a level where a combination of CAD plus manual drafting will provide a work capacity equal to that provided by the current fully manual work force. Because CAD would only affect drafting capabilities, the engineering staff would be unaffected. Comparing the reduction in personnel costs with the expenses attributed to CAD resulted in about a $100,000 net savings, as predicted by the cost-benefit analysis.

Although CAD system cost could be justified through staff attrition, larger cost benefits are possible by using the increased production capacity to do more work in house and reduce consultant contracts. In computing the savings in consultant costs that can be attributed to a CAD drafting system, it was assumed that the total CAD plus manual-drafting staff would remain the same size as the current staff, except that some manual-drafting positions would be transferred to the CAD unit. The actual increase in in-house capacity attributable to CAD is then the difference between a CAD plus manual-drafting operation and a fully manual operation with equal numbers of personnel.

To increase overall in-house capability, the added drafting capacity of CAD must be supported by an increased engineering capability. To do this would require adding engineering positions to the design staff. The total cost of this increase in in-house capacity attributed to implementing CAD in this manner is the sum of the CAD equipment plus overhead costs and the cost of the added engineering staff to meet the increase. To determine potential savings, this total cost is compared with the cost of hiring consultants to do the same amount of work. The increased real dollar savings by increasing staff rather than reducing personnel stem largely from the difference in overhead costs between in-house and consultant work. However, it is the addition of a CAD system that provides this capability at the least cost.

Other Benefits

In addition to the cost savings for structural drafting, the CAD system would provide benefits to other applications, both in the Structures Division and in highway design. These added applications would be developed by a CAD applications unit, and as terminal time becomes available through increased drafting productivity, they will be put into production. Major benefits, other than drafting, in structures include the following:

1. Detail checking: Although detail checking can never be eliminated, CAD-produced details will reduce checking and correcting time requirements by producing drawings with fewer errors. This will occur over time as an inventory of standardized details is reused many times, thus eliminating any repetition of errors for these details. This benefit will occur with virtually no added development work necessary.
2. Estimating: CAD software now available for drafting systems can enable the operator to automatically compute areas and volumes of the shapes being detailed. This will eliminate the need for manual computations for these values and reduce the total man hours needed for estimating. Future developments would include integrating a reinforcing-bar list computation and plotting programs with the CAD drafting system, allowing automatic-bar list generations from the CAD-produced details.
3. Standard sheets: Current standard detail drawings now maintained manually by the Structures Division would be stored on CAD files. As specification or policy changes dictate revisions to these details, the modifications can be readily made on the CAD files without the need of manual redrawing.
4. Layout: A CAD system would provide an interactive means to do bridge layouts, eliminating the slow trial-and-error manual methods involving retracing proposed layouts. Future developments in CAD highway design applications will also be applicable to bridge layout. In addition to productivity in terms of time, the CAD operations would produce more accurate layouts than the manual-scaling methods now used.
5. Design: An interactive CAD system would provide the designer with ongoing feedback and opportunities for response and control during an automated design, resulting in faster and more thorough final designs. CAD design systems allow designs to be visualized and provide an efficient means of setting up and producing finite-element or grid models for complex structures and dynamic analyses.

CONCLUSION

Based on the findings of this project, CAD works and can be highly productive in terms of time required to produce an engineering drawing. Key factors enhancing drawing productivity include the use of CAD technicians experienced in the drafting application, a sufficient flow of work, as well as CAD hardware, software, and plotting capabilities geared to the drafting application. The use of a drafting pool provides a better overall production environment but requires careful planning in work scheduling and drawing review.

CAD can also be justified on a cost basis. If the CAD equipment is used sufficiently, the savings from increased productivity can overcome the equipment and support expenses involved. However, the CAD use needed for a significant positive cost-benefit ratio may demand more than a one-work-shift operation. Consideration must be also given to the organizational effects of any increased drafting work capacity due to CAD in a combined design and drafting operation.

For the NYSDOT application evaluated by this study, CAD is cost justified. The required productivity and the minimum cost-effective CAD work load can be provided without significantly affecting the design and drafting production balance. Based on the demonstration project findings and cost evaluation, it is shown that a CAD operation with two work shifts and six work stations will provide at least a net 20 percent savings in the production cost per drawing. Further productivity increases through experience, new applications software, and drawing standardization will increase this net savings.

Publication of this paper sponsored by Committee on General Structures.

Superstructure Envelope Generation with Conversation-Mode Software

WILLIAM C. McCARTHY, GEORGE GROSSMAN, and JOHN GREY

ABSTRACT

The versatile qualities associated with the IBM conversational monitor system (CMS) were used in the development of a computer program to generate shear and moment envelopes and maximum and minimum reactions for bridge superstructures. Carefully contrived questions throughout the envelope program, made possible through CMS, solicit a free-format user response that guides the direction of the program run. This conversation mode permits selected application of program segments, flexible input and output control, and repetition of analytical steps. A matrix-displacement approach is applied to the production of maximum positive and negative shear and moment values at every 20th point along a span for up to as many as 10 continuous spans. The program models the superstructure as a continuous beam with many user options governing the input of material and cross-sectional properties. The properties for nonprismatic spans may be input over user-designated length segments. An HS truck load, its corresponding lane, and, by request, the Interstate equivalent are positioned on the structure according to AASHTO specifications. The optimum magnitudes are found by way of analytically derived influence lines. Output may consist of shear, moment, and reaction influence lines, optimum magnitudes at selected points in the beam, and the shear and moment envelopes. A secondary program dead-load function may result in output that includes the reactions and shear and moment diagrams for both simple and continuous support conditions. The extent of the output is at the discretion of the user.

The New Mexico State Highway Department Bridge Design Bureau has an ongoing software development program to employ the latest in computer technology toward the solution of bridge problems. The goal of the bureau is to update existing software where feasible and, when necessary, to develop new material. Ultimately the bureau expects to have an interactive system that transfers information to and from a central core of data, uses direct input with immediate feedback, and may draw on the services of one or more programs, depending on the extent of the problem. The sequencing of the programs will offer a user the flexibility of moving forward to a next logical step or of digressing to a previous point in order to repeat a step or steps. The repetition of steps brings no loss in pertinant data because the data are stored in a central core for the user to modify or not, as desired.

Updating of existing programming has begun along with the establishment of a central data core or standard file. Software designed to generate the shear and moment envelopes and optimum reactions for bridge superstructures was considered an essential start in new program development. This new FORTRAN program, termed MAXMIN, was targeted to be diverse in its capacity and to lend itself for use in an existing beam design program. The many qualities associated with the IBM conversational monitor system (CMS) (1) were directed toward this goal. MAXMIN, the development and range of which are detailed in subsequent paragraphs, exceeded the objectives of the bridge design bureau.

CONVERSATIONAL MONITOR SYSTEM

The IBM CMS (1) may be incorporated into the larger IBM or Amdahl Corporation computers. When available, the interactive CMS editing, storage, and input capabilities give the programmer as well as the user a powerful tool. Simple edit commands allow the programmer to modify, add to, or take away from an existing program with relative ease. Although a MAXMIN user would not normally edit the program, an exception may be the occasional modifications to reflect future changes in AASHTO (2) specifications. Toward this end, the bridge design bureau has required the identification and extensive documentation of program segments dealing directly with AASHTO specifications.

CMS is divided into storage files; the first, or A, file is typically assigned as the primary work region. As such, main programs with their subroutines are often placed in file A in a packed form that reduces the amount of needed storage. Programs stored in a packed form must be unpacked before being compiled or executed. Main programs may also share subroutines, which eliminates duplication. CMS permits the use of EXEC programs to automatically control the extent of main programs. An EXEC program, for example, may compile a main program, identify and define the size of input and output files, and then direct execution of the program. Input data are not restricted to a file by CMS but may be read directly through a cathode-ray tube (CRT) terminal. In the current form, data are entered into MAXMIN through a CRT, whereas output is partly stored in a secondary file B and partly through a CRT. The user is given an opportunity to study the data in the file before he requests a hard copy.

The bureau's standard file has preassigned regions to store relevant bridge data. CMS permits the selective retrieval of data from this file. A main program or subroutine read statement identifies the file line and, through format control, the line segment containing the desired information. A like process with write statements may be used to place information in the file. In this way, the data, such as span lengths or cross-sectional properties, may be withdrawn from the file before the operation of a program. An empty file at the relevant positions automatically sends the program to the CRT for the required data. However, a user may designate early in the process that the material be entered only through the CRT to avoid working with data in the file not applicable to the problem at hand. Similarly, CRT input or program output or both may

be sent to the file at the user's prerogative for use in subsequent program runs. MAXMIN is not operational through the standard file at this time even though the mechanism for doing so may be readily inserted into the program. This convenient process will not be made operational in MAXMIN until an interface with a pier analysis program, under development, is complete.

The CMS conversation-mode capability is of direct benefit to the MAXMIN user. Carefully contrived questions have been inserted into MAXMIN with formatted write statements at pivotal locations. The user response, through a CRT with a free format that uses commas to separate individual data terms, dictates the direction of the program. The anticipated response, in many cases, is either a yes or no. Instead of an alphanumeric answer, the bridge design bureau prefers the convenient 1 for yes and 0 for no. When data are requested, the bureau employs a subroutine that gives the user up to three chances to verify the data. Once this has been done, the program moves to the next step. The user may replace the previous data in any of the three chances. Failure to verify terminates the program run.

PROGRAM EXTENT

The program has as its principal objective the development of shear and moment envelopes and the maximum and minimum reactions for a bridge superstructure or individual girder modeled as a continuous beam. Loads consist of an AASHTO HS truck, the corresponding lane, and, when specifically requested, the military or Interstate equivalent. A truck load selection ranging from an HS15 through an HS30 designation is offered to the user. With the loads specified, the program is geared to produce the maximum positive and maximum negative (minimum) shear and moment at every 20th segment along each span for up to a 10-span beam. This process involves three steps. First a matrix-displacement continuous-beam analysis for unit loads at the 20th points precedes the development of influence lines. Simple statics is then applied, one point at a time, toward the resolution of the influence lines. Finally the loads are located over the influence lines in positions that create optimum values. The latter process follows AASHTO (2) guidelines with regard to truck-axle spacing and load placement.

A secondary program objective encompasses the reactions and shear and moment diagrams for dead load. The dead-load capacity was designed to handle three possible cases: simple span, continuous span with a noncomposite deck, and continuous span with a composite deck. The user may designate simple-span dead load for the girder weight and then follow through with a second continuous treatment involving the weight of the deck. The program permits, at the user's discretion, the addition of dead load beyond the weight of the deck and girder. Thus a user may incorporate random uniform or concentrated dead loads (e.g., signposts, road surface, and so on) into the analysis.

The question-and-answer format establishes the direction of the analysis, so the user may decline some of the dead-load portion and move directly to a live-load analysis. The user may also work with only the dead-load portion and skip the live-load portion. Normal application, however, would have the user build on the analysis, step by step, from dead-load to live-load analysis.

ANALYTICAL THEORY

The analytical choice was the matrix-displacement continuous-beam analysis detailed by Wang (3). Static equilibrium at the supports ties external generalized forces (P) to internal generalized forces (F) by a statics matrix ([A]). A conjugate beam establishes a member stiffness matrix ([S]) that bonds F to internal displacements (e). Manipulation of the statics and deformation-matrix equations with an application of the conservation of energy produces the two key equations:

$$\{F\} = [SA^T]\{X\} \quad (1)$$

$$\{P\} = [ASA^T]\{X\} \quad (2)$$

Once the load matrix ({P}) has been established, Equation 2 is solved simultaneously to obtain the external displacements ({X}). Insertion of {X} into Equation 1 leads to the internal forces ({F}) or span moments at the supports.

A span is subdivided into 20 equal segments for analytical purposes. A concentrated load multiplied by the influence line value directly beneath yields the associated quantity. Second-order interpolation is used to obtain the influence value when a load is not over a 20th point. A uniform load multiplied by the region beneath the influence line segment over which the load acts again yields the associated value. This region is derived by using Simpson's one-third rule.

MAXMIN determines optimum magnitudes by first identifying peak positive and negative influence values. Distances between peaks are found to correctly define trailer-axle spacing. The truck is passed over the influence peaks, both back to front and front to back, for up to five sections before and after a peak. The central axle is always positioned directly over a 20th section. A reaction, shear, or moment value is found for each truck placement and tested against the previous value to identify the larger. The maximum (or minimum) truck value is compared against the corresponding quantities derived from the Interstate and lane loads to obtain the optimum.

In some cases the truck and Interstate loads may be placed over the influence line so as to immediately create a maximum or minimum. The end reactions are an example. MAXMIN is designed to account for these special cases.

The 20-segment breakdown ensures a high degree of accuracy when nonprismatic sections are involved. The nonprismatic member stiffness coefficients and the fixed-end shears and moments are generated with a subroutine based on a flexibility approach outlined by Kardestuncer (4). Thus the force-deformation relationships are not predefined as they are for prismatic spans. The resultant fixed-end moments serve as an equivalent load in the matrix-displacement technique.

INPUT REQUIREMENTS

Three types of data are solicited by MAXMIN--the beam dimensions, properties, and load. The program requests data first for a dead-load analysis and at its conclusion proceeds to the live-load or principal analysis. Dimension and property data entered for the dead-load analysis are carried forward to the live-load analysis. However, a program inquiry to the user with regard to property changes allows the user to modify the material before the next step begins. As previously mentioned, the user is given the option to skip unwanted analytical segments.

The dead-load portion may involve only a few data requests or become quite extensive, at the user's discretion. The dead-load support conditions (simple or continuous), the number of spans, and the

span lengths are established first. Then the cross-sectional dimensions (or moment of inertia and area) and the material properties are entered one span at a time. MAXMIN calculates the moment of inertia and area given the cross-sectional dimensions and establishes the uniform dead weight of the span. Beyond this, the user may designate additional combinations of concentrated and uniform loads. The process concludes with a matrix-displacement dead-load analysis.

The case may arise in which additional dead load is placed on the structure after the simple spans have been made continuous. MAXMIN accounts for this possibility, permitting a second dead-load analysis with an equal capacity to enter an extensive array of uniform and concentrated loads. Again the user is queried as to changes in properties or cross-sectional dimensions.

Many options are possible with regard to the structural make-up. It is necessary to have a modulus of elasticity and moment of inertia to achieve a matrix-displacement solution. The dead-weight calculations require a cross-sectional area and specific weight. When the beam is composed of two different materials, MAXMIN carries out a section transformation by using a modular ratio. A moment of inertia and area may be input without definition of a specific cross section. However, a cross section may be constructed as shown in Figure 1. The height and width for each rectangular component of Figure 1 are input at the request of the program. A component that does not exist is given zero dimensions. The height and width of each rectangular component are assigned a number. On a cue from the program, a change is implemented by specifying the dimension number followed by the new magnitude. Thus, a change is quickly made without alteration of the other values. The user may make as many changes as desired. An empty record, as would occur when no data are entered, sends the program forward to the next series of statements. In this way the user concludes the changes by hitting the CRT return key without first entering data. MAXMIN continues to cue the user for new material until an empty record is encountered.

One moment of inertia or set of cross-sectional dimensions is required for a prismatic span. A nonprismatic span, on the other hand, needs these values for 20 equally spaced intervals along the span. Although these values could be entered one interval at a time, this would be cumbersome in most instances. Thus, MAXMIN has a procedure for entering data in length segments. A set of values is input that defines the cross section at the beginning of the segment. These values are automatically assigned to the intervals within the length segment. The web depth for an established cross section may vary over the length according to linear or parabolic formulations shown in Figure 2. Additional

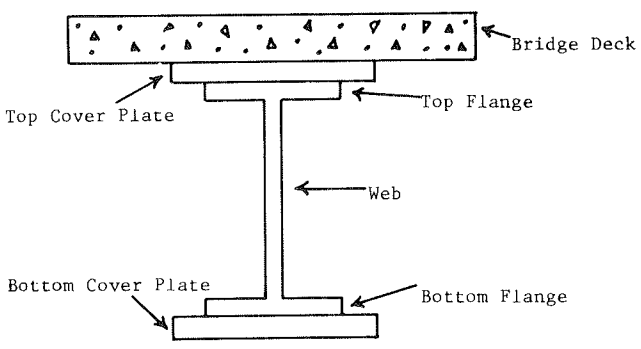

FIGURE 1 Cross-sectional components.

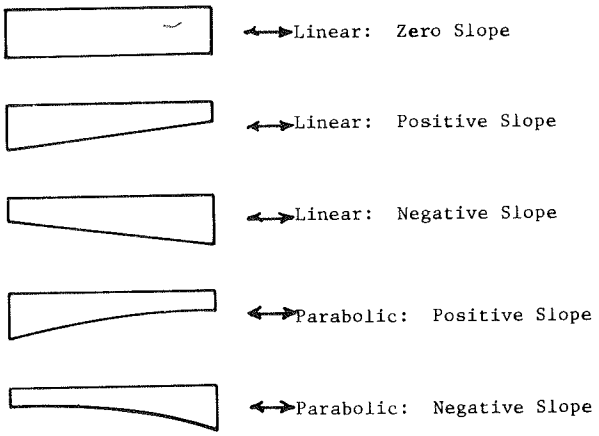

FIGURE 2 Web-depth variations.

web depth at the end of the segment is all that is required.

When a span is symmetric, the inertia or dimensions need only be input for the first half of the span. A change in section is accomplished as before, except that the user designates the beginning and end of the length segment for which the modifications are to be made.

The live-load portion typically needs the least amount of input data. Unit loads are automatically positioned at the 20th points to generate influence lines. The user is queried as to the truck load type and whether to include the Interstate equivalent. MAXMIN calculates the equivalent lane and Interstate load. No other data are required.

PROGRAM OUTPUT

The flexibility featured in the input requirements is carried forward to the output. For dead load the reactions are automatically printed, whereas the shear and moment diagrams are printed by user request only.

Shear and moment envelopes may not necessarily be the end result when live load is involved. The user may request a printout of influence lines for reactions or for shear and moment at selected points along the beam. In addition, the user may ask for maximum and minimum reactions or for maximum and minimum shear and moment at user-designated points along the beam. This process may be repeated again and again with either the same live load or a different load, as specified.

MAXMIN live-load output includes the optimum magnitudes, both positive and negative, and at the user's request, the load type and position over the beam that caused these values. If the truck load controls, the result is the location of the central axle from the left beam support and whether the truck is moving right to left or left to right. Similar treatment is given to the Interstate equivalent except that the location is to the front axle. Finally, if the lane load controls, the concentrated load (or loads in the case of negative moment) is again located relative to the left support whereas the uniform load is placed over the positive or negative influence region.

A shear or moment envelope is composed of a maximum positive and maximum negative value at every 20th span segment over the length of the beam. Although possible, a double listing of load type and position accompanying the optimum magnitudes is not generally requested. Instead a more reasonable approach is to generate the shear and moment envelope

followed by a selective request for additional data at selected points along the beam.

SAMPLE PROBLEM

The two-span nonprismatic beam in Figure 3 illustrates the kind of problem routinely handled by a MAXMIN analysis. The cross section is a cover-plated wide flange with a web depth of 40 in. at the supports, varying parabolically to a depth of 20 in. at the span centerlines.

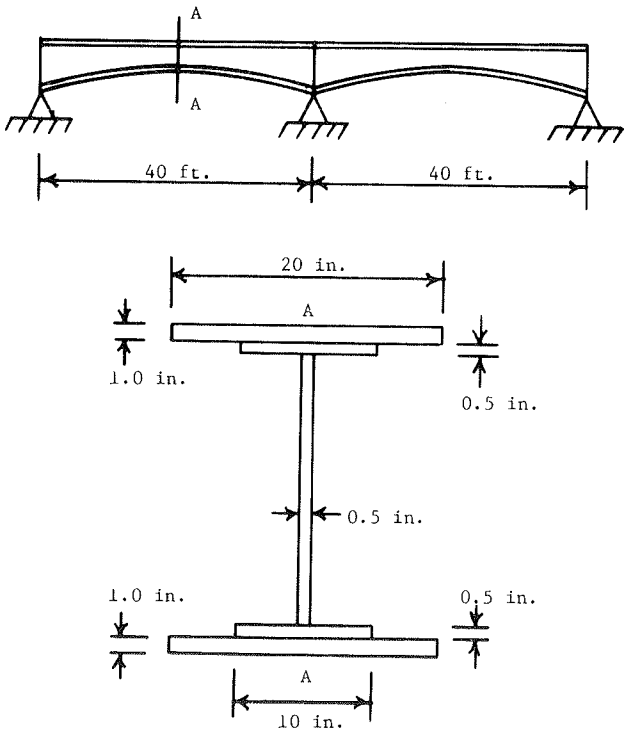

FIGURE 3 Sample problem: nonprismatic beam.

The MAXMIN input sequence started with a request for the analysis type, which for this example was live load only. A series of requests followed to establish the number of spans, span lengths, and span type (prismatic or nonprismatic). Under the continued guidance of the program, a segment a half-span long was defined by entering the distance to and web depth at the beginning and end of the segment. A positive-slope parabolic web-depth variance was designated for the segment. MAXMIN calculated the intervening 20th-span property values after the flange and cover-plate dimensions had been entered. In response to the user-specified symmetry, MAXMIN assigned these properties to their counterpart on the other half of the span. An HS20 to 44 truck load (military) was specified to conclude the input.

For brevity the MAXMIN output was restricted to a few representative items. Table 1 presents the MAXMIN-generated influence coefficients for the first two reactions. The maximum and minimum reactions with the pertinent load data are contained in Table 2. MAXMIN was asked to produce maximum and minimum shear and moment values at user-selected points along the beam. These values are found in Table 3. ICES STRUDL II (5) supplemented with hand computations was used to verify the MAXMIN results.

TABLE 1 Reaction Influence Coefficients

Left Reaction		Central Reaction		Left Reaction		Central Reaction	
Span 1	Span 2	Span 1	Span 2	Span 1	Span 2	Span 1	Span 2
1.000	0.000	0.000	1.000	0.318	−0.125	0.814	0.701
0.934	−0.024	0.083	0.998	0.270	−0.117	0.860	0.634
0.867	−0.046	0.166	0.993	0.226	−0.107	0.898	0.563
0.801	−0.067	0.248	0.984	0.186	−0.094	0.929	0.488
0.735	−0.085	0.329	0.971	0.149	−0.080	0.953	0.410
0.670	−0.101	0.410	0.953	0.115	−0.065	0.971	0.329
0.606	−0.114	0.488	0.929	0.083	−0.049	0.984	0.248
0.544	−0.124	0.563	0.898	0.054	−0.033	0.993	0.166
0.483	−0.130	0.634	0.860	0.026	−0.016	0.998	0.083
0.425	−0.132	0.701	0.814	0.000	−0.000	1.000	0.000
0.370	−0.130	0.761	0.761				

TABLE 2 Maximum and Minimum Reactions

	Value	
Characteristic	Maximum	Minimum
Left reaction		
Load type	HS20-44	HS20-44
Movement	Left to right	Left to right
Back axle spacing (ft)	14	14
Central axle location (ft)	14 from left	64 from left
Reaction magnitude (kips)	50.88	−7.12
Central reaction		
Load type	HS20-40	–
Movement	Left to right	–
Back axle spacing (ft)	14	–
Central axle location (ft)	44 from left	–
Reaction magnitude (kips)	68.76	–

TABLE 3 Select Shear and Moment Envelope Values

	Value	
Characteristic	Maximum	Minimum
First span, midpoint		
Shear		
Load type	Military	Military
Back axle location (ft)	16 from left	20 from left
Magnitude (kips)	15.36	−27.54
Moment		
Load type	HS20-44	HS20-44
Movement	Left to right	Left to right
Back axle spacing (ft)	14	14
Central axle location (ft)	20 from left	64 from left
Magnitude (ft-kips)	314.58	−142.48
First span, intermediate support		
Shear		
Load type	–	HS20-44
Movement	–	Right to left
Back axle spacing (ft)	–	14
Central axle location (ft)	–	26 from left
Magnitude (kips)	–	−59.92
Moment		
Load type	–	HS20-44 lane
Magnitude (ft-kips)	–	−358.12

COMPARISON WITH GEORGIA BEAM

The MAXMIN program solves problems by user interaction that are currently handled by noninteractive programs of which GEORGIA BEAM (6) is typical. The two programs carry out many of the same functions. GEORGIA BEAM is more thorough in that it can develop optimum displacements and stresses. However, GEORGIA BEAM is goal oriented toward beam design. MAXMIN, on the other hand, is directed toward load

distribution with a supplement to beam design as a secondary consideration.

A further comparison with GEORGIA BEAM reveals other differences. MAXMIN uses an exact matrix-method solution whereas GEORGIA BEAM uses one-step moment distribution. MAXMIN also derives intermediate influence magnitudes with a higher-order interpolation and generates shear and moment envelope values for twice the number of points along the beam. Finally, MAXMIN calculates uplift reactions at intermediate supports.

Differences in the computational time are difficult to access. Attempts at such a comparison have led to no definite conclusions except that the differences appear to be negligible. A choice, then, as to whether to use one or the other of the two programs comes down to an assessment of the problem objective and the individual's preference for interactive input.

CONCLUSION

CMS provides a diverse yet comprehensive tool to the programmer and program user. Valuable CMS options include storage manipulation, flexible input and output features, straightforward program modification procedures, and support program features. The CMS interactive mode gives the user a sense of being in control in that not only the end result but the process of obtaining it is in the hands of the user. This freedom quickly overcomes the resistance to CMS often exhibited by the novice.

Many of the CMS user qualities have been incorporated into MAXMIN. The user-initiated question-and-answer free format, repetition of steps with accompanying data changes, file storage, and the omission of analytical segments is the result. The accuracy was verified by numerous comparisons against American Institute of Steel Construction tables (7) of moments, shears, and reactions for continuous highway bridges. Further confirmation of the MAXMIN results were provided by a series of ICES STRUDL II (5) analyses.

An extensive number of potential analytical directions or choices have been built into the MAXMIN program. Thus, the total operational time may also vary extensively. The principal goal, shear and moment envelopes, normally involves the most computational time. Toward this end, a four-span beam operates on a time scale of approximately 2 min once the required data have been entered.

MAXMIN has two major deficiencies. The program does not as yet have a graphics capability and so the output is restricted to tabular form. As a result, the visual impact of the output is not realized. MAXMIN was designed as an Interstate program or for bridges subjected to an HS truck loading. Other categories of truck load were not considered.

The MAXMIN program is of immediate benefit in the application of the beam-design program of a bridge design bureau. The goal in the near future is an extension of MAXMIN to include a lateral distribution of the load culminating in a pier analysis and design.

REFERENCES

1. CMS for Programmers: A Primer. IBM Corporation, Poughkeepsie, N.Y., 1978.
2. Standard Specifications for Highway Bridges, 12th ed. AASHTO, Washington, D.C., 1977.
3. C.K. Wang. Matrix Methods of Structural Analysis, 2nd ed. International Textbook Co., Scranton, Pa., 1966.
4. H. Kardestuncer. Elementary Matrix Analysis of Structures. McGraw-Hill, New York, 1974.
5. ICES STRUDL II, the Structural Design Language, Vol. 1. Massachusetts Institute of Technology, Cambridge, 1971.
6. J.M. Nieves-Olmo. The Analysis of Continuous Beams for Highway Bridges, Volume 1: GEORGIA BEAM. State Highway Department of Georgia, Atlanta, 1962.
7. Moments, Shears, and Reactions for Continuous Highway Bridges. American Institute of Steel Construction, New York, 1966.

Publication of this paper sponsored by Committee on General Structures.

Computer Analysis of AASHTO Plate Girders in Pure Bending with Load-Factor Design

PAUL G. NORTON

ABSTRACT

A computer program has been developed to perform the calculations to analyze AASHTO plate-girder cross sections in pure bending with load-factor design. The program is based on an extensive search of current design specifications and will analyze a straight girder or curved girder with hybrid or homogeneous steel elements. The procedure used by this computer program to analyze plate girders is described. Several interpretations of the AASHTO specifications made during the development of this computer program are described.

A computer program has been developed to calculate the stresses and allowable stresses to analyze steel plate-girder cross sections in pure bending by using the AASHTO load-factor design method. The program module, located in an IBM 4341 computer, operates in the interactive mode under the IBM conversational-mode system environment. Currently plans are under way to incorporate the program to run on an IBM PC/XT microcomputer.

The program listing is based on an extensive search for current design considerations (1-6). It was necessary to refer to these reports to determine the assumptions made in the AASHTO allowable-stress formulas. For example, the basic allowable compression-flange stress for a straight girder is based on a prismatic flange within the unbraced length. In continuous bridges, the compression flange is often nonprismatic within the unbraced length. A U.S. Steel technical report (1) addresses this problem and proposes a design procedure. Discrepancies between the specifications and the research reports have been corrected. Specification modifications have been incorporated into the program where engineering judgement required them.

Input for the program includes basic geometric properties such as diaphragm spacing, radius of curvature, width and thickness of top and bottom flanges, depth and thickness of web, and material properties such as ultimate strength of the concrete slab and yield strength of the web and of each flange. The program's analysis is for pure bending, so all the moments (nonfactored) at the cross section are needed, including not only the normal moments but also the lateral bending moments and the fatigue moments. The allowable fatigue stress and the distance from the extreme tension fiber in the web to the fatigue point under consideration are also required.

Normal and lateral bending stresses are computed for the dead-load-1 (DL1) and total stress conditions. Normal and lateral fatigue stresses are computed for the live loads.

Special features in the program include (a) identification of compact compression flanges for curved girder sections, (b) specification limits of compression flange width-to-thickness ratios, (c) different yield strengths of the flanges, and (d) an option of composite action in the negative moment regions of continuous bridges.

All the results of the analysis for one cross section are printed on a single 8.5 x 11-in. sheet (Figure 1). Included are all input information, normal and lateral bending stresses, and the allowable bending stresses. Determination of the allowable bending stresses requires calculating the basic allowable bending stress for each flange and, when appropriate, the hybrid reduction factor or the three curvature-reduction factors or both.

PURPOSE AND SCOPE

The AASHTO specifications have evolved from liter-

```
********************* LOAD FACTOR HYBRID SECTION **********************
* SLAB=  7.00 FT X   8.00 IN.       MODULAR RATIO(N)= 8   F'C=3500 PSI *
* TOP FLANGE = 12 X 1.250 IN.       TOPFLG FY= 50 KSI   BOT FY= 50 KSI *
* BOT FLANGE = 20 X 1.813 IN.       UNBRACED LENGTH = 25.00 FT         *
* GIRDER WEB = 78 X 0.625 IN.       WEB FY   = 36 KSI                  *
*****************************************************************************
******************** NON-FACTORED DESIGN MOMENTS **********************
*                          DL1    DL2    L+I   TOTAL                  *
* NORMAL BENDING MOMENTS    4438   1441   3029    8908                 *
*                                  +(L+I) -(L+I)                      *
* NORMAL FATIGUE BENDING MOMENTS     2406    600                       *
*    NOTE:BOTTOM FLANGE IS IN TENSION, DIST. TO FATIGUE PT. =  0.00 IN.*
*****************************************************************************
***************************** DESIGN STRESS *****************************
*                        DL1     DL2     L+I     TOTAL                 *
* TOP FLANGE STRESS(KSI)  34.195  5.237   8.588  48.020                *
* BOT FLANGE STRESS(KSI)  22.639  6.166  19.619  48.424                *
* TOP FLANGE SEC MOD(IN3)   2025   4293    9170                        *
* BOT FLANGE SEC MOD(IN3)   3058   3646    4014                        *
*---*---*---*---*---*---*---*------*---*---*---*---*---*---*---*---*---*
* TOP FLANGE DL1 STRESS= 34.195KSI      F= 29.81KSI             NO GOOD *
*    FB= 29.813KSI  R= 1.000                                           *
* TOP FLANGE STRESS= 48.020KSI          F= 48.74KSI                OK   *
*    FB= 50.000KSI  R= 0.975                                            *
* BOT FLANGE STRESS= 48.424KSI          F= 48.74KSI                OK   *
*    FB= 50.000KSI  R= 0.975                                            *
* FATIGUE STRESS RANGE=  8.638KSI       F= 13.00KSI                OK   *
* CONCRETE SLAB STRESS= 1687PSI         F= 2900PSI                 OK   *
*****************************************************************************
```

FIGURE 1 Sample output.

ally hundreds of research reports published by scholars from industry and from prestigious engineering schools. The AASHTO specifications are guide specifications and are meant to serve as a reference for bridge engineers (1,2). They are analogous to the laws of the United States in that bridge engineers must interpret the intent of the words that make up the specification just as lawyers and judges must interpret the laws. As stated in NCHRP Synthesis 23 (8, p. 13): "Squanto showed the Pilgrims how to plant corn. The Pilgrims survived. Had Squanto written them a set of instructions [specifications], the outcome may have been quite different." Attempting to correctly assess the intent of the AASHTO specifications is not a life-or-death struggle, but the specifications can be misinterpreted by the practicing bridge engineer.

Unlike the codes of the American Institute of Steel Construction and the American Concrete Institute, the AASHTO code does not have instructive textbooks, engineering handbooks, and expanded-commentary books dealing with it. Both industry and university researchers are busy developing new concepts and ideas. The intent of the AASHTO specifications is left to the interpretation of the bridge engineer.

The intent in this paper is to share some ideas on what are perceived to be the intent of the specifications and to describe the procedure used by a specific computer program to analyze plate girders. The program's scope is limited to welded plate girders. The program assumes an AASHTO group 1 loading. Plates that are grade 36 or grade 50 are the acceptable materials. In addition, the analysis is independent of the action of shear.

COMPUTATION OF STRESS

DL1 Normal Stress

The stress due to the DL1 moment is computed for the compression flange by using the moment-of-inertia method. The tension flange is not a design consideration at this loading stage, because the total normal or total tip stress would control. However, a check of the DL1 normal stress is necessary for the top compression flange of a composite section. The fullest use of the flange steel will yield a final stress close to the allowable stress for each flange. Because the partly composite and the fully composite sections have their neutral axes closer to the top flange than the noncomposite section, most of the stress in the top flange is from DL1. The combination of a high DL1 stress and low allowable stress can control the size of the top flange. For a curved girder the top flange stress for the DL1 loading stage is even more critical. Therefore, the calculation of the DL1 stress is important for the proper design of the top flange of a composite section.

Total Normal Stress

The stress due to the group 1 loading combination 1.3 [DL1 + DL2 + 5/3(L + I)] is computed for the top flange and the bottom flange by using the moment-of-inertia method. Calculation of the total normal stress in the top and bottom flanges is necessary to properly design each flange in composite or noncomposite straight girders or curved girders.

Total Tip Stress

The stress due to nonuniform torsion, lateral flange bending, in a horizontally curved girder is computed for the group 1 loading combination by using the moment-of-inertia method. The total lateral bending stress at the tips of the flange added algebraically to the total normal bending stress results in the maximum and minimum values of the nonuniform stress distribution experienced by the flange. The maximum value is defined as the total tip stress.

The top flange of a composite section must have its lateral bending stress calculated by adding the individual stresses experienced at each loading stage. The flange is attached to the deck slab by shear connectors. This connection results in the partly composite and fully composite horizontal inertia of the slab resisting the lateral bending moments along with the flange for the dead-load-2 (DL2) and live-load loading stages. This composite action significantly reduces the lateral bending stress experienced by this flange.

The total tip stress is crucial for the design of horizontally curved girders. It will tend to control the size of the flange for sharp radii (large lateral bending moments) or narrow flange choices (small horizontal section modulus).

Fatigue Stress Range

The fatigue stress range is computed for the fatigue point under consideration. The stress range is calculated at a designated point on the girder. For a curved girder design, the lateral fatigue stress range is added to the normal fatigue stress range to give the total fatigue stress range.

When shear connectors are provided in the negative-moment region of a continuous girder, it is the longitudinal reinforcing bars, not the concrete deck in tension, that act compositely. The fatigue stress range is computed in the reinforcing bars by extrapolating the straight-line stresses on the girder to the center of the top layer of reinforcement.

The fatigue stress range at the critical fatigue point is an important design consideration. For imposed loadings larger than HS20, the fatigue stress range can control the size of the flanges at almost every point of a horizontally curved girder with welded diaphragm connection plates.

COMPUTATION OF ALLOWABLE STRESS

The allowable stresses needed to properly analyze a girder cross section include the following:

1. Compression-flange allowable normal stress at the DL1 loading stage,
2. Top-flange allowable normal stress at maximum load,
3. Top-flange allowable tip stress (for a curved girder),
4. Bottom-flange allowable normal stress at maximum load,
5. Bottom-flange allowable tip stress (for a curved girder), and
6. Allowable fatigue stress range.

The computation of the allowable stresses includes calculation of the basic allowable compression-flange normal stress, calculation of the hybrid reduction factor for a hybrid girder, and calculation of the curvature correction factors for a curved girder. These values in combination with the minimum yield point of the flange (F_y) equal the allowable stresses for a straight or curved girder. The allowable fatigue stress range is specified by the engineer.

The process of calculating the allowable stress is represented in terms of a flowchart in Figure 2.

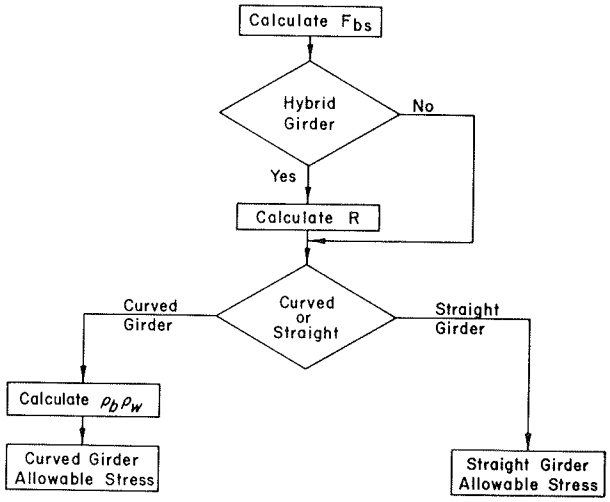

Legend

F_{bs} = Basic Allowable Compression Flange Normal Stress
R = Hybrid Reduction Factor
$\rho_b \rho_w$ = Curvature Correction Factors

FIGURE 2 Computation of allowable stress.

Basic Allowable Compression-Flange Normal Stress

The basic allowable compression-flange normal stress is computed for a straight girder from AASHTO 1.7.59B or AASHTO 1.7.59D (1,2) and for a curved girder from CURVED AASHTO 2.12B (3).

It is appropriate at this point to note that an ordinary plate-girder web will not conform to the severe D/t_w constraint specified in AASHTO 1.7.59A1b (Figure 3). Accordingly, the program will not analyze a straight girder as a compact section or a straight girder in transition as defined by AASHTO 1.7.59C.

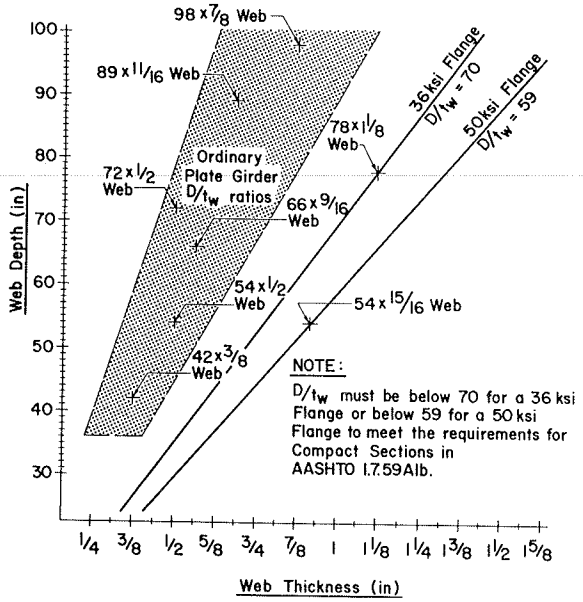

FIGURE 3 Compact section web requirement for straight girder.

The formula for the maximum strength of an unbraced section for a straight girder is given in AASHTO 1.7.59D. It is the same formula proposed by Vincent (4). Note that it is similar to the allowable stress design formula given in AASHTO Table 1.7.1A in that both formulas have the constant F_y/E. However, the allowable stress design specification also lists simplified formulas for each value of F_y.

The computer program described here uses simplified formulas based on the equation given in AASHTO 1.7.59D. The simplified formulas are as follows:

1. If F_y = 36,000 psi and the section is symmetrical, $F_{bs} = 36{,}000 - 13.6(L/b)^2$.
2. If F_y = 36,000 psi and the section is unsymmetrical, $F_{bs} = 36{,}000 - 16.8(L/b)^2$.
3. If F_y = 50,000 psi and the section is symmetrical, $F_{bs} = 50{,}000 - 26.2(L/b)^2$.
4. If F_y = 50,000 psi and the section is unsymmetrical, $F_{bs} = 50{,}000 - 32.3(L/b)^2$.

Note that all these formulas are similar to the practical and familiar formula, $F_b = 20{,}000 - 7.5(L/b)^2$, listed in AASHTO Table 1.7.1A. Also note that the term F_{bs}, the basic allowable compression-flange normal stress, is expressed in pounds per square inch. The original formula (1.7.59D), defined as the maximum strength, is expressed as the resisting moment (M_u). In order to analyze a composite section, the magnitudes of the stresses experienced at each loading stage by the extreme fibers of each flange are required. The stresses, not the individual resisting moments, are of practical use. This concept is similar to the curved-girder specification, CURVED AASHTO 2.12B, which describes the resistance in terms of maximum flexural stress. The simplified formulas are different for a symmetrical and a nonsymmetrical girder; the nonsymmetrical girder conforms to AASHTO 1.7.60A, in which the term b is replaced by 0.9b.

The derivation of the original formula (AASHTO 1.7.59D) assumed a prismatic compression flange within its unbraced length. In continuous bridges the compression flange at an interior support is often nonprismatic within the unbraced length. A U.S. Steel technical report (7) addresses this condition and proposes a design procedure that involves calculating F_{bs} by using the flange width at the low-moment side (assumes narrower flange) of the unbraced length. The program can analyze a nonprismatic compression flange. The design flange width at the low-moment side is input and F_{bs} is calculated, substituting the design flange width for the flange width at the section under consideration.

For a straight girder design, AASHTO 1.7.59D allows an increase of 20 percent of the resistance at any point along the length of the girder when the ratio of stresses at the two ends of the unbraced length is less than 0.7. Because the possibility of a nonprismatic compression flange exists, the 20 percent increase should be based on the ratio of forces (not stresses) in the flange at each end of the unbraced length. The decision to increase the allowable stress by 20 percent is made by the engineer. It is believed that the 20 percent increase would be best applied within the unbraced length at the interior supports only.

If the unbraced length of the compression flange is less than that specified in AASHTO 1.7.59B1c, the section is braced.

A flowchart of the calculation of the basic allowable compression-flange normal stress is shown in Figure 4.

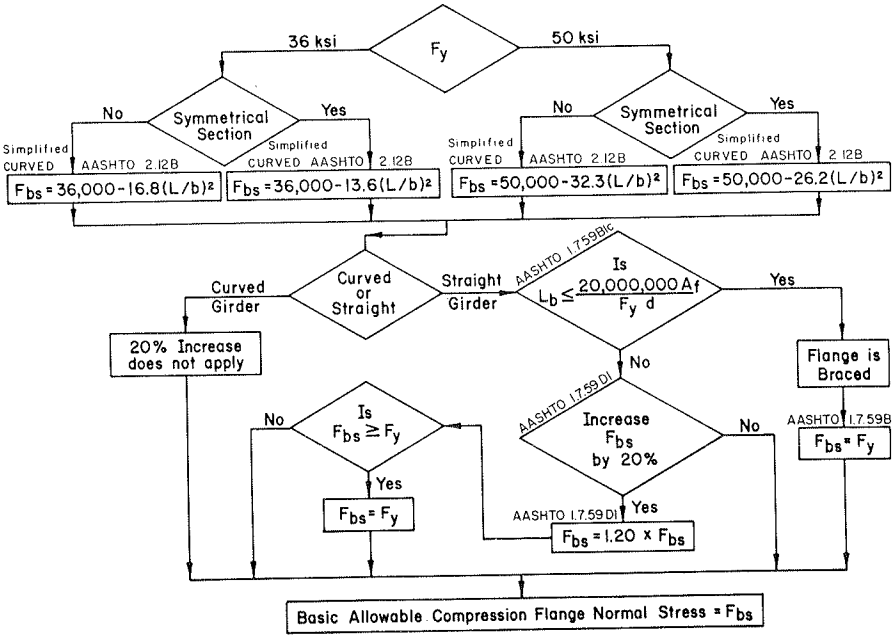

FIGURE 4 Computation of basic allowable compression-flange normal stress (F_{bs}).

Hybrid Reduction Factor

The hybrid reduction factor is calculated for a girder that uses a 36-ksi web and one or two 50-ksi flanges. For a homogeneous girder, the reduction factor is set equal to 1.000.

At this point in the program, the local buckling requirement for the unbraced compression flange is checked. If the requirement is not met, the flange is defined as illegal and the reduction factor is set equal to zero. For a composite section the top flange is checked at the DL1 loading stage only. For a curved girder the local buckling requirements in CURVED AASHTO 2.12B1 and 2.12B2 are compared with the compression-flange ratio of width to thickness.

The hybrid reduction factor is calculated for a straight girder by using the formulas in AASHTO 1.7.67B. These are the original formulas proposed by the ASCE subcommittee on hybrid beams and girders (9).

For the case of the nonsymmetrical girder, the formula is similar to AASHTO 1.7.50 (service load design method), in which the ratio of web yield strength to tension flange yield strength is designated "alpha." The same variable is designated "rho" in AASHTO 1.7.67B. In the figures for this paper "alpha" is used for this variable to make the specification terminology consistent.

The hybrid reduction factor is calculated for a curved girder by using the formulas in CURVED AASHTO 2.19Aa and 2.19Ab. The formulas, derived by Culver (6), are for a compact section and a noncompact section as defined by the compression-flange ratio of width to thickness.

A flowchart of the calculation of the hybrid reduction factor is shown in Figure 5.

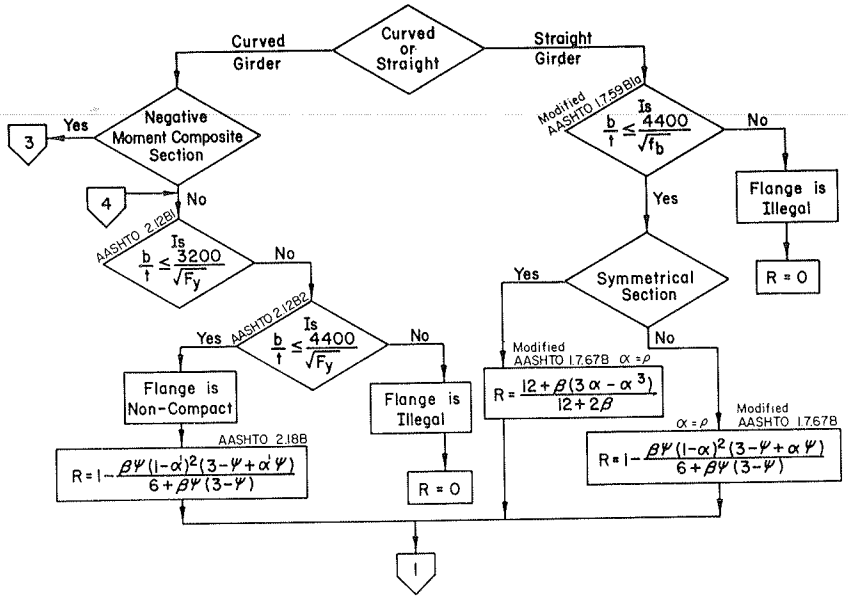

FIGURE 5 Computation of hybrid reduction factor (R).

After the reduction factor has been calculated, the program determines whether the reduction factor applies to each flange. If the stress in the extreme tension fiber of the web is larger than the minimum yield point of the web, the hybrid reduction factor applies to the tension flange. A similar check is made at the extreme compression fiber of the web to determine whether the hybrid reduction factor applies to the compression flange. It is believed that the reduction factor can properly be applied to the tension flange and not to the compression flange. This condition often occurs at a composite section.

The derivation of the hybrid reduction formula for a composite section is based on the tension capacity of the girder (5). It does not consider whether the compression flange yields or not because of normal bending moments. Because the fullest use of the top flange of a composite section will result in a high magnitude of flange stress, the application of the reduction factor to the top flange of a composite section will affect the size of the flange.

For a curved girder design, the allowable normal stress is usually reduced because of curvature correction factors. If a 36-ksi flange is chosen for the top flange of a composite curved girder, for example, the application of the curvature correction factors could reduce the allowable normal stress to 30 ksi. It is now necessary to decide whether the top flange, which has the same F_y as the web and a stress at least 20 percent less than the F_y of the web, should have the hybrid reduction factor applied to it. It is believed that the hybrid reduction factor should not be applied for this case.

After determining whether to apply the reduction factor to each flange, the program then checks whether the compression-flange area is greater than or equal to the tension-flange area. If the compression-flange area is less than the tension-flange area, the reduction factor is set equal to zero.

A flowchart showing the process of deciding whether the reduction factor applies to each flange and checking of the compression-flange area is given in Figure 6.

For a curved girder, the hybrid reduction factor is adjusted, depending on the ratio of lateral bending stress to normal bending stress in the tension flange, in accordance with CURVED AASHTO 2.19A. If the ratio of lateral bending stress to normal bending stress is high, the flange is controlled by the tip stress. In this case the hybrid reduction factor does not apply, and the program sets the reduction factor equal to 1.000.

Finally, for a curved hybrid girder that uses the deck-slab reinforcement to achieve composite action in the negative-moment region, the ratio of lateral bending stress to normal bending stress is checked for the compression flange in accordance with CURVED AASHTO 2.19B. This check results in either an adjustment in α' or the recognition that the lateral bending stress controls the design of the flange (6), in which case the hybrid reduction factor does not apply and the program sets the reduction factor equal to 1.000.

A flowchart of the adjustment of the hybrid reduction factor is given in Figure 7.

Curvature Correction Factors

The curvature correction factors are computed for a curved girder from CURVED AASHTO 2.12B. The compression-flange ratio of width to thickness is compared with the specification limit in CURVED AASHTO 2.12B1. If the ratio does not exceed this limit, the flange is defined as compact and the curvature correction factors are calculated by using the formulas in CURVED AASHTO 2.12B1. Note that the severe web constraint (D/t_w) for compactness, as specified in AASHTO 1.7.59A1b (Figure 3), does not apply for a curved girder (6). However, it should be noted that a compact straight girder is not the same as a compact curved girder.

If the compression flange does not meet the compact-flange requirements, the program checks its ratio of width to thickness against the noncompact requirement as defined in CURVED AASHTO 2.12B2. If the flange does not meet this requirement, it is defined as illegal and both correction factors are set equal to zero. For a flange that is noncompact, the curvature correction factors are calculated by using the formulas in CURVED AASHTO 2.12B2.

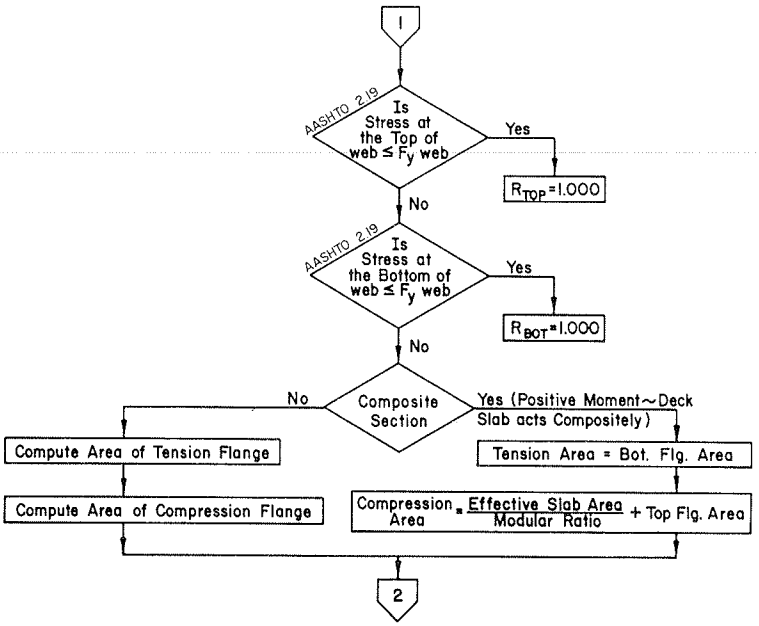

FIGURE 6 Application of hybrid reduction factor (R).

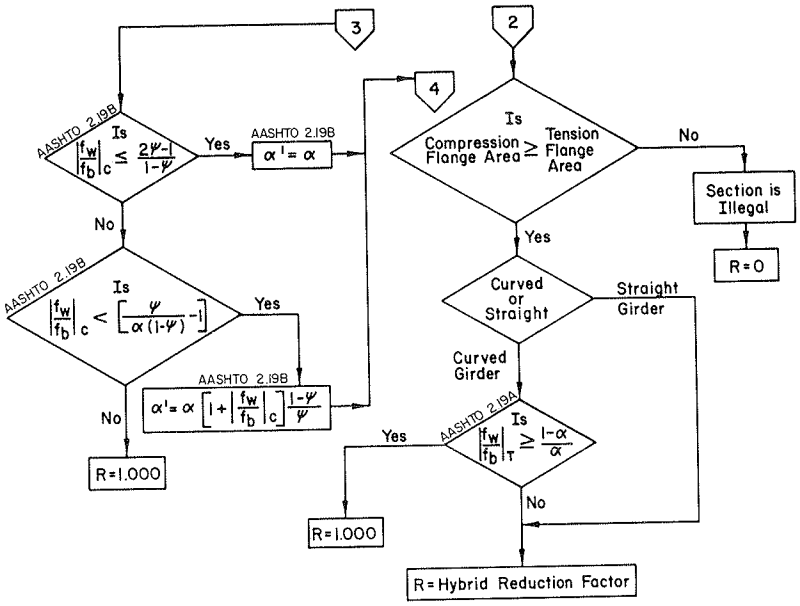

FIGURE 7 Adjustment of hybrid reduction factor (R).

The correction factors are based on the length of the unsupported compression flange between cross frames or diaphragms. They reduce the allowable compression-flange stress because the flange is unstable and will buckle laterally, torsionally, or locally under the influence of high stress. The top flange of a composite section is attached to the deck slab by shear connectors and partly encased in concrete. It is believed that the curvature correction factors should not be applied to the top flange of a composite section. However, CURVED AASHTO 2.16 uses the conservative approach and applies the curvature correction factors to the compression flange regardless of the presence of composite action. The program uses this conservative AASHTO approach.

The flowchart for calculation of the curvature correction factors is given in Figure 8.

Straight-Girder Allowable Stress

The compression-flange allowable stress at the DL1 loading stage and the compression-flange allowable stress at maximum load are calculated by using combinations of the basic allowable compression-flange normal stress and the hybrid reduction factor. The tension-flange allowable stress is calculated by using combinations of the minimum yield point of the flange material and the hybrid reduction factor.

The flowchart for calculation of the straight-girder allowable stress is given in Figure 9.

Curved-Girder Allowable Stress

The compression-flange allowable normal stress at the DL1 loading stage and the compression-flange

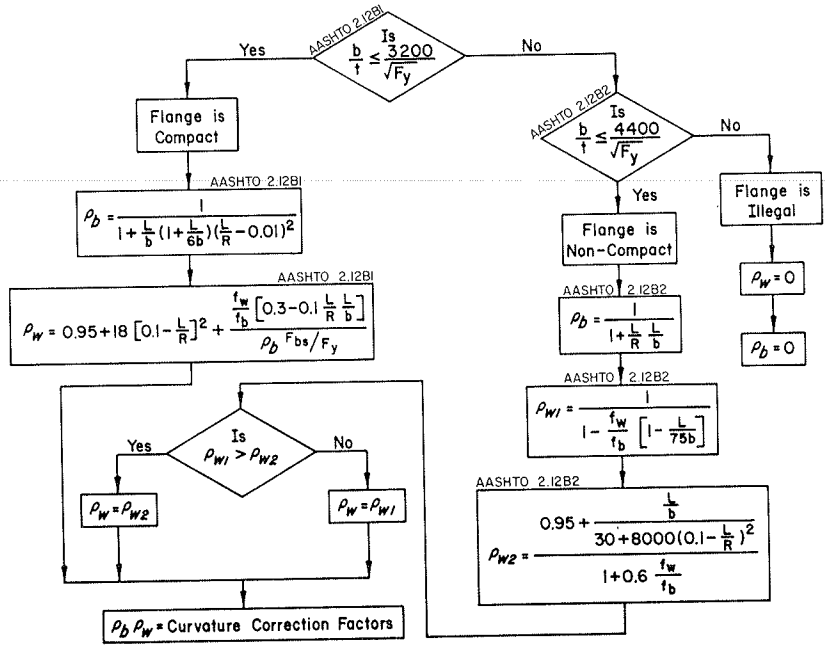

FIGURE 8 Computation of curvature correction factors (P_bP_w).

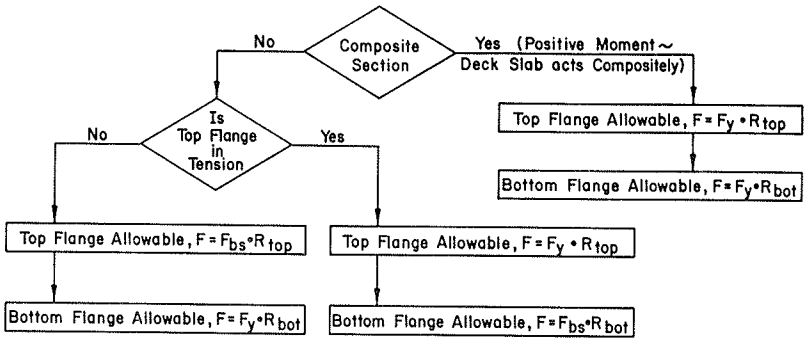

FIGURE 9 Computation of straight-girder allowable stresses.

allowable normal stress at maximum load are calculated by using combinations of the basic allowable compression-flange normal stress, the hybrid reduction factor, and the curvature correction factors. The tension-flange allowable normal stress is calculated by using combinations of the minimum yield point of the flange material and the hybrid reduction factor.

Curvature correction factors are not applied to the tension flange because it will not buckle. However, the AASHTO 2.12B specification is written in such a way that it could easily be interpreted that the rho factors are applied to the tension flange. This interpretation can be shown in three steps, as follows:

1. $F_{by} = F_{bs}P_bP_w$,
2. For the tension flange, $F_{bs} = F_y$, and
3. Therefore, for the tension flange, $F_{by} = F_yP_bP_w$.

It is believed that compact and noncompact curved-girder flanges should have the maximum flexural stress for the tension flange defined as follows:

1. $F_{by} = F_y$ (noncompact) and
2. $F_{bu} = F_y$ (compact).

This judgment is based on the service load design method, which defines the allowable tension-flange normal stress, in CURVED AASHTO 1.10B, in relation to F_y.

The flowchart for calculation of the curved-girder allowable stress is given in Figure 10.

The maximum allowable tip stress experienced by a tension or compression flange for a homogeneous or hybrid girder is equal to the minimum yield point of the flange material.

Allowable Range of Fatigue Stress

The allowable range of fatigue stress is given in AASHTO Table 1.7.2A1 for redundant load-path (multi-girder) structures and for nonredundant load-path (fracture-critical) structures. The location of the critical fatigue point and the allowable range of fatigue stress are input to the program. However, at any girder cross section with case 1 roadway load cycles, there are three choices of fatigue moments: lane fatigue moments, truck fatigue moments, and truck fatigue moments at a live-load distribution of S/7.0. At any girder cross section there may be numerous locations of fatigue design points.

For a girder with case 1 roadway load cycles, the determination of which live-load distribution to use for the truck fatigue moments is necessary. The stress range due to the distribution S/7.0 is 21.4

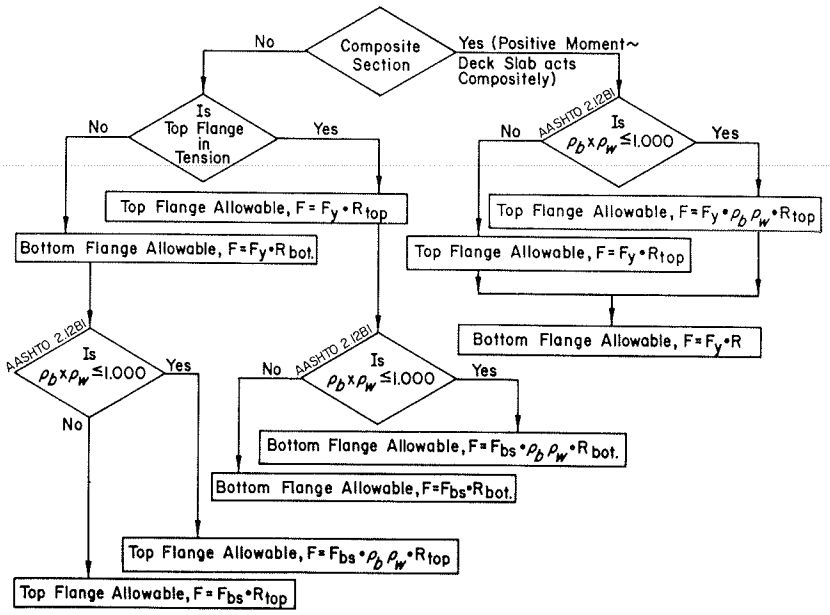

FIGURE 10 Computation of curved-girder allowable normal stresses.

percent less than the stress range due to the distribution S/5.5. The allowable range of fatigue stress for more than 2 million cycles is equal to or less than the allowable range for 2 million cycles for all fatigue categories, as shown in AASHTO Table 1.7.2A1. If the allowable range of fatigue stress for more than 2 million cycles is more than 21.4 percent of the allowable range for 2 million cycles, the truck fatigue moments at a distribution of S/7.0 will control the truck fatigue-stress range. This will occur for fatigue categories D and E** for a fracture-critical girder and for fatigue categories C, D, and E' for a multigirder system (Table 1).

TABLE 1 Case 1 Roadway: Allowable Fatigue Stresses

	Multi-Girder Structures			
Category	Lane Allowable (Ksi)	Ratio	Truck Allowable (Ksi)	Controlling Truck Distribution
A	36	1.50	24	S/5.5
B	27.5	1.72	16	S/5.5
C	19	1.90	10	S/7.0 ←
C*	19	1.58	12	S/5.5
D	16	2.29	7	S/7.0 ←
E	12.5	2.50	5	S/7.0 ←
E'	9.4	3.62	2.6	S/7.0 ←
F	12	1.50	8	S/5.5

	Fracture Critical Structures			
Category	Lane Allowable (Ksi)	Ratio	Truck Allowable (Ksi)	Controlling Truck Distribution
A	24	1.00	24	S/5.5
B	18	1.13	16	S/5.5
C	13	1.44	9	S/5.5
C*	13	1.18	11	S/5.5
D	10	2.00	5	S/7.0 ←
E**	8	3.20	2.5	S/7.0 ←
F	9	1.29	7	S/5.5

Legend
← Indicates that one truck at a distribution of S/7.0 for "over 2 million" stress cycles controls over a truck distribution of S/5.5 at "2 million" stress cycles.

Next the determination of whether the truck fatigue moments or the lane fatigue moments will control is necessary. This comparison is made in the same manner as the determination of the controlling truck fatigue moments. The ratio of lane fatigue moments to truck fatigue moments must be larger than the ratio of allowable stresses for the lane fatigue moments to control. The ratio of allowable stresses and appropriate controlling truck distribution are given in Table 1.

In addition to the considerations cited, the location of the fatigue point is also important. The fatigue-point location is input to the program.

Common controlling fatigue design points for a fracture-critical or multigirder system are shown in Figure 11.

SUMMARY AND COMMENTS

During the development of the computer program, several interpretations of the AASHTO specifications had to be made. The key ideas in this paper may be summarized as follows:

1. Ordinary plate-girder webs will not conform to the severe D/t_w constraint for a compact straight girder. Therefore, ordinary straight plate girders will not be compact.
2. Because ordinary straight plate girders will not be compact, the stress and allowable stress are of practical use but not the moment and resisting moment.
3. The design of nonprismatic compression flanges can be based on the narrower flange width at the low-moment side of the unbraced length.
4. The hybrid reduction factor is not applied to a flange until its adjacent extreme web fiber stress becomes larger than the web F_y.
5. It is believed that the curvature correction factors should not be applied to the top flange of a composite section. However, unless AASHTO clearly adopts this concept into the specification, the factors will be applied to the flange.
6. It is believed that the tension flange should not have the curvature correction factors applied to it, because it will not buckle.

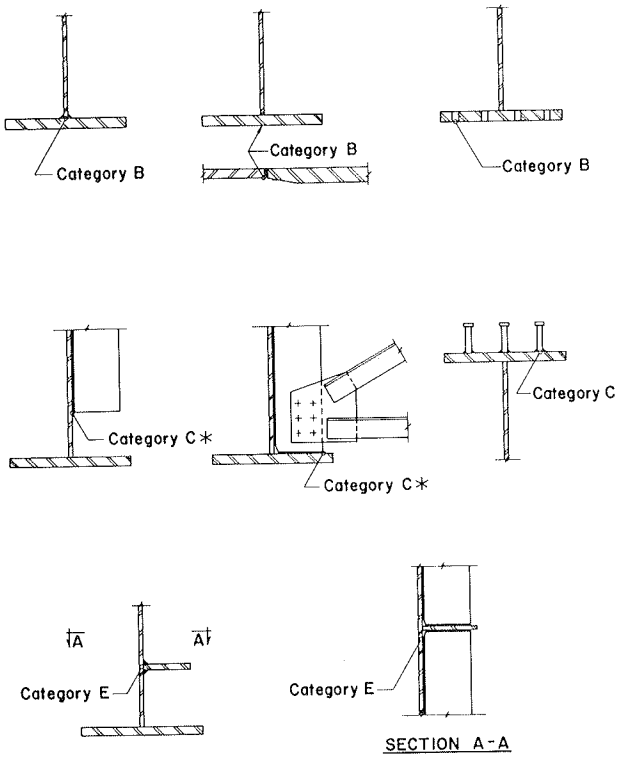

FIGURE 11 Common fatigue design points.

This program enables the engineer to evaluate AASHTO plate-girder cross sections quickly, which in turn minimizes the actual design time. However, it is only the first step of a much larger program that would make the decisions that the engineer must now make.

ACKNOWLEDGMENT

The ideas reported here are the result of a study conducted during the development of Computer Program 060G for Gannett Fleming Transportation Engineers, Inc., Camp Hill, Pennsylvania. Thanks are given to Marc H. Soto for his encouragement during the development of the program. Special thanks are extended to Gerald K. Gillan, who acted as friend and advisor at the inception and during the development of this paper. Marie Gantt and Kelly Eckert typed the manuscript. The figures were prepared by Thomas Dormer. Their contribution is appreciated.

REFERENCES

1. Standard Specifications for Highway Bridges, 12th ed. AASHTO, Washington, D.C., 1977.

2. Interim Specifications: Bridges. AASHTO, Washington, D.C., 1978, 1982.
3. Specifications for Horizontally Curved Highway Bridges. AASHTO, Washington, D.C., 1980.
4. G.S. Vincent. Tentative Criteria for Load Factor Design of Steel Highway Bridges. Bull. 15. American Iron and Steel Institute, New York, 1969.
5. C.G. Shilling. Bending Behavior of Composite Hybrid Beams. Journal of the Structural Division of ASCE, Aug. 1968.
6. C.G. Culver. Design Recommendations for Curved Highway Bridges. Final Report, Research Project 68-32. Civil Engineering Department, Carnegie-Mellon University; Pennsylvania Department of Transportation, Harrisburg, 1972.
7. Lateral Buckling of Highway Bridge Girders. U.S.S. Technical Report ADUSS 88-6506-01. U.S. Steel Corporation, Pittsburgh, Pa., 1974.
8. Getting Research Findings into Practice. NCHRP Synthesis of Highway Practice 23. TRB, National Research Council, Washington, D.C., 1974.
9. Design of Hybrid Steel Beams: Report of the Subcommittee 1 on Hybrid Beams and Girders, Joint ASCE-AASHO Committee on Flexural Members. Journal of the Structural Division of ASCE, June 1968.

Publication of this paper sponsored by Committee on Steel Bridges.

The ideas expressed in this paper are those of the author and not those of any sponsor or of AASHTO.

Finite-Element Program for Analysis of Folded-Plate Bridge Superstructures

FAHIM A. BATLA, PATRICK R. REISNOUR, and DIVAKAR V. PATHAK

ABSTRACT

The behavior of bridge superstructures such as box girders and T-beams is similar to that of a folded-plate structure. A simplified finite-element program, FAP, specifically developed for the elastic analysis of constant depth and straight folded-plate type structures is presented. Being a specific-purpose program, it can be used by a bridge engineer without the extensive training, knowledge, and effort that may be required for finite-element programs developed for the analysis of a wide range of structural types. Most of the data for FAP analysis is generated by the program from minimal and straightforward input information. FAP has been developed with particular emphasis on practical design and construction considerations. It has already been used for the design of several bridge superstructures. FAP can facilitate the design of many folded-plate type bridge superstructures, especially in those cases in which the design may otherwise be a difficult and time-consuming effort because of the complex geometrical, loading, support, or construction conditions. The illustrative examples presented indicate that the results of analyses using FAP are in good agreement with those based on more exact theories and experimental data.

The finite-element method of structural analysis has become progressively more practical and economical as the availability and use of digital computers have increased. In the finite-element method complicated geometric forms, arbitrary loading and support conditions, and other structural parameters can be accurately and readily represented without extensive use of simplifying assumptions. This method, therefore, offers several advantages over conventional methods of structural analysis.

In recent years several computer programs based on the finite-element method have been developed for structural analysis and design. These programs have been developed for the analysis of a wide range of structural types and usually involve a large number of variables and complicated and extensive input data. This in turn requires a substantial amount of user effort, computational time, and computer capacity, which may not be necessary for the analysis of certain types of structures for which the modeling of the structural behavior can be simplified without affecting the acceptability of results for the purpose of design.

A large number of structures can be categorized as folded plates because of their behavior under loads and their cross-sectional shapes. The spatial rigidity of a folded-plate structure is provided by the out-of-plane (plate bending) and in-plane (membrane) behavior of its component plates, which join at folds (1-6). The width of these plates between folds in the transverse direction of the structure is small in comparison with their respective lengths between supports of the structure. As a result, the bending of these plates is predominantly a one-way behavior in the transverse direction of the structure.

The behavior of box girders, T-beams, and similar types of bridge superstructures is similar to that of a folded-plate structure. A finite-element computer program, FAP, for the elastic analysis of

constant depth and straight folded-plate structures under static loads is presented. The program is based on a simplified plate-bending finite element specifically modeling the folded-plate behavior (6). As a result, the number of computations and variables is substantially reduced in comparison with general-purpose finite-element programs. FAP requires less computer time and memory capacity and a minimal amount of input data and user effort. It has been developed with emphasis on the practical concerns of a structural engineer and facilitates the design of folded-plate type bridge superstructures in terms of both structural and functional considerations. The program is capable of the analysis of a folded-plate structure subjected to surface, gravity, or concentrated loads; prestressing forces; temperature loading; and arbitrary boundary conditions. It has been used for the analysis and design of folded-plate type bridge superstructures (7-9) and for determination of the lateral distribution of wheel loads for multi-T-beam bridges (10).

DESCRIPTION OF PROGRAM

The program is based on the displacement (stiffness) approach of the finite-element method of structural analysis. The theory and the development of mathematical models used in the program to represent plate-bending and membrane (plane stress) actions of component plates of the structure are described in detail elsewhere (6). The following sections provide an overview of the development of the simplified plate-bending finite-element analysis used in FAP, input data requirements, output of analytical (response) results, and other highlights of the program.

Simplified Plate-Bending Model

The differential equations of the classical two-way plate-bending theory are expressed as follows (11,12):

$$M_x = -D[(\partial^2 w/\partial x^2) + \mu(\partial^2 w/\partial y^2)]$$
$$M_y = -D[\mu(\partial^2 w/\partial x^2) + (\partial^2 w/\partial y^2)]$$
$$M_{xy} = -D(1-\mu)(\partial^2 w/\partial x \partial xy) \quad (1)$$

where D is the plate rigidity and μ is Poisson's ratio.

The basic assumptions used in the development of a plate-bending model are as follows (Figure 1):

1. Each finite element is rectangular; of uniform thickness; and made of an elastic, isotropic, and homogenous material.
2. The force-displacement relationship is linear, so that the principle of superposition is valid.
3. The displacement field within each element can be uniquely defined in terms of its out-of-plane nodal displacements.
4. The plate-bending moments within each element (Equation 1) can be determined from its displacement field.

The following 12-term polynomial, therefore, may be used to represent the displacement field of the two-way plate-bending model shown in Figure 1:

$$w(x,y) = \alpha_1 + \alpha_2 x + \alpha_3 y + \alpha_4 x^2 + \alpha_5 xy + \alpha_6 y^2 + \alpha_7 x^3 + \alpha_8 x^2 y + \alpha_9 xy^2 + \alpha_{10} y^3 + \alpha_{11} x^3 y + \alpha_{12} xy^3 \quad (2)$$

In light of the dominant one-way bending behavior of the plates of a folded-plate structure, the following additional assumptions are used in the development of the simplified plate-bending element shown in Figure 1:

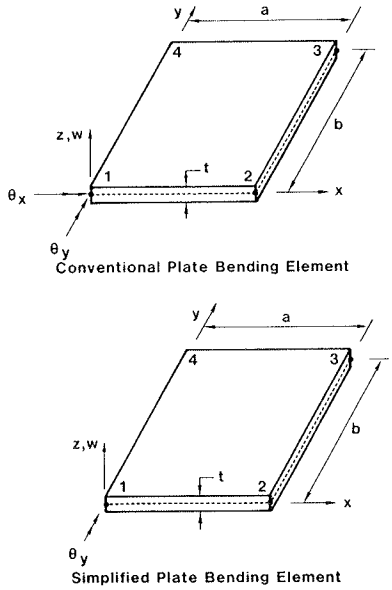

FIGURE 1 Conventional and simplified plate-bending elements.

5. The plate-bending strain ($\partial^2 w/\partial y^2$) in each plate in the longitudinal (y) direction of the structure contributes little to the total strain energy of deformation of the structure and therefore can be neglected.
6. The transverse bending moment within each finite element is constant with respect to the longitudinal direction of the structure; that is, $\partial M_x/\partial y = 0$.
7. The twisting moment (M_{xy}) in each element is constant.

By using these additional assumptions, the 12-term displacement field (Equation 2) is reduced to the following 6-term displacement field:

$$w(x,y) = \beta_1 + \beta_2 x + \beta_3 y + \beta_4 x^2 + \beta_5 xy + \beta_6 x^3 \quad (3)$$

The following conditions are then used to define the six-term displacement function (Equation 3) in terms of the following boundary displacements (Figure 1):

1. At a typical node i, $w = w_i$;
2. At $x = 0$ and $y = b/2$, $-\partial w/\partial x = \theta_0$; and
3. At $x = a$ and $y = b/2$, $-\partial w/\partial x = \theta_a$.

The final displacement function for the simplified plate-bending element is

$$\begin{aligned} w(x,y) = {} & [1 - (x/2a) - (y/b) - (3x^2/2a^2) + (xy/ab) + (x^3/a^3)]\,w_1 \\ & + [(x/2a) + (3x^2/2a^2) - (xy/ab) - (x^3/a^3)]\,w_2 \\ & + [(-x/2a) + (3x^2/2a^2) + (xy/ab) - (x^3/a^3)]\,w_3 \\ & + [(x/2a) + (y/b) - (3x^2/2a^2) - (xy/ab) + (x^3/a^3)]\,w_4 \\ & + [-x + (2x^2/a) - (x^3/a^2)\theta_0 + (x^2/a) - (x^3/a^2)]\,\theta_a \end{aligned} \quad (4)$$

Because the rate of change of $\partial w/\partial x$ with respect to $y(\partial^2 w/\partial x \partial y)$ is constant (Equation 4), θ_0 and θ_a are further related to the nodal angular displacements (θ_{yi}) as follows:

$$\theta_0 = (\theta_{y1} + \theta_{y4})/2$$
$$\theta_a = (\theta_{y2} + \theta_{y3})/2 \quad (5)$$

The stiffness matrix of the total 8-df simplified plate-bending element is given elsewhere (6).

A 2-df/node rectangular plane stress element with in-plane flexural modes (13) is used in FAP to represent the in-plane behavior of the plates of the structure. The overall representation of the behavior of a folded-plate structure is therefore reduced from a conventional 6-df/node idealization to a 4-df/node idealization (Figure 2).

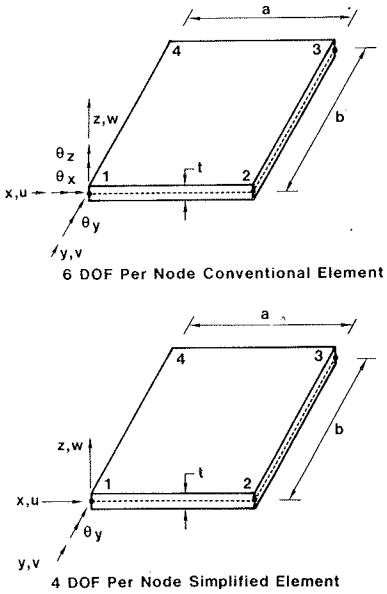

FIGURE 2 Conventional and simplified elements.

Idealization of Prestressing Forces

Another practical feature of FAP is the representation of prestressing forces and tendon profiles in concrete structures. The exact representation of the variation of prestressing forces along the tendon length and the geometry of tendon profile for finite-element analysis is usually a complex and time-consuming effort. For the analysis by FAP, a prestressing tendon is represented by piecewise straight segments (Figure 3). The tendon is divided into as many segments as the number of elements through which it passes. The prestressing force is assumed to be constant within each segment of the tendon. This method allows the study of the structural response under a tendon of arbitrary length and facilitates the optimum use of prestressing (9). The overall effort of representing the tendon profile and the prestressing force is also reduced. The approximation converges rapidly to an almost exact condition with the refinement of the finite-element idealization of the structure. The initial and final prestressing forces along the tendon length are estimated by conventional methods (14-16); the program does not compute them.

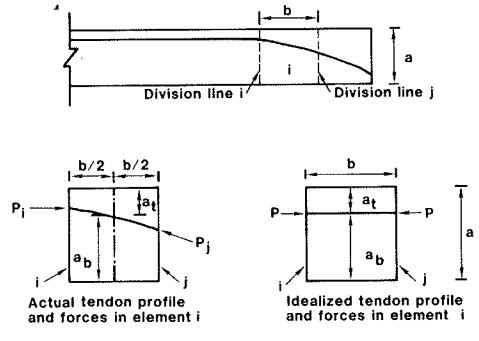

FIGURE 3 FAP idealization of prestressing forces and tendon profiles.

Idealization of the Structure and Input Requirements

The finite-element idealization of the structure for FAP analysis is shown in Figure 4. In order to understand this idealization and the subsequent input requirements, certain terms are defined as follows:

1. Longitudinal joints are the transverse lines that divide the structure into (idealized) segments longitudinally.
2. Nodal lines are parallel to the longitudinal direction of the structure and divide the structure transversely.
3. Nodes are the location at which nodal lines intersect with longitudinal joints. Node numbering is defined once and is same for all joints.
4. A segment is a portion of the structure between two consecutive longitudinal joints.
5. An element is the rectangular plate portion of the structure bounded by two consecutive longitudinal joints and nodal lines. Element numbering is defined once and is same for all segments.
6. The structural coordinate system is shown in Figure 4. To simplify the transformations between the element and structural coordinate systems, the y-axis is always parallel to the longitudinal direction of the structure; x- and z-axes are interchangeable.
7. The element coordinate system is shown in Figures 1 and 2. Again, the element y-axis is always parallel to the longitudinal direction of the structure. In the element coordinate system, x- and z-axes are not interchangeable.
8. The degrees of freedom correspond to a nodal displacement due to the deformations of the structure. Each degree of freedom also refers to the directions of loads applied to a node. Each node can be displaced or loaded four ways: three translational displacements per load corresponding to x-, y-, and z-directions and one rotational displacement per load about the y-axis (Figure 4).
9. Constrained nodes are those at which one or more degrees of freedom are constrained because of the physical conditions existing at a support or in cases where symmetry is used in the analysis. A controlled displacement, such as that due to support settlement, is also considered a constrained degree of freedom.

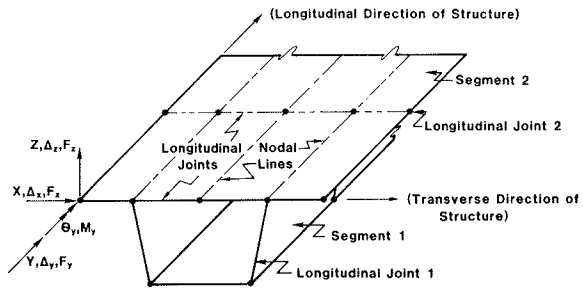

FIGURE 4 FAP idealization of folded-plate structure.

10. Nodal loads are concentrated loads directly applied to a node. These loads are indicated in the structural coordinate system.

11. Element loads are uniformly distributed surface loads on the element. These loads are indicated in the element coordinate system. Element loads also include gravity load due to the self weight of the material and forces produced by the temperature differential existing across the depth, width, or the length of the structure.

12. Stagewise analysis is automated analysis of the same structure for varying length, support, and loading conditions and changes in other structural parameters during construction of the structure or its service life (Figure 5).

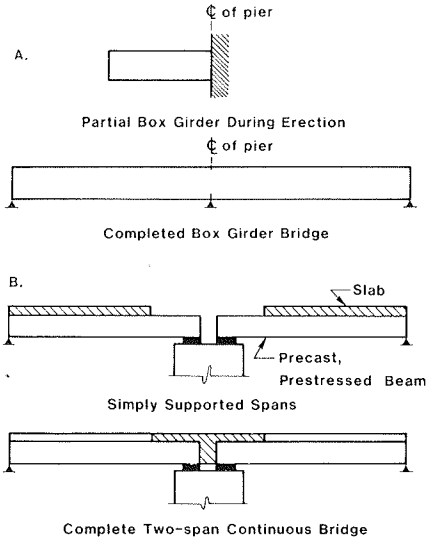

FIGURE 5 Stagewise analysis.

13. Load case is a particular combination of loads for which analysis of the structure is desired.

The flowchart in Figure 6 indicates the sequential order of input data requirements. A brief description of each requirement is as follows:

1. Structure comment cards are used to provide information about the structure, which is echo-printed and has no influence on the analysis.

2. Structure control data provide the following information: total number of segments in the structure, number of nodes per longitudinal joint, number of elements per segment, number of segment types (a segment type is defined according to segment properties, described in the following), and number of stages to be analyzed.

3. Segment type code indicates the type of each segment in the structure in sequential order according to its location in the structure.

4. Segment properties provide the following information for each type of segment: segment width between longitudinal joints and elastic modulus, thickness, Poisson's ratio, and unit weight of material for each element in the segment.

5. Element connections indicate the numbers of the two nodal lines that bound each element transversely. The first number refers to node 1 and the second number refers to node 2 of the element. These two numbers together establish the element coordinate system shown in Figures 1 and 2. This information is provided once and element locations for the whole structure are generated by the program.

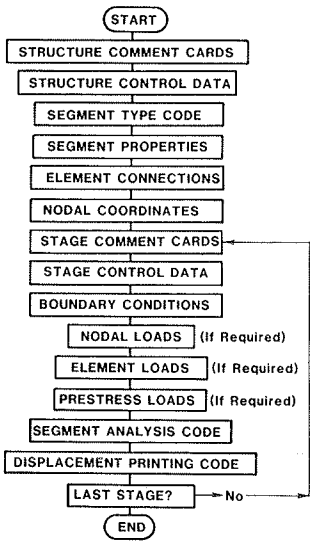

FIGURE 6 Sequence of input information for FAP.

6. Nodal coordinates indicate the x- and z-coordinates of each node in the structural coordinate system. This information is provided once and the nodal coordinates for the whole structure are generated by the program.

The following information is provided for each stage of analysis:

7. Stage comment cards are the same as the structural comment cards.

8. Stage control data provide the following information for a particular stage of analysis: number of segments to be included in the stage, number of constrained nodes, number of nodal load cases, number of element load cases (surface loads in any of the three directions, self weight of the material, and temperature differential between elements), and number of prestress load cases.

9. Boundary conditions indicate, at this step, each degree of freedom of the constrained nodes, as indicated in the stage control data, individually coded for its constrained or free condition.

10. Nodal loads provide the magnitude, location, and direction of each nodal load, according to the nodal load cases. The term "load" is used for either an applied force or a displacement condition corresponding to each degree of freedom. If a degree of freedom is free, the corresponding load is considered an applied force; if the degree of freedom is constrained, the corresponding load is considered a forced displacement including zero displacements.

11. Element loads provide the data for three different types of element loads, as required. It is not necessary that all the elements of a segment, or all the segments in a particular stage of analysis, be loaded for any element load case.

12. Prestress loads (tendons) can also be grouped in different load cases. For each prestress load case, the following information is provided: number of tendons in the load case, number of segments through which each tendon passes, and location of tendon and average prestressing force within each element (Figure 3).

Output Information

The output consists of an echo print of all input data and the following response quantities for each

stage of analysis. All information refers to the load case number, longitudinal-joint number, segment number, element number, and nodal-line number, as required. The response quantities are units consistent with the units of the input information:

1. Longitudinal in-plane (membrane) stresses at midpoints of the edges of each element,
2. Transverse in-plane stresses at the center point of each element,
3. Transverse bending moments at midpoints of the longitudinal edges of each element, and
4. Displacements and reactions corresponding to each degree of freedom of a node.

The preceding information is printed only for segments and longitudinal joints desired by the user. At the end of the analysis for each load case, the external equilibrium conditions in the x-, y-, and z-directions are checked and printed.

Error Messages

Any error in the input data for which the analysis cannot be executed stops the program from further execution. In this case an error message or messages are printed indicating the possible source of error to assist the user in locating it in the input information.

ILLUSTRATIVE EXAMPLES

The complete analysis of various types of folded-plate structures, including stagewise analysis, loading, and boundary conditions, is beyond the scope of this paper. The intent of the following examples is to provide representative illustrations of the use and the accuracy of FAP.

Example 1

The structure for example 1 is taken from a study by Goldberg et al. (17). The dimensions and loading of the single-span, simply supported structure are shown in Figure 7. The structure has diaphragms at both ends that are assumed to be infinitely rigid in their planes but completely flexible for out-of-plane deformations. The elastic modulus and Poisson's ratio are 10,600 ksi and 0.33, respectively. Table 1 represents the vertical and horizontal displacements of point A, as shown in Figure 7. These include the elasticity and experimental results (17), results based on the simplified 4-df/node plate element, and results using the conventional 6-df/node plate element (18).

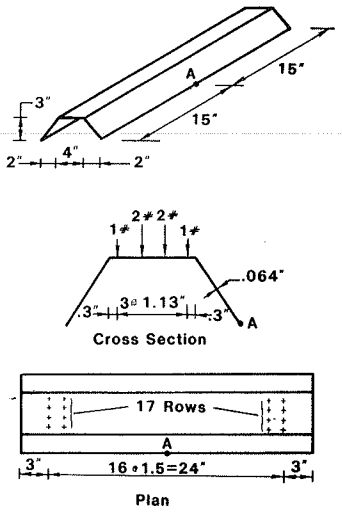

FIGURE 7 Example 1: single-span folded-plate structure with loading.

TABLE 1 Example 1: Horizontal and Vertical Displacements of Point A

Type of Displacement	Displacement (in.)			
	Elasticity	Experimental	4 df[a]	6 df[b]
Horizontal	0.032	0.030	0.0306	0.0306
Vertical	0.016	0.012	0.0146	0.0150

[a] Total df = 840.
[b] Total df = 1,260.

Example 2

The idealization of a prestressing tendon with a varying force for a two-equal-span box beam with symmetrical prestressing is described in example 2. The structure, its FAP idealization, and the idealization of the tendon profile and the prestressing force are shown in Figure 8. The representative results of analyses by FAP are presented in Table 2. These results are compared with the results of accurate elastic analysis considering the exact tendon profile and prestressing force variation along the tendon length.

Example 3

This example is of a three-cell, two-equal-span, symmetrically loaded box girder (Figure 9); the example is taken from a study by Scordelis (19). The finite-element idealization for FAP is also shown in Figure 9. The representative results are presented in Figures 10, 11, and 12 (in pounds-force per square foot, foot-pounds per foot, and feet x 10^5, respectively) along with the elasticity solutions by Scordelis (19) and the results obtained by using a computer program based on a 6-df/node element (6).

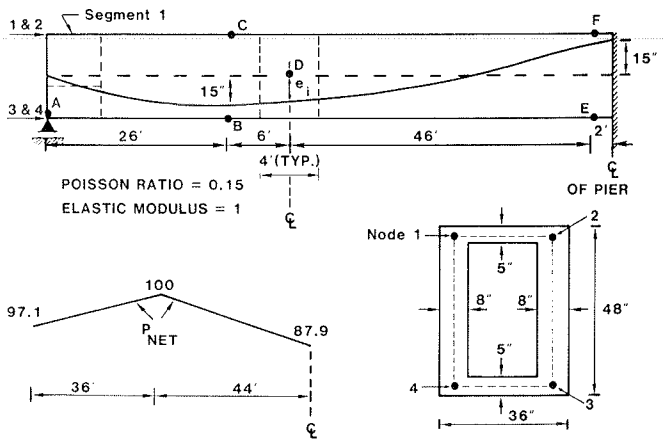

FIGURE 8 Example 2: finite-element idealization of structure and prestressing force.

TABLE 2 Example 2: Representative Results of Prestress Analysis

Analysis	Reaction at A	Stress at B (psf)	Stress at C (psf)	Vertical Deformation at D (ftx100^5)	Stress at E (psf)	Stress at F (psf)
FAP	0.316	−224.7	23.7	369.83	45.8	−228.5
Exact	0.316	−224.3	23.4	371.11	44.8	−227.6
Difference (%)	0	0.18	1.28	0.35	2.23	0.40

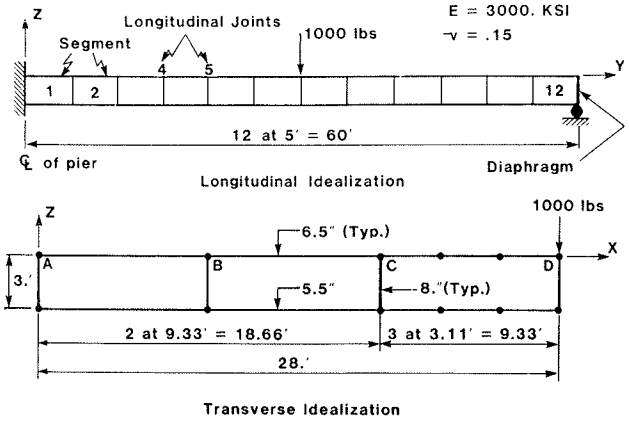

FIGURE 9 Example 3: finite-element idealization of three-cell box girder.

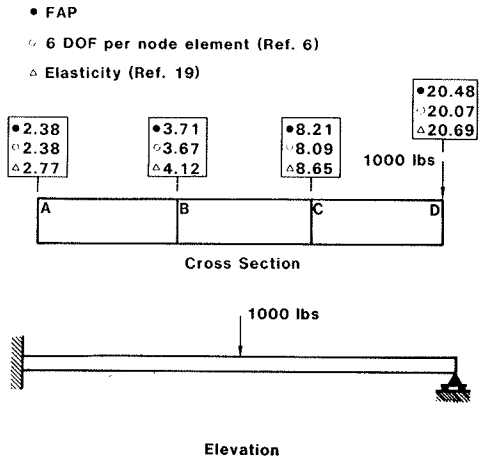

FIGURE 12 Example 3: vertical deflection at center line of span.

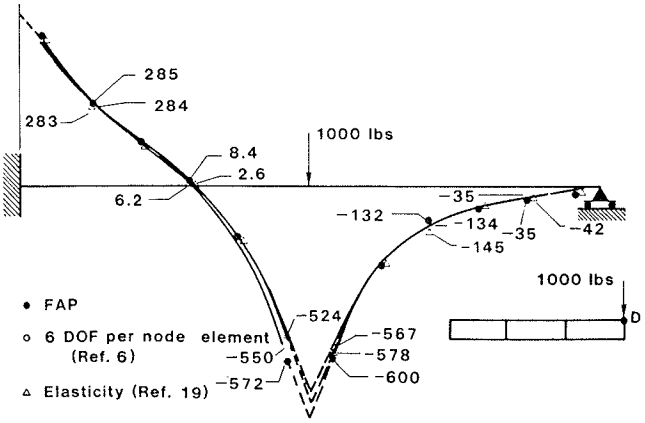

FIGURE 10 Example 3: longitudinal stresses at point D.

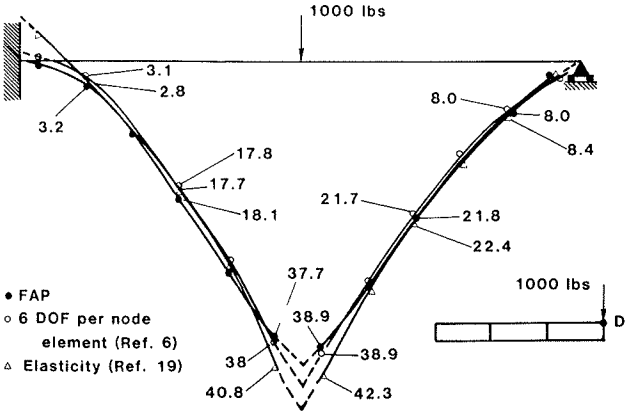

FIGURE 11 Example 3: transverse moments at point D.

SUMMARY AND CONCLUSION

The FAP finite-element program was specifically developed for the elastic analysis of constant depth and straight folded-plate type structures. The program can facilitate the design of folded-plate type bridge superstructures such as T-beams and box girders. Most of the data for the finite-element analysis is generated by the program from minimal and straightforward input information. The bridge superstructure can be analyzed under all the loading conditions, which are common in a bridge design and for arbitrary boundary and stagewise erection conditions. The analytical results consist of deflections of the structure, transverse bending moments, and in-plane stresses in the component member plates, which are the practical strength and serviceability concerns in a design. Being a specific-purpose program, FAP may be used by a bridge engineer for the purpose of design of several types of structures without the extensive training, knowledge, and effort that may be required for the use of those finite-element programs that have been developed for the analysis of a wide range of structural types. FAP has been tested, as much as is practically possible, for accuracy of its analysis for the purpose of design of bridge superstructures.

The FAP element uses only 4 df/node compared to a conventional 6-df/node plate model. The results from FAP also converge more rapidly to acceptable results, thus requiring fewer nodes for the overall analysis. These two factors are significantly advantageous if the saving of user effort, computer time, and capacity requirements is to be considered.

ACKNOWLEDGMENT

The authors express their appreciation to the faculty and all the staff of the Civil Engineering

Department and Computer Center of the North Dakota State University for their assistance and encouragement in the preparation of this paper. The principal author of the paper especially wishes to express his deep appreciation to his major advisor, V.J. Meyers, and his Ph.D advisory committee at Purdue University for their timely and highly valuable advice in the development of the simplified plate-bending element used in FAP. Sincere thanks are also extended to E.W. Walters and the staff of the Indiana State Department of Highways for their assistance and encouragement during the initial phase of the development of FAP.

REFERENCES

1. J.E. Goldberg and H.L. Leve. Theory of Prismatic Folded Plate Structures. Journal of International Association of Bridge and Structural Engineering, Vol. 17, 1957.
2. J. Born. Folded Plate Structures. Unger Publishing Co., New York, 1962.
3. A.C. Scordelis. Analytical and Experimental Studies of Multicell Concrete Box Girder Bridges. Presented at Symposium on Folded Plates and Spatial Panel Structures, International Association for Shell and Spatial Structures, Madrid, Spain, Sept. 1974.
4. G.H. Powell. Comparison of Simplified Theories for Folded Plates. Journal of the Structural Division of ASCE, Dec. 1965.
5. H.R. Evans and K.C. Rockey. A Critical Review of the Methods of Analysis for Folded Plate Structures. Proc., Institute of Civil Engineers, London, June 1971.
6. F.A. Batla. Finite Element Analysis of Prestressed Concrete Box Girders. Ph.D thesis. Purdue University, West Lafayette, Ind., Dec. 1976.
7. R.J. Holman. Development of an Instrumentation Program for Studying Behavior of a Segmental Concrete Box Girder Bridge. Project JHRP-77-4. Purdue University-Indiana State Highway Commission Joint Highway Research Program, West Lafayette, Ind., March 1977.
8. S.P. Wanders, D.A. Winslow, and C.D. Sutton. Study of the Segmental Box Girder at Turkey Run: Construction, Instrumentation, and Data Collection. Project FHWA/IN/JHRP-79/25. Purdue University-Indiana State Highway Commission Joint Highway Research Program, West Lafayette, Ind., Dec. 1979.
9. F.A. Batla and P.R. Reisnour. Optimum Use of Prestressing in Concrete Structures: Design of Post-Tensioned Concrete Bridge Over Park River, Grafton, North Dakota. North Dakota State University Project 0025. North Dakota State Highway Department Research Project, Fargo, in preparation.
10. P.R. Reisnour. Study of Lateral Distribution of Wheel Loads for Multi-tee Beam Bridges. M.S. thesis. North Dakota State University, Fargo, Sept. 1982.
11. S. Timoshenko and S. Woinowski-Krieger. Theory of Plates and Shells. McGraw-Hill, New York, 1959.
12. R. Szillard. Theory and Analysis of Plates. Prentice-Hall, Englewood Cliffs, N.J., 1974.
13. R.H. Gallagher. Finite Element Analysis. Prentice-Hall, Englewood Cliffs, N.J., 1975.
14. T.Y. Lin and N.H. Burns. Design of Prestressed Concrete Structures. Wiley, New York, 1981.
15. A.E. Naaman. Prestressed Concrete Analysis and Design. McGraw-Hill, New York, 1982.
16. A.H. Nilson. Design of Prestressed Concrete. Wiley, New York, 1978.
17. J.E. Goldberg, M.J. Gutzwiller, and R.H. Lee. Analytical and Model Studies of Continuous Folded Plates. Journal of the Engineering Mechanics Division of ASCE, Vol. 94, No. EM5, Oct. 1968.
18. K.J. Bathe, E.L. Wilson, and F.E. Peterson. SAPIV: A Structural Analysis Program for Static and Dynamic Response of Linear Systems. U.S. Department of Commerce, June 1973. NTIS: PB 221 967.
19. A.C. Scordelis. Analysis of Continuous Box Girders. U.S. Department of Commerce, Nov. 1967. NTIS: PB 178 355.

Publication of this paper sponsored by Committee on Concrete Bridges.

The results, views, and conclusions presented in this paper are solely based on the authors' experience and knowledge and do not necessarily represent the policies of any educational, governmental, or public agency or the opinions of any other individual.

Cost-Effective Decision Models for Maintenance, Rehabilitation, and Replacement of Bridges

RICHARD E. WEYERS, PHILIP D. CADY, and RICHARD M. McCLURE

ABSTRACT

Methodology has been developed to determine whether a deteriorated bridge should be rehabilitated or replaced based on minimum life-cycle costs. Mathematical models were developed from the generalized cash-flow diagrams to facilitate the conversions of cash flow to equivalent values. The equivalent alternative values (equivalent uniform annual costs) are compared by means of a parameter called the value management (VM) term. The sign of the VM term indicates the decision (rehabilitate or replace) and the magnitude of the cost savings. The true cost of long-term borrowing is considered in the interest rate. Inflation's opposite effects on receipts and disbursement are evaluated. Examples of the mathematical models are presented. A microcomputer program was developed to solve the mathematical model. It is a prompt-type program that asks for the input parameters and presents the results and the VM term.

Although highway conditions vary among the states, the national trend is toward deteriorating highway conditions and need for additional funding. Reflective of this trend is Pennsylvania's enormous bridge problem. Pennsylvania has approximately 54,500 bridges longer than 8 ft. About 7,200 of these bridges are structurally deficient or functionally obsolete or both. The cost of improving these structures has been estimated to be $3.0 billion (1). Pennsylvania's reaction to this staggering problem was the enactment of a $1.4 billion bridge program, but even with the implementation of this program a significant amount of bridge work will remain. In addition, of the 22,500 bridges in Pennsylvania that are 20 ft or longer, 400 (2 percent) become deficient each year (2). By 1990 the cost to repair the backlog of bridges after the billion-dollar program has been finished was estimated to be $4.6 billion (2). Therefore, a management tool that will optimize the use of available funds through cost-effective solutions is urgently needed. The purpose of this paper is to present a standardized methodology for cost-effectiveness comparisons in order to generate least-cost solutions to bridge work.

COST EFFECTIVENESS

Cost effectiveness can be achieved through a standardized methodology of comparison in order to generate least-cost solutions, which account for all of the costs incurred over the service life of a structure considering the time value of money. This is in fact the meaning of cost effectiveness. Decisions based on initial costs or individual events will generally not result in a least-cost solution.

Basis

By using standard engineering economic analysis procedures, cost effectiveness is based on comparison of alternatives. The alternatives are as follows:

1. Force-account rehabilitation of the existing structure followed by eventual replacement,
2. Contract rehabilitation of the existing structure followed by eventual replacement, and
3. Replacement of the structure immediately.

Because the rehabilitation alternatives (1 and 2) include eventual replacement, the replacement alternative (3) is evaluated first because it becomes an input parameter for the first two.

The rehabilitation alternatives are compared first, and the one that has the lowest cost is compared with the replacement alternative in the calculation of a parameter called the value management (VM) term, which is obtained by subtracting the equivalent structure rehabilitation cost from the equivalent structure replacement cost. The sign of the VM term indicates the decision (positive sign, rehabilitate; negative sign, replace) and the magnitude of the cost savings if the decision is rendered as indicated by the sign.

The equivalent values are determined as equivalent uniform annual costs (EUAC) for perpetual service. The choice of perpetual service is based on the long use of bridge sites (50 years or more), and the difference between equivalent values for 50 years or more and for infinity (perpetual service) is small in comparison with the uncertainties in predicting future cash flows. Note that the equivalent replacement and rehabilitation costs can be expressed in terms of capitalized cost (present worth of perpetual service) simply by multiplying by the reciprocal of the interest rate, which is, of course, the value for the uniform series present worth factor for infinite time.

Cost Data

Costs for rehabilitation and maintenance work by force account should include the following:

1. Maintenance overhead (equipment and facilities),
2. Design (personnel plus overhead),
3. Maintenance or rehabilitation work (personnel plus material and work contracted, if any),
4. Traffic maintenance and protection, and
5. Road user costs, if appropriate.

Rehabilitation and maintenance work performed by contract should include the following items:

1. Design (personnel plus overhead),
2. Contract administration,
3. Bid price,
4. Inspection costs (including overhead), and
5. Traffic maintenance and protection and road user costs, if applicable.

The major replacement cost items should include the following:

1. First cost (replacement structure cost, engineering, and contract administration);
2. Annual maintenance, rehabilitation, and repair costs (including the items previously listed);
3. Salvage values; and
4. Traffic maintenance and protection and road user costs, if applicable.

Interest Rate and Inflation

The interest rate is the expression of the time value of money in engineering economic evaluations. Prevailing lending rates are generally not appropriate because they include an inflation factor. The true cost of long-term borrowing is generally considered to be of the order of 4 to 6 percent (3).

Classical engineering economic evaluation methodology, for the most part, ignores the effects of inflation. The rationale for this posture is that if inflation affects all aspects of cash flow in the same manner, its net effect on economic decision making is nil. However, in the financing of highway maintenance and construction, this is not true. Funds for new construction, capital improvements, and maintenance of the nation's highways at both the state and federal levels are derived primarily from fixed cents-per-gallon motor fuel taxes. Revenues in the past increased as fuel consumption increased, and at relatively low inflation rates funding pretty well kept pace with costs. However, after the 1973 oil embargo a pronounced change occurred. Rapid increases in fuel costs resulted in marked reduction in fuel consumption because of economizing by motorists and the rapid changeover to smaller, more fuel-efficient automobiles. Also, in order to provide incentives for the development of alternative fuel sources, tax exemptions were provided for gasoline-alcohol blends. These factors produced a drastic reduction in the rate of growth in revenues. During the same period the costs increased sharply because of rapidly rising inflation rates. Although future rates may be tempered somewhat, there is every reason to believe that this trend will continue. Thus, we are faced with a scenario in which inflation affects receipts and disbursements oppositely, creating a situation in which engineering economic analysis must take into account the effects of inflation.

The true interest rate for the conditions described in the preceding paragraph is a function of three factors:

1. Prevailing interest rate,
2. Inflation rate, and
3. Rate of increase in funding.

It has been shown (4) that the applicable relationship is as follows:

$$i^* = \{[(1 + i)(1 + q)]/(i + f)\} - 1 \quad (1)$$

where

i^* = true interest rate,
i = prevailing interest rate,
f = inflation rate, and
q = rate of increase in funding.

(All rates are expressed in decimal form.) Note that when the effects of inflation are ignored, $i^* = i$.

Using data for the period 1970-1979 from a 1981 General Accounting Office report to the Congress (5), the following values for inflation and funding rates were determined:

1. Inflation rate for highway construction costs: 9.4 percent,
2. Inflation rate for highway maintenance costs: 7.4 percent, and
3. Increase in funding for highway maintenance and construction: 4.8 percent.

The Models

To facilitate the conversions of cash flows to equivalent values that can be compared and used in the VM term, generalized models were developed. The generalized replacement and rehabilitation models, in the form of cash-flow diagrams, are presented in Figures 1 and 2, respectively. The mathematical relationships follow.

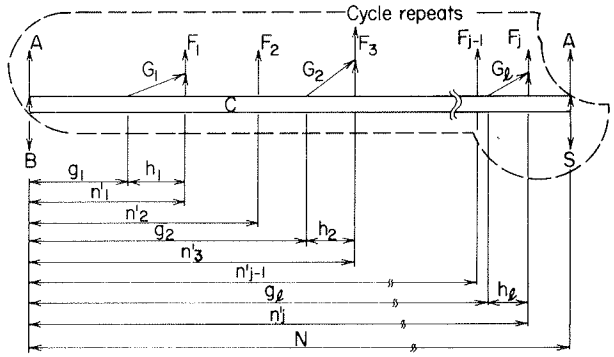

FIGURE 1 Replacement cash-flow diagram, mathematical model, and notation.

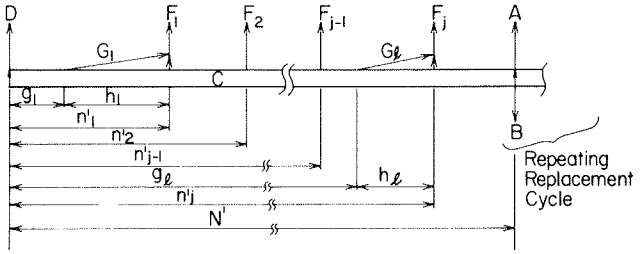

FIGURE 2 Rehabilitation cash-flow diagram, mathematical model, and notation.

Replacement Model

$$EUAC_{Replace} = (A/P, i, N)\left[(A - S) + \sum_{m=1}^{\ell} G_m(P/G, i, h_m + 1)(P/F, i, g_m - 1) + \sum_{k=1}^{j} F_k(P/F, i, n'_k)\right] + (S - B)(i) + C \quad (2)$$

where

A = replacement structure first cost;
B = salvage value of present structure;
S = salvage value of replacement structure;
C = annual maintenance cost for cleaning deck, drainage system, and so on;
F = single future expenditures (e.g., deck overlay, abutment underpinning, painting);
N = life of replacement bridge;
G = annual increase in maintenance cost due to progressive deterioration (e.g., deck patching);
n' = time to single future expenditure;
g = time to beginning of increasing maintenance costs due to progressive deterioration;

h = duration of increasing maintenance costs due to progressive deterioration; and
i = interest rate;

(A/P) = capital recovery factor (A/P, i percent, n)

$$= i(1 + i)^n/[1 + i)^n - 1] \quad (3)$$

(P/F) = single payment present-worth factor (P/F, i percent, n)

$$= 1/(1 + i)^n \quad (4)$$

(P/G) = gradient present-worth factor (P/G, i, n)

$$= (1/i)\left(\{[(1 + 1)^n - 1]/i(1 + i)^n\}\ [n/(1 + i)^n]\right) \quad (5)$$

Rehabilitation Model

$$EUAC_{Rehab} = (EUAC_{Replace})(P/F, i, N') + i\left[D + C(P/A, i, N') + \sum_{m=1}^{\ell} G_m(P/G, i, h_m + 1)(P/F, i, g_m - 1) + \sum_{k=1}^{j} F_k(P/F, i, n'_k)\right] \quad (6)$$

where

D = initial repair cost,
N' = time to require replacement, and

(P/A) = uniform series present-worth factor

$$= (P/A, i, n) = 1/(A/P) = [(1 + i)^n - 1]/i(1 + i)^n \quad (7)$$

EXAMPLES

The manner in which the mathematical models are applied and the effects of inflation are accounted for in the selection of interest rate is illustrated in the two examples that follow. The values for the capital recovery factor (A/P, i percent, n), single payment present-worth factor (P/F, i percent, n), uniform series present-worth factor (P/A, i percent, n), and the gradient present-worth factor (P/G, i percent, n) used in the examples may be found in any engineering economy text or calculated from the formulas presented.

Example 1

The cash flows associated with replacement and rehabilitation (by force account and by contract) for a certain bridge are shown in Tables 1 and 2. The cost-effective approach is determined as follows:

1. Assume that the interest rate is the mean of the 4 to 6 percent usually considered to represent the range of the true interest values for long-term investments; that is, i = 5 percent.
2. Replace structure (see Figure 3):

$$EUAC_{Replace} = \underset{5.101}{(A/P,5\%,40)}\ \{(45,000 - 1,500) + \underset{0.5847}{[(100)(P/G,5\%,3 + 1)}\underset{0.2812}{(P/F,5\%,12 - 1)} + (100) \times \underset{5.101}{(P/G,5\%,3 + 1)}\underset{0.4810}{(P/F,5\%,27 - 1)}] + [(8,000) \times \underset{0.3769}{(P/F,5\%,15)} + (1,500)(P/F,5\%,20) + (6,000) \times \underset{0.2314}{(P/F,5\%,30)}]\} + (1,500 - 1,000)(0.05) + 500 = \$3,424/year.$$

TABLE 1 Cash-Flow Table for Bridge Replacement: Example 1

End of Year	Cost ($)	Symbol	Item
0	45,000; 1,000	A, B	Replacement bridge minus salvage beams of current bridge
1-12	500	C	Annual maintenance and cleaning
13	500; 100	C, G_1	Annual maintenance and cleaning + deck patching
14	500; 200	C2G_1	Annual maintenance and cleaning + deck patching
15	500; 300; 8,000	C, 3G_1, F_1	Annual maintenance and cleaning + deck patching + deck and drainage repair
16-19	500	C	Annual maintenance and cleaning
20	500; 1,500	C, F_2	Annual maintenance and cleaning + underpinning and bearing repair
21-27	500	C	Annual maintenance and cleaning
28	500; 100	C, G_2	Annual maintenance and cleaning and deck patching
29	500; 200	C, G_2	Annual maintenance and cleaning and deck patching
30	500; 300; 6,000	C, 3G_2, F_3	Annual maintenance and cleaning + deck patching + deck and abutment repair
31-39	500	C	Annual maintenance and cleaning
40	500;1,500	C, S	Annual maintenance and cleaning minus salvage value of railings and beams

Note: Bridge replaced after 40 years.

TABLE 2 Cash-Flow Table for Rehabilitation of Current Structure: Example 1

End of Year	Force Account[a]			Contract[b]		
	Cost ($)	Symbol	Item	Cost ($)	Symbol	Item
0	7,500	D	Point abutment, repairing wings, widening and patching deck, treating railing, and painting beams	12,000	D	Point abutment, replacing wings, deck, and railings
1-5	300	C	Annual maintenance and cleaning	200	C	Annual maintenance and cleaning
6	300, 100	C, G_1	Annual maintenance and cleaning + deck patching	200	C	Annual maintenance and cleaning
7	300; 200	C, 2G_1	Annual maintenance and cleaning + deck patching	200	C	Annual maintenance and cleaning
8	300; 300	C, 3G_1	Annual maintenance and cleaning + deck patching	200	C	Annual maintenance and cleaning
9	300; 400	C, 4G_1	Annual maintenance and cleaning + deck patching	200	C	Annual maintenance and cleaning
10	300; 500; 1,200	C, 5G_1, F	Annual maintenance and cleaning + deck patching + underpinning wings and abutment and painting beams	200; 1,000	C, F_1	Annual maintenance and cleaning + painting
11-15	300	C	Annual maintenance and cleaning	200	C	Annual maintenance and cleaning
16-19				200	C	Annual maintenance and cleaning
20				200; 1,000	C, F_2	Annual maintenance and cleaning + painting
21-25				200	C	Annual maintenance and cleaning

[a] Bridge replaced after 15 years.
[b] Bridge replaced after 25 years.

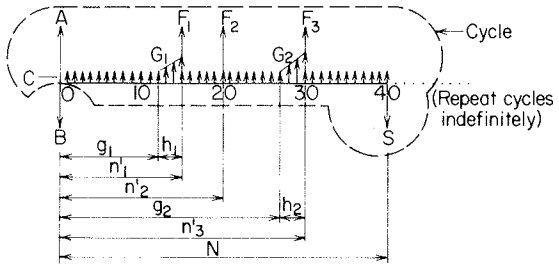

FIGURE 3 Example 1: replacement model.

3. Rehabilitate structure (force account) (see Figure 4) by using the rehabilitation model:

FIGURE 4 Example 1: force-account rehabilitation model.

$$EUAC_{Rehab} = (3,424)(P/F,5\%,15)_{0.4810} + (0.05)_{10.3796} \times {}_{11.966}[7,500 + (300)(P/A,5\%,15)_{0.8227} + (100)(P/G,5\%,6)_{0.6139} (P/F,5\%,4) + (1,200)(P/F,5\%,10)] = \$2,264/year.$$

4. Rehabilitate structure (contract) (see Figure 5):

$$EUAC_{Rehab} = (3,424)(P/F,5\%,25)_{0.2953} + (0.05)_{14.094} \times {}_{0.6139}[12,000 + (200)(P/A,5\%,25)_{0.3769} + (1,000)(P/F,5\%,10) + (1,000)(P/F,5\%,20)] = \$1,802/year.$$

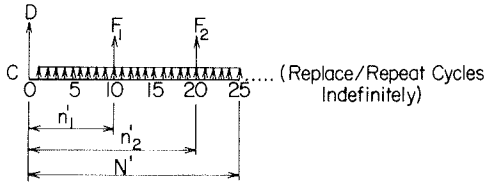

FIGURE 5 Example 1: contract rehabilitation model.

5. Compare rehabilitation methods:

$1,802/year < $2,264/year.

Therefore, contract repair would be chosen.

6. Compare repair versus replacement cost:

VM = $3,424/year - $1,802/year = +$1,622/year.

Therefore, the structure should be rehabilitated (by contract). The annual saving is $1,622/year and the capitalized saving is $1,622/0.05 = $32,440.

Example 2

The cash flows associated with replacement and rehabilitation (by force account and by contract) for a certain bridge are shown in Tables 3 and 4. The most cost-effective approach is determined as follows:

1. Assume that the interest rate is based on the technique that takes into account rates of inflation and funding. As previously discussed, the historical rates for the 1970s are 9.4 percent inflation rate for highway construction costs, 7.4 percent inflation rate for highway maintenance costs, and 4.8 percent increase in funding for highway maintenance and construction. Because it is not practical to use two interest rates in the same analysis, assume that the combined inflation rate is the average of the rates for construction and maintenance costs; i.e., f = (9.4 + 7.4)/2 = 8.4 percent. Assume that the prevailing interest rate for long-term public financing during the period is 10 percent. There-

TABLE 3 Cash-Flow Table for Bridge Replacement: Example 2

End of Year	Cost ($)	Symbol	Item
0	44,000; 2,000	A, B	Replacement of bridge minus salvage beams of current bridge
1-11	500	C	Annual maintenance and cleaning
12	500; 50	C, G_1	Annual maintenance and cleaning and deck patching
13	500; 100	C, $2G_1$	Annual maintenance and cleaning and deck patching
14	500; 150	C, $3G_1$	Annual maintenance and cleaning and deck patching
15	500; 200	C, $4G_1$	Annual maintenance and cleaning and deck patching
16	500; 250	C, $5G_1$	Annual maintenance and cleaning and deck patching
17	500; 300	C, $6G_1$	Annual maintenance and cleaning and deck patching
18	500; 350	C, $7G_1$	Annual maintenance and cleaning and deck patching
19	500; 400	C, $8G_1$	Annual maintenance and cleaning and deck patching
20	500; 450; 8,800	C, $9G_1$, F_1	Annual maintenance and cleaning and deck patching + deck overlay
21-29	500	C	Annual maintenance and cleaning
30	500; 1,030	C, F_2	Annual maintenance and cleaning + underpin abutment and cleaning channel
31	500; 50	C, G_2	Annual maintenance and cleaning and deck patching
32	500; 100	C, $2G_2$	Annual maintenance and cleaning and deck patching
33	500; 150	C, $3G_2$	Annual maintenance and cleaning and deck patching
34	500; 200	C, $4G_2$	Annual maintenance and cleaning and deck patching
35	500; 250, 10,000	C, $5G_2$, F_3	Annual maintenance and cleaning and deck patching and deck overlay
36-39	500	C	Annual maintenance and cleaning
40	500; 900	C, F_4	Annual maintenance and cleaning and repair bearing areas
41-49	500	C	Annual maintenance and cleaning
50	400; 4,000	C, S	Annual maintenance and cleaning minus salvage value of beams and railings

Note: Bridge replaced after 50 years.

TABLE 4 Cash-Flow Table for Rehabilitation of Current Structure: Example 2

End of Year	Cost ($) Force Account	Contract	Symbol	Item
0	20,000	26,000	D	Underpin and pressure point abutments
1	600	500	C	Annual maintenance and cleaning
2	600; 50	600; 50	C, G_1	Annual maintenance and cleaning and deck patching
3	600; 100	600; 100	C, $2G_1$	
4	600; 150	600, 150	C, $3G_1$	
5	600; 200; 28,000	600; 200; 25,000	C, $4G_1$, F_1	Annual maintenance and cleaning and deck patching and deck replacing and adding more stringers
6-14	600	600	C	Annual maintenance and cleaning
15	600, 3,000	600, 3,500	C, F_2	Annual maintenance and cleaning + painting
16-24	600	600	C	Annual maintenance and cleaning
25	600; 3,000	600; 3,500	C, F_3	Annual maintenance and cleaning + painting
26-30	600	600	C	Annual maintenance and cleaning

Note: Bridge replaced after 30 years.

fore, the true interest rate is calculated as follows:

$$i^* = \{[(1 + i)(1 + q)]/(1 + f)\} - 1$$
$$= \{[(1 + 0.10)(1 + 0.048)]/(1 + 0.084)\} - 1$$
$$= 0.063 = 6.3 \text{ percent.}$$

a. Replace structure (see Figure 6) by using the replacement model:

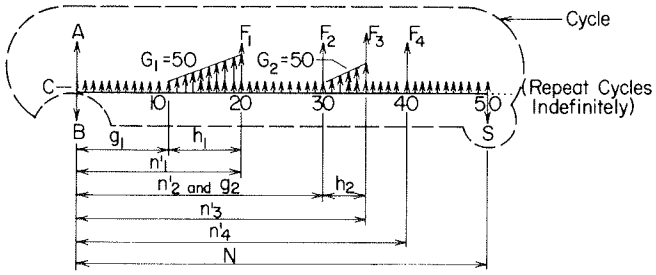

FIGURE 6 Example 2: replacement model.

$$EUAC_{Replace} = (A/P,6.3\%,50)\{(44{,}000 - 4{,}000) + \underset{29.020}{(50)(P/G,6.3\%,10)}\underset{0.5428}{(P/F,6.3\%,10)} + \underset{11.312}{(50)(P/G,6.3\%,6)}\underset{0.1700}{(P/F,6.3\%,29)}] + [(8{,}880)\underset{0.2947}{(P/F,6.3\%,20)} + (1{,}030)\underset{0.1600}{(P/F,6.3\%,30)} + (10{,}000)\underset{0.1179}{(P/F,6.3\%,35)} + (900)\underset{0.0868}{(P/F,6.3\%,40)}]\} + (4{,}000 - 2{,}000)(0.063) + 500$$
$$= \$3{,}595/\text{year.}$$

b. Rehabilitate structure (see Figure 7) (same cash-flow diagram applies to force-account and contract repairs in this case; only values of factors are different):

(1) Force account by using the rehabilitation model:

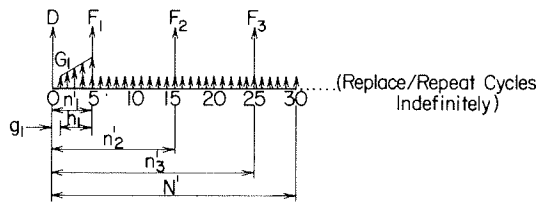

FIGURE 7 Example 2: force-account and contract rehabilitation model.

$$EUAC_{Rehab} = (3{,}595)\underset{13.3340}{(P/F,6.3\%,30)} + 0.063 \times \underset{7.847}{\{20{,}000 + (600)(P/A,6.3\%,30)} + (50)\underset{1.000}{(P/G,6.3\%,5)}(P/F,6.3\%,0) + [(28{,}000) \times \underset{0.7368}{(P/F,6.3\%,5)} + (3{,}000)\underset{0.4000}{(P/F,6.3\%,15)} + (3{,}000) \times \underset{0.2171}{(P/F,6.3\%,25)}]\} = \$3{,}780/\text{year.}$$

(2) Contract by using the rehabilitation model:

$$EUAC_{Rehab} = (3{,}595)\underset{13.3340}{(P/F,6.3\%,30)} + (0.063) \times \underset{7.847}{\{26{,}000 + (600)(P/A,6.3\%,30)} + (50)\underset{1.000}{(P/G,6.3\%,5)}\underset{0.7368}{(P/F,6.3\%,0)} + [(25{,}000)\underset{0.4000}{(P/F,6.3\%,5)} + (3{,}500)\underset{0.2171}{(P/F,6.3\%,15)} + (3{,}500)(P/F,6.3\%,25)]\}$$
$$= \$4{,}038/\text{year.}$$

c. Compare cost:

(1) Rehabilitation by force account: $3,780/year.
(2) Rehabilitation by contract: $4,038/year.
(3) Replacement: $3,595/year.

Therefore, the structure should be replaced.

2. In the same situation as that just described but without considering inflation (f = q and therefore i* = i = 10 percent), the calculations are exactly the same as those in the immediately preceding case except that the interest rate is 10 percent. The results will be as follows:

a. Rehabilitation by force account: $4,722/year.
b. Rehabilitation by contract: $5,152/year.
c. Replacement: $4,958/year.

Therefore, the structure should be rehabilitated by force account.

3. In the same situation as that just described, ignoring inflation changes the choice of alternative from replacement to rehabilitation (by force account) and has an effect on the magnitude of the real present value. Because the relationship used in accounting for inflation is based on the real present value of inflated future costs, comparisons will have to be based on present worth.

The EUAC computed by using the model are for perpetual service. The present worth for perpetual service, also called the capitalized cost, is EUAC divided by the interest rate (expressed as a decimal). Therefore, the capitalized cost for the choice

when taking inflation into account (replacement) is calculated as follows:

$3,595/i* = $3,595/0.063 = $57,063.

And the capitalized cost for the choice when inflation is ignored (rehabilitate by force account) is calculated as follows:

$4,722/i = $4,722/0.100 = $47,220.

Therefore, if inflation is ignored in this case, the real present value for the least-cost alternative is understated by nearly $10,000 (17.2 percent).

MICROCOMPUTER PROGRAM

A microcomputer program that simulates the mathematical models presented in this paper and outputs the least-cost solution was written for the Apple IIe. It is a user-friendly prompt-type program that asks for the input parameters (interest rate, if inflation is to be considered; maintenance and rehabilitation costs; time parameters; etc.). The program is available on request from Richard Weyers or Philip D. Cady.

SUMMARY

A standardized cost-effectiveness solution to whether a bridge should be rehabilitated or replaced has been developed. The alternatives were evaluated by means of appropriate mathematical models that have been developed from generalized cash-flow diagrams. Inflation's opposite effects on receipts and disbursements were evaluated and illustrated by an example. The example showed that if inflation is ignored, the wrong decision can be reached and the real cost will be significantly understated. The standardized methodology presented for cost-effectiveness comparison of alternatives for bridge operations should aid in optimizing the use of limited available funds.

ACKNOWLEDGMENT

The authors wish to acknowledge the support of the Pennsylvania Department of Transportation and FHWA in funding the work described here as part of a larger project. The authors also wish to acknowledge and thank Knud E. Hermansen, instructor of civil engineering at Pennsylvania State University, for developing the computer program discussed here.

REFERENCES

1. R.M. McClure, C.L. Brodeur, and S.W. Marquiss. Bridge Problems and Policies in Pennsylvania. PTI 8301. Pennsylvania Transportation Institute, Pennsylvania State University, University Park, May 1983, 246 pp.
2. Bridges 83: An Economic Analysis. Pennsylvania Economy League, Western Division, Pittsburgh, April 1983, 101 pp.
3. J.R. Craig, D.S. O'Conner, and J.J. Ahlskog. Economics of Bridge Deck Protection Methods. Presented at National Association of Corrosion Engineers Annual Convention, March 22-26, 1982, (Paper 82).
4. P.D. Cady. Inflation and Highway Economic Analysis. Journal of Transportation Engineering of ASCE, Vol. 109, No. 5, Sept. 1983, pp. 631-639.
5. Deteriorating Highways and Lagging Revenues: A Need to Reassess the Federal Highway Program. Report CED-81-42. General Accounting Office, March 5, 1981, 90 pp.

Publication of this paper sponsored by Committee on Structures Maintenance.

The authors are responsible for the accuracy of the data and the conclusions and opinions.

Economic and Performance Considerations for Short-Span Bridge Replacement Structures

J.J. HILL and A.M. SHIROLE

ABSTRACT

Bridges with span lengths up to 100 ft often can be replaced with many different types of structures. This paper is based on a study covering economic and performance aspects of 3,692 bridge replacements in Minnesota during the period 1973 to 1983. Initial and subsequent costs as well as performance problems and considerations for different types of concrete, steel, and timber structures are discussed.

During the past decade new bridge construction and reconstruction activities in the United States have increased significantly. Many different types of structures have been and are being built to replace a large number of deteriorated and deficient bridges. This paper is based on a study that covers 3,692 bridge replacement structures constructed in Minnesota during 1973 to 1983. For the purposes of this study, bridges with main-span lengths of up to 100 ft are considered as short-span structures. Table 1 indicates different types and numbers of bridge replacement structures included in this

TABLE 1 Type and Number of Structures, 1973-1983

Material and Type of Structure	No. of Bridge Structures: State Routes	No. of Bridge Structures: Other Than State Routes
Concrete		
Deck and box girder, rigid frame, arch	1	9
Slab	2	24
Channel	0	59
Culvert		
Box	24	68
Box (precast)	45	98
Pipe (round)	0	8
Pipe arch	75	1,499
Precast arch	4	3
Steel		
Beam	82	251
Truss	6	20
Through, deck, and box girder	6	20
Arch	1	4
Culvert		
Pipe	5	60
Pipe arch	1	280
Long span	8	41
Other	6	17
Prestressed concrete		
Beam	202	88
Slab and voided slab	2	26
Box girder	3	1
Double-T	2	33
Quad-T	0	133
Bulb-T	2	30
Channel and other	0	12
Timber and other		
Timber		
Beam	10	66
Slab	1	327
Box culvert	0	8
Masonry arch	2	11
Wrought iron girder	0	1
Aluminum box culvert	0	5

Note: Construction period 1973 to 1983.

study. Available information on construction costs as well as subsequent performance and required maintenance for these structures are evaluated to determine economic and performance considerations that should justifiably influence the selection of certain types of structures.

AVAILABLE INFORMATION

During the past 11 years, many different types of structures (see Figures 1-4) have been used in replacing 3,692 bridges in Minnesota. For structures other than culverts, construction cost data have been available in terms of contract prices. Tables 2 and 3 give construction costs per square foot for different types of concrete, steel, prestressed-concrete, and timber structures over state trunk highways and routes other than state trunk highways. For culverts, however, construction costs per square foot were not available. Most recent installed costs per linear foot for commonly used types of culverts are presented in Table 4.

Annual inspection reports, field observations, and special reports indicating problems for different types of structures under severe Minnesota conditions were reviewed. History of the type and extent of required maintenance activities as well as information on maintenance costs for different types of structures in different age groups have also been available. This information was analyzed to determine apparent performance patterns, if any, for different types of structures.

ANALYSIS OF AVAILABLE INFORMATION

Concrete Bridge Structures

General Observations

For both trunk highways and other routes, concrete culverts have been used in large numbers as replacement structures. Concrete culverts are relatively simple and quickly constructed and are well suited for rural regions. The Minnesota Department of Transportation has been replacing steel and concrete structures with concrete box culverts (mostly precast) and concrete pipe arches. Slabs and channel sections have been used, although in relatively

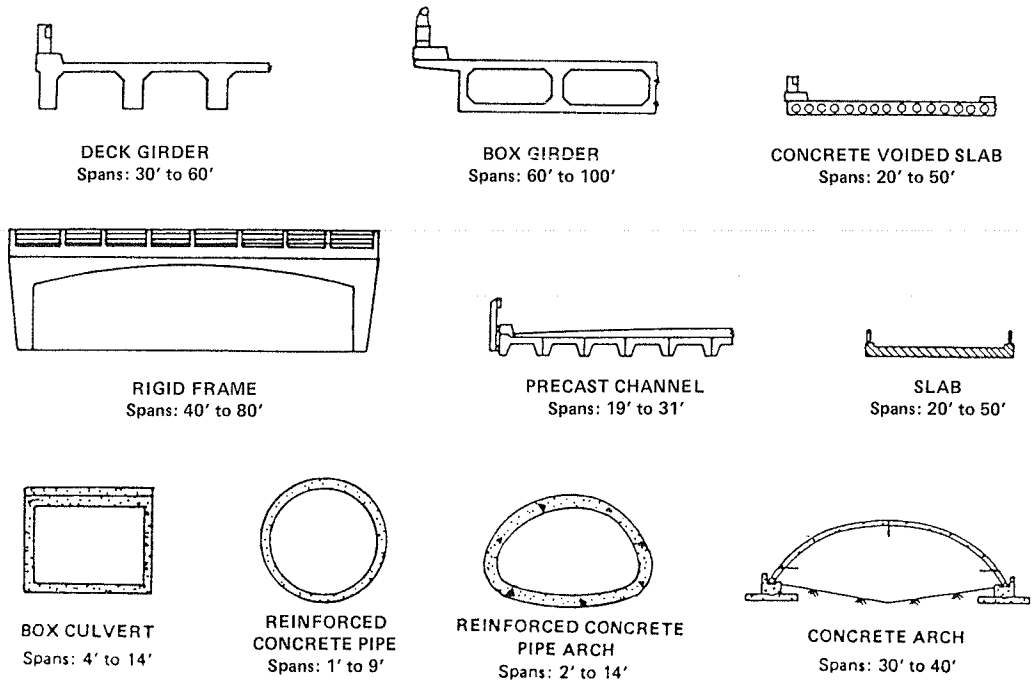

FIGURE 1 Concrete bridge structures.

TRUSS
Spans: 30' to 100'

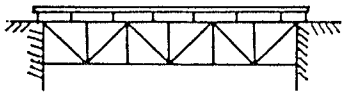

DECK TRUSS
Spans: 40' to 100'

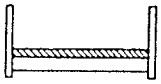

THROUGH GIRDER
Spans: 20' to 80'

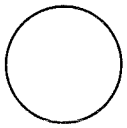

METAL PIPE
Spans: 3' to 10'

METAL PIPE ARCH
Spans: 3' to 20'

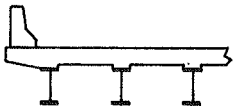

I BEAMS
Spans: 30' to 100'

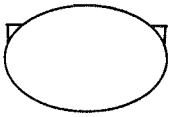

METAL ELLIPSE
Spans: 10' to 30'

FIGURE 2 Steel bridge structures.

BULB TEE
Spans: 40' to 95'

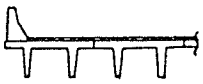

DOUBLE TEE
Spans: 30' to 65'

QUAD TEE
Spans: 30' to 65'

I BEAMS
Spans: 30' to 100'

FIGURE 3 Prestressed-concrete bridge structures.

TIMBER BEAM
Spans:30' to 60'

TIMBER SLAB
Spans: 18' to 32'

FIGURE 4 Timber bridge structures.

TABLE 2 Construction Cost, 1973-1983: Trunk Highway Bridges

Year of Construction	Item	Type			
		Steel Beam	Steel Continuous Beam	Prestressed Concrete Beam	Timber Beam
1973	Range ($)	32.00-41.00	12.00-27.00	16.00-24.00	15.00-32.00
	Avg ($)	37.50	22.27	19.57	25.20
	No.	4	22	49	5 (pedestrian)
1974	Range ($)	29.00	19.00-48.00	22.00-32.00	
	Avg ($)	29.00	28.00	27.33	
	No.	1	7	18	
1975	Range ($)		26.00-31.00	20.00-32.00	34.00
	Avg ($)		29.25	26.42	34.00
	No.		4	24	1
1976	Range ($)		24.00-46.00	22.00-47.00	
	Avg ($)		33.43	28.21	
	No.		7	48	
1977	Range ($)		22.00-44.00	23.00-43.00	
	Avg ($)		33.80	30.64	
	No.		15	22	
1978	Range ($)		24.00-68.00	25.00-48.00	
	Avg ($)		45.44	34.64	
	No.		18	26	
1979	Range ($)	57.00-127.00	35.00-100.00	29.00-66.00	
	Avg ($)	91.50	58.59	42.69	
	No.	6	17	36	
1980	Range ($)	69.00-112.00	45.00-115.00	54.00-62.00	
	Avg ($)	83.33	69.75	56.80	
	No.	3	17	5	
1981	Range ($)	97.00	44.00-120.00	27.00-94.00	
	Avg ($)	97.00	60.71	54.40	
	No.	1	7	5	
1982	Range ($)	85.00-102.00	28.00-72.00	30.00-61.00	54.00-58.00[a]
	Avg ($)	92.50	49.55	40.57	56.33
	No.	1	22	14	3
1983	Range ($)		40.00-71.00	29.00-70.00	
	Avg ($)		55.24	46.64	
	No.		21	14	

[a] One timber slab bridge was built at a cost of $53.00/ft^2.

TABLE 3 Construction Cost, 1973-1983: Bridges on Other Than Trunk Highways

Year of Construction	Item	Concrete							
		Beam	Continuous Beam	Rigid Frame	Slab	Voided Slab	Box Culvert	Channel Span	Continuous Slab
1973	Range ($)	16.00-28.00	25.00-26.00			31.00-32.00		14.00-29.00	
	Avg ($)	20.66	25.57			31.37		18.44	
	No.	7	1			1		6	
1974	Range ($)	17.00-31.00					38.90	15.00-23.00	
	Avg ($)	21.29					38.90	18.57	
	No.	10					1	7	
1975	Range ($)	21.00-36.00		37.00-38.00	25.17	29.45		27.00-32.00	
	Avg ($)	27.40		37.12	25.17	29.45		24.91	
	No.	6		1	1	1		9	
1976	Range ($)				19.18				22.00-28.00
	Avg ($)				19.18				25.44
	No.				1[a]				4
1977	Range ($)							21.00-38.00	25.00-26.00
	Avg ($)							26.92	25.24
	No.							11	1
1978	Range ($)							27.00-42.00	27.00-32.00
	Avg ($)							33.75	29.22
	No.							4	4
1979	Range ($)						36.51	37.00-43.00	47.00-94.00
	Avg ($)						36.51	40.26	70.75
	No.						1	2	2
1980	Range ($)			157.00-158.00					30.00-38.00
	Avg ($)			157.35					30.29
	No.			1					3
1981	Range ($)	26.00-27.00			77.00-78.00				34.00-35.00
	Avg ($)	26.26			77.51				34.68
	No.	1[c]			1				1
1982	Range ($)	26.26		41.00	26.00				36.00-62.00
	Avg ($)			41.00	26.00				52.00
	No.			1	1				3
1983	Range ($)				72.00-125.00		48.44		
	Avg ($)				98.00		48.44		
	No.				2		1		

[a] RCC pipe arch, related to slab, voided-slab, and box-culvert styles.
[b] Two slab prestressed-concrete bridges were built at a cost of $37.76/ft^2.
[c] Related to beam style.

TABLE 4 Construction Cost, 1982: Culvert Structures

Type of Structure	Size	Cost ($/linear ft)	Size	Cost ($/linear ft)
Concrete				
Box culvert	7 ft x 3 ft	220	12 ft x 9 ft	600
Pipe arch	22 in.	30	169 in.	430
Pipe	12 in.	20	84 in.	160
Precast long-span arch	31 ft	670	40 ft	1,200
Steel				
Pipe (corrugated)	12 in.	10	90 in.	190
Arch (corrugated)	17 in.	10	71 in.	55
Long span (full ellipse)	23 ft	700	30 in.	400

smaller numbers, for county and local bridges. Because of the need for time-consuming falsework, formwork, cure, and field quality control for such construction during Minnesota's limited construction season, there apppears to be a definite trend to minimize or eliminate cast-in-place reinforced-concrete construction. Further, because of their generally better quality and strength, standard prestressed concrete beam sections are being favored over both precast and cast-in-place reinforced-concrete sections.

Economic and Performance Considerations

The cast-in-place reinforced-concrete structures are quite labor intensive, take longer to construct, and generally cost more. This is particularly true in the case of cast-in-place reinforced-concrete beam and deck-girder type structures. For spans up to 50 ft, cast-in-place slab-type structures are simpler to form and support and are less expensive to build as well. Precast channel sections make economical and speedy modular construction possible and eliminate the need for expensive field forming and falsework. These channel sections have been competitive in price for spans up to 30 ft and have been widely used by county and local governments. Since 1979, however, their use has been discontinued because of severe concrete spalling around the reinforcement located in their legs.

A review of required maintenance and cost data for concrete structures in the age groups of 0-10, 11-20, 21-30, and more than 31 years indicates the main problems to be decks and railings. This is especially true for bridges more than 31 years old, for which the maintenance costs have been considerably higher. Better protection of surfaces exposed to winter salt and sand is therefore necessary. This, however, is not critical for concrete culverts because they do not have exposed deck systems.

Steel Bridge Structures

General Observations

Steel beam is the predominantly used section for structures on state routes. They are lighter in weight than concrete and offer possibilities of year-round construction. They can be easily built

Steel				Prestressed Concrete						Timber	
Beam	Deck Girder	Continuous Beam	Continuous Deck Girder	Beam	Voided Slab	Precast Channel	Double-T	Bulb-T	Quad-T	Beam Span	Slab Span
	30.00-31.00 30.38 1			20.00-21.00 20.76 1						15.00-19.00 17.26 6	14.00-15.00 14.43 4
				17.00-28.00 22.82 5		29.00 29.00 1				17.00-20.00 18.60 2	19.00-21.00 19.66 3
				23.00-32.00 25.13 5						21.00-26.00 23.46 3	18.00-38.00 23.59 10
		21.00-26.00 22.83 3	23.00-24.00 23.83 1	21.00-42.00 29.20 9	37.76 37.76 1[b]					25.00-26.00 25.87 1	18.00-24.00 21.23 8
		25.00-41.00 30.88 13		21.00-34.00 30.86 11	44.00-45.00 44.54 1	22.00-29.00 24.99 3			28.00-41.00 31.79 6		20.00-30.00 23.90 32
25.00-29.00 26.69 2		25.00-51.00 35.08 27		25.00-53.00 35.46 12	41.00 41.00 1		27.00-28.00 27.50 1	28.00-56.00 41.97 4	23.00-60.00 32.62 39	26.00-44.00 34.39 9	24.00-35.00 28.79 63
		31.00-54.00 38.40 24		20.00-80.00 39.02 15	35.00-50.00 42.45 2		31.00-42.00 34.86 10	34.00-77.00 44.93 10	29.00-72.00 40.40 33	31.00-32.00 31.39 1	15.00-69.00 28.43 28
		22.00-51.00 38.78 8		61.00-80.00 73.31 3	35.00-36.00 35.59 1		36.00-64.00 36.82 5		33.00-40.00 37.47 6		30.00-45.00 35.43 30
		34.00-46.00 39.15 11		30.00-54.00 38.32 10			24.00-36.00 30.91 5	35.00-37.00 35.86 2	29.00-50.00 34.30 18	54.00 54.00 1	29.00-64.00 36.38 21
		25.00-49.00 38.06 17		34.00-50.00 40.50 6			30.00-43.00 34.13 3	32.00-44.00 35.50 5	29.00-37.00 33.25 8		29.00-46.00 34.27 22
		32.00-57.00 41.57 9		37.00-64.00 41.60 6			27.00-42.00 33.46 5	39.00-44.00 41.70 4	31.00-39.00 34.65 10		30.00-37.00 34.19 8

on large skews and curves and are adaptable to flared geometry. This is a great advantage, especially for state trunk highway bridges. The steel beam sections are widely used for replacement structures on other than state routes as well. However, steel pipe and pipe arch culverts are relatively simple and faster to install and are well suited for rural regions. Therefore, these sections are predominantly used as replacement structures for other than state routes. Steel continuous-beam and plate-girder sections have also been used, although in relatively smaller numbers, for county and local bridges. The fabrication and erection of steel built-up sections require skilled labor and extensive inspection.

Economic and Performance Considerations

The steel beam structure lends itself easily to simplified and faster construction. For county and local structures, therefore, its cost has been quite competitive with costs of prestressed-concrete beam bridges. For state trunk highway bridges, however, the cost appears to be 15 to 20 percent higher than that of prestressed-concrete beam structures. Special skews and curves and flared geometry, which is more common with state trunk highway bridges, could be reasons for such a difference in costs. Corrosion at connections as well as under leaky expansion joints and fatigue cracking at or near welds are of concern in steel structures. Fire and accident damage to critical structural components is also of serious consequence.

A review of the required maintenance and cost data for steel structures in the age group of 0 to 20 years indicates that decks, beams, and joints have the most problems. Subsequently, problems with bearings appear to develop in the age group of 21 to 30 years and with substructures in the category of more than 31 years. In general, well over 50 percent of the maintenance costs relate to decks and beams. Better protection for surfaces exposed to winter salts and better drainage systems are necessary.

Prestressed-Concrete Bridge Structures

General Observations

Use of prestressed-concrete sections for bridge construction in Minnesota has been extensive. Modern precasting, pretensioning, and transportation facilities have made lighter, longer span sections economically available. Such sections are manufactured year-round in plants by using higher-strength concrete and under stricter quality control. The standard beam sections are therefore predominantly used for structures on state routes. Prestressed double-T, bulb-T, and quad-T sections, which were introduced in Minnesota in 1977-1978, do not require any deck forming and make truly modular system bridge construction possible. These sections are widely used for structures on other than state routes.

Economic and Performance Considerations

For structures on state trunk highway routes, prestressed-concrete beams are commonly used. The standard prestressed-concrete beam structures have, in general, been 15 to 20 percent more economical than steel beam structures. Double-T, bulb-T, and quad-T sections, because they eliminate the need for deck forming, have been more economical than prestressed beam sections. Further, the shallower depths of these sections necessitate less extensive grading work for the bridge approaches. This has been particularly important for counties and local governments, because Minnesota bridge funds are not available for approach-grading work. Shallower sections therefore reduce the dollar amounts of local participation as well. Prestressed-concrete beam sections have been used for state trunk highway bridges primarily because of heavy traffic loads and concern over damage to joints if quad-T sections are used.

Double-T and bulb-T sections have also been used for state trunk highway bridges because of their longer span capabilities and less problems from the number of bearings required. These sections are used with 5 to 6 in. of cast-in-place concrete slabs over them to eliminate joint-cracking problems between sections.

A review of required maintenance and cost data for prestressed-concrete structures in the age group of 0 to 10 years does not indicate any major problems. In the age group of 11 to 30 years, however, expansion joints appear to require major maintenance and in the category of more than 31 years beams need major maintenance.

Timber Bridge Structures

General Observations

Timber bridge structures present a natural and aesthetically pleasing appearance. However, their use is somewhat limited to short span lengths. They are seldom used for structures on state trunk highway routes. Timber bridges offer the possibility of year-round construction with basic tools and minimal maintenance costs. Further, they require a much less sophisticated inspection than concrete or steel bridges. Timber beam and slab spans are therefore widely used on local and county routes. They are, however, vulnerable to damage by fire, accidents, and insects.

Economic and Performance Considerations

Of the timber-beam and slab span types commonly used by counties and municipalities, the slab type has been somewhat more economical than the beam type. Although their construction costs are somewhat comparable to sections such as the prestressed-concrete quad-T, their maintenance costs are normally low. Except for icy conditions, the Minnesota environment has not been detrimental to timber bridges. Carefully placed ice breakers and use of slanted members have successfully minimized ice damage. Use of ring-shank nails and similar hardware has successfully prevented lamination of timber members.

A review of required maintenance and cost data does not indicate any major problems for bridges in the age group of 0 to 30 years. In general, major maintenance of timber decks appeared to become necessary for bridges in the category of more than 31 years.

Culvert Structures

General Observations

A variety of concrete and metal culvert types have been commonly used in Minnesota when there is a small stream flow. The soil pH and resistivity determine whether a concrete or a metal culvert would be appropriate for a particular location. Since their introduction in the mid-1970s, longer-span metal culverts have been well accepted by counties and municipalities. They have also been accepted for state trunk highway routes. In 1976, precast concrete box culverts were introduced in Minnesota. These have gained wide acceptance because of their rapid construction. Precast concrete arch sections are particularly suitable when headroom limits the use of round pipe sections. Their wide-bottom shape fits well into small stream bottoms. A new longer-span precast concrete arch type has been recently introduced in Minnesota. This type consists of complete precast arch sections set on cast-in-place concrete footings.

Economic and Performance Considerations

Table 4 gives installed costs for different types of culverts. Precast concrete arch sections have been the most commonly used because of their competitive price, faster construction, and suitability under a variety of soil conditions. The less costly prefabricated metal culverts are appropriate when conditions are less corrosive. Their ability to be assembled away from the site and placed by cranes makes them economical. Concrete floors, headwalls, and dropwalls have been necessary to prevent the scour problems of long-span metal culverts.

Concrete culverts need a good bedding and need to be tied together to alleviate settlement and piping problems. Concrete arch-type culverts have a tendency to fill in under low flow conditions and restrict waterway openings. Inverts of metal culverts disintegrate and need relining or replacement. Also, poor compaction of soil during installation can result in distortion or total failure of metal culverts.

A review of required maintenance of culverts indicates problems to be related to either poor construction practices or scour.

CONCLUSION

Certain definitive patterns have become apparent as a result of this study of 3,692 bridge replacements in Minnesota over the last 11 years. Some of the conclusions are as follows:

1. There is a definite trend away from labor-intensive and time-consuming types of construction;
2. A stronger emphasis exists on precast rather than cast-in-place construction;
3. Although steel beam and prestressed-concrete beams or double-T sections are mostly used for state trunk highway bridges, counties and municipalities have shown their preference for steel beams, quad-T's, and timber spans;
4. Different culvert types not only are a workable alternative but are widely used as economical bridge-replacement structures for state, county, and local routes; and
5. Provisions for adequate protection of surfaces exposed to corrosive environments are necessary to improve bridge performance and reduce future maintenance costs.

Publication of this paper sponsored by Committee on Structures Maintenance.

Close-Range Photogrammetry for Bridge Measurement

FRED B. BALES

ABSTRACT

Studies have been conducted to determine the applicability of close-range photogrammetry for the measurement of bridges. Included are steel-beam deflection measurement, records of deck deterioration, and drawings for the documentation of historic structures. Measurement and documentation by photogrammetric methods are of sufficient accuracy for a variety of measurements involving structures. When structures are measured by the traditional hand-measurement method, particularly for as-built and historic documentation, the field work becomes the most labor-intensive phase. The photogrammetric method can be effective by reducing the manual labor, scaffolding, and other support equipment required to accomplish such measurement by hand. It can also minimize interruption to the flow of traffic.

Close-range photogrammetry is another precise tool in the arsenal of measuring techniques now available to the highway and transportation profession. Any time that the simultaneous recording of a large number of points is required, close-range photogrammetry can become most effective in minimizing interruption to traffic. It is also helpful in cases where heavy traffic makes ordinary survey techniques unsafe and inefficient.

This technology, sometimes referred to as nontopographic photogrammetry, has been used in Europe for several decades in the architectural field for the documentation of historic structures and monuments and for accident investigations. The academic community in the United States has been active in close-range photogrammetric projects for a number of years, as have various industrial groups such as the aircraft, automobile, and shipbuilding industries. Unfortunately, photogrammetry has been slow to attain recognition in the transportation field (1-3).

BACKGROUND

It was not until the director of the Virginia Highway and Transportation Research Council (VHTRC), Howard Newlon, became aware of work being accomplished at the Miami-Dade Community College by Joel Kobelin that the potential of close-range photogrammetry was recognized by Virginia. It appeared to have possibilities for the measurement and preparation of drawings as required by the National Historic Preservation Act of the 1960s and subsequent federal-aid highway acts of the late 1960s and 1970s.

Close-range photogrammetry has been approached with guarded optimism. The first attempt in 1979 at taking close-range photography was through the use of a camera owned by the Virginia Department of Highways and Transportation (VDHT), a World War II surplus Fairchild F-56 aerial camera. This camera produced a negative 7 x 7 in. and was equipped with a long-focal-length lens of 210 mm.

The camera was rather unwieldy and had to be hand held in a horizontal position, supported on the top of a stepladder, and leveled in a crude fashion. Single photographs were taken; the camera then was repositioned over another point. By doing so, overlapping pairs of photographs suitable for stereoscopic viewing were exposed. Because of the long-focal-length lens, the camera had to be positioned some distance from the object being photographed in order to obtain sharp focus. This increased the likelihood that obstructions such as trees, utility poles, embankments, buildings, railway cars, and automobiles would block the line of sight. Of course, this photography revealed the potential of a close-range photogrammetric system but was lacking in image quality so essential for the preparation of adequate structure drawings. However, it was discovered from these early experiments that a fairly large-format camera (large negative size) and a fairly short-focal-length lens (distance from lens to film) are needed, particularly when conventional stereoscopic mapping instruments such as those now available to most departments of highways and transportation are used.

VDHT has a completely equipped and fully staffed aerial photogrammetric section, which has worked cooperatively with the VHTRC to develop and implement a close-range photogrammetric system to meet new and expanding needs.

Research projects were approved for Highway Planning Research funding by FHWA during the fall of 1980 to study the application of close-range photogrammetry to the measurement of highway- and transportation-related structures. A search was initiated at that time for a metric camera to meet the necessary criteria.

Actually, there are a limited number of manufacturers of close-range cameras worldwide, and few are willing to rent their equipment on a short-term basis. The U.S. representative of Zeiss Jena was willing to rent a metric camera, the UMK 10/1318, equipped with a lens of 100-mm focal length and with variable focus for exposures as close as 12 ft (camera to object). The camera produces a negative 5 x 7 in. on glass plate for image stability, flatness, and enhanced accuracy.

During the course of this research effort, a variety of transportation-related sites were photographed. Twenty-four sites were photographed, not all of which were bridges. There were unique highway markers, a tunnel portal, a cut-stone masonry culvert, and archaeological sites. A test beam was also measured in the civil engineering laboratory at the University of Virginia.

Certain field measurements are needed for control of horizontal and vertical scale within each stereoscopic overlapping pair of photographs and for use in the orientation of the photography in a mapping instrument. Small contrasting black-and-white targets 5 x 8 in. large have served adequately for marking horizontal and vertical control positions within the region being imaged (Figure 1). They have been printed on card stock by using either diazo equipment or a printing press. These were tacked or taped to wood or taped to steel structures. Others have been printed on adhesive-backed material and placed on steel beams, and still others have been placed on steel beams by using magnets. On some concrete bridges where the surface would not accept adhesives, a template was used and the target was spray-painted on.

Inasmuch as VDHT is using conventional optical-

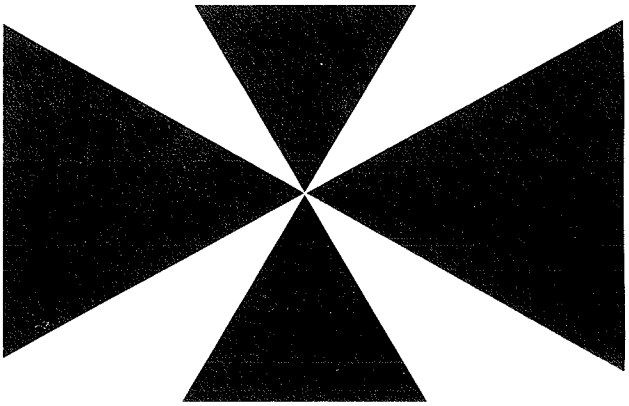

FIGURE 1 Targets used to mark horizontal and vertical control positions.

mechanical stereoscopic mapping equipment, certain constraints are imposed by the design of the instruments. The close-range camera movement is limited to about 5 degrees of tip and tilt. Stated in photogrammetric terms, this is 5 degrees of omega, phi, and kappa along the three rotational axes of the instrument. It is also necessary to position the camera along a line essentially parallel with the object being photographed. Otherwise, a condition is created similar to an aircraft's losing altitude between aerial camera exposures.

Close-range photogrammetry is a little different in many respects from aerial photogrammetry. Its reliability must be proven by comparing the results obtained with an acceptable, time-honored conventional method of measurement.

Structures were photographed under a variety of weather and lighting conditions. Most were taken under excellent lighting conditions, but some were taken under overcast skies. Several sites were photographed through light rain, and one structure was photographed at night with floodlights. The camera platforms varied from creek bottoms, with the photographer standing in waist-deep water, to a special cherry-picker mount and a boat moved on a line parallel to the bridge by using lines and anchors.

This report will be confined to the methodology for measuring deflections on a laboratory test beam, measuring deflections for one bridge, recording one bridge deck, and historic documentation for two bridges.

METHODOLOGY

Test Beam

The hydraulically actuated test bench at the University of Virginia was located within a convenient distance from a flat stationary wall. This wall in the laboratory was suitable for the placement of targets for photogrammetric control measurements (Figure 2).

Control was arranged in a quadrilateral with all sides and diagonals chain measured. Close-range photographs were taken with the camera positioned 25 ft from the test I-beam and also were taken under various loading conditions from two camera stations. Dial gauges reading to 0.001 in. were used to physically measure the test I-beam deflection.

Image positions were measured on the photographs by using a comparator that had 1-micron accuracy for use in an analytic aerotriangulation computer program. Manual and photogrammetric measurements were

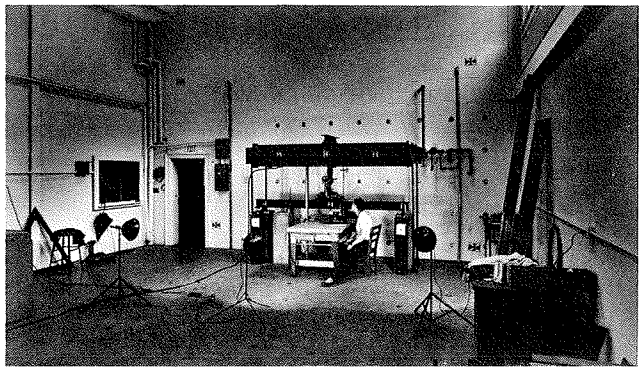

FIGURE 2 Set-up to photograph test beam.

in close agreement. The beam with maximum loading deflected 0.408 in. The disagreement between close-range photogrammetry and measurement by the conventional method was 0.040 in.

Bridge Deflections

One of the structures on which the deflections was measured was a new bridge under construction. It was of the continuous-beam design with a total length of 464 ft. The distance between piers of the span measured was 170 ft (Figure 3). The camera was positioned under the center of the span with the lens axis pointing upward. Distance from the bottom of the beams to the three camera stations required at this site was 36 ft.

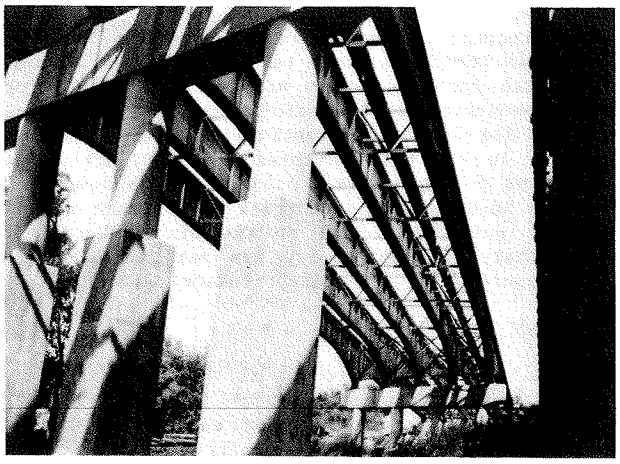

FIGURE 3 Fifth Street Bridge, Lynchburg, Virginia (under construction).

Control targets were placed on the beams by using adhesive-backed targets. The horizontal and vertical positions on the targets were measured with a precision theodolite by using the triangulation method from a measured baseline. The deflection of the beams was also measured by differential leveling.

Two sets of photographs were taken, one set at the time of placement of the steel beams and the other set after the pouring of the concrete deck (Figures 4 and 5). Here again the comparator with an accuracy of 1 micron and the analytic aerotriangulation method were used for the computation of position.

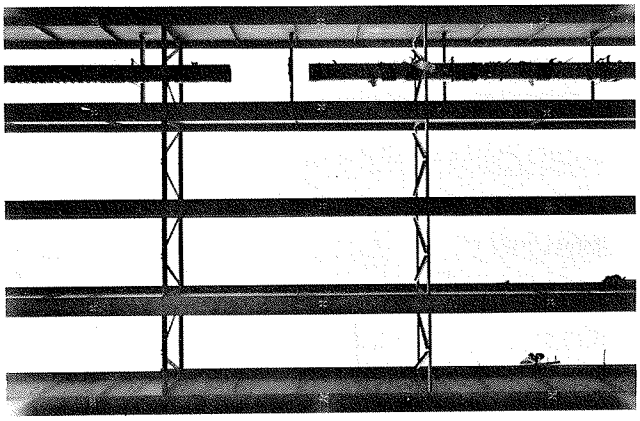

FIGURE 4 Fifth Street Bridge after placement of steel beams.

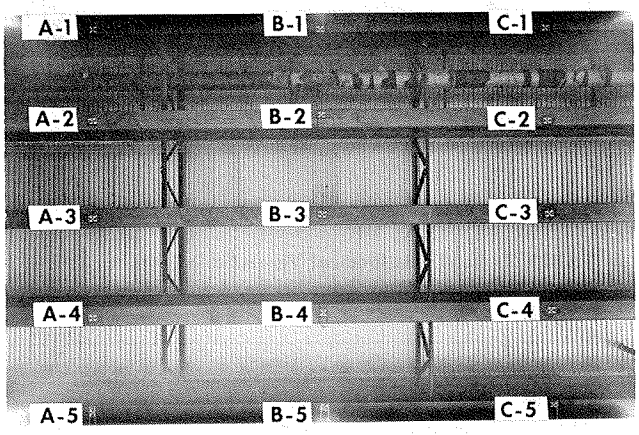

FIGURE 5 Fifth Street Bridge after pouring of concrete deck.

According to the design calculations, the maximum dead-load beam deflection should have been 2 in. However, by both photogrammetric analytic aerotriangulation and differential-leveling techniques, the maximum deflection was determined to be only 3/8 in. (see Table 1).

Bridge Deck

The bridge deck selected for this study is near Harrisonburg where VA-33 crosses Interstate 81. Close-range photography was taken following the conventional bridge inspection team. While the travel lanes were still cordoned off for the normal bridge inspection, the photographic crew moved in with the cherry picker to take vertical photography. The necessary horizontal and vertical control as required for the photogrammetric work had been premarked on the bridge deck just before photography.

The inspection team had made the normal survey, including the use of drag chain, to determine delamination. The delaminated regions were marked by using chalk on one section and spray paint on another for ease of identifying them with the close-range photography (Figure 6). Figure 7 shows the photogrammetric record of the delamination shown in Figure 6.

A bridge deck could be photographed rapidly if it was not for mandatory safety rules that require the boom of the cherry picker to be returned to a neutral position before it is moved to the next camera station. Even with all the precautionary measures, exposures were taken at intervals on an average of 8 min.

TABLE 1 Summary of Elevation Measurements on Fifth Street Bridge, Lynchburg, Virginia

	No Load (September 18, 1981)		Loaded (April 21, 1982)		
Point	Differential Leveling (ft)	Photogrammetry (ft)	Differential Leveling (ft)	Photogrammetry (ft)	Ground Triangulation (ft)
A-1	714.88	714.85	714.86	714.85	714.85
A-2	714.65	714.64	714.66	714.66	714.65
A-3	714.49	714.49	714.51	714.51	714.49
A-4	714.31	714.32	714.34	714.34	714.32
A-5	714.13	714.14	714.14	714.12	714.13
B-1	715.02	715.02	714.99	714.99	714.98
B-2	714.80	714.80	714.79	714.79	714.78
B-3	714.63	714.62	714.64	714.64	714.62
B-4	714.45	714.46	714.46	714.46	714.44
B-5	714.27	714.27	714.27	714.27	714.23
C-1	715.11	715.08	715.09	715.09	715.07
C-2	714.90	714.90	714.89	714.89	714.89
C-3	714.73	714.73	714.73	714.73	714.73
C-4	714.55	714.55	714.54	714.54	714.53
C-5	714.35	714.36	714.33	714.33	714.30

Historic Documentation

The two structures selected for inclusion in this paper to show historic documentation illustrate measurements and drawings prepared under favorable and unfavorable conditions. As mentioned earlier, the close-range photographs were taken under a variety of weather and lighting conditions. A bedstead pony truss bridge was photographed under overcast skies in a drizzling rain with a fairly large object-to-camera distance (Figure 8). This is the type of condition to be avoided if at all possible. The drawing of this bridge, a side elevation, was prepared to a scale of 1 in. = 3 ft (Figure 9).

Hand measurements of the actual bridge were compared with dimensions taken from the photogrammetric drawing by using an engineer's scale. In making such a comparison, it should be remembered that even the width of a pencil line on the drawing can represent a measurement as large as 1 in. Paint and corrosion build-up on the bridge sometimes amount to as much as 3/8 in.

Some of the hand measurements differed by as much as 3/4 in. from the scaled measurements. The results are favorable when considered as a percentage of the total dimensions. Of the 15 points checked, 60

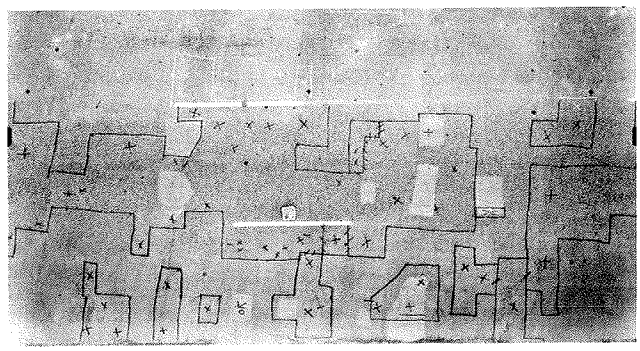

FIGURE 6 Bridge over I-81, Harrisonburg, Virginia, showing regions of delamination.

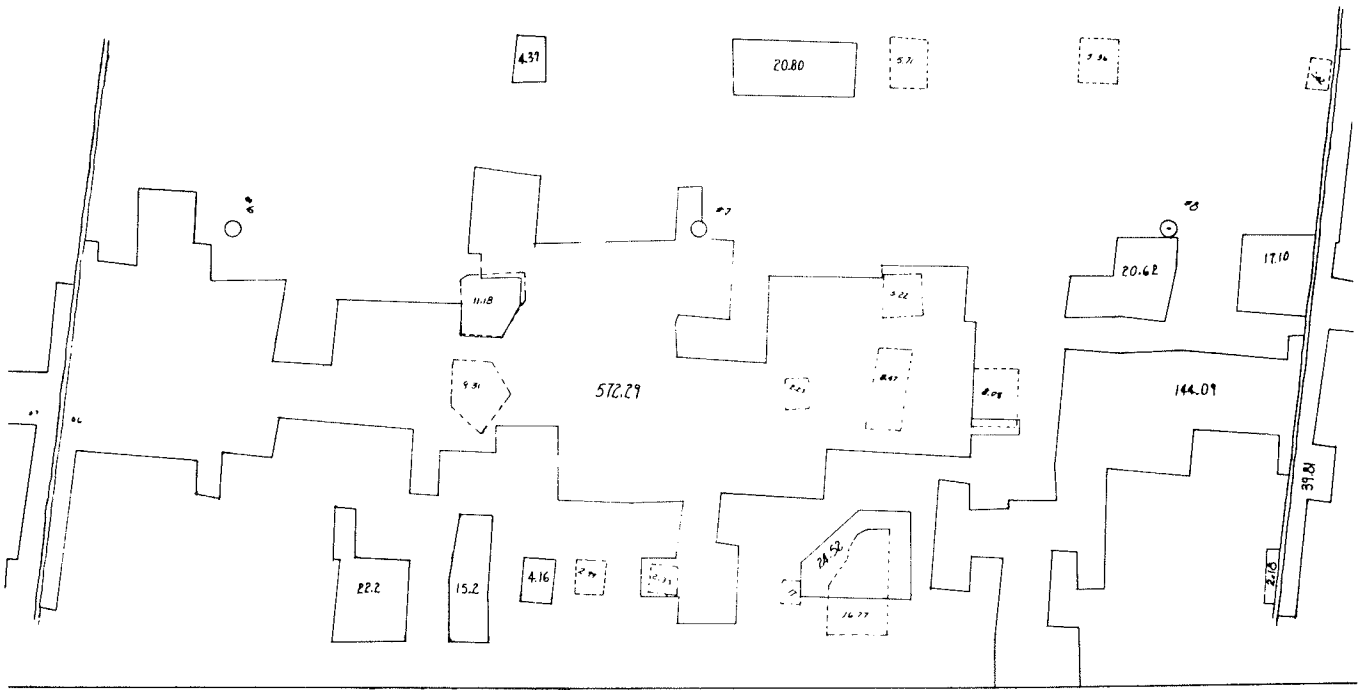

FIGURE 7 Photogrammetric record of delamination shown in Figure 6.

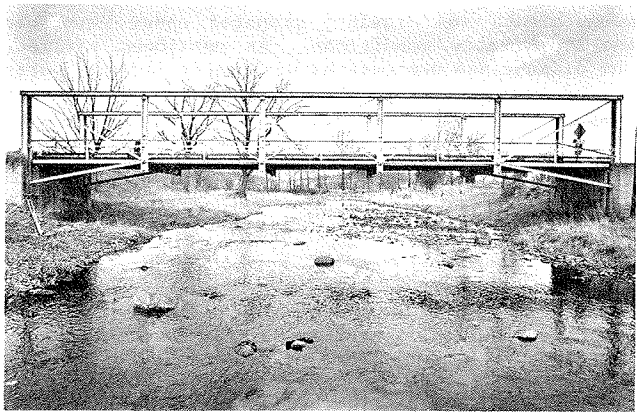

FIGURE 8 Pony truss bridge, Augusta County, Virginia.

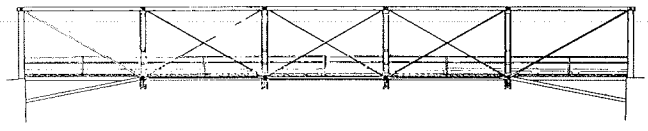

FIGURE 9 Intermediate-stage photogrammetric documentation of pony truss bridge.

percent differed less than 2 percent; 87 percent differed less than 5 percent; and only 2 readings out of 15 were greater than 5 percent in error (Table 2).

The cross-sectional measurements (those measured perpendicular to the elevation plane) fared somewhat better. Of 17 readings, 4 were difficult to read by photogrammetry as well as by manual methods. Rust and paint build-up apparently caused erratic readings, and the largest error of these four was as great as 1/4 in. All other errors were less than 1/8 in. There were 4 other points of the 17 that were in error by only 1/64 in. (Table 3). Actually, on a percentage basis, 65 percent of the cross-sectional measurement was less than 3 percent in error; 85 percent was less than 5 percent in error.

TABLE 2 Hand Measurement Versus Scaled Dimensional Comparison, Pony Truss Bridge, Augusta County, Virginia

Location	Hand Measurement (in.)	Scaled Measurement (in.)	Difference (in.)
1	71.376	71.400	0.024
2	11.184	10.800	0.384
3	90.120	90.000	0.120
4	90.240	90.600	0.360
5	90.480	90.000	0.480
6	90.120	89.400	0.720
7	90.480	89.700	0.780
8	6.312	6.000	0.312
9	5.064	4.800	0.264
10	6.372	6.600	0.528
11	7.188	6.900	0.288
12	9.564	9.600	0.036
13	6.000	5.700	0.300
14	56.880	56.700	0.180
15	183.480	183.600	0.120

Results similar to those for the overall elevation of the bedstead pony truss were experienced in checking the elevation of the joint detail of this bridge (Figures 10 and 11). The results were better, in most part because of a shorter object-to-camera distance. From a percentage standpoint, 67 percent of the errors in measurement were less than 1/16 in. and 92 percent were less than 1/8 in. (Tables 4 and 5).

Despite the unfavorable conditions encountered on this bridge, the comparative results from hand and scaled measurements were favorable. The engineers concluded that drawings produced by photogrammetric methods for this site were as accurate as a hand-

TABLE 3 Cross-Sectional Dimensional Comparison, Pony Truss Bridge, Augusta County, Virginia

Location	Photogrammetric Reading (in.)	Hand Measurement (in.)	Difference (in.)
1	2.172	2.187	0.015
2	1.692	1.813	0.121
3	1.224	1.375	0.151
4	2.328	2.313	0.015
5	2.292	2.250	0.042
6	1.296	1.359	0.063
7	4.260	4.250	0.010
8	3.528	3.469	0.059
9	3.960	3.750	0.210
10	2.040	2.000	0.040
11	0.972	1.000	0.028
12	2.316	2.375	0.059
13	12.000	12.016	0.016
14	0.888	0.906	0.018
15	2.772	2.875	0.103
16	1.620	1.688	0.068
17	6.792	6.875	0.083

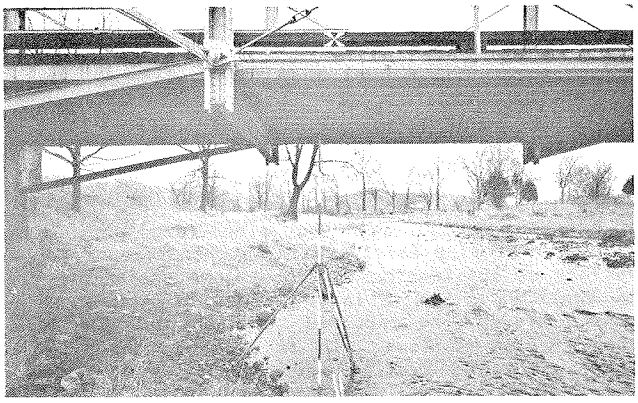

FIGURE 10 Pony truss bridge: joint detail.

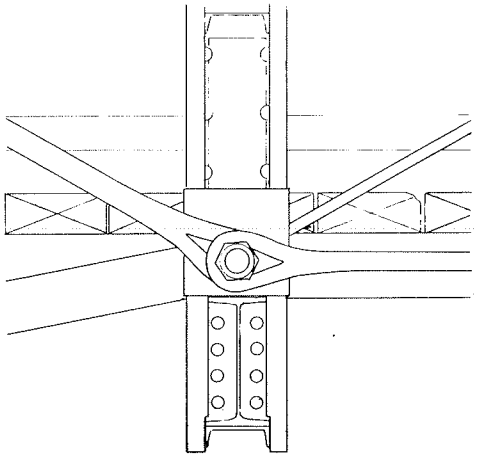

FIGURE 11 Intermediate-stage photogrammetric documentation of joint detail of pony truss bridge.

measured documentation drawing, given a reasonable scale drawing and a short object-to-camera distance. The lesson to be learned is never to photograph a site under conditions that are less than ideal.

A structure photographed under ideal weather conditions is a bascule span, which is one of the few remaining movable spans in Virginia and the only Scherzer rolling lift highway bridge known to remain in the state. Two views were taken of this bridge, known locally as the Hodges Ferry Bridge (Portsmouth, Virginia). The first view, consisting of two overlapping pairs of photographs, was exposed from a motorboat anchored in the river. The boat was moved 59 ft with anchors along a line parallel to the side of the bridge. The photograph and drawing are shown in Figures 12 and 13.

The second view is of the rocker-arm detail, which was used for dimensional analysis. It was

TABLE 4 Hand Measurement Versus Scaled Dimensional Comparison, Pony Truss Bridge: Joint Detail

Location	Hand Measurement (in.)	Scaled Measurement (in.)	Difference (in.)
1	2.3125	2.3	0.0125
2	3.9375	3.9	0.0375
3	0.2500	0.3	0.0500
4	1.7500	1.7	0.0500
5	5.1875	5.3	0.1125
6	2.375	2.3	0.0750
7	9.500	9.45	0.050
8	6.000	6.05	0.050
9	0.375	0.40	0.025
10	14.500	14.5	0
11	5.625	5.4	0.225
12	2.167	2.05	0.117

TABLE 5 Cross-Sectional Dimensional Comparison, Pony Truss Bridge: Joint Detail

Location	Photogrammetric Reading (in.)	Hand Measurement (in.)	Difference (in.)
1	1.032	1.000	0.032
2	1.944	1.969	0.025
3	0.456	0.375	0.081
4	2.1096	2.2125	0.015
5	7.2876	7.250	0.0376
6	1.4496	1.406	0.0436
7	0.336	0.3125	0.0235
8	0.462	0.500	0.038
9	2.352	2.375	0.023
10	8.844	8.875	0.031

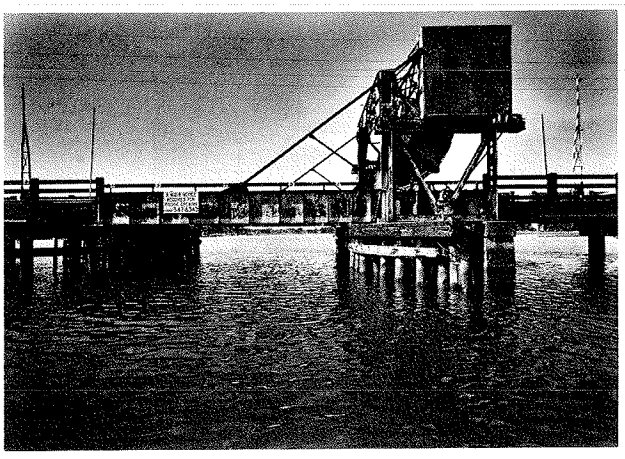

FIGURE 12 Hodges Ferry Bridge, Portsmouth, Virginia.

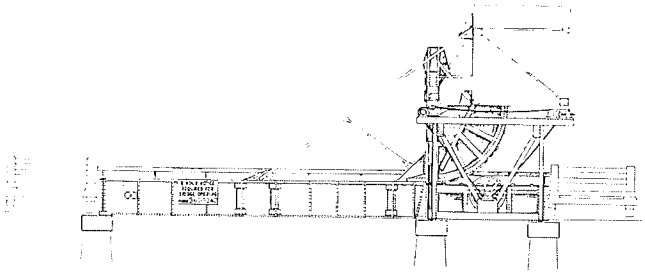

FIGURE 13 Intermediate-stage photogrammetric documentation of Hodges Ferry Bridge.

selected as an example of a site that would be prohibitively time-consuming to hand measure, to say nothing of the dangers involved (Figures 14 and 15). The high traffic volume on the narrow bridge and its height above the water made hand measurements hazardous.

Of the 18 points used for analysis, all measurements show less than 1/8 in. difference between hand and photogrammetric measurements. Of these, eight show less than 1/64 in. difference, three show less than 1/32 in., and six others show less than 1/16 in. difference between the two methods (Table 6). The conclusion from this site is that the photogrammetric method is potentially a reliable technique for making documentation drawings and for cross-sectional measurements on structures (4).

TABLE 6 Cross-Sectional Dimensional Comparison, Hodges Ferry Bridge

Location	Photogrammetric Reading (in.)	Hand Measurement (in.)	Difference (in.)
1	4.488	4.5156	0.0276
2	4.872	4.875	0.003
3	0.384	0.375	0.009
4	0.696	0.750	0.054
5	0.372	0.375	0.003
6	3.192	3.250	0.058
7	2.700	2.6875	0.0125
8	5.616	5.625	0.009
9	9.036	9.0625	0.0265
10	5.604	5.5625	0.0415
11	4.848	4.750	0.098
12	59.964	59.96875	0.00475
13	5.520	5.500	0.020
14	2.736	2.6875	0.0485
15	0.300	0.3125	0.0125
16	0.408	0.375	0.033
17	0.684	0.6875	0.0035
18	1.092	1.125	0.033

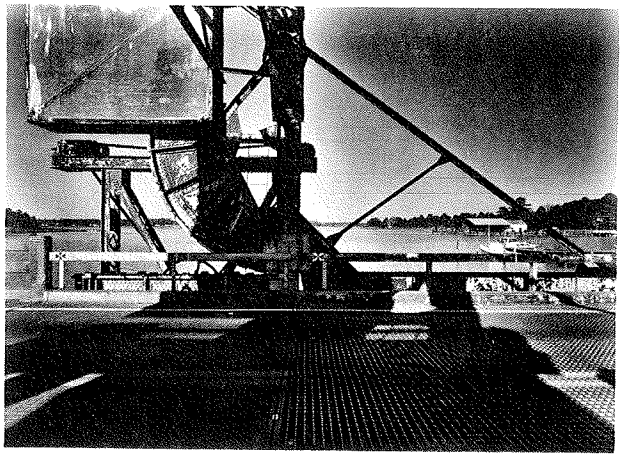

FIGURE 14 Rocker-arm detail, Hodges Ferry Bridge.

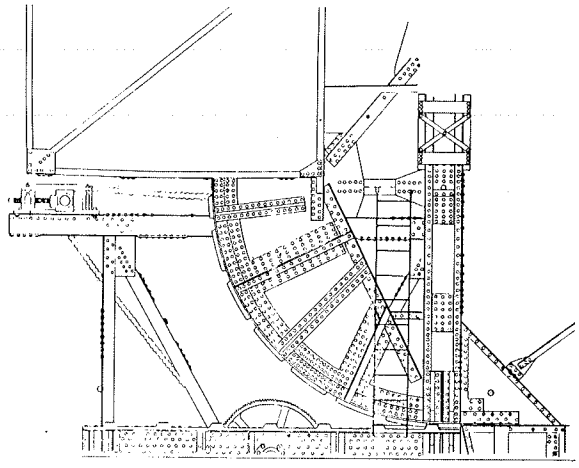

FIGURE 15 Photogrammetric documentation of rocker-arm detail, Hodges Ferry Bridge.

CONCLUSIONS

It has been demonstrated that close-range photogrammetry can provide fairly reliable measurements for a variety of applications. Close-range photogrammetry is applicable when a large number of points on a bridge need to be recorded simultaneously or in a short period of time. It is also applicable when interruption to traffic needs to be minimized or when ordinary survey techniques are unsafe, ineffective, or inefficient. It is recommended that photographs be taken only under ideal lighting conditions.

Close-range photography provides a permanent set of records for immediate or future use in the evaluation and documentation of bridges. It can be used for as-built plans for new bridge structures as well as for the documentation of historic bridges.

The results obtained from beam deflection were rather inconclusive; therefore, it is recommended that additional work be accomplished on this subject.

REFERENCES

1. J.-P. Agnard and R. Sanfacon. Photogrammetry Study of French Architecture. Proc. of the Symposium on Close-Range Photogrammetric Systems, American Society of Photogrammetry, Falls Church, Va., 1975, pp. 1-3.
2. S.A. Veress and L.L. Sun. Determination of Motion of a Gabion Wall. Photogrammetric Engineering and Remote Sensing, Feb. 1978.
3. Manual of Photogrammetry, 4th ed. American Society of Photogrammetry, Falls Church, Va., 1980.
4. P.A.C. Spero. The Photogrammetric Recording of Historic Transportation Sites. Report 83-R35. Virginia Highway and Transportation Research Council, Charlottesville, June 1983.

Publication of this paper sponsored by Committee on Structures Maintenance.

Application of Load Spectra to Bridge Rating

FRED MOSES, MICHEL GHOSN, and RICHARD E. SNYDER

ABSTRACT

Important safety decisions are made each time a bridge is evaluated. Field inspections have concentrated on estimating deterioration and dimensions of load-carrying members. How to measure and use a load spectrum at the site is described. Information on truck loads, dynamic impact, and girder distribution can provide additional data for rating bridges. Five sites in Ohio are reported. In addition, almost 100 other instrumented bridges have been studied by a similar weigh-in-motion operation, which uses existing bridges to provide equivalent static weights of passing vehicles. Weight data are unbiased because the field operation is undetected by drivers. The measured bridge load spectra can replace conservative AASHTO rating recommendations for impact and girder distribution factors. In order to enhance this application a reliability or probabilistic approach incorporates the measured site load spectra in evaluating the bridge safety. Loading is modeled by random variables including truck weight, traffic volume (affecting multiple presence), axle spacings and loads, impact, girder distribution, and measured stresses. A load simulation forecasts the maximum response for periods corresponding to inspection intervals. The calculation incorporates uncertainties and provides a reliability measure for comparing bridge safety. Examples include ultimate strength and fatigue-limit states. Strategies are described for using the load spectra and the reliability model to develop load factors for rating, schedules for inspection intervals, posting control, and redundancy evaluation.

The evaluation or rating of existing bridges is a continuous activity for most bridge bureaus. Vital safety decisions must be made to repair, rehabilitate, post, close, or replace an existing bridge. Existing manuals provide inspection techniques and guidelines for rating. The field inspection establishes deterioration and dimensions of load-carrying members. The rating (strength) checks generally follow procedures similar to AASHTO design including specified design loads, girder distribution and impact factors, and allowable stresses. Some flexibility in choosing safety factors is usually available.

Recent proposals for rating modifications include load-factor design and reliability-based load and resistance safety factors (1). One goal is to modify rating values if additional field inspection effort or analysis and load response are carried out (2).

BRIDGE LOADING SPECTRA

Ideally, the bridge rating engineer is in a better position than a designer to establish more precisely both the loading spectrum and the capacity for an existing structure. The uncertainties that should affect the safety factors are quite different for an existing bridge from those needed for a design that is not yet built. The acquisition of dimensions and material properties is routine and will not be described here. However, the acquisition of load and bridge response data is not routine, even though hundreds of bridges have been tested in many countries. One reason for its limited use in rating may be the need for a simplified measurement system. Bridge tests are costly and often use specialized equipment and processing programs. Equipment and test procedures must be available for routinely measuring load spectra. A second difficulty is the incorporation of a measured load spectrum into the formulation of rating factors.

In this paper some field methods for routinely acquiring bridge load spectra and response statistics and a probabilistic model for applying this information will be described. The field measurement system for obtaining load spectra is an extension of the weigh-in-motion (WIM) concept developed at Case Western Reserve University for the Ohio Department of Transportation (ODOT) and FHWA (3). It was originally developed to provide truck weight and traffic statistics. A recent test program extended the methodology to obtain bridge performance data also (4). This information on truck loads, bridge girder stresses, and dynamic response can provide valuable data for evaluating an existing bridge.

In order to utilize this data base of acquired load spectra a reliability-based formulation is described. It can calibrate appropriate load factors in conjunction with predictions of the maximum expected truck loading and can even account for parallel-redundant load paths. The reliability model also incorporates the measured statistics of girder distribution and impact. Risk assessments of ultimate strength and fatigue lives are given. Strategies based on the acquired site-specific load spectra are discussed for inspection, rehabilitation, and permit control.

LOADING ANALYSIS

For most short- and medium-span bridges, the critical loading is self-weight and heavy truck traffic. Self-weight can be estimated during inspection from cores and recorded dimensions. The repetitive heavy vehicle loads may cause fatigue cracks, instability, permanent displacement, or collapse.

Each live-load event depends on truck weight and axle loads and intervals between closely spaced vehicles (headways). In a critical component, stresses also depend on load distribution and bridge dynamics, which for the design were estimated from simplified models. Current load specifications also reflect the truck traffic in existence many decades ago. Changes in truck traffic, including heavier legal and permit vehicles and other trends, are important. Such changes are as follows:

1. Increased gross weights: unless accompanied by longer axle lengths, heavier vehicles induce greater longitudinal bending moments;
2. Influence of closely spaced axles: increased tandem and triaxial weight combinations significantly affect component stresses sensitive to concentrated wheel loads;
3. Traffic increases: the frequency of platoons

of closely spaced vehicles, superimposing their load effects, increases with higher volumes;

4. Enforcement: there is concern that citizen-band (CB) radio communication and by-pass options have decreased legal load enforcement; also, little is known about whether posting signs has any effect on restricting loads;

5. Maintenance: bridge load spectra measurements show that the major influence on dynamic response is roadway roughness (4,5); and

6. Bridge lives: it is evident that initial estimates of 40 to 70 years for bridge lives are often being surpassed.

Live-Load Variables

The random girder stress (S) caused by a truck movement across a bridge in a typical multistringer bridge may be written as

$$S = mWghI/S_x \quad (1)$$

where

W = the vehicle weight,
m = a factor to convert gross weight to bending moment,
g = girder distribution factor (stringer analysis),
h = variable to account for influence of multiple vehicles on overloading (function of traffic volume),
I = impact due to dynamic response, and
S_x = girder section modulus.

In design or rating manuals the load (W) and moment factor (m) are specified by the recommended axle or lane loads. The analysis or load distribution to individual girders is also specified, for example, girder spacing divided by 5.5, for steel girders (6). These factors nominally assume some multiple-presence arrangement, represented here by h. The dynamic allowance is also specified and formulas are usually given for calculating effective section moduli. The prediction of the loading either for repeated spectra (fatigue) or maximum response (strength) must include the uncertainties in W, m, g, h, I, and S_x.

For a new design, uncertainty in W and m and the volume (affecting h and fagitue life) will be large, especially when projected over long periods. Similarly the analysis uncertainties g, I, and S_x will be significant even with accurate finite-element analysis because of variations in stiffness factors, dimensions, and long-term changes.

In a bridge evaluation, there should be considerably lower levels of uncertainties if measurements of load spectra can be made. In addition, if the inspection or evaluation intervals are short (less than 5 years), the impact of uncertainty in future traffic projections should be minimized. A description of how the load spectra study can be performed is given later.

Reliability Modeling

A safety criterion is needed for evaluating existing bridges or designing new structures. Basing the safety criterion on the traditional allowable stress method may lead to inconsistent designs. A better approach has been shown to be load-factor design in which different load factors for dead and vehicle loading can account for respective levels of uncertainty (1,6). A rational safety goal is to keep the failure risk below some economically acceptable limit. The difficulty lies in calculating risks in the likely range of usefulness, typically less than 0.001 failure rate per year.

As a consequence a reliability model has been introduced in developing design codes in the United States and abroad for buildings, offshore structures, and so forth (7). It has also been adopted in Canada for bridge design (1). It is based on a nominal measure of reliability, namely, a safety index, which can be implemented without detailed probabilistic calculations. The safety index (often called beta) can be used in bridge rating for two major purposes: establishment of priorities for bridge rehabilitation based on safety measures and incorporation of past experience to establish target safety indices for rating limits.

A general model for reliability begins with a failure function (g) such that $g < 0$ implies failure. A simple case would be a structural element with strength R loaded with dead (D) and vehicle (L) loads. Thus,

$$g = R - D - L \quad (2)$$

expresses the safety criterion. The safety index can then be expressed as follows:

$$\text{Safety index} = \text{mean of g/standard deviation of g} \quad (3)$$

Accurate calculations of β have been developed that for many distribution functions provide a good agreement with risk determined from simulations. Risk is given as follows:

$$\text{Risk} = F(\beta) \quad (4)$$

where F is the normal (Gaussian) distribution.

An excellent source for this material is the recent report on the formulation of the ANSI A-58 building code (7). It also contains a computer program for calculating β given an equation for g. An important application of β is the calibration of load factors (γ) and resistance safety factors (ϕ). A target β (typically in the range of 2 to 4) is determined from existing specifications and field performance. The calibration finds the safety factors in a load- and resistance-factor safety check similar to load-factor design:

$$\phi R > \gamma_D D + \gamma_L L \quad (5)$$

γ's and ϕ's are found to provide the target β over a full range of applications. For example, an analysis of the current AASHTO code showed how load factors can be chosen to give more constant β's for different spans and ratios of dead to live load (8). The input in the β calculation is the means and variances of each of the load and resistance variables. Although data may be limited, a sensitivity study showed that the calibration exercise reduces the importance of small changes in the data base. This occurs when both the target β's and the safety factors use the same data base.

Subsequently, β's are calculated for the fatigue-limit states and the maximum-load-limit state.

FIELD MEASUREMENT OF LOAD SPECTRA

The most important ingredient in the load model is accurate truck weight statistics. Avoidance of static scales is well recognized and by-pass routes make such scales ineffective for obtaining accurate highway weight statistics. For several years there has been worldwide interest in producing an undetectable system for automatically weighing trucks moving at normal highway speeds. A variety of pavement insert scales have been tested. These flexible

plates respond to vertical forces and are calibrated to give histograms of recorded wheel loads. The problems encountered are due to scale flexibility and the bounce when a massive flexible vehicle moves on a rough pavement at high speeds. The vehicle is typically on the scale for only a portion of its natural period, and large systematic errors may occur because of force oscillation. As a consequence, pavement scales are more accurate for low-speed sorting at busy weigh stations.

Recently the authors and their colleagues at Case extended a system of bridge measurements (5) used to obtain strain histories to also obtain truck weight information. The weighing system has reached the stage of relatively routine operation by ODOT (3,4), FHWA (9), and other groups to monitor truck weights. Thus far, more than 100 sites have been surveyed.

Briefly, the WIM system uses existing bridges as equivalent static scales. Trucks move at normal speeds and drivers cannot detect the weighing operations. Vehicle speeds and dimensions are obtained via tapeswitches bonded to the roadway (Figure 1). Bridge girder response comes from reusable strain transducers clamped to steel flanges or bolted to concrete beams. The girder influence line provides a simulated strain record. The vehicle axle weights are obtained by automatically matching the measured and simulated strains (10). The data recording, monitoring, and weight calculation are done in real time on a minicomputer in an instrument van usually parked beneath the bridge. A known calibration truck is used to establish a relationship between strains and truck weight.

Sites monitored by this procedure have included single-span and continuous steel girders and reinforced and prestressed-concrete beams. The accuracy of the WIM weighing has been verified in several studies by comparing it with static weighings (3,9). It is important for planning that the weight predictions be unbiased. The WIM surveys have provided general weight trends, which, however, are still limited for bridge load and fatigue-spectra modeling.

In a recent modification to the system, strain and traffic data were taken on a continuous basis (4). This provides a total picture of truck traffic including weights, lane occupancy, headways in each lane, maximum stresses, girder distributions, impact, and so forth. Field operations were performed during the summer of 1982 at five sites in northeast Ohio including four steel and one concrete-beam bridge. An example of a recorded event is given in Figure 2. The event shown is two trucks moving side by side. The processing of the strain record gave a 68.3-kip vehicle in the driving lane and a 31.4-kip vehicle in the passing lane with axle weights as shown. This processing required influence coefficients for each lane and girder, which are obtained with the calibration vehicle run at normal speeds in each lane position. One influence example is shown in Figure 3.

Some 8-16 hr of continuous recording were typically obtained at each of the sites investigated. On a routine basis it is expected that a site could be monitored in about 2 days, including set-up, calibration, data acquisition, and processing. It should be noted that the truck weight and traffic data are applicable to any bridge along the same highway, whereas the bridge response parameters (impact, girder stresses) apply only to the structure being studied. Thus, either a rehabilitation or a replacement structure would also benefit from the load spectrum.

To illustrate the acquisition of a load spectrum, a typical site study is outlined. The application to reliability models for rating, fatigue, and load prediction is given in the next section. Table 1 contains the truck weight distribution measured by the WIM system at a site in Ohio on I-90. It shows average gross weight, standard deviation, and average axle distributions for the most common truck categories. An example of a maximum stress distribution is given in Figure 4, which illustrates the low stress levels (less than 6 ksi) observed in most bridge studies. Table 2 shows average measured girder distribution factors for the several steel girder sites; the corresponding AASHTO values are included. Note that when trucks are occupying both lanes, the AASHTO distribution generally is conservative.

Dynamic factors in Table 3 were calculated from examination of the strain oscillation. This has not yet been automated because the dynamic oscillation can be confused with static strain variations caused by axle spacings. It is inaccurate to use spectral

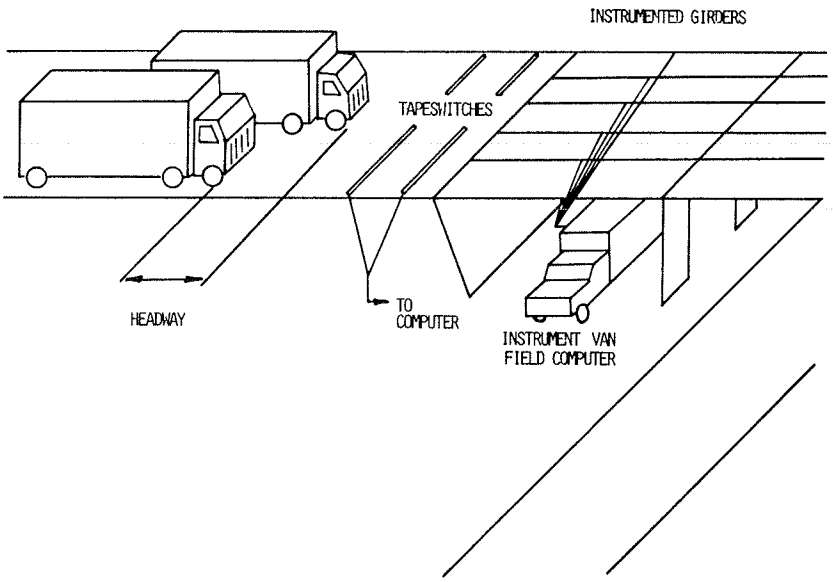

FIGURE 1 Typical WIM installation.

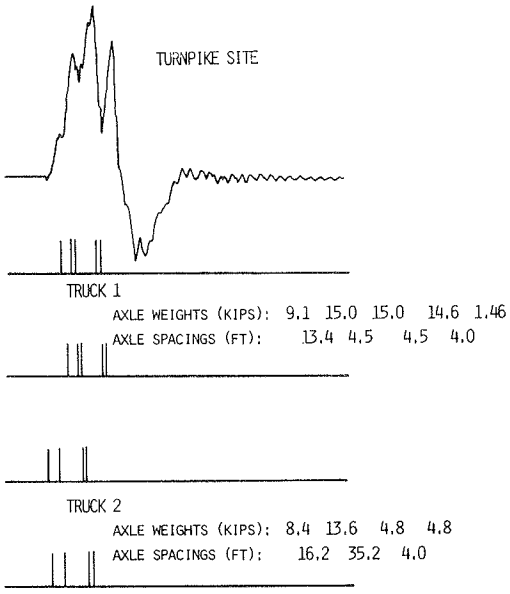

FIGURE 2 Sample record of two side-by-side trucks.

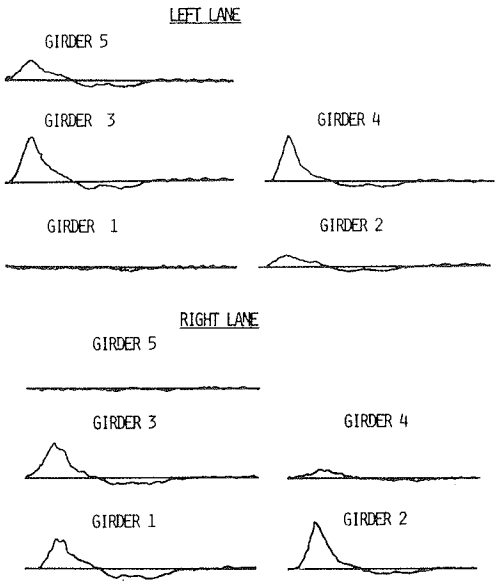

FIGURE 3 Influence lines for a five-girder bridge.

TABLE 1 Truck Statistics Obtained by WIM System (Ohio, I-90)

Category	No. of Vehicles	Percentage of Total	Gross Weight (kips)		Axle Weight Distribution (%)		
			Avg	SD	Front	Drive	Rear
Two-axle single							
Lane 1	63	12	15.8	5.94	33.57		66.44
Lane 2	9	2	15.8	4.14	30.34		69.62
Three-axle single							
Lane 1	29	5	27.9	6.74	30.09		69.46
Lane 2	5	1	25.6	5.09	36.12		63.85
Four-axle semitrailer							
Lane 1	45	9	32.4	12.12	17.89	38.25	43.80
Lane 2	4	1	32.9	5.06	23.87	35.07	41.03
Five-axle semitrailer							
Lane 1	217	42	50.8	17.73	13.86	48.08	38.03
Lane 2	52	10	48.8	18.49	14.04	48.43	37.49
Five-axle split							
Lane 1	37	7	53.87	17.55	11.93	47.54	40.50
Lane 2	10	2	39.98	15.50	19.86	45.72	34.38

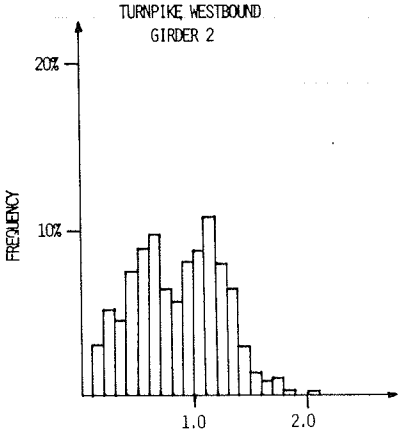

FIGURE 4 Histogram of maximum stress distribution.

TABLE 2 Average Girder Distribution Factors

Site	Percentage of Total Stress by Girder						AASHTO Value (6) (%)
	1	2	3	4	5	6	
I-90							
Case 1	6.4	19.1	40.6	25.9	7.1	0.8	
Case 2	0.2	7.4	19.2	29.9	29.6	13.6	
Case 3	3.3	13.3	29.9	27.9	18.4	7.2	36
I-71							
Case 1	7.6	27.2	33.9	20.5	9.5	1.5	
Case 2	-0.3	14.0	22.5	30.1	23.0	10.6	
Case 3	3.7	20.6	28.2	25.3	16.3	6.1	36
I-80 westbound							
Case 1	18.2	37.9	34.0	9.7	0.1	NA	
Case 2	-0.1	9.9	34.2	37.2	18.9	NA	
Case 3	9.1	23.9	34.1	23.5	9.5	NA	33
I-80 eastbound							
Case 1	23.7	37.9	25.9	11.8	0.6	NA	
Case 2	0.3	11.0	27.2	42.9	18.6	NA	
Case 3	12.0	24.5	26.6	27.4	9.6	NA	33

Note: Case 1: truck in right lane (measured); case 2: truck in left lane (measured); case 3: side-by-side trucks of same weight (hypothetical). NA = not applicable.

TABLE 3 Dynamic Factors for Typical Truck Records (Ohio, I-90)

Record	Impact[a] (%)	Record	Impact[a] (%)
1	15	13	26
3	13	17	26
6	11	18	23
8	17	19	14
10	20	20	19
12	23		

[a]Measured on most heavily loaded girder.

analysis for finding dynamic response for bridges with spans less than 125 ft. Figures 5 and 6 show headway spacings between moving trucks in the same lane or moving in different lanes. This gives the data for constructing the load superposition model or the headway variable (h) defined earlier. Data on section modulus S_x can also be inferred by taking the bending moments and dividing by the girder stresses. In the instances studied, such data might be misleading because the bridges were designed to be noncomposite but obviously exhibited considerable composite action. More detailed study of the variable S_x is still needed.

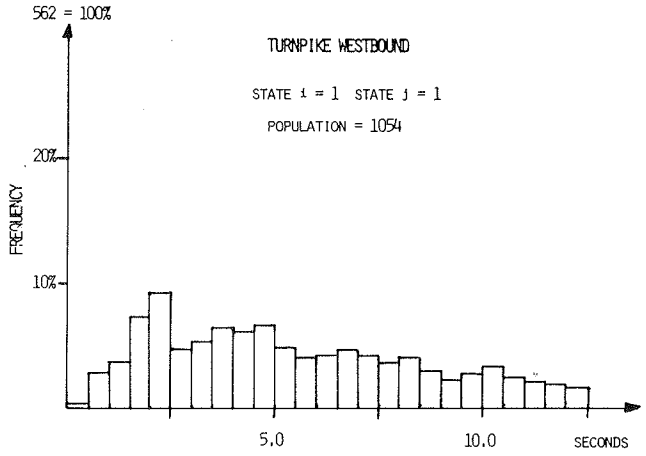

FIGURE 5 Histogram of headway for trucks in right lane.

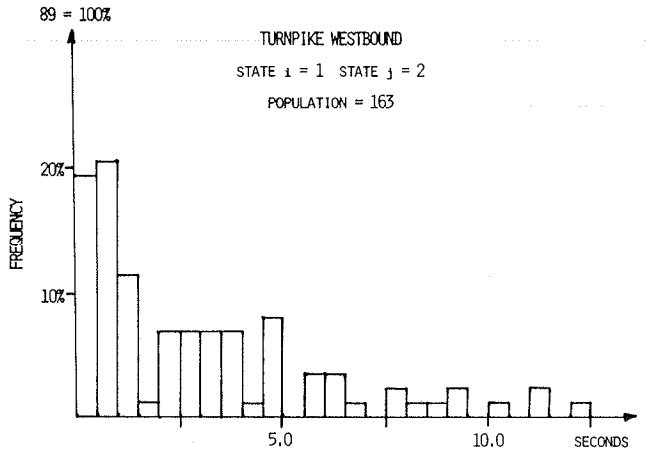

FIGURE 6 Histogram of headway for trucks in left lane approaching trucks in right lane.

RELIABILITY ASSESSMENTS

The previous section showed how a load spectrum data base could be acquired. This section provides application of the data to load forecasting and calculation of safety indices for ultimate strength (component and system) and fatigue.

Load Forecasting

Load spectrum data have been typically taken for 1- or 2-day periods at each site. Adjustments for daily, weekly, and seasonal variations can be made by using more extensive weight survey information gathered for pavement, enforcement, and other planning purposes. The first step in bridge reliability modeling is to forecast maximum bending moments. These depend on the truck weight distribution, axle spacing and axle weight distribution (variable m given previously), and truck volume (which affects headway). As an illustration the load data taken at an I-90 (Ohio) site are used to forecast distribution of maximum bending moment for a 100-ft simple supported span. Several types of load-modeling programs have been used in such forecasting, including simulation, Markov renewal models, and simplified approximations, all of which are in general agreement (11). Figure 7 shows a maximum moment distribution for a 10-year forecast by using five-axle vehicles with constant axle spacings and weight distribution. These forecasts, which ignore future growth in truck weights, are in the form of probability distributions. The mean and variance are the most important parameters needed in the failure function (Equation 1) to calculate β. This was done by using a level-2 reliability analysis (7). The data for dead load, live load, and strength are presented in Table 4. Using the failure function in Table 4 provided a β of 3.1. It should be noted that the live-load data are based only on a limited number of sites.

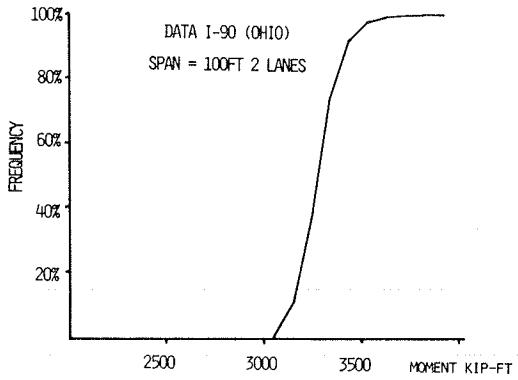

FIGURE 7 Distribution of maximum bending moment for a 10-year forecast.

For study of design safety and load factors, β's should be calculated for different span and support configurations. The aim is to obtain reasonably uniform β's over the range of code applicability. Because the current load specifications do not match measured load spectra, there will likely be scatter in β's. Taking an average of these β's gives an appropriate target and choosing the dead- and live-load factors (7,8) can also smooth out any variations in β.

TABLE 4 Data Base for β Calculations Without Measured Load Spectra at Site

Random Variable	Mean	Coefficient of Variation (%)	Comments
R	1.1 AASHTO (1,676.4 kip·ft)	15	Resistance: nominal AASHTO strength
D	1,673 kip·ft	10	Dead load[a]
m, W, h	4,450 kip·ft	20	Obtained from simulation of maximum moment by using measured truck data and average truck volume (V = 2,500/day)
g	0.3	11	Maximum girder distribution factor: based on 4 sites (4)
I	1.11	11	Impact factor: based on 10 sites (13)
Total live load	1,482 kip·ft	25	Calculated: live load = mWhgI

Note: Failure function = R - D - mWhgI (assume log normal distributions); 100-ft span (span length affects R, D, m).

[a] Based on data from Moses and Ghosn (8).

Rating

An important fact in rating is that the bridge is available for making observations relating to both capacity (deterioration) and the load spectrum. The rating should be viewed as part of an important control process in producing acceptable safety. A model of demand (load) and capacity (resistance) for a bridge similar to the fundamental reliability model may appear as shown in Figure 8. The load and strength frequency distributions for the as-built conditions will show little overlap, indicating high reliability. Over time, the strength deteriorates and the loads generally increase. If nothing is done to rehabilitate any damage or control the loads, the risk may increase to unacceptable levels. Inspection is part of this control process.

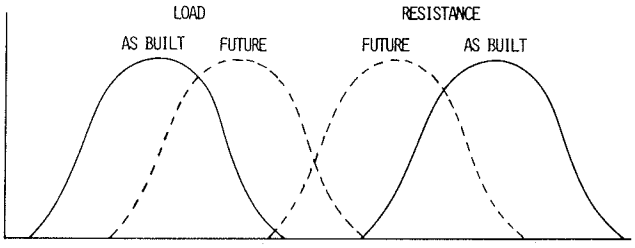

FIGURE 8 Reliability model for bridge rating.

To illustrate, consider the load model described previously. Figure 9 shows a simulated distribution of the maximum bending moments for periods of 1 day, 1 month, 1 year, and 5 years. The increasing load suggests that the inspection interval is important.

In the absence of a measured load spectrum, the design specification must be used to calculate design moments. These values will have greater uncertainty than a measured load spectrum determined at the site. For example, the overall live-load coefficient of variation is 25 percent without a measured spectrum, which compares with 15 percent in Table 5 when measurements have been taken. Note that only a few sites have yet been monitored, so the data base in Tables 4 and 5 must be viewed as still tentative.

As one application of this data, Figure 10 compares β's for different estimates of section deterioration for the case of an available load spectrum with the case in which measurements are not made. The higher β's reflect the lower uncertainties with measured load spectrum. In fact, another advantage of the measured spectrum is the identification of the mean load, which may differ significantly from the specification loads. For the same

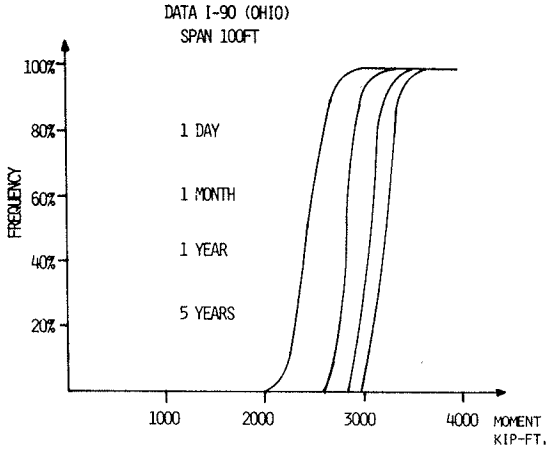

FIGURE 9 Distribution of maximum bending moment for different rating periods.

TABLE 5 Data Base for β Calculations with Measured Load Spectra (Ohio, I-90)

Random Variable	Mean	Coefficient of Variation (%)	Comments
S_X	404.8 in.^{3}		Section modulus: from site plans[a]
F_y	40 ksi	10	Yield stress (7)[a]
D_{et}	0.8	15	Deterioration factor: mean assumed from inspection[a]
D	186 kip·ft	10	Dead load: estimated from site plans
m, W, h	1,092 kip·ft	12	Obtained from simulation based on I-90 volume
g	0.30	8	Measured maximum girder distribution factor
I	1.2	11	Measured impact

Note: Failure function = $S_X F_y D_{et}$ - D - mWhgI (assume log normal distribution); 40-ft span, two lanes.

[a] $R = F_y \cdot S_X \cdot D_{et}$.

parametric data in Table 5, Figure 11 shows reduction in β with the increase of the mean value of the load spectrum. Figures 12 and 13 show the effect on β with measured impact and girder distributions as compared with using AASHTO specification values.

Redundancy

It is generally recognized that redundant or parallel load paths are necessary in case of accidental loadings or component failures (caused by fatigue and brittle or even ductile behavior). It is pos-

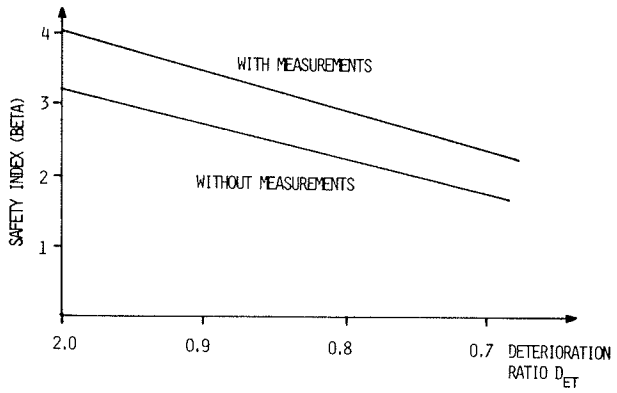

FIGURE 10 Beta for different estimates of deterioration (40-ft span).

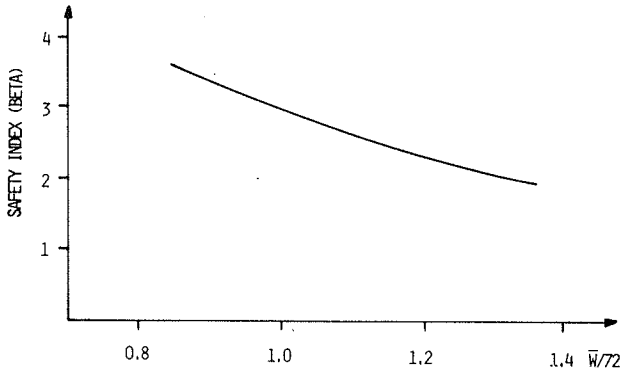

FIGURE 11 Beta for different values of mean load (40-ft span).

sible to compare, for example, a two-girder with a five- parallel-girder system, as shown in Figure 14. If the first yield capacity is the same for both systems, the five-girder system has both a higher collapse load and greater reserve capacity if one of the girders should fail. Different component failure sequences or failure trees have been modeled in a reliability framework and are reported elsewhere (11,12). A damage index (similar to β) is introduced to integrate the consequences of load occurrences beyond the initial component failure. Redundant systems will have lower expected damage indices than statically determinate structures. These damage indices may also be included in a rating strategy, but further work is needed to make the system methodology easy to apply.

Fatigue

Fatigue checks are not normally part of a bridge evaluation, because it would appear imprudent to recommend precautions such as posting based only on a calculation and no observation of cracks. Laboratory tests of similar specimens often show variations with orders of magnitude in fatigue life. Nevertheless, a fatigue check may often identify critical components for detailed field inspection and perhaps also schedule inspection intervals. A load spectrum can also be introduced in the risk assessment for fatigue damage.

The fatigue of steel bridge members is determined by an averaging process. Each vehicle crossing at time t contributes to the cumulative damage [D(t)]. The failure function may be written as follows:

$$g = D_f - D(t) \tag{6}$$

D_f is the damage at failure, which should have a mean of 1.0 according to Miner's linear cumulative damage rule. Summing over the frequency histogram of stress range cycles (S_i) gives (13)

$$D(t) = (Vt/c)\ \Sigma\ S_i^3\ f(S_i) \tag{7}$$

where V is the truck volume. The cubic term derives

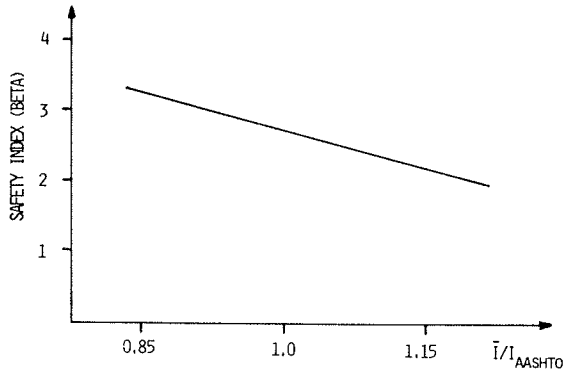

FIGURE 12 Beta for different values of mean impact (40-ft span).

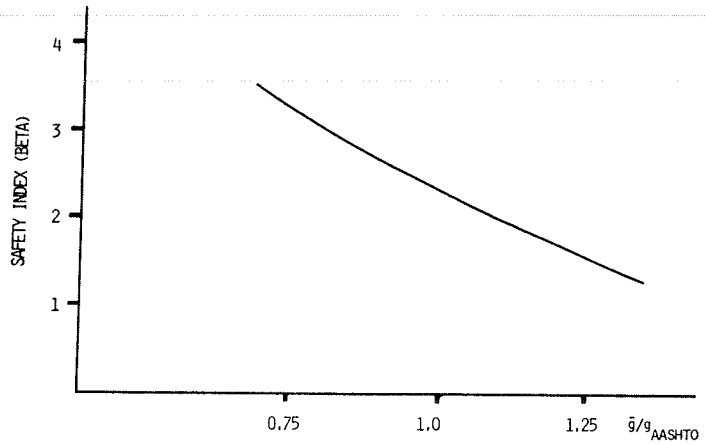

FIGURE 13 Beta for different values of girder distribution factor (40-ft span).

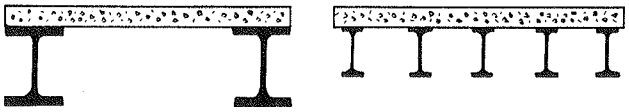

FIGURE 14 Example of bridge configurations.

from the slope of typical welded attachment S-N curves, whereas the intercept c depends on the fatigue category. The stress range (S_i) may be replaced by respective random variables by using Equation 1. The iterative safety index (7) program was run with typical AASHTO design factors and data (4,13). The results showed β's in the range of 2 to 3 for redundant cases and higher values for nonredundant cases. Proposals to modify the specification to produce a more uniform range of β's include the following:

1. Use a standard fatigue vehicle to calculate design moments rather than the AASHTO design with variable axle spacing (6).
2. Adjust the allowable stress ranges to produce similar β's for different attachments.
3. Allow more categories of heavy volumes instead of the single category of more than 2,000,000 because there are many roadways with an excess of 5,000 trucks per day. Beta is reduced with increased volume.
4. Allow more categories of heavy vehicle weight classification because some roadways are known to carry considerable numbers of heavy and overloaded vehicles. Beta decreases with increases in average vehicle weights.

It should be noted that the average weight that produces the same damage as the total population has been reported as 50 kips based on FHWA loadometer studies (14). Recent WIM studies, however, show regions with much heavier vehicles. These data are presented in Table 6 in terms of average vehicle weight to give the same overall damage intensity for a number of sites nationwide (9). This may show higher or lower β's than when the FHWA data base, which is averaged from many sites, is used. If the site is one with a high load spectrum, the β calculated may be low. This evaluation should be used to guide inspection frequency and the location of potential flaws.

TABLE 6 Fatigue Damage: Equivalent Truck Weight (9)

Site (9)	Equivalent Truck Weight (kips)	Site	Equivalent Truck Weight (kips)
CA-1	59.3	TX-1	54.3
CA-2	54.3	TX-2	58.3
CA-3	57.5	TX-3	57.1
CA-4	47.1	TX-4	54.3
CA-5	47.6	TX-5	52.2
CA-6	49.7	TX-6	58.3
GA-1	49.7	TX-7	67.1
GA-2	39.9	IL-1	69.8
GA-3	43.5	IL-2	48.2
ARK-1	53.5	IL-3	60.4
ARK-2	53.1	IL-4	52.2
ARK-3	44.7	NY-1	52.6
ARK-4	52.6	NY-2	44.7
ARK-5	51.2	NY-3	46.0
ARK-6	55.2	NY-4	56.4
OH-1	53.9		
OH-2	60.4		

CONCLUSIONS: STRATEGIES FOR BRIDGE EVALUATION

The routine acquisition of site-specific bridge load and response spectra has been outlined. In addition, a reliability assessment measure, namely, the safety index, could be used to rate the safety of a particular design. There are several possible applications of load spectra measurements that can lead to more efficient strategies for inspection, evaluation, and permit and load control.

Inspection

Funds are limited and reliability assessments may identify critical elements and assist in identifying inspection intervals. Fatigue-calculated β's may identify bridge locations where detailed crack investigation is warranted.

Posting

If low safety indices are found for maximum loading conditions, posting is warranted until repair or rehabilitation can be undertaken. WIM operations can assist in determining whether posting limits are obeyed.

Legal Load Limits

The impact of higher load limits will be reflected in the reliability model with lower safety indices.

Permit Loads

Reduced load factors may be warranted if loading is carefully controlled, as in the case of escorted permit vehicles. This can be reflected by reduced load uncertainties giving higher β's in the reliability model.

Enforcement

Evaluation of enforcement effectiveness is important in reducing load uncertainties. The impact of such enforcement becomes apparent in the calculated β values. The cost of increased enforcement should be balanced by the improvements in bridge safety.

Rating

Load and resistance factors in rating calculations need to be different from values used in design because of exposure period and available performance data (1). The existence of a measured load spectrum at a site should permit reduced load factors. Flexibility in incorporating the measurements in rating decisions will encourage bridge engineers to seek more field data to corroborate their calculations and enhance bridge safety.

ACKNOWLEDGMENT

The research and field work reported here has been supported by ODOT, FHWA, and the National Science Foundation.

REFERENCES

1. P.F. Csagoly and R.A. Dorton. The Development of the Ontario Highway Bridge Design Code. In Transportation Research Record 665, TRB, National Research Council, Washington, D.C., 1978, pp. 1-12.

2. R. Imbsen. Structural Strength Evaluation of Existing Reinforced Concrete Bridges. NCHRP Interim Report, Project 10-15. TRB, National Research Council, Washington, D.C., 1983.
3. F. Moses and M. Ghosn. Weighing Trucks-In-Motion Using Instrumented Highway Bridges. Final Report., Case Western Reserve University, Cleveland, Ohio, 1981.
4. F. Moses and M. Ghosn. Instrumentation for Weighing Trucks in Motion for Highway Bridge Loads. Case Western Reserve University, Cleveland, Ohio, 1983.
5. F. Moses, G.G. Goble, and A. Pavia. Application of a Bridge Measurement System. In Transportation Research Record 579, TRB, National Research Council, Washington, D.C., 1976, pp. 36-47.
6. Standard Specifications for Highway Bridges. AASHTO, Washington, D.C., 1977.
7. B. Ellingwood, T.V. Galambos, J.G. Macgregor, and C.A. Cornell. Development of Probability Based Load Criteria for American National Standard A58.1. Special Publ. 577. National Bureau of Standards, Gaithersburg, Md., June 1980.
8. F. Moses and M. Ghosn. Bridge Load Data and Reliability Assessments. Presented at International Conference on Short- and Medium-Span Bridges, Toronto, Canada, Aug. 1982.
9. R.E. Snyder, G.E. Likins, Jr., and F. Moses. Loading Spectrum Experienced by Bridge Structures in the United States. Report FHWA/RD-82/107. FHWA, U.S. Department of Transportation, Sept. 1982.
10. F. Moses and G.G. Goble. Feasibility of Utilizing Highway Bridges to Weigh Vehicles in Motion. Report FHWA-RD-75-33. FHWA, U.S. Department of Transportation, Nov. 1974.
11. F. Moses and M. Ghosn. Reliability-Based Design and Evaluation of Highway Bridges. Presented at ASCE Special Conference on Probabilistic Mechanics and Structural Reliability, Berkeley, Calif., Jan. 1984.
12. F. Moses and M. Ghosn. Requirement for Reliability-Based Bridge Code. Presented at ASCE National Meeting, St. Louis, Mo., Oct. 1981.
13. F. Moses and A. Pavia. Probability Theory for Highway Bridge Fatigue Stresses: Phase II. Final Report., Ohio Department of Transportation, Columbus, Aug. 1976.
14. C.G. Schilling. Section 2 Fatigue Stress. In U.S. Steel Highway Structures Design Handbook, U.S. Steel Corporation, Pittsburgh, Pa., 1982, Chapter i-vi.

Publication of this paper sponsored by Committee on Structures Maintenance.

A Pragmatic Approach in Rating Highway Bridges

SHIH C. PENG

ABSTRACT

A procedure is presented for rating highway bridges for regulation loads without causing yielding of the bridge materials. The procedure consists of three major parts: the measurement of regulation loads with a load measure, the yield capacity calculations of bridge members, and the ratings for various traffic conditions. The importance of accurate ratings, which will form the basis for making decisions pertaining to bridge upgrading and traffic control, is recognized. The results of the actual application of the procedure were found to be satisfactory in the strengthening programs of many existing bridges and in issuing overload permits. The procedure is considered to be simple, direct, and practical.

Highway bridges can have different ratings under different loading conditions. Because the actual traffic conditions are basically controlled by state regulations, it is logical to assume that regulation or legal loads resemble the various highway loadings. For upgrading an existing bridge economically, issuing overload permits, or posting for load limits, more reliable ratings for the regulation loads are desirable. Because any standard loading, such as HS20, as given in the AASHTO specifications (1) or a statistical truck model, is incapable of simulating all the load effects caused by the action of regulation loads of innumerable combinations of axle loads and spacings on various bridge members, it cannot yield reliable ratings. But by using a load measure, the actual traffic condition can be closely measured and thus more reliable ratings can be obtained.

A standard loading can easily be made into a load measure, for instance, by changing HS20 to HSW, where W is the variable combined weight on the first two axles. This simple transformation will make HS no longer a standard loading but rather a system of measurement. Like feet or meters for measuring lengths, the HS load measure may be used to obtain the load effects of various highway loadings. The proportional configuration of the HS load measure suggested is identical to that of the HS loading, which consists of either a three-axle truck or the corresponding lane loading. The only exception is that the spacing of the last two axles is fixed at 14 ft for the HS load measure.

The basic principle followed in this paper is to rate highway bridges for regulation loads without causing yielding of the bridge materials. Because

the bridges will not be considered usable after permanent yielding, the ultimate strength of the bridge members beyond yield will not be used in the rating.

It is estimated that without changing the design criteria, such as impact and load distribution, and by adopting the modified capacity formulas for the load-factor design as given in the current AASHTO specifications, a rating procedure for the regulation loads of any state could be developed and made operational within a short period, say, 2 to 3 months, by using the approach described in this paper.

BRIDGE LOADS

Three basic loads--dead, live, and impact--are considered in the rating of most highway bridges. For any existing bridge, the dead loads can be accurately estimated from plans or field measurements, the live loads are the regulation loads, and the impact loads may be calculated according to the AASHTO specifications.

Because it is rather cumbersome to apply the regulation loads directly in structural analyses and calculations, the HS load measurements are substituted for the regulation loads. The method of determining the HS measurements is described in the following.

Almost all the regulation loads have numerous truck configurations. In order to determine the maximum load effects (moment and shear in a simple span), repetitious calculations for the numerous configurations are apparently inevitable. However, because the main features of most regulations are similar in defining the maximum axle load, the minimum axle spacing, and the combinations of the axles, a simple structural rule, that the heaviest total load within the shortest distance will produce the largest load effect, can be used to eliminate many truck configurations. Once the maximum load effect has been found, the equivalent HS loading or HS measurement can be determined by proportion. The HS measurement represents a loading that will produce the same load effect as that produced by the governing regulation loads. The word "governing" is used to indicate that the loads will cause the maximum load effect.

Listed in Table 1 are the maximum load effects (moments and shears) caused by HS20 loading acting on simple spans. A similar table may be found in Appendix A of the AASHTO specifications.

To illustrate for typical regulation loads, listed in Table 2 are the maximum moments and shears and their corresponding HS measurements for the Northwest Territories (NWT) governing regulation loads (2) on simple spans. To account for the multiple presence of regulation trucks on short-span bridges, only two trucks tailgating at an assumed spacing of 40 ft between the rear axle of the first truck and the front axle of the following truck were used. The values in Table 2 would differ if different regulation loads and truck spacings were chosen, and they are not recommended for use except in this paper. A graphic representation of the HS measurements for spans up to 300 ft is shown in Figure 1.

As an example, for a moment of 759.3 ft·kip caused by an NWT governing truck acting on a 50-ft span (Table 2), the HS measurement is calculated as follows:

$$HS_m\ [(759.3 \times 20)/627.9] = HS_m 24.2,$$

where 627.9 is the maximum moment in foot kips caused by HS20 loading acting on the 50-ft span (Table 1).

Table 2 is the most important tool in rating and it also requires the most time to develop. Table 2 remains useful as long as the regulations are enforced and provided that there is no substantial change in the traffic pattern.

APPLICATION OF HS LOAD MEASURE

The HS measurements for the maximum load effects of the NWT regulation loads in a structural member can be found in Table 2 if the equivalent simple-span length is known. It is assumed that the equivalent simple-span length is equal to the loaded-span length for the structural member obtained by using the principle of influence lines. The loaded-span length is the length on which the loads can be placed to produce the maximum load effect in a structural member and is not necessarily the length of the member. The technique for determining the loaded-span length, or the equivalent simple-span length, is to match the general shapes of the influence lines for the structural member concerned with the maximum moment or shear influence line for a simple span as shown in Figure 2.

It is quite clear that for a simple beam, the loaded-span length is equal to the length of the beam for both the maximum moment and maximum shear.

TABLE 1 Maximum Moments and Shears of HS20 on Simple Spans (One Lane)

Span (ft)	Moment (ft·kips)	Shear (kips)	Span (ft)	Moment (ft·kips)	Shear (kips)	Span (ft)	Moment (ft·kips)	Shear (kips)	Span (ft)	Moment (ft·kips)	Shear (kips)	Span (ft)	Moment (ft·kips)	Shear (kips)
1	8.0	32.0	21	168.0	42.7	42	485.3	56.0	100	1,524.0	65.3	400	14,600.0	154.0
2	16.0	32.0	22	176.0	43.6	44	520.9	56.7	110	1,703.6	65.9	420	16,002.0	160.4
3	24.0	32.0	23	184.0	44.5	46	556.5	57.3	120	1,883.3	66.4	440	17,468.0	166.8
4	32.0	32.0	24	192.7	45.3	48	592.1	58.0	130	2,063.1	67.6	460	18,998.0	173.2
5	40.0	32.0	25	207.4	46.1	50	627.9	58.5	140	2,242.8	70.8	480	20,592.0	179.6
6	48.0	32.0	26	222.2	46.8	52	663.6	59.1	150	2,475.1	74.0	500	22,250.0	186.0
7	56.0	32.0	27	237.0	47.4	54	699.3	59.6	160	2,768.0	77.2	520	23,972.0	192.4
8	64.0	32.0	28	252.0	48.0	56	735.1	60.0	170	3,077.1	80.4	540	25,758.0	198.8
9	72.0	32.0	29	267.0	48.8	58	770.8	60.4	180	3,402.0	83.6	560	27,608.0	205.2
10	80.0	32.0	30	282.1	49.6	60	806.5	60.8	190	3,743.1	86.8	580	29,522.0	211.6
11	88.0	32.0	31	297.3	50.3	62	842.4	61.2	200	4,100.0	90.0	600	31,500.0	218.0
12	96.0	32.0	32	312.5	51.0	64	878.1	61.5	220	4,862.0	96.4			
13	104.0	32.0	33	327.8	51.6	66	914.0	61.9	240	5,688.0	102.8			
14	112.0	32.0	34	343.5	52.2	68	949.7	62.1	260	6,578.0	109.2			
15	120.0	34.1	35	361.2	52.8	70	985.6	62.4	280	7,532.0	115.6			
16	128.0	36.0	36	378.9	53.3	75	1,075.1	63.1	300	8,550.0	122.0			
17	136.0	37.7	37	396.6	53.8	80	1,164.9	63.6	320	9,632.0	128.4			
18	144.0	39.1	38	414.3	54.3	85	1,254.7	64.1	340	10,778.0	134.8			
19	152.0	40.4	39	432.1	54.8	90	1,344.4	64.5	360	11,988.0	141.2			
20	160.8	41.6	40	449.8	55.2	95	1,434.1	64.9	380	13,262.0	147.6			

TABLE 2 Maximum Moments, Shears, and HS Measurements of NWT Regulation Loads on Simple Spans (One Lane)

L_s (ft)	M (ft-kips) (1)	M (ft-kips) (2)	V (kips) (1)	V (kips) (2)	HS_m (tons) (1)	HS_m (tons) (2)	HS_v (tons) (1)	HS_v (tons) (2)
1	5.0		20.0		12.5		12.5	
2	10.0		20.0		12.5		12.5	
3	15.0		20.0		12.5		12.5	
4	20.0		21.4		12.5		13.4	
5	25.0		23.4		12.5		14.6	
6	30.4		25.4		12.7		15.9	
7	36.7		26.9		13.1		16.8	
8	44.8		27.9		14.0		17.4	
9	52.9		28.9		14.7		18.1	
10	61.2		29.8		15.3		18.6	
11	70.1		30.5		15.9		19.1	
12	79.1		31.3		16.5		19.6	
13	88.1		32.1		16.9		20.1	
14	97.9		32.6		17.5		20.4	
15	107.8		33.0		18.0		19.4	
16	117.7		33.5		18.4		18.6	
17	128.0		34.8		18.8		18.5	
18	138.6		36.7		19.3		18.8	
19	149.1		38.5		19.6		19.1	
20	160.0		40.3		20.0		19.4	
21	171.7		41.9		20.4		19.6	
22	183.4		43.4		20.8		19.9	
23	195.1		45.0		21.2		20.2	
24	207.7		46.3		21.6		20.4	
25	220.3		47.6		21.2		20.7	
26	232.9		48.9		21.0		20.9	
27	248.2		50.0		20.9		21.1	
28	264.4		50.9		21.0		21.2	
29	280.6		51.9		21.0		21.3	
30	299.2		52.9		21.2		21.3	
31	320.6		53.9		21.6		21.4	
32	341.9		54.9		21.9		21.5	
33	363.3		55.9		22.2		21.7	
34	384.6		56.8		22.4		21.8	
35	406.0		57.7		22.5		21.9	
36	427.3		58.6		22.6		22.0	
37	448.9		59.4		22.6		22.1	
38	470.5		60.2		22.7		22.2	
39	492.1		61.1		22.8		22.3	
40	514.1		61.8		22.9		22.4	
42	558.6		63.0		23.0		22.5	
44	603.7		65.3		23.2		23.0	
46	649.4		68.2		23.3		23.8	
48	704.3		70.0		23.8		24.1	
50	759.3		71.3		24.2		24.4	
52	814.6		73.1		24.6		24.7	
54	869.6		74.4		24.9		25.0	
56	924.5		75.7		25.2		25.5	
58	979.8		76.9		25.4		25.5	
60	1,035.1		78.0		25.7		25.7	
62	1,090.4		79.0		25.9		25.8	
64	1,145.3		80.0		26.1		26.0	
66	1,200.2		81.1		26.3		26.2	
68	1,255.5		81.9		26.4		26.4	
70	1,310.6		82.7		26.6		26.5	
75	1,448.4		84.6		26.9		26.8	
80	1,585.9		86.0		27.2		27.0	
85	1,724.1		87.4		27.5		27.3	
90	1,861.6		88.7	89.7	27.7		27.5	27.8
95	1,992.2		89.9	92.6	27.9		27.7	28.5
100	2,137.0		90.5	95.5	28.0		27.8	29.2
110	2,412.8		92.6	102.8	28.3		28.1	31.2
120	2,688.2		94.2	110.3	28.5		28.4	33.2
130	2,964.0	2, 984.1	95.5	117.1	28.7	28.9	28.3	34.6
140	3,239.2	3,358.9	96.4	125.2	28.9	30.0	27.2	35.4
150	3,514.8	3,845.7	97.3	131.4	28.4	31.1	26.3	35.5
160	3,790.5	4,346.3	98.1	137.2	27.4	31.4	25.4	35.5
170	4,066.3	4,847.7	98.9	142.0	26.4	31.5	24.6	35.3
180	4,341.4	5,349.0	99.4	146.4	25.5	31.4	23.8	35.0
190	4,617.1	5,867.7	100.0	150.2	24.7	31.4	23.0	34.6
200	4,892.9	6,412.4	100.5	153.7	23.9	31.3	22.3	34.2
220	5,443.6	7,503.4	101.4	159.9	22.4	30.9	21.0	33.2
240	5,995.1	8,596.5	102.1	164.9	21.1	30.2	19.9	32.1
260	6,546.0	9,691.0	102.8	169.1	19.9	29.5	18.8	31.0
280	7,096.8	10,787.0	103.4	172.9	18.8	28.6	17.9	29.9
300	7,648.0	11,883.0	103.9	176.0	17.9	27.8	17.0	28.9
320	8,199.1	12,980.4	104.2	180.1	17.0	27.0	16.2	28.1
340	8,752.7	14,078.6	104.5	181.3	16.2	26.1	15.5	26.9
360	9,304.0	15,176.7	105.0	183.5	15.5	25.3	14.9	26.0
380	9,855.2	16,275.6	105.2	185.4	14.9	24.5	14.3	25.1
400	10,406.5	17,375.2	105.4	187.2	14.3	23.8	13.7	24.3
420	10,957.7	18,474.8	105.6	188.7	13.7	23.1	13.2	23.5
440	11,509.0	19,574.4	105.8	190.1	13.2	22.4	12.7	22.8
460	12,060.2	20,674.8	106.1	191.4	12.7	21.8	12.3	22.1
480	12,611.5	21,774.4	106.3	192.7	12.2	21.1	11.8	21.5
500	13,162.7	22,875.4	106.4	193.8	11.8	20.6	11.4	20.8
520	13,714.0	23,975.8	106.5	194.9	11.4	20.0	11.1	20.3
540	14,265.2	25,076.8	106.7	195.8	11.1	19.5	10.7	19.7
560	14,816.5	26,177.1	106.8	196.7	10.7	19.0	10.4	19.2
580	15,367.7	27,278.2	106.9	197.6	10.4	18.5	10.1	18.7
600	15,919.0	28,379.2	107.0	198.2	10.1	18.0	9.8	18.2

Note: L_s = span length, M = moment of governing regulation loads, V = shear of governing regulation loads, HS_m = HS measurement for moment effect, HS_v = HS measurement for shear effect, (1) = single regulation truck, and (2) = two regulation trucks with 40-ft spacing between them.

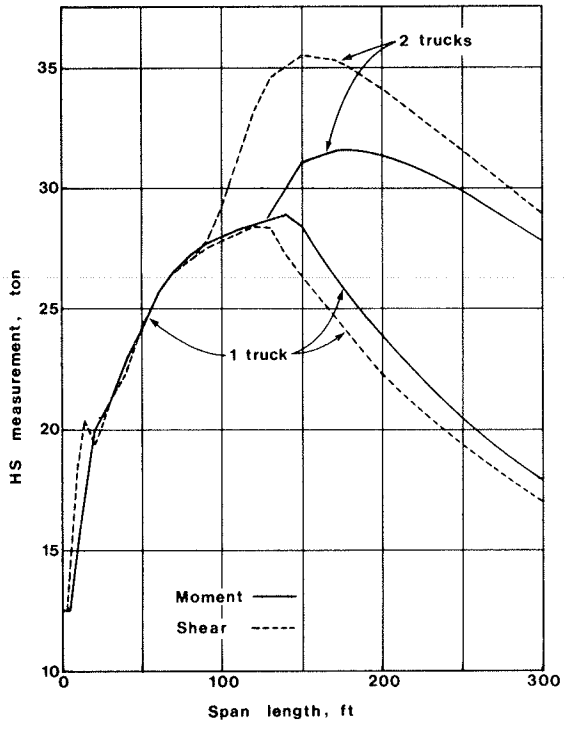

FIGURE 1 HS measurements of NWT regulation loads.

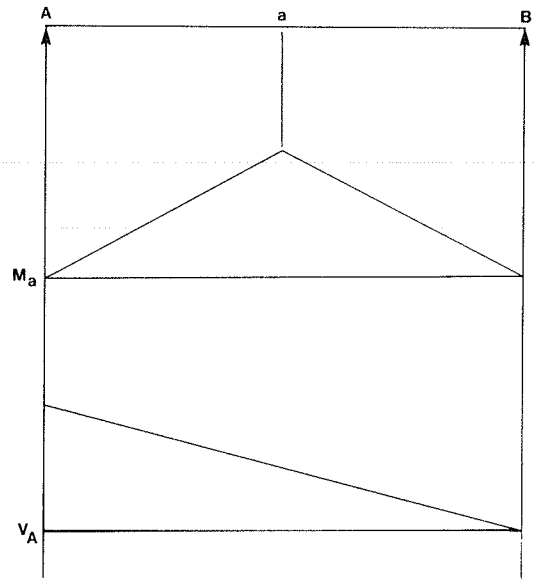

FIGURE 2 Influence lines of maximum moment and shear for a simple span.

Thus the corresponding HS measurements can be obtained easily from Table 2.

For a continuous beam as shown in Figure 3, the HS measurement for moment (HS_m) is selected when the shape of the influence line appears to be a moment influence line for a simple span and the HS measurement for shear (HS_v) is selected when the shape of the influence line appears to be a shear influence line for a simple span. For the reaction R_B at the interior support B, because the shape of the influence line ABC is similar to that of the moment influence line for the simple span AC, the loaded-span length of 220 ft is used and $HS_m30.9$ is selected for two trucks tailgating.

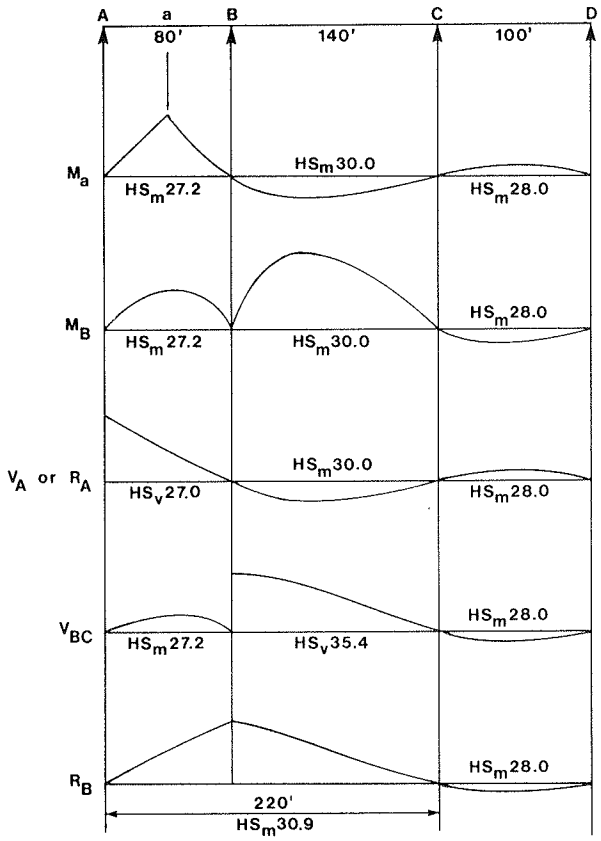

FIGURE 3 Influence lines and HS measurements for a continuous beam.

For a truss, as shown in Figure 4, the loaded-span length for the chord members is the length of the truss, whereas for the diagonals and verticals, the loaded-span lengths are determined by their corresponding influence lines. It can be seen that whether to select HS_m or HS_v is not so clear as it was in the case of beams. However, HS_m may be used for chord members and hangers and HS_v for diagonals and verticals other than hangers.

For floor beams perpendicular to traffic, the loaded-span lengths are determined by using the beam spacings rather than the lengths of the beams, as shown in Figure 5. Otherwise the determination of the loaded-span lengths for selection of the HS measurements for these beams is similar to that for the reactions in a continuous beam, as shown in Figure 3.

A concrete deck slab with main reinforcement perpendicular to traffic (Figure 6) may be assumed a continuous beam just as it is if the main reinforcement is parallel to traffic. In most state regula-

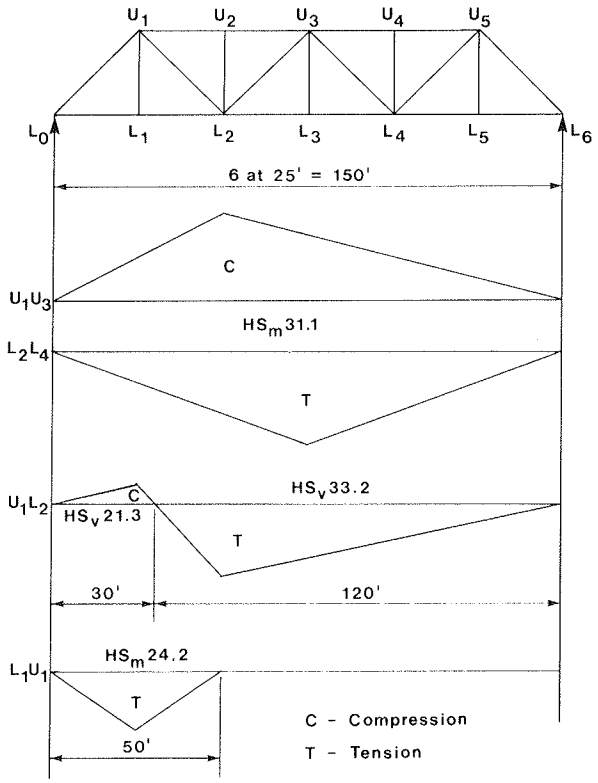

FIGURE 4 Influence lines and HS measurements for a truss.

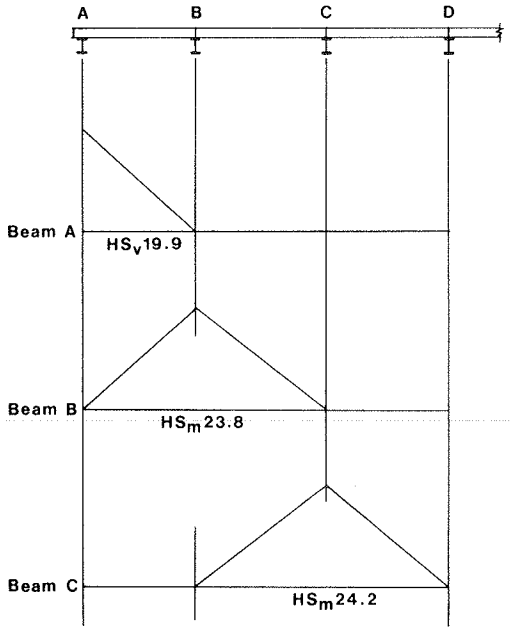

FIGURE 5 Influence lines and HS measurements for floor beams.

tions the minimum axle spacings are generally less than but could be close to the wheel spacing of HS trucks as specified in the AASHTO specifications. The approximately equal axle and wheel spacings make Table 2 also useful for slabs. The HS measurements would be slightly conservative, because the minimum

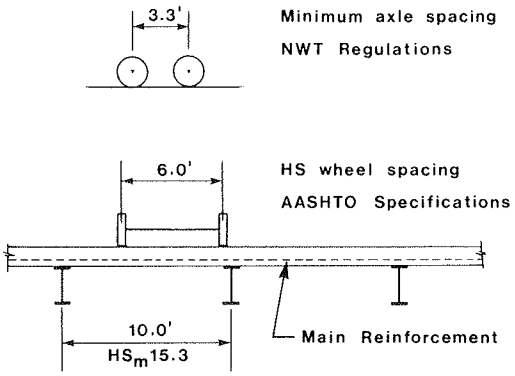

FIGURE 6 HS measurement for concrete deck slab with main reinforcement perpendicular to traffic.

axle spacing given in the NWT regulations is less than the wheel spacing of HS trucks.

BRIDGE MEMBER CAPACITIES

The bridge member capacities may be calculated by using the capacity formulas in the load-factor designs as given in the AASHTO specifications (1). All the formulas given for the reinforced-concrete design are directly applicable to the rating. The capacity formulas for the prestressed-concrete and the structural-steel bridges require two modifications. One is to introduce a capacity or strength reduction factor (ϕ) to all the formulas. The other is to replace the ultimate strength with the yield strength if the ultimate strength is present in the formula.

The capacity reduction factor is normally less than 1, which will reduce the yield capacity to an available capacity for the estimated dead, live, and impact loads and other important loads if required. The remaining capacity ($1 - \phi$) is reserved to account for all the miscellaneous effects acting simultaneously with the estimated loads. These miscellaneous effects include aging and deterioration of the structures, variations in material strength, workmanship and dimensions, and so forth. The values of ϕ found in many design codes (1,3-5) do not take aging and deterioration into consideration. For use in the rating exercise, these values may be adjusted to suit the existing general conditions of the structures.

The use of the material yield strength instead of the ultimate strength is simply to emphasize the concept that the failure modes and permanent deformation are not considered in the rating of the bridges.

The following are a few commonly used capacity formulas for prestressed concrete and structural steel, which have been modified:

1. The flexural strength of a rectangular section of prestressed concrete is expressed as follows:

$$\phi M_y = \phi A_s^* f_y^* d[1 - 0.6p^*(f_y^*/f_c')] \quad (1)$$

where

A_s^* = area of prestressing steel,
d = distance from extreme compressive fiber to centroid of prestressing force,
f_c' = compressive strength of concrete at 28 days,
f_y^* = yield stress of prestressing steel,
M_y = yield moment strength of a section,
p^* = ratio of prestressing steel, and
ϕ = capacity reduction factor.

The preceding formula is identical to that for reinforced concrete.

2. For structural steel Equations 2, 3, and 4 give bending, axial tension, and axial compression, respectively:

$$\phi M_y = \phi S F_y \quad (2)$$

$$\phi T_y = \phi A_n F_y \quad (3)$$

$$\phi P_y = 0.85\phi A_s F_{cr} \quad (4)$$

where

A_n = net effective area,
A_s = gross effective area,
F_{cr} = buckling stress,
F_y = yield stress of steel,
P_y = yield compressive strength,
S = elastic section modulus, and
T_y = yield tensile strength.

The compact sections will be treated the same as the noncompact sections, and the plastic section modulus will not be used.

BRIDGE RATING

The bridge rating is a measure of the bridge member capacity available for the maximum live and impact loads and is expressed as a number in terms of the regulation loads. A rating of 1.3 for a bridge member means that the member can carry 1.3 times the regulation load. Also, the rating can be regarded as the live-load factor.

The general equation for rating is as follows:

$$\text{Rating} = [(\phi - D)/\Sigma L(1 + I)](HSW/HS) \quad (5)$$

where

D = dead-load effect expressed as a fraction of yield capacity,
I = impact fraction,
L = live-load effect expressed as a fraction of yield capacity,
HS = HS loading used in analysis, and
HSW = HS measurements for the regulation loads.

If HS measurements are used in the analysis, Equation 5 becomes

$$\text{Rating} = (\phi - D)/\Sigma L(1 + I) \quad (6)$$

An example of the rating of an interior steel girder of a two-lane bridge for NWT regulation loads is outlined in the following. Girder characteristics are as follows: length, 85 ft; spacing, 8 ft; section: W36 x 260, $S = 952$ in.^{3}, $F_y = 36$ ksi; dead load, 0.8 kip/ft of girder length; live load, HS20 used for analysis; and design code, AASHTO specifications for 1977 (1).

1. Compute the yield moment capacity of W36 x 260:

$\phi M_y = \phi S F_y = \phi(952)(36)(1/12) = 2{,}856\phi$ ft•kip,
$M_y = 2{,}856$ ft•kip.

2. Compute dead-load moment and D at midspan:

$M_D = 0.125(0.8)(85)^2 = 722.5$ ft•kip,
$D = 722.5/2{,}856 = 0.253$ ft•kip.

3. Compute maximum live-load moment (M_L) and L. The distributions of wheel loads for the concrete deck are 8/5.5 = 1.455 for two lanes and 8/7.0 = 1.143 for one lane. From Table 1, for an 85-ft span the maximum moment near midspan is 1,254.7 ft•kip per lane for HS20. Then M_L and L are calculated as follows:

M_L = 0.5(1,254.7)(1.455) = 912.8 ft•kip for two lanes,
M_L = 0.5(1,254.7)(1.143) = 717.1 ft•kip for one lane,
L = 912.8/2,856 = 0.320 for two lanes, and
L = 717.1/2,856 = 0.251 for one lane.

4. Compute impact fraction:

I = 50/(85 + 125) = 0.238.

5. Compute the rating for a girder in good condition with ϕ = 0.9. From Table 2, for L_S = 85 ft, HS_m = 27.5. The following calculations are for both lanes loaded and one lane loaded:

Rating (both lanes) = [(0.9 - 0.253)/0.320(1 + 0.238)](20/27.5) = 1.188.

Rating (one lane) = [(0.9 - 0.253)/0.251(1 + 0.238)] x (20/27.5) = 1.514

The results indicate that the girder could carry about 20 percent overload for both lanes loaded and about 50 percent overload for only one lane loaded.

6. Compute the rating for a girder in a heavily corroded condition with ϕ = 0.75:

Rating (both lanes) = [(0.75 - 0.253)/0.320(1 + 0.238)](20/27.5) = 0.912.

Rating (one lane) = [(0.75 - 0.253)/0.251(1 + 0.238)] x (20/27.5) = 1.163.

The rating of 0.912 indicates that the girder would require either strengthening or posting if both lanes were frequently loaded.

7. Compute rating for the same condition as in step 6 except that only one-half the impact load is used:

Rating (both lanes) = [(0.75 - 0.253)/0.320(1 + 0.119)](20/27.5) = 1.009.

Rating (one lane) = [(0.75 - 0.253)/0.251(1 + 0.119)] x (20/27.5) = 1.287.

Low speed may be posted to reduce impact. The girder could still carry about 30 percent overload if single-lane traffic at reduced speed is enforced.

DISCUSSION

Instead of indiscriminately using a standard loading in the evaluation of bridges, the approach and the method of rating presented here would enable practicing engineers to use their own judgment in dealing with local and many particular traffic conditions.

The rating example shows that there are many ratings for many different traffic conditions. It is believed that the rating results are easily understood by engineers, truckers, and regulation enforcement agencies. On the other hand, a rating based on a standard loading would only indicate whether the structure was adequate for that loading. Decisions made according to such a rating would be questionable if the regulation loads are actually carried by the bridges. Any loading that does not represent the actual traffic loads could result in either an uneconomical use of the bridge materials or an unsafe structure. In general, upgrading for the standard HS loading would often result in higher cost for shorter bridge members and lower cost for longer members, whereas upgrading for the regulation loads would yield the opposite results.

In order to have accurate ratings, many aspects need to be considered. One way of simulating the regulation loads is offered in this paper. Other aspects, such as the determination of member capacities and the methods of structural analyses, must depend on the judgment of the practicing engineers for accuracy. The reason for choosing the HS configuration as a measuring device is that the HS loading has been commonly used in the past and thus it is familiar to bridge engineers and will retain the usefulness of the old calculations.

The technique used in the rating could also be adopted in design. The corresponding HS measurements may be used instead of the standard HS20 loading if the bridge is to be designed to carry the regulation loads. It is seen in Table 2 and Figure 1 that bridge members having different span lengths would have different HS measurements. If the design live loads closely resembled the regulation loads, the load factor applied to the live load in the AASHTO specifications could be appreciably reduced.

The treatment of other load effects, such as live-load deflection, fatigue, and the uncracked condition of the prestressed-concrete section, are beyond the scope of this paper. In the current codes (1,3-5) these effects are dealt with under specified service loads. It is suggested that the service loads also be scrutinized and that some of the effects may be redefined. For instance, suppose that a live-load deflection under a given service load exceeds the code limit. What is to be done about this? Is the strengthening of the member required or should the deflection be ignored? Also, how can the tension allowed in the precompressed tensile zone of a prestressed-concrete section with bonded reinforcement be maintained under a load heavier than the service load? The tension would disappear forever when the service load was exceeded and the section became permanently cracked.

The concept of the load measure is quite different from that of the standard loading. Essentially, a standard loading must be related to a set of traffic conditions, which are largely based on a survey, and the method of determining a standard loading is usually a statistical one. Unless the survey data are inclusive and timeless and the statistical assumptions are accurate enough, the standard loading would not be able to cope with all traffic conditions. On the other hand, because a load measure has no built-in assumptions of any traffic condition, it is able to measure the load effects of any loading adequately.

CONCLUSION

For more realistic ratings, it is important to use the regulation loads in conjunction with local traffic conditions. There will be different ratings for different traffic conditions. A load measure is more adaptable than a standard loading in simulating the regulation loads. The rating procedure presented has been applied satisfactorily in the strengthening programs of many Canadian federal bridges and is believed to be simple, direct, and practical.

ACKNOWLEDGMENT

The author acknowledges many contributions and sug-

gestions made by his colleagues R.H. Pion, G.S. Hibbert, and H.I. Nadler and expresses thanks to J.C. Beauchamp, Chief Bridge Engineer of Public Works Canada, for his permission to apply the rating procedure in the strengthening programs of many federal bridges.

REFERENCES

1. Standard Specifications for Highway Bridges. AASHTO, Washington, D.C., 1977.
2. Large Vehicle Control Regulations. Northwest Territories, Canada, March 31, 1974.
3. Design of Highway Bridges. CAN3-S6-M78. Canadian Standards Association, Rexdale, Ontario, Canada, 1978.
4. Steel Structures for Buildings--Limit-State Design. CAN3-S16.1-M78. Canadian Standards Association, Rexdale, Ontario, Canada, 1978.
5. Ontario Highway Bridge Design Code. Ministry of Transportation and Communications, Downsview, Ontario, Canada, 1979.

Publication of this paper sponsored by Committee on Structures Maintenance.

The opinions expressed in this paper are those of the author and not necessarily those of Public Works Canada.

A Rational Procedure for Overweight Permits

BAIDAR BAKHT and LESLIE G. JAEGER

ABSTRACT

A rational procedure for calculating safe permit loads for vehicles as governed by the bridges on the route without having to analytically evaluate all the bridges is given. The basis of the procedure is the worst combination of maximum vehicle weights that a bridge is likely to have sustained during its lifetime. With the severest load combination as the datum, maximum increases over legal loads for normal traffic are calculated for control vehicles. Expressions for calculating the modification factors corresponding to two- and three-lane loadings are also provided.

Applications are quite often made for permission to let a much heavier vehicle cross a bridge than that legally permitted for normal traffic. The maximum safe weight for such a vehicle can be obtained by an analytical evaluation of the bridge. Alternatively, according to the procedures developed in this paper, the maximum safe weight of a special-permit vehicle can be obtained from the heavy vehicle traffic that a bridge is known to have carried during its lifetime.

The design capacity of a highway bridge carrying normal traffic safely implicitly takes account of the following factors:

1. Legally permitted normal vehicle weights as represented by the design vehicle and possibly a portion of the live-load factor,
2. Bridge type,
3. Number of lanes on a bridge,
4. Length of span,
5. Accidental and deliberate exceedance of legally permitted weights,
6. Transverse vehicle position,
7. Simultaneous presence of more than one vehicle in the transverse direction,
8. Simultaneous presence of more than one vehicle in a lane,
9. Vehicle width, and
10. Vehicle speed as represented by the dynamic load allowance or impact factor.

In the case of a special-permit vehicle, factors 5-10 are either known beforehand with some degree of certainty or can be prescribed as a condition for the permit. More reliable knowledge of these factors can be used to advantage to permit a substantially heavy special-permit vehicle without compromising the safety of the structure.

A safe estimate of the maximum load of a special-permit vehicle for a bridge can be obtained by the procedure given here without analytical evaluation of the structure. This procedure requires the knowledge of one of the following:

1. The maximum vehicle weights corresponding to the code-specified factors 1-10, given previously, that a bridge is capable of sustaining and
2. The worst combination of maximum vehicle weights that the bridge is likely to have sustained in its lifetime.

The former can be obtained from the design calculations but only if the design vehicle has a direct relationship with the actual vehicle weights, as it does, for example, in the case of the Ontario Highway Bridge Design Code (1,2). As pointed out by Buckland and Sexsmith (3), the AASHTO (4) design loads are not in close correspondence with actual traffic. Therefore, the knowledge that a bridge has been designed to AASHTO specifications is not always sufficient to establish the maximum vehicle weights that the bridge can sustain.

The determination of the maximum loads that a bridge is likely to have sustained in the past requires a probabilistic analysis, which is given in the following section.

PROBABILISTIC ANALYSIS

Factors 5-10 listed earlier are probabilistic in

nature. For example, it is not known beforehand what fraction of the total vehicle population will exceed legally permitted weights nor what the probability is that such overweight vehicles will travel in extremely eccentric positions. It is usual to include the most unfavorable of these factors in design or evaluation calculations. However, calculations based on estimating the probability of individual occurrence of these unfavorable factors rapidly leads to the conclusion that certain combinations of them are extremely unlikely even once in the lifetime of a bridge. Hence it is suggested that it is unrealistic to design a new bridge on the basis that all of these factors are present simultaneously and to the maximum extent possible.

Similarly, in assessing the load-carrying capacity of an existing bridge it should not be assumed that the bridge has already safely carried a load combination in which all of the factors were simultaneously present at their worst. Instead it is recommended that a technique be used in which a realistic estimate is made of the worst combinations of normal traffic that have already been experienced and that this estimate be used as the basis for calculating the permissible size of an overweight vehicle.

The probability of the simultaneous presence of vehicles in two adjacent lanes is studied in the following simple example.

Example

Consider a two-lane bridge with a span 300 ft long that carries a low density of heavy trucks, estimated at 300 per day. Let it be supposed that the bridge is 20 years old and that the coefficient of variation of the heavy truck weights is 20 percent. The statistical distribution of heavy truck weights is assumed to be as shown in Figure 1. An estimate is sought of the probability that two trucks at least 60 percent heavier than the mean will be simultaneously situated on the middle third of the bridge, one in each lane, at least once during the 20-year life of the bridge.

It is first necessary to establish a time interval within which any given truck may be on the central 100 ft of the bridge. Taking a slow vehicle speed of 20 ft/sec, a time interval of 5 sec is postulated. From the properties of the normal distribution, it is found that 0.00135 of the total heavy vehicle population has weights of 60 percent or more above the mean. This fraction is shaded in Figure 1. Thus, the expected number of heavy vehicles per day that cross the bridge and are this heavy is 300 x 0.00135 = 0.405 vehicle per day.

In one day there are 1,728 time intervals of 5 sec each. Hence, the probability that a vehicle 60 percent or more heavier than the mean will be on the middle third of the span during any single 5-sec interval is $0.405\ (1/17{,}280) = 2.34 \times 10^{-5}$. The probability that two such vehicles will be present during any given 5-sec interval is the square of this quantity:

$$P = 5.47 \times 10^{-10} \tag{1}$$

The combination of a low probability that such an event will happen in a given 5-sec interval together with the large number of intervals that represent the lifetime of a bridge is ideally suited to the use of the Poisson distribution of probability of occurrence. With the customary notation, the probability that the stated occurrences will happen in any given 5-sec interval is denoted by p and the total number of time intervals by N. The product Np is the Poisson parameter α_1:

$$Np = \alpha_1 \tag{2}$$

If the probability of m occurrences is defined as P(m), the following equations are obtained by using Poisson distribution theory:

$$P(0) = \exp(-\alpha_1)$$

$$P(1) = \alpha_1 \exp(-\alpha_1)$$

$$P(2) = (\alpha_1^2/2!)\exp(-\alpha_1) \tag{3}$$

During the 20-year life of the bridge the total number of 5-sec intervals (N) is equal to 1.26×10^8. Hence α_1 is found to be 0.069, and Equations 3 then give the following:

$$P(0) = 0.933$$

$$P(1) = 0.063 \tag{4}$$

It is concluded that on the basis of the assumptions made it is unlikely (only a 6.7 percent chance) that the two vehicles, each at least 60 percent heavier than the mean, will be on the middle third of the bridge simultaneously.

However, the situation changes swiftly if the simultaneous presence of somewhat lighter vehicles is investigated. For example, for vehicles 40 percent heavier than the mean, α_1 is found to equal 19.65 and P(0) to be approximately 10^{-8}. Thus it is virtually certain that there will be two vehicles, each at least 40 percent heavier than the mean, simultaneously present on the middle third of the bridge at least once during its lifetime.

The large probability change associated with the reduction of the vehicle weight is at the basis of the generalized treatment given in the following. What is demonstrated in the foregoing is that

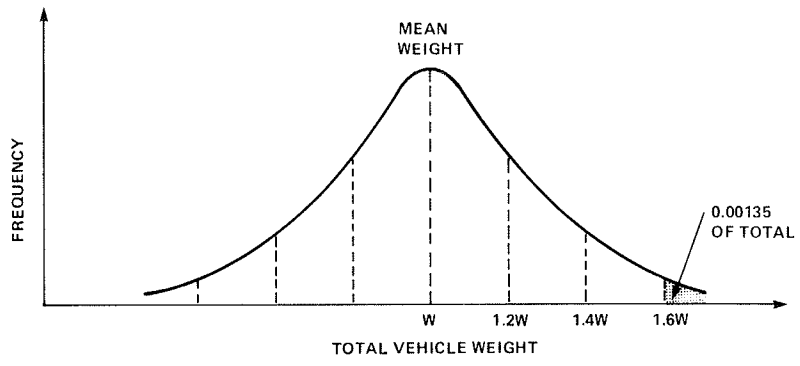

FIGURE 1 Assumed distribution of heavy vehicle weights.

changes in weight levels considered have effects many times larger than the values of other parameters. For example, if the time interval was estimated as 2.5 sec instead of 5 sec, the value of N would double. However, the same value of α_1 would be obtained by halving the value of P, and this would affect the load level only slightly.

Simultaneous Presence of Two Vehicles

For the multiple presence of vehicles, it is recommended that the Poisson approach be used. A value of the parameter α_1 is first selected, the value being so chosen as to make it likely that the event has already occurred in the life of the bridge. It is recommended that $\alpha_1 = 3.0$ on the basis that this corresponds to a 95 percent probability of at least one previous occurrence of the event. The weights of vehicles corresponding to this value of α_1 are then ascertained.

Let the two simultaneously present vehicles be r standard deviations above the mean of the vehicle weights, the number of vehicles per day crossing each lane of the bridge be n, the time interval for presence on the middle third of the bridge be T sec, and the previous life of the bridge be B years.

Figure 2 defines the fraction [q(r)] of all heavy vehicles that are at least r standard deviations higher than the mean. Values of q(r) for various r-values can be obtained from Figure 3.

The expected number of heavy vehicles per day that cross each lane of the bridge and have weights at least r standard deviations above the mean is nq(r). The probability of having such a vehicle present during any one time interval of T sec is Tnq(r)/86,400. Hence the probability (P) that two such vehicles will be simultaneously on the middle third of a span during a given interval of T sec is as follows:

$$P = T^2 n^2 [q(r)]^2/(86{,}400)^2 \quad (5)$$

The number of T-sec time intervals (N) in B years is given by

$$N = (B \times 365 \times 86{,}400)/T \quad (6)$$

Hence

$$\alpha_1 = \{B \times 365 \times T \times n^2 [q(r)]^2\}/86{,}400 \quad (7)$$

Adopting $\alpha_1 = 3.0$ as the criterion, Equation 7 gives

$$q(r) = (26.65/n)[1/BT]^{0.5} \quad (8)$$

From known values of B, T, and n, q(r) can be obtained from Equation 8, and values of r can be obtained from known properties of the normal distribution shown in Figure 3. The value of r thus obtained corresponds with 95 percent probability to the number of standard deviations above the mean for the weights of two trucks that will be simultaneously present on the middle third of the bridge during its previous history.

Using the procedure just described, values of r for B = 20 and 50 years and values of T = 3 and 5 sec were calculated for various values of n. These values are plotted in Figure 4 with respect to n.

Physical Significance of r

From the results of a vehicle weight survey, Csagoly and Knobel (5) confirmed that the distribution of heavy vehicles is indeed nearly normal. They also showed that the maximum observed loads corresponding to various base lengths (6) are approximately equal to $\mu + 3.5\sigma$, where μ is the mean heavy vehicle weight corresponding to a particular base length and σ is the relevant standard deviation. Values of r obtained from Equation 8 and plotted in Figure 4 imply that two vehicles of weight $\mu + r\sigma$ are most likely to be simultaneously present within the middle third of a span at least once during the time period considered. Thus the familiar modification factor F_2 for simultaneous loading of two lanes is given by

$$F_2 = (\mu + r\sigma)/(\mu + 3.5\sigma) \quad (9)$$

Substituting σ in terms of μ and the coefficient of variation (COV), Equation 9 can be rewritten as follows:

$$F_2 = [1 + r(COV)]/[1 + 3.5(COV)] \quad (10)$$

Values of F_2 for various time intervals T for B = 50 and 20 years and 20 percent COV are plotted in Figure 5. Thus if the value of F_2 is, for example, 0.90, it can be assumed that the bridge has at least once in its lifetime sustained in the middle third of its span two side-by-side vehicles, each of which weighed 0.90 times the maximum expected weight for a single vehicle.

Simultaneous Presence of Three Vehicles

The same approach that has been developed for two vehicles can be applied to investigate what the size of the vehicle will be such that three such vehicles will be simultaneously present with 95 percent probability during a given time period. Using the same

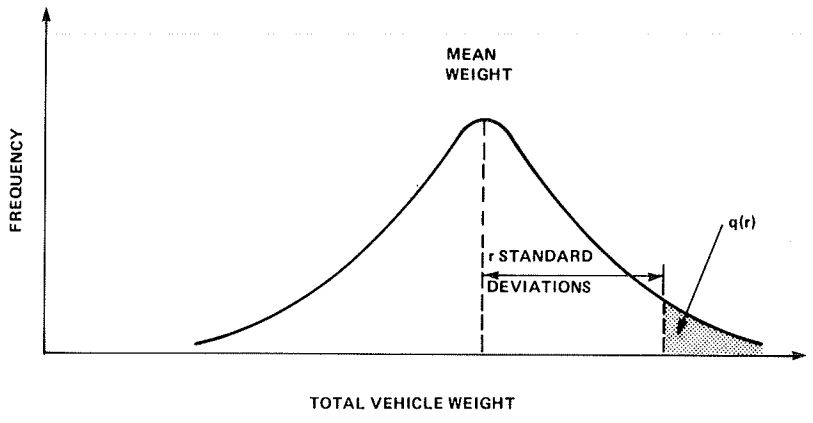

FIGURE 2 Vehicle weight distribution.

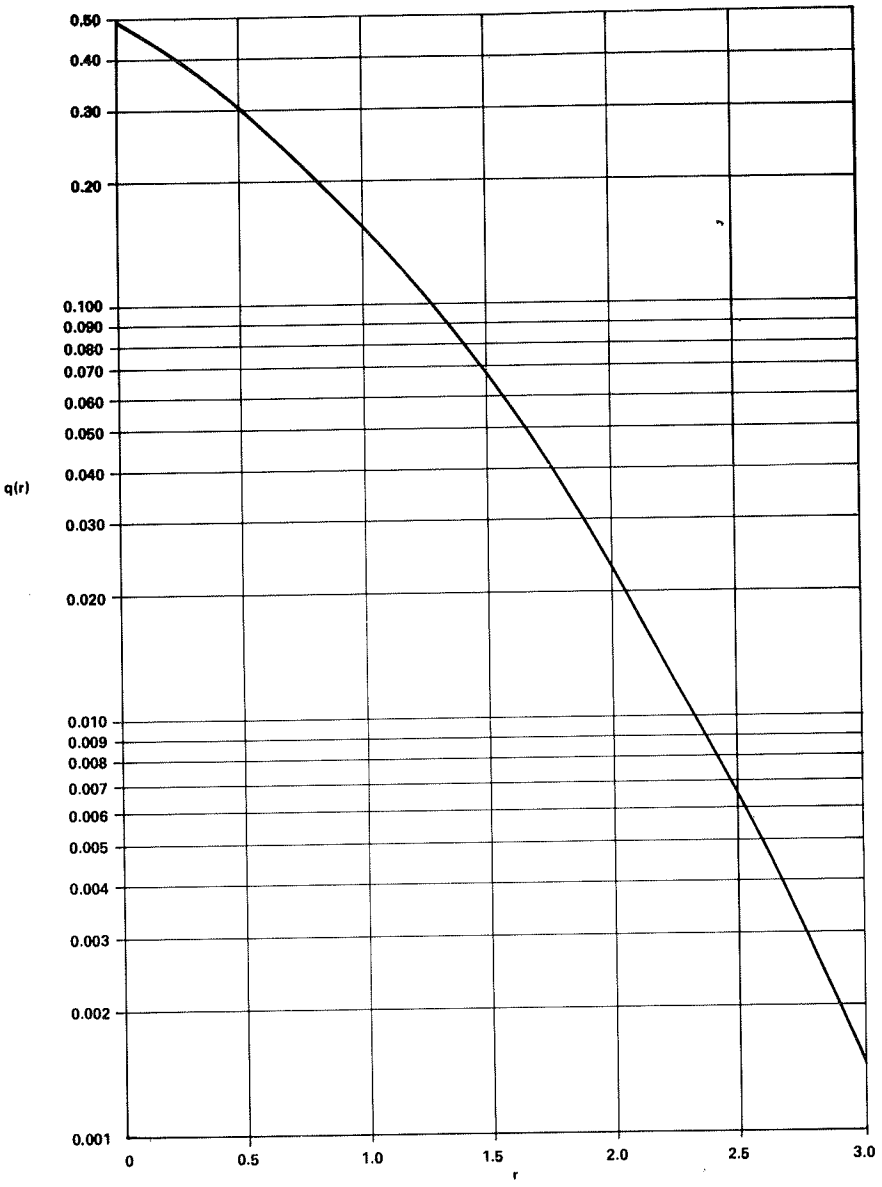

FIGURE 3 Variation of q(r) with r.

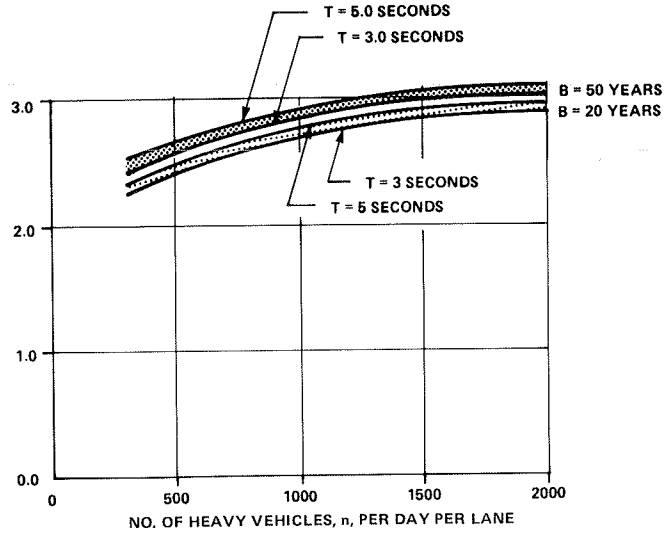

FIGURE 4 Values of r for simultaneous presence of two vehicles.

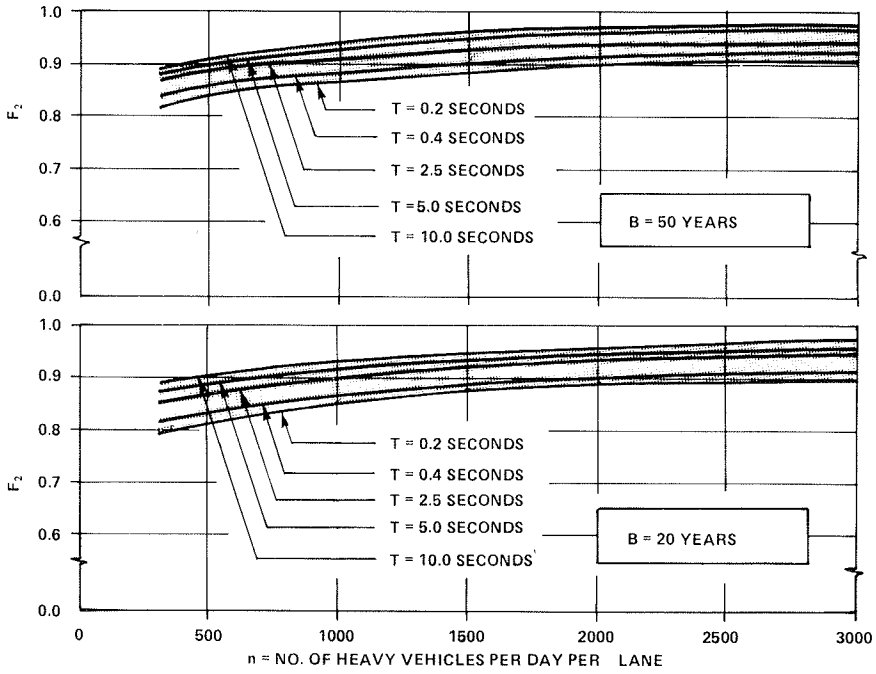

FIGURE 5 Two-lane loading modification factors for evaluation of safe overweights.

notation as before, the probability (P) that three such vehicles will be simultaneously present on the middle third of a span during a given time interval of T sec is as follows:

$$P = T^3 n^3 [q(r)]^3/(86,400)^3 \quad (11)$$

Substituting the value of N from Equation 6, α_1 is given by the following:

$$\alpha_1 = \{B \times 365 \times T^2 \times n^3 [q(r)]^3\} (86,400)^2 \quad (12)$$

Again adopting $\alpha = 3.0$ as the criterion, Equation 12 gives

$$q(r) = (394.41/n)[1/BT^2]^{0.33} \quad (13)$$

From Equation 13 the value of r can be obtained as for the case of two vehicles. The modification factor F_3 corresponding to the simultaneous presence of three vehicles is given by

$$F_3 = [1 + r(COV)]/[1 + 3.5(COV)] \quad (14)$$

Comments on Assumptions Made

In connection with the development of a design vehicle for the forthcoming bridge design code of the Canadian Standards Association (CSA), vehicle survey data from seven Canadian provinces were processed (Cheung and Agarwal, unpublished data). The COVs for heavy vehicles with different numbers of axles obtained from this study are plotted in Figure 6, which also defines the weight limit below which the vehicles were not included in the COV calculations. It can be seen that the value of COV generally decreases with the increase in the number of axles, suggesting a smaller spread of total weight for heavier vehicles.

Overall moments and shears in a bridge are usually governed by vehicles with five or more axles. For such vehicles, as shown in Figure 6, the COV for total weight rarely exceeds 20 percent, thus justifying the 20 percent value assumed earlier. A higher value of COV was not chosen because it would have resulted in a more benign value of the modification factor. The effect of changes in the COV values on F_2 is shown in Figure 7. It can be seen that a smaller COV leads to a more conservative value of F_2.

Derivation of the Poisson parameter α_1 has been based on finding two vehicles on the middle third of a bridge span. This fraction of the span is chosen because, in arriving at the longitudinal bending moments, a vehicle placed anywhere in the middle third of a span produces moments that are quite close to the maximum moments in the span. Similarly for longitudinal shears, the same kind of reasoning applies to the simultaneous presence of two vehicles in the end third of the span, and indeed the same reasoning can be applied to moments in continuous bridges.

The assumption that the maximum expected vehicle weight is equal to $(\mu + 3.5\sigma)$ is a safe one if the modification factors based on this assumption are used to assess the most severe load combination that a bridge may have experienced. However, if modification factors thus obtained are to be used for design purposes, it may be prudent to assume that the maximum expected vehicle weight is equal to $(\mu + 3.0\sigma)$. This revision of the assumption will lead to slightly larger, hence safer, values of the modification factors. With this assumption, modification factors for the simultaneous loading of two and three lanes, that is, F_2 and F_3, respectively, are calculated for various cases by the preceding procedure. Values thus obtained are plotted in Figure 8.

It is interesting to compare the previously calculated modification factors with those specified in the AASHTO (4) and Ontario (1) codes. The AASHTO specified values of F_2 and F_3 are 1.0 and 0.90, respectively. As can be seen in Figure 8, these values are safe upper limits for all cases shown, some of which are quite unrealistic. A high volume of heavy vehicle traffic, say, more than 1,000 vehicles per day per lane, is possible only when the speed of the vehicles is 55 mph or more. For such a

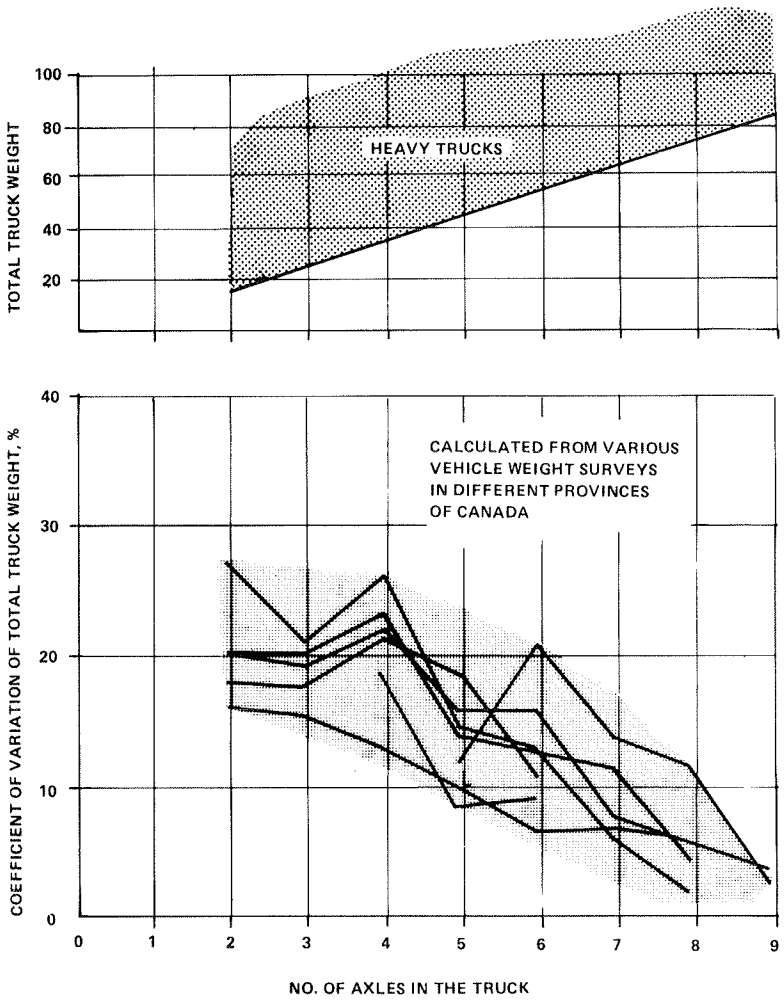

FIGURE 6 COVs of heavy truck weights.

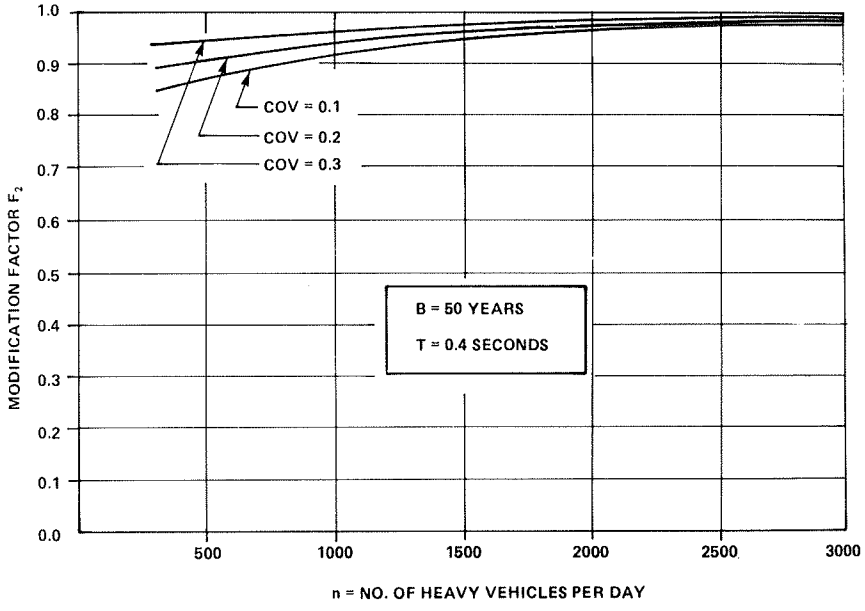

FIGURE 7 Effect of COV on F_2.

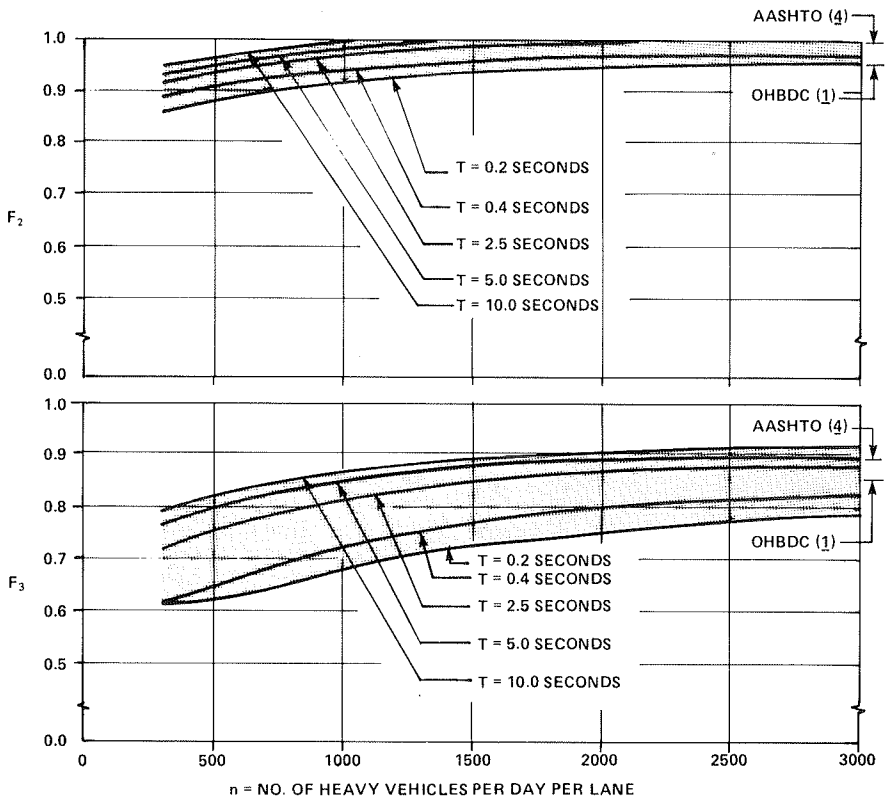

FIGURE 8 Modification factor for multilane loading for 50-year bridge life.

speed and a large span of 300 ft, T is equal to about 1.20 sec. For this case, the procedure gives F_2 and F_3 values of 0.96 and 0.79, respectively. Compared with these values, the AASHTO values of F_2 and F_3 appear quite conservative. The Ontario code (1) values of F_2 and F_3 are 0.95 and 0.85, respectively. These values compare well with the previously calculated values. It should be noted that in the second edition of the Ontario code (2) F_2 and F_3 values have been reduced to 0.90 and 0.80, respectively. These reductions result from the amalgamation of the modification factors for vehicle weights and dynamic load allowances, that is, impact factors (7), which were given different values in the first edition (1).

Application of Modification Factors

Although most bridges in North America are designed to the same specifications, legally permitted weights for normal traffic vary widely in different jurisdictions. These variations may represent conscious decisions to maintain certain margins of safety required by the various jurisdictions. Besides the vehicle weight regulations for normal traffic, maximum vehicle weights are the result of the accidental exceedance of legal weights and deliberate violations of weight laws. An estimate of the former can be obtained from the load factors given in the Ontario code (2) for normal traffic vehicles and for special-permit vehicles for which the loads can be closely obtained: The former is 1.40 and the latter, 1.25. Thus if it is ensured that the permitted weights will not be deliberately exceeded, normal traffic weights increased by a factor (R_1) of 1.40/1.25 = 1.12 may be permitted for special-permit vehicles flowing without restrictions with normal traffic.

It should be noted that the factor of 1.12 is applicable to Ontario and other jurisdictions with similar weight enforcement measures. In jurisdictions with strict enforcement, the factor should be reduced. It may, however, be prudent not to increase the factor beyond 1.15 even if the degree of enforcement is lenient. For most jurisdictions a factor of 1.10 may be appropriate.

An implicit assumption in the previous calculations is that during the bridge's lifetime, its load-carrying capacity remains unaffected. It is often argued that the condition of a bridge may change in such a way that at a given time it may not be able to safely carry the worst load combination that it once did. Such an argument may be convincing for unusually heavy test loads but not for normal traffic. If the condition of a bridge has changed so much that it is unable to carry the most severe load combination that it once did, the bridge is unsafe for normal traffic because such a load combination, being the result of chance, may occur again. In this paper only those bridges that are expected to carry normal traffic safely are involved.

If it is ensured that on a multilane bridge, a special-permit vehicle is the only one present, a single vehicle weight that would produce the same maximum effects as those produced by the most severe load combination can be calculated by procedures given in the following section.

DETERMINISTIC ANALYSIS

The permissible safe weight of a vehicle for a multilane bridge can be substantially increased above normal traffic weights if the vehicle is prescribed to travel along the bridge centerline and during its passage other vehicles are excluded from the bridge. An accurate assessment of this permis-

sible increase requires a knowledge of the load distribution properties of the bridge. In this section a general method, which does not explicitly require the load distribution characteristics of the bridge, is developed for two-lane bridges. The conclusion could also be applied to bridges with more than two lanes with the knowledge that the results will be more conservative than those for two-lane bridges.

One Central Vehicle on the Bridge

It has been established (8; Jaeger et al., unpublished data) that for the purpose of load distribution, right single-span bridges can be idealized by two dimensionless parameters (α and θ). The former parameter establishes the relationship of the torsional properties of the bridge with its flexural properties; the latter is based on a relationship between the flexural properties of the bridge and its ratio of span to width. Expressions for the two parameters are given in the Ontario Highway Bridge Design Code (2) and by Jaeger et al., who show that bridges of different types have different but distinctly identifiable ranges of α. As shown in Figure 9, for timber bridges α is between 0.001 and 0.02; for slab-on-girder bridges with steel or concrete girders α is between 0.06 and 0.2; for slab, voided-slab, and cellular bridges α is equal to 1.0; and for box-girder bridges α is between about 1.5 and 2.0. For all bridges θ is between 0.5 and 2.5.

A bridge with the smallest α-value and the largest θ-value has the worst, that is, the most unfavorable, transverse load distribution pattern. Conversely, a bridge with the largest α-value and smallest θ-value is one in which the load distribution is as uniform across its width as is possible for bridges of its type.

Eight two-lane bridges representing those with the best and worst load distribution characteristics in the four categories mentioned earlier were analyzed by the orthotropic plate theory (9) for different load cases. The values of the characterizing parameters are shown in Table 1, and the width of the bridge together with the details of the various load combinations are given in Figure 10. The load case shown in Figure 10a corresponds to the most severe load combination according to the AASHTO specifications (4). The transverse vehicle positions also correspond to the most severe load combination according to the Ontario code (2). Normal transverse positions for vehicles in the two lanes are shown in Figure 10b. Figures 10c-f show centrally placed single vehicles with wheel spreads (distance between the two lines of wheels) of 1.83, 2.00, 2.50, and 3.0 m, respectively. The contact area for each concentrated load was the same as that used by Bakht et al. (8) and shown in Figure 10h.

If the intensity of longitudinal moments (M_X) is taken as the basis for equivalence, two load combinations are equivalent to each other if each of the two cases produces the same maximum intensity of longitudinal moments. Using this criterion and taking the load case shown in Figure 10a as the datum, the percentage of increase (K) in vehicle weight for the other five load cases was calculated from the orthotropic plate analyses. It is noted

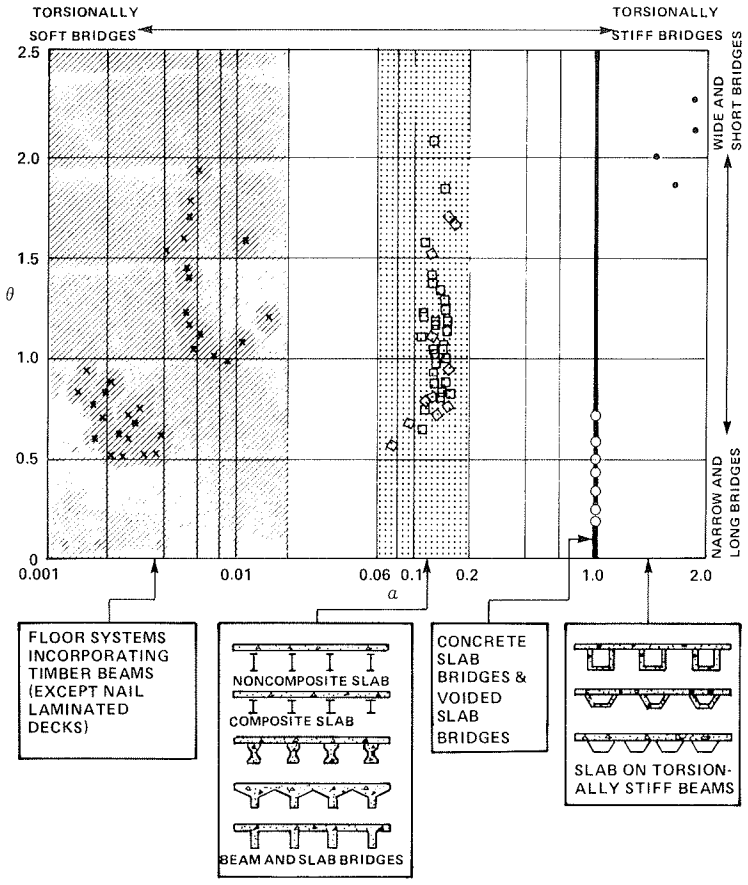

FIGURE 9 Values of α and θ for practical bridges.

that the datum load case corresponds to the most severe transverse position as specified by the AASHTO and Ontario codes. The percentage of increase depended on the bridge type and also on whether the bridge had the worst load distribution characteristics or the best. For each bridge type, the governing value of K was taken to be the smaller of the two for the best and the worst load distributions. It was found that going from the datum load case to the case with two vehicles in normal traveling positions (Figure 10b) did not result in any significant advantage for slab bridges; for box-girder bridges, the weights could be increased 3 percent, for slab-on-girder bridges 5 percent, and for timber bridges 8 percent. K is significant for single vehicles and depends on the bridge type and the wheel spread. Values of K for the datum case under consideration are plotted as case I in Figure 11 with respect to different values of wheel spread (W). As shown in Figure 11, values of K are the same for timber bridges and slab-on-girder bridges.

The preceding exercise was repeated by using the load case shown in Figure 10b as the datum. The resulting values of K are plotted as case II in Figure 11. This datum load case corresponds to the normal traveling positions of two vehicles. Thus case II in Figure 11 can be used when the only information available about the bridge is that it has been carrying normal traffic safely.

The curves for K-values given in Figure 11 for a specific bridge type can be used to calculate the permissible weight if the special-permit vehicle is known to traverse only one bridge or one type of bridge. Alternatively, when the vehicle has to pass over several bridges, the curves for timber bridges, which give the smallest values of K, can be used.

The curves given in Figure 11 are based on the assumption that each axle has two concentrated loads for which the effective contact region is as shown in Figure 10h. Axles with wider wheel spreads may each have four sets of double tires, resulting in four concentrated loads instead of the two assumed in the analysis. For such cases, the actual values of K will be higher than those given in Figure 11.

K-values given in Figure 11 correspond to two normal vehicles with full loads, that is, vehicles with maximum weights. As discussed earlier, a bridge may not have experienced two such vehicles in its

TABLE 1 Values of α and θ Used in the Analyses

	Load Distribution by Type of Bridge							
	Timber		Slab on Girder		Slab and Voided Slab		Box Girder	
Parameter	Worst	Best	Worst	Best	Worst	Best	Worst	Best
α	0.06	0.06	0.06	0.30	1.00	1.00	1.50	2.00
θ	2.0	0.5	2.0	0.5	1.5	0.5	2.5	1.5

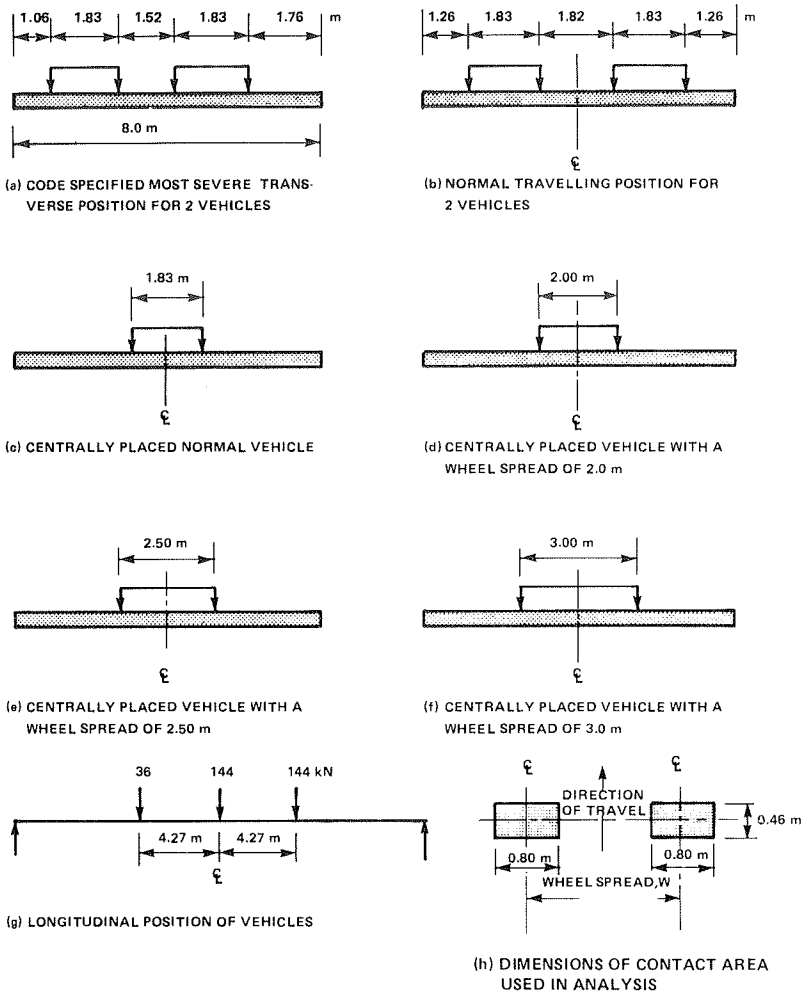

FIGURE 10 Details of loads.

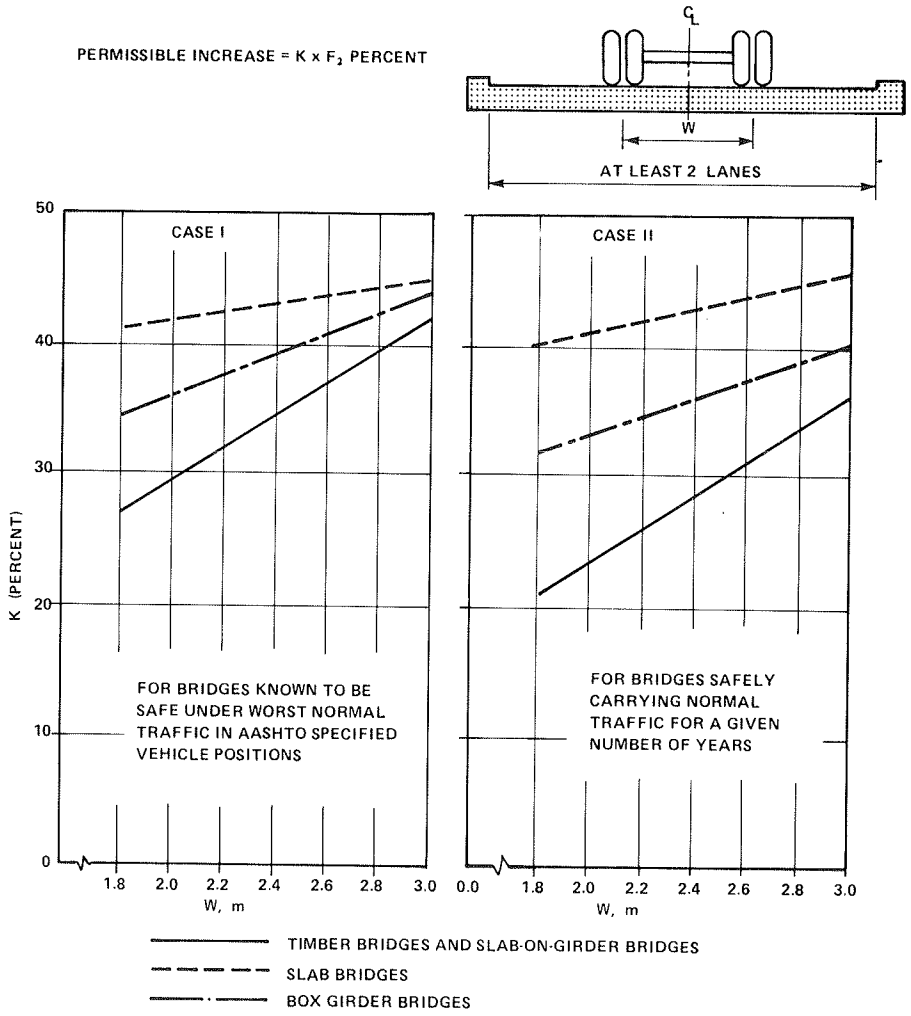

FIGURE 11 Values of K for single vehicles.

lifetime. However, it is certain that the bridge would have sustained two vehicles of weights equal to F_2 times full weight. Thus the factor R_2 by which a single vehicle weight can be increased to account for the presence of two vehicles is given by

$$R_2 = F_2[(1 + K)/100] \quad (15)$$

Long Spans

For the AASHTO HS20 loading, a single design vehicle governs moments for spans of up to 140 ft, and for the Ontario code this limit is about 80 ft. For both codes the design loadings beyond these limits incorporate a uniformly distributed load to account for the effect of more than one vehicle in a lane. The ratio of simple-span moments due to a single design vehicle and the corresponding moment due to the design loading incorporating the lane load is denoted by R_3. Values of R_3 corresponding to various simple spans are plotted in Figure 12 for both the AASHTO and Ontario loads. These curves can be used to estimate a permissible increase beyond the normal for the special-permit vehicle weight on longer spans if other vehicles are excluded from the bridge. The curves corresponding to the Ontario loads may be found to be more appropriate because, unlike the AASHTO loads, they are based on modern traffic conditions.

Dynamic Load Allowance

By restricting the speed of the permit vehicle on a bridge, the dynamic load allowance (DLA), which is usually known as the impact factor, can be reduced. Advantage can be taken of this reduced DLA in permitting a proportionally higher weight for the permit vehicle.

The Ontario code (2) specifies that the DLA for a single controlled vehicle crossing a bridge at restricted speed can be multiplied by the following reduction factors:

1. For a speed limit of 6 mph or less, 0.30;
2. For speed limits between 6 and 15 mph, 0.50; and
3. For speeds in excess of 15 mph, 1.0.

In arriving at an increase of the static vehicle weight that is equivalent to the reduction of the DLA, it should be remembered that the total load effects due to a single control vehicle are being compared with those due to two normal vehicles. The increase of vehicle weight to account for the reduction of the DLA is denoted by R_4. Taking 0.25 as the smallest DLA value specified by the Ontario code (2) and 0.7 as the modification factor for DLA due to two vehicles (1), R_4 for vehicle speeds of less than 6 mph is obtained as follows:

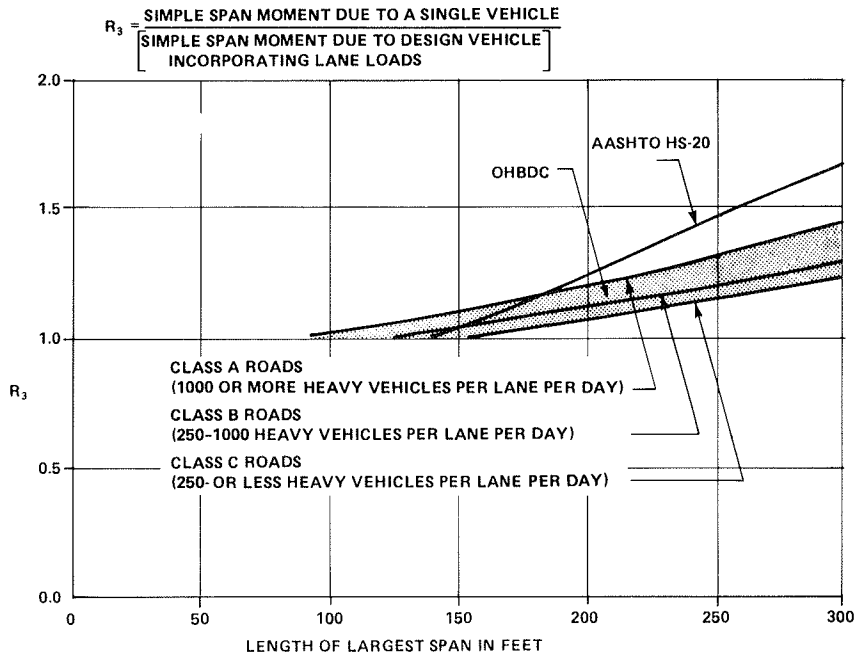

FIGURE 12 Values of R_3 for AASHTO and Ontario loads.

$$R_4 = (1 + 0.25 \times 0.7)/(1 + 0.25 \times 0.3) = 1.09 \quad (16)$$

R_4 for speeds between 6 and 15 mph works out to 1.04. It is noted that taking higher values of DLA would have resulted in larger and therefore less conservative values of R_4.

SUMMARY OF PROCEDURE

For a special-permit vehicle traveling along the centerline of a bridge with at least two lanes and with other traffic excluded from the bridge, an estimate of permissible vehicle weight increase above legal loads for normal traffic can be obtained as follows:

1. Allowance for confidence in weight: The factor R_1 accounts for the confidence that the weight of the permit vehicle will not be deliberately exceeded. Assume that R_1 is equal to at least 1.10.
2. Allowance for multilane loading: Using Equations 8 and 10 and assuming that COV = 0.2, calculate the value of F_2. Use T = 0.2 sec if there are many bridges involved in the trip. If the life of the bridge is 20 or 50 years, read F_2 directly from Figure 5 corresponding to the number of heavy vehicles per lane per day on the highway under consideration. Remember that the smaller values of F_2 lead to more conservative results. Using the value of F_2, calculate R_2 from Equation 15.
3. Allowance for presence of more than one vehicle in one lane: If all bridge spans are larger than, say, 80 ft, corresponding to the smallest span, read R_3 from the relevant curve for the Ontario code, R_3 = 1.0.
4. Allowance of speed restrictions: For vehicle speeds less than 6 mph assume R_4 equal to 1.09; for speeds between 6 and 15 mph, take R_4 equal to 1.04. For higher speeds R_4 is equal to 1.0.
5. Total weight increase: The final factor, R, which combines all allowances, is equal to $1 + (R_1 - 1.0) + (R_2 - 1.0) + (R_3 - 1.0) + (R_4 - 1.0)$, or $(R_1 + R_2 + R_3 + R_4 - 3.0)$.

EXAMPLE

To illustrate the use of the method, the example of a two-lane slab-on-girder bridge having three spans of 131, 164, and 131 ft is considered. The bridge is 20 years old and safely carries an average of 1,000 vehicles per lane per day at an average speed of 55 mph. According to the vehicle weight regulations of the jurisdiction a certain five-axle truck in normal traffic is allowed to carry only 49 tons. The maximum weight that this vehicle can carry as a special-permit vehicle is derived as shown in the following paragraphs. These restrictions were imposed:

1. Strict control of weight,
2. Travel along bridge centerline,
3. Travel speed on bridge less than 6 mph,
4. Other traffic excluded from the bridge, and
5. Wheel spread increased to 9 ft.

Because of weight control, R_1 is taken as 1.10.

For the middle third of the 131-ft span, T = 0.53 sec. From Figure 5 for B = 20 years, n = 1,000, and T = 0.53 sec, F_2 is approximately equal to 0.86. From case II of Figure 11, K is equal to about 33 percent for slab-on-girder bridges and W = 9 ft. Thus from Equation 15,

$$R_2 = 0.86\ [1 + (33/100)] = 1.17.$$

From Figure 12, for a span of 131 ft, R_3 is nearly equal to 1.0.

For vehicle speeds of less than 6 mph, R_4 = 1.09. Therefore,

$$R = 1.10 + 1.17 + 1.00 + 1.09 - 3 = 1.36.$$

The maximum permitted vehicle weight is therefore equal to 1.36 x 49 = 66.64 tons.

If an evaluation had shown the bridge to be safe for normal traffic corresponding to the most severe transverse load positions and the modification factor F_2 according to the AASHTO specifications (4), F_2 would be equal to 1.0, and case I of Figure 11 would give K = 40 percent. Then

$$R_2 = [1 + (40/100)] = 1.40.$$

In this case R would be equal to 1.59 and the permitted vehicle weight would be equal to 78.84 tons.

CONCLUSIONS

It has been shown that the modification factors for multilane loading can be obtained statistically and that these factors depend on the life of the bridge, the number of vehicles per day, the length of the span, and the speed of the vehicles. Expressions are developed for calculating this factor for two- and three-lane loadings. The corresponding AASHTO (4) factors are found to be quite conservative, whereas those of the Ontario code (1), although calculated by a different procedure, were found to be more realistic. A method is developed by which safe maximum weights for special-permit vehicles can be obtained without analytically evaluating the bridges on the route.

REFERENCES

1. Ontario Highway Bridge Design Code, 1st ed. Ministry of Transportation and Communications, Downsview, Ontario, Canada, 1979.
2. Ontario Highway Bridge Design Code, 2nd ed. Ministry of Transportation and Communications, Downsview, Ontario, Canada, 1983.
3. P.G. Buckland and R.G. Sexsmith. A Comparison of Design Loads for Highway Bridges. Canadian Journal of Civil Engineering, Vol. 8, 1981, pp. 16-21.
4. Standard Specifications for Highway Bridges. AASHTO, Washington, D.C., 1977.
5. P.F. Csagoly and Z. Knobel. The 1979 Survey of Commercial Vehicle Weights in Ontario. Research Report 221. Ministry of Transportation and Communications, Downsview, Ontario, Canada, July 1981.
6. P.F. Csagoly and R.A. Dorton. Proposed Ontario Bridge Design Load. Research Report 186. Ministry of Transportation and Communications, Downsview, Ontario, Canada, Oct. 1973.
7. Commentary to the Ontario Highway Bridge Design Code, 2nd ed. Ministry of Transportation and Communications, Downsview, Ontario, Canada, 1983.
8. B. Bakht, M.S. Cheung, and T.S. Aziz. Application of a Simplified Method of Calculating Longitudinal Moments to the Proposed Ontario Highway Bridge Design Code. Canadian Journal of Civil Engineering, Vol. 6, No. 1, 1979.
9. A.R. Cusens and R.P. Pama. Bridge Deck Analysis. Wiley, London, 1979.

Publication of this paper sponsored by Committee on Structures Maintenance.

Bridge Weight-Limit Posting Practice in the United States

ROY A. IMBSEN and RICHARD V. NUTT

ABSTRACT

Bridge weight limits allow the continued, limited use of a weak bridge that would otherwise present a significant safety hazard while protecting the legal and economic interests of the bridge owner. For weight limits to be effective, however, bridges must be posted for the proper weight limit, and the posting must be observed and enforced. The federal government became involved in bridge weight-limit posting in 1968 with the creation of National Bridge Inspection Standards (NBIS), which required states to inspect, inventory, and evaluate bridges on federal-aid routes. Weight-limit posting was required for bridges found to have insufficient structural capacity. The results of a survey of state posting practices are presented and the findings of a study on weight-limit posting in the United States are summarized. NBIS provides some engineering guidance for inspecting, evaluating, and posting highway bridges, but considerable engineering judgment is still required to fill the gaps. As a result, even within the limits set by NBIS, engineering practices vary among the states, which leads to differences in posting methods. This is evident from the results of the survey of the states. Development of a simple, uniform posting criterion by which the legitimate differences that exist between states can be rationally considered is recommended.

The United States is currently faced with a massive bridge replacement and rehabilitation problem. FHWA has estimated that there are currently more than 126,600 structurally deficient bridges within the United States (1). Many of these bridges should be rehabilitated or replaced, but they must compete for funding with an equally large number of bridges that have become functionally obsolete because of narrow widths and poor alignments. Because of the cost of modernizing all bridges on the U.S. highway system, it is necessary to delay improvements on many of these bridges for several years. In the meantime, it will be necessary to regulate the traffic on these bridges. This is normally done by establishing weight limits for vehicles using the bridge.

The weight and axle configuration of vehicles allowed to use the highways without special permits is governed by statutory law. In most states, this

legal weight limit is 80,000 lb or less, but several states allow higher weights. Michigan, which has the highest, allows nonpermit vehicle weights of 154,000 lb. Weight limits on deficient bridges are used to further restrict nonpermit vehicle weights. Failure to establish weight limits on a bridge with insufficient strength to carry the legal vehicle weight may subject the bridge owner to liability claims for injuries or damage resulting from a bridge failure. Weak bridges without weight limits may also become damaged, necessitating excessively costly repairs and unwarranted inconvenience to motorists.

In establishing bridge weight limits, the need to protect safety and property must be weighed against the need for an unrestricted highway system that enhances economic activity. Because some of the parameters are not clearly defined, it requires considerable judgment to achieve a balance. Thus, bridge weight-limit posting practices are not always uniform. Some of the administrative and engineering aspects of current bridge-posting practices in the United States are summarized in this paper, including the differences and similarities in the practices of the various states. This information was obtained from a survey of the states conducted by Engineering Computer Corporation as part of a study by NCHRP.

WEIGHT-LIMIT POSTING PROCESS

Bridge weight-limit posting, hereafter referred to as posting, is closely related to bridge maintenance inspection and structural strength evaluation. When a bridge is found to have insufficient structural capacity, weight-limit posting is only one of several available alternatives. The speed and volume of traffic can also be regulated. In many cases, standard evaluation methods may be overly conservative. When such an evaluation is questioned, a more detailed analysis or physical testing can often demonstrate the true strength of the bridge. A careful monitoring of the physical condition and load history of a marginally deficient bridge through frequent inspections could eliminate the need for posting. Minor repairs or reinforcement of weak components that can be made quickly and at a relatively minor cost are also alternatives to posting. Because of the severe restrictions imposed by posting, each of these alternatives should be given serious consideration.

Signs must be placed near bridges to clearly indicate to motorists the weight limits. Although standard signing is included in the Manual of Uniform Traffic Control Devices (MUTCD) (2), many jurisdictions have found it necessary to deviate from these standards to avoid ambiguities that could lead to misinterpretation under the provisions of their own weight-limit laws. The method of notifying the public of bridge weight limits also varies among the states.

Posted bridges remain an integral part of the highway system and must be operated accordingly. Continued inspection, usually at more frequent intervals and in greater detail than routine bridge inspections, will be necessary to detect any distress or deterioration that could affect structural strength.

Enforcement of bridge postings is important because a significant number of bridge failures have resulted from the use of a posted bridge by overweight vehicles. Proper maintenance of posting signs is necessary to make a posting enforceable.

Finally, it may be in the public interest to allow overweight vehicles to use posted bridges under strictly controlled conditions. This special allowance is often made through the overweight-permit process, but it may also be mandated by state law for certain types of vehicles.

The bridge-posting procedure, including its relationship to other aspects of bridge maintenance engineering, is summarized in the flowchart shown in Figure 1.

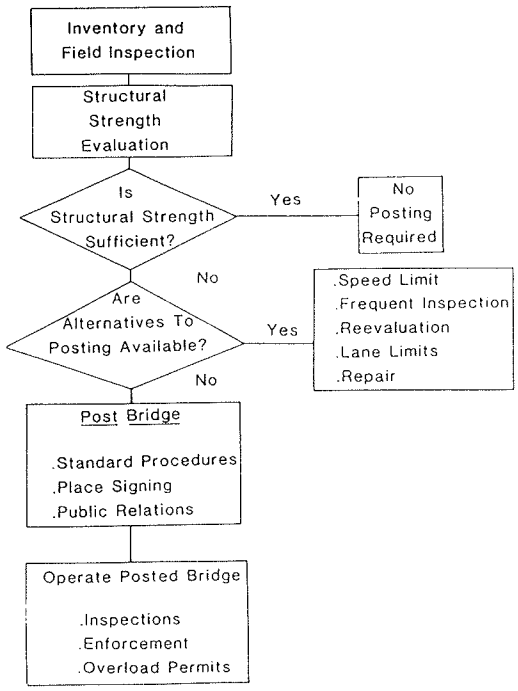

FIGURE 1 Bridge-posting procedure.

NATIONAL BRIDGE INSPECTION STANDARDS

In 1968, in the wake of the collapse of the Silver Bridge over the Ohio River at Point Pleasant, West Virginia, Congress passed the Federal-Aid Highway Act, which called for the development of National Bridge Inspection Standards (NBIS) (23 CFR, Section 650, 1968).

NBIS was developed by the U.S. Department of Transportation in consultation with state highway departments and other interested and knowledgeable parties. NBIS currently requires states to inventory their bridges and to inspect them at least once every 2 years. Specific items have been established that must be included in the inventory data. Those in charge of bridge inspection organizational units must be registered engineers or have 5 years of bridge inspection experience and must complete a comprehensive training course based on the bridge inspector's training manual, which was developed by a joint federal-state task force.

NBIS also requires that every bridge be rated for its safe live-load-carrying capacity according to guidelines in the manual published by AASHTO entitled Manual for Maintenance Inspection of Bridges (3), hereafter referred to as the AASHTO manual. When these ratings indicate that a bridge has insufficient strength to carry legal-weight vehicles, NBIS requires that the bridge be posted for reduced live loads.

Subsequent federal legislation made matching funds available for bridge rehabilitation and replacement. The Surface Transportation Assistance Act of 1978 extended the federal program to include bridges not on the federal highway system. This

legislation included the requirement that the inventory and inspection of these off-system bridges comply with the requirements of NBIS. As a result of this legislation, virtually every highway bridge in the country was made subject to NBIS requirements.

The AASHTO manual, in addition to prescribing inspection procedures, also discusses the rating of bridges and provides specifications for checking the capacities of existing bridges. The specifications are written to allow for variations in practice. Specific reference is made in many instances to the use of engineering judgment in determining loadings, resistance, and structural response. In addition, two levels of load-limit rating are described. One level, the inventory rating, is the load level that can safely use an existing structure for an indefinite period of time. The other level, the operating rating, is the maximum load level permissible under any circumstances. Because the AASHTO manual requires bridge weight limits to be set between the inventory and the operating ratings, there is considerable variation in posting practices among the various state and local jurisdictions.

CURRENT STATUS OF BRIDGE POSTING

A 1981 spot check conducted for Congress by the United States Comptroller General (4) indicated that several states were not in total compliance with the NBIS posting requirements. This lack of compliance occurred mainly at the local government level. The problem at the local level is compounded by the location of most of the nation's highway bridges in need of posting on local, off-system roads.

Engineering Computer Corporation (ECC) surveyed the state highway departments to determine bridge-posting practices in the United States. The statistics on the number and types of posted bridges for each of the states responding to the survey are summarized in Table 1. Although a few states did not respond, these statistics bring out some important features of current U.S. bridge-posting problems.

Few bridges on the Interstate highway system were reported as being posted. There are at least two reasons for this lack of posting. One is that the Interstate system is relatively new and constructed to high design standards. The other is that the

TABLE 1 Bridge Posting Statistics, 1983

State	Interstate		Other Federal Aid		Off-System		Total	
	No. of Bridges	No. Posted	No. of Bridges	No. Posted	No. of Bridges	No. Posted	No. of Bridges	No. Posted
Alabama	1,058	0	6,387	221	7,897	964	15,342	1,185
Alaska	120	1	420	18	310	27	850	46
Arizona	–	–	–	–	692	55	5,032	72
Arkansas	622	0	5,206	439	8,860	1,495	14,708	1,934
California	–	–	–	–	–	–	24,116	676
Colorado	959	0	2,615	100	3,895	1,908	7,469	2,008
Connecticut	754	0	2,314	102	1,662	149	4,730	251
Delaware	–	–	–	–	244	70	686	96
Florida	1,416	0	4,055	120	3,555	555	9,026	675
Georgia	–	–	–	–	6,738	797	6,738	797
Hawaii	103	0	599	53	402	63	1,104	116
Idaho	–	–	–	–	–	–	–	–
Illinois	1,861	0	5,939	99	17,272	2,159	25,072	2,258
Indiana[a]	1,809	0	3,350	78	10	2	5,169	80
Iowa	644	0	6,715	–	20,127	–	27,486	–
Kansas	1,301	0	9,071	2,202	14,543	6,087	24,915	8,289
Kentucky	–	–	–	–	–	–	–	–
Louisiana	1,201	0	4,644	222	8,787	1,119	14,632	1,341
Maine	225	0	1,044	15	1,406	115	2,675	130
Maryland	487	0	1,420	27	268	18	2,175	45
Massachusetts	915	0	2,457	450	1,165	418	4,537	868
Michigan	1,054	0	4,598	484	4,517	1,948	10,169	2,432
Minnesota	1,158	0	4,429	279	7,828	1,842	13,415	2,121
Mississippi	937	16	6,620	2,234	9,951	0	17,508	2,250
Missouri	1,107	0	7,317	1,493	15,383	2,496	23,807	3,869
Montana	779	0	1,593	50	2,912	453	5,284	503
Nebraska	330	0	4,806	1,137	11,270	4,704	16,406	5,841
Nevada	465	0	498	3	212	11	1,175	14
New Hampshire	372	0	1,159	24	1,926	556	3,458	580
New Jersey	626	0	2,672	320	1,754	488	5,090	808
New Mexico	1,087	0	1,825	39	638	28	3,550	67
New York	1,690	0	7,177	169	8,381	1,675	17,248	1,844
North Carolina	–	–	–	–	–	–	–	–
North Dakota	405	0	1,511	77	3,839	670	5,755	947
Ohio	2,176	0	9,912	619	16,787	6,004	28,875	6,623
Oklahoma	1,541	0	6,476	201	14,551	2,376	22,568	2,577
Oregon	–	–	–	–	–	–	–	–
Pennsylvania	–	–	–	–	–	–	21,300	3,466
Rhode Island	144	0	425	27	124	26	693	53
South Carolina	519	0	3,622	111	4,979	1,056	9,120	1,167
South Dakota	480	0	2,326	326	4,230	2,334	7,036	2,660
Tennessee	1,286	0	6,887	576	9,381	5,539	17,554	6,115
Texas	6,898	0	19,471	4	19,493	2,516[b]	45,820	2,520[b]
Utah	–	–	–	–	–	–	–	–
Vermont	385	0	841	43	1,357	186	2,583	229
Virginia	–	–	–	–	–	–	13,170	3,736
Washington	1,100	0	3,191	88	2,995	365	7,286	453
West Virginia	–	–	–	–	193	27	6,835	2,106
Wisconsin	849	0	5,336	72	6,579	1,242	12,764	1,314
Wyoming	995	0	984	30	892	165	2,871	195
Washington, D.C.	70	0	156	20	16	4	242	24

[a] State highway statistics only.
[b] Approximate number.

Interstate system is so important to U.S. economic and security interests that deficiencies are usually corrected relatively quickly.

More than 80 percent of the posted bridges are on local, off-system roads. The survey indicated that 21 percent of all local, off-system bridges are posted. In addition, many of the reported federal-aid bridges are probably owned by local jurisdictions. Many local bridges are not reported as being posted because some local agencies fail to comply with the NBIS posting requirements. Therefore, it follows that bridges with insufficient structural capacities are usually under the jurisdiction of local governments.

State bridge engineers were asked to estimate the number of bridge collapses over the past 10 years for four different bridge types on three different types of highway systems. Although their answers are only estimates, the results reported in Table 2 from the 45 states responding show some definite trends. Bridge failures are far more frequent with off-system bridges than with bridges on the federal-aid system. Many of the bridges that collapsed were not posted with a weight limit. Most failures occurred on steel or timber bridges, whereas reinforced-concrete bridges, which will show signs of distress before collapse, were not nearly so vulnerable. No collapses were reported for prestressed-concrete bridges, which are relatively modern in construction and design.

TABLE 2 Estimated Bridge Collapses During Past 10 Years

Route Type	No. of Collapses by Bridge Type			
	Steel	Timber	Reinforced Concrete	Prestressed Concrete
Interstate	0	0	0	0
Other federal aid	38	43	1	0
Off-system	169	344	1	0
Total	207	387	2	0

Note: 45 states responded to survey; number of bridges posted by type is as follows: steel, 127; timber, 144; reinforced concrete, 2; prestressed concrete, 0.

ADMINISTRATIVE ISSUES OF BRIDGE POSTING

Compliance with NBIS requires a close working relationship between state and local agencies. Not unexpectedly, many administrative problems have been encountered, including conflicts with existing state laws, local governments with insufficient resources to provide for necessary engineering, and a large number of weak local bridges for which few records are available. Despite the administrative difficulties, 28 of the 45 states responding to the ECC survey reported that they have completed the inventory of their off-system bridges. A report published for Congress on the status of the bridge replacement and rehabilitation program estimates that 98 percent of all off-system bridges had been inventoried as of December 31, 1981. The inventory of bridges on the federal-aid system is essentially complete.

In spite of the difficulties inherent in the NBIS requirements, more bridges are currently posted as a result of these standards. Table 3 shows the effect of the NBIS requirements on the number of bridges posted in the states surveyed by ECC.

The administrative practices related to implementing bridge postings and to operating and monitoring posted bridges also vary. There are variations in the ways states relate to the public, inspect posted bridges, enforce bridge postings, and issue permits for posted bridges.

TABLE 3 Effect of Federal Legislation on Number of Posted Bridges

Effect	No. of States
More than doubled	19
Increased 25-100 percent	7
Increased <25 percent	8
No increase	7
Reduced	1

Public Relations

In many cases there is considerable resistance to bridge posting from trucking companies, local residents, industry, or other individuals or groups who would be inconvenienced. The ECC survey of the states showed that state officials had different perceptions about the amount of public pressure and the degree of public confidence toward the posted weight limits within their states. In Figure 2 the opinions of state officials regarding the amount of public pressure against bridge posting are summarized. Figure 3 is a summary of the opinions of state officials about the level of public confidence in posted weight limits.

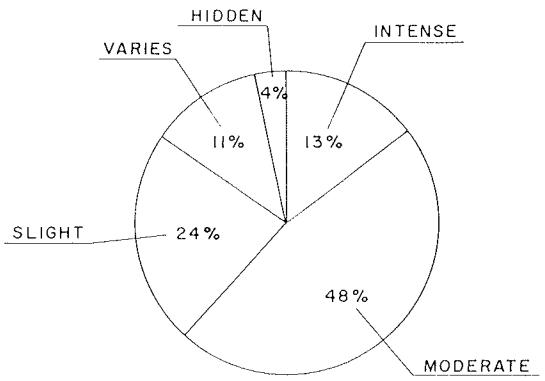

FIGURE 2 Perception of public pressure against posting by states.

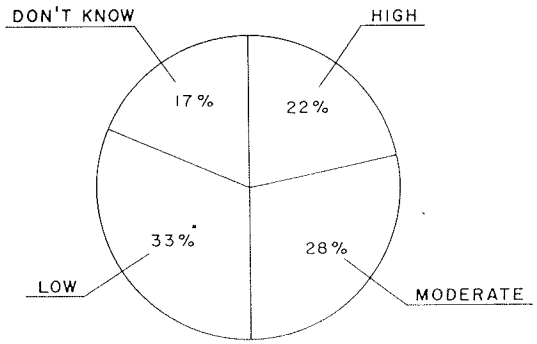

FIGURE 3 Perception of public confidence in posted load limits by states.

It is desirable to give advance notice of the posting so truckers can make arrangements to use detours or to limit their loads to the maximum weight allowed. When truckers are not informed of a scheduled posting, they are more likely to violate the weight limit. Various methods used by the

states to notify truckers of a posted bridge include news releases, special notification given to trucking associations, legal notices, published lists of restricted bridges, and advisory signs on routes with posted bridges. In Table 4 the methods used to notify the public are summarized and the number of states surveyed that use these methods is shown.

TABLE 4 Methods for Notifying Public of Bridge Posting

Method Used	No. of States
News release	23
Special notice to trucking association	20
Legal notice	4
Advance advisory signs	3
Notice posted at weigh stations	1
Notification of other agencies	6
Weight-limit maps or lists	5
Public hearings before posting	3
Regulatory signing only	9

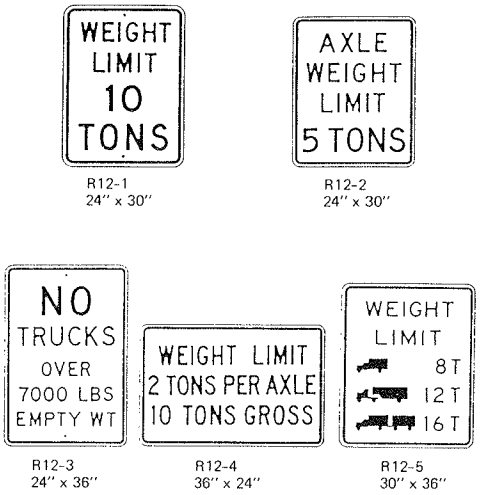

FIGURE 4 MUTCD standard bridge-posting signs.

Inspection

A posted bridge is typically an older structure that has not been designed to carry modern traffic. Often the structure is in a deteriorated condition and may have experienced some distress due to live load. It is necessary to monitor the condition of such bridges continually by frequent inspections to verify that the posted weight limits are appropriate.

Although local agencies have primary responsibility for their own bridges, many of them lack the qualified personnel or resources to perform bridge inspections in conformance with NBIS. In many states the state agency has taken over responsibility for bridge inspection, yet in others this practice is prohibited by state law. Many local agencies without qualified staff have retained consultants for bridge inspection. The responsibilities for local bridge inspection for the states responding to the ECC survey are summarized as follows:

	No. of Bridges by Type of Highway	
Inspector	Federal-Aid	Off-System
State agency	23	18
Local agency	16	20
Combination of state and local agencies	4	4
Consultant	3	3

Signing Practices

The AASHTO manual requires that the standards contained in the MUTCD (2) be followed when regulatory signing is placed on posted bridges. The current edition of the MUTCD recommends five standard bridge-posting signs, as shown in Figure 4. These signs do not always give precise definitions of axle loads and spacings and may have to be modified slightly to conform with local regulatory statutes. In addition to many variations of the standard signs, these modifications have also led to the development of many new nonstandard signs (J.C. Porter, unpublished data, February 1981).

A recent survey by Halstad revealed that there is considerable variation among the states with respect to the type of signs preferred for posting bridges. About half the states prefer the standard R12-5 sign or some similar, modified version. The next most popular sign is type R12-1, which is preferred by 17 states for bridges with span lengths less than 40 ft and by 11 states for bridges with span lengths more than 40 ft. Type R12-4 is preferred by only three states, whereas types R12-2 and R12-3 are not preferred by any state. Nine states preferred nonstandard signs of their own design.

Posting Enforcement

Truckers often disregard bridge weight limits because the penalties for exceeding the posted weight limits are low and enforcement is limited. One of the difficulties in enforcing bridge weight limits is that portable scales to check the weights of individual trucks are often necessary.

Most of the states responding to the ECC survey can assess fines against offenders and a few have the power, at least in theory, to sentence violators to jail. Fine structures vary considerably among the states. In some states maximum fines may be based on the number of previous offenses, whereas in others the fine is based on the amount of overweight. At least two states require that offenders pay for any damage done to the bridge, whereas one state reported that it can revoke the offender's vehicle registration. The possible legal consequences for violating a posted weight limit as reported by each of the states that responded to the ECC questionnaire are summarized in Table 5.

Permits for Posted Bridges

Because the hardship caused by bridge weight limits can be critical and even life-threatening (as in the case of fire-fighting equipment), it is sometimes in

TABLE 5 Consequences of Violation of Posted Weight Limit

Consequence	No. of States
Fine	
Maximum < $500	8
Maximum between $500 and $1,000	9
Maximum > $1,000	2
Maximum based on overweight	13
Jail	
Maximum < 30 days	1
Maximum between 30 and 180 days	7
Maximum > 180 days	3
Other	
Liability for cost of repair	2
Revocation of vehicle registration	1

the public interest to allow certain overweight vehicles on a posted bridge. This is usually done through the use of special permits.

Most of the states surveyed by ECC indicated that they have issued overload permits for posted bridges, but many of these states said that such permits were rare. Figure 5 shows the degree to which the states surveyed use such permits.

In certain states overload permits for posted bridges are never issued. In California, for example, permits are not issued for posted bridges, but state law allows fire-fighting equipment to use a bridge, provided the fire-fighting agency pays for any bridge damage.

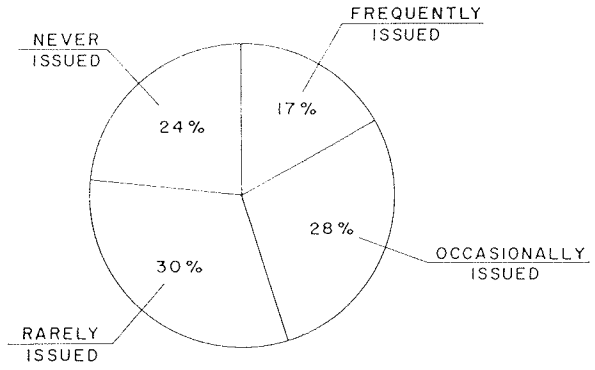

FIGURE 5 State practice of issuing overload permits on posted bridges.

ENGINEERING ASPECTS OF BRIDGE POSTING

NBIS provides some limited engineering guidance for inspecting, evaluating, and posting highway bridges, but considerable engineering judgment is still required to fill the gaps. As a result, even within the limits set by the NBIS, engineering practices vary among the states. This variation in practice leads to a difference in posting criteria that reflects different philosophies, different jurisdictional needs, and different traffic conditions.

INSPECTION

Bridge maintenance inspection is an art involving the application of both scientific principles and considerable engineering judgment gained from years of experience. Inspection relating to bridge-posting practice is most conveniently divided into inspections that are required before and those required after load-limit posting. Before a bridge can be posted, a thorough field inspection must be conducted. This is required so that a reliable structural-strength evaluation can be made. Subsequent to bridge posting, continued field inspection is required to monitor the condition of the posted bridge.

Before Posting

The primary purpose of inspecting a bridge before rating it is to determine information that is necessary to properly evaluate the strength of the bridge and its action under load. For this reason, it is desirable that inspectors become involved, at least to a certain degree, in the rating of bridges. The degree to which bridge maintenance inspectors are involved in the rating process in each of the states surveyed by ECC is shown in the following:

Involvement	No. of States
Performs calculations	9
Reviews calculations	5
Provides information and judgment	36
Not directly involved	7
Varies	2

After Posting

The majority of the states surveyed by ECC indicated that they reinspect their posted bridges more thoroughly or frequently than other structures. Many states also reported that they have the road maintenance personnel who drive the roads on almost a daily basis monitor posted structures for obvious signs of distress.

RATING

Bridge postings are usually based on the results of an analytical evaluation of the structural strength of the given bridge. Although the AASHTO manual (3) provides some guidance for evaluating or posting bridges, it also allows for a considerable amount of engineering judgment.

Posting Level

NBIS specifically states that posting is required if the AASHTO operating rating is less than the maximum legal weight of vehicles allowed to use the highways. Bridges need not be posted for loads below the AASHTO inventory load. Therefore, posted loads vary between the operating and the inventory levels. Although the AASHTO manual implies that frequency of inspection may be considered when a proper posting level is selected, it offers almost no additional guidance.

The ECC survey of the states showed considerable variation in the posted load level. There was also variation within some states in how they posted different bridge types. The posting levels of all states responding to the questionnaire are summarized in Table 6.

TABLE 6 Posting Levels Used by States

	No. of States by Bridge Type			
Posting Level	Steel	Timber	Reinforced Concrete	Prestressed Concrete
Operating	19	18	20	19
Inventory	14	15	12	13
Intermediate	8	8	7	8
Variable	5	5	5	5
Deferred	—	—	2	—

Loading

The traffic live load used for rating a bridge should be representative of the actual vehicles using the bridge. Only a few hypothetical rating-vehicle configurations are necessary to envelop the moments and shears caused by actual vehicles.

The vehicle configurations used for rating bridges vary among the states. Approximately 40 percent of the 45 states responding to the ECC survey use the typical AASHTO legal trucks. The remaining states use specially developed legal truck configurations, AASHTO H or HS design trucks, or some combination of truck types. The types of rating vehicles used by the states are summarized as follows:

Vehicle Configuration	No. of States
AASHTO legal vehicle	17
Modified legal vehicle	16
AASHTO design vehicle	5
Combination of AASHTO legal and design vehicles	4
Combination of AASHTO and modified vehicles	3

Of equal importance to the vehicle types is the number of vehicles assumed to be on the bridge at any one time. The AASHTO manual specifies that all lanes should be loaded when the rating is determined unless, in the judgment of the engineer, traffic movement and volume warrants the consideration of fewer lanes. Most of the states surveyed make only occasional use of the lane-reduction clause; however, five states consider only one vehicle at a time on the bridge.

Analysis Methods

Experience has shown that only a few structural components or failure modes control the maximum allowable live load for a bridge. These structural components or failure modes vary, depending on the type of bridge. Some of the less critical components and failure modes and the number of states surveyed by ECC that usually do not include these components or failure modes in bridge evaluations are listed in Table 7.

TABLE 7 Components or Failure Modes Not Considered in Rating

Component or Failure Mode	No. of States by Bridge Type			
	Steel	Timber	Reinforced Concrete	Prestressed Concrete
Concrete deck slab	19	15	16	–
Girder shear	19	7	14	16
Negative girder moment	3	3	3	3
Bent cap	23	15	25	23
Substructure	29	23	31	29
Other	3	3	3	3

The AASHTO manual allows the rater to use either working-stress or load-factor methods when a bridge is rated for its weight limit. Most of the states surveyed by ECC use working-stress methods exclusively for rating their structures. However, some states use load-factor methods for some structures and working-stress methods for others. Only one of the states surveyed used load-factor methods exclusively. The analysis methods used by each of the states surveyed (46 responded to the survey) are summarized as follows:

Method	No. of States
Working stress	26
Load factor	1
Combination	19

RECOMMENDATIONS

At this time there is too much variation in the posting criteria used by the different states. These differences are often justified; however, the current AASHTO manual and NBIS, although allowing for some variation, provide almost no guidance for rationally selecting the most appropriate criteria. Improved criteria need to be developed that will allow states and local jurisdictions to take into account those factors that legitimately affect the posted weight limits.

REFERENCES

1. Highway Bridge Replacement and Rehabilitation: Third Annual Report of the Secretary of Transportation to the Congress of the United States. U.S. Department of Transportation, July 1982.
2. Manual of Uniform Traffic Control Devices. AASHTO, Washington, D.C., 1981.
3. Manual for Maintenance Inspection of Bridges. AASHTO, Washington, D.C., 1978.
4. Better Targeting of Federal Funds Needed to Eliminate Unsafe Bridges. Report to the Honorable James R. Sasser, United States Senate, U.S. General Accounting Office. U.S. Comptroller General, Aug. 11, 1981.

Publication of this paper sponsored by Committee on Structures Maintenance.

Overloading of Prestressed-Concrete Spread Box-Beam Bridges

TERRY D. HAND and CELAL N. KOSTEM

ABSTRACT

An analytical scheme is developed that simulates the elastic and inelastic flexural response and the mechanism of damage initiation and propagation for prestressed-concrete spread box-beam bridges under any loading. The scheme employs the finite-element displacement method in which the nonlinear structural response is simulated by piecewise linearization of the tangent stiffness formulation. Damage initiation and propagation are simulated by dividing plate and beam elements into multiple layers, each in plane stress. The influence of box-beam torsional stiffness on the transverse flexure of the superstructure is incorporated into the model by introducing rod finite elements possessing the St. Venant torsional rigidity of the actual box section into the plane of the bridge slab. The coupled flexural and axial components of the box-beam contribution to composite bridge action are retained in twin I-beams, each corresponding to half the box beam. The model is applied to a field-tested bridge and found to yield reasonably good, slightly conservative predictions of elastic bridge deflections and girder moments. Results of postelastic simulations of several box-beam bridges are compared with those of flexurally identical or comparable I-beam bridges. Spread box-beam bridges are found to possess superstructure stiffness and strength approximately 30 percent higher than their I-beam counterparts. The lateral distribution of moment among box girders, more favorable at elastic load levels, is maintained almost proportionately well into the inelastic range, whereas progressive and unstable concentration of moment toward the loaded girder or girders is observed in comparable I-beam superstructures.

The majority of highway bridges in the United States are periodically subjected to loads far in excess of the service loads anticipated in the design process.

Investigations have been conducted over the years by various agencies to determine the overload response of bridges and to predict the deleterious effects of overloads on the various components of the superstructure. Analytical and limited experimental investigations to date have focused on the inelastic behavior of prestressed-concrete I-beam (1,2), reinforced-concrete cellular (3), and steel multigirder bridges (4). Little is known, however, about the post-linear-elastic response of prestressed-concrete spread box-beam bridges (Figure 1).

It has traditionally been assumed that these types of bridges are somehow stronger than corresponding I-beam bridges and that if the latter are able to carry given loads without damage, the same should be true of similarly dimensioned box-girder bridges. This assumption has led to ambiguity among many bridge engineers as to the meaning of strength and the definition of the damage initiation mechanism for such bridges.

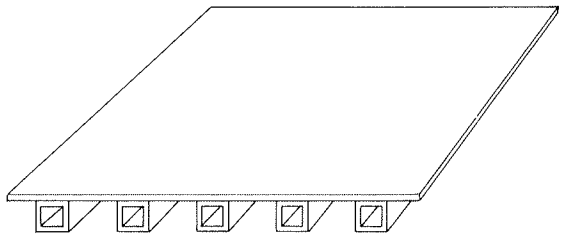

FIGURE 1 Typical prestressed-concrete spread box-beam bridge.

An analytical investigation was undertaken specifically to define the inelastic response and the mechanism of damage initiation and propagation of beam-slab prestressed-concrete spread box-beam bridges and to compare the overload characteristics of these types of bridges with those of equivalent bridges designed by using prestressed-concrete I-beams. The results clarify many questions regarding the structural response and strength differences in both the elastic and postelastic load ranges and may be used as a basis for decisions to permit overloads.

The investigation employed the finite-element displacement method. Nonlinear structural response was simulated by piecewise linearization of the tangent stiffness formulation, and damage initiation and propagation were simulated by dividing plate and beam elements into multiple layers, each in plane stress. The important influence of beam torsional stiffness on bridge behavior was incorporated into the model by introducing torsional rod elements into the plane of the slab.

DEVELOPMENT OF THE MODEL

Background

The development of a finite-element-based scheme for analysis of spread box-beam bridges proceeded from an earlier model developed principally by the second author to analyze I-beam bridges (1,2). In this model the three-dimensional elasticity problem presented by the flexure of a beam-slab superstructure was simplified and reduced to the problem of an eccentrically stiffened plate. The beam-slab bridge discretization consisted of beam and slab (plate bending and plane stress) elements. Finite-element nodes possessing in-plane (u and v) and bending (w, θ_x, and θ_y) degrees of freedom (df) are located at the middle surface of the slab (Figure 2). Coupled in-plane and bending stiffness coefficients are defined for the slab elements with respect to all 5 df, whereas major-axis bending and axial stiffness coefficients for beam elements are

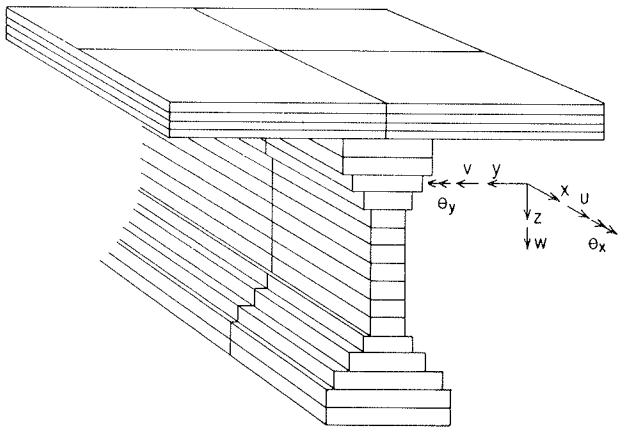

FIGURE 2 Layered beam and slab finite elements.

defined with respect only to u, w, and θ_y, thus precluding representation of weak-axis bending of the beams. Figure 2 shows the slab and beam layering scheme that allows elements to exhibit a stress variation through their depth and to experience progressive cracking, crushing, or yielding. At the same time, the layering provides the basis for redefining element stiffnesses after each load step through the appropriate summing of individual layer stiffnesses. In this scheme each layer is assumed to be in plane stress.

One of the principal shortcomings of this early model lies in its inability to incorporate the torsional stiffness of girders into the overall bending response of the superstructure. As a result, its application has been limited to bridges with beams that have negligible torsional stiffness, such as I- or T-beams. A second difficulty with the earlier model, which precluded its use in the analysis of box-beam bridges, was the question of how to treat torsional shear flows within the restricted context of the vertically layered beam stems.

Incorporation of Torsional Stiffness into the Model

Figure 3 illustrates a concept by which the torsional stiffness of box girders may be incorporated into the global stiffness of the superstructure. Notional linear finite elements, which possess the St. Venant torsional rigidity calculated for the actual box beam, are introduced longitudinally between nodes that lie over the centerline and stems of the box beams. Mathematically these elements are connected only to the θ_x df (Figure 2), which had formerly been used only in defining the transverse bending and twisting stiffnesses of the slab elements. On assembly into the global-stiffness equations, the additional stiffness provided by the torsion elements simulates the transverse stiffening effect caused by the actual beams in the real bridge. The flexural and axial stiffnesses of the box beams are retained in twin I-beams, which may continue to behave as the pure, planar beam columns of the original model.

Assumptions and Limitations

The proposed scheme for introducing the torsional stiffness of box beams into the otherwise purely flexural model necessitated several assumptions:

1. That the true torsional response of a box beam whose geometry is typical of those in the bridges under study can be reasonably approximated by St. Venant torsion alone,
2. That stresses from local transverse bending of box-beam walls in typically proportioned beams do not dominate over the primary flexural stresses and flexural and torsional shear stresses, and
3. That the usual assumptions of small deflection and small strain beam theory hold at least as well as for the original I-beam inelastic bridge model.

The first two assumptions have been validated by research by the authors and are reported elsewhere (5). The research consisted of theoretical and finite-element analyses of a box beam loaded in torsion and in combined flexure and torsion. Comparison of analytical results was made with limited benchmark data from the laboratory testing of a full-size prototype box beam (6).

The third assumption may be justified by the consideration that a bridge having torsionally stiff beams will exhibit less transverse dishing (indicative of less twisting of beams and more even distribution of moment among beams) than a bridge with flexurally equivalent, but torsionally flexible beams. This implies that box beams will more closely approximate plane bending than their I-beam counterparts. Moreover, although one generally associates box sections with torsion, their vastly higher torsional strength and smaller twist angles result in lower shear strains, which when coupled with the reduced warping tendency of closed sections results in a closer adherance to the assumption of key plane sections. Last the significantly smaller deflections and curvatures exhibited by box-beam superstructures as compared with corresponding I-beam superstructures make the small deflection and small strain assumptions all the more valid.

In addition to the assumptions just stated, the bridge model, with or without the torsional elements, is limited by the inherently flexural nature of its finite-element formulation. Because transverse shear deformations and stresses are neglected, the predicted bridge response and failure mechanism

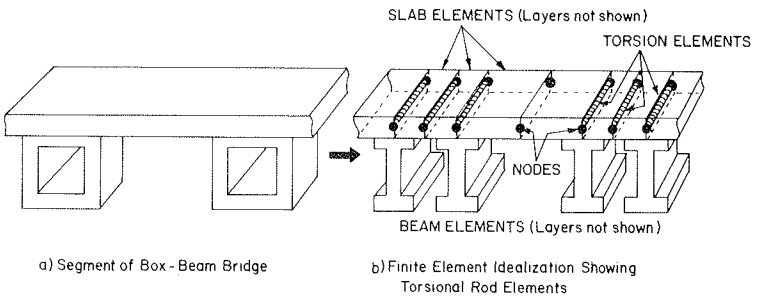

FIGURE 3 Incorporation of torsional stiffness.

is necessarily a flexural one. Thus, a bridge for which the actual overload response would lead to diagonal tension or shear cracking near the supports would be a poor candidate for analysis with this model. Because such cases are difficult to predict in advance, this model includes provisions for calculating, after each load step of the finite-element solution, the average flexural and torsional shear stress in each beam element. Torsional stresses are appropriately added or subtracted to flexural shears in each box-beam stem. Diagonal tension is then calculated, and if it approaches a preset threshold based on the rupture modulus of the concrete, the analysis is stopped. A message is printed by the computer program indicating that shear will govern the failure mechanism of the bridge, and further iterations with this model should be considered inaccurate.

VERIFICATION OF MODEL IN ELASTIC RANGE

The torsional rod element concept for simulating box-girder behavior was verified for loads in the elastic range by comparing the predicted response with corresponding measured data taken in field tests of an actual box-beam bridge (Hazleton Bridge) (7). Because measured data from the prototype were limited to midspan deflections and moment distribution coefficients derived from strain readings, an additional (elastic) finite-element model of the bridge was created to serve as a surrogate for loadings and response parameters not covered by the field tests. This second model employed a conventional finite-element package (SAP IV) and treated the bridge as a three-dimensional continuum with rectangular plate-bending elements and with membrane stiffness capability, including all parts of the slab and each wall of the girders.

Figures 4 and 5 show transverse deflection profiles at midspan as measured in the field tests versus those predicted by the SAP IV model and those predicted by the overload analysis model with special torsion elements [Bridge Overload Analysis (BOVA)]. The profiles correspond to two different transverse positions of the 333-kN (74.8-kip) test truck used in the tests (lanes 1 and 4). In each case the truck was positioned longitudinally to produce maximum bridge moment. Note that whereas the SAP IV model predicts the measured data almost exactly, the BOVA model consistently overestimates the deflection in the most heavily loaded girders.

Figures 6 and 7 show the moment distribution coefficients as derived from data taken in the field test versus values predicted by the SAP IV and BOVA

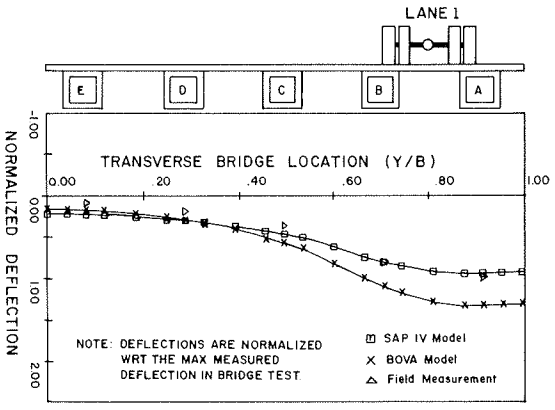

FIGURE 4 Midspan deflection profile: comparison of alternative models with test results (lane 1).

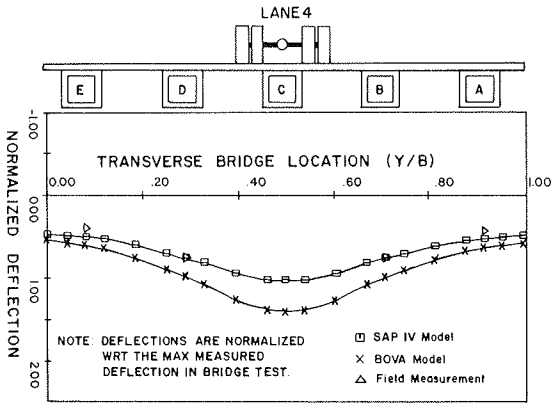

FIGURE 5 Midspan deflection profile: comparison of alternative models with test results (lane 4).

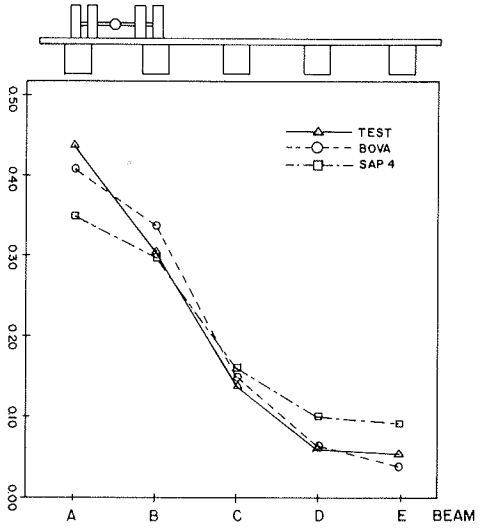

FIGURE 6 Distribution coefficients (percentage of total moment carried by beams) (lane 1).

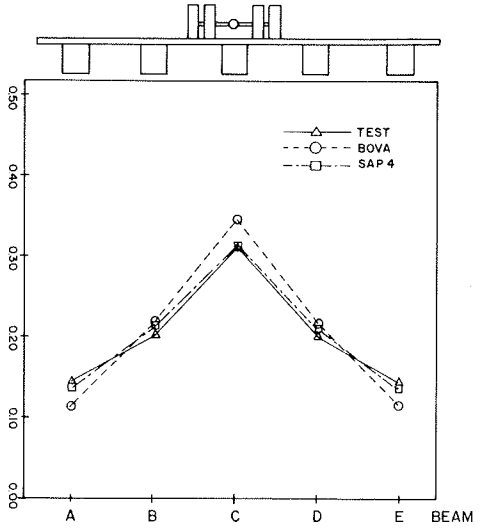

FIGURE 7 Distribution coefficients (percentage of total moment carried by beams) (lane 4).

models, respectively. These plots show good agreement generally. However, the BOVA-generated values again tend to be somewhat higher than the others, which indicates a slight overestimation of the portion of the bending moment carried by the most heavily loaded beams.

Figures 8 through 12 are longitudinal plots of internal beam torque for each of beams A through E for the case of the test truck in lane 2 (straddling girder B, the second beam from the right). Note again that although the predictions of the two models show reasonable agreement on order of magnitude, the BOVA formulation again predicts larger values.

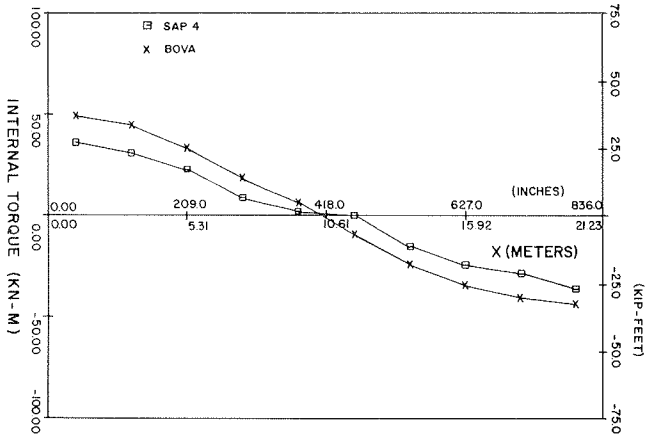

FIGURE 8 Internal torque versus longitudinal location: girder A, Hazleton Bridge (lane 2).

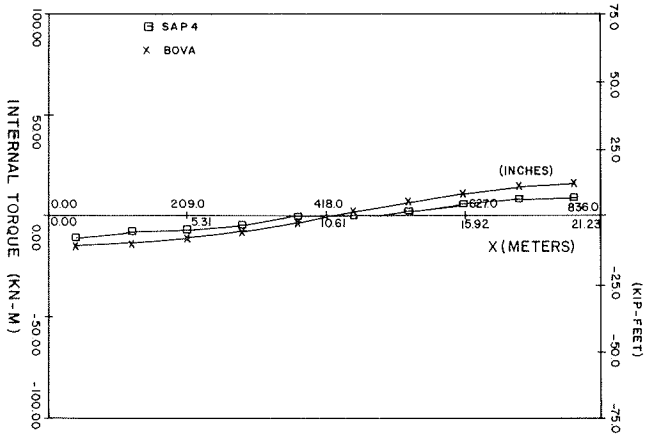

FIGURE 9 Internal torque versus longitudinal location: girder B, Hazleton Bridge (lane 2).

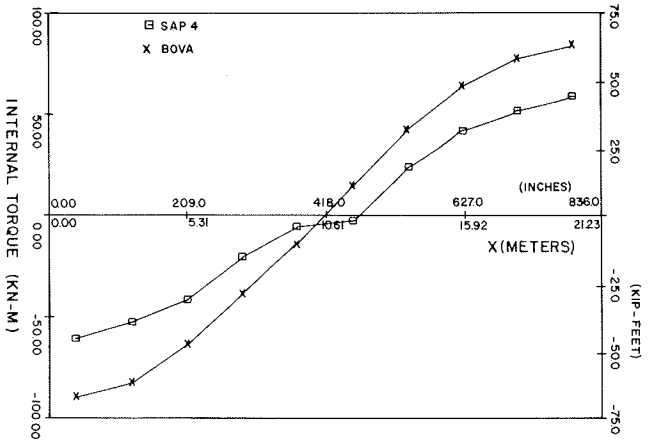

FIGURE 10 Internal torque versus longitudinal location: girder C, Hazleton Bridge (lane 2).

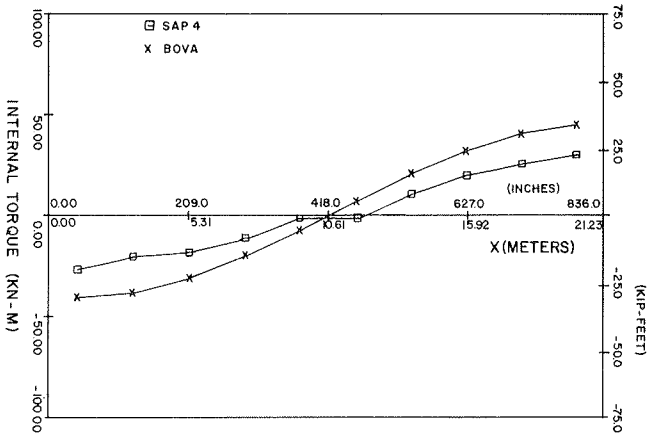

FIGURE 11 Internal torque versus longitudinal location: girder D, Hazleton Bridge (lane 2).

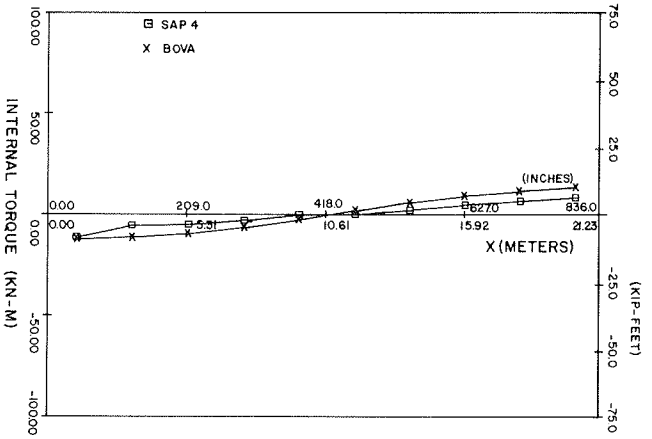

FIGURE 12 Internal torque versus longitudinal location: girder E, Hazleton Bridge (lane 2).

The response of the BOVA formulation for box-beam bridges (i.e., with torsion elements) is compared with that of the equivalent twin I-girder bridge (identical except without torsional elements) in Figure 13, which clearly shows the intended transverse stiffening effect contributed by the torsion elements. The loading for this plot was an AASHTO lane load in lane 2, that is, over beam B.

These results of analyses conducted at loads in the elastic range show that the response of a box-beam superstructure is quite well modeled qualitatively and reasonably well modeled quantitatively by the insertion of torsional rod elements into the layered beam-slab model as described earlier. The results suggest that in the elastic range at least, the inelastic model (BOVA) tends to overestimate somewhat the deflections, moments, and torques in the critical girder. The consistent overestimation, although problematic, is on the conservative side.

APPLICATIONS OF BOVA (BOX) IN INELASTIC RANGE

Extension of the box-beam overload model into the

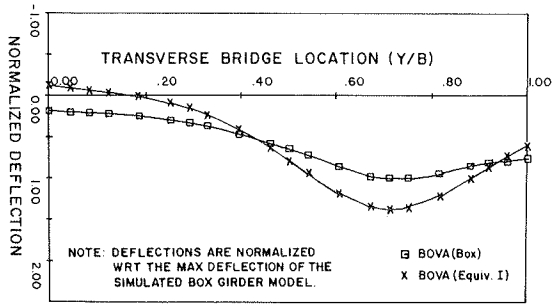

FIGURE 13 Midspan deflection profile: comparison of alternative models.

inelastic range proceeded in two stages. In the first stage the two BOVA versions of the Hazleton Bridge model (i.e., the simulated box-beam and the equivalent twin I-beam models) were each loaded to a point near the ultimate strength of the superstructure. The purpose was not only to predict the post-elastic response and failure mechanisms of the box-beam version but to investigate the differences in response between a box-beam bridge and a notional I-beam bridge identical in every detail except for the presence of the torsion elements.

The second stage involved a comparison of the responses of three distinct prestressed-concrete beam-slab bridges, each designed to Pennsylvania Department of Transportation (PennDOT) standards for the same span, width, and loading. The purpose was to evaluate the differences in behavior of actual alternative designs--bridges with eight I-beams, eight box beams, and five box beams.

Overload Analysis of Hazleton Bridge

In Figure 14 the load-deflection response of the Hazleton Bridge box-beam model is compared with that of the twin I-beam control model discussed previously. The loading consisted of monotonically increasing patch loads corresponding to the wheel footprint of the three-axle test truck used in the field tests (7). The truck was positioned in lane 2 straddling beam B. The ordinate is the total vertical load. The abscissa is the vertical deflection at midspan on the outer stem of the loaded beam.

Critical events in the overload history of each model are annotated on the curves, and the overload simulation was stopped in each case when the predicted flexural cracks in both stems of the loaded beam extended into the bottommost web layer. In the case of the box-girder model this occurred at a load of 2,259 kN (508 kips) and a deflection of 24.2 mm (0.954 in.). At this point the curve has clearly become nonlinear but retains a large positive slope, indicating that the bridge as a whole is not yet approaching its collapse load. By comparison, the equivalent I-beam bridge revealed the same damage level at a total load of 1,077 kN (377 kips) and a deflection of 23.8 mm (0.936 in.). The slope of the curve in this case, however, has become nearly horizontal, which implies that the bridge is near its ultimate load.

Figures 15 and 16 are based on data from the same overload simulation runs but show instead the predicted midspan deflection profiles at the same total loads as those annotated on the load-deflection curves. In addition, the box-beam profile (Figure 15) has a curve for a load of 333 kN (74.8 kips), the actual test-truck weight.

Examination of the two families of curves in

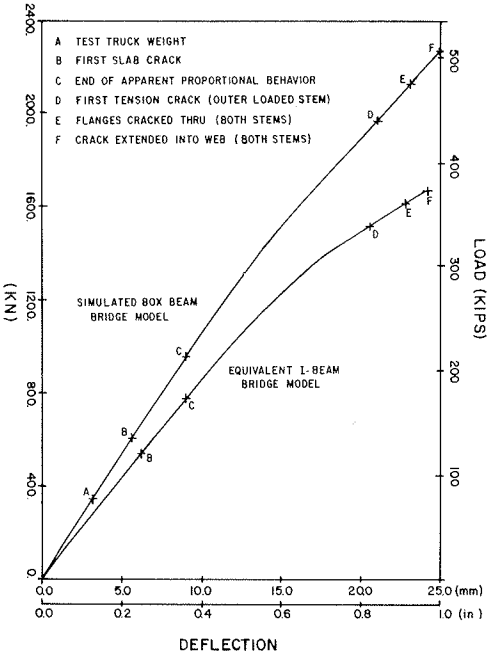

FIGURE 14 Load-deflection response of Hazleton Bridge models.

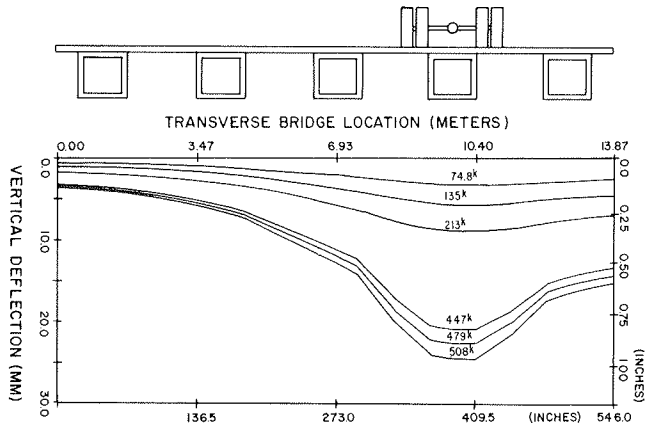

FIGURE 15 Midspan deflection profiles at various load stages: Hazleton Bridge, box-beam model.

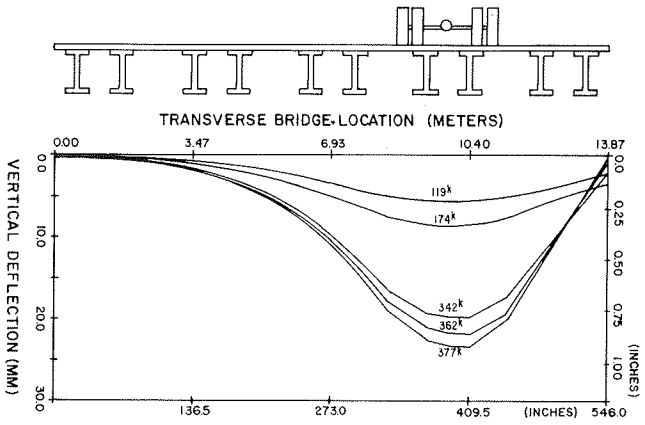

FIGURE 16 Midspan deflection profiles at various load stages: Hazleton Bridge, equivalent I-beam model.

conjunction with the load-deflection curves indicates that although critical damage occurs in both bridges at approximately the same maximum bridge deflection, the box-beam version reaches that deflection at a total load about 35 percent higher. Moreover, at this point in the equivalent I-beam bridge the loaded beam is taking on an increasing share of the total load as shown by the apparent unloading of the right-hand beam. By contrast, in the box-beam bridge the distribution of load to all beams appears to be maintained, even at high loads and severe deck and beam damage levels.

Analysis of Alternative PennDOT Bridges

The final series of analyses in the study compared the responses of three hypothetical bridges, each designed fully in accordance with PennDOT bridge standards (8) to meet the following requirements: span, 18.29 m (60 ft); total superstructure width (including curb and parapet), 14.22 m (46 ft 8 in.); and design loading, HS20 to 44, unskewed, and simply supported. From a design standpoint the bridges represent valid alternative structures with nominally equivalent capacities. These three cross sections are shown in Figure 17.

Overload simulations of the three bridges had two purposes: (a) to assess the behavior and strength differences between a typical spread box-beam bridge and an I-beam bridge having the same number of beams and beam spacing (as opposed to the equivalent I-beam version of the Hazleton Bridge, which was identical to the box-beam version except for the torsion elements but which did not represent an actual properly designed bridge) and (b) to determine differences in response between a box-beam bridge with many closely spaced small beams and one with fewer more widely spread large beams.

Figures 18, 19, and 20 show the comparative load-deflection curves and midspan deflection profiles at various load levels of the I-beam bridge and the bridge with eight box beams. The loading pattern for these analyses was a uniformly distributed lane load 3.05 m (10 ft) wide down the bridge centerline. The overload simulation was stopped at the first tension crack in the bottom flanges of the two loaded beams (both stems had to be cracked in the case of the simulated box beams).

These plots show a situation similar to the Hazleton Bridge, in which the box-beam bridge exhibits both stiffer transverse behavior and significantly greater strength. Also apparent in this comparison (not in the Hazleton Bridge) is the greater deflection capacity of the box-beam bridge at an equivalent damage level. [Actually, the box-beam bridge showed far less predicted slab damage at the 1,553-kN (349-kip) load level than the I-beam bridge showed at its 850-kN (191-kip) load level.]

The midspan deflection profiles of the bridge with eight box beams and the bridge with eight I-beams illustrate markedly different behavior at the higher postelastic load levels. In the I-beam bridge (Figure 19), what little lateral distribution of load to the exterior girders existed at the beginning appears to be degraded as (primarily) deck damage spreads. On the other hand, this lateral distribution, which is better initially in the box-beam bridge, is degraded little as deck damage propagates. Clearly the contribution of the torsional stiffness of the girders to the transverse stiffness of the superstructure maintains the transverse integrity of the system in spite of severe deck damage (Figure 20).

Figures 21 and 22 show load-deflection plots and families of midspan deflection profiles for the box-beam bridges with eight and five beams, respectively. The comparisons are not nearly so graphic or informative as the I-versus-box simulations. For these two bridge models, however, the load-deflection curves predict stiffer behavior by the five-beam bridge as opposed to greater strength and capacity for deformation in the eight-beam bridge. The loading and termination criteria were the same as those for the previous simulations. The profiles show a similar response character, particularly in regard to maintenance of lateral distribution of load.

CONCLUSIONS

In this investigation a rational analytical approach was developed for simulating the elastic and post-

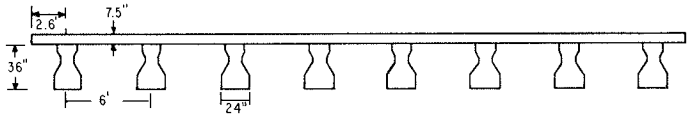

a) PENNDOT 24/36 I-Beam Bridge

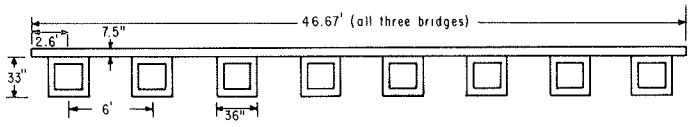

b) PENNDOT 36/33 Box Beam Bridge

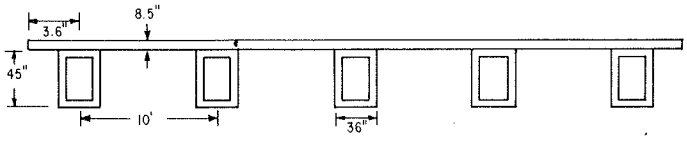

c) PENNDOT 36/45 Box Beam Bridge

(1 inch = 25.4 mm, 1 ft = 305 mm)

FIGURE 17 Bridge cross sections.

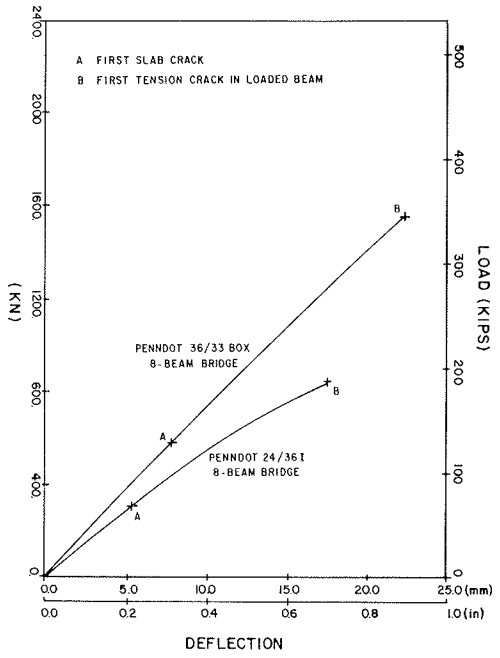

FIGURE 18 Load-deflection curves: PennDOT 36/33 box versus PennDOT 24/36 I eight-beam bridges.

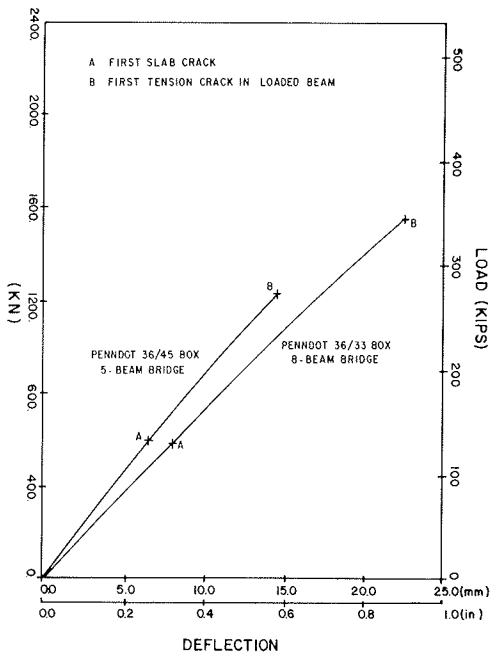

FIGURE 21 Load-deflection curves: PennDOT 36/45 five-beam versus PennDOT 36/33 eight-beam box-beam bridges.

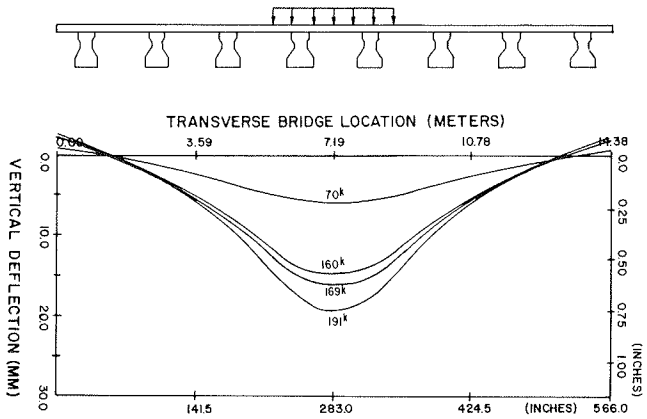

FIGURE 19 Midspan deflection profiles at various load stages: PennDOT 24/36 I-beam bridge.

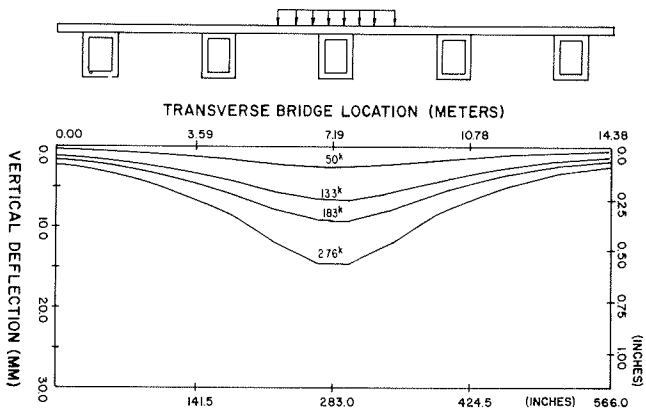

FIGURE 22 Midspan deflection profiles at various load stages: PennDOT 36/45 box-beam bridge.

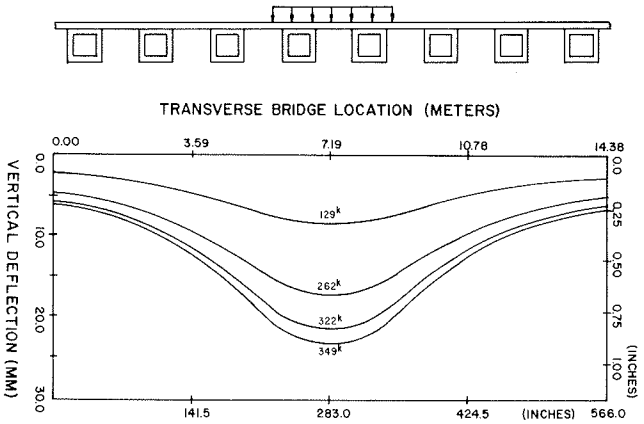

FIGURE 20 Midspan deflection profiles at various load stages: PennDOT 36/33 box-beam bridge.

elastic response of prestressed-concrete spread box-beam bridges. The scheme was shown to be a valid representation of true bridge behavior in the elastic load range, whereas its verification in the inelastic range must be deferred until prototype or scale-model bridges are tested to failure. Based on elastic studies, the model tends to err on the conservative side, suggesting that its results, extrapolated into the inelastic range, may reasonably be expected to give useful quantitative estimates of postelastic response, failure loads, and failure mechanisms.

Applications of the model to overload simulations of box-beam superstructures in comparison with equivalent or alternative I-beam superstructures suggest the following tentative conclusions:

1. Spread box-beam bridges exhibit significantly greater load-carrying capacity than their I-beam

counterparts with an identical or slightly greater major-axis moment of inertia.

2. Spread box-beam bridges exhibit higher overall flexural stiffness than comparable I-beam bridges, although the maximum bridge deflection reached at equivalent beam damage levels is about the same for the two bridge types.

3. In box-beam bridges transverse distribution of load to beams not directly loaded is higher initially and is effectively maintained through the entire load range as compared with I-beam bridges in which the initially poor transverse distribution becomes worse as total applied load is increased into the postelastic range.

REFERENCES

1. J.M. Kulicki and C.N. Kostem. The Inelastic Analysis of Prestressed and Reinforced Concrete Beams. Fritz Engineering Laboratory Report 378B.1. Lehigh University, Bethlehem, Pa., Nov. 1972.
2. W.S. Peterson and C.N. Kostem. The Inelastic Analysis of Beam-Slab Highway Bridge Superstructures. Fritz Engineering Laboratory Report 378B.5. Lehigh University, Bethlehem, Pa., March 1975.
3. J.G. Bouwkamp, A.C. Scordelis, and S.T. Wasti. Ultimate Strength of a Concrete Box Girder Bridge. Structural Division Journal of ASCE, Vol. 100, No. ST1, Jan. 1974.
4. J.C. Hall and C.N. Kostem. Inelastic Overload Analysis of Continuous Steel Multigirder Highway Bridges by the Finite Element Method. Fritz Engineering Laboratory Report 432.6. Lehigh University, Bethlehem, Pa., June 1981.
5. T.D. Hand. The Inelastic Analysis of Prestressed Concrete Spread Box Girder Highway Bridges. Ph.D dissertation. Lehigh University, Bethlehem, Pa., Sept. 1984.
6. R.M. McClure and R.M. Barnoff. Conventional and Through-Voided Box Beams Subjected to Combined Loading. In Transportation Research Record 785, TRB, National Research Council, Washington, D.C., 1980, pp. 15-21.
7. Y.L. Chen and D.A. VanHorn. Structural Behavior of a Prestressed Concrete Box-Beam Bridge--Hazleton Bridge. Fritz Engineering Laboratory Report 315A.1. Lehigh University, Bethlehem, Pa., Dec. 1970.
8. Standards for Bridge Design (Prestressed Concrete Structures). Standard BD-201. Pennsylvania Department of Transportation, Harrisburg, March 1973.

Publication of this paper sponsored by Committee on Structures Maintenance.

Overloading of Steel Multigirder Bridges

CELAL N. KOSTEM

ABSTRACT

The overloading of steel multigirder highway bridges may have deleterious effects on the structural integrity of the superstructure. The overloading of steel bridges is closely linked with the fatigue-life determination of the connection details. It is observed that the actual structural response of these bridges is different from the assumptions made in the design. Results obtained from a computer-based analytical model and simulation scheme are presented. The method provides a reliable tool to predict the linear-elastic and inelastic response of bridge superstructures up to the collapse load level. The observations from case studies have indicated that (a) interface slip between the girders and the bridge deck can be neglected for any practical overloadings, (b) high stresses due to overloading tend to be more prominent in the vicinity of the details that are prone to fatigue-crack initiation, (c) residual stresses play a nonnegligible role in the inelastic response of primary steel girders, (d) buckling is an important but not a critical phenomenon, and (e) damage initiation due to overloading can initiate in girders or in the deck, depending on the design details. It was also noted that bridges with a high degree of internal and external structural indeterminacy are less prone to damage induced by catastrophic overload.

Most highway bridges are subjected to overloading of varying degrees of severity with varying frequency. It is quite rare that all structural components of a bridge superstructure will not be subjected to stresses and deformations that will be equal to or below the values assumed by the designers. The overloading of a given bridge and its components will not necessarily occur only when a vehicle traversing the bridge is heavier than the design vehicle. Vehicles with close axle spacings, even if they are lighter than the design vehicle, can cause overloading. Thus, the issue of overloading is prevalent for all bridges. The frequency of the overloading cannot be accurately estimated unless the traffic count, including the axle spacing and weights of the axles, is monitored. Because some steel bridge components are known to be susceptible to fatigue, fatigue-crack initiation, and propagation, the overloading of steel bridges is closely related to the fatigue life of the bridges.

The current bridge design specifications (1) and bridge rating provisions (2) do not address the overloading with sufficient specificity. Even with these guidelines, much is still left to engineering judgment. The prudent deployment of engineering judgment requires a firm technical understanding of the structural response of highway bridges when subjected to overloaded vehicles.

A detailed research program on the overloading of prestressed concrete I-beam highway bridges has provided the needed information on the elastic and inelastic response of these bridges (3-6). The pilot research programs on the prestressed concrete spread box-beam bridges have also provided the comparative results between the I- and the box-beam construction (7).

The extensive analytical research and laboratory and field-test comparisons, where possible, have clearly indicated that the actual structural response of highway bridge is three dimensional. This differs substantially from the basic design premise of proportioning each structural component individually with little, if any, consideration for the interaction among these structural components. Thus, in the overload and even in the design-load assessment of the bridges with acceptable accuracy, the three-dimensional interaction among the structural members must be taken into account.

PRELIMINARY CONSIDERATIONS

In view of the difference between the presumed and the actual structural behavior of the bridge superstructure, certain factors with questionable validity have been examined, and their contributions have been identified. In the overloading response of steel multigirder highway bridges it is expected, but not quantified, that the cross framing will provide a more uniform distribution of the vehicular loading among the girders. The contribution of the cross framing in load distribution is not as high as was expected. Furthermore, the effectiveness of the cross framing in distributing the live load is dependent on load location (3,8).

If the cross bracings are to be as effective as expected, another problem surfaces. If the cross bracing is transmitting substantial forces in order to provide a more uniform distribution of the vehicular loads, the forces in these members need to be transmitted to some part of the structure. The cross framings are traditionally connected to the tension flange or to a bracket attached to the web at the vicinity of the tension flange. For increased load levels the forces transmitted by the bracing members cause out-of-plane deformations in the web-to-flange connection. These deformations, however small in magnitude, cause large local stresses. This type of action is known to be the source of the displacement-induced fatigue-crack initiation (8). Thus the possible positive contribution of the cross bracings is offset by adverse structural effects.

ANALYTICAL MODEL FOR OVERLOAD SIMULATION

If information is needed for the stresses, deformation, possible damage to the superstructure, and type and location of the damage, a more sophisticated analytical method needs to be developed. An approach that has been fully successful for prestressed concrete I-beam bridges was modified to simulate the behavior of the types of bridges in question (4-6,9-11). The bridge deck is simulated by a series of plate-bending finite elements with membrane stiffnesses. The girders were also divided into a series of beam finite elements. In order to account for the initiation and the propagation of material nonlinearity and any form of damage, the plate and beam elements were divided into a series of layers (Figure 1). The model developed and the method require computers. The computer program Bridge Overload Analysis--Steel (BOVAS) has been applied to all known field and laboratory test cases to verify its accuracy (11). The complexity of the mathematical derivation of the model prevents its inclusion in this paper; however, the details may be found in other publications (9,10).

One of the case studies conducted was the AASHTO Road Test bridge (12). The characteristics and the loading sequence of this bridge are widely known in bridge engineering. Figure 2 shows the finite-element layering of the bridge deck and the girder. The complexity of the geometry in Figure 2 clearly demonstrates the need for computer-based solution. All the details defined in Figure 2 were automatically generated by the computer program (11).

The experimental tests results and the analytical prediction by program BOVAS may be seen in Figure 3. Good agreement between the test results and the prediction may be noted. The other case studies have also resulted in similar favorable comparisons.

GENERAL OBSERVATIONS

Any investigation as detailed as this but without a detailed parametric investigation would yield observations that are applicable to the types of bridges being studied. However, the lack of a detailed parametric investigation would not permit the development of formulas to quantify the findings.

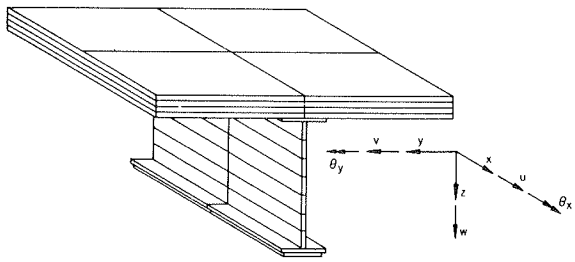

FIGURE 1 Slab and girder layering.

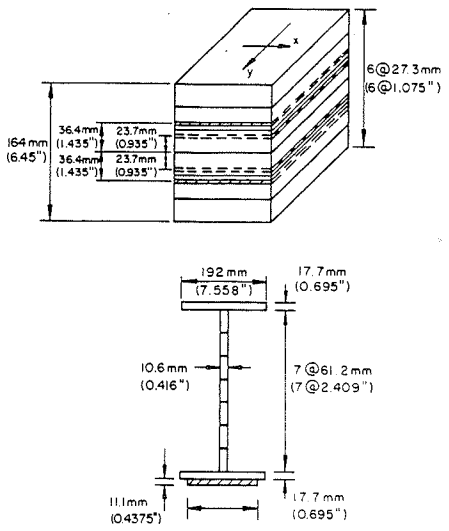

FIGURE 2 Slab and beam layering of test bridge (12).

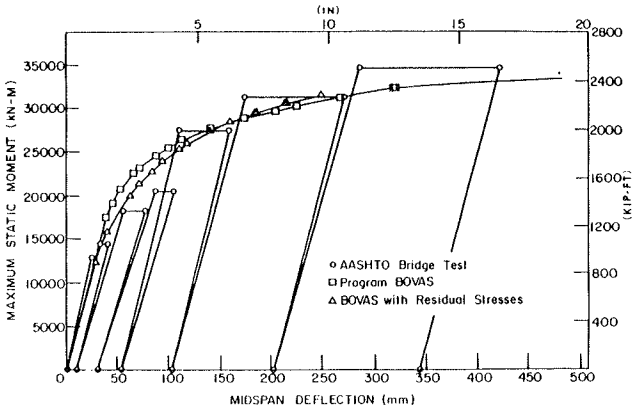

FIGURE 3 Moment versus deflection of test bridge.

Slip

The analytical research combined with the verification of the reported experimental research and field observations have indicated that slip is not a major concern in the structural response of steel multigirder bridge superstructures (13). Because of the friction between the deck and the steel girders, even for noncomposite construction, there exists a composite interaction. For increased load levels intermittent slips occur, but a fully noncomposite response cannot be achieved. In the case of partial or fully composite design until the occurrence of any noticeable slip, the bridge deck slab and the steel girders undergo substantial nonrecoverable damage (10,13).

High Stress Fields

As expected, the highest stresses are observed in the tension flanges and compression flanges (near the support in the case of continuous construction). For design loadings the magnitude of the stresses is within that of the design stresses. However, as the overloading occurs, these stresses increase proportionally to the gross weight of the vehicle. The contributions of the cross bracings do not enter into the lateral live-load distribution until the occurrence of the stress redistribution in the structure because of plastification or limited damage.

RESIDUAL STRESSES

The presence of the residual stresses should be noted in two situations: (a) the determination of the stress fields for the fatigue and fracture analysis of various members and details and (b) its effect on the overall structural response. The former has been well studied and quantified by many researchers and bridge engineers. As far as the latter is concerned, it is interesting to note that in the essentially linear-elastic response regime of the superstructure, the magnitude and the distribution of residual stresses do not play any role (Figure 3). Similarly, the collapse load level of the structure is not greatly affected by the residual stress field in the structural components. However, the variations in the residual stress intensities and their distribution play a predominant role in the structural response after the initiation of the nonlinear behavior and before the collapse (Figure 3).

The magnitude and the distribution of the residual stresses are highly affected by the fabrication procedures. In the absence of more reliable information, the residual stresses need to be considered as a factor that has adverse effects on the integrity of the superstructure.

Connection Details

Unfortunately past and present steel bridge engineering design practice places some critical details in the vicinity of the tension flanges. These details are known to have low fatigue life (1). Usually the stress ranges for these details are computed by using the reverse-design procedure, thereby neglecting the contributions of the out-of-plane deformations. This underestimates the stress range and thus overestimates the fatigue life of the actual connection.

In all case studies that have been conducted and verified with the field test results where available, it was observed that because of overloading the most stressed location in the tension flange is the tip of the cover plate, which is known for its low fatigue strength. Thus, through the visualization of this simple example, it is important to realize that overloading of steel bridges requires consideration of the fatigue provisions. This presupposes that the passage of the overloaded vehicle is not an extreme rarity.

Buckling

It has been observed that in the case of rolled girders, with or without cover plating, web buckling is uncommon. However, in the case of deep built-up girders, and especially in the case of plate girders, the stability of the web becomes a critical issue. This is more notable near the supports. Research has indicated that if the vertical stiffeners are properly designed, the web may buckle as a shear panel defined by the top and bottom flanges and the vertical stiffeners. This buckled web then develops a diagonal tension field and behaves like a truss member (Figure 4). Research has indicated that through the proper use of vertical stiffeners web buckling can be isolated to a few panels and does not initiate progressive spread of buckling. Buckling of the web causes a jog in the load-deformation curve of the structure, indicating a temporary shift in the stiffness. In the case of buckled panels, it would be premature to condemn the load-carrying capacity of the bridge.

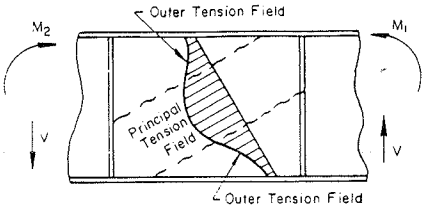

FIGURE 4 Typical transversely stiffened plate-girder web-plate panel under combined moment and shear.

The lateral buckling of the compression flange can occur for high load levels. However, in view of the current detailing practice there are always sufficient supports provided to brace the compression flange. The studies have not revealed the danger of lateral buckling due to the overloading.

Deck Damage

In prestressed concrete I-beam bridges it was noted

that the damage was always initiated by the cracking of the reinforced-concrete deck slab (5). These cracks were essentially parallel to the beams. For indiscriminately increased overload levels, the cracking formed partial hinges similar to the formation of the yield lines. The beams did not show any discernible damage until after substantial damage to the bridge deck. In the case of steel multigirder bridges with reinforced-concrete deck, such a generalization cannot be made. Depending on the proportioning of the steel girders, the damage to the superstructure can take place both at the girder as initiation of plastification or web-panel buckling and in the deck slab as cracking of the concrete. In the case of continuous construction, substantial cracking of the concrete over the interior supports takes place before any other damage to the rest of the deck and usually before any damage to the steel components. After the formation of pseudo-yield lines over the support, additional concrete cracking is observed between the girders. It should also be noted that even though such damage to the deck is not desirable, if cracking over the supports is noted and also if no inelastic behavior in the girders has taken place, through the rebound of the superstructure these cracks will close. All the deck concrete cracks, both in steel and prestressed concrete bridges, should be considered working cracks, provided that the girders do not undergo any loss of rebound capability.

Major Girder Damage and Structural Redundancy

In some cases deep cracks were observed, usually by coincidence, in the main girders of the bridges while the bridge was carrying a routine traffic load. An inference should not be drawn that such a bridge can carry overloaded vehicles. Various case studies undertaken by the author have demonstrated that in multigirder steel bridges if the superstructures have a high degree of internal and external structural indeterminacy, major damage to a girder will not result in the immediate loss of the bridge. The redistribution of the stresses permits the structure to hold up, perhaps after undergoing some noticeable deformations, and carry the regular traffic. Through the redistribution of the stresses other members may be highly overstressed. The misleading corollary to this is that if a bridge can carry some overloading and does not exhibit any distress, it should be able to carry some additional overloads. Without a full inspection and engineering computations, additional overloads to the structures should not be permitted without full cognizance of the incipient damage in the structure. The high degree of internal and external indeterminacy built into relatively old steel bridges is, in many cases, a blessing in disguise. The damage, if any, can in many instances go unnoticed for a prolonged period of time; with this probability in mind, the rating of these bridges should not be increased liberally.

RATING OF BRIDGES

If two highway bridges (one prestressed concrete I-beam and the other steel multigirder, designed and built using the same specifications for the same design loading and having equal span lengths and traffic lanes) are to be rated by using the current rating provisions (2), they may not have the same rating. This discrepancy is due to the current AASHTO guidelines for bridge rating (2). The prestressed concrete bridge will probably be rated for heavier loads than the steel bridge. It has been suggested that the rating provisions be revised so that the rating of the steel bridge is increased to that of the prestressed concrete bridge. Regardless of how reasonable this argument may sound, it has major flaws. In the rating of a steel bridge the residual stresses are not taken into account. The reduction of the allowable stresses in part can account for the number of unquantified parameters. Increase in the allowable stresses may result in permission for excessive stresses in some critical members.

CONCLUSIONS

The various findings discussed in this paper are the conclusions, and they will not reiterated. One concept that requires reexamination is overload versus inelastic response versus bridge inspection. It has been observed that depending on the dimensioning of the bridge and especially the detailing, it is possible that portions, and critical portions for that matter, may exhibit material or geometric nonlinearity even under service loads. The issuance of overload permits for such structures, especially if the structure has not been meticulously field inspected, should not be considered. In the case of structures with a high degree of indeterminacy, the possible adverse effects of previous overloadings may go unnoticed. Rating for higher loading requires the uncovering of built-in damages, if any. In the case of bridges with low structural indeterminacy, overloading permits or higher rating factors should be considered with extreme caution.

ACKNOWLEDGMENT

The study reported was sponsored in part by the Pennsylvania Department of Transportation (Research Project 77-1) and by FHWA. Jeffrey C. Hall, Stephen C. Tumminelli, and Carl A. Heishman participated in various phases of the reported investigation. The support of the sponsoring agencies and the participation of the project staff are gratefully acknowledged.

REFERENCES

1. Standard Specifications for Highway Bridges. AASHTO, Washington, D.C., 1977.
2. Manual for Maintenance Inspection of Bridges. AASHTO, Washington, D.C., 1982.
3. E.S. deCastro and C.N. Kostem. Load Distribution in Skewed Beam-Slab Highway Bridges. Fritz Engineering Laboratory Report 378A.7. Lehigh University, Bethlehem, Pa., 1975.
4. C.A. Heishman and C.N. Kostem. Inelastic Overload Analysis of Steel Multigirder Highway Bridges. Fritz Engineering Laboratory Report 432.7. Lehigh University, Bethlehem, Pa., 1983.
5. C.N. Kostem. Overloading Behavior of Beam-Slab Type Highway Bridges. Fritz Engineering Laboratory Report 378B.8. Lehigh University, Bethlehem, Pa., 1977.
6. C.N. Kostem and G. Ruhl. User's Manual for Program BOVAC. Fritz Engineering Laboratory Report 434.1. Lehigh University, Bethlehem, Pa., 1980.
7. T.D. Hand. The Inelastic Analysis of Prestressed Concrete Spread Box-Beam Highway Bridges. Ph.D. dissertation. Civil Engineering Department, Lehigh University, Bethlehem, Pa., May 1984.
8. T.A. Fisher and C.N. Kostem. The Interaction of Primary and Secondary Members in Multigirder Composite Bridges Using Finite Elements. Fritz Engineering Laboratory Report 432.5. Lehigh University, Bethlehem, Pa., 1975.
9. J.C. Hall and C.N. Kostem. Inelastic Analysis

of Steel Multigirder Highway Bridges. Fritz Engineering Laboratory Report 435.1. Lehigh University, Bethlehem, Pa., 1980.
10. J.C. Hall and C.N. Kostem. Inelastic Overload Analysis of Continuous Steel Multigirder Highway Bridges by the Finite Element Method. Fritz Engineering Laboratory Report 432.6. Lehigh University, Bethlehem, Pa., 1981.
11. C.N. Kostem. User's Manual for Program BOVAS. Fritz Engineering Laboratory Report 435.3. Lehigh University, Bethlehem, Pa., 1983.
12. Special Report 61D: The AASHO Road Test: Report 4--Bridge Research. HRB, National Research Council, Washington, D.C., 1962.
13. S.C. Tumminelli and C.N. Kostem. Finite Element Analysis for the Elastic Analysis of Steel Multigirder Highway Bridges. Fritz Engineering Laboratory Report 432.3. Lehigh University, Bethlehem, Pa., 1978.

Publication of this paper sponsored by Committee on Structures Maintenance.

The Ontario Bridge Code: Second Edition

ROGER A. DORTON and BAIDAR BAKHT

ABSTRACT

Based on the limit-state design philosophy, the Ontario Highway Bridge Design Code was first published in 1979. A brief account is given of the implementation of the first edition of the code and the problems associated with the implementation. The second edition of the code was published in late 1983. Major changes in the code provisions are identified, and some details of a computer system that is currently being developed to support the code are given.

Despite the diversity of vehicle weight regulations in various jurisdictions, most highway bridges in North America are designed by the same AASHTO specifications (1) or the Canadian Standards Association (CSA) bridge code (2), which is only a slight variation of the former. The Province of Ontario used the AASHTO specifications until 1979, when the first edition of the Ontario Highway Bridge Design Code (OHBDC) (3) was published. The AASHTO specifications were used by choice, because Ontario, like other Canadian provinces, has full jurisdiction over its highways and related matters, which include the formulation and enforcement of vehicle weight laws and the choice of design codes for its highways and bridges. In 1976 the Ministry of Transportation and Communications (MTC) of Ontario decided to write a highway bridge design code of its own, mainly for the following reasons:

1. The lack of conformity between heavy vehicles in Ontario and the AASHTO design vehicles. It is noted that Ontario permits much heavier vehicles on its highways than do most other jurisdictions in North America.
2. The difficulty and tardiness in the incorporation of latest research findings, however significant, in the AASHTO specifications.
3. A belief that the limit-state philosophy would lead to economy of design and uniform, predictable levels of safety in bridges.
4. The need to have a code in SI units in compliance with the government's commitment to metric conversion.

The first edition was written by 17 technical subcommittees under the steering control of an 11-member Code Development Committee in the relatively short time of about 3 years. This first highway bridge design code with a limit-state design format was written by a team of about 80 engineers from both within and without Ontario. Details of its development have been given elsewhere (4).

Soon after the publication of the first edition, work was started on the revision of the code. This work led to the second edition of OHBDC, which was published in late 1983. The purpose of this paper is to give a brief account of the implementation of the first edition and also to identify major changes that have taken place since the first edition.

IMPLEMENTATION OF FIRST EDITION

Following the limit-state format of the code, designers were required to consider both the ultimate and the serviceability limit states. The former limit state corresponds to the maximum load-carrying capacity, and the latter, which includes cracking, vibration, fatigue, and permanent deformations, is associated with loadings for normal use. The resistance and load factors specified in the code were calibrated to a target safety index value of 3.5 (5). The calibration was carried out for reinforced-concrete, prestressed-concrete, and steel structures from relevant available statistical data. Such data were not available for substructures, wood bridges, and soil-steel structures. Because of the lack of prior knowledge of the limit-state methods for these items, the relevant design equations were calibrated less rigorously: The calibration could only be done with respect to designs obtained from other North American codes.

Most problems in implementation of the code related to sections on foundations, wood bridges, and

soil-steel structures. The conservative approach to calibration of these items resulted in designs that, by comparison with designs from other codes, appeared uneconomical. Where possible, relevant code provisions were revised through a series of addenda (6-8). Because of the expectation of extensive revisions, the section on wood bridges was withdrawn, and until the second edition of OHBDC, wood bridges were required to be designed by the AASHTO specifications.

The code provisions did not always appear to result in any significant reduction of materials except for reinforcement in concrete deck slabs. This can be attributed to the design vehicle which, in conformity with heavy trucks in Ontario, is more than twice as heavy as the AASHTO HS-20 truck. The design computation time increased by about 30 percent. However, because there was no change in the drafting time, the net effect on the cost of contract document preparation was an increase of about 10 percent, and this is expected to decline as designers become more familiar with the code and the SI system of units. It should be noted that a 10 percent increase in the cost of contract document preparation corresponds to an increase of less than 1 percent in the total cost of the bridge. This increase appears justifiable on the grounds of more uniform and consistent safety levels, and the use of a more rational design philosophy that has the potential of improvement as more statistical data become available.

Mainly because of the new design philosophy, there were a number of problems in the implementation of the code. The code writers had to provide an interpretation service for clauses that they were either responsible for or familiar with. A Code Implementation Committee was set up to gather feedback from users so that the problems could be identified and addressed in the second edition of the code. Results of the feedback can be summarized as follows:

1. There was a general reluctance to use refined methods of analysis, and an extension of the range of application of simplified methods was sought.
2. There was a resistance to the complexity of the simplified method of analysis, which, for the cases analyzed, gave answers similar to those given by the AASHTO method.
3. The introduction of the new provisions for the dynamic load allowance (DLA), which required the calculation of the natural frequency of the bridge, did not appear to pose any problem.
4. The empirical method for design of deck slabs, which results in a considerable reduction of reinforcement, was widely used.
5. The serviceability limit state of cracking appeared to govern the design of concrete bridges.
6. The limit state of fatigue governed the design of steel bridges more frequently than is the case when AASHTO specifications are followed.
7. Earthquake loading substantially increased the footing sizes and the number of piles and generally governed the design of fixed piers.
8. There was a general concern that the code provisions relating to shear resistance of concrete beams were overly conservative.

Although called the design code, the OHBDC also covers explicitly the evaluation of the load-carrying capacity of existing bridges. The code has now been applied to the evaluation of more than 60 bridges. The multiple-level posting, which can be established through the code provisions, is now used for posting of some bridges in Ontario.

As discussed earlier, the level of safety in a bridge was measured by a quantity called the safety index and denoted by β (9). To compare the values of β as obtained for OHBDC design with those obtained by the AASHTO specifications a large number of steel and concrete bridges were designed by the two codes, and values of β were calculated (9). As shown in Figure 1, β for AASHTO designs varied from about 1.5 to 14, illustrating the nonuniformity of safety levels. β-values for OHBDC designs remained close together.

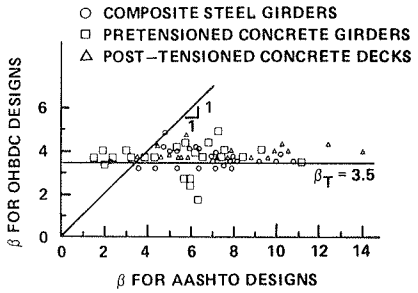

FIGURE 1 Comparison of safety index values.

THE SECOND EDITION

After the publication of the first edition of OHBDC, the technical committees were formed again, with a slight reduction in numbers, to start updating the code. The committee structure was generally the same as that for the first edition. The distribution of the affiliations of code writers remained unchanged, and professional fees were paid to consultants as before. The process of technical committee drafts and Code Development Committee reviews followed by public comments, as adopted for the first edition, was followed for the second edition.

The number of code sections was reduced from 17 to 14 by consolidating several sections dealing with loads.

In the following, major changes in specific code sections with respect to the provisions of the first edition of the code are identified and discussed.

Loads

The major change in the section on loads relates to the consolidation of the following three sections from the first edition:

1. Live and Dead Loads and Load Factors,
2. Dynamic Load and Vibration, and
3. Miscellaneous Loads and Movements.

The committee structure dealing with the three topics was the same as before. However, provisions under the three preceding headings were placed in a logical sequence under one heading. All clauses dealing with loads and load effects, which in the first edition were found in a number of locations, were consolidated under one heading.

A limited vehicle weight survey conducted in 1979 (10) indicated that the Ontario design vehicle still represented the vehicle population in Ontario quite closely. Consequently no change in the design-vehicle and live-load factors was sought.

As shown in Table 1 different values of modification factors for multilane loading were specified in the first edition for static loads and for DLA. Because of this, the governing multilane loading could not be established beforehand, and even when simplified methods of analysis were used, a designer had

TABLE 1 Modification Factors for Multilane Loading

No. of Loaded Design Lanes	Modification Factors in First Edition of OHBDC		Combined Modification Factors
	Static Load	DLA	
1	1.00	1.0	1.00
2	0.95	0.70	0.90
3	0.85	0.60	0.80
4	0.75	0.50	0.70
5	0.67	0.50	0.60
6+	0.60	0.50	0.55

Note: DLA = dynamic load allowance.

to investigate all the loaded-lane conditions separately. It was decided to amalgamate the modification factors for static and dynamic loads into one value in such a way that the resulting load effects were not substantially different. The amalgamated values of the modification factors as they appear in the second edition of the code are also given in Table 1.

In conformity with the usual practice, in the first edition of OHBDC it was specified that for the limit state of fatigue the single design vehicle should be placed in the most eccentric position. The fatigue response of a bridge component should depend on the normal transverse positions of traveling vehicles rather than some imaginary positions that may result in the worst load effects. With this in mind, it is now specified in the second edition that for the limit state of fatigue, the single design vehicle should be placed at the center of a traveled lane. It is anticipated that because of this change, economy will be justifiably affected, especially in bridges with wide shoulders.

After the publication of the first edition, an extensive and thorough dynamic testing program was undertaken. In this program 27 bridges of different types, span lengths, and so on, were tested. Details of bridges tested together with some relevant results have been given elsewhere (11). From test results the premise of the DLA provisions of OHBDC that DLA depends mainly on the first natural frequency of the bridge was validated. It was also found that the DLA values as given in the first edition of the code can be slightly reduced. Figure 2 shows the first- and second-edition DLA values corresponding to various values of the first natural frequency of the bridge. It is noted that the frequency of multispan bridges can be conveniently calculated by the simplified method given by Billing (12).

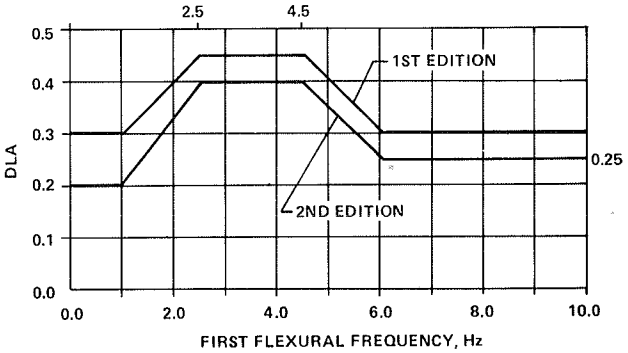

FIGURE 2 DLA values.

Deflection limitation criteria, which are concerned with human response to vibrations, have also been slightly relaxed in the second edition. These criteria are shown in Figure 3 together with the corresponding criteria given in the first edition.

The rather large number of load combinations specified in the first edition has been considerably reduced, and load combination factors have been eliminated by modifying the load-factor values.

Analysis of Bridge Superstructures

Provisions of the section on analysis of bridge superstructures have been the most controversial ones, mainly because of the reluctance of designers to be subjected to methods of analysis that are not so simple as the AASHTO load-distribution criterion (1). Because of the specification of different multilane modification factors for static load and DLA, the specified simplified methods became tedious, if not complex. The amalgamation of the two modifica-

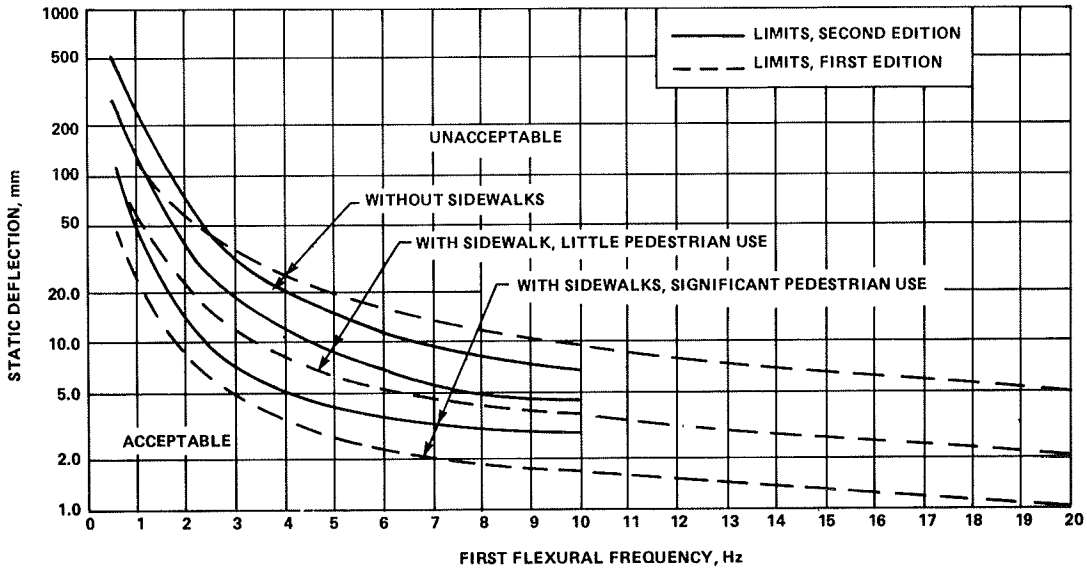

FIGURE 3 Deflection limitations.

tion factors into one, as discussed earlier, meant that the governing load cases could be established beforehand and the simplified methods made even simpler.

To extend the scope of the simplified methods and to make the analysis provisions easier to comply with, the following revisions have been incorporated:

1. The code clauses have been rearranged entirely to follow a logical sequence of operations.
2. Provisions for analysis of dead loads and live loads and the respective limitations for the use of relevant simplified methods have been separated.
3. Limitations on the applicability of simplified methods have been relaxed. It is now explicitly permitted to exercise engineering judgment in deciding whether a bridge is within the prescribed limits sufficiently closely for a simplified method to be applicable.
4. Unlike the first edition, the second edition contains simplified methods for both external and internal girders.
5. The simplified method for longitudinal shears has been revised and further simplified.
6. Based on recent research (13), a simplified method is provided for the calculation of transverse shear intensity in multibeam bridges.
7. An additional simplified method is provided for the analysis of multicell box girders.
8. A simplified method is provided to incorporate the effects of increased vehicle edge distance on longitudinal moments. This method is expected to prove useful for the analysis of bridges for the limit state of fatigue in which a vehicle is placed at the center of a traveling lane, thus increasing the vehicle edge distance considerably in many cases.
9. A simplified method of analysis is also provided to account for the presence of edge stiffening, for example, as provided by barrier walls.

Most of the simplified methods given in the code are derived from computer-based refined methods; they are presented in such a way that a designer, using methods similar to that of the familiar AASHTO load distribution criterion, can use the results of refined analyses, reduced to a graphical or tabular form, without having to perform the refined analysis computation.

Deck Slabs

One of the more compelling reasons for a bridge design code written for Ontario was a belief that concrete deck slabs of slab-on-girder bridges were usually overdesigned by a large margin. The basis of this belief was a large number of laboratory and full-scale tests showing that the failure mode for these components was that of punching shear and not flexure, for which the deck slabs are usually designed. From the studies it was concluded that a deck slab can safely sustain modern heavy vehicle traffic if it has a ratio of span to thickness of 15 and two meshes of orthotropic reinforcement with a minimum area of reinforcement in each direction and each mesh of 0.3 percent of the concrete area. Details of the basis of this empirical approach have been given elsewhere (14).

In the first edition of OHBDC, the deck slab thickness for new designs was required to be at least 190 mm. This limit has been increased to 225 mm in the second edition. The requirement for minimum slab thickness is not related to the strength of the slab but to considerations of durability. It is believed that slabs exposed to deicing salts should have reinforcement with a minimum cover of 50 mm from the salt-exposed surface. A recent survey of depths of cover conducted in Ontario showed that the standard deviation of the depth of cover is about 10 mm. Hence to ensure that in 97.5 percent of cases the actual depth of cover would be at least 50 mm, a depth of cover of 70 mm has been specified. This requirement, together with the requirement of a minimum spacing of 25 mm between two layers of reinforcement, results in an overall minimum deck slab thickness of 225 mm.

There was some ambiguity about the applicability of the empirical method in concrete slab-on-girder bridges without intermediate diaphragms. This ambiguity has been removed by clearly stating that the empirical method can be applied to concrete slab-on-girder bridges without diaphragms.

The empirical method for deck slabs was only an alternative permitted in the first edition if certain conditions, for example, a certain deck slab overhang width, were met. Confidence in the empirical method has grown since 1979. In Ontario several deck slabs have been designed by the empirical method and are performing well, and independent tests done in New York (15) have also confirmed the validity of the basis of the method. With the growing confidence in the empirical method it was decided to make the method mandatory rather than permissible in the second edition for all deck slabs that conform to conditions necessary for the application of the method.

The empirical method as given in the first edition was not applicable to bridges having skew angles larger than 20 degrees. Since the first edition, several tests have been conducted by MTC on deck slabs of bridges with large skew angles. From tests results it was concluded that away from the skew supports the deck slab behavior is similar to that of deck slabs in right bridges. Consequently, in the second edition it is specified that 0.3 percent isotropic reinforcement be provided in the middle regions of the decks and 0.6 percent in the end regions. The two regions are identified in Figure 4.

Wood Structures

A major change in the section on wood structures was the introduction of a set of design provisions for prestressed wood decks. As discussed in various publications (16,17), this new structural system consists of laminated decks that are transversely posttensioned. The purpose of prestressing in this case is to hold the laminates together so that the interlaminate slip is avoided. The system has been successfully applied to rehabilitate existing nail-laminated decks and also has been incorporated into the design of a new bridge (18).

The second edition of the code contains design

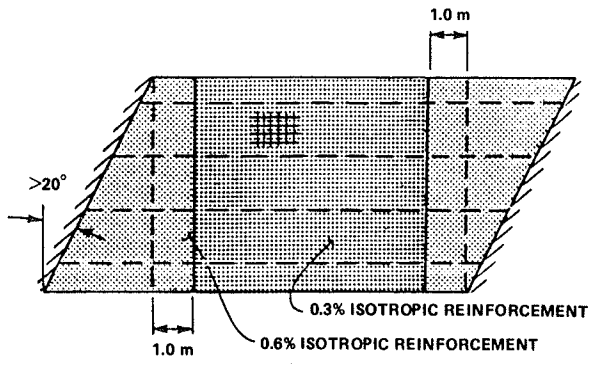

FIGURE 4 Reinforcement in deck slabs of skew bridges.

provisions for prestressed wood decks and details of approved prestressing systems. The code also has provisions for the design of wood-concrete composite bridges and gives approved details of the wood-concrete interface.

An extensive study was undertaken to compare the designs of wood bridges resulting from the AASHTO and OHBDC provisions. Details of the study have been reported elsewhere (19). A summary of the results of the study for sawn stringer bridges with transverse-laminated decks is shown in Figure 5. It can be seen that the AASHTO specifications result in deeper stringers when the stringer spacing is less than about 900 mm, but the situation reverses for larger stringer spacings; that is, the OHBDC provisions lead to deeper stringers.

COMPUTER SUPPORT SYSTEM

When a new code is implemented quickly, it is unlikely that there will be existing computer programs immediately available for use with it. In anticipation of the code, the MTC library of bridge programs had been metricated and converted to a load-factor format so that they could be used, at least in a limited way, with the new code. A new live-load routine was developed, but there was still a good deal of manual transfer and combining of required data. The level of sophistication of these converted programs was below that for programs that were available for calculations with the AASHTO specifications.

The current MTC library of bridge programs has been developed over the past 20 years and has undergone extensive modifications. The rapid change of programming techniques over the years has resulted in substantial nonuniformity between the various programs, making maintenance and modifications quite difficult. For the library of programs to be able to support the new code, two alternatives were considered: updating existing programs individually or developing a new modular system. The latter alternative, although incorporating a high initial cost, was chosen because of its long-term benefits. Because the system was modular in nature, it could easily accommodate changes and would be easy to maintain.

The computer system chosen to be developed is called the Ontario Modular Bridge Analysis System (OMBAS). Although called the analysis system, it also incorporates routines for design. The system includes a number of large modules, a data base, and a number of utilities. Each large module will perform a separate and unique function that is recognizable to the designer and constitutes a normal design step. Broadly speaking, the application subsystem includes 11 large modules carrying out the following functions:

1. Control,
2. Input,
3. Geometry-related calculations,
4. Idealization,
5. Generation of dead-load-related data,
6. Solution,
7. Generation of live-load-related data,
8. Generation of load combinations,
9. Calculation of resistances,
10. Detailing, and
11. Output.

The utilities system contains modular units that facilitate system development, operation, and maintenance. Details of OMBAS are given elsewhere (20).

The work on OMBAS is planned in two phases; phase 1 is scheduled for completion soon after the publication of the second edition of the code. It is expected that at the end of this phase the system would be suitable for code testing. The second phase is expected to take another 3 years.

The projected cost of the development of OMBAS is $840,000. The work on the project is being carried out by an MTC project team. An established project management system is being followed that calls for regular reviews by a user review group and a quality review group; the membership of the former includes consulting engineers and MTC staff. The latter group includes an external computer systems adviser. All Ontario users will have access to OMBAS, as they now do to the existing library of programs.

IMPLEMENTATION PLANS

A new commentary volume has been issued with the second edition of the code. This commentary explains the derivation of code clauses and cites references. With this commentary available, implementation by designers already familiar with the first edition should not be a problem. Seminars are planned, however, to ensure that users understand the new provisions and have a chance to discuss them with the authors.

Implementation of the new OMBAS computer system will represent a larger change, and special sessions of instruction will be held. The changeover from the current system to OMBAS will be a gradual one,

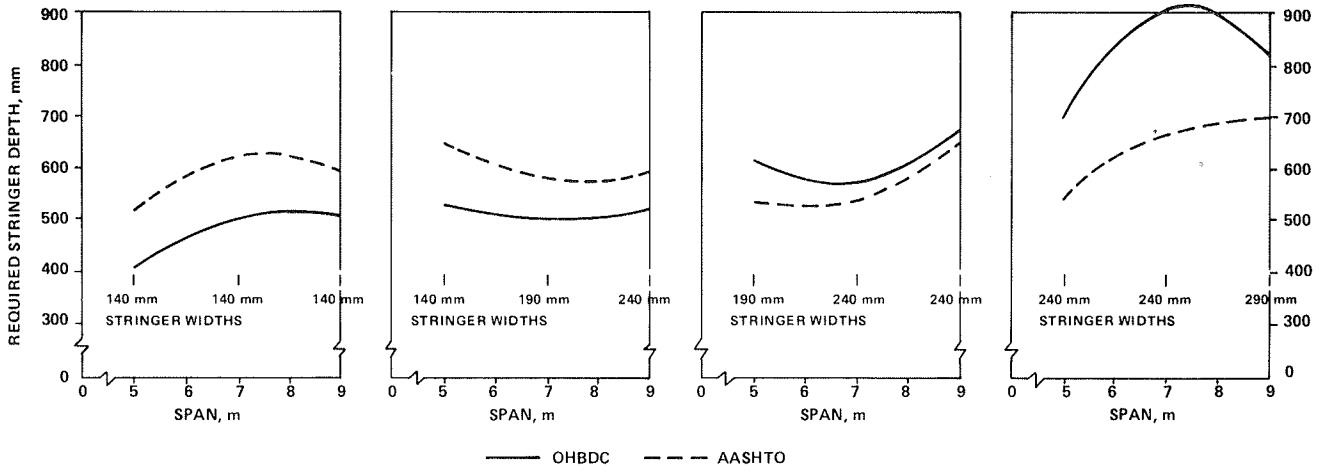

FIGURE 5 Comparison of AASHTO and OHBDC designs for bridges with sawn stringers and transverse-laminated decks.

and the existing programs will not be dropped until the full capability of OMBAS has been tested in the production mode.

The OHBDC first edition has been used on all MTC bridges for several years but has been optional in application to municipally owned bridges in Ontario. By the end of 1984, when OMBAS is fully operational, the second edition will become mandatory for the design and evaluation of all bridges in the province. All drawings will then require the seal of two professional engineers, one the designer and the other the checker, thus assuring that all designs have been carried out and checked in conformity with the code.

CONCLUDING REMARKS

The code has had wide acceptance in Ontario with no more problems in implementation than anticipated. The simultaneous issuing of a commentary and a reasonable lead time for familiarization are key items to ease the introduction of a new code. The code provisions, where appropriate, have recently been incorporated into the design criteria for elevated structures for a light rail transit system in the Toronto region, and the same limit-state format and calibration process has been followed. Within Canada the CSA Highway Bridge Committee is considering adoption of a number of OHBDC provisions and is also producing a limit-state design specification for the next edition. The AASHTO Bridge Committee has shown interest in some clauses, such as the deck slab empirical design method, as have code writers elsewhere, particularly those in Australia, New Zealand, and Japan.

Although introduction of the OHBDC has not brought about large changes in material quantities or costs, it does provide for the heavy Ontario truck loads in a more rational manner and with more consistent safety levels than before. The limit-state format appears to be the best to accommodate future changes as more statistical data become available and improvements are made in probabilistic design techniques.

In most jurisdictions there is an increasing emphasis on maintenance and rehabilitation, which will continue in years to come. Although the OHBDC covers the evaluation of existing bridges, the code provisions for bridge rehabilitation need to be expanded. This will be a major topic of study in preparation for the third edition, as will the provisions of design methods for partially prestressed concrete. Most future structural research and development projects in MTC will be generated by code needs. This continued development and the active participation of the code writers and users should ensure that the OHBDC remains in the forefront of available bridge codes.

REFERENCES

1. Standard Specifications for Highway Bridges. AASHTO, Washington, D.C., 1977.
2. Specifications for the Design of Highway Bridges. Canadian Standards Association, Rexdale, Ontario, Canada, 1974.
3. Ontario Highway Bridge Design Code, 1st ed. Ministry of Transportation and Communications, Downsview, Ontario, Canada, 1979.
4. P.F. Csagoly and R.A. Dorton. The Development of the Ontario Highway Bridge Design Code. In Transportation Research Record 665, TRB, National Research Council, Washington, D.C., 1978, pp. 1-12.
5. H.N. Grouni and A.S. Nowak. Safety Criteria in Calibration of the Ontario Bridge Code. Presented at International Conference on Short and Medium Span Bridges, Aug. 8-12, 1982, Toronto, Canada.
6. Ontario Highway Bridge Design Code: Addendum 1. Ministry of Transportation and Communications, Downsview, Ontario, Canada, Sept. 1979.
7. Ontario Highway Bridge Design Code: Addendum 2. Ministry of Transportation and Communications, Downsview, Ontario, Canada, Dec. 1980.
8. Ontario Highway Bridge Design Code: Addendum 3. Ministry of Transportation and Communications, Downsview, Ontario, Canada, May 1982.
9. A.S. Nowak and N.C. Lind. Practical Bridge Code Calibration. Journal of the Structural Division of ASCE, Vol. 105, No. 12, Dec. 1979.
10. P.F. Csagoly and Z.K. Knobel. The 1979 Survey of Commercial Vehicle Weights in Ontario. Research Report 230. Ministry of Transportation and Communications, Downsview, Ontario, Canada, July 1981.
11. J.R. Billing. Dynamic Loading and Testing of Bridges in Ontario, 1980. Presented at International Conference on Short and Medium Span Bridges, August 8-12, 1982, Toronto, Canada.
12. J.R. Billing. Estimation of the Natural Frequencies of Continuous Multispan Bridges. Research Report 219. Ministry of Transportation and Communications, Downsview, Ontario, Canada, Jan. 1979.
13. B. Bakht, L.G. Jaeger, and M.S. Cheung. Transverse Shear in Multibeam Bridges. Journal of the Structural Division of ASCE, Vol. 109, No. 4, April 1983, pp. 936-949.
14. P.F. Csagoly, M. Holowka, and R.A. Dorton. The True Behavior of Thin Concrete Slabs. In Transportation Research Record 664, TRB, National Research Council, Washington, D.C., 1978, pp. 171-179.
15. D.B. Beal. Load Capacity of Concrete Bridge Decks. Journal of the Structural Division of ASCE, Vol. 108, No. 4, 1982, pp. 814-832.
16. R.J. Taylor and P.F. Csagoly. Transverse Post-Tensioning of Longitudinally Laminated Bridge Decks. Research Report 220. Ministry of Transportation and Communications, Downsview, Ontario, Canada, June 1979.
17. R.J. Taylor, B. deV. Batchelor, and K. Van Dalen. Prestressed Wood Bridges. Presented at International Conference on Short and Medium Span Bridges, August 8-12, 1982, Toronto, Canada.
18. R.J. Taylor. A Prototype Prestressed Wood Bridge. Structural Research Report 83-SRR-07. Research and Development Branch, Ministry of Transportation and Communications, Downsview, Ontario, Canada, 1983.
19. R.J. Taylor. Wood Bridge Calibration Study for the OHBDC. Structural Research Report 83-SRR-04. Research and Development Branch, Ministry of Transportation and Communications, Downsview, Ontario, Canada, 1983.
20. B.S. Richardson and A. Fam. Ontario Modular Bridge Analysis System. Presented at Annual Conference, Canadian Society for Civil Engineering, June 1-3, 1983, Ottawa, Canada.

Publication of this paper sponsored by Committee on General Structures.

Design Provisions for Dynamic Loading of Highway Bridges

J.R. BILLING and R. GREEN

ABSTRACT

The Ontario Highway Bridge Design Code (OHBDC) contains provisions for dynamic load and vibration that differ substantially from those of other codes. In these provisions it is considered that the dynamic effects of vehicles crossing highway bridges can still be described in terms of an equivalent static effect that is a fraction of the design vehicle load, but the magnitude of this effect is described in terms of the natural frequency of the structure rather than the span length. Few codes are based on a limit-state design philosophy for both design and evaluation. Accordingly, new provisions were required for OHBDC that adequately represent the random effects of the dynamic component of load as typical design and evaluation vehicles traverse a span. A review of existing code provisions for impact, a discussion of vehicle-bridge interaction, and dynamic tests of bridges carried out in the Province of Ontario during the past 25 years are provided. The results of the tests are presented and discussed in the context of a design code for highway bridges. Some existing provisions were found unconservative for structures having a first flexural frequency between 2.0 and 5.0 Hz. Calibration of the load factors for dynamic load allowance for a reliability-based limit-state design code is described. In summary, the dynamic response of modern bridges to modern vehicles is reviewed and how this response can be catered to in a design code is described.

Investigations of the static and the dynamic responses of bridges to loading by both commercial and test vehicles have been part of routine test programs carried out by the Ontario Ministry of Transportation and Communications (MTC) in Canada during the past two to three decades. Investigations of dynamic behavior have been directed toward the response of new forms of construction for intermediate-span and long-span structures and assessment of pedestrian reaction to vehicles crossing flexible structures.

This test experience, together with a trend toward limit-state design for both bridge evaluation and bridge design, led to the development of the Ontario Highway Bridge Design Code (OHBDC). The OHBDC, first published in 1979 and revised in 1983, is a limit-state document. Development of the OHBDC by MTC required an almost complete evaluation of current design procedures. In particular, new provisions were required to represent the random nature of the dynamic component of load as representative design vehicles traversed a span or spans of a structure.

Old and current provisions for dynamic load allowance, the term favored here for impact, are reviewed. This review shows that many different dynamic load allowances have been used in design and that it is not clear that traditional non-limit-state codes model the physical behavior of vehicle-bridge interaction. The process by which the dynamic load allowance provisions of the OHBDC were developed is presented together with the test evidence and code provisions. The OHBDC provisions are believed representative of the principal characteristics of typical vehicle-bridge systems and include recognition of quasi-resonance between vehicle and bridge.

A HISTORY

A first step in the development of the OHBDC was to assess whether design provisions currently in use in North America and elsewhere for highway bridge dynamic loading were appropriate. This was based not only on a survey of those provisions but also on consideration of their derivation and intent.

Allowances for dynamic load, customarily referred to as impact factors, used by several countries are shown in Figure 1 in terms of span. There is general agreement that the allowance should be higher for short spans and should decrease as the longer span increases.

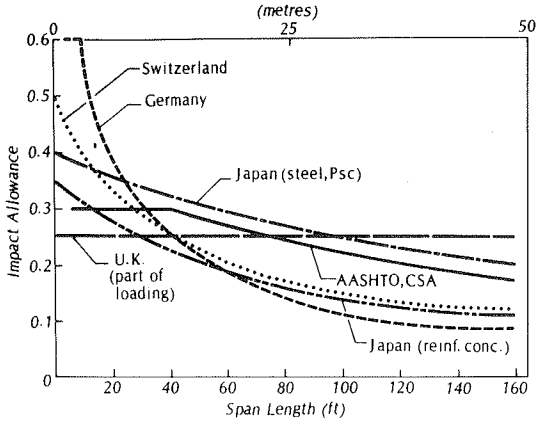

FIGURE 1 Typical impact provisions.

The development of impact factors in North America is of interest. In 1910, Thomson (1) suggested an impact stress allowance having the following form:

$$IS = (LLS)^2/2(DLS + LLS) \quad (1)$$

where

IS = impact stress due to live load,
DLS = stress due to static dead load, and
LLS = stress due to static live load.

The physical background leading to the design equation was neither given nor referenced, but it should

be noted that the ratio of live-load to dead-load stress is the main parameter in the design equation rather than span.

North American highway bridge impact provisions were derived from railway engineering, where designers were required to recognize the hammer-blow effect of steam locomotive drive wheels. This hammer-blow effect produces a sinusoidal force having a frequency proportional to locomotive speed and gives rise to large impactive forces. In 1922, the American Railway Engineering Association (AREA) adopted the following relationship (2):

$$I = 50/(L + 150) \quad (2)$$

where I is the impact factor, not to exceed 0.30, and L is the span length in feet. In the same year AASHO suggested (2) the following (L in feet):

$$I = (L + 250)/(10L + 500) \quad (3)$$

A joint conference committee of AREA and AASHO in 1927 adopted this form (2) (L in feet):

$$I = 50/(L + 125) \quad (4)$$

Thus, the main imput to highway bridge impact allowance was experience with railway bridges and steam locomotives.

The first thorough investigation of highway bridge dynamic loading was conducted from 1922 to 1928 by an ASCE committee (2). This committee identified that decks and deck support components had different response characteristics from those of main longitudinal members. An impact allowance of 0.25 was recommended for decks, and for main longitudinal members the committee suggested the following (L in feet):

$$I = 50/(L + 160) \quad (5)$$

with I not greater than 0.25. Test data were obtained from 10 bridges by using a 15-ton truck driving at speeds up to 15 mph. The recommendation for main longitudinal members included the statement: "Data are too meager to establish a relationship between impact and span." One of the main concerns at this time was the difference in response between vehicles having solid and those having pneumatic tires.

Major studies in the 1950s and 1960s included those carried out by the University of Illinois (3) and as part of the AASHO Road Test (4). These were both analytical and experimental studies and identified roughness and undulation of the riding surface and the approach and bridge as major contributors to the dynamic response of a bridge.

A speed parameter (α) associated with a smoothly rolling axle crossing a span was considered important:

$$\alpha = V/2Lf \quad (6)$$

where

V = truck speed (ft/sec),
L = span (ft), and
f = first flexural frequency (Hz).

In addition, the ratio of axle spacing to span length was found significant. This work at Illinois achieved significant agreement between analytical and observed results and identified the broad scope of the problem, especially for simple-span bridges (3). Three-span continuous bridges were also examined and found to be more complex than simple spans. Neither a quasi-resonance effect of close truck and bridge frequencies nor torsional responses were noted.

An alternative impact factor was suggested as a consequence of this work (5,6):

$$I = 0.15 + \alpha \quad (7)$$

The first term represents the effect of initial oscillation of the truck entering the span and the second the effect of a smoothly rolling mass crossing the span. This form was not, however, adopted in any design code.

Computer simulations in the early 1970s resulted in a rather complicated set of impact factors for the various components of horizontally curved steel bridges (7). This appears to be the only addition to the familiar Equation 4, adopted in 1927 and still widely used some 57 years later (8,9).

The AASHTO specifications (8) use the impact factor to increase member stresses, not to increase loads, although it is not unusual for Equation 4 to be used in design offices as a factor to increase loads rather than member stresses.

This brief survey has shown that the provisions used for dynamic loading of highway bridges are based on early railroad and highway experience. Structures and materials in use then were not typical of current construction. Vehicles were also quite different from typical heavy highway loads currently legal in Ontario and other provinces of Canada, where up to 63,500 kg (630 kN) may be carried on an eight-axle vehicle having a length of 21 to 23 m (10).

Even in the 1920s, when these provisions were developed, a clear relationship between span and impact was not evident. Nevertheless, the AASHTO impact formula has not been unsatisfactory, at least from the point of view that few (if any) bridge failures can be attributed directly to dynamic response of the bridge.

Two consistent patterns emerge from the literature on dynamic loading of bridges. First, the problem is too difficult and complex to address in the context of a design code by analytical means. Second, test data are difficult to obtain and difficult to interpret in a manner relevant to the design provisions of a code. Perhaps, therefore, these considerations have contributed to an apparent lack of need for change in dynamic loading provisions.

VEHICLE-BRIDGE DYNAMIC INTERACTION

To appreciate the design of bridges for vehicles, a discussion of vehicle and bridge characteristics is of value. When a moving load crosses a span that is at rest, the span deflects from an equilibrium position. Forces acting on the span are a combination of those due to the vehicle and span masses. These forces combine to give maximum static and dynamic effects at or near the midspan in simple-span structures. The dynamic response of the bridge will be a combination of the flexural and torsional modes of vibration and a forced response associated with the load oscillating on its suspension system. Elastic resistance of the superstructure tends to restore the span to an equilibrium position, and frictional forces (damping) within the span dissipate energy transferred to the span by the moving load. A typical deflection-time trace for the midspan of a simple-span structure is given in Figure 2. This trace can be thought of as an influence line for deflection at the instrument location, the midspan point.

A steady force is applied to the riding surface by the tires of a vehicle traveling along a smooth

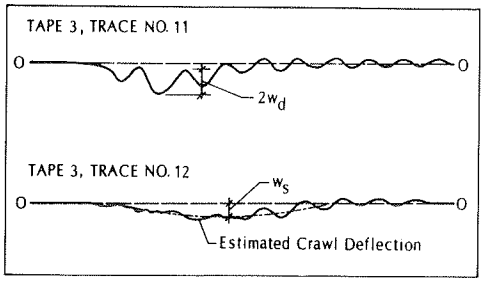

FIGURE 2 Typical deflection-time trace.

horizontal rigid riding surface at a constant velocity. This is an idealized situation, and the application of any external force caused by wind, steering, or braking will result in a change of applied tire force to the riding surface, as will variations in the profile of the riding surface. As a vehicle crosses a bridge superstructure, the superstructure deflects and further variation in vehicle axle load occurs. The instantaneous deflection of the superstructure is a function of the position of the vehicle, the previous deflection history, and the axle load variation. The vehicle and superstructure are inseparably coupled [Figure 3 (11)].

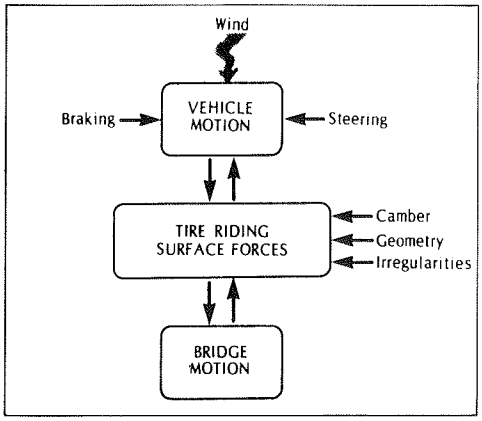

FIGURE 3 Vehicle and bridge interaction.

Thus, any description of the dynamic response of the vehicle-bridge system should include at least the mass distribution, natural frequencies, modes of vibration, and damping characteristics of the bridge superstructure; mass and dynamic characteristics of the vehicle; initial conditions of both vehicle and structure, including vertical displacements and velocity; and riding surface profile. Undulations and irregularities in the approach riding surface caused by repair, weathering misaligned expansion joints, snow, and ice all influence the initial condition of the vehicle. Camber variations, settlement, temperature-induced curvature, and badly maintained surfacing will also affect the superstructure riding surface profile. In addition, the superstructure may not be at rest because of other vehicles on or off the span. All the quantities noted previously cannot be easily monitored or measured within the normal limitations of budgets for either analyses or field tests.

Notwithstanding the complexity of the problem, simple models of vehicles and bridges can be used to gain insight into the principal vehicle and bridge characteristics governing response.

A single axle traversing a simple span without riding surface irregularities and response so small that the load is negligibly different from the static value corresponds to a point force crossing at constant velocity (V). The span deflection is increased over the static value by an amount dependent on the speed parameter α (Figure 4). For typical highway bridges and legal highway speeds, the speed parameter α is in the range 0.08 to 0.20, and the ratio of maximum to static deflection is bounded above by $[(1 + \alpha)/(1 - \alpha)]$ for all α. For typical bridges it is bounded above by $(1 + \alpha)$ (12-15).

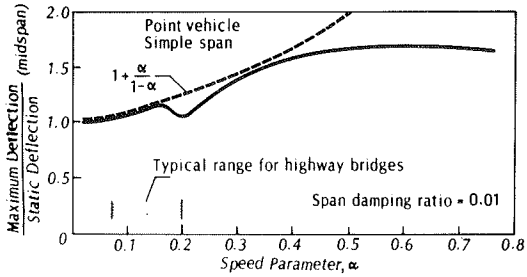

FIGURE 4 Simple-span dynamic amplification for moving-point load.

Now consider a constant force P combined with a constant-amplitude oscillatory load Q of circular frequency Ω, so that a force $(P + Q \sin\Omega t)$ traverses a simple-span bridge. This force represents an upper bound on the real situation because irregularities of the riding surface excite vehicle vibration but no energy is absorbed by the vehicle suspension. The dynamic deflection amplification factor (Δ) is strongly dependent on the ratio of vehicle frequency (Ω) to bridge fundamental frequency ($\omega = 2\pi f$), as shown in Figure 5 for two levels of bridge damping in terms of the fraction of critical damping (γ). The response (Figure 5) is akin to resonance of a system with a single degree of freedom (12) but is not infinite for zero damping

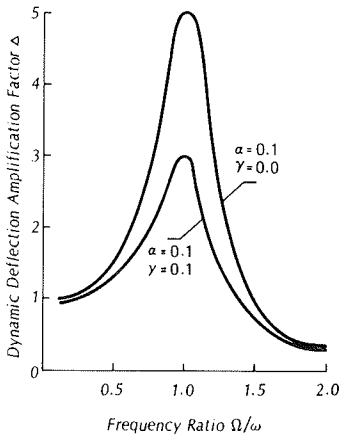

Total Dynamic Amplification of Deflection $= 1 + Q\Delta/P$

FIGURE 5 Dependence of dynamic amplification on frequency ratio and damping.

because passage of the load limits the time the bridge is exposed to the force (13). This large amplification of deflection when the load frequency (Ω) corresponds to the bridge frequency (ω) can be thought of as quasi-resonance.

There are other parameters that affect bridge dynamic response to vehicle passage, such as the ratio of live load to dead load, tire stiffness, and suspension stiffness (11-16). These simple models examine vehicle and bridge dynamic interaction for the first mode of a simple span. Continuous and multigirder bridges may have several modes with frequencies close together. Vehicles have heave frequencies of 2 to 5 Hz, so it is likely that one of the lower modes of any bridge with a span of 20 to 25 m is in the same frequency range. For longer spans for which the first mode of the bridge is below 2 Hz, coincidence of vehicle frequency and frequency of a higher mode of the bridge is likely (17), as is the amplification of response.

In summary, dynamic amplification increases with speed for a moving force but decreases with speed for a sprung mass without damping. The initial conditions for even the simplest case of a moving force and mass entering a span are uncertain, and the initial conditions for a sprung vehicle entering a bridge are even more difficult to assess.

1956-1957 TEST SERIES

A group of 52 bridges known to vibrate was selected for test (18,19). A variety of differing types, spans, and cross-sectional geometry was chosen. Approach and deck conditions varied widely and included marked irregularities or undulations.

From the more than 2,000 individual records of bridge motion for the calibration and other vehicles, it was possible to obtain vehicle speed and axle spacing, maximum static deflection for a given vehicle, amplitude of vibration, and frequencies of vibration. The stiffness of the structure was calculated from the calibration-vehicle data and was used to obtain an equivalent load of all other vehicles. The equivalent load of a vehicle is related through an unknown load-distribution and axle-spacing function to the calibration vehicle.

The importance of the ratio of maximum dynamic deflection (w_d) to maximum static deflection (w_s) in dynamic response studies (Figure 2) is well known. Hence the ratio of maximum dynamic deflection (amplitude) to equivalent load, referred to as the amplitude factor, was used to obtain the amplitude developed by a vehicle of unit equivalent load.

Typical results of interest are shown in Figures 6 and 7 in terms of amplitude factor versus speed and vehicle load, respectively. Figure 6 indicates that the amplitude factor is a function of speed and can have a form associated with a constant moving mass traversing a structure. The influence of increasing equivalent weight on amplitude factor is clearly shown in Figure 7.

The frequency of vibration of the loaded structures was generally the first longitudinal flexural frequency, suitably corrected for the additional mass of the vehicle, or a forced frequency the value of which ranged from 2 to 3 Hz. This range corresponds to the bounce frequency normally reported for heavy commercial vehicles sprung only by tires and having an inactive suspension system (4). Among the various correlations attempted, the tendency of the median amplitude factor to decrease with static stiffness (not shown) and to increase for bridges with observed frequencies in the range of the 2 to 5 Hz was apparent (Figure 8) (18).

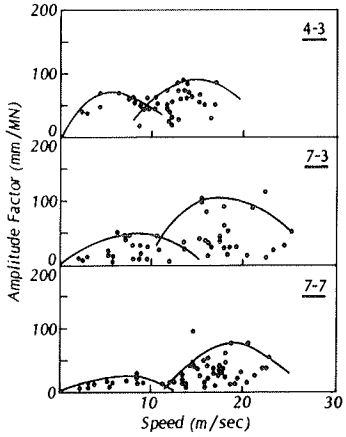

FIGURE 6 Amplitude factor versus speed.

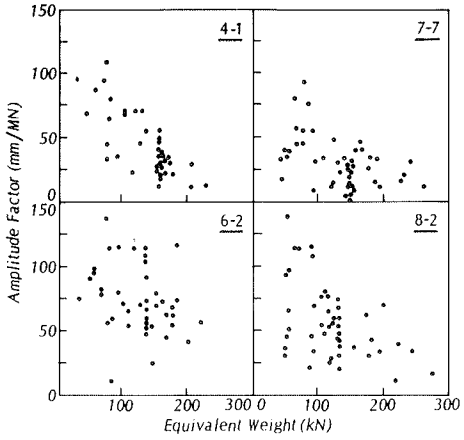

FIGURE 7 Amplitude factor versus equivalent weight.

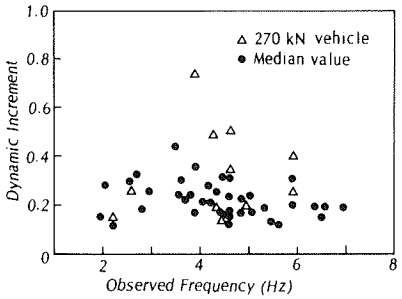

FIGURE 8 Dynamic increment versus observed frequency.

1969-1971 TEST SERIES

During this period a series of tests was completed on continuous concrete bridges by using a five-axle tractor-trailer combination weighing 400 kN (20). Calculated frequencies corresponded with observed values in most cases. The maximum observed dynamic amplification of deflection varied from 0.30 to 0.85 for bridges in the measured frequency range of 2 to 5 Hz because of a single test vehicle.

The observations from this test series led to the design concepts used for the Conestogo River Bridge

(21) in which by relaxing the live-load deflection to span requirements of AASHTO (8), it was possible to provide a distribution of longitudinal stiffness that yielded a first flexural frequency outside the quasi-resonance range associated with 2 to 5 Hz. The importance of the frequency content of the loading function on the magnitude of dynamic effects is clearly illustrated in Figure 9 (21) in which the footfall frequency of a horse drawing a buggy produced a greater dynamic response than a heavy truck did. The latter, however, produced the larger static response.

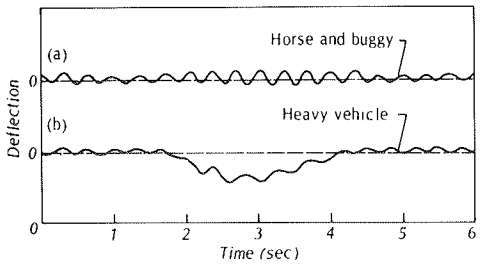

FIGURE 9 Deflection-time trace, sample span.

1980 TEST SERIES

The 1980 tests were carried out to ensure that values of mean dynamic response and the associated coefficient of variation used in calibration of the OHBDC were representative of modern vehicles and bridges. Test results indicated that reductions could be made in the values specified for dynamic effects in the first edition of OHBDC (22) as part of the second edition (23).

A total of 27 structures were selected at 22 locations, 5 of which were twin structures. They included 14 steel spans of 22 to 122 m, 10 concrete spans of 16 to 41 m, and three timber spans of about 5 m (24). The approaches, expansion joints, and deck of all of these bridges were in good to excellent condition.

Four test vehicles were used. TV1 and TV2 were five-axle tractor-trailer combinations having gross weights of 391 and 414 kN, TV3 was an eight-axle combination having a gross weight of approximately 580 kN, and TV4 was a three-axle service vehicle (241 kN). The vehicles are representative of heavy commercial vehicles operating in Ontario and all were loaded close to their legal limit.

More than 100 individual runs were recorded for each bridge by both test vehicles and normal traffic crossing the spans at a variety of speeds. In addition, the response of the bridge to truck passage was assessed subjectively by technicians associated with the tests; they used the Reiher-Meister scale (25).

The FM tapes of acceleration values recorded during the test were used to determine frequencies, mode shapes, and damping ratios of the bridge vibration modes (26). Between 6 and 12 modes of vibration of longitudinal flexure, torsion, and transverse flexure could normally be identified with certainty for longer-span continuous bridges (Figure 10). In contrast, the three timber bridges tested did not appear to have any vibration modes.

Values of the first flexural frequency are shown against the longest span of the bridge in Figure 11. Although there is a clear trend, with only a few data points covering a diversity of construction, it is unreasonable to suggest a simple relationship between frequency and span that could be

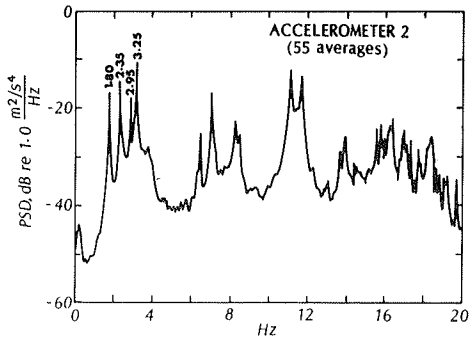

FIGURE 10 Power spectra, Gull Lake.

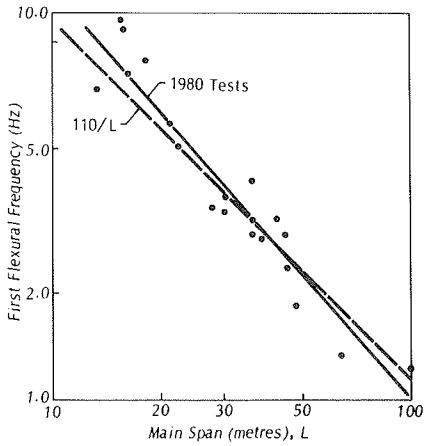

FIGURE 11 Frequency versus main span.

codified. A simple relationship such as f = 110/L (meters) appears to be useful for the preliminary design estimate of frequency. The test series did indicate that all components of the structure resist the action of both static and dynamic load.

By using the typical responses shown in Figure 12 for a three-span continuous bridge, three response

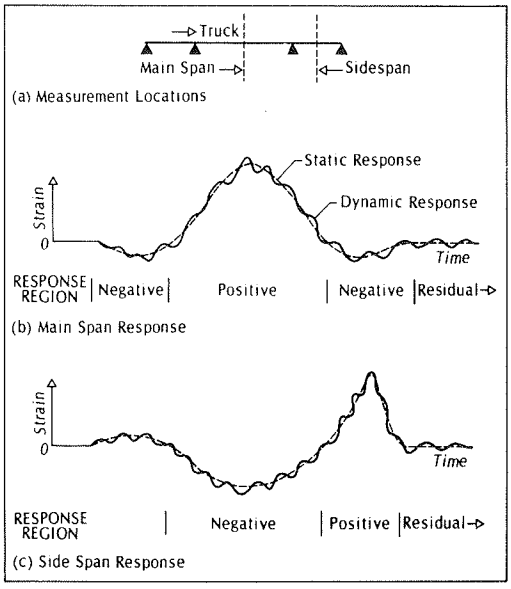

FIGURE 12 Typical responses.

regions were defined. Dynamic amplifications were computed for the three response regions by using the greatest static response for any instrument location. The overall statistics of dynamic amplification are presented in Table 1. These data include for each bridge all single-truck runs by test vehicles and by other traffic at all speeds in any one lane. The mean dynamic amplifications are not large, even though some individual test dynamic amplifications greater than 0.5 were observed. The coefficients of variation are large, varying between 0.56 and 1.11 with a mean of 0.85. The data of Table 1 show that the mean dynamic amplifications of continuous bridges are approximately equal for both positive and negative regions of the influence line for deflection at a given point.

Test vehicles TV1 and TV2 were similar in overall dimensions and weight. TV2 had an air suspension, whereas TV1 had leaf springs. The mean dynamic amplification by TV2 was about 60 percent of that for TV1 for all runs on all bridges. Presumably the air-spring and parallel shock-absorber suspension system provides damping under all conditions, whereas the leaf-spring assembly only absorbs energy for large displacements or high rates of loading (4).

The mean dynamic amplification for all runs generally decreased with increase in weight of trucks for spans greater than about 30 m (Figure 13). This reduction is presumably because additional axles are required for an increase in legal gross vehicle weight, and these axles are not in phase, which moderates the dynamic effect. If the product of truck weight and mean dynamic amplification is used as a measure of total dynamic load associated with a vehicle, Figure 14 shows the dynamic load for various test vehicle weights, corresponding to the data of Figure 13. The dynamic load for each of the four bridges shown is sensibly constant for each test vehicle weight; the different magnitudes are associated with different pavement irregularities for each bridge.

HUMAN RESPONSE

During a test technicians and others were asked to stand on the bridge and provide a subjective rating of bridge vibration caused by passing trucks. The Reiher-Meister descriptors (25) were used: not perceptible, slightly perceptible, distinctly perceptible, strongly perceptible, disturbing, and very disturbing. No training or calibration was given. The threshold of perception was found to be in the range of 0.015 to 0.025 g. The slightly, distinctly, and strongly perceptible ratings had mean accelerations of 0.039, 0.052, and 0.076 g, respectively. For one structure with a measured frequency of 0.75 Hz, the highest and mean of observed accelerations under normal traffic were 0.062 and 0.036 g, respectively. This particular structure had a live-load deflection to span ratio nearly twice that permitted by AASHTO (8).

OHBDC deflection criteria for pedestrian service-

TABLE 1 Overall Statistics of Dynamic Amplification

Bridge No.[a]	Positive Region Mean	Positive Region CV	Negative Region Mean	Negative Region CV	f (Hz)	Location[b]
1	0.129	0.67			4.00	
4	0.069	0.74			3.13	
6	0.136	0.90			5.00	
7	0.057	1.00			10.63	
8	0.110	1.11			12.00	
9	0.305	0.91				
10	0.093	0.84				
11	0.156	0.98			10.38	
12	0.077	0.65			3.13	
13	0.098	1.04			8.06	
14	0.150	0.85	0.105	1.18	7.13	a
	0.119	0.69	0.033	0.88		b
15	0.068	0.61	0.006	1.00	5.88	a
	0.031	0.72	0.003	0.76		b
16	0.161	0.72	0.134	0.79	3.31	c
	0.205	0.77	0.104	0.98		d
17	0.164	0.70	0.123	0.42	2.94	a
	0.141	0.72	0.100	0.57		
18	0.191	0.55	0.192	0.56		
19	0.174	0.56	0.171	0.48	1.80	c
	0.112	0.60	0.084	0.66		d
20	0.194	0.76			2.31	
21	0.210	0.93			2.88	c
	0.167	0.82				e
23	0.177	1.03	0.137	0.85	3.63	
24	0.236	1.05	0.204	0.78	2.69	
26	0.079	0.73	0.097	0.63	3.44	a
	0.062	0.83	0.041	0.85		b
27	0.090	0.63	0.092	0.52	0.75	a
	0.099	0.67	0.061	0.66		b
	0.084	0.59	0.075	0.55		d

Note: CV = coefficient of variation, f = mode frequency.

[a] See report by Billing (24).

[b] Location: a = main span, b = side span, c = midspan, d = support, e = floor beam.

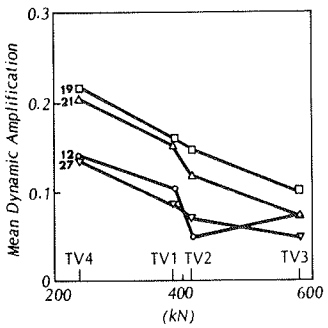

FIGURE 13 Mean dynamic amplification versus test vehicle weight.

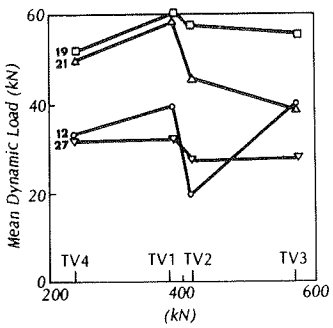

FIGURE 14 Mean dynamic load versus test vehicle weight.

ability are compared with results obtained from tests in Figure 15; observed deflections are scaled to provide values appropriate to a serviceability limit-state truck load. None of the bridges tested had significant pedestrian use. However, the criteria appear appropriate even though the bridges in the field behaved in such a way as to include the stiffening effects of curbs and barrier walls.

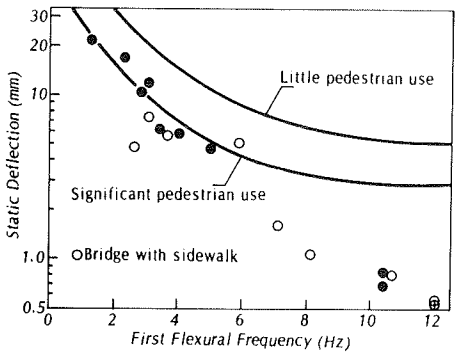

FIGURE 15 Pedestrian serviceability.

DESIGN OF OHBDC PROVISIONS

The OHBDC was undertaken to implement into design and evaluation various recent research findings regarding structural design and response (27). It was also undertaken to make design loads representative of actual and legal heavy truck traffic in the Province of Ontario (10).

The existing provisions for dynamic loading of bridges were elementary and familiar to design engineers, so they were easy to apply. However, as also noted previously, the dynamic components of loads arise from a complex process of vehicle and bridge dynamic interaction. It was therefore likely that any provisions that would require a significant increase in computation or complexity for what was often only a few percent of the total design load would not be accepted readily by design engineers. The question of whether the impact formula could or should be retained was carefully considered. It became apparent that change was not only necessary but essential, for three reasons. First, continued use of a formula bearing little relation to observed behavior of bridges in some span ranges would inhibit future editions of OHBDC and other code developments. Second, the need for a realistic representation of bridge loading becomes more important as analysis methods improve and as bridges become more slender and fatigue more important to design. Finally, because OHBDC was to be one of the first codes in North America developed by using an approach based on limit-state reliability, if any substantive change was to be made to the dynamic loading effects, it should be made with the first edition of that code. Once the need for change was realized, it was possible to focus on the task of developing a form and values for the provisions that would jointly satisfy the designer's need for simplicity and adequately represent the main dynamic effect of vehicle loads.

The literal interpretation of the term "impact factor" was considered too narrow to express the complex interaction of vehicle components, undulation and roughness of approach and bridge riding surface, bridge dynamics, and vehicle speed. It was discarded in favor of the term "dynamic load allowance."

The OHBDC provisions on dynamic loading were written with future developments in mind. The designer was therefore permitted to use any approved dynamic analysis or test or both to develop a dynamic load allowance. In lieu of these, which would probably only be in special circumstances, a dynamic load allowance was prescribed as an increase to and a fraction of the prescribed highway live load. This contrasts with other codes in which dynamic effects are accounted for by an increase in stresses in designated components and members caused by the live load (8,9).

This change means that the components of a bridge need not be defined with respect to their load-carrying function, because the appropriate allowance will automatically be included in the load applied to a particular component. It also represents the process actually used by designers.

The principal dynamic loading provisions of the second-edition OHBDC (23) are as follows:

1. The dynamic load allowance for a single wheel or axle unit of the OHBDC truck, shown in Figure 16, shall be 0.4. This allowance will be used primarily for design of deck slabs, short-span floor beams, and other components governed by the local effects of the impactive action of wheel load.

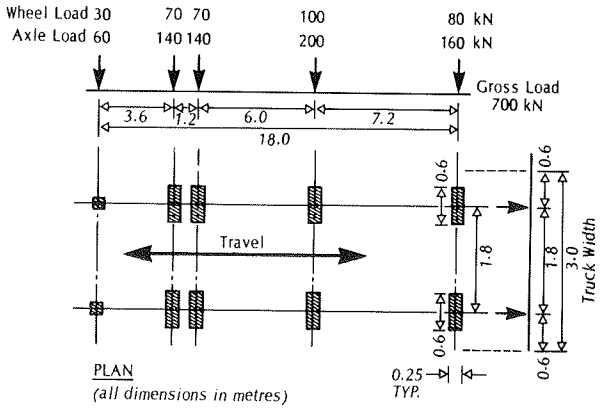

FIGURE 16 OHBDC truck.

2. The dynamic load allowance for more than a single axle of the OHBDC truck acting on a structure having no span in excess of 22 m shall be 0.3. This allowance will be used primarily for design of simple and continuous spans, transverse floor beams, and diaphragms where strong interaction between truck and bridge is unlikely. Typically, a span of 22 m would have a frequency no less than 5 Hz.

3. For a structure having any span greater than 22 m, the dynamic load allowance for the truck portion of the lane load shall depend on the first flexural frequency of the bridge, as shown in Figure 17. The dynamic load allowance for the uniformly distributed portion of the lane load shall be 0.1. This allowance will be used for design of main longitudinal members of the bridge where significant response of the bridge modes of longitudinal and torsional vibration is likely.

4. The dynamic load allowance for soil-steel structures shall be 0.4 for zero cover, reduced as depth of cover increases.

5. The dynamic load allowance for timber bridges shall be reduced by a factor of 0.7. This recognizes the higher damping of this type of construction.

6. For evaluation a reduced dynamic load al-

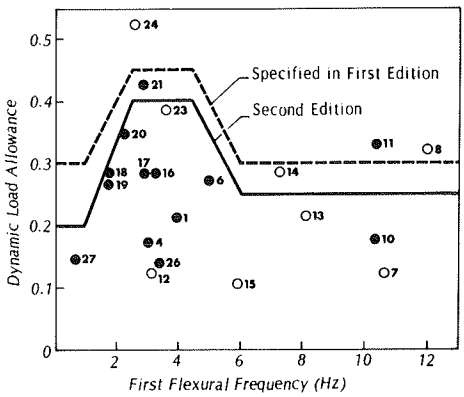

FIGURE 17 Dynamic load allowance versus frequency.

lowance shall be used for passage by a single vehicle carrying an exceptional load at low speed.

The values just given apply to loading in a single or multiple traveled or design lane or lanes. Multiple presence factors for dynamic loading in more than one lane were taken as 0.7 for two lanes, 0.6 for three lanes, and 0.5 for four or more lanes, and these factors were incorporated in the multiple presence factors for highway live load; this disguised the reduction in the dynamic load allowance due to multiple presence but facilitated calculation.

The values for dynamic load allowance given earlier are those that resulted from code calibration (28). Calibration was a process carried out to define load factors that would result in a reasonably uniform safety index (β) for all members of all bridge types. The load factor accounts for uncertainty in load and analysis and may include a professional factor. Although there are significant differences in longitudinal and transverse distributions of live load and dynamic load and in their variability, it was decided that a common load factor should be used for both live and dynamic loads as a convenience.

$$\alpha_{LL}I = \alpha_I\bar{I} \tag{8}$$

where

α_{LL} = specified live load factor, also to be used for dynamic load;
I = specified dynamic load allowance;
α_I = computed load factor for dynamic load based on $\bar{I}$, and
$\bar{I}$ = mean dynamic amplification

Therefore

$$I = \alpha_I\bar{I}/\alpha_{LL} \tag{9}$$

A typical value of α_I might be 2.5, and α_{LL} was specified as 1.4; hence a specified dynamic load allowance of 0.4 (say) would result from a mean observed dynamic amplification of only 0.22.

Values of mean dynamic amplification obtained from the tests (Table 1) were scaled by using Equation 9 and appropriate ratios of load factors (α_I/α_{LL}) ranging from 1.6 to 2.2 depending on the coefficient of variation (26) and the results plotted in Figure 17. The high dynamic amplification present for the majority of bridges in the region of 2 to 5 Hz is captured through the OHBDC provisions. AASHTO values at 2 and 3 Hz would be 0.16 and 0.20, respectively, for typical spans.

SERVICEABILITY

Some codes retain limitations on the ratio of depth to span of main longitudinal members and of deflection to span (8,9) introduced by railroad engineers during the 19th century. A review of these limitations in 1958 was unable to establish a basis for the limitations nor was change recommended (29).

The OHBDC considered specific provisions covering span-depth and span-deflection limitations but noted that such limitations might inhibit future innovation in design. Finally, because deflection was not regarded as a limit state, these limitations were discarded in favor of bridge vibration as a serviceability limit state. Pedestrians on a bridge are sensitive to acceleration of the superstructure produced by passing vehicles. Because it is difficult for the designer to compute accelerations, they were transformed to equivalent deflections at the edge of the structure, assuming average truck weights and bridge dynamic response. Three levels of vibration control were identified, and the two lower deflection levels are presented in Figure 15. The upper level (not shown) applies to bridges without sidewalks, which would be traversed only by maintenance personnel. The lowest level might apply to bridges in cities or in rural regions where they might be used for viewing or fishing. The second level is for bridges with sidewalks where few pedestrians are expected. Data from tests show that even the lowest level will generally be unrestrictive for spans greater than 20 m (26).

DISCUSSION

The recent report by the ASCE Committee on Loads and Forces on Bridges (30) focused attention on the problem of impact on bridges. Some assistance may be offered by this paper based on Ontario's experience in the resolution of the research problems identified by that committeee. The dynamic response of a vehicle subsequent to traversing an undulating approach and irregular expansion joint is unlikely to be quantified for use in the analysis of vehicle-bridge interaction. The mean value of the undulating component of vehicle load is influenced by vehicle suspension systems and vehicle length and appears to be sensibly constant for a given bridge and approach condition (Figure 14); it is not a function of gross vehicle weight for spans longer than the vehicle. The importance of suspension system characteristics and riding surface to the mean dynamic load associated with vehicles is not new (4-6,15,18). The structural engineer has little or no control over either suspension or riding surface properties and hence must rely on the results of field observations.

The Ontario studies, even as early as the mid-1950s, indicated that dynamic amplification values for individual bridges with frequencies in the region of 2 to 5 Hz were on the average greater than the similar mean values for bridges with spans of 15 to 20. This trend (Figure 11) is also apparent in the 1968-1971 data (not shown) (20) and in the 1980 data (Figure 17), and it is not unreasonable to consider that a dynamic property of a structure should be a primary variable in the dynamic response. There is no reason, even noting the variability of dynamic amplification, to expect this trend to be only an Ontario phenomenon, and indeed, as recent Swiss data (31) (Figure 18) illustrate, it is not. The Swiss data, for maximum response on smooth pavements, are from new bridges proof-tested by using similar vehicles (160 kN) traveling along the longitudinal centerline of the structure. The amplification values are bounded by a line having the same

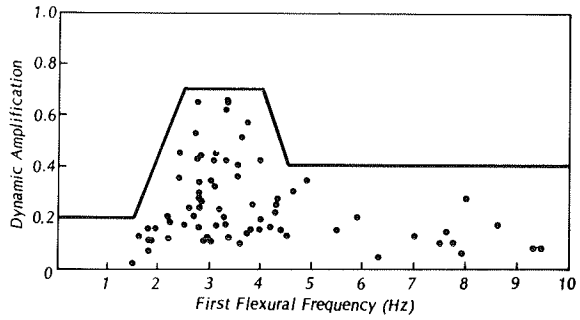

FIGURE 18 Peak dynamic amplification versus frequency, Swiss results.

form but not the same numerical values as those for the OHBDC (Figure 17).

Thus it does appear that first flexural frequency should be considered as a major variable for dynamic load allowance, particularly for spans with frequencies less than 5 Hz. Although the frequency range (2 to 5 Hz) may appear troublesome for design, no attempt should be made to avoid this frequency range, because dynamic load allowance values are available. On the other hand, designs can be created to reduce the large allowances associated with quasi-resonance (21).

The question of the need to consider dynamic effects at the ultimate limit state and what value should be used is for the calibration experts. Perhaps future design codes will incorporate an allowance for dynamic effects directly into the design loads at the ultimate and serviceability limit states and provide appropriate models for the analysis of vehicle effects at both limit states that reflect both static and dynamic response characteristics.

CONCLUSIONS

The provisions regarding dynamic loading of highway bridges in use in North America have been essentially unchanged for more than 50 years. It is questionable whether these provisions were representative of bridge behavior at the time they were developed. They are certainly not representative for large, heavy trucks on bridges that are becoming more slender and of longer span in the interests of economy.

The OHBDC has developed a new terminology and form for dynamic loading. The code attempts to represent the principal mechanisms of bridge loading and response in a manner that the designer can use with little change from current methods. The provisions have been written so as not to restrict further developments and are essentially independent of design vehicle geometry. All provisions of the 1983 OHBDC are discussed in another paper in this Record (Dorton and Bakht).

The OHBDC provisions have been built from the experience of the past by retaining values of dynamic load allowance for short spans but have added to this experience by considering the impactive manner of single-axle loads acting on the riding surface and vehicle-bridge interaction over a wide range of bridge types. The parameters used in the provisions refer to a dynamic characteristic of structure, frequency, rather than just span. The change in form of dynamic loading as a function of frequency has been supported by tests completed by others.

ACKNOWLEDGMENT

Support and coordination for this work was provided by the Research and Development Branch, MTC; this support is greatfully acknowledged. Additional support was provided through an operating grant awarded to the second author by the Natural Sciences and Engineering Research Council of Canada. Thanks are due many members of OHBDC committees who contributed to the development of the code and the provisions discussed here.

REFERENCES

1. W.C. Thomson. Bridge and Structural Design. McGraw-Hill, New York, 1910.
2. Impact in Highway Bridges. Transactions of ASCE, Vol. 95, 1931.
3. W.H. Walker. Final Report of the Investigation of Impact on Highway Bridges. Project IHR-9. Engineering Experiment Station, University of Illinois, Urbana, June 1969.
4. Special Report 61D: The AASHO Road Test: Report 4--Bridge Research. HRB, National Research Council, Washington, D.C., 1962.
5. W.H. Walker and A.S. Veletsos. Response of Single-Span Highway Bridges to Moving Vehicles. Bull. 486. Engineering Experiment Station. University of Illinois, Urbana, 1966.
6. R.N. Wright and W.H. Walker. Vibration and Deflection of Steel Bridges. Engineering Journal, Jan. 1972.
7. Tentative Design Specifications for Horizontally Curved Highway Bridges. AASHTO, Washington, D.C., 1975.
8. Standard Specifications for Highway Bridges, 12th ed. AASHTO, Washington, D.C., 1977.
9. Design of Highway Bridges. CAN3-S6-M78. Canadian Standards Association, Rexdale, Ontario, Canada, 1978.
10. P.F. Csagoly and R.A. Dorton. Proposed Ontario Bridge Design Load. Research Report 186. Ontario Ministry of Transportation and Communications, Downsview, Ontario, Canada, Nov. 1973.
11. Ontario Highway Bridge Design Code: Supplements. Ontario Ministry of Transportation and Communications, Downsview, Ontario, Canada, 1979.
12. J.M. Biggs. Introduction to Structural Dynamics. McGraw-Hill, New York, 1964.
13. L. Fryba. Vibration of Solids and Structures Under Moving Loads. Noordhoff International Publishing, Groningen, Netherlands, 1972.
14. Steel Guideways for Mass Transit. American Iron and Steel Institute, Washington, D.C., 1977.
15. H.H. Richardson and D.N. Wormley. The Coupled Dynamics of Transportation Vehicles and Beam-Type Elevated Guideways. Journal of Dynamic Systems, Measurement and Control, June 1974.
16. A.S. Veletsos and T. Huang. Analysis of Dynamic Response of Highway Bridges. Journal of the Engineering Mechanics Division of ASCE, Vol. EM5, Oct. 1970.
17. J.R. Billing. Estimation of the Natural Frequencies of Continuous Multi-Span Bridges. Research Report 219. Research and Development Division, Ontario Ministry of Transportation and Communications, Downsview, Ontario, Canada, Feb. 1979.
18. D.T. Wright and R. Green. Highway Bridge Vibration, Part II. Ontario Test Programme. OJHRP Report 5. Ontario Joint Highway Research Programme, Queen's University, Kingston, Ontario, Canada, 1964.
19. R. Green. The Motion of Highway Bridges Under Moving Loads. M.S. thesis. Queen's University, Kingston, Ontario, Canada, 1958.

20. P.F. Csagoly, T.I. Campbell, and A.C. Agarwal. Bridge Vibration Study. Research Report 181. Ontario Ministry of Transportation and Communications, Downsview, Ontario, Canada, 1972.
21. R.A. Dorton. The Conestogo River Bridge Design and Testing. Presented at Canadian Structural Engineering Conference, Montreal, Quebec, Canadian Institute of Steel Construction, Toronto, Canada, 1976.
22. Ontario Highway Bridge Design Code, Vols. 1 and 2. Ontario Ministry of Transportation and Communications, Downsview, Ontario, Canada, 1979.
23. Ontario Highway Bridge Design Code, 2nd ed. Ontario Ministry of Transportation and Communications, Downsview, Ontario, Canada, 1983.
24. J.R. Billing. Dynamic Loading and Testing of Bridges in Ontario, 1980. Presented at International Conference on Short and Medium Span Bridges, Canadian Society of Civil Engineering, Toronto, Canada, Aug. 1982.
25. H. Reiher and F.J. Meister. The Effect of Vibration and People. Forschung auf dem gebeite des Ingenieurwesens, Vol. 2, No. 11, 1931, p. 381 (translation: Report F-TS-616-RE, Headquarters Air Materiel Command, Wright Field, Ohio, 1946).
26. J. R. Billing. Dynamic Tests of Bridges in Ontario, 1980: Data Capture, Test Procedures and Data Processing. Report SRR-82-02. Research and Development Branch, Ontario Ministry of Transportation and Communications, Downsview, Ontario, Canada, 1982.
27. P.F. Csagoly and R.A. Dorton. The Development of the Ontario Highway Bridge Design Code. In Transportation Research Record 665, TRB, National Research Council, Washington, D.C., 1978, pp. 1-12.
28. A.S. Nowak and H.N. Grouni. Calibration of the Ontario Bridge Design Code, 1983 Edition. Canadian Journal of Civil Engineering, in preparation.
29. Deflection Limitations of Bridges. Journal of the Structural Division of ASCE, Vol. 84, No. ST3, May 1958.
30. Bridge Loading, Research Needed. Journal of the Structural Division of ASCE, Vol. 108, No. ST5, May 1982, Proc. Paper 17064.
31. R. Cantieni. Dynamic Load Tests on Highway Bridges in Switzerland--60 Years Experience EMPA. Report 211. Eidgenössische Materialprüfungs- und Versuchsan-stalt, EMPA, Dübendorf, Switzerland, 1983.

Publication of this paper sponsored by Committee on Dynamics and Field Testing of Bridges.

Notice: The conclusions presented in this paper are those of the authors and not necessarily those of any sponsor.

Implementation of the Analytical Capabilities Required for the Aseismic Design of Bridges

ROY A. IMBSEN and J. LEA

ABSTRACT

The design of a highway bridge located in a region of high seismic risk must include a detailed and accurate analysis of the bridge to determine its maximum anticipated seismic loads. To comply with newly developed code requirements and to ensure the utmost confidence in the predicted response, the seismic analysis should be performed by using the appropriate analytical procedures. The recently developed computer program Seismic Analysis of Bridges (SEISAB) used to conduct seismic analyses that comply with both the current AASHTO specifications and the Applied Technology Council seismic design guidelines is described. In addition, a description is given of the single-mode spectral method developed for the new guidelines for a specific category of bridges with low to moderate seismic vulnerability. An example is included to demonstrate the applicability of this method to a two-span bridge. A second example is included to illustrate how SEISAB-I was used to conduct a response spectrum dynamic analysis on a six-span curved bridge. Included also is a description of the nonlinear dynamic analysis capabilities to be included in the next version, SEISAB-II. The implementation of SEISAB-I through workshops funded by the National Science Foundation and the acceptance of the program based on trainee evaluations are also briefly described.

Both the current AASHTO bridge specifications (1), which were upgraded following the 1971 San Fernando earthquake, and the more recently adopted AASHTO Seismic Design Guidelines for Highway Bridges (2) require that a single-mode or multimode response spectrum analysis be conducted in the design of bridges to be located in zones of higher seismic activity. Because the analytical procedures involved in seismic analyses are new to many bridge de-

signers, it has been difficult to implement these new methodologies within the United States. Recognizing this problem, the National Science Foundation elected to fund a project to develop the computer program Seismic Analysis of Bridges (SEISAB) and conduct pilot workshops to aid in this implementation effort.

In addition to being used as a design tool to facilitate the implementation of the new design codes, SEISAB is also being extended to bring to the profession the nonlinear capabilities that were developed at the University of California, Berkeley, as part of an investigation into the adequacy of bridge structural resistance to seismic disturbances (3). These nonlinear capabilities of SEISAB are being designed for use by the researcher or bridge designer involved in the following design-related activities:

1. Conducting parametric studies to establish procedures and design coefficients for new or improved aseismic design specifications,
2. Conducting detailed dynamic analyses on complex bridges,
3. Investigating newly developed aseismic design strategies that include energy dissipation, and
4. Developing design procedures that include the complex effects of soil-structure interaction.

Extending SEISAB to include both newly developed elements unique to bridges and nonlinear analysis capabilities provides a vehicle for implementing the state-of-the-art methodologies emerging from the universities for the bridge engineering profession.

In line with the primary objective of developing a usable design tool, SEISAB-I was developed by incorporating a problem-oriented language written specifically for the bridge engineer (4,5). The free-format SEISAB language consists of simple, easy-to-remember commands natural to the bridge engineer in describing a bridge. Using a minimum amount of user input data, the program generates a mathematical model completely. SEISAB-I, which contains linear dynamic analysis capabilities, was well received in its initial pilot workshop in which it was presented to a selected group of highly qualified bridge engineers from the California Department of Transportation. Three subsequent workshops that included the use of SEISAB-I for both the design and the retrofitting of bridges were equally successful.

BACKGROUND

FHWA recently sponsored a series of workshops entitled Seismic Design of Highway Bridges to implement the latest principles of aseismic design (6). During these workshops, it was obvious that one of the most complicated tasks for a bridge engineer in attempting to apply these new design principles is conducting the dynamic analysis of the structural system. This problem faces most bridge designers today, whether they use the current AASHTO design specifications or the newly adopted Applied Technology Council (ATC) seismic design guidelines (2). The introduction of structural dynamics to the bridge design process requires that bridge designers learn both the basic principles in dynamics and the use of computer programs having dynamic analysis capabilities. This also implies that the designer has had at least introductory training in the art of mathematical modeling.

Because of the new concepts introduced in the AASHTO and ATC-6 design specifications, a major effort is required to train practicing bridge engineers in the latest principles of seismic design. In addition, if this training is to broaden the base so that further advancements in seismic design can be made, it must stimulate the interest of the profession as a whole.

Although the application of structural dynamics to the bridge engineering field is somewhat in its infancy, it has become apparent that certain types of bridges may be idealized so as to be more easily analyzed mathematically. Penzien and Imbsen developed the single-mode spectral method (SMSM) presented in the ATC-6 guidelines in an effort to simplify the task of implementing structural dynamics within the field of bridge engineering (7).

The SMSM is used to calculate the seismic design forces of a bridge that can be characterized as having its major dynamic response in a single mode of vibration. This method, although quite rigorous from a theoretical point of view, reduces a complex dynamics analysis to the performance of just two statics analyses. The first statics analysis is conducted to obtain the structural period and its corresponding displaced shape, the second to apply inertial forces consistent with that displaced shape. The intensity of the inertial forces is determined from a response spectrum selected for the bridge site by using the calculated structural period.

The SMSM as formulated can be applied to many types of bridges, including those with either continuous or discontinuous superstructures. Boundary conditions at the abutments and piers can be modeled to include the effects of the foundation. A bridge engineer can readily apply the SMSM by using a hand calculator and conventional statics structural analysis procedures. For the more complex bridges in the higher seismic zones, the seismic design guidelines recommend the multimode spectral method (MMSM), which is a response spectrum analysis. The SEISAB-I user has the option of using either the SMSM or the MMSM.

DEVELOPMENT OF THE SMSM FOR CONTINUOUS BRIDGE SYSTEMS

Bridges are generally continuous systems made up of many components, each component having distributed mass and elasticity and contributing to the overall response of the system. The response displacement of continuous systems, such as the one in Figure 1, can be shown at any time to be a linear combination of the individual modes of vibration. Restricting the number of modes to one and recognizing that the true vibration shape is unknown results in the following displacement approximation for transverse displacements:

$$v(x,t) = v_s(x)v(t) = v_s(x)A \sin(\omega t - \phi) \quad (1)$$

where

$v_s(x)$ = assumed vibration shape,
$v(t)$ = generalized coordinate representing the amplitude,
A = arbitrary scaling factor, and
ω = circular frequency.

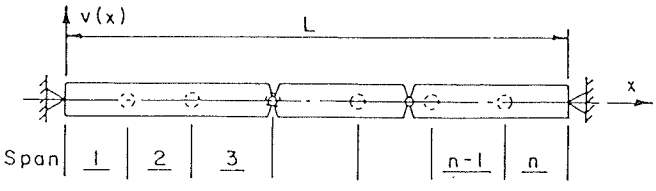

FIGURE 1 Typical bridge configuration.

Because the true mode shape is unknown, the best approximation to it should be obtained.

The process of selecting the closest possible approximation of the shape function, such as the approximation shown in Figure 2, can be facilitated by taking advantage of the free vibration displacements that result from inertial forces. Because inertial forces are proportional to the mass distribution, a transverse distributed load proportional to the mass should produce a good approximation of the true mode shape. Because the mass is usually distributed uniformly in bridge decks, application of a uniformly distributed load, p_o, shown in Figure 3, will displace the bridge deck into the approximate shape of the mode. This method of obtaining an approximating shape results in the consistency of $v_s(x)$ with the support conditions and intermediate expansion joints in the deck.

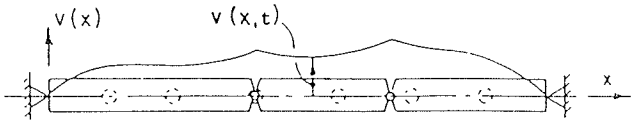

FIGURE 2 Displacement function.

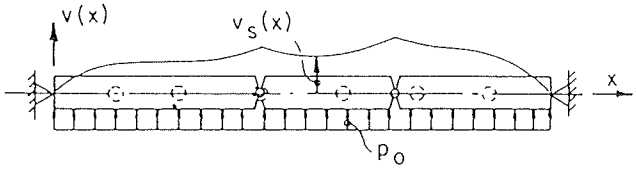

FIGURE 3 Mode shape due to uniform static loading.

Determining Period of Assumed Mode Shape

The vibration period associated with the assumed mode shape can be determined by using Rayleigh's method, which consists of equating the maximum strain energy with the maximum kinetic energy. The maximum strain energy is the stored internal energy resulting from the application of the load p_o and is equal to the work done on the system in displacing the bridge deck into the displaced shape $[v_s(x)]$, which can be expressed mathematically as follows:

$$W_E = (1/2)\int_o^L P_o v_s(x)dx = (P_o/2)\,\alpha \tag{2}$$

where

$$\alpha = \int_o^L v_s(x)dx \tag{3}$$

The kinetic energy (K) is expressed as follows:

$$\begin{aligned} K &= (1/2)\int_o^L m(x)[\dot{v}(x,t)]^2\,dx \\ &= (1/2)\int_o^L m(x)[\omega\cos(\omega t-\phi)v_s(x)]^2\,dx \\ &= (\omega^2/2g)\cos^2(\omega t-\phi)\int_o^L w(x)[v_s(x)]^2\,dx \end{aligned} \tag{4}$$

where $w(x)$ is the weight distribution along the deck. Equation 4 will be at its maximum when $\cos^2(\omega t - \phi)$ is equal to 1, or

$$K_{max} = (\omega^2/2g)\int_o^L w(x)[v_s(x)]^2\,dx = (\omega^2/2g)\,\gamma \tag{5}$$

where

$$\gamma = \int_o^L w(x)[v_s(x)]^2\,dx \tag{6}$$

Equating Equation 2 to Equation 5 and noting that $T = 2\pi/\omega$ results in the following:

$$T = 2\pi(\gamma/P_o\,\alpha g)^{1/2} \tag{7}$$

Pseudoinertial Loading

The maximum value of v(t) can be obtained by applying the concepts of the response spectrum method. The equation of motion for a continuous system approximated by a single generalized coordinate is found by using Hamilton's principle, which states that the first variation of (K - V), where K is the kinetic energy and V is the strain energy, plus the first variation of all nonconservative forces (W_{nc}) is equal to zero. Mathematically, calculating the first variation of I will produce the equation of motion:

$$I = \int_{t_1}^{t_2}(K - V)dt + \int_{t_1}^{t_2} W_{nc}\,dt \tag{8}$$

It can be shown (8) that the first variation of Equation 8 will result in the following:

$$m^*\ddot{v}(t) + c^*\dot{v}(t) + k^*v(t) - p^*_{eff}(t) = 0 \tag{9}$$

where

$$m^* = \int_o^L m(x)[v_s(x)]^2\,dx \tag{10}$$

$$c^* = \int_o^L c(x)\,[v_s(x)]^2\,dx \tag{11}$$

$$k^* = \int_o^L E^*I^*(x)[\partial^2 v_s(x)/\partial x^2]^2\,dx \tag{12}$$

$$p^*_{eff} = -\ddot{v}_g(x,t)\int_o^L m(x)v_s(x)dx \tag{13}$$

$E^*I^*(x)$ is the equivalent bending stiffness of the deck and $\ddot{v}_g(x,t)$ is the horizontal ground acceleration. Dividing Equation 9 by m^*, noting that c^*/m^* is $2\xi\omega$ and k^*/m^* is ω^2, and defining

$$\beta = \int_o^L w(x)v_s(x)dx \tag{14}$$

results in

$$\ddot{v}(t) + 2\xi\omega\dot{v}(t) + \omega^2 v(t) = -\ddot{v}_g(x,t)(\beta/\gamma) \tag{15}$$

By using the response spectrum method with a desired acceleration spectrum, noting that $S_d = S_a/\omega^2$, and given that $C_s = S_a/g$, $v(t)_{max}$ is calculated by the following equation:

$$|\,v(t)\,|_{max} = (\beta C_s g/\gamma\omega^2) \tag{16}$$

Substituting Equation 16 into Equation 1, v(x,t) becomes

$$v(x,t)_{max} = (\beta C_s g/\gamma\omega^2)v_s(x) \tag{17}$$

Equation 17 defines the maximum spectral displacements of all points on the bridge deck due to an assumed acceleration spectrum. The pseudoinertial load ($\overline{F}_I$) that is associated with this displacement and that approximates the inertial effects is found by noting that $S_a = \omega^2 S_d = \omega^2 v(x,t)_{max}$:

$$\begin{aligned} \overline{F}_I &= m(x)a \\ &= m(x)S_a \\ &= m(x)\omega^2 S_d \\ &= m(x)\omega^2 v(x,t)_{max} \\ &= [C_s\beta w(x)/\gamma]\,v_s(x) \end{aligned} \tag{18}$$

When the inertial load defined by Equation 18 is applied to the deck as a uniformly tranverse dis-

tributed load, as shown in Figure 4, the resulting static forces become the pseudoseismic forces.

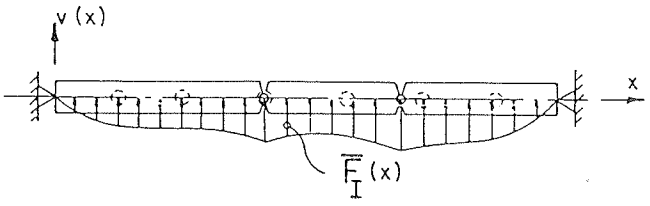

FIGURE 4 Pseudoinertial loading.

Summary of SMSM Procedure

The SMSM procedure is performed in the following steps:

1. Apply a uniformly distributed load (p_o) transversely to the bridge deck and calculate the displacements of the deck. The displacements will define $v_s(x)$.
2. Using $v_s(x)$, calculate α, γ, and β by using Equations 3, 6, and 14, respectively.
3. Calculate the period of the approximating vibration shape by using Equation 7.
4. Select an acceleration spectrum with damping ratio ξ and compute the dimensionless seismic coefficient (C) associated with the period calculated in step 3. Use C to compute the pseudoinertial load by using Equation 18.
5. Apply the pseudoinertial loading transversely to the bridge deck and compute the displacements and forces for design.

Comparison of SMSM and MMSM on Two-Span Bridge

The applicability of the SMSM can be demonstrated by comparing the results obtained from its use with those obtained from using the MMSM. The South Turlock Overcrossing is used for the comparison. The two-span straight bridge, which is supported on a single-column bent, is subjected to transverse earthquake loadings. Two separate test cases are considered for the transverse constraints at the abutments. In the first case, the abutments are fixed in the transverse direction, whereas in the second case, springs in the transverse direction are inserted to model the flexibility of the soil at the abutments. A spring coefficient of 1.0 x 10 kips/ft is used for the soil flexibility. Longitudinal movement of the superstructure is permitted in both cases.

SEISAB is used to perform the SMSM and the MMSM for both cases. The results of the SMSM and MMSM response analyses are tabulated for test cases 1 and 2 in Tables 1 and 2, respectively. The coefficients obtained by evaluating Equations 3, 6, and 14 for the SMSM are included in the tables. The first 10 modes are included in the results for the MMSM. The first transverse mode of response from the MMSM is also included in the tables for comparison.

The results from both test cases show that the structural period was closely approximated by using the SMSM. In addition, the SMSM calculations of the transverse shear force at the abutments and the bent are also close to the forces obtained by the MMSM.

TABLE 1 Test Case 1 Comparison

Location	Displacement Due to $p_o[Y(x)]$ (ft)	Pseudoinertial Loading ($\bar{F}_I$) (kips/ft)	Forces Due to $\bar{F}_I$ (kips)	Response Spectrum (kips)		Normalized Transverse Displacements		
				First Transverse Mode	Three Transverse Modes (RMS)	Uniform Load p_o	Inertial Load $\bar{F}_I$	First Transverse Mode Shape
Abutment 1	0.0	0.0	278	287	291	0.0	0.0	0.0
Span 1								
One fourth	0.0122	3.582				0.524	0.499	0.488
One half	0.0203	5.960				0.873	0.846	0.839
Three fourths	0.0233	6.841				1.000	0.992	0.989
Bent 2	0.0232	6.811	1,045	1,134	1,134	0.988	1.000	1.000
Span 2								
One fourth	0.0233	6.841				1.000	0.922	0.989
One half	0.0203	5.960				0.873	0.846	0.839
Three fourths	0.0122	3.582				0.524	0.494	0.488
Abutment 3	0.0	0.0	278	287	291	0.0	0.0	0.0

Note: $\alpha = 5.460$ ft^2, $\beta = 34.644$ kip·ft^2, $\gamma = 0.749$ kip·ft^3, $T_{SMSM} = 0.41$ sec ($T_{MMSM} = 0.40$ sec).

TABLE 2 Test Case 2 Comparison

Location	Displacement Due to $p_o[Y(x)]$ (ft)	Pseudoinertial Loading ($\bar{F}_I$) (kips/ft)	Forces Due to $\bar{F}_I$ (kips)	Response Spectrum (kips)		Normalized Transverse Displacements		
				First Transverse Mode	Three Transverse Modes (RMS)	Uniform Load p_o	Inertial Load $\bar{F}_I$	First Transverse Mode Shape
Abutment 1	0.00707	2.066	355	301	349	0.286	0.221	0.201
Span 1								
One fourth	0.01701	4.971				0.688	0.636	0.616
One half	0.02316	6.768				0.937	0.911	0.900
Three fourths	0.02472	7.224				1.000	1.000	1.000
Bent	0.02415	7.057	1,196	1,253	1,254	0.977	0.988	0.993
Span 2								
One fourth	0.02472	7.224				1.000	1.000	1.000
One half	0.02316	6.768				0.937	0.911	0.900
Three fourths	0.01701	4.971				0.688	0.636	0.616
Abutment 3	0.00707	2.066	355	301	349	0.286	0.221	0.201

Note: $\alpha = 6.600$ ft^2, $\beta = 41.877$ kip·ft^2, $\gamma = 0.9093$ kip·ft^3, $T_{SMSM} = 0.41$ sec ($T_{MMSM} = 0.41$ sec).

SEISMIC ANALYSIS OF SIX-SPAN CURVED BRIDGE WITH SEISAB

SEISAB was developed to meet the need for a computer program with MMSM capabilities written specifically for bridge designers. By using SEISAB, a complete, lumped-parameter structural model can be generated with only a few simple, free-form input commands. To illustrate the use of SEISAB, a response spectrum analysis was performed on a six-span curved bridge. An ATC-6 acceleration spectrum was used for the dynamic loading.

Description of the Bridge

The bridge is six-span curved box-girder bridge with single-column bents. The prismatic superstructure is continuous, with the exception of span 3, which contains an intermediate hinge. The intermediate hinge is outfitted with earthquake restrainer units to provide longitudinal restraint. Shear keys at the hinge provide transverse restraint between the two superstructure sections.

The seat-type abutments are radially oriented with transverse abutment-to-superstructure shear connections. Longitudinal restraint at the abutments is provided by restrainer units. The radially oriented, single-column bents are founded on pile groups.

Modeling and Program Input Details

As is conventionally done, the SEISAB program models a bridge by lumping properties at discrete locations along the superstructure and columns. The structural characteristics of the bridge are input into SEISAB in modular blocks called input data blocks. The subheads in this section are arranged according to data blocks to illustrate the SEISAB commands required to conduct a seismic analysis of a six-span curved bridge.

Initiating a Response Spectrum Analysis

The user initiates a response spectrum analysis by specifying the appropriate command in the SEISAB data block. In addition, the number of intermediate node points to be used on the superstructure and columns (i.e., the degree of accuracy of the analysis) may also be specified. Because the curved geometry of this bridge would result in coupling effects, the default number of three nodes on the superstructure was increased to 4. The input in the SEISAB data block is as follows:

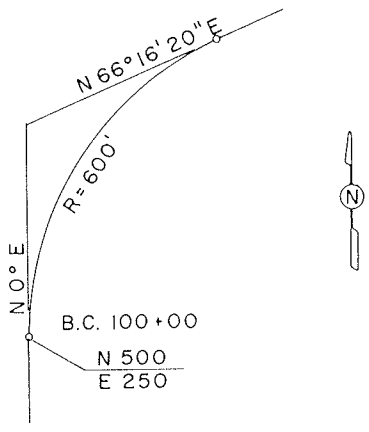

FIGURE 5 Horizontal alignment.

```
SEISAB 'RESPONSE SPECTRUM ANALYSIS, 6-SPAN CURVED
  BRIDGE'
RESPONSE SPECTRUM
SUPERSTRUCTURE JOINTS 4
```

Describing the Horizontal Geometry

To develop an accurate model, the location of the bridge centerline must be described correctly. This information is supplied to SEISAB in the ALIGNMENT data block. Alignment information for this bridge was taken directly from bridge plans and input into SEISAB. The alignment of the bridge is shown in Figure 5, and the input for the ALIGNMENT data block is as follows:

```
ALIGNMENT
C                              INITIAL REFERENCE POINT
STATION        100 + 0.0         INFORMATION
COORDINATES    N 500.0         E 250.0
BEARING        N 0 E
C                              CURVE INFORMATION
BC         10000.0
RADIUS     R 600.0
BEARING    N 66 16 20 E
```

Superstructure

The stiffness and mass characteristics of the superstructure were obtained from its cross-sectional properties. Because the spans are prismatic, only the properties of span 1 were input. The torsional moment of inertia was calculated by using expressions based on thin-walled, enclosed regions. The input for the SPAN data block is as follows:

```
SPANS
LENGTHS    100.0, 143.0, 3*117.0, 100.0
AREAS       86.0    $ PROPERTY GENERATION WILL BE USED
I11        862.0    $ FOR SPANS 2-6.  ALSO, PROGRAM
I22      13000.0    $ DEFAULTS WILL BE USED FOR THE
I33        360.0    $ MODULUS AND DENSITY.
```

Defining the Structural Members

Another user input feature of SEISAB is that any structural member that appears at more than one location in the bridge is described once in the DESCRIBE data block and then placed at the appropriate locations. The structural members in the six-span bridge that required defining are the bent columns and the longitudinal restrainers. Because the five columns are identical in cross section, only one needed to be defined. The input in the DESCRIBE data block is as follows:

```
DESCRIBE
COLUMN     'TYPE 1'    "TYPICAL PRISMATIC COLUMN"
AREA        33.0
I11        146.0
I22         73.0    $ PROGRAM DEFAULTS WILL BE USED
I33        143.0    $ FOR THE MODULUS AND DENSITY
RESTRAINER 'TYPE 1' "GALV. H.S. ROD"
LENGTH       5.0
AREA         3.068E-03
E            2.010E+06
RESTRAINER 'TYPE 2' "GALV. STEEL CABLE"
LENGTH      20.0    $ PROGRAM DEFAULTS WILL BE USED
AREA         0.01   $ FOR THE MODULUS
```

Abutment Information

The modeling of the bridge's two abutments was accomplished through the ABUTMENT data block. The connectivity between the superstructure and the

abutment was assumed to provide translational constraint in the transverse and vertical directions and rotational constraint about a horizontal axis perpendicular to the centerline of the abutment. The shear keys provided the translational constraint, and the width of the superstructure was assumed to provide the torsional constraint. The input in the ABUTMENT data block is as follows:

```
ABUTMENT STATION  100 + 0.0
ELEVATION         152.5  155.5
WIDTH NORMAL      35.0   $ GENERATION IS USED FOR
                            ABUT 7
RESTRAINER NORMAL LAYOUT 'TYPE 1' 8.0, 8.0 'TYPE 1'
  AT 1,7
```

Bent Information

The number, type, and spacing of bent columns are specified in the BENT data block. In addition, the user may also input into this data block the type of connectivity to the superstructure, the column end conditions, and the locations of any restrainers. The bridge under consideration has only single-column bents, and the columns are oriented radially to the superstructure. The column end conditions are fixed at both ends. Many program defaults in the BENT data block have been used for this bridge. The required input for the BENT data block is as follows:

```
BENT
ELEVATION TOP   153.0, 153.5, 154.0, 154.5, 155.0
HEIGHT           25.0  $ HEIGHTS GENERATED FOR OTHER
                           BENTS
COLUMN  'TYPE 1'   AT 2 3 4 5 6
```

Foundation Information

Modeling the connection of the columns and abutments to the foundation may be accomplished either by assuming complete fixity or by allowing for a flexible support. Complete fixity is a program default, whereas movement of the column bottoms or abutments or both is allowed by modeling soil as uncoupled springs. These soil springs are input into the FOUNDATION data block. The direction of the springs is normal and tangential to the centerline of the bent. The input for the FOUNDATION data block is as follows:

```
FOUNDATION
   AT BENT   2 3 4 5 6
       KF1  4.084E+08
       KF2  4.084E+08
       KM1  2.704E+10
       KM2  1.292E+10
       KM3  2.220E+10
```

Span Hinge Information

Discontinuities in the superstructure between bents are input into the HINGE data block. The mathematical modeling of the expansion joint or hinge is done by using a special zero-length element that has the unique property of being able to release the moment along the centerline of the hinge. Translational connectivity is specified for a horizontal axis perpendicular to the centerline of the superstructure at the location of the hinge. In addition, longitudinal restrainers may be placed across the hinge.

Because the joint has transverse shear keys, the transverse force condition is input as fixed. Longitudinally, the only restraint is provided by the restrainers. The width of the bridge is sufficient for transmitting torsional moment across the hinge. The input for the HINGE data block is as follows:

```
HINGE
AT  3   102.00          $ HINGE IS IN SPAN 3;  102 FT
WIDTH NORMAL   33.5        FROM BEGIN.
TRANSVERSE FIXED
REST NORMAL LAYOUT 'TYPE 2' 4.5,4.0,4.0,4.5 'TYPE 2'
  AT 1
```

Earthquake Information

The last data block, LOADINGS, specifies information about the loads applied to the bridge. The required loading for a response spectrum analysis is an acceleration spectrum. The SEISAB program has the ATC-6 spectra stored away; therefore, because the default is not applicable in this case, the only input needed to define the acceleration spectrum is the soil type. Soil type 3 (30 ft or more of soft to medium stiff clays) is present at the bridge site. Two loading cases are desired, one along an axis connecting the two abutments (in a chord or longitudinal direction) and one transverse to that axis. Because both of these loading cases are required by ATC-6, they are included in SEISAB as a program default and no input is needed. The input for the LOADINGS data block is as follows:

```
LOADINGS
   RESPONSE SPECTRUM
   SOIL TYPE III
```

EXTENDED NONLINEAR DYNAMIC-ANALYSIS CAPABILITIES OF SEISAB-II

In regions of high seismicity it has generally not been economically feasible to design and build bridges that resist earthquake loads elastically. Thus, in order to achieve acceptable performance, designers have relied on the postelastic behavior of certain components. This has generally meant that columns or piers could be expected to yield during a major earthquake. This design strategy also requires that other nonductile components, such as bearings, be designed to resist seismic forces elastically.

Recently, however, there has been growing interest in using different design and retrofitting strategies in regions of high seismicity (9,10). These strategies, which use concepts such as isolation, energy dissipation, and restraint, often employ special bearing devices designed to behave nonlinearly during a major earthquake. However, many of these design strategies are relatively new and lack histories of performance during an earthquake. In addition, the effect of these strategies cannot be adequately evaluated by experimental research that investigates only the performance of isolated components. Because full-scale testing of prototype designs is expensive, such testing is not usually economically feasible. Therefore, analytical techniques must be relied on if these new aseismic design strategies are to be properly evaluated. In many cases the analytical methods currently used to evaluate these strategies are based on simple, single-degree-of-freedom idealizations of a given bridge. However, the geometry and articulation of most bridges makes the validity of such simple idealizations questionable, especially in view of the presence of other nonlinear components in the bridge. To properly evaluate these new strategies and identify those situations where they will be the most beneficial, bridge designers must be able to realistically analyze the true nonlinear behavior of

various types of bridge structures employing many different design and retrofitting strategies.

Nonlinear dynamic-analysis capabilities would also facilitate much of the research recommended in recent workshops on the seismic aspects of bridge design (11,12). The objectives of much of this recommended research could be accomplished more efficiently if such analytical capabilities were readily available in a form that practicing bridge engineers could use.

The nonlinear program SEISAB-II will consider, along with the nonlinear behavior of bridge bearings, the effects of column flexural yielding and the formation of plastic hinges. An efficient method for considering column yielding in a finite-element computer program is to use nonlinear beam elements in which flexural yielding can occur at the ends of each element. An axial load and biaxial moment interaction yield surface can be described by using the conventional theory of ultimate strength of reinforced concrete. By assuming a transition from ideally elastic behavior to ideally plastic behavior at the yield surface, engineers can write (and have written) algorithms that include the nonlinear behavior of reinforced bridge columns (13-15).

CONCLUSIONS

Previous efforts by Imbsen et al. (6) to implement computer programs capable of assessing the dynamic response of bridges indicated that there was a need to develop both simplified methodologies and a computer program written specifically for bridge designers.

A simplified procedure such as the SMSM, which is applied by using conventional techniques of statics analysis, is easily understood. The procedure is applicable to bridge configurations that can be characterized as having their major dynamic response in the first mode of vibration. The current AASHTO seismic design guidelines (2) recommend that this method be used on such bridges in zones of both moderate and high seismic activity (i.e., seismic performance categories C and D). The guidelines also recommend that the SMSM be used on all bridges in a zone of moderately low seismic activity (i.e., seismic performance category B). The SMSM, included in SEISAB, was formulated by using the pseudo-dynamic-analysis procedures described in this paper. This procedure was included in SEISAB-I to provide the bridge designer with an easy-to-use analytical tool capable of handling space-frame structures required for lateral static loadings.

For the more geometrically complex bridges (e.g., curved alignments, varying column lengths, highly skewed supports) the response spectrum method (i.e., the multimode response method) is recommended as a minimum for the response analysis. Although most general frame analysis computer programs (e.g., STRUDL, SAP, EASE, and NASTRAN) have the capabilities needed to conduct an adequate response spectrum analysis, they tend to be quite difficult for most bridge designers to use. To model a bridge and select the appropriate commands from the ensemble of commands typically available in these general analysis programs, a designer must have a working knowledge of structural dynamics. In addition, boundary conditions at intermediate expansion joints and supports on a skew are difficult to model by using these general analysis programs. A special element developed by Tseng and Penzien (13) for intermediate hinges has been incorporated into SEISAB-I to model force releases that will accommodate movements along the bridge centerline and moment releases that are directed along a skewed support centerline nonorthogonal to the bridge centerline. In addition, because SEISAB-I has been developed specifically for bridges, it automatically generates a bridge model that simulates the inertial characteristics of a vibrating bridge. A special element has also been developed and included in SEISAB to model the stiffness characteristics of a bent cap embedded in the superstructure. Other features that are unique to bridges have also been included in the program to make it a convenient, easy-to-use program for conducting a seismic analysis of a bridge. SEISAB's output results have been tailored and formatted to report only those qualities needed for model verification and design.

Pilot workshops sponsored by the National Science Foundation were given initially to bridge engineers in California who were familiar with seismic design and subsequently to engineers less familiar with seismic design. Both groups of engineers indicated an overwhelming acceptance of SEISAB-I. The availability of SEISAB-I concurrent with AASHTO's adoption of seismic design guidelines and completion of the ATC seismic retrofitting guidelines (ATC-6-2) has also contributed to the acceptance of SEISAB. The four 2-day intensive workshops that have been conducted to date have included hands-on experience in using SEISAB on problem assignments for both seismic design and retrofitting. Because these workshops are geared toward the engineer involved in bridge design on a day-to-day basis, they fill a specific need by helping to equip bridge engineers with the skills needed to apply the newly developed methodologies and guidelines for aseismic bridge design.

ACKNOWLEDGMENT

This work was supported by the National Science Foundation under the direction of John B. Scalzi.

REFERENCES

1. Standard Specifications for Highway Bridges, 12th ed. AASHTO, Washington, D.C., 1977.
2. Seismic Design Guidelines for Highway Bridges. Report ATC-6. Applied Technology Council, Berkeley, Calif., Oct. 1981.
3. W.G. Godden, R.A. Imbsen, and J. Penzien. An Investigation of the Effectiveness of Existing Bridge Design Methodology in Providing Adequate Structural Resistance to Seismic Disturbances: Phase VII Summary. Report FHWA-RD-79-90. Office of Research and Development, FHWA, U.S. Department of Transportation, Dec. 1978.
4. R.A. Imbsen, J. Lea, V.N. Kaliakin, K.J. Perano, J.H. Gates, and S.L. Perano. SEISAB-I User Manual. Engineering Computer Corporation, Sacramento, Calif., Oct. 1982.
5. R.A. Imbsen, V.N. Kaliakin, and J. Lea. SEISAB-I Example Problems. Engineering Computer Corporation, Sacramento, Calif., Oct. 1982.
6. R.A. Imbsen, R.V. Nutt, and J. Gates. Seismic Design of Highway Bridges: Workshop Manual. Report FHWA-IP-81-2. FHWA, U.S. Department of Transportaton, Jan. 1982.
7. J. Penzien and R. Imbsen. Seismic Analysis of Bridges by a Single Mode Spectral Approach. Proc., Advances in Earthquake Engineering, Continuing Education in Engineering, University of California, Berkeley, June 1980.
8. R.W. Clough and J. Penzien. Dynamics of Structures. McGraw-Hill, New York, 1975.
9. R.A. Imbsen and R.A. Schamber. Earthquake Resistant Bridge Bearings, Vol. 1: Concepts. Report FHWA/RD-82/165. FHWA, U.S. Department of Transportation, 1983.

10. R.A. Imbsen and R.A. Schamber. Earthquake Resistant Bridge Bearings, Vol. 2: NEABS Computer Program. Report FHWA/RD-82/166. FHWA, U.S. Department of Transportation, 1983.
11. Proceedings of a Workshop on Earthquake Resistance of Highway Bridges. Applied Technology Council, Berkeley, Calif., Jan. 1979.
12. Comparison of United States and New Zealand Seismic Design Practices for Highway Bridges. Applied Technology Council, Berkeley, Calif., Aug. 1982.
13. W.S. Tseng and J. Penzien. Analytical Investigations of the Seismic Response of Long Multiple Span Highway Bridges. Report EERC 73-12. Earthquake Engineering Research Center, University of California, Berkeley, June 1973.
14. J. Penzien, R.A. Imbsen, and W.D. Liu. NEABS User Instructions. Earthquake Engineering Research Center, University of California, Berkeley, May 1982.
15. K. Kawashima and J. Penzien. Correlative Investigations on Theoretical and Experimental Dynamic Behavior of Nodal Bridge Structures. Report EERC 76-26. Earthquake Engineering Research Center, University of California, Berkeley, July 1976.

Publication of this paper sponsored by Committee on General Structures.

Prototype Prestressed Wood Bridge

R.J. TAYLOR and H. WALSH

ABSTRACT

The transverse prestressing of wood was conceived of in 1976 as a method for rehabilitating nailed laminated wood decks. Using high-strength prestressing steel, a permanent pressure is introduced normal to the direction of the laminations to provide high interlaminate shear strength and improved load distribution. The success of this new concept in rehabilitation resulted in its becoming the subject of a major research and development program conducted by the Ontario Ministry of Transportation and Communications (MTC). The extensive work performed by MTC over the past 7 years has led to the formulation of a set of comprehensive design specifications for prestressed wood. The objective of this paper is to outline the design, construction, and load testing of the world's first new prestressed wood bridge. The bridge was designed by MTC and constructed by the Ontario Ministry of Natural Resources (MNR) over the West River, on a logging access road, near Espanola, Ontario, in 1981. The design process with reference to the new design specifications, which have since been adopted by the Ontario Highway Bridge Design Code, is discussed. The field construction is outlined highlighting the prefabrication and assembly of the prestressed wood superstructure. The load testing of the bridge in 1982 and the subsequent evaluation of the test results are described. The MNR determined that the West River bridge cost only two-thirds of the steel structure originally proposed for that site. The load testing and subsequent evaluation indicated that this prestressed wood bridge is an extremely rigid structure with considerable reserve strength.

The transverse prestressing of laminated wood decks was conceived of in 1976 (1) as a method of rehabilitating existing nailed decks. The success of this new concept in rehabilitation resulted in a major research and development program (2) conducted by the Ontario Ministry of Transportation and Communications (MTC). Extensive research and development work led to the formulation of a comprehensive set of design specifications (3,4) devoted entirely to the design of prestressed wood decks. These new specifications have been included in the 1983 edition of the Ontario Highway Bridge Design Code (OHBDC) (4).

To evaluate the effectiveness of these new specifications, MTC and the Ontario Ministry of Natural Resources (MNR) designed and constructed the first new prestressed wood bridge in 1981. The objective of this paper is to outline the design, construction, and load testing of this prototype prestressed wood bridge.

The design analysis, with reference to the new OHBDC specification, and several computer analysis techniques are described in this paper. The fabrication and erection procedures are also outlined with particular emphasis on the field construction conducted by the MNR field construction crew. The load testing and subsequent evaluation of the completed bridge, performed by MTC in 1982, are also summarized.

STRUCTURAL DESCRIPTION

The main objective of the structural selection was to optimize the use of the prestressed wood concept while minimizing on-site construction requirements. The use of this prototype to demonstrate the design flexibility of the prestressed wood system was of secondary importance.

The bridge is located on the MNR Fox Lake logging access road near Espanola, Ontario. It is believed this bridge, which spans the West River near the

southern highway entrance, will be subjected to some of Ontario's heaviest commercial loadings.

The site, shown in Figure 1, consists of about a 7.0-m-wide fast-moving waterway surrounded by large bedrock formations. A typical elevation at the narrowest crossing is shown in Figure 2 along with the proposed structural form. To avoid the costly removal of the surrounding bedrock and limit the fill requirements the economic structure length would have to be about 13 meters. To satisfy the site requirements, while demonstrating the flexibility of the prestressed wood system, the wood frame structure shown in Figure 2 was proposed. This structure uses inclined legs providing a clear opening of 7.7 m. It maintains the required bridge elevation with minimum foundation requirements. It also takes advantage of two naturally formed rock ledges situated symmetrically on either side of the waterway.

The legs and the deck were to be constructed as an integrated, prestressed, laminated system. The individual leg laminations were to be prespliced to the deck laminations using galvanized nail-plate connectors. The prefabricated frames were then to be shipped to the site and assembled, and the entire structure was to be prestressed to form a continuous, rigid-frame structure.

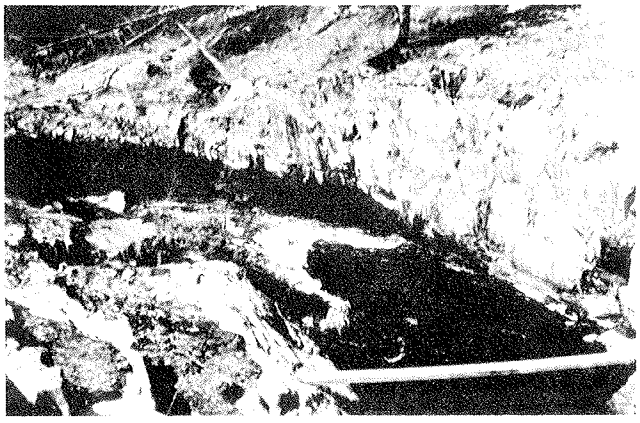

FIGURE 1 Proposed West River crossing.

DESIGN

The OHBDC specifications do not cover some of the requirements for the design of this frame structure, particularly those of load distribution. Therefore a number of computer analyses are presented as well as some laboratory testing of the deck-leg connection.

A preliminary evaluation indicated that using Ontario red pine graded No. 2 and better would require laminations of 38 mm x 292 mm for the deck and 38 mm x 190 mm for the legs. In addition, only one-half of the deck laminations would require full leg supports in terms of moment and axial capacity. The latter was to be achieved by spacing groups of four laminate frames as shown in Figure 3. Some additional construction details are provided in Figure 4.

The deadline imposed for MNR construction resulted in the commencement of the bridge, based only on a preliminary analysis. Because of its availability Douglas fir was substituted for red pine, so the following analyses and evaluation are based upon Douglas fir graded No. 2 and better.

Analysis

Because of the structure's low span-to-depth ratio it was believed that simplified static analysis would not properly represent the distribution of load in the structure. However, the application of a costly three-dimensional analysis was not considered practical. Instead, two complementary two-dimensional analyses were performed.

The first, a two-dimensional frame analysis program developed by R.K. Ayres as an MTC research project in 1975, represented the structure in elevation and so did not consider any lateral distribution of load. This provided maximum moments, shears, and reactions per line of wheels of the design vehicle.

The second analysis represented the deck in plan as an orthotropic plate (5) and simulated the legs as flexible columns. This type of analysis had

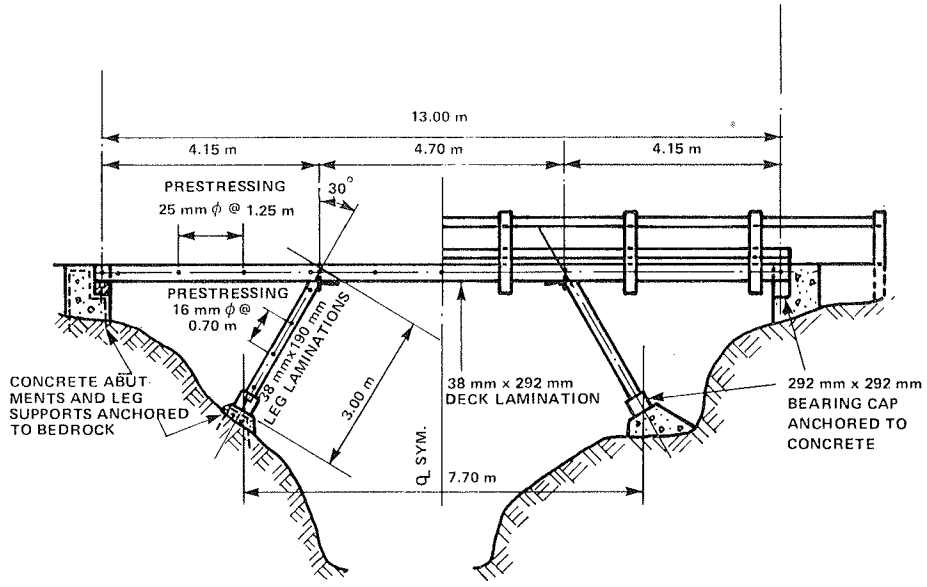

FIGURE 2 Elevation of Fox Lake Road bridge.

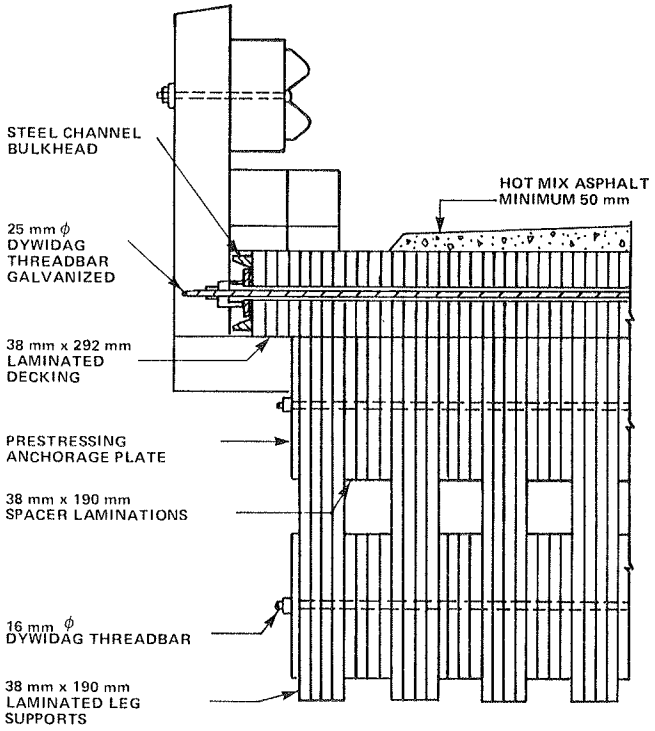

FIGURE 3 Partial section at leg.

already proven to be a fairly accurate representation of prestressed wood decks (1,2) and so was used to derive the distribution criteria needed to produce the design forces.

Frame Analysis

Figure 5 shows the frame arrangement used to represent the structure for analysis. The analysis was performed producing influence lines under the effects of a 100 kN wheel load. The influence lines were later used to determine the maximum forces under the effects of the OHBDC design vehicle.

This analysis was also used to determine dead load forces and vertical movement of the deck at the leg support under live load. The latter information enabled the determination of a representative support flexibility for use in the subsequent orthotropic analysis, where the leg supports were simulated by flexible columns.

Orthotropic Analysis

The orthotropic analysis represents the prestressed deck as a two-dimensional plate with flexural and torsional properties that may be different in two directions. The determination of rigidities for the analysis was based on the idealizations presented in the analysis section of the OHBDC (4).

Figure 6 shows the geometry and boundary conditions used to represent the structure in the orthotropic analysis. The abutment supports were repre-

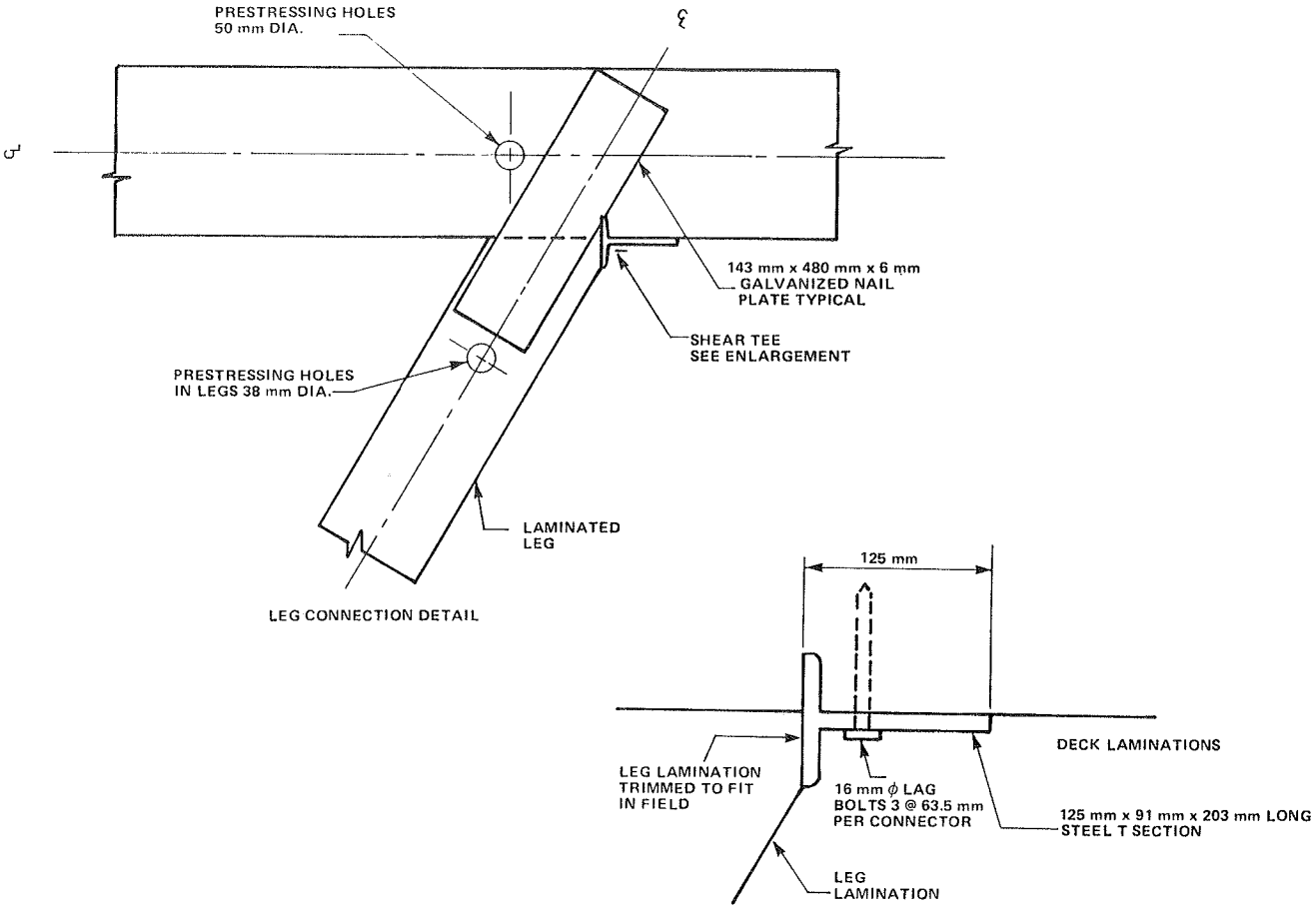

FIGURE 4 Leg details.

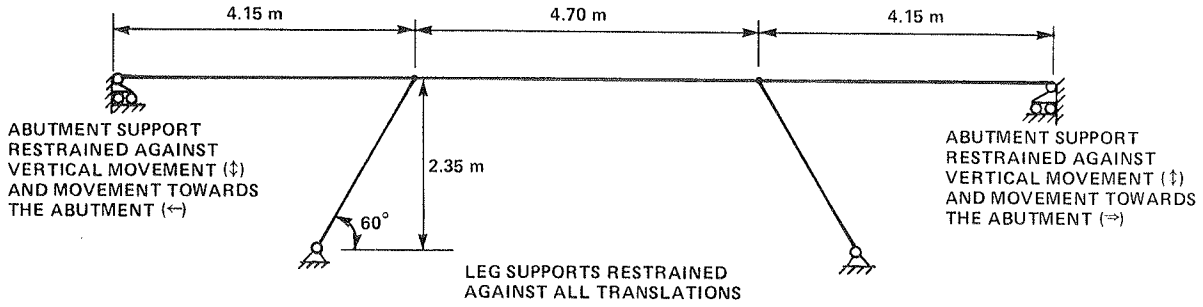

FIGURE 5 Geometry assumed for frame analysis.

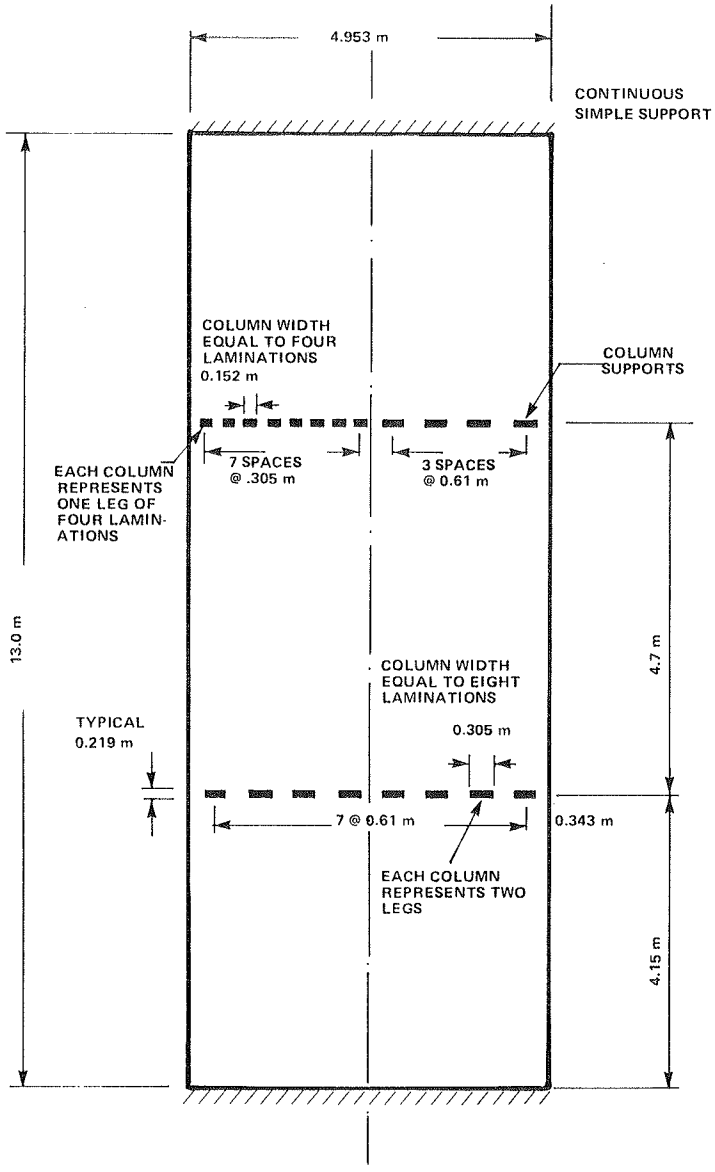

FIGURE 6 Orthotropic deck layout.

sented by line supports and the legs by flexible columns. Because of the limited number of columns that can be given in this program, only one-half of one support was represented in detail. Each leg, consisting of four laminations, was simulated by a column with dimensions equal to the horizontal projection of the leg-deck connection. All other columns represented two legs combined.

The orthotropic analysis was used to produce influence lines as a means of determining the critical vehicle placement. The unit load was a 100 kN axle with dimensions representing the OHBDC design

vehicle. All the force modes considered in the design of the bridge are listed in the following table.

Structural Component	Force Mode
Deck	Moment[a], vertical shear, interlaminate shear, axial force[a], and bearing
Leg	Moment[a] and axial force[a]
Leg-deck connection	Moment[a], horizontal shear[a], and bearing

[a]Evaluated as combined effects

Because the analysis did not properly represent the leg supports, the determination of moments and shears in the leg was based on the following assumptions. The distribution of load used to determine moment at the top of the leg was assumed to be the same as for negative moment in the deck over the leg, as determined from the orthotropic analysis. The distribution of load used to determine horizontal shear in the leg-deck connection was assumed to be the same as that for the maximum column reaction determined from the orthotropic analysis. These distribution widths were then applied to the undistributed leg moment and horizontal shear as determined from the frame analysis program.

OHBDC Specifications

MTC Report SRR-83-03 (3) details the design of prestressed wood bridges using the OHBDC specifications. Except for the case of the deck-leg connections, which will be discussed separately, all design modes for this bridge followed a similar design process. Therefore only the design for maximum positive moment is presented as an example of the design process using the new OHBDC requirements.

Design for Maximum Positive Moment

The following is a sample of the design calculations for maximum positive moment based on the OHBDC specifications (3). (OHBDC clause references are given in parentheses for possible future reference.)

Factored moment capacity is expressed:

$$Mu = f_{bu}\ S\ k_d\ k_m\ k_s \qquad (13.22.6.)$$

ϕ = performance factor = 0.9 (13.4.4.)

f_{bu} = specified strength = 10.0 MPa (13.11.2(a).)

S = section modulus = $bd^2/6$ = 0.75 [(1000 mm x 292^2)/6] mm

The maximum moment was assumed to occur at a transverse line of butt joints. Therefore the section modulus considers every fourth lamination to be discontinuous.

$S = 10.66 \times 10^6\ mm^3$

k_d = duration of load effect = 1.0 (13.5.3.)

k_m = load sharing effect = 1.5 (13.5.6.)

k_s = size effect = 1.0 (13.6.2.1.)

Therefore

$Mu = 0.9(10.0)\ (10.66 \times 10^6)\ (1.5)$

and

factored moment capacity Mu = 144 x 10^6 N•mm/m width

Total factored load effect is expressed:

Maximum unfactored live load moment M_{LL}

M_{LL} = 64.6 kN•m/m width

Corresponding dead load moments M_{DL}

asphalt M_{DL1} = 2.96 kN•m/m width

wood M_{DL2} = 2.91 kN•m/m width

Load factors at ULS α (Table 2.5.1.b)

live load and dynamic load allowance $\alpha_L = 1.4$

dead load (asphalt) $\alpha_A = 1.5$

dead load (wood) $\alpha_W = 1.2$

For dynamic load allowance, DLA, a single axle governs maximum positive moment. Therefore

DLA = 0.4 (2.4.3.2.3.)

DLA must be adjusted by a factor of 0.7 for wood components (2.4.3.2.10). Therefore

DLA = 0.7(0.4) = 0.28

Total factored load effect M_{TOT}

$$M_{TOT} = \alpha\ M_{DL1} + \alpha_W\ M_{DL2} + \alpha_L\ (M_{LL})\ (1 + DLA)$$
$$= 1.5(2.96) + 1.2(2.91) + 1.4(64.6)\ (1.28)$$

M_{TOT} = 124 kN•m/m width

The factored moment capacity, Mu = 144 kN•m/m width, is 16 percent greater than the total factored load effect, M_{TOT} = 124 kN•m/m width.

Deck-Leg Connection

The as-built leg connection is shown in Figure 4. Originally only the galvanized nail plate was to be used. According to the analysis and subsequent evaluation using the OHBDC specifications, the moment and shear capacity of the nail-plate connectors were more than adequate at the ultimate limit state. However, concerns were raised about the durability of the nail plates alone under repeated loadings. Therefore the additional steel T shear connector shown in Figure 4 was proposed. This type of connector had already proven to be resilient to the effects of repeated loads in part of another MTC research project for the development of a steel-wood composite (6).

Because of the deadline for construction and the uniqueness of this particular bridge, extensive development of the connection detail was not considered practical. However, some ultimate static testing was performed in an effort to establish the mode of failure and the ultimate strength of the proposed connection.

The first test was performed on the steel T section alone, as shown in Figure 7. The typical load-versus-slip response is shown in Figure 8 indicating linear performance up to about 200 kN. This would represent 100 kN per steel connector, one of which is used per leg. The total factored horizontal shear from the design analysis is only 48 kN per leg; therefore the connector is more then adequate.

Subsequently a full-size connector test was con-

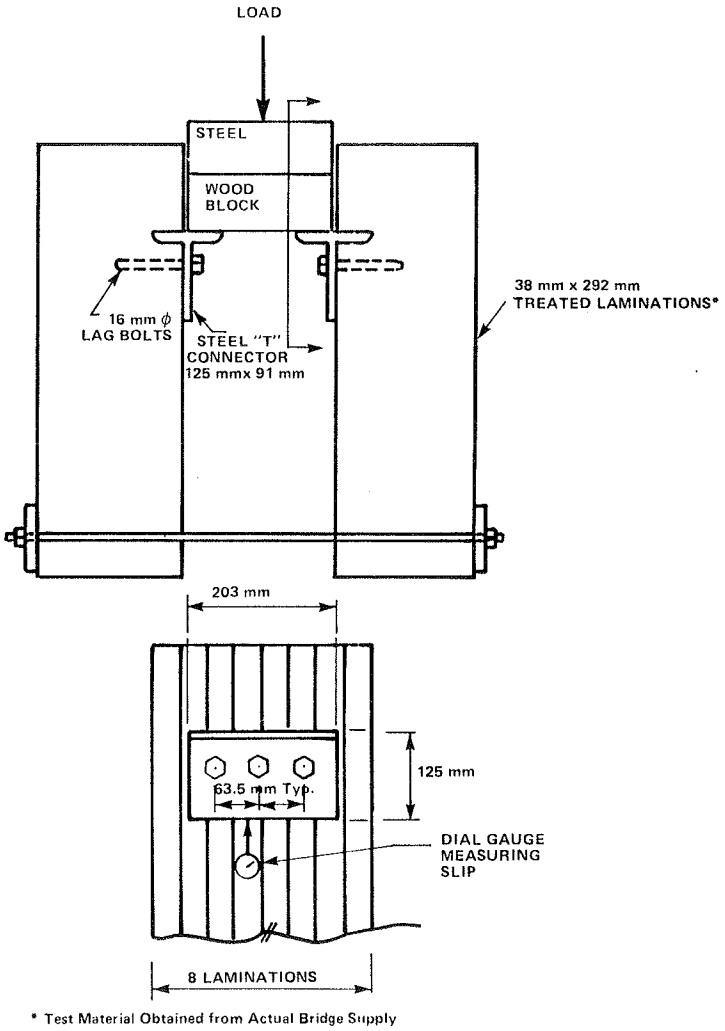

FIGURE 7 Test set-up for shear connector.

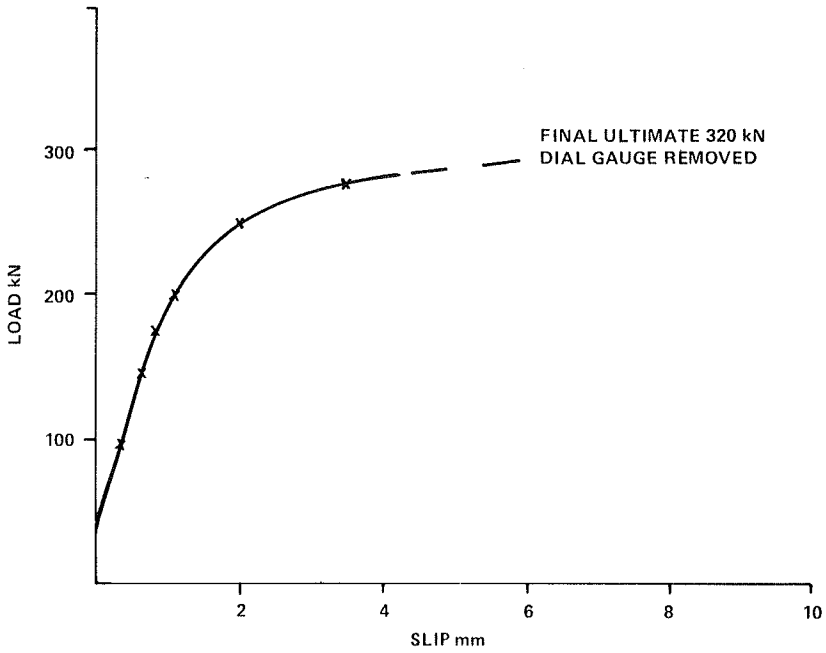

FIGURE 8 Load versus slip of shear connector.

ducted with both the nail plate and the steel T section installed. The ultimate failure mode was in bearing perpendicular to the grain of the wood deck as shown in Figure 9. The load at which the first sign of failure occurred was 385 kN per leg, and the ultimate crushing load was 508 kN per leg. No measurable slip movement of the steel T connectors occurred. The 385 kN would represent a horizontal shear capacity of about 190 kN per leg and 330 kN per leg in bearing--a value far in excess of that required.

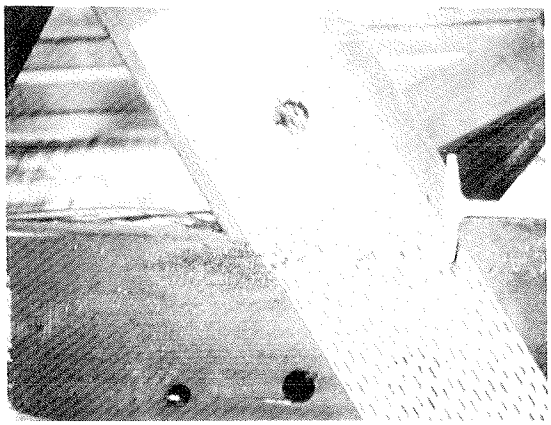

FIGURE 9 Failure of leg connection.

Scaling down the leg connection for more efficient material use was not considered justified. The nail-plate connectors were already as thin as practical, and a reduction in the steel T would not represent any significant savings because of the small number used.

Summary

The moment capacity as determined in the design example accounts for the occurrence of butt joints in the deck. Actually, these joints could be ignored because they have been spliced with nail plates and because they are not in the highest moment region. This would increase the total factored moment capacity from 144 kN•m to 192 kN•m. This is over 50 percent greater than the total factored load effect. Because of the substitution of Douglas fir for the originally proposed red pine, all of the design modes were determined to be conservative.

CONSTRUCTION

The fabrication and construction of the bridge were carried out by the MNR field construction crew under occasional supervision of the MTC design engineer. The crew consisted of three experienced construction people. This crew was, for a period of several weeks, supplemented by as many as three additional men who were available from other local MNR forces.

All steel hardware, including the nail-plate connectors and prestressing materials, were hot-dip galvanized for protection. All the wood materials, including the curbs, posts, and bearing caps, were cut and drilled before undergoing pressure preservative treatment with creosote. Only the holes in the deck, necessary to attach the deck to the supports and the curbs and posts to the deck, were drilled on site. These areas were surface treated according to the requirements of the OHBDC specifications.

Foundations

The abutments and footings were cast in place on sound bedrock and were anchored to the bedrock by grouted reinforcing tendons. This enables the structure to resist the negative reaction forces and high longitudinal forces that this light frame structure exhibits. Its dead load is very low so, in contrast to continuous structures of steel and concrete, the negative live load reactions are not overcome by gravity.

Solid sawn 290 mm x 290 mm bearing caps were tied down to the concrete supports as shown in Figure 10. This provided flexibility for the tie-down of the laminated deck and legs with lag bolts after prestressing had been performed.

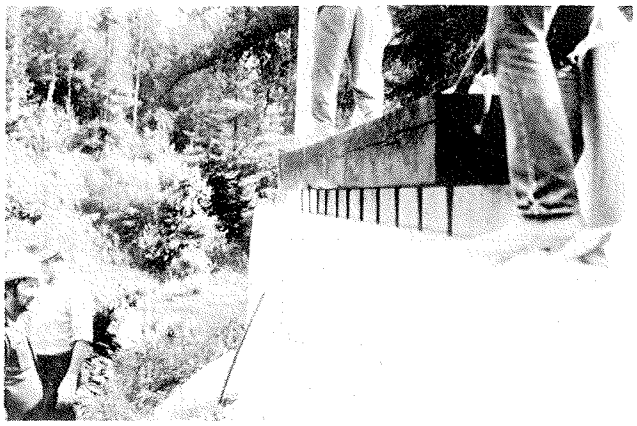

FIGURE 10 Wood bearings anchored to concrete supports.

Fabrication and Erection

The deck and leg laminations were fabricated at a nearby MTC yard to form the required frame geometry. First the deck laminations were spliced to form full-length laminations equivalent to the overall bridge length. Subsequently the legs were attached using a marked template to ensure proper locations and angle. When completed the individual laminate frames, ready for assembly, were shipped to the site. The prefabricated units were lifted into place by crane and nailed together to maintain alignment before prestressing. The completed wood frame structure is shown in Figure 11 with the prestressing bars and steel bulkheads installed and ready for prestressing.

Prestressing was performed using a new 24-jack hydraulic system assembled by MTC. This enabled the prestressing of the entire bridge to be done at the same time. The completed bridge, shown in Figure 12, was opened to traffic in the fall of 1981 and has since been used consistently by the local heavy logging traffic.

LOAD TESTING AND EVALUATION

In 1982 MTC performed a live load test on the bridge as part of the evaluation of its structural performance. The primary objective was to develop a better understanding of structural response in order to evaluate the analytic model used in the design. In addition, using MTC's special load testing vehicles, the bridge would be proof tested to a static load of more than two and one-half times the legal load.

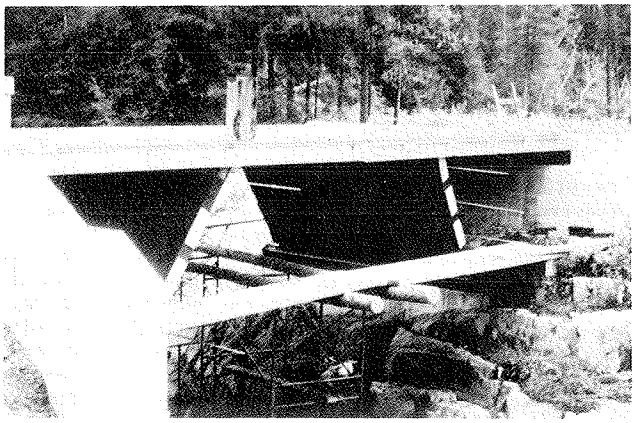

FIGURE 11 Assembled structure before prestressing.

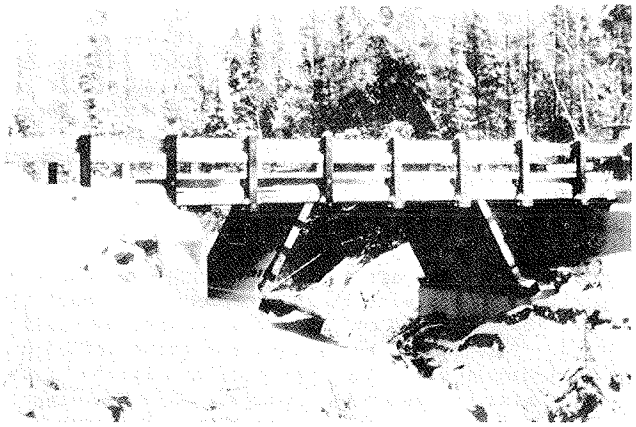

FIGURE 12 Completed structure opened in 1982.

Instrumentation

The bridge was instrumented primarily with linear displacement transducers, located as shown in Figure 13, to monitor the vertical displacement contour of the deck under load. A number of transducers were also installed to measure relative movement of the deck at the abutments and at the leg-deck connections, but these gauges registered no appreciable movements.

Nine demountable strain gauges developed at MTC's Testing and Instrumentation Laboratory (7) were also used to measure extreme fiber flexural strain in the deck. These were located immediately adjacent to the nine displacement transducers in the center span of the bridge.

Vehicle Loading

Using the influence lines produced by the design analysis, a number of critical vehicle positions were selected for one of MTC's load testing vehicles. The vehicle was moved through two transverse positions that represented an extreme eccentric lane loading and a concentric lane loading. In each lane the vehicle stopped at five longitudinal positions, providing a total of ten different static positions of the vehicle. At each of these static positions, all the instrument readings were recorded.

Load Testing

Load testing of the bridge was conducted without major difficulties and a maximum tandem loading of 42.5 kg (425 kN) was successfully applied. However, during the test it became apparent from visual observation that the leg supports were not resting evenly on the bearing caps. In fact some movement of leg was required before the support legs became fully engaged. Four additional displacement transducers were installed at the bottom of the legs to monitor this movement. Although the movement was only about 3 mm, its importance, as will be discussed in the next section, is reflected in the fact that the overall maximum vertical deflection of the bridge was only 9 mm.

Evaluation of Load Test Results

A preliminary review of the load test results indi-

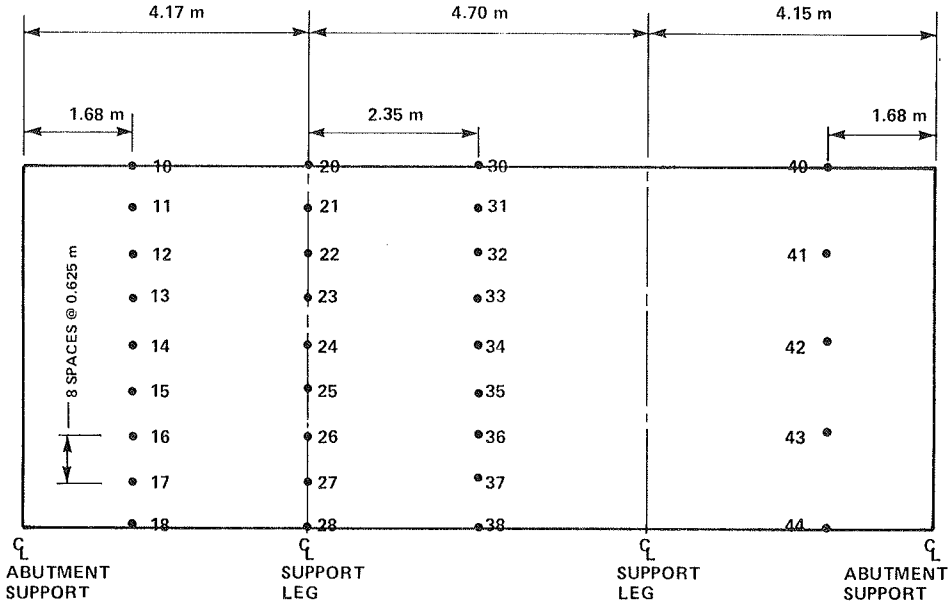

FIGURE 13 Plan layout of deflection transducers.

cated that the vertical deflection contour and the flexural strains would provide excellent data for evaluating the analytic model used in design. However, the movement of the legs would affect the overall deflection contour and subsequently the distribution of load. Therefore it would be necessary to account for this movement in the analytic model. This, in turn, would require better knowledge of the material stiffness.

Modulus of Elasticity

Usually, when comparing the deflection contours of experimental data with those produced by an analytic model, the comparison is made using normalized curves. This procedure offsets the error introduced by assuming a value for the modulus of elasticity, but it also assumes the structure behaves elastically. Because of the movement of the leg supports, this structure did not perform elastically. Therefore it was necessary to consider the measured leg displacements in the analysis and use a realistic value for the modulus of elasticity.

A sample of 17 full-size deck laminations from the actual treated material supplied for the bridge was retrieved at the time of construction. This made possible the determination of a representative modulus of elasticity for use in the analysis. The average modulus of elasticity, which was utilized in the subsequent computer analysis, was about 13 300 MPa. This average ignores the highest and the lowest measured values. The coefficient of variation was about 27 percent.

When reviewing the subsequent deflection and strain comparisons, this wide variation in material property should be kept in mind. The analytic model assumes uniform properties where in reality the distribution and magnitude of the material properties are quite varied.

Analytic Design Models

The bridge was initially reanalyzed using the same orthotropic analysis that was used in the original design described earlier. Only the loading was changed to represent the actual test vehicle used in the field. This analysis was designated orthop 1, and some results compared with the experimental data are shown in Figures 14 and 15. These figures display deflection contours at the midspan cross section under the eccentric and the concentric loading condition. In both cases the experimental results are of greater magnitude than those of the orthop 1 analysis. Though the analysis provides for some elastic shortening of the leg support, it does not account for the magnitude of movement that was measured in the field. Therefore the apparent deflections, as demonstrated by the experimental results, are much greater. The same is true for the longitudinal deflection contour shown in Figure 16.

The orthotropic analysis was then repeated, introducing prescribed settlements for the columns based upon the deflections measured at the west leg. This analysis was designated orthop 2. Because only the west leg was fully instrumented, as shown in Figure 13, it was not possible to represent all of the load positions. However, for the symmetrical loading with the tandem axle at the center of the

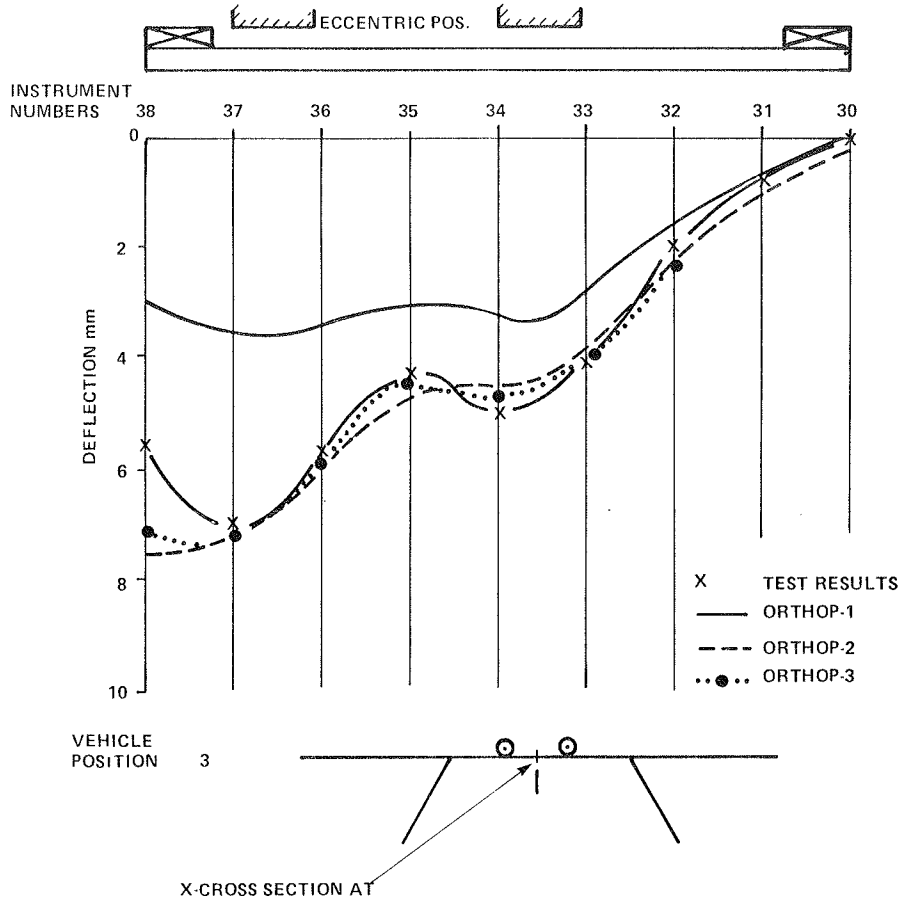

FIGURE 14 Vertical displacements, center span, eccentric loading.

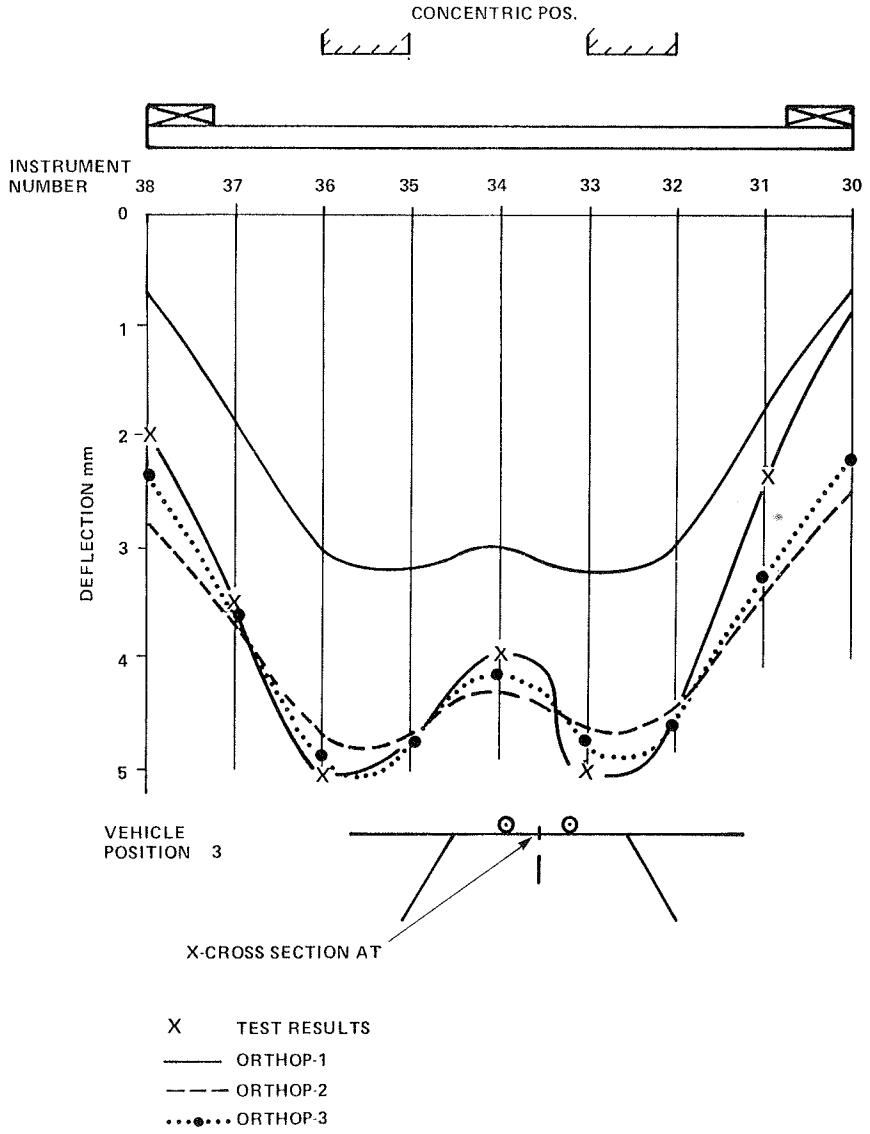

FIGURE 15 Vertical displacements, center span, concentric loading.

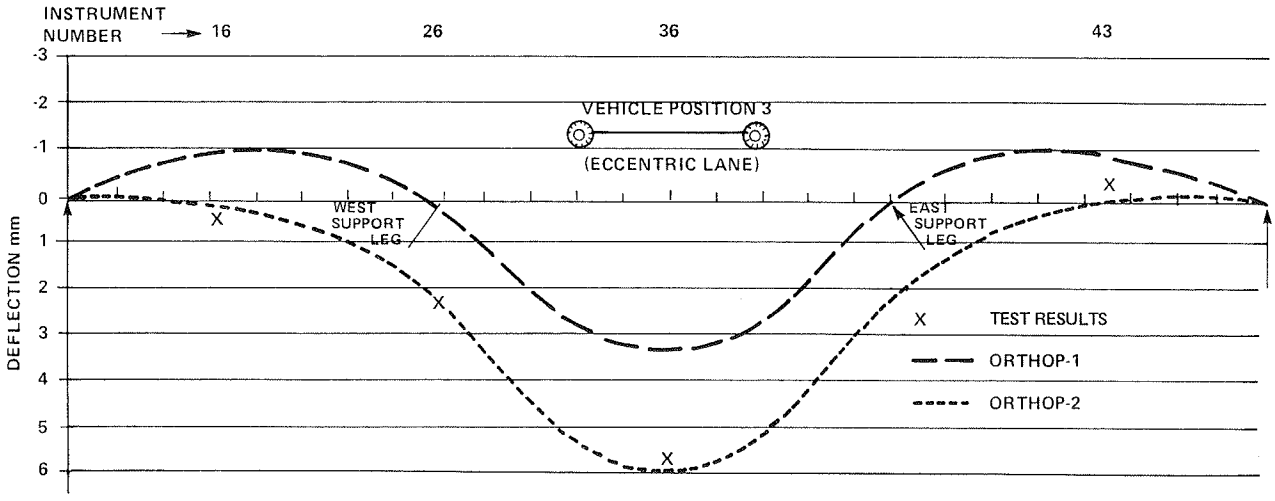

FIGURE 16 Vertical displacements, vehicle position 3, eccentric loading.

middle span, the east leg movement was assumed to be the same as that measured for the west leg.

The results of the analysis are shown in Figures 14, 15, and 16. The orthop 2 analysis provided deflections that were surprisingly close to the experimental deflection contours. The major discrepancy was at the outside edge of the deck. However, the orthop 2 analysis did not consider the increased edge stiffness caused by the curb, guardrail, and steel prestressing bulkhead. One additional, orthotropic analysis was performed that is designated orthop 3. It was performed primarily to demonstrate the sensitivity of the structural performance to variations in the material property assumptions.

The OHBDC specifies the shear modulus G_{LT} at $0.065E_L$, and the transverse modulus of elasticity E_T at $0.05E_L$ where E_L is the longitudinal modulus of elasticity. These values were used in the orthop 1 and orthop 2 analyses. However, a recent investigation (2) indicated that these structural properties for prestressed wood decks are much lower. Based upon the results of that investigation new values of $G_{LT} = 0.055E_L$ and $E_T = 0.037E_L$ were selected.

In addition to the material property changes, the orthop 3 analysis included the stiffness of the wood curb as an edge beam, in an attempt to better represent the real edge conditions.

The results of the orthop 3 analysis are shown in Figures 14, 15, and 16, and although the changes are not dramatic they do indicate a trend. The reduction in torsional and transverse stiffness has caused the transverse curvatures to become more pronounced, and the new deflected shapes are closer to the experimental results.

The increase in edge stiffness reduced the edge deflections bringing them closer to the experimental results. If the edge stiffness of the steel channel prestressing bulkhead could also be accommodated the representation would become even better.

Flexural Strains

In addition to the vertical displacement comparisons several strain comparisons were made with the analytic models. The transverse line of demountable strain gauges used at the center of the bridge provided a contour of the flexural strain on the underside of the deck. Figures 17 and 18 compare the experimental strains with those derived from the moments produced by the analytic models. In this derivation the average experimental modulus of elasticity was used and a uniform deck thickness was assumed.

Given the variation in the modulus of elasticity that exists between the actual laminations, the comparison between analytic and experimental results is considered fair. The applicability of demountable gauges to wood structures was still under investigation at the time of this test, and this particular application was considered part of that investigation.

Figures 17 and 18 also illustrate a very important consideration with respect to the three analytic models: Flexural strain distributions directly reflect moment distributions. According to the figures, these distributions changed very little

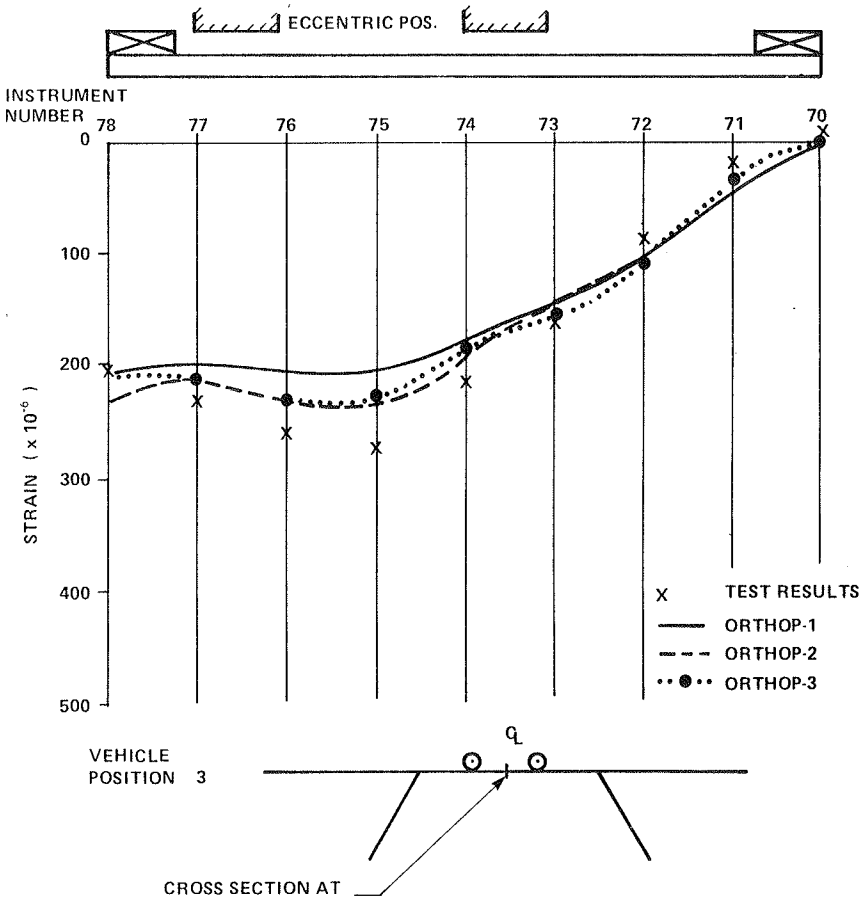

FIGURE 17 Flexural strains, vehicle position 3, eccentric loading.

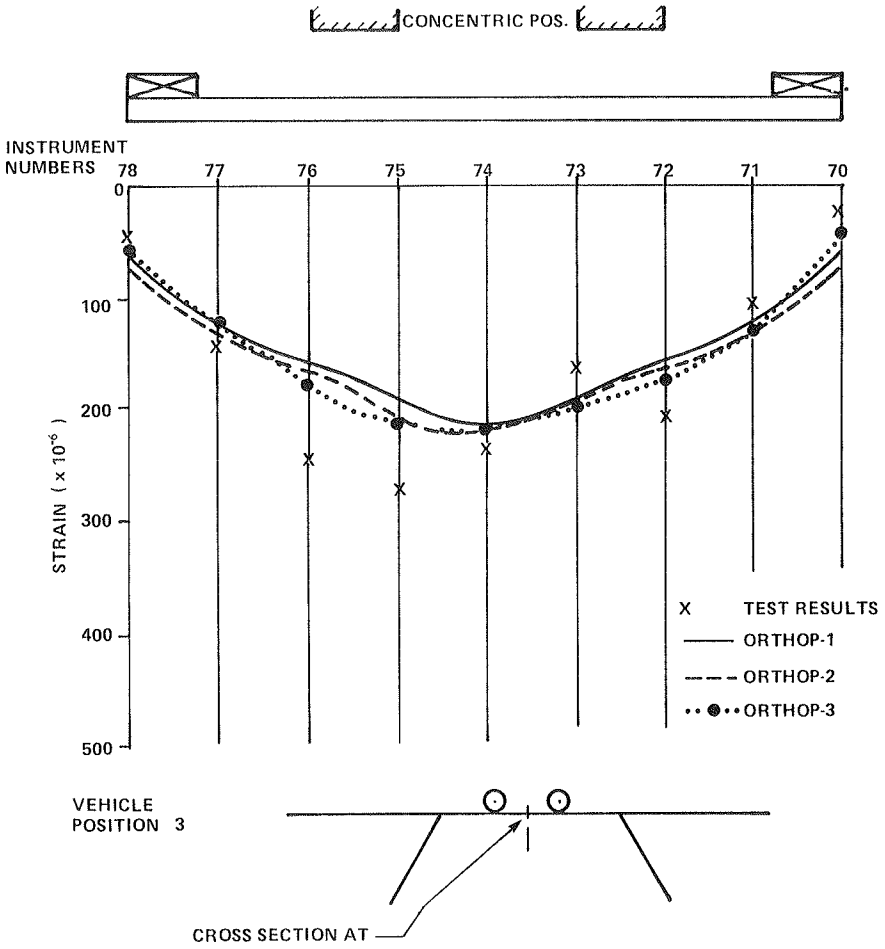

FIGURE 18 Flexural strains, vehicle position 3, concentric loading.

between the original design model and the introduction of leg movements in orthop 2 and orthop 3. Even the magnitude did not change appreciably, considering that the positive moment at the center of the bridge should increase when the intermediate supports undergo settlement. The increase in maximum positive moment in the center span was only 15 percent from the original analytic design model, orthop 1, to the final model, orthop 3, as shown in Figure 17.

Summary

The use of orthotropic analysis to represent the structural response of a prestressed wood deck system appears to be fairly accurate for displacement contours. The use of lower torsional and transverse flexural stiffness should be considered in design, although they apparently have limited effect on the distribution.

In this particular bridge, the leg movements do not appear to affect the force distributions appreciably. According to the analytic models only the maximum positive moment in the center span is increased by the settlement of the leg supports. All other design force modes were reduced. The apparent 15 percent increase in the positive design moment is comfortably accommodated by the moment capacity, which was determined to be 16 percent larger than the original factored moment determined earlier.

Further modification of the analytic model was not considered justified because small changes in the parameters do not appear to change the structural response to any appreciable degree.

Conclusions

This prototype bridge successfully carried MTC's maximum load testing vehicle that represents over two and one-half times the legal load. Under this load the maximum vertical displacement of the deck was around 9 mm.

The structural performance of the bridge was found to be representative of an orthotropic plate where the leg supports could be simulated as flexible columns. The analytic model indicated that the apparent leg movements have no adverse effects on the capacity of this structure to carry the full design load.

SUMMARY AND CONCLUSIONS

The design and construction of this prototype wood bridge demonstrated the flexibility in application of the prestressed wood system. The resulting structure is a strong and durable rigid frame that has a life expectancy of more than 50 years (8).

The bridge was constructed by what may be considered semiskilled labor. Very little special equipment, other than MTC's hydraulic prestressing system and a light construction crane, was required for construction of the prototype. A minimum of on-site work was required because the majority of

the fabrication was performed before transportation to the site.

The MNR estimated the cost of this prototype bridge to be only two-thirds the cost of the originally proposed steel structure (9). According to the load testing and the subsequent analytic evaluation, the capacity of the bridge is more than adequate to carry the full OHBDC design loads.

It is believed that the prestressed wood system can now be considered an economical alternative for new short-span bridges (2) as well as a method for rehabilitation (1). The system is being evaluated for use as a transverse laminated wood deck on steel girder bridges to replace the old nailed deck system. Two prototypes have been designed and were expected to be implemented in the fall and winter of 1983.

ACKNOWLEDGMENT

The authors wish to acknowledge P.F. Csagoly who conceived of the original rigid frame and prestressed wood system for this site. As Principal Research Officer for MTC until 1981, Csagoly was also the major driving force behind the successful development of the transverse prestressing system.

The following persons and organizations are also acknowledged for their contributions to the successful construction and testing of this new prototype wood bridge. S. Cross, Foreman, and the Huntsville field construction crew, MNR; J. Klubal, Senior Structural Research Technician, MTC; B. Kwok, Senior Laboratory Research Technician, MTC; L. Pena and G. Giles, Laboratory Research Technicians, MTC; and A. Messervia, Foreman, Thunder Bay District bridge crew, MTC.

REFERENCES

1. R.J. Taylor and P.F. Csagoly. Transverse Post-Tensioning of Longitudinally Laminated Timber Bridge Decks. Research Report RR.220. Ontario Ministry of Transportation and Communications, Downsview, Ontario, Canada, June 1979.
2. R.J. Taylor, B.deV. Batchelor, and K. Van Dalen. Prestressed Wood Bridges. Structural Research Report SRR-83-01. Ontario Ministry of Transportation and Communications, Downsview, Ontario, Canada, 1983.
3. R.J. Taylor. Design of Prestressed Wood Bridges Using the Ontario Highway Bridge Design Code. Structural Research Report SRR-83-03. Ontario Ministry of Transportation and Communications, Toronto, Ontario, Canada, April 1983.
4. Ontario Highway Bridge Design Code. Ontario Ministry of Transportation and Communications, Downsview, Ontario, Canada, 1983.
5. B. Bakht and R.C. Bullen. HECB/B/15, ORTHOP: Analysis of Orthotropic Right Bridge Decks. Version 2.0. Highway Engineering Computer Branch, Department of the Environment, London, England, n.d.
6. P.F. Csagoly and R.J. Taylor. A Development Program for Wood Highway Bridges. Structural Research Report 79-SRR-7. Ontario Ministry of Transportation and Communications, Downsview, Ontario, Canada, 1979.
7. J.W. Wagner. Development of a Demountable Reusable Transducer for the Measurement of Strain in Steel Structures. Laboratory Research Report LAB-82-03. Ontario Ministry of Transportation and Communications, Downsview, Ontario, Canada, Aug. 1982.
8. P.F. Csagoly and R.J. Taylor. A Structural Wood System for Highway Bridges. International Association for Bridge and Structural Engineering, Vienna, Austria, 1980.
9. ASKI News Publication. Ontario Ministry of Natural Resources, Sudbury, Ontario, Vol. 9, No. 1, Jan. 1983.

Publication of this paper sponsored by Committee on General Structures.

Evaluation of Seven Aluminum Highway Bridges After Two to Three Decades of Service

GORDON A. ALISON

ABSTRACT

Between 1948 and 1963 six aluminum highway bridges were erected in the United States and one was erected in Canada for highway overpasses and river crossings on Interstates and state highways. Girder types used vary from conventional built-up I and box to more radical triangular cross sections. Either riveting or welding was used depending on the structure. Recent reports from several owners and designers indicate that the performance of these bridges, particularly their corrosion resistance, is outstanding. This fact, coupled with the awesome number of obsolete bridges on the nation's roads and the impetus given to the Bridge Replacement Program by the Surface Transportation Assistance Act of 1982, resulted in a survey of the seven aluminum bridges in 1983. The results of this survey--based on inspection data provided by state highway officials--illustrate how the corrosion resistance of the alloys selected and how the design, details, test, construction, and erection methods employed are being verified by excellent performance in the field. Aluminum provides the bridge engineer and owner with a proven construction material for bridges where light weight and a long maintenance-free life are required.

There are an estimated 250,000 bridges in the United States in need of major repair or replacement. In 1982 the U.S. Congress passed the Surface Transportation Assistance Act that allocated $97.7 billion over a 5-year period for rebuilding the American infrastructure, including bridges. The following year the Aluminum Association, with the responsible state officials, surveyed seven aluminum highway bridges, erected between 1948 and 1963 in the United States and Canada for overpass and river crossings on Interstate and state highway systems, to determine their condition. Data were gathered on a variety of factors affecting performance such as traffic volume; environment; and the condition of superstructure, substructure, and approaches.

BACKGROUND

Before elaborating on the results of this examination, it might be useful to go back and review the reasons that justified the use of aluminum and the designs that were chosen. The potential of aluminum as a structural material has been amply demonstrated in its use for airframes since the 1930s. The first use of aluminum as a material for bridges was, appropriately enough, in Pittsburgh where the Smithfield Street Bridge was redecked in 1933 with a lightweight aluminum deck (plate plus stringers). Aluminum permitted the existing structure to sustain higher traffic loadings. In 1946 the possibility of using aluminum in railroad bridges was investigated by the Aluminum Company of America on a line serving a company aluminum smelter at Massena, New York. A riveted plate girder bridge was erected to span the Grassi River at the plant site. This was the first totally aluminum bridge built in North America.

Following this, the Aluminum Company of Canada erected a 504-ft riveted bridge over the Saguenay River in Quebec in 1950 to demonstrate the practicability of aluminum for constructing highway bridges. The bridge is located near a generating station that supplies power to Alcan's Arvida works, the largest aluminum smelter in the world.

The Interstate Highway Program was the impetus for the next major thrust. This resulted in the first welded aluminum highway bridge in the United States being erected in Des Moines, Iowa, in 1958. Since the completion of the riveted Arvida bridge in 1950 a wealth of new technology had been developed on specifications, equipment, and procedures for welding aluminum. At the same time, stronger, more weldable, corrosion resistant alloys had become available. Because welding is normally a faster process than riveting and had become the standard joining method for steel bridges, the decision was made to weld the Iowa plate girder bridge. The aluminum structure was designed to work compositely with the reinforced concrete deck through shear lugs. Expansion joints were also aluminum.

The stimulus for building the next group of aluminum bridges in 1960 was the desire of Robert Moses to specify an alternate material to steel and concrete in order to improve delivery and erection schedules. The firm of Andrews and Clark, Consulting Engineers, New York City, was commissioned to design two overpass bridges on the Long Island Expressway. These were conventional riveted plate girder structures. During the planning phase the performance of the Arvida bridge was carefully studied to determine if there was any excessive cracking in the concrete deck as a result of differential expansion between the concrete deck and the aluminum structure. It was concluded that not only was there little or no cracking but that the contraction of the aluminum structure in the winter had the potentially beneficial effect of preventing the ingress of moisture and road salt into the deck. Of the bridges reviewed in this paper these Long Island Expressway bridges are the most important in proving the feasibility of aluminum because of the high traffic density they sustain.

The next step in the evolution of the aluminum bridge was an attempt to drastically reduce weight and initial cost. The first embodiment of this concept was the Fairchild Bridge, a semimonocoque, riveted girder consisting of a series of triangular boxes. Each box is made from stiffened aluminum sheet, with the sheets connected via longitudinal extrusions. With this construction, the weight of the aluminum structure was reduced substantially (one-quarter to one-fifth the weight of a steel structure) without sacrificing performance. Full-scale fatigue tests at Lehigh University suggested that a life of over 100 years could be anticipated. No failure occurred during the test period. Four bridges of this type were erected between 1960 and 1963.

RESULTS OF 1983 SURVEY

How have these bridges performed? Are the designs and details used meeting the test of time? What about corrosion resistance--particularly to road salt? What about overall maintenance? Answers to these questions are summarized in Table 1.

Arvida Bridge

The Arvida, Quebec, bridge was the first all-aluminum highway bridge and the largest aluminum structure ever built at the time of its erection in 1950. Total length is 504 ft including approach spans. Length between skewbacks is 290 ft. Rise of the fixed arch is 47.5 ft. Width of roadway is 24 ft plus two 4-ft sidewalks. The arch shape was chosen for aesthetic reasons although it was realized that a truss structure would be lighter and more economical. Because only three aluminum bridges had been erected prior to 1950 (the Alcoa bridge at Massena, a bascule bridge at Sunderland, England, and a footbridge in Scotland), it was thought necessary to record the behavior of the Arvida bridge for a period of time after it was erected to compare its actual performance with assumed design values in such areas as stress levels, temperature effects, and corrosion behavior.

The bridge, located near the city of Jonquiere, was designed by C.J. Pimenoff, chief engineer, Dominion Bridge Company, Ltd., and fabricated by that company at their Lachine, Quebec, works. Dead loads were based on a unit weight of 175 lb per square foot. Arches were designed for a live load of 80 lb per square foot plus two 20-ton trucks abreast. The floor system and floor slab were designed for a live load of 100 lb per square foot plus two 20-ton trucks abreast. An alternate live load for arch, floor system, and floor slab design was a 50-ton electrical transformer on a 12-ton trailer pulled by an 18-ton tractor traveling at 10 mph. Wind loads included (a) a horizontal force of 30 lb per square foot on 1.5 times the projected area of the structure plus 200 lb per linear foot applied 7 ft above the roadway or (b) a uniform load of 50 lb per square foot on 1.5 times the projected area of the unloaded structure.

The structure was designed to resist stresses due to temperature variation of plus or minus 70°F from a normal temperature of plus 30°F (a range from plus 100°F to minus 40°F). Aluminum alloy 2014-T6 (clad) was used for plates and for extruded structural shapes (unclad). Rivet alloy was 2117-T4, bolt alloy 2024-T4. Unit axial tension stress used for alloy 2014-T6 (net section) was 21,000 lb per square inch. The maximum compression stress could not exceed this level. Values used for shear and bearing were 12,500 lb per square inch and 30,000 lb per square inch, respectively. These levels of stress are consistent with those currently specified by AASHTO for alloys of comparable strength to be used in aluminum bridge-type structures.

The Arvida bridge has performed well during its 34 years of service. The bridge has not been painted despite the original concern about the relatively low resistance of alloy 2014-T6 to corrosion. In fact, Alcan inspectors advise that the bridge is generally in good condition and the only cost of maintaining the structure to date has been $5,000 for repairs to the base plates in 1971. The asphalt wearing surface on the bridge deck has required only normal maintenance over the years and was replaced in 1983. It should be noted that although traffic density is relatively light on this bridge, road salt is used to melt snow during a 6-month winter period from November to the end of April.

Long Island Expressway Bridges

In 1959, A.A. Trinidad, Jr., of Andrews and Clark, Inc., Consulting Engineers, New York City, presented a paper to the New York State Association of Highway Engineers titled "Problems Involved in the Developing and Designing of the Aluminum Bridges for the Long Island Expressway" in which the following points were made.

After inspecting the Arvida aluminum bridge in 1957, one thing stood out to Andrews and Clark: Under critical inspection, the structural aluminum showed no signs of corrosion or distress after 7 years of continuous exposure to the elements and to varying traffic loads. It was therefore agreed that with good design and construction practice a safe, durable, corrosion-free structural aluminum bridge with a concrete deck was practical. Further, preventing corrosion of the aluminum alloy by concrete and providing for differential thermal expansion would not be problems.

Two bridges carry the Long Island Expressway over the divided lanes of the Jericho Turnpike and have single spans of approximately 77 feet on a skew of over 30 degrees and a width of over 110 feet (Figure 1). They are typical of many medium-span bridges where vertical clearances are critical and large skews are common. Designing the aluminum girders to act compositely with the concrete deck enabled girder depths of 4 instead of 5 ft to be used while meeting a live-load deflection requirement of 1/800 of the span. After this 1-ft reduction, girder depth is still one foot greater than that of a steel structure.

Aluminum alloy 6061-T6 was chosen for both structurals and rivets because of its good strength, availability in a wide variety of product forms, high resistance to corrosion, and good fabricating qualities. Also, structural specifications for this alloy had been fully developed (American Society of Civil Engineers, Proceedings Paper 970). Recommended tensile design stress was 15,000 lb per square inch based on a specified ultimate strength of 42,000 lb per square inch and a yield strength of 35,000 lb per square inch.

Aluminum alloys work efficiently with concrete as a composite beam because of the relative closeness of the elastic moduli of the two materials. To reduce fabrication, two flange angles were developed that required special extrusion dies. These angles have an outstanding leg thicker, as well as longer, than the leg connected to the web plate. They were extruded for the full girder length to eliminate splices and cover plates. Top flanges were painted with zinc chromate to reduce attack on aluminum from the concrete. The steel shear connectors were hot-dip galvanized. A 7-in. reinforced concrete slab supports a 2.5-in. asphalt-concrete wearing surface.

The superstructure is designed for a standard HS-20 loading with 17 girders on the westbound bridge and 18 girders on the eastbound bridge. Girders are spaced 7 ft on center. Rivets are 3/4 in. in diameter, driven cold. These were the first riveted aluminum highway bridges built in the United States.

The total amount of aluminum used in the two bridges was approximately 270,000 pounds or about 14 pounds per square foot of bridge surface. This compares with an estimated 35 pounds per square foot for steel. The total cost of each bridge including abutments, wing walls, and deck was approximately $350,000 or an estimated 18 percent above the cost of a comparable steel structure. (In a recent 1984 study Andrews and Clark estimate that this premium could be reduced to around 5 percent). Plans and specifications were prepared by Andrews and Clark for the New York State Department of Public Works.

TABLE 1 Results of 1983 Survey of Aluminum Bridges

Location	L.I. Expressway over Jericho Tpke, Nassau County, NY (2 bridges)	Rte 36 over Appomattox R Chesterfield Co., VA.	Sykesville MD, Route 32 over River Rd.	Amityville, NY (2 bridge) Sunrise Hwy @ Rte 110 Sunrise Hwy @ Wellwood Av.	DesMoines, IA 86th St./I-80 overpass	Arvida P.Q. over Saguenay River
Date Completed	1960	1961	1963	1963	1958	1950
Designer	Andrews & Clark, NYC, NY	Hayes, Seay, Mattern & Mattern, Roanoke, VA	Maryland Hwy Admin. & Inter. Alum. Str. Inc.	Kaiser & N.Y.D.O.T.	Ned L. Ashton Iowa City, IA	C. J. Pimenoff
Owner	NY State D.O.T.	VA, DOT	Maryland Hwy Admin.	NY State D.O.T.	Iowa DOT	City of Jonquires P.Q.
Fabricator	Pullman Standard, Chicago, IL	Reynolds Metals Co. Sanford Constn. Co, Inc	International Alum. Str. Inc., & Globe Iron Construction Co., Inc.	Traveller Mfg. Co. Sub. Stanray Corp.	--	Dominion Brdg Co. Ltd., Lachine P.Q.
Type of Construction	Riveted pl. girder with extruded flange reinforced concrete deck.	Alum triangular girder. Gravity abutments on solid rock reinforced concrete deck.	Alum girder with concrete deck, abutments & piers. Riveted triangular box stiffened sheet girders, reinforced concrete deck with asphalt wear surface.	Riveted triangular Box Stiffened Sheet Girders, reinforced concrete deck.	Welded plate girder reinforced concrete deck.	Riveted aluminum arch, concrete deck, rock foundation
Span	76'-9"	100'-4"	93'-6", 94'-2", 105'-9"	30'-76'-76'-30'	41'-3", 68'-9",68'-9", 41'-3"	290' clear, 504' overall
Width	61'	28' clear roadway	30' roadway, 37' overall	96'-0"	24' roadway, 36' overall	24' roadway, 2-4 ft sidewalks
Girder Depth	4'-6"	4'-10"	5'-7"	6'-0"	3'-2"	4'x6'-2" deep box girders
Alloy:	6061-T6 pl. & ext'n 6061-7/8" Rivets	6061-T6 pl. & ext'n AN5 & AN10 bolts & rivets	6061-T6 pl. & ext'n girders field spliced	6061-T6 pl. & ext'n Al. plate type shear connectors	5083-H113 pl. 5183 weld wire	2014-T6 pl. 2117 rivets
Design Load	HS-20	H20 & HS15, wearing surface 20 psf, sidewalk live load 60 psf	HS-20	HS-20, future wearing surface 20 psf., sidewalk live load 60 psf.	HS-20+19 p.s.f.	50 ton transformer on 18 ton tractor and 12 ton trailer
Avg. No. Vehicles/Day /Year	140,000 50 million	8050 -	6100 -	7050/21,800 2,573,250/7,957,000 46,318,500/143,226,000 (18 years)	Less than typical, but rising	
Aluminum Superstructure						
a. Condition	Good-Excellent	good, slight pitting, bent stiffeners	good, some corrosion	good	Quite well, many 1/8"-2" long hairline cracks in welds connecting diaphram and stiffener to webs of beams.	Good-excellent
b. damage	none	longitudinal-stiffeners damaged by flood debris	none	minor-no repairs	Section loss in bottom flange beams 1-4 due to collision damage caused by high vehicle.	None reported
c. repair	none	none	none	none, will be difficult to jack structure to free frozen bearings.	Grinding to remove notch in flanges damaged.	Base plates repaired in 1971 at cost of $5,000
Bridge Deck	OK	fair-20ft^2 spalled	not visible	deck in good shape no unusual cracking	OK, random cracking, hair-line transverse crack,s a little leaching	OK
Condition of Roadway Surface	poor due to heavy vehicle traffic, asphalt wearing surface replaced.	OK	bitumen wearing surface patched at bridge joints otherwise good.	good, no problems	Fair	OK, resurfaced in 1983

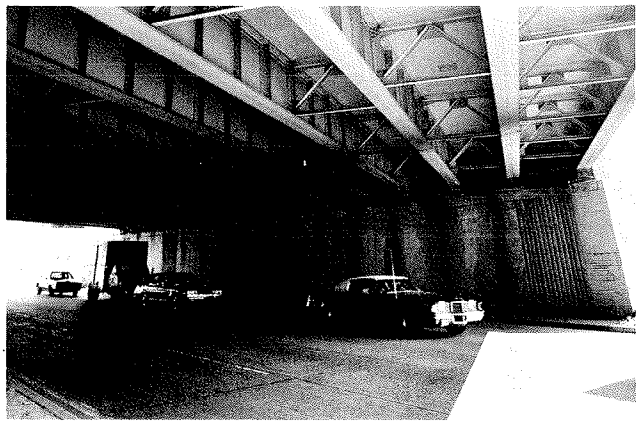

FIGURE 1 Aluminum superstructure of Long Island Expressway bridge.

This department supervised construction with its own engineering staff. Pullman Standard Car Manufacturing Company of Chicago was the fabricator, and the general contractor was Hendrickson Bros., Inc., Valley Stream, New York.

In the 1983 survey, New York State engineers reported that the aluminum structures were holding up very well. The engineers were particularly impressed with the speed of erection and suggested there might be a market for aluminum structures as replacement bridges on heavily used highways. Of the bridges surveyed, these Long Island bridges have by far the greatest traffic density. The estimated average daily traffic count is 140,000 vehicles; the yearly count is 50 million vehicles. This suggests that close to 1 billion vehicles have passed over these bridges since they were erected in 1960. Automobiles and light trucks accounted for 82 percent of the traffic with buses and heavy trucks (tractor-trailer) accounting for the remainder. Normal temperature range is 0°F to 100°F (58°F average). Road salt is used for more than 4 months per year.

The condition of the aluminum bridge structures was rated as good to excellent after an inspection of girder webs, flanges, stiffeners, diaphragms, and connector plates. There had been no structural damage. No corrosion was reported except of steel parts adjacent to the aluminum structure. The concrete deck is in good condition and has not required replacement. No water is leaching through the deck and there is no spalling concrete. Because of the traffic density the asphalt-concrete surface is rough and has some pot holes.

Iowa Bridge

The Iowa bridge is the only welded aluminum highway bridge in the United States. As noted earlier, welding was chosen over riveting to minimize weight and to gain experience with the type of construction being used on steel bridges. Erected in 1958, the Iowa bridge predates all the other highway bridges described in this paper except the Arvida bridge. The Iowa bridge was designed by Ned L. Ashton, Consulting Engineer, Iowa City, Iowa, for the Iowa State Highway Commission. The bridge is the 86th Street I-80 overpass and is located in the northwestern suburbs of Des Moines. It is a 220-ft-long x 30-ft-wide continuous aluminum girder bridge with a composite concrete deck. It has two 69-ft center spans and two 41-ft end spans.

The bridge is designed for AASHTO HS20-HS16 live loads plus 19 lb per square foot. The aluminum alloy specified for the structure was 5083-H113 welded with 5183 welding wire. The shielded inert gas metal arc welding process was specified to meet welding qualifications of Section IX of the ASME Boiler and Pressure Vessel Code. Fabrication conformed to ASCE Paper 970-ST3. Estimated weight of structural aluminum was about 75,000 pounds or approximately 12 pounds per square foot of bridge surface. Aluminum main beams weighed an estimated 53,144 pounds, diaphragms 17,288 pounds, and expansion joints about 4,000 pounds.

Traffic over the Iowa bridge, although less than typical, has increased in the past 2 years and is expected to continue rising. According to the Iowa Department of Transportation, the bridge has needed little maintenance and most of this was due to structural damage caused in 1978 by a vehicle exceeding the maximum height limits colliding with the superstructure. This overheight load struck the right exterior beam of span 3 causing a 2-in.-deep notch in the bottom flange. This notch was smoothed out by grinding to prevent it being the point of origin for a crack. In addition, weld cracks were observed between the ends of diaphragms 2, 3, and 4 and the web of beam 3. These cracks are being monitored and in a 1981 inspection were reported as numerous, fine, 1/8 to 2 inch cracks in the welds connecting diaphragms and stiffeners to the web of beams. The cracking is thought to be due to the welder pulling away when ending a weld. These cracks continue to be monitored.

The remaining four aluminum bridges in the survey represented attempts to substantially reduce metal content and cost by applying aircraft design principles to reduce weight and to use the production facilities of a number of fabricators supplying riveted aluminum structures to the transportation industry.

Amityville, New York, Bridges

In 1965 the New York State Department of Public Works (NYSDPW) let contracts for two aluminum bridges with riveted triangular box stiffened sheet girders. These structures were designed by Kaiser Aluminum & Chemical Corp. and NYSDPW. Both are located near Amityville, N.Y., one on Route 110 and Sunrise Highway, the other at Wellwood Avenue and Sunrise Highway. The bridges are 212 ft long and 96 ft wide and have two center spans of 76 ft and end spans of 30 ft (Figure 2). Loading was AASHTO HS-20

FIGURE 2 Amityville bridge.

with a 20 lb per square foot provision for a future wearing surface.

Sidewalk live load is 60 lb per square foot. Specifications called for an approved semimonocoque design for the superstructure with the skin braced by stiffeners or diaphragms for additional strength. The girders work compositely with the concrete slab. Individual inverted triangular beams made of alloy 6061-T6 support the concrete deck. They measure 10 ft wide x 6 ft deep overall and have 0.081-in.-thick side sheets and a 0.032-in.-thick corrugated top sheet. A bottom sheet, 0.102 in. thick, bridges the apices of the triangles. These sheets are riveted to specially designed longitudinal extruded sections and to lateral extruded bulb angle stiffener beams.

Falsework was eliminated by casting the concrete slabs directly on the corrugated top sheets that run longitudinally on top of the beams. A layer of 2.5 in. of asphaltic concrete covers the slabs. In designing the bridges as composite beams, stresses created by the difference in thermal expansion between aluminum and concrete are reacted to by thermal beams that run the full width of the structure near bulkheads. The aluminum superstructure of each of the Amityville bridges weighs 356,000 lb or about 17.5 lb per square foot.

As of 1982, the traffic count on the Route 110 and Sunrise Highway bridges was 7,050 vehicles per day, 2,573,000 vehicles per year. The estimated 18-year total was 46,318,500 vehicles. The equivalent figures for the Wellwood Avenue bridge are 21,800 (daily), 7,957,000 (yearly), and 143,226,000 (18 years).

These bridges are located in a light industrial seacoast region with minimum and maximum temperatures of 0°F and 100°F, respectively. Humidity varies between 50 and 100 percent. Road salt is used over a 4-month winter period. Annual snowfall is relatively light at 12+ inches.

Structural damage to the bridges has been minor and has required no repair. A major potential maintenance problem will be servicing rusted steel bearings. The problem is caused by the difficulty of jacking up the triangular beams due to lack of clearance and a fear of overstressing the structure locally at supports. (Shortly after erection the webs of both the Amityville and Sykesville bridges required reinforcement to resist the high shear loads at supports.) It was suggested, however, that the maintenance problems with the bearings could have been eliminated if aluminum or elastomeric bearings had been used initially. Other observations included the presumed difficulty in making repairs if a truck should hit the bridge, possible problems in obtaining a new triangular box girder, close placement of girders during construction that affects expansion and contraction, and difficulty in obtaining proper camber and correct beam length during fabrication. The bridge decks of both Amityville bridges were reported to be in excellent condition and have not been repaired or patched in 18 years. No maintenance of the aluminum superstructure has been required.

Sykesville, Maryland, Bridge

The Sykesville, Md., bridge (Figure 3) is similar to the Amityville bridges in design and construction. It was designed by the Maryland State Highway Administration and International Aluminum Structures, Inc., in 1963. It is located on Maryland Route 32 (Sykesville bypass). It spans River Road, the South Branch of the Patapsco River, and the B&O Railroad. There are three spans of 93 ft 6 in., 94 ft 2 in., and 105 ft 9 in. Depth of the triangular girders is 5 ft 7 in. (Figure 4). Overall width of the structure is 37 ft (30 ft clear roadway). AASHTO design loading is HS-20.

FIGURE 3 Sykesville bridge.

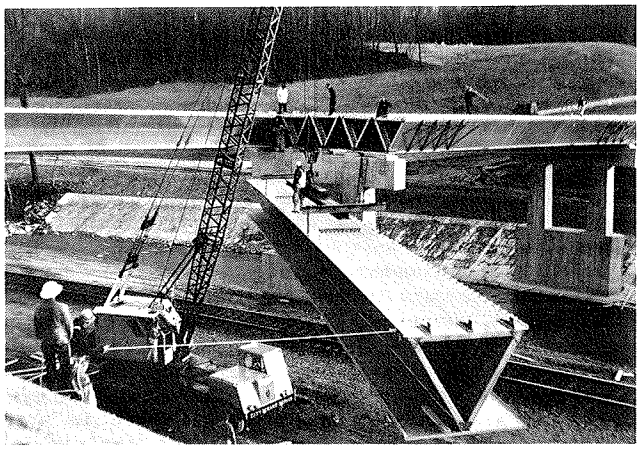

FIGURE 4 Erection of cell beam on Sykesville bridge.

The estimated traffic count in 1983 was 6,100 vehicles per day, up from 4,800 vehicles per day in 1980. The region is rural; average annual temperatures vary from plus 100°F to minus 5°F. Road salt is used over a 3-month winter period to handle an average snowfall of 22.5 in.

The aluminum beams were reported to be in good condition with no repairs necessary although there is some visible corrosion including discoloration at the longitudinal joints connecting the bottom plates. Steel bearings are rusted. The slab is constructed of lightweight concrete with a bituminous wearing surface that has been patched at the joints. Spot repairs to the concrete deck are anticipated. The effect of road salt leaching through the deck awaits coring data to determine if there has been any effect on the aluminum.

Appomattox, Virginia, Bridge

The Appomattox bridge also employs semimonocoque triangular beam girders, but its details are worth studying because they differ somewhat from those used in the triangular beam bridges in Maryland and New York (Figure 5). Located on Route 36 over the Appomatox River in Chesterfield County, Virginia, the bridge has a single span of 100 ft 4 in. and, due to clearance restrictions, a depth of 4 ft 10

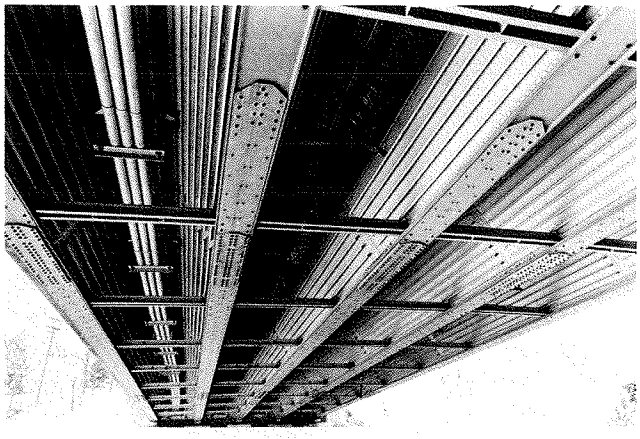

FIGURE 5 Aluminum superstructure of Appomattox River bridge.

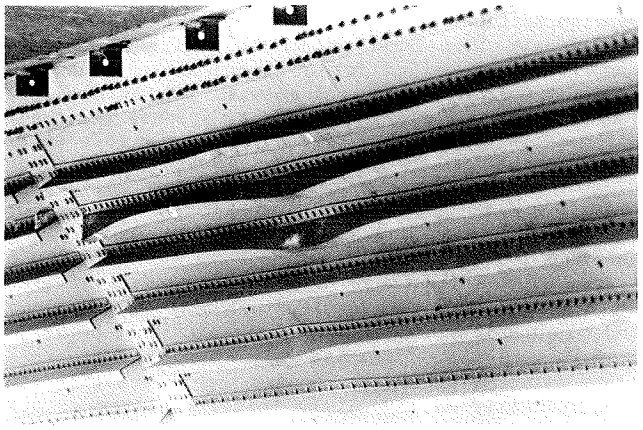

FIGURE 6 Appomattox River bridge: stiffeners damaged by flood debris.

in. This provides a span-to-depth ratio of 20.7 to 1, which is somewhat higher than that of most other bridges in this survey and results in minor vibrations when a heavy vehicle crosses the structure. Clear width of the roadway is 28 ft. AASHTO design load is H20 and HS15. Alloy 6061-T6 was used for all sheets, plates, extrusions, and rivets; connectors include aluminum AN5 and AN10 bolts and rivets. The bridge was designed by Hayes, Seay, Mattern & Mattern, Roanoke, Va., fabricated by the Reynolds Metals Company, and erected by the Sanford Construction Company in 1961.

Unlike the other triangular bridges, there are no continuous lower plates so the girders are open on their underside. Exterior longitudinal stiffeners reinforce the side sheets of the triangular beams; there are also interior stiffeners. There is provision for jacking the bridge to service bearings.

The estimated average number of vehicles per day is 8,050; 95 percent of these vehicles are automobiles and light trucks and the remainder are heavy vehicles. The bridge is located in an industrial region. Road salt is used, as required, over a 5-month period each year.

The structure is reported to be in good condition. The condition of individual aluminum components such as flange extrusions, side sheets, diaphragms, stiffeners, and connector plates is reported to be good but with slight pitting. The aluminum has taken on a typical rough granitelike appearance. Cadmium plated steel bolts and nuts are rusted and steel bearing plates and rocker assemblies need painting.

The longitudinal stiffeners of the upstream fascia girder have been bent by pounding from large timbers, power poles, and other large flood debris (Figure 6), but no structural repair has been required. There has been no adverse reaction between the aluminum structure and the concrete deck. The condition of the roadway surface is classed as fair with about 20 square feet spalled.

SPECIFICATIONS, DESIGN DATA

Current aluminum specifications available to bridge designers include aluminum chapters in both AASHTO Standard Specifications for Highway Bridges and AASHTO Standard Specifications for Support for Highway Signs, Luminaires and Traffic Signals. The Aluminum Association's Specification for Aluminum Structures or Specifications for Aluminum Bridge and Other Highway Structures are referenced in both cases. In 1983 the American Welding Society (AWS) published the first edition of AWS D1.2 Structural Welding Code--Aluminum. This code was approved by AASHTO in 1983.

Aluminum Standards and Data provides detailed information on nomenclature, product forms, mechanical and physical properties, fabricability, dimensional tolerances, and so forth for a wide variety of alloys. Additional design information is also available in Commentary on Specification for Aluminum Structures. These publications are available from the Aluminum Association, Inc., Washington, D.C.

SUMMARY

This 1983 inspection revealed that no painting or other major maintenance has been required for the aluminum superstructure of the seven bridges studied. Fascia girders of two of the bridges have been hit but the only repair required was grinding out a notch on the flange of one beam. The satisfactory performance of concrete decks and aluminum superstructures continues to verify the validity of the design principles, specifications, details, fabrication, and erection practices used initially. No fatigue cracking was reported for any of the riveted structures, and the type of fatigue cracking found in the one welded aluminum structure could be avoided in future bridges by modifications in fabrication and design.

The life of a typical bridge is expected to be at least 50 years although there are obvious exceptions. Based on an estimated total traffic count of 1 billion vehicles, an average of 114,000 vehicles have traveled across the aluminum Long Island, N.Y., bridges each day since they were opened to the traffic in 1960. This billion-vehicle performance represents a life expectancy of at least 50 years for similar aluminum bridges if the lifetime average daily traffic count is 55,000 vehicles rather than the 140,000 carried by the Long Island superstructures.

In addition, the premium for aluminum bridges appears to be narrowing according to studies made by Andrews and Clark Consulting Engineers in 1960 and in 1984. In 1972, in a paper entitled "Aluminum Bridges--An Evaluation," presented to a combined

meeting of the American Society of Civil Engineers and the Engineering Institute of Canada, John Clark of Alcoa concluded: "In the main, it has been shown that aluminum in bridges give trouble-free, maintenance-free service--up to 28 years in the examples cited."

Ten years later, the 1983 survey of these same bridges leads to a similar conclusion. On the basis of engineering applicability, aluminum is now a proven material for bridge construction. Any initial cost premium is more than justified by low maintenance and long life.

Publication of this paper sponsored by Committee on General Structures.

Finite-Element Load Distribution Factors for Multi-T-Beam Bridges

PATRICK R. REISNOUR and FAHIM A. BATLA

ABSTRACT

In this paper the determination of the lateral distribution of wheel loads on multi-T-beam bridges using the finite-element method is presented. The results are compared with existing applicable AASHTO specifications and other methods found in the literature. The evaluation of lateral wheel load distribution is of importance because of the significance of the localized effects of wheel loads on stresses and deflections of individual T-beams and must be determined with sufficient accuracy. It is found that significant differences exist in wheel load distributions determined using applicable specifications and other methods compared with distributions determined using the finite-element method of structural analysis.

The use of precast concrete components for the construction of multi-T-beam bridge superstructures with short to medium span lengths is increasing because of the ease of construction and relative economy associated with this type of superstructure. Because of the complexity of the behavior of multi-T-beam superstructures, the bridge engineer must often rely on design aids to avoid the complicated mathematical procedures of a rigorous analysis. These design aids should be simple to use yet lead to sufficiently accurate designs.

For bridges with short to medium spans, considerable emphasis must be placed on the calculation of stresses and deflections due to wheel loads. This emphasis is necessary because the local effects of these loads are of considerable significance in comparison with those effects caused by the other loads on the superstructure that are better distributed both longitudinally and transversely. Therefore the lateral distribution of wheel loads on multi-T-beam superstructures must by determined with a considerable degree of accuracy.

In this paper a comparison of factors used for the lateral distribution of wheel loads on nonskewed multi-T-beam superstructures obtained by several methods is presented. The load distribution factors that are based on existing design aids and other methods are compared with distribution factors determined using modern techniques of structural analysis based on the finite-element method. In the finite-element method, T-beam-type or similar structural systems are represented as an assemblage of plate finite elements and the overall behavior of the structure is then represented by the interaction of in-plane and out-of-plane plate deformations of the plate elements.

A multi-T-beam bridge superstructure is constructed by placing single-, double-, or multiple-stem T-beams side by side on the supports (Figure 1). In this investigation the flanges of adjacent T-beams are assumed to be connected throughout the length of the superstructure in a manner that provides full transfer of transverse shear and bending moments between the beams. The behavior of a multi-T-beam superstructure can be represented as the interaction of the longitudinal bending, transverse bending, and torsional behaviors of the superstructure (Figure 2). These individual aspects of the overall behavior of the structure are in turn dependent on structural parameters such as span lengths and thickness of the flanges and stems. The distance between the stems, width of the superstructure, depth of the stems, and position of wheel loads also affect the behavior of the superstructure. The parameters, which influence the distribution of wheel loads, that are varied in this study include

1. Span length,
2. Width of the superstructure,
3. Depth of the superstructure,

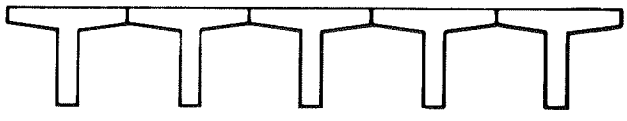

FIGURE 1 Cross section of multi-T-beam superstructure.

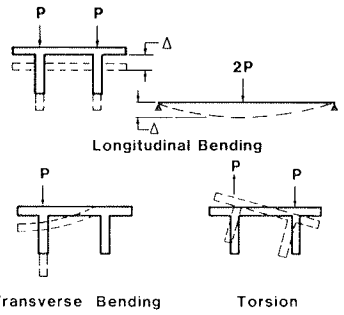

FIGURE 2 Deflection behavior.

4. Transverse position of the wheel loads,
5. Longitudinal position of the wheel loads, and
6. Number of traffic lanes.

The following parameters influence the lateral distribution of wheel loads and are the same for all the superstructures analyzed in this study.

1. Spacing of beams,
2. Flange thickness,
3. Thickness of stems,
4. Location of diaphragms, and
5. Span-to-depth ratio.

It should be noted that, in the course of developing final design aids for determining wheel load distribution factors for multi-T-beam superstructures, the influence of the parameters that may affect the lateral distribution of wheel loads must be thoroughly investigated. This is a monumental task. However, this task can be made easier and the results more accurate by use of the finite-element method of structural analysis.

To initiate the comparison of wheel load distribution factors based on various methods of analysis, it is useful to first discuss the theories on which the analysis methods and design aids are based. The discussion of theories and methods of analysis is presented in the next section. This is followed by the presentation and discussion of the results of the investigation described previously.

METHODS OF ANALYSIS

The finite-element method, the provisions of Article 1.3.1(B) of AASHTO Standard Specifications for Highway Bridges (1), and procedures developed by Aziz et al. (2) are used to determine distribution factors for wheel loads in this study. The finite-element method is used to determine the distribution of stresses and deflections in multi-T-beam superstructures and single T-beams. These distributions are in turn used to calculate the distribution factors. Distribution factors are determined using AASHTO design aids based on the spacing between the stems (1) and, in the procedures presented by Aziz (2), the calculation of distribution factors requires the evaluation of several dimensionless stiffness coefficients of the superstructure.

The AASHTO provisions for load distribution on beam and slab bridges, which are revisions to the specifications proposed by Sanders and Elleby (3), and the procedure presented by Aziz et al. (2) are based on analyses of bridge superstructures using orthotropic plate theory and tests conducted on actual bridges.

In orthotropic plate theory, the behavior of the superstructures is modeled as the behavior of a plate with uniform thickness and uniform but different flexural properties in the transverse and longitudinal directions (4-6). The actual flexural properties in the transverse direction of a multi-T-beam superstructure are not uniform across the width because of the localized contribution of the torsional stiffness of the stems to the transverse bending stiffness of the flange. However, in orthotropic plate theory, the transverse bending stiffness of the orthotropic plate is taken as the uniform distribution of the actual flexural stiffness.

In addition to the assumption of uniform flexural properties in the transverse and longitudinal directions, assumptions pertaining to classical thin plate theory are also used in the orthotropic plate approach (4-6). Furthermore, the following assumptions are used by Sanders and Elleby (3).

1. Poisson's ratio is equal to zero,
2. All connections transfer full moment and shear,
3. The spacing between beams and diaphragms is uniform,
4. The superstructure is rectangular in plan,
5. The beams are of equal stiffness, and
6. The superstructure behaves elastically.

With the exception of the first of these assumptions, the same assumptions were used for the analyses of multi-T-beam superstructures by Aziz et al. (2). Furthermore, in the analyses it is assumed that no intermediate diaphragms are used in the superstructure (2).

Application of the orthotropic plate model to represent the behavior of a multi-T-beam superstructure consists of representing the superstructure as a flat plate simply supported at the ends and free along the longitudinal edges. In superstructures where the spacing between stems or the depth of the stems is large in comparison with other dimensions of the T-beams, the orthotropic plate model presents a gross simplification of the actual behavior of the superstructure because of the manner in which the transverse and longitudinal bending stiffnesses and the torsional stiffness are treated.

In superstructures with large spacings between the stems, or deep stems, or both, the localized transverse stiffness of the flange in the vicinity of the stems creates a condition of transverse bending similar to the bending of a beam that is continuous over elastic supports (Figure 3). These elastic supports (stems) provide resistance to rotation (due to torsional stiffness of the stem) and resistance to vertical translation (due to longitudinal bending stiffness of the superstructure). Therefore, to arrive at a sufficiently accurate solution for the behavior under load of a multi-T-beam superstructure, the use of orthotropic plate theory is limited to those superstructures where the dimensions of the individual T-beams are such that the uniform transverse bending stiffness of the orthotropic plate

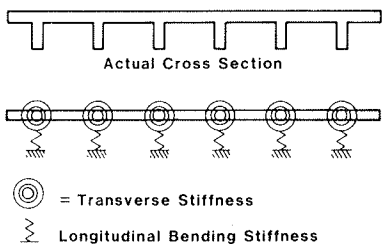

FIGURE 3 Continuous beam analogy.

does not differ greatly from the actual stiffness at any transverse location in the flange.

As noted previously, the lateral distribution of wheel loads is affected by the longitudinal and transverse bending behavior and the torsional behavior of the superstructure. The longitudinal bending behavior of the superstructure produces longitudinal in-plane stresses in the flange and stems (Figure 4). The transverse bending moments produce transverse distortions of the stems and flanges in the plane of the cross section that in turn influence the torsional properties of the cross section.

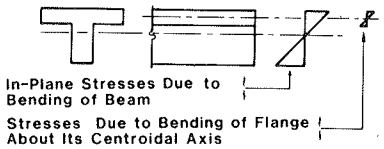

FIGURE 4 Longitudinal stresses caused by bending.

In Figure 4 it can be seen that the thickness of the flanges is small in comparison with the overall depth of the structure. The longitudinal in-plane stresses in the flange due to longitudinal bending of the flange plates about their centroidal axes are quite small in comparison with the longitudinal in-plane stresses in the flange due to the longitudinal bending of the T-beam cross section about its neutral axis. Hence, the longitudinal plate bending stresses of the flange due to bending about its centroidal axis can be neglected. Furthermore, because the longitudinal dimensions of the flange are much greater than the transverse dimensions between the stems, the bending of the flange may be treated as predominantly one-way (transverse) bending. Similar reasoning can be applied to the stems to show that they are also subject to one-way bending in the direction across the depth of the stem. Multi-T-beam superstructures can therefore be classified as folded plate structures that consist of long flat plates joined at the folds.

The finite-element method of structural analysis provides a means of accurately representing the actual geometry of multi-T-beam superstructures as well as the actual loading and support conditions. Furthermore, the finite-element method eliminates the need to make several simplifying assumptions typically used in the analysis of folded plate structures with other analytic techniques and formulations (7,8). Modeling of a multi-T-beam superstructure using the finite-element method eliminates the need to assume that the transverse bending stiffness is a uniform distribution of the actual stiffness because the actual distribution of the transverse bending stiffness is represented by the model. Finite-element modeling also provides an accurate representation of the longitudinal and twisting behavior of the structure. The finite-element method of structural analysis in general uses the assumptions of classical thin plate bending and in-plane elasticity theories because model developments are typically based on these theories. If these assumptions are satisfactory, the finite-element method leads to a much more accurate and straightforward analysis than do simplified methods of analysis. The accuracy of the finite-element models used in this study is demonstrated elsewhere (9-11) where results of finite-element analyses are compared with experimental results and results based on elasticity solutions that are considered exact.

Two finite-element programs are used for the analysis of multi-T-beam superstructures in this study. The finite-element program FAP, which was developed by Batla (11) specifically for the elastic analysis of constant-depth, straight folded, plate structures, is used as is the finite-element program SAPIV (12). The FAP program is used to determine the distribution of stresses and deflections due to wheel loads (two wheel loads per traffic lane) in all the multi-T-beam superstructures considered in this study. The SAPIV program is used as a finite-element analysis to provide independent verification of the results. The stresses and deflections, due to one wheel load on the beam, are also determined in a single T-beam. The longitudinal location of the wheel loads is the same for the superstructure and the single T-beam. The transverse locations of the wheel loads on the superstructures are discussed in the next section. The load factor representing the lateral distribution of wheel loads is determined as the ratio of the maximum stress in the superstructure to the maximum stress in the single T-beam. Load factors are determined from comparison of maximum peak stresses that occur in the flange above the stems, comparison of the maximum tensile stresses that occur at the bottom of the stems, and comparison of the maximum deflections that occur in the superstructure and single T-beams. The load factors determined using the finite-element analysis and those determined using the methods discussed previously are presented in the next section. The load factors based on comparison of the compressive stresses, tensile stresses, and deflections using the SAPIV finite-element program (12) are also presented to compare the load factors determined using different finite-element models.

DETERMINATION OF WHEEL LOAD DISTRIBUTION

The multi-T-beam superstructures for which wheel load distributions are determined in this study are assumed to be constructed of single-stem T-beams. The span-to-depth ratio, spacing between stems, flange thickness, and stem width are the same for each superstructure (Figure 5). The superstructures considered here consist of two overall widths: two-lane superstructures constructed of five T-beams, and superstructures constructed of seven T-beams. The latter are analyzed as both two-lane and three-lane bridges (Figure 6).

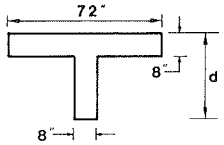

Span Length Feet	d Inches
40	24
60	36
80	48
100	60

FIGURE 5 Cross section of typical single T-beam.

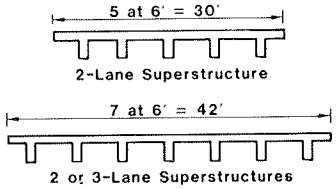

FIGURE 6 Superstructure cross sections.

In the finite-element method, the superstructures and single T-beams are modeled as simply supported with end diaphragms that are infinitely rigid in their own plane but completely flexible in the direction normal to the plane of the diaphragms; no intermediate diaphragms are used. The wheel loads on the superstructure are applied at midspan as well as at a distance from the midspan that represents the location of the wheels of an AASHTO HS 20-44 truck load with the center of gravity of the truck near the midspan (Figure 7). The lateral location of wheel loads considered for the evaluation of load factors is such that the loads act in the plane of the stems (Figure 8).

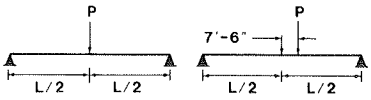

FIGURE 7 Longitudinal location of wheel loads.

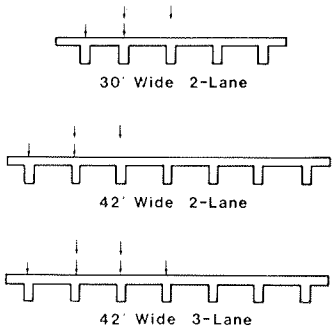

FIGURE 8 Transverse location of wheel loads.

As shown in Figure 8, two wheel loads are applied on stems that are common to two lanes. For convenience the finite-element idealization of the structure is done so that concentrated loads can be applied at the nodes. The wheel load cases shown in Figure 8 represent cases in which trucks are side by side and their wheel loads are close enough together to be assumed to be acting at the same point. The wheel loads are applied directly above the stems to ensure that the maximum compressive and tensile stresses occur at the top and bottom of the stems, respectively.

The maximum stresses and deflections in the multi-T-beam superstructures shown in Figure 6 and corresponding single T-beams are presented by Reisnour in his study of the lateral distribution of wheel loads on multi-T-beam bridges (10). The distribution of compressive stresses, due to single wheel loads placed at midspan, in the flange of a two-lane, 40-ft-span superstructure is shown in Figures 9 through 11. Figure 9 shows the stresses due to a wheel load over the stem of the central T-beam. The stress distributions shown in Figures 10 and 11 are due to single wheel loads placed on the T-beam adjacent to the central beam and the rightmost T-beam, respectively. Figures 12 and 13 show the distribution of compressive stresses in the flange due to two wheel loads in two positions at midspan. To illustrate the difference in the distribution of stress and deflections, the distribution of deflections due to the similar loading conditions for the same superstructures is presented in

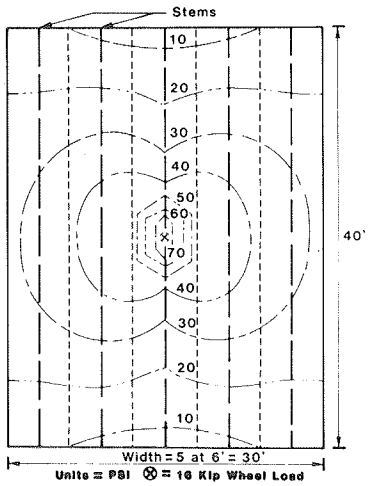

FIGURE 9 Compressive stresses in flange caused by single wheel load over stem of central T-beam.

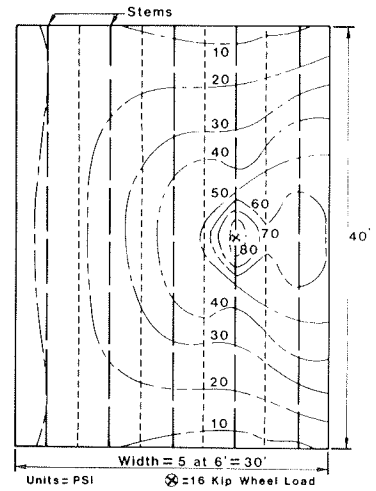

FIGURE 10 Compressive stresses in flange caused by single wheel load on T-beam adjacent to central stem.

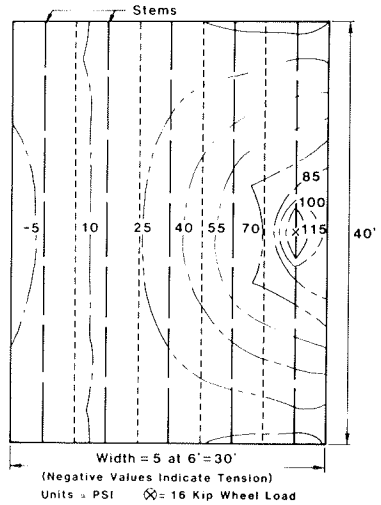

FIGURE 11 Compressive stresses in flange caused by single wheel load on rightmost T-beam.

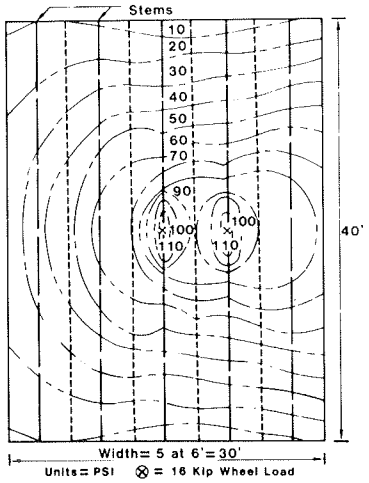

FIGURE 12 Compressive stresses in flange caused by two wheel loads: position 1.

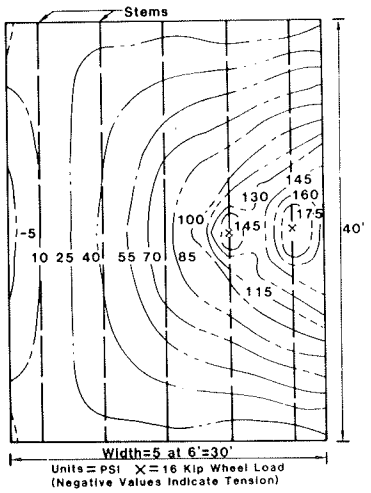

FIGURE 13 Compressive stresses in flange caused by two wheel loads: position 2.

Figures 14 through 18. The deflections shown in Figures 14 through 16 are those due to single wheel loads, and Figures 17 and 18 show the deflections due to two wheel loads.

The wheel load distribution factors based on maximum peak compressive stresses in the flange, maximum tensile stresses at the bottom of the stems, and maximum deflections as determined using the finite-element program FAP for the analysis of the superstructures shown in Figure 6 are presented in Table 1. Also given in Table 1 are the load factors calculated using the SAPIV finite-element program (12) for the 30-ft-wide, 40-ft-span superstructure to indicate the reliability of load factors determined using the different finite-element models. These distribution factors are calculated using the stresses and deflection due to wheel loads placed at the midspan of the superstructures and single T-beams. Distribution factors calculated using the stresses and deflections due to wheel loads placed at a distance from the midspan are not presented because they are similar to those shown in Table 1.

According to AASHTO provisions [1, Article

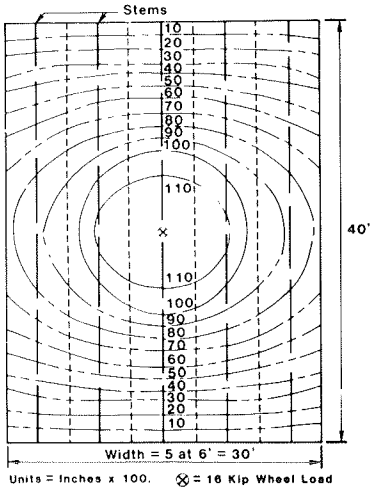

FIGURE 14 Deflections caused by single wheel load: position 1.

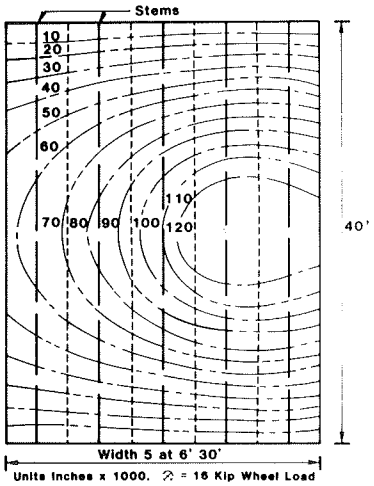

FIGURE 15 Deflections caused by single wheel load: position 2.

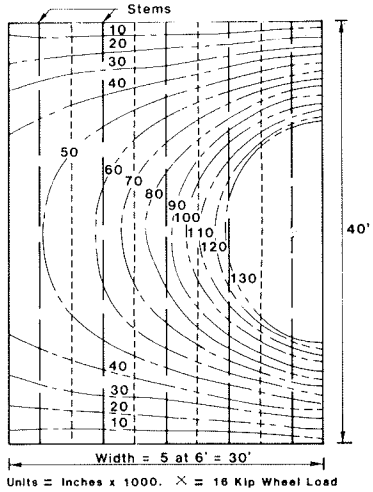

FIGURE 16 Deflections caused by single wheel load: position 3.

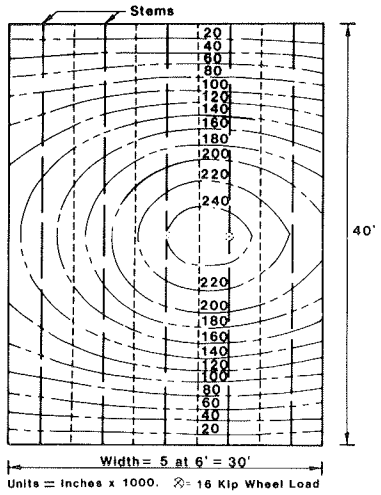

FIGURE 17 Deflections caused by two wheel loads: position 1.

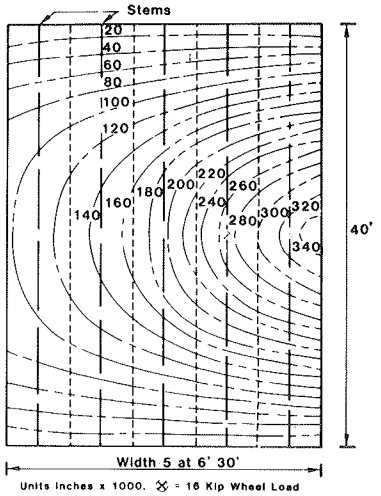

FIGURE 18 Deflections caused by two wheel loads: position 2.

TABLE 1 Load Distribution Factors Based on Compressive Stresses, Tensile Stresses, and Deflections as Determined Through Finite-Element Analyses

Span (ft)	Width (ft)	No. of Lanes	Based on Compressive Stresses	Based on Tensile Stresses	Based on Deflections
40	30	2	1.23	1.14	1.04
	30	2	1.29[a]	1.10[a]	1.02[a]
	42	2	1.19	1.06	0.93
	42	3	1.47	1.34	1.19
60	30	2	1.25	1.16	1.11
	42	2	1.17	1.07	0.96
	42	3	1.46	1.35	1.19
80	30	2	1.28	1.15	1.10
	42	2	1.19	1.06	0.99
	42	3	1.45	1.34	1.22
100	30	2	1.30	1.14	1.11
	42	2	1.20	1.05	0.99
	42	3	1.47	1.33	1.24

[a]Based on analyses using SAPIV; all other results are based on use of FAP.

1.3.1(B)], the wheel load distribution factor for a beam and slab superstructure, with two or more traffic lanes, constructed of concrete T-beams is determined as

$$LF = S/6$$

where

S = spacing between stems (feet).

Because the spacing between stems of all the superstructures considered in this study is 6 ft, the distribution factors for these superstructures are all equal to 1.

The procedure for determining distribution factors for multi-T-beam superstructures using the design aids presented by Aziz et al. (2) involves calculation of two nondimensional coefficents that are functions of the stiffness parameters of the superstructure. These coefficients are used to determine the coefficient D from charts presented in their paper (2). This coefficient D is corrected using a parameter that is a function of the width of the traffic lanes. The distribution factor is then calculated as

$$LF = S/D'$$

where

S = spacing between stems (feet) and
D′ = corrected D (feet)

The maximum wheel load distribution factors for each superstructure calculated using the finite-element method presented in Table 1 are given in Table 2 along with the distribution factors determined using the design aids of AASHTO (1) and Aziz et al. (2).

TABLE 2 Load Distribution Factors Based on Various Methods

Span (ft)	Width (ft)	No. of Lanes	Method: Finite Element	Method: AASHTO (1)	Method: Aziz et al. (2)
40	30	2	1.23	1.00	1.11
	42	2	1.19	1.00	1.17
	42	3	1.47	1.00	1.15
60	30	2	1.25	1.00	1.09
	42	2	1.17	1.00	1.13
	42	3	1.46	1.00	1.07
80	30	2	1.28	1.00	1.08
	42	2	1.19	1.00	1.17
	42	3	1.45	1.00	1.11
100	30	2	1.30	1.00	1.07
	42	2	1.20	1.00	1.17
	42	3	1.47	1.00	1.09

SUMMARY AND DISCUSSION

The data presented in Table 1 indicate that wheel load distribution factors based on comparison of compressive stresses, tensile stresses, and deflections all differ for each of the given superstructures. Figures 9 through 13 and 14 through 18 illustrate the differences between the distribution of compressive stresses in the flange and deflections. The difference between distribution factors based on tensile stresses and those based on compressive stresses indicates that there is a difference in the manner in which these stresses are distributed. This difference in the distribution of compressive

and tensile stresses is due to the presence of shear lag at the junction of the flange and stems; there is no shear lag effect at the bottom of the stems. The stress distributions shown in Figures 9, 10, and 12 show the occurrence of shear lag where the space between consecutive contours decreases more sharply along the loaded stem of the T-beam than at other locations across the width.

Figure 11 shows a region in the flange where a longitudinal stress reversal occurs at one side of the superstructure when the wheel load is located near the other edge. In the orthotropic plate model the superstructure is treated as a flat plate simply supported on the ends, free along the edges, and with uniform properties in the transverse and longitudinal directions. For this reason, under general wheel loading conditions, the orthotropic plate model of the superstructure will not be capable of predicting this stress reversal in the longitudinal direction of the superstructure, which may cause tensile stresses in the flange. Although the longitudinal stresses in the flange will be compressive when the dead load and other wheel loads are placed on the superstructure of the bridge shown in Figure 11, there may be cases, especially in structures where the width-to-span ratio is high, where the tensile stresses in the flange of the superstructure are quite significant and the net stress due to the superposition of all the loads may result in a longitudinal tensile stress in the flange.

Comparison of the distribution factors determined using the provisions of Article 1.3.1(B) (1) with the distribution factors calculated using the results of finite-element analyses (10) and the procedure presented by Aziz et al. (2) (Table 2) indicates that the latter methods of determining the lateral distribution of wheel loads on multi-T-beam superstructures are substantially different. The distribution factors determined using the stress distributions obtained from finite-element analyses and the procedure presented by Aziz et al. (2) are expected to be slightly higher because in both situations the superstructures are assumed to have no intermediate diaphragms. In the study by Sanders and Elleby (3) the superstructures were assumed to have intermediate diaphragms. It is interesting to note, however, that for the structures considered in this study, the wheel load distribution factors determined using the distribution of compressive stresses in the flange are quite conservative in comparison with the load factors calculated using the provisions of the AASHTO specifications.

To arrive at sufficiently accurate results of analyses of multi-T-beam superstructures, the model used to represent the behavior of the superstructure under load must be selected with great care. The use of orthotropic plate theory for the analysis of multi-T-beam superstructures must be limited to those superstructures where the uniform distribution of transverse bending stiffness does not differ greatly from the actual transverse bending stiffness at any point in the flange. The finite-element method is not limited to any particular geometrical configuration, loading or support conditions, or structural and material parameters. This method may be used, in conjunction with experimental testing of actual bridges, as the basis of simplified design aids without encountering the limitations found in other methods of analysis.

No matter what method of analysis is used for developing design aids for determining lateral wheel load distribution factors for multi-T-beam superstructures, it is important to discuss and clearly indicate in the specifications the limitations of application of the design aids in determining the lateral distribution of wheel loads. This will prevent inadvertant gross overdesigns or underdesigns.

ACKNOWLEDGMENT

The authors wish to express their appreciation to the staff of the North Dakota State University (NDSU) Computer Center and the faculty of the Department of Civil Engineering at NDSU for their encouragement, timely assistance, and advice throughout this project. Sincere thanks are also extended to R. Rogness of the Department of Civil Engineering for his advice and assistance in the preparation of this paper.

REFERENCES

1. Standard Specifications for Highway Bridges. 12th ed. AASHTO, Washington, D.C., 1977.
2. T.S. Aziz, M.S. Cheung, and B. Bakht. Development of a Simplified Method of Lateral Load Distribution for Bridge Superstructures. In Transportation Research Record 665, TRB, National Research Council, Washington, D.C., 1978, pp. 37-44.
3. W.W. Sanders and H.A. Elleby. Distribution of Wheel Loads on Highway Bridges. NCHRP Report 83. TRB, National Research Council, Washington, D.C., 1970, 56 pp.
4. R. Szillard. Theory and Analysis of Plates. Prentice-Hall, Englewood Cliffs, N.J., 1974.
5. A.C. Ugural. Stresses in Plates and Shells. McGraw-Hill, New York, 1981.
6. S. Timoshenko and S. Woinowski-Krieger. Theory of Plates and Shells. 2nd ed. McGraw-Hill, New York, 1959.
7. J. Born. Folded Plate Structures, Their Theory and Analysis. Translated by C.V. Amerongen. Fredrick Ungar, New York, 1962.
8. J.S.B. Iffland. Folded Plate Structures. Journal of the Structural Division, ASCE, Vol. 105, No. NST1, Jan. 1979, pp. 111-123.
9. F.A. Batla, V.J. Meyers, and P.R. Reisnour. Simplified Finite Element Analysis of Prismatic Folded Plates. Proc., International Symposium on Spatial Roof Structures, Dortmund, Federal Republic of Germany, Sept. 10-14, 1984.
10. P.R. Reisnour. Study of Lateral Distribution of Wheel Loads for Multi-Tee Beam Bridges. M.S. thesis, North Dakota State University, Fargo, 1982.
11. F.A. Batla. Finite Element Analysis of Prestressed Concrete Box Girders. Ph.D. dissertation, Purdue University, West Lafayette, Ind., 1976.
12. K.J. Bathe, E.L. Wilson, and F.E. Peterson. SAPIV: A Structural Analysis Program for Static and Dynamic Response of Linear Systems. PB-221 967. National Technical Information Service, U.S. Department of Commerce, June 1973.

Publication of this paper sponsored by Committee on General Structures.

Design, Fabrication, and Erection of a Curved, Prestressed Concrete Bridge with Continuous Girders

ROBERT M. BARNOFF, GORDON NAGLE, MARIO G. SUAREZ,
LOUIS F. GESCHWINDNER, JR., H. WILLIAM MERZ, JR., and HARRY H. WEST

ABSTRACT

A five-span, prestressed concrete bridge has been constructed for the Pennsylvania Department of Transportation at the Philadelphia Airport. The five curved, post-tensioned, box girders for the bridge are continuous over two and three spans, respectively. Approximate lengths are 139 and 126 ft for the two-span girders and 92, 135, and 92 ft for the three-span girders. Radius of curvature is 478 ft for the two-span girders and 326 ft for the three-span girders. Curvature of the girders was achieved by incremental chords 20 ft long, and field splicing was done only at piers with cast-in-place diaphragms. The bridge was analyzed assuming that the girders and diaphragms act as a two-dimensional grid system. A conventional program based on a matrix method of analysis was used to find the bending moments, shear forces, torsional moments, and displacements. Post-tensioning forces were analyzed using a space frame matrix method of analysis. Girders were prefabricated in lengths corresponding to the five spans and were transported by truck to the job site. Each span length of the girder was partly post-tensioned for shipment, and final post-tensioning for continuity over the piers was done in the field. The design, fabrication, transportation, erection, and final post-tensioning of the continuous curved girders are described in this paper. Details of the composite deck are also discussed.

A five-span, prestressed concrete bridge has been constructed for the Pennsylvania Department of Transportation on Legislative Route (LR) 795 (Interstate 95) in Philadelphia, Pennsylvania. This structure, which is located on a compound horizontal curve, is identified as ramp K over LR 67054. The ramp provides vehicular access to the Philadelphia International Airport.

The original design of ramp K was a curved, steel-plate-girder bridge, but an alternate design for a continuous, curved, prestressed, concrete bridge was submitted and approved. I.A. Construction Corporation was the general contractor for this project, and the prestressed concrete components were fabricated and supplied by Schuylkill Products, Inc., Cressona, Pa. Schupack Suarez Engineers, Inc., were the designers for the project with assistance from R.M. Barnoff and Associates, Inc., who performed the analysis of the continuous structure.

DESCRIPTION OF STRUCTURE

The compound horizontal curvature of ramp K dictated the use of two separate structures as shown on Figure 1. A two-span continuous structure, with spans

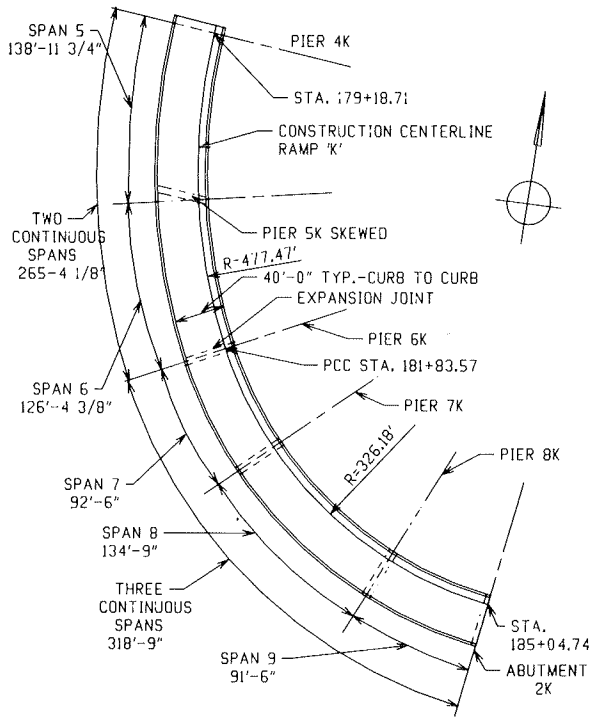

FIGURE 1 General layout of ramp K at Philadelphia International Airport.

of 138 ft 11-3/4 in. and 126 ft 4-3/8 in., was selected for the portion of the curve that has a radius of 477.41 ft. Three continuous spans of 92 ft 6 in., 134 ft 9 in., and 91 ft 6 in. were used for the remainder of the ramp that is located on a curve with a radius of 326.13 ft. One end of each of these structures has a common bearing on pier 6 as shown in Figure 1. All dimensions shown in Figure 1 and given previously are on the construction centerline.

Ramp K has a roadway width of 24 ft plus a 10-ft shoulder on the outside of the curve and a 6-ft shoulder on the inside. The overall width of the structure is 43 ft 6 in., and a slope of 0.05 ft/ft is maintained across the roadway. A vertical curve along the entire length of the bridge further complicates the geometry.

Five precast, post-tensioned, concrete box girders were selected as the main structural components for the two structures. Figures 2 and 3 are framing plans showing the geometry of the girders and the location of the exterior cast-in-place diaphragms. The girders were curved by fabricating them with incremental chords 20 ft in length. End chords of all girders deviated from the 20-ft length to accommodate the required center-to-center bearing length of the girders. Radially curved girders were not feasible because of fabrication difficulties.

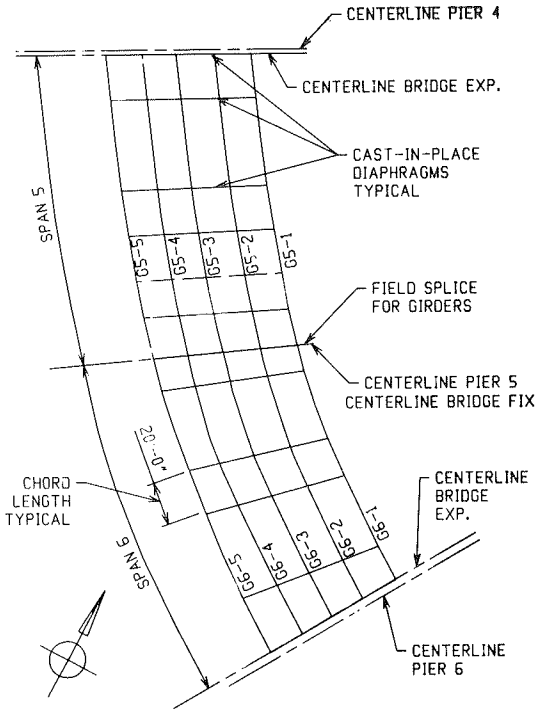

FIGURE 2 Framing plan for spans 5 and 6.

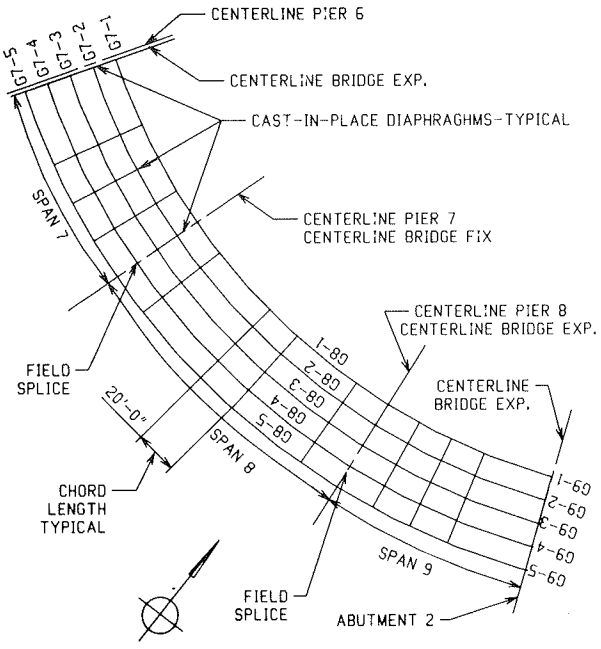

FIGURE 3 Framing plan for spans 7, 8, and 9.

The girders were fabricated and shipped in lengths corresponding to the five different spans. Continuity for the two- and three-span bridges was provided by splicing the girders at the piers with exterior cast-in-place diaphragms and applying post-tensioning for the full length of the spliced girders. For ease of fabrication all girders in spans 5 and 6 were fabricated with a common radius at the horizontal centerline of the 20-ft chords, and all girders in spans 7, 8, and 9 also have a common radius.

Dimensions and details of the girder cross section are shown in Figure 4. Voids were formed in the girders with Styrofoam, and internal diaphragms were provided at the junction of each 20-ft segment. Polyethylene ducts were provided for the multistrand post-tensioning tendons. Each girder received some post-tensioning at the fabricating plant to counteract the dead load stresses produced by the weight of the girders. Final post-tensioning of the continuous structure was done in the field after the diaphragms were constructed. The ducts for the tendons were in the voids of the box beam and the tendons were not bonded to the girder.

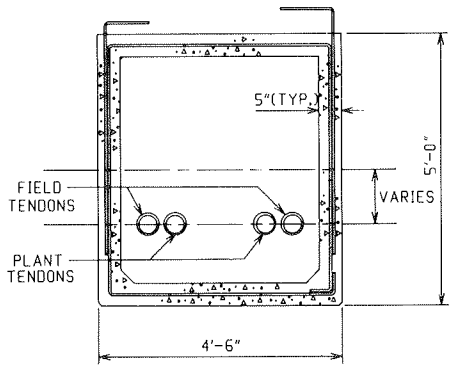

FIGURE 4 Typical girder details.

External cast-in-place diaphragms were heavily reinforced and tied into the girders. Post-tensioning was used to provide continuity in the direction transverse to the span of the girders. Essentially, the diaphragms were constructed so that the continuity between the girders and diaphragms resulted in a structural grid in the horizontal plane.

A composite deck was placed over the grids, and Pennsylvania Department of Transportation (PennDOT) standard parapets and safety curbs were constructed to complete the structure. The composite deck consisted of 2.5-in.-thick precast, prestressed concrete panels that span the box girders and a 5-in.-thick cast-in-place topping over the panels. Details of the deck are shown on the typical cross section in Figure 5. Mild steel reinforcement used in the cast-in-place portion of the slab was epoxy coated in accordance with PennDOT specifications.

ANALYSIS AND DESIGN

The location of the structure, the method selected for fabrication, the transportation of the girders, and the existence of roadways and utilities under the bridge created several design constraints. Some of these were

1. The five girders for each span were fabricated individually for the full span length between supports.
2. During construction the girders were erected and functioned as simple beams between supports to carry their own dead load plus the dead load of the exterior diaphragms. Plant post-tensioning was supplied to accommodate the dead load stresses in the simple beams. Obstructions at the site prevented the use of temporary shoring.
3. A constant radius of 477.41 ft was used for all girders on spans 5 and 6, the two-span continuous structure. Girders in spans 7, 8, and 9, the three-span continuous structure, were fabricated with a radius of 326.13 ft.
4. Pier 5K, the interior support for spans 5 and

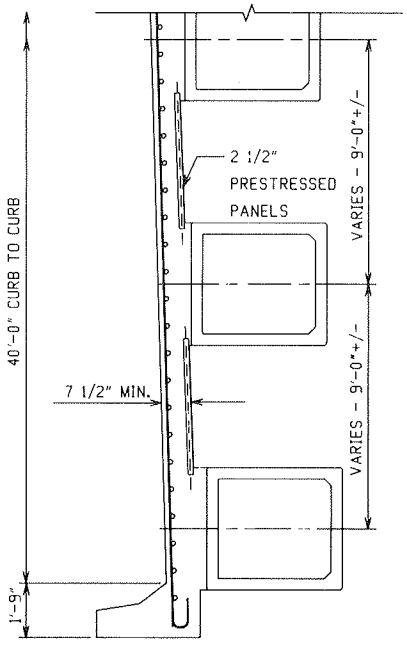

FIGURE 5 Typical cross section and deck details.

6, was skewed in relation to a radius of the curve. This resulted in all girders for these two spans having significantly different lengths. All other piers, and the abutment at the far end of span 9, were oriented so that their transverse centerline was on a radius.

5. Curvature of the girders caused a torque at each end when the simple spans were erected and before the diaphragms were placed. Struts were cast on the ends of the girders and jacks were used during erection to counteract this torque. The struts became part of the diaphragms at the supports after the cast-in-place concrete construction was completed.

6. The post-tensioned grids consisting of the continuous girders and the exterior diaphragms were designed so that the deck could be removed and replaced without overstressing any of the structural components. This condition required that the post-tensioning of the continuous girders be done before the deck concrete was placed.

The five individual girders for each span were analyzed in the conventional manner as simple beams. Stresses were computed for the dead load of the girders and dead load of the exterior diaphragms. Stresses due to the lifting and transporting operation were also evaluated. The magnitude of post-tensioning required to counteract these stresses was found and applied at the fabricating plant before the girders were moved from the casting bed.

Analysis of the two-span and three-span grids consisting of the girders and their connecting external diaphragms was accomplished using a stiffness matrix method of analysis. Each straight beam segment and diaphragm were considered to be a structural member of the grid, resulting in 114 members and 75 joints for the two-span structure and 133 members and 90 joints for the three-span structure. Coordinates for each joint were computed and became part of the input data for the analysis, along with assumed cross-sectional properties.

Moments, shears, torque, and displacements at each end of each member were found for the following loading conditions.

1. Dead load of beam haunches,
2. Dead load of 2.5-in.-thick prestressed panels over the entire length of the bridge, and
3. Dead load of cast-in-place deck concrete in the positive moment portion of the girder spans.

All of these data were found using a STRUDL grid analysis program. After the dead load actions were determined, the section properties in the girder were modified to account for the composite action of the deck slab. The grids were then analyzed for the following loading conditions.

1. Dead load of cast-in-place deck concrete in negative moment portion of the girder spans,
2. Dead load of parapets,
3. Dead load of future wearing surface, and
4. Live loads plus impact.

Preliminary analyses were conducted to determine the positions and types of live loadings that would produce the maximum actions in the various members of the grid. AASHTO HS20 loading was used in the live load analysis. Truck loads, lane loads, and overloads were investigated; and the maximum internal member actions at the joints were used in the final analysis for stresses.

Analysis of the continuous grids for stresses due to field post-tension, which had a variable eccentricity, was done by modeling the structures as three-dimensional rigid frames. Typical profiles of the field post-tensioning tendons are shown in Figure 6. Forces from the field post-tensioning were applied at the interior diaphragms and at each end of the grids. At each end of each member the applied forces consisted of an axial force (adjusted for friction loss), a vertical force, and a moment about the horizontal axis of the cross section. At the ends of each structure the applied actions consisted of the axial prestressing force and a moment, due to the eccentricity of the prestressing force, about the horizontal centroidal axis. Five separate analyses were done for each span with an assumed value of the prestressing force applied to individual girders for each of the five analyses. Results

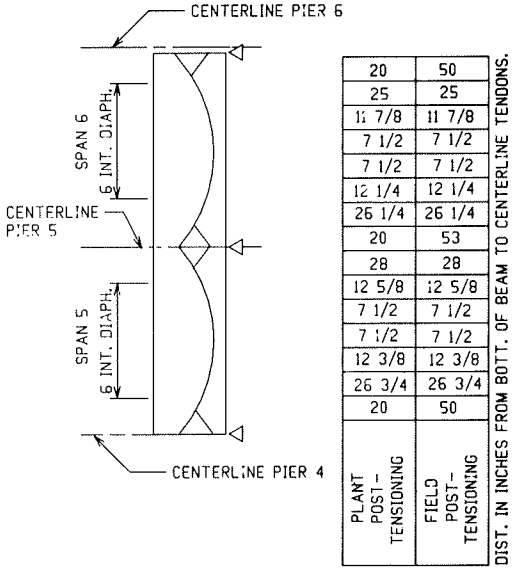

FIGURE 6 Strand profile for spans 5 and 6.

from the five analyses were combined using various percentages of prestressing force for individual girders and combining the prestress with stresses due to the various loading conditions until the required prestressing force in each girder was determined. Normal losses due to shrinkage and creep were also considered.

Special attention was given to the torsional moments in the girders that were caused by the gravity loads acting on the curved, continuous, grid systems and by the eccentricity and change in direction of the prestressing force. Additional mild steel reinforcement, in the form of stirrups and longitudinal reinforcement, was used where needed to accommodate the stresses caused by the torsional moments.

Conventional design procedures were used in selecting the reinforcement and prestressing tendons for the deck components. The prestressed deck panels were designed to support the full dead load of the deck and to act in a composite manner with the cast-in-place topping to carry the superimposed dead and live loads. AASHTO HS20 loading was used as the design live load for the deck. PennDOT specifications and design standards were used to select concrete components and reinforcement for the deck.

FABRICATION AND ERECTION

The twenty-five individual girders were fabricated by Schuylkill Products Inc., at their Cressona, Pennsylvania, plant. Steel forms were used on the two sides and bottom of the girders and Styrofoam was used to form the internal voids. Reinforcement was preassembled into cages and secured in the forms. Polyethylene post-tensioning ducts were used for the multistrand tendons. Because the tendons could not be bonded to the girder concrete except at the internal and cast-in-place diaphragms, care was taken to electrically insulate the tendons to reduce the possibility of corrosion. Fabrication methods used in producing the girders are shown in Figures 7 through 10.

Lifting hooks were provided at the internal diaphragms that were closest to the balance points of the girders. After the plant post-tensioning was applied the girders were moved from the casting bed and stockpiled. All girders were shipped by truck from the Cressona plant to the construction site at Philadelphia, a distance of approximately 94 miles. Large tractors with hydraulically steerable dollies were used to transport the girders, some of which weighed 115 tons, were 147 ft long, and had a maximum shipping width of 13 ft 6 in. and a shipping height of 12 ft. To equalize tire loads and eliminate static overturning moment, the girders were loaded so that their weight was transferred to the vehicle through their balance points. The size and magnitude of the loads dictated use of a vehicle with eight axles and thirty wheels.

The individual girders were set in position on the piers and temporary torque forces were applied at the girder ends to counteract the moment due to the curvature of the girders. After the girders had been set in place the external diaphragms were placed. Post-tensioning was then applied to the grid framework consisting of the continuous girders and the external diaphragms. The conduits housing the tendons were filled with grout to act as corrosion protection for the prestressing steel.

Construction of the deck followed the normal procedure for decks with partial depth prestressed panels. The 2.5-in.-thick 8-ft-wide panels were set to grade on grout haunches. The haunches were placed using timber forms bolted to the sides of the box girders and inserts cast into the concrete.

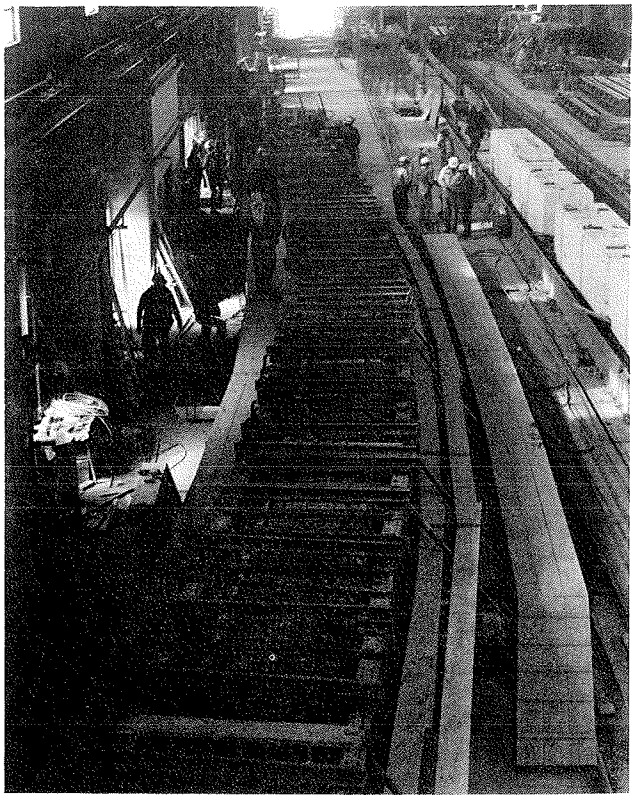

FIGURE 7 Steel forms with reinforcement and voids in place.

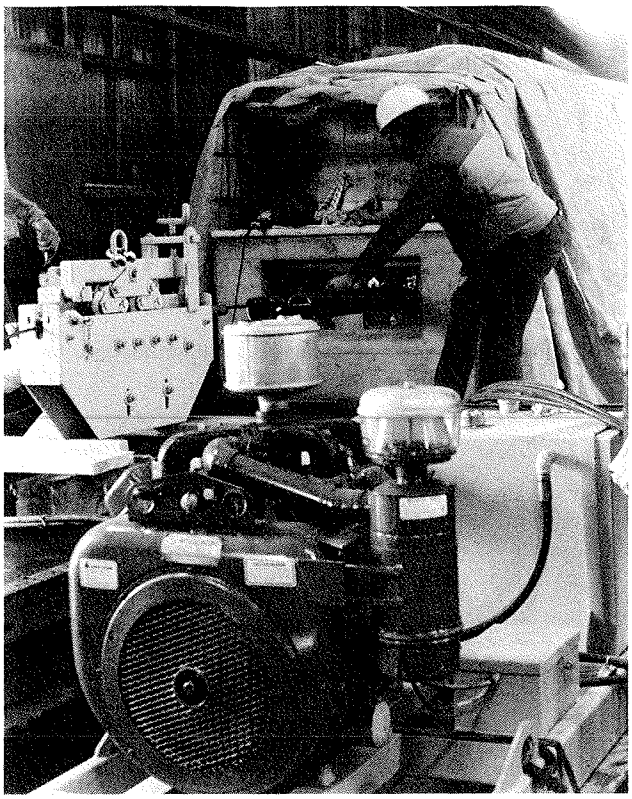

FIGURE 8 Placing tendons for post-tensioning in plant.

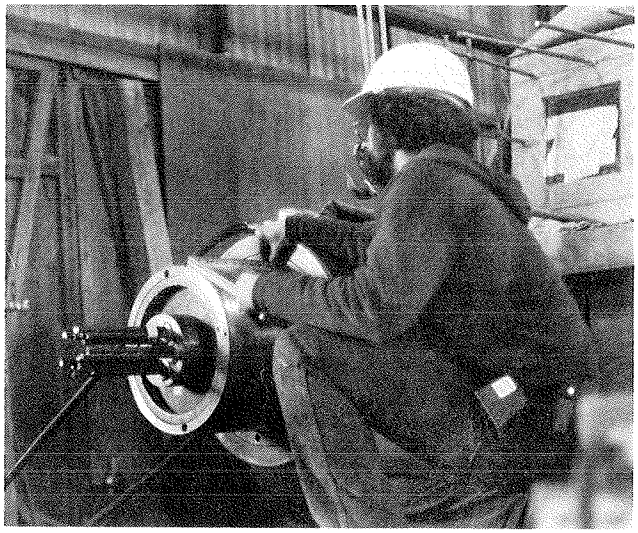

FIGURE 9 Post-tensioning in plant before shipping.

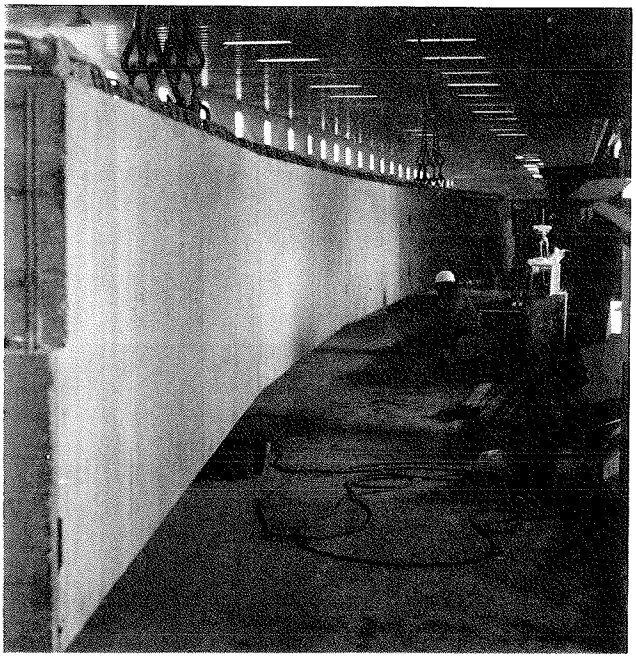

FIGURE 10 Completed girder being prepared for shipment to bridge site.

After the prestressed panels were placed, the top mat of reinforcing steel was set and the cast-in-place concrete topping was placed using conventional screeding and finishing equipment.

The cast-in-place concrete topping was placed in segments along the length of the continuous spans with the first placement being made in the positive moment portions of the continuous structures. This was followed by placement of the deck concrete over the piers in the negative moment portions. Additional longitudinal reinforcing steel was used in the deck slab in the negative moment areas to reduce cracking due to the tensile stresses in the slab and tops of the girders. Concrete and reinforcement for the parapets and safety curbs were placed in the conventional manner using standard forming techniques.

SUMMARY AND CONCLUSIONS

Continuous, curved, prestressed concrete bridges can be built economically using a combination of plant and field post-tensioning. Prefabrication of large girders is necessary to reduce field labor, construction time, and costs. Current technology and modern equipment allow plant fabrication and shipment of girders that are 160 ft long and weigh 90 tons.

Proper analysis and design of curved, continuous, prestressed concrete bridges is essential to achieve proper behavior of the completed structure. Close cooperation among the fabricator, erector, and designer is necessary to prevent overstressing any of the components during the fabrication and erection process. Ingenuity is required of all members of the design, fabrication, and erection teams to develop techniques that will reduce costs and assure good structural behavior of the bridge.

Conventional methods of matrix analysis can be used to find the dead and live load moments, shears, and torques in the prestressed grid. Care is required in evaluating the prestressing forces applied as loads to the structural framework. It was observed that the internal moments and torques were sensitive to slight discrepancies in the applied loads. The complicated geometry of the framework amplifies slight imbalances in the loads and results in computed torques and moments, of small magnitude, that do not agree with recognized theory.

Publication of this paper sponsored by Committee on Construction of Bridges and Structures.

Construction of Post-Tensioned Bridges in Germany

GUNTHER PLUEMER

ABSTRACT

A system for producing crack-free prestressed concrete by avoiding the temperature differentials due to escaping heat of hydration and sunshine is discussed. A description of girder production is followed by a report on slab production. The requirement of the strictest possible homogeneity of girders and slab is covered, and the structural, organizational, and economic advantages of the system are enumerated. If applied according to specifications, this system produces crackless prestressed concrete of such density and appearance that almost no maintenance is required. The system also yields considerable savings in material, labor, and overhead.

Concrete, an artificial conglomerate, has been in existence for more than 4,000 years. Until about two centuries ago the high compressive strength of its main ingredient, the aggregate, could not be taken advantage of because of the low compressive strength of its other ingredient, the binding agent.

The development of modern cement was a great improvement. It increased the compressive strength of the binding agent to approximately half that of the average aggregate, which meets most requirements. Unfortunately, concrete cannot withstand tension and therefore cannot endure bending. Wherever particular tensile stresses occur they result in cracks.

A century and a half ago Sir Marc I. Brunel thought of taking up the tensile share of a concrete section by iron rods and thus became the first person to apply the idea of reinforced concrete. It is now known that reinforced concrete does not fulfill its original purpose: reinforcement does not prevent cracking of concrete.

A further attempt to eliminate cracks was made about 50 years later by P.H. Jackson of San Francisco. Because the tensile strength of rebars is scarcely used unless the concrete has cracked, Jackson tried to prestress them, but the attempt failed because the prestress was reduced to almost nothing by shrinking and creeping of the concrete. Jackson's idea was finally realized by E. Freyssinet who introduced the first useful stressing system and built the first prestressed concrete bridge in 1939 near Oelde in Westphalia. This was made possible by the development of high-grade steel.

Modern reinforcing steel has such high tensile strength that not one-tenth of its allowable tension is used if the concrete is not cracked--and cracked concrete is precisely what reinforcement was intended to prevent.

After World War II, when many bridges in Germany had been destroyed and the price of steel rose enormously, prestressed concrete experienced a veritable boom. At the same time statically indeterminate systems became popular. Impressed with the possibilities of the latter, (e.g., continuous steel girders, or rigid frames, or boxes) most engineers tried to combine the two by developing methods for building continuous prestressed concrete structures.

Unfortunately, none of the methods yielded crack-free concrete. Because nobody knew what caused cracks they were considered inevitable. One might as well accept cracks and enjoy the fringe benefits of prestressing, such as larger spans or more slender beams. The idea of crack-free prestressed concrete was gradually forgotten.

A similar fate befell an article by Philipp Schreck (1) wherein he exposed the causes of cracks: the temperature differentials due to escaping heat of hydration and to sunshine. In a later supplement he proved that crackless continuous prestressed concrete structures cannot be built economically. This article too went unheeded by the profession.

Schreck was undaunted and finally realized Jackson's idea. Schreck developed a construction system that, by avoiding the detrimental effects of temperature differentials, produces crack-free prestressed concrete in the field and eliminates most problems associated with concrete bridges. Although cracks in reinforced concrete tend to be somewhat evenly distributed, rather numerous, and therefore narrow, theory tells us that with prestressed concrete just the opposite is true. Cracks occur in prestressed concrete in small numbers, are comparatively wide, and appear close to the supports. Such cracks are an effect of the two temperature differentials mentioned previously.

The notion of evenly distributed cracks in a continuous prestressed concrete structure is a pipe dream. Four conditions would have to be fulfilled:

1. The tension at the underside of the member would have to be constant;
2. The critical tension that induces cracking of the concrete would have to be constant;
3. The shear between grout and tendon and between rebars and concrete would have to be constant; and
4. The sectional area of reinforcement and of prestressing steel would have to be constant.

Note that none of these conditions is fulfilled in current practice.

Another point must be considered: A steel bridge announces its failure far in advance by visible alterations that allow its remaining service life to be determined fairly correctly. In contrast, prediction of the time of rupture of a tendon in a prestressed concrete bridge is virtually impossible. This implies that, if such a bridge has cracks, there is a constant danger of imminent collapse.

During the development of his system Schreck found, by theoretical deduction as well as by trial and error, that to avoid cracks each member of a prestressed concrete structure must be designed and treated as homogeneously as possible in all respects. This most important and peremptory condition explains the simplicity of the system (G. Pluemer, The Viaduct System, presented at annual meeting of TRB Committee on Construction of Bridges and Structures, Washington, D.C., January 20, 1982).

GIRDER PRODUCTION

The temperature differentials due to escaping heat of hydration and to sunshine affect structurally indeterminate systems of considerable height, such as box girders and continuous structures. This led

to using only simple T-beams. Although the construction height of the girders may amount to 1/16, 1/15, or even 1/14 of the span, the thickness of the slab may vary only from 24 to 28 cm, with negligible temperature difference between top and bottom. And although the girders span lengthwise from pier to pier, the slab spans crosswise from girder to girder. This distinction between the two components of a T-beam is clearly reflected in the separate production of girders and slab.

The use of a structurally determinate system all but eliminates the effect of the temperature differential due to sunshine. This leaves the problem of the escaping heat of hydration. Common sense as well as experience indicate that forced changes in the temperature of a concrete member, such as cooling its outside with cold water or heating it with steam, do not prevent a detrimentally large temperature difference between the outside and the core.

The safest and most practicable way to avoid temperature differentials is to heat the outside of the concrete member with warm air that, thanks to the development of unit heaters that use all kinds of fuel, is very economical and easy to do. A hollow steel form is required to serve as a warm air duct, and thermostats must be imbedded in the concrete section to monitor the unit heaters. The walls pointing away from the future girder must be insulated; this is most readily achieved by spraying their inside with plastic foam.

No falsework is needed because the double-walled form is self-supporting. To give it even more strength and the necessary camber, the form is prestressable. Inside the wall facing the future girder are extra-heavy-duty vibrators that can be activated individually for external compaction. The bottom plate, rigidly connecting the two side parts, is also double walled and foam insulated. The top of either side part is secured by removable railings. The gap between the two can be closed by insulated flaps and the ends can be closed by special plates designed to support the anchorage bearings.

The whole apparatus thus serves as

1. A form for the girders,
2. Its own falsework,
3. A compacting tool,
4. A heating device,
5. A curing container,
6. Shuttering gear,
7. An adjusting utensil,
8. A working space, and
9. A footbridge.

The girders have a cross section like an inverted T. They consist of a web and a bottom flange. The latter stands out 45 cm on either side of the web. The flange slopes outward with a pitch of 8 degrees and has an average thickness of 25 cm. The web has a thickness of 30 or 35 cm, making the flange 1.20 or 1.25 m wide. The height of the web depends, of course, on the span length. The top of the web ends, temporarily, at about the level of the underside of the future deck. For subsequent connection of the web and deck two parallel rows of stirrups shaped like inverted U's stick out of the web. With the exception of a slight widening at both ends, to accommodate the anchor plates, the cross section of the girder is constant throughout its entire length.

The girders are cast in place onto the bearings. These are of three kinds: (a) laminated steel-elastomer deformable in all directions, (b) laminated steel-elastomer that slide lengthwise, and (c) laminated steel-elastomer that are adjustable lengthwise. The adjustment of (c) is done by turning bolts and can be done under full load. To facilitate removal of the form its bottom part is slotted at the bearings, and the slot is closed with adjustable plates on high-speed bolts.

Two transportation trusses, 1.5 spans long, move the equipment forward into the next field where it serves as a gangway from pier to pier and as a working platform for the assembly of the reinforcing cage. Because the latter is too wobbly to be picked up at the ends, it is hooked onto the reinforcement carrier, a prestressed lightweight truss. A pair of hoisting frames affords vertical and lateral movement of the equipment, which is completed by an air compressor and a group of unit heaters with flexible ducts.

First the bearings are set on their concrete pads and the bottom part of the form is installed around them. Then one side part is connected to the bottom and the form is oiled very lightly. In the meantime the reinforcing cage including conduits has been assembled at the working platform on top of the transportation trusses; it is now lifted into place by the reinforcement carrier. Then the other side part of the form is moved over and connected to the bottom. After setting of the end plates and connection of the anchors thereto, the form is linked up with heater and compressor and is ready to be prestressed.

The concrete should at least be B 35 with a 28-day compressive strength of 5,000 psi. Usually B 45 with 6,500 psi is used, but an intermediate value of B 42 with 6,000 psi will suffice in most cases. The aggregate should be of constant mix, quality, and low cement demand. The water-to-cement ratio should be around 0.38; additives should be avoided.

The concrete is pumped into the form in the afternoon. The depositing starts at the far, or front, end and proceeds without interruption to the near end of the girder, so that there is no working joint whatsoever. Vibrators are individually activated as required to compact the concrete without segregation.

After the top has been covered by the flaps the new girder is completely enclosed and insulated so that curing is not influenced by the weather. When the concrete temperature rises, due to hydration of the cement, the unit heaters are automatically switched on and warm air is circulated through the hollow form parts so that the temperature of the core and the outer layers rises simultaneously. In this way a temperature differential due to escaping heat of hydration is avoided because the heat cannot escape. In fact, there is a heat gain that accelerates the hydration and thus the curing. This in turn speeds up the hardening of the concrete so that it reaches a rather high strength much earlier than under normal circumstances. Note that the major purpose of the warm air is to cause an even increase in temperature over the whole cross section. Faster curing is merely an additional bonus.

Shortly before midnight, when the girder has reached its peak temperature, the unit heaters are turned off automatically. After that the temperature starts to fall very slowly. Although it took about 6 hours for the temperature to rise to maximum, it takes at least 6 days or longer for it to come down to ambient level. However, 14 hours after pouring, the concrete has attained 55 to 65 percent of its 28-day strength. Not only can the form be removed, the girder can be partially prestressed; and it is now strong enough to be exposed to the air without damage.

This is the most important moment in the life of the girder. Remember that the form itself was prestressed, giving it a camber to make up for the added weight of the girder, the slab, and part of the traffic load. Now, before removal, the form is

slowly relieved of that stress while the girder is just as slowly and simultaneously partly prestressed. This avoids all vertical and lateral movement that would be detrimental to the young concrete. The new girder has been minutely shortened and the form has been considerably extended. Thus they come apart by themselves without application of external force. This explains why the system can afford wide bottom flanges with a slight slope.

One side and the bottom part of the form are now shoved into position for the next girder, and the other side part is lifted up and over the finished girder and placed next to the first side and bottom part. The inside is swept clean and oiled lightly, the new reinforcing cage is dropped in, the form is closed and prestressed, and so forth. By afternoon the next girder can be cast. One girder is produced per day.

When all girders of a span are finished, the transportation trusses are shoved over the front pier into the next field. They are then lined up with two adjacent new girders to form a two-span rail on which all the other equipment is rolled forward by casters and trucks. For this purpose the crossrails of the hoisting frames are lowered to lower their center of gravity.

The whole move takes about 1 working day, but to stay on the safe side 2 days are usually allocated. The handling of all the equipment for girder production normally requires four trained men and one helper.

SLAB PRODUCTION

About a week later, as soon as the girders are fully prestressed and the equipment for their production has cleared the span, the driveway slab is built in daily increments. Within any span the number of these segments equals the number of girders plus two, so that the speed of deck production coincides with that of girder production. On a bridge 15 m wide, for example, 3 girders and therefore 3 days are required; 2 days are scheduled for the move into the next field. This makes 5 days per span, so there will be 5 daily segments.

The major part of the equipment for slab production is the movable platform. Its front part is a little longer than a daily segment and made of rough boards. It serves as a stage for the reinforcing of the deck. Its hind part is exactly one segment long and lined with either sheet metal or Duraply. It serves as a form for the slab. The whole movable platform is divided lengthwise into strips. Those in the center are located between the girders; the outer two for the overhanging parts of the slab are supported by suspension trusses, which are lightweight steel space frames. The front ends of the trusses hang from the crossboom, a king post steel truss running on the webs of the girders between the stirrups; and their rear ends hang from cantilever carts that roll on the finished slab. The platform is built on wooden joists and blocking and is supported by steel form carts that run on casters on the bottom flanges of the girders and are adjustable in height by jacks.

When the slab section of the previous day has attained the necessary strength and when the reinforcement for the new segment has been prepared and temporarily suspended, the whole movable platform is lowered and rolled forward two increments so that it is in front of the reinforcement and fully accessible. The front part, the working stage, is swept while the rear part, the form, is cleaned and oiled. Then the platform is rolled back one increment, so that the form is now underneath the reinforcement, and raised into position. Thereafter the temporary suspension of the reinforcement is removed, the new working joint is set with a slotted board, and the form is adjusted to the girders. The next segment can now be cast.

Pumping of the concrete takes place in the early afternoon. The segment is divided into several subsections the size of the vacuum equipment. First the concrete is distributed by spade and shuffle; therefore it has a water-to-cement ratio of 0.42. Then it is compacted by bottle vibrators until it is of normal density, rather even, and about 0.25 inch too thick. Now a motor screed is passed slowly over the concrete. The screed runs on adjustable steel straightedges and gives the slab the specified slope and an evenness unobtainable manually. It condenses the concrete a second time to 0.125 inch above design thickness.

The third compaction is achieved by the vacuum technique. The concrete is covered with a two-ply mat, the bottom layer of which is perforated so finely that air or water can seep through it but cement cannot. The top layer is airtight, and its rim is carefully pressed down. A transparent hose connects the vacuum mat to a suction pump with a water meter. Within 20 to 25 minutes between 10 and 15 percent of the water is extracted from the concrete that thus loses around 1.5 percent in volume and attains the specified thickness.

While the first subsection is vacuum treated, the second section is poured, distributed, vibrated, and screeded. In this manner one subsection after the other is cast. Subsequently each subsection is finished with a skim floater, a rotating power trowel, to get a specially dense and smooth surface. Finally the new segment is covered with burlap and a tarpaulin to protect it from the weather and to prevent cooling of the surface. The whole procedure takes about 2 hours. Around noon the next day the concrete has attained the necessary strength and the process begins again. Another 24 hours later the segment can be post-tensioned and driven over by heavy equipment. The handling of the complete outfit for slab production normally requires five trained men and one helper.

HOMOGENEITY

This system offers a number of advantages in design, calculation, estimation, implementation, organization, logistics, handling of equipment, and comprehensibility for all persons involved because of its amazing simplicity and--in the broadest sense of the word--its homogeneity. Homogeneity of material is important. The concrete of the girders is treated differently than that of the slab. The former has a water-to-cement (w/c) ratio of 0.38 and is compacted once externally, and the latter has a w/c ratio of 0.42 and is compacted three times: first internally by hand vibrators, then externally by motor screed, and finally by water extraction. But the result is the same: the loss of 10 percent of the water gets the w/c ratio down from 0.42 to 0.38, and the density of both girder and slab is about 3 percent greater than that of concrete that was merely hand vibrated.

Research on vacuum dewatering has been done at the U.S. Bureau of Reclamation; the Chalmers Institute of Technology at Göteborg, Sweden; and at the Technical University of Hannover, Germany. The findings were impressive.

1. In a customary concrete slab the w/c ratio increases from bottom to top and the strength decreases; therefore the surface is less dense than the underside. In a vacuum treated slab the w/c ratio decreases from bottom to top and the strength

increases; therefore the surface is denser than the underside. Skim floating can only be done with vacuum treated concrete; customary green concrete is much too soft before setting, and after setting it is too hard.

2. Permeability is cut 60 percent with each percent of increase in density. If a concrete is made 3 percent denser, its permeability is cut to 0.4 x 0.4 0.4 = 0.064 or 6.4 percent. The additional skim floating reduces it further to about 5 percent. This was corroborated by numerous tests in which customary concrete showed a water penetration of 20 mm but vacuum treated concrete was permeated less than 1 mm.

3. The vacuum does not remove air from the concrete, but it expands the individual bubbles due to loss of pressure. When the voids are enlarged the air therein gets thinner. Frost resistance of the concrete thereby is increased considerably without raising the air demand.

4. As a result of the triple treatment (screeding, dewatering, and skim floating) the surface not only gets stronger, denser, and less permeable but also more wear resistant. This is a rather important feature to the traffic engineer if it causes a deck to last three, four, or even five times longer.

5. Carbonization of the cement by reaction with the carbon monoxide of the surrounding air is retarded by the cube of the lowering of the w/c ratio. If the latter is cut in half, the edifice lasts 8 times longer; if it is reduced by two-thirds, the duration increases 27-fold. Obviously, even a slight reduction is significant.

6. The strength attained by customary concrete after 28 days is reached after 1 week by dewatered concrete, and after 28 days is surpassed from 20 to 30 percent.

More tests have been made with similar results: shrinking and creeping are reduced considerably, there is no edge rising of slabs, the method is applicable to vertical or curved surfaces, and so forth.

The resistance of dewatered concrete to extreme changes in ambient temperature and tremendous pressure is demonstrated by the fact that it was used to line the fire chamber and exhaust tunnels of the space shuttle launching pad at Vandenberg, Calif., where the temperature reaches 6,000° F.

Just as important as homogeneity in material is constancy in all other respects. It has already been mentioned that, with the exception of a slight widening at the ends of the webs to accommodate the anchor plates, there is no enlargement or reduction of the girders; there are no cutouts; there are no crossbeams; there are no diaphragms.

Constancy in statics means a structurally determinate system; an elastic cross section, not a rigid one; and no constraints. That is why this system uses simple beams, a T-beam section, and direct, three-dimensionally elastic bearings.

Constancy in function means clear differentiation of the carrying direction of the members. The girders are prestressed longitudinally, but the slab is prestressed transversely. Continuous structures, both T-beam and box girder, under average loading conditions have positive moments in the field and negative ones over the supports. Ideally, the superstructure should be upside down. But because such a structurally correct solution is rather impractical, it is replaced by heavy reinforcing over the supports. The concrete is thicker and proportionately more mild steel is used. This system is utterly heterogeneous.

Homogeneity in treatment during construction means steady and even pouring, condensing, heating, and cooling of the concrete until it has attained the strength necessary to withstand any deviation. It means no movement, neither vertical nor lateral, during removal of forms. Transfer of carrying function from form to girder should be compensated by temporary shoring or by partial prestressing. Homogeneity means no transport of the member because that requires measures (such as a makeshift upper flange or special reinforcement) that later on, under service conditions, have no function whatsoever. The transport itself is expensive and constitutes a stress to which young concrete should not be subjected. Homogeneity also means gradual loading, with a safe time lag between increasing strength and corresponding stress. All these requirements are met by the system discussed herein.

Homogeneity in behavior under service load means constancy of structural conditions. This requirement automatically excludes use of the continuous beam because of the reversal of moments and consequent wrong position of tendons as well as because of considerations of inversion and continuity.

STRUCTURAL ADVANTAGES

Forty-eight hours after production the slab is fully integrated into the T-beam section. Creeping of the girder causes the daily working joints to be pressed together. There is also a transfer of stresses from the web to the deck that takes over its share of the compressive zone. The effective width of this upper flange is 12 times its thickness plus the width of the web, namely 3.60 m or three times as wide as the lower flange. Because the latter is situated within the precompressed tensile zone its area is adequate to withstand that precompression. It is built rather shallow and 1.20 m wide for three reasons: First it raises the moment of inertia (I) of the concrete section. Second it allows the lower two tendons to spread apart 1.00 m center to center so that the next pair may come down all the way; this increases the value of both I_x and I_y. Third it affords a track for the form carts and other equipment.

Another way to considerably raise the I_x is an increase in construction height because height enters the formula by the third power. For aesthetic reasons the height should not surpass 1/12 of the span and not fall short of 1/18. The mean value of 1/15 of the span length turned out to be the most effective and economic. The result is a wide flange section, with a high moment of inertia, made of a material with a high modulus of elasticity.

Naturally such a beam has a rather low deflection and consequently an equally small end rotation, less than half that of a standard precast girder. This in turn sharply reduces the negative moments within the slab that is continuous over the piers. The gap between the girders is 50 cm or 1 ft 8 in. The bond between girder and slab is broken on either side for another 50 cm. Thus the slab is given 1.50 m or 5 ft 0 in. for slight negative bending. Within this stretch it is reinforced a little more with mild steel in both directions, and the transverse prestressing tendons are closer than along the major part of the span where they usually are installed at 1.00 m center to center. A thickening of the slab is unnecessary, so it too is constant throughout the length of the bridge. The only heterogeneities are the expansion joints that occur at intervals of approximately 300 meters or 1,000 feet.

The goal of the system is to construct crackless concrete. One more way to avoid cracks is full prestressing. This means that each member is under constant compression in its particular carrying direction and that tensile stresses in other direc-

tions within the concrete, if they occur at all, are limited in origin, time, location, and intensity, never surpassing the allowable tensile strength of the concrete diminished by a substantial safety factor.

In prestressed crack-free concrete the slack reinforcement contributes less than 5 percent to the tensile strength of the member, and prestressing steel is more than five times more effective than slack reinforcement. It therefore makes neither structural nor economic sense to replace part of the prestressing steel by slack reinforcement or to partially stress reinforced concrete. There is no continuous transition from reinforced concrete, via restricted prestressing, to fully prestressed concrete. One cannot mix cracked concrete with crackless concrete.

Furthermore, the system uses full bond. Prestressing steel without bond "does not participate in transfer of stresses, nor contribute to the limitation of the width of cracks" (2), and it contributes not at all to their avoidance. The system also uses subsequent bond, or post-tensioning, because immediate bond, or pretensioning, is suited only for the precasting of parts that are limited in size and purpose.

The continuity of concreting ensures homogeneous material. Each girder is cast in a single operation, and the slab is built in successive portions small enough to be easily and quickly handled by the crew. While the girders are still relatively warm the deck is built at a considerably lower temperature level that, by transfer of heat from slab to web, averts the danger of cracks due to temperature differential.

ORGANIZATIONAL ADVANTAGES

This system is extremely industrialized, which means it achieves the largest output possible by employing the fewest personnel and least equipment possible and keeping them both constantly busy. The production cycle is as short as the material allows, and its course is fully adapted to the final product. Any and all operations that are not absolutely necessary are avoided, thus considerably reducing their number. Finally the system is as simple and as clearly arranged as possible. Five men handle the equipment for girder production, six men that for building the deck; including the supervisor this makes one dozen people.

Once the equipment is mounted it is easy to handle; it is self-propelling, so to speak. No heavy hoisting gear is required. For a 140-ft span the equipment weighs less than 100 metric tons or 220 kips. The heaviest part, one side of the form, weighs approximately 26 tons or 57 kips compared with the 113 tons or 250 kips of a girder.

Because of the special treatment of the concrete, the production cycle can be set at 24 hours for the girders as well as for the slab. Day after day both crews perform the same work. Every day the same equipment is handled at the same hour. Day after day the same type and amount of material are needed at the same time.

Because the slab can be driven over with heavy equipment 2 days after pouring, all supplies can be brought in over the bridge itself. The system is fully independent of the ground underneath, which needs never again be touched once the substructure is finished.

Reinforcing is easy: there are only four sizes of rebars, and more than half of them are straight and uncut. Most bent bars are used over and over with regular spacing. The number of conduits is relatively small and their positioning not at all problematic because there is no inversion; this also alleviates installation of the tendons. There are no coupler joints.

Because the system is repetitious, rational, and easily understood, break-in of the crew is fast and uncomplicated. The same holds true for all other people involved. The remarkable simplicity of the system results in considerable facilitation of the engineer's task: design, calculation, and supervision are much easier. Estimating, bidding, scheduling, organizing, implementing, settling of accounts, and dealing with subcontractors are easy for the contractor. And, of course, the job is just as easily manageable for the owner.

ECONOMIC ADVANTAGES

That a simple construction method like the one described herein yields savings in material, labor, overhead, and maintenance is not at all astonishing. The magnitude of these savings can be illustrated by a comparison of two different designs for the superstructure of a typical bridge, that across the 150-ft deep Waldnaab Valley near the town of Weiden, Germany. It has 8 spans 140 ft 3 in. long, a construction height of 9 ft 0 in., and a width of 46 ft 0 in., with 3 girders per span at 15 ft 4 in. on centers. This bridge was designed and costed out as a continuous box and as simple T-beam according to the system described here (Table 1). The latter was executed.

TABLE 1 Comparison of Continuous Box and Simple T-Beam

	Continuous Box	Simple T-Beam	T-Beam as Percent of Continuous Box
Concrete B 45 (yd^3/ft^2)	0.085	0.058	68.5
Reinforcing steel (lb/ft^2)	12.3	5.7	46.7
Post-tensioned steel (lb/ft^2)			
Longitudinal	3.3	2.9	87.5
Transverse	1.54	0.96	62.7
Working time (hr/ft^2)	0.186	0.093	50.0
Maximum compression (psi)			
During construction	3,570	800	22.4
In-service	2,175	1,203	55.3
Maximum diagonal tension (psi)	145	52	36.0

The continuous box must endure two-thirds more compression during construction than under service conditions, but the simple T-beam must endure one-third less. Under service conditions the maximum compression in the simple T-beam is only half that in the continuous box, the diagonal tension merely one-third. Because the concrete of girders and slab is of such density and appearance that it requires neither finishing nor upkeep, maintenance is practically nil.

If applied correctly and executed in the right manner, this system guarantees a superstructure without cracks, thereby avoiding most of the problems encountered with prestressed concrete today. This system also costs less both initially and in the long run.

CONCLUSION

Cracks are by no means inevitable, but they are fatally dangerous to prestressed concrete bridges. There is no way to predict the time of failure of such structures. Narrow cracks are barely less perilous than wider ones because their width increases in time. There is no way to distribute them evenly over a continuous prestressed concrete girder.

Because cracks are dangerous they must be avoided. Prestressed concrete, by virtue of its definition and of the idea which led to its invention, has no cracks. To avoid cracks need not necessarily be expensive.

The system described in this paper produces crack-free concrete economically. The success of the system is demonstrated by the bridges that have been built using it.

REFERENCES

1. P. Schreck. Risse im Spannbeton und deren Ursachen (Cracks in Prestressed Concrete and Their Causes). Die Bautechnik, Vol. 40, No. 8, 1963, pp. 130-138.
2. H. Wittfoht. Betrachtungen zur Theorie und Anwendung der Vorspannung im Brueckenbau (Contemplations on the Theory and Application of Prestress in Bridge Construction). Beton- und Stahlbetonbau, Vol. 76, No. 4, 1981, pp. 78-86.

Publication of this paper sponsored by Committee on Construction of Bridges and Structures.

Rehabilitation of Steel Truss Bridges Using a Superimposed Arch System

ROBERT J. BRUNGRABER and JAI B. KIM

ABSTRACT

A system for reinforcing steel truss bridges has been developed. The system consists of superimposed arches with hangers supporting the existing floor beams, which may be reinforced or replaced with new ones, as well as additional intermediate floor beams. To date this system has been applied to three bridges ranging in span from 74 to 136 ft. The first application was to a 100-year-old, 74-ft Pratt truss bridge at Coudersport, Pennsylvania. For a total cost of $62,000, including painting of the bridge, the borough of Coudersport was able to increase the posted weight limit of the bridge from 3 to 20 tons. Given reasonable routine maintenance, the bridge could provide service for another 100 years. During the installation of the reinforcing system, which took 3 weeks, traffic flow was maintained.

In the U.S. highway network there are still many steel and wrought-iron truss bridges of the prefabricated, pin-connected type built during a 50-to-60-year period around the turn of the century. These bridges were designed for loads considerably lighter than the AASHTO H-20 or HS-20 loadings, to say nothing of the trucks that are permitted and contemplated on our Interstate system. Over the years little has been done to improve the carrying capacity of these bridges; in fact, accidents and limited maintenance have usually led to serious deterioration.

There is ample evidence that many steel truss bridges on secondary highways and local roads are in need of replacement or major structural repair. These truss bridges typically have pin connections, and rust as well as corrosion and fatigue damage to the pins and the eyes of the truss members cannot be detected. It is clear that all of these bridges cannot be replaced and that the problem is worsening. When resources are limited, all bridges, particularly aged ones, should be looked after. Thus a cost-effective program of reinforcement and rehabilitation of these aging truss bridges is needed.

The present procedure for determining the maximum safe live load capacity of existing bridges is supposed to consider the effect of deteriorated portions of the bridge such as (a) rusted and dislocated end supports, (b) deformed and corroded members, (c) stretched or otherwise loosened I-bars that can no longer be counted on to carry their planned share of the load, and (d) inconsistent and uncertain quality of the material of the members.

The most critical regions, where most structures fail, are the joints. These portions are virtually impossible to inspect to determine the extent of deterioration. The only way to inspect such portions accurately is to completely disassemble the bridge joints, which would typically require the disassembly of the entire bridge. In the absence of such detailed inspection and evaluation of the joints, the presently posted weight limits for steel truss bridges are questionable, yet they severely limit the utility of many of our rural roads.

Many of the old, locally owned bridges are narrow. However, there is little evidence that serious accidents occur on these bridges, primarily because of the openness of the truss structure that permits easy visibility of oncoming traffic and the low volume of traffic on most of these bridges. Therefore it would be a low-priority use of public funds to provide wider bridges at many of these locations. Many of the roads leading to these bridges are only slightly wider than the bridges themselves; providing a modern-width, two-lane bridge would make little practical sense.

PROPOSED SOLUTION

Because it is virtually impossible to accurately predict the carrying capacity of even an individual member, not to say an entire bridge, it makes little practical sense to attempt the repair of any but the most obviously deficient members of a bridge. The resulting increased weight limit would still be highly uncertain and inadequate. What is needed is the superposition of a new structural system that will completely bypass all existing members and joints except those that can be expected to reliably carry modern loadings. The proposed reinforcement scheme to increase the load carrying capacity and to extend the life of a truss bridge consists of

1. Superimposed arches anchored to the existing abutments, or piers, or both. If necessary the piers and abutments are reinforced to resist the thrust of the arches.
2. Additional floor beams and hangers midway between existing floor beams.
3. Replacement or reinforcement of existing floor beams if they are deteriorated or overloaded.
4. Connection of the existing vertical members, which now act as hangers, to the arches and to the existing floor beams or replaced floor beams.
5. Additional stringers if needed.

Because the existing truss system, with braced portals and lateral bracing in the planes of the top and bottom chords, will provide lateral restraint for the superimposed arches, the arches can be of light rolled sections and thus quite economical. Doubling the number of floor beams, by adding a new floor beam between each pair of existing floor beams, cuts the effective stringer span in half so that live load moments are reduced by a factor of two and dead load moments are reduced by a factor of four. Because the new and replacement floor beams are installed from below, it is often possible to use the existing deck and stringer system without modification. Because the superimposed arches will pick up all floor beam loads, all existing members except the stringers and floor beams will be largely relieved of live load stresses. The arches can be designed to be strong enough to carry both dead load and live load forces. The hanger connections for the new intermediate beams as well as for the existing or replacement beams completely bypass all of the lower chord pin connections. Thus this reinforcement scheme would provide structural integrity even if existing bottom joint connections were to fail. Typically, such joints consist of several I-bars connected by a pin, and these bottom joints are usually in the most serious condition because of their proximity to the bridge roadway.

In a test of a 1-to-7 scale model of a typical bridge of this type, a simulated truck load of 40 tons was supported by the arch system even after both lower chords had been severed by the removal of a pin near midspan. The removal of the pin caused increased deformations in the loaded model, but the model did not collapse.

Some advantages of the system are that

1. Costs are reduced compared with replacement costs.
2. The reinforcing system can be designed to increase the load carrying capacity to any desired level so that, from the standpoint of structural safety, the bridge will be new.
3. By reducing the span of the stringers, the stresses in the floor system are reduced enough that, in many cases, the floor and stringers need not be involved in the rehabilitation.
4. In contrast with replacement bridges, the rehabilitated bridge involves no additional encroachment on the waterway or changing of the approaches to accommodate a higher roadway elevation.
5. The short construction period--the erection of a typical span will take 2 to 3 weeks--means that traffic can be maintained with little or no interruption.
6. The critical pin connections in the bottom chords are completely bypassed so that they are much less likely to fail, by fatigue or other causes, and failure of such a connection will not affect the overall integrity of the bridge.

APPLICATION

The system can best be described by referring to its first application, a 74-ft-long Pratt truss crossing the upper reaches of the Allegheny River on Seventh Street of Coudersport, Pennsylvania. This bridge was one of two connecting a group of about twenty-five homes to the rest of the borough. One bridge had been closed because of extensive corrosion of the stringers and floor beams, and the other, the bridge in question, had had its load limit reduced to 3 tons. Thus this part of the borough was effectively without the services of fire trucks, school buses, trash collection trucks, and large delivery trucks such as those carrying heating oil. A new bridge, built to current standards of width, was estimated to cost in excess of $180,000 and would have required the complete isolation of this part of the community for at least several months while the old bridge was removed and the replacement installed. Also, to maintain the necessary waterway opening with current standard bridge designs of steel or concrete girders would have required increasing the elevation of the approach roadways by at least 2 or 3 feet. This would have caused serious disruption of the front yards of several adjoining properties.

Figures 1 and 2 show the bridge in its original condition and after the rehabilitation system had been installed. The arches of this bridge consisted of 13-in. channel sections welded and bolted to form four segmental arches, one inside and one outside each existing truss. Each arch was shop welded to form three separate lengths, each about 25 feet long and weighing less than 800 pounds, that could be easily transported and erected. In fact, because of the proximity of power lines to one side of the bridge, two of the arches were completely erected by means of hand-operated hoists attached to the exist-

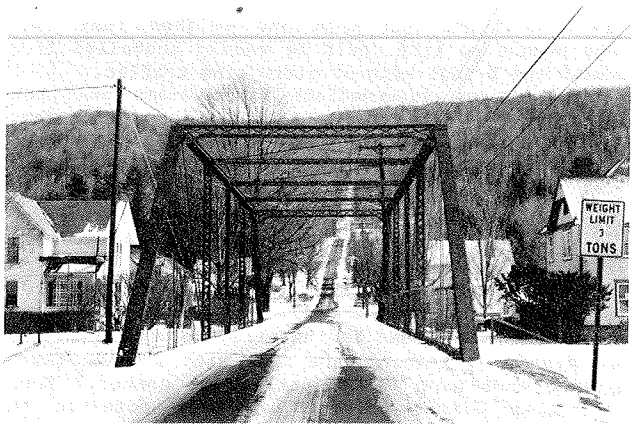

FIGURE 1 Coudersport bridge before rehabilitation.

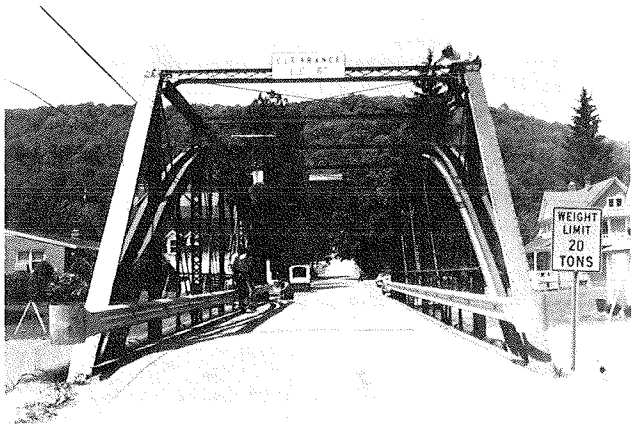

FIGURE 2 Coudersport bridge after rehabilitation.

ing truss. For this first application, the arches and floor beams were made of A-572 grade 50 steel and all other new members were of A36 steel. In the two additional applications of the system to date, all new members have been of A36 steel.

For the Coudersport bridge it was possible to use the existing abutments to resist the thrust of the arches. This was because the bridge had been raised 2.5 ft to accommodate the channel lining work that was done as part of a flood control project in 1953. At that time combined abutment and wing walls of reinforced concrete were cast in place on top of the earlier stone abutments. These concrete monoliths were found to be able to develop enough soil resistance to provide the required thrust. If the existing abutments had not been found adequate, two alternative solutions would have been possible: (a) reinforce the abutments with a facing of reinforced concrete or (b) resist the thrust by means of ties.

After the installation of the arches, the next task was the installation of hangers, additional intermediate floor beams, and stringers. The additional stringers were needed to reduce the span of the existing timber deck so that it could safely carry the wheel loads of an AASHTO H20 loading. If the floor deck had been metal grating or reinforced concrete, it might not have been necessary to add stringers because the introduction of intermediate floor beams cuts the span of the stringers in half thus reducing their bending moment by a factor of at least two. The intermediate floor beams were suspended from the arch by hangers, which were welded assemblies of light rolled shapes, and a pair of 1-in.-square hanger rods with 1.5-in. round threaded ends (Figure 3). The floor beams were 16-in.-wide flange sections, and each one weighed less than 1,000 pounds so they could be easily installed from beneath the bridge without disrupting traffic.

When the new intermediate floor beams had been installed, it was possible to replace the existing, laterally buckled floor beams. Because the number of floor beams had been doubled and only one existing floor beam was removed at a time, it was possible to keep the bridge open for traffic. Figures 4 and 5 show the original U-bolts supporting the existing floor beams and the new hangers for the replacement floor beams. The new hangers for the replacement floor beams are similar to those for the new intermediate beams in that they terminate in the same system of 1-in.-square rods with 1.5-in. round threaded ends used for adjusting the camber. However, they differ in that wherever possible an existing vertical truss member was used for the upper portion of the hanger. This permitted the

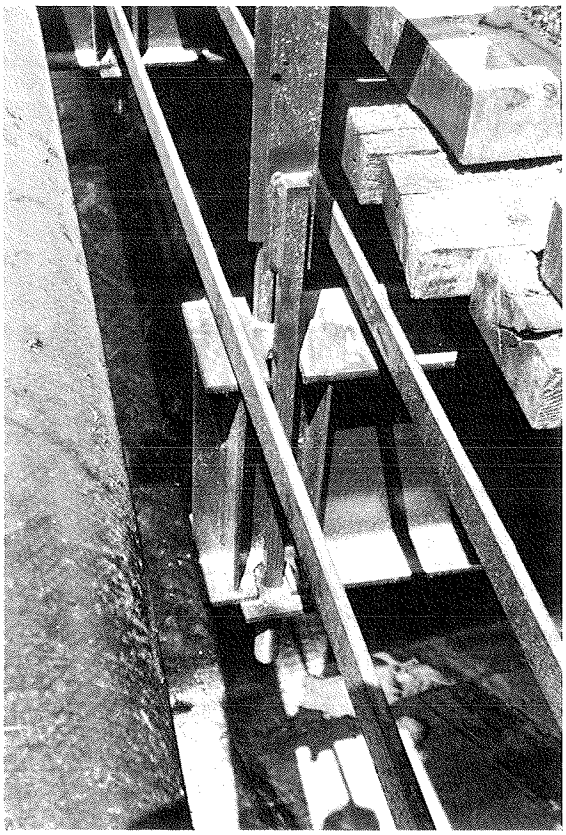

FIGURE 3 Intermediate floor beam supported by hanger rods.

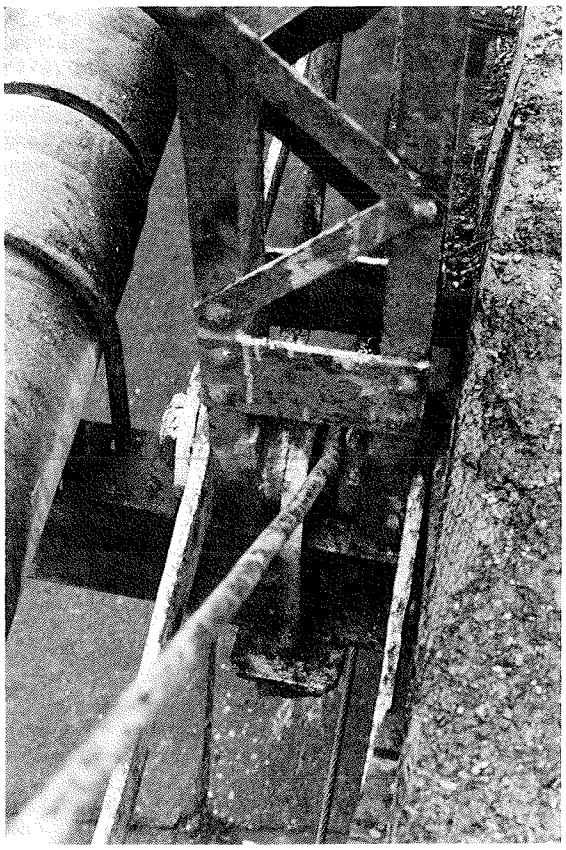

FIGURE 4 Original bottom pin-U-bolt joint for floor beam.

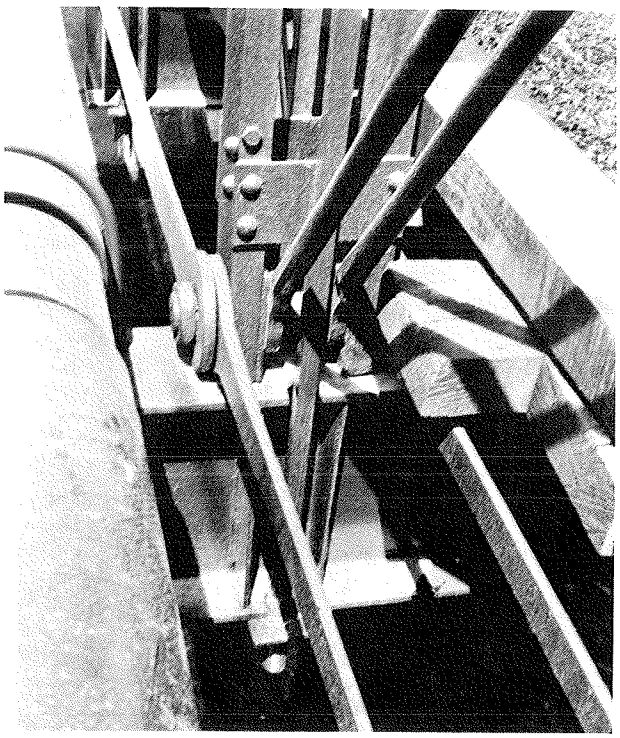

FIGURE 5 1-in.-square rods to support replaced floor beam.

complete bypassing of all the existing pin connections and rendered their condition unimportant to the future performance of the bridge. All that the old truss connections are called on to do is to provide enough continuity of the existing trusses to serve as lateral bracing for the slender sections of the new arches. Without the bracing of the existing truss the arch sections would have to be much heavier and thus more expensive. The entire erection operation took less than 3 weeks. The total cost for the rehabilitation, including painting, was about $62,000.

The most recent application of the rehabilitation system, a 139-ft-span, single-lane bridge in eastern Kentucky, went out for bids in early December 1983. The result was a low bid of $91,000, less than 25 percent of what the state of Kentucky had planned to spend for a new bridge. This installation was designed for an AASHTO HS-20 loading to accommodate coal trucks serving local strip mines. The Coudersport bridge installation was designed for an H-20 loading. In both cases the current AASHTO specifications were used.

LOAD TESTS

A series of load tests on the Coudersport bridge with the heaviest borough truck fully loaded with wet sand was conducted (Figure 6). The total weight of the loaded truck was 22.5 tons and this was judged to be the heaviest load that the bridge would be subjected to. (The heaviest fire truck in the borough is a fully loaded tanker weighing 17 tons.) The maximum deflection with the truck fully loaded with wet sand was 0.20 in. at the midspan of the bridge. For the load tests the bridge was instrumented with dial gauges clamped to the bridge. The stems of the gauges were tied by means of thin wires to concrete blocks placed in the bed of the stream. The thin wires provided such low resistance to the flow of water and air that there was little random

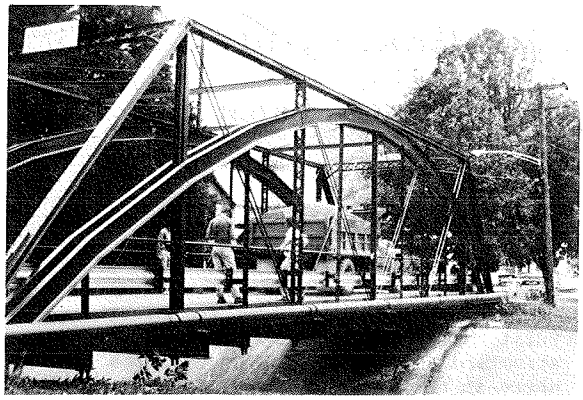

FIGURE 6 Load test with 22.5 tons.

fluctuation of the gauges and repeatability of measurements was adequate.

ADDITIONAL STUDIES

The authors are currently seeking support for a larger model, approximately 50 feet long, to be constructed and studied in the structural test facility that is being completed on the campus of Bucknell University. Such a model would be nearly full scale for some prototypes and thus would offer the following advantages: (a) It could be made of actual rolled shapes rather than the shapes milled from steel tubing that were necessary in the 1-to-7 scale model. (b) There would be no need to add weight to simulate dead load; the model could be tested to actual failure without as great likelihood of completely destroying the model. This would permit the determination of the actual failure load of the model under a variety of reinforcement configurations and loading conditions.

It is planned to use this larger model to provide three significant extensions of the previous studies: (a) more careful investigation of the need for and provision of lateral bracing for the arches, (b) the possibility of placing arches only on the outside of the main trusses so that there will be no encroachment on the width of the traffic lane, and (c) the possibility of placing the arches outboard from the main trusses so that, with the use of longer floor beams and remodeled end portal frames, the bridge can be widened. This would increase the availability of FHWA funds for these projects. Such funds can be made available for bridges of substandard width on the basis of state or county petitions for waivers; however, it may be feasible to include widening of the roadway as part of the rehabilitation system.

ACKNOWLEDGMENT

The authors wish to thank the Borough of Coudersport for providing an opportunity for the first field application of this reinforcement system. The authors are grateful to the American Iron and Steel Institute for sponsoring the initial model study of this system. Special thanks are due to Williamsport Fabricators, Inc., for their expeditious, high-quality fabrication and erection of the system. Finally, the authors wish to thank their students, Richard Haller, Vincent Mehringer, Paul Paino, and John Yadlosky, for their assistance with this project.

Publication of this paper sponsored by Committee on Construction of Bridges and Structures.

Renovation of the Third Avenue Bridge in Minneapolis

DAVID O. MILLER and RICHARD D. BECKMAN

ABSTRACT

The Third Avenue Bridge has the most dramatic setting and sophisticated design of all Minneapolis spans over the Mississippi. Built in 1918 this reinforced concrete structure had deteriorated to the point where it needed major renovation or replacement. Howard, Needles, Tammen, & Bergendoff, Architects, Engineers, and Planners, did a detailed inspection and evaluation of the bridge. They recommended replacement of the entire deck including roadway, barriers, sidewalks, railings, and lights; the spandrel caps and the upper portions of the spandrels; the entire approach spans, including the bents; and even the abutments and wing walls. Special challenges for the designers included estimating quantities and defining how much of the structure was to be replaced, improving sight distances, improving drainage by inducing a slight grade, protecting the top reinforcement, adding a new safety-shaped barrier between the roadway and the walkways, and developing special provisions for the use of shotcrete. In addition, the designers worked to preserve the historic and aesthetic values of the bridge. It became clear that a normal construction pace would not be acceptable. The bridge was too important to the traffic system to be closed any longer than really necessary. An incentive clause was added to the contract. Construction brought additional problems. The condition of the bridge was worse than expected. Decisions about the extent of the repairs had to be made daily. Nevertheless, the project was a success. The Third Avenue Bridge was reopened to traffic almost a year ahead of schedule and has been saved for decades to come.

The Third Avenue Bridge is one of eleven bridges (or bridge systems) crossing the 9-mile course of the Mississippi River through Minneapolis and connecting the east and west sides of the city. It carries State Highway 65 over the river and connects Third Avenue South on the west (downtown) side to Central Avenue on the east side of the river. These are both major city streets that carry high volumes of traffic.

Of all Minneapolis spans over the Mississippi, the Third Avenue Bridge has the most dramatic setting and sophisticated design (Figure 1). It angles across the river, just above Saint Anthony Falls, on seven low arches that are curved at each end and leads straight into downtown Minneapolis.

Built in 1918 at a cost of $850,000, this reinforced concrete structure had deteriorated badly over the years. The Minnesota Department of Transportation (Mn/DOT) thoroughly renovated the bridge between 1979 and 1981. Because the bridge was in a historic district, was itself a historic structure, spanned a developing park, and had obvious historic and aesthetic values, its renovation posed both special problems and opportunities.

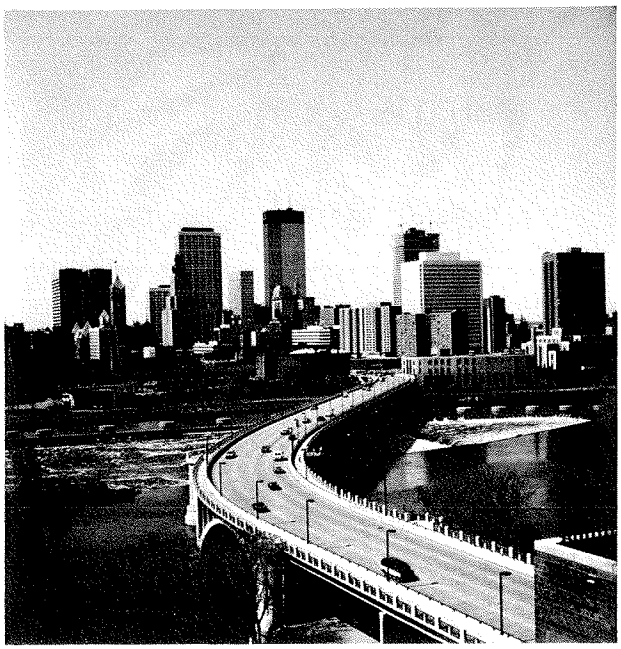

FIGURE 1 Third Avenue Bridge.

The Third Avenue Bridge, 1,864 ft long and 52 ft above the river, was built with four traffic lanes, two broad sidewalks, observation decks, and a spiral stair between the deck and Main Street, below. By the 1960s the bridge had deteriorated to the point where it needed major renovation or replacement. The concrete deck and sidewalks were disintegrating; the east abutment was split top-to-bottom; the spiral stair was a complete ruin.

As originally constructed between 1915 and 1918, the bridge consisted of six distinct units: the southwest abutment, four southwest approach spans over railroad tracks, five ribbed arch spans and two barrel arch spans over the water, four northeast approach spans over another track and Main Street, and the northeast abutment. The earth-filled abutments had reinforced concrete wing walls and abutment walls. Two of the southwest approach spans had sixteen reinforced concrete girders supported by three-column, reinforced concrete bents, and the other two had five steel girders supported by the same type of bents. The five ribbed arches had a clear distance between springing lines of 211 ft; the two barrel arches had a clear distance of 134 ft between springing lines. Open-spandrel columns were used above the ribbed arches, and spandrel walls were used above the barrel arches to support the deck. The four spans of the north approach had sixteen reinforced concrete girders supported by five-column reinforced concrete bents.

The asphalt-surfaced roadway was 56 ft wide between the faces of the traffic railings and was flanked on both sides by concrete sidewalks 9 ft 8 in. wide. The outer railings were decorative art-deco castings, added in 1939. The out-to-out width of the bridge was 82 ft 6 in.

The Third Avenue Bridge was added to the Minnesota Trunk Highway system in 1933 and now carries State Highway 65. The bridge is currently maintained by the city of Minneapolis through an agreement with, and at the expense of, the Minnesota Department of Transportation.

DESIGN

In 1967 Howard, Needles, Tammen, & Bergendoff (HNTB), Architects, Engineers, and Planners, was retained by the Minnesota Highway Department, the predecessor of Mn/DOT, to inspect the Third Avenue Bridge and conduct preliminary engineering for its rehabilitation. They found that localized and progressive failures could occur unless the deterioration was checked.

From the deck the bridge appeared to be in fair condition at that time. The in-depth investigation revealed that the concrete throughout the bridge had areas of severe spalling, which often exposed the reinforcement. Mineral deposits and scaling existed in areas where water had seeped through the concrete. These deposits were densest around the deck expansion devices and floor drains.

The corrosive action of locomotive exhausts had deteriorated the concrete beams and steel plate girders in the approach spans, significantly reducing their load carrying capabilities. Additional supporting members had been placed adjacent to the beams in both of the weakened approaches to reinforce them. The structural integrity of the bridge was also diminished by penetrating cracks in the cap beams of the concrete bents, in the spandrel columns and walls, and in the north abutment.

The remaining portions of the bridge were found to be in good general condition. These included the piers and their foundations, the arches, and portions of the spandrel columns and walls. Reconstruction would allow a substantial portion of the bridge to be saved at a cost considerably less than that of building a new bridge. In fact building a new bridge at the same location would have been impractical and perhaps impossible. The existing bridge stands on a thin limestone shelf and is carefully aligned to avoid several large breaks in that shelf. Demolition of the existing bridge would probably further damage the limestone shelf and render it unsuitable as a foundation for any new bridge.

In 1973 HNTB began the reconstruction plans for the Third Avenue Bridge. The designers made plans for a new deck. Drainage was to be improved by inducing a slight grade on the new deck and sidewalk. Neoprene expansion devices were to be used to help prevent deterioration of the concrete around the expansion joints. A type-J safety barrier was to be added to replace the existing tubular steel safety rail between the sidewalks and the traffic lanes. A concrete parapet and a new lighting system were proposed to replace the existing art-deco railing and lighting system.

Improvements below the deck were to include repairing or replacing the spandrel walls and columns. During the inspection, cracks and spalling had been found in the spandrels, but further investigation would be required to determine the full effect these had on the structural integrity of the spandrels. For this reason the plans specified that decisions on the extent to which the spandrels were to be replaced were to be made in the field during reconstruction.

The new design called for completely rebuilding both abutments and approach spans. Because of new design standards, the plans called for replacing the three bents at each approach with single bents of similar design (Figure 2). This was more economical than the three-bent design, and opened the space beneath the bridge. In addition, a 36-in.-diameter water main was to be added beneath the deck.

FIGURE 2 South approach bent.

The plans called for extensive use of shotcrete to repair the spalling and cracking concrete found throughout the structure. Quantities of shotcrete to be used were estimated in the plans but were to be finally determined in the field. The bridge was then to be coated in Thoroseal to give it an even color and texture. HNTB submitted the designs to the state for final approval in 1976.

Because the bridge was located in the Saint Anthony Falls Historic District and was itself of considerable historic and aesthetic value, Mn/DOT worked closely with two historical agencies to retain these values. When the Minnesota Historical Society and the Minneapolis Heritage Preservation Commission first reviewed the plans, they were concerned about some aspects of the proposed modernization. The original reconstruction plans were done with economy and function as primary considerations, and they were done to the standards of AASHTO and the bridge specifications of Mn/DOT. The plans did not include reconstruction of the spiral staircase, which had been closed for years and removed in 1976. The historical agencies wanted the stairway replaced. They believed that the stairway was a historic and aesthetic element of the bridge and that pedestrian access from the bridge to the newly redeveloped Main Street area below was essential.

Research of the old plans indicated that a redesign of the old stairway would not meet current safety codes. The spiral radius was too tight to meet today's standards. Redesign using a larger radius would require the purchase of additional right-of-way. The alternative finally agreed upon by all parties was a winding staircase of poured concrete with four straight runs and three round landings, all wrapped around a central pier (Figure 3). The design retained much of the sculptural value of the original design but in a safer and more functional form.

Another concern was the bridge lighting system. The original reconstruction plan called for 19 swanneck, standard freeway design, lighting fixtures. The argument was made that this lighting system would not be in character with the design and historic nature of the bridge. The parties concerned finally decided upon 53 architectural-style units, only 20 ft high (Figure 4). This lighting system satisfies functional standards and looks attractive

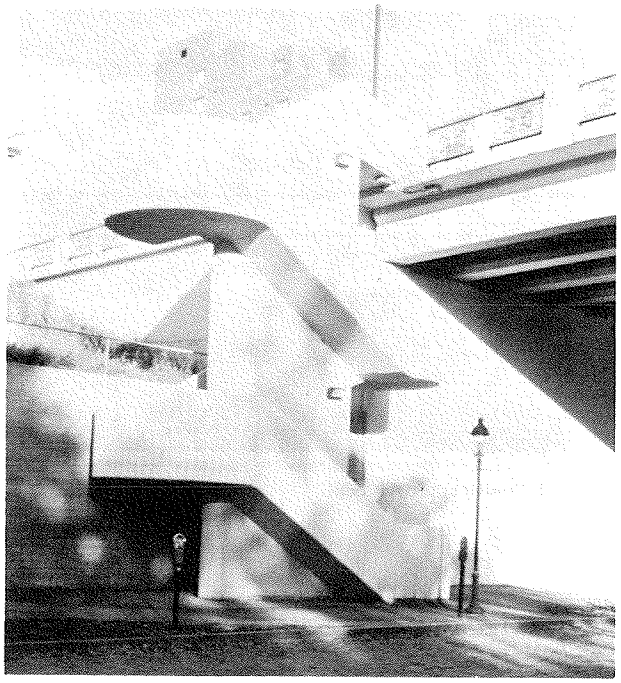

FIGURE 3 Reinforced concrete staircase.

FIGURE 4 Lighting system.

as it outlines the bridge and defines the curves at the ends.

The northeast approach bent was also changed. It was argued that the redesign was less aesthetically pleasing than the original arched bents and that the railroad crash barrier was not needed because the track was used rarely and at slow speeds. A vaulted bent without a crash barrier was finally decided upon (Figure 5). In addition the historic agencies objected to the proposed replacement of the art-deco

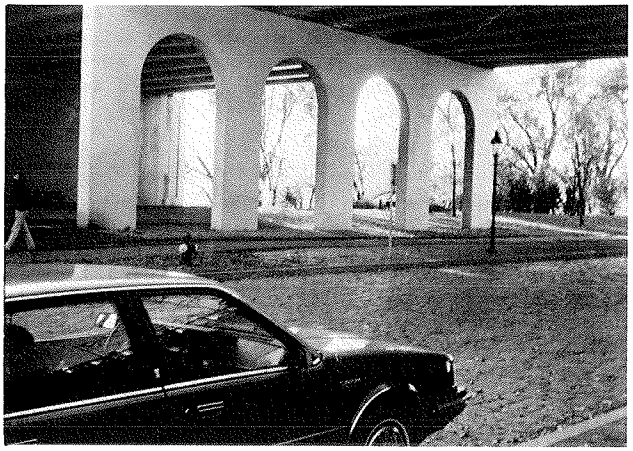

FIGURE 5 North approach to bent.

railing. Mn/DOT agreed that the railing should be salvaged and reinstalled (Figure 6).

Before the final plans were submitted in 1979, a few other changes were made. Vehicles approaching the bridge from 1st Street South could not obtain proper sight distances to cross Third Avenue. The vertical profile of the bridge was flattened to alleviate this problem. A flare that widened the bridge at the south approach was also added to the design to improve the sight distance.

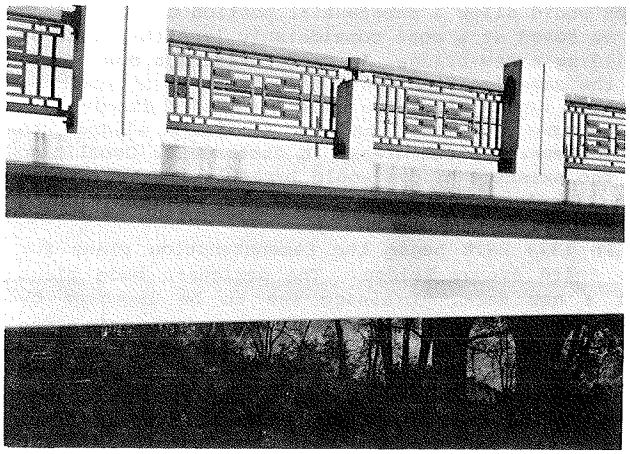

FIGURE 6 Art-deco railing.

Design practices had changed to some extent during the long design period, and the final plan reflected these changes. They included using A588 steel beams in the southwest approach spans and epoxy-coated reinforcing steel and a 2-in. dense concrete wearing course on the roadway of the deck. In addition, the entire reconstruction was redesigned using a load factor.

CONSTRUCTION

The practice of Mn/DOT is to get the construction engineer involved in a project as early as possible.

A field trip was planned well before the final plans were complete to acquaint the field staff with the structure. A "snooper" was scheduled so the substructure could be examined. Unfortunately the sidewalk geometrics were such that use of the snooper would have created a safety problem. Consequently a closeup inspection of the deterioration did not occur until construction began, leaving the extent of the problem a surprise. The more accessible areas were inspected and binoculars were used to view the rest. Another bridge was examined that, several years earlier, had undergone similar repairs, and the engineers and inspectors from that job were interviewed. That input was given to a Mn/DOT design liaison person who, in turn, conveyed it to the consultant. One significant item revised by the field input was the quantity of shotcrete. The initial quantity called for was 50 cubic yards. It was recommended that this be increased to 500 cubic yards. That amount was determined not by measurements but by the combined experience and judgment of field personnel. The actual final quantity came to about 600 cubic yards.

The next task was to determine the number of working days needed to complete the work. That number was to be a stipulation of the contract. Past records were used for production rates. Reports from other agencies gave typical times and production rates. The similar repair project, previously mentioned, was used as a guide. Contractors were called for their ideas. In the end the field personnel sat down with the plans and mapped out how the work would be accomplished and what would be the controlling operation. The fact that Minnesota does not charge working days between November 15 and April 15 was taken into account. Estimates were made of how much work could be done during this "free" time. Also taken into account was the fact that work pursuant to the contract, because of the letting date, could not start until late fall. One important question was how much leeway to allow to accomplish unanticipated repairs. At what point should repairs be stopped and the existing structure used? Another problem was the installation of the new water main; the city of Minneapolis typically prefers to use its own forces. Would that create a coordination problem? Still another problem was to maintain Northwestern Bell telephone service in existing ducts.

After much deliberation, a reasonable number of working days were determined. Taking into consideration the September 15 cutoff date for laying a bituminous wearing course, the October 15 cutoff date for the low-slump concrete deck overlay, and the typical 110 working days in a Minnesota bridge construction season, final completion was projected well into the second construction season.

The district staff was so advised. They in turn consulted with the city of Minneapolis, which determined that a closure of this vital link for that period of time would create a serious negative economic impact on the city. Meetings were held with city officials, the city council, and business associations. The bridge connects downtown with the historic Saint Anthony area (the beginnings of Minneapolis). The area was being redeveloped and the new merchants of the area were concerned that a closure would be devasting to their business. For obvious economic reasons they requested that the bridge not be closed during the first Christmas season.

How could the closure time be held to a minimum? To have a contractor accelerate the schedule would mean more cost to Mn/DOT. How much more was Mn/DOT willing to pay? The date of September 18, 1981, was established as the latest date Mn/DOT wanted to have traffic restored to the structure. An incentive of $5,000 per day, for up to a maximum of 100 calendar days, was offered for early completion. The amount was determined by calculating $3 per hour delay per vehicle, and $0.19 per mile per vehicle for a detour. These figures gave nearly a 2-to-1 benefit-cost ratio. The same amount per day would be assessed as damages if the contractor failed to open the bridge by September 18, 1981.

The contract was written to allow the contractor to use ingenuity in finding ways to earn the incentive. The city council revised a noise ordinance to allow around-the-clock work. The new water main was included in the contract, thus eliminating some possible coordination problems. A stipulation was included in the contract requiring that one lane of traffic be open in each direction until January 2, 1980, thus satisfying the Saint Anthony merchants.

Bids were opened at a special letting on July 6, 1979, and Johnson Brothers Corporation of Litchfield, Minnesota, was the low bidder at $9.1 million. They elected to maintain traffic on the upstream half of the bridge, and bolted portable traffic barriers to the in-place deck (Figure 7). Demolition began with removal of the bituminous surface and the sand layer that was over the structural slab (Figure 8). At that point it became apparent that the structure was in worse shape than anticipated (Figure 9). It was questionable how much construction equipment the slab could support. On the

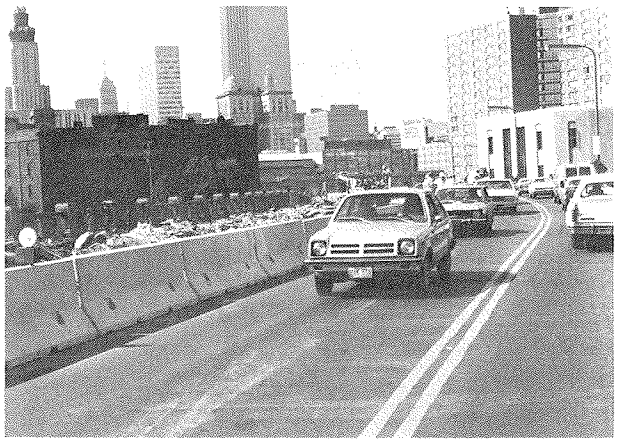

FIGURE 7 Traffic barrier on upstream half of bridge.

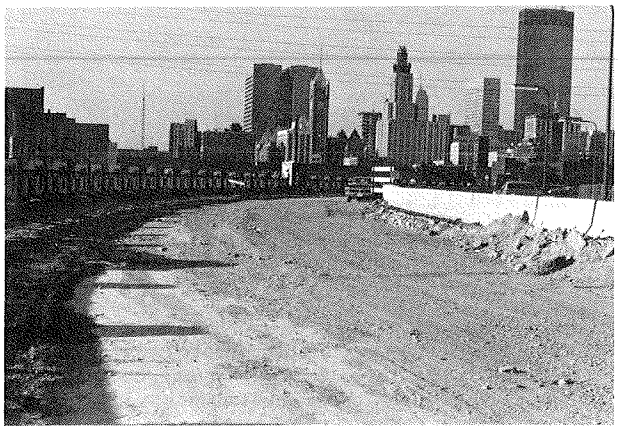

FIGURE 8 Sand layer removed.

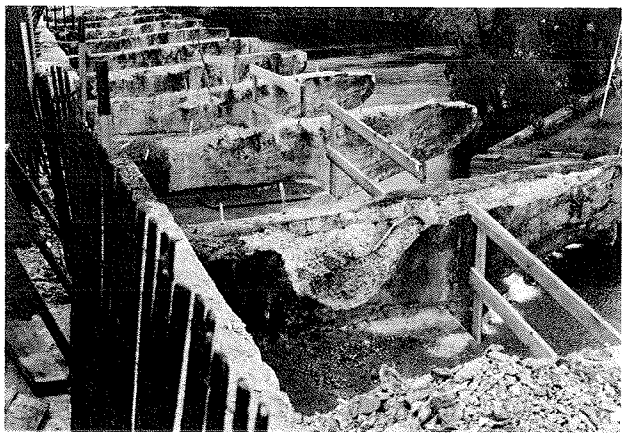

FIGURE 9 Deterioration of cap.

FIGURE 10 Holes in structural slab.

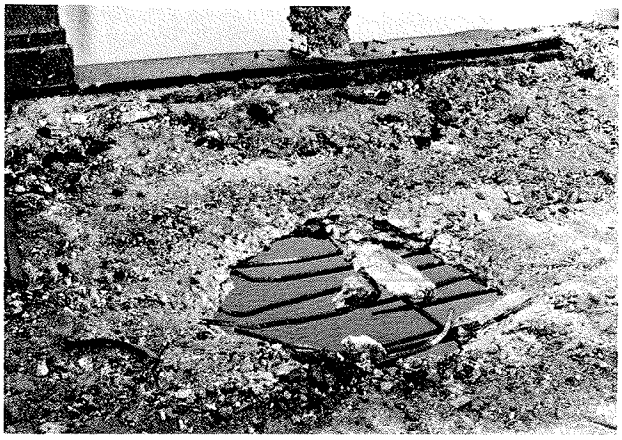

FIGURE 11 Hole opened by tire of front-end loader.

northeast approach spans, which had been underpinned, portions of the slab disintegrated leaving fairly large holes (Figure 10). On one occasion the tire of a front-end loader, which was removing the sand layer, fell through the structural slab (Figure 11). Another question was how the substructure would react to the unloading of just half of the superstructure. The plans suggested that a certain sequence be followed. Experience on a previous project indicated that the sequencing would create no problems. Traffic was still carried on the upstream half, and whether that half would hold up became a concern. In addition to the poor condition of the structural slab, it was found that some of the spandrel columns had deteriorated to the point where they were only half as wide as they should have been (Figure 12). The strength of the remaining concrete was questionable. At that point all trucks and buses were banned. The inspectors were on a continual lookout for signs of fatigue or failure. At one time Ames dials were installed, and it was found that the freeze-thaw in the "punky" concrete was causing it to move but that the movement was not progressive.

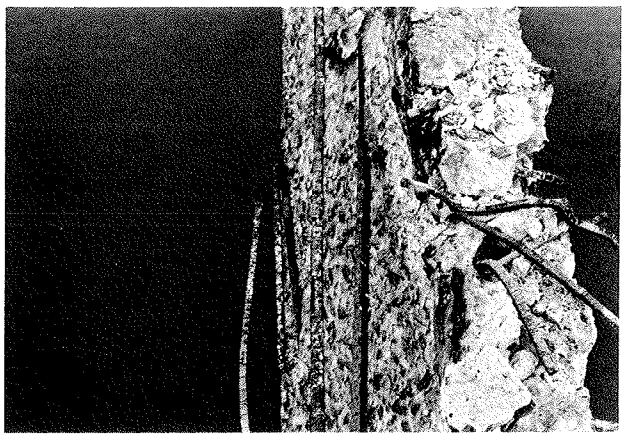

FIGURE 12 Spandrel cap deterioration.

When the sand layer had been removed the contractor began concrete removal. The method chosen to remove the old deck was to first saw it into large panels (Figure 13). The contractor devised a sling-type device that, when used with a mobile crane, held the slab while the reinforcing steel was cut. When the steel was cut the crane merely lifted the slab and set it on waiting trucks or on a spot from which it could be hauled away later. The deteriorated spandrel columns and walls were removed in a

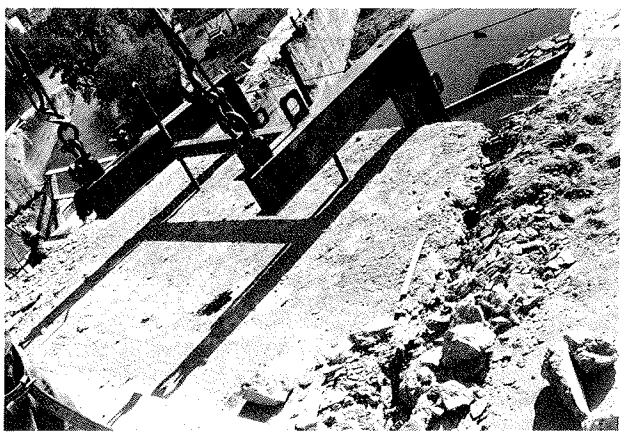

FIGURE 13 Deck removal.

similar way (Figure 14). Holes were drilled at the elevation to be cut, and splitters and torches were used so that large sections could be removed at a time. These methods helped control the rubble problem. The contract stipulated that rubble not be dropped into the river. Immediately after these removals the contractor built a false deck below the elevation of the new deck. This served not only as a replacement for safety nets but as a work platform to increase efficiency and to catch rubble. The removal operations continued around the clock until well into the winter when the contractor determined that the removals were no longer a factor affecting the efficiency of the daytime rebuilding crew.

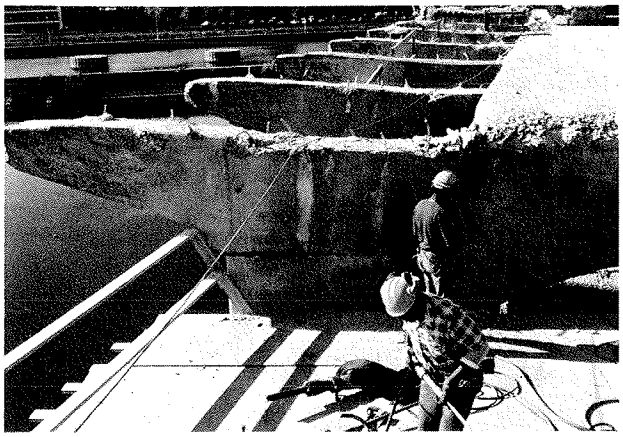

FIGURE 14 Spandrel removal.

Shortly after the bids were opened, the field engineering staff was forced to take a look at the different types of concrete repair. What did the contract say? When should the various types of repair be used? Until then it had not been anticipated that there would be such a drastic difference in the bid unit prices. For instance, the shotcrete was $2,000 per cubic yard; the mortar patch was $500 per cubic yard. Part of the reason some of the repair prices were so high was the specification that removal of unsound concrete be included in the price--jackhammering, chipping, and all the handwork.

One area that was anticipated to be a problem, but was not, was the repair of the spandrel columns. The actual elevation to which they were to be removed was to be determined by the engineer in the field. The method of determining whether the column should be repaired or completely removed and built anew was simple. The length of column and the square footage of shotcrete repair at which the cost would be equal were computed. If the needed shotcrete repair was greater than that, the decision was to remove the column down to the arch. This required inspectors to be on the spot while the demolition was taking place.

The determination was based on the results of visual inspection and sounding with a miner's hammer. This method worked quite well. In only one case was it determined, during subsequent repair, that a column should have been completely removed. The freezing weather during the initial inspection was apparently responsible for the sound appearance of the concrete. The "punky" concrete had been frozen and so had looked and sounded like sound concrete. Just prior to the shotcrete repair a more thorough inspection was made and specific areas were marked for removal. The removal crews were watched to verify the accuracy of the previous findings. Inspection consisted of not only viewing the material being removed but watching the equipment and the workmanship of the crews. It was specified that the removals be done with hammers not heavier than 5 lb. Larger hammers could cause costly and unnecessary damage.

Another area where it was difficult to determine which type of repair to use was the pier repair. The piers near the water line were in quite bad shape. The experience on the spandrel columns showed that the strength of the shotcrete was quite high. Strengths of 8,000 to 9,000 psi were experienced in just a few days. The low-slump concrete used on other deck repairs had given strengths of 6,000+ psi on 28-day tests. Considering that, it was determined that near the waterline shotcrete rather than forming and pouring should be used. The shotcrete method would also give a tighter bond that would be more resistant to freeze-thaw cycles and the water action of the river. During the repair of the piers, in many instances not just a few inches but several feet of bad concrete were removed (Figure 15). The shotcrete was applied in layers as specified.

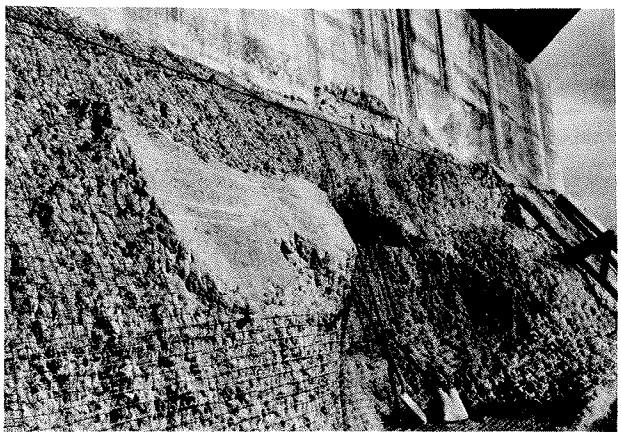

FIGURE 15 Pier repairs before shotcreting.

Mortar patch was to be used primarily on horizontal surfaces. An example of this was repairs on the tops of the arches. In most instances the contractor chose to use shotcrete but to be paid the mortar patch unit price.

The bridge was closed to traffic after the first of the year and the contractor continued work. The approach spans over land at the northeast end of the bridge were completely torn down. The approach spans over land at the southwest end were left in place until nearly the end of the job and were used by the contractor for access. The temporary Northwestern Bell trestle at the northeast end was also used for foot access by workmen. The upstream half of the bridge was used as an access road and not demolished until enough of the downstream half was rebuilt to allow it to be used for access. Except for a short time when the weather was too bitterly cold to work, rebuilding of the spandrel columns and the northeast pier continued all winter (Figure 16). Forms were insulated and the temperature of the concrete was continually checked to be sure that it did not freeze. The first section of structural deck was ready for concrete pouring by April (Figure 17).

During the rebuilding it soon became apparent

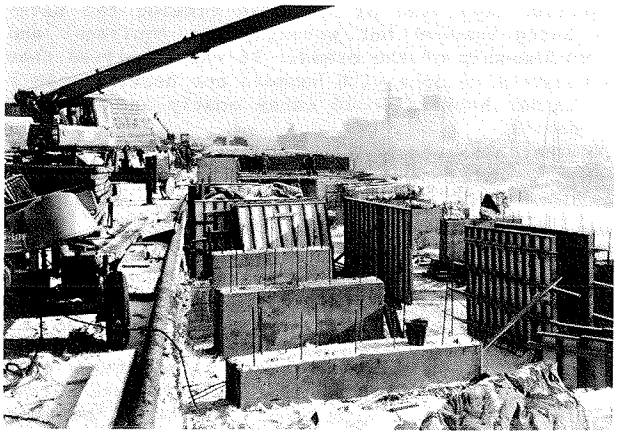

FIGURE 16 Winter work.

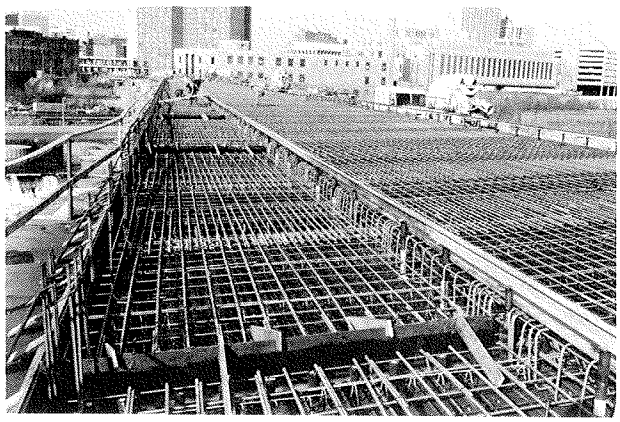

FIGURE 17 Structural deck ready for pouring of concrete.

that the as-built plans did not always represent the actual structure. Dimensions did not always agree. In-place reinforcing steel was not always where shown; in some places it was rusted through or even missing. This created a potential problem because the contractor was working to earn the full incentive. A misrepresentation on the plans, or a failure to make timely decisions, could leave Mn/DOT open to future claims. Luckily a good working relationship between the state and Johnson Brothers had been established. Workers were looking for and reporting potential problems early enough for timely modifications to be made. Mn/DOT and HNTB designers were available when needed for design modifications. Decisions had to be made daily, sometimes at the spur of the moment. Maintaining the intent of the plan and good workmanship were the primary objectives.

Demolition of the upstream half of the structure began after the new structural slab on the downstream half could be used for contractor access. Operations similar to those of the first half, except that no night work was scheduled, continued. The last sections of the structure to be demolished and rebuilt were the approach spans over land at the southwest end of the bridge.

The safety barrier was poured and the low-slump concrete wearing course pavement was placed by the October 1 cutoff date. An unexpected incident occurred during the placement of the low-slump concrete. The arches were contracting during the cool late summer evenings. In some cases the green low-slump concrete debonded before the joints could be sawed. All the joints were then checked for debonding. Where necessary they were cut out and repoured to leave room for temperature-induced movement.

Mn/DOT normally provides all the surveying on its construction projects, but in this case it was specified that the contractor would furnish it. There were two reasons for this: First, inspectors were busy on other projects. Second, with the shortage of manpower Mn/DOT did not want to be in a position of delaying the contractor. It was believed that the contractor should have flexibility and control scheduling if he was trying to earn the incentive.

By fall the art-deco railings, which had been removed before demolition, were reinstalled. The new lighting system was installed and operational. In late November, almost a year ahead of schedule, the bridge was reopened to traffic and the Johnson Brothers Corporation earned the full incentive payment. Work beneath the deck continued until the following summer. That work consisted of finishing the shotcrete repair and refinishing the entire structure to a uniform texture and color. Finally, the new staircase was built.

CONCLUSIONS

Mn/DOT believes that the renovation of the Third Avenue Bridge (Figure 18) was a complete success.

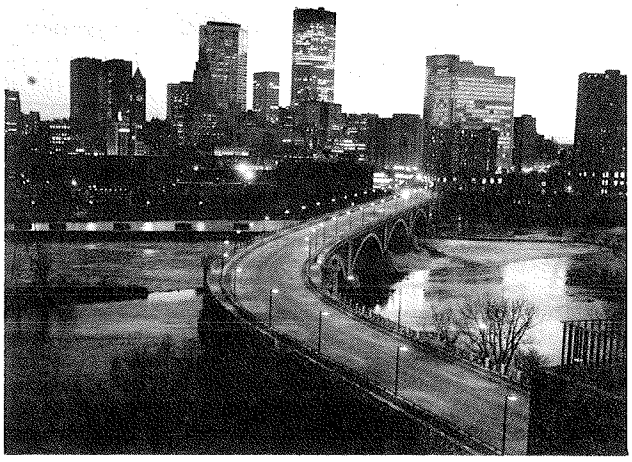

FIGURE 18 Night view of rehabilitated Third Avenue Bridge.

Almost all known renovation methods were used. Portions of the bridge were completely rebuilt. Portions were patched or repaired with shotcrete. New joints were watertight. Epoxy-coated reinforcement bars were used. The upper portion of the deck was low-slump concrete. The latest safety standards were incorporated. The historic and aesthetic integrity of the bridge was maintained. The structure was out of service for less than a year, which was a plus in the eyes of the public. Complete demolition and replacement, even if possible, would have taken several years. The project won a national third-place award from the FHWA for "excellence in design for historic preservation and cultural enhancement." The project was given an award for design excellence by the Minneapolis Committee on Urban Environment. Best of all, the useful and lovely Third Avenue Bridge has been saved for decades to come.

Publication of this paper sponsored by Committee on Construction of Bridges and Structures.

Test of Welding Technique for Repair of Steel Highway Bridges

T. MATSUMOTO and S. MOTOMURA

ABSTRACT

A welding technique for the repair of steel highway bridges is described. Recent inspection of steel bridges indicates that there are considerable fatigue cracks, which need some repair work, in bridges that have been in service more than 10 years. The demand for field welding in lieu of bolting has increased. The main problems of field welding are welding under the influence of stresses, welding under the influence of vibration, and rewelding a weld with fatigue cracks. These problems are not common in new bridge construction. A series of laboratory and field tests on plate girder bridges has been conducted to assess the influence of these problems on the welding technique used in field repair. A recommended practice for field weld repair is proposed, and test results showing the effect of stresses, vibrations, and so forth are given. The welding technique proposed here has been successfully applied.

There are approximately 3,700 steel bridges on the Hanshin Expressway, which is 123.6 km long. According to the results of a recent inspection, there was considerable fatigue cracking in bridges that had been in service more than 10 years. This meant that an effective repair method was needed.

Field welding can be more practical than bolting, but there are differences between shop and field welding. For example, it is common practice to keep a bridge open to traffic during repair. This causes traffic-induced vibration and load-induced stresses. The influence of such vibration and stresses on welding was not clearly understood.

In the last 5 years a series of laboratory and field tests of plate girder bridges has been conducted to assess the influence of vibration and stresses on the rewelding of fatigue cracks. A recommended procedure for field weld repair is proposed here, and test results showing the influence of stresses, vibrations, and so forth are presented. The welding technique proposed here has been successfully used in the repair of bridges.

QUESTIONS

The main open questions about weld repair are

For field welding under the influence of stresses:

1. What is the possibility of cracking due to stresses and cold cracking due to restraint of plate?
2. Are there excessive residual stresses due to stresses and restraint of plate?
3. Is there deformation due to welding under stresses and restraint of plate?

For field welding under the influence of traffic-induced vibrations:

1. What is the possibility of hot cracking due to vibrations during weld solidification?
2. What is the effect of vibrations on bead shapes?
3. What is the effect on the strength of joints of welding under the influence of vibrations?

For butt rewelding of fatigue cracks, to what extent is fatigue strength recovered in rewelded joints?

TEST AND MEASUREMENT

General Considerations

Tests of field weld repairs of plate girders include

1. Fillet welding tests with tensile-stressed specimens,
2. Vibration measurement of actual bridges,
3. Fillet welding tests of vibrating specimens, and
4. Fatigue tests of original and repaired butt weld joints.

The chemical composition and mechanical properties of test steel SM50 and SM58Q, specified in the Japanese Industrial Standard (JIS), are shown in Tables 1 and 2, respectively. SM50 steel is equiva-

TABLE 1 Chemical Composition of Test Steel

steel grade	Thickness (mm)	Chemical composition %				
		C	Si	Mn	P	S
JIS SM50 (ASTM A572 Grade 50)	9	0.14	0.40	1.29	0.020	0.004
	30	0.18	0.41	1.37	0.020	0.015
JIS SM58Q (ASTM A678 Grade B)	9	0.14	0.34	1.30	0.014	0.003
	30	0.12	0.29	1.31	0.011	0.003
	40	0.13	0.29	1.28	0.018	0.003

JIS : Japanese Industrial Standard
ASTM : American Society for Testing and Material

TABLE 2 Mechanical Properties of Test Steel

Steel grade	Thickness (mm)	Mechanical properties			Allowable tensile stress (kgf/cm^2)
		Yield strength (kgf/mm^2)	Tensile strength (kgf/mm^2)	Elongation (%)	
SM50 (ASTM A572 Grade 50)	9	42 (≧33)	56 (50~62)	25 (≧17)	2,100
	30	41 (≧32)	58 (50~62)	27 (≧21)	
SM58Q (ASTM A678 Grade B)	9	58 (≧47)	63 (58~73)	27 (≧19)	2,600
	30	55 (≧46)	63 (58~73)	29 (≧26)	
	40	58 (≧46)	66 (58~73)	30 (≧26)	

( ) : JIS provision

lent to ASTM A572 grade 50, and SM58Q corresponds to ASTM A678 grade B. Electrodes for fillet welding are the super low hydrogen type, LBM-52 (JIS D 5016, equivalent to AWS E 7610), and super low hydrogen-low strength type, LB-47A (JIS D 4316), which were selected based on nonpreheated weld metal cracking tests. For butt welding, an ultra low hydrogen electrode, LB-62UL (JIS D 5816, equivalent to ASW E 9016-G), which has strength equivalent to that of the test steel, was used.

Fillet Welding Test of Tensile-Stressed Specimens

Welding tests of thirty specimens were carried out in the laboratory to examine the effects of tensile stresses and restraints transferred from the surrounding plate on cracks, residual stresses, and welding deformation. Test specimens and conditions are shown in Figure 1 and Table 3, respectively. Tensile stresses are $0.8\sigma_{all}$ for web plates (thickness, t = 9 mm), and σ_{all} for flange plates (t = 30 mm), where σ_{all} is allowable tensile stress. In the tests, constant stress was applied during welding; then deformation was kept constant by controlling the gauge length for 48 hours after welding, and finally stress and restraint of deformation were released.

TABLE 3 Test of Welding Under Stress

Specimen	Direction of weld line	Steel grade	Thickness t(mm)	Stress (kg/mm^2)	Gauge length (mm)	Welding position	Electrode
V-1	Perpendicular	SM50	9	$\sigma_{all} \times 0.5$	400	Horizontal	(4ø) LBM-52
V-2	Ditto	SM50	9	$\sigma_{all} \times 0.8$	Ditto	Ditto	(4ø) LBM-52
V-3	Ditto	SM50	30	σ_{all}	Ditto	Ditto	(4ø) LB-47A
V-4	Ditto	SM58Q	9	$\sigma_{all} \times 0.8$	Ditto	Ditto	(4ø) LB-47A
V-5	Ditto	SM58Q	30	σ_{all}	Ditto	Ditto	(4ø) LB-47A
P-1	Parallel	SM50	9	$\sigma_{all} \times 0.8$	Ditto	Ditto	(4ø) LBM-52
P-2	Ditto	SM50	30	σ_{all}	Ditto	Ditto	(4ø) LB-47A
P-3	Ditto	SM58Q	9	$\sigma_{all} \times 0.8$	Ditto	Ditto	(4ø) LB-47A
P-4	Ditto	SM58Q	30	σ_{all}	Ditto	Ditto	(4ø) LB-47A
P-5	Ditto	SM50	9	$\sigma_{all} \times 0.5$	Ditto	Ditto	(4ø) LBM-52

Welding defects were sought using X-ray, magnetic particle, and microstructure and macrostructure tests in accordance with JIS. Welding residual stresses, $(S_x, S_y)_{RS}$, and maximum stresses, $(S_y)_{max}$, were measured by two-axis strain gauges. The maximum stress $[(S_y)_{max}']$ can also be expressed as

$$(S_y)_{max} = (S_y)_{TRC} + (S_y)_{RRC} \quad (1)$$

where $(S_y)_{TRC}$ is the stress due to constant applied load and welding, and $(S_y)_{RRC}$ is the stress increment at a constant gauge length. Deformation, or change in length, due to welding was measured using a gauge length of 40 cm that was marked on the specimens.

Vibration Measurement of Bridges

Before the test of fillet welding under the influence of vibration was conducted, field measurements of traffic-induced vibrations of main girders in three plate girder bridges were carried out to obtain basic data for laboratory tests. Span lengths of these bridges are 22.4 m, 34.3 m, and 37.4 m. Both vertical and horizontal vibration responses were measured in the frequency range of 0.3 to 300 Hz. The measured points were on the support, the flange plate, and the web plate (top, center, and bottom) of the main girder at midspan. The main girder vibrated irregularly in both the horizontal and the vertical direction.

The results of the frequency analysis of the measured horizontal and vertical irregular vibrations are shown in Figure 2. This figure depicts the relationship between mean and deviation of horizontal and vertical displacement ranges and frequencies.

Fillet Welding Tests Under the Influence of Vibration

The effect of vibration on bead shape and other weld defects were examined using specimens (Figure 3) that were connected by fillet welding under vibrating conditions.

The specimens are of SM50 and SM58Q steel with a thickness of 9 mm for the web plates and 30 mm for the flange plates of the plate girders. Frequencies in the tests were 0.3, 3, 30, 90, 150, and 300 Hz, and displacement ranges were Vs, 5 Vs, and 10 Vs. Vs is the mean value of the displacement ranges shown in Figure 2. In-plane or out-of-plane vibrations are applied to the specimens at each frequency.

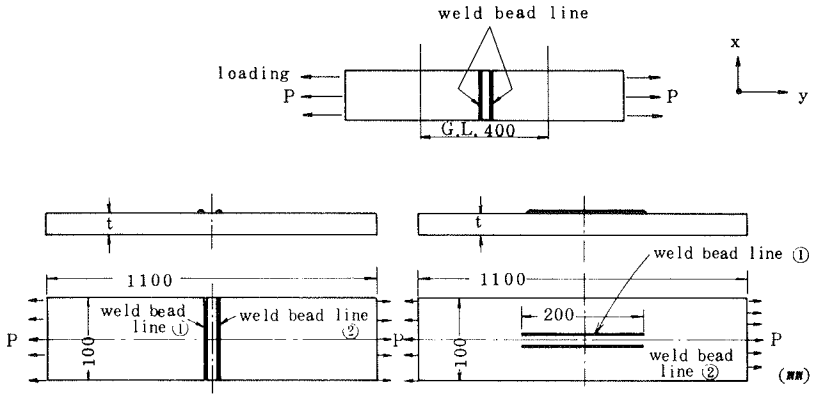

(a) Perpendicular welding to stress axis (b) Parallel welding to stress axis

FIGURE 1 Specimens for test of welding under stress.

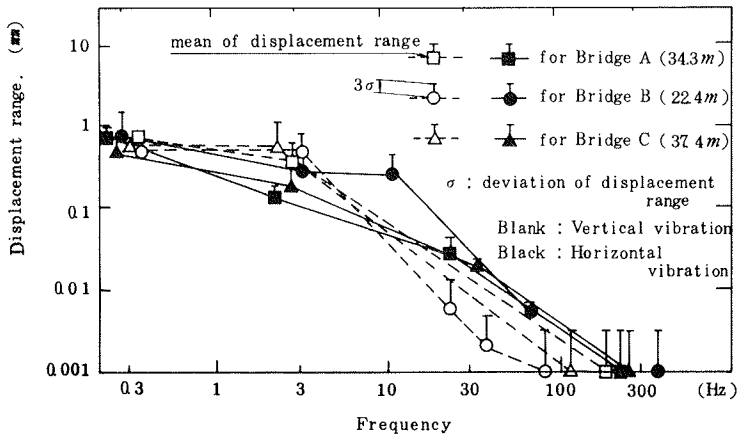

FIGURE 2 Results of frequency analysis of measured vibration.

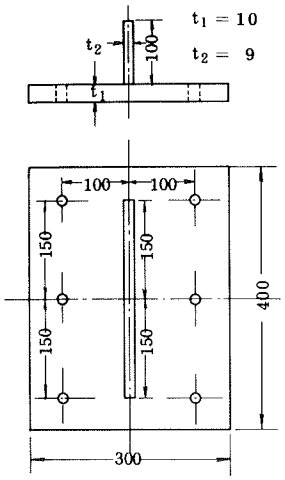

FIGURE 3 Specimen for test of fillet welding under vibration.

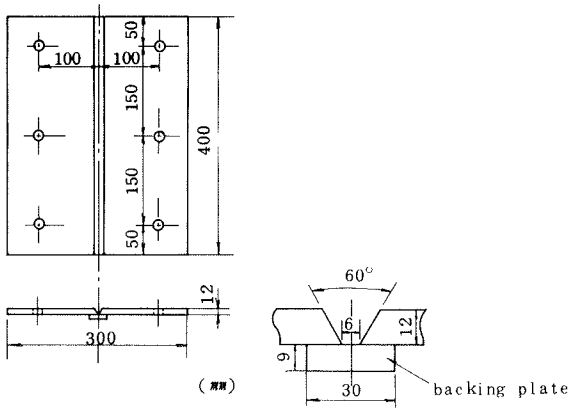

FIGURE 4 Specimen for test of groove welding under vibration.

Vertical up-welding, vertical down-welding, and overhead welding were used on the specimens to examine the effect of directions and positions of welding. Welding defects were sought and inspected using the methods mentioned earlier.

In addition to the fillet welding test, a groove welding test was carried out to examine the influence of vibration on the strength of welded joints (Figure 4). The electrodes used in this test were LB-47A and LBM-52.

Fatigue Strength Test of Repaired Weld Joint

Fatigue cracks often occur in the weld zone of steel bridges. Fatigue tests were conducted on four specimens (Figure 5). Two specimens were used for the original weld joint and weld metal tests, and two were used for the rewelded joint and reweld metal tests. Each specimen was of SM58Q steel 40 mm thick and was connected by submerged arc welding at the center. For the rewelding tests, two specimens, which had received proper gouging treatment after some fatigue damage, were manually welded with an LB-62UL electrode. The number of stress cycles in this test is shown in Table 4.

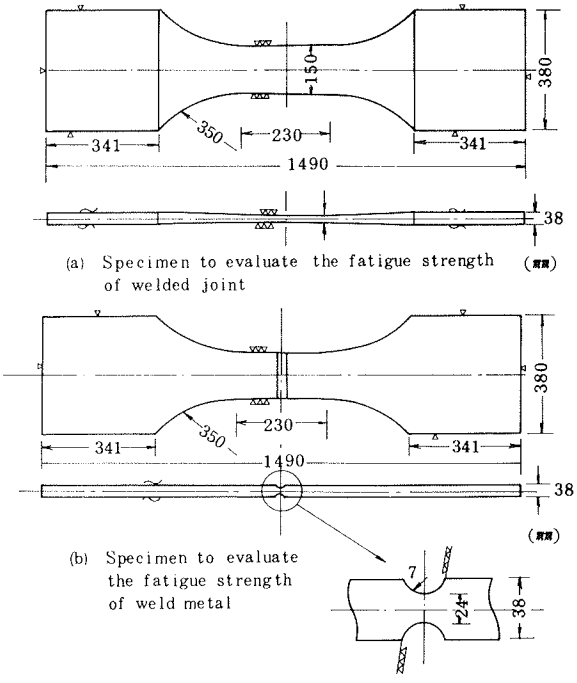

FIGURE 5 Specimens for test of fatigue strength of welded joint.

TABLE 4 Stress Range and Number of Cycles

Test specimen	Stress range (kgf/mm^2)	Number of cycles n	Fatigue damage n/Nf
re-welded joint	40	2.0×10^5	0.30
re-weld metal	35	1.0×10^5	0.34

Nf : Number of cycles to failure

TEST RESULTS

Fillet Welding with Tensile-Stressed Specimens

No weld cracks occurred, but a few pinholes, detected by magnetic particle test, and a few blowholes at the weld toe were found. Maximum stresses, $(S_y)_{max}$, in the load axis were almost equal to yield stress of the base metal for both perpendicular and parallel weld cases.

Residual stress, $(S_y)_{max}$, in the load axis is shown in Figure 6. These values are lower than 8 kgf/mm^2 for both cases. The deformations, due to the influence of welding and tensile stress, $0.8\sigma_{all}$ and σ_{all}, are less than 0.87 mm for a single weld line (Table 5).

Test of Fillet Welding Under the Influence of Vibration

In Figure 7 the results of visual examination are shown. Undercuts, leg length, and throat depth of the fillet weld for both vertical up- and vertical down-welding conditions are shown. Unacceptable defects are indicated by a black portion of a circle.

The interpretation of the results of the visual examination is based on the provisions of Japan Road Association (JRA) specifications (1). As shown in Figure 7, poor bead shapes, especially on the undercuts, occurred at a frequency of 3 Hz for vertical up-welding. The effect of in-plane vibration on bead shape is more significant than that of out-of-plane vibration. It is assumed that the specimen vibrates with large displacement amplitude at this frequency and that weaving is difficult for in-plane vibration. However, the vibration did not affect the leg length or the throat depth of the fillet welding. In the case of the vertical down-welding test conducted only for in-plane vibrations, the bead shapes were in the acceptable range. In the overhead welding condition, there were undercuts at a frequency of 3 Hz.

Blowholes were detected by the X-ray test. Results of the evaluation of vertical up-welding are shown in Figure 8. The figure shows blowholes at a frequency of 3 Hz and 5 Vs or more displacement range. No blowholes were observed in the case of vertical down-welding.

In Figure 9 typical photographs of the weld zone are shown for different test conditions. The first crystal structures with round shapes occur at vibration frequencies of 30 Hz or more.

Figure 10 shows the relationship between the tensile strength of the joint connected by groove weld-

TABLE 5 Results of Test of Welding Under Stress

Specimen	Steel grade	Electrode	Thickness	Load (ton) (Stress) (kgf/mm^2) Initiation	Load (ton) (Stress) (kgf/mm^2) Maximum	Deformation (mm) Weld Line (1)	Deformation (mm) Weld Line (2)	Direction of weld line	Crack
V-1-C	SM50	LBM-52	9	85 (9.4)	21.7 (24.1)	0.17	0.40	Perpendicular	NO
V-2-C	SM50	LBM-52	9	13.7 (15.2)	258 (28.7)	0.31	0.68	Ditto	Ditto
V-3-C	SM50	LB-47A	30	57.3 (19.1)	828 (27.6)	0.37	0.55	Ditto	Ditto
V-4-C	SM58Q	LB-47A	9	18.1 (20.1)	33.6 (37.3)	0.36	0.73	Ditto	Ditto
V-5-C	SM58Q	LB-47A	30	782 (26.1)	1050 (35.0)	0.51	0.71	Ditto	Ditto
P-1-C	SM50	LBM-52	9	133 (14.8)	3342 (38.0)	0.26	0.75	Parallel	Ditto
P-2-C	SM50	LB-47A	30	57.3 (19.1)	90.0 (30.0)	0.36	0.55	Ditto	Ditto
P-3-C	SM58Q	LB-47A	9	182 (20.2)	4450 (500)	0.36	0.87	Ditto	Ditto
P-4-C	SM58Q	LB-47A	30	780 (26.0)	116.7 (38.9)	0.51	0.70	Ditto	Ditto

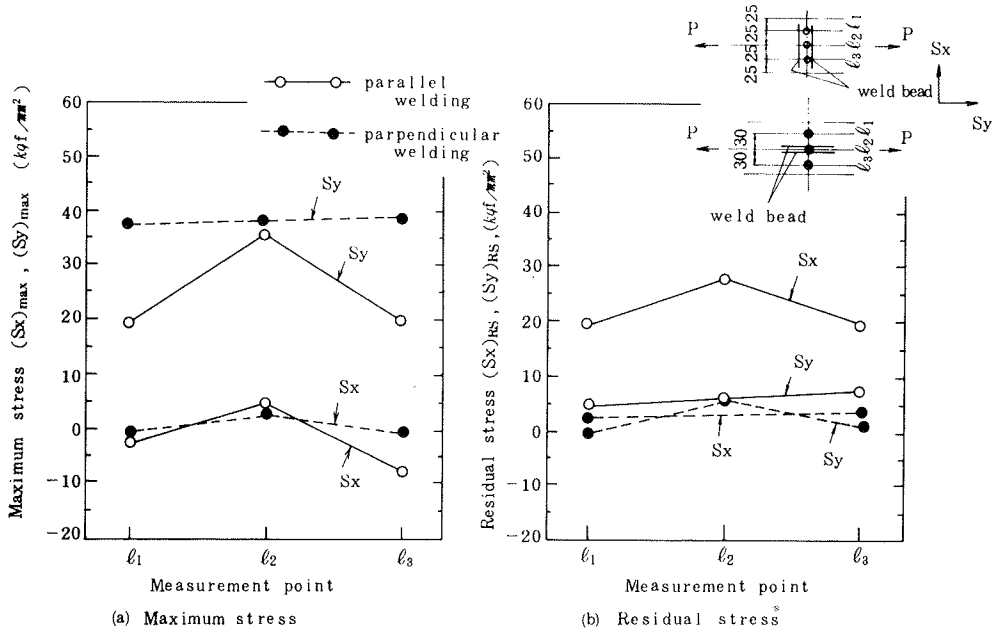

FIGURE 6 Maximum stress and residual stress of weld zone under stress.

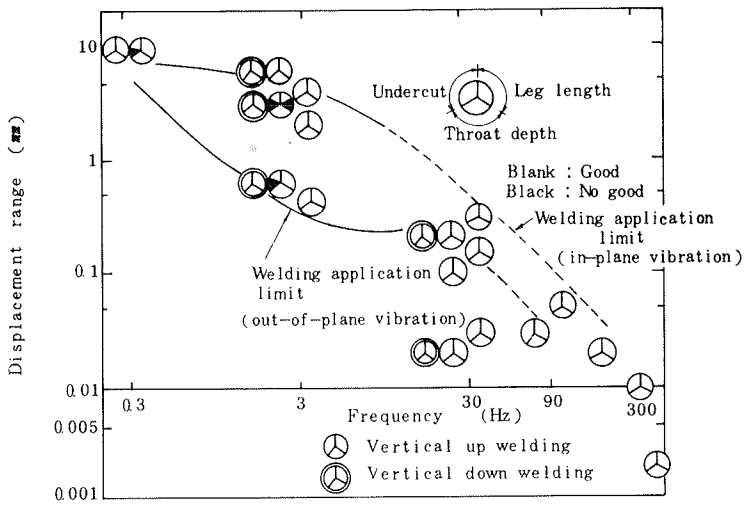

FIGURE 7 Visual examination results of test of welding under vibration.

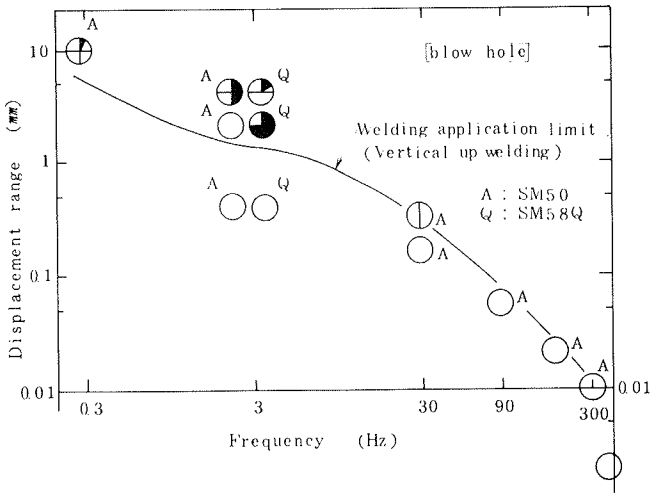

FIGURE 8 X-ray test result for welding under out-of-plane vibration.

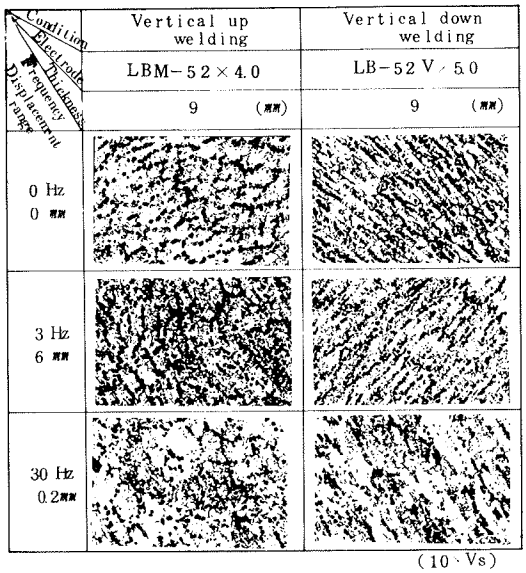

FIGURE 9 Microstructures of weld metal under vibration.

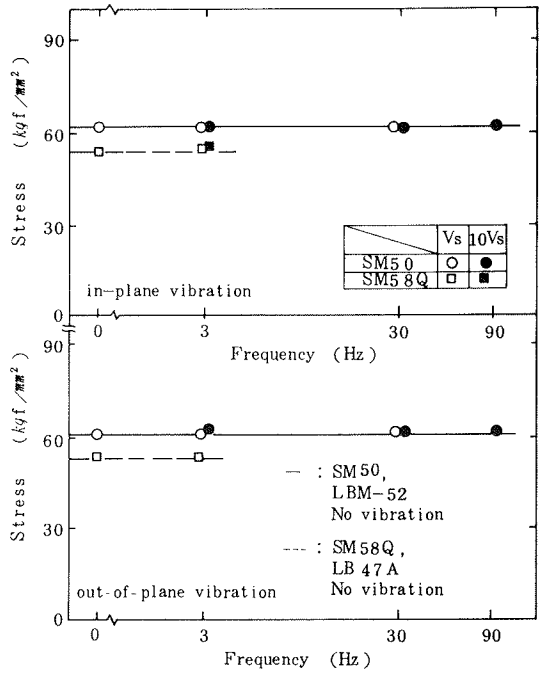

FIGURE 10 Tensile strength of groove welding joints under vibration.

ing and the frequencies of the vibration. The tensile strength of the welded joints is not influenced by vibration. There is a slight decrease in charpy impact at 3 Hz and 10 Vs vibration. The tensile strength of the joint welded with a super low hydrogen-low strength electrode, LB-47A, was lower than that of base metal, SM58Q.

In addition to the laboratory tests, field tests were carried out on a plate girder bridge with traffic-induced vibration. Three fillet test specimens (Figure 3) were welded to the plate girder. In spite of slightly poor bead shapes, weld defects were not detected and the strength of those fillet welded joints was in the acceptable range.

Fatigue Strength Test of Repaired Weld Joints

Stress number (S-N) lines for the fatigue strength test are shown in Figure 11. This figure illus-

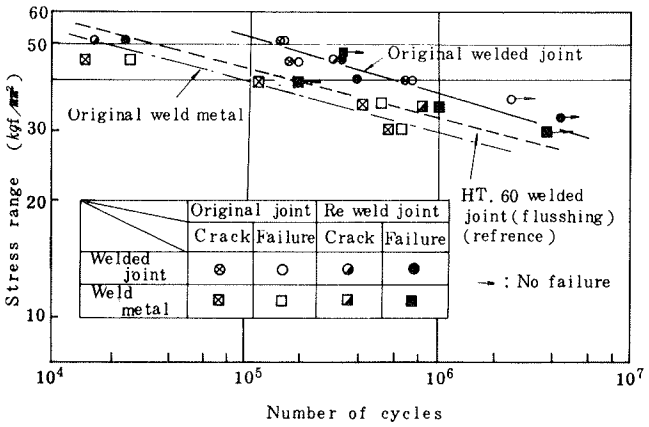

FIGURE 11 Fatigue strength test results.

trates the relationship among the applied stress range, $\Delta\sigma$, the number of cycles at the initiation of the crack, Nc, and the number of cycles at failure, Nf. Two straight S-N lines for the original welded joints and the weld metal can be approximately expressed as

$$Nf \cdot \Delta\sigma^{7.74} = 1.65 \times 10^{18} \quad (2)$$

$$Nf \cdot \Delta\sigma^{7.92} = 4.96 \times 10^{17} \quad (3)$$

The fatigue strength of the rewelded joint is almost equal to that of the original welded specimen, except in the case of the specimen for $\Delta\sigma$ = 50 kgf/mm². In the case of $\Delta\sigma$ = 50 kgf/mm², the fatigue strength was decreased by a weld defect (4 mm x 1 mm slag inclusion). The fatigue strength of repaired weld metal specimens is not lower than that of the original weld metal specimens.

SUMMARY AND DISCUSSION

Fillet Welding Under the Influence of Tensile Stresses

The influence of low tensile stresses on weld defects is almost negligible. Maximum stresses, $(S_y)_{max}$, approach the yield stress of the base metal, and the maximum residual stress is lower than 8 kgf/mm². Elongation of welding deformation is affected by tensile stresses, but deformation of this magnitude is not thought to cause problems in practical use. It is concluded from these results that fillet welding is applicable to repair work done under the influence of tensile stresses.

Fillet Welding Under the Influence of Compressive Stresses

Although a test for this condition was not conducted, it is assumed that welding deformation under compressive stresses will be magnified by shrinkages during the heat input and solidification process. Such deformation and welding heat will decrease the buckling strength of members under compressive stresses. These problems are being studied.

Fillet Welding Under the Influence of Vibration

For the web plate of the plate girder, vertical up- and vertical down-welding tests were conducted. In the case of vertical up-welding, blowholes that lower the strength of joints did not occur within the vibration range of 5 Vs, although bead shapes, especially undercuts, were slightly affected by vibration. In the case of vertical down-welding, bead shapes and blowholes were in acceptable ranges. The application limit of vertical welding is shown in Figures 7 and 8.

It is concluded that fillet welding can be used to repair web plates under the influence of vibration if visual examinations and the correction of defects are done carefully.

In the test of the fillet welding on the flange plate, blowholes were not detected although the possibility of undercuts exists. Fillet welding can be used in the repair of flanges under the influence of vibrations if visual examination and correction of defects are done carefully. It is noted that the leg length and the throat thickness of fillet welds have to be increased to give an equivalent strength to connections if it is necessary to use an electrode, such as an LB-47A, the strength of which is lower than that of the base metal.

Repaired Weld Joints

Recovery of fatigue strength to the original level in fatigue-damaged joints can be achieved by the butt rewelding method although the S-N data presented are based on only a few tests. The combined effect of the removal of the fatigue-damaged metal by gouging and the reheating of the weld metal is thought to be the main reason for this recovery.

CONCLUSION

The series of tests reported in this paper highlighted the importance of welding conditions and weldability considerations, limitations, and cautions for field weld repairs. It can be concluded that field weld repair is applicable to steel bridges, except in highly compressed areas, if there is sufficient assessment of the welding condition, inspection, and removal of defects.

RECOMMENDED PROCEDURE FOR FIELD WELD REPAIR

To secure the necessary quality of repair, field welding should be carefully done following the procedures given hereafter in addition to the provisions of the existing JRA specifications for the construction of new bridges.

1. Stresses of the bridge to be repaired should be checked and vibration should be measured and assessed.
2. A welding procedure test should be done using specimens attached to the actual bridge and under the same conditions as those under which actual repair work will be done. The same skilled welders should be employed for the test and the actual repair work.
3. Scaffolds for field weldings should be stiff enough to prevent the scaffolds from vibrating with a large amplitude.
4. Visual examination and correction of defects should be done carefully.
5. Bead shapes should be smoothed by grinding after welding to minimize stress concentration.

The Hanshin Expressway Public Corporation has recently published a manual for the repair of steel highway bridges (2) that includes field weld repair provisions based on these recommendations. The man-

ual has been successfully followed in repairing damaged bridges of the Hanshin Expressway.

ACKNOWLEDGMENT

The authors would like to thank many colleagues with whom they have discussed these tests, and they will be pleased if this paper is helpful to people concerned with bridge repair.

REFERENCES

1. Specification for Highway Bridges, Part II. Japan Road Association, Tokyo, Japan, 1980.
2. Manual for Repair of Steel Highway Bridges. Hanshin Expressway Public Corporation, Kobe, Japan, 1984.

Publication of this paper sponsored by Committee on Fabrication and Inspection of Metal Structures.

Scale-Model Tests for Full-Depth Precast Concrete Panel-Decked Composite Bridge Span

MRINMAY BISWAS, ROBERTO A. OSEGUEDA, and JAMES S. NOEL

ABSTRACT

The Texas Transportation Institute, under the joint sponsorship of the Texas State Department of Highways and Public Transportation and the FHWA, has undertaken a multiyear research program to investigate the strength and structural performance of a bridge deck system using full-depth precast concrete slab panel modules supported on steel stringers. The primary objective of the study is to evaluate the full range of behavior of a composite bridge deck system that uses epoxy mortar and shear studs as joint material for a modular construction using full-depth, full-width precast concrete panels with block-outs. Understanding this behavior would facilitate the use of such a method for rapid bridge deck construction and rehabilitation. The first phase of this program, a series of static load tests on a one-third scale laboratory model, has recently been completed. The design and detailed construction of the scale model, the details and results of the load tests, and the evaluation of the results are presented in this paper. The results indicate that, within the elastic stress range, the construction system described here would develop composite action in a satisfactory manner.

Use of full-depth precast concrete panels is a viable method of bridge deck construction and replacement. Such a method has been used since the early 1960s. More than a dozen transportation agencies have built at least twenty-five bridges using such a method. Many of the projects were for rehabilitation, and some were new constructions. Since 1973 many of these bridges have been constructed to provide composite action. Composite action is afforded, typically, by the use of mechanical shear connectors; or structural mortar based on epoxy, cement, or polymer; or both connectors and mortar. Except for some scattered and minor nonstructural failures, all the bridges are reported to be performing well.

In the case of noncomposite construction, the structural behavior of a span is not greatly dependent on the precast panel decks, although some incidental development of composite action has been reported. In the case of composite construction, on the other hand, structural behavior would be dependent primarily on the performance of the separate components as well as on that of the system as a whole.

Attempts to investigate structural behavior and strength of such construction have been rare. Because the rehabilitation and construction of structures on existing highways are done under extremely restrictive tactical constraints, a reluctance to engage in such research and investigation involving a bridge pressed for service is understandable. Because of the significance of such an investigation, the Texas State Department of Highways and Public Transportation, jointly with FHWA, has undertaken a research program conducted by the Texas Transportation Institute, Texas A&M University, involving laboratory tests, prototype construction, and subsequent tests of the prototype under field conditions. The first phase of this program, the design and construction of a one-third scale laboratory model and static load tests, has recently been completed. The progress and results of this research are described.

DESIGN PROTOTYPE

To establish a basis for design of the model, a typical design of a two-lane, 60-ft nominal span bridge was selected from the Standard Drawings of Steel I-Beam Bridges of the Texas Highway Department (1). A typical cross section is shown in Figure 1(a). The stringers are old standard 36WF150 rolled sections, spaced 8 ft center to center. One signif-

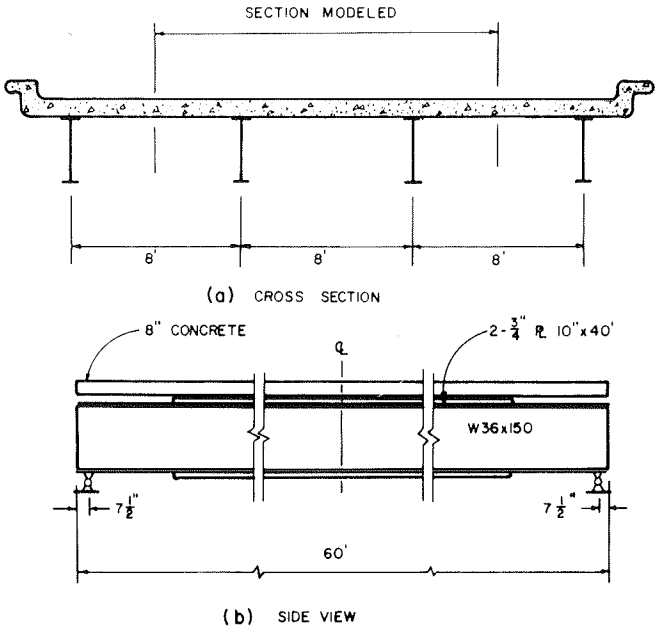

FIGURE 1 Schematic views of the prototype bridge (1).

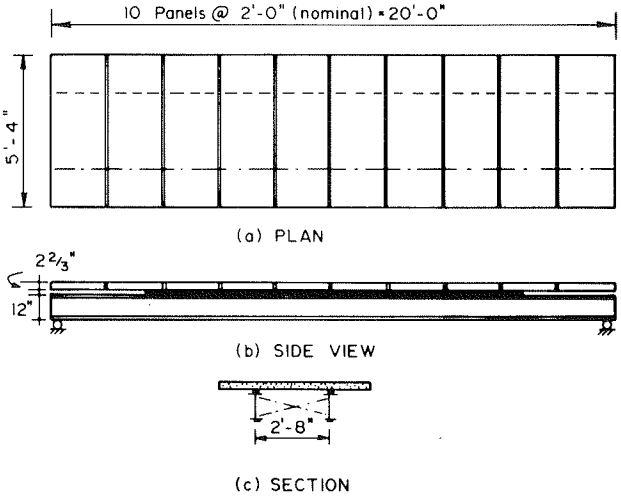

FIGURE 2 Layout of one-third scale model.

icant feature is that welded cover plates, 3/4 in. thick, 10 in. wide, and 40 ft long, were used top and bottom.

It was assumed that the existing deck of such a bridge would be replaced by a series of full-depth and full-width, 8-in.-thick, precast panels, typically 6 ft long. Standard welded stud shear connectors and epoxy mortars would be used (2). The average nominal gap between the top of the stringer and the bottom of the precast panel would be 3/4 in. A side view of the prototype stringer and replacement panel is shown in Figure 1(b). It was further assumed that an isotropic reinforcement system consisting of same size bars, spaced equally both ways top and bottom, would be used for the precast slabs. Such reinforcement for cast-in-place decks is specified by the Ontario Bridge Design Code (3) and has been used experimentally by the New York State Department of Transportation (4).

MODEL DESIGN AND COMPONENT CONSTRUCTION

General Considerations

After consideration of the facilities available and review of the experience with models at other installations, a one-third scale was selected. Dead load and mass density effects were not included because the composite action is usually and primarily engaged to resist live loads only. This greatly simplified the design and loading scheme of the model. Necessary dimensional analyses were done to simulate the structural mechanics parameters in relation to live load only (5).

A 16-ft typical width of the prototype, including two interior stringers, was modeled. It was considered important to physically include cover plates in the model to simulate a realistic construction situation. A schematic layout of the model is shown in Figure 2. The values of sectional property parameters of the prototype, an ideal one-third scale model, and the calculated values of the actual model design are given in Table 1.

TABLE 1 Composite Sectional Properties of Prototype, a One-Third Ideal Model, and the One-Third Design Model: Middle and End Sections

Section	Composite Sectional Parameter	Prototype	1/3 Ideal Model	1/3 Design Model
Midsection	I (in.^{4})	34,370	424.32	424.06
	Q (in.^{3})	871.32	32.27	32.55
	S_{top} (in^3)	2,878.08	106.04	105.92
	S_{bot} (in.^{3})	1,029.1	38.11	37.87
	I/Q (in.)	39.45	13.15	13.03
End section	I (in.^{4})	25,778.7	318.26	324.78
	Q (in.^{3})	713.77	26.43	27.08
	S_{top} (in.^{3})	2,453.7	90.88	91.37
	S_{bot} (in.^{3})	756.32	28.01	28.34
	I/Q (in.)	36.12	12.038	11.99

Note: I = moment of inertia, Q = horizontal shear, S = section modulus.

Model Stringers

The computed sectional properties of the stringers could ideally be obtained by welding plates cut to precise dimensions. However, a number of fabricators indicated that this would be impractical because proper alignment could not be maintained. Compromise design was reached by using W 12 x 19 beam sections modified in the following manner: Cover plates, 3/16 in. thick, 2-3/4 in. wide, and 13 ft 4 in. long, were welded top and bottom. Both sides of top and bottom flanges at each end (total of 8 locations per stringer) were coped by grinding away 3/8 in. of the edges of the last 34-1/2 in. The design of the model stringers is shown in Figure 3.

To simulate realistic construction, available standard headed studs, 1/4 in. in diameter and 2-1/2 in. long, were used. The shear studs were placed in pairs, with a lateral spacing of 1-3/4 in. and a longitudinal spacing of 6 in. center to center through the whole length of the stringer. The calculated horizontal shear strength of the system was designed to match the ultimate flexural strength of the composite model stringer when subjected to a third-point loading.

Model Precast Concrete Panel Modules

The overall dimensions of a typical, full-depth,

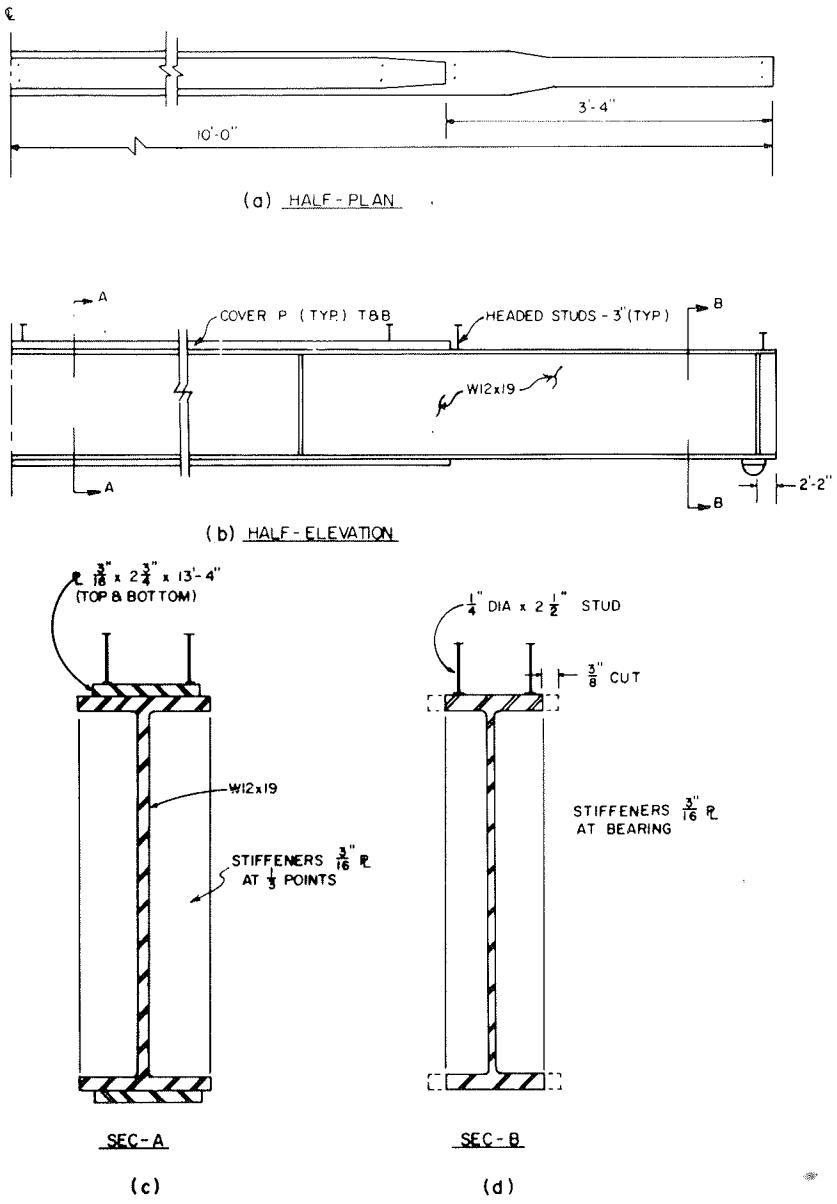

FIGURE 3 Details of model stringers.

one-third scale precast concrete model panel is shown in Figure 4(a). Ten such identical panels were used in series to form the deck of the model span. The blocked-out holes were designed and positioned to fit over the headed studs that had been previously welded on the model stringers. Figure 4(b) shows the details of the transverse joint between adjacent slabs.

Formwork

Clear acrylic sheets, 1/4 in. thick, were selected based on the experience of other researchers. The material can be cut precisely using standard woodworking equipment. It allows visual inspection of the underside and sides of the form. No bond release agent is needed. Smooth clean surfaces are obtained, which are amenable to bonding to epoxy mortar subsequently used at shear keys. The form does not absorb water, and it eliminates bleeding. The completed forms are light and can be easily handled. To facilitate vibration, the plastic formwork was placed on a plywood frame, which in turn was placed on a table-type vibrator. In addition, two pneumatic ball vibrators were used at each end of the plywood frame to assure consolidation of fresh concrete evenly throughout the form.

Reinforcing Steel

Deformed reinforcement under No. 3 bar size is not available. Welded-wire fabric (3 x 3--D3 x D3) was used as top and bottom reinforcement for the precast slab panels. This essentially eliminated all problems related to modeling the reinforcement. The mesh was equivalent to deformed 0.195-in.-diameter bars, placed at 3.0 in. center to center both ways. The steel area provided is 0.38 percent of the gross cross-sectional area of the slab. This is less than the conventional steel requirement for transverse flexure, and it slightly exceeds the usual longitudinal distribution steel requirements. The isotropic

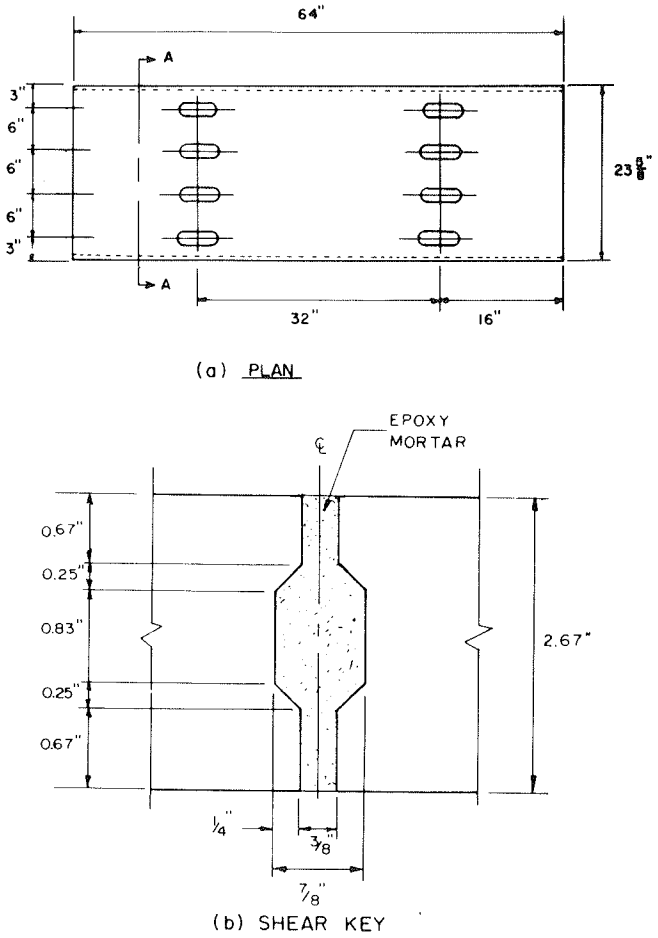

FIGURE 4 Details of model precast concrete panel.

reinforcement provided, however, exceeds the requirements of the specifications of the Ontario Highway Department and the practice of the New York State Department of Transportation.

Model Concrete and Slab Casting

To model the concrete to the extent possible, nominal 3/8-in.-max pea gravel, passed once through a 1/4-in. sieve, was chosen as the coarse aggregate and fine masonry sand was selected as the fine aggregate. The gradation of the coarse and fine aggregate was mostly within the geometrically scaled down limits of AASHTO requirements. Because of the presence of a larger amount of fines than is found in usual concrete, a larger amount of water was needed to obtain proper workability, and consequently a relatively large cement factor of 9 bags per cubic yard was needed to obtain the necessary strength.

Figure 5 shows the acrylic sheet formwork, the welded wire re-bar cage, and the block-out molds. Figure 6 shows a typical cast panel. One panel was cast every 3 days. The panels were cured using wet burlap. Test cylinders 2 in. x 4 in. and 4 in. x 8 in. were also cast. They all tested at over 6,000 psi in compression at 28 days.

Epoxy Mortar

Epoxy Compound

Texas Highway Department (THD) standard epoxy binder

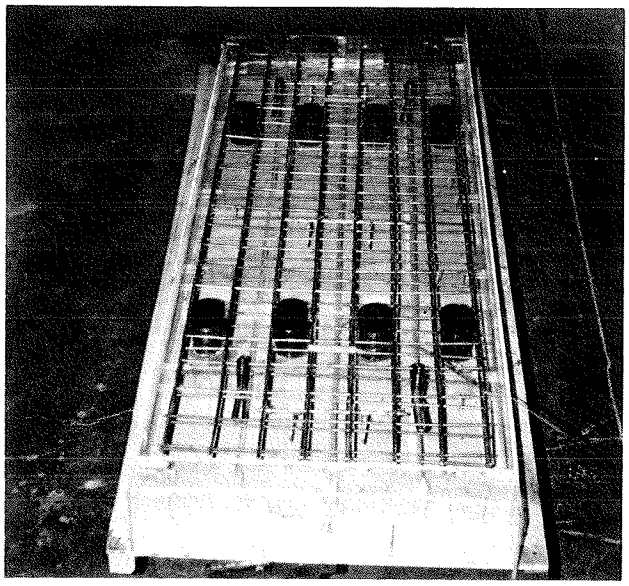

FIGURE 5 Acrylic plastic form including welded wire isotropic reinforcement and block-out molds.

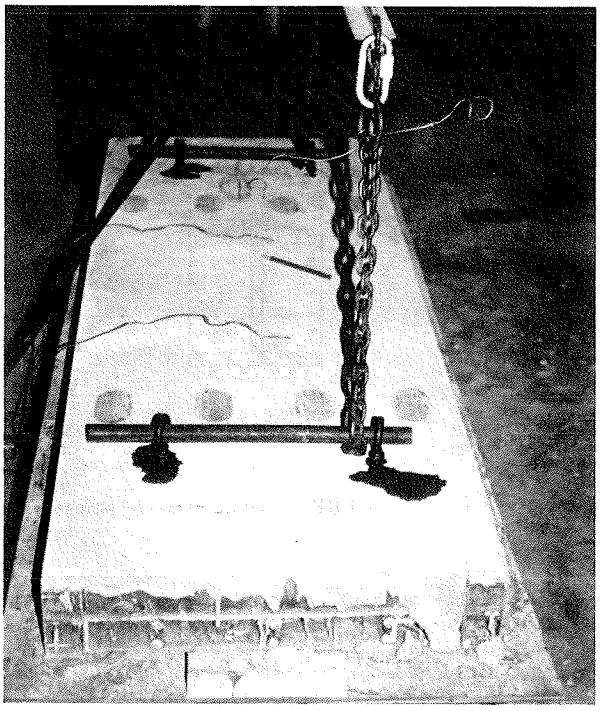

FIGURE 6 Concrete panel after casting.

B-102 was selected. It has customarily been used as a binder in a patching compound to repair existing concrete structures. It was not formally classified in accordance with the recent ASTM C-881 specifications. It, however, appeared to be similar to the ASTM type III, grade 1, class C epoxy.

Aggregate

A compromise was made between using graded silica sand and common construction sand. Commercially available sand blasting sands, namely Texblast grades No. 2, No. 3, and No. 4, were considered. On

the basis of sieve analyses, a 50-50 percent blend of Texblast No. 2 and No. 4 was selected. This blend meets the requirements of THD grade No. 1 aggregate that is specified for mixing with B-102 epoxy compound (6).

Mix Design

The design of epoxy mortar mix was based on needed workability. Trial batches were made with sand-to-epoxy weight ratios of 2.75 through 3.50 at increments of 0.25.

A sand-to-epoxy weight ratio of 3 to 1 was selected to produce a trowelable mix that would be used to cast the pockets around the pairs of shear studs. A weight ratio of 2.75 to 1 was selected to produce a flowable mix that would be poured into the transverse keyways between adjacent slab panels.

Cylindrical test specimens 2 in. x 4 in. were cast. The material exhibited consistently high strength of about 12,000 psi in compression and about 1,500 psi in (split cylinder) tension when tested at about 24 hours after casting. The average tangent modulus was about 1.4 (10^6) psi.

MODEL ASSEMBLY AND LOAD TESTS

The prefabricated components of the model were moved by truck to a site about 10 miles away for assembly and subsequent load testing. This simulated a realistic construction situation. Composite action develops in steps that follow the sequence of placement of slab panels and the subsequent grouting of various joints. The test sequences were designed to monitor such stepwise development of the composite action.

Loading System and Instrumentation

The layout of the load points and the key to locations of various sensors are shown in Figure 7.

Loading

A third-point loading was used with four identical RC-250 Blackhawk hydraulic rams. The rams were connected to a single pump through a four-way manifold. Calibrated load cells were used under each ram to monitor equal load application. Properly designed and fabricated AASHTO grade elastomeric bearing pads were placed between the loading devices and the top of the model.

Strain Gauges

Longitudinally oriented uniaxial strain gauges were placed at cross sections 1 through 8 (Figure 7) to measure flexural deformations. Surface bonded gauges were used at the flange and web of the stringers and on the underside of the concrete panels. In addition, small strain gauges were bonded to the reinforcement bars, and large capsulated concrete strain gauges, to be embedded in the precast concrete panels, were placed in the formwork. Strain gauge rosettes were placed at four sections, A through D, (Figure 7) to measure shear deformations.

Dial Indicators

A total of six dial indicators were used, placed at the quarter points on the underside of each stringer. A reference beam was used to measure relative deflection as a function of load.

Displacement Transducers

Four electrical displacement transducers were used to measure the relative horizontal slip displacement between the bottom of the precast panel and the top of the stringer. One transducer was placed 18 in. (longitudinally) away from each end of the two stringers. A typical installation is shown in Figure 8. In all there were 4 load locations and a total of 103 sensor locations.

Test 1: Noncomposite Stringer

The purpose of this test was to validate the loading system, the instrumentation system, and the calculated structural properties of the steel stringers. Only two precast panels were placed on top of the stringers, over a strip of elastomer, to provide horizontal loading planes at a suitable height under the rams. Figure 9 shows the setup of test 1. A maximum load of 5 kips per ram was applied. Figure 10 shows a flexural normal strain distribution of a typical section within the middle-third length. Figure 11 shows shear strain distribution at a section near the support. Midspan deflection as a function of load per ram is shown in Figure 12. The average flexibility is 0.094 in. per 1 kip third-point load per ram, or the average stiffness is 10.638 kips/ram/1 in. of midspan deflection.

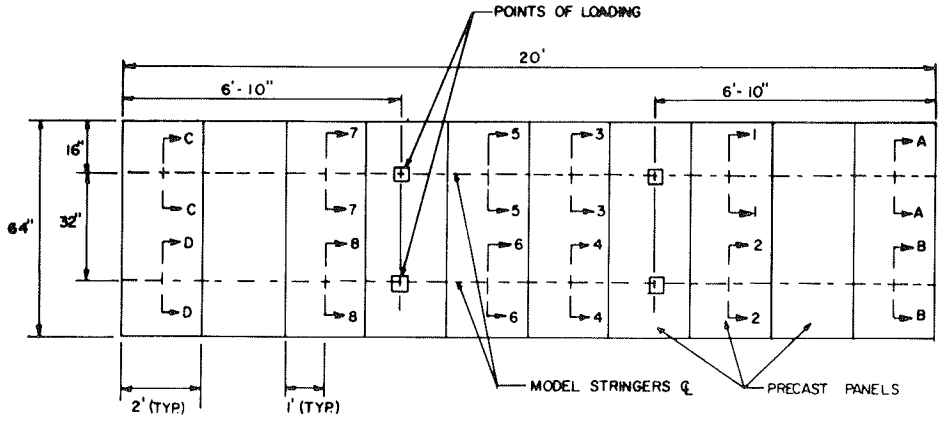

PLAN

FIGURE 7 Key to location of instrumented sections.

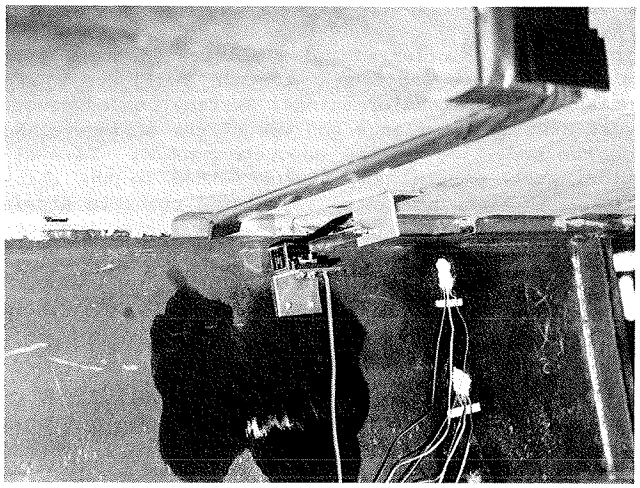

FIGURE 8 Typical displacement transducer installation to measure horizontal slip.

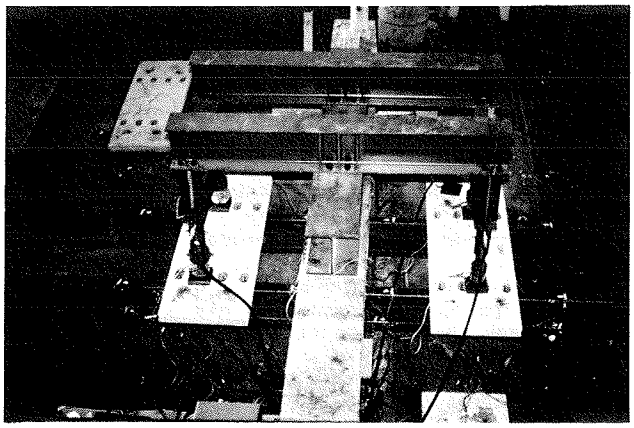

FIGURE 9 Setup for test 1 (noncomposite).

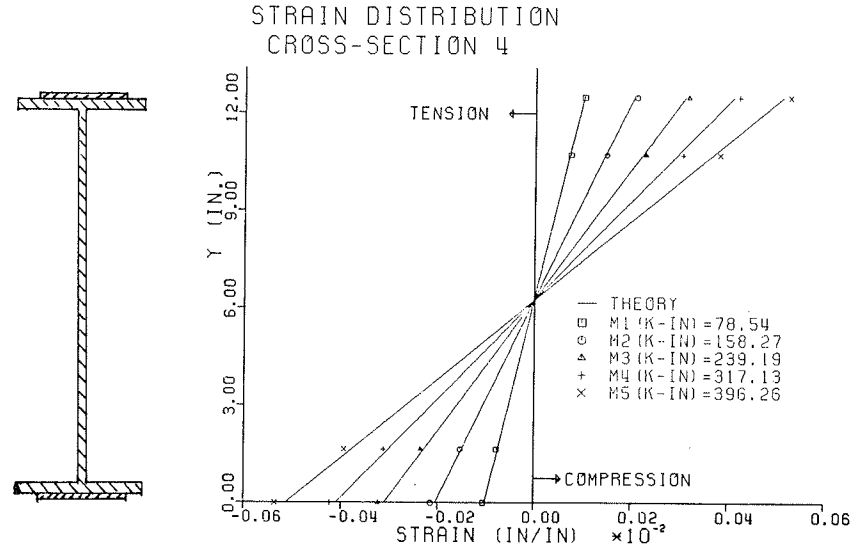

FIGURE 10 Flexural strain distribution at section 4-4: test 1.

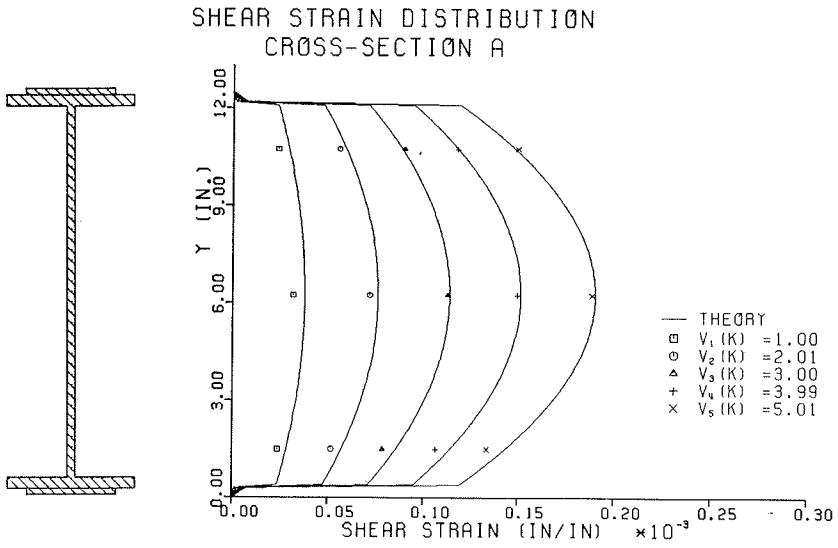

FIGURE 11 Shear strain distribution at section A-A: test 1.

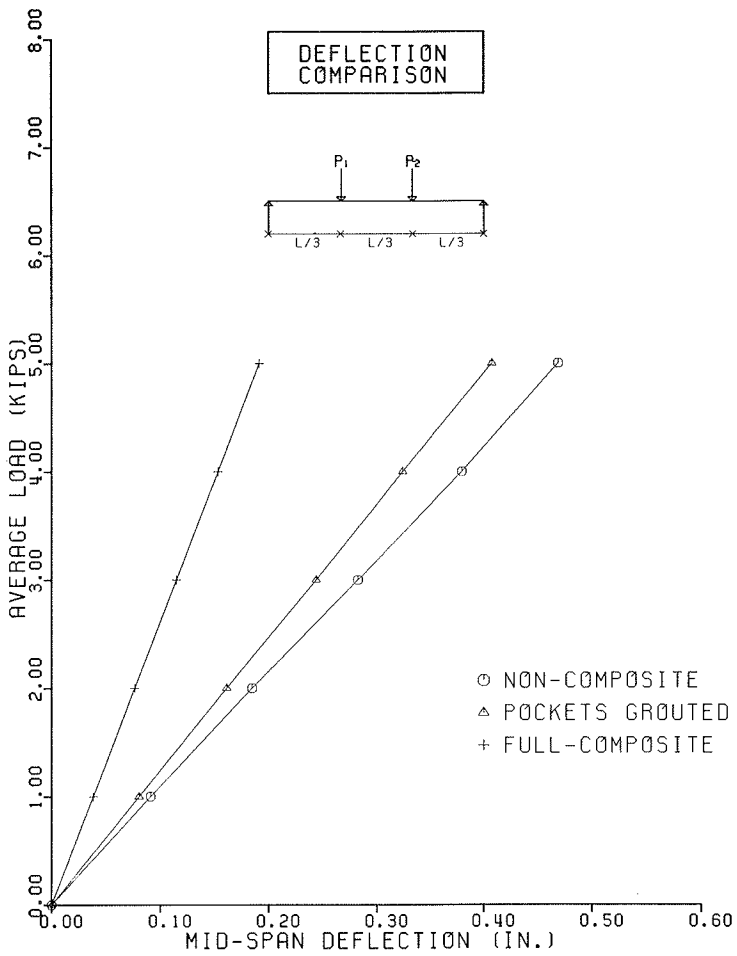

FIGURE 12 Comparison of midspan deflections for tests 1, 2, and 3.

Test 2: Partial Composite Stringer

For this test, only the pockets around each pair of shear connectors were grouted. The keyways between adjacent slab panels were left ungrouted. This simulates a situation where a bridge might need to be briefly opened to traffic in between stages of construction. To isolate the effect of incidental development of composite action due to adhesion of epoxy mortar bedding at the stringer and slab interface, the areas of the top of the flange in between the pockets were dammed using peel-back foam insulation strips. These also served as bearings for the precast panels and provided the necessary gap between the stringer and the panels. This arrangement is shown in Figure 13. The load test (Figure 14) was conducted 24 hr after grouting the pockets and a maximum load of 5 kips per ram was attained. The midspan deflection as a function of load per ram is shown in Figure 12. The average flexibility is 0.08 in. per 1 kip of third-point load per ram, or the average stiffness is 12.5 kips/ram/1 in. of midspan deflection. This indicates a 17.5 percent increase in stiffness due to grouting only the pockets.

Test 3: Full Composite Stringer

For this test all the transverse joint keyways between the adjacent slab panels were filled with a flowable epoxy mortar. Peel-back foam insulation strips, backed by 1 in. x 2 in. furring lumber, were used to seal all the potential leak locations. Figure 15 shows the deck after grouting all the joints. The load test was conducted, 24 hours after grouting of the transverse keyways, to a maximum of 6 kips per ram or a maximum total load of 24 kips for the model span. Readings were taken at intervals of 1-kip load per ram. Figure 16 shows the flexural normal strain distribution at a typical middle-third region of the span. Figure 17 shows the shear strain

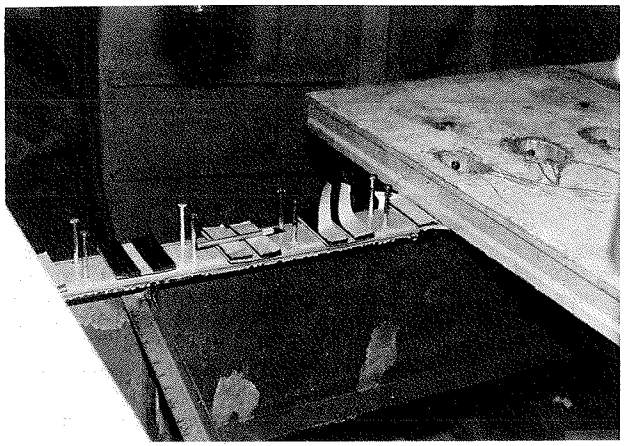

FIGURE 13 Peel-back foam insulation used to dam epoxy mortar and as bearings for precast panels.

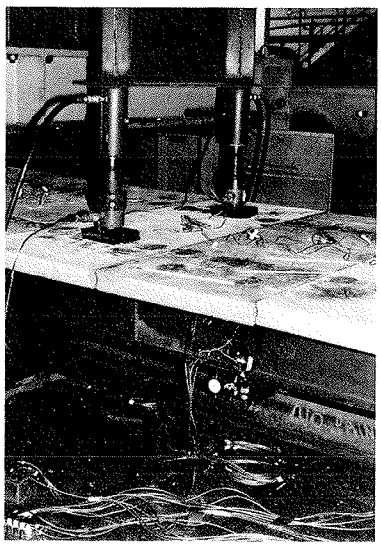

FIGURE 14 Setup for test 2 (partially composite).

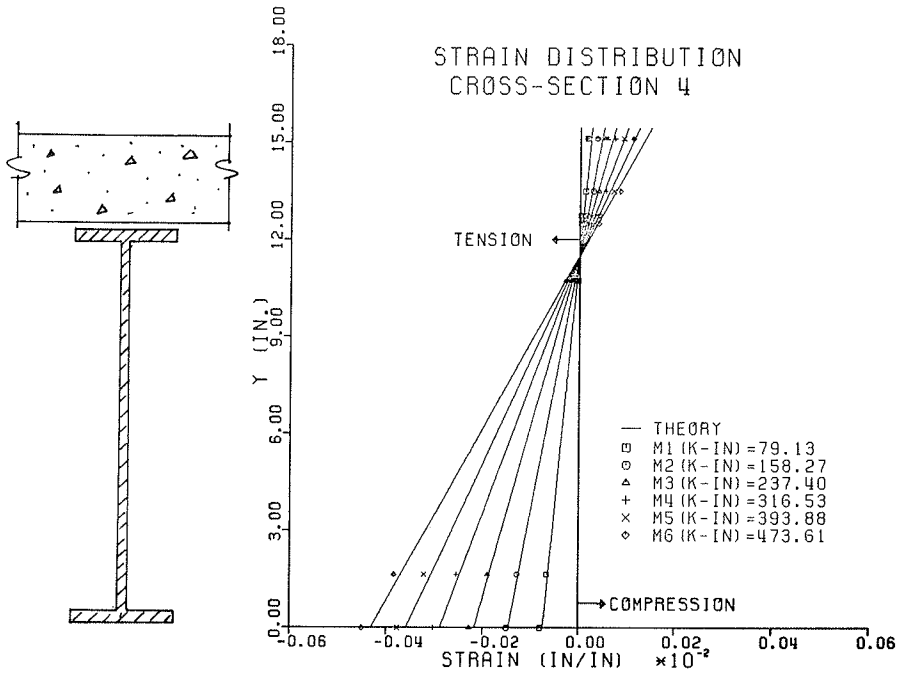

FIGURE 16 Flexural strain distribution at section 4-4: test 3.

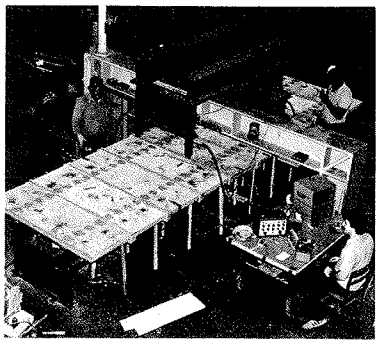

FIGURE 15 The one-third scale model after completion of all grouting before test 3 (fully composite).

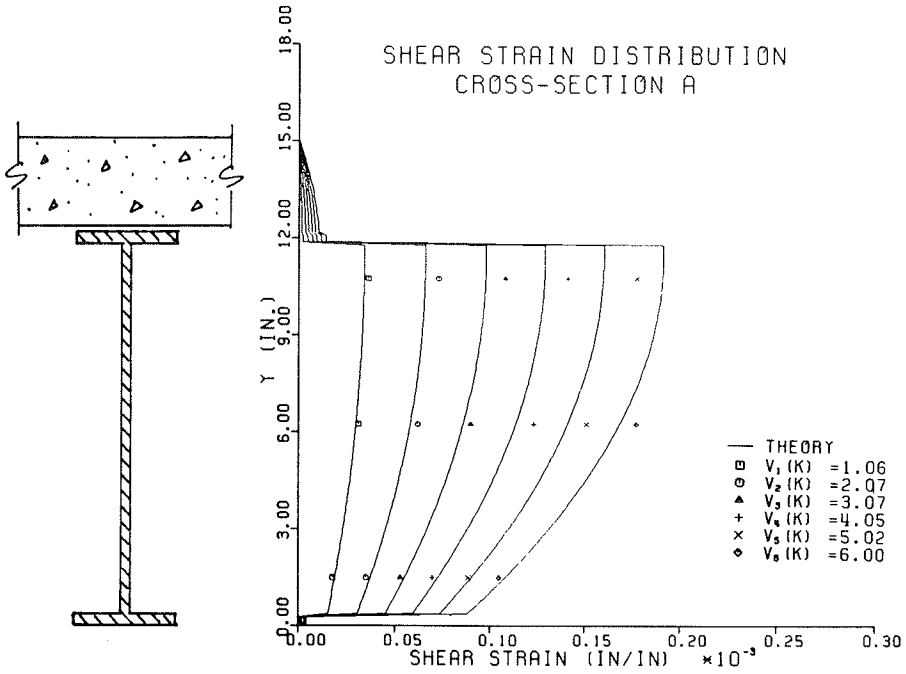

FIGURE 17 Shear strain distribution at section A-A: test 3.

distribution at a typical section near a support. The midspan deflection as a function of load per ram is shown in Figure 12. Average flexibility is 0.037 in. per 1 kip of third-point load per ram, or an average stiffness of 27 kips/ram/1 in. of midspan deflection. This is about a 155 percent increase in stiffness over the noncomposite section.

The maximum horizontal slip, measured at the displacement transducers, was about 0.001 in. A nearly linear relation between load and slip displacement was observed.

Summary of Results

The various test results have been reduced and compared with calculated theoretical values whenever possible (5). Generally good correlations have been obtained.

Figure 18 illustrates the advantages achieved by grouting the shear connectors to get composite action. A 40 percent increase in the live load carrying capacity is realized because of composite action.

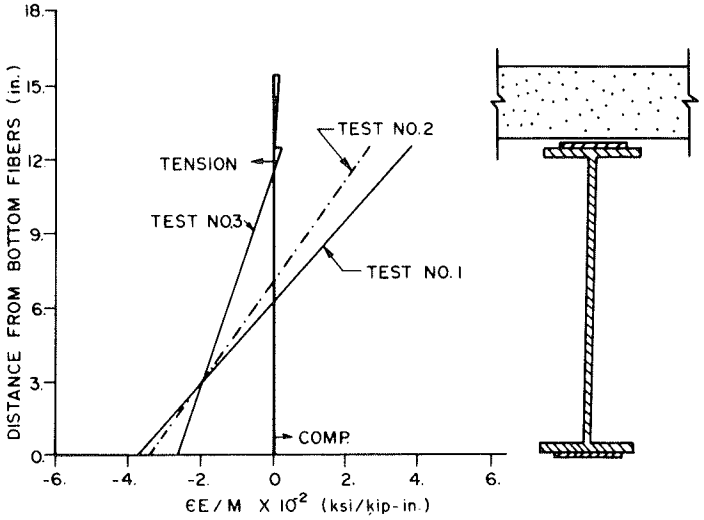

FIGURE 18 Comparison of flexural stress distribution for tests 1, 2, and 3.

Some of the results were scaled up to compare with the corresponding calculated values of the prototype. Figures 19 and 20 show the comparisons of normal strain at the bottom of a steel stringer and the (linearly projected) strain at the top of concrete, respectively. Figure 21 shows the comparison of midspan deflection.

Horizontal shear deformation or slip displacement was less than estimated. This may be due to adhesion of epoxy mortar at the shear pocket locations.

CONCLUSIONS

In concluding the first phase of this experimental investigation the maximum applied load was limited to keep the steel stresses within elastic limit without failing the horizontal shear transfer system. A stepwise development of composite action corresponding to modular construction sequence was observed. After the completion of construction using the full-depth precast panels, satisfactory composite action developed. Load-deformation relations, in general, were linear. Excellent correspondence between model behavior and calculated prototype behavior was obtained. For the prototype considered in this investigation the results indicated nearly 50 percent over load capacity com-

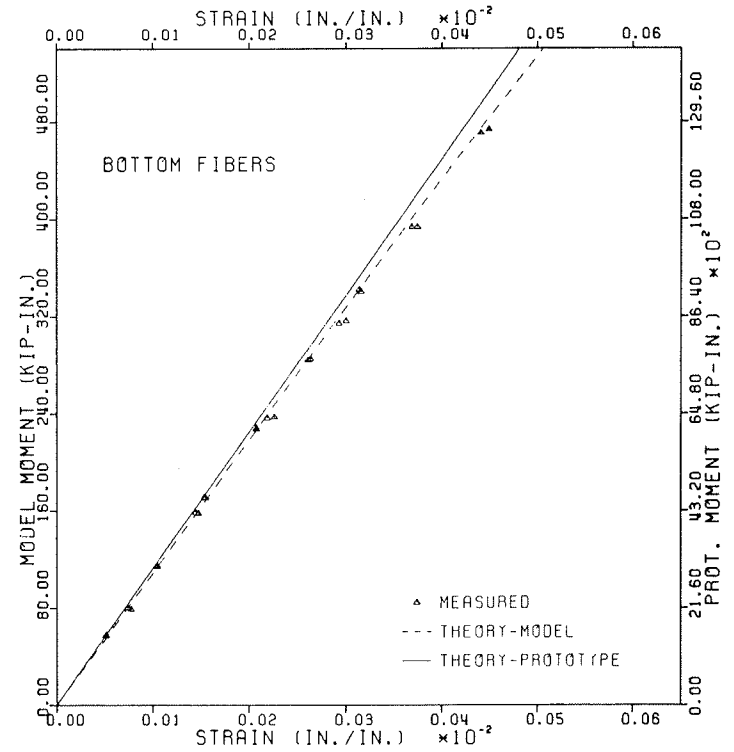

FIGURE 19 Comparison of flexural strains at the bottom fiber of composite model and prototype.

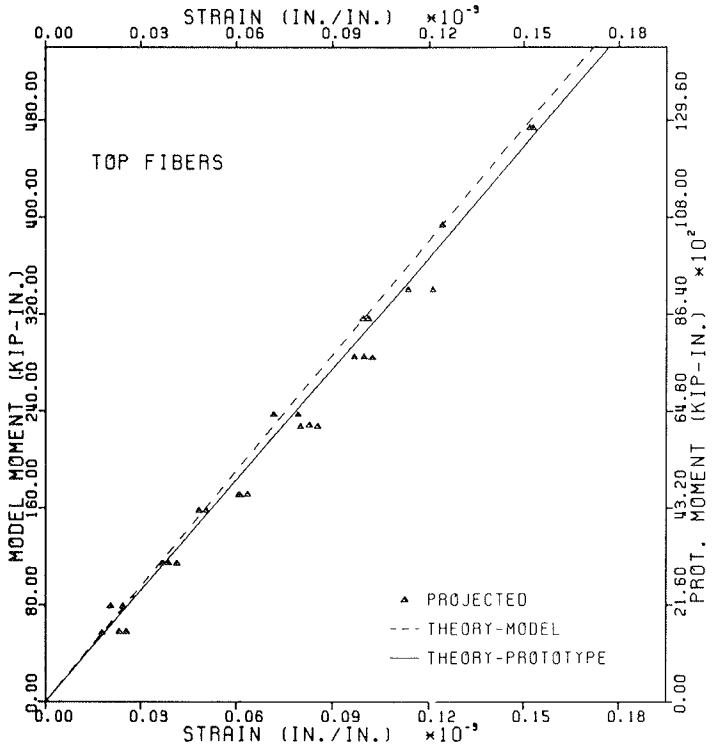

FIGURE 20 Comparison of flexural strains at top fiber of concrete deck panel of composite model and prototype.

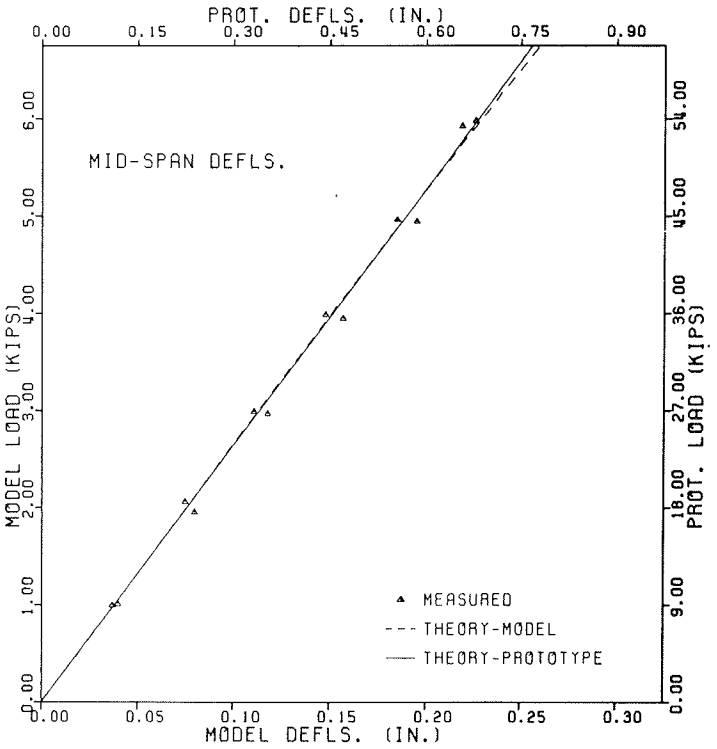

FIGURE 21 Comparison of midspan deflection of composite model and prototype.

pared to live load effects of an HS20-44 design truck.

The model is still intact and has been moved to a new testing facility about 10 miles away. Many other experiments to investigate other structural characteristics are anticipated.

ACKNOWLEDGMENT

The study is jointly supported by the Texas State Department of Highways and Public Transportation and the FHWA under Federal Contract No. HP0010(7). John Panak and R. Sanford are the contact persons for the state and federal agencies, respectively. David Beal of New York State Department of Transportation provided valuable suggestions about model construction.

REFERENCES

1. Drawing and Details for I-Beam Bridges. Revised edition. Texas Highway Department, Austin, 1962.
2. M. Biswas, J.S.B. Iffland, R.E. Schofield, and A.E. Gregory. Precast Bridge Deck Replacement Applications. In TRB Special Report 148: Bridge Replacements with Precast Concrete Panels, TRB, National Research Council, Washington, D.C., 1974.
3. Ontario Highway Bridge Design Code, Section 7. Ontario Ministry of Transportation and Communications, Toronto, Ontario, Canada, 1978.
4. D.B. Beal. Strength of Concrete Bridge Decks. Research Report 89. Engineering Research and Development Bureau, New York State Department of Transportation, Albany, 1981.
5. R.A. Osegueda. Rapid Bridge Deck Replacement. M.S. thesis. Texas A&M University, College Station, 1983.
6. Instructions for the Use of Texas Highway Department Epoxy Binder B-102. Report of the Materials and Test Division. Texas Highway Department, Austin, July 1965.

Publication of this paper sponsored by Committee on Structures Maintenance.

Ohio Turnpike Cuyahoga River Bridge Rehabilitation

WILLIAM S. FREEH

ABSTRACT

Opened to traffic in 1955, the twin two-lane Ohio Turnpike bridges over the Cuyahoga River valley span 2,650 ft and reach as high as 175 ft above the valley floor. Each bridge is comprised of four 100-ft-long girder spans and nine 250-ft-long truss spans supported by 12 reinforced concrete piers. As the use of deicing salts increased during the 1960s, so did deterioration of the concrete portions of the bridges. The original design permitted salt water to flow directly onto the surfaces of the piers. By the mid-1970s deterioration of the piers became evident. Efforts to patch the piers and divert drainage were made, but the piers had already become so saturated with chlorides that deterioration continued. In 1980, under contract to the Ohio Turnpike Commission, Howard, Needles, Tammen & Bergendoff inspected the piers and found that about 40 percent of their surface area was spalled or near spalled. Subsequently the firm recommended methods of repair to prevent recurrence of the condition, prepared plans and specifications for shotcreting (selected alternative), and provided resident construction inspection.

The Ohio Turnpike, opened to traffic in 1955, was designed and constructed before serious consideration was given to mitigating the potentially destructive effects of deicing salts. The twin, two-lane bridges over the Cuyahoga River valley are the longest on the turnpike, spanning 2,650 ft and reaching as high as 175 ft above the valley floor. Each bridge is comprised of four 100-ft-long girder spans and nine 250-ft-long truss spans supported by 12 reinforced concrete piers. The concrete decks, when originally constructed, had open curbs for drainage.

As the use of deicing salts increased during the 1960s, so did deterioration of the concrete portions of the bridges. The deck, where the reinforcing steel is close to the surface, and the edges of the deck slab, where the salt-laden water flowed through the open curbs, were the first areas to show severe spalling. The deck was patched with relative ease, but patching the vertical edges of the slab outside the railing was difficult. To prevent salt water flowing over the fascias, the open curbs were closed in 1967 and all drainage from the decks was diverted through open toothplate-type expansion joints located above all but two of the piers. Joints were located 25 ft from piers 4S and 4N to prevent drainge falling on railroad tracks passing close to these piers.

The piers had been subjected to some salt water flowing through the joints since the first use of deicing salts, but the closing of curb openings increased the flow directly onto the surfaces of the piers. By the mid-1970s there was visible deterioration of the piers (except 4S and 4N). There were some efforts by Ohio Turnpike Commission (OTC) maintenance forces in later years to patch the piers and to divert drainage away from them, but the piers had

already become so heavily saturated with chlorides that their deterioration continued.

By 1980 it was apparent that extreme measures were necessary to prevent further deterioration of the piers. The OTC selected the Howard, Needles, Tammen & Bergendoff (HNTB) Cleveland office to make a thorough inspection of the piers, recommend methods of repair to prevent recurrence of the condition, prepare plans and specifications for the repairs, and provide resident construction inspection.

With the aid of spider staging, the entire surface area of each pier (except 4S and 4N) was inspected by hammer sounding to locate delaminated areas in the apparently sound concrete. Hollow sounding areas were outlined in chalk and recorded on scale drawings of the piers as "near spall." Areas where spalling had already occurred were recorded as "spalled." The depth of most spalled areas was at the plane of the outside face of the main vertical reinforcement that ranged between 2.75 and 4 inches. Clearly, spalling and delamination were the result of expansion of the corroded reinforcement.

In the spalled areas it was observed that the horizontal tie bars were heavily corroded but that main vertical bars did not have large metal loss. Concrete was removed around a number of representative vertical bars revealing that corrosion was limited to the outside faces and that good bond remained on the inside portion of the bars. The surface area recorded as spalled or near spalled totaled about 54,000 square feet, representing approximately 40 percent of the surface area of the piers. Samples of concrete were removed from 26 locations in sound concrete and tested for salt content. Results indicated that large amounts of chloride occurred in virtually all exposed pier surfaces.

Several alternatives for repair of the piers were considered. The repair would have to provide protection against continuing deterioration resulting from the high chloride content found in much of the concrete that is sound at present. A routine repair alternative would have been to remove all deteriorated concrete down to sound concrete; replace heavily corroded reinforcement; and replace all missing concrete with conventional concrete, pneumatically placed mortar (shotcrete), or preplaced aggregate and pressure-injected grout. A latex additive could have been used to improve the bond and reduce the permeability of the shotcrete patches.

Following this type of repair, all surfaces of the piers could have been waterproofed to prevent additional water and chloride penetration. However, some moisture would still penetrate the concrete surfaces, migrate through parts of the piers, and combine with the chlorides already present in the sound concrete to cause corrosion of the reinforcement. This solution was therefore not considered sufficiently effective.

The second alternative considered was the use of cathodic protection. Cathodic protection reverses the electrochemical process of corrosion. Two organizations that specialize in cathodic protection and have installed successful systems in bridge decks were consulted. Although neither had ever attempted such a system on a vertical concrete face, both were of the opinion that a successful system could be devised.

The Harco Corporation, one of the cathodic protection specialists consulted, was hired by the OTC to do a corrosion evaluation and cathodic protection feasibility field study on sample piers. Harco prepared a report that stated that it would be feasible to protect the piers cathodically; however, for the cathodic protection to function properly, chlorides would have to be added to the new patches to closely match the chloride content of the adjoining concrete because cathodic protection is most effective in wet, chloride-laden concrete that serves as a conductor. It was also noted that if new concrete patches without chloride were placed adjacent to chloride-laden concrete and if cathodic protection were not used in these areas, a severe battery action would be created, significantly accelerating corrosion.

The method proposed for cathodically protecting the piers included removing all loose and deteriorated concrete, patching with new concrete containing chlorides, installing a system of wires on the surfaces, and then coating the surfaces of the piers with a conductive material. The recommended coating material would have been extremely high in carbonacious material and black in color. The cathodic protection alternative was rejected because it was expensive, experimental, had an obtrusive color, and would require an unknown amount of maintenance.

A third alternative, chloride removal, was considered. Two methods of removal have been successful in laboratory tests. One method uses a flushing technique with ion-free water. The other method involves an electrochemical process. The latter did show promise for bridge decks but would have been impractical for the large vertical surfaces of the piers.

Because the remaining sound concrete did contain potentially destructive amounts of chloride, the cost to remove and replace all surface concrete was investigated. It was found that a much better unit price could be obtained for removing and replacing the entire surface than for treating only the spalled and near spalled areas. Certainly the aesthetics of a patch job would have been undesirable.

HNTB's recommendation to the OTC was that all surface concrete on all piers (except piers 4S and 4N) be removed to a minimum of 1.5 in. behind the main reinforcing steel; that all surfaces be sandblasted; and that the surfaces be restored with either plain shotcrete or preplaced aggregate and pressure-injected grout, ensuring that the steel reinforcement would not be in contact with any chloride-contaminated concrete. To maintain the structural integrity of the piers it would be necessary to design a sequence of removal and replacement. The OTC accepted the recommendation and authorized HNTB to prepare plans and specifications.

It has been the experience of HNTB that some repair projects using shotcrete have not given good long-term results. For this project the objective was to achieve a repair that would last 50 years or more, and because this project would be one of the largest such pier repair projects ever undertaken, HNTB, with concurrence of the OTC, engaged the services of Thomas J. Reading, a nationally recognized authority on shotcrete. Reading has had some 30 years experience in this field, was formerly Chairman of the American Concrete Institute (ACI) Committee on Shotcrete, and is an active member of that committee. He assisted in writing the shotcrete specification, field testing and qualifying the nozzlemen, and organizing other field controls.

Plans were prepared showing the construction sequence necessary to maintain structural integrity, and bids were taken on the two recommended alternative methods of repair. Only one bid for the preplaced aggregate alternative was received, and it was significantly higher than the low bid of $2,731,176 for shotcrete repair submitted by the Pressure Concrete Construction Company. Pressure Concrete was awarded the contract and the project was begun on May 17, 1982.

Type 1A cement was specified. It was supplied in tank trucks for all piers east of the Cuyahoga River by the Dundee Cement Company and in standard sacks for the piers west of the river by the Medusa Cement Company. The fine aggregate, a natural sand, had to meet the requirements of the ACI specifications. Samples were taken for testing from all stockpiles in the supplier's yard and again at the site. Moisture content was frequently checked and was usually between 3.5 and 4.5 percent. The sand was covered to protect it from rain because an increase in moisture content would hamper pumping the sand-cement mix through the hoses. The water-cement ratio varied between 0.35 and 0.45 by weight. The mixing and curing water was hauled to the site in tank trucks from a local municipal supply.

Specifications required that cement and sand be batched by weight. The contractor was granted permission to batch volumetrically, provided periodic weight checks were made to ensure the specified ratio of cement to sand. Frequent calibration of the batching equipment--Concrete Mobiles--was found to be necessary. Periodically separate samples of cement and sand were taken and weighed just before combining. Additional tests were made to determine the ratio of cement to sand in the mixture before it was discharged into the shotcreting machine.

Dry-mix (i.e., except for the free moisture in the sand, all mixing water was added at the nozzle) shotcreting equipment was used. Shooting equipment consisted of four Jetcreters supplemented by one Micon and one Maynedier gun. The guns required frequent maintenance mainly because of wear. An ample supply of compressed air was provided with pressures as high as 110 psi at the gun. Air pressures at the nozzle were estimated at about 80 psi for most applications.

The shooting of test panels was required before shotcrete was applied to the structure to establish the mix proportions and qualify the nozzlemen. Although all of the nozzlemen had had prior experience, each was required to demonstrate his ability to apply shotcrete of the required quality. The test panels were 3 ft square at the back with sides flared out at a 60-degree angle. To simulate actual project conditions, the thickness of the panels and the location and size of reinforcing bars and wire mesh were the same as in the structure.

A 28-day strength of 4,200 psi on cores taken from the preconstruction panels was required--20 percent more than the 3,500 psi required in control test panels taken during construction. The panels were also required to be substantially free from lenses and sand pockets and have good bond of the shotcrete to the reinforcement. Because the reinforcing bars were as large as No. 11 and as closely spaced as 8 in. (5 in. at laps) some difficulty in obtaining sound shotcrete was anticipated.

The first series of panels was rejected because of low strength, attributable to insufficient cement resulting from improper batching. Several nozzlemen were disqualified because of the presence of sand lenses and pockets behind the reinforcing bars of their test panels. It was determined that a mix somewhat wetter than that used in ordinary shotcrete construction was necessary for the material to flow around the reinforcing bars without forming sand pockets. The mix proportions had to be adjusted to obtain the needed strength and to compensate for the small amount of added water. Because the mix was on the wet side, it was necessary to use a design of 1 part cement to 3.5 parts sand by weight. This generally gave strengths of about 5,000 psi. The high strength level was considered desirable because shotcrete is usually more variable than ordinary concrete. This mix design also provided good freeze-thaw resistance. Nozzlemen who failed to qualify on their first attempt were given the opportunity to gun another panel.

Field control testing was done on panels having the same size and features as those in the preconstruction tests. They were gunned on the same day as that portion of the structure that they represented, to provide an indication of the quality of shotcrete in the structure. Cores taken from the control test panels were required to have a 28-day strength of 3,500 psi. Seven-day strengths were also determined to compute the strength ratio for the two ages. This permitted an early estimate of the acceptability of the shotcrete.

A generous number of control test panels were made early in the work, but the number was reduced after the number of cores taken from the structure was sufficient to indicate a satisfactory correlation. In all, 42 control test panels were made. With few exceptions there were no problems in obtaining shotcrete of the required quality. The shotcrete was applied in two layers placed several weeks apart. The first layer was about 4.5 in. thick and encompassed the existing reinforcing bars. The second was about 2 in. thick and encompassed the newly installed wire mesh. The bottoms of the piers were usually shot first, and the remainder was done by working from the top down.

Because of the height of the piers (some 100 feet) the gunning on each pier extended over a 3- to 4-day period. This resulted in bonding problems. When working from the top down overspray and waste shotcrete diluted by water from the nozzle ran down over the piers and created a coating that could not be removed by water blast. In the early stages brooming of the surface of the first shotcrete layer was too light or was done too early (before bleeding was complete) to produce a good bonding surface. Also, a coating of the type described previously tended to develop on this surface when the second layer of shotcrete was applied.

Because these conditions could lead to poor bond, they were closely observed by the inspectors. Considerable sandblasting or material blasting (using the regular shotcrete mix with no water added at the nozzle) was required before these areas were covered with shotcrete.

After the shotcrete had hardened, each layer was sounded with a hammer to check for drummy areas. Particular attention was paid to locations where drumminess was thought to be most likely. Ten piers were found to have drummy areas, most of which were small. The total area involved was about 500 square feet, only 0.4 percent of the area of the shotcrete. Most of the drummy areas were found in the lower half of the piers where the coating problem was greatest. Virtually all drummy areas occurred between the two shotcrete layers. All drummy areas were chipped out and reshot.

The acceptability of the shotcrete was determined mainly from cores taken from the structure. These were usually taken through the two layers comprising the 6.5-in. thickness. Following the rationale in ACI Shotcrete Specification 506.2-77, it was required that the average of three 28-day tests from any day's work should not be less than 3,000 psi and no single test should be below 2,600 psi. In all about 120 cores were taken from the structure. The overall average strength exceeded 5,500 psi. The lowest average of three tests was 3,500 psi, and one core tested below the 2,600 psi requirement.

The low core had a 28-day strength of 2,215 psi. A proximate core had a 7-day strength of 2,100 psi. These cores were taken from the first layer of the top drop (the top 6 ft of the pier) of pier 8S on the south end where the quality of shotcrete was

suspect because of trouble in the batching operation. The shotcrete in the cores appeared sound to the eye. The apparent cause of the low strength was inadequate cement content resulting from faulty operation of the Concrete Mobile. The layer was sounded and no drummy areas were found. The matter was discussed with structural engineers who thought that this slight strength deficiency could be tolerated in this area where loading conditions are insignificant. The batching machine was adjusted, and cores taken from the next drop were very good. It was therefore decided to accept this drop and allow the contractor to proceed with the second shotcrete layer. The appearance of the shotcrete in the cores from the structures was very good; there were a minimum of lenses and sand pockets. Because of the favorable results obtained, the number of cores was reduced for the later piers.

HNTB is of the opinion that the aesthetics achieved by the contractor were much better than anticipated. The specifications called for a flashcoat finish, but at the suggestion of the contractor a sample with a finish struck off with a trowel was administered to a section of a pier and compared to a sample of the flashcoat. The finish with the trowel was selected. Wire guides were used on every corner and at about 3 or 4 foot centers on flat surfaces. The combination of trowel finish and wire controls produced very sharp lines much like those of a formed surface, except that there were no form marks.

In order to protect the repaired piers from new salt penetration they were treated with Chem-Trete BSM40 weatherproofing after the proper cure time had elapsed.

HNTB believes that the well-researched, clear, and strictly adhered to specifications will achieve the desired 50-year life expectancy of this major shotcrete repair project. A second rehabilitation contract for the bridges has been let. This contract will include a new deck, about 10 ft wider than the existing deck, with sealed expansion joints and a closed drainage system. The westbound bridge was rehabilitated in 1983, and the eastbound bridge is scheduled for completion in 1984.

Publication of this paper sponsored by Committee on Structures Maintenance.

Rivet Replacement Criteria

R.N. FAZIO and A.E. FAZIO

ABSTRACT

The New Jersey Transit Corporation (NJ Transit) is currently implementing a major capital improvements program to upgrade its physical plant. The rehabilitation of existing bridges is a major element of this work. The adoption of rivet replacement criteria for the various bridges programmed for rehabilitation is discussed in this paper. The rivet replacement criteria have been developed for use as a guideline by the engineer during inspection, design, and construction of the various bridges programmed for rehabilitation. The criteria developed are simple, reliable, and reproducible and provide a uniform evaluation scheme for the 600 railroad bridges found within NJ Transit's physical plant. In this paper the importance of loading conditions, type of connection, grip length, and cost as parameters to be considered in assessing if a rivet should be replaced is discussed.

The New Jersey Transit Corporation (NJ Transit) was created by the state legislature in 1979 and has been chartered to run all commuter passenger trains in the state of New Jersey. NJ Transit is the third largest commuter rail system in the nation and includes 490 route miles of track, 600 undergrade bridges, 75 locomotives, 968 passenger cars, and 142 stations. As a result of years of deferred maintenance, NJ Transit is in the process of implementing a major capital improvements program to upgrade its physical plant. The rehabilitation and replacement of various bridges within the rail system is a major element of this program. NJ Transit bridges vary in length from 5 ft to 2,926 ft and were found to have deficiencies that ranged from minor paint loss to major structural deterioration.

In this paper the adoption of uniform rivet replacement criteria for the various bridges that are programmed for rehabilitation is discussed. The criteria are developed to meet the following goals: (a) provide standard rivet replacement criteria that are simple, reliable, and reproducible for the 600 railroad bridges within NJ Transit's physical plant; (b) provide the various consulting firms, construction contractors, and in-house staff standard criteria to be used for the many bridges programmed for rehabilitation; (c) give guidance to the engineer during the inspection, design, construction, and quality control phases in selecting which rivets should be replaced; and (d) allow the development of more accurate rivet replacement costs for the bridges programmed for rehabilitation.

PROBLEM FORMULATION

Any structure consists of individual members that must be fastened together to create a structural system that is compatible with its intended service. If the connections are inadequate the structural

system will behave in such a manner that the design stresses of the individual connecting members will not be in agreement with the actual stresses experienced in the system. Therefore, no matter how efficiently the individual members are designed, proper attention must be given to the connections of the structure. The concept of a properly functioning structural system is especially important in the rehabilitation of railroad bridges.

After the bridges that were programmed for rehabilitation had been inspected it was observed that rivet head deterioration varied from zero to 100 percent. Field observations led to discussions centered around the following questions.

1. How will the riveted connections behave under the existing railroad loadings if the rivet is not able to hold the connection tight?
2. What minimum acceptable percentage of rivet head should be specified in order for the connection to remain tight?
3. Do the type of loading (i.e., direct shear, prying action) and the type of connection influence the minimum acceptable percentage of rivet head that is required for the connection to remain tight?
4. Can uniform rivet replacement criteria, which would be utilized by inspectors, design engineers, and field engineers, be established for the bridges programmed for rehabilitation?

RIVETS

The rivets found on NJ Transit's bridges were predominantly button head of a rounded shape with diameter of 1.5 D + 1/8 in., where D is the nominal diameter of the rivet shank. The height of the rivet head is 0.425 times its diameter. Rivet heads were also found to be flattened to 1/4 in., countersunk, and chipped flush as dictated by clearance requirements.

The hot riveting technique, which was used extensively, consists of heating a rivet to 1,800°F and then inserting the rivet into matching holes (sized 1/16 in. larger than the nominal diameter of the rivet) of the connecting materials. A head was formed on the protruding end of the plain shank by the rapid forging action of a pneumatic hammer. The force of the riveting causes the heated shank to expand laterally and nearly fill the hole. As the rivet contracts and squeezes together the parts being connected, a clamping action develops.

The squeezing effect actually causes some transfer by friction of stress between the materials being connected. The frictional forces developed between the materials being connected are not considered a dependable factor to be included in the calculation of the strength of the connection and were conservatively neglected in the design specifications. Yet the frictional force that is developed in the connection results from the rivet head providing the necessary restraining action to keep the joint tight. As can be seen from Figure 1(A), the equilibrium equations of statics show that the initial compressive force in the plates must equal the initial tensile force of the rivet. The initial tension in the rivet of the connection produces the compressive forces between the back of the connection and the adjacent surface. Figure 1(B) shows the approximate stress distribution developed by Rotsher that is most commonly accepted by the profession (1). This stress distribution depicts the transfer of forces that are generated on a small ring of contact between the fixed head of the rivet and the connecting steel members.

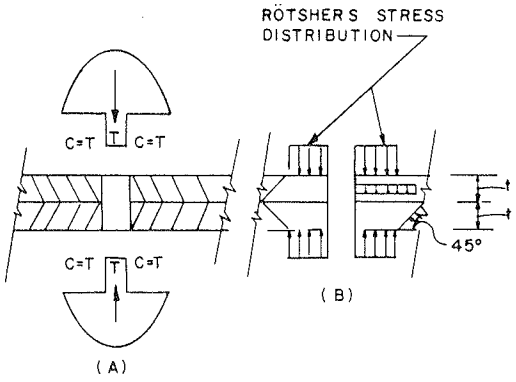

FIGURE 1 Rivet stress distribution.

LOADING CONDITIONS

Riveted connections are usually considered bearing-type joints and are designed in connection members to resist shear forces that must be transferred between the connection members. The clamping force in a rivet is difficult to control and cannot be relied on as can that of high-strength bolts. Therefore, in the analysis of a riveted connection subjected to an in-plane loading through the centroid of the rivet group, the following loading stages exist: (a) static friction prevents slip; (b) external load exceeds the frictional resistance and the joint slips until rivets are partly or all in bearing; (c) the rivet and plates deform elastically; and (d) yielding of the plates or rivets occurs until either the plate fractures or the rivet shears completely.

Three significant loading conditions exist for which the foregoing analysis is somewhat different and more complicated. These loading conditions are pure tension, combined tension and shear, and prying action.

Pure Tensile Load

When a tensile load is applied to a connection, the fastener will elongate and the precompressed members will tend to expand to their original thickness. If the plate expansion does not exceed the initial contraction of the plates, some contact pressure between the connecting members will remain, and the following relationship will hold true.

Rivet Force = Contact Forces + Tensile Load

A further increase in external tensile load will result in a decrease in member contact forces until the plates separate. When the connecting members separate, the rivet force is equal to the applied external load, and the following relationship will hold.

Rivet Force = Tensile Load

Combined Tensile and Shear Loads

Figure 2 depicts a typical girder-floor beam connection in which the rivets are subjected to combined shear and tensile forces. The vertical load being transferred tends to cause the connection to slide downward and is resisted by the shearing strength of the rivets. The downward externally applied load and upward resisting shear force of the rivets produce a couple. The moment produced is Pe. An equal and opposite couple must be produced by the tension

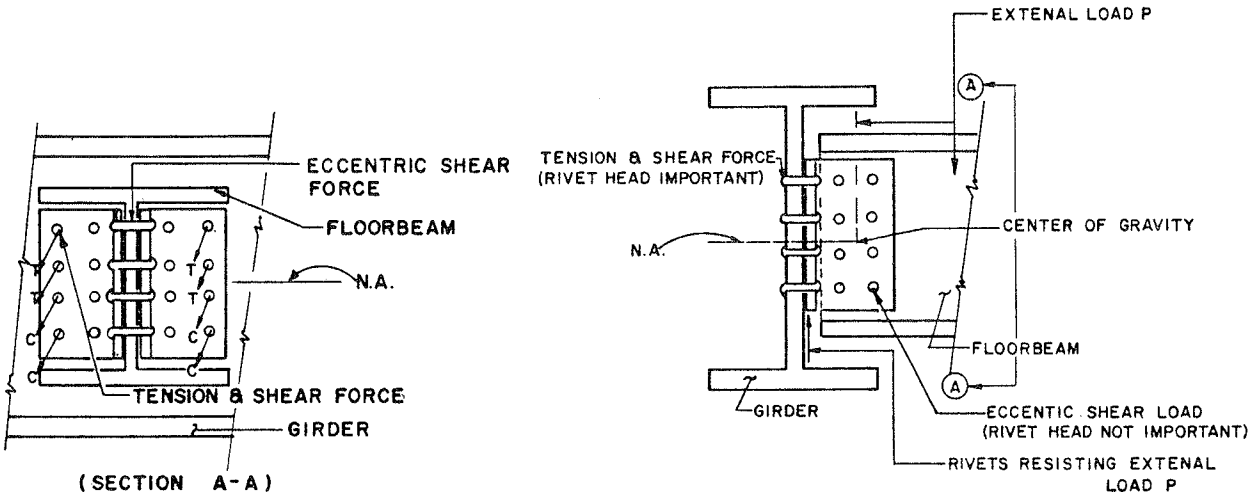

FIGURE 2 Typical girder-floor beam connection.

in the upper rivets and by the compression in the lower part of the connection. As shown in Figure 3 the stresses in the connection are assumed to vary linearly from the neutral axis. Figure 4 shows that the rivet head acts as a restraint in keeping the connecting material tight when tensile loading is experienced within the connection.

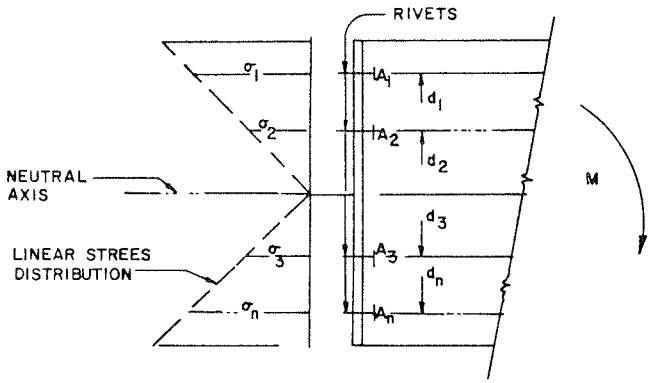

FIGURE 3 Fastener group stress distribution.

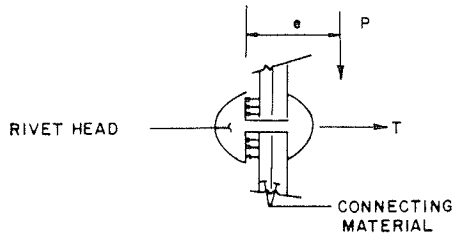

FIGURE 4 Detail of rivet connection.

Prying Action

Prying action forces develop depending on the flexural rigidity of the connection. If the connecting members are not fairly stiff, prying action forces will increase the tensile force in the rivets. Therefore, for equilibrium to exist, the total force in the rivet must equal the applied force plus the prying forces, and the useful capacity of the rivet is decreased by the prying forces developed in the connection. Therefore, depending on the relative stiffness of the rivet fasteners and the connecting material, the prying forces may be negligible or they may be a substantial portion of the total tension in the rivet.

FAILURE MODES OF RIVETED JOINTS

Failure of riveted joints occurs if the applied load exceeds the tensile capacity of the net section, the shear capacity of the rivet, or the bearing strength of the connecting material. It is assumed that the rivets are tight and that the heads are full and provide the area needed to develop a restraining force. Many of the rivets observed during bridge inspections had heads substantially reduced by corrosion. If the head of the rivet is corroded and is not able to provide the restraining action required to keep the joint tight, the rivet head should be considered in assessing whether the joint is adequate to resist the applied load.

Head Reduction

The type of connection (rigid, semirigid, or flexible joint) and the loading conditions experienced by the connection should be parameters to consider when assessing whether a rivet should be replaced because of rivet head deterioration.

In particular, it appears that reduction of the rivet head should be investigated when rivets are experiencing loading conditions of pure tension, combined shear and tension, and prying action. Thus, if the rivet is subjected to any type of tensile force, the reduction of the rivet head should be considered as an additional parameter in deciding if the rivet should be replaced.

Depending on the rotational characteristics under load, connections can be classified as simple, semirigid, and rigid. A rigid connection is one that does not rotate and has complete moment resistance; a connection that is flexible, free to rotate, and has zero moment resistance is a simple connection. A semirigid connection falls somewhere in between the rigid and flexible connection. The three classifications of joints can be characterized as follows.

- Rigid connection--resists greater than 90 percent of moment (2),

- Semirigid connection--resists 20 to 90 percent of moment (2), and
- Flexible connection--resists 0 to 20 percent of moment (2).

The type of structural connection in which the rivet head is significant is the flexible connection in which the three loading conditions discussed previously develop. A flexible connection is designed to rotate and, if the connecting angles are light connectors, the angles will deform. If the connecting angles deform, the rivets must also deform; thus it becomes apparent that the rivet head contributes to keeping the connection tight.

As illustrated in Figure 5 for the floor beam-to-stringer connection, the connecting angle deformation could exist. The applied loading tends to cause the connection to slide downward, and this tendency is resisted by the shear strength of the rivets. The heavy live loads experienced on the railroad bridges tend to rotate the connection by pulling the upper rivets away from the web by inducing a tensile force in these rivets. Thus the rivet head becomes an important parameter to investigate in assessing whether the connection is adequate when subjected to tensile force [see Figures 6(A) and 6(B)].

As shown in Figure 6(A), the rivet head acts as a restraining support that holds the joint in place as the rivet shank bends. It can be inferred that if the rivet head is 100 percent deteriorated [Figure 6(B)], the rivet connection will resist the shear force but not the tensile force (produced by the rotation of the joint) that develops from the heavy live loads experienced on railroad bridges. This logic seems to indicate that the rivet connection will fail in tension and that these stresses will be further redistributed to other rivets, causing an unbuttoning and failure of the connection. Thus, when any rivet experiences a tensile loading and the connection is not designed as a rigid connection, the rivet head should be considered as a structurally significant parameter when determining if the rivet should be replaced. A minimum acceptable percentage of rivet head should be defined to ensure that the rivet is able to resist the secondary tensile stresses produced by joint rotation.

Grip Length

Unless the connecting plates are rigid with respect to the rivets, the connection remains elastic, the load is transmitted from one plate to another, and the distribution of forces is not uniform. It must be emphasized that the longer the joint is, the greater will be the number of rows of rivets and the greater will be the proportion of the load transmitted by the outer rivets. The grip length of a rivet in the joint must be investigated to determine if the clamping force is adequate to keep the joint tight. In joints fastened with long rivets the individual plates have adjusted to the loads experienced and have assumed a curved shape within the connection. Tests on high-strength bolts have confirmed this behavior; shear tests of single bolts yield shear planes at almost 90 degrees to the bolt

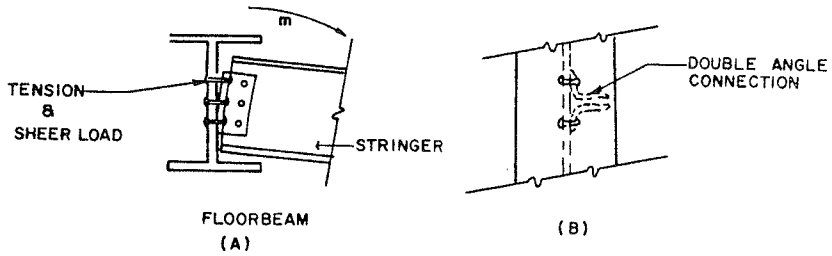

FIGURE 5 Typical deformation in floor beam-stringer connection.

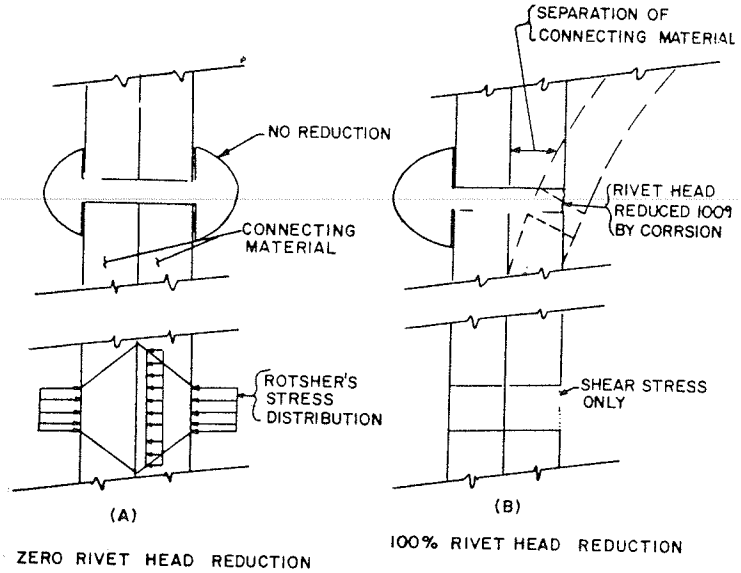

FIGURE 6 Example of reduction in rivet head.

TABLE 1 Field Report

Existing Rivet Condition	Rivet Replacement Criterion A	Rivet Replacement Criterion B	Rivet Replacement Criterion C	Rivet Replacement Criterion D
Percent of rivet head remaining	25	50	75	85
Rivets to be replaced (%)	5	10	15	20

TABLE 2 Relative Cost Values

Rivet Replacement Criterion	Unit Price ($/rivet)	Rivets to be Replaced (%)	Relative Cost Value ($)
Criterion A	60	5	300
Criterion B	60	10	600
Criterion C	60	15	900
Criterion D	60	20	1,200

by the total number of rivets to be replaced according to criteria A, B, C, and D (Table 1).

According to Table 2, rivet replacement based on criterion D will cost four times more than rivet replacement based on criterion A. Clearly, the rivet replacement criterion adopted for a particular bridge will influence rivet replacement cost.

In addition, a great variance in cost can develop if (a) the rivet replacement criteria used by the engineer in developing cost estimates are not identical to the rivet replacement criteria used by the contractor in developing the bid price or (b) each contractor in developing bid costs for rivet replacement uses different rivet replacement criteria. If standard rivet replacement criteria are incorporated in the contract documents, there should not be major variances between the engineer's estimated cost, the contractors' bids, and the actual cost of a particular bridge rehabilitation. Furthermore, as the magnitude of the job increases, so does the number of rivets to be replaced. This increases the cost of rivet replacement. For these reasons uniform rivet replacement criteria have been developed and adopted by NJ Transit for bridge rehabilitation work.

CONCLUSION

The need for and development of the uniform rivet replacement criteria adopted by NJ Transit for use in its programmed bridge rehabilitations have been discussed. In summary, it has been shown that the type of loading, type of connection, and grip length are important parameters to be considered when determining if a rivet must be replaced. The criteria developed and adopted by NJ Transit will (a) provide the various architectural and engineering firms, construction contractors, and in-house staff uniform rivet replacement criteria for the various bridge rehabilitations, (b) provide consistent and reasonable cost estimates for the various bridge rehabilitations, and (c) provide NJ Transit, for its 600 railroad bridges, standard rivet replacement criteria.

Further studies should attempt to determine the amount of rivet head reduction that would be acceptable to maintain service loads (highway, railroad). The following research should be undertaken to determine what structural impact the rivet head has in the connection.

- Empirical testing,
- Theoretical research, and
- Correlation studies of theoretical results and empirical testing results.

The results of such research should be incorporated in standard specifications such as those of the American Railway Engineering Association, the American Institute of Steel Construction, and AASHTO. This information would be beneficial to the practicing engineer tackling bridge rehabilitation problems.

REFERENCES

1. W. McGuire. Structural Analysis and Design. Prentice-Hall, Englewood Cliffs, N.J., 1968, Connections, pp. 787-1031.
2. J. McCormac. Structural Steel Design. 2nd ed. Intext Educational Publishers, New York, 1971, Riveted Connections, pp. 191-230.
3. J.W. Fisher and J.H. Struik. Guide to Design Criteria for Bolted and Riveted Joints. Wiley, New York, 1974.

Publication of this paper sponsored by Committee on Structures Maintenance.

Strengthening California's Steel Bridges by Prestressing

GUY D. MANCARTI

ABSTRACT

The Surface Transportation Assistance Act of 1982 that addresses increased truck sizes and weights has exacerbated maintenance problems of existing bridges designed to meet earlier loading criteria. In 1975 California implemented the Permit Design Live Load that allows substantial increases in live loads. Strengthening existing steel bridges on the highway system, in particular those bridges on California's State Highway Extra Legal Load network (SHELL routes), has assumed a high priority. Two steps can be involved: (a) All existing steel girder bridges are screened for potential overstress by a sophisticated computer program, CURVBRG. This program, which uses a plane grid analysis, was written at the University of California at Berkeley and adapted by the Structural Research Unit of the California Department of Transportation for use by the Office of Bridge Maintenance. For the heavier live loads, CURVBRG assesses stresses and deflections much more precisely than do usual design methods. If overstress is indicated, step (b) is implemented. (b) Longitudinal prestressing tendons are installed to enhance moment capacity in critical areas. Structural steel may be added as necessary to achieve balanced design stresses. This has been done on seven steel girder bridges to date and is planned for a dozen more. CURVBRG is described briefly, and several examples of prestressed installations are presented. Prestressing has proven to be a quick, economical, aesthetically pleasing method of strengthening steel bridges.

The Surface Transportation Assistance Act of 1982 mandated, among other things, increased truck sizes and weights. With this increase, many bridges designed by earlier live-loading standards became structurally inadequate. Several states, including California, have established even higher permit-loading criteria for special heavy-hauler routes. California's system, known as the State Highway Extra Legal Load or SHELL system, is being designed to accommodate California's maximum permit loads--trucks with up to 13 axles and gross weight of 314,000 lb (Figure 1).

Steel girder bridges, with relatively small dead-to-live load ratios, are especially affected by increases in live loads. Although California does not have a high percentage of steel bridges in its highway system, there are enough steel bridges, particularly on SHELL routes, to warrant comprehensive studies of system bridges to determine permit live-load ratings and identify bridges in need of strengthening on key routes. Several other methods have been used in unique cases, but the best developed technique thus far for increasing live-load capacity has been to strengthen steel girder bridges by prestressing.

BRIDGE INVENTORY RATING

All bridges on California's state highways have been inventoried by means of standard rating techniques

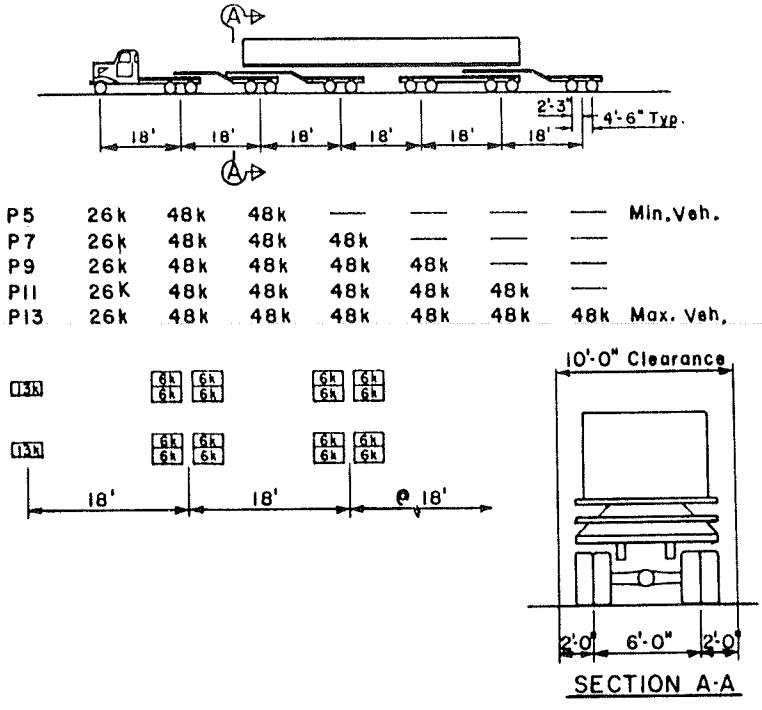

FIGURE 1 California permit loads.

to identify those with lower capacities. The computer program CURVBRG has been adapted by the Office of Bridge Maintenance for second-level analysis of more precise stresses and deflections under increased live load on bridges previously identified as overstressed.

The CURVBRG program was written in 1974 by Mondkar and Powell (1) at the University of California, Berkeley, and was modified as required for California Department of Transportation (Caltrans) computer equipment by the Structural Research Unit of the Office of Structures Design under the direction of R.E. Davis, Bridge Research Engineer. The program was introduced to the Office of Bridge Maintenance by Davis in 1977. For the benefit of engineers unfamiliar with computer technology, a second volume (2) provided annotated input forms and input and output for sample Caltrans problems.

Subsequent studies made in conjunction with field tests of instrumented structures subjected to measured loads clearly demonstrated that (a) CURVBRG could provide maximum envelope stresses at all points in a structure for any combination of loadings designated by the rater; (b) the program could readily account, with appropriate load factors, for dead loads, construction stages, arbitrary configurations of geometry and articulation, and arbitrary configurations of vehicle axles and combinations of load cases; (c) theoretical strains agreed closely with measured ones, and correlations were significantly better than those obtained by other methods; and (d) stresses obtained by the current AASHTO distribution factors were ultraconservative. For these reasons CURVBRG was adopted for day-to-day use and has been consistently demonstrating that steel girder bridges previously identified as substandard, based on current AASHTO criteria, are actually capable of carrying the new permit loadings without costly rehabilitation or replacement. Currently projected savings to the highway fund are large.

When refined analysis by CURVBRG demonstrates that bridges deemed substandard in the first-level screening have adequate load capacity to sustain permit loadings they are re-rated on the inventory and no further work is done.

Bridges found to be deficient by CURVBRG analysis are scheduled in systemwide priority for the strengthening program. Results of the detailed analyses, identifying critical areas and amounts of overstress, are made available to designers for preparation of contract plans.

STRENGTHENING BY PRESTRESSING

Steel girder structures are frequently found adequate for permit loadings in all respects except moment capacity, a deficiency susceptible to alleviation by prestressing. Compressive force is applied to tension flanges to provide a resisting moment sufficient to accommodate permit loadings. Deficiencies in negative moment areas of continuous structures may require the addition of steel to compression flanges to balance the sections. Concrete decks usually provide enough area in positive moment strengthening to keep compressive stresses within normal limits. These refinements will be illustrated in the examples.

CRITERIA FOR DESIGN

Normal prestressing criteria are used for the design of prestress tendons. Special tendon prestressing sequences are seldom required because applied forces are nominal in comparison with superstructure capacity. Special attention is paid to tendon paths, tendon encasement, and fastening devices, which are designed to match tendon ultimate values. These devices should not fail under any loading condition including seismic or accidental loading, and they are proportioned so that they will not cause failure of components of the structure to which they are attached.

Tendon paths are generally straight, although haunched girders may require angle points to align forces with girder flanges. Tendon paths must clear girder stiffeners and lateral bracing, which may require relocation or, if allowable, creation of an opening to accommodate tendons. Tendons are kept free from corrosion by encasement in galvanized pipes and grouting after tensioning. Anchorages are also sealed.

All strengthening by prestressing in California to date has employed strands, although specifications also permit use of high-strength rods. Only tendon forces and paths are shown on the plans. All prestressing systems and anchorage hardware must be tested and approved by the Caltrans Transportation Laboratory prior to installation.

DESIGN PROCESS FOR A SIMPLE SPAN

The steps of the design process are

1(a). Determine moments for applied dead load + live load + inertia (DL+LL+I) at center of span.

1(b). Calculate girder stresses.

2(a). Determine allowable girder stresses based on as-built material.

2(b). Calculate stressing force required to compensate for the difference between the allowable stresses and the DL+LL+I stresses in the tension flange. Assume an eccentricity for the stressing force that will allow adequate space for mounting the stressing anchorage brackets. Check compression flange steel and concrete stresses.

3(a). Repeat the process for other critical points within the span at flange reduction locations.

3(b). Determine location where stressing force may be terminated based on allowable unit stresses. Termination point must be between existing transverse stiffeners if anchorage brackets are mounted on the girder web.

4(a). Design anchorage brackets. Use sufficient transverse offset to clear girder stiffeners if brackets are mounted on the girder web. Check bracket size to ensure that its dimensions are consistent with the available space and the assumed stressing eccentricity.

4(b). Check the existing girder web for bearing stresses generated by the anchorage bracket.

EXAMPLES

Pit River Bridge and Overhead on I-5

One of the earliest strengthening jobs using prestressing was done in conjunction with the complete rehabilitation of the Pit River deck truss over Shasta Lake. Constructed to 1941 standards, the structure served for many years until wear and tear due to increasing truck traffic and deterioration due to salts necessitated complete deck replacement. Addition of a safety median barrier, replacement of portions of deck previously widened with lightweight concrete, addition of a deck seal and wearing course, and an increase in roadway width to accommodate exterior safety barriers required strengthening the stringer system and the cantilevered portions of floor beams.

Stringers were strengthened by prestressing tendons, affixed as shown in Figure 2, to reduce tensile stresses in negative moment areas over the

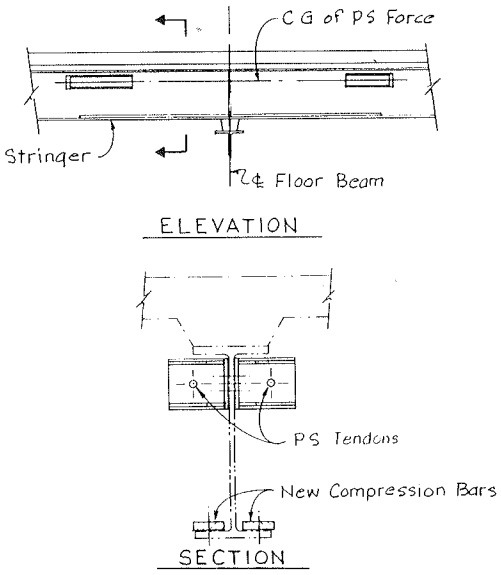

FIGURE 2 Pit River bridge stringers.

floor beams. Because prestressing increased compressive stress in the bottom (compression) flange, it was necessary to add the compression bars shown.

Floor-beam cantilevers were strengthened at their bases by fastening tension straps with tie plates alongside the original floor-beam cover plates before adding superstructure dead load (see Figure 3). The finished work is shown in Figure 4.

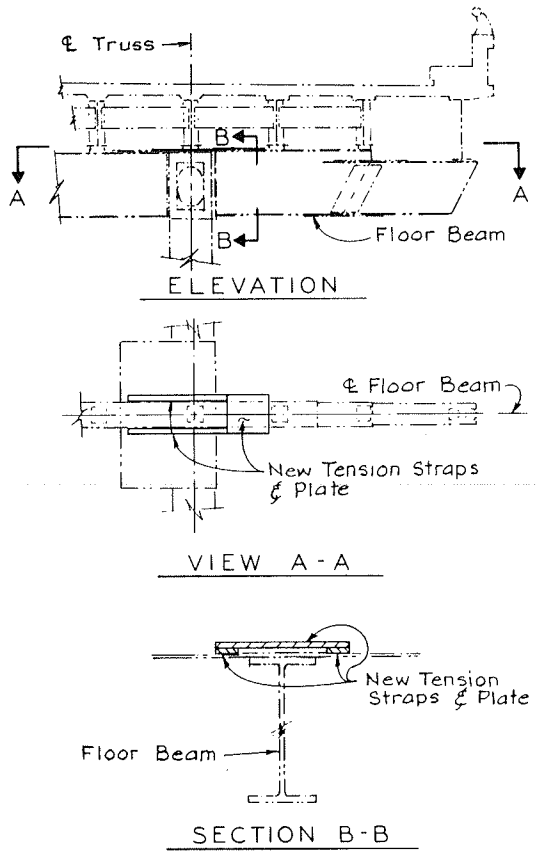

FIGURE 3 Pit River bridge floor beams.

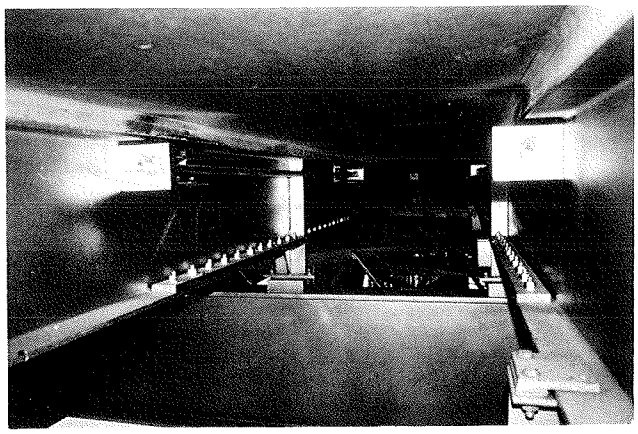

FIGURE 4 Pit River bridge—strengthened interior stringers.

Avenue 328 Overcrossing on CA-99

This composite steel girder structure, with six simple spans and five lines of girders, was designed for AASHTO HS20-44 live loading. The bridge was found to be deficient in moment capacity for permit loadings in the three central, 90-ft spans.

Strengthening was accomplished by adding 120 kips of force to each of the fifteen girders by means of two 60-kip tendons, 60 ft long, symmetrically placed on either side of the web 6 in. above the bottom flange. The attachment (Figure 5) was secured to the girder web by fourteen 7/8-in. high-strength bolts. All hardware was galvanized. Creep loss in the prestressing system was assumed to be 5,000 psi plus any losses characteristic of the prestressing and anchorage system. The tendons of each girder web were stressed simultaneously and enclosed in 2-in., standard, all galvanized pipe, which was grouted after stressing. The longitudinal centerline of the tendons was placed outboard of the girder stiffeners, and tendon supports (Figure 6) were placed at 15-ft intervals.

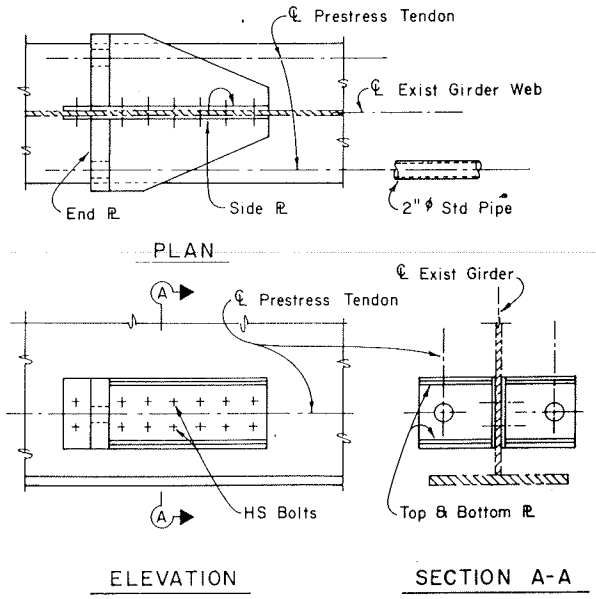

FIGURE 5 Prestress tendon anchorage—positive moment zone.

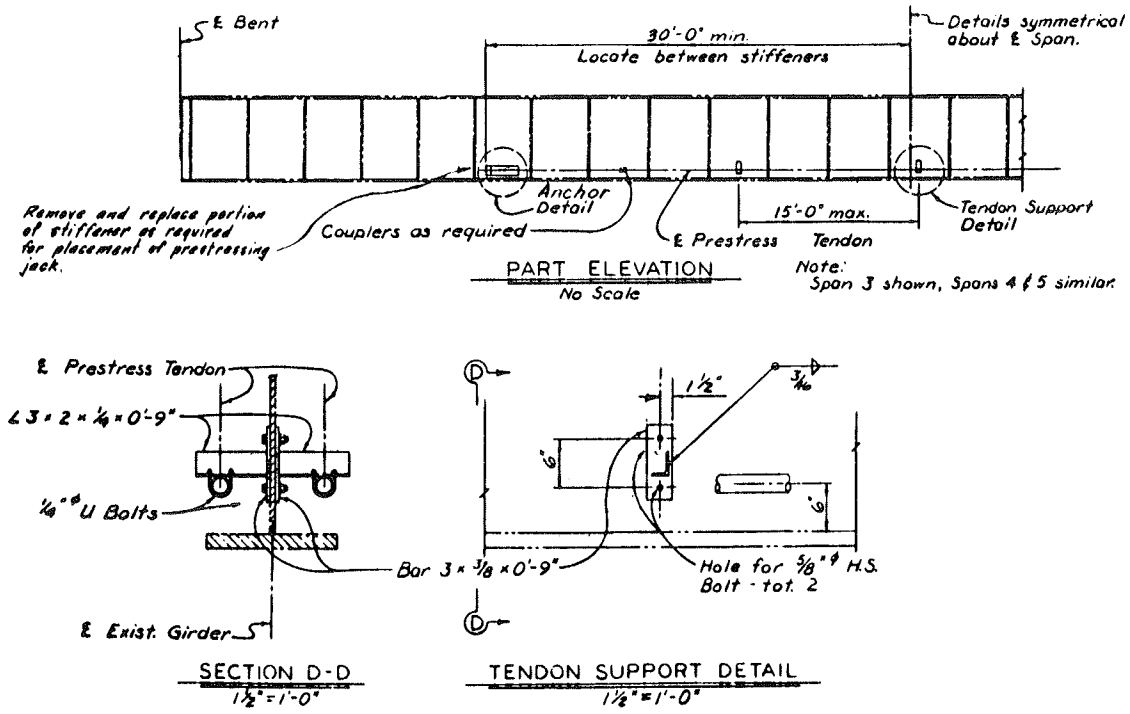

FIGURE 6 Avenue 328 overcrossing tendon supports.

Bid items and total bid amounts for the contract were

Traffic control system (lump sum)	$ 3,000
Prestressing steel girder (15 girders)	30,000
Miscellaneous metal (6,100 lb)	20,000
Contract total	$53,000

Drilling of bolt holes for the anchorages was included in the price of miscellaneous metal. All other work, including prestressing steel and grouting, was included in prestressing steel girder.

After anchorages were installed, prestressing was completed in less than a week; the contract allowed 50 days. Figures 7 through 9 are photographs of the installation during and after construction.

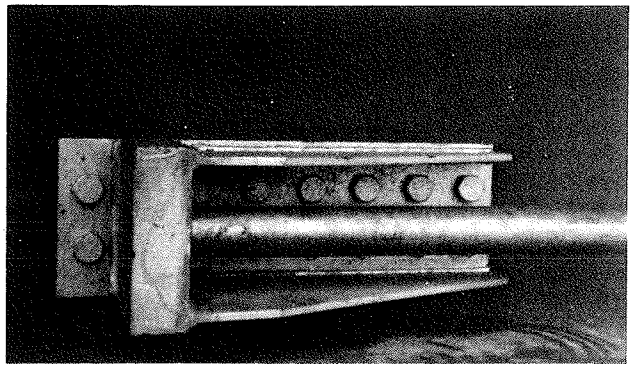

FIGURE 8 Tendon anchorage.

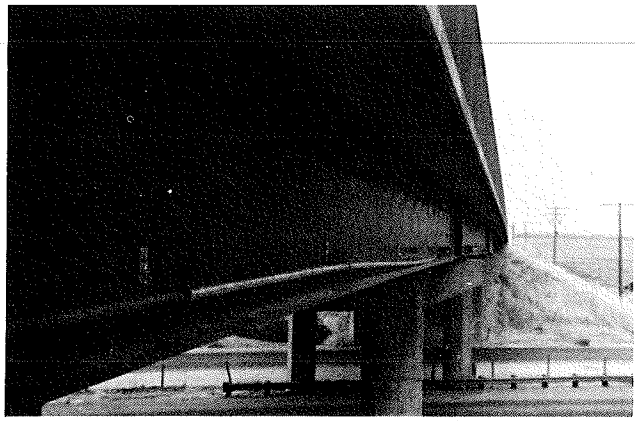

FIGURE 7 Two-inch pipe encasement for prestress tendon.

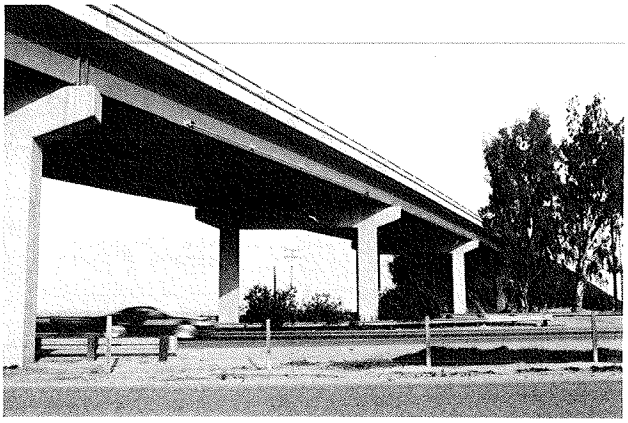

FIGURE 9 Completed exterior girder tendon.

Truckee River Bridges and Overheads on I-80

When I-80 was constructed through the Truckee River Canyon in 1955, high falsework for cast-in-place structures over deep canyons and segmental cantilever construction had not been developed to the present state of the art. Welded-steel girder structures were the best alternative for such sites. Seven crossings of the Truckee River and two high railroad overheads were constructed of steel. The Southern Pacific Transportation Company main line, which occupies the canyon, was used for the delivery of the girders. Designed for HS20-44 live loading, the majority of steel structures on this main truck route into California became deficient in load-carrying capacity with the introduction of the California permit load. Widening, deck replacements, seismic retrofitting, and upgrading to permit capacity for most of the steel structures from Auburn to the Nevada border are now under way. Spans shorter than 90 feet usually meet permit live-load requirements, but spans longer than 100 feet invariably have to be strengthened. The total anticipated cost of these improvements over the next 5 years will be more than $20 million.

Route Separations

Route separations, which are points of interchange on the SHELL system, are carefully screened and must be upgraded to permit live-load capacity. The route separation of CA-43 and CA-5 in Kern County is a typical steel girder structure that has been strengthened by prestressing. The two 145-ft spans have been strengthened by putting 350 kips of prestress force into each of the girders. For the four-girder section, a total force of 1,400 kips has been introduced into the superstructure. The largest force used in a steel girder superstructure thus far is at the Milpas Street separation structures in Santa Barbara. These composite, four-girder, dual structures, with single spans 122 ft long and 6 ft deep, have 360 kips of force in each girder, which makes a total of 1,440 kips on the cross section.

CONSTRUCTION

Construction problems reported by resident bridge engineers are minimal. Field adjustments and coping of intermediate interior web stiffeners may be required at some locations. Because California does not use intermediate stiffeners on exterior exposed webs, installation problems at those locations are nonexistent. Care, however, must be taken in placing tendons and encasements in position over traffic. Prestressing is checked by measuring both deformations and gauge pressures. Properly equipped and qualified prestressing contractors perform the work.

MAINTENANCE

Bridge maintenance engineers inspect the strengthened structures annually. They report no performance problems and all strengthened bridges are carried at full-permit live loading. No corrosion problems have been discovered even though several of the structures are located in aggressive mountain environments.

CONCLUSION

All structures strengthened by prestressing (see Table 1) have performed well thus far. There has been no evidence of loss of prestress due to slippage in the anchor systems. Permit loads on the SHELL system routes do not appear to pose a fatigue problem. Encasement of the tendons and anchorages has proven to be a wise precaution, particularly in coastal California and in the High Sierra where salting of bridges may expose unprotected prestress hardware and tendons to corrosive elements.

As structures have been identified and scheduled for strengthening in California's priority program, new problems in unique situations have been encountered. Innovative approaches taken by both designers and prestressors have solved these problems. Prestressing to upgrade the load-carrying capacity of steel girder structures has become the mainstay of California practice.

TABLE 1 California Bridges Strengthened by Prestressing

Bridge	Route	County	Strengthened		Force per Girder (kip)
			Date	Span (ft)	
Pit River bridge	I-5	Shasta	1979	35	70-100
Salinas River bridge	CA-101	Monterey	1980	89	190
Milpas Street separation	CA-101	Santa Barbara	1980	122	360
Bridge-street undercrossing	CA-101	San Luis Obispo	1980	74	75
Avenue 328 overcrossing	CA-99	Tulare	1982	90	120
Truckee River bridges	I-80	Nevada	1983	100	110
Route 43/5 separation	CA-43	Kern	1984	145	350

REFERENCES

1. D.P. Mondkar and G.H. Powell. CURVBRG--A Computer Program for Analysis of Curved Open Girder Bridges. Report No. UCSESM 74-17. Structural Engineering and Structural Mechanics, University of California, Berkeley, Dec. 1974.
2. R.E. Davis. Analysis of Steel Plate Girder Bridges with the Computer Program, CURVBRG. Report No. FHWA/CA/SD-79/1. Division of Project Development, California Department of Transportation, Sacramento, Sept. 1979.

Publication of this paper sponsored by Committee on Structures Maintenance.

Rehabilitation of Steel Deck Girder Bridges

STANLEY W. WOODS

ABSTRACT

Two 12-span bridges composed of two steel plate girders with a floor system were constructed in 1960. These were the first all-welded girder bridges built in Wisconsin. Plans were prepared to widen these bridges to carry a third lane and replace the existing deck. Several flaws that required repair were discovered in the welded girders. Before construction a transverse crack in the flange was found under the gusset plate used to attach the lower lateral bracing. The gusset plate was welded longitudinally and transversely to the bottom flange. During construction several other flaws were found: cracks under tack welds on the flanges, fatigue cracks in floor-beam webs, web butt welds with incomplete fusion, poor flange-to-web fillet welds, and improper termination of welded covered plates. These flaws were repaired to extend the life expectancy of the bridge by (a) removing the welded gusset plates, grinding the flange smooth, and bolting on new gusset plates; (b) removing the tack-welded piece and grinding out the cracks in the flanges; (c) removing the stringer-to-floor beam welded web connections, reattaching with bolted angles, and drilling stop holes; (d) drilling stop holes at the flange-web intersections in the tension area and providing bolted splice plates as required; (e) grinding the poor web-to-flange fillet welds into a smooth transition; and (f) placing bolted splice plates across the ends of the welded cover plates. The total rehabilitation was analyzed and found to be cost-effective.

Two bridges carry Interstate 94 across the Wisconsin River. These 12-span bridges are composed of two steel girders with a floor system and were designed in four segments of 3 continuous span units (Figure 1). The bridges were constructed in 1960 and were the first all-welded girder bridges built in Wisconsin. Rehabilitation plans were prepared in 1977 to replace the deteriorated concrete decks and to add four new girders to widen the bridges to three lanes. Lack of funding delayed bidding until September 1981. The contractor, working on an accelerated schedule, completed the contract in December 1983.

In March 1981 bridge maintenance personnel reported that the bottom flange of one of the main girders was cracked, resulting in a 75 percent loss of section. Traffic was rerouted until a bolted splice was placed on the flange. Further investigation revealed that the crack initiated where the bottom lower lateral system was attached to the gusset plate, which was welded to the bottom flange. Although the shop plans showed the gusset plate attached with longitudinal fillet welds, the plate was welded both longitudinally and transversely. The transverse fillet welds were believed to be the initiators of fatigue cracking. Because this detail was repeated at every lower lateral connection, the plans were modified to remove all these welded gusset plates and replace them with bolted plates in the positive moment areas. After the contract had been awarded and rehabilitation work had begun, several more problems with the steel girders were discovered. The repair of the gusset plates and the newly discovered problems are discussed in this paper.

REHABILITATION ANALYSIS

The original bridges were designed as two steel girders with a floor system because this structural system was thought to be more economical than a multiple-girder system. The bridges were supported on separate piers with a median width of 46 ft. To add an extra lane in each direction, it was decided to build a pier between the existing piers and add four steel girders (Figure 2). The new girders were designed to be the same depth as the existing girders, so that girder deflections would be comparable, although these girders were deeper than required for a multiple-girder system. Since the existing girders were assumed to be in good condition, with only a new deck required, it was determined that the extra cost of building the new girders deeper than required would be much less than

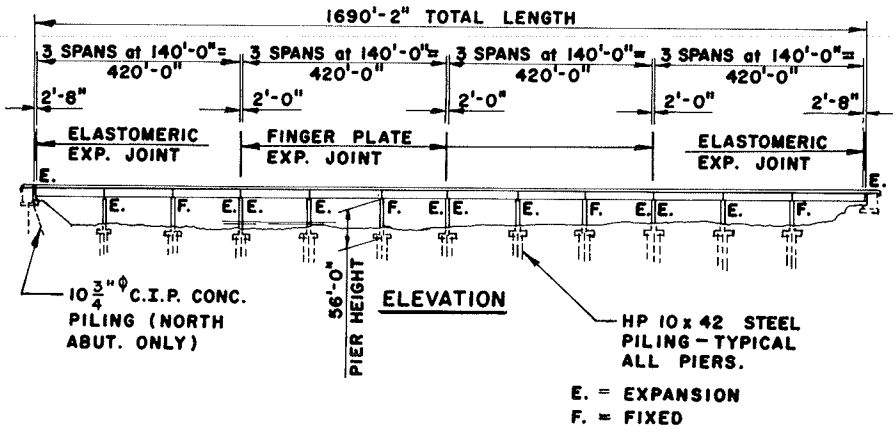

FIGURE 1 Design data.

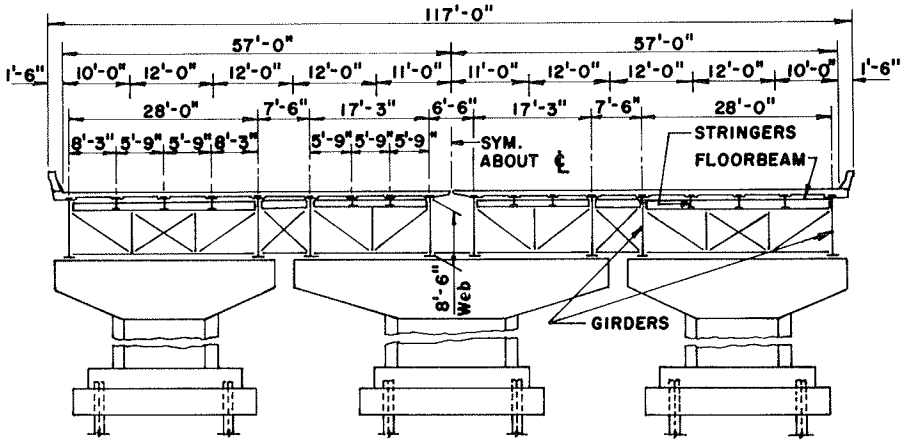

FIGURE 2 Cross section through roadway.

the cost of replacing the existing girders to create a multiple-girder system. The estimated cost to replace the welded gusset plates was considered reasonable and provided effective repair so it was included in the rehabilitation contract.

The properties of the existing bridge steel were evaluated before the contract was let. Charpy energies at 40° F were 80 ft lb for the flange and 56 ft lb for the cover plates. Nil-ductility temperatures were approximately -30° F for the cover plates and -100° F for the flanges. The steel was therefore considered adequate.

The contractor constructed the median piers, new superstructrue steel, and deck before starting deck removal on the existing bridges. As deck removal began on the first bridge, the need for more repair work was discovered. An estimate was made of these additional repairs and contract change orders were placed with the contractor. The following tables show the cost breakdown for the project, including the additional repairs that were required after the original contract was let.

Item	Cost ($)
Contract bid price	6,057,000
Gusset plates for lower lateral connection	257,000
Termination of cover plates	125,000
Top flange connections, flange-to-web welds, weld flaws at web butt weld near flange	60,000
Floor beam-stringer connections	450,000
Web cracking at butt welds	72,000
Ultrasonic testing	7,000
Substructure repair--pier encasement	166,000
Bolting cross bracing to existing bridges	37,000
Total project cost	7,231,000

Superstructure costs (in dollars) were

Widening only	2,315,000	or 28.24/ft²
New deck on existing bridge	792,000	
Girder repairs on existing bridge	1,008,000	
	1,800,000	or 15.20/ft²

Hindsight indicates that a more thorough inspection of the existing bridges should have been made before the rehabilitation plans were prepared. The estimated final costs of the rehabilitation plans could have been compared to the estimated cost of replacing the existing superstructure with a multiple-girder system, which would be a more redundant structure. This decision would have also had to be weighed against the public response to replacing a 20-year-old bridge.

However, at the time the rehabilitation plans were prepared, there was no reason to suspect the existence of faulty welds and poor construction practices. More and more was being learned about fatigue-prone details but thorough checks for them were just being initiated. Considerable cost and effort were required to repair the existing bridges, but it is believed that fatigue-prone areas have been eliminated or isolated and that these bridges will have a normal service life.

GUSSET PLATES FOR LOWER LATERAL CONNECTION

The bridges were fabricated entirely from A242 steel. The lower lateral system was attached to the main girders by gusset plates welded to the top side and inside of the bottom flange (Figure 3). The shop details showed the gusset plates to be attached with longitudinal welds only, but the fabricator had welded these plates on all sides. Flange butt welds also occurred under some of these gusset plates. Before the bidding on this bridge was opened, maintenance personnel discovered a crack in the bottom flange in the butt weld under a gusset plate. Ultrasonic testing indicated that the crack reduced the net section by 75 percent (Figure 4). A bolted splice detail (Figure 5) was developed using A588 steel to attach the lower lateral system as well as splice the flanges together. In addition, a hole

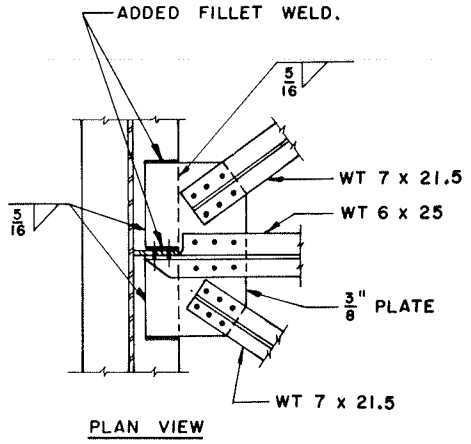

FIGURE 3 Lower lateral connection.

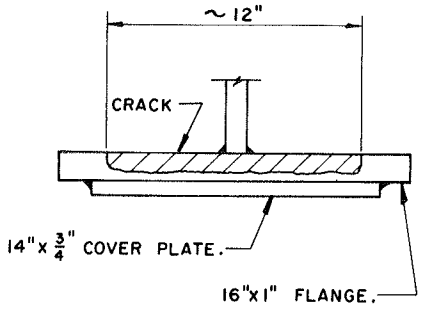

FIGURE 4 Crack location in bottom flange.

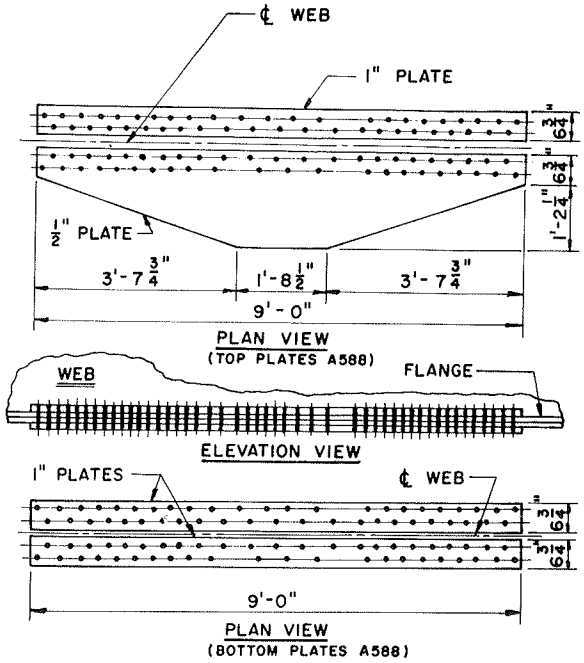

FIGURE 5 Bolted splice detail.

was drilled at the web-flange intersection to prevent crack growth into the web. The fillet welds connecting the cover plate to the flange were removed for 1 in. on both sides of the crack centerline to prevent crack growth into the cover plate.

This repair detail was added to the contract plans. The contractor was required to remove the welded gusset plates, grind the flanges smooth, and ultrasonically test the flange. Where serious flaws were discovered in the flange, full-strength flange splice plates were bolted to the flange. Otherwise only a gusset plate to attach the lateral bracing was bolted to the flange along with a corresponding plate on the bottom of the flange.

In several locations deep gouges (0.5 in. maximum) were discovered in some of the flange plates under the gusset plates. Full-strength flange splice plates were bolted to the flange at these locations. The shallow gouges were ground smooth before the new gusset plates were bolted to the flanges.

Ultrasonic testing was used to determine whether any fatigue-initiating cracks were present after removal of the gusset plates. If no such cracks were found it was assumed that the girder was all right. Where cracks or flaws were detected, the flange plates were isolated from the web by drilling holes, and the splice plates provided the required strength in case the cracks should grow.

Eventually the concrete deck over the first bolted splice repair that had been done 2.5 years earlier was removed. As a follow-up investigation, the splice plates were removed and the flange plates were examined with ultrasonic testing. These tests showed that the initial crack had now grown completely through the flange plate. Because the splice detail was designed for full strength, the plates were replaced and no further action was contemplated because the cracked flange plate now had a full-strength bolted splice.

TERMINATION OF COVER PLATES

The original plate girders had been fabricated with cover plates welded to the flange plates. This had been done to take advantage of the higher allowable stress for A242 steel with thicknesses of 0.75 in. or less. Because fatigue cracks were not found at the termination of these cover plates but stress levels were high enough to cause them, retrofit plans were prepared to reduce the chance of fatigue cracks starting.

Bolted splice plates were designed to connect both sides of the flange plate at the cover plate termination (Figures 6 and 7). It was assumed that the plane of failure for the flange would occur in this area. These full-strength splices were provided in the tension areas on both top and bottom flange plates to reduce the stresses at these locations and thus provide a longer fatigue life. If fatigue cracks develop in the flange the bolted splice plates will provide the required strength.

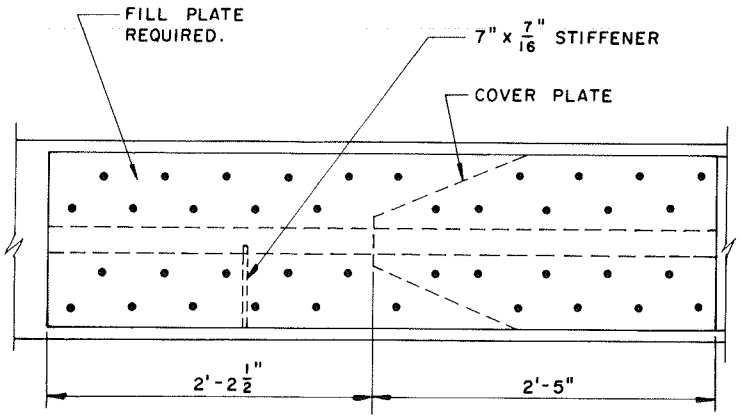

FIGURE 6 Splice detail at end of cover plate.

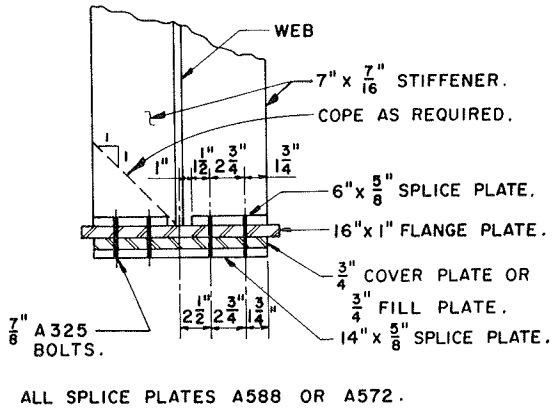

FIGURE 7 Cross section of cover plate.

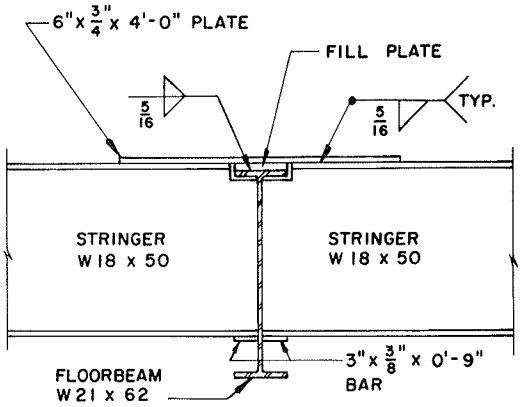

FIGURE 8 Stringer-to-floor beam connection.

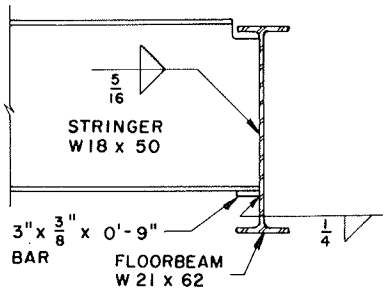

FIGURE 9 Stringer end-to-floor beam connection.

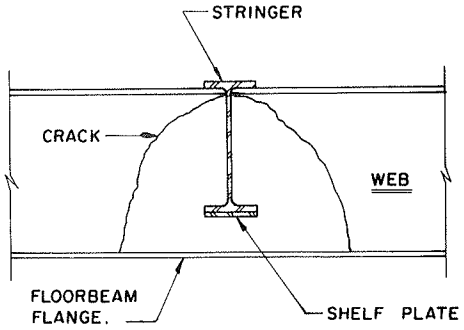

FIGURE 10 Floor-beam web fatigue cracks.

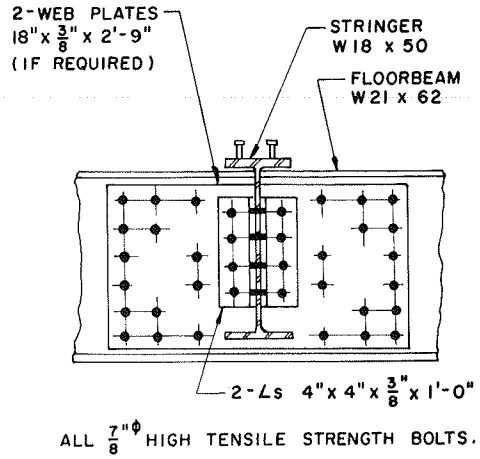

FIGURE 11 Stringer-to-floor beam repair attachment.

TOP FLANGE CONNECTIONS

The bridge was initially built with stay-in-place forms. The contractor used Z-angles at a 4-ft spacing that extended almost all the way across the flange to hold the forms in place. The Z-angles were attached to the flange with four tack welds. Cracks between 1/32 and 1/16 inch deep were discovered under all the welds transverse to the longitudinal axis of the girder flange. These flaws were repaired by removing the angle and grinding the top flange to remove the cracks. Magnetic particle testing was used to check for complete crack removal. These cracks were initially thought to be fatigue cracks but were later assumed to be caused by the tack weld replacement because they occurred under all the tack welds. The cracks also may have been a reaction caused by the galvanizing on the angle or the use of a non-low-hydrogen welding consumable. The original contractor also welded round pipe flanges to the top flange to support the rail for the paving machine. These pipe flanges were removed in the tension areas and the flange was ground smooth. No cracks were found in these areas, probably because more heat was applied to these fillet welds than was used for the tack welds.

FLOOR BEAM-TO-STRINGER CONNECTIONS

These two-girder bridges have a stringer-to-floor-beam system to support the slab. The 12-span bridge also has 4 units of three continuous spans with expansion joints at the ends of each unit. The stringers were designed as continuous members to cross over the floor beams (Figure 8) except at the ends where they were terminated (Figure 9).

Inspection of these connections revealed fatigue cracks beginning to form in the floor-beam webs where the stringers were continuous over them. These cracks were apparently caused by out-of-plane bending in the web caused by live load stresses. At the end floor beams where the stringers terminated, several fatigue cracks in the web had already propagated to the bottom flange (Figure 10) because there was more deflection occurring here due to lack of restraint because the stringer was not continuous.

To correct these flaws the stringers were removed from the floor beams by flame cutting the stringer flange and web adjacent to the fillet weld connections. The remaining material on the floor-beam web was ground smooth. The stringers were re-attached to the floor beams with clip angles (Figure 11), and studs were placed on the flanges to make the stringers composite with the slab. The composite action reduced the simple span stresses enough to

compensate for the loss of continuity. Stop holes were drilled at the crack tips on the floor-beam webs.

Even though fatigue cracking had grown more than a few inches into the web, full-bolted web splices were also made. These areas will have to be checked closely in future bridge inspections, but there is redundancy in the number of floor beams to provide a margin of safety.

WEB CRACKING AT BUTT WELDS

Weld flaws were discovered at the web-to-flange intersection where the webs were butt welded together (Figure 12). Apparently the flanges were attached to the web before the web butt welds were made. As a result weld flaws were made during fabrication where the web butt weld terminated near the flange.

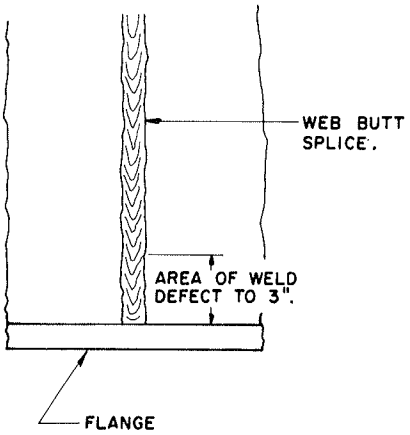

FIGURE 12 Web butt weld flaw.

Two 1-in. round holes were drilled through the web on each side of the weld at the base of the flange (Figure 13). The area between the holes was removed by sawing and the cuts were ground smooth. The portion of the web above the saw cut was checked with dye penetrant to be sure the flaw was completely removed. Further inspection of these web butt welds indicated that some of them had areas with cracks due to lack of fusion at the time of fabrication. A bolted web splice was provided at 33 out of 80 potential locations where the lack of fusion was more than 1 foot long. There was no indication that these flaws were growing but, where no splices were made, they will be checked during future inspections.

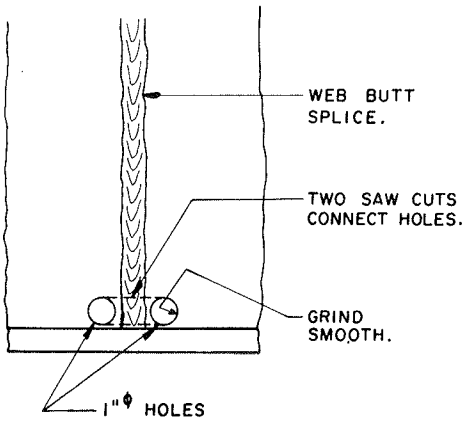

FIGURE 13 Web butt weld repair.

FLANGE-TO-WEB WELDS

Several areas were found where there was undercutting in the flange-to-web fillet welds. These areas were repaired in the tension zones only (top flange over piers and bottom flange in midspan) by grinding the areas with sharp contours. No welding was added because it was believed that there was sufficient weld present and grinding smooth would eliminate any crack initiators.

SUMMARY

After the field flaws were discovered a meeting was held to decide what retrofit action to take. Because the needed repairs were substantial, an estimate was made of the cost of completely removing the floor system and replacing it with two lines of full-depth girders. This estimate was compared with the estimated costs of repairing the existing girders. The cost of replacing the floor system was estimated to be more than the cost of repairing the existing girders ($2,000,000 versus $600,000) so this scheme was not used.

Fatigue cracking was found at the lower lateral gusset connections and at the stringer-to-floor-beam connections. All other cracks and flaws that were found were believed to be caused during initial girder fabrication. Removal or isolation of the fabrication flaws was considered adequate for bridge safety. The locations of the fatigue cracks were also isolated or changed to reduce or eliminate the chances of future crack growth. It is expected that these rehabilitated structures will perform satisfactorily throughout their life.

Publication of this paper sponsored by Committee on Structures Maintenance.

Thin Polymer Concrete Overlays for Bridge Deck Protection

MICHAEL M. SPRINKEL

ABSTRACT

The installation of thin polymer concrete (PC) overlays on portland cement concrete bridge decks during the past 3 years has demonstrated that overlays of low permeability and high skid resistance can be successfully installed with a minimum of disruption to traffic. The initial condition of the overlays has been excellent from the standpoint of permeability, skid resistance, and bond, although some overlays have been better than others. In this paper the potential of thin PC overlays for extending the service life of bridge decks is discussed. The bond achieved between the overlay and the deck concrete, the protection provided by the overlay, and the tensile properties of the resins and how they affect the performance of the overlays are described. The cost of a PC overlay is compared with that of a more conventional, latex-modified concrete overlay, and insight is provided about when to specify a PC overlay based on considerations of service life, traffic volume, discount rate, and the value of driving time.

Thin polymer concrete (PC) overlays have been installed on portland cement concrete bridge decks in Virginia and several other states during the past 6 years (1-5). The experimental overlay consists of four layers of resin and clean, dry, angular-grained, silica sand applied to the top of a portland cement concrete deck to provide a 0.5-in.-thick, relatively impermeable, skid resistant wearing surface (6). Typically the initiated and promoted resin is sprayed uniformly over the surface of the deck (Figure 1), and before it gels (10 to 20 minutes) the resin is covered to excess with broadcast fine aggregate (Figure 2). Usually, within the first hour a layer cures sufficiently to permit vacuuming the excess aggregate in preparation for placing a subsequent layer. Approximately 12 hours are required to place an overlay on one lane of a 350-ft bridge. Five to 8 hours are required to shotblast the deck and 5 to 6 hours to install the four layers of polymer--1 hr per layer plus 1 hr for curing before opening the lane to traffic. When a lane cannot be closed for 12 hours, the overlay can be placed on part of the lane, or the entire deck can be shotblasted and one layer of resin and aggregate applied one day and the subsequent layers on the next day.

The installation of PC overlays on five bridges on Interstate 64 near Williamsburg, Virginia, in 1981; a sixth bridge near Vienna, Virginia (Beulah Road bridge), in 1982; and a seventh bridge near Columbia, Tennessee (Big Swan Creek bridge), in 1983, has demonstrated that an overlay of low permeability and high skid resistance can be successfully installed by a contractor or by a state or federal force labor with a minimum of disruption to traffic and at a reasonable cost. The initial permeability, skid resistance, and bond condition of the overlays was observed to be excellent, but some overlays were better than others.

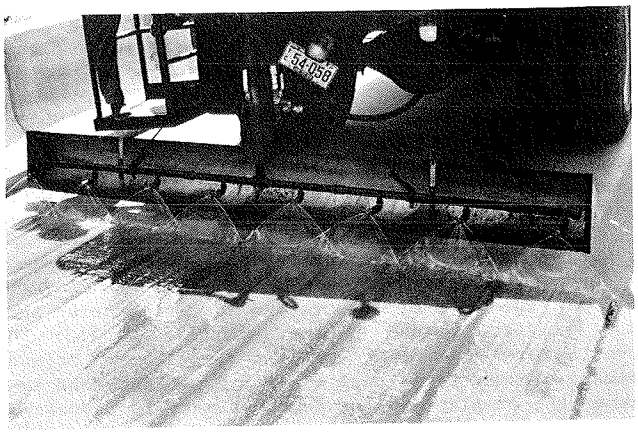

FIGURE 1 Polyester resin sprayed over deck surface.

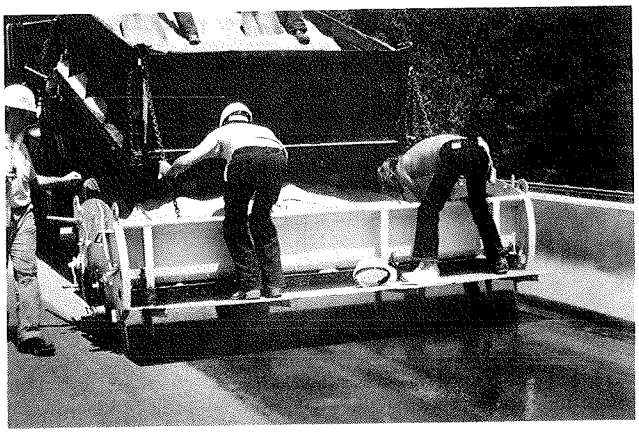

FIGURE 2 Silica aggregate broadcast over resin.

The resins used were clear, low-viscosity, highly resilient, general-purpose, unsaturated polyester resins designed for applications requiring resistance to wear and high impacts. U.S.S. Chemical blend LB183 was used on bridges near Williamsburg and on the northbound lane of the Beulah Road bridge; Reichhold Chemical blend Polylite 90-570 was used on the southbound lane of the Beulah Road bridge; and Dural International blend 317 was used on the Big Swan Creek bridge. The first course contained 1 percent Union Carbide A-174 coupling agent and 1 percent Surfynol S440 wetting agent to enhance bond strength and reduce surface tension. The second, third, and fourth courses contained 0.5 percent Union Carbide A-174 coupling agent and 0.5 percent Surfynol S440 wetting agent.

Two initiators were used. One was 60 percent

methylethylketone peroxide [MEKP ($C_4H_8O_2$)] in dimethyl phthalate and the other was 40 percent benzoyl peroxide dispersion (BPO-40) equal to Reichhold Chemical's formulation 46-742. Two promoters were also used. One was approximately 6 percent active cobalt in naphtha (CoN), and the second was N, N, dimethyl aniline [DMA ($C_6H_4N(CH_3)_2$)].

Before placement of the first layer of polymer and after all major spalls had been repaired, the deck was shotblasted with a machine equipped with a dust collector. The equipment recycles the steel shot, collects concrete cuttings, and rapidly provides, at low cost and with little or no environmental impact, a completely cleaned deck. The equipment cleans the deck at a rate of 100 to 150 yd^2 per hour depending on the size of the unit (2,3,5). It does not fracture the aggregate or paste as is common when jackhammers or scarification equipment are used (7), and it cleans more efficiently and completely than does sandblasting equipment.

The purpose of this paper is to report on the condition of the PC overlays after 1 year of service life--particularly the overlay on the Beulah Road bridge, which is representative of the others--and the knowledge gained of the potential of thin PC overlays for extending the service life of bridge decks. In the first part of this paper the bond between the overlay and the deck concrete is discussed and attempts are made to answer the question, "How long will the overlay stay down?" In the second part the protection provided by the overlay, which is intended to prevent the infiltration of water and salt and thereby prevent corrosion of the reinforcing steel, is examined. In the third part the tensile properties of the resins are compared and how these properties affect the performance of the PC overlays is noted. In the fourth part the cost of a PC overlay is compared to that of a more conventional, latex-modified concrete overlay and insight is given about when to specify a PC overlay based on considerations of service life, traffic volume, discount rate, and the value of driving time.

STRENGTH OF BONDS

Shear Strength

To obtain an indication of the shear strength of the bond at the interface between the PC overlay and the base and the shear strength of the portland cement concrete base, cores were subjected to two tests. For the former, the shear force was directed through the bond interface; for the second it was directed through the concrete approximately 2.5 inches below the interface. The load was applied at 10,000 lb per minute with the apparatus shown in Figure 3.

Table 1 gives the shear strength and the types of failures for cores taken from the Beulah Road bridge in 1982, 2 weeks after the overlay was placed, and in 1983, 47 weeks after the installation. Although the cores taken in 1982 were 2.75 in. in diameter and those taken in 1983 were 4.0 in. in diameter there is no evidence that the difference in size affected the results. As can be seen from the table, there was no significant difference between the shear strengths of the two sets of cores for the portland cement concrete, but the 1983 strengths for the bond interface were lower than those for 1982. Of particular significance is the deterioration in strength of the bond of LB183 resin during the first year. Whereas the strength of this bond was greater than that of the base concrete in 1982, in 1983 it had decreased an average of 56 percent to a value only 52 percent that of the base concrete. For the 90-570 resin there was a 25 percent loss in the strength of the bond during the first year, but the strength was still 89 percent that of the base concrete. The loss in shear strength may be attributed to the creep and thermal stress that occurred during the year in service and that can be expected to continue (8).

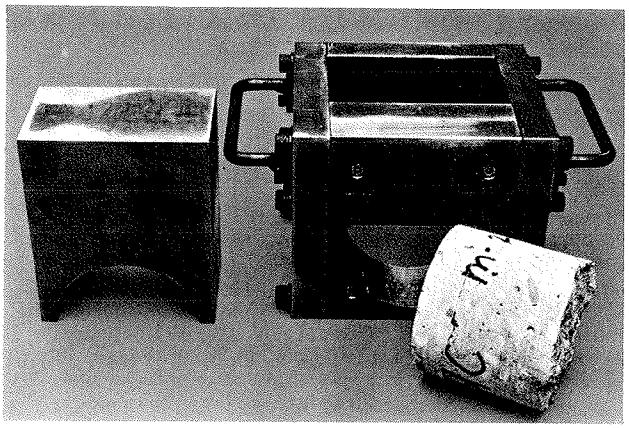

FIGURE 3 Apparatus used to subject cores to shear.

The modes in which the cores failed in the shear tests also provided evidence that the strength of the bond deteriorated during the first year. In 1982 the only failures were in the base concrete; in 1983 failures were noted in the bond interface, in the base concrete, and sometimes in both.

Further evidence of the breakdown in shear strength with cycles of temperature change is shown in Figure 4, which shows the results of shear tests on specimens prepared in the laboratory of the Virginia Highway and Transportation Research Council. The concrete base of each specimen consisted of a section 4 in. in diameter and 2.25 in. thick cut from a 4-in. x 8-in. cylinder. The base concretes were fabricated to have four different 28-day com-

TABLE 1 Shear Strength of Cores from Beulah Road

	LB183 Resin					90-570 Resin				
	Shear Strength ($lb/in.^2$)		No. Failures at Indicated Location			Shear Strength ($lb/in.^2$)		No. Failures at Indicated Location		
Year	Concrete	Bond Interface	Bond	Concrete	Both	Concrete	Bond Interface	Bond	Concrete	Both
1982	Avg 776	1,001	0	4	0	Avg 824	972	0	3	0
	SD 76	229				SD 164	175			
1983	Avg 838	436	1	1	1	Avg 823	730	0	0	4
	SD 38	140				AD 165	108			

Note: SD = standard deviation.

Physical Properties of Base Concrete

Mix	w/c	28-day Compressive Strength, lb./in.^{2}	Shear Strength, lb./in.^{2}
4	0.68	2200	877
3	0.54	3150	894
2	0.43	5450	1235
1	0.34	7350	1543

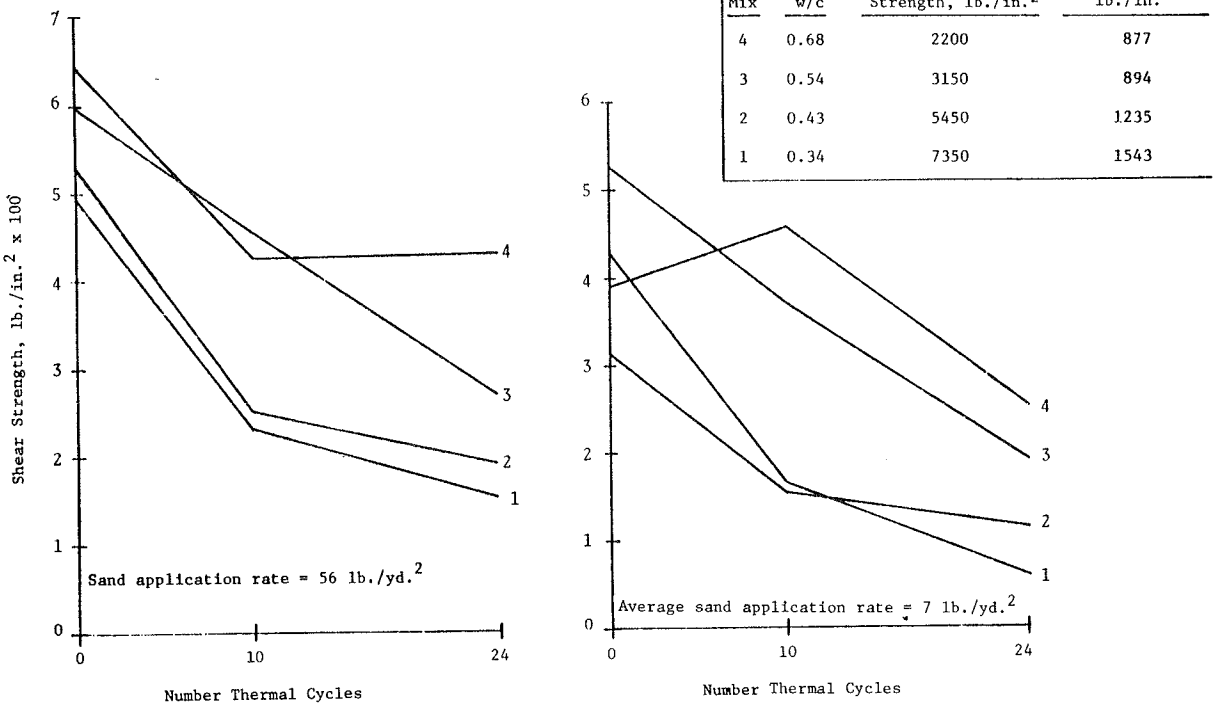

FIGURE 4 Shear strength of bond interface as function of number of thermal cycles for different base concrete strengths.

pressive strengths as shown in Figure 4. Following a 2-week period of moist curing and a 6-week period of air curing, a PC overlay constructed with 90-570 resin was placed on one sawn concrete surface of each specimen. Fine aggregate was applied to the overlays in an excessive amount (approximately 56 pounds per square yard) and at rates of 0 and 14 lb per square yard. The curves are based on the averages of tests on two specimens of concrete representing each level of design strength and subjected to either 0, 10, or 24 thermal cycles. The cycles were applied at the rate of 1 per day with the temperature changing from 0°F to 100°F. The overlays were 1 week old at the time the first thermal cycle was applied and 2 months old at the time the shear tests were conducted.

Figure 4 shows that, regardless of the strength of the base concrete, the shear strength of the bond interface decreased as the number of thermal cycles increased. Also, the highest shear strengths in the bond interface were achieved with the base concrete having the lowest design strength. This implies that the more permeable low-strength base concrete absorbed more resin, provided more mechanical bond, and yielded more under stress thereby subjecting the bond interface to less stress. Finally, Figure 4 shows that when an excess of aggregate (56 lb per square yard) was used in the overlay, the shear strengths at 0, 10, and 24 cycles were higher than when an average of 7 lb per square yard was used because the thermal and shrinkage stresses are less when an excess of aggregate is used in the overlay (8).

The mode of failure for the specimens prepared in the laboratory was similar to that of the cores taken from the Beulah Road bridge. At 0 cycles, which can be compared with the data for the cores taken in 1982 (Table 1), most failures were in the base concrete or involved the base concrete. At 10 and 24 cycles, which can be compared with the data for the cores taken in 1983, most failures were in the bond interface, and the few failures that involved the base concrete were in the two lower strength concretes.

Of additional interest is the fact that the shear strength of the bond interface at 0 cycles was lower for all specimens prepared in the laboratory than for the cores from the bridge. There are three possible explanations: First, the A174 coupling agent that is added to the resin helps bond the resin to the silica in the aggregate and this effect would be less pronounced for the siliceous gneiss coarse aggregate used in the laboratory specimens, which contain less silica, than for the chert aggregate used in the Beulah Road bridge. Second, the shear strengths of the base concrete in the laboratory specimens were generally higher than those of the base concrete in the bridge. Third, more surface contact was achieved with the shotblasted surface of the cores than with the sawn surface of the laboratory specimens.

Of particular importance is the fact that, despite the loss in bond strength that occurred with both resins as a result of thermal and shrinkage stresses, a second set of specimens identical to those that had been subjected to the shear tests and constructed with 90-570 resin and 56 lb per square yard of aggregate (Figure 5, right) withstood 300 thermal cycles without becoming debonded. The remaining specimens in the second set prepared with 0 and 14 lb per square yard of aggregate (Figure 5, left) delaminated in the vicinity of the bond interface. Based on the performance of these specimens, it is reasonable to expect that a PC overlay properly constructed with 90-570 resin will stay bonded for approximately 10 years.

Tensile Strength of Bond

One-inch-diameter cores were removed from the Beulah

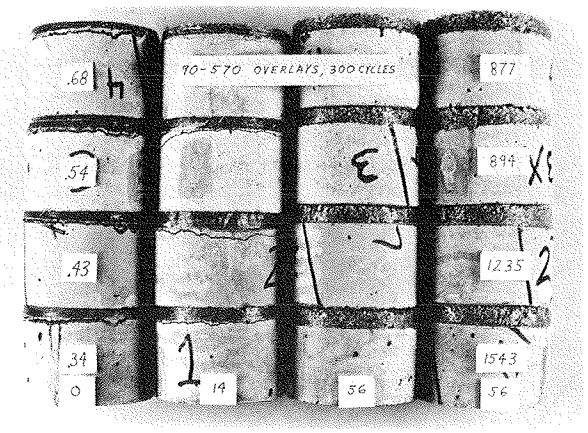

FIGURE 5 Condition of test specimens after 300 thermal cycles.

Road bridge in 1982 and again in 1983 and tested in tension in an attempt to pull the overlay from the base concrete. The average tensile strength of the composite and the mode of failure are given in Table 2. Note that the tensile strength of the cores with the LB183 overlay decreased an average of 28 percent during the first year but the tensile strength of the cores with the 90-570 resin did not change, which suggests that a longer service life can be expected for the 90-570 resin. The results of the tensile tests agree in pattern with those of the shear tests.

Delamination

As determined with the Delamtech, after 47 weeks of service life, 1.4 percent of the LB183 overlay on the Beulah Road bridge was delaminated whereas no delaminations were detected in the 90-570 overlay. Inspections of the delaminated area revealed that insufficent aggregate was placed on that portion of the overlay. The lower aggregate content resulted in an increase in shrinkage and in thermal stress during the first winter and thereby led to premature failures in the bond and in the base concrete. After 2 years of service life delaminations have not been observed in the LB183 overlays near Williamsburg.

In summary, overlays constructed with both resins were soundly bonded to the base concrete initially and after 1 year of service life. An area of the LB183 overlay on the south end of the Beulah Road bridge debonded during the first year because insufficient aggregate had been placed on that portion of the overlay. The bond strength of the LB183 overlay is decreasing more rapidly than that of the 90-570 overlay. Whereas it is anticipated that the properly constructed portion of the LB183 overlay will remain bonded at least 5 years (2), the 90-570 overlay should remain bonded a much longer time.

PROTECTION PROVIDED BY OVERLAY

Electrical Resistivity

Two weeks and 47 weeks after the overlay was installed on the Beulah Road bridge, electrical resistivity measurements (ASTM D3633-77) were made at grid points located 4 ft apart in the transverse direction and 5 ft apart in the longitudinal direction. Measurements were also made at half of these locations after 24 weeks of service life. The results are given in Table 3. Both materials exhibited good to excellent resistivity 2 weeks after they were installed. The resistivity of the LB183 overlay decreased to fair after 24 weeks of service life, but that of the 90-570 overlay was still good to excellent after 24 weeks and good after 47 weeks. The resistivity of the LB183 overlays placed near Williamsburg was fair to poor after 1 year of service life.

The test provides a good indication of the extent of cracking in an overlay. A low reading is indicative of a crack at the test location. The crack allows water to penetrate the overlay and lower the resistance in the electrical circuit. The 90-570 overlay is more flexible than the LB183 and therefore is less prone to cracking to relieve the stress caused by temperature changes, shrinkage, reflective cracking, and creep.

Permeability

A rapid test (9) recently developed by the Portland Cement Association for the FHWA was used to determine the permeability to chloride ion of 4-in.-diameter cores removed from the Beulah Road bridge, and the results are given in Table 4. A permeability of 2214 coulombs was determined for the base concrete. After 2 weeks of service life the permeability of the base concrete with a PC overlay was 2.9 coulombs for LB183 and 0.9 coulombs for 90-570. After 24 and 47 weeks of service life additional cores were taken. Cores containing the LB183 overlay showed an increase in permeability, but the permeability of the cores with the 90-570 overlay was about the same as when the overlays were installed. The permeability data support the electrical resistivity data in that both indicate a deterioration in the waterproofing characteristics of the LB183 material after only 24 weeks of service life. The deterioration was probably caused by a combination of shrinkage and thermal stresses.

Cores taken from the LB183 overlay after 47 weeks of service life showed a greater permeability than ones taken at 24 weeks, which suggests that the thermal stress to which the overlay was subjected during the first winter caused additional cracking. Of greatest significance is the fact that the cores taken from the 90-570 overlay exhibited a permeability of only 1 coulomb after 47 weeks of service.

TABLE 2 Tensile Strength of Cores from Beulah Road

	LB183 Resin				90-570 Resin			
		No. Failures at Indicated Location				No. Failures at Indicated Location		
Year	Tensile Strength (lb/in.^{2})	Polymer	Bond	Concrete	Tensile Strength (lb/in.^{2})	Polymer	Bond	Concrete
1982	Avg 337 SD 78	0	2	5	Avg 268 SD 93	0	0	6
1983	Avg 241 SD 48	0	2	4	Avg 266 SD 53	0	1	5

Note: SD = standard deviation.

TABLE 3 Electrical Resistivity Measurements, Percentage of Total Number of Readings

Age (weeks)	Product	Range of Electrical Resistivity (ohms/ft^2) Poor ($<10^4$)	Fair (10^4 to $<10^6$)	Good (10^6 to 10^8)	Excellent ($>10^8$)
2	LB183	0	6	15	79
	90-570	1	2	13	84
24	LB183	2	88	9	1
	90-570	0	1	41	58
47	LB183	2	80	17	1
	90-570	0	11	78	11

Clearly, this represents the best 1-year performance of any thin PC overlay placed in Virginia.

To further examine the permeability of the 90-570 resin, laboratory-prepared specimens identical to the ones subjected to the shear tests were subjected to 300 cycles of temperature change at the rate of 3 cycles per day, and permeability tests were conducted at 0, 10, 50, 100, 200, and 300 cycles. The results, which are based on the average of tests of two or more specimens at each number of test cycles, are shown in Figure 6. Also shown in this figure are the results of tests on cores removed from the Beulah Road bridge, the bridges in Williamsburg (3), and a bridge with a latex overlay. Recent tests of cores removed from 12 bridges with latex overlays ranging in age from 1 to 9 years have exhibited permeabilities in the range of 130 to 1298 coulombs with an average of 773 coulombs for an overlay thickness of 1.25 in.

It is not obvious that the 90-570 overlay is significantly better than the LB183 overlay from the standpoint of permeability (Figure 6). However, it must be remembered that the base concrete prepared in the laboratory had an average permeability of 7400 coulombs, a value significantly higher than that of the base concrete in the Beulah Road bridge. Test results for the overlay are affected by the

TABLE 4 Permeability Data, Coulombs

	Date of Sample and Age (weeks)						
	3/01/82 (-9)	5/18/82 (2)	10/20/82 (24)	3/29/83 (47)	5/18/82 (2)	10/20/82 (24)	3/29/83 (47)
	Material						
Span	Concrete	LB183	LB183	LB183	90-570	90-570	90-570
A	2308	0.5	52	809	–	–	–
B	–	0.7	–	–	0.5	0.3	2.2
C	–	3.7	248	859	–	–	–
D	–	–	–	–	2.2	0.0	5.1
E	–	53.0	447	521	–	–	–
F	2124	–	–	–	0.7	0.7	0.1
Log. Avg	2214	2.9	179	713	0.9	0.1	1.0

Note: Dash = no samples taken.

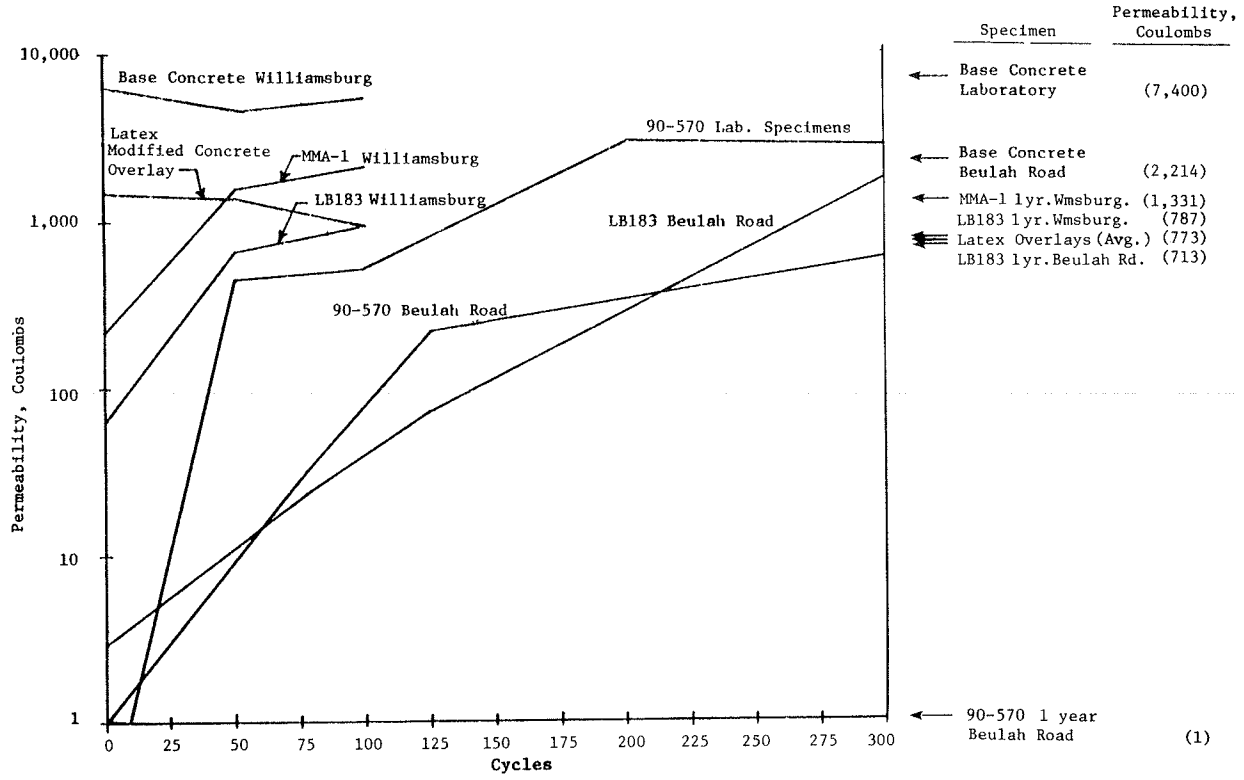

FIGURE 6 Permeability to chloride ion of PC overlays as a function of number of thermal cycles.

permeability of the base concrete because the 0.5-in.-thick PC overlay accounts for only 25 percent of the 2-in. thickness of the test specimen.

Based on the data shown in Figure 6, it can be concluded that both resins experienced an increase in permeability when subjected to cycles of temperature change. Also, if the results obtained with the laboratory specimens and the cores removed from the Beulah Road bridge are averaged, it can be concluded that after 300 cycles the permeability of a 0.5-in.-thick layer of 90-570 resin and aggregate was about equal to that of a 1.25-in.-thick overlay of latex-modified concrete. If it can be assumed that 1 year in service is equivalent to 50 thermal cycles, the 90-570 and the LB183 overlays should provide a permeability less than or equal to that of a 1.25-in.-thick latex overlay for at least 6 years. The performance of the overlays must be observed for a number of years to allow a more accurate projection of the permeability to be expected after 6 years.

Shrinkage

It was believed that the LB183 resin cracked more than 90-570 resin because it exhibited a higher shrinkage. However, recent measurements indicated no major differences among the shrinkages of the two resins and resin 317. The measurements indicated that a shrinkage of approximately 2 percent can be expected when no aggregate is used and a shrinkage of 0.2 percent is typical when the aggregate-to-resin ratio by weight is 4 to 1. It is obvious that the principal way to minimize shrinkage is to load the resin to excess with aggregate. Because the LB183 resin does not shrink significantly more than the other resins, one must conclude that it cracks more as a result of shrinkage-induced stress because it is less flexible and therefore less able to strain to accommodate stress.

Half-Cell Potential

Copper sulfate half-cell potentials (ASTM C876-77) were measured before, immediately after, and approximately 1 year after the installation of the PC overlays. The results of the measurements imply that there was a high probability that no corrosion was occurring before and approximately 1 year after the installation of the overlays. Values could not be determined immediately after the installation of the overlays because there were no cracks in the overlays to allow the completion of the electrical circuit.

Rutting in Wheelpaths

A 12-ft straightedge was used to measure rutting in the wheelpaths. The device has six scales spaced 2 ft apart. Measurements are made by depressing the six scales until they touch the surface of the deck and recording the readings. The rutting in a wheelpath is computed by subtracting the reading on the scale located in the center of the wheelpath from the average of the readings for the two adjacent scales. Measurements were made at 10-ft intervals along the length of the bridges. The amount of wear, computed by subtracting the measurements obtained after 1 year of service life from the measurements obtained immediately after the overlay was installed, was less than 1/32 in. for all the bridges.

Skid Numbers

Skid numbers (ASTM E501-76 and E524-76) were determined in tests at 40 mph in each lane 3 weeks before and 4, 13, and 50 weeks after the PC overlay was installed on the Beulah Road bridge. The results are given in Table 5. The concrete surface exhibited high numbers prior to the overlay and even higher numbers afterwards. The low reading found for the LB183 resin after 4 weeks of service life was caused by asphalt tracked onto the lane from an approach area that had been given a new surface the same week. After 50 weeks of service life the lane with the LB183 resin exhibited slightly higher skid numbers than the lane with 90-570 resin, but the numbers obtained in both lanes were excellent and higher than the ones determined for the base concrete prior to placing the overlays. The skid resistance of the lane with the 90-570 resin should be monitored over the next few years because it is the only overlay of its type in Virginia. After 1 year of service life the LB183 overlays near Williamsburg exhibited an average treaded tire number of 57 and a bald tire number of 44 (3).

TABLE 5 Skid Numbers for 40 mph Tests

		Treaded Tire		Bald Tire	
Date	Age (weeks)	Resin LB183	Resin 90-570	Resin LB183	Resin 90-570
4/15/82	-3[a]	52	51	39	36
6/03/82	4	44[b]	57	36[b]	51
8/02/82	13	53	55	47	49
4/19/83	50	58	56	49	45

[a] Three weeks before PC overlay was placed.
[b] Asphalt had been tracked onto bridge.

TENSILE PROPERTIES

The bond strength and the protection provided by the overlay constructed with the 90-570 resin were better than those of the overlays constructed with LB183 resin. For example, the shear and tensile strengths of the bond interface deteriorated much more for the latter than for the former during the first year of service life. Also, the resistivity of the LB183 overlay decreased and the permeability increased significantly during the first year of service life, whereas the 90-570 overlay exhibited good resistivity and low permeability after 1 year. Because both products are polyester resins, it was thought necessary to determine their physical properties, which explain the superior performance of the 90-570 overlay.

The most obvious differences between the two products were determined using ASTM D 638-80, "Standard Test Method for Tensile Properties of Plastics." The results of tests conducted in accordance with this procedure are given in Table 6 and shown

TABLE 6 Tensile Properties of Resins

	Tensile Strength (lb/in.^{2})		Elongation at Break (%)		Modulus of Elasticity (lb/in.^{2})[a]	
Resin	Avg	SD	Avg	SD	Avg	SD
317	2,858	301	23.3	8.1	4.69×10^4	0.99×10^4
LB183	5,089	1,928	8.0	3.8	7.81×10^4	0.91×10^4
90-570	2,836	373	49.2	11.4	3.52×10^4	0.21×10^4
MMA-1[b]	1,427	525	2.3	0.4	6.29×10^4	1.39×10^4
EP5LV	4,797	626	12.5	1.2	6.60×10^4	1.56×10^4
MMA-2[c]	4,821	262	6.7	0.0	7.19×10^4	0.58×10^4

Note: SD = standard deviation.
[a] Calculated at 0.05 in./in. strain except MMA.
[b] 63 percent MMA and 37 percent PMMA.
[c] FX822, PMMA unknown.

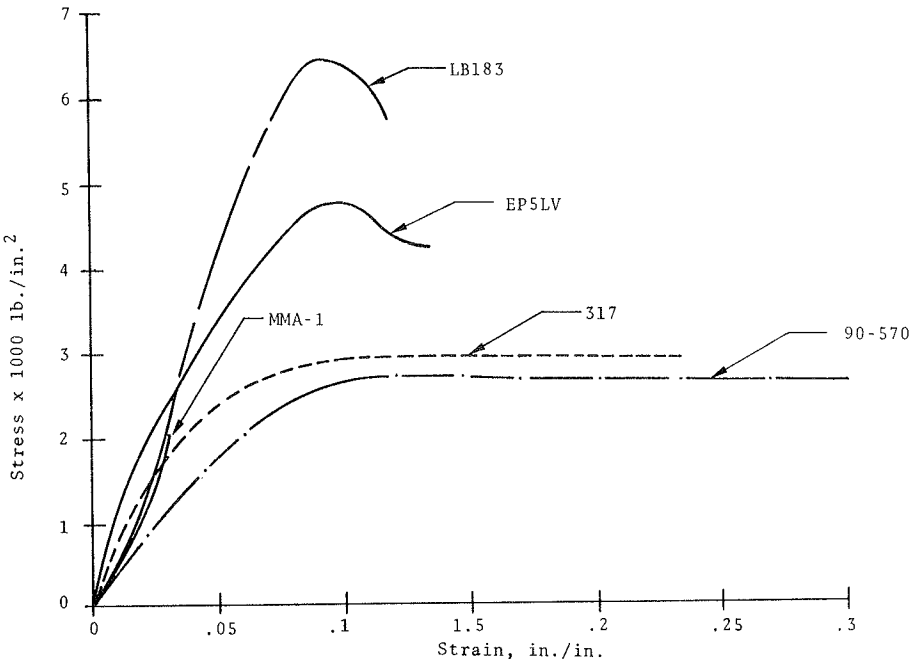

FIGURE 7 Stress-strain data based on average of three specimens of each resin.

in Figure 7 (unpublished memoranda from R.E. Steele to M.M. Sprinkel, July 13 and October 17, 1983). Data for resin 317, which was used on the Swan Creek bridge in Tennessee, data for methylmethacrylate (MMA-1) used on one of the bridges near Williamsburg, and data for an EP5LV epoxy currently being placed on several bridges in Virginia are included in the table and figure. The tests were conducted on specimens 0.13 in. thick, 0.50 in. wide, and 8.5 in. long. A 3.0-in. gauge was used, and the test speed was 0.2 in. per minute.

From Table 6 and Figure 7 it is obvious that the LB183 resin has a higher tensile strength and modulus of elasticity and a much lower elongation than the 90-570. Because the LB183 resin elongates only 8.3 percent it is more likely to crack when subjected to shrinkage, reflective cracking, or thermal stress than is the 90-570 resin. The more flexible 90-570 is able to elongate and accommodate the tensile stresses and thereby provide an overlay of high resistivity and low permeability. The 90-570 and 317 resins should be less prone to cracking than LB183, MMA-1, MMA-2, and EP5LV epoxy. Extensive cracking has occurred in overlays constructed with LB183 and MMA-1 (2,3). The EP5LV epoxy overlay system is being studied at this time. Based on the data in Table 6, it is reasonable to conclude that a resin should have a minimum elongation of 20 percent to minimize the formation of cracks and thereby ensure adequate protection. A specification requiring 20 to 40 percent elongation seems reasonable.

Thermal Stress

When two materials of different properties are bonded together, a shear stress develops when the composite is subjected to a change in temperature. The stress is a function of the temperature change and the coefficient of thermal expansion and moduli of elasticity of the materials. A shear failure in the vicinity of the interface can be expected if the shear stress exceeds the shear strength of either of the materials or the strength of the bond. A method for computing the theoretical stress is discussed in detail elewhere (2-8).

Reasonable values for the dynamic modulus of elasticity for a polyester resin, as determined by ASTM C215-60, are 0.4×10^6 lb per square inch for an overlay with no aggregate and 1×10^6 lb per square inch for an overlay sanded to excess (2). For the same aggregate application rates, reasonable values for the coefficient of thermal expansion for a polyester resin are 56×10^{-6} in./in./°F and 16×10^{-6} in./in./°F, respectively. Portland cement concrete typical of that used in bridge decks in Virginia has a dynamic modulus of elasticity of 4.2×10^6 lb per square inch and a coefficient of thermal expansion of 5.7×10^{-6} in./in./°F (2). Using these values, the theoretical shear stress at the bond line for a 1°F change in temperature is 18 lb per square inch for an overlay with no aggregate and 8.3 lb per square inch for an overlay with excess aggregate.

If an overlay is placed on concrete at 74°F and later cooled to 0°F, as was the case for the specimens shown in Figures 4 and 5, the bond interface is subjected to a stress of 1,300 lb per square inch if the overlay has no aggregate and 610 lb per square inch if it has an excess of aggregate. When no or a small amount of aggregate is placed in the overlay, the theoretical shear stress exceeds the shear strength of both the bond interface and the base concrete, which explains the failures shown in Figure 5. On the other hand, when an excess of aggregate is placed in the overlay, the theoretical shear stress is about equal to the shear strength of the bond interface and is less than the shear strength of the base concrete, which explains why the specimens shown in Figure 5 with an excess of aggregate in the overlay did not delaminate after 300 thermal cycles. Because the shear stress is great enough to fatigue the bond interface, the strength of the bond decreases with an increase in the number of thermal cycles, as shown in Figure 4.

Because of fatigue due to cycles of thermal stress, the service life of a PC overlay is finite but difficult to predict. A useful service life of 10 years seems reasonable for an overlay constructed with a high-elongation resin and an excess of sand. It will be necessary to continue to monitor the per-

formance of the overlays to make a more accurate projection.

WHEN TO SPECIFY THIN POLYMER CONCRETE OVERLAYS

Three cases are presented to illustrate when the use of a thin PC overlay instead of a more conventional latex-modified concrete overlay is justified. The comparison is based on consideration of the service life of the PC overlay, the volume of traffic, the discount rate, and the value of driving time. For each of the three cases, it is assumed that the following conditions exist.

1. The overlay is to be placed on a two-lane bridge on I-95, 40 ft wide by 350 ft long.
2. It is necessary to increase the skid resistance and curtail the infiltration of additional chloride.
3. It is not feasible to construct a temporary bridge or detour traffic.
4. A 0.5-in.-thick PC overlay can be installed with 12 hr of lane closure time, at a cost of $24 per square yard plus the cost of controlling traffic with cones, and will provide acceptable service for 5 to 15 years.
5. A 1.25-in.-thick latex-modified concrete overlay can be installed with 9 days of lane closure time, at a cost of $30 per square yard plus the cost for controlling traffic with median barriers, and will provide acceptable service for 30 years.
6. Because it is difficult to predict the relationship between interest rate and inflation over a 30-year period, calculations are made for discount rates of 0, 5, and 10 percent, where the discount rate is the annual rate at which money increases in value through investment.

Case 1

For case 1, the peak-hour volume-to-capacity ratio with both lanes open is 0.30. With one lane closed, the ratio for the open lane is 0.60. Traffic flow will not be impeded by closing one lane for an extended period of time.

The cost for traffic control while the PC overlay is being installed is $1 per square yard and the cost for the latex overlay is $5 per square yard. The present worth of the thin PC overlay at a discount rate of 0 percent and a service life of 10 years is $\$25/yd^2 + \$25/yd^2 + \$25/yd^2 = \$75$ per square yard compared with $35 per square yard for the latex. At a discount rate of 5 percent and a service life of 10 years the present worth of the PC overlay is $25 + (\$25) \div (1.05)^{10} + (\$25) \div (1.05)^{20} = \$50$ per square yard, and at a discount rate of 10 percent it is $38 per square yard. According to the data in Table 7, the latex overlay at $35 per square yard is the most economical alternative in case 1 unless for a service life of 10 years the discount rate exceeds 12.6 percent, which is highly unlikely, or for a service life of 15 years the discount rate exceeds 6.3 percent. It seems reasonable to conclude that for case 1 the latex overlay is the most economical alternative because a service life for the PC overlay in excess of 10 years and a discount rate in excess of 5 percent are not likely at this time.

Case 2

For case 2 the peak-hour volume-to-capacity ratio is 0.6 with both lanes open and 1.0 with one lane closed. The one open lane cannot carry the peak-hour traffic volume, and a major reduction in speed and level of service occurs. The PC overlay is justified because one lane of the bridge cannot be closed during peak-hour traffic, which is necessary for the construction of the latex overlay.

For case 2 the cost of traffic control for the latex is higher than in case 1 because of the higher volume of traffic. A cost of $20 per square yard seems reasonable. The cost of traffic control for the PC overlay would be the same as in case 1. The present worth of the latex overlay for the 30-year service life is $50 per square yard and, as can be seen in Table 7, the present worth of the PC overlay is less if the discount rate exceeds 5 percent for a 10-year service life and exceeds 0 percent for a 15-year service life. For case 2 the use of the PC overlay is justified because one lane cannot be closed during peak-hour traffic to allow the construction of a latex overlay. In addition, the PC overlay can be justified on the basis of present worth when the discount rate exceeds 5 percent for a 10-year service life and 0 percent for a 15-year service life.

TABLE 7 Present Worth ($/yd^2) of Thin PC Overlay as a Function of Discount Rate and Service Life

Service Life (yr)	Discount Rate (%)		
	0	5	10
5	$150	$89	$62
10	75	50	38
15	50	37	31

Case 3

For case 3 the peak-hour volume-to-capacity ratio with both lanes open is 0.5 and with one lane closed it is 1.0. It is reasonable to assume that an increase in the volume-to-capacity ratio from 0.5 to 1.0 will cause a decrease in the average speed of the motorist from 53 mph to 32 mph (10, p. 140). Assuming the speed reduction affects a 10-mile segment of the average trip, the average time lost per vehicle is 7.4 min. Furthermore, assuming an average wage rate of $1 per hour per vehicle, which is extremely conservative, the cost of reduction in speed to the motorist is 12 cents per trip. Assuming an average hourly traffic flow of 1,300 vehicles, which is reasonable (11, p. 20), the cost to motorists of the reduction in speed is $161 per hour. For the 12 hours of the lane closure required for the installation of the PC overlay the cost is negligible assuming the lane closure occurs during off-peak hours. For the minimum of 9 days required for the installation of the latex overlay, the cost is $15 per square yard assuming the delays associated with the lane closure last for 8 hours each day. The addition of the cost of travel time increases the present worth of the latex overlay to $65 per square yard, and for a service life of 15 years the polymer overlay is more economical. For a service life of 5 or 10 years, the polymer is more economical when the discount rate exceeds 9.2 or 1.5 percent, respectively. For case 3, if the value of travel time is taken into account, the PC overlay is generally the most economical alternative based on present worth.

The costs of accidents and increases in vehicle operating costs that result from a lane closure provide an additional incentive to use a PC overlay. Over a 30-year period the total lane closure time required for the construction of a latex overlay with a 30-year service life is 3, 6, or 9 times greater than that required for the construction of

PC overlays with useful service lives of 5, 10, or 15 years, respectively. It is reasonable to expect that the benefits from a reduction in lane closure time and, therefore, in the number of potential accidents would increase with an increase in the volume of traffic and the useful service life of the PC overlay. Research is needed to quantify these benefits.

CONCLUSIONS

PC overlays can be installed by maintenance forces or by a contractor with a minimum of disruption to traffic.

PC overlays constructed with two polyester resins, 90-570 and LB183, are securely bonded to the base concrete and provide low permeability and high skid resistance after 1 year of service life.

PC overlays constructed with resins 90-570 and 317 are exhibiting the highest bond strength, the least amount of cracking, and the lowest permeability because they have a tensile elongation at break in the range of 20 to 50 percent as determined by ASTM D638-80, which is higher than that of the other resins tested.

The PC overlay becomes more economical relative to a latex overlay with increases in the service life of the PC overlays, the volume of traffic, the discount rate, and the value of driving time. These factors can be used to determine the most economical alternative.

PC overlays are still experimental and should not be used where alternative methods for extending service life are practical. A useful service life of 10 years seems reasonable, but the performance of the overlays should be monitored so that a more accurate projection of service life can be made.

ACKNOWLEDGMENT

The study was sponsored by the Virginia Highway and Transportation Reserch Council in cooperation with the Demonstration Projects Division of the FHWA.

REFERENCES

1. The American Concrete Institute. Applications of Polymer Concrete. Publication SP-69. Detroit, Mich., 1981, pp. 21-43.
2. M.M. Sprinkel. Polymer Concrete Overlay on Beulah Road Bridge: Interim Report No. 1--Installation and Initial Condition of Overlay. VHTRC 83-R28. Virginia Highway and Transportation Research Council, Charlottesville, Va., Feb. 1983.
3. M.M. Sprinkel. Evaluation of the Construction and Performance of Polymer Concrete Overlays on Five Bridges: Interim Report No. 1--Construction and Condition of the Overlays Initially and After One Year in Service. VHTRC 83-R29. Virginia Highway and Transportation Research Council, Charlottesville, Va., Feb. 1983.
4. M.M. Sprinkel. Polymer Concrete Overlay on Beulah Road Bridge: Final Report--Condition of Overlay After One Year in Service. VHTRC 84-R12. Virginia Highway and Transportation Research Council, Charlottesville, Va., Nov. 1983.
5. M.M. Sprinkel. Polymer Concrete Overlay on Big Swan Creek Bridge: Interim Report No. 1--Installation and Initial Condition of Overlay. VHTRC 84-R26. Virginia Highway and Transportation Research Council, Charlottesville, Va., Feb. 1984.
6. Polymer Concrete Overlays, Interim Users Manual--Method B. FHWA-TS-78-225. U.S. Department of Transportation, Washington, D.C., Feb. 1978.
7. H. Walker. Memorandum to M.M. Sprinkel. File 26.5.29.47.83A. Sept. 8, 1983.
8. M.M. Sprinkel. Thermal Compatibility of Thin Polymer Concrete Overlays. In Transportation Research Record, TRB, National Research Council, Washington, D.C., forthcoming.
9. D. Whiting. Rapid Determination on the Chloride Permeability of Concrete. FHWA-RD-81/119. FHWA, U.S. Department of Transportation, Aug. 1981.
10. N.J. Petersen and D.R. Samdahl. Highway Traffic Data for Urbanized Area Project Planning and Design. NCHRP Report No. 255. TRB, National Research Council, Washington, D.C., 1982, 191 pp.
11. J.L. Memmott and C.L. Dudek. A Model to Calculate the Road User Costs at Work Zones. Research Report 292-1. Texas Transportation Institute, Austin, Texas, Sept. 1982.

Publication of this paper sponsored by Committee on Structures Maintenance.

Effect of Water Infiltration of Penetrating Cracks on Deterioration of Bridge Deck Slabs

TAKEAKI KATO and YUJI GOTO

ABSTRACT

The deterioration of bridge decks is a serious maintenance problem in Japan, but deterioration in Japan is different from that in the United States because all bridge decks in Japan are covered with an asphalt overlay about 7.5 cm thick. Deterioration to a depth of about 18 cm has been found in decks that were seldom treated with deicing salts. These decks exhibited partial depression and fall-off, not scaling or spalling. Fatigue tests of model slabs and field surveys of bridges were carried out to determine the mechanism of deterioration, investigate methods of repair, and evaluate existing bridge decks. A test specimen, faultily constructed and severely cracked in the laboratory, deteriorated rapidly due to water infiltration of cracks, leakage through cracks, and abrasive action caused by crack movement under repeated loading. The fatigue strength of this specimen was about one-third its static strength, which is remarkably low compared with the normal fatigue strength of reinforced concrete. The mechanism of deterioration of bridge decks is thought to be a combination of three conditions: break-out of penetrating cracks caused by faulty construction and drying shrinkage, infiltration and leakage of rainwater, and abrasion due to wheel loading. Experimental work on an actual bridge showed expansive concrete to be effective in preventing break-out of shrinkage cracks.

Nihon Doro Kodan (Japan Highway Public Corporation), which oversees all express highways in Japan, presently maintains 3200 km of expressway including 3,500 bridges. The deterioration of bridge deck slabs is a serious problem in Japan, but the deterioration is different from that in the United States because all bridge decks are covered with an asphalt overlay about 7.5 cm thick. Deteriorated bridge decks are often found where deicing chemicals are seldom used. These decks exhibit partial depression and fall-off, not scaling nor spalling. Because air-entrained concrete is used for all bridge deck slabs in Japan, deterioration due to freezing and thawing is seldom seen.

Bridge decks designed before 1970 exhibit a great deal of deterioration and damage. The span between main girders of these bridges is about 4 meters, and the depth of the slab is 16 to 18 cm. Concrete cover over both top and bottom reinforcement is 3 cm. Most of these bridges have been repaired by partial reconstruction of the bridge deck, reinforcement with additional stringers between girders, or steel-plate bonding.

The 1973 "Specification for Highway Bridges" (published by Japan Road Association) has been revised to require that the span between main girders be about 3.2 meters and slab depth 22 to 23 cm. The specification of a concrete cover over top reinforcement did not change. To study the cause of deterioration, investigate methods of repair and reinforcement, and establish a method of evaluating bridge decks, many fatigue tests of bridge deck slabs have been carried out in the laboratory of Nihon Doro Kodan since 1976.

The following results have been obtained from full-size model tests.

1. A full-size model bridge deck (18 cm in depth) designed according to the older standards had a static strength of about 490 kN and a fatigue strength of about 250 kN under midspan point loading (loading plate size is 20 x 50 cm) (1).
2. A model bridge deck (22 cm in depth) designed according to the newer standards had a static strength of about 930 kN and a fatigue strength of about 440 kN under the same loading (2).

The ratio of fatigue strength to static strength in the bridge deck (about 0.5) is consistent with the results of other tests that used small-size slab specimens (3). It can thus be confirmed that bridge decks ordinarily show the same fatigue conduct as do general reinforced concrete (RC) members. Maximum wheel loads measured on expressways in Japan are around 100 kN if tandem axle loads are converted to equivalent single axle loads for reinforcement design.

Judging from the results of the fatigue tests mentioned previously, fatigue strength of deck slabs far exceeds the actual wheel load level, so it is not expected that fatigue damage will occur even in thin slabs designed according to the old standard.

Observation of deteriorated bridge decks indicated that (4)

- Deterioration is found only in limited parts of bridges.
- Deterioration of one-lane roadways is heavier than that of two-lane roadways.
- Most deteriorated parts exhibit a gridlike pattern of cracks that progress because of water infiltration and leakage. Free lime, concrete powder, and rusty liquid from reinforcements are found on the bottom surface of bridge decks.

On the basis of these observations it was hypothesized that water leakage through cracks that run the entire depth of the deck (hereinafter called penetrating cracks) was one of the most important factors in deck deterioration. To test this hypothesis a model bridge deck that exhibited the characteristics that had been observed in the field was reconstructed in the laboratory. Model slabs with severe, artificially induced penetrating cracks were constructed and repeated loading tests were carried out in the presence of water leakage. The results were a great quantity of abraded concrete powder and many broken pieces that flowed out with water leakage. Progressive deterioration was clearly shown and as a result fatigue strength dropped considerably. In this paper the deterioration mechanism of

bridge deck slabs, evidenced by these test results and field surveys, is considered and countermeasures to deterioration are described.

FATIGUE TESTS OF ARTIFICIALLY CRACKED MODEL SLABS

Fabrication of Specimens

To artificially produce penetrating cracks in a slab, the slab can be turned upside down and loaded so that cracks are initiated on the top surface. But this method is not very effective because, when the slab is righted, cracks on the top surface close due to the self-weight of the slab. At the beginning of loading little water infiltration was observed. Soon thereafter slight water leakage was noted, but it soon stopped. The progress of deterioration could no longer be followed.

At this point another method was tried to artificially produce cracks. A model bridge deck slab was fabricated on model steel girders under unfavorable construction conditions. The properties of the cement of this slab were

- Compressive strength--21.9 Mpa,
- Water-to-cement ratio--0.70,
- Slump--21.3 cm,
- Entrained air--3.6 percent, and
- Temperature--30°C.

Weather conditions were

- Skies--cloudy,
- Temperature--30°C (86°F), and
- Relative humidity--70 percent.

The slab was dried by the artificial wind (velocity 2 to 8 meters per second) of an electric fan. There was no moisture curing.

Details of this specimen are shown in Figure 1. The result was that many cracks, mainly above the positions of reinforcements, were generated in about 30 minutes after the concrete was cast. By the beginning of the fatigue test, about 3 months after construction, these cracks had grown wider because of shrinkage of the concrete and restriction of the steel girders as shown in Figure 2(a). Some of the transverse cracks are more than 1 to 2 mm in width. Figure 2(b) shows that wider transverse cracks reached the bottom surface of the slab, and during rainfall some free lime with water leakage could be observed.

Loading Method and Repetition Patterns

Figure 1 shows the loading apparatus, the positions of the moving load, and the water that was ponded on top of the slab during fatigue loading of the top surface of the slab. As a preliminary loading, approximately 2,000 78.4-kN repeated loadings were applied to points 1 to 23 to produce a gridlike pattern of cracks over the entire bottom surface. Consequently, cracks occurred and finally crack density reached 10 m/m² (total crack length per unit area) as shown in Figure 2(c).

The fatigue loading patterns were as follows. The loading point was changed to the next point after every cycle (0.3 million repetitions).

Case 1. Fatigue load level was 78.4 to 24.5 kN; one cycle on points 3, 5, 13, 19, and 21, respectively; three cycles on points 4, 11, 12, and 20, respectively; 5.1 million repetitions total.

Case 2. Fatigue load level was 103 to 24.5 kN; one cycle on points 11, 12, 20, 101, and 102, respectively; 1.5 million repetitions total.

Case 3. The upper load level was decreased to 88.3 kN; three rounds of one-cycle loadings on the same points as in case 2; 4.5 million repetitions total.

Case 4. The loading point was moved to point 103, which was between points 101 and 102 where serious damage had been observed. Fatigue load level was 88.3 to 24.5 kN; and after 0.65 million repetitions at this point fatigue failure occurred.

Various kinds of measurement were carried out by the static loading of points 9 through 15 after one-cycle loadings had been applied to all points. Water that leaked was collected in a container under

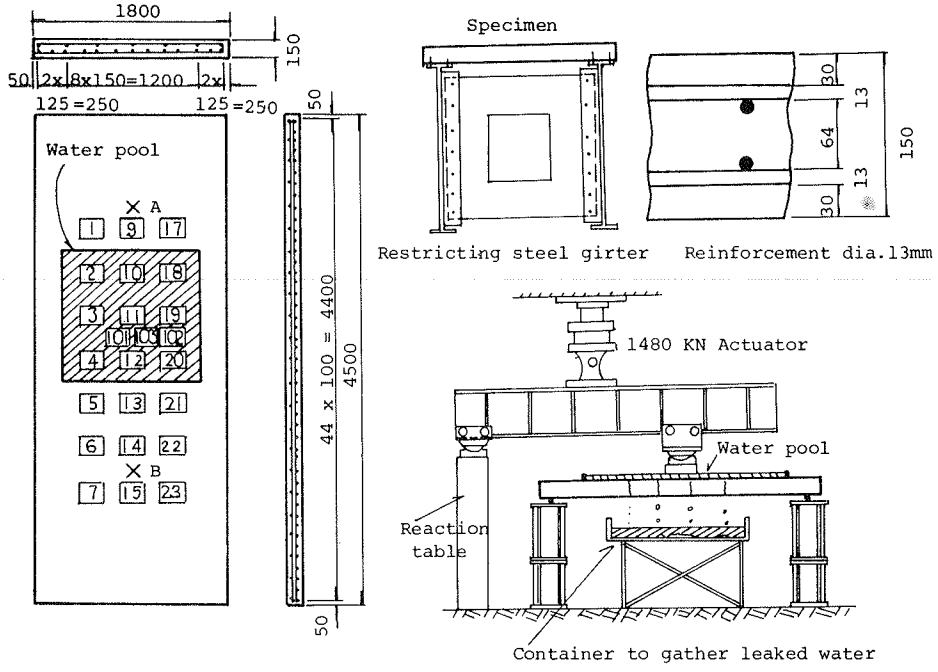

FIGURE 1 Shape of specimen, loading points, and loading apparatus.

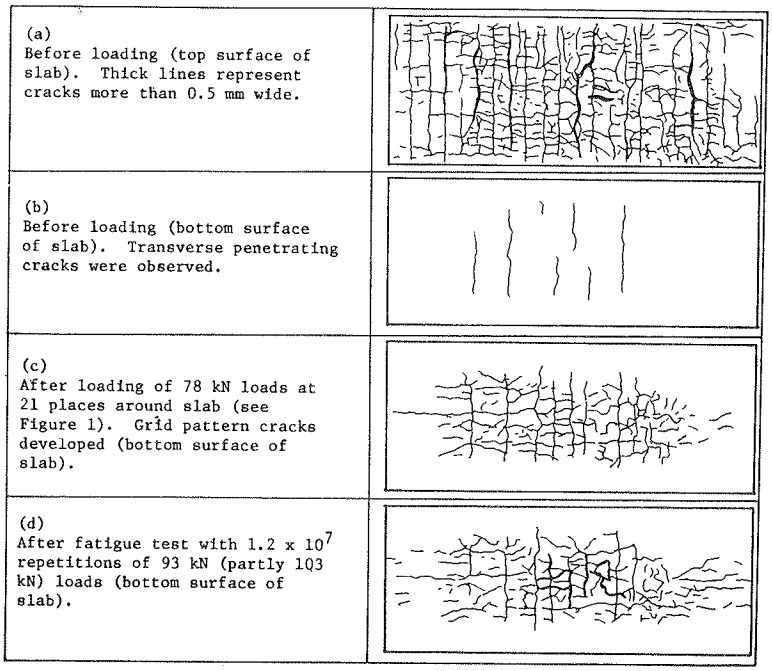

FIGURE 2 Change in cracks of slab specimen.

the specimen slab at every cycle on each point and its volume was measured. The water was then allowed to evaporate and any remains were measured as abrasion weight.

Fatigue Test Results

Progress of Deterioration

Figure 3 shows how the deterioration of the specimen progressed under repeated loading from case 1 through case 4. Figure 3(a) shows the loading process (one unit of the abscissa indicates one cycle or 0.3 million repetitions of load). In case 1 tensile strain of the bottom reinforcement was 400 ∿ 500 x 10^{-6} and the change in crack width was about 0.1 mm. Water leakage volume was slight and little deterioration occurred except for the flowage of some white, soft, free lime. In case 2 the upper limit of tensile strain of the reinforcements was arranged to be about 900 x 10^{-6} so that fatigue failure of the reinforcements would not occur, and the upper load level was increased to 103 kN. The result was that the volume of water leakage from cracks suddenly increased to 1000 to 2000 cm^3 per hour and abrasion weight during one cycle of loading reached 5 to 10 gm. The change of crack width due to loading was more than twice as large; clearly, deterioration was remarkably rapid [see Figure 3(b), (c), and (d)].

Because the tensile strain on the bottom reinforcement increased as deterioration progressed, the upper load was decreased to 88.3 kN and repeated loading was continued. As shown in Figure 3, deterioration progressed even as the load level was dropped to 88.3 kN.

Figure 4 shows that abrasion volume increased in proportion to the increase in total leakage volume. Apparently water infiltration of cracks and abrading action occurred. Figure 5 shows this abrading action. Figure 5(d) represents relative movement parallel to the crack direction near point 12 on the bottom surface. The sliding direction of a crack reverses when the loading point is moved from point

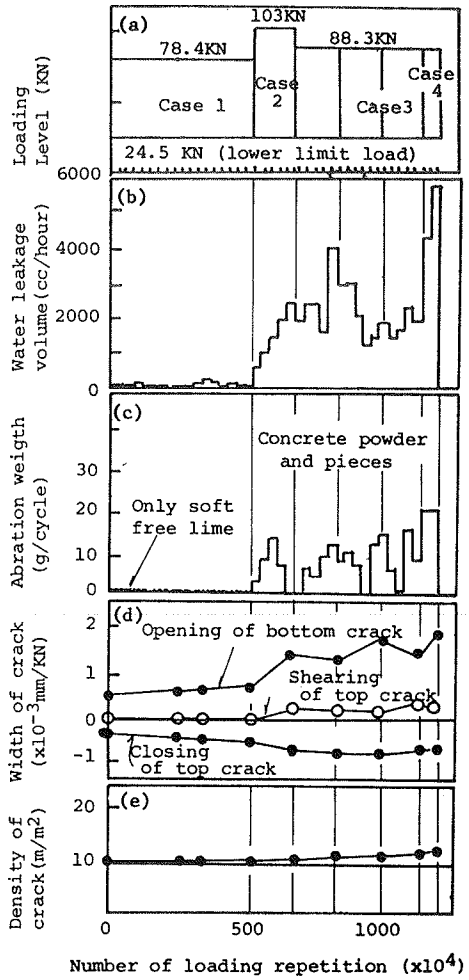

FIGURE 3 Progress of deterioration caused by loading repetition.

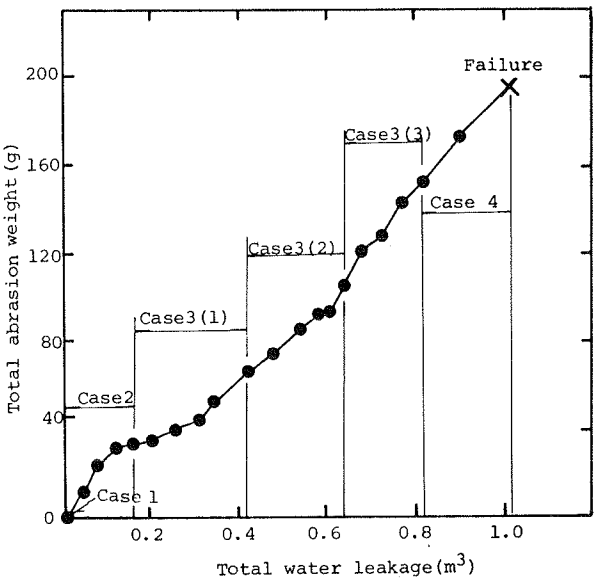

FIGURE 4 Relationship between total water leakage and total abrasion weight.

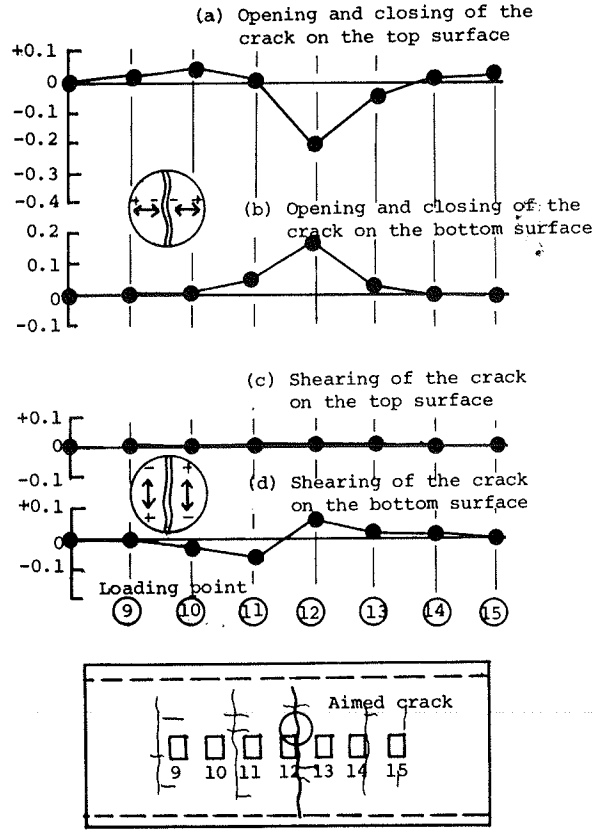

FIGURE 5 Change of representative crack caused by moving load.

11 to 12, abrading action occurs, and crack width is about 0.15 mm. After loading in case 3, the loading point was moved to point 103 in case 4. When point 103 was loaded, water leakage volume increased considerably to 4000 to 5000 cm^3 per hour, and at 0.65 million repetitions of load it suddenly increased significantly.

Therefore the loading machine was stopped and the specimen was observed in detail. On the top surface of the slab punching-shear cracks had occurred around point 103, and on the bottom surface shear cracks, which are different from bending cracks, had penetrated from the top surface. The vertical opening of a shear crack close to point 103 (measured with a dial gauge) was about 0.3 mm at a loading level of 0 to 88.3 kN. It was judged that punching-shear failure had occurred and the fatigue testing of this specimen ended.

State of Cracks

Later, fatigue test specimens were subdivided with a concrete cutter into small pieces and their cross sections were observed. Figure 6 shows a cross section connecting loading points 19 and 20. Fatigue punching-shear cracks, including vertical bending cracks generated at the position of reinforcement, were observed. Figure 7 shows cracks near point 20 magnified. Because of water infiltration and abrasion caused by loading, the inside width of the crack expanded to about 0.5 mm and its edge was round. The condition of the top surface of the slab is shown in Figure 8. A similar pattern of deterioration can often be seen on deteriorated in-service slabs after removal of the asphalt overlay.

Comparison with Static Strength

After fatigue tests were completed, static loading tests were carried out on points A and B shown in Figure 1. Static strength was 282 kN at point A and 273 kN at point B. If the average of these values is taken as the static strength of this slab, the ratio of fatigue upper loads of 88.3 kN and 103 kN

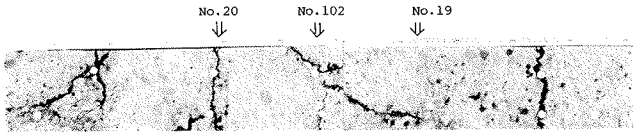

FIGURE 6 Cross section where punching-shear failure took place (seen from transverse direction).

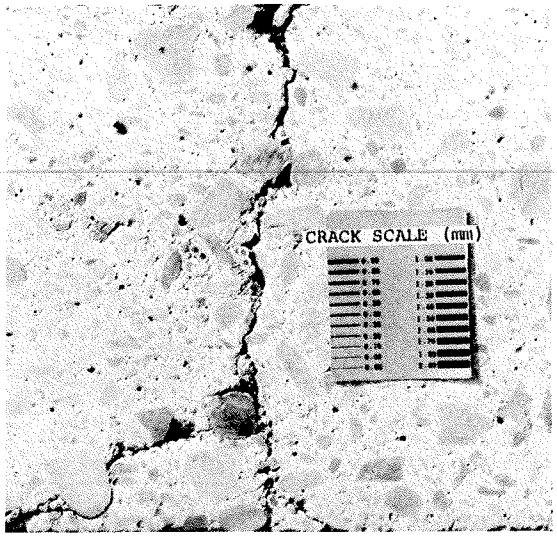

FIGURE 7 Magnified cross section under point 20 (width of crack expanded because of abrading action).

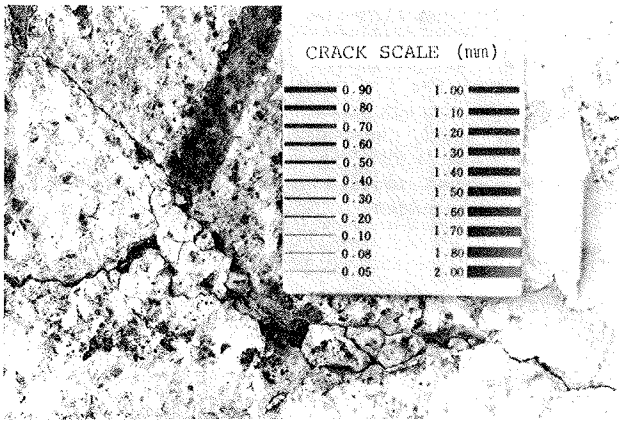

FIGURE 8 Deterioration of top surface of specimen.

to static strength is 0.32 and 0.37, respectively. These values are remarkably low compared with the value usually obtained without water infiltration. This is an example of a case in which the punching-shear strength of the concrete is less than the fatigue strength of the reinforcement.

DETERIORATION MECHANISM OF BRIDGE DECKS

It is assumed that the fatigue strength of the specimen with water leakage mentioned previously is about 88 kN. Because specimen depth was 15 cm and the steel ratio was different from that used in actual bridges, Kakuta's proposed formula (5), which gives a favorable calculation value of strength for this type of test specimen, was used. Conversion of these calculated values to the old standard (slab depth = 18 cm) gave about 120 kN. This is close to the maximum converted wheel load of 100 kN. To confirm this finding, full-size model tests need to be carried out. Investigation of this subject is now under way.

On the basis of the findings discussed previously, it may be concluded that the deterioration mechanism of bridge decks is a combination of three conditions:

1. Break-out of penetrating cracks that were caused by drying shrinkage and faulty construction,
2. Infiltration of cracks by rainwater and leakage of rainwater from cracks, and
3. Wheel loads great enough to cause abrasion.

It is widely known that bridge decks are thin compared with other concrete structures and that the influence on durability of slight construction errors and imperfections is serious. Furthermore bridge decks are loaded directly by traffic and subjected to severe curing conditions.

To confirm these findings, in 1983 the condition of cracks on the top surface of 24 bridge decks on the Tomei Expressway was investigated. Asphalt overlay sections 1 m x 2 m were torn off and the relationship between water leakage and cracks on the top surface of bridge decks was studied. Cracks, serious or not, occurred in all parts of the top surface of decks. Figure 9 shows serious cracking. From this figure it can be seen that cracks on the top surface of a deck are similar to those on the bottom surface and that rainwater is infiltrating penetrating cracks. (Only cracks on the bottom surface from which free lime flowed were considered.) In most places concrete over top reinforcement did not deteriorate even if there were cracks in it, and

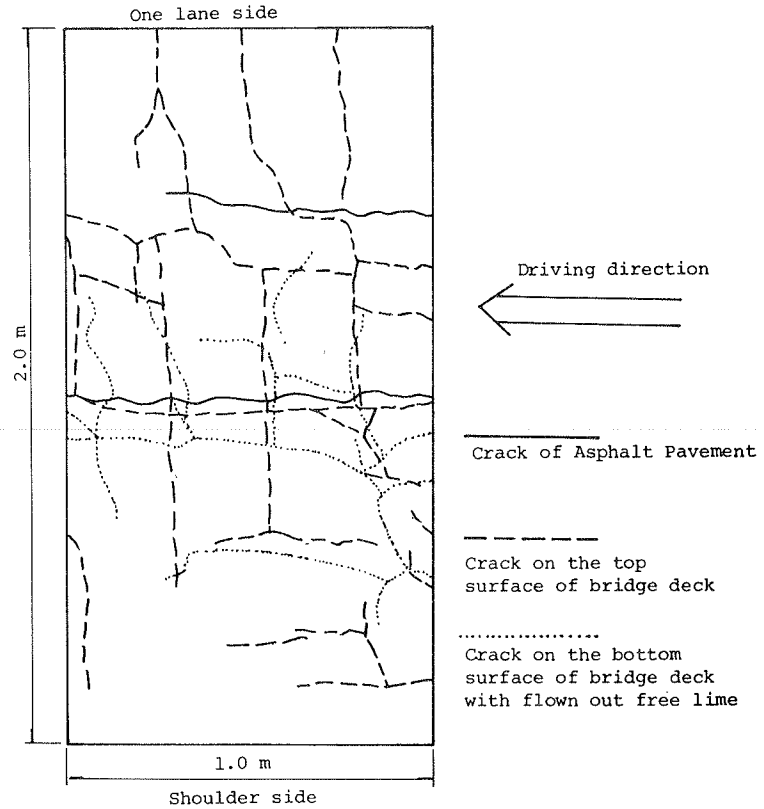

FIGURE 9 Typical crack pattern of deteriorated bridge deck in service.

minimal serious spalling of concrete and corrosion of reinforcement were found.

Table 1 shows the results of regression analysis of 24 investigated data. From the data in Table 1, it can be seen that in case 1 the correlation between asphalt overlay and bottom surface of the deck is not strong and that the correlation in cases 2 and 3 is fairly strong. In case 2, there is a difference between each coefficient of partial correlation. This difference shows that where there are cracks in the asphalt overlay there are always cracks in the top surface of the deck, but that there are not always cracks in the asphalt overlay where there are cracks in the top surface of deck.

In case 3 the difference between coefficients of partial correlation noted in case 2 obtains. The analysis of case 3 shows that where there are cracks in the bottom surface of a deck there are always cracks in the top surface of a deck, but that there are not always cracks in the bottom surface where there are cracks in the top surface.

From this analysis it is clear that rainwater infiltration of penetrating cracks results in damage to the bottom surface of a deck. Cracks in the top surface of a deck bring about reflection cracks in the asphalt overlay. In general, more deterioration was observed on one-lane than on two-lane bridges. This indicates that wheel load influences the rate of deterioration.

It is possible that the three previously mentioned conditions that contribute to deterioration occur at the same time. If this is the case, a method for maintaining deteriorated bridge decks can be devised based on the assignment of numerical values to the density of the gridlike pattern of cracks, from which free lime has flowed, on the bottom surface on bridge decks.

INFLUENCE OF DEICING CHEMICALS

Corrosion of reinforcement by deicing chemicals must also be considered. It is probable that such corrosion of reinforcement influences the progress of deterioration to some extent even if punching-shear failure due to wheel load does not occur. In the United States corrosion of reinforcement by deicing salts and spalling of covering concrete are known to be a problem (6). Even though asphalt overlays are less frequently used on bridge decks in the United States than in Japan, it is possible that the same type of deterioration occurs on the top surface of decks in both countries.

Figure 10 shows a concrete core taken from a severely deteriorated bridge deck where deicing chemicals were scattered. There are wide crack links between main reinforcing bars due to corrosion of the bars, and the covering concrete is spalling off. In this figure chlorine quantity inside the core far exceeds the specified value (in Japan NaCl weight in concrete must be less than 0.1 percent of sand weight).

Although deterioration due to deicing salts has not been observed frequently on bridge decks in Japan, it should be added to the three previously discussed conditions that accelerate deterioration.

COUNTERMEASURES TO DETERIORATION

The increase in the depth of bridge decks to 22 to 23 cm in the 1970 specification has been effective. Not only has shear strength increased, but adverse effects of construction errors and imperfections have decreased. In fact, if static strength were increased from 1.8 to 2.0, bridge decks would not fail because of wheel loads even if they were somewhat deteriorated.

The addition of stringers between main girders has been used for reinforcing bridge decks designed by the old standard. Because bending moment occasioned by wheel load is decreased by this rehabilitation method and crack movement due to wheel load becomes smaller, this method can be helpful. Al-

TABLE 1 Regression Analysis of Cracks in Asphalt Overlay: Top and Bottom of Slab

Case	Analysis	Coefficient of Multiple Correlation	Coefficient of Partial Correlation		
			Asphalt Overlay	Top of Slab	Bottom of Slab
1	Asphalt overlay versus bottom of slab	0.67	0.45	-	0.39
2	Asphalt overlay versus top of slab	0.77	0.77	0.27	-
3	Top of slab versus bottom of slab	0.84	-	0.55	0.83

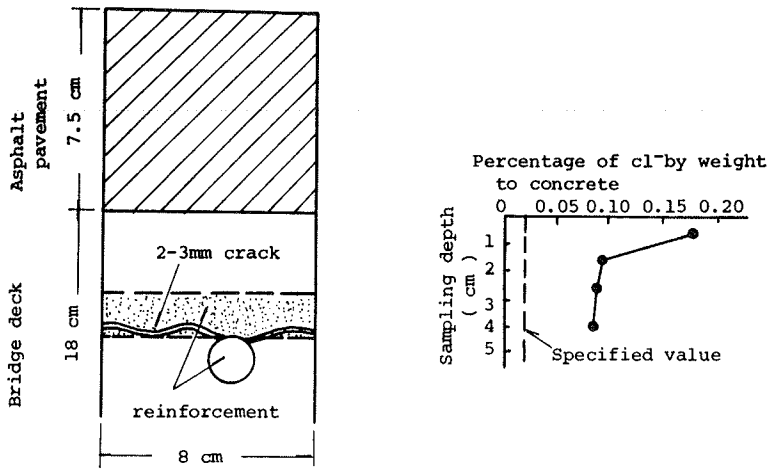

FIGURE 10 Cl^- content of concrete core of actual bridge deck and crack caused by corrosion of reinforcement.

though it slows the rate of deterioration, it is not a perfect method because a decrease of moment does not mean a decrease of shear force and an increase of shear strength of cross section.

Even with the new increased standard strength of bridge decks, the concrete cover top reinforcement remains 3 cm. Cracks caused by drying shrinkage and construction-induced cracks over reinforcements continue to occur. Therefore, reinforcements will continue to be corroded by infiltrating deicing chemicals, and covering concrete will eventually tear off.

There are two methods of preventing bridge-deck deterioration due to water infiltration of cracks. One method is to prevent the break-out of cracks due to factors such as drying shrinkage. Another method is to prevent water infiltration even if cracks occur. An example of the former will be given hereafter.

In 1980, for the first time in Japan, an expansive concrete bridge deck was constructed on a interchange ramp bridge (simple steel, composite plate girder) 41.5 m long and 8.5 m wide (7). The unit content of the expansive component is 35 kg/m³ estimated as part of cement content. Test specimens made with this mix proportion expanded to about 300 x 10^{-6} in a standard confined expansion test after 7 days of 20° C water curing. These test specimens had a steel-to-concrete ratio of 0.01.

Figure 11 shows the change in length of an expansive concrete deck in actual service compared with a like-shaped normal concrete deck constructed at the same time. Expansion of the expansive concrete deck reached its maximum value at 5 days, and expansive strain was measured as 160 x 10^{-6} longitudinally and 220 x 10^{-6} transversely. After about 700 days this expansion became nearly zero because of drying shrinkage. From this time on, expansive concrete completely compensated for the drying shrinkage of concrete. The normal concrete deck shrank to about 200 x 10^{-6} due to drying and, as shown in Figure 12, many cracks developed after 30 days. Few cracks developed in the expansive concrete deck. Another experimental construction of an expansive concrete bridge deck was carried out in 1982 on an expressway plate girder bridge with a span of 36.0 m. The results of this experiment were similar to those of the first.

It has been confirmed that expansive concrete is effective in preventing crack break-out. Therefore, Nihon Doro Kodan is now investigating the use of expansive concrete decks as a standard construction method.

To prevent water infiltration, waterproofing membranes were considered first, but, to date in Nihon Doro Kodan, membranes have been used only in limited projects, such as the reconstruction of a small area of deteriorated bridge deck. This is because

1. There were misgivings that asphalt overlays on the membranes would slide,
2. No reliable method of waterproofing had been established, and
3. Membranes are very expensive.

These problems will probably be solved in the future on the basis of recent technological developments. Large-scale experimental construction will determine

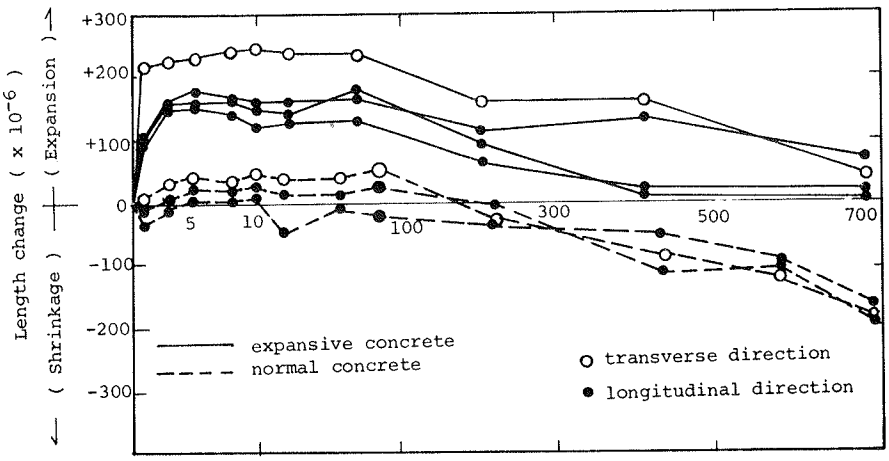

FIGURE 11 Change in length of normal and expansive concrete bridge deck.

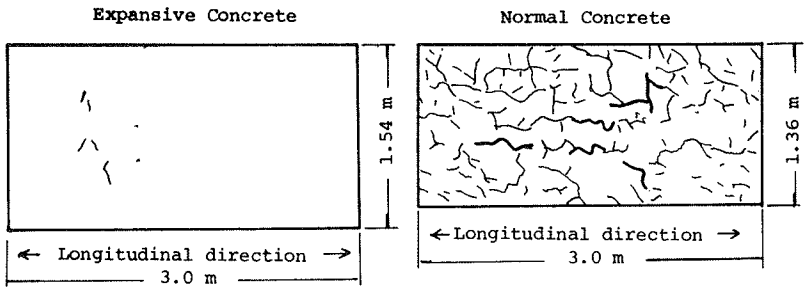

FIGURE 12 State of cracks on bottom surface of bridge deck 700 days after construction.

whether the practice of using waterproofing membranes will be adopted.

CONCLUSIONS

Mechanisms of bridge-deck deterioration, repair methods and methods of evaluating bridge-deck fatigue were investigated using tests of model slabs and field surveys of bridges in service.

The results may be summarized as follows:

Test specimens--constructed of low-quality concrete under adverse curing conditions and severely cracked by artificial means--deteriorated rapidly because of water infiltration of the cracks and abrasion caused by repeated loading.

Abrasive action was proved by the measurement of concrete powder and pieces that flowed out of penetrating cracks and by the measurement of abrading movement of cracks.

Fatigue failure, due to the punching shear of the slab, occurred. The fatigue strength of this specimen was about one-third its static strength, which was remarkably low compared with the usual fatigue strength of RC members.

From the test results and field surveys, the deterioration mechanism of bridge deck was estimated to be the combination of three conditions: breakout of penetrating cracks caused by drying shrinkage, infiltration and leakage of rainwater with and without dissolved deicing chemicals, and wheel loads that generate abrasive action.

Experimental constructions show that expansive concrete is extremely effective in preventing breakout of shrinkage cracks.

Some type of numerical characterization of the density of gridlike cracks from which free lime has flowed is needed to facilitate evaluation of existing bridge decks.

REFERENCES

1. Y. Iioka, T. Higai, and H. Muraki. Experimental Research on Fatigue Strength of Reinforced Concrete Slabs. Report of The Laboratory of Nihon Doro Kodan. Tokyo, Japan, Dec. 1977, pp. 132-142 (in Japanese).
2. Y. Iioka, T. Higai, and N. Fujita. A Fatigue Test of Reinforced Concrete Slab Decks. Report of The Laboratory of Nihon Doro Kodan. Tokyo, Japan, Dec. 1978, pp. 198-209 (in Japanese).
3. Y. Kakuta and Y. Fujita. Fatigue Strength of Reinforced Concrete Slabs by Punching Shear. Proc., Japan Society of Civil Engineering, Vol. 317, Jan. 1982, pp. 149-157 (in Japanese).
4. S. Fujita and Y. Kimura. Investigation of the Evaluation of Bridge Deck Slabs. Report of The Laboratory of Nihon Doro Kodan. Tokyo, Japan, Dec. 1980, pp. 134-146.
5. Y. Kakuta, A. Itoh, and Y. Fujita. Experimental Study on Punching Strength of Reinforced Concrete Slabs. Proc., Japan Society of Civil Engineering, Vol. 229, Sept. 1974, pp. 105-115 (in Japanese).
6. Durability of Concrete Bridge Decks. NCHRP Synthesis of Highway Practice No. 57, TRB, National Research Council, Washington, D.C., May 1979, 61 pp.
7. A. Takeda, S. Nakamura, and T. Toyofuji. Consideration on the Crack Control of Steel Bridge Deck Slabs. Concrete Journal, Vol. 21, No. 3, March 1983, pp. 31-39 (in Japanese).

Publication of this paper sponsored by Committee on Structures Maintenance.

TRANSPORTATION RESEARCH RECORD 950

Second Bridge Engineering Conference

Volume 2

Conducted by the Transportation Research Board,
National Research Council, and the Federal Highway
Administration, U.S. Department of Transportation,
September 24-26, 1984

TRB
TRANSPORTATION RESEARCH BOARD
NATIONAL RESEARCH COUNCIL
WASHINGTON, D.C. 1984

Transportation Research Record 950
Price $21.00
Edited for TRB by Naomi Kassabian, Scott Herman, Elizabeth Kaplan, and Jane Starkey

modes
1 highway transportation
3 rail transportation

subject areas
22 hydrology and hydraulics
25 structures design and performance
33 construction
34 general materials
40 maintenance

Transportation Research Board publications are available by ordering directly from TRB. They may also be obtained on a regular basis through organizational or individual affiliation with TRB; affiliates or library subscribers are eligible for substantial discounts. For further information, write to the Transportation Research Board, National Academy of Sciences, 2101 Constitution Avenue, N.W., Washington, D.C. 20418.

Printed in the United States of America

Library of Congress Cataloging in Publication Data
National Research Council. Transportation Research Board.
Bridge Engineering Conference (2nd: 1984: Minneapolis, Minn.)
Second Bridge Engineering Conference.
(Transportation research record; 950)
1. Bridges–Congresses. I. National Research Council (U.S.). Transportation Research Board. II. United States. Federal Highway Administration. III. Title. IV. Series.
TE7.H5 no. 950 380.5 s 84–14831
ISBN 0-309-03659-3 [624'.2] ISSN 0361-1981

Sponsorship of the Papers in This Transportation Research Record

GROUP 2–DESIGN AND CONSTRUCTION OF TRANSPORTATION FACILITIES
Robert C. Deen, University of Kentucky, chairman

Planning Committee for the Second Bridge Engineering Conference
John M. Hanson, Wiss, Janney, Elstner & Associates, Inc., chairman
James W. Baldwin, Jr., Robert M. Barnoff, Keith V. Benthin, Roland H. Berger, Bernard E. Butler, Robert C. Cassano, James D. Cooper, Robert N. Kamp, Jimmy D. Lee, Albert D.M. Lewis, Clellon L. Loveall, Frank D. Sears, Arunprakash M. Shirole, and A. Mainard Wacker

General Design Section
Samuel V. Fox, Texas State Department of Highways, chairman

Committee on Hydrology, Hydraulics and Water Quality
A. Mainard Wacker, Wyoming Highway Department, chairman
J. Sterling Jones, Federal Highway Administration, secretary
James E. Alleman, John J. Bailey, Jr., Harry H. Barnes, Jr., Darwin L. Christensen, Earl C. Cochran, Jr., Stanley R. Davis, Robert M. Engler, Samuel V. Fox, Benjamin M. Givens, Jr., John L. Grace, Jr., Richard B. Howell, William T. Jack, Jr., Kenneth D. Kerri, Floyd J. Laumann, Walter F. Megahan, Marshall E. Moss, Robert E. Rallison, Everett V. Richardson, Robert F. Shattuck, Michael D. Smith, Michael B. Sonnen, Charles Whittle, Henry B. Wyche, Jr.

Structures Section
John M. Hanson, Wiss, Janney & Elstner & Associates, chairman

Committee on General Structures
Clellon Lewis Loveall, Tennessee Department of Transportation, chairman
John M. Kulicki, Modjeski & Masters, secretary
John J. Ahlskog, Dan S. Bechly, Neal H. Bettigole, Edwin G. Burdette, Martin P. Burke, Jr., Jack H. Emanuel, Dah Fwu Fine, Richard S. Fountain, Frederick Gottemoeller, J. Leroy Hulsey, Walter J. Jestings, Robert N. Kamp, Heinz P. Koretzky, Celal N. Kostem, Wendell B. Lawing, Richard M. McClure, Gordon R. Pennington, David R. Schelling, Arunprakash M. Shirole, Marcello H. Soto, Robert F. Victor, Stanley W. Woods

Committee on Steel Bridges
Frank D. Sears, Federal Highway Administration, chairman
Chris S.C. Yiu, Pavlo Engineering Company, secretary
Pedro Albrecht, Dan S. Bechly, Chester F. Comstock, J. Hartley Daniels, David A. Dock, Jackson L. Durkee, Nicholas M. Engelman, John W. Fisher, Karl H. Frank, Louis A. Garrido, Wayne Henneberger, Robert B. Jarvis, B.F. Kotalik, Richard W. Lautensleger, Albert D.M. Lewis, Abba G. Lichtenstein, Joseph M. McCabe, Jr., Roy L. Mion, W.H. Munse, Robert H. Scanlan, Frederick H. Sterbenz, Carl E. Thunman, Jr., Carl C. Ulstrup

Committee on Concrete Bridges
Robert C. Cassano, California Department of Transportation, chairman
T. Alberdi, Jr., Craig A. Ballinger, W. Gene Corley, C.S. Gloyd, John M. Hanson, James J. Hill, Ti Huang, Cornie L. Hulsbos, Roy A. Imbsen, Hubert Janssen, Heinz P. Koretzky, H.G. Kriegel, John M. Kulicki, R. Shankar Nair, Edward G. Nawy, Walter Podolny, Jr., Adrianus Vankampen, Julius F.J. Volgyi, Jr., Donald J. Ward, W. Jack Wilkes

Committee on Dynamics and Field Testing of Bridges
James W. Baldwin, Jr., University of Missouri-Columbia, chairman
Charles F. Galambos, Federal Highway Administration, secretary
Baidar Bakht, Furman W. Barton, David B. Beal, Harold R. Bosch, John L. Burdick, William G. Byers, Gene R. Cudney, Bruce M. Douglas, Ismail A.S. Elkholy, Hota V.S. Gangarao, David William Goodpasture, Roy A. Imbsen, F. Wayne Klaiber, Celal N. Kostem, Robert H. Lee, Fred Moses, M. Noyszewski, Gajanan M. Sabnis, R. Varadarajan, William H. Walker, Kenneth R. White

Construction Section
Garland W. Steele, West Virginia Department of Highways, chairman

Committee on Construction of Bridges and Structures
Robert M. Barnoff, Pennsylvania State University, chairman
Mrinmay Biswas, John K. Bright, John F. Cain, David A. Dock, Jackson L. Durkee, Thomas H. Ellis, George A. Harper, Marvin H. Hilton, Frank J. Kempf, Andrew Lally, John P. Rutter, Michael M. Sprinkel, Man-Chung Tang, J.R. Wilder, Thomas G. Williamson, Kenneth C. Wilson

Committee on Fabrication and Inspection of Metal Structures
Robert N. Kamp, Byrd, Tallamy, MacDonald & Lewis, chairman
William G. Byers, Hubert F. Crick, Moss V. Davis, A.J. Dunn, Jackson L. Durkee, Nicholas M. Engelman, Philip F. Frandina, Karl H. Frank, G.A. Gix, Carl Hartbower, Kenneth F. Hurst, Frank J. Kempf, Michael Lauriente, Anthony Leone, Eric F. Nordlin, Jack P. Shedd, William F. Via, Jr., John P. Weisner

GROUP 3–OPERATION AND MAINTENANCE OF TRANSPORTATION FACILITIES
D.E. Orne, Michigan Department of Transportation, chairman

Committee on Structures Maintenance
Jimmy D. Lee, North Carolina Department of Transportation, chairman
Robert N. Kamp, Byrd, Tallamy, MacDonald & Lewis, secretary
John J. Ahlskog, Robert M. Barnoff, Roland H. Berger, Alfred G. Bishara, William G. Byers, A.J. Dunn, Ian J. Dussek, Nicholas M. Engelman, Ray W. James, Eldon D. Klein, Robert H. Krier, David G. Manning, Wallace T. McKeel, Jr., Richard J. Posthauer, Jack W. Roberts, George P. Romack, Steven J. Shecter, Arunprakash M. Shirole, Charles V. Slavis, Lloyd M. Smith, Marilyn H. Tobey, Robert G. Tracy, Alden L. West

Lawrence F. Spaine, Adrian G. Clary, William G. Gunderman, and Neil F. Hawks, Transportation Research Board staff.

Sponsorship is indicated by a footnote at the end of each report. The organizational units, officers, and members are as of December 31, 1983.

Notice: The Transportation Research Board does not endorse products or manufacturers. Trade and manufacturers' names appear in this Record because they are considered essential to its object.

Contents

Authors of the Papers in This Record

Barsom, J.M., Technical Center, United States Steel Corporation, One Tech Center Drive, Monroeville, Pa. 15146
Bellenoit, James R., Steinman, Boynton, Gronquist and Birdsall, Bourse Building, 21 S. 5th Street, Philadelphia, Pa. 19106
Blodgett, James C., 2800 Cottage Way, Room W2235, U.S. Geological Survey, Sacramento, Calif. 95825
Brice, James C., 345 Middlefield Road, U.S. Geological Survey, Menlo Park, Calif. 94025
Brown, Scott A., Sutron Corporation, 2190 Fox Mill Road, Herndon, Va. 22110
Buyukozturk, Oral, Department of Civil Engineering, Massachusetts Institute of Technology, 77 Massachusetts Avenue, Cambridge, Mass. 02139
Cantieni, Reto, EMPA, Swiss Federal Laboratories for Material Testing, Ueberlandstrasse 12a, CH-8600 Duebendorf, Switzerland
Chang, Howard H., Department of Civil Engineering, San Diego State University, San Diego, Calif. 92182
Cotton, George K., Simons, Li and Associates, 3555 Stanford Road, P.O. Box 1816, Fort Collins, Colo. 80522
Davis, Stanley R., Hydraulics Branch, FHWA, HNG-31, U.S. Department of Transportation, 400 Seventh Street, S.W., Washington, D.C. 20590
Fisher, John W., Department of Civil Engineering, Fritz Engineering Laboratory, Lehigh University, Bethlehem, Pa. 18015
Frank, William J., Berger, Lehman Associates, P.C., 550 Mamaroneck Avenue, Harrison, N.Y. 10528
Gee, D. Michael, Hydraulic Engineering Center, U.S. Army Corps of Engineers, 609 Second Street, Davis, Calif. 95616
Hanson, John M., Wiss, Janney, Elstner Associates, Inc., 330 Pfingsten Road, Northbrook, Ill. 60062
Hilton, Marvin H., Virginia Highway and Transportation Research Council, P.O. Box 3817, University Station, Charlottesville, Va. 22903
Hoffman, P.C., Department of Civil Engineering, Villanova University, Villanova, Pa. 19085
Holly, F.M., Jr., Iowa Institute of Hydraulic Research, University of Iowa, Iowa City, Iowa 52242
Holowka, M., Structural Office, Ontario Ministry of Transportation and Communications, 3501 Dufferin Street, Downsview, Ontario M3K 1N6, Canada
Imbsen, Roy A., Engineering Computer Corporation, 3217 Ramos Circle, Sacramento, Calif. 95827
Jones, J. Sterling, Federal Highway Administration, U.S. Department of Transportation, 6300 Georgetown Pike, HNR-10, McLean, Va. 22101
Keating, Peter B., Department of Civil Engineering, Fritz Engineering Laboratory, Lehigh University, Bethlehem, Pa. 18015
Kennedy, J.F., Iowa Institute of Hydraulic Research, University of Iowa, Iowa City, Iowa 52242
Kolmus, Russell J. III, Michael Baker, Jr., Inc., 4201 Dutch Ridge Road, Beaver, Pa. 15009
Koob, Michael J., Wiss, Janney, Elstner Associates, Inc., 330 Pfingsten Road, Northbrook, Ill. 60062
Kozy, William R., Michael Baker, Jr., Inc., 4301 Dutch Ridge Road, Beaver, Pa. 15009
Kulicki, John M., Modjeski and Masters, P.O. Box 2345, Harrisburg, Pa. 17105
Laursen, Emmett M., Department of Civil Engineering and Engineering Mechanics, University of Arizona, Tucson, Ariz. 85721
Li, Ruh-Ming, Simons, Li and Associates, Inc., 3555 Stanford Road, P.O. Box 1816, Fort Collins, Colo. 80522
McClure, Richard M., Department of Civil Engineering, Pennsylvania State University, University Park, Pa. 16802
Nakato, T., Iowa Institute of Hydraulic Research, University of Iowa, Iowa City, Iowa 52242
Osborn, Andrew E.N., Wiss, Janney, Elstner Associates, Inc., 330 Pfingsten Road, Northbrook, Ill. 60062
Out, Johannes M.M., Department of Civil Engineering, Fritz Engineering Laboratory, Lehigh University, Bethlehem, Pa. 18015
Prickett, Joseph E., Modjeski and Masters, P.O. Box 2345, Harrisburg, Pa. 17105
Rabbat, Basile G., Construction Technology Laboratories, Portland Cement Association, 5420 Old Orchard Road, Skokie, Ill. 60077
Richardson, E.V., Engineering Research Center, Colorado State University, Fort Collins, Colo. 80523
Russell, Henry G., Construction Technology Laboratories, Portland Cement Association, 5420 Old Orchard Road, Skokie, Ill. 60077

Sadler, C., Structural Office, Ontario Ministry of Transportation and Communications, 3501 Dufferin Street, Downsview, Ontario, M3K 1N6, Canada
Schamber, Robert A., Engineering Computer Corporation, 3217 Ramos Circle, Sacramento, Calif. 95827
Shen, Hsieh Wen, Department of Civil Engineering, Colorado State University, Fort Collins, Colo. 80523
Simons, Daryl B., Simons, Li and Associates, Inc., 3555 Stanford Road, P.O. Box 1816, Fort Collins, Colo. 80522
Stevens, M.A., P.O. Box 3263, Boulder, Colo. 80307
Trent, Roy E., Federal Highway Administration, HNR-10, Turner-Fairbank Highway Research Center, 6300 Georgetown Pike, McLean, Va. 22101
Vandershaf, David E., Engineering Computer Corporation, 3217 Ramos Circle, Sacramento, Calif. 95827
Waldner, H. Eugene, Modjeski and Masters, P.O. Box 2345, Harrisburg, Pa. 17105
Wang, Sang-yi, Department of Civil Engineering, Colorado State University, Fort Collins, Colo. 80523
West, Harry H., Department of Civil Engineering, Pennsylvania State University, University Park, Pa. 16802
Wium, Daniel J.W., Department of Civil Engineering, Massachusetts Institute of Technology, 77 Massachusetts Avenue, Cambridge, Mass. 02139
Yen, Ben T., Department of Civil Engineering, Fritz Engineering Laboratory, Lehigh University, Bethlehem, Pa. 18015

Preface

The most recent national bridge inventory of deficient bridges conducted by the Federal Highway Administration, U.S. Department of Transportation, indicates a continuous increase in the total number of bridges that are being classified as structurally deficient or functionally obsolete. Approximately 27,000 bridges in the federal-aid highway system alone are considered structurally deficient along with more than 123,000 bridges in the remainder of the system. The problem faced by railroad and transit agencies is just as severe. More than half of the one million bridges in the United States are more than 50 years old.

The problem is widely recognized, and increasing federal, state, and operating-agency appropriations are being made available for bridge construction, maintenance, and rehabilitation. Finding a solution to the rapid and continuous deterioration in existing bridge systems demands the best efforts of professional employees of state, federal, and local governments; private transportation agencies; consulting engineering firms; industry; planners; scientists; engineers; and other interested groups.

With an annual investment of billions of dollars in fixed transportation systems and the concomitant decision to protect the investment during an inflationary period has come a realization that the results of research and development and modern management methods must be applied to optimize the limited funds. Incremental savings that result from technical and administrative decisions will result in substantial long-term savings to owners and users.

The Second Bridge Engineering Conference was organized to facilitate an interchange of information on all aspects of planning, design, construction, repair, rehabilitation, replacement, and maintenance of vehicular bridges with specific emphasis on problems and solutions of interest to bridge engineers and administrators of highway, railroad, and transit agencies. The papers in these two volumes were prepared in advance and presented at the conference held September 24-26, 1984, in Minneapolis, Minnesota. Several of the papers are not included in the program because of limitations of time and space.

Organization and direction of the conference are the responsibility of the Planning Committee, whose members are listed on the reverse side of the title page. Technical reviews of papers were conducted by the several committees also listed on the same page.

The Bridge Engineering Conference was partly funded by the Federal Highway Administration. Financial contributions were also received from several contracting companies and suppliers in Minnesota.

The following organizations cooperated to make the conference possible:

COSPONSOR

Federal Highway Administration

COOPERATING AGENCIES

Associated General Contractors of America
American Railway Engineering Association
American Road and Transportation Builders Association
International Road Federation
Minnesota Department of Transportation
Minnesota Chapter, American Public Works Association
National Association of County Engineers

Fatigue Behavior of Weathered Steel Components

J.M. BARSOM

ABSTRACT

The effect of weathering on the fatigue behavior of fabricated weathering-steel components used for bare applications in bridges and other structures is discussed. The fatigue behavior of weathered weathering-steel and unweathered steel structural details is compared, and the applicability of AASHTO fatigue-design curves to predict their behavior is discussed. The data and discussion reveal that surface roughness of steels caused by weathering corresponds to localized stress (strain) raisers on the surface that may decrease the fatigue life of weathered weathering-steel components. Consequently, the effect of weathering on fatigue life is more pronounced for category A details. However, because the surface imperfections that correspond to the various AASHTO fatigue-design curves are more severe than those generated by weathering, the current AASHTO fatigue-design curves should be equally applicable to predict the fatigue behavior of weather and unweathered bridge-steel components.

Unprotected structural steels are oxidized by aqueous environments. This corrosion process occurs on the exposed surfaces and transforms the steel surface into corrosion products. Because of localized variations in the electrochemical reactions during the corrosion process and in the transport of the environment through the corrosion products, the oxidation process proceeds at slightly different rates in neighboring regions. This localized variation results in roughening of initially smooth surfaces that are exposed to the environment. Surface roughness corresponds to localized stress (strain) raisers on the surface that may decrease the fatigue life of weathered components.

Weathering steels (such as ASTM A588) subjected to full-immersion conditions in water corrode at the same rate as carbon steels. However, unlike carbon steels, weathering steels subjected to wet and dry weathering cycles form a highly adhering oxide layer that, with time, significantly retards further oxidation. During the time necessary to develop a protective oxide layer, the underlying surface of the steel is roughened by the wet and dry weathering process.

The effect of weathering on the fatigue behavior of fabricated weathering-steel components used for bare applications in bridges and other structures is discussed. The fatigue behavior of unweathered fabricated-steel details and the principles used in the development of the AASHTO fatigue-design curves are described. Then the effects of weathering, if any, on the fatigue behavior of fabricated-steel details are presented, and the applicability of the AASHTO fatigue-design curves to predict the behavior of weathered fabricated-steel components is discussed.

GENERAL FATIGUE BEHAVIOR OF STRUCTURAL COMPONENTS

The fatigue life of any structural component can be divided into an initiation life and a propagation life. The existence of stress raisers (such as changes in geometry, notches, or welding imperfections) minimize or may eliminate the initiation life. Stress raisers can be classified as geometry related (such as changes in cross section) or imperfections (such as gouges and weld imperfections). Fatigue cracks always initiate at the geometrical or imperfection stress raiser that causes the highest localized stress intensification. Thus, under identical test conditions, a machined and polished specimen would have a longer fatigue life than the same specimen that has mill surfaces that, in turn, would have a longer fatigue life than the same specimen that contains a severe gouge.

Once a crack is initiated the remaining life is governed by the stress range and the crack size, such that the fatigue life decreases as the magnitude of each of these parameters increases.

It can be concluded from the preceding discussion that, among other things, stress raisers decrease the fatigue life of structural components, and that the shortest life of otherwise identical details is obtained for the component that contains the most severe stress raiser.

FATIGUE BEHAVIOR OF UNWEATHERED STRUCTURAL-STEEL COMPONENTS

To evaluate the significance of weathering on the fatigue behavior of structural-steel components, the fatigue behavior of unweathered details and some of the principles used in the development of the AASHTO fatigue-design curves need to be understood. The behavior of unweathered details can then be used as reference to establish the significance, if any, of weathering on the fatigue behavior of structural-steel components.

AASHTO Fatigue-Design Curves

The current AASHTO fatigue-design specifications are based on experimental curves that relate the fatigue life to failure (number of cycles), N, of unwelded and welded details to the total (tension plus compression) applied nominal stress range, $\Delta\sigma$ (1). A large number of tests for a given detail were conducted and compared with other available data to generate statistically significant stress-range versus fatigue-life relationships. The design curves represent the 95 percent confidence limit for 95 percent survival of all available data for a given detail.

The extensive fatigue data that have been obtained by testing bridge details have been used to establish allowable stress ranges for various categories of details (Figure 1). Each category represents structural details that have approximately equivalent fatigue strengths. For example, all welded attachments that have a length (L) in the direction of stress equal to or less than 2 in. are considered to have equivalent fatigue strength. In reality, under identical fabrication and geometrical conditions, a 2-in.-long attachment results in a higher stress concentration than a shorter attachment and, therefore, would have a shorter fatigue life. Because the curve for each category corresponds to the 95 percent confidence limit for 95

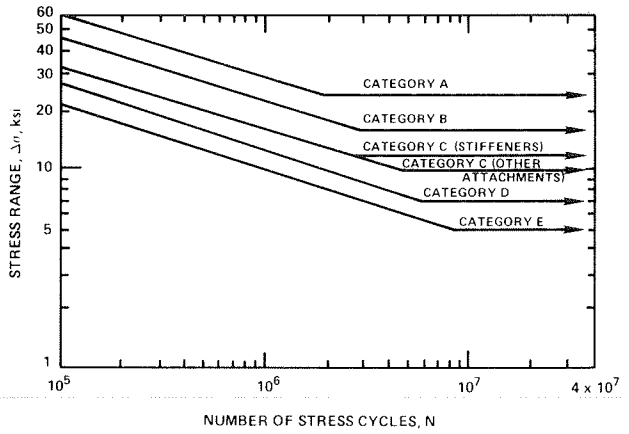

FIGURE 1 AASHTO design stress range curves for categories A-E.

percent survival of all the details in a given category, the fatigue-design curves correspond to approximately the shortest lives obtained for details in each category and are, therefore, governed by the details in that category that have the most severe geometrical or weld-stress concentration.

The existence of gouges and weld-imperfection stress raisers in a structural detail of a given geometry decrease the fatigue life of the detail. Consequently, significant variability (scatter) in fatigue-life data can be obtained by testing many details of identical geometry, but which contain different size imperfections. This variability in the data is apparent in the data base used to establish the AASHTO fatigue categories. For example, the longest life obtained for a category C detail (stiffener) that was tested at a stress range ($\Delta\sigma$) of about 25 ksi was about 4 times longer than the same detail that exhibited the shortest life. The difference in fatigue life for these two specimens was caused primarily by the difference in the size of the initial imperfections that existed in the specimens. The one that had the shortest life contained the most severe stress raiser. Because the shortest life is obtained for the specimen that contained the most severe imperfection, the AASHTO fatigue curve for each category is governed by the specimens that contained the most severe imperfection. Thus the AASHTO fatigue curves represent the 95 percent confidence limit for 95 percent survival of all the details in a given category and are governed primarily by the details in a given category that have the most severe geometrical discontinuities, imperfections, or both.

Imperfections in Structural Components

The AASHTO fatigue categories encompass base metal (category A) as well as weldments (categories B-F). Consequently, the imperfections that are the origin of fatigue cracks can be divided into three categories: (a) imperfections in base metal, (b) imperfections embedded in weld metal, and (c) imperfections at a weld termination or weld toe. The following is a brief characterization of the imperfections that are of primary significance to each of the AASHTO categories.

Category A

The AASHTO fatigue-design curve for category A determines the allowable stress ranges for base metal with as-rolled or cleaned mill surfaces and flame-cut edges that have a surface roughness value no greater than 1,000 microinches (μin.) R_a (arithmetic average roughness), as defined by the American National Standards Institute (ANSI) (2, p. 4).

The available data (3-8) indicated that "rolled beams provide the least severe flaw condition for structural elements and can yield extremely long lives at high stress-range levels; however, a large discontinuity in the surface or at the flange tip can reduce the fatigue life of the beam substantially" (4, p. 11). Thus a few rolled beams that contained large discontinuities, which are not permitted by the current specifications, yielded fatigue lives equivalent to the mean life for welded beams (category B).

Examination of welded-beam test results obtained at Lehigh University (3,4) indicated that, in general, the most severe imperfections resided in the fillet welds rather than at the flame-cut edges. The fatigue performance of good-quality [arithmetic average roughness (R_a) of 1,000 μin. or less] flame-cut edges was closer to that for rolled beams than for welded beams. Consequently, flame-cut edges that have an ANSI roughness of 1,000 μin. R_a or less are included in category A.

The notches introduced by good-quality flame cutting (R_a of 1,000 μin. or less) that caused failure were more severe and sharper than the notches introduced in rolled beams and plate surfaces by the rolling operation (4, p. 10). Because the shortest lives were obtained for the specimens that contained the most severe imperfections, the AASHTO fatigue-design curve for category A included those specimens that contained the most severe imperfections generated by good-quality flame cutting (R_a roughness $\leq$1,000 μin.).

Category B

The welded details that are encompassed in AASHTO category B are primarily fillet welds, groove welds with welds ground flush, and groove welds in transition joints that have generous slopes (no steeper than 1 to 2.5) and radii ($\geq$24 in.). These ground slopes and radii were selected to minimize the effects of the geometrical stress concentrations and thus force the fatigue cracks to initiate from subsurface weld imperfections.

Fatigue cracks in category B weldments originated at porosity, lack of fusion, weld repair, tack weld, stop-start position in the longitudinal flange-to-web fillet weld, or trapped slag (9). The majority of cracks initiated and propagated as subsurface cracks until they intersected the fillet-weld surface. The few cracks that started from the flange tip contained notches that were "visually apparent and more severe than the regular flange roughness caused by the flame-cutting procedure" (3, p. 22). Beams that failed by this mode yielded shorter lives than those that failed from weld imperfections. Despite the severe damage to the flange edges, the short lives for these beams exceeded the design life provided by the category B fatigue-design curve.

Because AASHTO specifications require the removal of severe gouges and notches from flanges, the most likely imperfection that would cause fatigue failure of plain welded beams is an internal weld imperfection.

Categories C-E

The majority of fatigue cracks in bridge girders initiate at a weld toe or at a weld termination near a stiffener, or other attachments such as a gusset plate or end of a cover plate. These are regions of high stress concentration and high residual stresses that may contain small weld imperfections such as

slag intrusion (9,10). Moreover, because the surface of the deposited weld metal is invariably rippled, the toe angle between the weld metal and the base metal can vary significantly at neighboring points along the weld toe, thereby resulting in variations in the stress concentration. For a cover plate with longitudinal fillet welds, the fatigue crack initiates at the termination of the weld. For a cover plate with transverse fillet welds, multiple fatigue cracks initiate at the toe of the weld.

Because fatigue cracks in categories C-E initiate from similar weld imperfections at weld toes and weld terminations, the decrease in fatigue life from category C to category E is related primarily to an increase in the severity of the geometrical stress raiser at the toe or termination of the weld. This severity is dependent on geometrical factors as well as on the quality of fabrication.

EFFECT OF WEATHERING ON THE FATIGUE PERFORMANCE OF WEATHERING-STEEL STRUCTURAL DETAILS

Surface roughening of steels that is caused by weathering corresponds to localized stress (strain) raisers on the surface that may decrease the fatigue life of weathered components. The change in fatigue life of a component caused by weathering depends primarily on the magnitude of the most severe stress raiser induced by weathering as compared with the magnitude of the most severe stress raiser residing in the component before weathering. Thus the decrease in fatigue life caused by weathering should be most pronounced for machined and polished components and negligible, if not beneficial, for components that contain severe surface notches or imperfections from other sources. Thus the magnitude of the effect of weathering on the mean fatigue life is strongly dependent on the intitial condition of the unweathered components, such that the mean fatigue-life curves for components with the smallest surface and subsurface imperfections exhibit the largest effects. Consequently, the effects of weathering on the AASHTO fatigue-design curves rather than on the mean fatigue-life curves should be investigated. Also, the correspondence between the most severe stress raiser encompassed by each AASHTO fatigue category and those induced by weathering need to be considered.

Surface Roughness Caused by Weathering

The arithmetic average surface roughness (R_a) for weathering-steel samples that have been weathered for up to 11 years was measured in accordance with ANSI procedures by using a standard roughness sampling length (cutoff) value of 0.03 in. The specimens weathered for 11 years had as-received mill surfaces and were exposed in a moderate marine environment. Specimens that were weathered for 6 years had either as-received mill-scaled surfaces or blast-cleaned surfaces and were weathered in a semi-industrial environment. All specimens were cleaned as recommended by ANSI/ASTM G1-72 in a 1 to 2 percent solution of sodium hydride in molten sodium hydroxide at 700°F.

Figure 2 shows the R_a values as a function of exposure time. The data indicate that the R_a values for all specimens and test conditions reach a constant maximum value of about 600 μin. between 2 and 3 years. Moreover, the peaks-per-inch count (of peaks greater than 50 μin., peak to valley) as a function of time, which is another surface roughness parameter, for all specimens and test conditions (Figure 2) also indicates that the surface roughness asperity density reaches a constant minimum value of about 100 peaks per inch between 2 and 3 years.

Because R_a, and therefore the depth of the surface pits, reaches a constant maximum value, and the peaks per inch reach a constant minimum value, the surface roughness induced by weathering corresponds to gentle craters rather than to sharp notches.

Effect of Weathering on AASHTO Fatigue Categories

The AASHTO fatigue-design curves represent the 95 percent confidence limit for 95 percent survival of all the details in a given category and, therefore, correspond to the fatigue behavior of the components that have the most severe geometry, imperfections, or both in that category. Therefore, most of the details in a given category should have longer fatigue lives than predicted from the design curve for that category. For example, a butt-welded component with the weld ground flush (category B) can be fabricated with minimum or no imperfections such that its fatigue life for a given stress range is as good as the life for the as-received plate or rolled beam (category A). The fatigue cracks for such a category B detail would more likely initiate from surface rather than from subsurface imperfections. Weathering, which is a surface phenomenon, would be expected to decrease the fatigue life of such a detail more than for a similar category B detail that contains a severe subsurface imperfection. Consequently, the effect of weathering on the fatigue

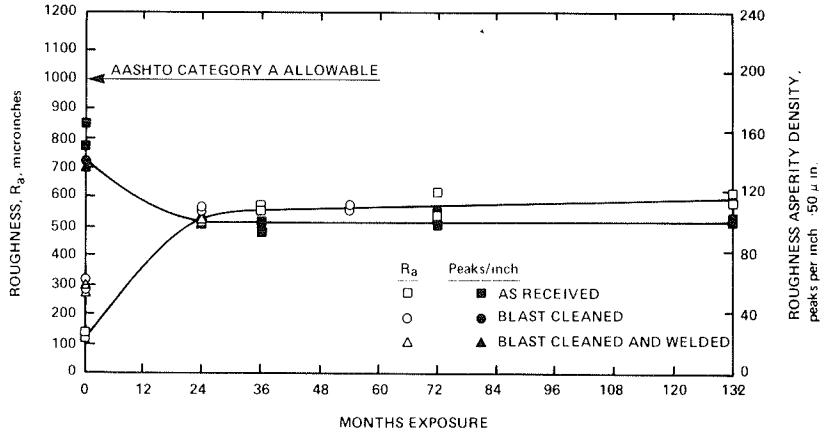

FIGURE 2 Surface roughness versus exposure time for weathering steels.

life of steel components must be considered in reference with its effect on the AASHTO fatigue curves rather than on the curves that correspond to the mean fatigue lives. The AASHTO fatigue curves represent the fatigue behavior of components that contain the most severe imperfections allowed for a given category, rather than the behavior of components that contain the least severe imperfections and therefore would exhibit superior fatigue behavior.

Category A

Fatigue tests conducted on unweathered category A type specimens indicated that the failure-causing notches introduced by good-quality flame cutting ($R_a \leq 1{,}000$ μin.) were more severe and sharper than the notches introduced in rolled-beam and plate surfaces by the rolling operation (4, p. 10). Consequently, the AASHTO category A fatigue curve corresponds to the fatigue behavior of components that contain notches that have a severity equivalent to at least the severity of a flame-cut edge with an R_a of 1,000 μin. Figure 2 shows that the ANSI roughness of weathered surfaces reaches a maximum of 600 μin., which is lower than the 1,000 μin. allowed for flame-cut edges. Therefore, the fatigue life of weathered weathering-steel surfaces should be longer than the life of flame-cut edges with 1,000 μin. roughness and, at a given stress range, longer than predicted by the AASHTO category A fatigue-design curve. This observation is supported by experimental data obtained at U.S. Steel Research for specimens with as-received mill-scaled surfaces and with blast-cleaned surfaces (Figure 3). (Note that these data are from an unpublished report by G.T. Blake, "Fatigue Tests of A588 Steel at Different Exposure Times During Six-Year Weathering," July 1982.)

Because weathering is a surface phenomenon that induces surface stress raisers, and because fatigue cracks for category A initiate at surface imperfections rather than from weld imperfections or from geometrical stress raisers as for categories B-E,

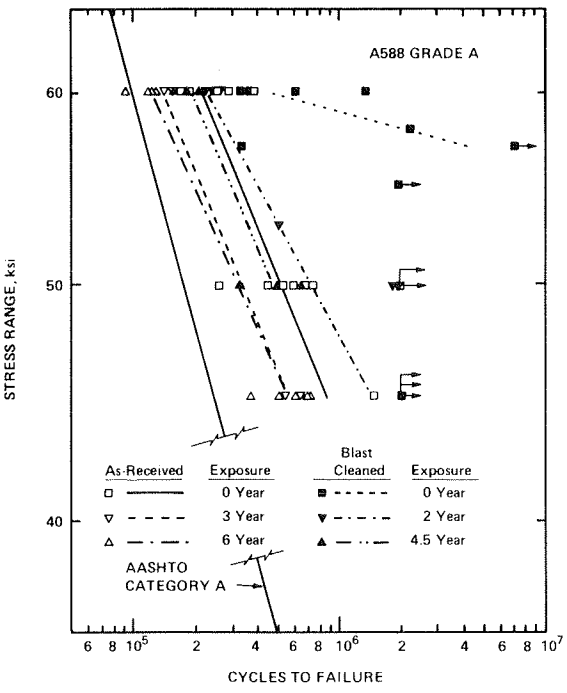

FIGURE 3 Fatigue data for as-received and blast-cleaned specimens.

the effect of weathering on the fatigue life of weathering-steel components should be most pronounced for category A type components than for any other component.

The fatigue behavior of weathered steel specimens was investigated by several Japanese organizations in a round-robin program reported by Kunihiro et al. (11). The investigation included (a) carbon steels and weathering steels, (b) two strength levels for each type of steel, (c) base metal specimens and butt-weld specimens that were ground flush, (d) three exposure sites that had different atmospheric severity, and (e) three exposure-time durations: 0, 2, and 4 years.

The following discussion presents an analysis of all the Japanese data for base metal specimens of the two grades of weathering steels that were exposed at three sites for 0, 2, and 4 years. These combined data have been reported by Albrecht (12) (Figures 4 and 5). These data indicate that, for stress ranges larger than about 35 ksi, some of the fatigue lives for weathered and, to a lesser extent, unweathered specimens were smaller than would be predicted by the AASHTO category A fatigue-design curve.

The data reported by Kunihiro et al. (11) were presented in a tabular form with comments that usually defined the location for the fatigue-crack initiation site. These comments indicate that the failure of many specimens was caused by cracks that initiated and propagated to failure outside the test section for the hourglass-shaped specimens (for example, fillet and radius regions of the transition from the test section to the shoulder, and in the shoulder and grip regions of the specimen). The fatigue life for these specimens was influenced by specimen preparation, specimen design, and test procedure, and it should not be used to characterize the behavior of unweathered or weathered specimens. Eliminating these test results from the total population presented in Figures 4 and 5 significantly decreases the number of data points that fall below the category A fatigue-design curve (Figures 6-8). Nevertheless, a few test results for both unweathered and weathered specimens still had fatigue lives that were lower than predicted by the design curve.

The data presented in Figures 6-8 represent the total population of test results for specimens whose failure was confined to the test (necked-down) section and for some specimens whose fracture origin was not identified and could have failed outside the test section. The data in Figures 7 and 8 also represent test results obtained from the three exposure sites that had significantly different atmospheric severity. One of the three sites, the Simonoseki site, was a marine environment and "was close to a tunnel where the exhaust from the vehicles [localized acid water] could have affected the results" (11). Unfortunately, the reported data were not identified by exposure site and, therefore, the effect of atmospheric severity on the fatigue life of the specimens, especially those exposed at the Simonoseki site, cannot be delineated.

Some of the unweathered-specimen test data fell below the AASHTO category A fatigue-design curve. Further analysis of the data presented by Kunihiro et al. (11) indicated that the yield strength for the SMA 50 grade steel varied between 47 and 64 ksi, and for the SMA 58 grade steel it varied between 67 and 74 ksi (the SMA 50 and 58 represent minimum tensile strengths in kg/mm²). The minimum stress for the fatigue tests was about 3 ksi. Consequently, the maximum stress for specimens subjected to stress ranges that exceeded 44 ksi would be higher than the yield strength of some specimens. The fatigue life for specimens subjected to such test conditions, as

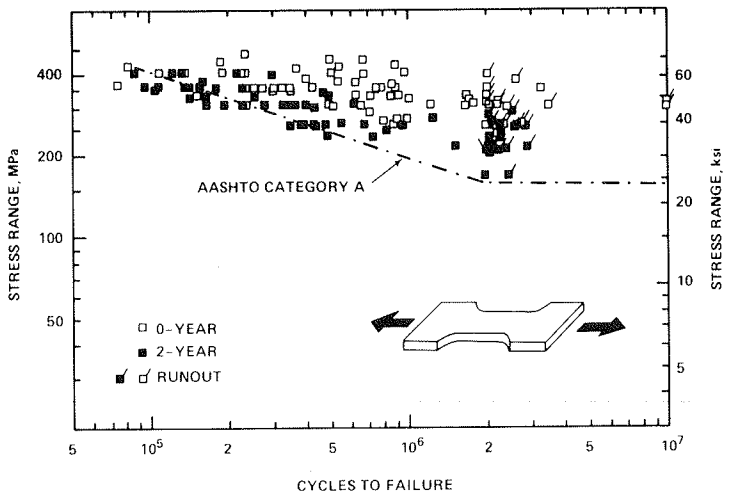

FIGURE 4 Fatigue strength of 2-year weathered plain plate specimens fabricated from Japanese atmospheric corrision resisting steels (SMA 50 and SMA 58).

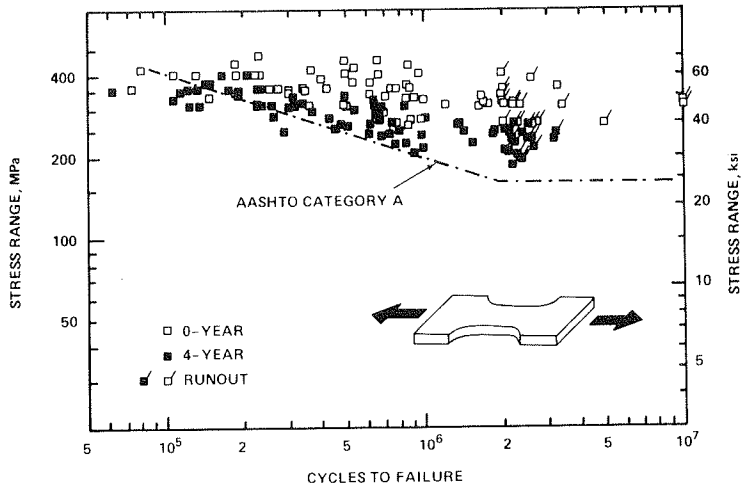

FIGURE 5 Fatigue strength of 4-year weathered plain plate specimens fabricated from Japanese atmospheric corrosion resisting steels (SMA 50 and SMA 58).

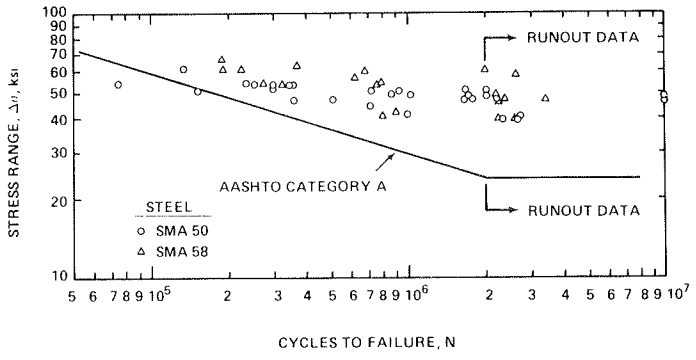

FIGURE 6 Fatigue data for plane specimens before atmospheric exposure.

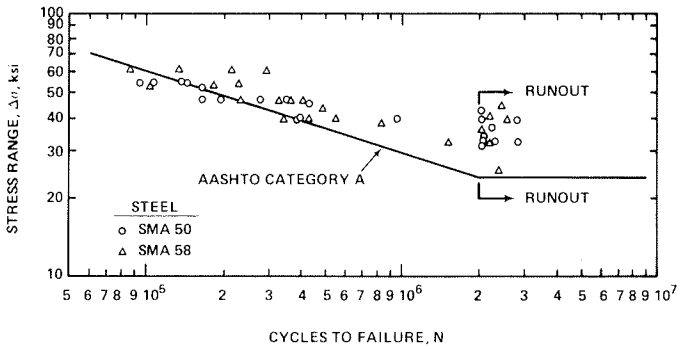

FIGURE 7 Fatigue data for plane specimens after 2-year exposure in three atmospheric environments.

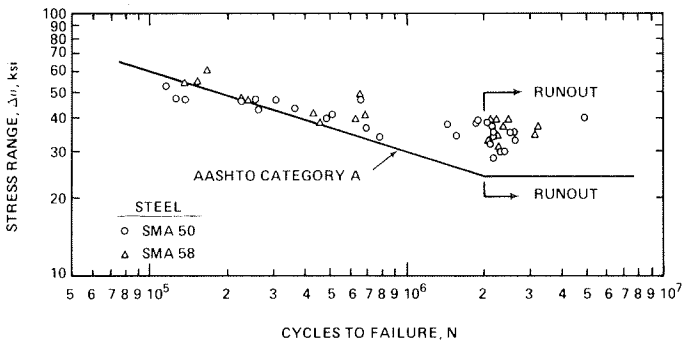

FIGURE 8 Fatigue data for plane specimens after 4-year exposure in three atmospheric environments.

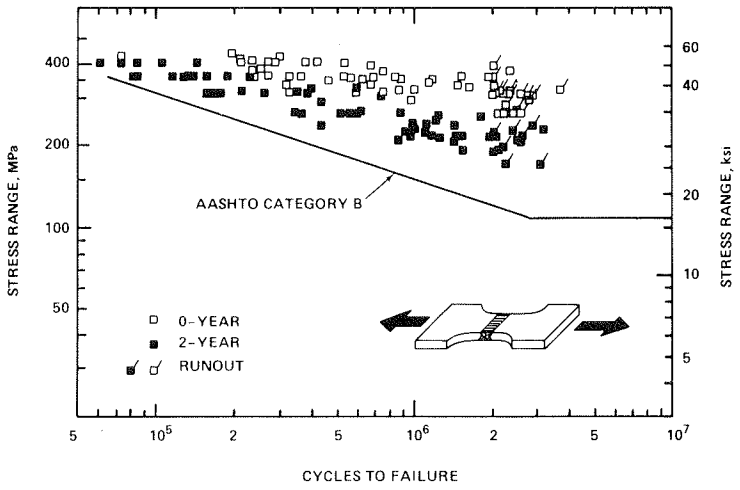

FIGURE 9 Fatigue strength of 2-year weathered butt-welded ground-flush specimens fabricated from Japanese atmospheric corrosion resisting steels (SMA 50 and SMA 58).

expected, is less than that predicted by the category A fatigue-design curve. In other words, the AASHTO design curve should not be used to characterize the behavior of these specimens. Unfortunately, although the yield strength for the steels that were obtained from different sources was reported, the source or yield strength for the individual fatigue specimens was not given.

Examination of the data presented in Figures 6-8 indicates that 10 of the 13 test results that exhibited fatigue lives shorter than those predicted for the AASHTO category A fatigue-design curve were of the lower-strength grade steel (yield strength $\geq$ 47 ksi). Nine of these 10 test results (two in Figure 6, four in Figure 7, and three in Figure 8) were at stress ranges ($\Delta\sigma$) equal to or higher than 47 ksi, with one (Figure 8) at a $\Delta\sigma$ of about 55 ksi. The corresponding maximum stress for these specimens was equal to or higher than 50 ksi, with one subjected to a maximum stress of 58 ksi. The remaining specimen (1 of the 10 in Figure 8) was subjected to a stress range of 43.5 ksi and a maximum stress of

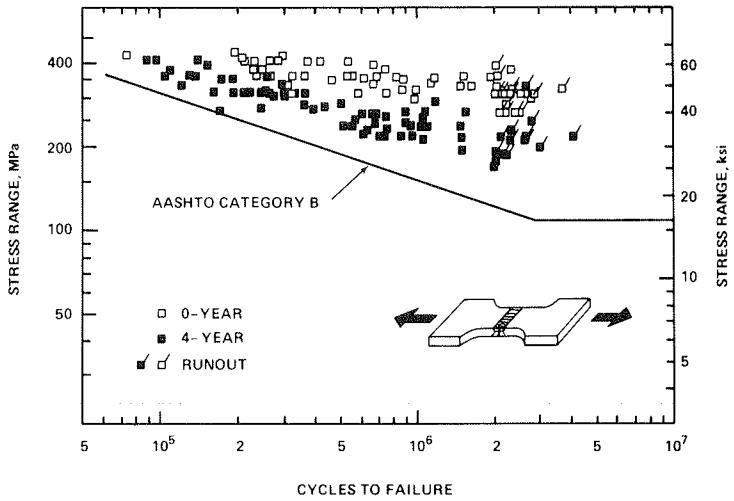

FIGURE 10 Fatigue strength of 4-year weathered butt-welded ground-flush specimens fabricated from Japanese atmospheric corrosion resisting steels (SMA 50 and SMA 58).

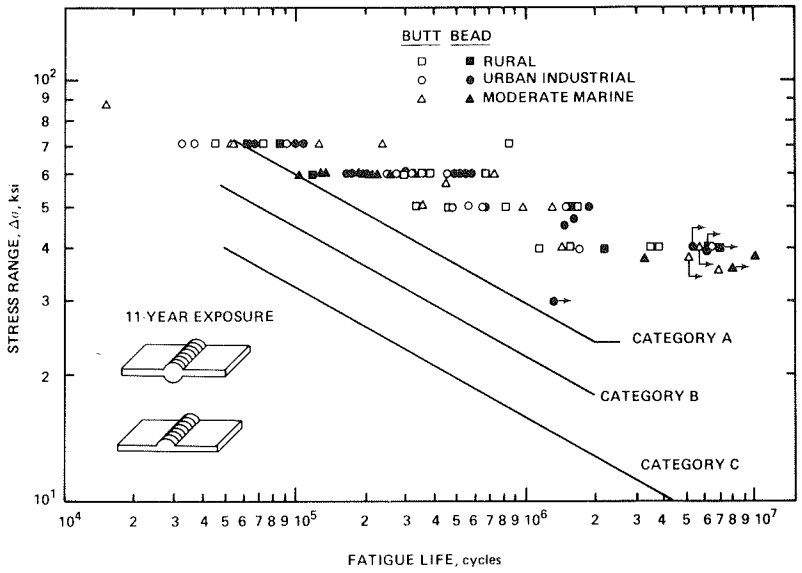

FIGURE 11 Fatigue data for butt-welded specimens and bead-on-plate specimens of ASTM A588 steel weathered for 11 years in three environments.

46.5 ksi, which is close to the minimum yield strength reported for the SMA 50 grade steel. The fatigue life for this specimen was 2.65×10^5 cycles, which is within 8 percent of the 2.85×10^5 cycles expected from the category A fatigue-design curve.

Based on the preceding observations and because the AASHTO fatigue-design curves represent the 95 percent confidence limit for 95 percent survival of all the details in a given category, the behavior for the data reported by Kunihiro et al. (11) appears to be consistent with the data base used in the development of the AASHTO fatigue-design curves.

Category B

Fatigue cracks in components that contain category B type details occur primarily at subsurface imperfections such as gas pockets. These imperfections are more severe than the surface or flame-cut edge imperfections allowable for category A type details. Because weathering is a surface phenomenon, it cannot alter the severity of subsurface imperfections. Consequently, the category B fatigue-design curve corresponds to a lower bound for weathered and unweathered category B details. These observations are supported by all available data (11,12) for weathered weathering steels (Figures 9 and 10), where all the test results for weathered and unweathered butt-welded ground-flush specimens exhibited longer fatigue lives than those predicted by the category B fatigue-design curve.

Categories C, D, and E

Fatigue cracks in specimens that correspond to categories C, D, and E initiate from similar weld imperfections that are equal to or smaller than 0.016 in. and that are located at weld toes and weld terminations. The decrease in fatigue performance from

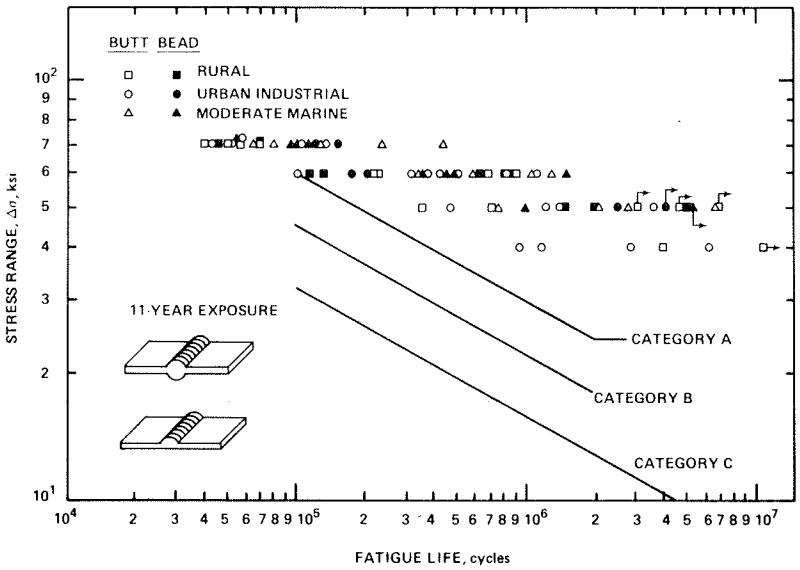

FIGURE 12 Fatigue data for butt-welded specimens and bead-on-plate specimens of ASTM A242 steel weathered for 11 years in three environments.

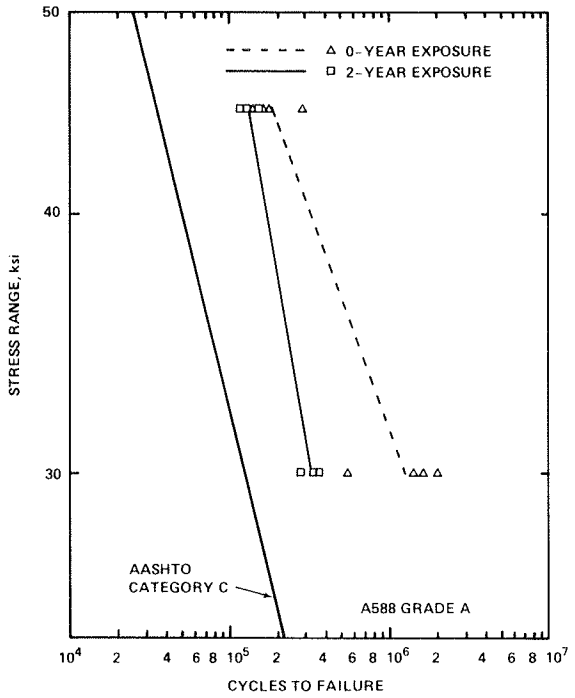

FIGURE 13 Fatigue data for blast-cleaned welded specimens (from Blake, unpublished data).

category C to D to E is related primarily to an increase in the geometrical stress concentration in the regions of the weld imperfections. Because metal removal due to weathering is negligible when weathering steel is used properly, and because weathering does not preferentially attack the weld metal or heat-affected zone over the base metal (13), it cannot increase the geometrical stress concentration inherent in the geometries for categories C, D, and E. Furthermore, because the size (0.016 in.) of the weld imperfections for these categories is small, the removal of a surface layer of metal by weathering may eliminate or at least decrease the size of the surface imperfections, thus resulting in a possible improvement in the fatigue lives for category C, D, and E details that initially contained severe imperfections. Improved fatigue life for fabricated components as a result of weathering has been documented by Yamada (14).

Figures 11-15 present fatigue data for unweathered and weathered weathering-steel category C details (12, 15, and unpublished data from Blake). These figures present data from specimens that have been weathered for up to 11 years. The combined data indicate that weathering had a negligible effect on the fatigue behavior of category C type details. More importantly, all the specimens exhibited better fatigue lives than those that correspond to the AASHTO category C fatigue-design curve.

Figure 16 (12) presents fatigue data for unweathered and weathered weathering-steel category D details. The data indicate that the fatigue behavior of weathered and unweathered specimens are identical, and that the AASHTO category D fatigue-design curve predicts their behavior conservatively.

No data are available for weathered category E type specimens; however, based on the preceding observation, weathering should not have any adverse effect on their fatigue behavior.

Based on all available data for the fatigue behavior of weathered weathering-steel components and on the discussion in the preceding sections, it can be concluded that the current AASHTO fatigue-design curves are equally applicable to predict the fatigue behavior of weathered as well as unweathered bridge-steel components.

SUMMARY

The data and discussion presented in this paper indicate that surface roughness of steels caused by weathering corresponds to localized stress (strain) raisers on the surface that may decrease the fatigue life of weathered components. Consequently, the effect of weathering on fatigue life is more pronounced for category A details of the AASHTO fatigue-design provisions. Nevertheless, because the most severe surface imperfections that correspond to the various AASHTO fatigue-design categories are more severe than those generated by weathering, the

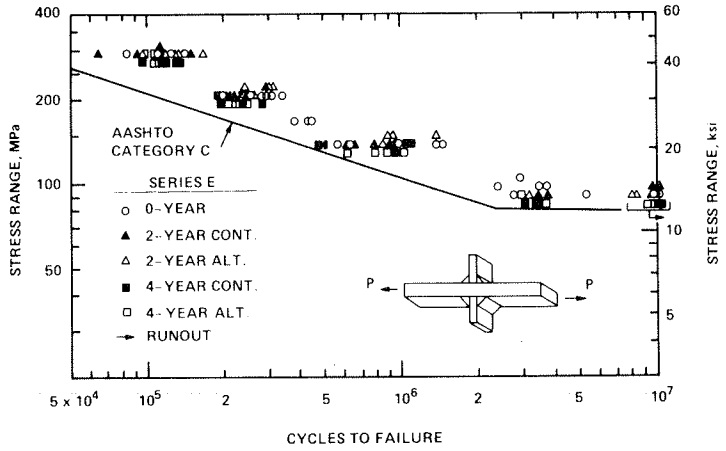

FIGURE 14 Comparison of data for specimens with transverse stiffeners and AASHTO allowable category C line (12).

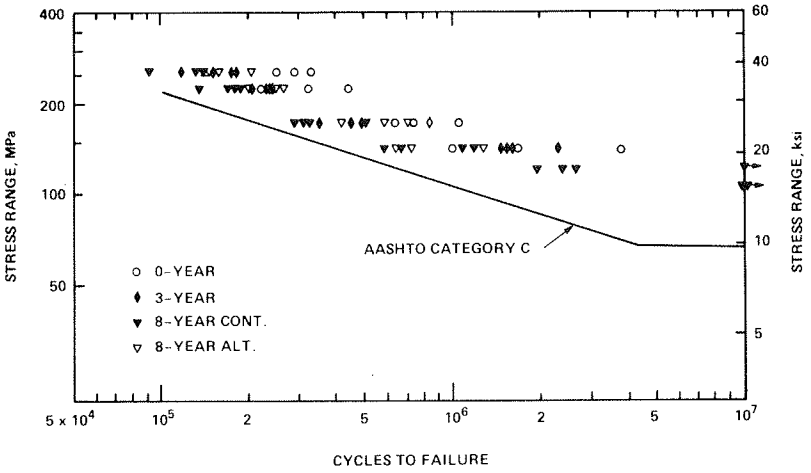

FIGURE 15 Comparison of category C type specimens and AASHTO allowable category C curve (15).

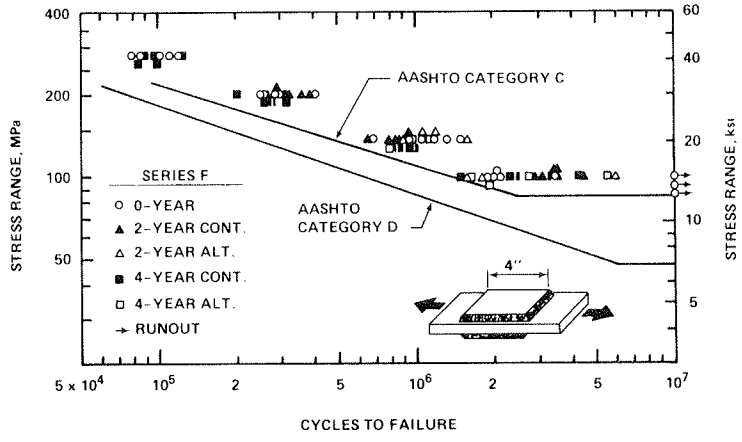

FIGURE 16 Comparison of all data for specimens with attachments (12).

current AASHTO fatigue-design curves should be equally applicable to predict the fatigue behavior of weathered as well as unweathered structural-steel components.

REFERENCES

1. Standard Specifications for Highway Bridges. AASHTO, Washington, D.C., 1977.
2. Surface Texture. Report ANSI B 46.1-1978. American National Standards Institute, New York, 1978.
3. J.W. Fisher, K.H. Frank, M.A. Hirt, and B.M. McNamee. Effect of Weldments of the Fatigue Strength of Steel Beams. NCHRP Report 102. TRB, National Research Council, Washington, D.C., 1970, 114 pp.
4. J.W. Fisher, P.A. Albrecht, B.T. Yen, D.J. Klingerman, and B.M. McNamee. Fatigue Strength of Steel Beams with Welded Stiffeners and Attachments. NCHRP Report 147. TRB, National Research Council, Washington, D.C., 1974, 85 pp.
5. F.C. Lea and J.G. Whitman. The Failure of Girders Under Repeated Stresses. Welding Research Supplement, Vol. 18, No. 1, Jan. 1939.
6. J.D. Nee. Fatigue Strength of USS "T-1" Constructional Alloy Steel Beams With and Without Stiffeners. Applied Research Laboratory, United States Steel Corporation, Monroeville, Pa., Feb. 1966.
7. D.R. Sherman and J.E. Stallmeyer. Fatigue of "T-1" Beams. Status Report of Fatigue Committee. Welding Research Council, University of Illinois, Urbana, May 1963.
8. W.M. Wilson. Flexural Fatigue Strength of Steel Beams. Engineering Experiment Station Bull. 377. University of Illinois, Urbana, Vol. 45, No. 33, Jan. 1948.
9. E.G. Signes et al. Factors Affecting the Fatigue Strength of Welded High Strength Steels. British Welding Journal, Vol. 14, No. 3, 1967.
10. F. Watkinson et al. The Fatigue Strength of Welded Joints in High Strength Steels and Methods for Its Improvement. In Proc., Conference on Fatigue of Welded Structures, The Welding Institute, Brighton, England, July 1970.
11. T. Kunihiro, K. Inoue, and T. Fukusa. Atmospheric Exposure Study of Weathering Steel. Research Laboratory Report 729. Ministry of Construction, Tokyo, Japan, 1972.
12. P. Albrecht. Fatigue Behavior of 4-Year Weathered A588 Steel Specimens with Stiffeners and Attachments. Report FHWA/MD-81/02. Department of Civil Engineering, University of Maryland, College Park, July 1978.
13. P.R. Simmon. Arc Welding of Weathering Steels. Welding Journal, Dec. 1968.
14. K. Yamada. Japanese Experience on Weathering Steel Bridges. Department of Civil Engineering, Nagoya University, Furo-Cho, Chikusa-Ku, Nagoya, Japan, 1983.
15. P. Albrecht and J.G. Cheng. Fatigue of 8-Year Weathered Automatically Welded A588 Steel Stiffeners. Department of Civil Engineering, University of Maryland, College Park, June 1982.

Publication of this paper sponsored by Committee on Steel Bridges.

Fatigue Strength of Weathered and Deteriorated Riveted Members

JOHANNES M.M. OUT, JOHN W. FISHER, and BEN T. YEN

ABSTRACT

A study has been performed on the fatigue resistance of corroded and deteriorated riveted members. The need for this study arose from the concern with the large number of riveted structures functioning today that have various degrees of corrosion and potential fatigue damage. The validity of AASHTO and American Railway Engineering Association category D that is generally used for riveted connections is uncertain, particularly near the fatigue limit. A series of fatigue tests was carried out on 80-year-old steel bridge stringers with a riveted built-up cross section. The stringers were significantly corroded along the compression flange and locally at the tension flange. The stress ranges that were applied were selected between the fatigue limits of design categories C and D. The corroded region of the tension flange proved to be the most severe condition, varying between categories C and E. The category D fatigue limit appears to be applicable to the rivet detail studied. The reduction of the compression flanges had no effect on the performance of the member. A strong frictional bond between section components was found to have a beneficial effect on fatigue life. A

series of reduced-temperature tests on a cracked stringer did not induce fracture of the cracked component and confirmed the redundancy of riveted built-up sections fabricated from mild steel.

Major concerns of bridge engineers today are the safety of old riveted structures and the potential fatigue damage that has accumulated. Many of these structures were fabricated and placed into service at the beginning of the century. The question of safety is of increasing importance as ever-intensifying traffic, deteriorating components, and accumulation of large numbers of cycles are a reality for highway, railroad, and mass transit bridges.

The criteria adopted for control of fatigue and fracture of new bridge structures are based on studies of modern welded construction and ongoing laboratory research on welded members. Most older bridges were constructed of riveted built-up members. Research is needed to establish better estimates of the fatigue resistance of riveted built-up sections.

Most of the previous laboratory work has been carried out on simple butt splices. A further limitation is that none of the previous testing has been performed with stress ranges less than 97 MPa. Both the AASHTO and the American Railway Engineering Association (AREA) specifications use a lower-bound estimate based on these limited data to classify the fatigue strength of riveted built-up members (1,2). This lower bound corresponds to category D in the joint classification system. A description and summary of the data base used are given in the commentary to the AREA specifications (2).

A recent literature survey by the authors confirmed the validity of category D as a lower-bound estimate for fatigue strength. Figure 1 shows the collected test results for normal clamping force and bearing ratios as permitted by the specifications. The test results for bearing conditions that exceed the specification limits are shown in Figure 2, which shows that some results fall below category D.

A pilot test program on the high-cycle fatigue behavior and fracture resistance of riveted built-up members in their weathered and deteriorated state is described. Stringers from an actual bridge were used in this study. The need for this investigation stems from the desirability to ascertain whether or not a difference exists between splices, built-up sections, cover-plate terminations, and other details of riveted built-up members. Category D fatigue restrictions impose an enormous penalty on fatigue resistance. It is of particular interest to investigate the applicability of this category near the fatigue or endurance limit because no experimental data are available at values less than 97 MPa.

FATIGUE TEST PROGRAM

Fatigue tests were conducted on four riveted built-up stringers taken from a railroad bridge. The purpose of the test program was to

1. Establish fatigue life data on rivet details, with particular focus on the high-cycle region; and
2. Establish the fatigue behavior of the deteriorated built-up member.

The second objective deals with the effect of force redistribution to the other section components as a result of crack extension at a rivet detail or corroded flange angle. This redistribution raises stresses and produces progressive crack initiation and propagation in those components. Note that riveted built-up members possess a degree of redundancy, which allows for an important increment of life after cracking develops in one component. The factor of redundancy did not appear in the majority of the previous experiments, which had been conducted on simple splices.

The project concentrated on high-cycle fatigue behavior; that is, near the constant cycle fatigue limit of AASHTO and AREA categories C and D of 69 and 48 MPa, respectively. This generally meant continuation of cycling beyond 10^7 cycles.

Test Specimens

The fatigue tests were conducted on members that had been removed from a railroad bridge. It was a three-span riveted truss bridge that supported a

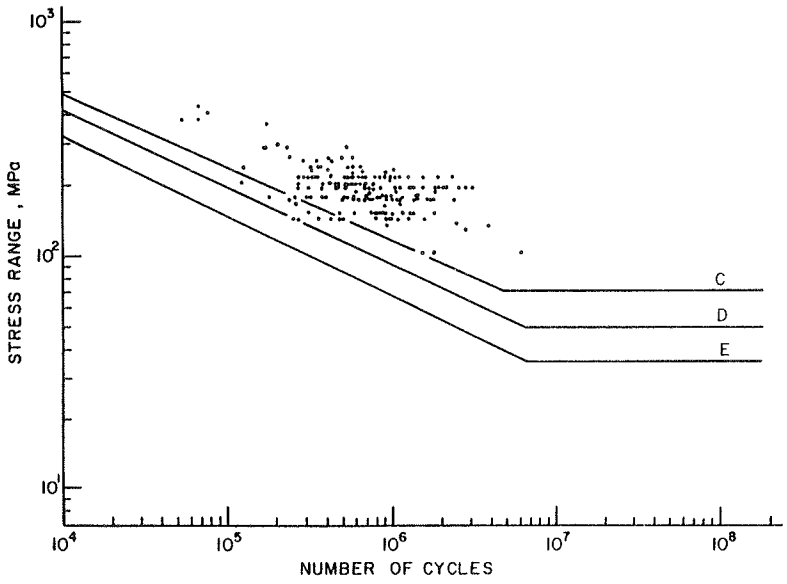

FIGURE 1 Fatigue resistance of riveted steel connections with normal clamping force and low bearing ratio ($\leq$ 1.5).

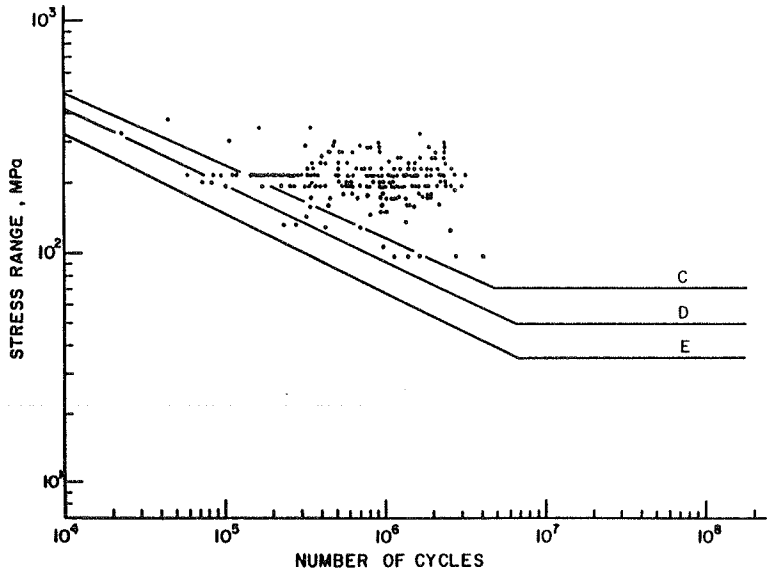

FIGURE 2 Fatigue resistance of riveted steel connections with normal clamping force and high bearing ratio (≥ 1.5).

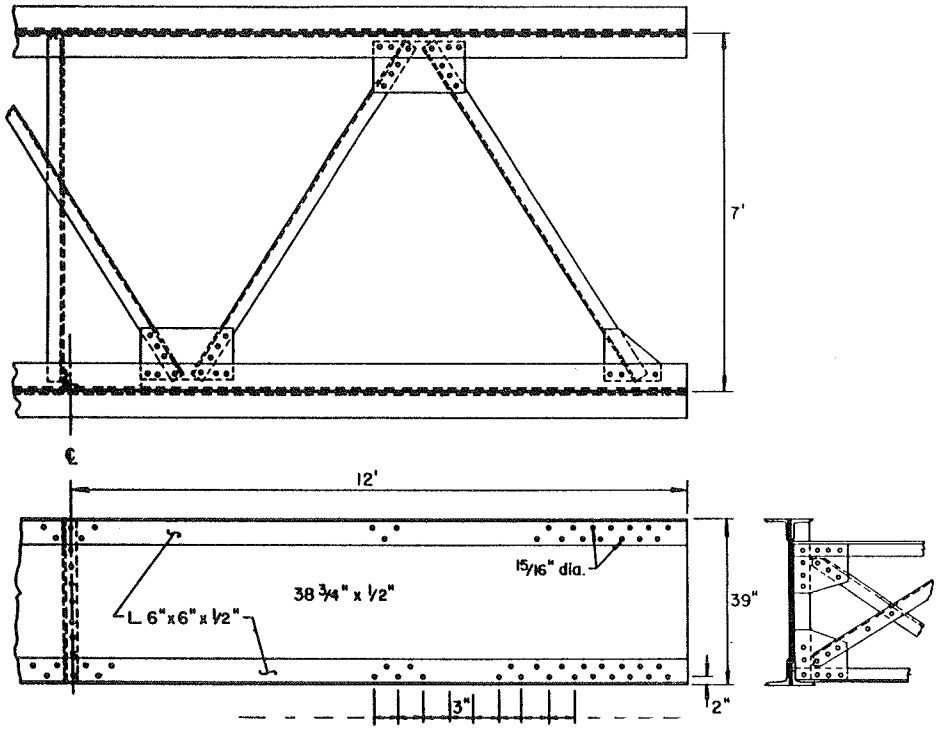

FIGURE 3 Stringers of the French Broad Ivy River Bridge.

single railroad track. The bridge was owned by the Southern Railroad Company and was located near Marshall, North Carolina, spanning the French Broad Ivy River. It was built in 1903 and demolished in 1982 for being obsolete rather than for malfunctioning. It was in service until demolition. Strain measurements made while in service indicate that about 1 percent of the stress cycles exceeded the category D fatigue limit; thus the cumulative fatigue damage from service was negligible (3). The bridge was constructed by the Phoenix Steel Company. The construction material used was medium steel, an early alloy steel. In 1903 alloy steels had just replaced wrought iron as the principal material for metal structures.

Fritz Engineering Laboratory acquired six of the stringers. They were built-up I-shapes that were 1 m deep and 0.32 m wide, and consisted of a web plate and four angles that were connected to the web by two rows of rivets (Figure 3). Their original length was 7.32 m. As cut from the bridge, they were about 6.10 m long.

The condition of the stringers appeared to be satisfactory. Their surface had been protected by a heavy tar coating and was eventually cleaned by sand blasting. Inspection indicated that the tension

flange was relatively undamaged except at sections where the cross frame had been connected to the web (Figure 4). The bottom inside flange angle is seen to be severely corroded, so that a reduced thickness resulted as well as a partly eliminated rivet head at that section. The regions of reduced thickness contained a set of notches and associated stress concentrations, which proved to be rather severe.

Significant deterioration was generally present along the compression flanges, as illustrated in Figure 5, which shows a thickness reduction of the flange where the cross ties had rested on the stringers. Several long cracks were found in the compression flange at the location of the lateral bracing connection plates, as illustrated in Figure 6. It appears that the bracing connection had provided restraint to the top flange adjacent to a tie-bearing point.

Test Setup

The stringers were tested in a four-point bending setup. The repeated loads were applied by two Amsler 245-kN hydraulic jacks and one pulsator, as illustrated in Figure 7. The distance between the jacks was 1.53 m. The loading signal had a constant amplitude, and the frequency of the cycle was 520 cycles per minute.

Lateral braces were attached adjacent to each jack to prevent lateral movement caused by the slight distortion and lack of symmetry of the deteriorated section. The high frequency of the variable loads required special care to prevent vibration of the setup and the jacks.

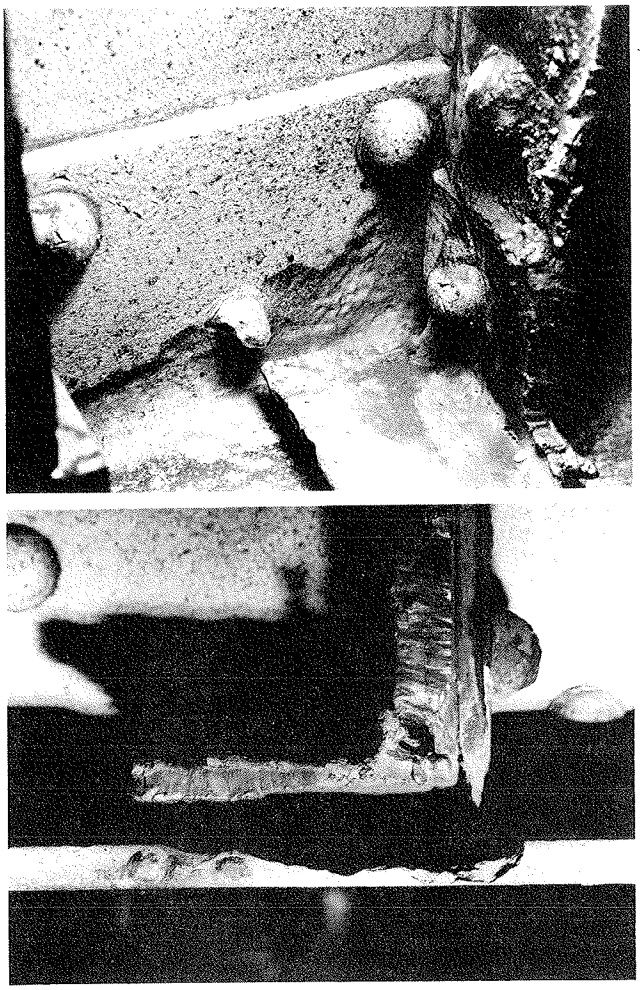

FIGURE 4 Flange angle corrosion at cross-frame connections.

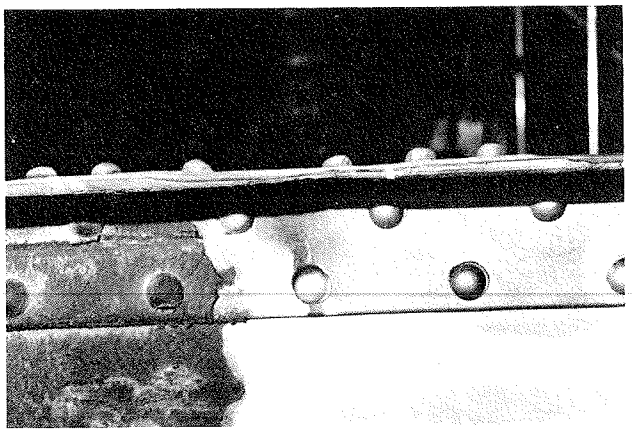

FIGURE 5 View of compression flange showing significant reduction in outstanding legs.

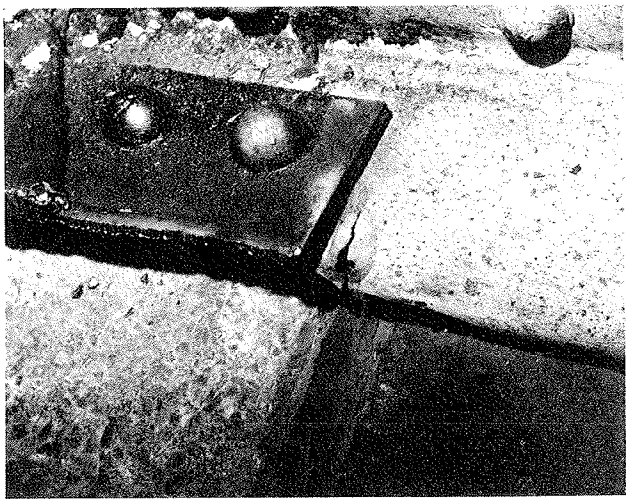

FIGURE 6 Preexisting crack in compression flange next to bracing connections.

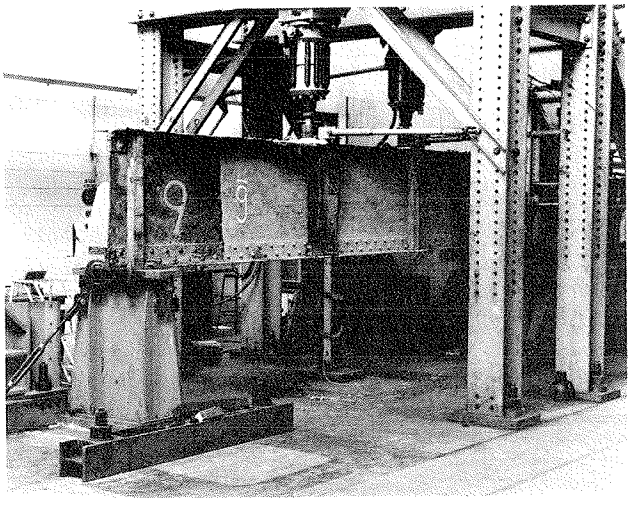

FIGURE 7 Fatigue testing setup.

Results of Fatigue Tests

General Remarks

Four of the stringers have been tested. The attention focused on the following details: (a) the corroded region of the flange angles, and (b) the riveted connection between the web and angles. The data in Table 1 summarize the test results for the fatigue strength of the corroded region. For each test beam, the gross section stress range (at the full section) and the net section stress range (at the section reduced by corrosion) are tabulated. Results are tabulated for the number of cycles until first detected cracking, until failure of the corroded angle, as well as the number of cycles until failure of the section, if applicable.

TABLE 1 Observed Cracking, Corroded Area

Test	$\Delta\sigma$ Gross[a] (MPa)	$\Delta\sigma$ Net[b] (MPa)	No. of Cycles (10^6)	Comment
1	73.4	75.2	3.77	Crack found >104 mm
			4.40	Angle severed
			4.99	Section failed
2	62.1	64.8	0.85	Angle severed
			1.45	Section failed
3	62.1	63.4	39.71[c]	No failure
4	55.2	57.2	1.19	Crack found >7.6 mm
			5.37	First hole drilled
			7.61[d]	Section spliced

Note: Ratio $R = \sigma_{min}/\sigma_{max} \approx 0.1$.
[a]Stress range at full section.
[b]Stress range at section reduced by corrosion.
[c]Test discontinued.
[d]Test stopped because of change in condition.

The test results on the rivet details are summarized in Table 2. Only the test data for those fatigue cracks that were not affected by cracking of the corroded section or other adjacent sections are listed. It was observed that progressing cracking of a section caused force redistribution from the cracked section components to the other cross-sectional elements. This redistribution often generated rapid cracking in those elements. This effect is shown in Figures 8 and 9. Soon after severing of the corroded angle, the opposite flange angle developed several cracks within a short period of time.

TABLE 2 Summary of Test Results at the Rivet Details

Test	$\Delta\sigma$ Net[a] (MPa)	No. of Cycles[b] (10^6) N_c	No. of Cycles[b] (10^6) N_f	Comment
1	65.9	6.52		Angle, bottom hole, top of hole
		7.34		Angle, bottom hole, top of hole
		8.70		Angle, bottom hole, top of hole
		12.98		Angle, bottom hole, top of hole
			18.25	Test stopped
2	59.3	36.50		Web plate, bottom hole, bottom of hole
			36.50	Test stopped
3	56.2	18.26	38.69	Angle, bottom hole, fillet, top of hole
			39.72[c]	Angle, bottom hole, fillet, top of hole
			39.72[c]	Angle, bottom hole, fillet, top of hole
	46.8	25.94		Angle, bottom hole, top of hole, shear span
	45.8	25.94		Angle, bottom hole, top of hole, shear span

Note: Only cracks at rivet holes not affected by a cracked section are included.
[a]Stress range at section reduced by corrosion.
[b]N_c = life until first cracking, and N_F = life until failure of component.
[c]Test stopped.

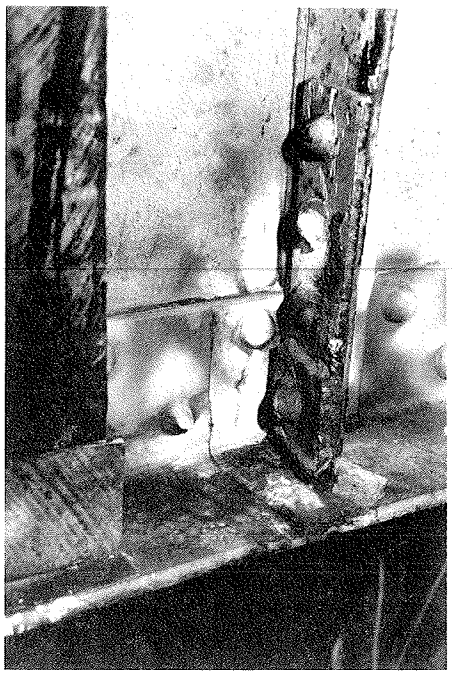

FIGURE 8 Crack at corroded area of test beam 1.

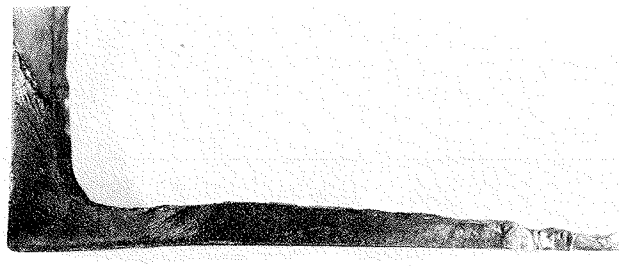

FIGURE 9 Surface of crack in corroded area of test beam 1.

Fatigue Resistance of Corroded Region

The four stringers tested all had the region of reduced thickness from corrosion. The degrees of reduction, however, were quite different and varied from 5 to 40 percent of the angle leg area. Figure 8 shows the cracked-reduced section of beam 1. The crack surface at this section is shown in Figure 10. Cracking was observed to initiate at multiple sites in the region near the edge of the angle where the thickness is minimal.

The corroded section of beam 2 after fracture is shown in Figure 11. Before the test a small existing crack had been detected in the corroded section, which was removed by grinding. This segment is shown in Figure 12.

The degree of corrosion of the third stringer is shown in Figure 13. No cracking was observed at

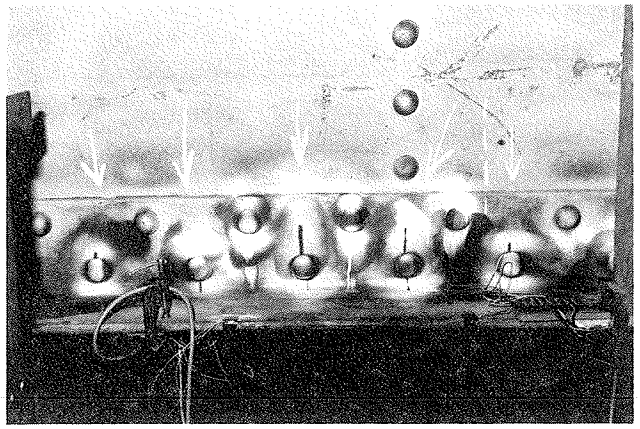

FIGURE 10 Set of cracks developed because of force redistribution in section.

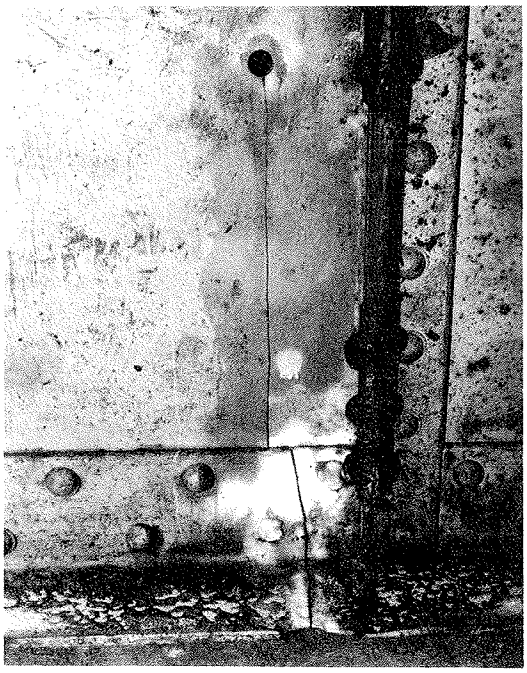

FIGURE 11 Cracked section at corroded area of test beam 2.

this section throughout the test. The thickness reduction was less than half the original thickness.

Figure 14 shows the crack in the reduced section of beam 4. This crack was arrested by drilling holes centered on the crack tip after it had grown to a length of about 64 mm. The crack subsequently reinitiated after 2.2 million additional stress cycles, and the section was finally spliced to permit continued testing of the stringer.

The fatigue test data of the corroded region detail of the flange angle are shown in Figure 15. The stress range is defined on the net section.

The corroded areas of stringers 2 and 4 (see Figures 11 and 14) had a fatigue life at the first observed cracking that was lower than that provided by category E. The corroded detail of stringer 1 (see Figure 8) had a fatigue resistance slightly lower than category C. Stringer 3 (see Figure 13) did not crack at this location.

The deterioration of the flange angle of beam 3

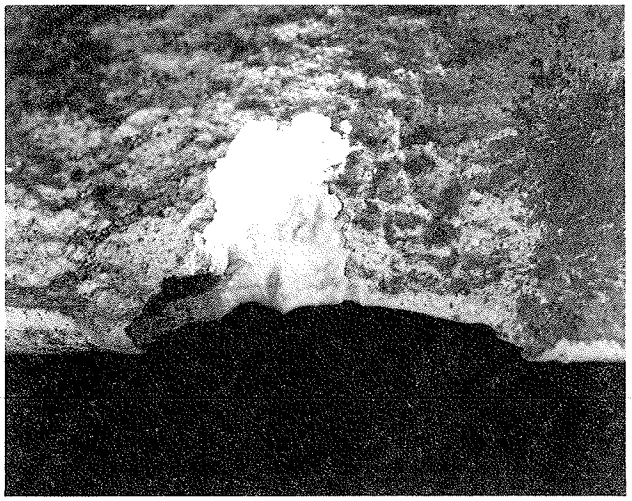

FIGURE 12 Initial crack in corroded area of test beam 2.

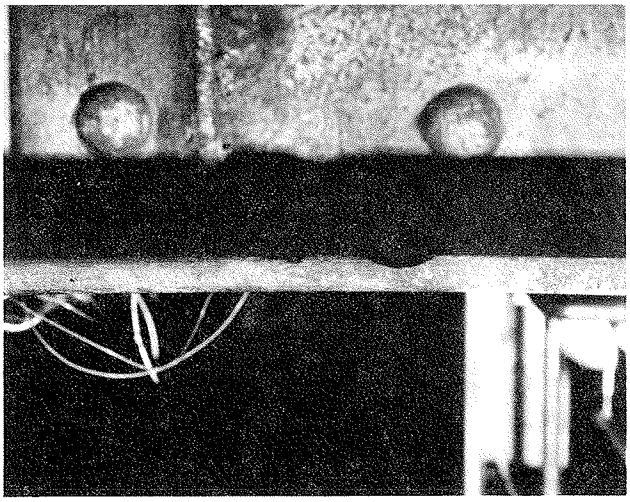

FIGURE 13 Corroded area of test beam 3.

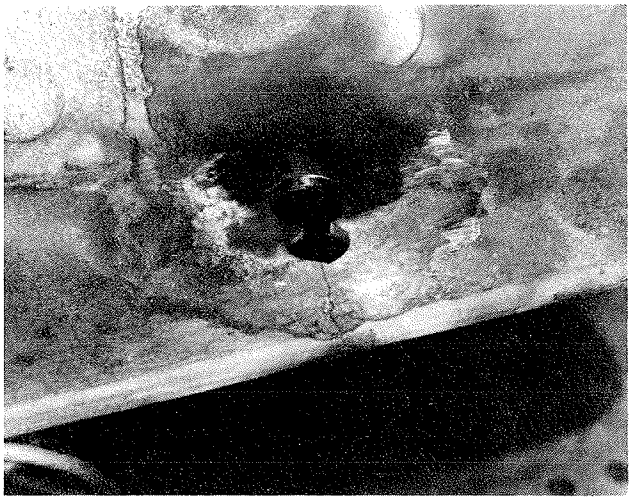

FIGURE 14 Corroded area of test beam 4 with crack, reinitiated after having holes drilled.

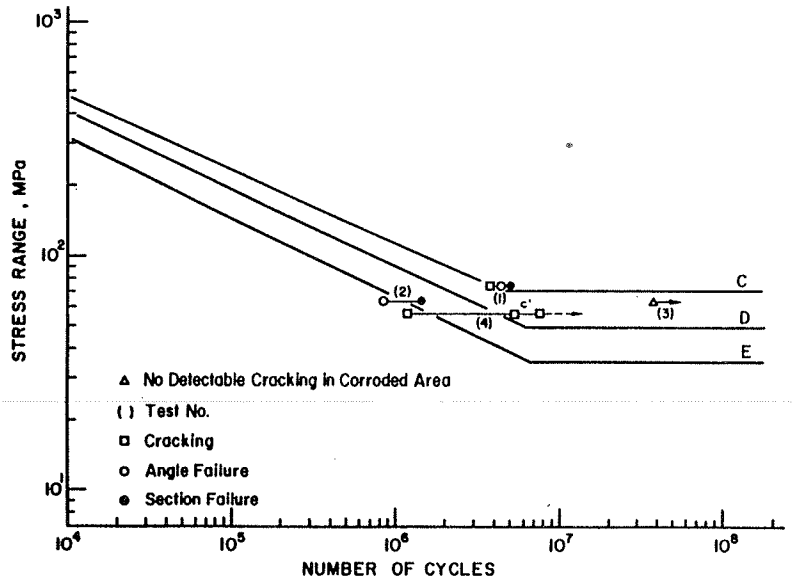

FIGURE 15 Fatigue resistance of corroded area details.

was not severe enough to have a crack initiate. The severity of the corroded regions of stringers 1, 2, and 4 were greater than that predicted by considering the loss of cross-sectional area only, as they all plot well below category A. Apparently, the roughness of the surface and the associated stress concentrations are the major factors in making this detail more severe than anticipated.

The mechanism of crack formation in the corroded area is as follows. First, several small cracks form on the rough surface at the deeper notches close to the angle tip. These cracks coalesce and form a long, shallow surface crack. This surface crack then propagates through the flange thickness at the tip and becomes an edge crack, whereas small cracks continue to form in the corroded surface and to coalesce with the edge crack. The crack length measured at the bottom surface significantly lags behind the length measured at the corroded top surface.

A final note should be made on the crack length at discovery in the various cases. For beam 4, the crack was small when detected--7.6 mm. This condition is identified in Figure 15 as cracking. The condition where the crack length has increased to approximately the length at discovery for beam 1 is represented by point C'. Hence the fatigue strength of the corroded sections of beams 1 and 4 are comparable.

All three stringers that developed cracks in the corroded section sustained a substantial number of additional stress cycles before the section failed. The numbers of cycles at failure of the angle of the cross section are indicated by angle failure and section failure, respectively.

Fatigue Resistance of Rivet Details

Fatigue cracks formed at rivet holes, as illustrated in Figure 16. The crack surface of one of these details is shown in Figure 17. The fatigue strengths of the rivet details that cracked independently of each other are summarized in Table 2 and plotted in Figure 18 as a function of the net section stress range. In Figure 18 cracking denotes first observed cracking. Failure of the flange angle developed for stringer 3 only. The cracked angles of the remaining stringers were retrofitted before failure could

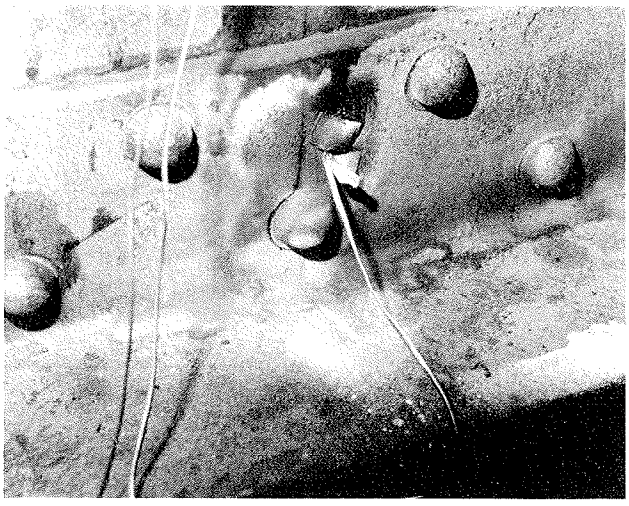

FIGURE 16 Fatigue cracked riveted section in test beam 3, after several reduced temperature tests.

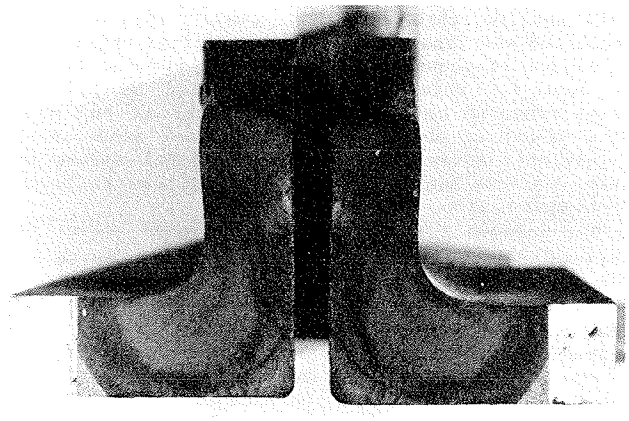

FIGURE 17 Cracked surface of crack at rivet hole running into bottom flange.

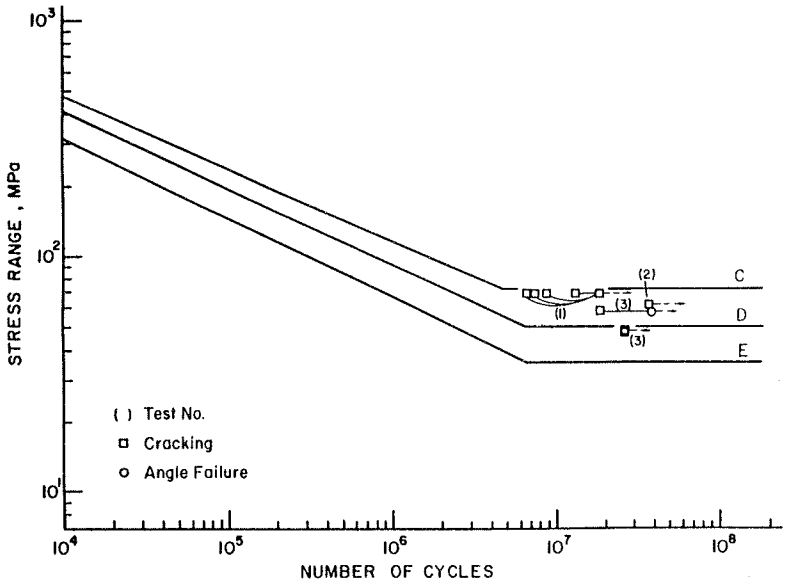

FIGURE 18 Fatigue resistance of rivet details.

occur. No tests were continued until failure of the riveted section because of cracking at rivet holes.

Fatigue cracking was observed to occur below the fatigue limit for category C (69 MPa). Two cracks developed below the fatigue limit of category D (48.3 MPa). Both of these cracks were located in a shear span. The stress condition that corresponds to bending and shear is slightly more severe than bending alone if the rivets are in bearing.

The literature review demonstrated that clamping force and bearing ratio were the principal variables influencing the fatigue behavior of riveted joints (4). Most of the cracked-rivet details are located in a constant moment region, so that the rivets do not transmit a bearing force. This is a favorable condition. At the same time, the rivets appear to be tight, which is favorable as well.

The available shop drawings do not indicate the method of hole preparation. The apparent distortion of the holes may be a result of punching or driving of the rivets.

There was no clear evidence of cracks existing at the beginning of the tests. In one or two instances a dark oxide was found on the crack surface, but sometimes this oxide was located away from the hole. In at least one instance it appeared this had occurred when the angles were flame cut from the section in order to expose the crack surfaces. None of these cracks corresponded to an appreciably different fatigue life than others without any indication of oxide.

The majority of the rivet details were observed to develop first cracking at the top of the hole, even though the nominal stress range is higher at its bottom. Most cracks initiated at the inner surface between web plate and angle at the edge of the hole. It is possible that fretting has aided crack initiation.

Observations during the test indicated that there was a significant influence of a frictional bond between the web plate and angles. This bond was from a paint and corrosion product. The significance of this influence lies in the effect it had on the propagation velocity of the crack. The frictional resistance between web plate and angle, which was adjacent to the crack as well as ahead of the crack front, reduced the compliance of the cracked plate and the crack opening displacement. This decreased the crack growth rate and extended the fatigue life. Crack growth measurements indicate that the crack growth rate was fairly constant with increasing crack length, as long as the crack propagated in the vertical leg of the angle. This phenomenon is treated in more detail elsewhere (5).

The fatigue resistance of the riveted stringers is compared with the category C and D resistance lines, which are shown to represent riveted members (2) in Figure 19. Also plotted are the results of other tests on riveted members. Fatigue life is defined as first observed cracking in all cases. The truss joints tested by Reemsnyder (6) and the hanger members tested by Baker and Kulak (7) were subjected to much higher stress range levels than the stringers and therefore yielded much shorter fatigue lives. All three sets of test data confirm that category D is a lower bound for the fatigue life, as defined by the development of a small crack.

Cracking of Deteriorated Compression Flanges

The significant loss of section of the compression flange apparent in Figure 5 was typical of every test beam. In extreme cases this loss was sufficient to result in the development of fatigue cracking in the outstanding legs of the angle. Figure 20 shows one such fatigue crack. The crack surfaces are shown in Figure 21.

The cracks always started at the section that had the largest thickness reduction. The explanation for this phenomenon is that the compressional stress cycle resulted in yielding on the net ligaments of the reduced section as a result of stress concentration and reduced area. During the unloading part of the stress cycle a residual tension stress field formed, which permitted crack initiation. In these circumstances the crack propagated toward the heel of the angle and arrested after having grown out of the region of yielding. None of the cracks propagated past the heel. Hence the cracks in the compression flange did not adversely affect the load-carrying capacity of any of the test beams.

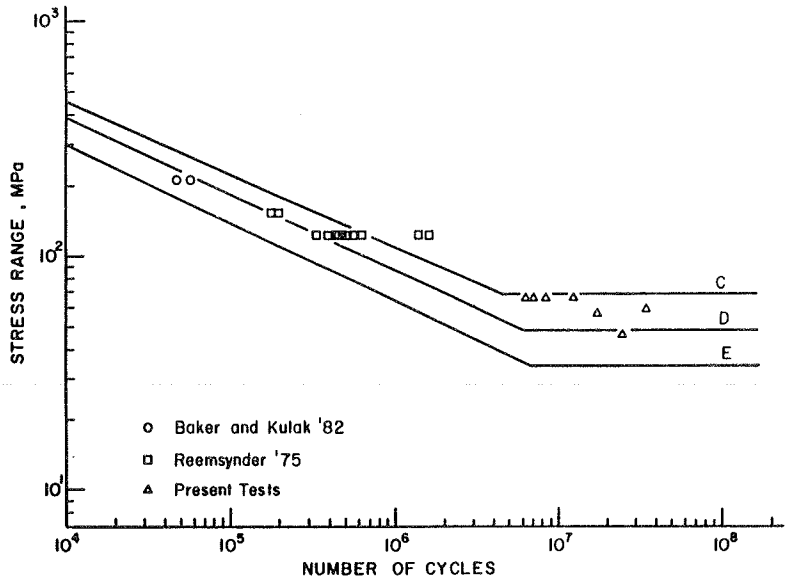

FIGURE 19 Fatigue resistance of riveted members.

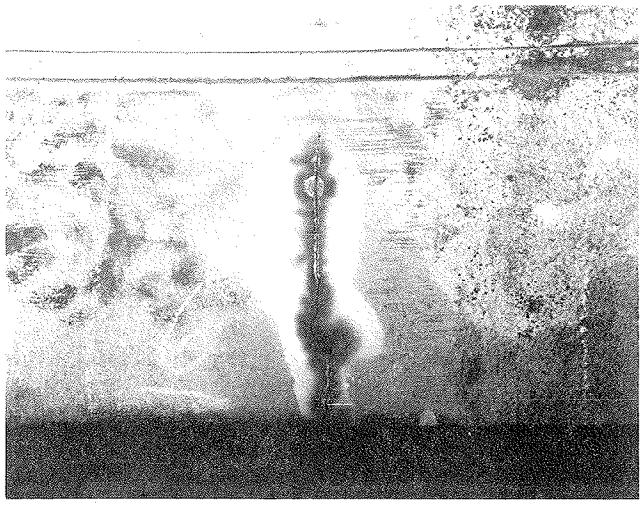

FIGURE 20 Fatigue crack in deteriorated compression flange of test beam 1.

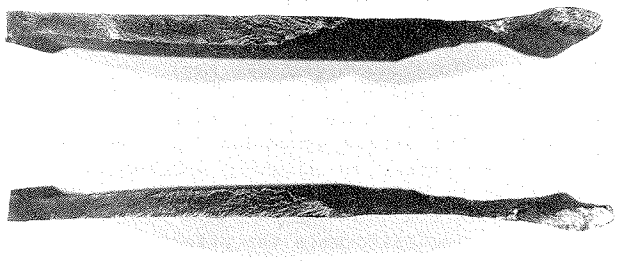

FIGURE 21 Fatigue crack surface in deteriorated compression flange of test beam 1.

REDUCED TEMPERATURE TEST

Objective and Procedure

A reduced temperature test was carried out on the third stringer. The objective was to evaluate the behavior of the member, given a fatigue crack, under low temperatures. More specifically, the objective was to determine if brittle fracture of a component would occur and how that would affect the behavior of the cross section. At the start of the test a fatigue crack extended from the top of the hole to the edge of the angle and from the bottom of the hole to the angle fillet, as shown in Figure 16. No cracking was observed in the other flange angle or in the web plate at that cross section.

The test procedure was as follows. The cyclic test was interrupted so that an insulating box of Styrofoam could be built around the section, which contained a grid of copper tubes with openings at regular distance through which liquid nitrogen could be injected into the closed space. By injecting the nitrogen, the temperature of the enclosed section of the stringer was decreased to approximately -40°C. The temperature was monitored by three temperature gauges attached to the web plate at mid-depth and to the top and bottom angles. After reaching the required temperature, the temperature was maintained by regulating the nitrogen flow.

With the cracked section being at this low temperature, a static load that corresponded to the maximum load of the repeated load cycle was applied. The cyclic loading was then resumed at a frequency of 260 cycles per minute. The crack front advanced in a stable, fatigue mode. The cyclic loading was continued for a period of approximately 0.5 hr at the reduced temperature. Then the crack was propagated at room temperature for an additional 12.5 to 25 mm. This procedure was then repeated.

Material Fracture Characteristics

An indication of the fracture characteristics of the material was obtained by performing a series of Charpy V-notch impact tests on 18 specimens taken from a tension flange angle of one of the stringers. Temperatures varied from -18° to 66°C. The results are shown in Figure 22.

A large variation in absorbed impact energy can be seen at test temperatures between 21° and 44°C.

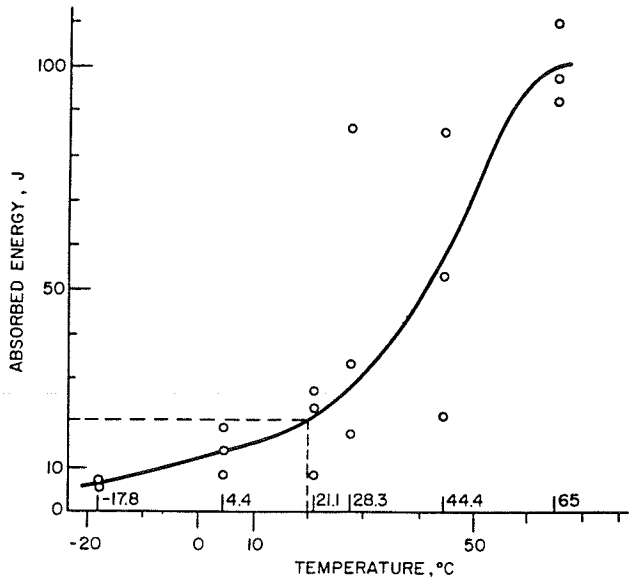

FIGURE 22 Charpy V-notch characteristics of flange angle.

The estimated 20.3 J transition temperature was about 20°C. Hence the material would satisfy the impact energy requirement for zone 2 of the AASHTO and AREA specifications.

Results of Reduced Temperature Test

The reduced temperature test was performed for a number of different crack lengths. These lengths and the number of stress cycles experienced under reduced temperature are given in Table 3.

TABLE 3 Reduced Temperature Test Results

Test	a_i (mm)	ΔN (cycles)
1	—[a]	19,000
2	27.9	0[b]
3	39.4	22,000
4	61.0	12,000
5	88.9	9,000
6	114.3	15,000
7	142.2	17,000
	152.4[c]	

Note: $T \simeq -40°C$. $(\sigma_{max})_g = 61$ MPa. $\dot{\epsilon} \simeq 2.6 \times 10^{-3}$ (S^{-1}). a_i = crack length at start of test measured at bottom of flange from angle corner to crack tip.

[a] Crack in fillet.
[b] Single static test.
[c] Test 7 discontinued; no fracture.

No unstable crack extension occurred in the cracked angle at any stage. During the process of crack extension the gross section stress increased by about 30 percent. It is apparent from the data in Table 3 that significant numbers of stress cycles were applied at each crack length increment.

The maximum estimated stress intensity factor during the test was 45 MPa$(m)^{1/2}$ if an edge crack was assumed from the heel of the angle. The test results suggest that a significant temperature shift is applicable because the dynamic fracture toughness at 21°C was this order of magnitude (8).

In addition, the results indicated that the frictional restraint between the cracked angle and the uncracked web, which was noted in the section on Fatigue Test Program, was beneficial because the crack opening was small. The associated stress intensity factor was probably smaller than predicated by assuming an edge crack.

No adverse behavior was experienced at the section when the flange angle cracked in two under the reduced temperature. The remaining resistance of the cross section was sufficient to carry the applied load.

SUMMARY AND CONCLUSIONS

The experimental studies carried out on four weathered and deteriorated riveted members provided information on the extreme life behavior of such members. In addition, they have also provided information on the behavior of severely corroded regions and their susceptibility to fatigue crack growth. The principal findings are as follows.

1. The extreme life fatigue resistance of the web flange riveted connection appears to be close to the category D fatigue limit. Several fatigue cracks were found to develop in the rivet details at stress ranges between 46 and 66 MPa after 8 to 30 million cycles.

2. The fatigue resistance of the corroded section was observed to vary between category E and C, depending on the severity of the corrosion and the loss of cross-sectional area. This degree of severity cannot be accounted for by considering only the loss of area. The four test results suggest that when the thickness of the outstanding flange angle is reduced until less than half remains, the proximity of the corroded area to the opposite surface reduces the fatigue resistance. Those stringers that had more than half of their flange thickness removed by corrosion initiated fatigue cracks near the category E resistance curve. When about half the thickness was available, initiation was observed to occur near the category C resistance curve. A lesser level of thickness did not result in crack initiation.

3. Severing of a component of the built-up section did not immediately impair the cyclic loading capacity of the members. Between 0.5 to 1 million cycles of a stress range of 62 to 69 MPa on the gross section were required before the load-carrying capacity was completely destroyed. Cracks formed slowly in the other angle and in the web plate. All four test beams exhibited redundant behavior once cracks developed that severed a flange angle.

4. Significant bond was observed to exist between the angles and web plate in their painted and corroded condition. This reduced the opening of the crack and extended the fatigue life.

5. Fatigue cracks that formed in the deteriorated legs of the compression flange were observed to arrest near the heel of the angle. None of these cracks affected the load-carrying capacity and the fatigue resistance of the stringers.

6. Reduced temperature tests at periodic intervals of extension of a crack grown from a rivet hole into the outstanding leg of an angle did not result in unstable crack growth. Even with 95 percent of the angle section cracked, the crack extension mode was stable.

ACKNOWLEDGMENT

This paper is based on a part of Fritz Engineering Laboratory Project 483, "The Fatigue Strength of Weathered and Deteriorated Riveted Members." The project was carried out under the sponsorship of the University Research Program, U.S. Department of

Transportation. The experiments were conducted at Fritz Engineering Laboratory, Lehigh University, Bethlehem, Pennsylvania.

Appreciation is due to the technical staff: Robert Dales, Charles Hittinger, Kermit Eberts, David Kurtz, Raymond Kromer, Peter de Carlo, and Russell Longenbach; to Ruth Grimes and Giovanni Vecchio; to Richard Sopko; to George Irwin for valuable advice; and to the sources that contributed test data.

REFERENCES

1. Interim Specifications: Bridges. AASHTO, Washington, D.C., 1979.
2. Manual for Railroad Engineering. American Railway Engineering Association, Washington, D.C., 1980, Chapter 15: Steel Bridges.
3. J.W. Fisher, B.T. Yen, W.J. Frank, and P.B. Keating. An Assessment of Fatigue Damage in the Norfolk and Western Railway Bridge 651 at Hannibal, Missouri. Tech. Report 484-1(83). Fritz Engineering Laboratory, Lehigh University, Bethlehem, Pa., Dec. 1983.
4. J.M.M. Out, J.W. Fisher, and B.T. Yen. The Fatigue Behavior of Weathered and Deteriorated Riveted Members--Phase I. Tech. Report 483-1(83). Fritz Engineering Laboratory, Lehigh University, Bethlehem, Pa., Sept. 1983.
5. J.M.M. Out. The Fatigue Behavior of a Weathered and Deteriorated Riveted Member. Master's thesis. Lehigh University, Bethlehem, Pa., May 1984.
6. H.S. Reemsnyder. Fatigue Life Extension of Riveted Connections. ASCE, Journal of the Structural Division, Vol. 101, No. ST12, Dec. 1975, pp. 2591-2608.
7. K.A. Baker and G.L. Kulak. Fatigue Strength of Two Steel Details. Structural Engineering Report 105. Department of Civil Engineering, University of Alberta, Edmonton, Alberta, Canada, Oct. 1982.
8. S.T. Rolfe and J.M. Barsom. Fracture and Fatigue Control in Structures: Applications of Fracture Mechanics. Prentice-Hall, Englewood Cliffs, N.J., 1977.

Publication of this paper sponsored by Committee on Steel Bridges.

Stresses in Hanger Plates of Suspended Bridge Girders

JAMES R. BELLENOIT, BEN T. YEN, and JOHN W. FISHER

ABSTRACT

Hanger plates in suspended span bridges are briefly examined for in-plane bending. The hanger plates are designed as tension members; however, measurements indicate that bending occurs as well. This bending is produced by the relative rotation at the ends of the plate and is caused by the frictional bond between the hanger plate, pin, and girder web assembly. A finite-element model of the hanger plates indicates that a nonuniform stress distribution exists across the width of the plate at the pinhole. The maximum stress concentration factors were calculated to be 4.6 and 1.8 for 6.9 MPa (1 ksi) axial and bending stress, respectively. A fatigue strength analysis was conducted to determine the life of the hanger plates.

A frequently adopted arrangement for short- and medium-span steel bridges is the three-span structure with a suspended portion in the middle (see Figure 1). The suspended steel girders are usually connected to the overhanging girders by hinges and hanger plates. This arrangement renders the suspended girders in a simply supported condition.

The hanger plates, which are attached to the girders by pins (as illustrated in Figure 2), are primary bridge components. The plates are designed to undertake the reactions of the rocker supports of the suspended span. Because the pins of hanger plates are assumed to rotate freely, the hangers are assumed to sustain tension forces.

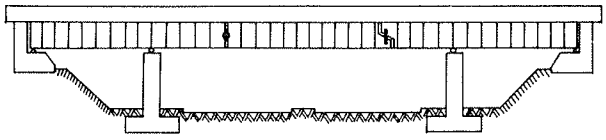

FIGURE 1 Three-span bridge with suspended girders.

In actual cases hanger plates may be subjected to in-plane bending because of friction at the pins, and to out-of-plane bending because of skewness of the bridge or other reasons. Broken hanger plates have been found in bridges (1). Some results of a brief study on in-plane bending of hanger plates are presented here.

MEASURED STRESSES

Because hanger plates are assumed to take tension forces, live-load stresses in hanger plates are expected to be tensile in nature. Measurements by electrical resistance strain gauges on hanger plates of two highway bridge girders indicated that strains varied from tension to compression, or vice-versa, as vehicles traversed the bridges (2).

Examples of recorded strain-time traces are shown in Figure 3. These results imply that the hanger plates were subjected to more than simple tension.

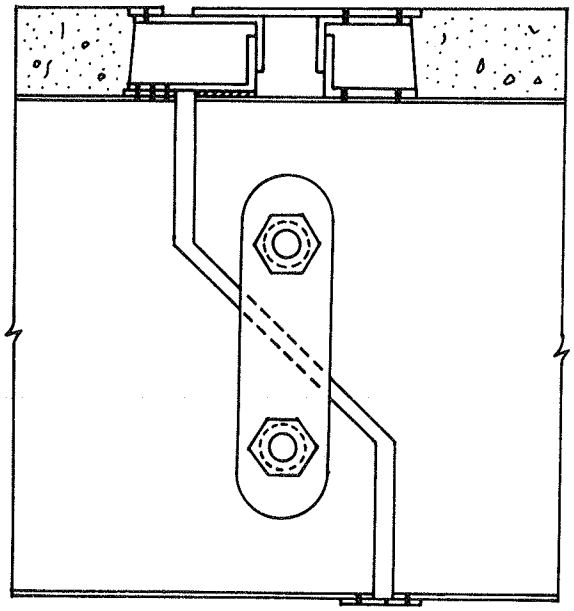

FIGURE 2 Hanger plate.

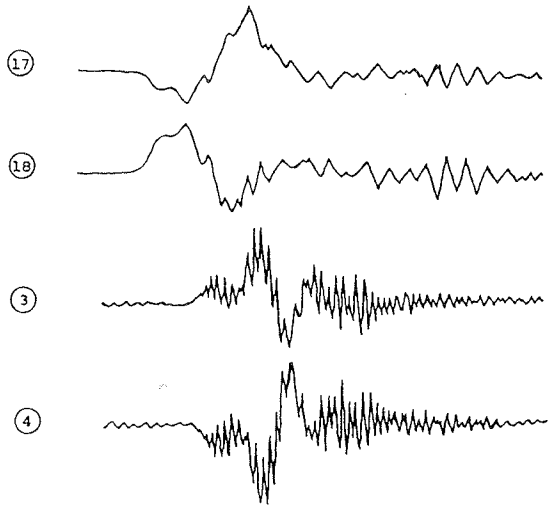

FIGURE 3 Recorded strain traces.

From the strain traces, stress distributions in hanger plates were established. Examples are plotted in Figure 4. These are estimated stresses across the hanger plates at a specific instance. The distributions clearly indicate that the hanger plates were subjected to bending in addition to axial forces. In other words, the hanger plates were not acting as simple tension members, as assumed.

CAUSE OF BENDING STRESSES

A hanger plate subjected to tension and in-plane bending may be modeled as a pin-connected tension member with restraints against end rotations (see Figure 5). The restraints could be induced by friction at the pins or bonding between the hanger plates and adjacent girder webs. When relative rotation or transverse displacement between the pinholes occurs, the hanger plate undergoes bending.

The relative rotation and transverse displacement of a hanger plate in a bridge are difficult to calculate. Their magnitudes depend on the geometry and configuration of the hanger plates and pins, as well as on the arrangement of the bridge girders and the roadway deck in the vicinity. If it is assumed that the hanger plates rotate with the girders such that the relative rotation between the ends of the hanger plate is equivalent to that between the ends of the cantilever and the suspended girder, and that the transverse displacement is compatible to this rotation, then the bending stresses in the hanger plate would be directly proportional to the relative rotation.

This postulation can be examined by comparing the influence lines of the relative rotation of the girder ends and the recorded live-load strains in the hanger plates. Figure 6 shows such a comparison. The recorded strains at a point of a hanger plate

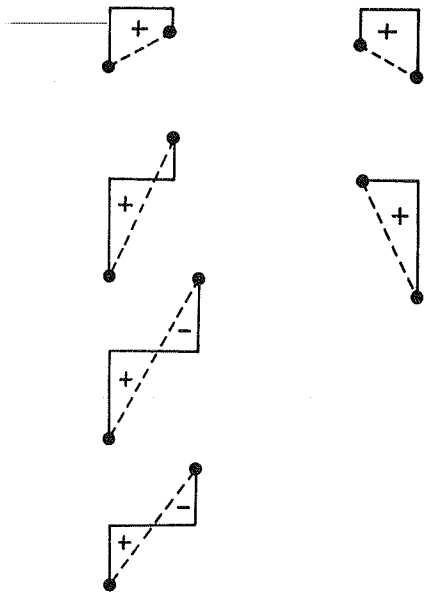

FIGURE 4 Stress distribution across hanger plate width.

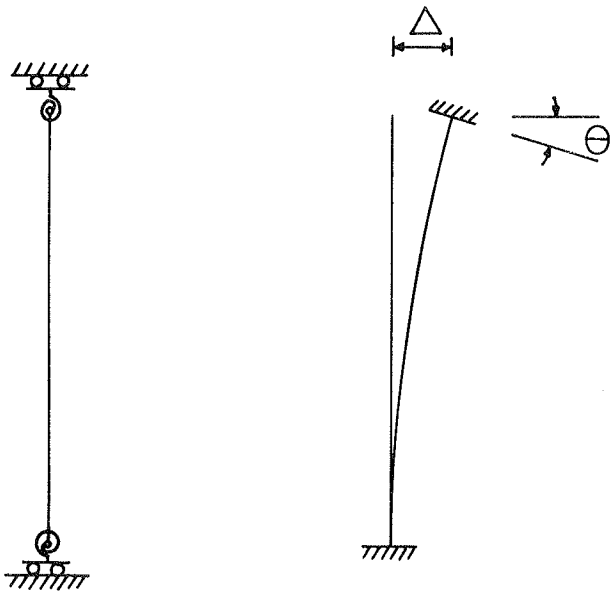

FIGURE 5 Model for hanger plate analysis.

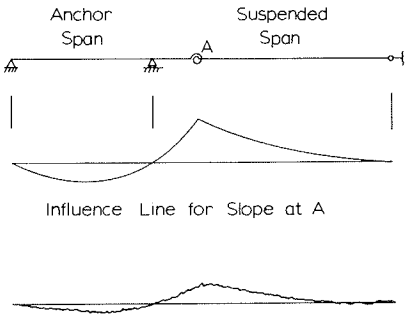

FIGURE 6 Influence line for slope versus recorded strain trace.

were produced by a single truck traversing a bridge at a crawl speed. The similarity of the curves is obvious.

To explore this further, the relative rotations at the 12 hanger plates of 6 girders of a bridge are estimated. The axial forces in the hanger plates, evaluated from measured strains in the plates, are applied to the respective girders. The resulting rotations are given in Table 1, together with the

TABLE 1 Bending Moment in Flange Plates

Girder	Hanger Plate	θ	$M_{comp.}$	$M_{meas.}$
G1	W	0.000451	22	0
	E			8
G2	W	0.000623	30	2
	E			0
G3	W	0.000935	45	8
	E			6
G4	W	0.000887	40	27
	E			24
G5	W	0.000216	10	33
	E			6
G6	W	0.000113	5	13
	E			0

respective computed bending moments, assuming that the ends of the hanger plates are bonded to the girder webs. The corresponding bending moments from measured strains are also listed. By comparing the computed and measured bending moments it is evident that the bending of the hanger plates is less than the computed value. Nevertheless, the hanger plates do appear to have rotated with the girders and to have sustained bending moment.

ESTIMATION OF FATIGUE STRENGTH

Under tensile axial forces and bending moments, live-load stresses at the pinholes of hanger plates could be quite high. The result is possible fatigue crack growth at the pinholes. To estimate the fatigue endurance, it is necessary to know the stress magnitudes and their variation with time (3).

The stress distribution at a pinhole of a hanger plate is evaluated by a finite-element analysis. The results are shown in Figure 7. The stress concentration factor (K_T) is 4.6 at the edge of the pinhole for a uniform axial stress, and is 1.8 for a maximum bending stress of 6.9 MPa (1 ksi). The nonuniform nature of stresses in the hanger plate produces nonsymmetrical stresses at the pinhole. For the case shown, the axial and maximum bending

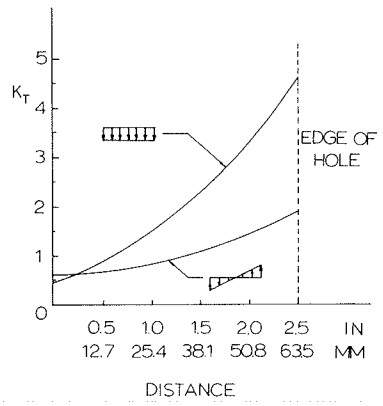

FIGURE 7 Stress distribution at pinhole.

stresses are equal, where the highest stress at the edge of the hole is 3.2 times the highest stress in the plate.

The variation of stresses at a pinhole can be estimated from the stress history of the hanger plate. For the plate discussed in Figure 7, the stress histogram from measurement is shown in Figure 8. Most of the stress ranges (live-load stresses)

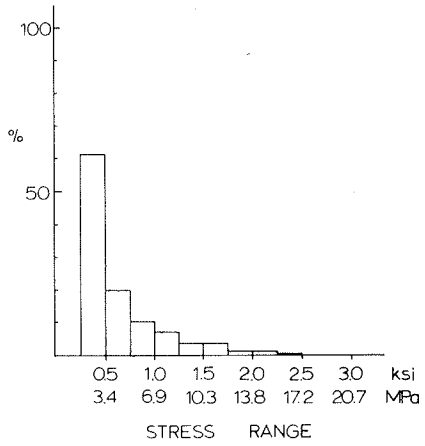

FIGURE 8 Histogram of stress range.

were low, with a maximum value of 20.7 MPa (3.0 ksi). By assuming that the stress distribution shown in Figure 7 is applicable all the time, the maximum stress range at the pinhole would be 66.2 MPa (9.6 ksi).

The fatigue strength of hanger plate pinholes has not been defined. Conservatively, category C of AASHTO allowable stresses may be adopted (4). For multigirder bridges, the threshold value for category C is 69.0 MPa (10 ksi). Because the maximum live-load stress could be higher than this threshold, fatigue crack propagation must be considered.

Results of studies have indicated that fatigue crack growth in ferrite-pearlite steels follow the rule (5) that

$$da/dN = 3.6 \times 10^{-10} \quad (\Delta K)^3 \qquad (1)$$

where

a = crack size,
N = number of cycles,

ΔK = range of stress intensity factor = $f(a) S_r \sqrt{\pi a}$,
S_r = constant amplitude stress range, and
$f(a)$ = correction factor for crack shape, stress gradient, and so forth (6).

Equation 1 may be rearranged and integrated to give an estimated life (N):

$$N = \int dN = \int_{a_i}^{a_f} \left(da / \{ 3.6 \times 10^{-10} [f(a) S_r \sqrt{\pi a}]^3 \} \right) \quad (2)$$

For the hanger plate shown in Figure 7, an initial corner flaw of a_i = 2.54 mm (0.1 in.) is assumed with a detectable final crack size of a_f = 25.4 mm (1.0 in.). The constant amplitude stress range is estimated from the stress histogram by using Miner's hypothesis and is equal to 5.8 MPa x 3.2 = 18.5 MPa (2.7 ksi). By incorporating the stress gradient of Figure 7 into an expression for the connection factor f(a), the resulting estimate life is 506 x 10^6 cycles. If 2,000 cycles per day are induced by trucks, it would take many years for the crack to grow. Thus, if the hanger plate is made of steel with adequate toughness against brittle fracture, there should be ample time for inspection if a crack would ever develop.

CONCLUSIONS

In conclusion, the following points are restated.

1. Hanger plates of suspended bridge girders are subjected to bending as well as axial forces.
2. In-plane bending results from friction at the pin and the relative rotations of the girders at the hanger plate.
3. Live-load stresses at the edge of pinholes are higher than those in the hanger plates.
4. Fatigue cracks could grow from pinhole edges.

For the case studied, there is ample time for inspection. Further studies are needed on the adequacy of current design assumptions and, particularly, on the behavior of plates in relation to girder geometry and bridge dimensions.

ACKNOWLEDGMENT

Field data and part of the results of this study were obtained under an FHWA research project. This sponsorship is acknowledged.

REFERENCES

1. J.W. Fisher. Fatigue and Fracture in Steel Bridges. Wiley Interscience, New York, April 1984.
2. J.R. Bellenoit, B.T. Yen, J.W. Fisher, and R. Roberts. A Fatigue and Fracture Investigation of Suspended Span Bridge Components. Report 449.2. Fritz Engineering Laboratory, Lehigh University, Bethlehem, Pa., June 1982.
3. J.W. Fisher. Bridge Fatigue Guide--Design and Details. American Institute of Steel Construction, Chicago, 1977.
4. Standard Specifications for Highway Bridges. AASHTO, Washington, D.C., 1977.
5. S.T. Rolfe and J.M. Barsom. Fracture and Fatigue Control in Structures: Application of Fracture Mechanics. Prentice-Hall, Englewood Cliffs, N.J., 1977.
6. J.W. Fisher, B.T. Yen, and K.H. Frank. Minimizing Fatigue and Fracture in Steel Bridges. Journal of Engineering Materials and Technology, Transactions of ASME, Vol. 102, Jan. 1980.

Publication of this paper sponsored by Committee on Steel Bridges.

Design of the Cable-Stayed Girder Weirton-Steubenville Bridge

WILLIAM R. KOZY and RUSSELL J. KOLMUS III

ABSTRACT

When completed, the Weirton-Steubenville Bridge will be the sixth cable-stayed girder bridge constructed in the United States. The design to be constructed at a $20 million cost was chosen in 1983 from three bridge designs presented for construction bids. Crossing the Ohio River between Weirton, West Virginia, and Steubenville, Ohio, the new bridge will be 1,965 ft from abutment to abutment and have a main span of 820 ft. A concrete, inverted Y-shaped tower, which rises 365 ft above the supporting pier, features above its apex a 140-ft-high pylon that supports a dual-plane cable system. Materials specified for the composite bridge were placed where their properties would provide the greatest advantages without sacrificing integrity and function. Fascia girders are I-girders with webs skewed at 10 degrees from the vertical, thus reducing cable-connection eccentricity, material quantities, and steel fabrication costs. The composite superstructure consists of longitudinal stringers, transverse floor beams, and a concrete deck--all treated as an orthotropic system. Further,

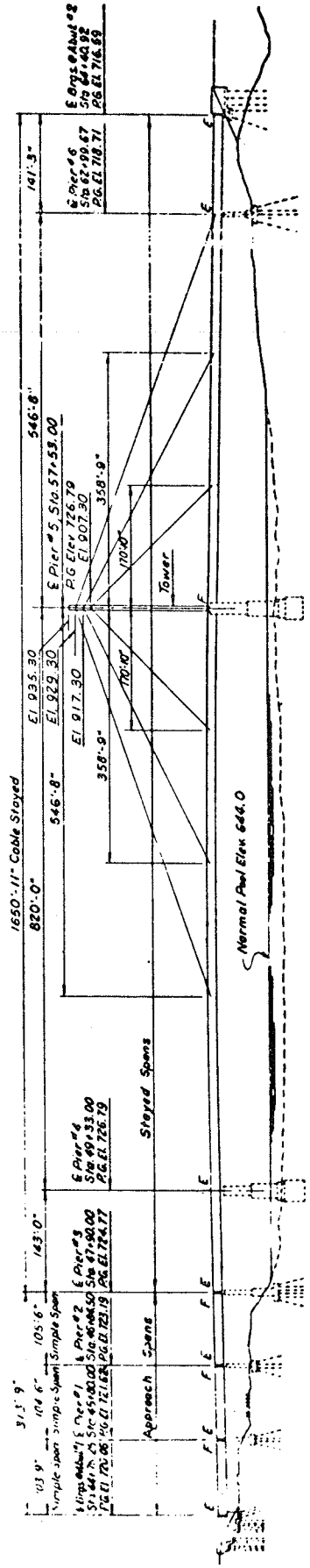

FIGURE 1 Steel alternate design 1.

horizontal trusses are placed at the bearings of the tower pier and at the outermost cable connections on the ends of the bridge to distribute axial load throughout the deck. The approach spans are continuous, composite, multigirder types. Load-factor design was used in the approach spans, substructure units, the tower, and the multigirder portions of the stayed spans.

In the early 1970s the West Virginia Department of Highways retained Michael Baker, Jr., Inc., to study and recommend a current state-of-the-art bridge to cross the Ohio River between the towns of Weirton, West Virginia, and Steubenville, Ohio. After studying the several bridge types proposed by Baker, the state of West Virginia requested that a cable-stayed girder bridge be designed for this river crossing.

STEEL ALTERNATE DESIGN 1

The initial bridge design consisted of a four-span, cable-stayed girder main river structure that had three simple-supported approach spans (see Figure 1). The approach spans were chosen so that future ramps could be added easily.

The cable-stayed girder portion of the bridge was a four-span continuous box girder that had spans of 143, 820, 547, and 141 ft. The superstructure consisted of a two-cell rectangular steel box girder with outriggers supporting the full six-lane bridge width. The deck was an orthotropic steel design that had an epoxy asphalt wearing surface. The tower was A-shaped with the deck passing through the steel box legs of the frame (see Figure 2). A single-plane, fan-shaped cable system was used that featured six cable lines. These cables connected to the tower and extended through the median, which was attached to the middle web of the two-cell box girder.

On the Ohio side the three 102-ft simple-sup-

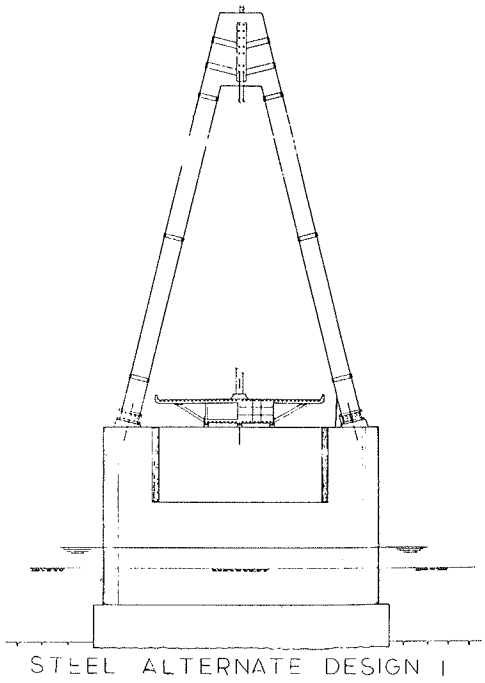

FIGURE 2 Typical cross section of cable-stayed bridge at pier 5 (design 1).

ported approach spans consisted of twin steel box girders with outriggers supporting an orthotropic steel deck that had an epoxy asphalt wearing surface.

Of the eight substructure units--six piers and two abutments--six were supported on steel H-piles driven to rock, whereas the two main river piers (piers 4 and 5) had footings founded on rock.

The abutments were standard U-shaped cantilevers with high back walls to accommodate the deep box girders.

All the piers were basic solid shaft design. Pier 6, as the anchor pier for the cable-stayed girder unit, was modified by a slot in the center to accommodate the tie-down assembly.

The configuration of pier 5 was dictated by the A-frame tower (see Figure 2).

CONCRETE ALTERNATE DESIGN

In 1978 the FHWA directed that an alternate concrete bridge be designed. Another engineering consultant was chosen to design the alternate by using the cable-stayed girder concept with concrete as the main material. This design used a concrete fascia girder, steel floor beam, and concrete deck and tower. This design was completed in 1983 and bid against the two steel alternates.

STEEL ALTERNATE DESIGN 2

The original steel alternate bridge was developed as a state-of-the-art bridge in 1974. Then nearly 7 years went by from the time that the original bridge design was initiated. This, along with the FHWA directive requiring a concrete alternate design, prompted the West Virginia Department of Highways in 1981 to request a redesign study to determine the economics of updating the original design or creating a new cable-stayed girder bridge design that reflected the current state of the art.

REDESIGN STUDY

In 1981 the West Virginia Department of Highways retained Baker to study whether or not a new cable-stayed girder design might have a lower construction cost than the original steel design. To arrive at a lower construction cost, two major cost areas were addressed: the first was the fabrication costs involved in different deck and tower cross sections; and the second was material quantities and types. These savings were to be made without sacrificing the serviceability or the structural integrity of the bridge. To accomplish these goals the study was divided into two phases. The first phase considered five superstructure cross sections of the bridge structure, as shown in Figures 3-7. The relative cost of the sections was estimated, and then each section was evaluated and ranked by using the criteria given in Table 1. On the basis of the results of the evaluation, Baker recommended cross-section type 2, which the West Virginia Department of Highways selected for use in the second phase of the study.

In the second phase of the study the bridge was investigated along its longitudinal axis. Pier and abutment locations already had been established in the original steel design. In addition, piers 4 and 5 had been constructed by this time. Consequently, the major items remaining to be determined were the cable arrangement and spacing as well as the tower height, cross section, and transverse configuration. Researching the literature, studying recent cable-stayed girder bridge designs, and performing preliminary calculations revealed that a dual plane of cables with connections spaced at about 60 ft was

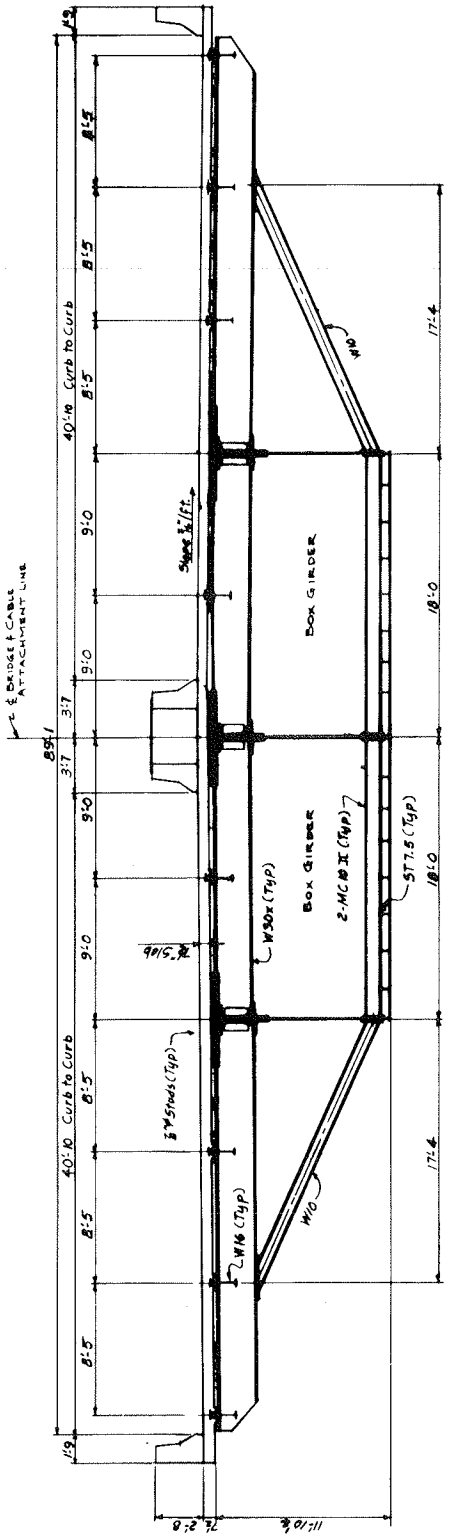

FIGURE 3 Redesign study: typical cross section, type 1.

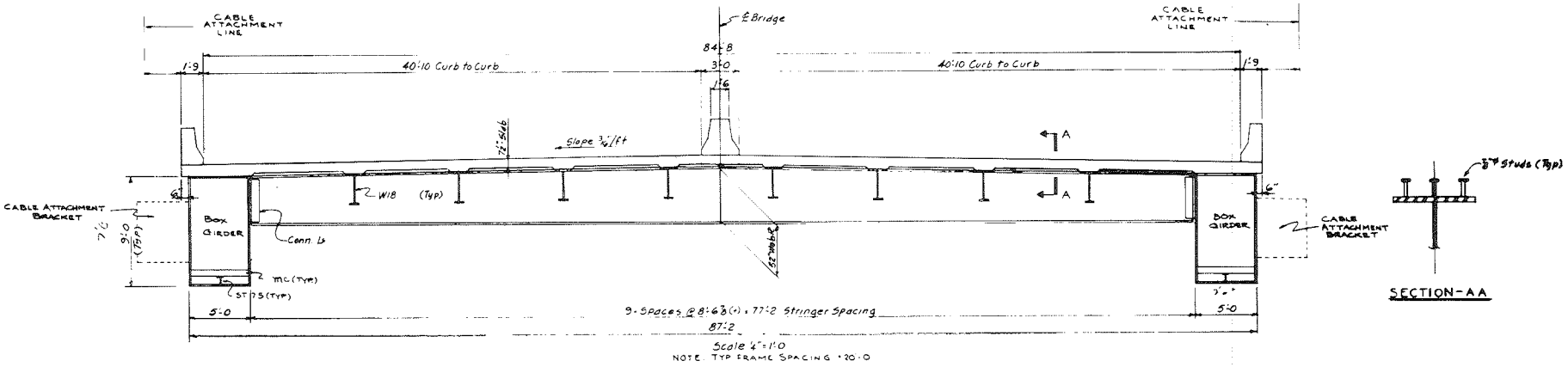

FIGURE 4 Redesign study: typical cross section, type 2.

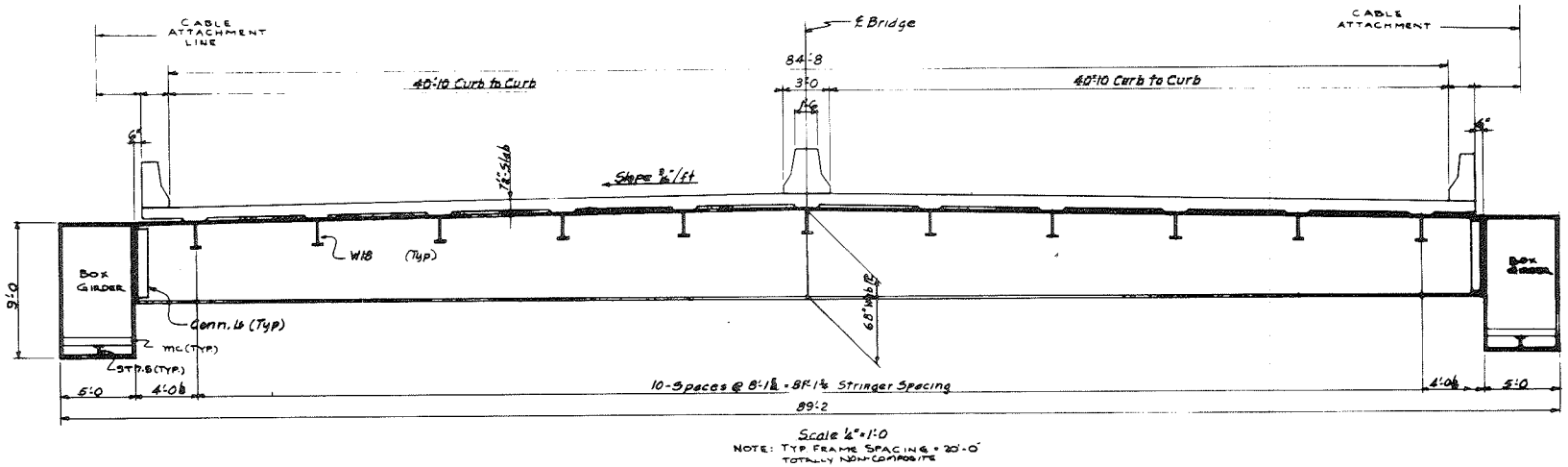

FIGURE 5 Redesign study: typical cross section, type 3.

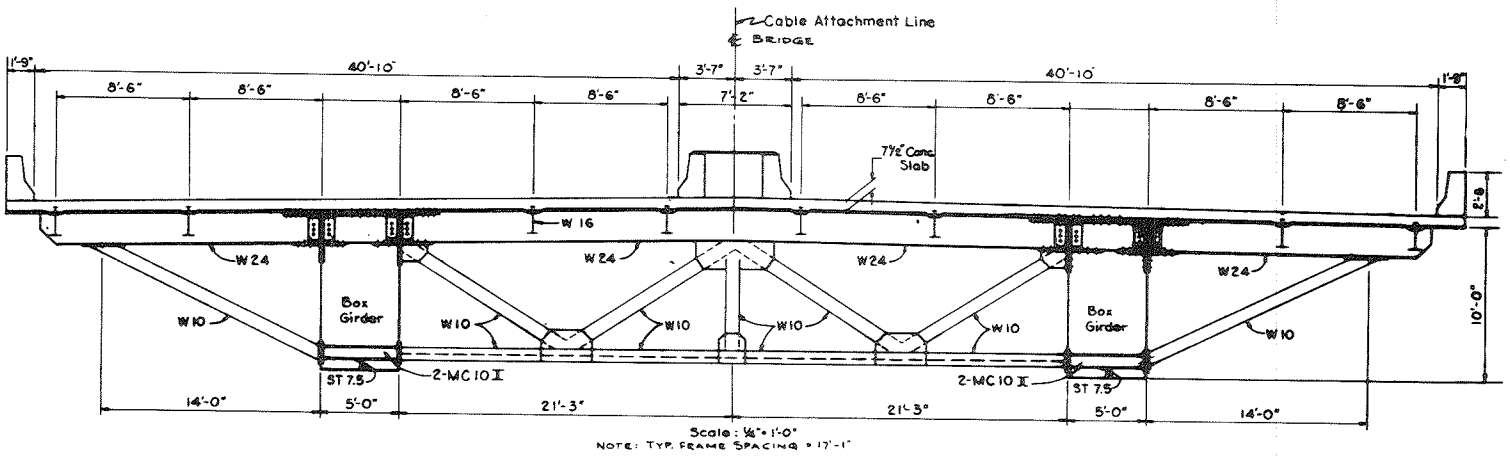

FIGURE 6 Redesign study: typical cross section, type 4.

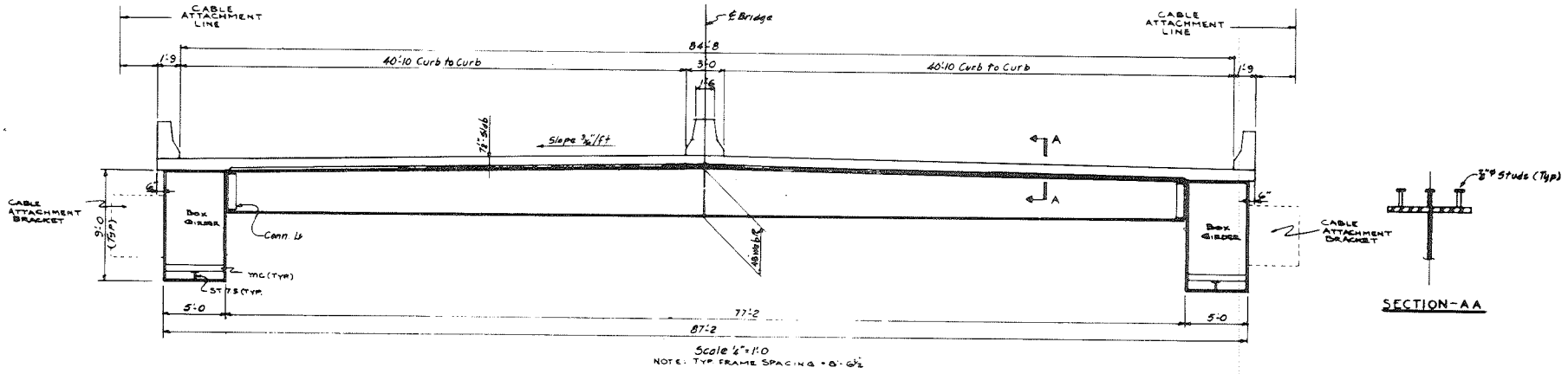

FIGURE 7 Redesign study: typical cross section, type 5.

TABLE 1 Redesign Study Type Comparisons

	Type 1[a]	Type 2[b]	Type 3[c]	Type 4[d]	Type 5[e]
Steel quantities (cross-frame only)	911#/lf bridge	1047#/lf bridge	2335#/lf bridge	845/lf bridge (transverse diaphram not included)	1843#/lf bridge
Concrete quantities	2.64 cy/lf bridge	2.5 cy/lf bridge	2.5 cy/lf bridge	2.64 cy/lf bridge	2.5 cy/lf bridge
Weld quantities (1 = most, 5 = least)	1	4	3	5	2
Constructability	Fair to good	Good	Good to excellent	Fair	Excellent
Wind stability	Proven excellent	Good	Good	Good	Good
Live-load stability (torsional rigidity)	Good	Excellent	Excellent	Fair	Excellent
Adaptability to existing pier 4	No modification required	Extensive modification required	Extensive modification required	Some modification required	Extensive modification required
Adaptability to precast deck units	Good	Good	NA	Fair	Excellent
Composite slab-girder efficiency	Good	Fair	NA	Good	Fair
Floor beam spacing adaptability	Poor aesthetically	Good aesthetically	Good aesthetically	Poor aesthetically	Good aesthetically
Slab removal for maintenance					
Degree of redundancy	Poor to good	Excellent	Excellent	Good	Excellent
Cable connection adaptability	Fair	Excellent	Good	Poor	Excellent
Adaptation to many cable connection points	Poor	Excellent	Good	Poor	Excellent
Fracture critical members	Poor	Good	Best; lower tension stress than 2	Worst	Good
Adaptation for multigirder approach spans	Poor	Excellent	Good	Poor	Excellent

Note: NA = not applicable.
[a] See Figure 3.
[b] See Figure 4.
[c] See Figure 5.
[d] See Figure 6.
[e] See Figure 7.

the most economical, stable configuration under the given conditions and with the chosen cross sections.

Supporting the cable system in this design is an inverted Y-shaped, reinforced-concrete tower that has a box section in the legs and an H-shaped section in the pylon. The approach spans were changed to a continuous composite steel, multigirder configuration. After sizing all the members and calculating the bridge quantities, $11 million was estimated as the savings in construction costs over the original steel design. Baker then recommended a total redesign of the bridge. Agreeing with Baker's recommendations, the West Virginia Department of Highways authorized the redesign of the bridge as shown in Figure 8.

FINAL DESIGN

In the final design of the bridge three goals guided the research and design approach to devise a cost-effective bridge for bidding. The load-factor design method, as described in the AASHTO Standard Specifications for Highway Bridges (1), was used wherever practical as opposed to the service load design method as described in the same publication. In addition, different materials (i.e., concrete or steel) were used in the most effective manner. Finally, the most cost-effective cross sections were used in appropriate areas. These goals were to be obtained without sacrificing member and section safety or function.

APPROACH SPANS

In the redesign the approach spans took on a new configuration. The superstructure changed from simple-supported, dual steel box girders over three spans to a 315-ft, three-span continuous, composite steel multigirder with a concrete deck (Figure 9). The greatest economy identified here was in steel fabrication costs. To accommodate this wider structure, the piers were changed from a straight concrete shaft to an open frame concrete bent, which resulted in lower concrete quantities.

STAYED SPANS

To use the most economical superstructure configurations in applicable areas, a continuous, composite steel multigirder with a reinforced-concrete deck again was used in the non-cable-supported portion of the cable-stayed girder spans (Figure 10). This, then, transitioned into a cross section by using stringers, floor beams, and fascia girders with a composite concrete deck. The arrangements are shown in Figures 11 and 12. This configuration is most effective because it permits combining the major deck support elements with the cable reaction points.

In the final design stage the superstructure took on a slightly different configuration than that used in the redesign study. A significant item that changed was the fascia girder. In the redesign study a box girder was thought necessary for handling the torque induced into the fascia girders by the cable connections. After further investigations of state-of-the-art designs and extensive studies of shear centers and centers of gravity, a modified I-type fascia girder cross section was found to be more feasible and economical than the box girder because of reduced material quantities and fabrication costs. The web of the fascia girder was skewed at 10 degrees from the vertical, which closely approximates the shallowest cable inclination transverse to the bridge. This then enables the web to follow the cable from the critical clearance areas to their point of connection, thus drastically reducing the eccentricity in the cable connections (about 40 in. with the box section to 10 in. with the weldment). Reducing the eccentricity drastically minimized the structural requirements of the cable connection. In addition, the floor beam was connected at the cable work points to aid in the stability of the fascia girder. The fascia girder was optimized further by using stringers in conjunction with the concrete

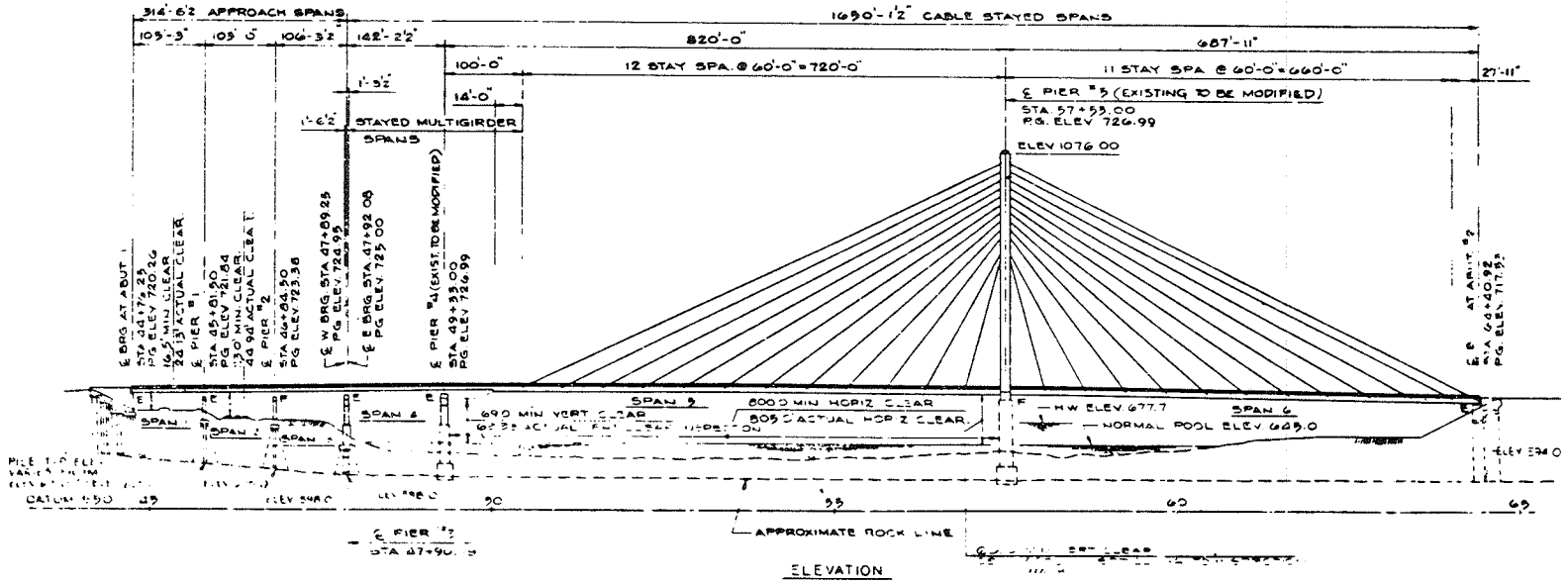

FIGURE 8 Redesigned bridge.

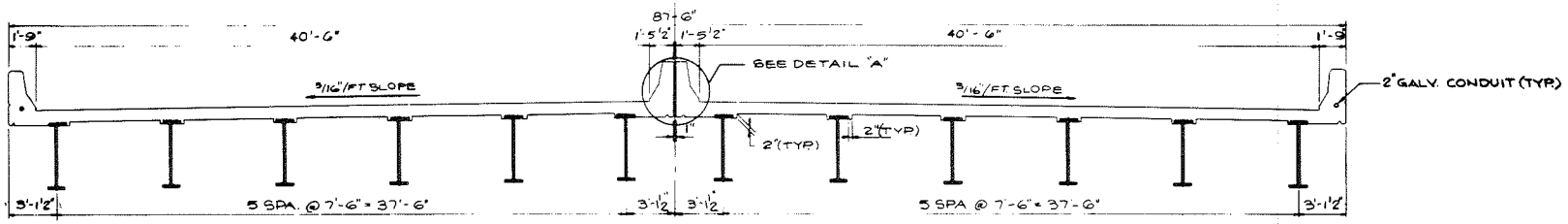

FIGURE 9 Approach spans cross section.

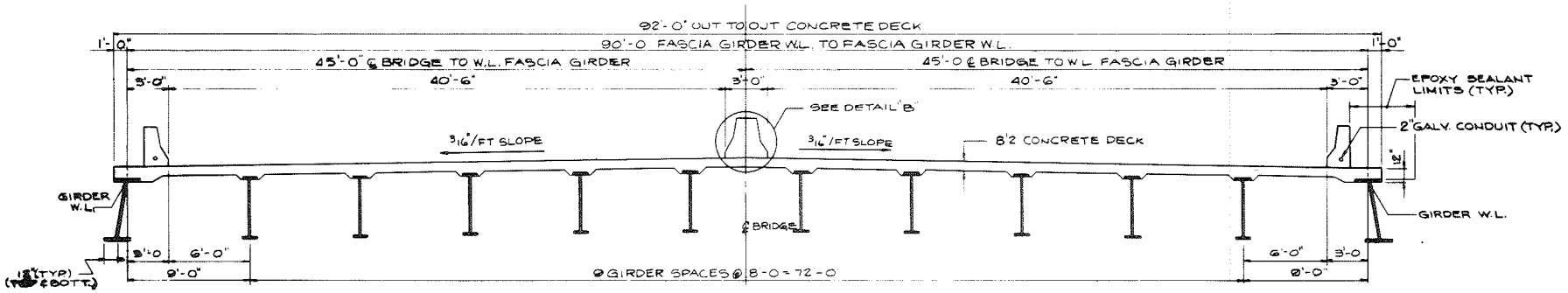

FIGURE 10 Stayed span multigirder cross section.

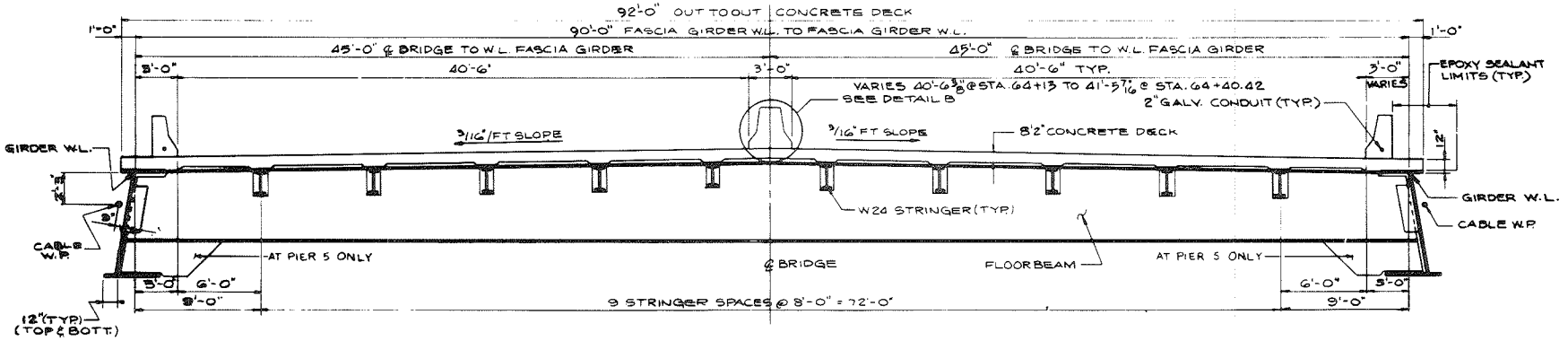

FIGURE 11 Cable-stayed girder span cross section at floor beam FB2-FB7 and FB9.

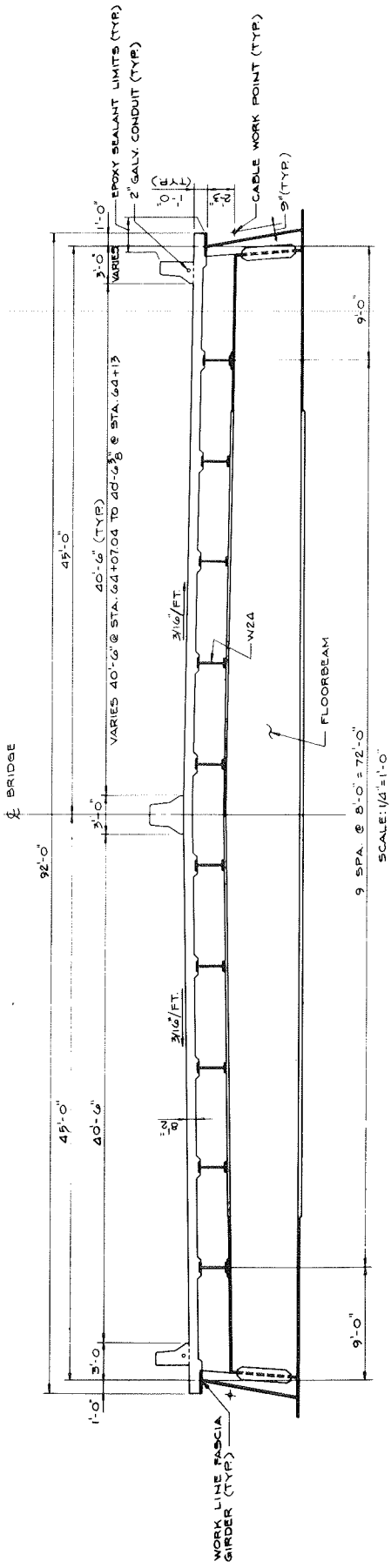

FIGURE 12 Cross section of cable-stayed bridge at floor beams FB1 and FB8.

deck to withstand the axial load induced by the cables into the superstructure. In doing this the deck with the wide flange stringers was analyzed as an orthotropic system. A finite-element computer analysis, which also checked the shear lag effect, proved this innovative approach to be reasonable.

The fascia girder also was optimized by requiring that (a) the construction of the superstructure be in 60-ft segments and (b) the fascia girder be shored until the cast-in-place concrete deck reached a specified strength. Therefore, the composite section supports the dead and live loads. As with all cable-stayed girder bridges, the dead-load moments were adjusted by selecting the proper cable tensions to optimize the superstructure cross section.

Horizontal trusses were then added at pier 5 (the tower pier) and at the last cable connections on the ends of the bridge. The end trusses ensured that the axial load induced by the end cable was distributed directly throughout the entire deck cross section, specifically in the stringers. The pier truss transferred the unbalanced stringer axial forces to the fascia girder bearings at pier 5. These trusses ensured that there was no shear lag effect at any of these locations.

These trusses also provide flexibility for bridge deck replacement while the bridge is still able to carry two lanes of traffic.

After a review by the American Institute of Steel Construction Bridge Committee of preliminary bridge design plans, the stringers were made continuous and the floor beams were lowered except at the truss locations. Doing so significantly cut the number and complexity of connections in the design and also lowered construction costs, despite an increase in steel weight.

TOWER

In this design the tower configuration changed from a 225-ft-high steel A-shape to a 365-ft-high concrete inverted Y-shape, as shown in Figure 13. As anticipated, with reduced fabrication and because the tower is basically a compression member, concrete was the most economic material to use.

After researching the literature on cable-stayed girder design and calculating preliminary estimates, the most economic cable-to-horizontal angle in the longitudinal plane was determined to be between 25 and 65 degrees. Cable 1A was close to 25 degrees; however, cables near the tower had to exceed 65 degrees to maintain proper overhead clearances in the transverse direction, according to West Virginia requirements.

By using these design criteria, the tower height was raised to 365 ft above pier 5 and 430 ft above normal pool elevation. To accommodate the expanded number of cables and to obtain optimum tower height, an H-shaped, concrete, single-leg pylon was used to anchor all the cables. Supporting this pylon are two concrete box-shaped legs.

The H-shaped pylon cross section was selected for its simplicity in designing and constructing the cable connections. A concrete fascia panel was used to protect the cable connections from the weather and to conceal inspection platforms and access ladders.

The posttensioning was placed in the pylon's web to counteract the tension induced by the cables, thus simplifying design and construction.

The height of the apex of the inclined legs that were accommodated required transverse clearances between the tower leg and traffic and between the cable and traffic. This then gave the pylon a total height of 140 ft above the apex.

The dual, inclined tower legs, each 225 ft high,

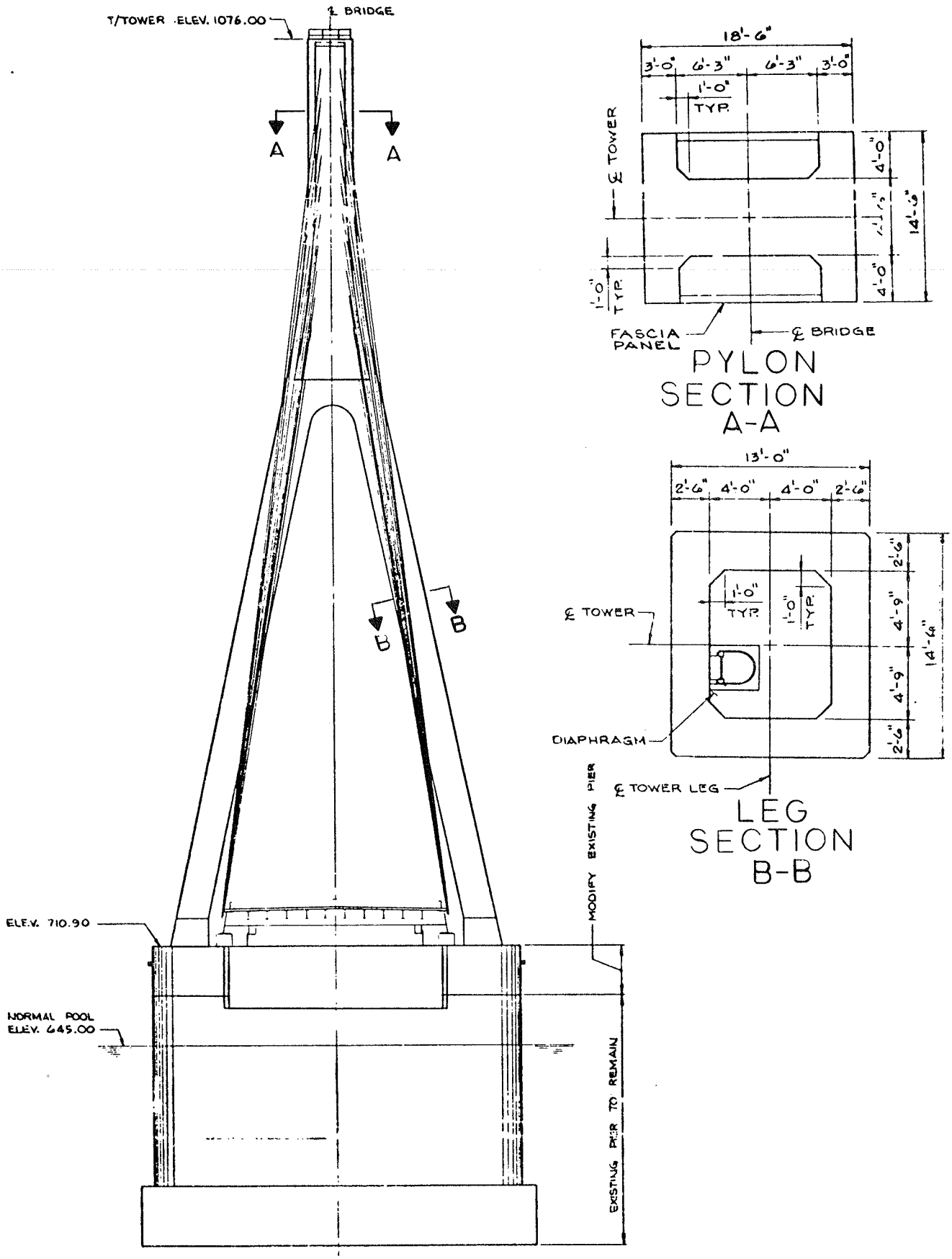

FIGURE 13 Tower, pier 5.

maintained minimum deck widths and fully used the conditions dictated by the already constructed pier 5. These legs will set on a concrete tower pedestal on a yet-to-be-constructed portion of pier 5. Dual access for cable connection inspections is provided by an elevator in one leg and a ladder in the other.

SUBSTRUCTURE

To arrange the cables symmetrically in the first steel design, pier 6 was placed between pier 5 and abutment 2. With the last cable anchored into it, pier 6 served as a tieback for the entire structure. In the second steel alternate design, the increased number of cables made abutment 2 the symmetrical tieback location. As a result, pier 6 was eliminated in the second steel design, thus leaving four substructure units in the stayed spans.

These units had to be designed to accept a much wider bridge--92 ft as opposed to 36 ft for the bottom flange of the box girder--than the original steel alternate. Pier 4 was modified from a straight pier to a hammerhead, and pier 3 was designed as a hammerhead; for this reason, and because the piers are in the river's flood plain, pier 5 was changed slightly to accommodate embedment of the bearing pedestal reinforcing steel.

Eliminating pier 6 meant that abutment 2 would tie back the entire structure. Under certain load cases, the uplift on the abutment became substantial.

The tiedown is a large mass of concrete placed beneath abutment 2. This mass is posttensioned to a weldment that attaches to the tiedown bars from the last floor beam and is supported on piles. The maximum pile load occurs in the construction phase before tensioning the tieback cable. The majority of the load on the piles is relieved when the superstructure tieback cable is tensioned. The abutment back wall and wing walls are cantilevered on pile footings.

DESIGN CONSIDERATIONS

As with all cable-stayed girder bridges, the dead-load moments in the stayed areas can be adjusted by changing the tension in the cable stays. This assisted in material optimization of the fascia girder. When the live-load moment envelope was obtained, the maximum negative moments at the interior hard points (piers 4 and 5) were large compared with the positive moment.

To reduce the effect of the large negative moments on the girder, the dead-load moment was made positive by adjusting cable tensions. The live-load moment envelope was investigated along the entire stayed span length, and the dead-load moment was then adjusted to optimize the superstructure sections.

Temperature and wind loads did not govern the deck stress design, but they did affect the tower design in some areas. Wind loadings were applied as recommended by A.G. Davenport of the University of Western Ontario in Canada, who also reviewed the wind stability studies and confirmed the stability of the bridge. Differential temperatures were applied between the concrete tower, steel cables, and the mixed concrete and steel deck. The loads that were induced affected the tower design only.

The method by which this bridge will be erected has an effect on the final stresses in the deck. Several erection schemes were investigated to optimize material use.

The first erection scheme specified that the bridge be built on falsework from abutment 2 to pier 5. It then used cantilever construction to erect the main span, tensioning the forestay and the backstay as the main span progressed. This scheme was abandoned in favor of balanced-cantilever construction because of the high cost of the falsework. The initial balanced-cantilever construction contemplated that all the steel be erected in the superstructure, and then the concrete deck poured. The vast majority of the dead-load stresses went into the steel by using this scheme. Because this type of construction required a great deal of steel, a panelized, shored-erection scheme working away from pier 5 in a balanced-cantilever manner was chosen. This scheme optimizes the superstructure cross section without penalizing the erection process significantly.

The tower, multigirder cross sections, and all substructure units were economized further by using the load-factor design method in these areas. The cable-supported areas of the bridge were designed by using the service load design method because the AASHTO code criteria do not address composite beam column design and design schedule constraints precluded developing such criteria.

CONCLUDING REMARKS

On September 9, 1983, construction bids were opened for the three alternate bridges. The lowest bid was made on the second steel alternate design, and the construction contract was awarded to S.J. Groves and Sons Company for its $20 million bid.

There were nine bids on the second steel alternate, one at $32 million on the first steel alternate, and none on the concrete alternate. Several contractors who bid the second steel alternate said that they priced the concrete alternate and estimated it to be about $4 million more than the second steel alternate.

All three alternates were satisfactory designs, with economic conditions and preexisting constraints creating advantages and disadvantages for all three. However, common practice states that concrete exerts its best qualities in compression and that steel exerts its best qualities in tension and bending. Exploiting the materials' best qualities and reducing the quantity and complexity of steel fabrication appeared to allow the second steel alternate design to gain final advantage over the other alternatives.

REFERENCE

1. Standard Specifications for Highway Bridges. AASHTO, Washington, D.C., 1977.

Publication of this paper sponsored by Committee on Steel Bridges.

Design of the Cable-Stayed Mississippi River Bridge at Quincy, Illinois

JOHN M. KULICKI, H. EUGENE WALDNER, and JOSEPH E. PRICKETT

ABSTRACT

Two alternative two-lane, cable-stayed bridges have been designed to carry US-24 over the Mississippi River at Quincy, Illinois. The design and detailing information on both alternatives are presented. Both bridges include main spans of 900 ft and both use concrete towers and a concrete deck. The concrete alternative uses 6,000-psi concrete precast segments that consist of edge beams, floor beams, stringers, and a deck slab. The steel alternative uses welded I-shaped edge girders, steel stringers, and floor beams, and a deck composed of precast, full-width, full-thickness slab panels that are posttensioned longitudinally in erection lengths (comparable to the cable spacing) and are then made composite with the stringers and main girders.

The new westbound US-24 Mississippi River bridge at Quincy, Illinois, has been designed for two alternative methods of construction. In the first alternative the deck system is entirely of concrete. In the other alternative the deck system consists of steel members with a concrete deck. Inasmuch as both alternative cable-stayed bridges have been designed by one consultant, the same philosophy of design and detailing has been applied to both alternatives. This should result in two genuinely equal alternatives in terms of the designers' attention to both the immediate and long-term costs to the owner.

The entire project consists of several thousand feet of approach structure, some ground and approach work, and a cable-stayed main bridge. The prime consultant is Booker Associates, Inc., which designed the approaches to the cable-stayed bridge, including the flanking transition spans. Modjeski and Masters designed the cable-stayed bridges. The owner is the Illinois Department of Transportation. The discussion in this paper is limited to a description of the cable-stayed bridge.

The general elevation of the concrete alternative bridge is shown in Figure 1. In both alternatives the general span arrangement consists of (from left to right) a transition span of 200 ft, a 440-ft side span of the cable-stayed unit, the main span of the cable-stayed unit at 900 ft, another side span at 440 ft, and a transition span of 200 ft. The span arrangement was preset by a separate engineering contract for alignment studies. The two-lane bridge is relatively narrow, being only 32 ft, 0 in. curb to curb. In both alternatives the tower is of concrete. In the concrete alternative the deck system, which consists of edge beams, floor beams, stringers, and a deck slab, is composed entirely of concrete. There are 96 cables on the concrete alternative structure.

The steel alternative is shown in Figure 2. This alternative contains 56 cables. The deck system consists of longitudinal welded steel girders, steel floor beams, and steel stringers. The longitudinal members are composite with the concrete deck after

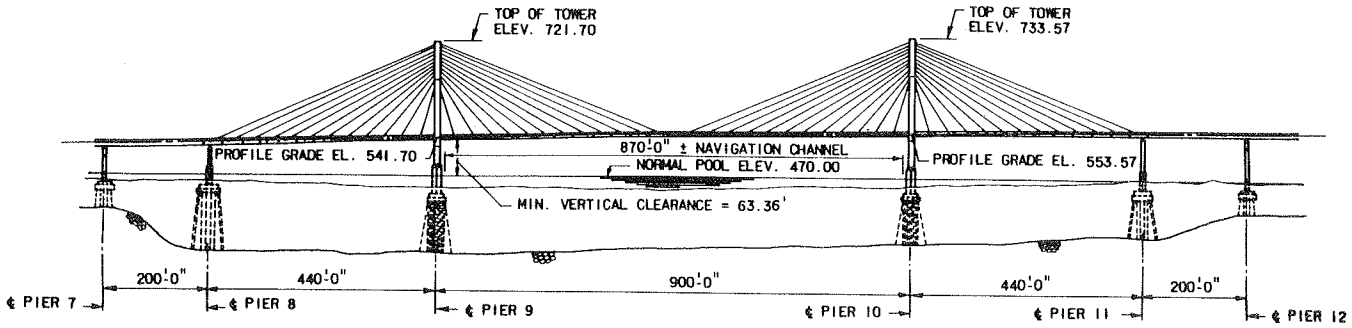

FIGURE 1 Elevation view of concrete alternative.

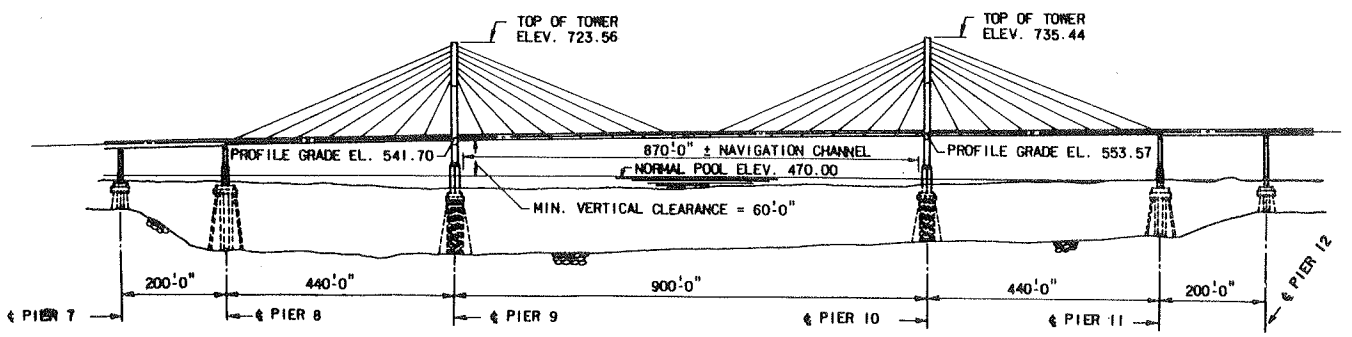

FIGURE 2 Elevation view of steel alternative.

posttensioning of the slab panels. The contract drawings contain the complete details for both alternatives. A third alternative is also being permitted wherein the main span may be of concrete construction and the transition spans may be of steel construction.

BASIC DESIGN PARAMETERS

Basic loads for both alternatives are given in Table 1, which is excerpted from the general note sheet of the contract documents. The basic design procedure used influence lines for all structural components. This imples a first-order analysis. The second-order effects were estimated from a limited number of iterative second-order analyses and were found to be relatively small. A percentage adjustment was made to in-plane and out-of-plane tower moments. The loading patterns that produced the largest second-order effects in the deck system, which were found to be quite small in absolute terms, were not the same as the loading patterns that produced the maximum first-order effect. Because these two effects offset each other, no adjustment in the deck moments was made. It is important to note that this conclusion is structure dependent and should not be generalized without further study.

The dead load of each of the bridges was balanced such that there was essentially no dead-load bending in the tower and only local (i.e., between-cable) bending in the deck structure. This was accomplished by selective cable adjustment and local ballasting. In order to allow for some tolerance in the actual as-constructed balance, an unbalanced dead load was applied, as explained in Table 1.

Dead-load moment and thrust curves, and live-load moment and thrust envelopes for the concrete and steel alternatives are shown in Figures 3 and 4, respectively. Both alternatives have been designed so that the concrete decks can be removed and replaced if necessary, and also so that any cable can be replaced without auxiliary support in the river.

Dynamic analyses and wind tunnel tests were performed for both alternative structures. The wind tunnel tests were performed at the low-speed aerodynamic test facility of the National Research Council, Ottawa, Ontario, Canada, under the direction of R.L. Wardlaw. Some alteration of both cross sections was required, as explained herein. A summary of the pertinent results is given in Table 2.

CONCRETE TOWERS

A front elevation, side elevation, and several sections through the tower are shown in Figure 5, as are the principal dimensions.

TABLE 1 Design Loads

DESIGN

EXCEPT AS NOTED HEREIN, THE BRIDGE IS DESIGNED IN ACCORDANCE WITH THE AASHTO STANDARD SPECIFICATIONS FOR HIGHWAY BRIDGES, 12TH EDITION, DATED 1977 AND, THE AASHTO INTERIM SPECIFICATIONS THROUGH 1982.

LOAD FACTOR DESIGN METHODS HAVE BEEN USED TO PROPORTION THE TOWER, EDGEBEAMS, STRINGERS, BEARING PLATES, TRANSITION SPANS, AND THE CONCRETE ALTERNATE (CABLE-SUPPORTED SPAN) DECK SLAB. THE TRANSITION SPANS HAVE BEEN DESIGNED FOR AASHTO LOADING. THE FOLLOWING FACTORED LOADS WERE USED IN THE CABLE-SUPPORTED SPANS:

GROUP I:	1.4 (BD) + 2.17 (L + I)
GROUP II:	1.4 (BD + W)
GROUP III:	1.4 (BD + L + I + 0.3W + WL + LF)
GROUP IV:	1.4 (BD + L + I + S + T + R)
GROUP V:	1.35 (BD + W + S + T + R)
GROUP VI:	1.35 (BD + L + I + 0.3W + WL + LF + S + T + R)
	B = 1.0, B = 0.875

NOMENCLATURE IS THE SAME AS AASHTO.

SERVICE LOAD DESIGN METHODS HAVE BEEN USED TO PROPORTION THE CABLES, AND FLOORBEAMS IN CABLE-SUPPORTED STRUCTURE (CONCRETE ALTERNATIVE) AND HAVE BEEN USED TO DESIGN THE DECK SLAB AND CABLES IN THE CABLE-SUPPORTED STRUCTURE (STEEL ALTERNATIVE).

EDGEBEAMS AND STRINGERS ON THE CABLE-SUPPORTED STRUCTURE (CONCRETE ALTERNATIVE) HAVE BEEN DESIGNED TO HAVE NO TENSION UNDER GROUP I SERVICE LOADS.

THE DEAD LOAD ON THE CABLE-SUPPORTED SPANS CONSISTS OF THE GEOMETRIC DEAD LOAD, PLUS AN UNBALANCED DEAD LOAD EQUAL TO 3% OF THE DEAD LOAD TREATED IN THE SAME MANNER AS A MOVING LIVE LOAD, I. E., THE PORTION OF THE STRUCTURE CONTRIBUTING TO A GIVEN MAXIMUM FORCE OR MOMENT WILL BE CONSIDERED TO BE 3% OVERWEIGHT.

SEISMIC LOADS

AASHTO, ZONE 1

TEMPERATURE (CABLE-SUPPORTED SPANS)

ASSUMED ERECTION TEMPERATURE	50^{0} F
ASSUMED MEAN TEMPERATURE	50^{0} F
TEMPERATURE DIFFERENTIAL - CABLE TO CONCRETE	40^{0} F
TEMPERATURE DIFFERENTIAL - CABLE TO STEEL	30^{0} F
TEMPERATURE RANGE FOR EXPANSION DAMS	$\pm$ 80^{0} F
TEMPERATURE GRADIENT THROUGH DECK STRUCTURE	20^{0} F
TEMPERATURE GRADIENT THROUGH TOWER	15^{0} F
ALL DIMENSIONS GIVEN AT	50^{0} F

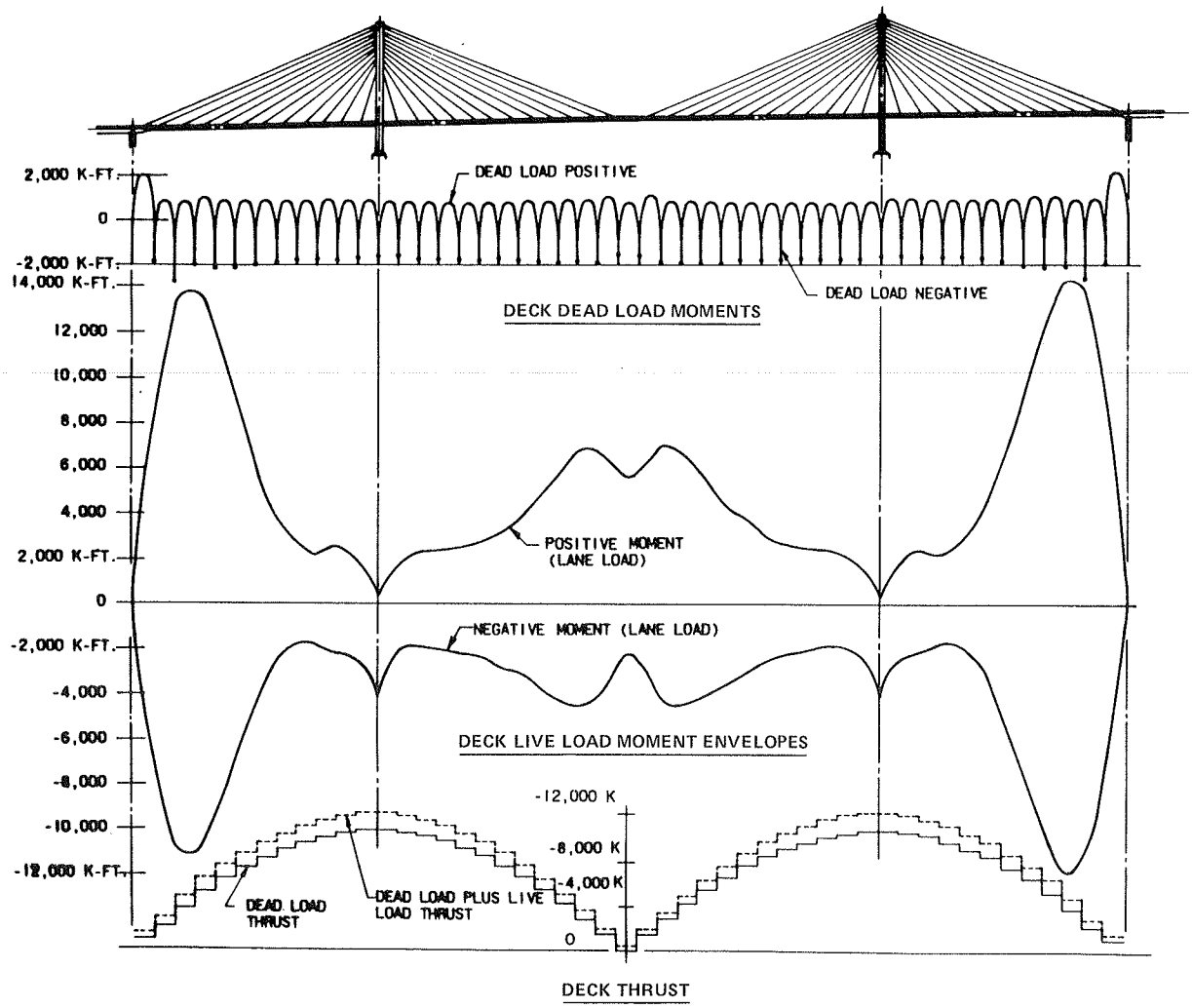

FIGURE 3 Moment and thrust envelopes for concrete alternative.

The bow-legged arrangement was chosen in order to simplify the structural arrangement of the cables. On this bridge the cables all lie in a vertical plane. This greatly simplifies the detailing of the anchorage of the cables in the tower and in the deck section, in that the geometry at each cable anchorage point can be defined by a single angle, which the cable makes with the horizontal plane. The cables all frame into the pylon, and because the lower cable connections are located in a plane vertically beneath the cable connections in the pylon and the deck passes between the tower legs, it is necessary to sweep the legs outward to provide clearance for the deck section. Below the deck at the level of the bottom strut, the tower legs are turned inward to minimize the width of foundation required. The concrete in the tower is 5,000-psi cast-in-place concrete.

Typical reinforcing details in the pylons are shown in Figure 6. The location of the cables is shown in each of the three views, which illustrate the problems in detailing the reinforcing to clear the cable anchor pipes. The principal vertical reinforcing is mechanically coupled for continuity and is distributed around the outer face of the column and the inner face of the void. The horizontal reinforcing consists of stirrups and other reinforcement distributed around the exterior face of the column and the inner face of the void.

A partial elevation view and section that shows the distribution of posttensioning in the tower pylon is shown in Figure 7. As can be seen in section A-A, the cables are designed to be socketed on the inside tower walls in a manner that applies tension to the long walls. It was possible to use this arrangement because the relatively narrow bridge resulted in cable loads that were low enough that posttensioning to resist wall tension was practical. The cable sockets could, therefore, be relatively well protected by being within the tower leg voids.

The cable locations and bearing corbels are also shown in Figure 7. The detailed location of the posttensioning shows that the posttensioning must clear the cable anchor pipes. The tower pylon is posttensioned vertically and in both horizontal directions, thus providing a state of triaxial posttensioning. The vertical posttensioning is heaviest in the upper portion of the pylon; however, a reduced amount continues down to the bottom of the upper strut. The horizontal bars are the 14-ft, 6-in. posttensioning bars, whose primary function is to carry the horizontal pull from opposing cable pairs across the tower pylon. The posttensioning shown as dots are the 7-ft-long posttensioning bars, whose function is to control the bending that results from the cable bearing on the corbel that spans between the tower walls, and also to provide

adequate shear friction for transfer of the cable load into the 14-ft, 6-in. posttensioning bars. The overall system of posttensioning is designed to keep the concrete in compression during all stages of erection and during the life of the structure; this will minimize crack formation in the pylon.

The pylon section has been subjected to a finite-element analysis, whereby it was found that the concrete is in compression at all service load stages during the life of the bridge, except for some minor tension from Poisson effects. It is important that these 7-ft posttensioning bars maintain the pylon concrete in compression. These bars are so short that a small amount of seating loss could seriously affect posttensioning. Additional requirements to assure that these bars will provide compression for the life of the bridge are included in the special provisions, which require restressing all of the horizontal bars in the tower pylon. The restressing shall take place no less than 30 days after the initial prestressing of each bar. The restressing will consist of two repetitions of jacking each bar to the desired tension and seating the anchor nuts on the anchorage. A test block was used to stress and restress a bar of 7-ft length as required on the contract drawings; based on that experience it is believed that the restressing operation as described will give satisfactory long-term performance of these short bars.

A cross section of a bottom tower strut is shown in Figure 8. The longitudinal and transverse reinforcing are shown as solid lines and small dots, and the longitudinal posttensioning is also shown. The longitudinal posttensioning extends out-to-out of the tower legs. The struts on these towers are structurally significant members that stabilize the tower legs and carry torsion, moment, shear, and thrust.

TABLE 2 Aerodynamic Characteristics

	Concrete Alternative	Steel Alternative
First bending frequency (Hz)	0.275	0.462
First torsional frequency (Hz)	0.631	0.706
Flutter		
Damping (% critical)	0.3	0.5
Speed (mph)	120	>130
Vortex: vertical		
Damping (% critical)	0.3	0.5
Speed (mph)	16	25
Displacement (in.)	0.5	0.5
Acceleration (% g)	0.4	1.1
Wind angle (degree)	0	0
Vortex: torsional	—[a]	—[a]

[a]None.

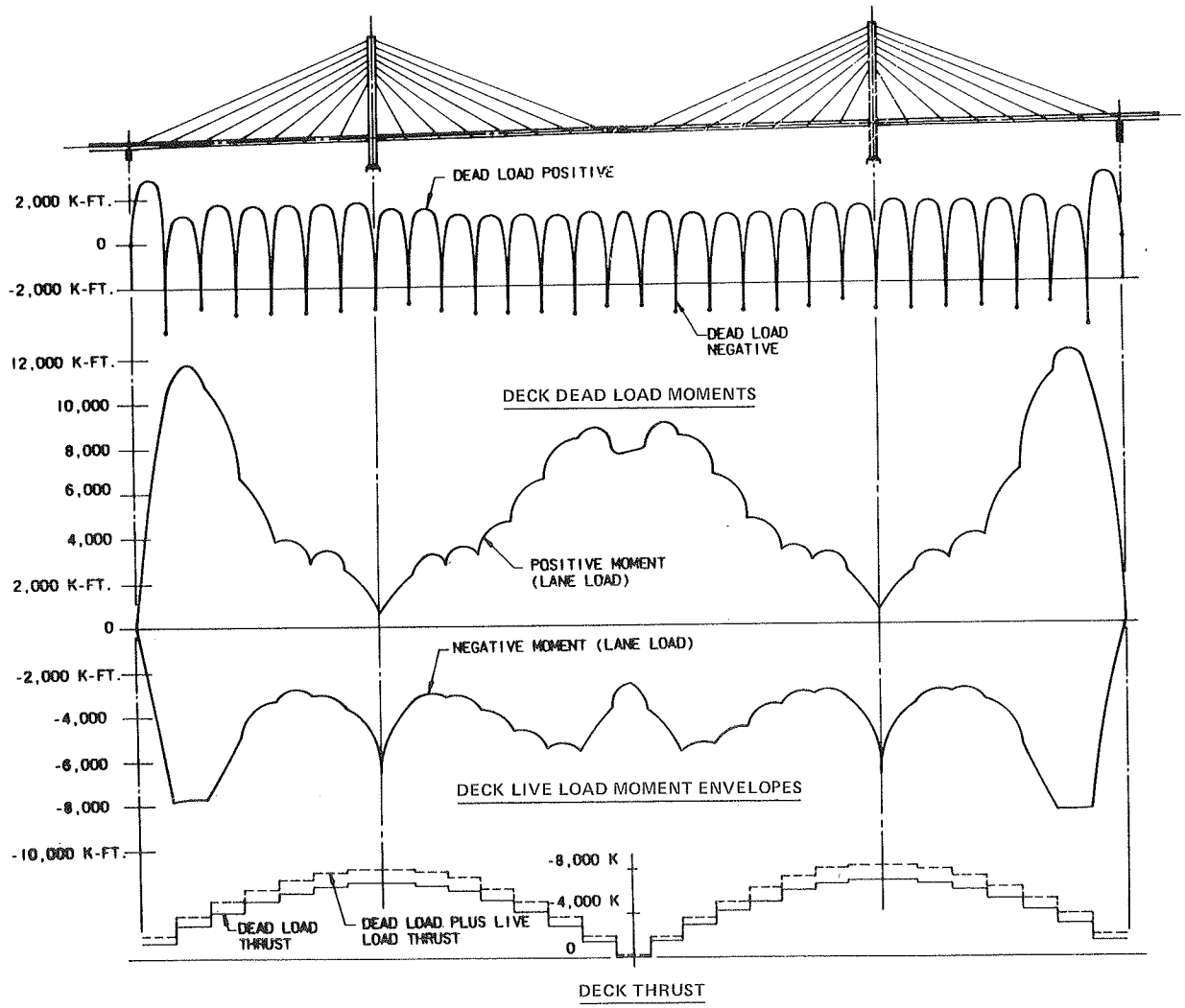

FIGURE 4 Moment and thrust envelopes for steel alternative.

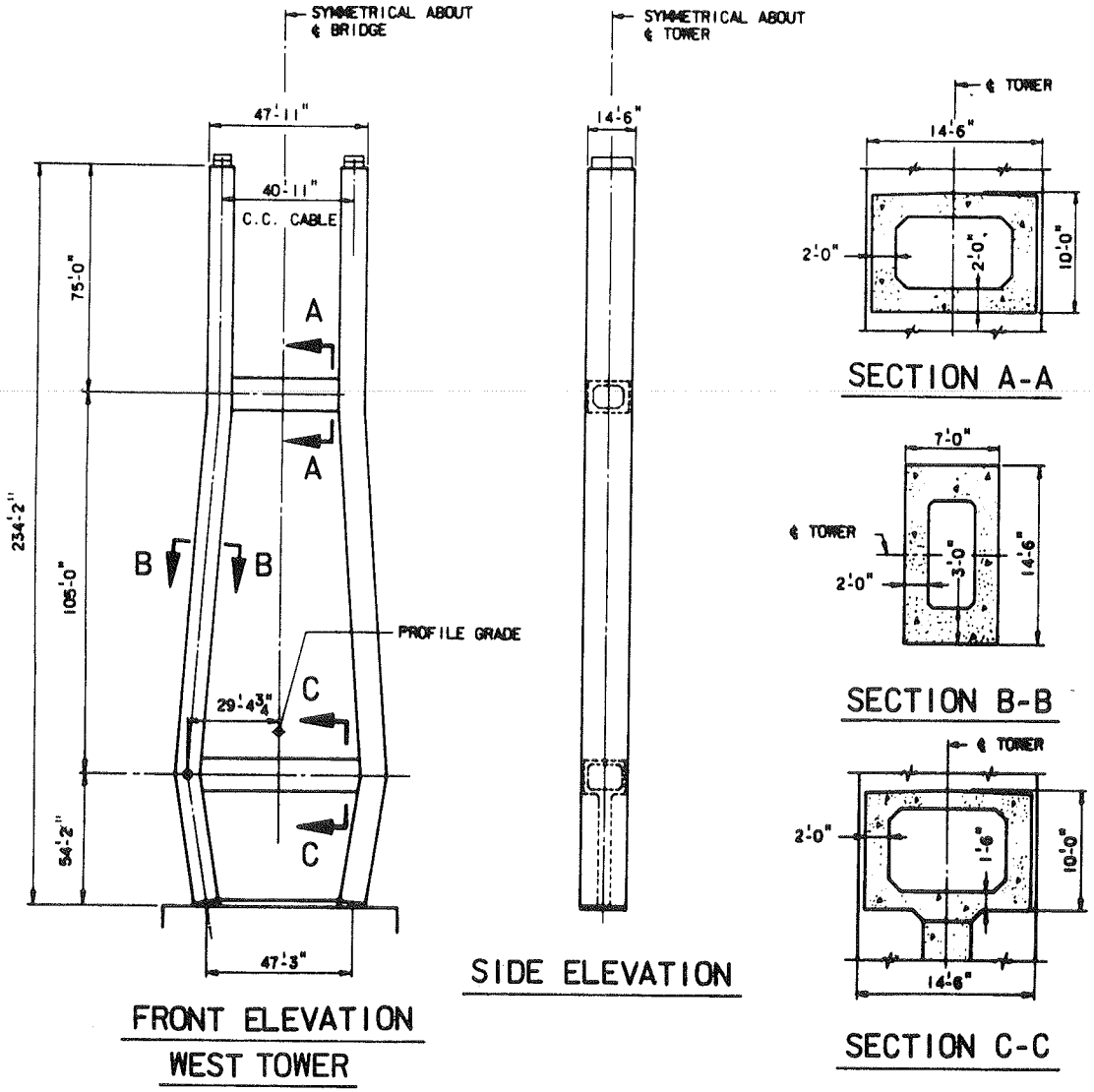

FIGURE 5 Concrete tower: elevations and sections.

CABLE SYSTEM

The cable system proposed for the Quincy bridge shown on the contract drawings consists of cables made of bundles of parallel wires of 0.25-in.-diameter, ASTM A421, grade BA that have 240-ksi tensile strength. In the socket the wires splay out and are buttonheaded and anchored by a locking plate that is attached to the socket. The splayed area in the socket is filled with a special epoxy casting material that further anchors the wires within the socket. Emerging from the socket, the wires are wrapped with a spirally wound wire strand and protected by a polyethylene pipe. In addition, near the socket a short length of steel sleeve is attached to the socket and surrounds the polyethylene pipe. These details are shown in Figure 9. The number of wires per cable in the two alternative structures varies from 81 to 283 wires per cable. The stress in each cable has been limited to 103 ksi. In some cases the cable design is based on a temporary design condition in which one cable is assumed to be removed and the adjacent cables must carry not only their load but also part of the load that would normally be carried by the cable that is removed.

As a matter of interest, this design calls for about 943 miles of wire for the concrete alternative and about 630 miles of wire for the steel alternative.

Tower attachment details for the proposed cable are shown in Figure 10. This is the dead end of the cable. It bears on a concrete corbel that is an integral part of the tower wall. The cable anchor pipe is welded onto the bearing plate, and the entire assembly is cast into the tower pylon. The cable and socket are threaded upward through the cable anchor pipe and anchored with split washers. An elastomeric washer is positioned at the lower end of the cable anchor pipe, along with a protective neoprene boot that is clamped to the polyethylene tube and to the cable anchor pipe.

The cable hardware at the deck connection is shown in Figure 11. First, there is a bearing plate that has an opening large enough to pass the socket. Next is the split bearing washer followed by the adjusting split shims. On top of that is a socket alignment shim, and finally, the cable socket. Nominal shim thickness of 6 in. is anticipated. The special provisions require that if the thickness of shims needed to adjust the cable to its required tension exceeds 12 in., the engineer must be con-

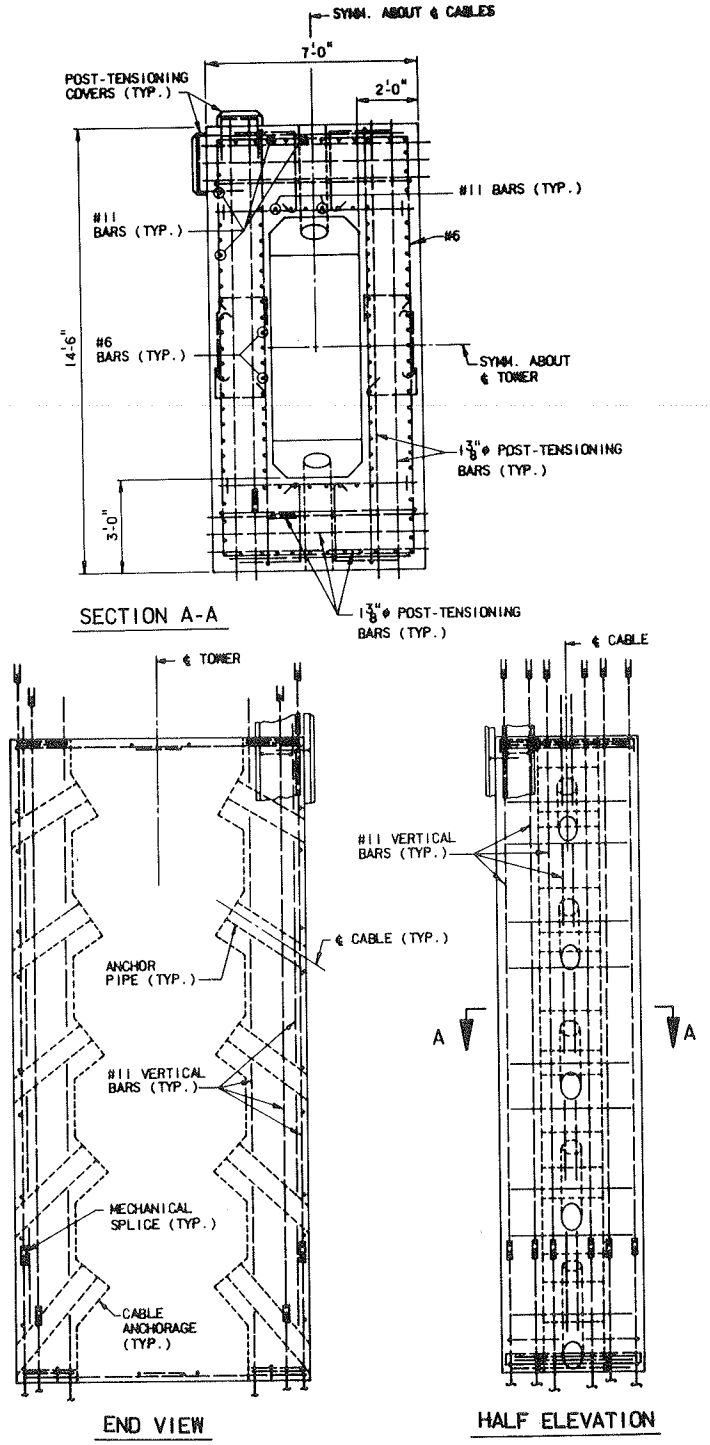

FIGURE 6 Concrete tower pylon: reinforcing details.

sulted. More than 12 in. of shims would be outside of the anticipated normal range; thus it would then be necessary to consider the reason for the discrepancy.

The special provisions provide for an alternative cable system that uses a 0.6-in.-diameter, low relaxation ASTM A416, grade 270, seven-wire strand in a parallel configuration. Such a system may be proposed by the contractor as summarized herein. The parallel wire cables, as shown on the contract drawings, have previously demonstrated acceptable fatigue characteristics. It is mandatory that any alternative cable system proposed shall demonstrate equivalent fatigue resistance. The total number of stays and the location of the cable work points may not be changed. If a socket with an external thread is proposed, the special provisions contain requirements for the amount of thread required. Any alternative system proposed shall provide cables of essentially the same stiffness and weight as those shown on the contract drawings; that is, the product of cable area times the effective modulus elasticity shall be the same as those shown on the plans. Note that some of the cables on the contract drawings

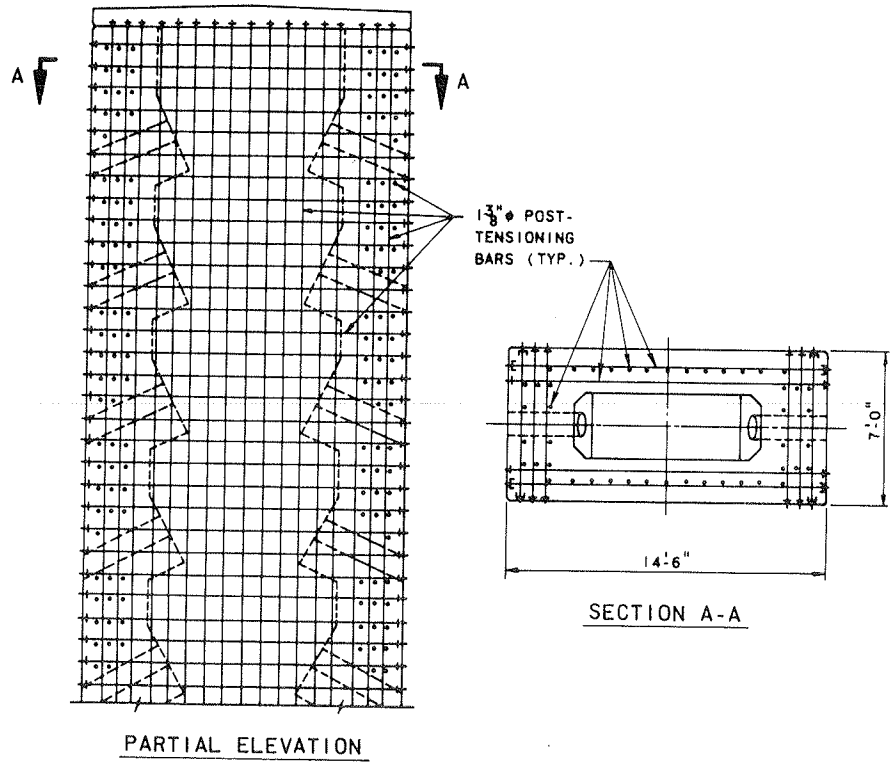

FIGURE 7 Concrete tower: posttensioning arrangement.

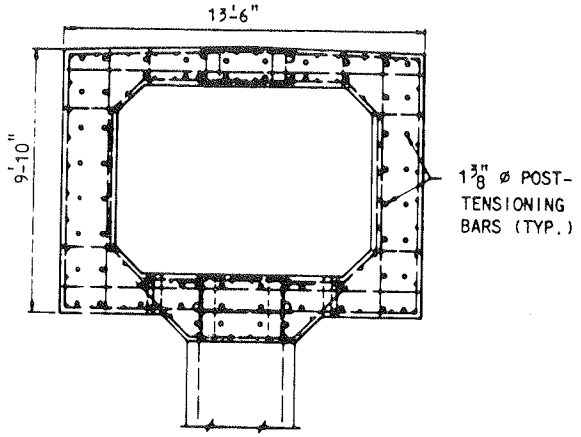

FIGURE 8 Concrete tower: section through lower strut.

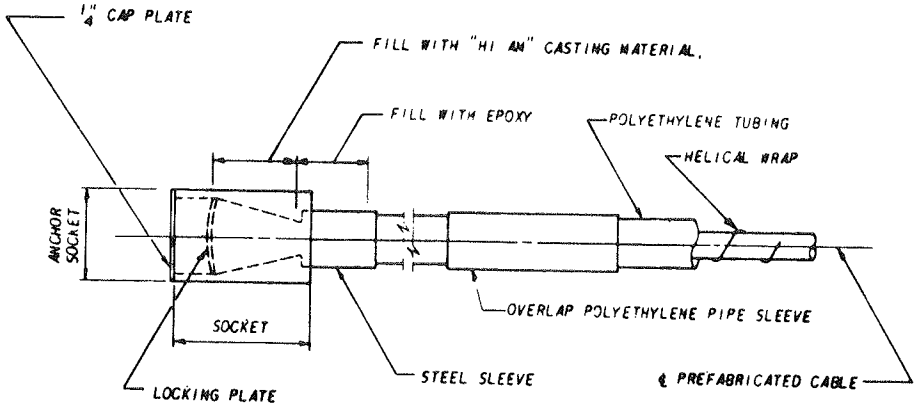

FIGURE 9 Cables: schematic of parallel wire cable.

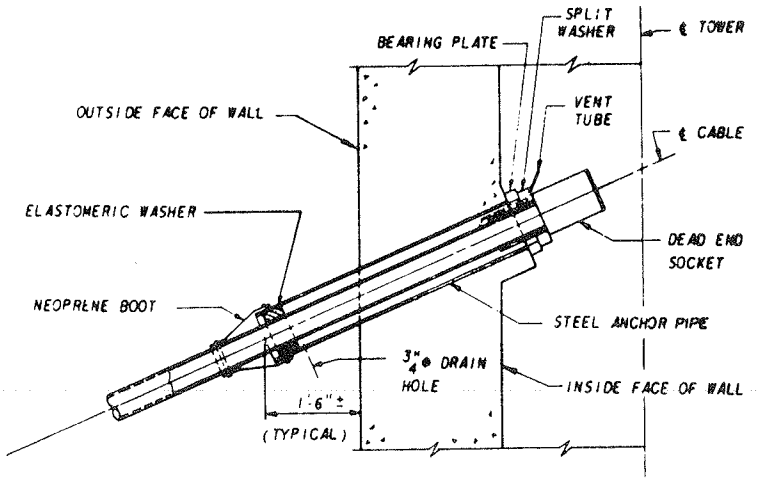

FIGURE 10 Cables: details of tower attachment.

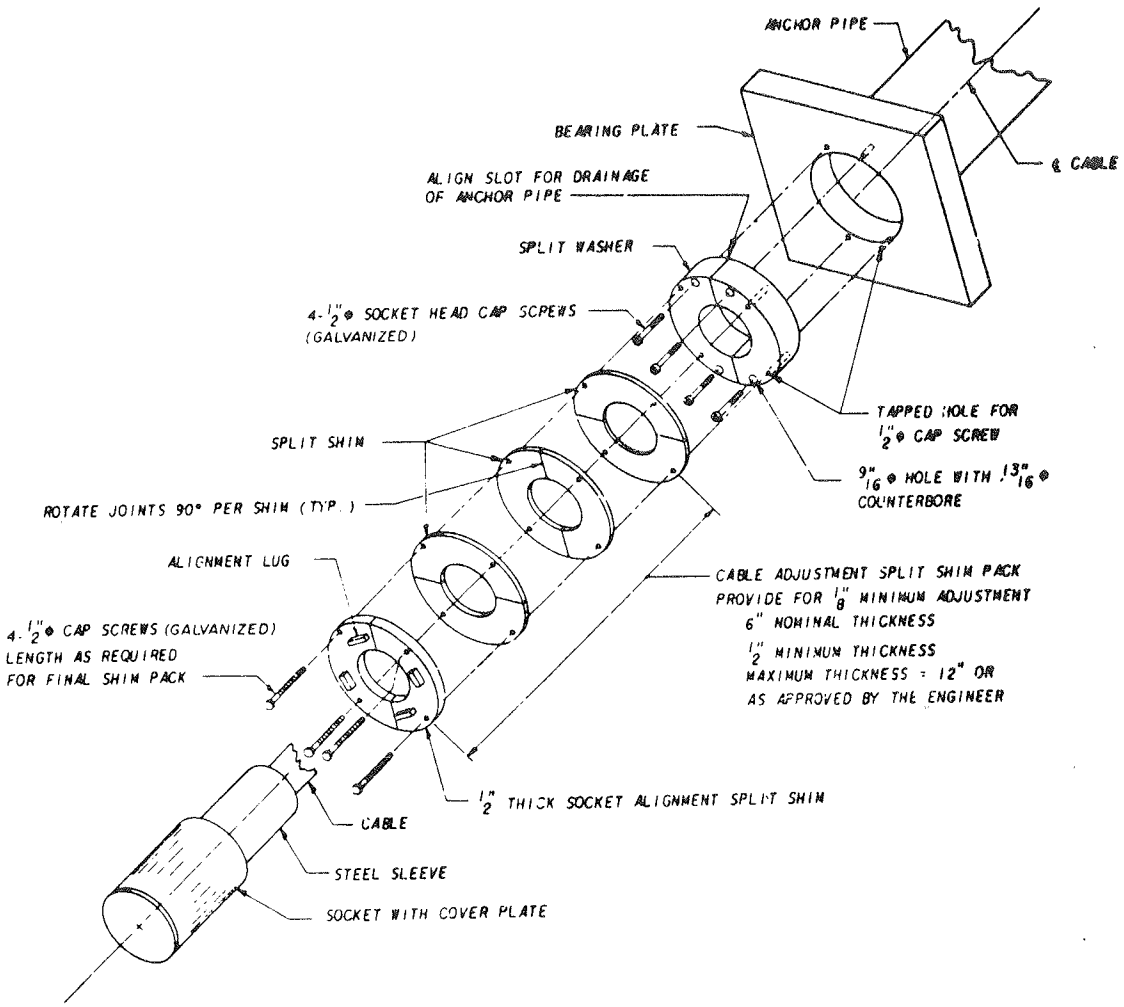

FIGURE 11 Cables: details of edge beam attachment.

have been oversized, either to provide additional stiffness to the structure or to provide for cable removal, and these requirements will also apply to any alternative cables proposed. It is desirable that an alternative cable system use anchor pipes no larger than those presently detailed. If the size of the anchor pipe were to be changed to accommodate a proposed alternative cable, many of the internal details within the edge beam and tower would have to be modified to a larger anchor pipe size.

Typical corbel details in the tower pylon are shown in Figure 12. The anchor pipe, bearing plate

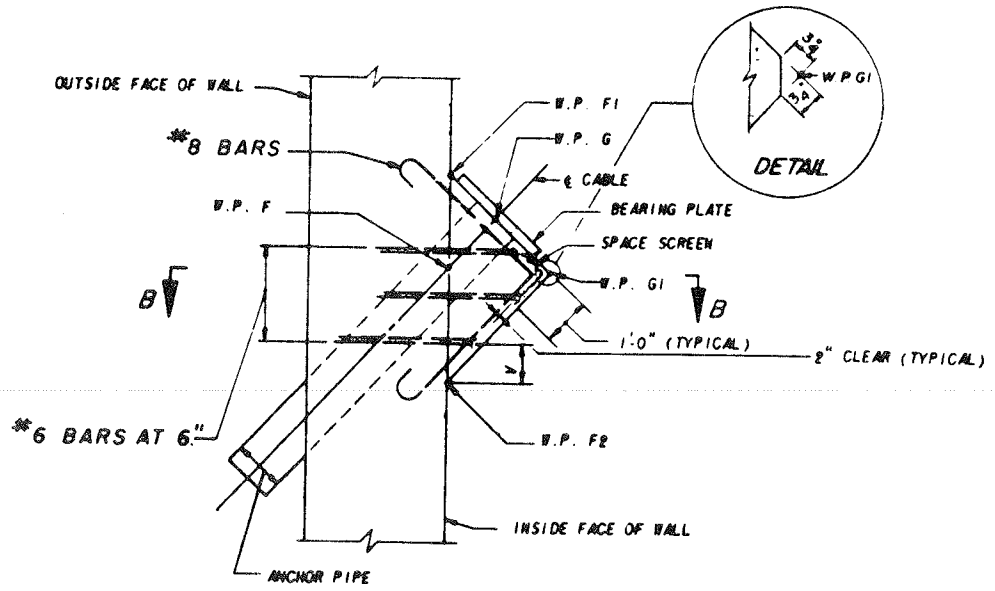

FIGURE 12 Cables: reinforcing at tower corbel.

assembly, and the location of the work points that completely describe the geometry of each corbel are shown. The extra reinforcing required at each corbel, and all other required reinforcing, is completely detailed on the contract drawings.

CONCRETE ALTERNATIVE DECK SYSTEM

A general elevation of the concrete alternative bridge is shown in Figure 1. This bridge is of segmental concrete construction. Beginning at each tower, the deck is cast-in-place. Then, proceeding in each direction from the tower, the deck is composed of precast segments. The closing sections at the centerline of the bridge and at the anchor piers are cast-in-place. The cast-in-place sections use 5,000-psi concrete, and the precast segments have a minimum strength of 6,000 psi. In each side span the cables are spaced at 36 ft, 8 in.; main span cable spacing is 36 ft, 0 in.; and generally the segments are the same length as the cable spacing. There are 12 cables on each side of each pylon for a total of 96 cables on the bridge.

A cross section of the deck section is shown in Figure 13. Cables are in a vertical plane, and on each side the edge beam is centered directly under the cables. The floor beams span transversely between the edge beams and carry the stringers and the deck. In this figure edge beams of different sizes are shown in the left and right half sections because the edge beam changes dimensions along the bridge. In the side span there are two major changes in edge beam dimensions. In the first major transition the edge beam is a constant 3 ft, 9 in. wide

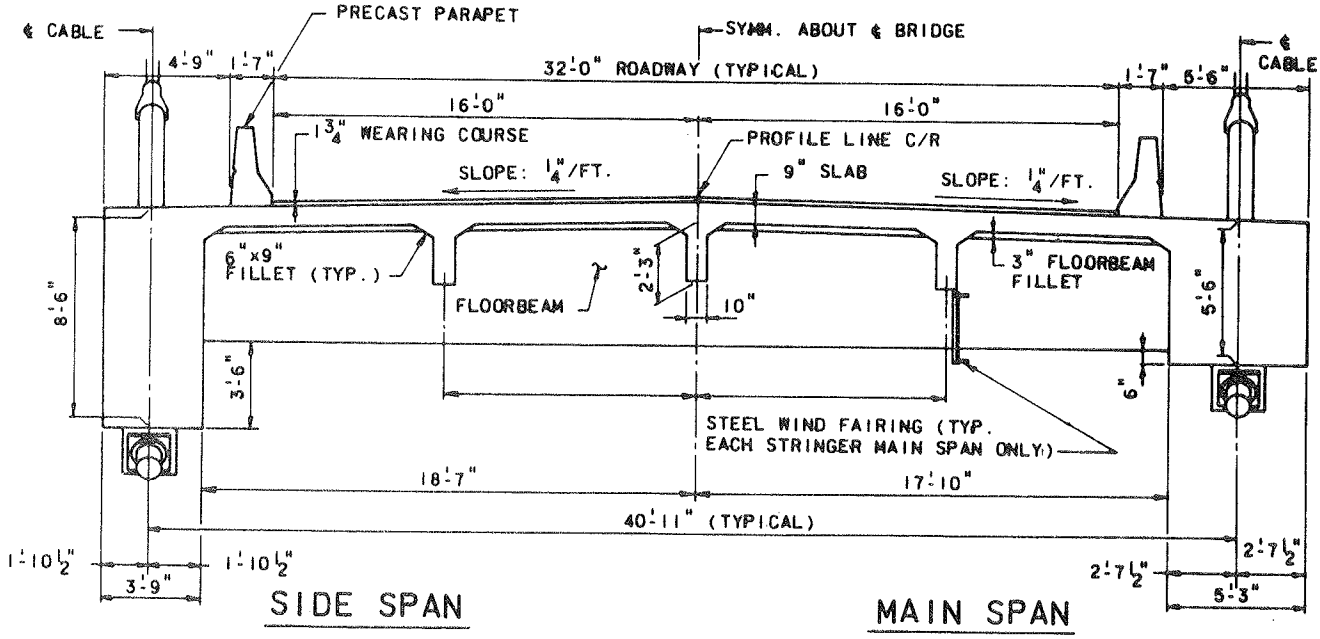

FIGURE 13 Concrete alternative: cross sections.

and varies from 8 ft, 6 in. to 5 ft, 6 in. in depth. In the second major transition the edge beam remains at 5 ft, 6 in. in depth and varies from 3 ft, 9 in. to 5 ft, 3 in. wide. It remains at this latter section across the tower pier to the centerline of the bridge. Thus, although the depth and the width of the edge beam vary at several different locations, only one dimension varies at any given location.

The floor beams are box sections that have a width of 2 ft, 6 in. The concrete stringers are 10 in. wide and 3 ft deep from the top of the roadway slab to the bottom of the stringer. The roadway slab is 9 in. thick, with a 1.75-in. bituminous concrete wearing course.

Steel wind fairing plates (to control wind vibration) are added to the structure beneath each stringer in the main span only; they extend from the bottom of the stringer to the same elevation as the bottom of the edge beam.

Figure 14 is a typical cross section of the deck that shows the mild steel reinforcing and the prestressing bars. There is longitudinal posttensioning in every longitudinal element (i.e., the edge beam, the deck, and the stringers). The amount of the posttensioning varies with the natural thrust in the bridge. At the towers, where the natural thrust in the bridge is the greatest, the amount of the posttensioning is the least. Generally, the longitudinal reinforcement within a segment is the same length as the segment itself. However, in the edge beam a percentage of the mild steel reinforcing is placed in ducts and mechanically coupled to the reinforcement in the adjacent segment. The ducts are then filled with grout, which produces some continuity of mild steel reinforcing between the segments in the edge beam.

A front elevation of the floor beam is shown in Figure 15. This is a reinforced-concrete member with no prestressing in it. Generally, there are two floor beams per segment. In addition to supporting the floor and its loads, the floor beam stabilizes the edge beam. A grid analysis was performed that shows that if a load is placed on one floor beam, that floor beam deflects and twists the edge beam, and as the edge beam rotates the adjacent floor beams are caused to deflect.

A cross section of a typical floor beam is shown in Figure 16; it is a hollow box, 2 ft, 6 in. wide with 5-in.-thick walls. Diaphragms are located at the stringer and intermediate points. At the center of the main span some of the floor beams are solid

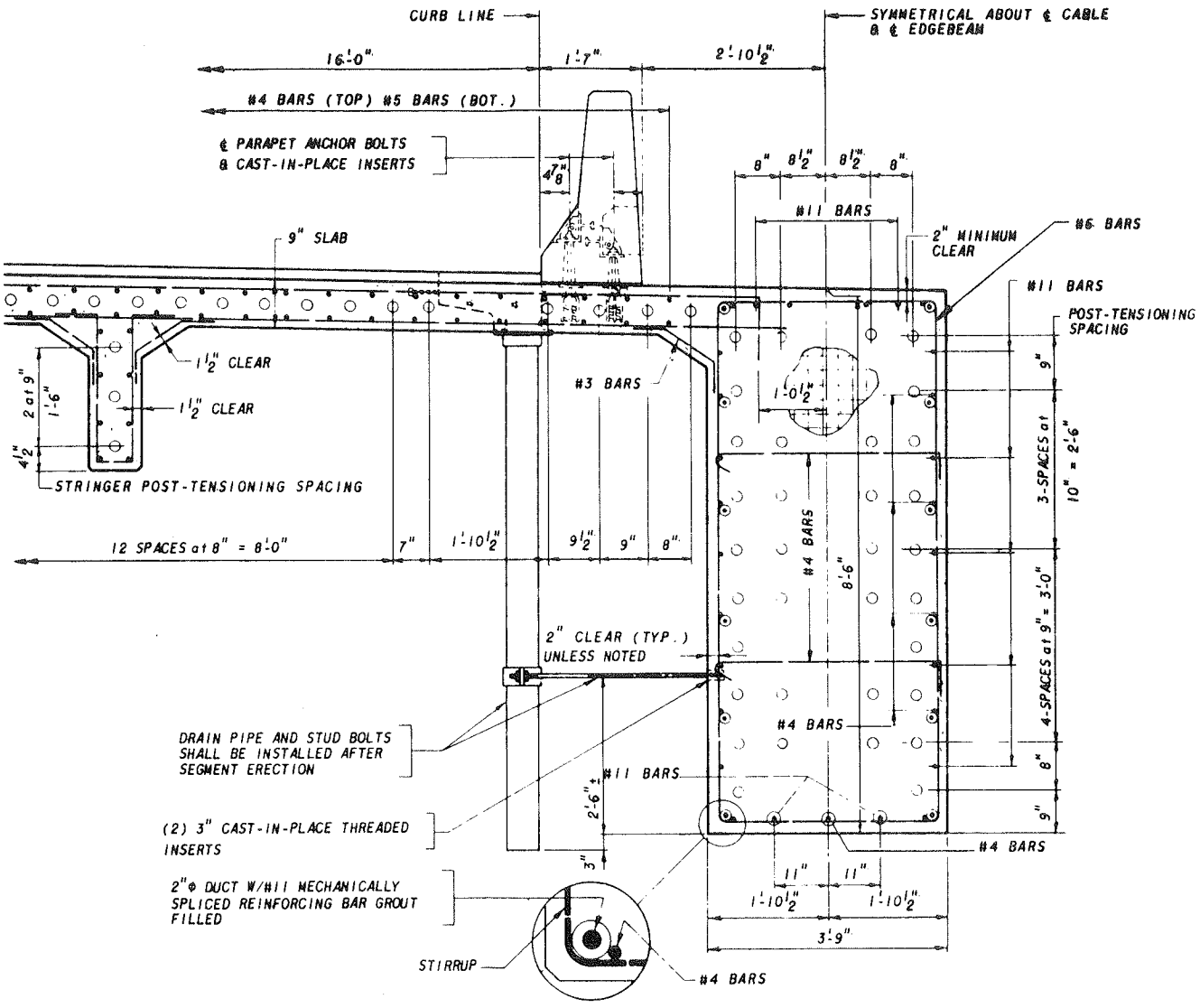

FIGURE 14 Concrete alternative: prestressing and reinforcing details.

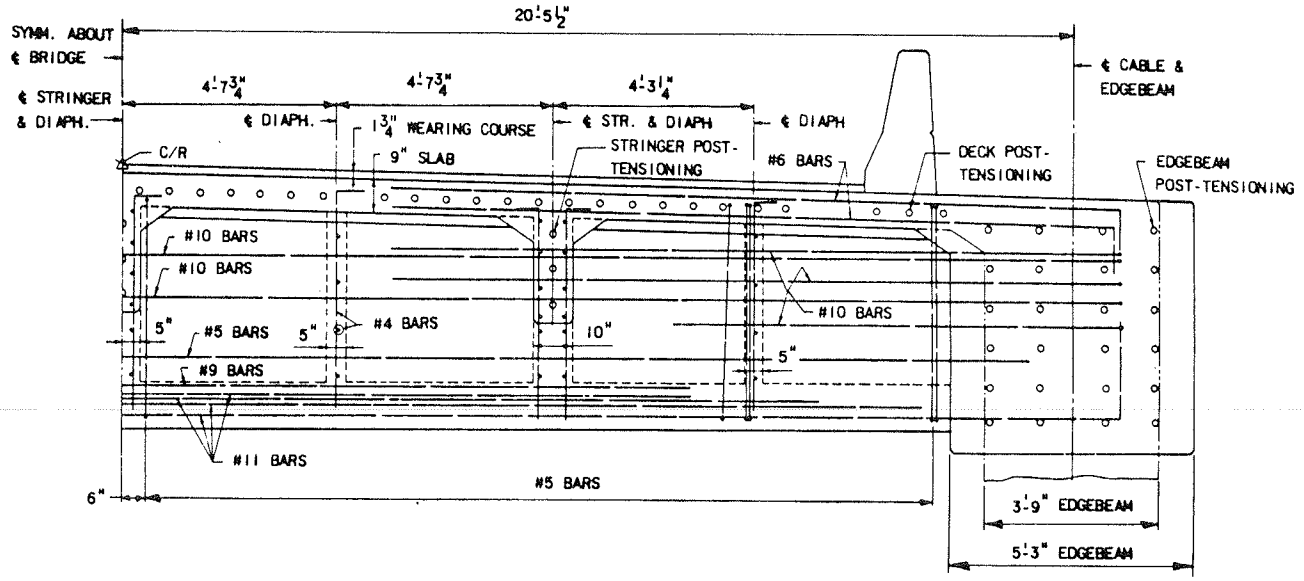

FIGURE 15 Concrete alternative: floor beam reinforcing details.

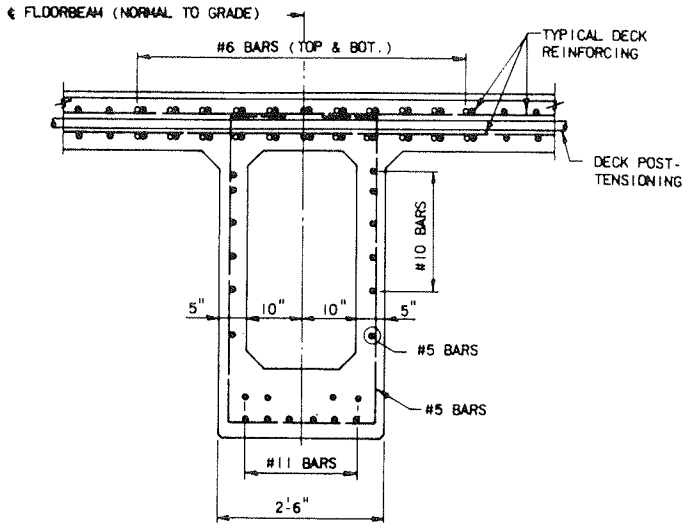

FIGURE 16 Concrete alternative: floor beam cross section.

where additional weight is required to balance the bridge.

The general deck arrangement is shown in Figure 17, which is a half plan for a typical superstructure segment. The following elements are shown: the deck, the edge beam shown at the bottom, and a cable anchor pipe passing through the edge beam. The stringers are shown running horizontally, and the floor beams are shown as vertical lines, with their diaphragms being horizontal.

Figure 18 shows an elevation view of the edge beam with the reinforcing and the embedded cable anchor pipe terminating at the steel bearing plate under the edge beam at the corbel. Detailing of the reinforcing and the prestressing to maintain clearances for the cable anchor pipe was a problem.

The hardware associated with the anchorage of the cable at the edge beam is shown in more detail in Figure 19. A neoprene boot is fastened to the anchor pipe and to the cable. An elastomeric washer is located at the upper end of the steel anchor pipe. The cable and the anchor pipe pass through the edge beam to the bottom of the corbel where the anchor pipe is welded to a bearing plate. The bearing plate supports the split washers, the shim pack, and the cable socket.

The edge beam cross section in Figure 20 shows the posttensioning and the embedded bearing plate and cable anchor pipe. The shear rings welded to the cable anchor pipe are also shown. This figure shows the tight clearances that exist between the posttensioning and the cable anchor pipe with its welded shear rings.

Erection of the bridge is basically the contractor's responsibility. However, an erection sequence has been assumed and analyzed on a preliminary basis. The contractor may choose to be guided by the procedure shown or may develop a totally different erection procedure.

The first stages of the erection of the superstructure are shown in Figure 21a. The tower construction has been completed. The auxiliary erection stays have been tied off to the top of the tower, and falsework has been erected adjacent to the tower

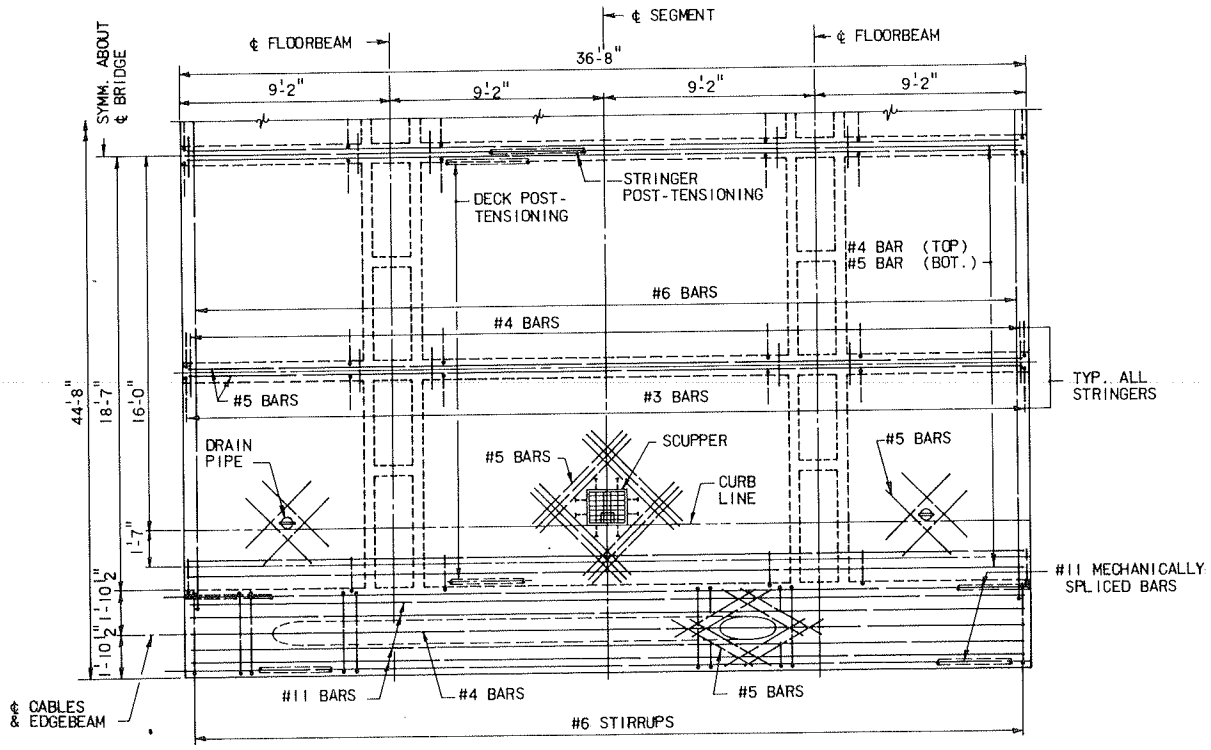

FIGURE 17 Concrete alternative: segment reinforcing details.

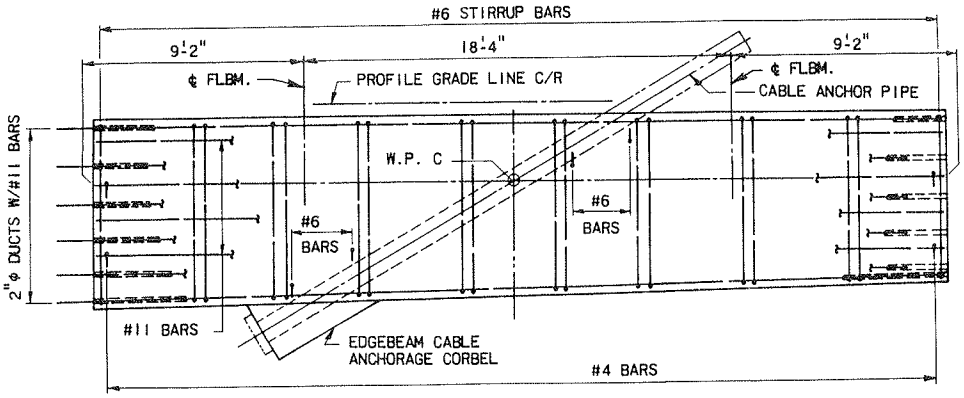

FIGURE 18 Concrete alternative: edge beam reinforcing details.

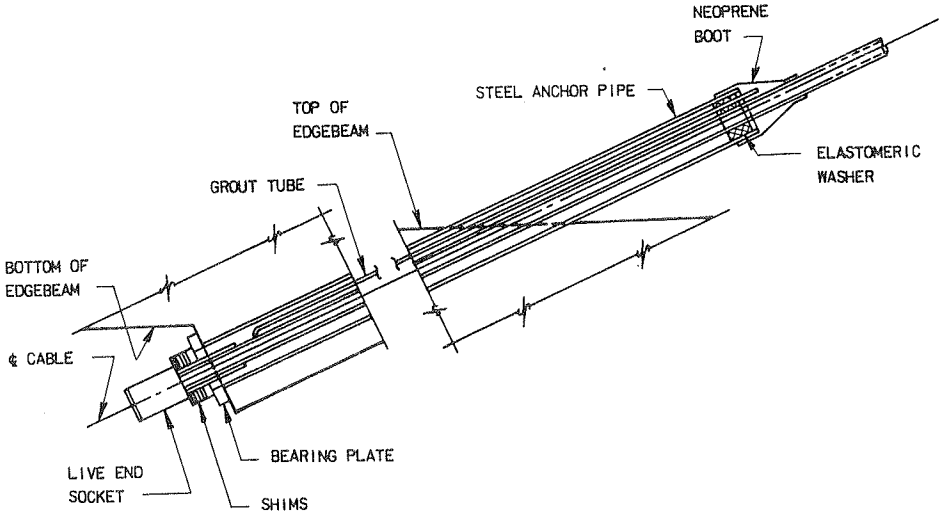

FIGURE 19 Concrete alternative: edge beam cable attachment details.

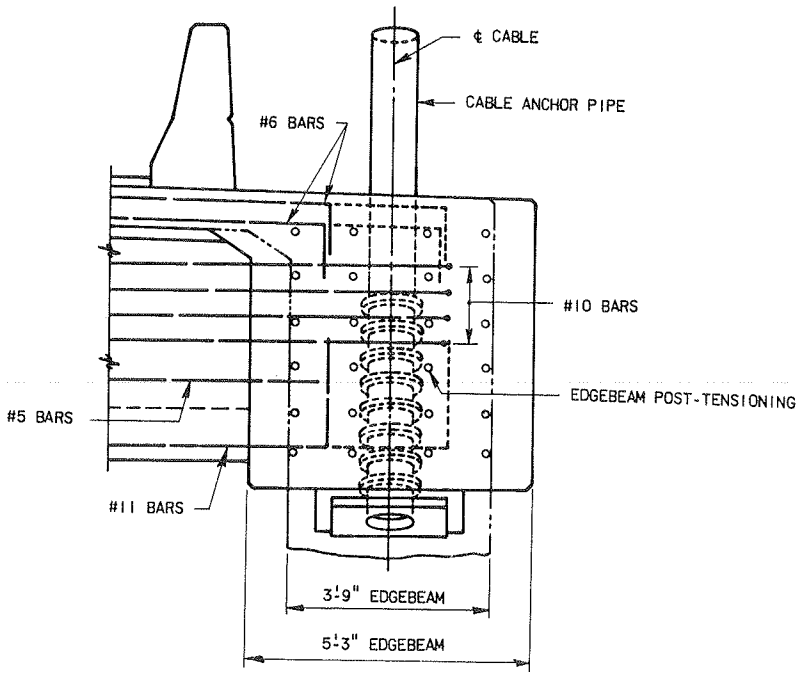

FIGURE 20 Concrete alternative: edge beam reinforcing and cable pipe details.

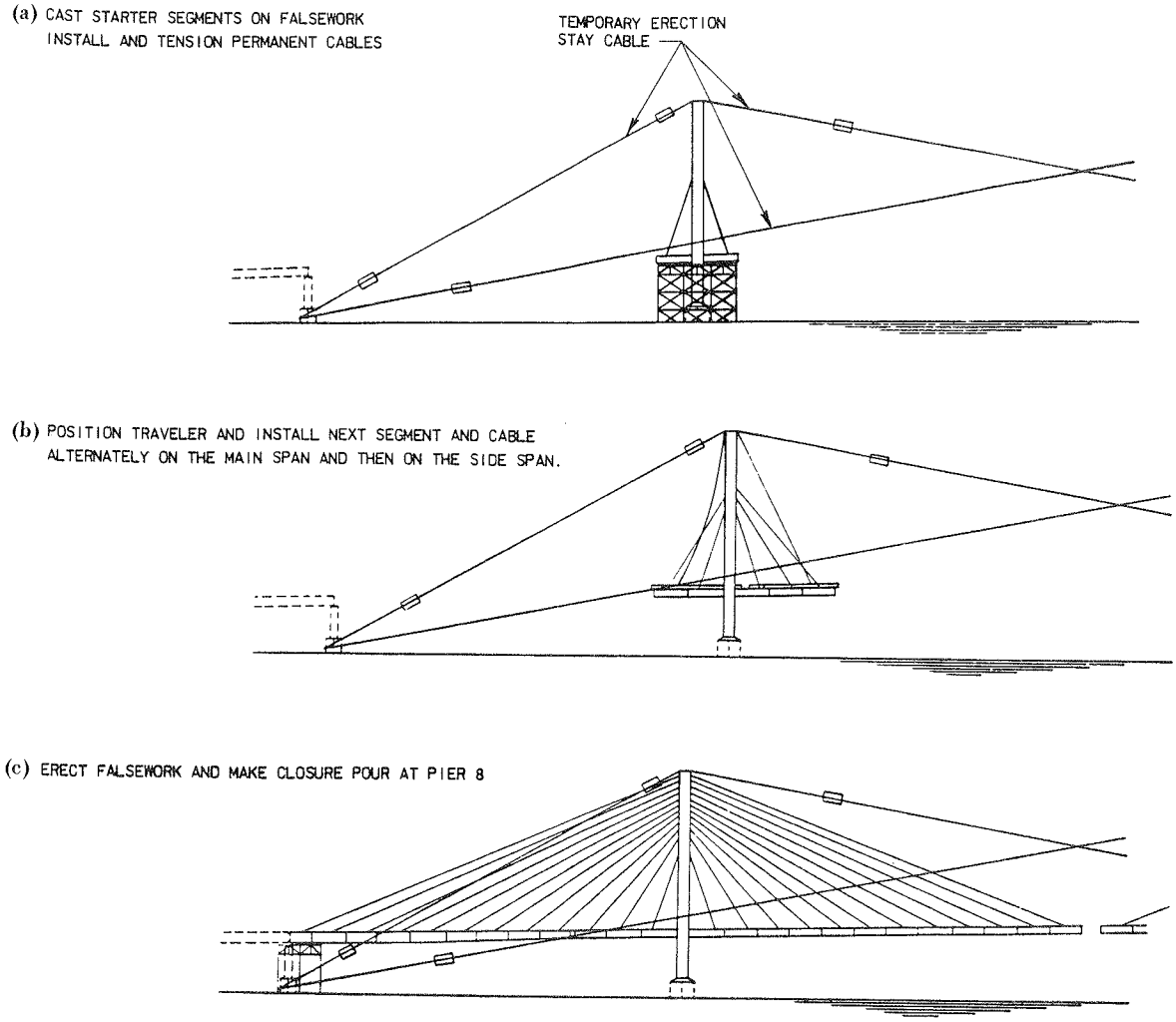

FIGURE 21 Concrete alternative: selected stages of erection.

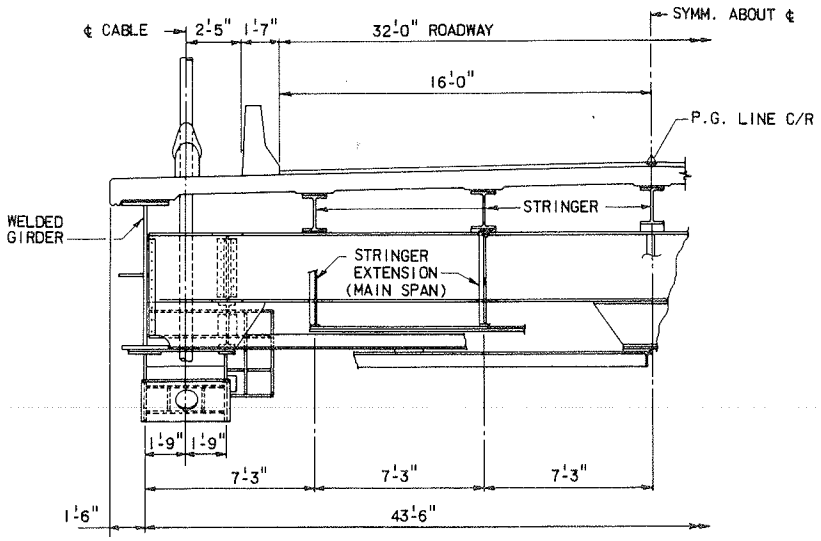

FIGURE 22 Steel alternative: typical cross section.

to support the initial cast-in-place deck segments, which have been cast and are supported on their stays.

Figure 21b shows an early stage in the erection with two travelers in position on the deck. The left traveler is shown in the rest position and the right traveler is erecting a precast segment.

An elevation view of the bridge with all the precast segments erected is shown in Figure 21c. Falsework has been erected at the anchor pier, and the cast-in-place segment has been constructed.

STEEL ALTERNATIVE SUPERSTRUCTURE

A general elevation of the steel bridge layout is shown in Figure 2. The span lengths are the same as the concrete bridge. The structural arrangement includes two single-web welded steel girders, rolled section floor beams, and rolled stringers. The system includes a precast, composite, concrete deck. There are 7 cables on each side of each of the pylons, for a total of 56 cables in all. The cables are spaced at 60 ft in the main span and 63 ft in the side spans.

A typical cross section is shown in Figure 22. The deck slab is detailed to be precast full width. The two main girders are made up of 72-in. constant-depth webs and are spaced at 43 ft, 6 in. The stay cables are inboard of the girders at 40-ft transverse spacing.

Typical floor beams are W36x260 sections. The stringers are two different sizes, depending on location: either W18x119 or W18x97. The stringers are heavier than might normally be required because the deck is under compression and the stringers are required to function as compression members.

Generally, the fabricated steel members are shop welded, and all field connections use high-strength bolts.

Certain details are somewhat unconventional, partly because of the combination of features built into the structure. The composite section is required to accommodate both the bending and compression stresses that the structure loads create. The strength requirements were not obtainable by post-tensioning the slab section after it was composite with the steel. A system of precasting the deck slab unit, then continuously posttensioning it, and subsequently making it composite with the steel was devised to meet all strength requirements.

Certain aerodynamic features were necessary on the 900-ft main span, but not on the side spans. Plates were added beneath each stringer, which in effect extend the stringer webs down to the level of the bottom flanges of the girder, as shown in Figure 22. The plates are 0.375 in. thick and are appropriately stiffened and braced.

The wind tunnel testing also led to the addition of wind fairing plates located outside of the main girders. These plates are 30 in. wide and are positioned horizontally in the plane of the bottom flanges of the girders.

A partial cross section view is shown in Figure 23. The W36x260 beam spans longitudinally between floor beams only in the panels that contain cable anchorages. Its purpose is to react the vertical component of the cable. Because the cable is eccentric with respect to the main girder, this beam is required to carry half of the vertical component of the load in the cable.

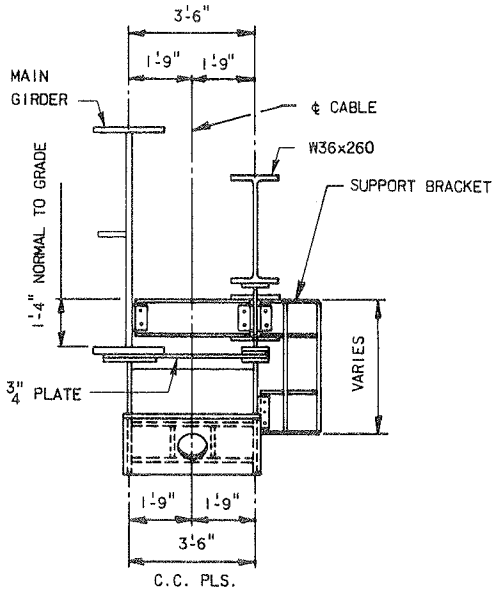

FIGURE 23 Steel alternative: framing at cable locations.

Figure 24 shows a plan and elevation of the deck framing at a typical cable anchorage. The horizontal component of the cable load is applied out of the plane of the main girder, and the transverse framing provides a means of stabilizing the forces without overstressing the girders. The frame is also effective in accommodating cable loads that are unequal in the two cables in a pair on opposite sides of the roadway.

Figure 25 shows a detailed plan view at a cable attachment location. The 0.75-in. plate, which is connected to the girder and the longitudinal W36 beam, helps to react the horizontal component of the cable load. The connections on all four edges of the plate transmit the loads into the horizontal frame.

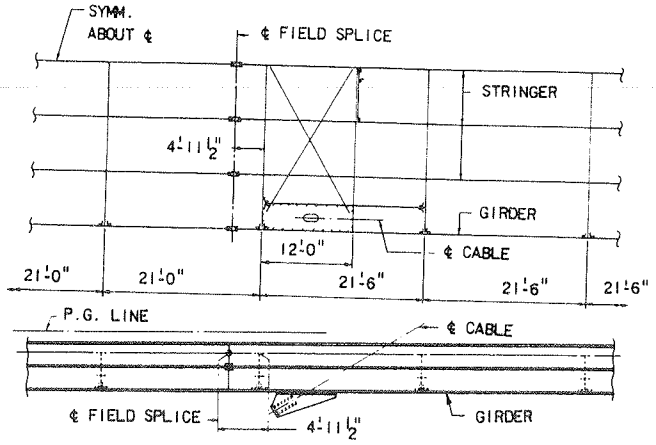

FIGURE 24 Steel alternative: plan and elevation of deck framing at cable anchorage.

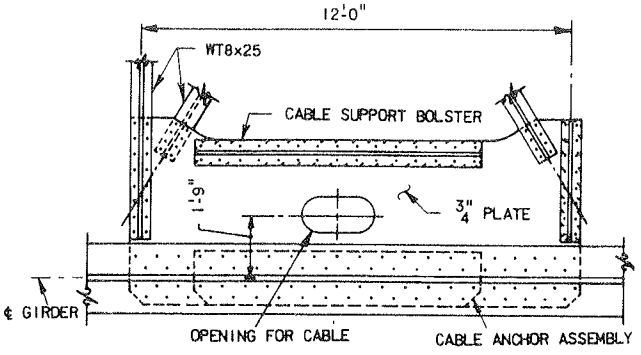

FIGURE 25 Steel alternative: cable frame attachment details.

The connection of the cable to the girder is accomplished by a weldment that accommodates the cable socket. A typical cable anchorage is shown in Figure 26. The weldment is bolted to the bottom flange of the girder and to the framing members inboard of the girder. Shims are provided to allow for initial adjustment of the assembly to assure that it is in proper orientation with respect to the vertical plane of the cable.

Figure 27 shows an elevation view of the lower end of a typical stay cable. The hardware for this type of cable is basically the same as shown previously in Figure 11 for the concrete bridge. The cable penetrates the deck slab through a steel pipe that is embedded in the precast unit.

Details of a typical girder field splice are shown in Figure 28. The girder functions in both bending and axial compression, which requires that the splice details include a heavier connection in the web than is normally required in a typical beam splice. The girder web is considerably heavier than is typical for the same reason. The splices are designed to be consistent with the load factor design for the member and are specially designed for the combined state of stress that occurs at the specific location of each splice. Depending on the erection scheme, it may be possible to erect longer sections and eliminate some of the splices shown on the plans. The splice locations shown on the contract drawings are consistent with the assumptions that were made for the preliminary erection scheme shown on the plans.

Typical features of the precast deck slab units are shown in cross section in Figure 29. The slabs are detailed to be cast full width and full thickness. It is specifically required that the deck erection must follow closely behind the steel erection, because the superstructure design is based on the composite section carrying most of the compressive dead load that is caused by the horizontal components of the cable loads. The slab units cannot assume compression loads until the slab is made composite with the longitudinal girders because the stress occurs initially in the girder and is then distributed into the slab.

The deck units are full width and vary from 9 to 11 ft in length. The slabs contain adjusting screws that allow the units to be placed on the supporting

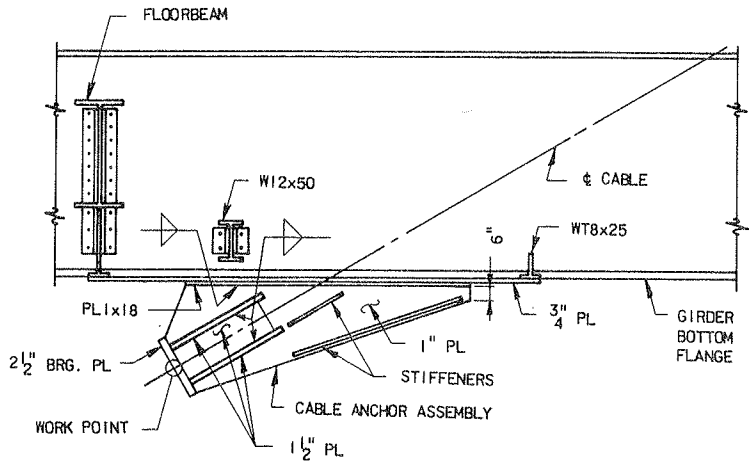

FIGURE 26 Steel alternative: cable anchor assembly details.

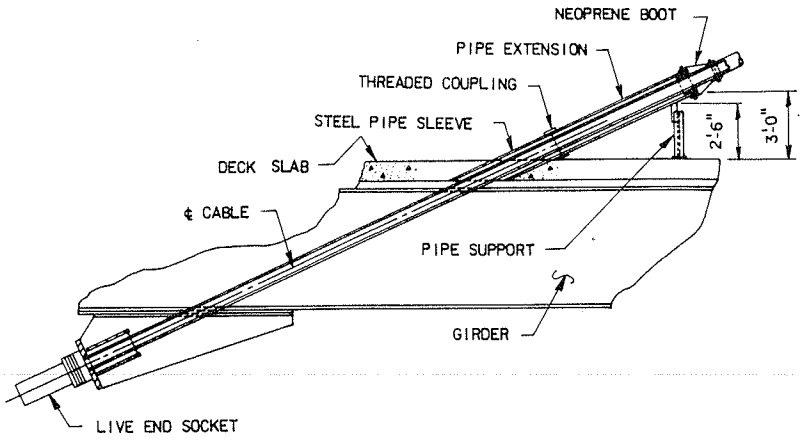

FIGURE 27 Steel alternative: cable details at deck level.

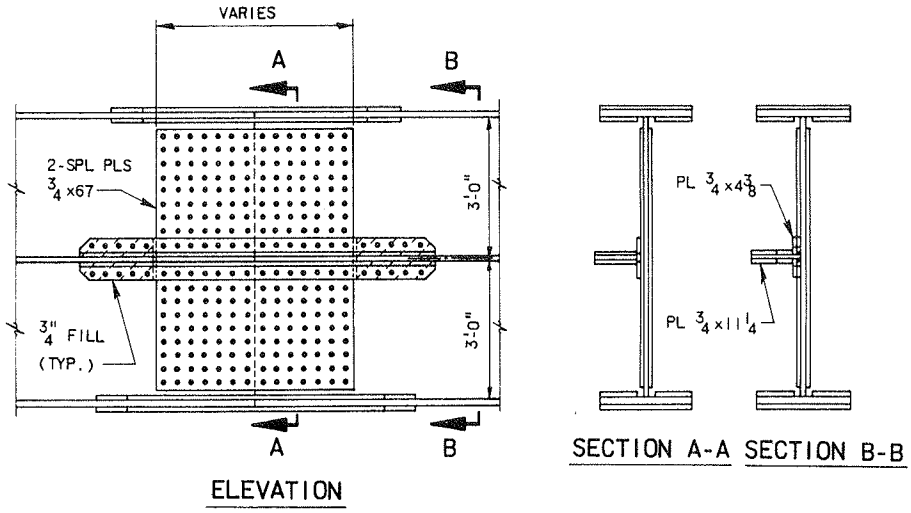

FIGURE 28 Steel alternative: typical splice details for girders.

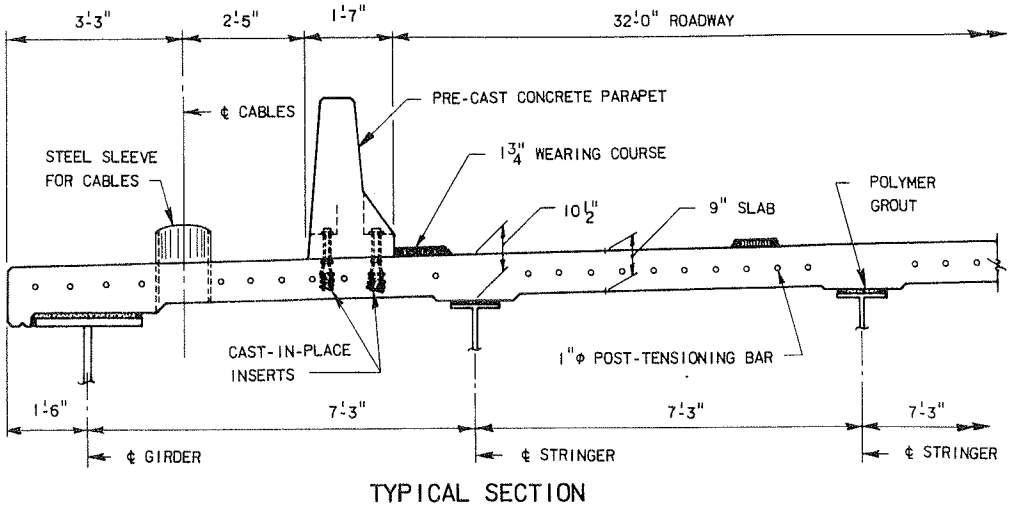

FIGURE 29 Steel alternative: details for precast slab panels.

steel members with a space between the slab and the flange that is later filled with grout to complete the haunch. This sequence permits the slab to be posttensioned before making it composite with the steel beams. The slabs are reinforced both longitudinally and transversely and are posttensioned longitudinally in groups of three to five panels. The posttensioning takes place after the slabs are erected on the steel supporting elements, but before they are made composite with the girders and stringers. The slabs are cast with openings to allow placement of the steel studs. The studs are attached to the beams after the slab has been erected and finally positioned. The openings at the stringer locations allow enough room for normal application of the studs, but the openings over the girder flanges are restricted, and special testing procedures are required for the studs. The normal bend test would require a larger opening than the available space allows.

After the studs are installed and grouting of the openings and the haunch between the underside of the slab and top of the beam is completed, the grout hardens and the slab becomes composite with the steel girder.

An investigation was made of an assumed erection procedure to determine the feasibility of the scheme shown on the contract plans. Computations generally indicated that no major reinforcement of the members will be required, but adjustment of some cables may be necessary to avoid overstress as the erection proceeds. A general sequence similar to that shown for the concrete bridge was assumed, except that the individual pieces are not as heavy, which allows somewhat greater flexibility in maintaining balance with respect to tower bending. The concept is based on installing temporary stays on the tower top and erecting the initial steelwork at the tower, which is supported by appropriate falsework. The deck slab at the tower is cast-in-place and posttensioned after it cures. The typical sequence outlined in the following paragraphs is then followed in a balanced-cantilever arrangement.

The details shown in Figure 30 outline the items comprising one section of deck erection. The process is then repeated for the other sections. The typical required sequence, referring to Figure 30, is described as follows.

- The first step is to erect the steel framing members, cantilevered from the previously completed section.
- The precast slab panel at the cable location is then placed in its required position, as shown in step 1.
- Step 2 is erection of the cable. Because the slab at that location is already in place, the cable must be pulled through the opening in the slab.
- In steps 3-5 the precast panels are placed. With the cable in place, the additional dead loads are supported by the cable and are not dependent on cantilevering.
- At step 6 the posttensioning bars are placed and spliced to the preceding bars at the location of the cast-in-place joint.
- At step 7 the cast-in-place joint is placed and allowed to cure.
- The bars are posttensioned and the studs are placed through the openings in the slab at step 8. The grout is then placed to fill the stud openings and the haunches between the slab and the tops of the flanges. At this point the section becomes composite and the sequence can be repeated for the next section.

At the final closure stage at the center of the main span, first the steel members are closed and the joints bolted, and then a 4-ft section of slab is cast-in-place to complete the deck section. The remaining items can then be completed, such as completion of the installation of parapets, placement of the roadway wearing surface, and final adjustment of the cables.

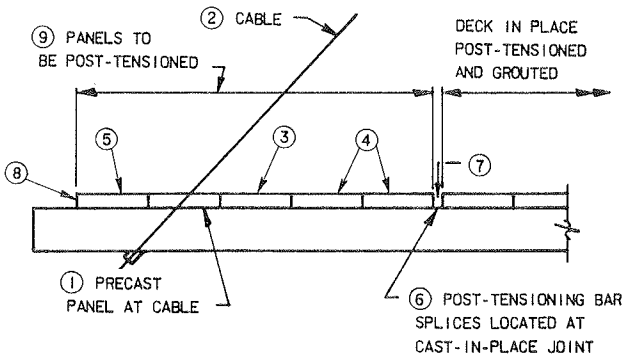

FIGURE 30 Steel alternative: deck panel erection sequence.

CONCLUSION

Both alternative structures were advertised for bid in November 1983. Bids were taken in February 1984. The winning alternative was the steel bridge, which was bid at a total cost of $17,230,461.

ACKNOWLEDGMENT

This project was designed for the Illinois Department of Transportation, District 6-0. The assistance and cooperation of Carl E. Thunman, Jr., chief of bridges and structures, and William E. Burns, district engineer, are acknowledged, as is the cooperation of Ronald D. Williams, project manager for Booker Associates, Inc., the engineering prime contractor for the total project.

Publication of this paper sponsored by Committee on Steel Bridges.

Deflections and Camber Loss in Heat-Curved Girders

MARVIN H. HILTON

ABSTRACT

To check the camber loss in heat-curved girders, a 140-ft, simply supported span was instrumented during the construction of a bridge. The span was composed of four steel plate girders that have radii of curvature varying from 802.51 ft on the inside to 834.51 ft on the outside of the alignment curvature. Girder deflection and camber loss were measured before and after construction of the bridge deck. Some loss in camber from construction loading occurred shortly after placement of the concrete deck. The amount of loss, however, was only one-fourth of that determined from the AASHTO equation for predicting such loss. In addition, no significant camber losses were caused by service loading over a 6.5-month period subsequent to construction.

The construction of a number of curved girder bridges during the past few years has given rise to at least one question relating to the fabrication of the steel girders. This involves the requirement that additional camber be provided in steel girders that are to be heat curved. This additional camber is to allow for subsequent losses from the dissipation of residual stresses imposed by the heat-curving process during fabrication of the girders. The AASHTO specifications suggest that approximately 50 percent of the camber loss relating to the heat-curving process occurs during construction of the bridge, and an additional 50 percent occurs after a few months under service loading (1). Therefore, the increase in camber should be included in bridge forming during construction, and after construction is complete the bridge profile should be higher than the plan grade between the supports. If the additional camber is lost as suggested by the AASHTO specifications, then the final profile should be attained after several months of traffic loading.

Many bridge engineers and steel fabricators, however, question whether the additional camber is necessary. The fabricators would prefer that they not be required to provide the additional camber in heat-curved girders because, in most cases, this adds to the time and expense of fabrication. To determine the nature of the deflections and camber loss in a heat-curved girder bridge, one bridge was instrumented and measurements were taken both during and after construction. The camber losses measured do not include those that may have occurred between the steel fabrication plant and the job site, or those that may have occurred before placement of the instrumentation on the structure.

STRUCTURE STUDIED

A curved girder bridge consisting of three simply supported spans, two of them relatively short at 36 and 18 ft, and the third 140 ft, was studied during its construction. All the measurements, however, were confined to the 140-ft span. A general view of the curvature of the steel girders is shown in Figure 1.

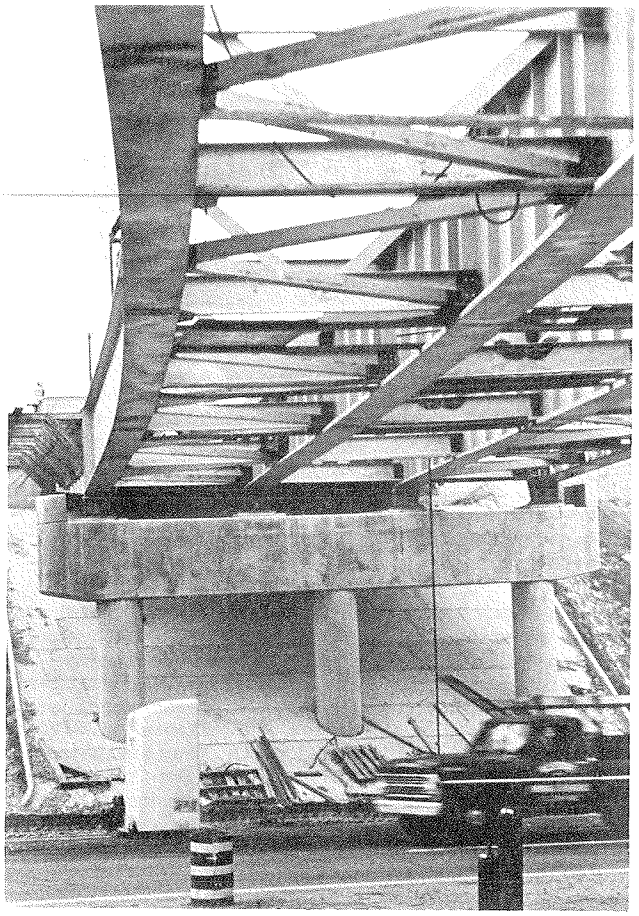

FIGURE 1 View showing curvature in the girders and design of diaphragms and lateral cross bracing.

The bridge has four steel-plate girders spaced at 10 ft, 8 in. on center. The girders of the 140-ft span are connected by truss-type diaphragms, and lateral cross bracing is used on the exterior bays, as illustrated in Figure 1. The girders were fabricated from A588 steel and were heat treated to obtain the required degree of curvature. They are curved on radii varying from 802.51 ft on the inside to 834.51 ft on the outside of the alignment curvature. On the centerline of the bridge the alignment is equal to a 7-degree highway curve.

INSTRUMENTATION, TESTS, AND PROCEDURES

Girder and Bearing Deflection Instrumentation

Because some of the deflection increments to be measured were expected to be on the order of hundredths of an inch, a high precision, modified Wild N-III level was selected for use. The level, which is marked in 0.001-in. increments, was mounted on a trivet set in stationary bronze lugs on the top of the pier cap at the north end of the span. The line of sight of the level was thus slightly below the bottom flanges of the girders. Special design

scales were installed at the midspan points of each girder and adjusted vertically to intersect the line of sight of the level. To measure and account for possible dead-load deflections of the bridge bearings, dial gauges were set as close as possible to the centerline of bearing of each girder.

Thermal Instrumentation

Thermocouples were placed on the top and bottom flanges at the midspan of the girders. They were also placed at the quarter-span points of the girders and at selected positions on the web of the girders.

During placement of the concrete deck and parapet walls a 24-channel temperature recorder scanned each gauge every 12 min. Other temperature measurements were taken before the concrete was placed and after each phase of the construction was completed to determine the effect of solar radiation on the deflection of the girders.

Tests on Plastic Concrete

Tests of the plastic concrete were restricted to the measurement of properties that would have the most direct influence on the girder deflections during deck placement. These included the times of initial and final set, unit weight, and temperature of the concrete.

Procedures

The instrumentation was installed on the test span while construction was in progress, and initial readings were taken on all systems as soon as the installation was complete. Subsequent measurements were taken during a full day after each major stage of construction to determine the effects of differential thermal conditions. With the exception of brief delays during deck placement for taking measurements, the contractor's normal procedures were used during construction.

After construction was completed, the positions of the deflection rods and scales were marked on the girders to establish their horizontal and vertical position. Initial readings were then taken on the vertical position of the girders, and the thermocouples were scanned to obtain data that were used to establish the differential temperature conditions. These data were then used as the basis for measurements of the long-term loss in camber after the bridge had been put into service. The gauges were then dismantled and later installed after the removal of the forming and painting of the structural steel.

RESULTS

Thermally Induced Deflections in Steel Section

With the forming for the deck in place, the lower portion of the steel girders are shielded from the sun. Consequently, the top flanges of the girders are exposed to solar radiation, whereas the lower portion is exposed to only the ambient air temperature. Because the alignment of the bridge is in a generally southerly to northerly direction, in the early morning the sun strikes the web and lower flange of the eastern girder and in late afternoon it strikes the web and lower flange of the western girder. The effect is a net thermal differential between the upper and lower flanges that develops an internal moment over the cross section of each girder (2). The internal moment causes the girder to deflect upward by an amount relating to the intensity of the solar radiation, time of day, and so forth. The differential temperatures shown in Figure 2 were recorded at eight times from 7:30 a.m. to 3:20 p.m. on a typical sunny day in early August. At 7:30 a.m. the lower flanges were warmer than the upper flanges for all the girders, probably because they were somewhat protected from the elements during the night. However, with time the upper flanges heated up. By 3:00 p.m. a maximum temperature differential of 36°F was recorded on each of the two center girders.

The deflections that correspond to each of the reported differential temperatures are shown in Figure 3. The initial reference elevations of the girders were recorded at 7:30 a.m. As can be noted from these data, the maximum upward midspan deflections of the girders were on the order of 1.25 in. at 3:00 p.m. These data indicate that the thermal effects on girder deflections must be taken into account if there is an attempt to measure deflections that result from loading and from sustained losses of camber caused by dead weight or service loads.

To determine the thermal gradients through the depth of the girders, thermocouples were placed on the webs of girders 5, 7, and 8. One was located at mid-depth of the web and another approximately 2 in. below the lower side of the top flange. The thermal gradients for girder 7 (Figure 4) indicate that the temperature increase caused by solar radiation on the top flange was transmitted downward through the web. Thus any calculations performed to determine thermal deflections must consider that the upper portion of the web above the neutral axis participates in the development of the forces and moments. In some instances, as the data in Figure 4 suggest, a portion of the web below the neutral axis was warmer than the lower flanges of the girders.

For the bridge tested in this study, the plate girder design incorporates changes in the moment of inertia at points of increasing flange plate thickness. This, in addition to the action of the rigid diaphragm connections between the giders, creates a complex system. The rigid diaphragm connections cause the thermally related deflections to be distributed across the width of the span, as indicated by the data in Figure 3. Because the 3:00 p.m. thermal deflection data were more uniformly distributed across the span width, theoretical calculations were made to determine the agreement with the field results. The calculated deflections were based on the following relationship:

$$F = AE\alpha\Delta T \quad (1)$$

where

- F = force developed by expansion of the heated steel,
- A = area of the section above the neutral axis,
- E = modulus of elasticity of steel,
- α = thermal coefficient of expansion for steel, and
- ΔT = difference in temperature between the upper and lower flanges.

Because the internal moment in the girder is developed by the product of the force and the distance to the neutral axis, the deflection (Δ) is

$$\Delta = (A\alpha\Delta T d L^2)/8I \quad (2)$$

where

- d = distance from the force center to the neutral axis,
- L = length of span, and
- I = moment of inertia.

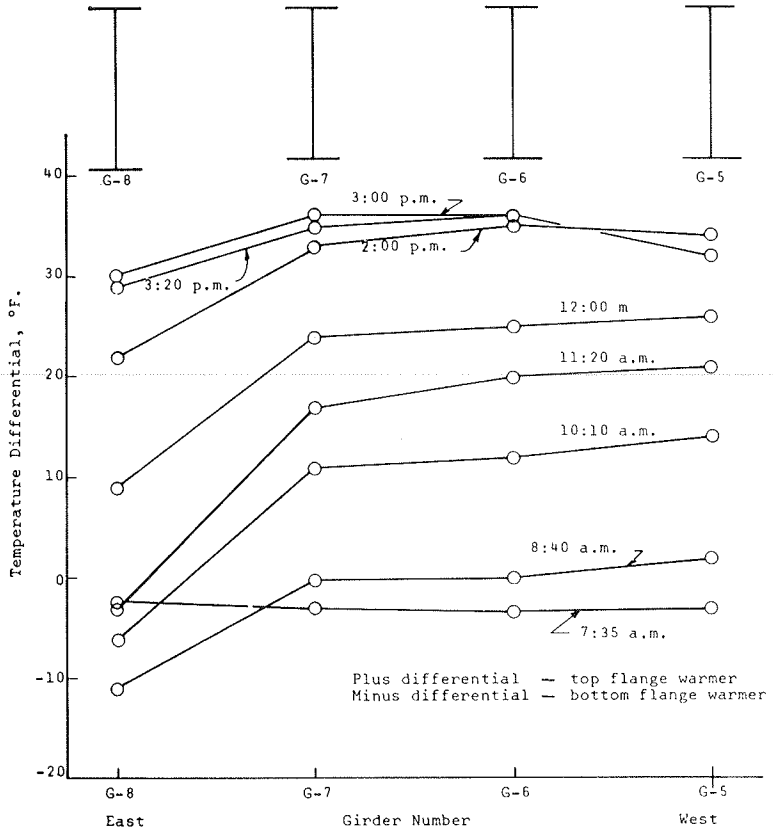

FIGURE 2 Temperature differential between top and bottom flanges of curved girder span with deck forming in place; before deck placement.

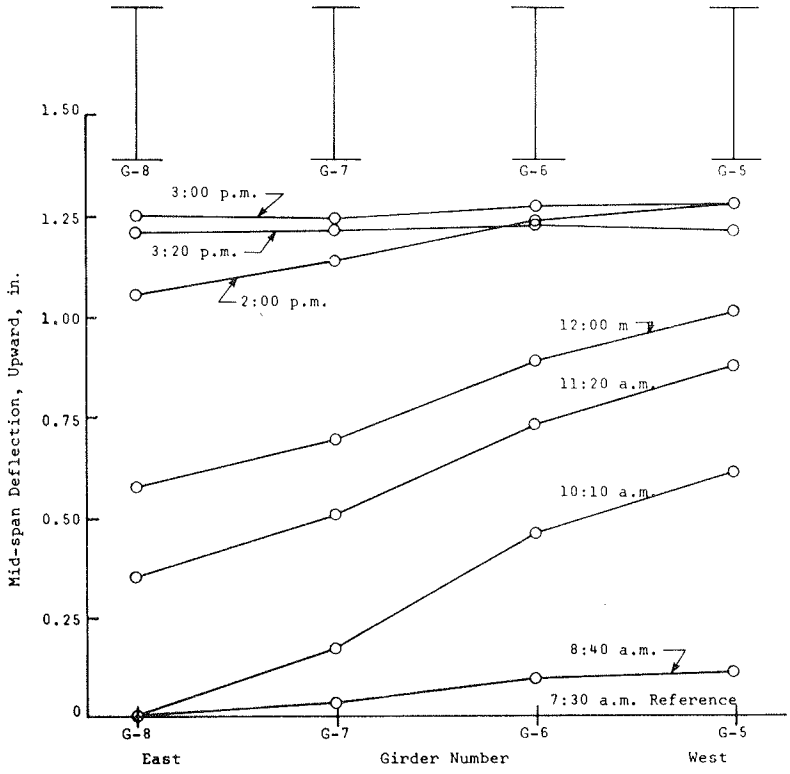

FIGURE 3 Upward deflections at midspan of curved girder span resulting from solar radiation; deck forming shielded lower portion of girders from sun.

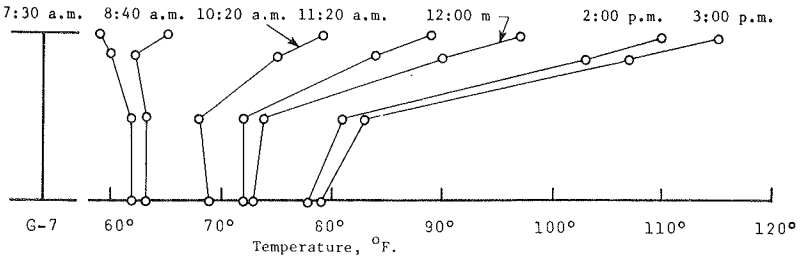

FIGURE 4 Thermal gradients through the depth of girder 7 caused by solar radiation; deck forming in place.

By using the midspan properties of the steel section, the thermal deflections calculated from Equation 2 were within less than 1 percent of the thermal deflections measured in the field at 3:00 p.m. in early August. Thus Equation 2 gives a reasonably satisfactory estimate of the deflections caused by differential temperatures that are relatively uniform across the width of the span.

Dead-Load Deflections in Steel Section

Reinforcing-Steel Placement

The first deadweight loading on the span (excluding the deck forming) was the reinforcing steel. Temperature measurements and deflection readings taken on the girders before placement of the deck concrete were compared with the initial readings taken approximately 12 days earlier. The thermal differentials were the same for these two periods except for a 0.5°F difference on two of the girders. By using Equation 2 and applying a correction to the measured deflections for those two girders, the thermal differentials were neutralized. The resulting deflections thus reflected only the downward movement caused by the deadweight of the reinforcing steel. The midspan dead-load deflections that result from the weight of the reinforcing steel were on the order of 0.15625 in. (Table 1).

TABLE 1 Midspan Dead-Load Deflections of Steel Girders Caused by Placement of Deck Reinforcing Steel and Concrete

	Midspan Dead-Load Deflection (in.) by Girder			
Loading	G-8	G-7	G-6	G-5
Reinforcing steel	0.144	0.165	0.171	0.209
Concrete	2.494	2.568	2.662	2.690
Steel plus concrete	2.638	2.733	2.833	2.899
Bearing settlement	-0.018	-0.007	-0.012	-0.002
Total	2.620	2.726	2.821	2.897
Plan values	3.625	3.75	3.25	3.375
Difference	+1	+1	+0.4375	+0.46875

Note: Thermally neutral deflections.

Concrete Deck Placement

Concrete was placed on the 140-ft span beginning at 6:30 a.m. on August 21. At the beginning of the deck placement the temperature on the steel girders indicated that they were not in a thermally neutral position. Because the lower flanges were warmer than the top flanges, the girders were initially deflected downward. As the day went by, the temperature differential between the top and bottom flanges changed. By 10:00 a.m. the upper flanges were warmer than the lower flanges, but by 11:15 a.m. all the concrete had been placed on the span and the temperature on the top flanges began to drop relative to that on the lower flanges. By 2:24 p.m. the temperature differential between the flanges was slight, and the span was, for all practical purposes, in a thermally neutral state.

Figure 5 shows the deflections of the girders at the various stages of concrete placement. These deflections existed at the stage of concrete placement indicated on the graph and include any amount caused by thermal differentials. At 11:25 a.m., approximately 5 hr after the beginning of placement, all of the concrete was in the forms. At that time, however, the top flanges were warmer than the lower, so it could be expected that a counter-deflection upward existed. Therefore, additional deflection measurements were taken at 2:45 and 3:20 p.m., when the span was close to a thermally neutral position. As would be expected, the downward deflection was greater at these times, although the dead load on the girders remained unchanged from that which had existed at 11:25 a.m. Applying the corrections previously discussed to account for the initial thermal differentials yielded the final thermally neutral dead-load deflections that resulted from the weight of the concrete deck. These final values are shown by the lower curve in Figure 5 and are reported in Table 1.

Before calculating the thermal corrections for the deflection data, it was necessary to consider the setting time of the concrete. This is an important consideration because once the concrete begins to set, some degree of composite action between the concrete and steel begins. To determine the times of initial and final set, two samples--one at the beginning and one midway through the placement operation--were tested by using ASTM C403-68 procedures. It was found that the time of final set was approximately 5:45 p.m. for the first concrete placed on the span. For the concrete located in the midspan region, the final set occurred at 10:30 p.m. Based on these data, no composite action between the steel girders and concrete could be expected at 3:20 p.m., when the last deflection measurements were recorded. Accordingly, all calculations to determine thermal corrections to the girder deflections that occur during deck placement are based on the section modulus of the steel action only. Corrections to the deflections measured subsequent to the final set of the concrete, as discussed later, must be calculated based on some degree of composite action between the girders and the concrete deck.

Some slight movements of the bearing assemblies did occur during the placement of the concrete deck. The average final deflections, or settlements, in the bearings at the north and south ends of the span are given in Table 1. As would be expected, the placement of the concrete caused some downward settlement of the bearings. These average

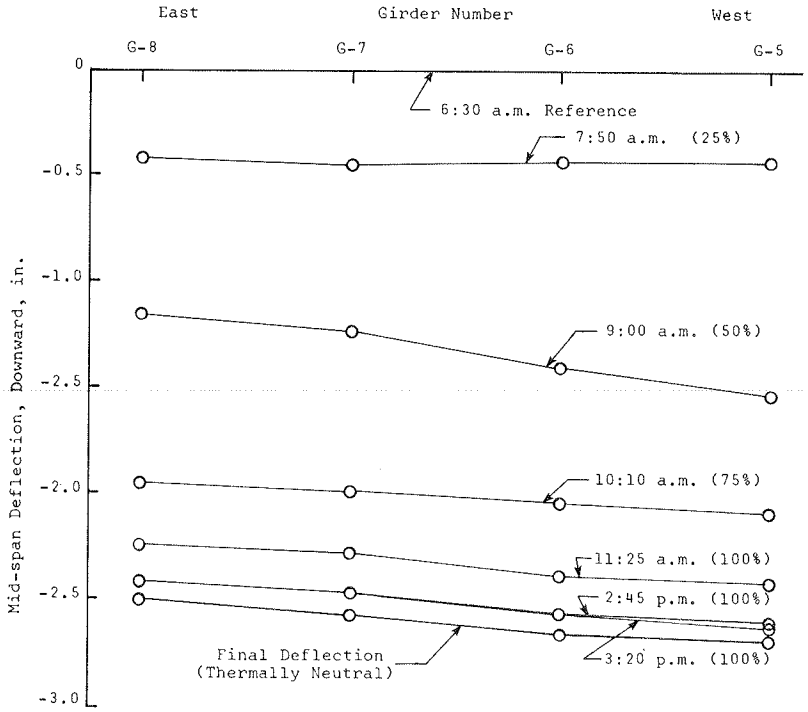

FIGURE 5 Downward deflections at midspan caused by placement of concrete deck.

values are thus deducted from the girder deflections measured on completion of the placement of the concrete deck.

The total measured deflections of the curved girders caused by the weight of the reinforcing steel and concrete are given in Table 1 and are lower than those given in the bridge plans. In addition, the measured deflections were progressively larger from the inside girder to the outside girder, whereas the plan deflections alternate from lower to higher values between girders. This suggests that the diaphragm action between the girders tends to even out the actual deflection patterns. It is interesting to note that the average of the measured deflections is 2.766 in. Theoretical calculations that include deflections from shear forces at the diaphragms yield an average deflection of 2.77 in. Thus, based on the average deflection, which tends to allow for diaphragm action between girders, there was excellent agreement between the measured and theoretical dead-load deflections.

Two additional deflection measurements were recorded the day after the deck was placed. By this time the heat of hydration of the concrete was causing the top flanges of the girders to be warmer than the lower flanges. Temperature differentials on the order of 17° to 24°F existed at 10:00 a.m. on August 22, and it was expected that the girders would be at a higher elevation at midspan than they had been at 2:45 p.m. the day before. The 10:00 a.m. data in Figure 6 show this to be the case, as the deflections were at that time less than the thermally neutral final deflections for the previous day. The thermal deflections were calculated by using Equation 2 and are shown in the upper portion of Figure 6. By applying these as corrections to the measured data of August 22, the thermally neutral deflections shown by the lower curve in Figure 6 were within 0.01 in. or less of those measured on the previous day. Therefore, no deflections resulting from camber loss in the steel girders occurred during the first day after the deck was placed.

Thermally Induced Deflections and Short-Term Camber Loss in Composite Section

As discussed earlier, the data for 2:45 p.m. on the day the concrete deck was completed best represent a thermally neutral condition of the span under study. Therefore, these deflections and thermal data were used as a new base reference for the comparison of the deflections resulting from subsequent thermal, dead-loading, or other conditions. Nineteen days after completion of the deck additional temperature-deflection data were recorded to determine their order of magnitude under the new condition of the concrete deck and steel girders acting as a composite section. Unlike the thermal effects discussed earlier for the steel section only, the top flanges of the girders were then protected from the sun, whereas the remaining portion of the girders was exposed to ambient conditions as well as to direct solar radiation on the east side of the bridge in the morning and on the west side in the evening. In addition, because of the composite action of the deck and girders, the moment of inertia and location of the neutral axis differ from those of the steel section only. Consequently, thermal deflection data were collected during a day in early September for two purposes: (a) to obtain data that could be used for making thermal corrections to all subsequent deflection measurements that would be recorded, and (b) to determine if any loss of camber in the heat-curved girders had occurred in the 19-day period since the application of the sustained dead loading of the concrete deck and reinforcing steel.

The results of these measurements, given in Figures 7 and 8, show the net thermal differentials between the top and bottom flanges of the steel and the deflections that result from the thermal loads, respectively. These data were recorded at seven times during the day, with the first measurement being used as a reference. Therefore, for the thermal data shown in Figure 7, the net temperature differ-

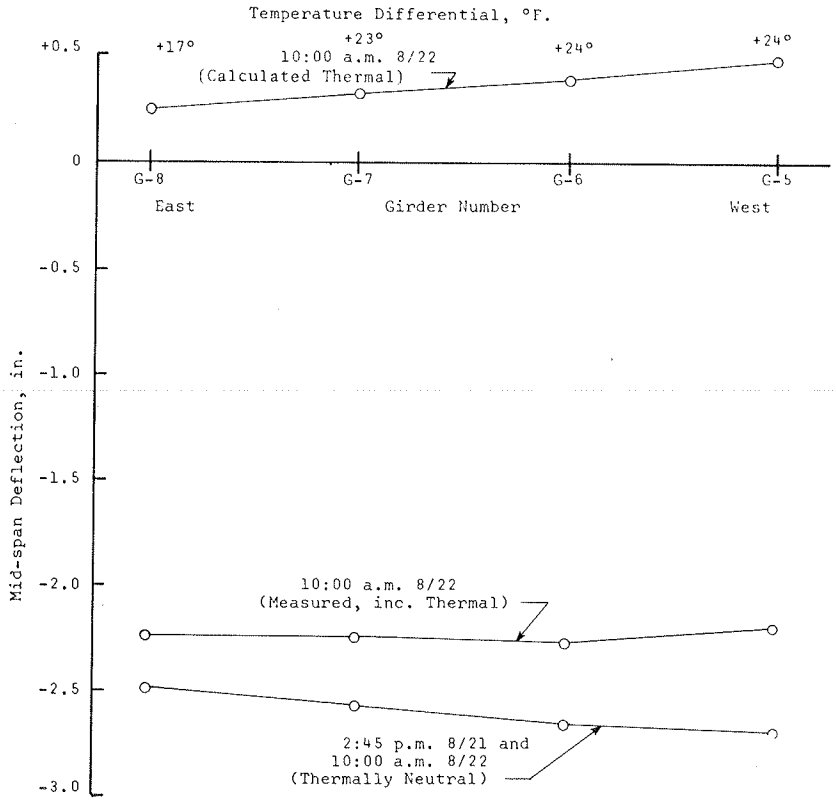

FIGURE 6 Deflections of girders 1 day after deck placement, showing effect of differential temperatures resulting from heat of hydration of concrete.

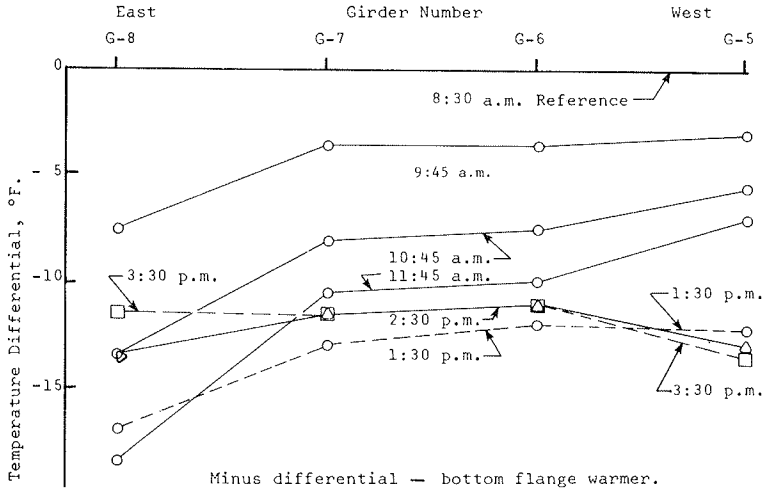

FIGURE 7 Temperature differentials between top and bottom flanges in composite section 19 days after deck placement.

ential between the top and bottom flanges of each girder is the algebraic difference between the differential at 8:30 a.m. and that at the time of the subsequent measurement. In all cases measurements taken subsequent to the 8:30 a.m. reference indicated that the exposed lower portion of the steel girders was warmer than the top flanges within the concrete deck. Net temperature differentials on the order of 11° to 14°F developed downward deflections of the composite girders on the order of 0.25 in. or more, as shown in Figure 8.

Because of the uneven distribution of the temperatures measured on the lower flange and web of each girder, it was difficult to use Equation 2 to calculate the thermal deflections of the composite section. Although the calculated thermal deflections were reasonably close to those measured, the temperature variation within the web of each girder made it virtually impossible to assume, with a reasonable degree of confidence, that the true effects were being reflected in the calculations. Therefore, the experimental data were used for making thermal corrections to the composite section deflections. To determine the deflections that occurred between the

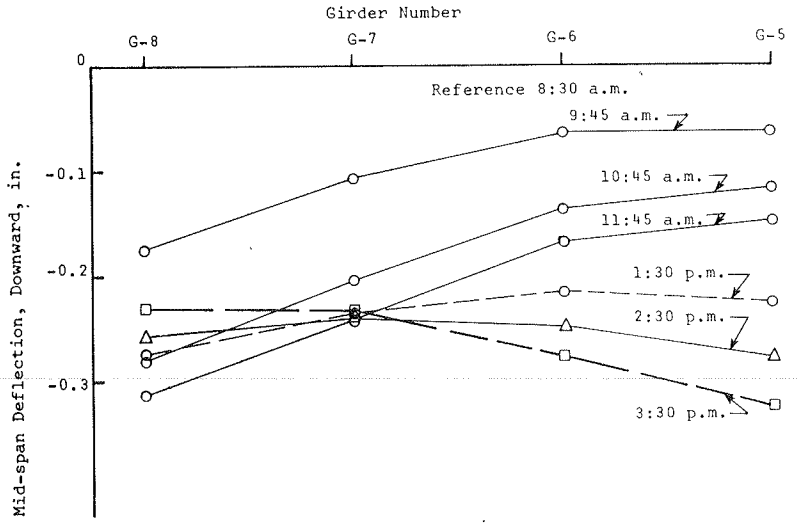

FIGURE 8 Downward deflections at midspan caused by differential temperatures between top and bottom flanges of steel girders in composite section 19 days after deck placement.

completion of the deck and 19 days later, the deflections that existed at 2:45 p.m. on August 21 were used as a base for comparison with those measured at 3:30 p.m. on September 9. The former data were selected because they were nearly thermally neutral. The latter data, however, indicated that the lower flanges were approximately 12°F warmer than the upper flanges. By using the 3:30 p.m. differential temperatures from Figure 7 and the corresponding deflections from Figure 8, thermal corrections were calculated by proportioning. Because the differential temperatures were nearly the same for each set of data, only a small reduction in the 3:30 p.m. thermal deflections had to be made. After calculating the corrections for the thermally induced deflections and subtracting these algebraically from the measured changes in deflections occurring between August 21 and September 9, deflections ranging from 0.243 in. on girder 6 to 0.313 in. on girder 8 still remained. These remaining deflections reported in Table 2 are thus a loss of camber in the steel girders that occurred sometime during the 19-day period.

TABLE 2 Deflections and Camber Loss 19 Days After Deck Replacement

Girder No.	Deflection and Camber Measurement (in.)		
	Total Measured Deflections[a]	Thermal Deflections (corrections)	Remaining Deflection[b] (camber loss)
G-5	-0.505	-0.226	-0.279
G-6	-0.504	-0.263	-0.241
G-7	-0.501	-0.201	-0.300
G-8	-0.510	-0.197	-0.313

[a] Difference between 2:45 p.m. August 21, and 3:30 p.m. September 9 (19 days).
[b] Algebraic difference between measured and thermal deflections.

The camber loss, which ranges between 0.25 in. for girder 6 to 0.3125 in. for girder 8, probably occurred within the first few days subsequent to placement of the deck. This is substantiated by a set of deflection measurements taken 5 days subsequent to the placement of the deck, which indicated a camber loss on the order of 0.25 in. for all four girders.

Dead-Load Deflections in Composite Section

Twenty-two days after the deck was completed concrete was placed for the last of the two parapet walls. The walls were placed on different days, thus allowing for the measurement of the steel girder deflections resulting from the weight placed first on the east and then on the west sides of the bridge.

The dead-load deflections of the girders from the weight of both walls are given in Table 3. The net deflection after correction for differential temperatures was about the same for each girder, that is, approximately 0.5 in. Compared with the values given on the bridge plans, the actual deflections were lower on all girders except number 8, which was 0.125 in. higher.

TABLE 3 Midspan Dead-Load Deflections of Steel Girders Caused by Placement of Parapet Walls

Loading	Midspan Dead-Load Deflection (in.) by Girder			
	G-8	G-7	G-6	G-5
West wall	0.048	0.169	0.351	0.412
East wall	0.429	0.293	0.183	0.094
Total	0.477	0.462	0.534	0.506
Plan values	0.5	0.625	0.625	0.75
Difference	–	+0.15625	+0.125	+0.25

Note: Thermally neutral deflections.

Long-Term Camber Losses

With both the east and west parapet walls placed, the dead loading on the test span was essentially complete. Therefore, it was once again necessary to monitor the temperature-deflection characteristics of the completed span. To allow the east parapet wall concrete to gain sufficient strength to be representative of that which would be effective over

the next several months, 4 days were allowed to elapse before the thermal deflection data were recorded. These final temperature-deflection data were recorded in mid-September, but are not reported here because they were similar to those data recorded on September 9. In general, however, a maximum downward deflection on the order of 0.21 in. was caused by a 10°F thermal difference between the upper and lower flanges. Thus, for reasonably uniform differential thermal conditions, a deflection of 0.021 in. per degree F could be expected.

At the same time that the data just discussed were collected, initial readings for the measurement of long-term camber loss were recorded for each girder. Based on the thermal deflection data, corrections were applied to these initial readings to obtain a thermally neutral basis for subsequent comparisons.

On October 10, 24 days after the initial camber readings were taken, the bridge was opened to traffic. On April 29 of the following year, 202 days after the bridge was placed in service and 226 days after the initial long-term camber readings were recorded, the final camber measurements were recorded. By using the thermal data that were recorded simultaneously, the final readings were corrected to obtain the thermally neutral position of the girders. With the exception of girder 5, the initial and final readings were virtually the same. For girders 6, 7, and 8 there was a 0.01- to 0.02-in. increase in camber. Because a difference of this order of magnitude is well within the expected experimental error involved in reinstalling the deflection scales, it is reasonable to conclude that there was no long-term camber loss of any practical consequence in either of these girders. Although these data indicate that girder 5 experienced an increase in camber of 0.13 in., it is not likely that this was the case. It is more likely that this result can be attributed to experimental error, although it is higher than expected. Therefore, it is concluded that there was no camber loss of any practical significance in the span during the 226-day period, which included 202 days under service loading.

CALCULATED VERSUS ACTUAL CAMBER LOSS OF HEAT-CURVED GIRDERS

When bridge girders are to be heat treated to obtain horizontal curvature, the current AASHTO specifications for highway bridges require that an additional amount of camber be included in them during fabrication to compensate for possible losses during service as residual stresses dissipate (3). The amount of camber (including that which would be needed to offset anticipated dead-load deflections) is given in the specification as

$$\Delta = (\Delta_{DL}/\Delta_m)[\Delta_m + (0.02L^2F_y/EY_o)] \quad (3)$$

where

Δ_{DL} = camber (in.) at any point along the length L calculated by usual procedures to compensate for deflection caused by dead loads or any other specified loads,
Δ_m = maximum value of Δ_{DL} (in.) within the length L,
E = modulus of elasticity (ksi),
F_y = specified minimum yield point (ksi) of the girder flange,
Y_o = distance from the neutral axis to the extreme outer fiber (in.) (maximum distance for nonsymmetrical sections), and
L = span length (in.) for simple spans or the distance between a simple end support and the dead-load contraflexure point for continuous spans.

[Note: Part of the camber loss is attributable to construction loads and will occur during construction of the bridge; total camber loss will be complete after several months of in-service loads. Therefore, a portion of the camber increase (approximately 50 percent) should be included in the bridge profile. Camber losses of this nature (but generally smaller in magnitude) are also known to occur in straight beams and girders.]

Actually, only the second portion of the AASHTO formula pertains to the additional camber allowance for heat curving. This part of the relationship was presented by Brockenbrough (3) in 1970 as

$$\Delta_r = 0.02L^2F_y/EY_o \quad (4)$$

where Δ_r is the residual deflection to be offset by an increase in vertical camber at the point of maximum dead-load camber.

Because the test structure is a simple span, the maximum dead-load camber is at midspan. In addition, the flange plate thickness changes at certain points along the length of the girder, which results in a nonsymmetrical section. Noting that the specifications assume that 50 percent of the camber loss occurs during construction and the remainder occurs under service loading, the values for additional camber were calculated from Equation 4. For the construction loading, the steel section Y_o was used, and for the service loading the composite section Y_o was used. This resulted in separate calculations for the construction and the service loadings. The calculated camber loss values are compared with the measured values in Table 4.

The camber losses calculated for the construction loads ranged from 1.16 to 1.20 in., with an average of 1.19 in. for the four girders. The measured camber losses ranged from 0.24 to 0.31 in., with an average of 0.28 in., only 24 percent of that predicted by the formula. The camber losses calculated for the service loads ranged from 0.90 to 0.95 in., with an average of 0.92 in. for the four girders. As discussed earlier, no service load camber loss was detected in the field.

The total camber loss calculated for the four girders ranged from 2.09 to 2.11 in., with an average of 2.10 in. The total camber losses measured were only those classified as construction losses and averaged 0.28 in., only about 13 percent of the average of those calculated for the four girders.

It should be noted that the radii of curvature of the four girders comprising the test span were greater than 800 ft, whereas those investigated by Brockenbrough were curved to radii in the 200- to 500-ft range (3). The shorter radii of curvature were developed by applying heat to a greater portion of the flange width. The relative residual vertical curvature remaining after loading was also greater in the shorter radii girders. Of the five girders investigated by Brockenbrough, all had radii of curvature less than 300 ft when curved with type 3 heat (one-quarter of the flange width heated) and less than 470 ft when curved with type 2 heat (one-sixth of the flange width heated). Brockenbrough's relationship for the increase in vertical camber (Equation 4) would thus appear to be applicable to girders heat curved to considerably shorter radii than those tested in this study. Because the degree of heating and the radius of curvature appear to be related, residual stresses and thus loss of camber

TABLE 4 Calculated Versus Actual Camber Loss of Heat-Curved Girders

Girder No.	Span Length (ft)	Radius of Curvature (ft)	Steel Section Y_o (in.)	Construction Loading Camber Loss (in.)		Composite Section Y_o (in.)	Service Loading Camber Loss (in.)	
				Calculated	Actual		Calculated	Actual
G-5	138.45	834.51	41.1	1.16	0.28	49.6	0.95	0
G-6	138.58	823.84	39.9	1.20	0.24	52.2	0.91	0
G-7	138.72	813.18	40.3	1.19	0.30	52.5	0.91	0
G-8	138.91	802.51	40.4	1.19	0.31	53.3	0.90	0
Avg				1.19	0.28		0.92	0

Note: A588 steel; yield of 50 ksi. E = 29,000 ksi.

would probably be greater in girders curved to shorter radii.

The results of this study suggest that the AASHTO specifications relationship (Equation 4) might not be applicable to girders heat curved to radii of 800 ft or greater. Considering the magnitude of difference between the camber losses measured on the test structure and those calculated, Equation 4 may not be completely applicable to girders heat curved to radii in the 500- to 800-ft range. In addition, the results suggest that the radius of curvature might be a factor in calculating the potential camber loss in heat-curved girders.

SUMMARY OF CONCLUSIONS

1. The results of the study suggest that the relationship given for the calculations of the potential camber loss in heat-curved girders [article 1-7-14(c), AASHTO Standard Specifications for Highway Bridges (1)] may not be applicable to girders that have radii of curvature greater than 800 ft.
2. Some camber loss from construction loading occurred shortly after placement of the concrete deck. The amount of camber loss, however, was significantly less than that which would be predicted from the specifications. The camber loss from construction loads was approximately one-fourth (24 percent) of that determined from the AASHTO equation.
3. There was no significant camber loss caused by service loading after the bridge had been in service for approximately 6.5 months.
4. The average total camber loss, including both construction and service loading, was approximately 13 percent of that predicted by the AASHTO equation.
5. Considering the magnitude of the differences between the camber losses measured on the test structure and those calculated, the AASHTO equation might not be completely applicable to girders heat curved to radii in the 500- to 800-ft range.
6. Because the amount of heat applied to the girders is related to the degree of curvature required, the results suggest that the radius of curvature might be a variable that should be considered in calculating potential camber losses.

ACKNOWLEDGMENT

The author thanks the Virginia Department of Highways and Transportation for sponsoring this research. The help of Larry Ichter, graduate assistant, and Jimmy French, technician supervisor, in conducting the field study is appreciated.

REFERENCES

1. Standard Specifications for Highway Bridges. AASHTO, Washington, D.C., 1977.
2. M.H. Hilton. A Study of Girder Deflections During Bridge Deck Construction. Virginia Highway Research Council, Charlottesville, June 1971.
3. R.L. Brockenbrough. Criteria for Heat Curving Steel Beams and Girders. ASCE, Journal of the Structural Division, Vol. 96, No. ST10, Oct. 1970.

Publication of this paper sponsored by Committee on Steel Bridges.

The opinions, findings, and conclusions in the paper are those of the author and not necessarily those of the sponsoring agency.

Observations from Tests on a Segmental Bridge

RICHARD M. McCLURE, HARRY H. WEST, and P.C. HOFFMAN

ABSTRACT

The Pennsylvania Department of Transportation designed and constructed a posttensioned segmental concrete box-girder bridge at the Pennsylvania Transportation Research Facility (Test Track) located at Pennsylvania State University. The bridge consists of two independent curved girders with a simply supported span length of 121 ft (36.9 m). The cross section of each girder consists of a box section with side cantilevers. The main objectives of the research program for the segmental bridge were to make field measurements on the full-scale bridge, to study the behavior of the bridge under normal truck loadings, and to study the overload behavior to establish actual safety factors. The accomplishment of these objectives required temperature studies, static load testing of the bridge, overload testing of the bridge, laboratory testing of individual segments, and theoretical studies. This research resulted in many observations for the design of segmental bridges concerning temperature, longitudinal bending, and transverse bending.

The United States is faced with the severe problem of bridge deterioration. It has been reported that 105,000 of the 564,000 bridges in the United States are in critical need of repair or replacement (1). There is no simple answer to solving the problem of replacing and repairing these deteriorated bridges. The task of correcting the structures will undoubtedly require many different technologies and methods.

One of the answers to this problem is the use of precast, prestressed-concrete segmental construction in which the benefits of both precasting and posttensioning can be combined advantageously. This combined method has been shown to be an efficient and economical method of construction (2).

Segmental bridge construction originated in the United States about three decades ago. In 1952 the Freyssinet Company designed a segmental I-girder bridge in New York State; however, the technique of segmental construction was not commercially applied on a large scale until 1962, when the Choisy-le-Roi Bridge was built over the Seine River in Paris (2). Since then segmental construction has spread throughout Europe, and the technique has been continuously refined (3). Segmental construction is now gaining worldwide acceptance, with much use in the United States.

Engineers concerned with the problems of bridge repair or replacement are constantly looking for innovations and improvements in bridge quality and economy. To this end, an experimental segmental bridge was designed and constructed by the Pennsylvania Department of Transportation (4).

A letter survey was also conducted as part of the project. The purpose of the letter survey was to gather information on current designs and construction problems as well as to assess the state of the art concerning segmental concrete box-girder bridges in the United States. The results of this survey pointed out the need for the establishment of national design and construction criteria (5). Since this survey, two reports on the subject have been published by the Prestressed Concrete Institute (PCI) (6,7).

The main objectives of the research program for the experimental segmental bridge were to make field measurements on the full-scale bridge, to study the behavior of the bridge under normal truck loadings, and to study the overload behavior to establish actual safety factors. The accomplishment of these objectives required temperature studies, static load testing of the bridge, overload testing of the bridge, laboratory testing of individual segments, as well as theoretical studies.

TEST BRIDGE

The experimental segmental bridge was constructed at the Pennsylvania Transportation Research Facility (Test Track), which is located at Pennsylvania State University. This facility is an oval-shaped highway, 1 mile in length, which was built primarily for pavement and bridge research.

The configuration of the bridge had to match the existing alignment of the facility, and the span length was controlled by the existing abutments. Because of the curvature at the bridge locations, the curved girders have full superelevation and are on a grade. The general plan, elevation, and cross section of the experimental bridge are shown in Figure 1. The bridge consists of two identical

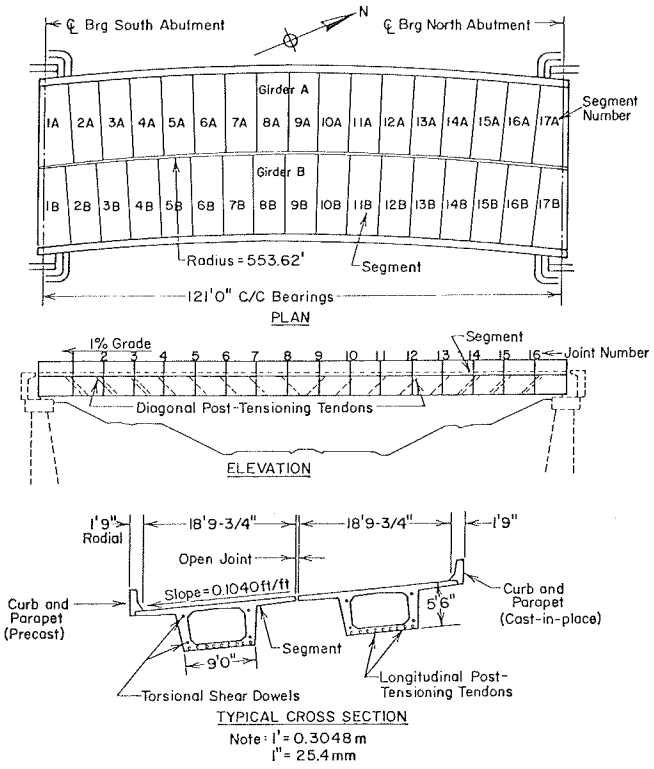

FIGURE 1 General plan, elevation, and typical section.

simply supported girders with segments and joints numbered as shown. It should be noted, however, that most segmental bridges have continuous spans. Each independent girder consists of 17 segments that are tied together with longitudinal bar or strand posttensioning tendons plus diagonal bar posttensioning tendons. Steel shear dowels were used to achieve alignment during construction and to transfer torsional moment after the girders were built. Epoxy was used as the main jointing material between the segments. An open longitudinal joint between the girders was selected to allow an independent comparison of the two girders.

The design specifications for the experimental bridge were from the Standard Specifications for Highway Bridges of AASHTO (8). These were supplemented by the Pennsylvania Department of Transportation's Design Manual (9).

The curved box girder was designed for longitudinal moment by using straight beam theory for the dead load, AASHTO HS20-44 live loading, and prestress. The design was made by using allowable stresses and was checked for ultimate strength. For transverse moment, the segments were designed elastically as a box frame with side cantilever flanges. At the bottom of the webs the frame was assumed to be simply supported.

Each girder was analyzed for torsion as a horizontally curved beam with eccentric loads. Torsional design was based on a method presented by Zia and McGee (10). The cross section of the segments was approximated as a box section with the flanges neglected.

The ability of the joints to provide friction was considered only for ultimate strength conditions. Accommodations for flexural shear were provided by the posttensioned diagonal bar tendons, and the steel shear dowels were designed to resist torsional shear between segments. These joint details are not necessarily representative of current practice.

End diaphragms were introduced in the end segments, which were ample in size to take the substantial reaction forces from the neoprene bearings pads and torsional anchorages and to provide room for the posttensioning end anchorage plates. In addition, an opening was made to allow easy access by researchers to the inside of the box section.

The segments for the experimental bridge were cast individually at a fabrication plant by the short-line method in one steel form with provisions for adjustments. They were then hauled about 100 miles (161 km) to the facility, where they were erected on steel scaffolding-type falsework.

TEMPERATURE STUDY

The main purposes of this study were to determine the dimensional level that needs to be considered in the heat flow problem for a bridge structure; to observe the temperature distributions that occur within a cross section over a 1-year period, as well as to identify the meteorological conditions associated with extreme temperature distributions; and to measure bridge movements under the different observed temperature distributions.

Instrumentation

The instrumentation for measuring temperatures consisted of an Estherline Angus-Model E 1124 E multipoint recorder and 24 copper versus constantan thermocouples that were located at various positions on the cross section (11,12). The thermocouple placement was performed after bridge erection by drilling and filling the void with an epoxy that was specified by the manufacturer as thermally compatible with the concrete (11).

The average vertical deflections at midspan were measured by using six dial gauges, with two placed at each end and two placed at midspan. The dial gauges were mounted to produce vertical deflections that were perpendicular to the bottom of the girder (11).

Longitudinal Variation

The initial portion of the thermal study considered the possibility of a longitudinal temperature variation. This investigation compared 10 thermocouple readings at hourly intervals for 3 different daily cycles between segments 2A and 5A, and segments 2A and 9A (see Figure 1).

The collected ordered pairs of readings for like thermocouple positions were then analyzed by simple linear regression. From the regression analysis it was concluded that there was no significant longitudinal temperature variation (11). The longitudinal study reduced the heat-flow problem from a three-dimensional analysis to one with no more complexity than two dimensions.

Transverse Variation

The second portion of the study observed the transverse temperature distributions of the bridge for 18 daily cycles during the period starting on October 25, 1978, and ending on October 16, 1979. The set of 18 daily observations was designed to indicate seasonal extremes as best as could be predicted by the researchers before the measurements. Each transverse temperature distributon was compiled hourly from the 24 thermocouple readings (11).

It was found that there was little transverse temperature variation in the horizontal direction. Therefore, the heat-flow problem could be further reduced from a two-dimensional to a one-dimensional state with the vertical temperature variations resulting in vertical deflections only (11).

Vertical Deflection and Vertical Temperature Distribution

The effect of the seasonal variation on vertical deflection has been reported previously (11,12). The observations indicated that the maximum upward deflection was 0.72 in. (18.29 mm); it occurred on July 7, 1979. Also, the maximum downward deflection was 0.11 in. (2.79 mm); it occurred on January 4, 1979. The thermal conditions on the two dates were completely opposite (11).

The thermocouple readings on July 7, 1979, that corresponded to the maximum upward deflection of 0.72 in. indicated a maximum surface temperature differential of 51°F (28.3°C) between the top and midheight to the girder.

Specifications

Currently, U.S. design codes do not specify the consideration of a vertical temperature distribution. However, the New Zealand specification requires the consideration of a fifth-power temperature distribution for webs and cantilever flanges, as shown in Figure 2a. Also, the deck slab above the cells and the soffit are subjected to a linear temperature distribution, as shown in Figure 2a. The PCI and the Post-Tensioning Institute (PTI) recommended as simplier vertical thermal distribution, as shown in Figure 2b, where the flange is uniformly warmer than the remaining cross section (12).

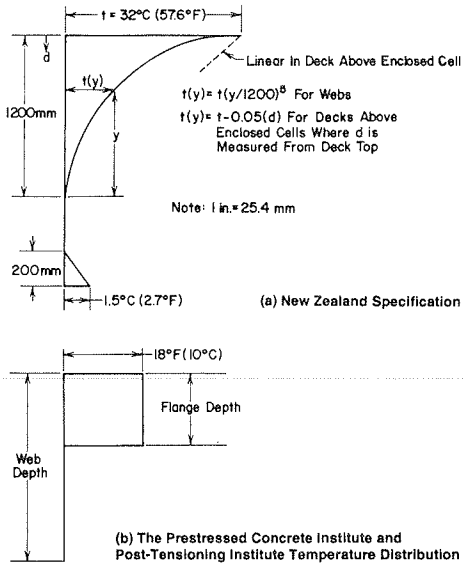

FIGURE 2 Thermal distribution assumptions for design.

Comparisons

A comparison of the temperature distributions with the New Zealand specification indicates satisfactory agreement. The observed maximum surface temperature differential of 51°F is reasonably close to the New Zealand recommendation of 57.6°F (32°C). Also, the field observations for the webs indicate that the critical temperature distribution that causes maximum upward bowing can be approximated by a fifth-order polynomial. In addition, the slab above the box cell showed a linear temperature distribution (11).

The observed curvature, which was calculated from measured vertical deflections, was compared with theoretical curvatures, which were calculated from both the modified New Zealand specification and the modified PCI-PTI temperature distribution. In the modified New Zealand specification the vertical temperature distribution varied as a fifth-order polynomial from 51°F at the top surface to 0°F (-17.8°C) at a depth of 47.24 in. (1200 mm). In the modified PCI-PTI method the temperature was assumed to be 35.8°F (19.9°C) in the 8-in. (203-mm) flange, which is approximately twice the recommended value, and 0°F elsewhere. The observed curvature for a 0.72-in. (18.3-mm) midspan deflection agreed closely with curvatures calculated from the modified New Zealand and PCI-PTI distributions (12). However, residual temperature stresses calculated from the two vertical temperature distributions differed markedly (12).

STATIC LOAD TESTING

The main purpose of the static load testing of the full-scale experimental bridge was to study the elastic longitudinal bending behavior of girder A under actual live-load conditions. The tests focused mainly on the determination of experimental deflections and strains from which stresses were determined. The test results were compared with results from a finite-element analysis and from a conventional analysis. Numerous comparisons were made between observed and calculated quantities, but only two are reported here. More comparisons are available in a report by McClure and West (13).

Testing and Instrumentation

The test vehicle for these tests was loaded to conform as closely as possible to AASHTO HS20-44 live loading plus additional loading to account for the effects of impact (8). The loading arrangement for the vehicle is shown in Figure 3. The test vehicle traveled from north to south and occupied three lateral positions on girder A during the static load tests. First, the center of the vehicle was 5 ft (1.52 m) to the left of the girder centerline while the vehicle crossed. On the next two passes the center of the vehicle was centered and 4 ft (1.22 m) to the right of girder centerline, respectively (13).

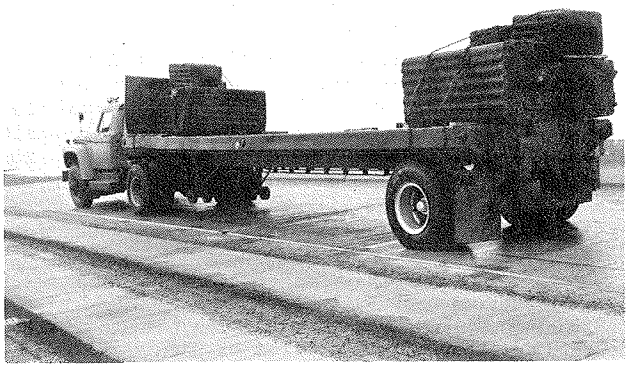

FIGURE 3 Test vehicle for static load tests.

During the tests measurements were made to determine live-load deflections by using dial gauges, and live-load strains were determined by using electrical resistance strain gauges. The readings for the deflections when using dial gauges were taken manually, which required the test vehicle to be stopped when the front axle was at odd-numbered joints so that the readings could be taken. The readings for strains were recorded continuously by using a Honeywell Accudata System with a half-bridge hookup for temperature compensation as the test vehicle traveled at approximately 1.0 mph (1.6 km/h). Therefore, two separate runs were needed to obtain a complete set of readings (13).

The live-load deflections for various positions of the test vehicle were measured by using six dial gauges that were located on the bottom of girder A. At each end, two dial gauges were located at the lower corners of the box approximately 1.5 in. (38 mm) from the abutment pedestal. Two dial gauges were similarly located at midspan. The desired deflection was taken as the average value at the center of the span with respect to the average values at the end gauge locations. All measurements were perpendicular to the bottom of the girder, which resulted in deflections that were also perpendicular to the bottom (13).

Measurements to determine live-load strain for all positions of the test vehicle were made by using electrical resistance strain gauges located at the middle of segment 9A, which is at midspan. This segment was chosen because of the high live-load bending moment at that location (13). The locations of the metal foil electrical resistance strain gauges are shown in Figure 4.

Deflections

Both experimental and theoretical values of vertical deflection are plotted in Figure 5 according to the

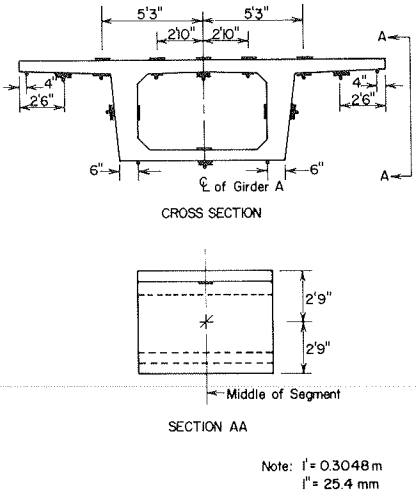

FIGURE 4 Locations of electrical resistance strain gauges on segment 9A for static load tests.

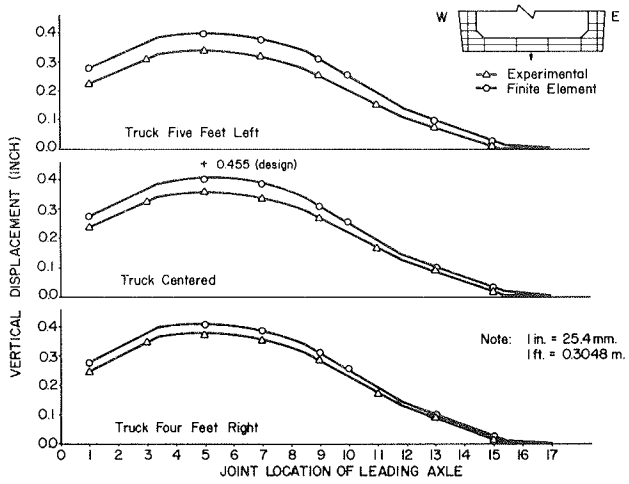

FIGURE 5 Midspan centerline vertical deflections for static load tests.

position of the leading axle of the truck loading. The main theoretical values were determined by using an elastic finite-element analysis for prestressed-concrete structures with the use of SAP IV. The structural analysis program (SAP) is a general purpose finite-element program that was developed at the University of California at Berkeley. The SAP IV version, first released in June 1973 and revised in April 1974, was used in this study (14).

The variation in midspan deflection as a function of load position is theoretically composed of straight-line segments when all three axles are either to the left or the right of midspan. Discontinuities occur in the straight-line segments when an axle enters or leaves the span. However, the variation is curved in those regions where there are axle loads on both sides of midspan (13). The curves shown in Figure 5 are drawn through the data points to reflect these conditions.

An examination of the data in Figure 5 indicates that the experimental results are consistently lower in value than the finite-element results, with a maximum discrepancy of about 15 percent. This tendency for the actual bridge to be stiffer than the finite-element model was reflected throughout the study (13).

Also displayed in Figure 5, for the truck-centered case, is the midspan deflection associated with the leading axle at joint 5 based on the conventional beam theory approach. This deflection of 0.455 in. (11.56 mm) is about 14 percent greater than the corresponding finite-element value, which indicates that the conventional approach used in the design employs a model that is even less stiff than the finite-element model (13).

Longitudinal Stresses

If the bridge is treated approximately as a straight member, and if it is assumed to be loaded and to respond in the vertical plane, then the maximum midspan moment will vary piecewise linearly as the truck moves across the span. Discontinuities occur as an axle enters the span, crosses over midspan, or leaves the span (13). A standard influence line approach gives a maximum midspan moment of 2,228 ft-kips (3021 kN•m) when the leading truck axle is at joint 7. This moment reduces slightly to 2,133 ft-kips (2892 kN•m) when the leading axle is at joint 5. Because longitudinal flexural stress is a direct function of bending moment, this stress will have the same piecewise-linear variation as does the moment when the truck passes over the bridge (13).

The longitudinal stresses on the bottom centerline surface of the box section for segment 9A are compared in Figure 6. The variation patterns in stress as the truck passes over the span show excellent correlation between the experimental and finite-element results. Also, the trend observed earlier in the displacement comparisons is substained here; that is, the experimental results are approximately 15 percent less than the finite-element results (13).

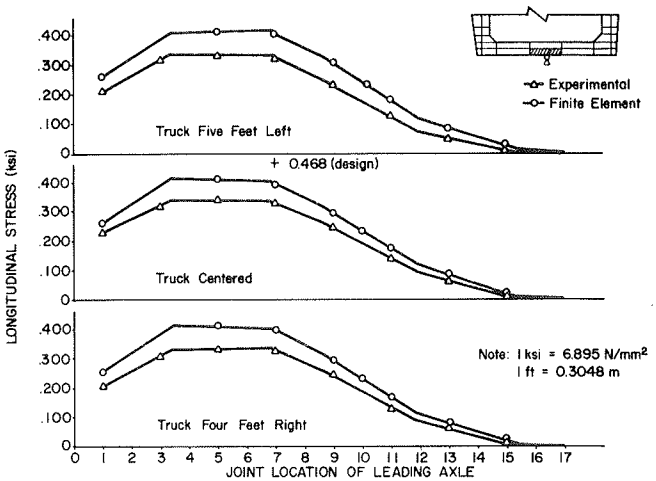

FIGURE 6 Bottom flange longitudinal stresses for middle of segment 9A for static load tests.

Based on standard flexural stress calculations, and by using the maximum midspan moment of 2,228 ft-kips for the simplified straight beam and the section modulus from the design computations, the maximum flexural stress is 0.468 ksi (3.23 N/mm²) (13). This stress is shown in Figure 6 for the truck-centered case with the leading axle at joint 7, and it is seen to be larger than both the finite-element and experimental values.

OVERLOAD TESTING

The main purpose of the overload testing was to study the inelastic longitudinal bending behavior of girder B under overload conditions. The tests focused mainly on the determination of experimental deflections and strains from which stresses were determined. The test results were compared with the results from a finite-element analysis and from a conventional analysis. Numerous comparisons were made between observed and calculated quantities, but only a few will be reported here. More comparisons are available in a report by McClure et al. (15).

Testing and Instrumentation

Girder B was tested with static loading by using the loading frames shown in Figure 7. The loading frames include four hydraulic tension jacks. Four openings

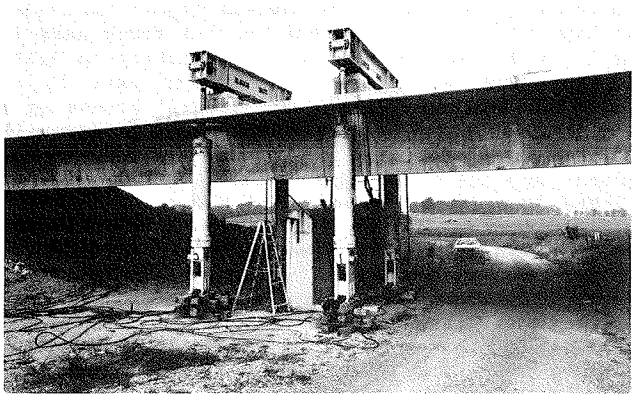

FIGURE 7 Loading frame for overload tests.

for the jacks were cut through the concrete bridge deck directly above the jacks. The jacks were hinge-connected to the steel loading beams at their top ends and attached to the anchor assembly of the rock anchors at their lower ends. The rock anchors were drilled and grouted approximately 75 ft (23 m) below the ground level, 20 ft (6 m) of which were in sound bedrock. Each rock anchor was capable of developing a load of 500 kips (2225 kN), which was equal to the capacity of the loading beams used for the testing. Each loading beam consisted of two 27 x 114 wide flange beams placed on a roller support at one end and a hinged support at the other. The beams delivered the loads through 2-in.-thick (50.8-mm) steel plates to concrete pedestals located over the webs to give a longitudinal bending type failure. The load schedule called for an initial load of 186 kips (887.4 kN), with daily increments of 100 kips (444.8 kN) until failure occurred. The loads were monitored by separate pressure gauges for each jack and verified from strain readings on each ram (15).

Deflections for all load increments were measured by using dial gauges. Three gauge lines located at the bottom of the girder were used as was previously described for the static load tests. All dial gauges determined the displacements in a direction perpendicular to the bottom surface of the girder. After the girder started yielding, the deflections were measured with an engineer's level, which was set up at a distance from the girder, and two level rods, which were permanently mounted at the midspan of the girder (15).

Strains at the middle of segment 9B were measured at each load increment by using metal foil electrical resistance strain gauges. This segment, which is at midspan, was chosen because of the large bending moment at that location. These longitudinal strain gauges were placed as shown in Figure 8. Only longitudinal gauges were used because bending was of primary interest. All strains were read with a Model P-350 Budd Strain Indicator, which used a half-bridge circuit with temperature compensation gauges (15).

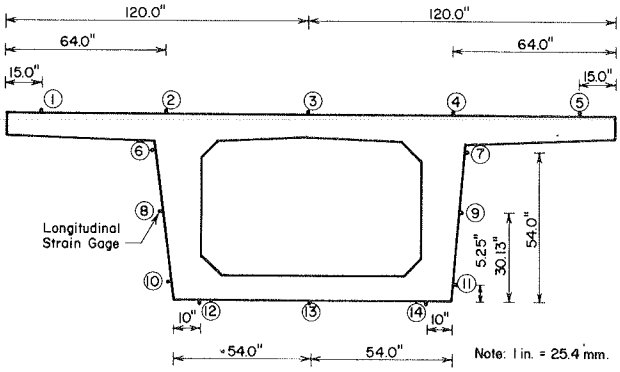

FIGURE 8 Location of electrical resistance strain gauges on segment 9B for overload tests.

Deflections

To obtain the total experimental deflection at midspan for any load, the permanent set was added to the measured deflection. This was necessary so that all experimental deflections were measured from the same origin. The experimental and theoretical midspan deflections are shown in Figure 9. The data in

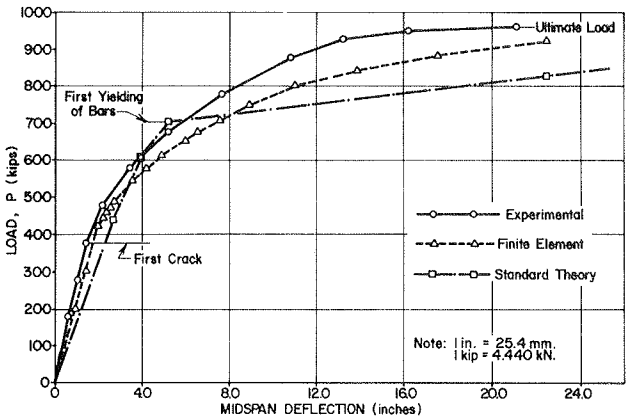

FIGURE 9 Load deflection diagrams for girder B for overload tests.

the figure indicate satisfactory agreement between finite-element and observed deflections at all load levels, with the finite-element model once again indicating less stiffness than the real structure. The finite-element analysis was once again performed by using SAP IV, which was extended beyond yielding by using the inelastic properties of the materials (15). Figure 9 also shows the results of a conventional prestressed-concrete beam analysis by using strain compatibility (16), which indicates satisfactory agreement with experimental values up to first yielding.

Longitudinal Stress

The permanent set strains should be added to the measured strains to obtain the absolute surface strains that should be with the theoretical strains. However, permanent set strains were not measured. Comparison of measured and finite-element strains did indicate fair agreement up to first yielding, where permanent set strains were small but did reveal a deviation of results above first yielding where the permanent set strains were relatively large (15). Figure 10 shows the comparison of observed and finite-element strains at the middle of segment 9B for a load of 376 kips (1672 kN), which is below first yielding.

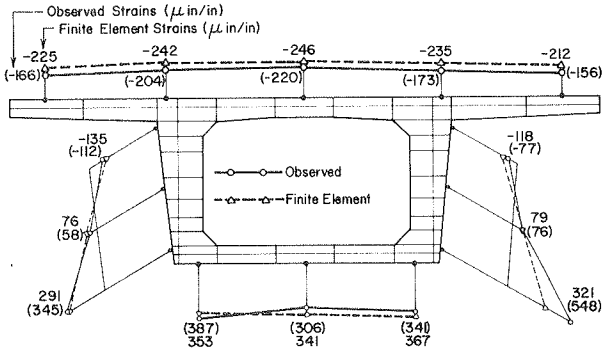

FIGURE 10 Longitudinal surface strains at middle of segment 9B for a load of 376 kips (1672 kN) for overload tests.

Cracking and Failure

In the first and second days of testing, up to load P = 276 kips (1228 kN), there was no visible cracking on the bottom surface of the bridge. In the third day of testing, at load P = 376 kips (1672 kN), the first visible cracking was observed at the bottom surface between the points of loading. As the load was increased, cracks increased in number, and those between the points of loading widened and extended toward the compression zone. Nothing unusual was noticed until the eighth day of testing at a load of 876 kips (3896 kN), when two loud sounds were heard at different times and the pressure gauge readings for the jacks dropped down slightly. It sounded like a strand or bar tendon had broken each time. At this load the cracks at joints 8 and 9 opened widely and extended upward toward the top slab.

In the last day of testing, at load P = 945 kips (4203 kN), two events occurred: first, a noise was heard and the deflection increased suddenly by 0.25 in. (6.35 mm); second, two strong sounds, similar to those that occurred at P = 876 kips were heard, and again, deflection increased suddenly by another 0.25 in. Pressure readings started to fall off, but then reached a constant value. As the load was slightly increased to a load of 955 kips (4248 kN), the crack at joint 8 opened widely and the concrete in the compression zone crushed and spalled on the surface. The mode of failure of the bridge is shown in Figure 11. On inspection of joint 8, it was found that all the longitudinal strands were broken and only the bar tendons were holding the bridge in place.

The finite-element load at first cracking was estimated at P = 420 kips (1868 kN), which is 12 percent larger than the observed value. The cracking load calculated from conventional theory was P = 439 kips (1953 kN), which is 5 percent larger than the corresponding finite-element value. Also, the finite-element load at failure was estimated at P = 920 kips (4092 kN), which is 4 percent smaller than the observed value. The failure load calculated from conventional theory by using strain compatibility was P = 901 kips (4000 kN), which is 2 percent smaller than the corresponding finite-element value (15).

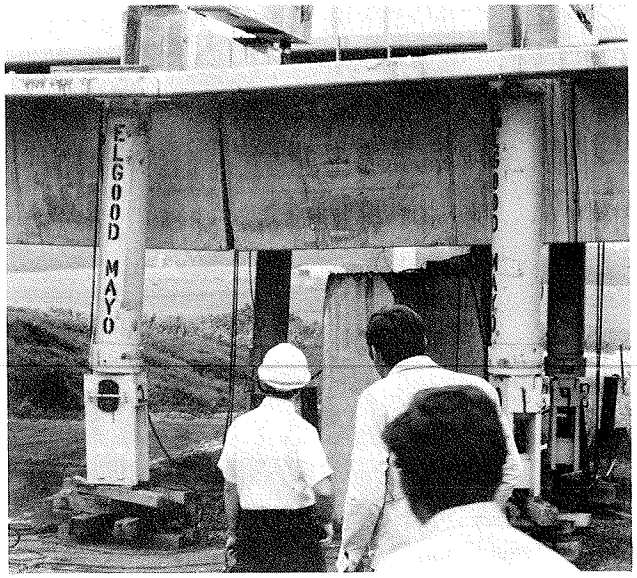

FIGURE 11 Mode of failure of girder B.

LABORATORY TESTING

The main purpose of the testing of individual segments was to establish transverse bending behavior to augment the data obtained from field testing the experimental bridge. The individual segments were tested under simulated field conditions to determine failure modes. Experimental results were compared with the results from a conventional approach that used a frame analysis in the elastic range and yield-line theory to predict ultimate behavior of the slab. Numerous comparisons were made between observed and calculated quantities, but only a few will be reported here. More comparisons are available in a report by McClure et al. (17).

Testing and Instrumentation

Four individual segments were tested under simulated field conditions in the structures laboratory at Pennsylvania State University. Each concrete segment was supported between two steel end frames approximately the shape of the segment, as shown in Figure 12. The end frames had provisions for torsional shear dowels, diagonal tendons, and longitudinal posttensioning bars that could be tensioned to induce the desired longitudinal stress conditions. The four segments were tested statically for several loading positions. In the tests the loads were positioned along the middle of the segment to simulate wheel loads from a standard truck.

Measurements were taken with dial gauges to determine transverse deflections at the middle of the segment. Measurements were also taken with wire electrical resistance strain gauges to determine strains at the middle of the segment. All strains were read with a Model P-350 Budd Strain Indicator, which used a half-bridge circuit with temperature compensation gauges (17).

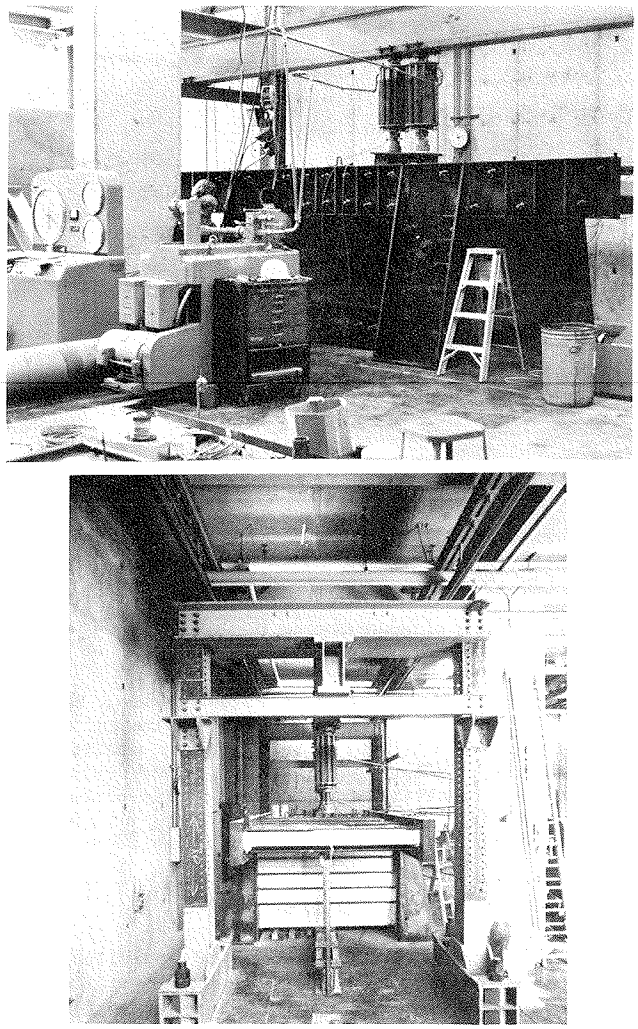

FIGURE 12 Test setup for testing of segments: front view (top), and side view (bottom).

Deflections

The results of the tests indicated that the only significant deflections were the vertical deflections of the top slab that were maximum at the ends of the cantilevers. Deflections at other locations were extremely small. Deflections at the end of the flange are shown in Figure 13. The data in this figure indicate that the amount of longitudinal posttensioning stress in the slab also affects the flange deflection.

The theoretical flange deflection curves shown in Figure 13 are for a simple cantilever without friction along the edge of the flange. The theoretical curve used elastic theory up to first cracking and was modified for inelastic stresses above first cracking.

Moments

Experimental and theoretical transverse moments were compared to determine the reliability of the frame design process in the transverse direction. All of the experimental and theoretical moments were for the middle of the segment, where the moments are a maximum because the loads are applied at the middle of the segment. The moments are for two static loads of 20 kips (89 kN), which represent the standard AASHTO wheel loads plus an allowance for impact.

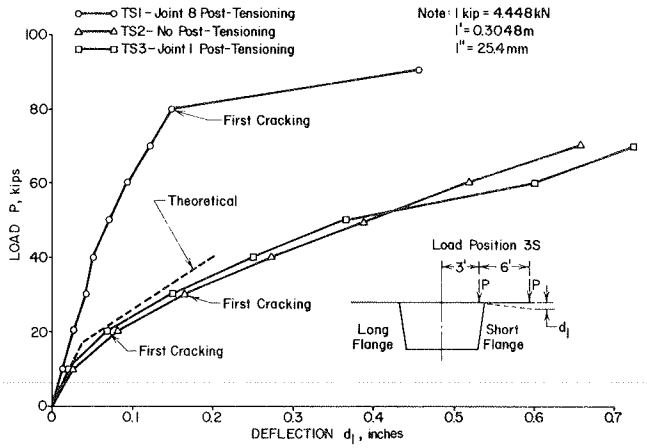

FIGURE 13 Deflection of flange in transverse direction at middle of segment.

Strains from the electrical resistance strain gauges were used to establish the experimental strain distribution at any section. The stresses and forces at that section could then be determined, and the experimental transverse moments were calculated by using statics. The theoretical transverse moments were calculated by the method used for the design of the segments. This procedure is based on the moment distribution method of analysis for a rigid frame, and the load is assumed to be distributed over a length of segment (17).

A comparison of experimental and theoretical moments indicated that transverse bending moments are the largest in the top slab, and that in almost all cases the experimental moments are smaller than the theoretical moments (17).

Cracking and Failure

All cracking and failures during the laboratory transverse bending tests occurred in the top slab of the segments. Theoretical cracking loads were calculated by neglecting the end frames and treating the sections as doubly reinforced slabs. The flanges were treated as cantilevers, and the top slab of the box section was treated as a part of a rigid frame. Theoretical ultimate loads were calculated by using yield-line theory for the top slabs. A simple support was assumed at the end frames, and a fixed support was assumed along the tops of the webs. Satisfactory agreement was observed between experimental and theoretical cracking and failure loads (17).

OBSERVATIONS

- Curvature because of temperature is constant along the length of girder. Therefore, the heat-flow problem can be reduced from a three-dimensional to a two-dimensional state.
- Little transverse temperature variation occurs in the horizontal direction. Therefore, the heat-flow problem can be further reduced from a two-dimensional to a one-dimensional state, with temperature variation occurring in the vertical direction only.
- For a statically determinate or indeterminate structure, residual stresses develop because of restrained strain from a nonlinear vertical temperature variation. These residual stresses can be calculated by direct analysis if the vertical variation in temperature is known.

- For a statically indeterminate structure, the curvature from vertical temperature variation is also important in the design. Either a fifth-order vertical temperature distribution across the entire cross section (New Zealand gradient) or a uniform vertical temperature distribution in the top slab (PCI-PTI gradient) can be used to predict the curvature.
- Reinforcing steel must be provided to carry the total tensile force if the temperature stresses caused by the nonlinear vertical temperature distribution or continuity-induced stresses exceed the ultimate tensile stress of the concrete.
- Elastic deflections and stresses from longitudinal bending can be adequately predicted by using the finite-element method, with the finite-element values about 15 percent larger than the actual values. A conventional design can also be used to conservatively predict the values, with the conventional values consistently larger than the finite-element values. Some economy in design might be achieved by using the finite-element method of analysis in the design.
- Inelastic deflections and stresses from longitudinal bending can be adequately predicted by using the finite-element method. The conventional design approach of using strain compatibility can be used to conservatively predict the failure load, but it should not be used to predict inelastic deflections.
- The only significant transverse deflections in a segment are in the top slab. These deflections occur under the wheel loads and are maximum at the end of the cantilever flanges. The elastic transverse deflections can be predicted by treating the cross section as a rigid frame.
- Transverse moments have a maximum value at a cross section under the wheel loads. Elastic transverse moments can be conservatively predicted by using a frame analysis, where the frame consists of a box section with side cantilevers.
- Transverse bending failures of the top slab were the primary mode of failure, with the flanges being the weakest part of the segment. Theoretical transverse cracking loads can be predicted by treating the cross section as a rigid frame. Theoretical transverse failure loads can be predicted by using yield-line theory for the slab, with a simple support assumed at the edge of segment and a fixed support assumed along the top of webs.

ACKNOWLEDGMENT

A portion of a major 6-year investigation on an experimental segmental bridge that was conducted at the Pennsylvania Transportation Institute, located at the Pennsylvania State University, was presented in this paper. The study was sponsored and funded by the Pennsylvania Department of Transportation and FHWA.

REFERENCES

1. One in Six U.S. Highway Bridges is Deficient. Engineering News Record, March 10, 1977, pp. 18-21.
2. J. Muller. Ten Years of Experience in Precast Segmental Construction. Prestressed Concrete Institute Journal, Vol. 20, No. 1, Jan.-Feb. 1975, pp. 28-61.
3. C.A. Ballinger, W. Podolny, Jr., and M.J. Abrahams. A Report on the Design and Construction of Segmental Prestressed Concrete Bridges in Western Europe--1977. FHWA, U.S. Department of Transportation, July 1978.
4. H.P. Koretzky and A.T. Tscherneff. Final Report--Research Project No. 72-9 on the Design of an Experimental Posttensioned Segmental Concrete Box Girder Bridge. Publication 118. Pennsylvania Department of Transportation, Harrisburg, Sept. 1974.
5. H.P. Koretzky and P.H. Kuo. Letter Survey on "State of the Art in the U.S.A. of Segmental Concrete Box Girder Bridges." Publication 114. Pennsylvania Department of Transportation, Harrisburg, July 1974.
6. Prestressed Concrete Institute, Joint PCI-PTI Committee on Segmental Construction. Recommended Practice for Precast Posttensioned Segmental Construction. Prestressed Concrete Institute Journal, Vol. 27, No. 1, Jan.-Feb. 1982, pp. 14-61.
7. Prestressed Concrete Institute, Bridge Committee. Tentative Design and Construction Specifications for Precast Segmental Box Girder Bridges. Prestressed Concrete Institute Journal, Vol. 20, No. 4, July-Aug. 1975, pp. 34-42.
8. Standard Specifications for Highway Bridges, 11th ed. AASHTO, Washington, D.C., 1973.
9. Design Manual. Publication 15. Pennsylvania Department of Transportation, Harrisburg, 1973, Part 4: Structures.
10. P. Zia and W.D. McGee. Torsion Design of Prestressed Concrete. Prestressed Concrete Institute Journal, Vol. 19, No. 2, March-April 1974, pp. 46-64.
11. P.C. Hoffman, R.M. McClure, and H.H. West. Temperature Studies for an Experimental Segmental Bridge. Interim Report. Pennsylvania Transportation Institute, Pennsylvania State University, University Park, June 1980.
12. P.C. Hoffman, R.M. McClure, and H.H. West. Temperature Study of an Experimental Segmental Concrete Bridge. Prestressed Concrete Institute Journal, Vol. 28, No. 2, March-April 1983, pp. 78-97.
13. R.M. McClure and H.H. West. Field Testing on an Experimental Segmental Bridge. Interim Report. Pennsylvania Transportation Institute, Pennsylvania State University, University Park, June 1980.
14. H.H. West and R.M. McClure. Full Scale Testing of a Prestressed Concrete Segmental Bridge. Proc., International Conference on Short- and Medium-Span Bridges, Toronto, Ontario, Canada, Aug. 1982.
15. R.M. McClure, H.H. West, and M. Abdel-Halim. Overload Testing of an Experimental Segmental Bridge. Interim Report. Pennsylvania Transportation Institute, Pennsylvania State University, University Park, July 1982.
16. A.H. Nilson. Design of Prestressed Concrete. Wiley, New York, 1978.
17. R.M. McClure, D.B. Anderson, and T.E. McDevitt. Laboratory Testing of Segments for an Experimental Bridge. Interim Report. Pennsylvania Transportation Institute, Pennsylvania State University, University Park, Feb. 1980.

Publication of this paper sponsored by Committee on Concrete Bridges.

Problems in Designing Prestressed Segmental Concrete Bridges

DANIEL J.W. WIUM and ORAL BUYUKOZTURK

ABSTRACT

Prestressed segmental concrete bridge construction offers unique advantages over conventional methods of bridge construction. As a result, this relatively new method has gained wide popularity in the construction industry. However, as with any innovative technique, there are some design problems associated with these bridges that require attention. Experience has indicated that damage may occur at local details in these bridges. Some design problems that can be solved with the use of advanced analysis methods to obtain a better understanding of bridge behavior are discussed. The finite-element method, in conjunction with representative material models, is ideally suited for providing a better understanding of the structural behavior and for obtaining accurate response predictions. Two representative examples are analyzed and discussed to demonstrate how to use these procedures in the design process. Response predictions obtained from the application of these advanced analysis methods to segmental concrete bridges can be used as a basis for improving designs. Further examples are given, and finally the importance and implementation of such methods in routine design are briefly discussed.

A damaged local detail in a precast segmental bridge can adversely affect the stability or safety of the bridge as a whole. Therefore, special attention should be given to the design of these details. However, in some cases standard design methods may not sufficiently cover all critical conditions in these details. The objective of this paper is to emphasize that these problems can be solved with the use of advanced analysis methods during the design process.

As a result of the need for efficient, economical, and maintenance-free structural systems, structural designers optimize their designs by using structural components and materials as efficiently as possible. Precast segmental bridge technology is an example of such a development, by which construction costs have been reduced in many cases. These bridges consist of small prefabricated segments that are assembled and prestressed on site (1,2).

Despite the advantages associated with the structural efficiency and low maintenance of the structures, damages have been observed in some field applications. Little information is available on the long-term performance of these structures. A few examples of previous problems on these bridges are joints that failed, spalling and honeycombing of concrete, instabilities during construction, and various problems at local details.

In the following sections typical structural problems that have been encountered in precast segmental bridges are discussed. Two specific problems are then analyzed and discussed to illustrate the use of advanced design methods. Finally, the implications for future designs are examined.

STRUCTURAL PROBLEMS IN PRECAST SEGMENTAL BRIDGES

A large number of precast segmental bridges have been constructed over the past 10 years, and on the whole the construction method has proved to be economically viable. Nevertheless, a number of engineering problems that are unique to these types of bridges have been encountered (2). Some problems that can be resolved in the design stage are briefly discussed. Other problems that usually occur during construction are not covered, but they have been discussed elsewhere (2).

Concrete has spalled off or cracked on several of these bridges. Gerwick (3) and Lin and Redfield (4) reported that concrete was crushed at prestressing tendon anchors in the Columbia River crossing bridges. A large number of prestressing ducts in thin slabs also caused spalling on these structures. Casey (5) indicated that an overly complex cross section made it difficult to compact the concrete, and this led to honeycombing. Expensive remedial measures then offset much of the cost savings. In a box-girder bridge with external tendons, severe cracks developed in the anchor diaphragm, which resulted in closure of the structure to traffic (6). Additional vertical prestressing and extensive grouting were necessary to prevent further crack growth. A similar example is analyzed and discussed in more detail in the next section of this paper.

Cracks and thermal deformations occurred on a number of bridges while manufacturing and curing the segments. For example, large cracks developed in the segment wings of the Zilwaukee Bridge after curing, but the majority of these cracks closed after transverse prestressing was applied. Shrinkage and thermal expansion and contraction probably caused these cracks (7). The remaining large cracks were filled with epoxy, and additional prestressing was added to limit further cracking during operational use.

Creep and shrinkage deformations of concrete significantly affect the deflections of the structure. Thus the shapes of the segments have to be adjusted so that large secondary moments are not introduced when two adjacent sections of the bridge are joined together. This problem is especially troublesome when the two parts do not deflect by the same amount. Several research projects have focused on the time-dependent behavior of segmentally constructed bridges, and a number of numerical methods have been developed to predict the creep, shrinkage, and elastic deflections during the life of the bridge (8-11). These methods have been used with varying degrees of success. On the majority of bridges the actual deflections compared favorably with the predicted values, but discrepancies occurred on some projects (12). In cast-in-place bridges these differences can be remedied while casting the new segment. However, shims or special wet segments have to be used for precast bridges,

but these methods may not provide a satisfactory solution.

Shear keys on the contact faces between segments provide shear strength and ensure that adjacent segments can be positioned accurately during construction. Epoxy bonding agents are usually applied on these surfaces to protect the prestressing tendons from corrosion, to provide additional shear strength, and to assist in placing the segments while erecting the bridge. On a number of earlier bridges the epoxy failed to reach the required strength before additional segments were added, and some of these shear keys were crushed (5,12,13).

Analysis of Local Distress

The large costs that are involved in constructing prestressed segmental bridges require that precautions be taken to prevent damages in these bridges, such as damaged bearings and delaminations and cracks in the concrete. Cracks should be prevented from forming or kept to a minimum because they might result in corrosion of the reinforcement and deterioration of the concrete. The complex geometries and material behaviors of these bridges differ substantially from those of normal building-type structures, and therefore conventional techniques may not apply in designing details.

One example is the design of anchor blocks, where standard design methods are based on the behavior of rectangular beams. If the geometry differs from this form, the calculated stress distributions will be incorrect and the design might be unconservative. Material properties also play an important role in the behavior of a structure. The engineer should use realistic and representative values and models for the strength, stiffness, and time-dependent properties of the materials. Often empirical data are not sufficiently accurate for complex structures. If there is any doubt about the characteristics of the concrete, representative tests should be performed to ensure that the design data are consistent with the material that will finally be used in the bridge. Further, it might be necessary to make additional adjustments during construction if the concrete properties change.

Two selected problems are considered in the following subsections to demonstrate how refined methods can be used to more closely approximate the actual deformations and stress distributions in a bridge. The objective is to indicate that these methods can provide realistic answers to complex problems in bridge design. The effect of sharp deviations in the prestressing tendons are first investigated. Then the creep and shrinkage deformations under dead loads and prestressing forces are calculated.

The specific details assumed in these analyses do not refer to any particular structure. The objective of this presentation is to provide an understanding of the problems in general, and to describe methods that can identify and clarify these problems during the design stages.

Spalling and Cracking of Concrete at Prestressing Tendon Locations

Stress concentrations generally occur at positions where prestressing tendons are sharply curved or at anchor locations. An analysis is presented of a torsion diaphragm that also serves as an anchor block for prestressing tendons. This diaphragm is located above the supports of a multispan continuous bridge. The tendons are sharply curved in this anchor diaphragm, and the concern is whether cracks might develop in this region.

Analysis

The anchor region of the bridge in Figure 1 is analyzed to determine whether cracks might develop from the stress concentrations around the tendons. The finite-element method is used for this purpose. No details will be given regarding this method, and readers are referred to the available texts on this topic (14,15). What assumptions have been made in these analyses, and how the prestressing forces have been incorporated, are discussed. The results of these analyses are discussed later in this subsection.

Two different two-dimensional plane stress analyses are performed on the concrete box girder. These analyses are for an assumed cross-sectional detail at the anchor diaphragm, as shown in Figure 2, and for a corresponding long section of the anchor region, as shown in Figure 3. These sections are assumed to be symmetrical about their centerlines. Figures 4 and 5 show the finite-element meshes and the boundary conditions that are adopted to represent the symmetry.

Concrete is a nonlinear material in which deformations are not proportional to applied loads and strains are not proportional to the applied stresses (16). This is especially true at high compressive stresses that are close to the failure strength of the concrete. But in tension the stress-strain response is approximately linear. The purpose of the present analysis is to predict the formation of

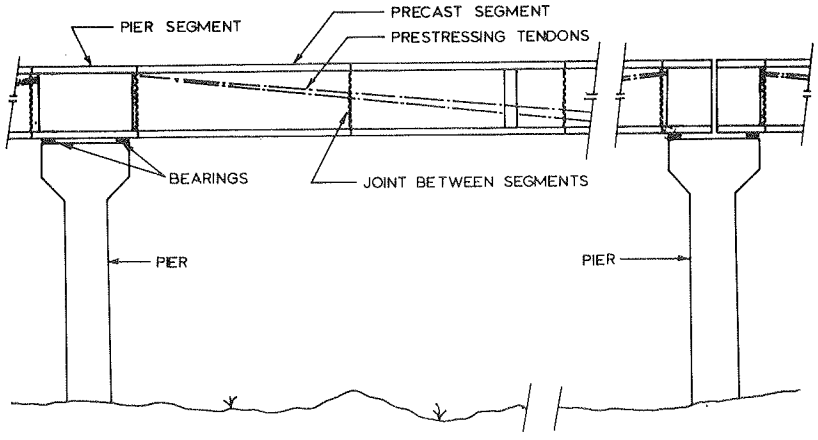

FIGURE 1 Typical span.

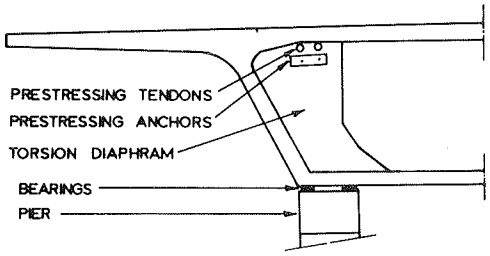

FIGURE 2 Details of cross section at support.

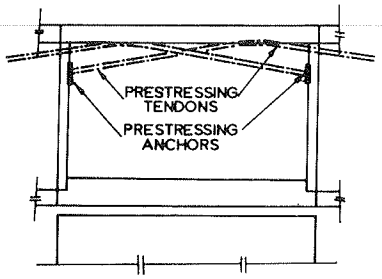

FIGURE 3 Details of long section through pier segment.

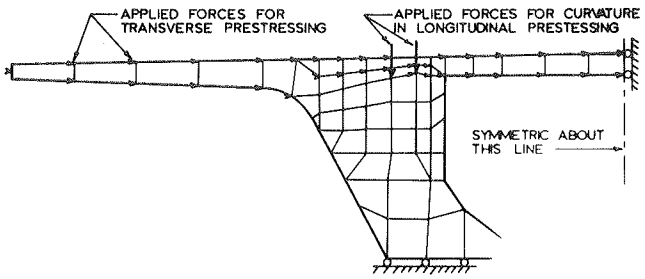

FIGURE 4 Finite-element mesh for cross-section analysis.

cracks in the diaphragm caused by the tensile stresses that occur at the locations where the prestressing tendons are sharply curved. Because tensile cracks form in concrete at relatively low stresses, a linear analysis provides sufficiently accurate answers.

Reinforcing steel introduces additional stiffness and strength in concrete, and in the finite-element analysis of a reinforced-concrete structure the effect of reinforcement may be conveniently modeled with the use of the smeared-reinforcement concept (17). The finite-element analysis program used for the present study includes this capability. But light reinforcement usually included in the torsion diaphragm under consideration does not significantly affect the crack predictions, and thus it may be ignored.

In both cases a thin section of the anchor block is analyzed so that the stresses do not change significantly through the thickness. Thus it is not necessary to perform a three-dimensional analysis; a two-dimensional (plane stress) approach is considered to be adequate.

For the purpose of this example, a bridge is considered that is prestressed in both the longitudinal and the transverse directions. Transverse prestressing is applied in the top slab of the box section by bonded pretensioned reinforcement. Prestressing in the longitudinal direction is applied

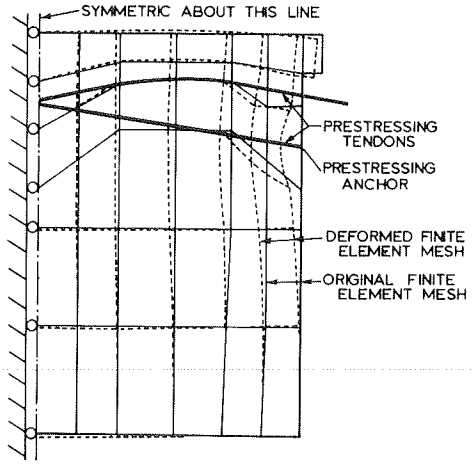

FIGURE 5 Finite element for long section analysis.

with posttensioned bonded tendons. The longitudinal prestressing tendons are sharply curved in the anchor block. This introduces large vertical forces on the cross section, which are taken into account in both analyses.

In the analysis the transverse prestressing forces are applied as nodal forces on the finite-element nodes. Equivalent forces are calculated to represent the prestressing as accurately as possible. Because the pretensioned tendons are fully bonded to the concrete, it can be assumed that the total prestressing force is transmitted to the concrete by uniformly distributed bond stresses. These forces act along the tendon, and all forces should therefore be applied along that line. This restriction would dictate where the finite-element nodes should be placed. As an alternative, equivalent nodal forces can be calculated to represent the effect of the prestressing force at the boundary of each finite element. Displacement interpolation functions for the finite elements provide the basis for allocating the representative forces to the two or three nodes on each boundary (14).

The vertical forces that result from the curved longitudinal prestressing tendons are applied as distributed forces on the nodes. The displacement interpolation functions are again used to convert these distributed loads to equivalent nodal loads.

Experimental results indicate that the failure strength of concrete is greatly influenced by the stress level. Kupfer et al. (18) tested concrete under biaxial compression and compression and tension. They found that under biaxial compression, the compressive strength of the concrete exceeds the usual uniaxial strength. However, when concrete is subjected to tensile and compressive stresses in two perpendicular directions, the tensile strength of the material is less than the tensile strength under uniaxial stresses. These phenomena are best represented by the failure envelope in Figure 6a. This envelope represents the biaxial stress combinations under which concrete fails. In Figure 6a the two principal stresses at a point (σ_1 and σ_2) are normalized with respect to the uniaxial compressive strength of the concrete. If the stresses lie outside the failure envelope, it can be expected that the concrete will have failed. The mode of failure depends on the type of stresses. If both stresses are compressive, the concrete will be considered crushed; if one or both of the stresses are tensile, the concrete will be cracked.

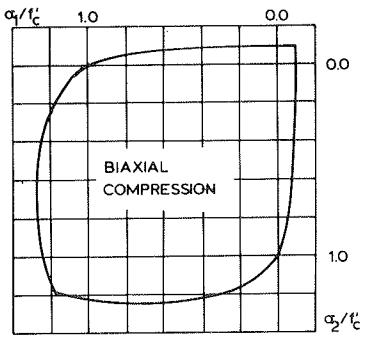

(a) Experimental biaxial failure envelope

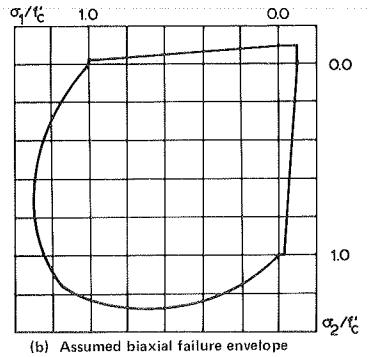

(b) Assumed biaxial failure envelope

FIGURE 6 Failure envelopes of biaxially loaded concrete.

Several numerical methods have been proposed to represent these experimental results (17,19). A simplified model is used for this analysis (20). It consists of the criteria for the biaxial compression region (21), a bilinear model in the tension-compression region, and a constant strength in the biaxial tension region. This postulated failure envelope is shown in Figure 6b.

Therefore, the proposed strategy to determine whether cracks might form in the concrete is to analyze the details with the use of a linear elastic method, and then to compare the predicted stresses with the established failure criterion for concrete.

Discussion of Results

The results of the finite-element analyses are presented in Figures 5, 7, and 8. The deformed shape (indicated by broken lines in Figure 5) is exaggerated to indicate the effect more clearly. Note the effect of the boundary conditions, as well as the influence of the prestressing forces on the deformation. Figure 7 shows the maximum principle stress contours. In this figure full lines represent tensile stresses and broken lines represent compressive stresses. It is particularly important to notice the large tensile stresses above the prestressing tendons in the cross section.

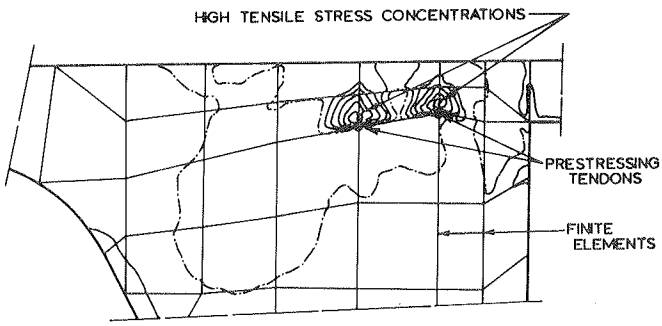

FIGURE 7 Results of cross-section analysis.

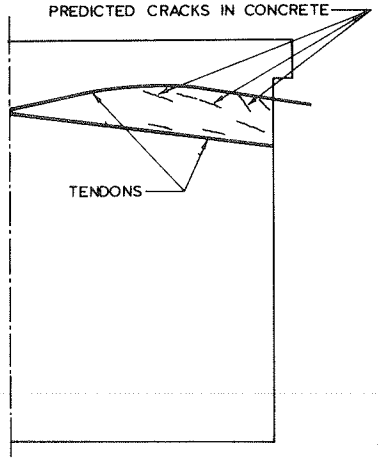

FIGURE 8 Predicted crack location in long section.

The directions of the principal stresses and their relative magnitudes have been obtained from the finite-element analyses. Of particular interest are those locations where large tensile stresses occur in conjunction with the compressive stresses. This is the case at positions above and behind the tendons anchors (see Figure 8). If such an analysis is performed while designing a bridge, the engineer can take precautions to prevent these cracks from forming or to prevent them from extending if they do form.

Creep in Concrete

The time-dependent behavior of segmentally constructed precast and cast-in-place bridges is of great importance in the design and construction of these structures. Sections of a structure can be deformed or overstressed if the time-dependent deformations are not predicted correctly. Therefore, it is necessary to use accurate models for the structure as well as for the material so that they represent the actual bridge. These deformations are used to calculate the prestressing forces and to determine the initial shape of the bridge.

A number of numerical models are available to calculate these long-term deformations. The methods of the American Concrete Institute (ACI) (22) and the Comite Europeen du Beton (CEB) (23) are widely used. However, these standard methods for predicting creep and shrinkage have been questioned for their accuracy. Bazant and Panula (24) recently suggested a model for better predictions. Also, attention should be paid to variations in the local climatic, material, and environmental conditions in computing long-term deformations.

A method for predicting the long-term shortening of a multispan bridge with finite elements is described. The method offers advantages in (a) computing accurate material models for long-term deformations, and (b) allowing flexibility for better structural representation.

It has been shown that the long-term deformation of concrete can be predicted more accurately if some tests are performed on the concrete (24). Therefore, it is possible to reduce the uncertainty in the creep and shrinkage predictions. The method described in this subsection is well suited for incor-

porating such test results in the design of such a structure.

Numerical Model for Creep

Bazant (25) and Anderson (26) proposed a method for calculating long-term creep and shrinkage deformations with the finite-element method. The method for the uniaxial creep of concrete is based on the following assumptions.

1. The total deformation of the concrete at time t is the sum of those deformations that result from the applied stress $[\epsilon_\sigma(t)]$ and those deformations that are independent of the applied stress $[\epsilon^0(t)]$:

$$\epsilon(t) = \epsilon_\sigma(t) + \epsilon^0(t) \tag{1}$$

2. The stress-related deformations can be divided into the instantaneous and the long-term deformations, such that

$$\epsilon_\sigma(t) = \left\{[1/E(t')] + C(t;t')\right\}\sigma = \sigma\, J(t;t') \tag{2}$$

where

$\sigma/E(t')$ = instantaneous deformation at age t',
$\sigma C(t;t')$ = creep deformation, and
$J(t;t')$ = total time-dependent compliance.

Bazant indicated that a time-step integration method can be developed from these basic assumptions to calculate the time-dependent deformations under varying stress conditions. This material law can be written as

$$\Delta\epsilon = (\Delta\sigma/E'') + \Delta\epsilon'' + \Delta\epsilon^0 \tag{3}$$

where

$\Delta\epsilon$ = change in strain during a time step,
$\Delta\sigma$ = change in stress during the time step,
$1/E''$ = time-dependent compliance,
$\Delta\epsilon''$ = incremental inelastic (creep) strain, and
$\Delta\epsilon^0$ = non-stress-related strain increment.

This model for creep has been incorporated in a finite-element program for the analysis of plane stress and plane strain specimens.

Finite-Element Model of Prestressed Span

The center span of a five-span continuous bridge with posttensioned tendons is analyzed to determine time-dependent deformations. It is assumed for the purpose of this analysis that the tendons are located outside the concrete and that they are only attached to the concrete at the anchors and at two intermediate diaphragms, where the tendons change direction (see Figure 1). The main objective is to calculate the shortening of this span as a result of creep and shrinkage in the concrete so that the expansion joints and bearings can be designed accordingly. Therefore, because the end spans are far removed from this span, and because only long-term effects at the expansion joints will be calculated, it can be assumed that the ends of this span are prevented from rotating.

Only dead-load effects are considered, and because these do not introduce torsional or any other nonplanar effects, plane stress finite elements can be used to model the concrete box girder. Also, it is assumed that the shear lag effect in the flanges of the box girder will not affect the long-term deformations, and that this effect can therefore be ignored in this analysis. Elements of different thicknesses are used. These correspond to the total thickness of concrete on the particular level, and no special provision is made for the hollow box. One-dimensional elements with axial stiffness are used to represent prestressing tendons. Initial strains in the tendons introduce the prestressing forces in the bridge. The advantage of using this approach, rather than applying equivalent external forces at finite-element nodes, is that prestressing losses caused by concrete creep and shrinkage are taken into account through deformations in the bridge. The additional stiffness of the tendons is also taken into account.

The initial strains in the prestressing tendons are calculated as follows. The bridge span is analyzed with linear elastic material properties that represent the stiffness of the concrete at the time of stressing. Unit forces are consecutively applied at the finite-element tendon anchors. The force P_{ji} in tendon section i caused by the unit force at anchor j is obtained from these analyses:

$$f_i = f_i^0 - (P_{1i}f_1^0 + P_{2i}f_2^0 + \ldots + P_{ni}f_n^0) \tag{4}$$

if there are n tendons. These forces, with the additional forces introduced by the dead loads, can be written as

$$[f] = \left\{[I] - [P]\right\}[f^0] + [f^{DL}] \tag{5}$$

where

[f] = vector that contains the prestressing forces in the tendons (f_i) at the time of stressing,
[I] = n by n identity matrix,
[P] = stress influence matrix with entries P_{ji},
$[f^0]$ = initial prestressing force vector, and
$[f^{DL}]$ = vector that contains the forces in the tendons from the dead loads.

The initial tendon forces can then be obtained from

$$[f^0] = \left\{[I] - [P]\right\}^{-1}[f - f^{DL}] \tag{6}$$

The corresponding initial strains are calculated from these initial stresses.

Bazant (25) suggested that the total time-dependent compliance in Equation 2 can be expressed as a Dirichlet expansion such that

$$J(t;t') = a_0 + b_0(t')^{-n_0} + \sum_{m=1}^{N}[a_m + b_m(t')^{-n_m}]\left\{1-\exp[-(t-t')/\tau_m]\right\} \tag{7}$$

where a_i, b_i, and n_i are experimentally determined coefficients, and τ_i are retardation times. Also, the shrinkage strain can be expressed as

$$\epsilon_{sh}(t) = \epsilon_{sh\infty}\, k_d \sqrt{(t-t')/[(t-t')+\tau_\alpha]} \tag{8}$$

where $\epsilon_{sh\infty}$, k_d, and τ_α are coefficients that depend on the concrete properties.

Note that the particular method does not merely require one single creep coefficient, but several coefficients (as shown in Equation 7) are needed to fully represent the time-dependent behavior of the concrete. It is important that the correct coefficients are used in this model. These coefficients can be obtained either from experimental data or by calibrating Equation 7 to available creep curves.

In this analysis data from previous tests are used to illustrate the method (27,28). These coefficients are adjusted for the particular concrete compressive strength of approximately 5,000 psi.

The finite-element mesh and the deformed shapes

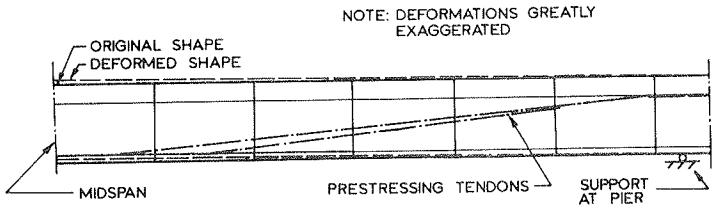

FIGURE 9 Configuration used for creep analysis.

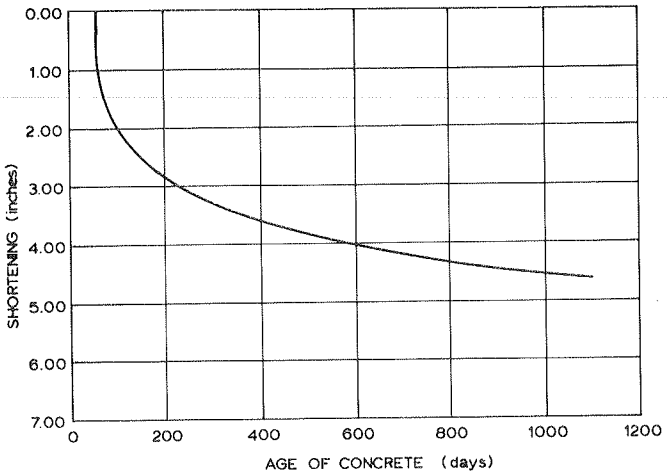

FIGURE 10 Long-term shortening.

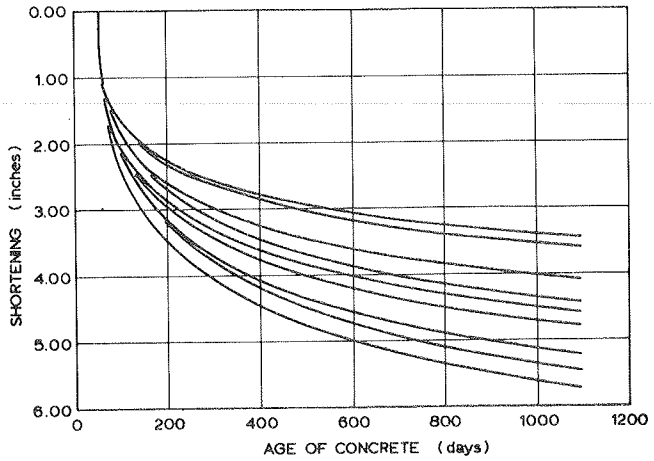

FIGURE 11 Variability in the shortening.

are shown in Figure 9, and the shortening of the bridge is shown in Figure 10. Note that the deformations initially increased rapidly, but then the rate of change in deformations decreased. These deformations only take elastic, creep, and shrinkage effects into account, but short-term effects of temperature changes and horizontal traffic loads should also be considered in the final calculations.

Variability of Concrete Properties

Because of variations in the way concrete is batched and cured, and because of variations in aggregate properties, composition of different mixes, and environmental conditions, concrete from different batches have different stiffness, creep, and shrinkage properties. This is so even for concretes with similar strengths. Therefore, it is not possible to accurately predict these properties with empirical expressions. Because of these uncertain properties the structural response is also uncertain. An uncertainty analysis should be performed to explore how the response of the structure is affected by the uncertainty in the material properties.

The present case study is extended in this subsection to illustrate how the shortening of the bridge is affected by the variability in the long-term concrete properties. It has been found that the predicted stiffness, creep, and shrinkage properties have standard deviations of 20, 22, and 33 percent, respectively, with respect to the average material properties (24). To study the behavior of the bridge under these variable conditions, a number of analyses can be performed with different material properties. For this example, three different values are assigned to each of the material properties. In terms of the average (predicted) value (α) and its standard deviation (σ_α), these three values are ($\alpha - \sigma_\alpha$), α, and ($\alpha + \sigma_\alpha$). The predicted response for nine selected cases are presented in Figure 11, where different combinations of each of the three material properties (stiffness, creep, and shrinkage) are used.

Note the wide range in the predicted shortening. It is clear that it is not possible to accurately predict the shortening of the bridge; the bearings and other supporting structures can also not be designed to close tolerances, but this uncertainty should be taken into account.

The finite-element method, as previously described, is ideally suited for this analysis, where the material properties have to be incorporated in the actual design. The example indicates that it is important to determine whether the deformations are sensitive to variations in the material properties.

APPLICATION OF REPRESENTATIVE CONCRETE MODELS TO BRIDGE ANALYSIS

Current design codes incorporate many safety margins that have been built up through many years of experience. However, design conditions only reflect the sometimes limited experience of previous designs and experiments, and usually it is not possible to extend these standards beyond those limits on which they are based. Therefore, in applying innovative design concepts that do not adhere to these limits, alternative methods have to be explored to verify the designs.

Research has been conducted on the fundamental behavior of concrete when it is subjected to various load and environmental conditions. This information reflects the actual material response, whereas current concrete design codes tend to reflect the properties of members or structural systems. Although these research results may not be used directly in the design process, finite-element programs have been developed in which they have been incorporated. As was illustrated in the previous examples, these methods can be used to study the nonstandard details to ensure that the material strengths are not exceeded.

Apart from these cases, several more examples can be given where standard building codes would not be directly applicable. Simplifying assumptions are often implicitly incorporated in design rules and can be justified for smaller members. In larger applications these simplifications may introduce inaccuracies that might not be compensated for by the redundancies in the structure. A few examples are discussed in the following paragraphs.

Various theories have been proposed for designing shear and torsional reinforcement in beams, but tests indicate that current design expressions may be unconservative for certain conditions (16). More advanced material behavior should therefore be applied in the analysis of deeper beams and box girders. In these instances the members resemble plane stress conditions for which biaxial properties should be considered to more accurately incorporate the failure and shear transfer behavior of concrete.

Current design methods should be improved in accounting for the effects introduced in statically indeterminate structures by prestressing and thermal gradients at ultimate loads. Approximations would introduce inaccuracies that can lead to cracking and crushing under design conditions. The use of incorrect creep and shrinkage data in the design can likewise cause inaccuracies in deformation predictions, which would result in distress.

Local details also deserve special attention, especially where high stress concentrations can be expected. Tendon anchors, abrupt directional changes in prestressing tendons, supports, joints, holes, and cavities can also introduce high stress concentrations. Again, current design methods should be improved for these cases.

SUMMARY

In this paper a brief discussion is presented of the problems that have occurred on some precast segmental bridges. Some of these problems may be attributed to conventional design methods that may not correctly incorporate the complex behavior of these bridges. Two typical problems are analyzed and discussed to show how the finite-element method can be used in conjunction with a representative material model to study specific details. These material models can provide more accurate information on the serviceability and ultimate limit strength of these structures. Therefore, such methods should be incorporated in the design process of these bridges.

REFERENCES

1. W. Podolny and J. Muller. Prestressed Concrete Segmental Bridges. Wiley, New York, 1982.
2. D.J.W. Wium and O. Buyukozturk. Precast Segmental Bridges--Status and Future Directions. Journal of Civil Engineering for Practicing and Design Engineers, Vol. 3, No. 1, 1984, pp. 59-79.
3. B.C. Gerwick. Construction Problems and Solutions: I-205 Columbia River Bridge. Proc., Segmental Concrete Bridge Conference, Prestressed Concrete Institute, Kansas City, Mo., 1982.
4. T.Y. Lin and C. Redfield. Some Design Issues for American Constructors. Proc., Segmental Concrete Bridge Conference, Prestressed Concrete Institute, Kansas City, Mo., 1982.
5. G.J. Casey. Zilwaukee Bridge Construction. Proc., Segmental Concrete Bridge Conference, Prestressed Concrete Institute, Kansas City, Mo., 1982.
6. R.J. Woodward. Cracks in a Concrete Bridge. Concrete, Vol. 17, No. 7, 1983, pp. 40-45.
7. Early Decisions and Delays on the Zilwaukee Michigan Bridge Project. U.S. General Accounting Office, 1983.
8. S. Kashima and J.E. Breen. Construction and Load Tests of a Segmentally Precast Box Girder Bridge Model. Res. Report 121-5. Center for Highway Research, University of Texas, Austin, 1975.
9. K.N. Shiu, J.I. Daniel, and H.G. Russel. Time-Dependent Behavior of Segmental Cantilever Concrete Bridges. Final Report. Illinois Department of Transportation, Springfield (in preparation).
10. M.K. Tadros, A. Ghali, and W.H. Dilger. Long-Term Stresses and Deformations of Segmental Bridges. Prestressed Concrete Institute Journal, Vol. 24, No. 4, 1974, pp. 67-87.
11. S.F. van Zyl and A.C. Scordelis. Analysis of Curved, Prestressed Segmental Bridges. ASCE, Journal of the Structural Division, Vol. 105, No. ST11, 1979, pp. 2399-2417.
12. A.C. Harwood. I-205 Columbia River Bridge Design and Construction. Proc., Segmental Concrete Bridge Conference, Prestressed Concrete Institute, Kansas City, Mo., 1982.
13. E.A. Lamberson and J.M. Barker. Kishwaukee River Bridges. Concrete International, Vol. 3, No. 3, 1981, pp. 93-101.
14. K.J. Bathe. Finite Element Procedures in Engineering Analysis. Prentice-Hall, Englewood Cliffs, N.J., 1982.
15. O.C. Zienkiewics. The Finite Element Method. McGraw-Hill, New York, 1982.
16. R. Park and T. Paulay. Reinforced Concrete Structures. Wiley, New York, 1975.
17. Finite Element Analysis of Reinforced Concrete. ASCE, New York, 1982.
18. H. Kupfer, H.K. Hilsdorf, and H. Rüsch. Behavior of Concrete Under Biaxial Stresses. Journal of the American Concrete Institute, Vol. 66, No. 8, 1969, pp. 656-666.
19. W.F. Chen. Plasticity in Reinforced Concrete. McGraw-Hill, New York, 1981.
20. O. Buyukozturk and T.-M. Tseng. Behavior of Concrete in Biaxial Cyclic Compression. ASCE, Journal of Structural Engineering, Vol. 110, No. 3, March 1984, pp. 461-476.
21. K.J. Willam and E.P. Warnke. Constitutive Model for the Triaxial Behavior of Concrete. Paper III-1. Presented at Seminar on Concrete Structures Subjected to Triaxial Stress, International Association of Bridge and Structural Engineers, Bergamo, Italy, May 17-19, 1974.
22. Building Code Requirements for Reinforced Concrete. Report ACI-318-77. American Concrete Institute, Detroit, 1977.
23. CEB-FIP Model Code for Concrete Structure. Federation International da la Precontrainte, Wexham Springs, Slough, England, 1978.
24. Z.P. Bazant and L. Panula. Creep and Shrinkage Characterization for Analyzing Prestressed Concrete Structures. Prestressed Concrete Institute Journal, Vol. 25, No. 3, 1980, pp. 86-122.
25. Z.P. Bazant. Mathematical Models for Creep and Shrinkage of Concrete. In Creep and Shrinkage in Concrete Structures (Z.P. Bazant and F.H. Wittman, eds.), Wiley, New York, 1982, pp. 163-256.
26. C.A. Anderson. Numerical Creep Analysis of Structures. In Creep and Shrinkage in Concrete Structures (Z.P. Bazant and F.H. Wittman, eds.), Wiley, New York, 1982, pp. 259-303.

27. Z.P. Bazant and S.T. Wu. Dirichlet Series Creep Function for Aging Concrete. ASCE, Journal of the Engineering Mechanics Division, Vol. 99, No. EM2, 1973, pp. 367-387.
28. R.D. Browne. Properties of Concrete in Reactor Vessels. Paper 13. Proc., Conference on Prestressed Concrete Reactor Pressure Vessels, Institution of Civil Engineering, London, England, 1967, pp. 11-113.

Publication of this paper sponsored by Committee on Concrete Bridges.

Edge-Stiffening Effect of New Jersey Barrier Walls on Cantilever Slabs

C. SADLER and M. HOLOWKA

ABSTRACT

The policy of using New Jersey type barrier walls along all major highways has been endorsed by the Ontario Ministry of Transportation and Communications. Consequently, new bridges and deck rehabilitations have massive barrier walls along outside edges of bridge decks. These barriers act as edge stiffening for cantilever slabs and have a significant effect on the distribution of live load on cantilever slabs. The current code specifications for the design of concrete cantilever slabs were established for slabs with rigid supports and with no edge stiffening. These specifications are conservative when edge stiffening is present. The load distribution of a typical cantilever slab supported by an exterior longitudinal girder was investigated by using three-dimensional finite elements. The study considered various edge-stiffening conditions and varying flexibility of longitudinal deck support. The results are compared with the methods given in the Ontario Highway Bridge Design Code and with other simplified methods. As a result of the enhanced load distribution, a significant potential saving in the quantity of cantilever reinforcing steel and in the cost of deck rehabilitation can be realized.

During the past few decades the nature of highways and vehicular traffic has changed rapidly. The highway system has developed with the objectives of providing for increased traffic volumes, increased truck loads, faster speeds, and greater safety. The vehicular traffic, in particular truck traffic, has dramatically changed in size and weight. As the heavy trucks have become more numerous and traffic has become more congested, a greater need to confine out-of-control trucks has arisen. Consequently, the nature of the restraining elements, which are designed to keep trucks within their right-of-way, has also changed.

Initially, the railings, parapet walls, or barrier walls were of simple form, consisting of a post and railing type. The initial use of wood gave way to the stronger materials of steel and concrete. However, as truck size increased, the post and railing type were not sufficient to resist collision loads and could not redirect out-of-control trucks back onto the highway. Consequently, the province of Ontario adopted a standard barrier wall that consisted of a continuous reinforced-concrete barrier wall. The typical barrier wall used for controlled-access highways is shown in Figure 1. This barrier wall is 450 mm wide at the base and just more than 1 m in height, with a total mass of 760 kg/m. Also shown is a barrier wall with railing that is used for roads with pedestrians. These massive barrier walls are considered a restraint mechanism and are used to redirect traffic, but not in a structural sense.

In Ontario a popular form of bridge construction is the concrete slab on longitudinal concrete or steel girders. Economically, it is advantageous to minimize the number of girders; consequently, the use of a cantilever slab is common. A typical cross section of a recently designed continuous steel box-girder bridge is shown in Figure 2. The design of the cantilever is governed by (a) dead loads, (b) vertical live loads, and (c) horizontal collision loads. The dead-load effects are secondary compared to the live-load effects. The ratio of factored live-load effect to factored dead-load effect is approximately 2.5 to 3.5 for a cantilever span of 1.5 m.

Current design specifications do not take into account the presence of these massive barrier walls. The design specifications have not kept pace with the development of the barrier walls and their structural effect on the design of the supporting slab. The effect of the presence of continuous concrete barrier walls on the design of the supporting cantilever slab is investigated. The presence of barrier walls affects only the distribution of vertical live loads and collision loads. Dead-load effects are not altered by the presence of barrier walls.

CODE SPECIFICATIONS FOR CANTILEVER SLABS

Current codes have been developed so that the canti-

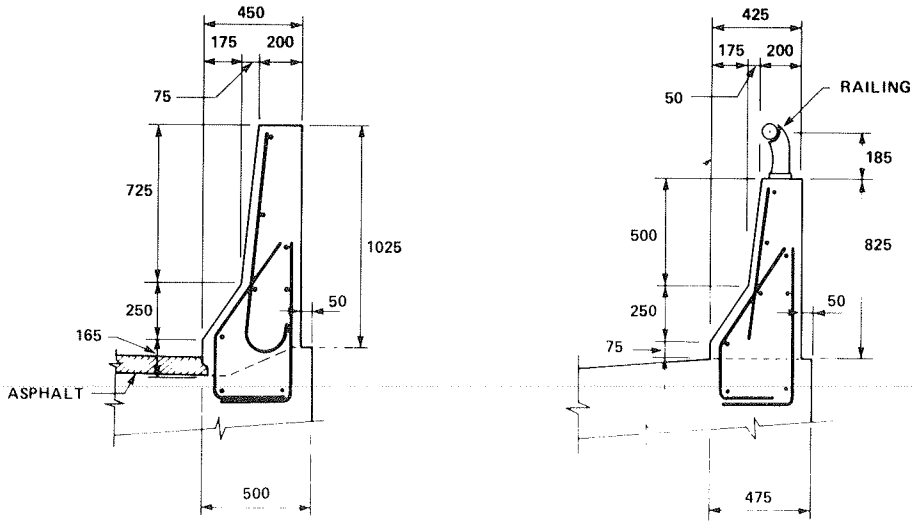

FIGURE 1 Typical barrier walls, Ontario Ministry of Transportation and Communications.

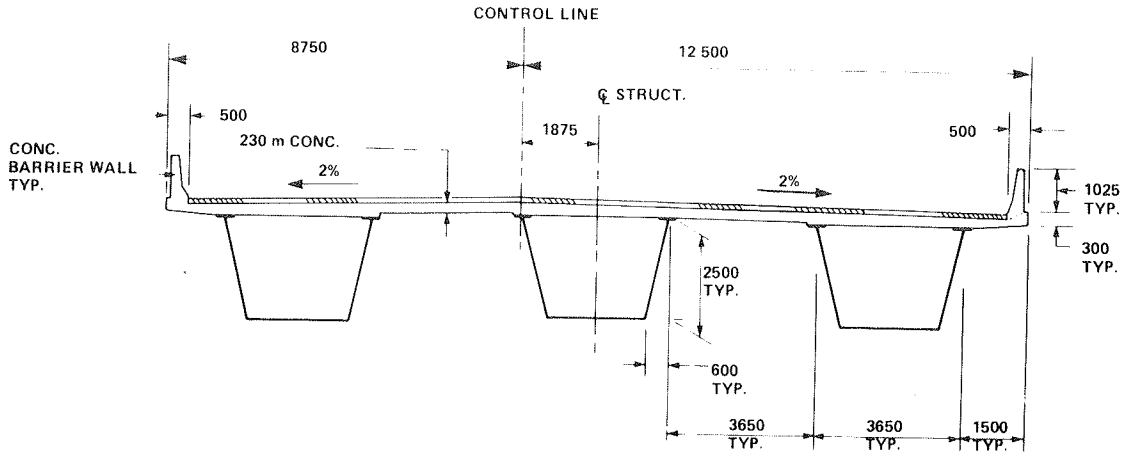

FIGURE 2 Typical section of a steel box-girder bridge.

lever slab can be designed on a unit length basis. The unit length is parallel to the support line of the cantilever. The AASHTO specifications (1) for the distribution of live load have not changed over the past 35 years. The formulas for determining the effective length of slab-resisting live load were developed so that the slab is designed to support the load independent of the end support along the cantilever. For railing or collision loads, the provisions do attempt to take into account the presence of a parapet; however, they do not take into account the length of the cantilever. The design moments are calculated by distributing the moment caused by a concentrated vertical wheel load or a collision load over a prescribed effective length (E):

$$M \text{ (per unit length of slab)} = (P \cdot X)/E \quad (1)$$

where

M = moment resultant;
P = concentrated vehicle load caused by wheel or collision load;
X = moment arm, distance from wheel load to supported end, or distance from location of collision load to base of barrier wall; and
E = effective length of cantilever slab resisting live-load moments (see Table 1).

The recently published Ontario Highway Bridge Design Code (OHBDC) (2) bases its formulas for cantilever slabs partly on Westergaard's (3) elastic method (AASHTO) and partly on a semigraphical elastic method (4), as shown in Table 1. In the cases of (a) cantilever slabs spanning less than 1.2 m and supporting wheel loads and (b) barrier wall collision loads, the applicable equations are identical to those of AASHTO. In the case of wheel loads applied to cantilever slabs greater than 1.2 m and where the cantilever span is small in comparison to the length of the supported end, the semigraphical elastic method proposed by Bakht and Holland (4) is specified. The design moment for live load is given in the form:

$$M \text{ (per unit length of slab)} = (PA'/\pi)\{1/\cosh[A'y/(C - x)]\} \quad (2)$$

where

A' = coefficient (see Figures 3 and 10);
y = distance measured along supported end from the wheel load;

C = distance of concentrated wheel load from support end, measured along the x-axis; and
x = distance measured perpendicular to and from the supported end.

Equation 2 is applicable to slabs with linearly varying thickness, but it does not account for the presence of edge stiffening. The coefficient A' is dependent on the slab thickness ratio, the position of the load on the slab, and the location of the reference point, as shown in Figure 3, which is taken from the OHBDC. For the majority of bridges, the cantilever span is less than 1.2 m in length; consequently, the AASHTO format was retained in lieu of the more general form of Equation 2 because for small spans the variation between the two equations is minimal. It should be noted that for both codes the cantilever span for slab-on-girder bridges is limited in length to 1.8 m.

SCOPE OF INVESTIGATION

The present study was undertaken to determine the effect of the presence of edge stiffening or barrier walls on the distribution of live-load effects in typical cantilever slabs. A typical cantilever deck section (Figure 2) was considered in the formulation of the mathematical models.

The distribution of live-load effects in cantilever slabs is affected by the following structural parameters:

1. Length of slab in the direction of the overhang,
2. Thickness of the slab overhang,
3. Material properties of the slab (modulus of elasticity),
4. Presence of edge stiffening,

TABLE 1 Moment and Distribution Length Formulas

Load Case	Direction of Force Effect [distribution length (E), m]	
	Transverse Moment	Longitudinal Moment
AASHTO		
Wheel loads	0.8X + 1.143	0.35X + 0.98 ≤ 2.134
Collision loads		
With barrier wall	0.8X + 1.524	—
Without barrier wall	0.8X + 1.143	—
OHBDC		
Wheel loads		
Cantilever span ≤ 1.2 m	0.8X + 1.15	
Cantilever span > 1.2 m	$M = (PA'/\pi)\{1/\cosh[A'y/(C - x)]\}$	0.35X + 1.0 ≤ 2.1
Collision loads		
With barrier wall	0.8X + 1.15	—
Without barrier wall	0.8X + 1.15	—

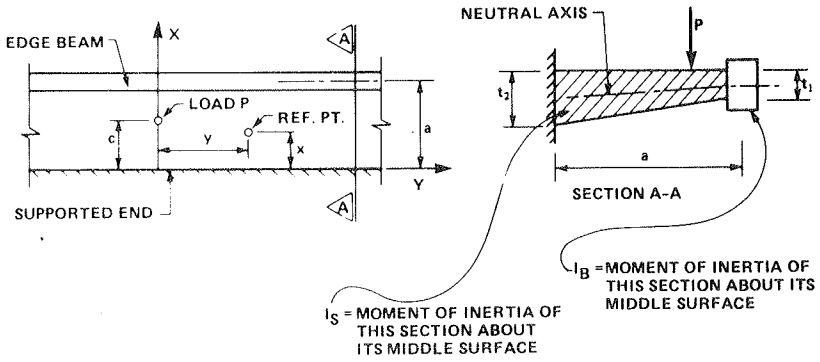

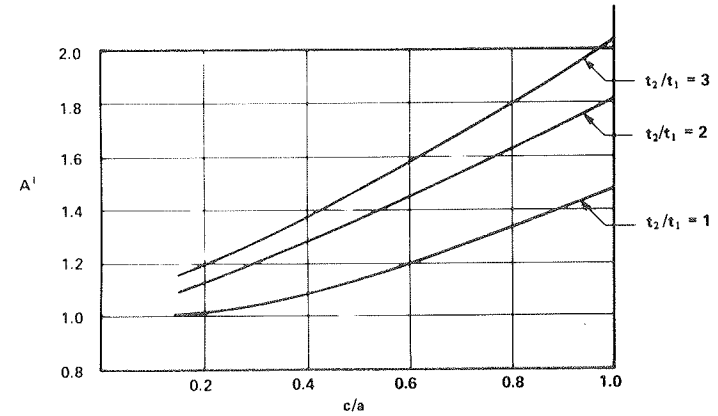

FIGURE 3 Value of coefficient A' at Y = 0.

5. Longitudinal stiffness of supporting girders, and
6. Location and type of load.

Several of these parameters are kept constant or specified in order to simplify the analysis. The first three items are established as follows: slab span = 1.5 m, slab thickness = 230 mm, and material property of the concrete slab (E_{slab}) = 27 700 MPa. (Note that E_{slab} = Young's modulus of elasticity of a concrete deck.)

The parameters studied are 4, 5, and 6. The degree of edge stiffening is varied by assigning appropriate values of the modulus of elasticity to the barrier wall. The longitudinal stiffness of the supporting girder is varied by assigning different boundary conditions to the supports. The location and magnitude of the applied vertical and horizontal live loads are as specified in the OHBDC.

The results from the mathematical model were then compared with both code methods and with other existing methods of analysis (4,5).

FINITE-ELEMENT ANALYSIS

Analysis of cantilever slab configurations was carried out by using the finite-element program QUEST (6). The computer program was used to perform a linear elastic analysis of a bridge by representing structural elements with quadrilateral thin shell finite elements capable of simulating both membrane and flexure behavior. The program is based on the displacement formulation of the finite-element method and considers all six degrees of freedom at each element node. The method allowed any one or more of the six degrees of freedom (three translatory and three rotational) to be constrained at a nodal point.

Three different cantilever slab configurations were investigated. The cases chosen represent extreme structural or boundary states. In the first case a cantilever slab fixed at the supported end against all translations and rotations and has no edge stiffening along the free edge is modeled. In the second case a cantilever slab, again, is modeled; it is fixed at the supported end but has edge stiffening along the free edge. In the third case a cantilever slab that has the supported end resting on a flexible media is modeled; for example, a steel plate girder parallel to the direction of traffic. The free edge is edge stiffened. These three conditions are shown in Figure 4.

The load cases for each of the three cases are shown in Figure 5 and are as follows:

1. An 80-kN horizontal collision load applied at the top of the barrier wall,

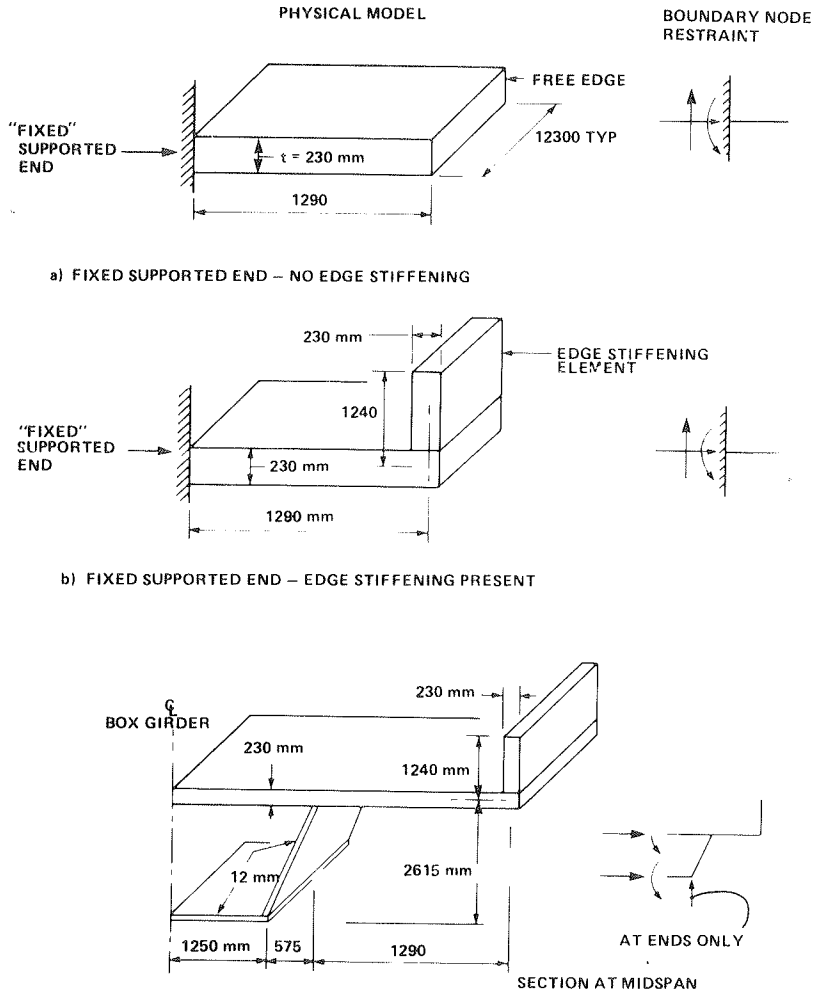

FIGURE 4 Cantilever slab configurations used to model structural response for finite-element analysis.

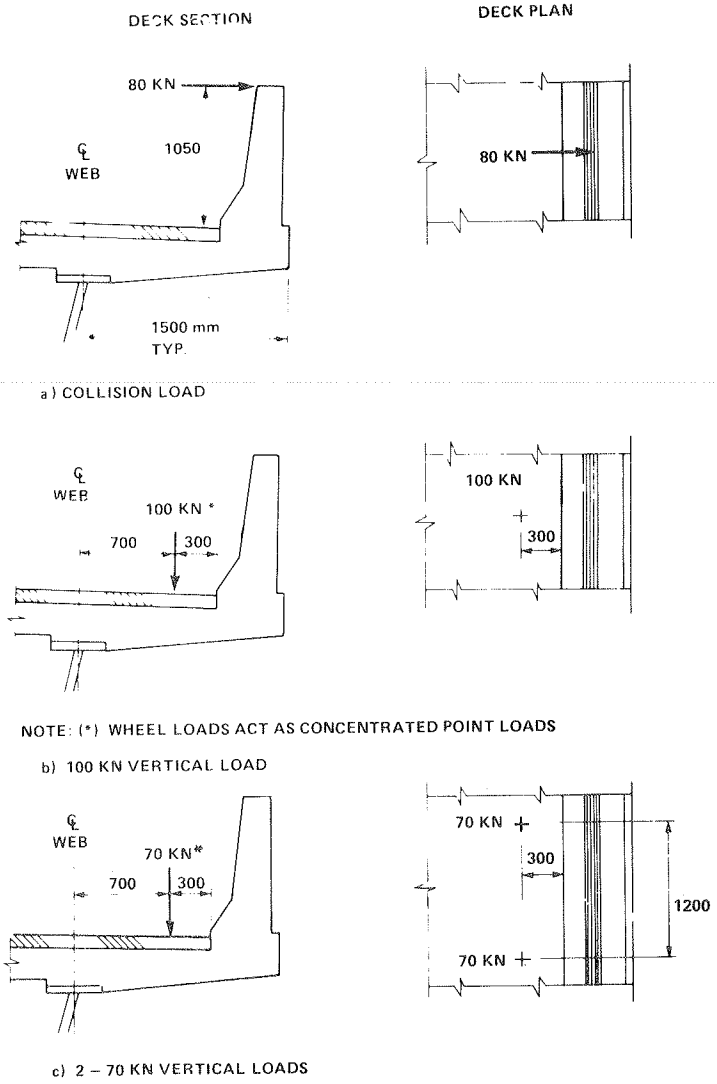

FIGURE 5 Load cases: magnitudes and positions.

2. A single 100-kN vertical wheel load acting on the slab, and
3. Two 70-kN wheel loads that act on the slab and are 1.2 m apart in the direction normal to the span of the slab.

The vertical loads were applied at 300 mm from the face of the barrier wall. Dynamic load effects were not included in this investigation because the effect simply affects the magnitude and not the distribution of the live load.

The process of modeling the structural behavior of a cantilever slab requires an arrangement of quadrilateral elements so as to closely approximate the load-distribution characteristics of the real structure. Figure 6 illustrates the subdivision of the idealized structure into finite elements. The arrangement shown provides reasonable element aspect ratios and provides for an element layout that results in a reasonable resolution of the resulting force effects. To avoid local effects caused by slab discontinuities, a width 8 times the cantilever slab span is used. In this way the condition of an infinitely wide cantilever slab is modeled. Structural components that comprise the barrier wall, slab, and support beam are all modeled. In modeling the barrier wall it was decided to replace the actual barrier wall shape with elements of a rectangular cross section to simplify the modeling for the finite-element analysis. The only requirement is that the overall height and moment of inertia of the barrier wall about the base of both the model and actual barrier wall be the same. This facilitated the correct application of the horizontal collision load and at the same time closely approximated the vertical stiffness of the edge-stiffening element.

OBSERVATION AND DISCUSSION OF RESULTS

A total of three different idealizations, each with the same three load cases, were investigated. The results of the analysis are given in Figures 7-9. The bending moments in the direction of the cantilever span are shown as contours on a plan of the mathematical model.

Figure 7 shows the distribution of moments for the collision load of 80 kN. As can be expected, the maximum moment occurs at the free edge of the cantilever slab. The first contour is representative of the condition where no barrier wall stiffening is considered. The second and third contours are representative for the cases where barrier wall stiffening is considered. The peak moment decreases by almost 30 percent when barrier walls are consid-

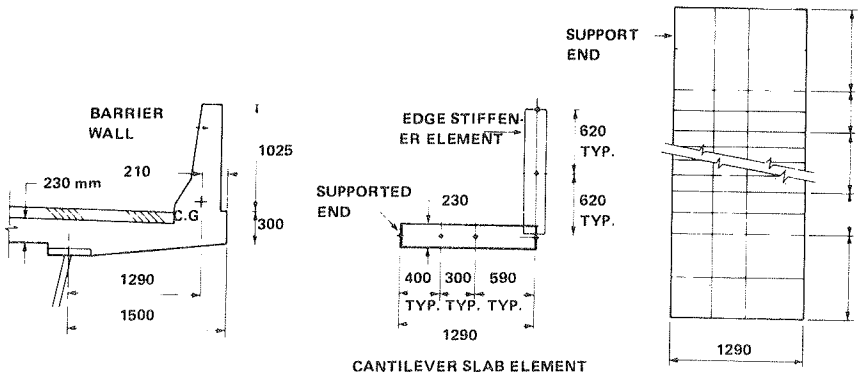

a) STRUCTURE IDEALIZATION FOR QUEST RUN No. 1 & 2

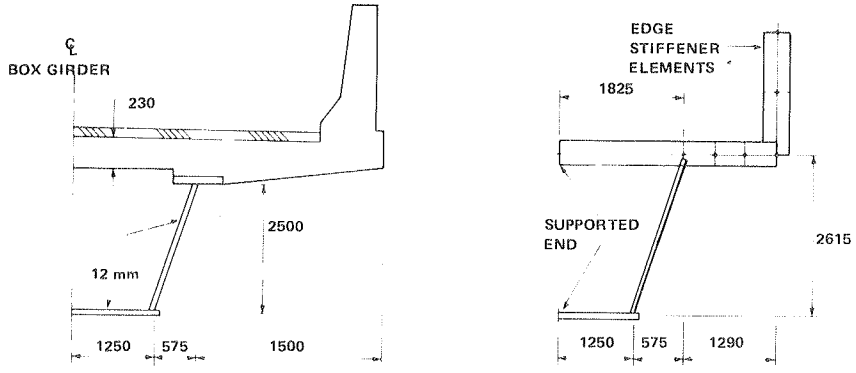

b) STRUCTURE IDEALIZATION FOR QUEST RUN No. 3

FIGURE 6 Finite-element arrangement.

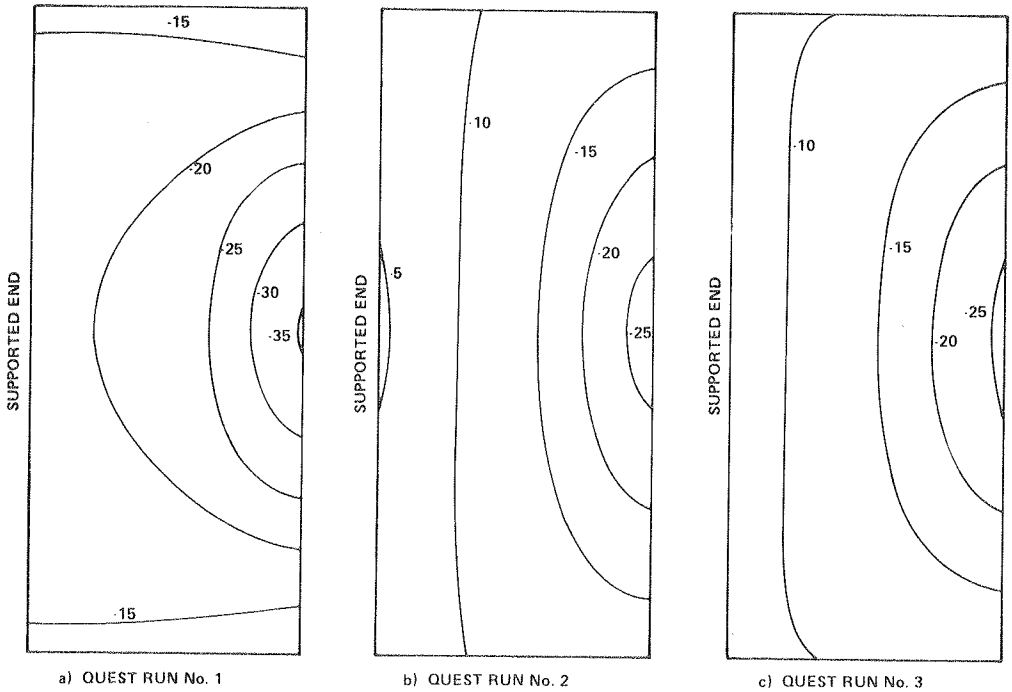

a) QUEST RUN No. 1 b) QUEST RUN No. 2 c) QUEST RUN No. 3

FIGURE 7 Moment diagram, 80-kN collision (kN·m/m).

TABLE 2 Comparison of Results of Analysis (moments at centerline web)

Load Case	Maximum Moment Results (kN·m/m)							
	AASHTO		OHBDC		QUEST 1: Fixed-End Support Without Barrier Wall	Bakht(5): Fixed-End Support With Barrier Wall	QUEST 2: Fixed-End Support With Barrier Wall	QUEST 3: Flexible-End Support With Barrier Wall
	With Barrier Wall	Without Barrier Wall	With Barrier Wall	Without Barrier Wall				
80-kN collision	39.2	45.5	39.2	45.5	18.8	–	10.3	9.0
	66.1[a]	86.3[a]	66.1[a]	86.3[a]	35.0[a]	–	28.0[a]	25.0[a]
100-kN wheels	–	41.2	–	36.3	35.4	25.5	24.0	11.6
2- to 70-kN wheels	–	–	–	32.5	32.5	26.3	21.8	11.9

[a]Moment at face of barrier wall.

ered. The boundary condition of the supported end has little effect on the moment distribution at the free edge.

The comparison of results for the various methods of analysis is given in Table 2. For this load case, moment values at both the supported and free edge are tabulated. Both code methods (AASHTO and OHBDC) give the same results. The finite-element analysis gives moments that are significantly smaller than the code requirement. If the barrier wall is treated as a cantilever slab supported by the deck, then the moments at the base of the barrier wall can be calculated in the same fashion as for vertical loads and in accordance with the code methods. Consequently, E = 0.8X + 1.15 = 2.142 m, and the live-load moment = PX/E = 46.3 kN•m/m. This is 72 percent greater than that predicted by the finite-element analysis, but it is only 70 percent of the code predictions. At the supported end of the cantilever slab the finite-element results are at least 50 percent smaller than the code values. It is obvious that for the cantilever slab with this type of concrete barrier wall, the provisions of both codes are extremely conservative.

Figure 8 shows the distribution of bending moments for a 100-kN vertical load. Directly under the wheel loads and for all three conditions there are local positive bending moments. At the supported end of the cantilever slab the moments are negative. As expected, there is no moment at the free edge of the unstiffened case; however, there are small negative moments at the free edge for the stiffened cases. With no barrier wall, the finite-element result of 35.4 kN•m/m indicates satisfactory correlation to the OHBDC value of 36.6 kN•m/m and the AASHTO value of 41.2 kN•m/m (see Table 2). With the addition of a barrier wall, the moments decrease to 24.0 and 11.6 kN•m/m, depending on the support condition. For the case of a rigid support, this is a 33 percent reduction. It should be noted that local positive moments directly under the wheel point are of the same magnitude as the negative moment when the presence of barrier walls is taken into account. These are present for the extreme case of point loads. If a distributed load that represents the actual tire print is used, this moment would be much smaller.

Figure 9 shows the moment contours for the loading case of two adjacent wheel loads. This case represents typical dual-axle loads where there is an interaction of the two closely spaced loads. The AASHTO code does not address this condition. The

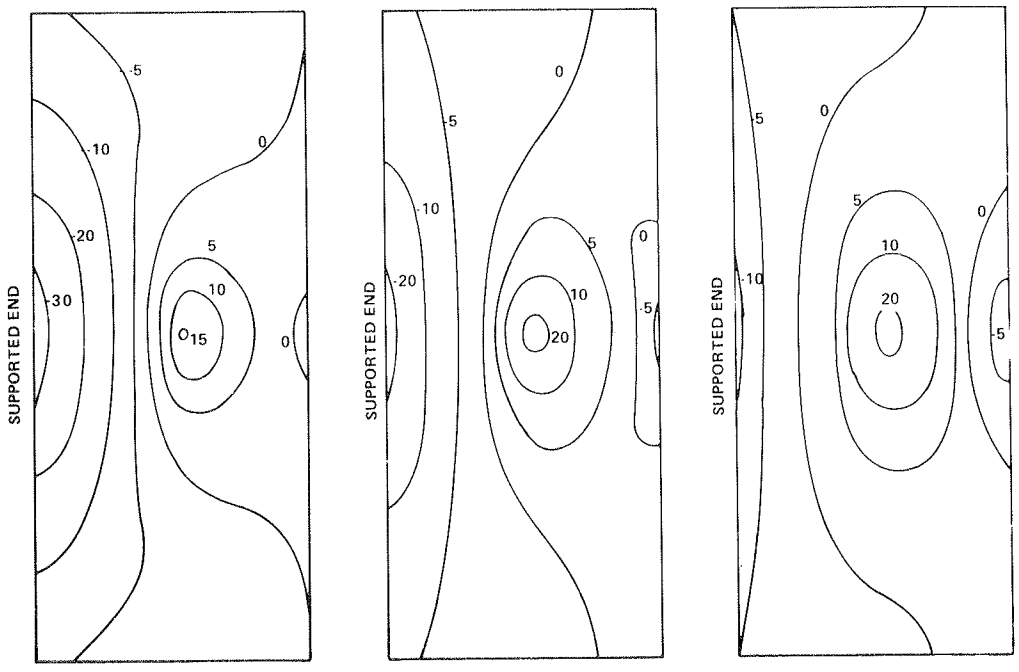

a) QUEST RUN No. 1 b) QUEST RUN No. 2 c) QUEST RUN No. 3

FIGURE 8 Moment diagram, 100-kN wheel (kN·m/m).

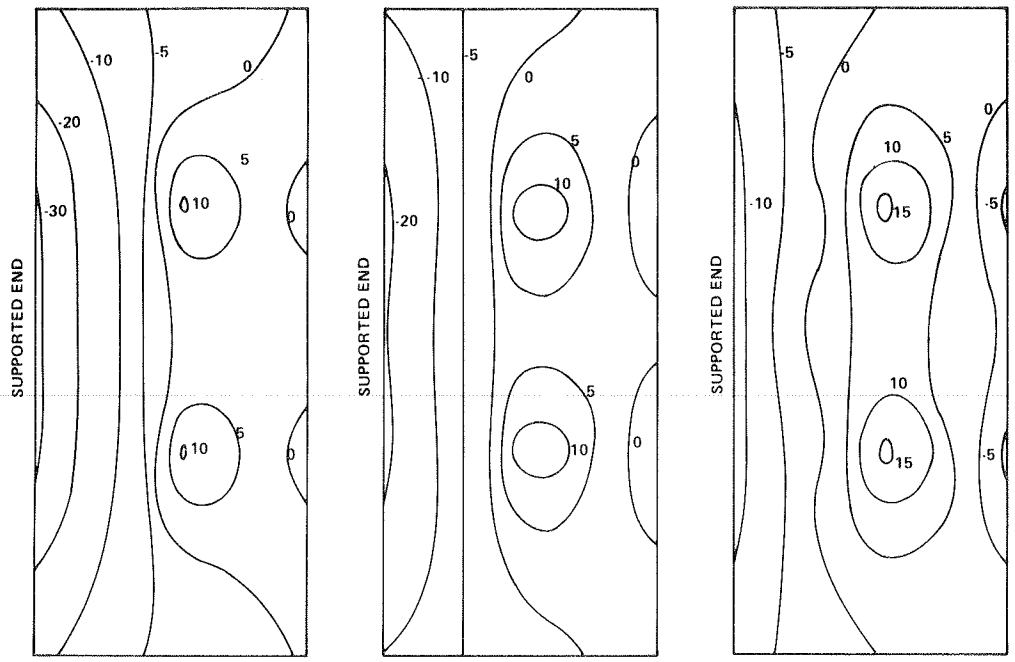

a) QUEST RUN No. 1 b) QUEST RUN No. 2 c) QUEST RUN No. 3

FIGURE 9 Moment diagram, 2- to 70-kN wheels (kN·m/m).

method outlined in the OHBDC for cantilever spans greater than 1.2 m can handle this condition. Figure 3 is used to compute the value for the coefficient A' (Equation 2). A comparison of Figures 8 and 9 clearly shows the difference between the two load conditions. Local effects are present at the two points of loading. At the support end the moments are more uniform because the loading has been spread into two discrete point loads. The various bending moments are given in Table 2. The OHBDC method and the finite-element method yield the same result (32.5 kN•m/m) for the condition of no barrier wall. The maximum negative moment decreases to 21.8 kN•m/m when the barrier wall effect is introduced, and it further decreases to 11.9 kN•m/m when a flexible support is introduced.

The results indicate that the OHBDC analysis, based on the method for spans greater than 1.2 m, shows a satisfactory comparison to the finite-element results, not including edge stiffening. The introduction of a continuous barrier wall causes a significant reduction in the maximum moment effect. A flexible support causes a further reduction in moment. None of the designer-oriented formulations given in Table 1 takes into account the significant effect that end support flexibility has on the load-distribution characteristics of the cantilever slab.

ANALYSIS OF EDGE-STIFFENED CANTILEVER SLAB

The finite-element results for unstiffened cantilever slabs compared favorably with the OHBDC method for slabs with spans greater than 1.2 m. The OHBDC method is based on a manual method developed by Bakht and Holland (4). The method gives a simple procedure to analyze the problem of concentrated loads on elastic cantilever slabs of linearly varying thickness made of isotropic materials. However, the effect of edge stiffening is not included. A subsequent paper by Bakht (5) takes into account the effect of edge stiffening by elaborating on the method given by Bakht and Holland (4). Equation 2 can be used with a new series of curves for A' that take into account the effect of the edge stiffening as a parameter of the ratio of the moment of inertia of the edge stiffening to the moment of inertia of the section of slab about its middle surface. The introduction of an edge-stiffening beam in the cantilever slab does not change any of the essential conditions. Figure 10 shows the graphs for the new values of the coefficient as developed by Bakht (5).

The data in Table 2 give the results for these coefficients in the column titled Bakht. A comparison of the finite-element results for the second case to these methods indicates a satisfactory comparison, with the former results generally being smaller. For the single wheel load, the method by Bakht (5) underestimates the moment by 6 and 20 percent for the single and the dual wheel load, respectively. Consequently, the results indicate that the simplified methods outlined by Bakht and Holland (4) and by Bakht (5) can reasonably predict moments in cantilever slabs that have rigid support. These methods can be also used for cantilever slabs of semi-infinite length.

The flexibility of the cantilever slab support has a significant effect on the bending moment. However, only an elaborate method of analysis can reasonably predict the moment values. The flexibility of the support will vary with span; consequently, the cantilever slab should be designed for a variable moment along the supported end and consequently should have a varying amount of reinforcing steel along the length of the support end. From a practical point of view this may not be economical. The effect of nonrigid supports appears to be a difficult aspect to incorporate in a design office.

The effect of edge stiffening is shown in Figure 11. The coefficient A' is plotted as a function of the ratio I_B/I_S. (Note that I_B = moment of inertia of edge beam about the middle surface, and I_S = moment of inertia of longitudinal section of slab about its middle surface.) This graph shows that increasing the edge stiffness to cantilever slab stiffness ratio to beyond 15 results in a minimal

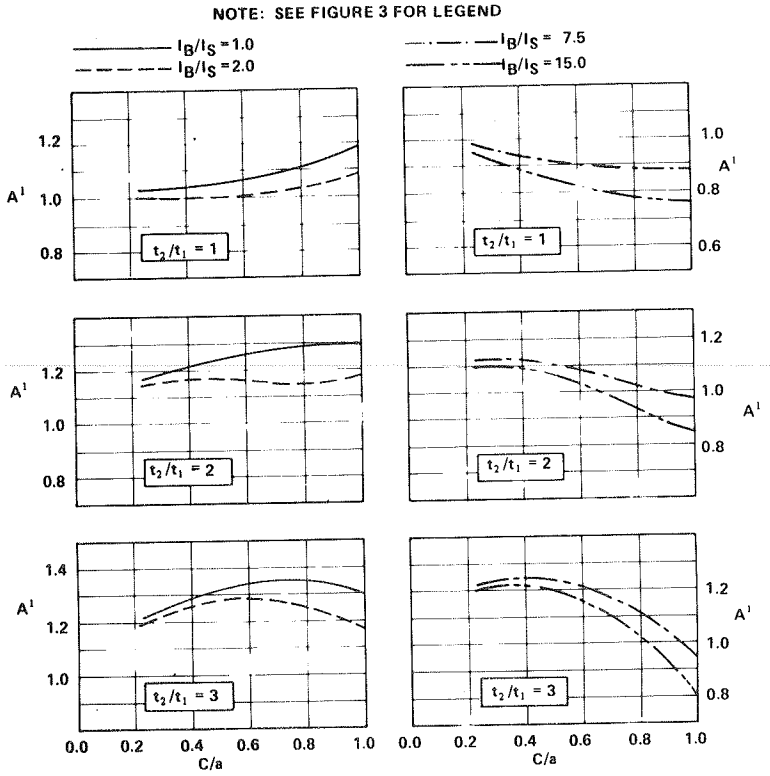

FIGURE 10 Value of coefficient A′ at Y = 0.

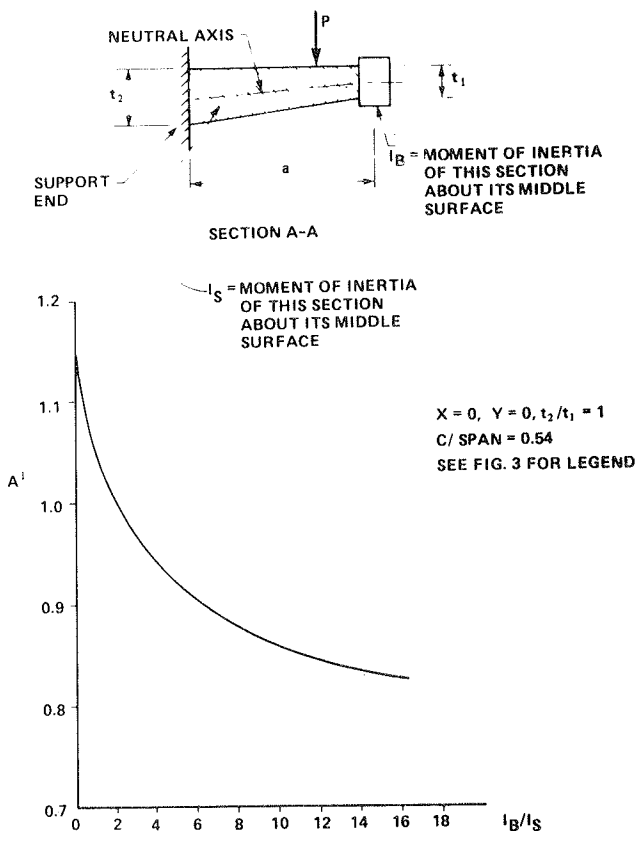

FIGURE 11 Variation of coefficient A′ with ratio I_B/I_S.

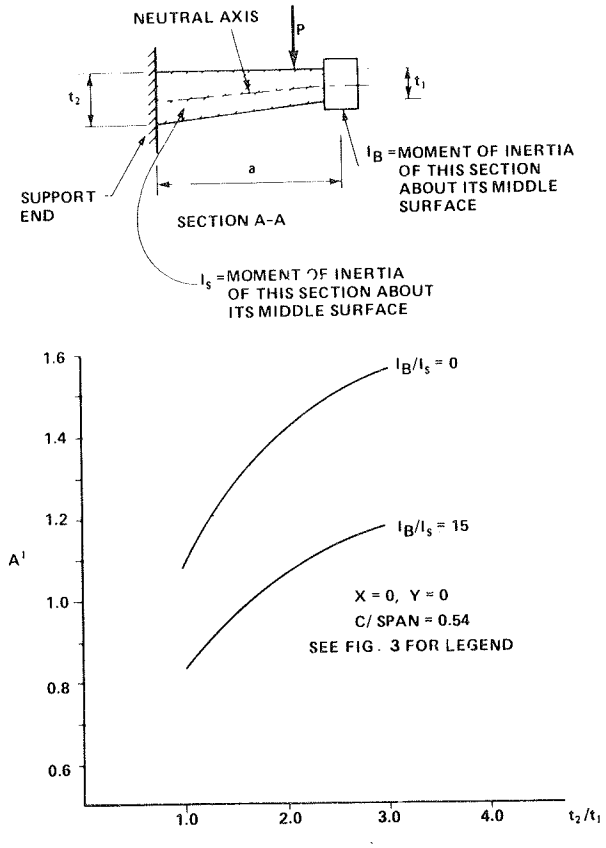

FIGURE 12 Variation of coefficient A′ with ratio t_2/t_1.

decrease to the design moment. For the case shown, the coefficient A', which is proportional to maximum moment, can decrease by as much as 30 percent.

The barrier walls shown in Figure 1 would generally result in a I_B/I_S ratio greater than 15. Sidewalks and curbs can also act as edge stiffening. The ratio of stiffness of a sidewalk compared to that of the supporting cantilever slab, which is typically between 1 and 3, is of a much lower magnitude than for barrier walls. This reduced degree of edge stiffening can still result in a reduction of the maximum moment on the order of 10 to 15 percent.

The effect of varying slab thickness is not considered by AASHTO and was not considered in the finite-element analysis. However, the methods given by Bakht and Holland (4) and Bakht (5) do consider slab thickness variations. For the geometry considered, increasing the slab thickness ratio (t_2/t_1) has the effect of increasing the peak support moments. (Note that t_1 = slab thickness at free edge, and t_2 = slab thickness at supported end.) Figure 12 shows that this increase can be as high as 30 to 40 percent. Consequently, varying thickness could effectively eliminate any beneficial effect of edge stiffening. Generally, the ratio t_2/t_1 does not vary significantly in the typical cantilever slab considered and thereby has little effect on its design.

ECONOMIC CONSIDERATION

By adopting the method of analysis given by Bakht (5), a cost saving can be achieved. By using the current version of the OHBDC for the design of the cantilever slab, the 100-kN wheel load will produce a factored maximum bending moment of 92.5 kN•m/m at the ultimate limit state. To resist this moment, the 230-mm slab with a nominal cover of 70 mm would require 2200 mm² of reinforcing steel per meter of slab. This translates into 20M bars at 135-mm centers. By considering the effect of the barrier wall, the maximum bending moment is only 71.2 kN•m/m. The reinforcing-steel requirement is 1600 mm², or 20M bars at 185 mm.

It can be seen that a savings of 27 percent, or 600 mm²/m length of cantilever, can be achieved. If it is assumed that the cantilever steel is terminated approximately 1.5 m past the centerline of the girder (see Figure 1), the total length of the reinforcing-steel bars would be 3.0 m. With a cantilever slab along each side of the bridge, this translates into a mass savings of 28 kg/m of bridge length. For a bridge length of 60 m, the savings in mass would be 1700 kg and would result in a total savings of approximately $2,100 (assuming cost of epoxy-coated reinforcing steel to be $1,250/t). (Note that $1 Canadian = $0.810 U.S.)

Less reinforcing steel is necessary when the barrier wall is taken into account; therefore, smaller bars or a larger concrete cover can be used. These two features increase the durability of the concrete slab when it is exposed to deicing chemicals.

A potential savings is also possible for rehabilitation. During rehabilitation the existing substandard barrier walls of many bridges are upgraded to current standards. Often there is also a need to widen the existing bridge deck. A narrow widening could be achieved by simply adding to the cantilever length. By taking into account the better distribution of the live load caused by the presence of the barrier wall, the structural capacity of the existing cantilever slab may be sufficient; otherwise, the existing cantilever slab would have to be removed and replaced or somehow strengthened.

CONCLUSIONS AND RECOMMENDATIONS FOR FURTHER RESEARCH

The finite-element analysis confirms that standard barrier walls significantly enhance the distribution of live-load effects in cantilever deck slabs. The maximum live-load bending moments in the direction of the span decrease by 33 percent.

A general simplified method of analysis based on the extension of a method specified in the OHBDC (2) and developed by Bakht (5) can be used for the design of cantilever deck slabs with barrier walls. This method can be used for determining moments anywhere along the slabs, including areas of the slab near deck expansion joints.

Several parameters that affect the behavior of a cantilever slab subjected to live load have not been considered.

1. The effect of construction joints in the barrier walls was not considered. These construction joints have no reinforcement passing through them, and consequently a weak link exists. Because these joints are still effective in compression but not in tension, their presence needs to be considered. The local discontinuity should not have a significant effect on the deflection characteristic of the system because the overall stiffness of the barrier wall would not be affected. Consequently, these discontinuities should have little effect on the distribution of moments.
2. The investigation considered only point loads. In reality, the wheel loads are patch loads of finite area, thereby spreading the concentrated load over a larger area. This effect may result in an even better distribution and a decrease in the local moment effect directly under the wheel loads.
3. The effect of nonhomogeneity of the concrete slab (such as cracking, honeycombing, and so forth) on the load distribution was not considered.

These three items should be investigated. Prototype full-scale models should be constructed and monitored to ensure satisfactory behavior and agreement with the theoretical approach.

REFERENCES

1. Standard Specifications for Highway Bridges, 12th ed. AASHTO, Washington, D.C., 1977.
2. Ontario Highway Bridge Design Code, 1979. Ontario Ministry of Transportation and Communications, Downsview, Ontario, Canada, Jan. 1979, Vol. 1, Section 7.
3. H.M. Westergaard. Computation of Stresses in Bridge Slabs due to Wheel Loads. Public Roads, Vol. 2, No. 1, March 1983, pp. 1-23.
4. B. Bakht and D.A. Holland. A Manual Method for the Elastic Analysis of Wide Cantilever Slabs of Linearly Varying Thickness. Canadian Journal of Civil Engineering, Vol. 3, 1976, pp. 523-530.
5. B. Bakht. Simplified Analysis of Edge Stiffened Cantilever Slabs. ASCE, Journal of the Structural Division, Vol. 107, No. ST3, March 1981, pp. 535-550.
6. HECB/B/14 (QUEST). Highway Engineering Computer Branch, Department of the Environment, London, England, undated.

Publication of this paper sponsored by Committee on Concrete Bridges.

Proposed Replacement of AASHTO Girders with New Optimized Sections

BASILE G. RABBAT and HENRY G. RUSSELL

ABSTRACT

Structural efficiency and cost-effectiveness of bridges built with pretensioned I-sections and T-sections and a cast-in-place deck were evaluated. Selected precast, prestressed sections produced in the United States were compared with AASHTO and Prestressed Concrete Institute (PCI) girders. Spans in excess of 80-ft (24.4 m) were considered. Bulb-T, Colorado, and Washington girders were more structurally efficient than AASHTO-PCI girders. Cost analyses were performed on existing Bulb-T, Colorado, Washington, and AASHTO girders, and on modified counterparts with 6-in.-thick (152-mm) webs. Bulb-T's were found to be the most cost-effective girder, with estimated cost savings of 17 percent on the in-place cost of girders and deck compared with the AASHTO girders. For equal span length, girder spacing, and truck loading, modified Bulb-T's required up to 25 percent less prestressing force than the AASHTO girders. Modified Bulb-T's are recommended for use as national standards. Ways of implementing the proposed new optimized sections are suggested.

The standard AASHTO and Prestressed Concrete Institute (PCI) girders, types I through VI, were developed in the late 1950s and early 1960s. Standardization has led to simplified design and economical bridge construction (1). In the past 25 years there have been significant advancements in the technology of prestressed-concrete design and construction. Individual state highway departments developed their own standards for improved efficiency and economy. With new designs entering the market, the question became: How efficient are the standard AASHTO girders?

OBJECTIVES

This investigation was undertaken to evaluate the latest prestressed-concrete bridge girder designs being used in the United States and to determine which designs represent optimum designs that could be promoted as national or regional standards. The investigation was limited to bridges built with pretensioned I-sections and T-sections, for spans in excess of 80 ft (24.4 m), and with concrete compressive strengths up to 7,000 psi (48.3 MPa).

SCOPE

The objectives were accomplished within the following scope:

1. Current precast, prestressed-concrete girders with composite cast-in-place deck designs being used in the United States were summarized;
2. Creative new concepts becoming available through research were reviewed;
3. Girders representing optimum designs and exhibiting strong potential for standardization were determined; and
4. Recommendations for standardization of the most practical and cost-effective designs were made.

RESEARCH APPROACH

The project was divided into two phases. In phase 1 information was collected throughout the United States on a regional basis from selected highway agencies and producers. Advantages and disadvantages of the concepts inventoried were assessed.

In phase 2 structural efficiency and cost-effectiveness of the best existing designs, as well as some modified ones, were evaluated relative to the efficiency of AASHTO sections. This included evaluation of structural parameters such as girder spacing, span length, concrete strength, and deck thickness.

A computer program was developed for use in the parametric studies. A relative unit cost index was assigned to girder and deck-slab concretes, prestressing strands, and reinforcing steel. The cost index reflected in-place relative costs for the finished girder and deck. Costs of materials and labor were included. Data generated by the computer program were used to determine the most cost-effective girders and to develop design charts.

Survey results of phase 1, computer program documentation, and results of phase 2 analyses are available in a detailed report (2). A summary of the cost-effectiveness analyses and a sample design chart are presented in this paper.

COST-EFFECTIVENESS ANALYSIS

Cross Sections Analyzed

Comparisons of the structural efficiency of existing girders indicated that the most efficient sections were Bulb-T, Washington series, and Colorado G54 and G68 sections (2). Bulb-T's have been used successfully in the Pacific Northwest. A set of Bulb-T sections was developed in 1959 by Anderson (3). These sections, as well as the Washington series and Colorado G68, have 5-in.-thick (127-mm) webs. Strands deflected within the webs of these sections are bundled. End blocks are also used in these girders.

Several survey participants expressed concern about possible difficulties in manufacturing and transporting girders with 5-in.-thick webs. The main concerns were consolidation of the concrete in thin and deep members and stability of such slender members during transport. On the other hand, some survey participants believed that current AASHTO girders can be improved by reducing their web thickness.

At a meeting held in April 1980, members of the PCI Committee on Bridges were asked about the minimum practical web width to place and consolidate the concrete in precast, prestressed I-sections. All committee members were in favor of a minimum web thickness of 6 in. (152 mm). (Note that these data

are from the minutes of the PCI Committee on Bridges meeting held April 15, 1980, at the Ramada O'Hare Inn, Des Plaines, Illinois, J. Barker, chairman.)

Standard AASHTO bridge girders types I and II have 6-in.-thick webs. In all regions of the United States, concrete has been placed and consolidated in these sections without difficulty. Therefore, in phase 2 sections with 5-in.-thick webs were evaluated and compared with similar sections with 6-in.-thick webs. Sections with 6-in.-thick webs should be easier to manufacture and transport than sections with 5-in.-thick webs.

Existing and modified sections analyzed for cost-effectiveness are shown in Figures 1 and 2.

Structural Parameters

The sections were evaluated through a detailed

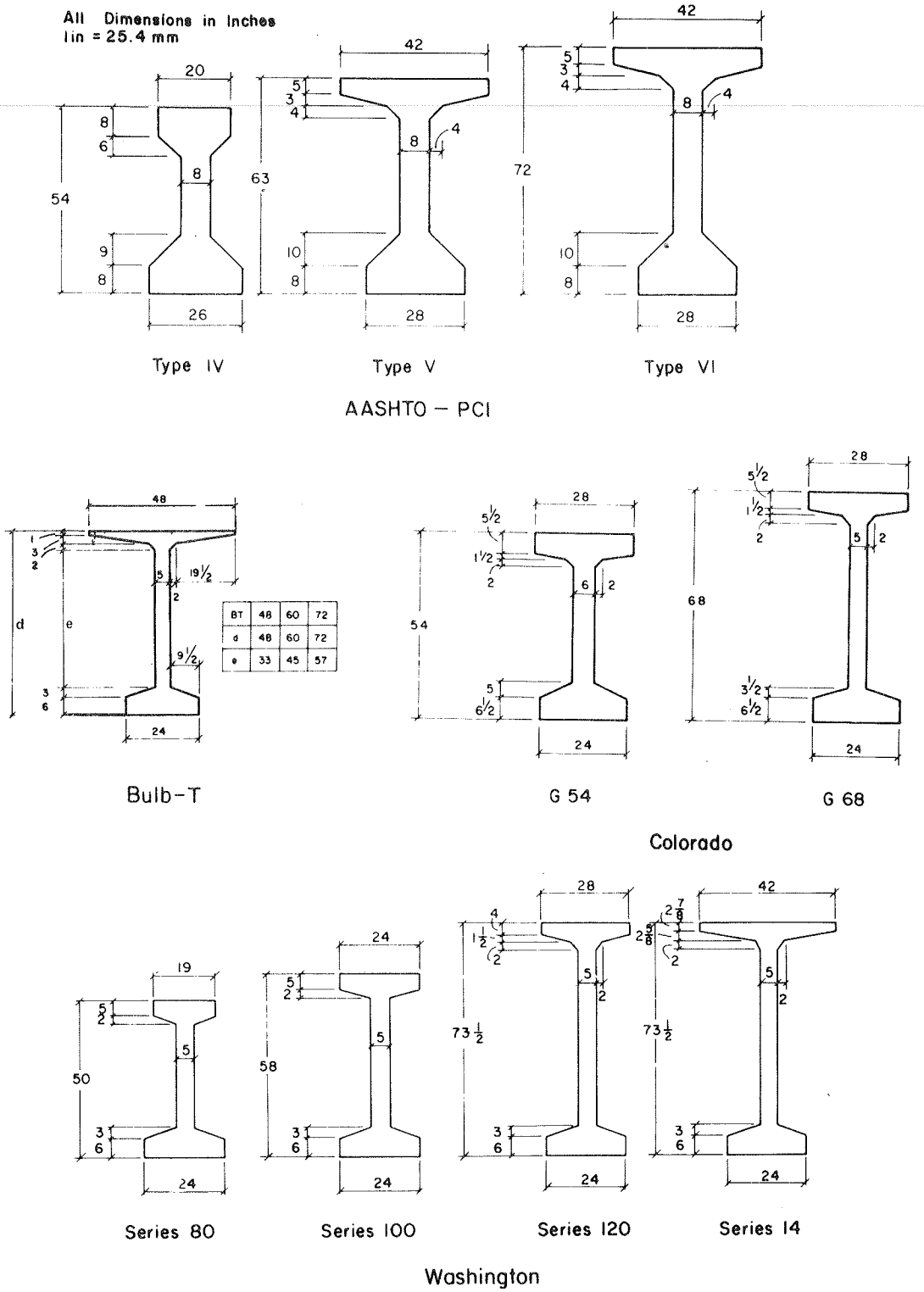

FIGURE 1 Existing girders analyzed.

structural analysis. Parameters considered in the analysis included girder spacing, span length, deck thickness, and concrete strength. Girder spacing was varied between 4.5 and 10 ft (1.37 and 3.05 m). Spans in excess of 80 ft (24.4 m) were considered. Deck thickness varied with girder spacing. Concrete strength for girders was varied between 5,000 and 7,000 psi (34.5 and 48.3 MPa).

Development of Computer Program

To evaluate the effect of each variable, a parametric study was carried out. The number of variables necessitated preparing a computer program to analyze each case and to generate cost data. This program, called BRIDGE, required input of girder span, spacing, and cross section; concrete and strand characteristics; and relative costs of materials. The program determined deck thickness and reinforcement, required number of strands, and cost index per unit surface area of bridge deck.

The following assumptions were made in program BRIDGE:

1. Design conforms to AASHTO specifications (4).
2. Live load consists of HS20-44 loading.
3. Girders are simply supported.
4. A typical interior girder is considered.
5. Concrete deck is cast-in-place and acts compositely with the girder. Deck formwork is sup-

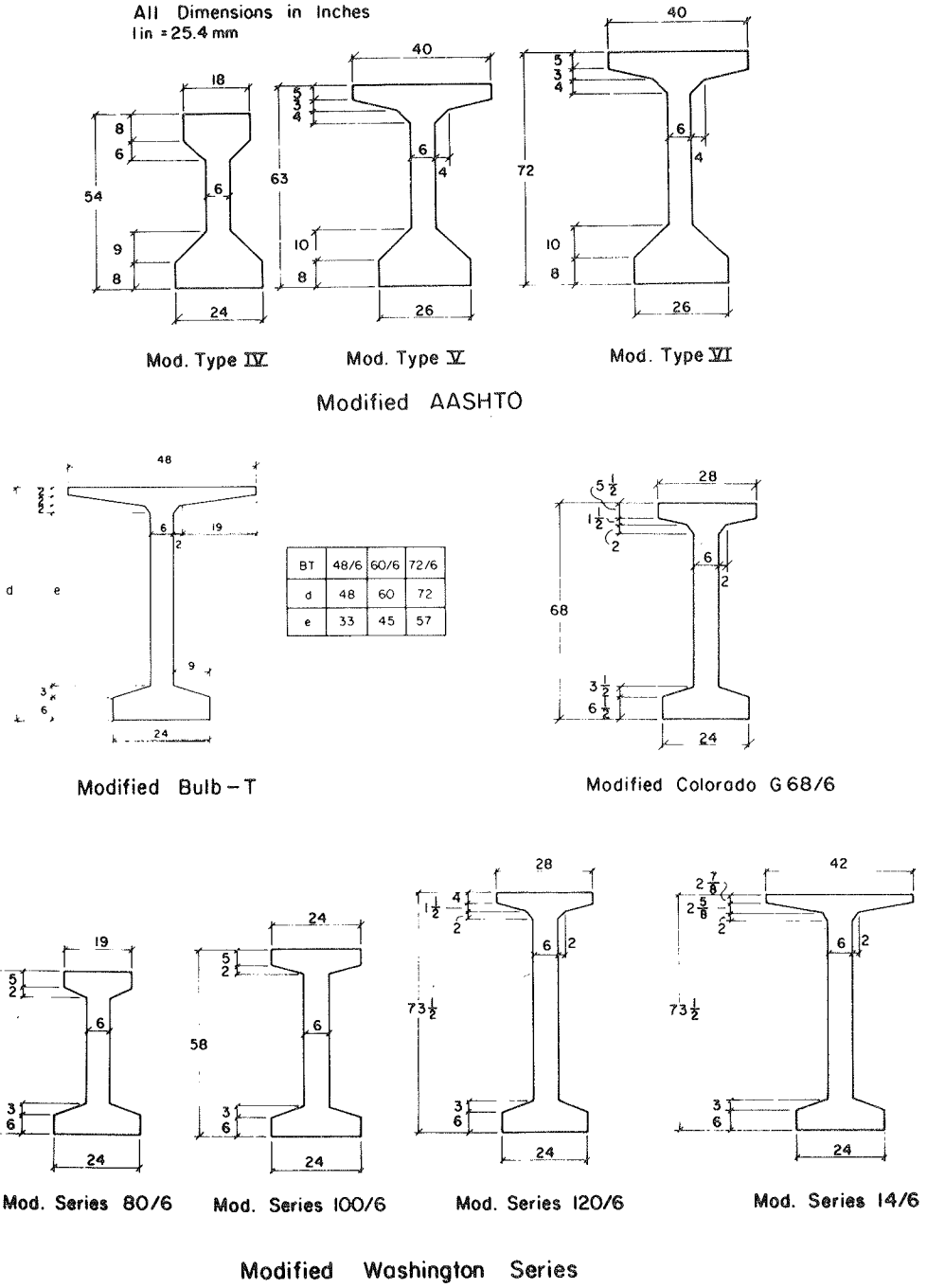

FIGURE 2 Modified girders analyzed.

ported on the girder. In calculations of the composite section properties, the transformed area of strands is neglected.

6. Concrete compressive strength of the deck is constant and equal to 4,000 psi (27.6 MPa) at 28 days.

7. Strands are grade 270 (1862 MPa) stress relieved, with 0.5-in. (12.7-mm) diameter and have an idealized trilinear stress-strain curve.

8. Total prestress losses are constant and equal 45,000 psi (310 MPa).

9. Initial or long-term camber or sag does not govern design, as the AASHTO specifications (4) do not specify deflection limits for concrete bridges.

10. Cost of materials, labor, transportation, and erection of girders with concrete compressive strengths between 5,000 and 7,000 psi (34.5 and 48.3 MPa) is assumed constant. The effect of increasing the girder concrete strength from 5,000 to 7,000 psi on the in-place cost of the girder is negligible.

11. Relative unit costs of materials and labor are constant for the cost analysis. All girders are compared on a common basis.

12. Cost analysis comparisons are for precast girders and a cast-in-place deck. Cost of substructure and approach fills are not considered.

13. Additional costs from the use of end blocks in all girders that have 5-in.-thick (127-mm) webs are ignored.

Relative Unit Cost Indexes

Several factors affect the cost of the superstructure. Costs of material and labor vary from region to region, between states of a region, between districts of a state, and within a district according to bridge location. An assessment of local and regional factors was not possible within the scope of this investigation. However, a cost analysis was possible by comparing the cost of the recommended sections on a common basis.

From survey data an average cost was determined for girder concrete, deck concrete, reinforcing steel, and prestressing strands. These average costs included materials and labor. For girder concrete, the cost also included transportation and erection. Average costs were then reduced to relative costs per pound of in-place material. The following relative unit costs for in-place materials (including labor) were used for the cost analyses: concrete (girders and deck), 1 unit per pound; strands, 8 units per pound; reinforcing steel, 9 units per pound; and epoxy-coated reinforcing steel, 12 units per pound.

Girders were compared based on the same unit costs. The relative costs of materials were taken as the product of material weight and relative unit costs. The summation of relative costs of materials was then divided by deck area to give a cost index per square foot. Additional weight and therefore cost of concrete required for the end blocks of girders that have 5-in.-thick webs were ignored.

Optimum Cost Index Charts

By using the BRIDGE program, a cost chart (2) was prepared for each of the sections shown in Figures 1 and 2. The same relative unit costs for in-place materials (material and labor), as well as material properties, were assumed for all girders and decks. A representative chart is shown in Figure 3. This figure shows the cost index per square foot of deck versus span length for an AASHTO type VI girder. The solid lines are for selected girder spacings. Maximum girder spacing was set at 10 ft (3.05 m). The dashed line is an optimum cost curve.

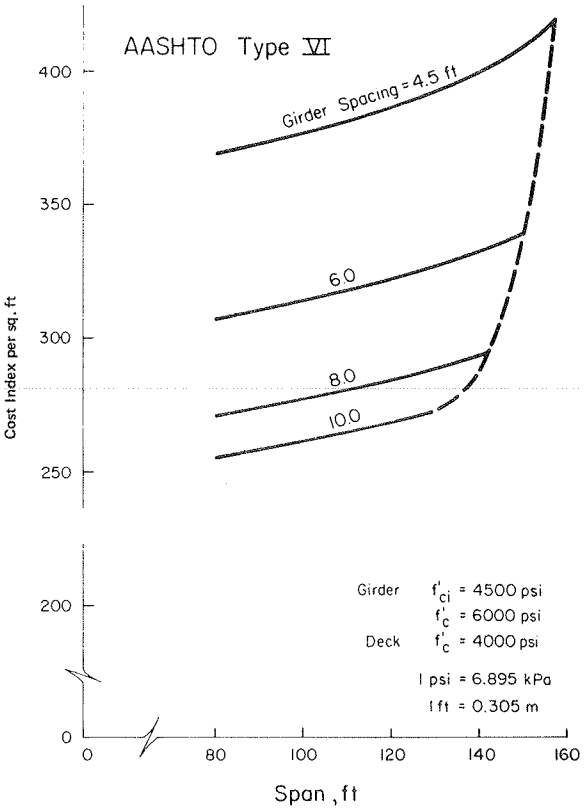

FIGURE 3 Cost chart for AASHTO type VI girder.

Figure 3 illustrates the effect of girder spacing on cost. For a given span, as girder spacing increases, unit cost per square foot of bridge deck decreases. For an AASHTO type VI section, if girders are spaced 10 ft apart, the cost per unit area of bridge deck is 30 percent less than if girders are spaced 4.5 ft (1.37 m) apart. Therefore, it is most economical to place girders at the largest practical girder spacing. This fact has already been suggested by Scott (5) and Jacques (6).

COST-EFFECTIVENESS COMPARISONS

Optimum cost curves were used to compare the cost-effectiveness of selected girders. Girder spacing ranged between 4.5 and 10 ft (1.37 and 3.05 m). A few selected cases are compared here.

Overall Comparisons

Optimum cost curves for AASHTO type VI, Colorado G68, Washington series 14, and Bulb-T BT72 girders are compared in Figure 4. These girders are intended to be used for spans in excess of 100 ft (30.5 m). The data in Figure 4 indicate that the Bulb-T BT72 is the most economical girder for spans up to 135 ft (41.2 m), and that the AASHTO type VI girder is the most expensive.

Modified girders G68/6, series 14/6, and BT72/6 are compared with an AASHTO type VI girder in Figure 5. For spans up to 140 ft (42.7 m), the modified Bulb-T BT72/6 is the most economical and is, on average, about 3 percent cheaper than a modified Washington series 14/6 girder.

Modified Bulb-T's are compared with AASHTO sections in Figure 6. For spans from 80 to 120 ft (24.4 to 36.6 m), modified Bulb-T's yield savings of about 17 percent when compared with the AASHTO

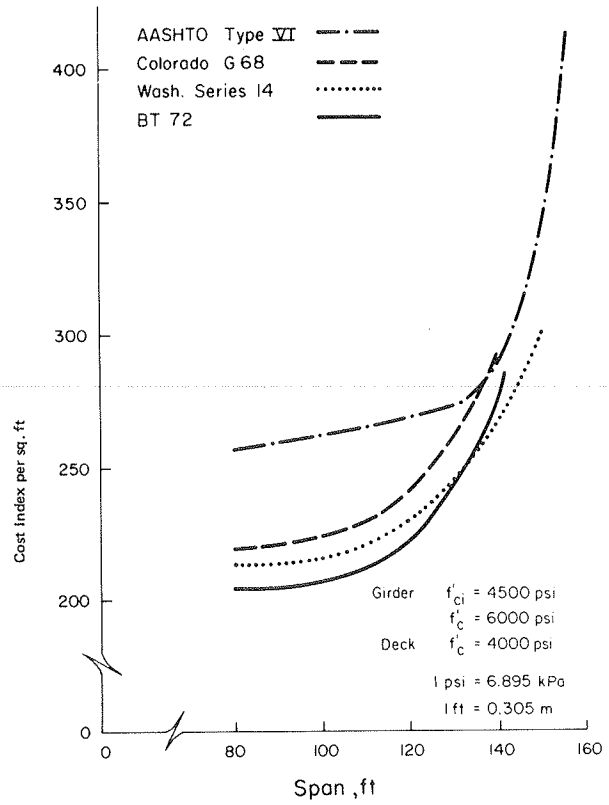

FIGURE 4 Comparison of optimum cost curves for AASHTO type VI, Colorado G68, Washington series 14, and Bulb-T BT72.

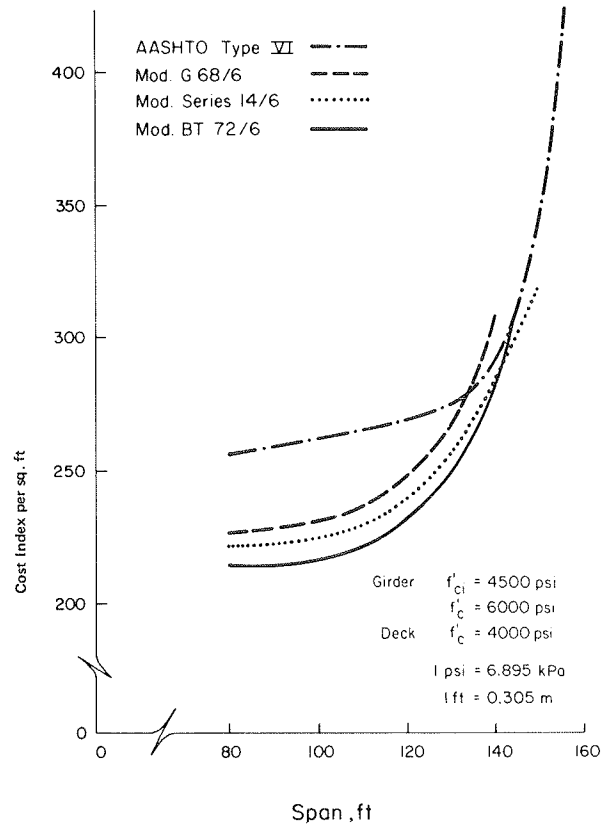

FIGURE 5 Comparison of optimum cost curves for AASHTO type VI and modified G68/6, series 14/6, and BT72/6 girders.

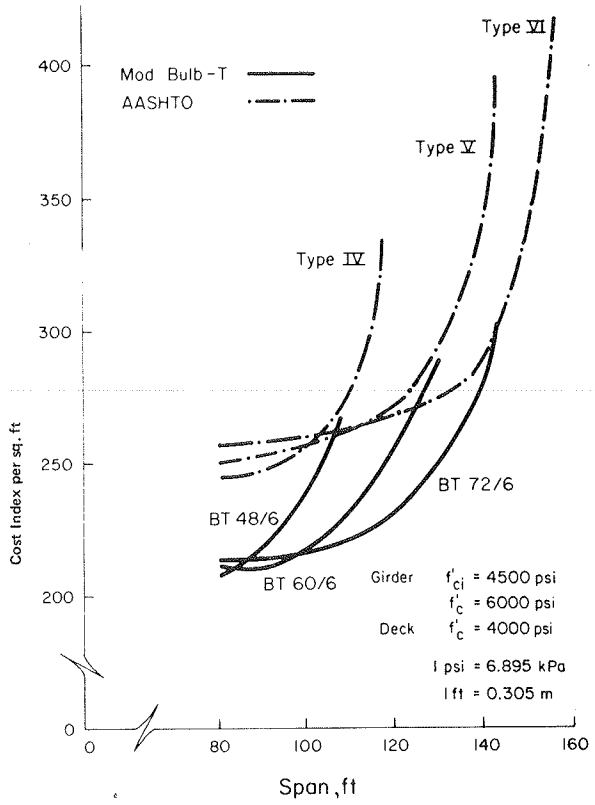

FIGURE 6 Comparison of optimum cost curves for modified Bulb-T's and AASHTO girders.

girders. For spans of 120 to 140 ft, cost savings vary from 17 down to 2 percent.

Web Thickness

Comparisons of Bulb-T, Washington series, and Colorado G68 sections with 5-in.-thick (127-mm) webs and similar sections with 6-in.-thick (152-mm) webs indicate that girders with 6-in.-thick webs cost 3 to 5 percent more than similar girders with 5-in.-thick webs. However, survey results from phase 1 indicate that sections with 6-in.-thick webs are easier to manufacture throughout the United States. All sections with 5-in.-thick webs have end blocks. Additional labor and material costs and girder weight resulting from the use of end blocks were ignored. However, if costs of end blocks are considered, differences in costs of sections with 5-in.-thick web versus sections with 6-in.-thick web would be somewhat less than indicated.

Comparisons between AASHTO sections and modified AASHTO sections with 6-in.-thick webs indicated that modified AASHTO sections yield cost savings of 6 percent when compared with AASHTO sections.

Effect of Concrete Strength

In all comparisons the concrete compressive strength of the girder was assumed to be 6,000 psi (41.4 MPa). Some girders were analyzed assuming 5,000 and 7,000 psi (34.5 and 48.3 MPa) concrete. The effect of concrete compressive strength on optimum cost curves is shown in Figure 7 for an AASHTO type VI girder. Comparisons indicate that by increasing the concrete compressive strength of the girder from 5,000 to 7,000 psi, maximum span capability of a section was increased by about 15 percent.

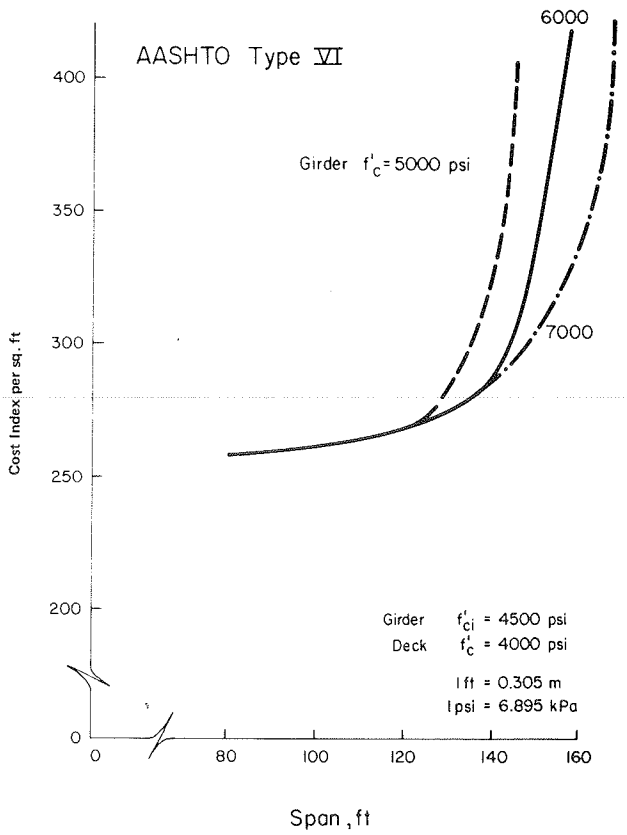

FIGURE 7 Variation of optimum cost curves with concrete compressive strength for AASHTO type VI girder.

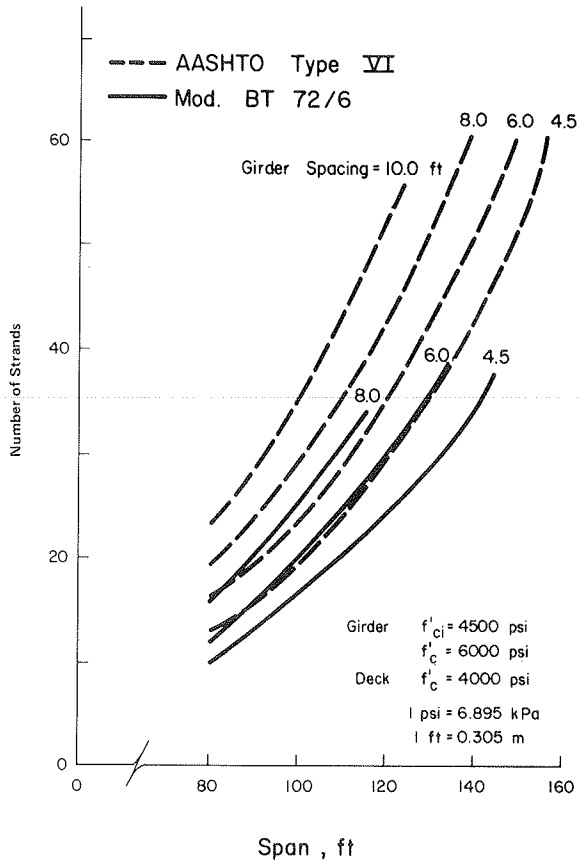

FIGURE 8 Required number of strands in AASHTO type VI girder and modified Bulb-T BT72/6.

Effect of Bundling Strands

In the comparisons given in the previous subsection strands were assumed to be spaced 2 in. (50.8 mm) on center at midspan. Strands were positioned as low as practical in the section to obtain maximum eccentricity of the prestressing force. Some girders were analyzed by assuming that strands were bundled at midspan. Comparisons indicated that overall cost savings and an increase in span capability from bundling of strands were negligible.

REQUIRED PRESTRESSING FORCE

Both modified Bulb-T BT72/6 and AASHTO type VI girders are 72 in. (1.83 m) deep. The number of seven-wire 0.5-in.-diameter (12.7-mm) stress-relieved strands needed in these girders is shown in Figure 8. Plotted are the number of required strands versus girder span for different girder spacings.

Because the modified Bulb-T BT72/6 is 35 percent lighter than the AASHTO type VI girder, it requires fewer strands. Therefore, the magnitude of the initial prestressing force is smaller. Consequently, existing prestressing abutments for AASHTO type VI girders would be adequate for prestressing the modified Bulb-T BT72/6.

The data in Figure 8 indicate that AASHTO type VI girders can be used at a girder spacing of 10 ft (3.05 m). Maximum girder spacing for the modified Bulb-T BT72/6 is approximately 8.5 ft (2.6 m) (2). For equal span, girder spacing, and truck loading, the modified Bulb-T BT72/6 requires 15 to 25 percent fewer strands than the AASHTO type VI girder.

SI CONVERSION

Recently, new International System of Units (SI), metric, sections were adopted in Canada under an arrangement agreed to by the prestressed-concrete producers. For an unspecified period of time, bridges in Canada will be designed by using the new metric sections, but alternate designs will be produced based on existing nonmetric sections. Because the new sections are more efficient than the existing ones, it was believed that the changeover would be accelerated by the competitive need to use the new sections. Some of the new metric sections are currently being produced in Ontario.

CONCLUSIONS

Based on the cost-analysis results discussed previously, the following conclusions have been drawn.

1. For girders with 5-in.-thick (127-mm) webs, the most cost-effective sections are Bulb-T's. For spans from 80 to 120 ft (24.4 to 36.6 m), Bulb-T's have 20 percent less in-place cost for girder and deck compared with AASHTO girders. For spans of 120 to 135 ft (36.6 to 41.2 m), the cost reduction for Bulb-T's varies from 20 to 5 percent. The next most cost-effective sections with 5-in.-thick webs are the Washington series.
2. In most regions of the United States it may not be easy to consolidate the concrete in girders with 5-in.-thick webs. Moreover, in these girders the strands must be bundled at midspan, and end blocks are needed to conform with minimum concrete cover requirements.

3. By using girders with 6-in.-thick (152-mm) webs, it will be possible to economically consolidate girder concrete in all regions of the United States. However, the use of girders with a 5-in.-thick web will be beneficial where experience has demonstrated the thickness to be satisfactory.
4. For girders with 6-in.-thick webs, the most cost-effective sections are modified Bulb-T's. For spans of 80 to 120 ft, modified Bulb-T's have 17 percent less in-place cost for girder and deck compared with AASHTO girders. For spans of 120 to 140 ft (36.6 to 42.7 m), the cost reduction varies from 17 to 2 percent.
5. Reduction of top and bottom flange widths and web thicknesses of AASHTO types IV, V, and VI girders by 2 in. (50.8 mm) reduces the overall inplace cost of girders and deck by about 6 percent. Span capability of the modified sections is not affected by these changes in width.
6. The overall in-place cost of girders and deck is decreased substantially by placing girders at the largest practical girder spacing.
7. An increase in the concrete compressive strength of the girder from 5,000 to 7,000 psi (34.5 to 48.3 MPa) increases the span capability of AASHTO girders by about 15 percent.
8. Bundling of strands at midspan to increase eccentricity of prestress does not lead to any significant overall cost reduction for the girders considered.
9. For equal span and girder spacing, modified Bulb-T's require up to 25 percent less prestressing force than the AASHTO girders.

RECOMMENDATIONS

Based on the conclusions in the previous section, the following actions are recommended:

1. Modified Bulb-T girders with 6-in.-thick (152-mm) webs are recommended for use as national standard precast, prestressed-concrete bridge girders in the United States for spans from 80 to 140 ft (24.4 to 42.7 m);
2. Girder spacing should be as large as possible; and
3. If metrication is adopted in the United States, modification of the previous sections to SI units should be considered as part of any standardization.

IMPLEMENTATION

Construction of the Interstate highway system has been completed in some states. In most states it is close to completion. Therefore, the rate of bridge construction on the Interstate system is much slower than it was from the late 1950s to the early 1970s. Nevertheless, according to statistics prepared by the Bridge Division of the FHWA, considerable new bridge construction and major reconstruction is ongoing.

The cost of new prestressed-concrete bridge construction and bridge rehabilitation with participation of federal funds authorized during calendar year 1982 totaled $767 million. Based on bridge inventory and inspection records, it is anticipated that "in the next 20 to 30 years, we will have over $30 billion worth of bridge construction based on the value of the dollar today" (7). Revenue from the recently legislated $0.05 tax on gasoline has increased the funds allocated for bridge construction by about 25 percent.

As previously mentioned, selection of bridge type is based on economy. Safety standards for Interstate and other high-speed highways require greater clearances. Therefore, there is need for construction of bridges with spans of 110 to 130 ft (33.5 to 39.6 m). In all states surveyed, except California, the most economical bridges for spans of approximately 70 to 130 ft (21.3 to 39.6 m) are constructed with pretensioned bridge girders.

Cost analyses indicate that modified Bulb-T's can yield savings of 17 percent on the overall cost of girder and deck compared with AASHTO girders. Also, the modified Bulb-T's are about 35 percent lighter than AASHTO girders for comparable spans. A 140-ft (42.7-m) AASHTO type VI girder is extremely heavy and therefore difficult to transport on highways. Lighter sections with 140-ft spans have been transported on highways with no difficulty.

Although steel forms constitute a capital investment, their life span is limited to about 10 years. Where new forms are needed, new plants built, or improved sections sought, optimized sections should be considered. Capacity of existing stressing beds or abutments will be adequate for the modified Bulb-T's, as these sections require up to 25 percent less prestressing force than the AASHTO girders.

The implementation of new sections should be gradual over a period of time. It will require effort on the part of both departments of transportation and producers. Preparation of design aids for the new sections will encourage and facilitate implementation of the new sections. A sample preliminary design chart is shown in Figure 8, where design curves have been superimposed for the modified Bulb-T BT72/6 and the AASHTO type VI girder.

Highway agencies should be informed of the economic benefits that can be achieved with optimized sections. Departments of transportation will have to design with old and new sections over a transition period. The Canadian experience in switching to new metric sections sets an example of implementation of new sections under an arrangement agreeable to producers and highway agencies.

ACKNOWLEDGMENT

This investigation was sponsored by FHWA. Thomas Krylowski was the contract manager, and his cooperation was greatly appreciated.

Several states and producers participated in the survey. The Prestressed Concrete Institute, members of the PCI Committee on Bridges under James H. Barker, chairman, and other individuals provided information. Their numerous contributions are gratefully acknowledged.

This investigation was conducted under the direction of W. Gene Corley, divisional director, Engineering Development Division, Construction Technology Laboratories, a division of the Portland Cement Association. This paper is based on Portland Cement Association Research and Development Bulletin RD80.

REFERENCES

1. Precast Concrete Elements for Transportation Facilities. NCHRP Synthesis of Highway Practice 53. TRB, National Research Council, Washington, D.C., 1978, 48 pp.
2. B.G. Rabbat, T. Takayanagi, and H.G. Russell; Construction Technology Laboratories. Optimized Sections for Major Prestressed Concrete Bridge Girders. FHWA, U.S. Department of Transportation, July 1981, 172 pp.

3. A.R. Anderson. Systems Concepts for Precast and Prestressed Concrete Bridge Construction. In TRB Special Report 132: Systems Building for Bridges, TRB, National Research Council, Washington, D.C., 1972, pp. 9-21.
4. Standard Specifications for Highway Bridges, 12th ed. AASHTO, Washington, D.C., 1977, 496 pp.
5. N.L. Scott. Suggestions for Reducing Costs in Prestressed Concrete Bridges. In Highway Research Record 34, HRB, National Research Council, Washington, D.C., 1963, pp. 117-129.
6. F.J. Jacques. Study of Long-Span Prestressed Concrete Bridge Girders. Journal of the Prestressed Concrete Institute, March-April 1971, pp. 24-42.
7. L.A. Herr and F.D. Sears. Bidding and Contract Arrangement in Bridge Construction. Journal of the Prestressed Concrete Institute, July-Aug. 1980, pp. 38-40.

Publication of this paper sponsored by Committee on Concrete Bridges.

Proposed Limit State Strength Evaluation of Existing Reinforced-Concrete Bridges

ROY A. IMBSEN and ROBERT A. SCHAMBER

ABSTRACT

Because of several catastrophic bridge failures, bridge safety has been emphasized during the past decade. As a result there has been a concerted effort to develop and disseminate procedures for systematic bridge inspection and rating. Although bridges with concrete superstructures rarely fail catastrophically, gradual deterioration and increased loads can affect their structural capacity. Existing procedures for inspecting and rating bridges with concrete superstructures are limited. A summary of a methodology proposed for rating reinforced-concrete bridges is presented. The methodology was developed in the first phase of an NCHRP project to improve strength evaluations of existing reinforced-concrete bridges. The methodology is presented in a limit-states format by using approximate load and resistance factors. By using this format a basis is provided on which probability theory and engineering judgment can be rationally combined to allow for independent consideration of each of the major variables that can affect the determination of the load capacity of a bridge. This methodology includes consideration of the level of effort in maintenance and inspection, the degree of load-limit enforcement, the quality of construction, the refinement used in simulating the bridge, the effects of deterioration on the load-carrying capacity, and the degree of refinement in determining the load-distribution factors.

Currently, the procedure for evaluating reinforced-concrete bridges in the United States is based on AASHTO guidelines published in the Manual for Maintenance Inspection of Bridges (1). Experience has demonstrated that the structural capacity of reinforced-concrete bridges usually exceeds the capacity calculated by the conventional techniques presented in this manual.

Many engineers recognize the built-in conservatism in the current approach to the evaluation of bridge strength. Factors that tend to cause the capacity of reinforced-concrete bridges to be underestimated include

1. Material strengths that exceed nominal values used for evaluation,
2. Conservative assumptions used in calculating structural resistance (i.e., zero tension in concrete),
3. Interaction of structural components in resisting and distributing the loads,
4. Structural redundancies, and
5. Overestimation of the loads.

INTRODUCTION

To make improvements in the bridge evaluation process that will lead to more realistic evaluations while still preserving public safety requires a rational consideration of each of the five factors previously mentioned. One method for making such improvements is through a limit-states approach based on probabilistic concepts. This approach was used in the recently developed Clause 12 of the Canadian Standards Association Bridge Code (2-4).

The proposed methodology for evaluating existing bridges incorporates such a limit-states approach. Although the methodology represents a significant change in the current philosophy, from the user's

point of view it is similar to the current AASHTO load-factor approach. It should be emphasized that the user need not understand the statistical basis of the methodology to effectively apply it to the evaluation of a structure. The specific values included in this paper for load and resistance factors are based on a combination of preliminary statistical data and engineering judgment. These values should be considered as preliminary and are intended only to illustrate the overall approach of the methodology.

DEFINITION OF PROPOSED LIMIT-STATES EVALUATION

When a structure or structural element becomes unfit for its intended purpose, it is said to have reached its limit state (5,6). Limit states fall into two categories: safety limit states and serviceability limit states. Structural reliability is the probability that a given structure will perform satisfactorily by not reaching its limit state over a specified time period.

Safety limit states (i.e., ultimate limit states) correspond to the ability of the structure or structural component to support the applied loads. Serviceability limit states either restrict the normal use of a bridge or affect its durability. The acceptable level of structure reliability will vary, depending on the type of limit state used in the calculations.

EVALUATION PROCESS

The limit-states evaluation process (see Figure 1) described in this paper consists of the following steps.

Step 1--collection of information: field inspection, office records, and special testing;
Step 2--selection of rating vehicle: standard vehicle, overload vehicle, and special permit vehicle;
Step 3--analysis: identification of critical failure mode(s), determination of nominal load effects, and determination of nominal resistance;
Step 4--selection of load and resistance factors: charts and engineering judgment; and
Step 5--determination of rating factors.

The results of the structural strength evaluation may be used to determine restrictions on the use of the bridge by normal traffic (load limit posting), the maximum weight of the occasional overload vehicle allowed to mix with normal traffic (unsupervised overload permit), or the absolute maximum weight of any vehicle allowed on the bridge under controlled circumstances (supervised overload permit). In addition, a substandard live-load capacity may also be justification for future repairs or replacement or both.

PROPOSED RATING EQUATION

The basic structural engineering equation states that the resistance of a structure must equal or exceed the demand placed on it by loads. Stated mathematically,

$$R \geq \sum_{k=1}^{n} Q_k \qquad (1)$$

where R is the resistance and Q_k is the effect of load k. The solution of this simple equation encompasses the whole art and science of structural engineering, including the disciplines of strength of materials, structural analysis, and load determination. This equation applies to design as well as to evaluation. In structural evaluations the objective is to select the maximum allowable live load. In the case of bridge evaluations, this usually means the maximum vehicle weight.

Any rational and tractable approach to the analytical solution of the basic structural engineering equation requires that the modes of failure be identified to establish the resistance. The location, types, and extent of the critical failure modes must be determined. The equation must be solved for each of these potential failure modes.

Because neither the resistance nor the load effect can be established with certainty, safety factors must be introduced that give adequate assurance that the limit states are not exceeded. This may be done by stating the equation in a load and resistance factor format.

Separate load or resistance factors that will account for each of the major sources of uncertainty may be introduced to the equation. The basic rating equation used in the proposed approach is simply a special form of the basic structural engineering equation, with load and resistance factors introduced to account for uncertainties that apply to the bridge evaluation problem; that is,

$$RF = \left[(\phi R/\alpha) - \sum_{i=1}^{m} \gamma_i^D D_i - \sum_{j=1}^{n} \gamma_j^L L_j (1.0 + I)\right] / [\gamma_R^L L_R (1.0 + I)] \qquad (2)$$

where

RF = rating factor (the portion of the rating vehicle allowed on the bridge),
ϕ = capacity reduction factor,
m = number of elements included in the dead load,
α = simulation factor,
R = nominal resistance,
n = number of live loads other than the rating vehicle,
γ_i^D = dead-load factor for element i,
D_i = nominal dead-load effect of element i,
γ_j^L = live-load factor for live load j other than the rating vehicle(s),
L_j = nominal traffic live-load effects for load j other than the rating vehicle(s),
γ_R^L = live-load factor for rating vehicle,
L_R = nominal live-load effect for rating vehicle, and
I = live-load impact factor.

Equation 2 should be evaluated for both the safety and the serviceability limit states. The following subsections discuss the philosophy and parameters considered for each of the variables in this proposed rating equation.

Simulation Factors

The capacity of an existing bridge is evaluated by simulating the hypothetical failure scenario that is most likely to occur within the life expectancy of the bridge. A mathematical model, field inspection, test results, and engineering judgment are typically used in this simulation. A simulation factor (α) is introduced to account for the refinement or level of effort used in simulating the actual failure scenario. Three levels of simulation were selected initially (see Table 1). Requirements for field inspection, analysis, and the rater/checker must be met or exceeded before the tabulated simulation factors can be used.

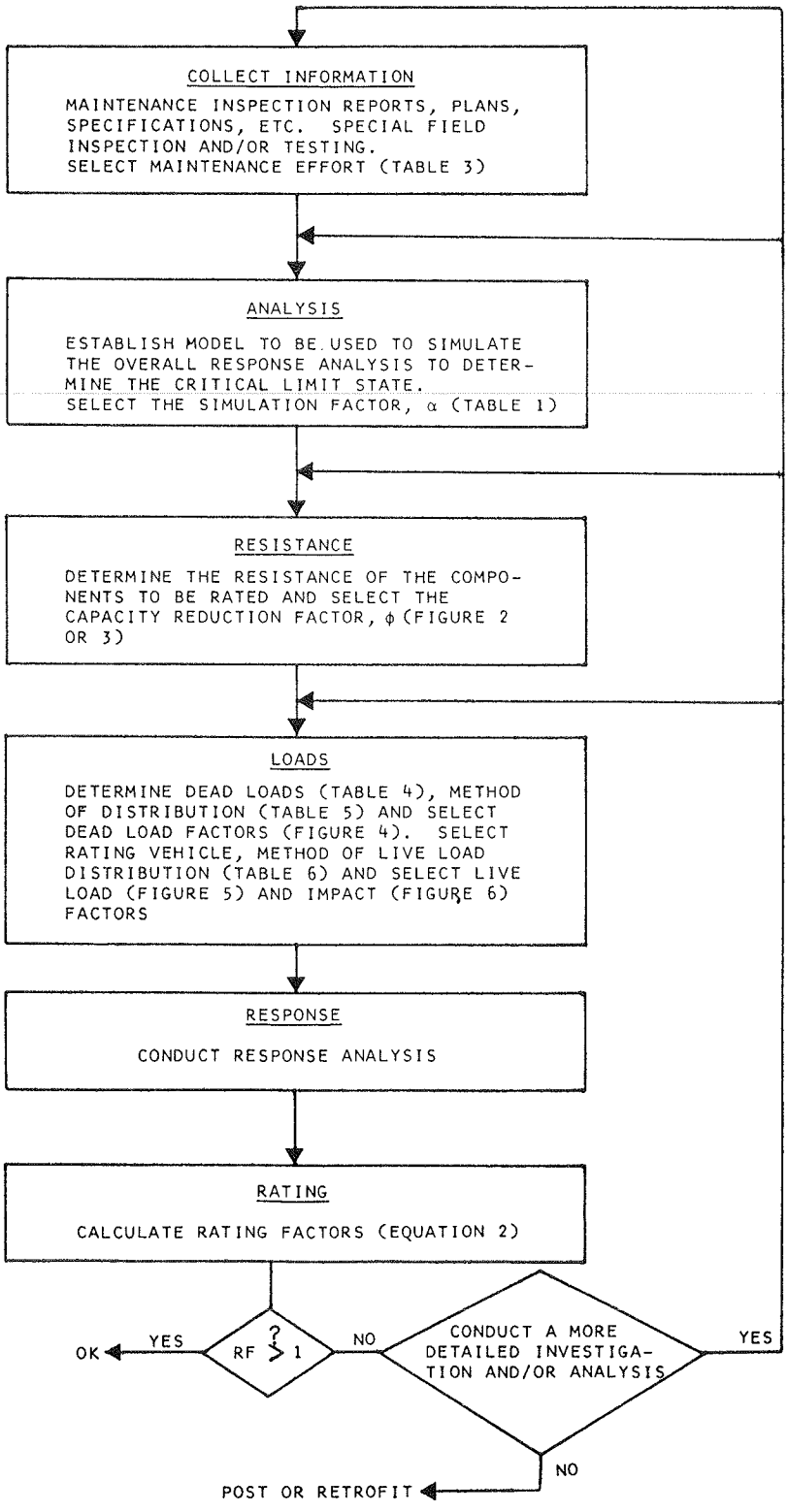

FIGURE 1 Flowchart of evaluation process.

TABLE 1 Simulation Factors

Factor	Field Inspection	Analysis	Rater/Checker
0.95	Detailed: conducted by rater or checker; will include determination of location and extent of deterioration; structural dimension verified by field measurement; some field testing may be required	Detailed: some secondary structural effects considered (finite element, grid, orthotropic plate, three-dimensional space frame in conjunction with influence surfaces)	Both rater and checker are professional engineers with at least 1 year of experience in rating bridges
1.0	Normal biennial maintenance inspection conducted by professional engineer or qualified inspector; structural dimensions taken from plans; rater to review maintenance records	Detailed: only primary effects considered (two-dimensional plane frame in conjunction with AASHTO live-load distribution factors)	Either rater or checker is professional engineer with at least 1 year of experience in rating bridges
1.05	Normal biennial maintenance inspection; some structural dimensions assumed; maintenance records not reviewed	Approximate: simplified idealization of structure that includes only the most critical primary effects (neglect structure continuity, and so forth)	Rater is a professional engineer with at least 1 year of experience; no independent check conducted

Resistance

The determination of the structural resistance (R) of a structure or structural component is one of the primary tasks in the evaluation process. In a limit-states approach it is necessary to define the limit states at which resistance will be determined. Regardless of the material or structure type, these limit states should provide for similar structural performance.

Safety Limit States

Safety limit states are those states that correspond to the maximum load-carrying capacity of a structure or component. These limit states should be set at a low probability of occurrence because failure of the structure or component can lead to loss of life as well as to major financial losses. Safety limit states include

1. Loss of equilibrium of all or part of the structure considered as a rigid body (e.g., overturning, sliding, uplift);
2. Loss of load-bearing capacity of members because of insufficient material strength, buckling, fatigue, fire, corrosion, or deterioration;
3. Overall instability of the structure (e.g., P delta effect, wind flutter, seismic motions); and
4. Extremely large deformation (e.g., transformation into a mechanism).

In the case of reinforced-concrete structures subjected to traffic live loads, the safety limit state is assumed to occur when an individual component such as a girder reaches its ultimate capacity and forms a plastic hinge. In most cases this state does not present a serious threat to safety. The actual threat to safety occurs when enough plastic hinges are formed within the structure to result in a collapse mechanism. Many studies have indicated that this will normally occur at a loading significantly greater than the load at which the first plastic hinge was formed. This is because most reinforced-concrete structures have a high level of structural redundancy. Therefore, what is currently defined as the safety limit state would in most cases be more appropriately called a severe damage limit state.

The nominal resistance of reinforced-concrete members at the safety limit state is the ultimate strength of any given member. Strength calculations should take into consideration the observable effects of deterioration, which may include (but are not limited to) loss of concrete or steel cross-sectional area, loss of composite action, or reduced material strengths.

It is proposed that the strength of sound concrete shall be assumed to be equal either to the values taken from the plans and specifications or to the average of the construction test values. When neither of these values are available, the ultimate stress of sound concrete may be assumed to be 3,000 psi. A reduced ultimate stress should be assumed for unsound or deteriorated concrete, unless evidence to the contrary is discovered by field testing.

To allow for undetected structural weaknesses, it is proposed that the area of tension steel to be used in computing the ultimate flexural strength of reinforced-concrete members should not exceed 75 percent of the reinforcing required for a balanced condition. The steel yield stresses proposed for various types of reinforcing steel are given in Table 2.

TABLE 2 Yield Stress of Reinforcing Steels

Reinforcing Steel	Yield Stress, F_y (psi)
Unknown steel (before 1954)	33,000
Structural grade	36,000
Intermediate grade and unknown after 1954 (grade 40)	40,000
Hard grade (grade 50)	50,000
Grade 60	60,000

Serviceability Limit States

Serviceability limit states either restrict the normal use of the bridge or affect its durability. These limit states include

1. Excessive deflection or rotation that affects the use or appearance of the structure or of nonstructural components;
2. Excessive local damage (e.g., cracking, splitting, spalling, local yielding, slip of connection) that affects the use, durability, or appearance of the structure; and
3. Excessive undesirable vibrations.

The most important serviceability limit states in a bridge evaluation are those that tend to affect the durability of the structure and shorten its useful life. Two types of serviceability failures are considered critical for reinforced concrete.

One of these critical serviceability failures is fatigue in the reinforcing steel. This will occur when a large number of repetitive live loads result in large variations in the steel stresses. The critical number of load repetitions is only likely to occur as a result of normal traffic. Because evaluation of the serviceability limit state for fatigue is not used to restrict live loadings, its primary function is to alert the engineer to a potential problem that will warrant more frequent field inspections.

TABLE 3 Maintenance Effort (safety limit states)

Inspection	Preventive Maintenance	Repair	Maintenance Effort
Annual inspections by professional engineer involved in performing or checking structural strength evaluation	Steps taken to prevent further damage	Within 5 years, when capacity is currently impaired or when it may possibly become impaired	1
Annual inspections by professional engineer or qualified inspector	None	None	2
No special inspection	None	None	3

Crack control is the other critical serviceability limit state considered in the evaluation of existing reinforced-concrete bridges. The effect that crack width has on the rate of deterioration of structures exposed to severe environments is still unknown. Nevertheless, there is some concern that excessive crack width can cause an increase in the rate of deterioration, although several other factors not associated with the level of live loading also play a role.

The allowable steel stress limitations are based on fatigue and crack control requirements as described in AASHTO Sections 1.5.38 (Fatigue Stress Limits) and 1.5.39 (Distribution of Flexural Reinforcement) (7). The following conditions are recommended for serviceability limit states:

1. Restrictions of normal traffic (i.e., below posted weight limits) should not be required to maintain serviceability;
2. Fatigue stress limitations should not be considered for occasional overload trucks; and
3. Frequent inspections should be conducted on bridges subject to live loadings that produce steel stresses beyond the recommended allowable stresses for serviceability.

Capacity Reduction Factor

A capacity reduction factor (ϕ) is included in the basic rating equation to account for variation in the calculated resistance. It takes into consideration the dimensional variations of the structure, differences in material properties, future deterioration, and potential inaccuracies in the theory for calculating resistance.

The capacity reduction factor also accounts for variations in inspection and maintenance efforts that limit the ability of the inspector to detect or prevent future deterioration or distress that can potentially result in losses in live-load capacity. The maintenance effort for bridges that show signs of deterioration distress is categorized into three proposed levels (Table 3). The inspection, preventive maintenance, and repair conditions must be met or exceeded before the tabulated value for the maintenance factor is used. Note that maintenance efforts on structures with no observable deterioration or distress, which are inspected biennially by a professional engineer or by a qualified inspector, shall be classified as maintenance effort 1. Maintenance efforts on bridges with observable deterioration shall be classified as either maintenance effort 2 or 3, depending on the amount of deterioration and the frequency of inspection.

The proposed capacity reduction factors for safety limit states shall be taken from Figure 2 for flexure and from Figure 3 for shear. The capacity reduction factor for serviceability limit states shall be equal to 1.0.

Dead-Load Factors

Dead loads, which shall be determined from dimensions on the plans or from field measurements, shall include the weights of each of the permanent parts and appendages of the bridge. Partial dead-load factors are proposed to reflect both the various degrees of control used in producing the structural and nonstructural components of the bridge and the degree of analytical refinement used to determine the distribution of dead load to the structural components. The minimum unit weights of materials to be used in computing the dead load are taken from Table 4.

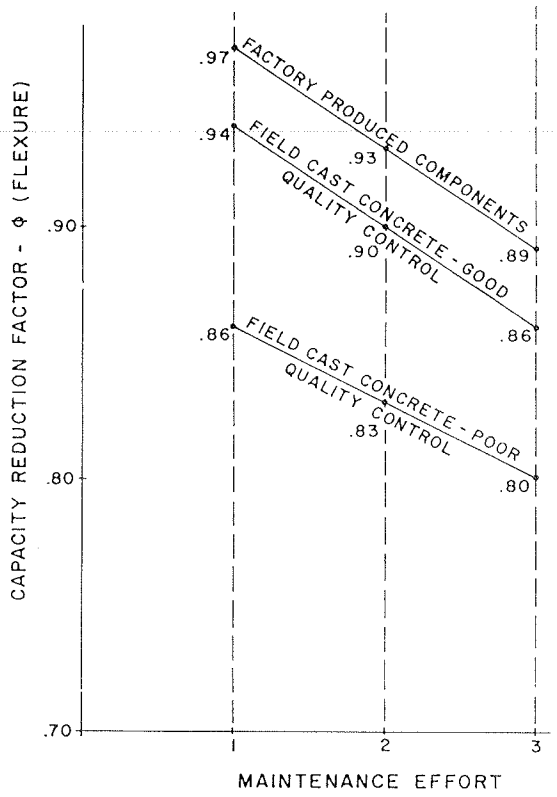

FIGURE 2 Capacity reduction factors—flexure.

The effort used to determine dead-load distribution is categorized into three proposed levels of refinement (Table 5). Once the level of refinement for the dead-load distribution has been selected, separate dead-load factors (γ^D) are obtained for each type of component in the bridge. The dead-load factors proposed for use in the evaluation of safety limit sates are shown in Figure 4. Dead-load factors for serviceability limit states shall be equal to 1.0.

Live-Load Factors

Highway vehicles come in a wide variety of sizes and configurations. No single vehicle can accurately reflect the effects of all of these vehicles. Because it is necessary to limit the number of vehicle configurations to a manageable level in order to

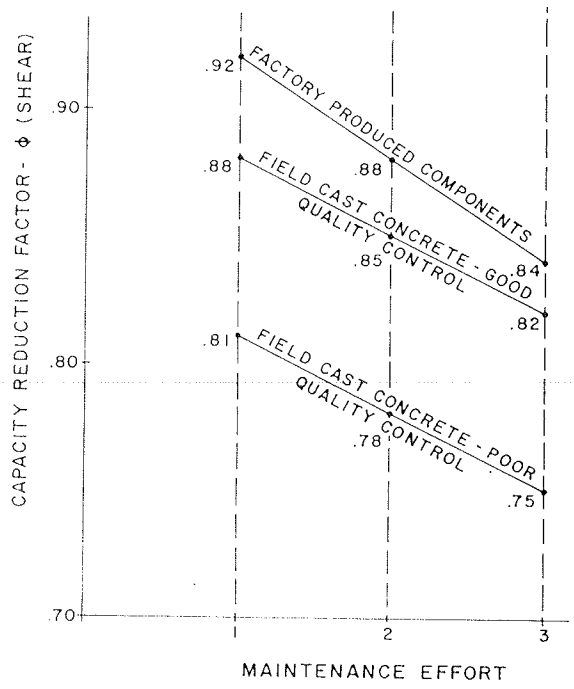

FIGURE 3 Capacity reduction factors—shear.

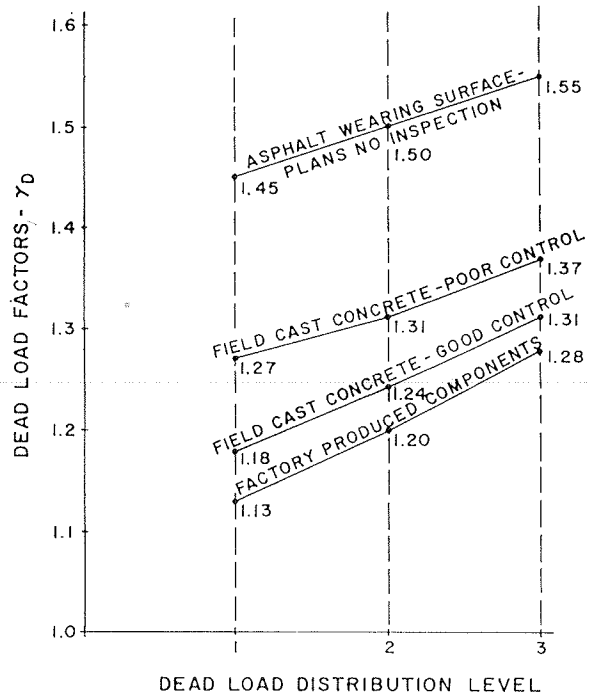

FIGURE 4 Dead-load factors.

keep the evaluation process from becoming too cumbersome, the effect of the actual traffic live loads will vary from predicted values. This variation will usually be greater than the variation in dead-load effect.

Live-load factors (γ^L) are used in the evaluation to account for variations in the maximum live-load effects that are likely to occur during the life of the bridge. Because the effect must be measured in relation to the maximum weight of the vehicles actually allowed on the bridge, it is affected by the amount of control exercised over weight limits. If load limits are strictly enforced or if there is close control of the types of vehicles granted overload permits, the variation in maximum live load will be less, and a smaller live-load factor is justified. If, on the other hand, load limits cannot be adequately enforced and violations are likely, then a higher live-load factor must be used to provide for higher overloads.

The degree of refinement or sophistication used to determine the distribution of live loads to the load-carrying components is also included in the live-load factor. The three proposed levels of refinement are given in Table 6.

The live-load factors proposed for use in the evaluation of safety limit states are shown in Figure 5. Live-load factors for serviceability limit states shall be equal to 1.0.

TABLE 4 Dead-Load Unit Weights

Material	Unit Weight (lb/ft^3)
Asphalt surfacing	144
Concrete, plain or reinforced	150
Steel	490
Cast iron	450
Timber (treated or untreated)	50
Earth (compacted), sand, gravel, or ballast	120

TABLE 5 Dead-Load Distribution Levels

Level	Description
1	Grillage analogy, orthotropic plate, finite element
2	Loadings from tributary areas in which reactions are computed by including the continuity of the structure
3	Loadings from tributary areas in which reactions are computed by assuming simple supports

TABLE 6 Live-Load Distribution Levels

Level	Description
1	Grillage analogy, orthotropic plate theory, finite element, or specially prepared influence surfaces developed by using one of these methods
2	Load distributions based on formulas that have been derived for specific loads, such as AASHTO design live-load distribution factors for AASHTO design loads
3	Load distributions based on formulas that are not specifically intended for the loading under consideration or load distributions based on simple support reactions

Impact Factors

It is proposed that the dynamic effects of moving live loads shall be included in the evaluation of both the safety and serviceability limit states. As part of the development effort for the Ontario bridge code (8), comprehensive studies were conducted on the dynamic effects of moving vehicles. The findings from these studies led to the development of impact factors (I) that are dependent on the dynamic frequency of the bridge deck. The method for calculating impact in the proposed rating equation is specified in the Ontario bridge code.

The impact factor for components of deck slabs with designs governed by a single-axle or dual-axle unit shall not be less than 0.40. In addition, the impact factor for the following items shall not be

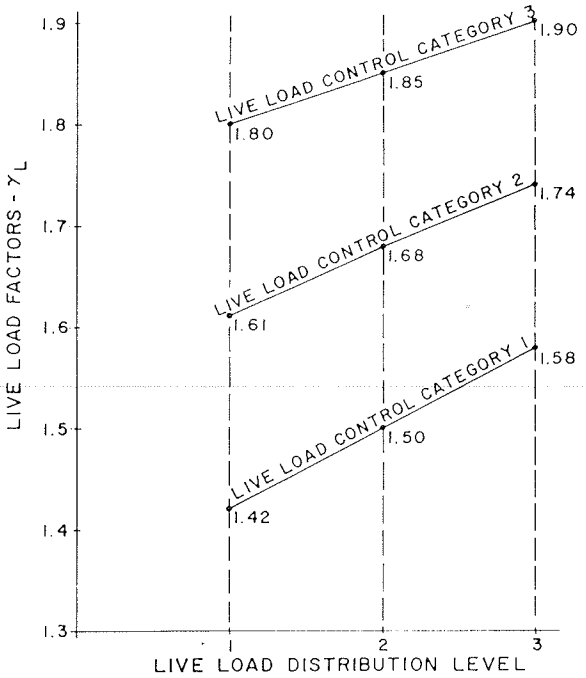

FIGURE 5 Live-load factors.

less than 0.35: (a) floor beams supporting deck slabs, (b) other beams with spans less than 40 ft, and (c) slabs with spans less than 40 ft.

The load factor for each of the main longitudinal components other than those previously mentioned is taken from Figure 6 as a function of the first flexural frequency of the given component. The first flexural frequency may be determined from a dynamic analysis, tests, or an approximate formula (see Equation 3). The impact factor shall be the maximum value obtained from Figure 6 for any frequency within ±10 percent of the calculated value.

For the purpose of determining the impact factor, the first flexural frequency shall be calculated by using the static properties of the materials. In the absence of advanced mathematical modeling techniques or tests, the following approximate formula may be used to obtain the frequency:

$$\text{Frequency (in hertz)} = 400/\text{span (in feet)} \quad (3)$$

ILLUSTRATIVE EXAMPLE

This example is intended to illustrate the application of the proposed methodology. Note that, as mentioned previously, the factors included in the proposed procedure are based on limited statistical data and are only included to illustrate the overall procedure. The bridge selected for this example is a single-span, T-beam structure; its dimensions and member properties are shown in Figure 7. The bridge was constructed in 1925, and it is assumed in this illustrative example that a thorough field inspection revealed insignificant deterioration. Given this assumption, the bridge is to be evaluated for normal traffic loadings. Rating factors will only be calculated for flexure in the interior girders for the following vehicles: AASHTO HS20-44; and legal vehicles: type 3, type 3S2, and type 3-3 (1).

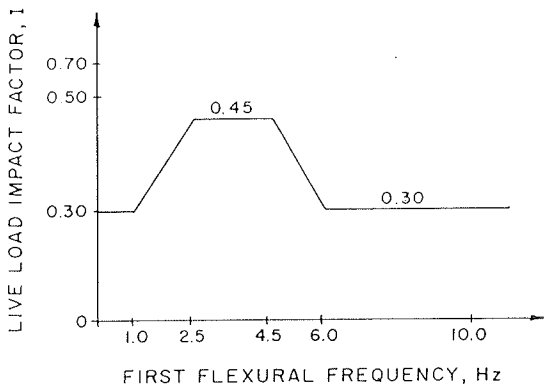

FIGURE 6 Diagram of impact factor.

Simulation Factor

The bridge has been inspected by a qualified inspector as part of the normal biennial inspection. The analysis was performed by using a two-dimensional idealization of the bridge in conjunction with AASHTO load-distribution factors. This evaluation was performed by registered engineers experienced in bridge evaluation. By using the data in Table 1, the appropriate simulation factor is 1.0.

Resistance: Safety Limit States

Concrete

The field inspection revealed that the concrete was sound. Because the plans contained information on the design concrete strength and because construction records are not available, assume that f'_c = 3,000 psi.

Reinforcing Steel

Because the structure was built in 1925 and the reinforcing steel type is unknown, assume f_y = 33,000 psi (Table 2). To calculate the ultimate moment capacity, the following properties were determined from the dimensions on the bridge plans:

1. Gross steel area: A_s = 6.89 in.^{2};
2. Depth of steel: d = 2.22 ft;
3. Depth of concrete compression block: a = 1.14 in. (0.095 ft); and
4. Ultimate moment capacity (resistance): R = $A_s f_y[d - (a/2)]$ = 494 kip-ft.

Resistance: Serviceability Limit States

Because f_y = 33,000 psi is less than the f_y = 40,000 psi limit, serviceability limit states will not be critical. Therefore, no calculations for fatigue or cracking are made.

Capacity Reduction Factor

No deterioration is present, the quality of construction appears satisfactory, and the bridge is on the biennial inspection program. Therefore, the capacity reduction factor (ϕ) taken from Figure 2 is 0.94.

Dead-Load Factors

A summary of the calculated dead loads is as follows:

Concrete section = 0.87 kip/ft,
Rail = 0.22 kip/ft, and
Asphalt concrete (AC) overlay = 0.40 kip/ft.

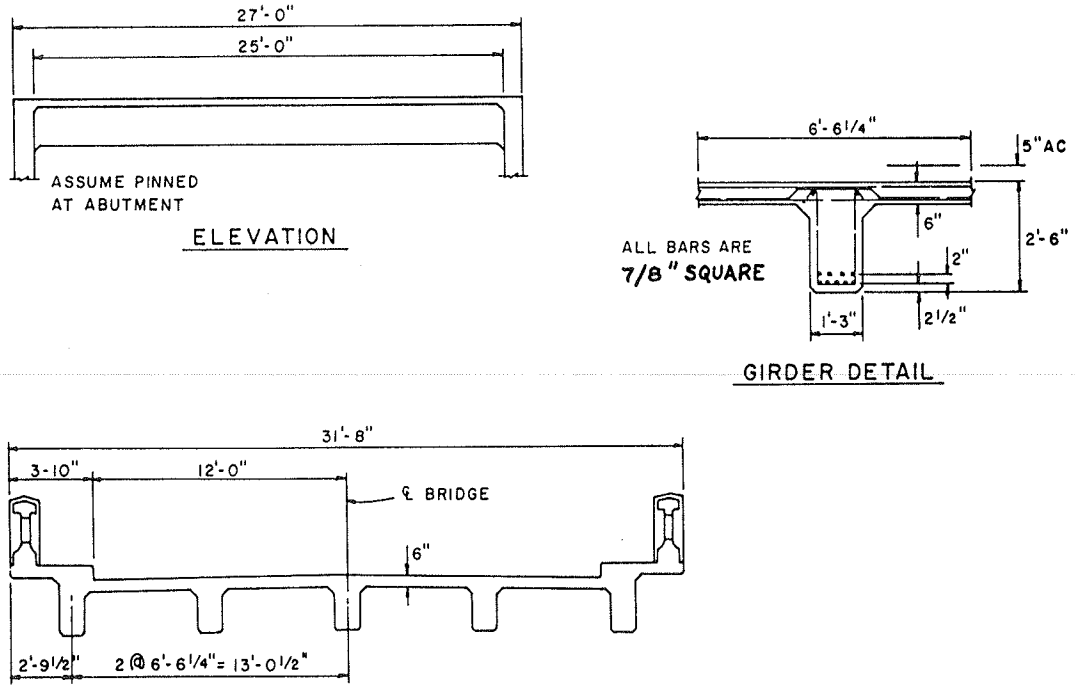

FIGURE 7 Single-span, T-beam bridge evaluated in example.

Different dead-load factors apply to each portion of the dead load. These factors will be selected from Figure 4, level 2, which is based on the tributary areas in which reactions are computed by including the continuity of the structure.

1. Total factored dead load:

$$\gamma_i^D \times w_{DL_i} = \gamma_i^D \times w_{DL_i} \quad (4)$$

Concrete section: 1.24 x 0.87 kip/ft = 1.08 kips/ft,
Rail: 1.31 x 0.22 kip/ft = 0.29 kip/ft, and
AC overlay: 1.50 x 0.40 kip/ft = 0.60 kip/ft.

Thus the total factored dead load = 1.97 kips/ft.

2. Dead-load moment (sum of dead-load effects):

$$\Sigma\gamma_i^D D_i = (\Sigma\gamma_i^D w_{DL_i} L^2)/8 = [1.97 \times (26)^2]/8 = 166 \text{ kip-ft} \quad (5)$$

Live-Load Factors

The live-load moments per wheel line of typical legal vehicles are taken from the AASHTO Manual for Maintenance Inspection of Bridges (1). The live-load moment for the HS20-44 truck was taken from the AASHTO Standard Specifications for Highway Bridges (7): type 3 = 93.5 kip-ft, type 3S2 = 90.2 kip-ft, type 3-3 = 77.0 kip-ft, and HS20-44 = 104.0 kip-ft.

Number of wheel lines = S/6 = 6.52/6 = 1.09 wheel lines.

The live-load distribution factors are based on formulas from AASHTO (level 2 live-load distributions from Table 6). In addition, the control of legal loads is vigorously enforced (category 1 live-load control from Table 7). Therefore, the live-load factor from Figure 5 is 1.50.

TABLE 7 Live-Load Control Categories

Load Limit Enforcement	Overload Sources	Category
Vigorously enforced: roadside weighing of trucks	Reasonable control of overloads at the source	1
Moderate enforcement of weight limits: no roadside weighing of trucks	Limited sources of overloads	2
Weight limits difficult to enforce	Many potential overload sources (mining, logging, and so forth)	3

Impact Factor

By using Equation 3, the calculated frequency is 15 Hz for a span length of 26 ft. The impact factor I = 0.30 is obtained from Figure 6.

Live Load Plus Impact Effect

Calculating the live-load moment effects for a typical interior girder with 1.09 wheel lines gives the following:

Type 3: $L_R(1.0 + I)$ = 93.5 x 1.09 x 1.30
= 132 kip-ft.
Type 3S2: $L_R(1.0 + I)$ = 90.2 x 1.09 x 1.30
= 128 kip-ft.
Type 3-3: $L_R(1.0 + I)$ = 77.0 x 1.09 x 1.30
= 109 kip-ft.
HS20-44: $L_R(1.0 + I)$ = 111.1 x 1.09 x 1.30
= 157 kip-ft.

Evaluation

The evaluation [rating factor (RF)] is calculated as follows:

$$RF = [(\phi R/\alpha) - \Sigma\gamma_i^D D_i]/[\gamma_R^L L_R (1.0 + I)] \quad (6)$$

The evaluation produces the following calculations:

Type 3: RF = [(0.94 x 494)/(1.0 - 166)]/(1.50 x 132) = 1.51.
Type 3S2: RF = [(0.94 x 494)/(1.0 - 166)]/(1.50 x 128) = 1.55.
Type 3-3: RF = [(0.94 x 494)/(1.0 - 166)]/(1.50 x 109) = 1.82.
Type HS20-44: RF = [(0.94 x 494)/(1.0 - 166)]/(1.50 x 157) = 1.27.

In order to compare the results, both the current AASHTO rating factors for HS20 loads that the California Department of Transportation calculated for this bridge by using the load-factor method and the rating factors that the Illinois Department of Transportation calculated by using the allowable stress method are given:

1. Inventory rating factor--California (load factor): RF = 0.97; and Illinois (allowable stress): RF = 0.86; and
2. Operating rating factor--California (load factor): RF = 1.61; and Illinois (allowable stress): RF = 1.44.

CONCLUSIONS

A proposed methodology for evaluating the structural strength of existing reinforced-concrete bridges that was developed in the first phase of an NCHRP project is presented. This methodology for rating bridges rationally combines probability theory with engineering judgment by using a limit-states format that contains both load and resistance factors. A somewhat general approach was taken in preparing the methodology so that all of the relevant variables, including some that have not yet been evaluated by scientific means, can be included in the rating process. The numerical values assigned to the load and resistance factors are based on limited statistical data and some preliminary calibration efforts.

The primary purpose of the proposed procedure is to place all of the variables involved in perspective so that they can be addressed, researched (if needed), and proportionally weighted in order that an overall evaluation procedure can be developed.

ACKNOWLEDGMENT

The authors are particularly grateful for the guidance, assistance, and contributions of Peter Buckland and Fred Moses.

REFERENCES

1. Manual for Maintenance Inspection of Bridges. AASHTO, Washington, D.C., 1982.
2. Design of Highway Bridges. CSA Standard CAN3-S6-M78. Canadian Standards Association, Toronto, Ontario, Canada, Aug. 1978.
3. Design of Highway Bridges, Supplement No. 1-1980. CSA Standard CAN3-S6-M78. Canadian Standards Association, Toronto, Ontario, Canada, April 1980.
4. R.L. Foster, C.W. Peterson, and P.G. Buckland. Commentary on Clause 12, Existing Bridge Evaluation of CAN3-S6-1978, Supplement No. 1-1980. Canadian Journal of Civil Engineering, Vol. 8, 1980, pp. 196-205.
5. J.G. MacGregor. Load- and Resistance-Factor Design of Concrete Highway Bridges. In Transportation Research Record 711, TRB, National Research Council, Washington, D.C., 1979, pp. 1-7.
6. J.G. MacGregor. Safety and Limit States Design for Reinforced Concrete. Canadian Journal of Civil Engineering, Vol. 3, 1979, pp. 484-513.
7. Standard Specifications for Highway Bridges, 12th ed. AASHTO, Washington, D.C., 1977.
8. Ontario Highway Bridge Design Code. Ontario Ministry of Transportation and Communications, Downsview, Ontario, Canada, 1979.

Publication of this paper sponsored by Committee on Concrete Bridges.

Thermal Effects in Concrete Bridge Superstructures

ROY A. IMBSEN and DAVID E. VANDERSHAF

ABSTRACT

The findings of a current research project entitled Thermal Effects in Concrete Bridge Superstructures are highlighted. The research project is sponsored by NCHRP. A brief discussion of the mechanisms of heat transfer as they relate to bridge structures is presented, including the thermal coefficients of various types of different concrete composed of different aggregates. Also included are brief discussions on mean effective bridge temperatures, temperature differentials, and the response analysis for nonlinear temperature gradients. Two case studies of longitudinal thermal response selected from those conducted in the research project are included in this paper. The thermal gradients used in New Zealand, England, and Ontario, Canada, plus those recommended by the Post-Tensioning Institute, are included in the response analysis. In addition, specific recommendations for improving the U.S. design provisions for thermal effects are included.

Traditionally, bridges have been designed to resist only the overall longitudinal movement arising from temperature strain. However, with the recent changes in bridge types, it has become apparent that temperature differentials also exist in bridge superstructures. These temperature differentials cause stresses that should be included in the design procedures. Although the current AASHTO specifications include probable temperature ranges of mean temperature conditions that affect expansion and contraction of concrete bridge superstructures, there is no recommendation for temperature differentials that may occur in individual superstructure sections.

The purpose of this paper is to highlight some of the findings in a current research project, Thermal Effects in Concrete Bridge Superstructures (1), which reviews and evaluates the various procedures that have been proposed for use in considering thermal effects on bridge superstructures. The ultimate goal of the research is to upgrade the current AASHTO code for thermal effects.

There are only a few published accounts of concrete bridges damaged by differential temperature effects. In 1981 Zichner (2) described the fundamentals for determining temperature effects in concrete bridges and indicated that cracks such as those shown in Figure 1 were observed during thorough inspections of several different bridges. The cracks, located in the bottom slabs and girder stems of these box-girder bridges, resulted in part from temperature differences that existed within the individual bridge superstructures.

Recently in Colorado, cracking was experienced in the webs and bottom deck soffits of four cantilever, segmental, prestressed bridges. Two of the bridges are approximately 747 ft long, the third is about 516 ft long, and the fourth is about 449 ft long. The three longer bridges have four spans, whereas the shorter one has three. The three-span bridge, shown schematically in Figure 2, exhibited the greatest amount of cracking (3). The crack patterns on the single-cell bottom deck soffit and webs are also shown in Figure 2. The largest crack width reported is approximately 0.13 in.

HEAT TRANSFER BY RADIATION

Heat transfer by radiation is generally considered to be the most important contribution of heat energy exchange on concrete bridge superstructures. During the daylight hours when the structure is exposed to the sun, especially during the warm summer months, a net gain of heat energy occurs throughout the depth of the structure, primarily as a result of solar radiation impinging on the surfaces of the structure. Conversely, primarily as a result of reradiation to the surrounding environment of the heat energy stored in the structure, a net loss of heat energy occurs during the night. During the summer the temperature in the top surface of the bridge deck is warmer than the soffit, which results in a positive gradient. A negative gradient develops on typical winter nights when the top surface is cooler than the soffit.

THERMAL PROPERTIES OF CONCRETE

The thermal coefficient of expansion for concrete is greatly dependent on its aggregate type and mix proportions (4-7). The cement paste of normal concrete usually has a higher thermal coefficient of expansion than the aggregate in the mix; however, because the aggregate occupies about 75 percent of the volume, it is the thermal expansion characteristics of the aggregate that dictate the anticipated volumetric change during a given temperature change.

Most codes specify an average thermal coefficient of 0.000011 to 0.000012 per degree Celsius (about 0.000006 per degree Fahrenheit) for reinforced concrete. The actual coefficients from laboratory tests on concrete samples (Table 1) vary by as much as 22 percent above and 64 percent below the higher value, depending on the aggregate type.

MEAN TEMPERATURES

Mean or effective bridge temperatures are associated with the long-term (seasonal) movements of a bridge. Bridge codes typically provide detailed guidelines for the calculation of overall longitudinal movements by specifying a range of temperatures that depend on the geographical location of the bridge and the structure type. The specified range of effective temperatures represents the average range to be considered in design. At times, a given range of effective temperatures may have to be adjusted to compensate for unusual conditions, such as frost pockets or sheltered, low-lying areas.

Emerson (8) defines the effective temperature of a bridge as that temperature that governs the longitudinal movement of the bridge deck. The effective temperature may be derived by performing a calculation that includes both the product of the areas between isotherms and their mean temperatures divided by the total area of cross section of the deck. Emerson (9) and Black et al. (10) have correlated the extreme values of effective bridge temperatures

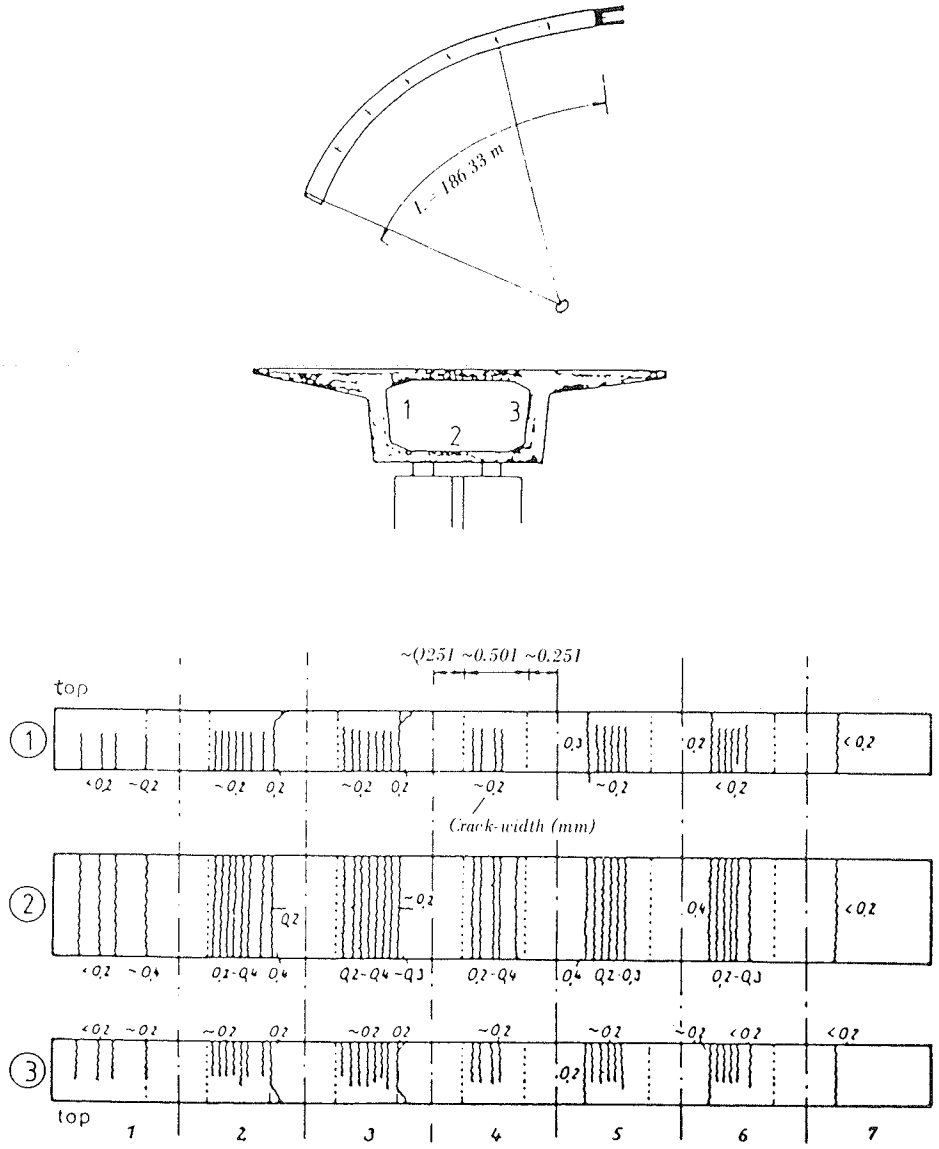

FIGURE 1 Cracks in a multispan box-girder bridge.

with shade temperatures. Emerson correlated shade temperatures with the temperatures obtained from structures instrumented with thermocouples, whereas Black et al. correlated shade temperatures with bridge movements to obtain the extreme values of effective bridge temperatures.

TEMPERATURE DIFFERENTIALS

Because of the unsatisfactory thermal conductivity of concrete, the diurnal temperature effects on a concrete bridge superstructure usually produce temperature gradients. Large, positive temperature gradients occur during days with high solar radiation, clear skies, a large range of ambient temperatures, and a light wind. Negative temperature gradients develop during periods associated with night and winter conditions. The temperature gradients that form in a given structure are governed by heat flow through the body and are a function of the density, specific heat, and thermal conductivity of the concrete.

One-dimensional heat flow in the vertical direction is generally considered to be sufficiently accurate to conduct most analyses of bridge superstructures. Researchers have conducted both analytical and experimental studies to determine temperature differentials that occur in bridge superstructures. The research efforts that led to the development of the codes in New Zealand, England, and Ontario, Canada, are briefly discussed.

New Zealand

Priestley (11,12) analyzed the effects of several assumed thermal gradients and compared the results with measured data available at the time. One of the assumed thermal gradients consisted of a linear temperature distribution through the top deck slab, as proposed by Maher (13), and which was supported by measured temperatures from three bridges located in the British Isles (14,15). Other assumed thermal gradients included the temperature distribution proposed by the Ministry of Works of New Zealand, and distributions in which temperatures vary with depth

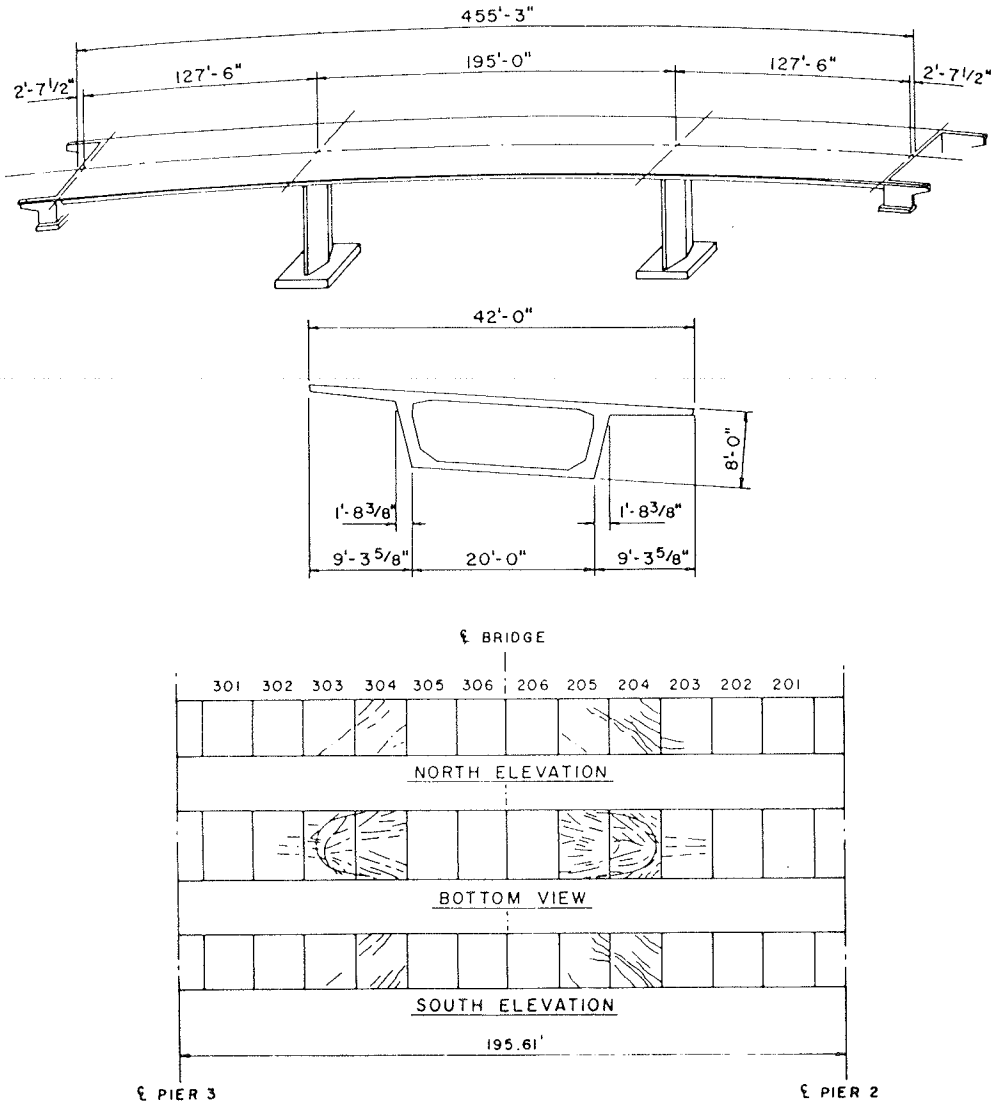

FIGURE 2 Miller Creek Bridge in Colorado.

TABLE 1 Thermal Coefficient of Concrete (-0.000001 per degree Celsius)

Aggregate Type	PCA (6)	Emerson	Browne (5)	Ontario
Quartzite		12.7	11.7-14.6	12.8
Quartz	11.9		9.0-13.2	
Sandstone	11.7	11.7	9.2-13.3	11.7
Gravel	10.8	13.2	9.0-13.7	13.1
Granite	9.5	9.6	8.1-10.3	9.5
Dolerite		9.6		9.5
Basalt	8.6		7.9-10.4	
Marble			4.4- 7.4	
Limestone	6.8	7.3	4.3-10.3	7.4

as second-degree, fourth-degree, and sixth-degree parabolas. The sixth-degree parabola was found to be in satisfactory agreement with measured data, and its use was recommended for superstructure depths between 1200 and 1500 mm (47 and 59 in.).

In 1976 Priestley (15,16) proposed a revised temperature distribution that consisted of three individual parts, as shown in Figure 3. In the first part, temperatures are assumed to decrease nonlinearly from a maximum at the top surface of the deck slab to a minimum at a depth of 1200 mm. The nonlinear variation is represented by a fifth-degree parabola. The second part of the revised distribution applies only to a deck slab over an enclosed cell of a box girder, in which case temperatures are assumed to decrease linearly. The third and final part of the revised distribution assumes a linear variation of temperatures over the bottom 200 mm (8 in.) of the cross section.

Priestley also found that the maximum temperature at the top of the concrete deck slab would decrease linearly with the thickness of bituminous overlay because of the insulating properties of this material.

Great Britain

In 1973 Emerson (8,17) described a method for calculating the one-dimensional heat flow within a concrete-slab bridge by using an iterative, finite-difference solution scheme. The method relates the bridge temperature to solar radiation, ambient air temperature, and wind speed. The model of the structure in this case is composed of several layers, and a starting time is assumed, at which point

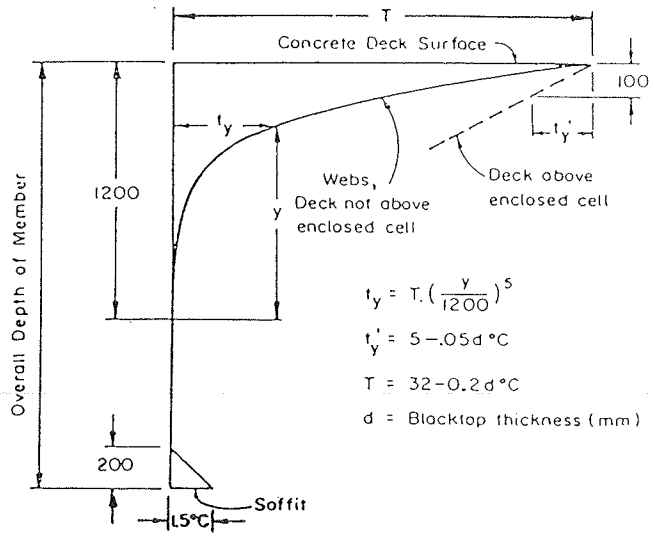

FIGURE 3 Temperature difference from the New Zealand design brief.

the equations governing the boundary conditions are applied.

The assumption of boundary conditions requires an estimation of the times at which the nonlinear differential distribution is at a minimum. It is further assumed that the temperature throughout the structure is a constant at this time. Emerson (8) estimated that the beginning time for concrete bridges was 0800 hours for the heating phase and 1600 hours for the cooling phase. By using these input parameters, a nonlinear differential temperature distribution was computed at 15-min intervals until a maximum gradient was reached at approximately 1500 hours. Temperatures predicted by the model correlated well with measured prototype summer and winter temperature distributions. The current British Standard BS 5400 (18) has been updated to include the temperature distributions determined in these research efforts, as shown in Figure 4.

Ontario

In 1975 Radolli and Green (19) developed a one-dimensional heat-flow analysis similar to the one used by Emerson (8). Although acknowledging that the assumption of one-dimensional heat flow is not technically correct, they cited comparisons that indicated that satisfactory correlations exist between observed and predicted temperature gradients obtained from a one-dimensional heat-flow analysis. They were able to use this approach to develop simplified formulas for use in design.

Comparisons between the British standards (18), Maher (13), the New Zealand Ministry of Works (20), and Priestley's sixth-degree parabola to an I-girder indicate that the resulting stresses are strongly dependent on the temperature differences and temperature gradients. Comparisons between the gradients proposed by Leonhardt et al. (21), Priestley, Maher, and the one-dimensional heat flow were presented for varying superstructure depths. The results were decomposed into continuity and self-equilibrating stresses. Radolli and Green proposed that simple design formulas be used for designs that do not require an understanding of the temperature gradient.

RESPONSE ANALYSIS

Having selected a given temperature gradient or loading, the bridge designer is next faced with performing the response analysis. There are several ways to accomplish this; the two most useful methods follow.

General Method

The general method procedure, shown in Figure 5a, involves separating the arbitrary gradient into three components: axial, bending, and residual. It is first necessary to solve these three problems, and then to superimpose the resulting three stress distributions, as shown in Figure 5b.

Equivalent Prestress Method

The equivalent prestress method procedure, which is much easier to apply than the preceding one, is based on an analogy between thermal strains and prestress strains. In this method the stresses from a completely restrained structure are superimposed with the stresses that result from the removal of the restraints, as shown in Figure 5c. Removal of the restraint is accomplished by dividing the restrained stress field into a series of equivalent negative prestress forces, as shown in Figure 5d.

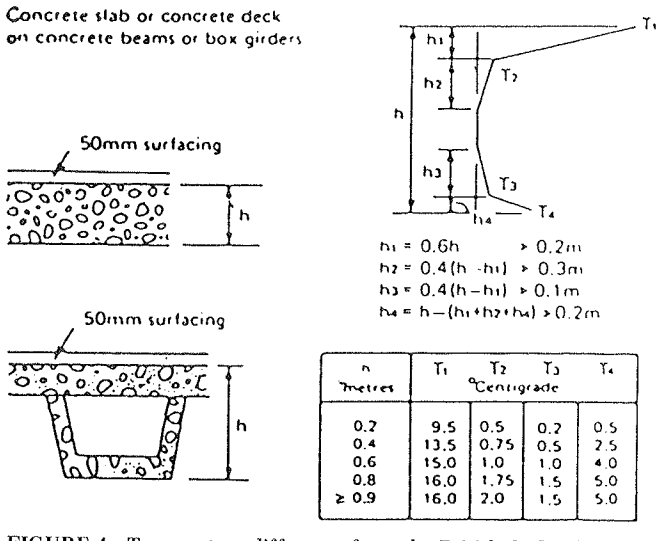

h metres	T_1 °Centigrade	T_2 °Centigrade	T_3 °Centigrade	T_4 °Centigrade
0.2	9.5	0.5	0.2	0.5
0.4	13.5	0.75	0.5	2.5
0.6	15.0	1.0	1.0	4.0
0.8	16.0	1.75	1.5	5.0
≥ 0.9	16.0	2.0	1.5	5.0

h metres	T_1 °Centigrade	T_2 °Centigrade	T_3 °Centigrade	T_4 °Centigrade
0.2	3.5	0.5	0.25	1.5
0.4	6.5	0.75	0.5	3.5
0.6	8.5	1.0	1.5	5.0
0.8	10.0	1.5	2.5	6.5
≥ 0.9	10.5	2.0	3.5	7.0

FIGURE 4 Temperature difference from the British Code of Practice, BS 5400.

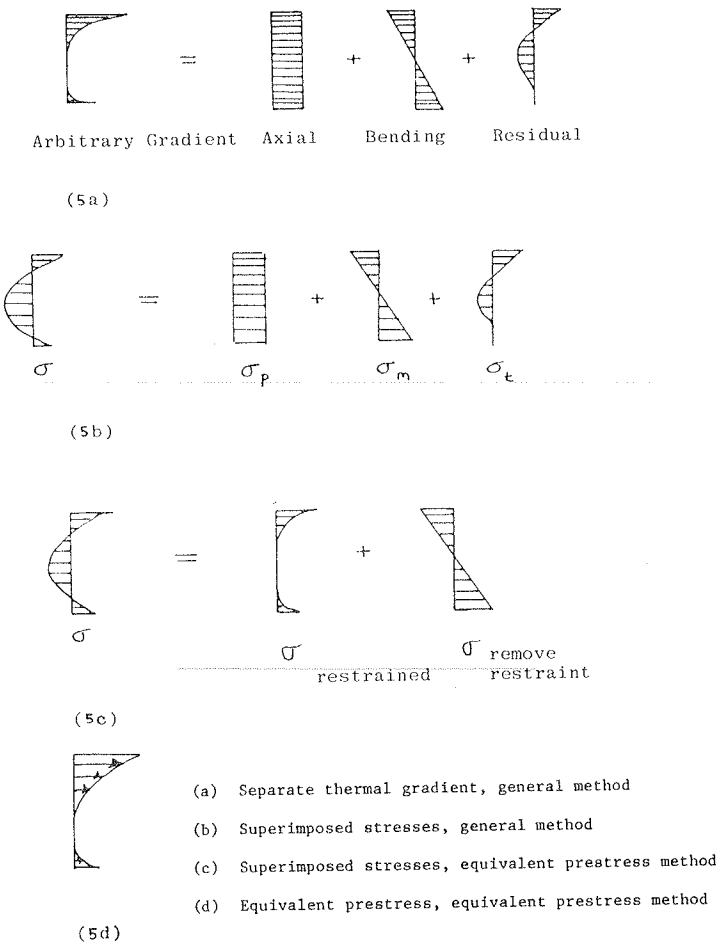

(a) Separate thermal gradient, general method

(b) Superimposed stresses, general method

(c) Superimposed stresses, equivalent prestress method

(d) Equivalent prestress, equivalent prestress method

FIGURE 5 Response analyses.

Most of the case studies presented in the following sections were analyzed by this method.

ALTERNATIVE APPROACHES

The bridge design codes of different countries provide the designer with many different approaches to help account for thermal effects. The codes basically differ in the refinement used to determine the meteorological conditions at proposed bridge sites, the types of thermal loadings considered, and the methods used to accommodate these thermal loadings.

The codes in most countries are similar in that they contain provisions for some sort of thermal gradient that produces a corresponding stress distribution; this corresponding stress distribution is then grouped with other stresses (e.g., dead load, live load, prestress) so as to modify the design. This usually results in an increase in the prestress force, sometimes by a relatively large amount.

However, researchers in Switzerland and Germany are currently developing a new approach based on the concept that partial prestressing is sufficient to accommodate thermal gradient stresses and strains. This design procedure leaves the prestress force unchanged, and relies instead on mild steel reinforcement to resist the thermal stresses. This, at least in part, explains why the large number of existing prestressed concrete bridges that were designed and built without consideration given to thermal gradient effects have continued to perform satisfactorily for so many years of service.

The minimum design requirements for bridges in the United States are governed by the AASHTO design specifications. In certain cases additional, more detailed design criteria may be used. With respect to temperature, the design recommendations of the Post-Tensioning Institute (PTI) are often used in the design of prestressed-concrete bridges. Several individual states have also developed their own design procedures for considering thermal effects, which in most cases are similar to those recommended by PTI. A detailed description of the procedures, compiled from a survey of the states, is contained in the NCHRP report (1).

CASE STUDIES

Longitudinal and transverse temperature effects were applied to a selected group of U.S. bridges as part of the NCRHP research project. Four thermal gradients were used to study the longitudinal effects, whereas two thermal gradients were used to study the transverse effects.

Four thermal gradients (Figure 6) were selected for the case studies on longitudinal temperature effects. These gradients were selected because they are representative of those currently being used. They include those specified in the New Zealand, British, and Ontario codes. In addition, the gradient recommended by PTI was included because it is somewhat representative of the gradients currently used in the United States. A summary of the bridges included in the NCHRP project on case studies for

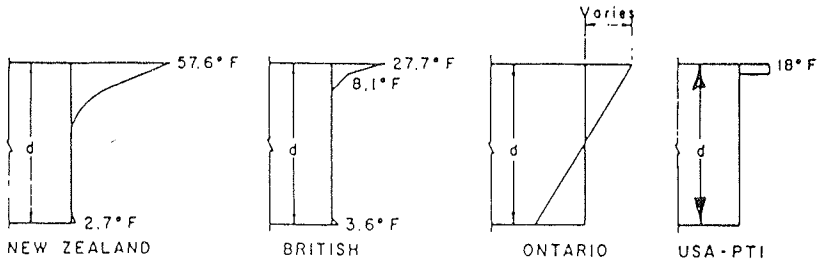

FIGURE 6 Thermal gradients used for case studies.

TABLE 2 Summary of Bridges Included in Case Studies for Longitudinal Temperature Effects

Case No.	Name and Location	Superstructure	Substructure	Length	Depth	Depth/Span Ratio	No. of Spans	No. of Hinges	No. of Frames	Comment
1L	Colorado River Bridge, California and Arizona	Precast, prestressed I-girder	Pier wall	565 ft, 6 in.	6 ft, 3 in.	0.056	5	0	1	Representative I-girder
2L	West Silver Eagle Road overhead, California	Cast-in-place pre-stressed box girder	Double column	750 ft, 0 in.	5 ft, 0 in.	0.037	6	0	1	Representative box girder
3L	Turkey Run Creek Bridge, Indiana	Precast, prestressed segmental box girder	Single column	317 ft, 0 in.	9 ft, 0 in.	0.057	2	0	1	Segmental cantilever
4L	Kishwaukee River Bridge, Illinois	Precast, prestressed segmental box girder	Single column	1,096 ft, 0 in.	11 ft, 8 in.	0.047	5	0	1	Segmental cantilever
5L	Columbia River Bridge, Washington	Cast-in-place pre-stressed segmental box girder	Single column	1,870 ft, 0 in.	9 ft, 0 in.[a] 24 ft, 0 in.[b]	0.053	5	0	1	Segmental and haunched cantilever
6L	West Silver Eagle Road overhead (falsework), California	Cast-in-place pre-stressed box girder	Double column	750 ft, 0 in.	5 ft, 0 in.	0.037	6	1	2	Falsework loading
7L	East Connector, California	Cast-in-place rein-forced box girder	Single column	1,104 ft, 0 in.	6 ft, 0 in.	0.055	11	2	3	Multiframe
8L	Miller Creek F-11-AK, Colorado	Precast, prestressed segments and box girder	Single column	445 ft, 3 in.	8 ft, 0 in.	0.041	3	0	1	Case history

[a]Minimum. [b]Maximum.

longitudinal effects is given in Table 2. The results of two of these case studies (case numbers 5L and 8L) are included in this paper. The applicable portions of the codes are those that pertain to the positive gradients that occur during the day when there is high solar radiation.

Plots of top and bottom fiber stress versus the distance longitudinally along the bridge are presented in this paper for both of the case studies. In addition, section stresses are included at selected points along the bridge to show the stress variations at different depths.

The plots show that maximum fiber stresses usually occur at the pier or column supports adjacent to the abutments. The plots also show that changes in superstructure cross sections caused by flares in the bottom slab and girder stems or in the haunched superstructure cause significant changes in fiber stresses.

The bridges analyzed were assumed to have a coefficient of thermal expansion of 0.000006 per degree Fahrenheit, uncracked section properties, and no reductions in thermal gradients for surfacing, elevation, and so forth.

Case 5L: Columbia River Bridge

The Columbia River Bridge was included in the case studies because it is a major structure and because it uses a customized and optimized cross section. Another reason for selecting this bridge is to evaluate the effect of the pronounced variation in the depth of its structure caused by the haunches at the interior supports. This bridge was designed according to the Washington State criteria on thermal effects. For longitudinal thermal effects of box girders, the criteria specify a temperature increase of 20°F in the top slab. The stresses caused by this increase in temperature are combined with dead load for a service loading. In addition, another service load condition, which results from one-half the temperature gradient (i.e., 10°F), is combined with the dead load and full live load.

This structure, shown schematically in Figure 7, is a five-span, 1,870-ft-long bridge.

Figures 8 and 9 are plots of top and bottom fiber stresses, respectively, along the bridge centerline. The Ontario code was not considered in this case because it was not apparent how this code should be applied to nonprismatic sections.

Figures 10 and 11 show plots of the variation in stresses, with section depth for the three gradients considered for 9- and 24-ft-deep sections, respectively.

Case 8L: Miller Creek Bridge

The Miller Creek Bridge and several other bridges in the same area developed severe cracking problems shortly after completion of construction. Because thermal gradient effects are suspected as being one of the causes of this distress, this bridge was included in the case studies.

This structure, shown schematically in Figure 12, is a three-span, 455-ft-long bridge.

Figures 13 and 14 are plots of top and bottom fiber stresses, respectively, along the bridge centerline.

The Miller Creek Bridge is of special interest because the structure developed relatively severe cracking in the bottom flange and girder stems at approximately the one-quarter and three-quarter

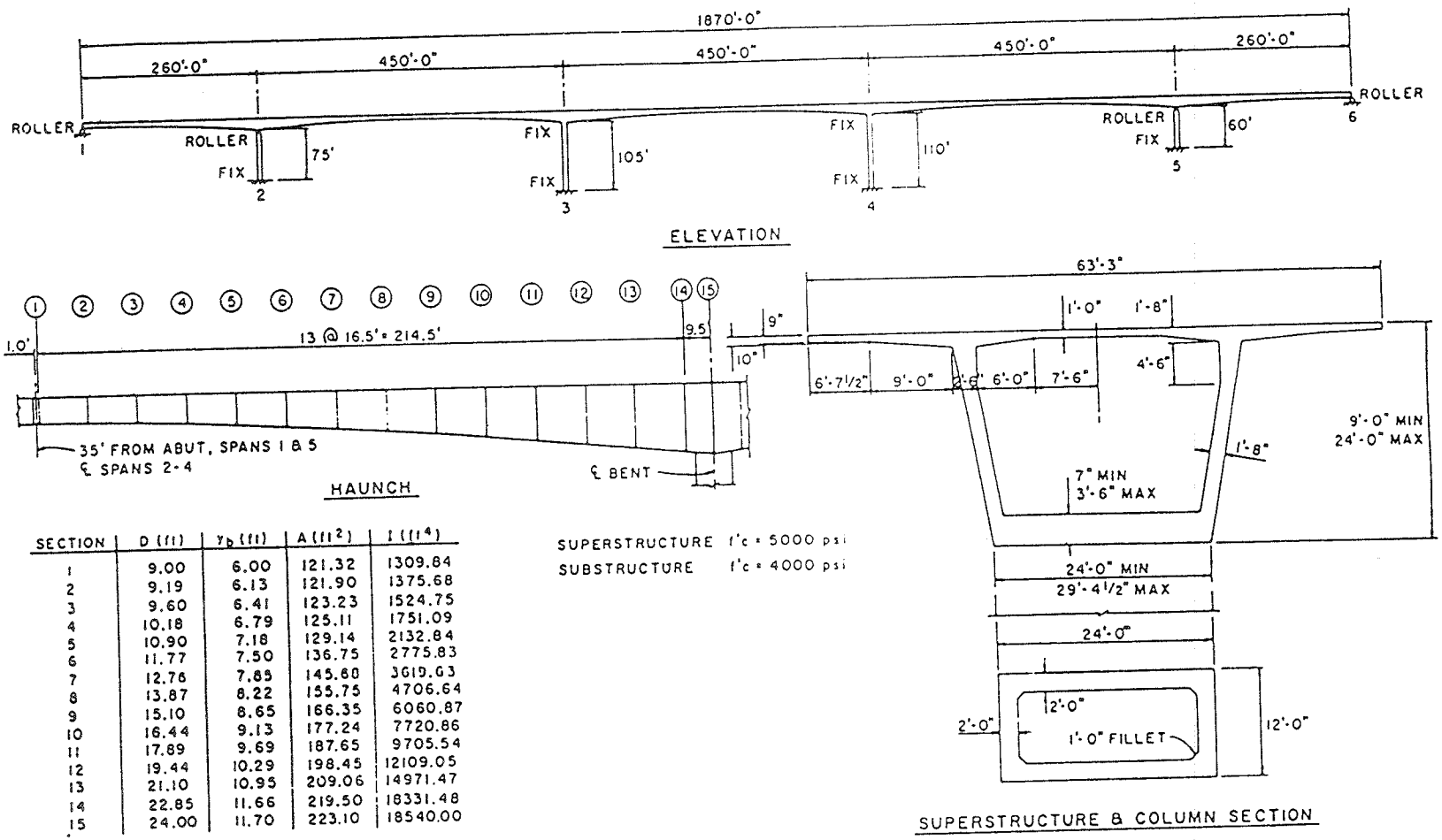

SECTION	D (ft)	y_b (ft)	A (ft^2)	I (ft^4)
1	9.00	6.00	121.32	1309.84
2	9.19	6.13	121.90	1375.68
3	9.60	6.41	123.23	1524.75
4	10.18	6.79	125.11	1751.09
5	10.90	7.18	129.14	2132.84
6	11.77	7.50	136.75	2775.83
7	12.76	7.85	145.68	3619.63
8	13.87	8.22	155.75	4706.64
9	15.10	8.65	166.35	6060.87
10	16.44	9.13	177.24	7720.86
11	17.89	9.69	187.65	9705.54
12	19.44	10.29	198.45	12109.05
13	21.10	10.95	209.06	14971.47
14	22.85	11.66	219.50	18331.48
15	24.00	11.70	223.10	18540.00

SUPERSTRUCTURE f'c = 5000 psi
SUBSTRUCTURE f'c = 4000 psi

FIGURE 7 Case 5L: Columbia River Bridge superstructures and substructure details used for analysis.

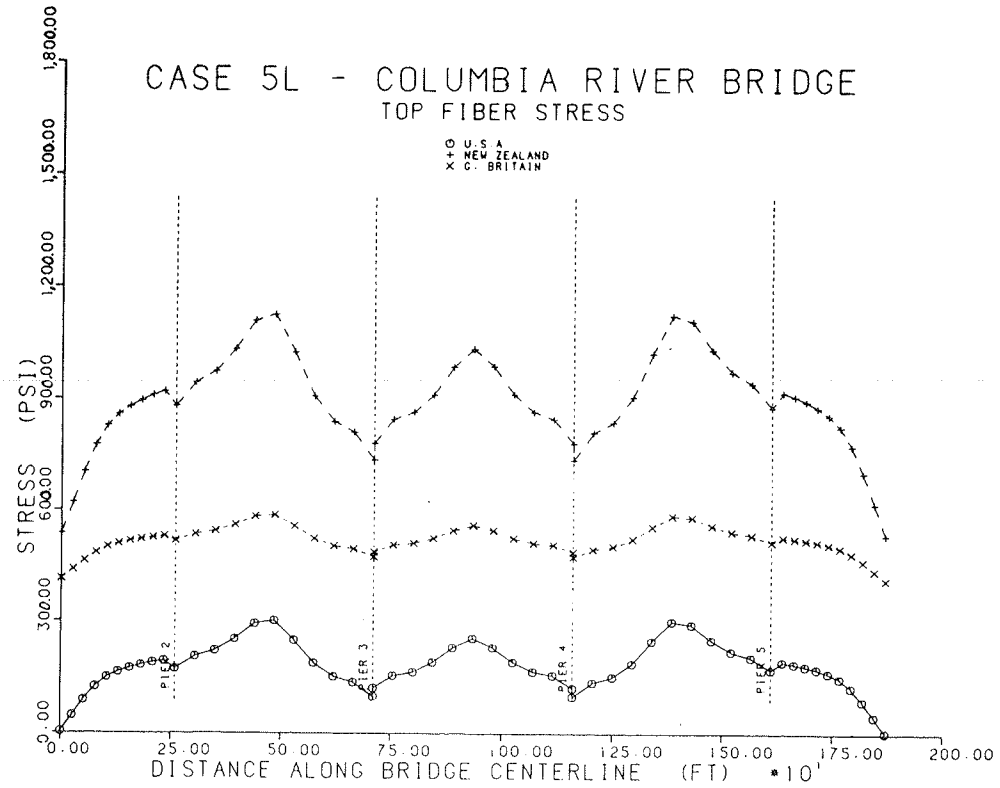

FIGURE 8 Case 5L: longitudinal variations in top fiber stresses along a girder centerline caused by positive temperature gradients.

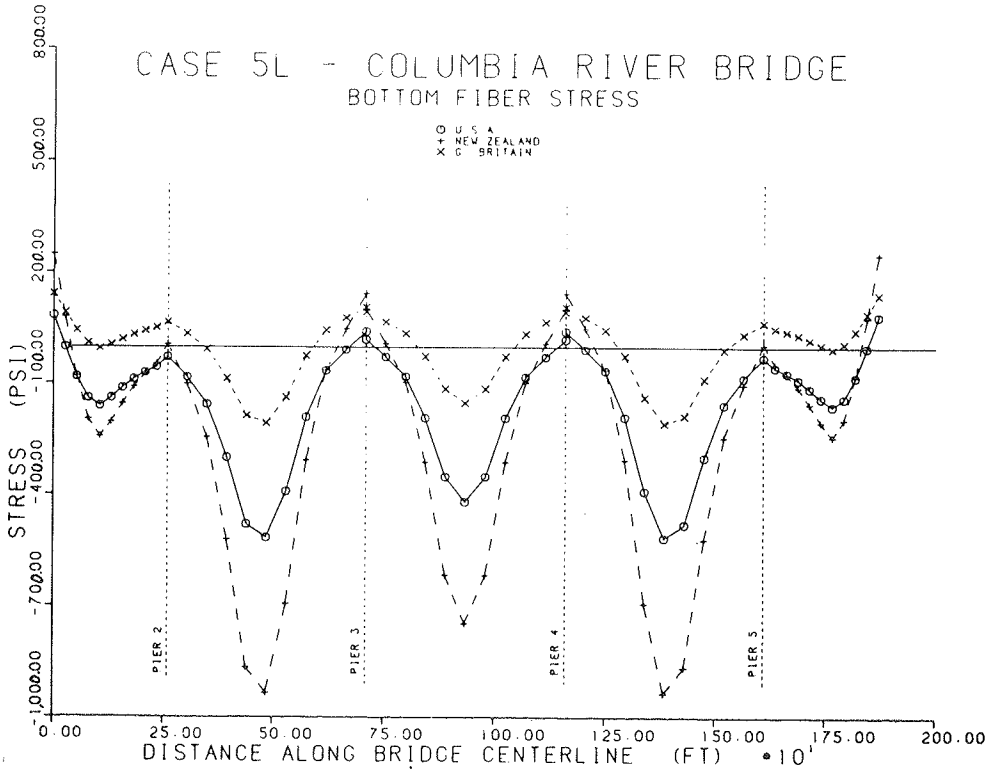

FIGURE 9 Case 5L: longitudinal variation in bottom fiber stresses along a girder centerline caused by positive temperature gradients.

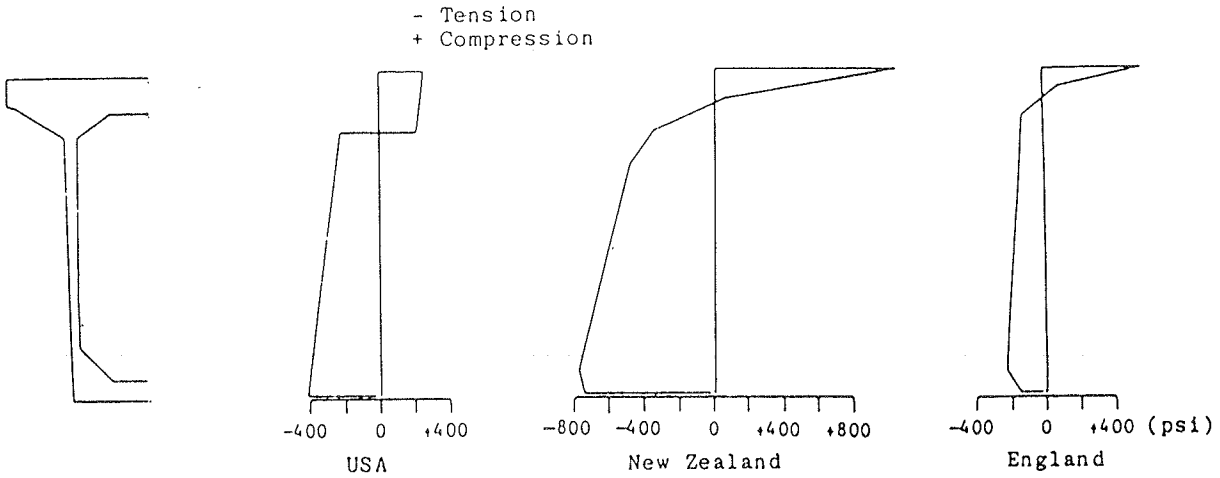

FIGURE 10 Case 5L, 9-ft deep cross section: variation in girder cross-section stresses with depth caused by positive temperature gradients.

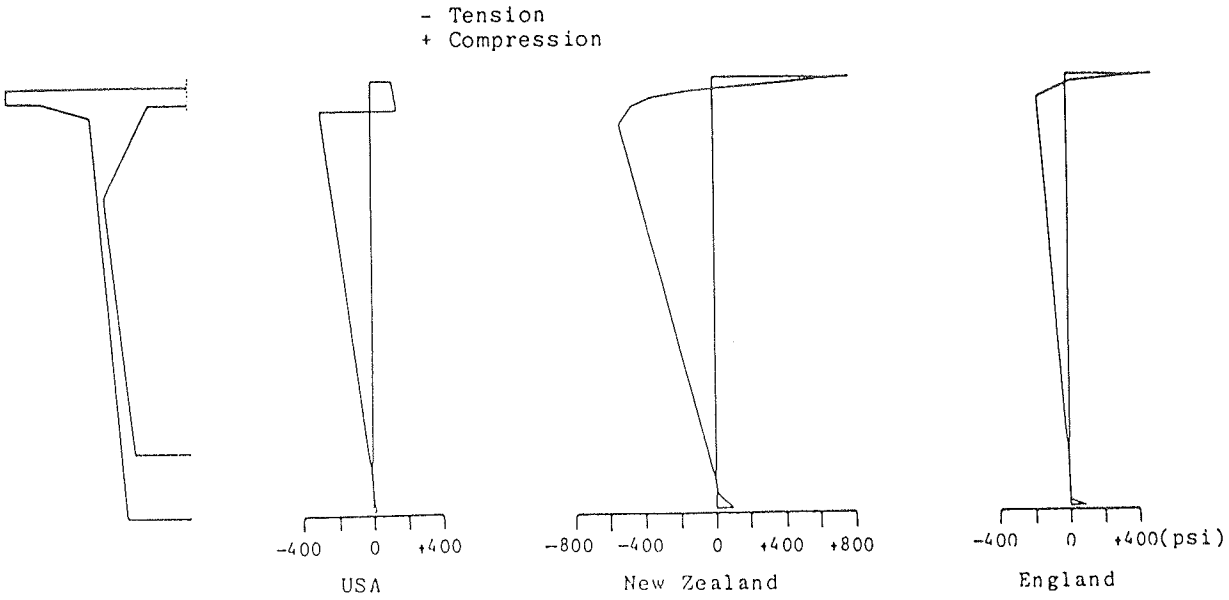

FIGURE 11 Case 5L, 24-ft deep cross section: variation in girder cross-section stresses with depth caused by positive temperature gradients.

points of span 2 (see Figure 2) a short time after completion of construction. Thermal gradient effects are thought to have been a significant contributing factor to this distress. The crack widths, in fact, were observed to be opening and closing on a daily basis, generally correlating reasonably well with daily temperature fluctuations.

This structure was constructed by the segmental, balanced-cantilever method. Prestress tendons are typically placed in the bottom slab within the center portion of the span to resist positive bending moments that can result from creep after the cantilevered portions of the superstructure are tied together. In this bridge these tendons terminated in the vicinity of the cracking. Several other similar bridges constructed nearby at about the same time have developed similar cracking patterns.

A plot that shows dead-, prestress-, and U.S. thermal-load stresses is shown in Figure 15. This plot shows that tensile stresses occur in the bottom fiber at the same location where the cracks developed in the Miller Creek Bridge.

Based on the details of construction and the characteristics of the observed cracking, it is postulated that the reasons for the cracking appear to be some combination of the following:

1. Greater inelastic redistribution of stress (i.e., increase of positive moment from creep) than anticipated,
2. Stress concentrations in the prestress anchorage zone, and
3. Thermal gradient stresses.

Although the primary cause of the distress cannot be precisely determined, it appears that the inelastic redistribution of stress that results in an increase of positive moment (reason 1) is probably the most important single factor. Local tension stresses caused by prestress anchorages and thermal

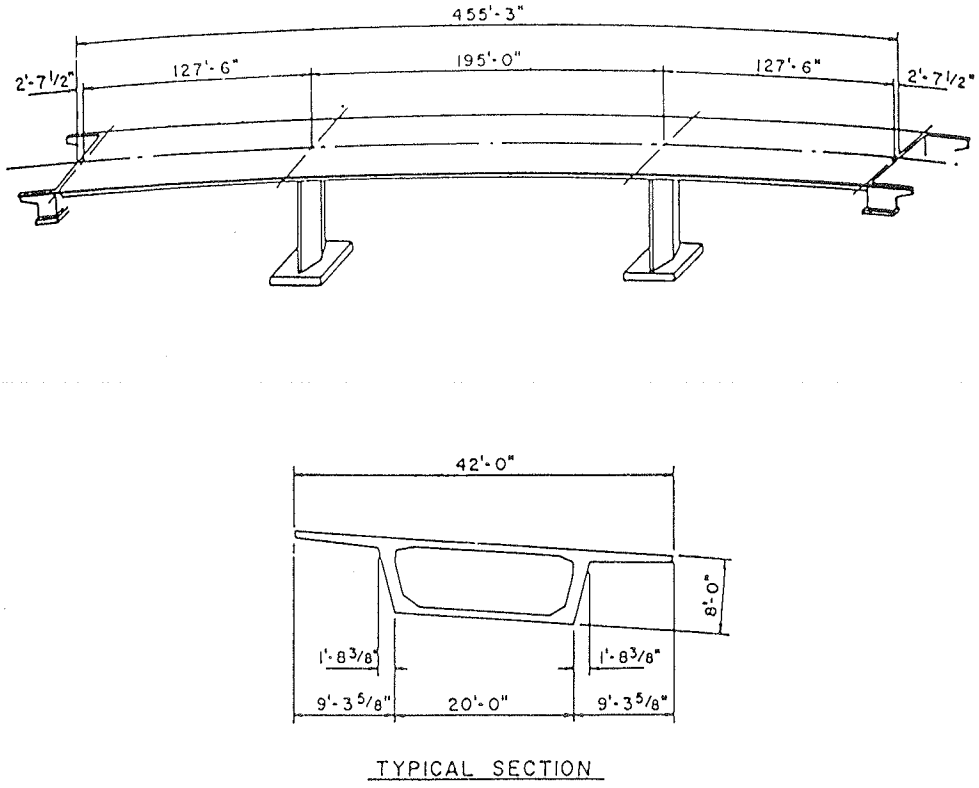

FIGURE 12 Miller Creek Bridge superstructure and substructure details used for analysis.

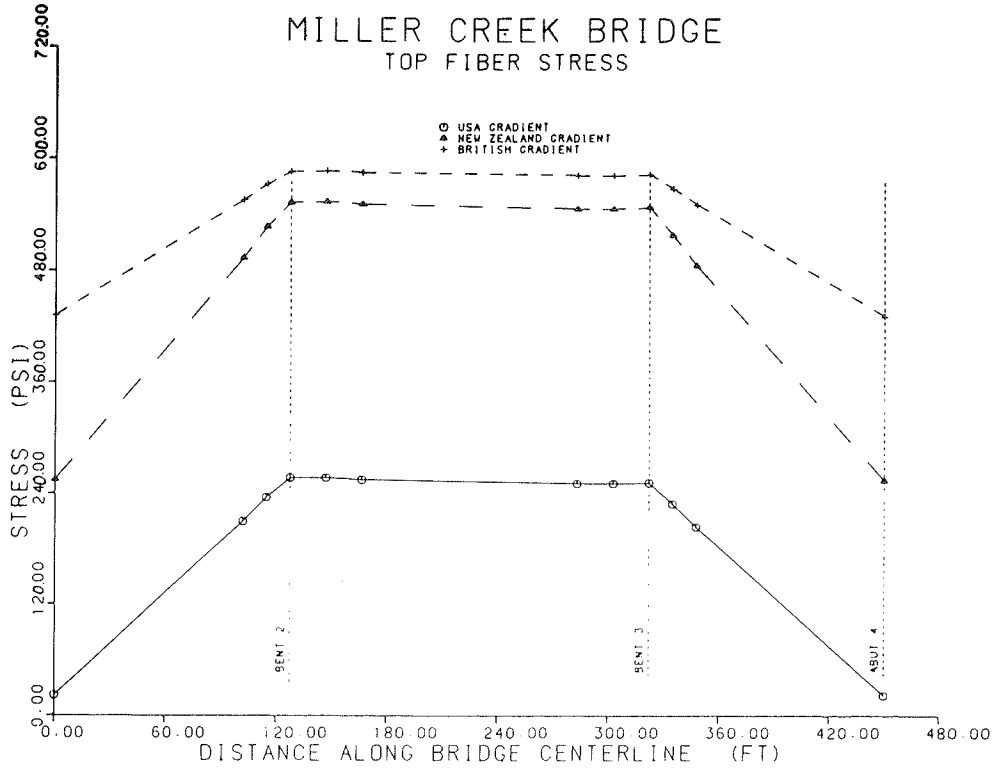

FIGURE 13 Case 8L: longitudinal variation in top fiber stresses along a girder centerline caused by positive temperature gradients.

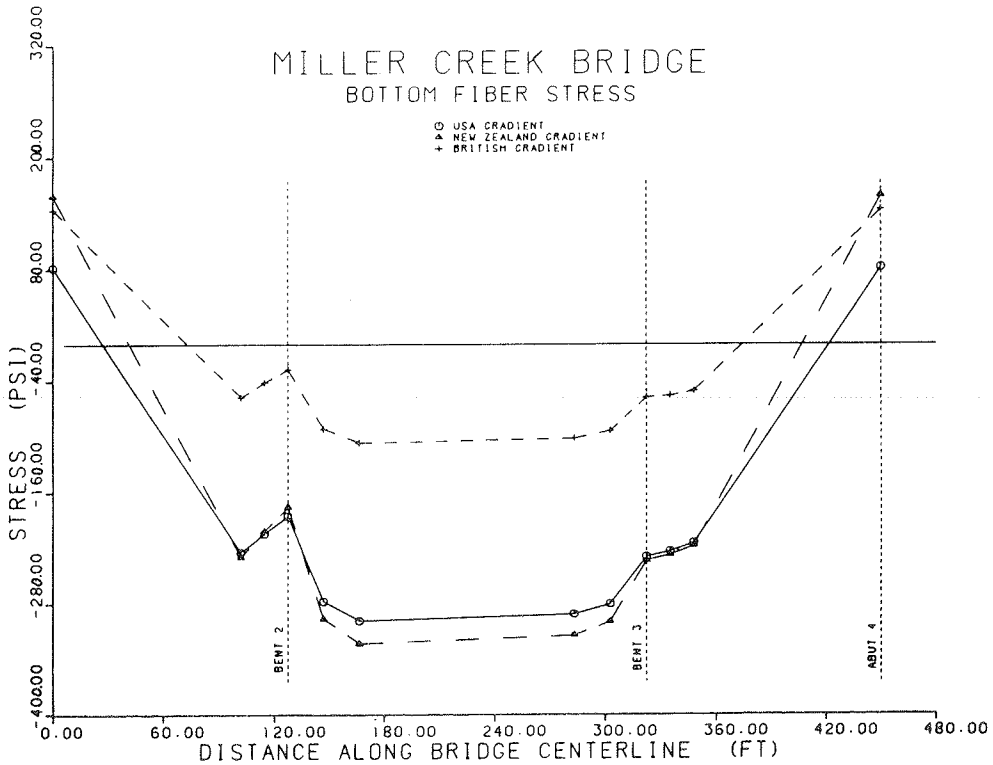

FIGURE 14 Case 8L: longitudinal variation in bottom fiber stresses along a girder centerline caused by positive temperature gradients.

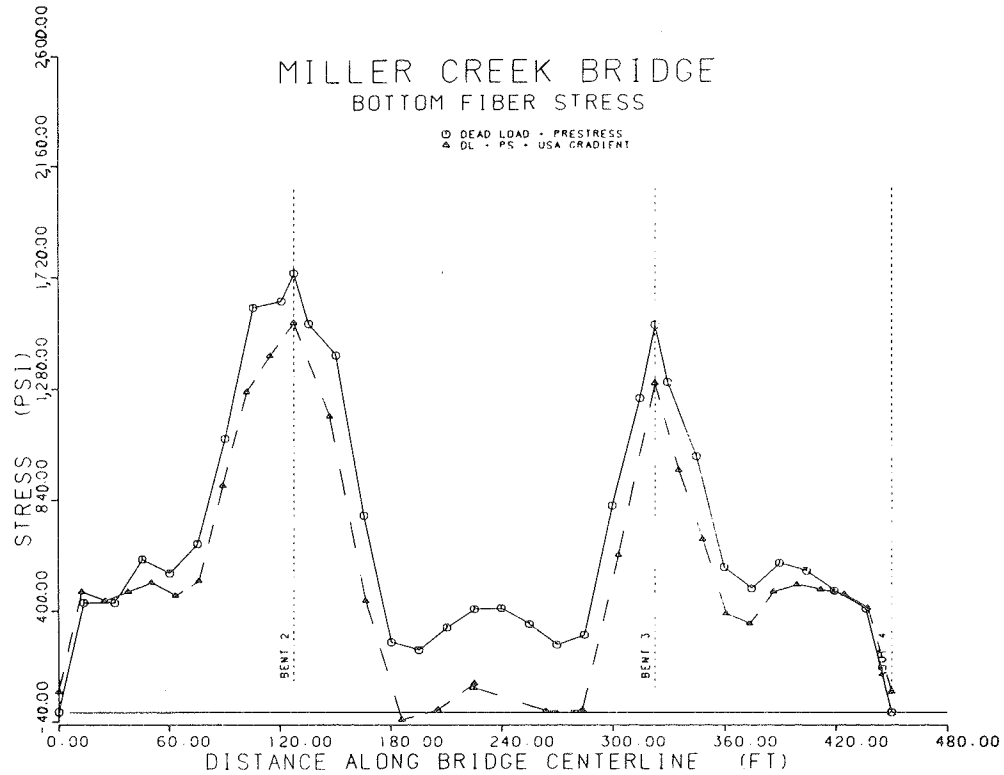

FIGURE 15 Case 8L: longitudinal variation in bottom fiber stresses along a girder centerline caused by combined dead load, positive temperature gradient, and prestressing.

gradient stresses, although significant, are probably of secondary importance.

The cracking probably could have been avoided by extending the bottom slab prestress tendons in the zones of high bottom-fiber compression, thus anchoring them much closer to bents 2 and 3.

In summary, it appears that although the thermal gradient stresses do contribute to the cracking problem, they are not the basic cause of it.

CONCLUSIONS AND RECOMMENDATIONS

Several case studies were conducted to investigate the effects of various assumed thermal gradients on the longitudinal and transverse fiber stresses induced in various types of concrete bridge superstructures. The following conclusions about the nature of thermal effects on concrete bridges are drawn from an assessment of the results of these case studies.

1. Although fiber stresses induced in different bridges by any single thermal gradient may vary in magnitude, the stress patterns are generally similar.
2. Cross-sectional changes such as bottom slab flares and haunches have a significant effect on the fiber stresses induced by thermal gradients.
3. The calculated fiber stresses were sensitive to the type of temperature gradient assumed. Although some gradients produced similar, extreme fiber stresses, the differences in fiber stresses between the extreme fibers within the girder section were significant. In many cases this difference was sufficient to affect the requirements for longitudinal reinforcement. This could be a contributing factor in some cases where concrete cracking has been observed.

Based on the results from these case studies and a review of the design approaches used in other countries, it is apparent that U.S. bridge design requirements should be expanded to include the effects of a thermal gradient. The current AASHTO procedures for considering longitudinal movement are basically adequate, although it would be desirable to include a more accurate method for determining seasonal variations in temperature. In light of these observations, the following recommendations are made for improved thermal design procedures in the United States.

1. Maps that reflect climatic variation, similar to maps used in the British design standard and the Ontario bridge code, should be included in the AASHTO specifications. Data contained in these maps can be used to develop the much-needed methods for determining structure temperatures.
2. An AASHTO guide specification should be developed to provide for the effects of thermal gradients. Because there is little or no evidence of distress caused by a temperature gradient in conventionally reinforced-concrete bridges, this guide specification should be directed toward the larger, prestressed-concrete bridges, which past experience has demonstrated are more likely to develop problems from temperature differentials. This guide specification should include the following:
    a. Methods for determining both longitudinal and transverse stresses;
    b. A nonlinear temperature gradient with a shape similar to that used in the British design standard; actual temperature differentials will vary;
    c. An option to accommodate the gradient stresses by increasing the prestress force or by determining the amount of auxiliary mild reinforcement by the partial prestressing concept;
    d. A map that indicates the maximum probable solar radiation in different geographical areas to help determine the maximum temperature differential for a given bridge site; and
    e. Transverse analysis consideration of the effects of a temperature differential caused by solar radiation on the top deck slab.
3. In developing a method for designing bridges for thermal effects, there are several points that must be kept in mind. These points, which relate to the current state of the art and design practices, are as follows:
    a. The format of the design specifications should be general enough to include advances in the state of the art as they are developed and allow for extension of the procedures to other bridge types in the future,
    b. The procedures should provide for maximum simplicity without sacrificing significant accuracy,
    c. The need for future training to implement the procedures must be considered, and
    d. In light of the limited number of cases in which temperature-induced distress has been observed, there is a potential problem with designer acceptance of elaborate thermal design procedures.

REFERENCES

1. R.A. Imbsen, D.E. Vandershaf, and C.F. Stewart. Thermal Effects in Concrete Bridge Superstructures. NCHRP Interim Report 12-22. TRB, National Research Council, Washington, D.C., May 1983.
2. Ing. T. Zichner. Thermal Effects on Concrete Bridges. Presented at Comite Europeen du Beton Enlarged Meeting, Commission 2, Pavia, Italy, Oct. 1981.
3. Memorandum: In-Depth Inspection of the Creeks and Spalls Developing in the Walls and Bottom Slabs of the F-11-AK, F-11-AL Structures over Miller Creek on I-70. Colorado Department of Highways, Denver, July 29, 1982.
4. S.G. Fattal, T.A. Reinhold, and B. Ellingwood. Analysis of Thermal Stresses in Internally Sealed Concrete Bridge Decks. Report FHWA/RD-80/085. HRS-20, Office of Research and Development, FHWA, U.S. Department of Transportation, April 1981.
5. R.D. Browne. Thermal Movement of Concrete. Concrete, Nov. 1972.
6. Building Movements and Joints. Portland Cement Association, Skokie, Ill., 1982.
7. Concrete Manual, 7th ed. Bureau of Reclamation, U.S. Department of the Interior, Denver, 1966.
8. M. Emerson. The Calculation of the Distribution of Temperature in Bridges. TRRL Report LR 561. Transport and Road Research Laboratory, Department of the Environment, Crowthorne, Berkshire, England, 1973.
9. M. Emerson. Bridge Temperatures Estimated from the Shade Temperature. TRRL Report 696. Transport and Road Research Laboratory, Department of the Environment, Crowthorne, Berkshire, England, 1976.

10. W. Black, D.S. Moss, and M. Emerson. Bridge Temperatures Derived from Measurements of Movement. TRRL Report 748. Transport and Road Research Laboratory, Department of the Environment, Crowthorne, Berkshire, England, 1976.
11. M.J.N. Priestley. Effects of Transverse Temperature Gradients on Bridges. Report 394. Ministry of Works, Wellington, New Zealand, Sept. 1972.
12. M.J.N. Priestley. Temperature Gradients in Bridges--Some Design Considerations. New Zealand Engineering, Vol. 27, Part 7, July 1972, pp. 228-233.
13. D.R.H. Maher. The Effects of Differential Temperature on Continuous Concrete Bridges. Civil Engineering Transactions, Institute of Engineers of Australia, Vol. CE12, Part 1, April 1970, pp. 29-32.
14. W.I.J. Price. Discussion of Papers Entitled Medway Bridge: Design, by O.A. Kerensky and G. Little; and Medway Bridge: Construction, by M.F. Hansen and J.A. Dunster. Proc., Institution of Civil Engineers, Vol. 31, June 1965, pp. 162-166.
15. M.J.N. Priestley. Linear Heat-Flow and Thermal Stress Analysis of Concrete Bridge Decks. Res. Report 76/3. Department of Engineering, University of Canterbury, Christchurch, New Zealand, Feb. 1976.
16. M.J.N. Priestley. Design Thermal Gradients for Concrete Bridges. New Zealand Engineering, Vol. 31, Part 9, Sept. 1976, pp. 213-219.
17. M. Emerson. Temperature Differences in Bridges: Basis of Design Requirements. TRRL Report 765. Transport and Road Research Laboratory, Department of the Environment, Crowthorne, Berkshire, England, 1977.
18. Steel, Concrete, and Composite Bridges--Part I: General Statement. British Standard BS 5400. British Standards Institution, Crowthorne, Berkshire, England, 1978.
19. M. Radolli and R. Green. Thermal Stresses in Concrete Bridge Superstructures Under Summer Conditions. In Transportation Research Record 547, TRB, National Research Council, Washington, D.C., 1975, pp. 23-36.
20. M.J.N. Priestley and I.G. Buckle. Ambient Thermal Response of Concrete Bridges--Bridge Seminar, 1978. Summary Volume 2. Structure Committee, Road Research Unit, National Roads Board, Wellington, New Zealand, 1979.
21. F. Leonhardt, G. Kolbe, and J. Peter. Temperature Differences Endanger Prestressed Concrete Bridges. Brefon-und Stahlbetonau, No. 7, July 1965, pp. 157-163.

Publication of this paper sponsored by Committee on Concrete Bridges.

Fatigue Behavior of Welded Wrought-Iron Bridge Hangers

PETER B. KEATING, JOHN W. FISHER, BEN T. YEN, and WILLIAM J. FRANK

ABSTRACT

The behavior of fatigue crack growth and fatigue strength of welded lap splice wrought-iron hangers in a railroad bridge was studied. The original wrought-iron hangers were lap spliced with steel plates for the purpose of tightening the members. Field inspection revealed cracks in the welded lap splices. Examination of simulated test joints and cracked hanger splices in the laboratory indicated that fatigue cracks would develop from weld deposits at the cut of the wrought-iron bar, propagate into the steel splice plate, and cause failure. Fatigue cracks could also propagate into the wrought-iron bars but would be arrested by the slag (iron silicate) stringers. Breaking of the wrought-iron bar only occurred when the applied stress was quite high in comparison with the yield point. Measured live-load stresses in the actual bridge member were relatively low. Evaluation of traffic and load records indicates that the effective live-load stresses would be well below the fatigue strengths of these spliced joints. No imminent problem of fatigue failure is expected in the hangers.

Before the refinement of the steel-making process, wrought iron was widely used as the principle structural material in bridge construction. It was used in many railroad structures during the period from the late 1800s to the early 1900s. Although the material properties of wrought iron have been well known since the beginning of its use, the welded fatigue behavior has never been adequately quantified. Thus a study on the fatigue behavior of welded wrought-iron splice plate repairs on Norfolk and Western Railway Bridge No. 651 in Hannibal, Missouri, is presented. Welded repairs are known to result in low fatigue strength details with steel components. Because the structural members were wrought iron with steel reinforcement, it was desired to evaluate the seriousness of the resulting welded details and to assess the degree of cumulative damage that may have occurred.

BRIDGE DESCRIPTION

The Norfolk and Western Railway Bridge was originally built for the Wabash Railroad in 1888 by the Detroit Iron and Bridge Works. The bridge spans the Mississippi River with seven truss spans and one continuous swing span for a total length of 1,580 ft (Figure 1). It carries a single track and has a truss spacing of 18 ft. The bridge members are con-

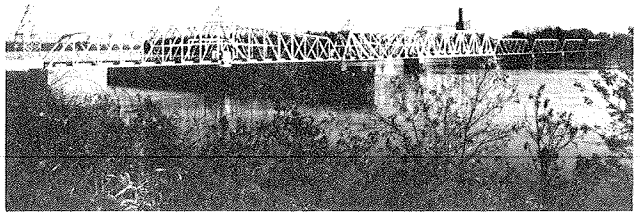

FIGURE 1 View of bridge.

structed of riveted built-up wrought-iron sections and eyebars. Span F, which contains the most severe welded repair detail, is a nine-panel, 176-ft, 4-in.-long simply supported span (Figure 2). All diagonals, bottom chord members, and the U1-M1 and U8-M8 hangers are comprised of eyebar pairs.

Throughout its history, the bridge has undergone an extensive number of repairs and revisions (note that these data are from the records and summarizations of repairs to Bridge 651 of the Norfolk and Western Railroad). This includes span shortening and relocation, stringer replacement, and eyebar tightening. Beginning in 1937, a period during the early development of the welding process, many of the repairs incorporated welding, some to an extreme. Common to old, pin-ended truss bridges, many of the eyebar members loosened with time and required tightening. The corrective repair procedure used on this bridge was to cut the eyebar body and then to weld steel lap shear splices over the cut. A small length was cut out of the eyebar body and the two cut ends were drawn together so as to retension the member. Splice plates were welded on either side, thus overlapping the cut (Figure 3). The steel lap plates were of A7 material.

A continuous fillet weld was placed around the entire perimeter of each lap plate, which resulted

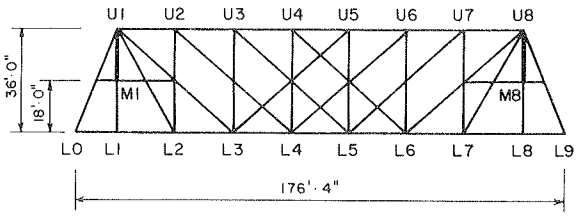

FIGURE 2 Profile of span F.

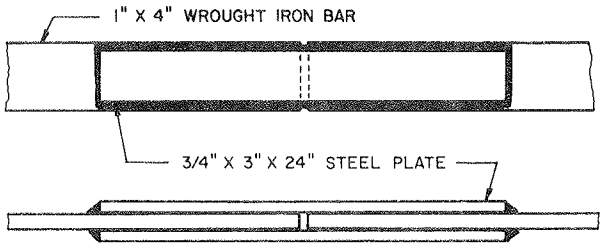

FIGURE 3 Plan of lap splice repair.

FIGURE 4 Toe crack in transverse weld.

in both transverse and longitudinal welds, the latter bridging the exposed gap between the two wrought-iron plate ends. This was done on many of the diagonals, bottom chord members, and on six of the eight eyebar hangers in span F, as well as eyebar members in the other seven spans. For the hangers in span F, the original cross-sectional area of the wrought-iron bar is 4.0 in.^{2}. The addition of the splice plates increases the total area by 12 percent to 4.5 in.^{2}. This type of tightening procedure was a common method of repair before the fatigue strength of weldments became known. The American Railway Engineering Association (AREA) specifications now provide procedures for eyebar tightening by heating and upsetting of the eyebar body.

FIELD INSPECTION

A detailed inspection of the bridge revealed fatigue cracks in the welded lap splices. The most severe cracking was found in the transverse welds in the hangers of span F, where the cracks had coalesced across the toe of the transverse weld. Figure 4 shows the presence of the crack along the entire length of the transverse fillet weld. Also, fatigue cracks were found in the welded gap at the center of the lap splice (Figure 5). Although each hanger is comprised of a pair of eyebars, with a combined cross-sectional area of 8.0 in.^{2}, the inspection revealed that only one eyebar was carrying the load. The other eyebar was found to be slack, even during live loading of the span. This may have occurred from pin wear, pin rotation, or improper tensioning during repair. This condition effectively doubled the stress range level in the active member, which resulted in a more serious situation. A study was undertaken to determine the severity of the cracking and to determine what corrective measures were necessary to prevent failure of the member.

FIELD MEASUREMENTS

Concurrent with the field inspection was the strain gauging and monitoring of one hanger in span F. An electrical resistance strain gauge was mounted on the load-carrying member of hanger U1-M1. Strain readings were taken during passage of several freight trains and of a test train of known weight at various speeds. This allowed for the correlation of the field-measured stresses with the stresses ob-

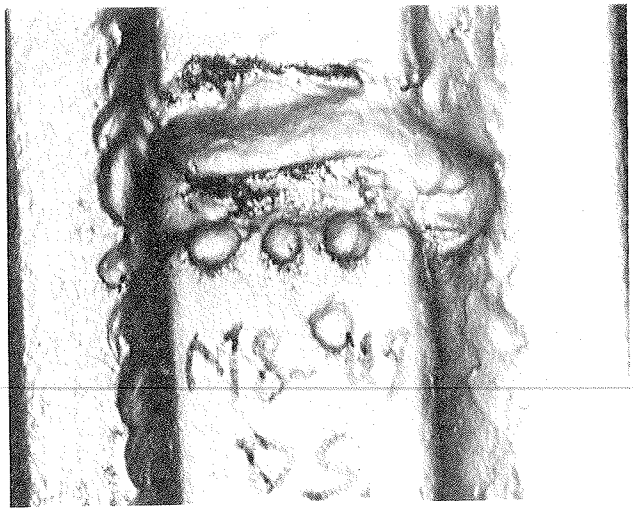

FIGURE 5 Crack in welded gap.

tained from a computer model of the structure. Also, it permitted the effective stress range for the recording period and, subsequently, for the entire life of the bridge to be estimated.

Figure 6 shows the frequency of maximum stress for 10 trains during the recording period, excluding stress ranges less than 7 ksi. The maximum recorded stress range was 16 ksi, which accounted for only 3.5 percent of the total number of cycles. The effective stress range (S_r Miner) was calculated to be 10.6 ksi. Examination of the stress histories indicated that there occurred one load cycle per car or locomotive for the hanger members. Each wheel group (the two trucks from adjoining cars) gave one complete cycle.

PHYSICAL PROPERTIES

Wrought iron is a two-component metal that consists of high purity iron and iron silicate, a particular type of glasslike slag. Originally, the slag content of wrought iron (2.5 percent by weight) was thought to be an undesirable impurity. But it was eventually realized that the slag was responsible for the desirable properties of wrought iron--its resistance to corrosion and to fatigue.

Nineteenth century furnace temperatures were not high enough to keep the refined iron from solidifying and trapping some of the molten slag during the final stages of the refining operation. Bessemer's development of steel making was originally intended to produce wrought iron of higher quality and lower cost than what was currently available. But the process resulted in steel that did not contain the slag. It had superior mechanical properties and could be manufactured in greater quantities and at a lower cost.

In wrought iron, slag is distributed throughout the iron matrix, generally in the form of threads of fibers that extend in the direction of rolling. Approximately 250,000 of the siliceous fibers are present in each cross-sectional square inch. Corrosion resistance is attributable to the purity of the iron base, freedom from segregated impurities, and the presence of the slag fibers distributed throughout the metal base. The slag fibers are present in sufficient numbers to form an effective barrier to the process of corrosion, forcing it to spread over the surface of the metal rather than to pit or penetrate (1).

Tensile tests of wrought iron bars taken from the structure gave a minimum yield stress of 26 ksi at 0.002 offset. The tensile strength was measured as 45 ksi. These results agree with ASTM specifications for A42-13 wrought-iron plates.

FATIGUE TESTS

The laboratory fatigue tests of the hanger lap splice were conducted in two parts to accurately assess the severity of the transverse weld cracks. Initially, specimens were fabricated and tested by using pieces of wrought-iron bars salvaged from span E. This span was replaced when the original span was knocked into the river during a barge collision. Later, as a result of the replacement of the cracked hangers, the actual welded joints from span F became available. These were also fatigue tested, examined, and then compared with the fabricated specimens. Figure 7 shows a lap splice repair of span F in the alternating stress testing machine.

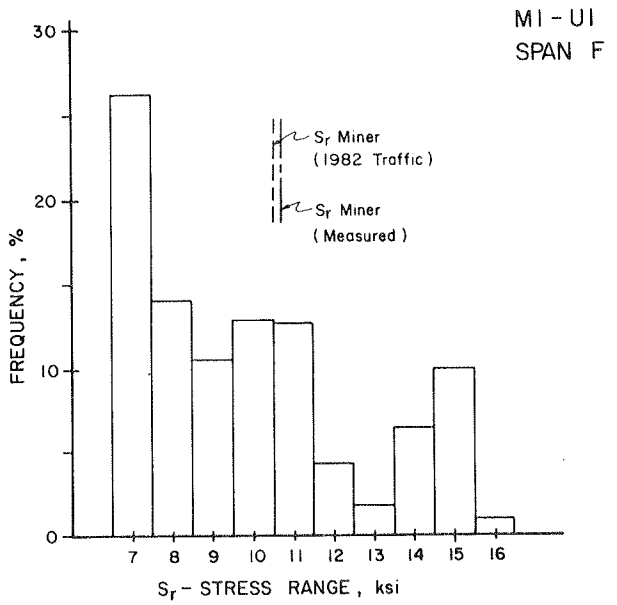

FIGURE 6 Histogram for hanger, span F.

Testing of Fabricated Specimens

A total of seven tests were conducted by using three different constant amplitude stress ranges and two variations of the weld orientation. The first three test specimens were run at a stress range of 12 ksi. Although there was noticeable cracking along the toe of the transverse weld, failure of these three specimens did not occur at this location. The first two specimens incorporated the center junction, which was subjected to a stress range of 10 ksi. This resulted in failure of the specimen at this location at 2.1 million cycles for specimen 1 and 3.6 million cycles for specimen 2. The cracks initiated in the longitudinal weld that bridged the gap between the wrought-iron plates and propagated into the steel plates. These failures correspond to the fatigue life for ordinary steel and plot near the category D fatigue strength curve, as can be seen in Figure 8. However, the test sample is so small that assessing the resistance using category E is a reasonable lower bound. Clearly, it was this location that controlled the fatigue life of the lap splice connection.

After failure of the steel plates, both specimens 1 and 2 were regripped to continue testing of the

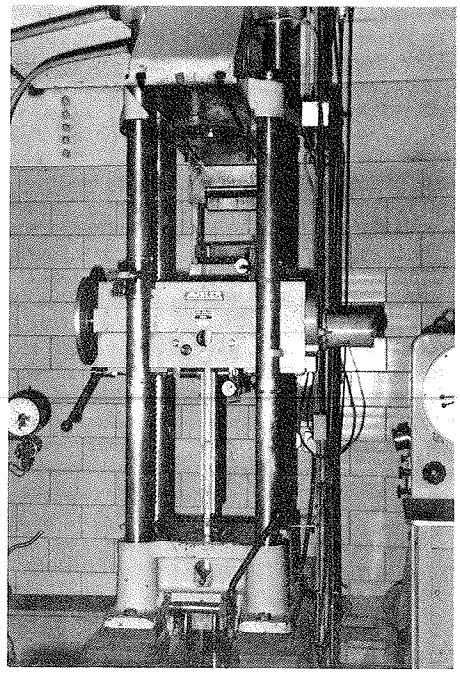

FIGURE 7 Alternating stress test machine.

Because the properties of wrought iron are not isotropic but are directionally dependent, a seventh test specimen was fabricated with the steel plates welded to the edges of the wrought-iron bar. The specimen was tested at a constant stress range of 15 ksi, and the fatigue crack propagated perpendicular to the edges of the elongated stringers. This did not result in crack arrest, and the failure occurred at 0.46 million cycles. This failure life plots within the scatter band of a category E detail and is shown by the cross in Figure 9.

In order to evaluate the fracture toughness of the toe crack, the temperature was lowered on two specimens during testing. Specimens 1 and 4, run at stress ranges of 12 and 18 ksi, respectively, did not fail by fracture with a reduction in temperature to -40°F. The test results indicate that the welded wrought iron had a relatively high resistance to crack instability at reduced temperatures. It was concluded that the toe-cracked eyebars would not fail because of brittle fracture.

Testing of Span F Hangers

Six of the eight hangers in span F that contained the lap splice repair were removed from the structure. The six lap splice joints were cut from the members and shipped to the laboratory for detailed examination. Several were fatigue tested, and the remainder were cut open to reveal the extent of the cracking.

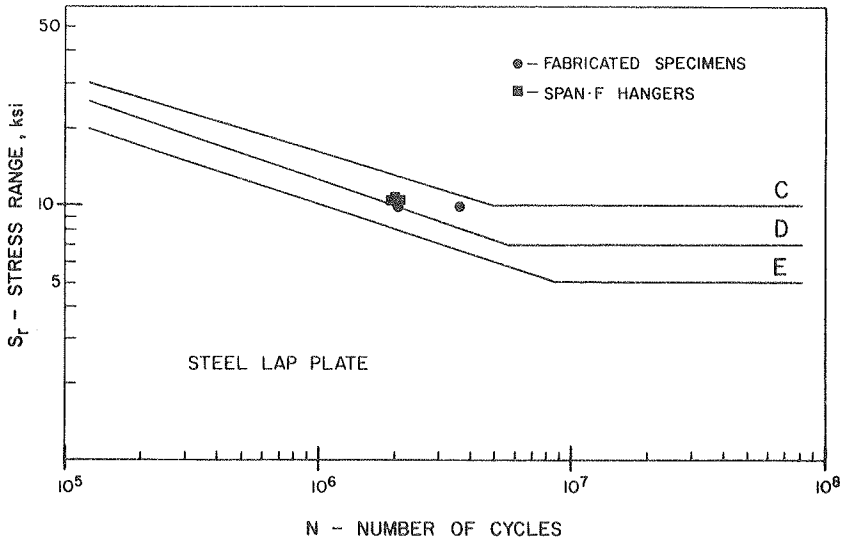

FIGURE 8 Plot of steel lap plate data on S-N curve.

transverse welds that provided a cover plate detail. Both specimens were tested to 20 million cycles without failure at this location, although noticeable cracking at the weld toe and in the weld occurred. Specimen 3, which incorporated only the end detail, was tested to 6 million cycles without failure and then was destructively examined to evaluate the cracking.

Because failure at the toe weld of the wrought-iron plate did not result in failure at 12 ksi, the stress range was increased to 18 ksi for the next three specimens. At the higher stress level failure occurred at the toe of the transverse weld beginning at approximately 0.74 million cycles. This was still well above the fatigue strength expected at a category E detail. All fatigue test results applicable to the wrought-iron members are plotted in Figure 9. Those tests that were stopped before failure are indicated with an arrow.

The actual bridge lap splices were found to be of lower quality with respect to the welding and workmanship when compared to the laboratory-fabricated specimens. These repairs were conducted in 1937, when the welding process had not been adequately developed, and they were made under field conditions. The majority of the transverse welds were found to be undersized for the given plate thickness. The weld sizes ranged from 0.1875 to 0.25 in. for a 0.875-in. plate. Current design specifications require a minimum weld size of 0.3125 in. In addition, the welds exhibited porosity and undercutting of the wrought-iron plate. Many of the weld profiles had a contact angle that greatly exceeded 45 degrees.

One full-sized joint was placed in the alternating stress machine and fatigue tested at a stress

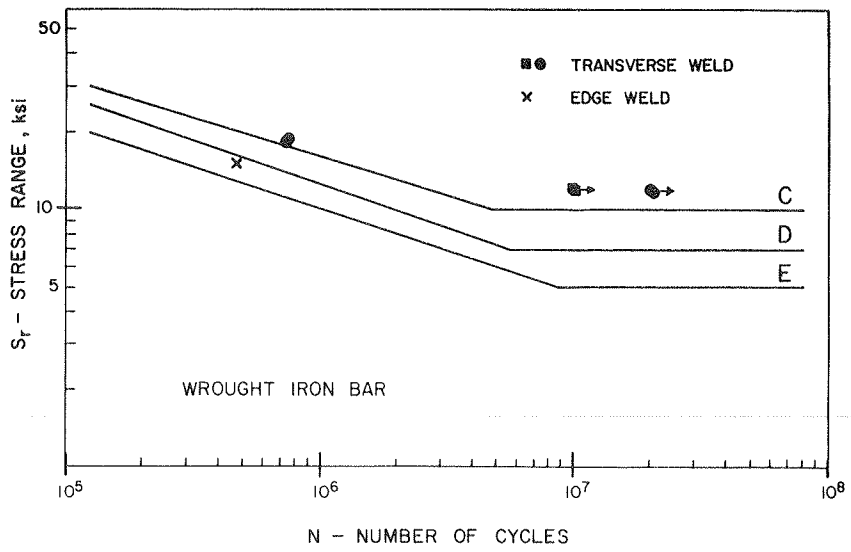

FIGURE 9 Plot of wrought-iron data on S-N curve.

range of 12 ksi in the eyebar. As expected, failure occurred, with a fatigue crack orginating at the center gap, where the stress range was 10.7 ksi, and propagated into the steel plates. Final failure occurred at 1.9 million cycles; the results are plotted in Figure 8. This obviously is a lower-bound estimate of the life, as it did not consider the stress cycles experienced by the detail in the bridge. Each of the two resulting halves of the original joint were then tested separately to evaluate the fatigue resistance of the visible transverse weld toe cracks. Although each piece experienced toe cracks in the wrought iron and root cracking of the welds, the tests were carried to 10.0 million cycles without any evidence of failure or inability to continue to resist the cyclic loads. These tests are also plotted in Figure 9; the arrows indicate that they had not failed. Two additional joints were tested to determine the fatigue strength of the steel splices. These tests are plotted in Figure 8 as solid squares. All three joints provided slightly less fatigue resistance than the fabricated specimens as a result of their prior cyclic loading in the structure.

The remaining lap splice joints were cut open to expose cracks that might have occurred in the welds during service. For most joints, cracks were found on only one side of the joint. This was generally observed at the weld with the greater reinforcement angle. Also, toe cracks were found toward the center portion of the transverse weld, and root cracks were found at the outer ends of the weld. No cracking was found in the longitudinal welds, except at the center gap location. Here the crack had propagated through the entire weld, but in no case was the crack observed to enter the steel lap plates. Figure 10 shows an exposed surface at the member gap. The two lap plates were partly cut with a saw before pulling the member apart at a reduced temperature. No significant crack extension can be seen in the splice plates. Cracking was visible in the welds at each edge only.

Examination of Results

The mechanism of crack formation and propagation is as follows. Fatigue cracks were found to begin at the toe of the transverse weld in the welded center portion of the wrought-iron plate. Visible cracks

FIGURE 10 Exposed welded gap.

were first noticed at approximately 0.5 million cycles at a stress range of 12 ksi. Initially, the toe cracks propagated perpendicular to the thickness of the wrought-iron plate until they encountered a significant slag stringer. The crack may then reinitiate out of the stringer at a location that is further into the joint. The crack continues to encounter stringers, and this process continues to a depth of approximately 0.1875 to 0.125 in. at an approximate angle of 45 degrees. At this point the crack is arrested as the crack turns and extends vertically into the joint, parallel to the stress. The angle of growth corresponds to the plane perpendicular to the stress field through the fillet weld. The crack growth results in a staircase effect, as can be seen in Figures 11 and 12.

The importance of the stringers in the wrought iron appears to be their ability to arrest the transverse crack and deflect the growth of the crack into the joint. A similar joint geometry in steel would result in the toe crack propagating through the thickness of the main plate. In the welded wrought iron, the crack is arrested and turned parallel to the plate and cyclic stress. There is an obvious redistribution of the stress in the vi-

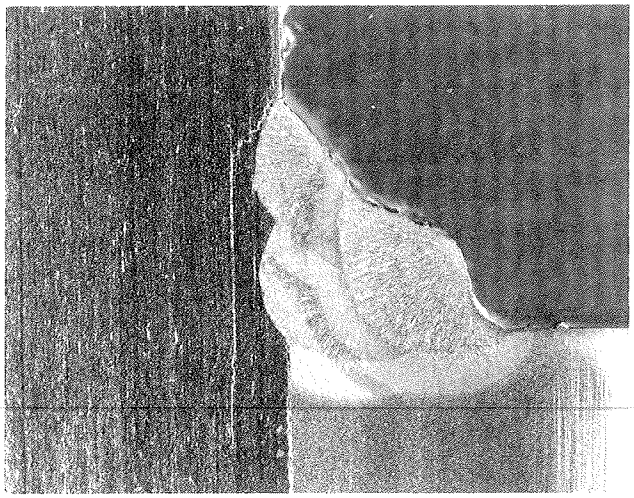

FIGURE 11 Crack growth in test specimen.

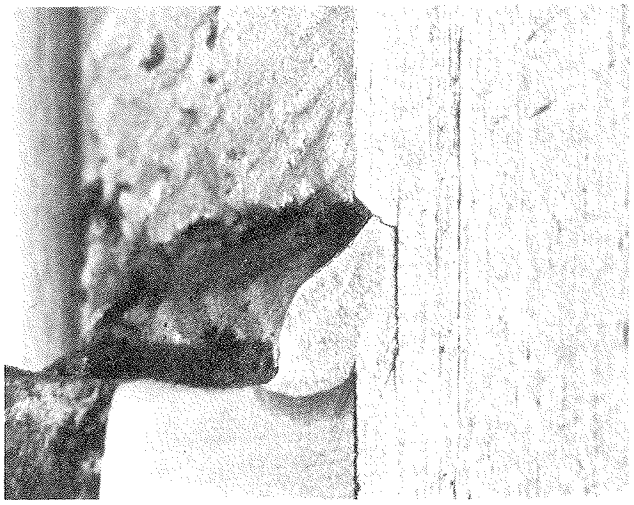

FIGURE 12 Crack growth in span F hanger.

cinity of the crack front. As the crack moves into the joint following the laminated stringers, the stress is redistributed to the longitudinal welds. The redistribution of the stress to the outer portions of the joint results in root cracking in both the longitudinal welds and in the outer portions of the transverse welds because the weld sizes were small. Eventually all the load was transferred through the longitudinal welds, which resulted in continued crack extension along the weld throat.

Fatigue testing at a high stress range of 18 ksi resulted in a maximum stress level of 21 ksi. This maximum stress corresponds to approximately 80 percent of the measured yield stress of the wrought iron. As the fatigue crack propagated into the joint, the cross section of the wrought-iron plate was reduced. This resulted in yielding of the net section of the wrought-iron plate and also resulted in continued crack extension, with the eventual failure of the section. Such high stress ranges would not be expected in a wrought-iron structure.

The test results from the welded wrought-iron specimens and the actual hangers are summarized in Figures 8 and 9. These tests demonstrate that the fatigue resistance is much greater than that provided by category E--the expected fatigue category for such welded steel details. None of the details tested at a stress range of 12 ksi failed as a result of the crack that formed at the weld terminations. These cracks were arrested and did not impair the load-carrying capability of the joint. Failure, should it occur, was shown to develop at the gap region.

TRAFFIC STUDY AND FATIGUE ASSESSMENT

To accurately assess the severity of fatigue cracking in welded lap splices, the stress history spectrum for the hanger member must be determined. By reviewing the traffic that the structure has experienced and its relation to the stress levels in the hanger, an estimate can be made of the cumulative fatigue damage and the remaining life of the structure.

Because of the long history of the bridge and a change in ownership, limited traffic data were obtainable from the Norfolk and Western Railway. Available data included the following: train timetables from 1936 to 1963, annual gross tonnage figures from 1971 to 1981, and a listing of all train movements during 1982. Because these data were insufficient for an adequate traffic study, it became necessary to supplement it with other sources of data. Correlation was made with traffic data from Canadian National (CN) Rail at bridges that were on lines similar to that of the line that Bridge 651 traverses (2,3). CN has done extensive traffic studies on many of their lines, which allows them to develop useful averages and to indicate particular trends from an extensive data base.

Given the limited amount of traffic data, the traffic frequency and distribution must be estimated. There are several important parameters that can be used to generate the necessary information. These are the number trains per day, locomotive weights, engine units per train, annual gross tonnage, and carload distribution. Although not all parameters are known for each year under study, not all are needed for any one particular year. The method used in a particular time period was dictated by the available information.

The period of concern for the hangers is from 1937, when the welded repairs were performed, to the present. Also, an estimation for the future (to the year 2000) was made. For each year, the number of locomotives and cars that crossed the bridge was estimated. Studies by CN concluded that only cars more than 60 gross tons have a significant effect on the fatigue life, and all other lighter traffic could be ignored (4). From 1937 to 1954 it was assumed that only the locomotives contributed to fatigue damage because carloads seldom exceeded 60 tons. Assuming one locomotive per train (typical with steam locomotives), the yearly total was calculated from the timetables. Because extra freight trains were run in a given time slot, the number of scheduled trains, both passenger and freight, was increased by 10 percent. Beginning in 1955, with the complete conversion to diesel, carloads began to increase. The number of cycles per year from the carloads was determined by multiplying the annual gross tonnage by the percentage of cars greater than 60 tons and dividing by the root-mean-square value for carloads greater than 60 tons. The number of locomotive loadings was determined from available timetables, with the realization that more than one diesel unit could be used on one train. Beginning in 1962, when train tables were no longer available, the number of locomotive units was determined by dividing the annual gross tonnage by the estimated average gross tons pulled by one unit. Carload cycles were determined as previously mentioned.

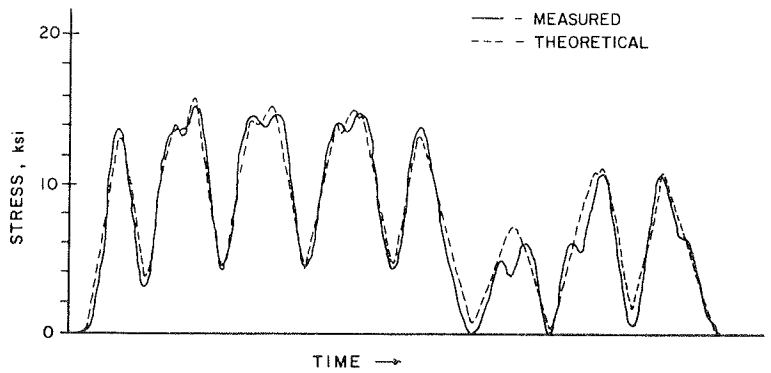

FIGURE 13 Comparison of measured and theoretical response.

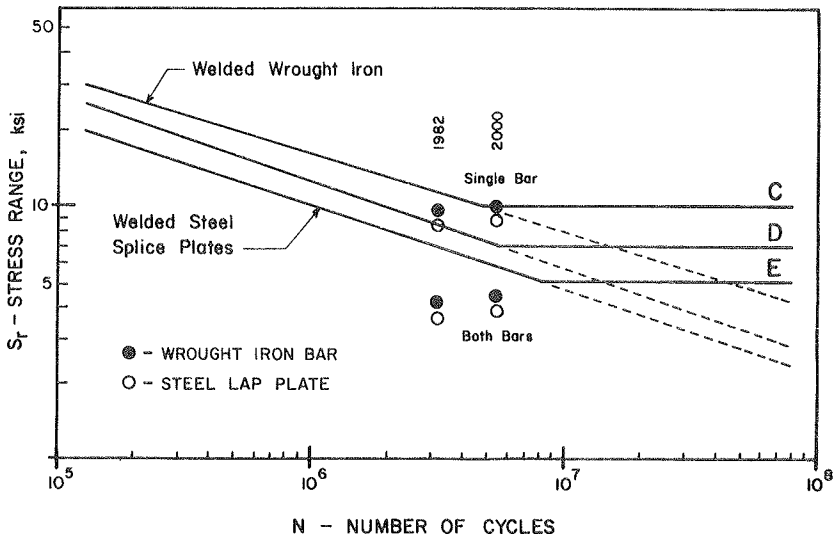

FIGURE 14 Plot of estimated fatigue life for hangers, span F.

Having the number of loading cycles caused by both locomotives and carloads for each year, it was necessary to determine the stress ranges caused by them. A three-dimensional linear finite-element model of the span was developed and calibrated with the strain-gauge data obtained during the field investigation. This examination demonstrated that impact effects were negligible and that a space-frame analysis was applicable to the structure. The influence of dynamic effects is reduced on the structure because of the presence of a sharply curved tunnel immediately adjacent to the bridge site. This imposes speed restrictions on all train traffic. Figure 13 shows the correlation between the theoretical and measured stress history for a given train passage. From the computer analysis an influence diagram was developed for the hanger member. A typical wheel-spacing configuration was assumed for both a steam and diesel locomotive and a typical car. Each was given a unit weight and passed across the influence diagram; then the stress range was determined. Then, by using the estimated static values for locomotive and car weights, the effective stress range could be determined for each year. By using Miner's linear fatigue damage relationship, the extent of the fatigue damage could be estimated by summing the number of cycles at a particular stress range for a given year.

A problem of determining the correct effective stress range that corresponded to all damage cycles arose because of the slackness in some in the eyebars. The actual accumulated fatigue damage estimate for a given loaded member is bounded by the condition of both bars carrying the load and by the condition that only one carries the entire load for the member. Assuming that both eyebars were loaded resulted in an effective stress range (S_r Miner) equal to 4.3 ksi for 3.1 million variable load cycles. Projected to the year 2000, the figure increases to 4.5 ksi for 5.2 million cycles. With only one bar participating, the 1982 value increases to 9.8 ksi for 3.1 million cycles, and the future damage increases to 10.3 ksi for 5.2 million cycles. These points are plotted in Figure 14 and are compared to AASHTO fatigue categories and the fatigue test data developed on the welded wrought-iron joints.

The predicted effective stress range and accumulated cycles of the variable loading plot well below the fatigue resistance provided by welded wrought-iron end details. The tests on laboratory-welded specimens and on cracked details removed from span F demonstrated that a stress range of 12 ksi would not produce failure, even after 20 million cycles of loading. The effective stress range and cumulative cycles in 1982, as well as those projected to 2000, are well below those resistance values. Had both hangers been effective and the stress range decreased, an even greater margin of reserve life would exist.

Because the lap plate splices are more critical at the cross section at the center of the joint where the eyebar was cut, those values are plotted in Figure 14. The increased cross-sectional area decreases the effective stress range to 3.8 ksi in 1982 if both bars are effective and to 8.7 ksi if only a single bar is carrying the load. The small degree of cracking observed in the field and in the eyebars removed from the structure suggests that both hangers were carrying the load throughout much of their life. Had both hangers shared the load, no appreciable damage would have developed for the traffic projected to the year 2000.

SUMMARY AND CONCLUSIONS

As a result of the fatigue tests of welded wrought iron with welded lap splice repairs and the correlation with the load history of the bridge, the following conclusions were reached.

1. Surface cracks were found to develop at the toe of the splice plates that were welded to the surface of the wrought-iron eyebars at cycle lives comparable to welded steel components. These cracks were found to have no adverse effect on the fatigue resistance of the wrought-iron members because they were arrested by the wrought-iron slag stringers.
2. An evaluation of the load history to which the members were subjected indicated that the weld toe cracking would be expected. It primarily resulted because the two eyebar hangers were not sharing the load. One eyebar was found to be loose, and this increased the cyclic stress in the other eyebar by slightly less than 50 percent.
3. Laboratory fatigue tests were carried out on simulated welded joints and on several of the cracked eyebar hanger splices. The simulated test joints demonstrated that the wrought iron would arrest the fatigue cracks that formed at the weld toe at stress levels expected in the structure. The weld toe cracks encountered the flattened longitudinal stringers and were arrested as the crack deflected parallel to the cyclic stress. The crack-arrested details were able to sustain 20 million stress cycles at 12 ksi without any further evidence of distress. The cracked hangers were also fatigue tested, and they yielded comparable results.
4. The laboratory tests also demonstrated that the steel splice plates were the more critical detail. The four tests carried out provided a fatigue resistance comparable to category D, although they are classified as category E details. Because the stress range at the critical steel section was less than the wrought-iron bar, the hangers had not experienced much growth at those sections.
5. The stress history analysis and laboratory evaluation demonstrated that the other weld-repaired members (such as chord and diagonals) were not susceptible to any appreciable crack growth and would not be fatigue critical.
6. A pilot test on the edge-welded wrought-iron splice demonstrated that the stringers were not effective in arresting fatigue crack growth.

ACKNOWLEDGMENT

This study was sponsored by the Norfolk and Western Railway. The authors are indebted to E. Bond, assistant chief engineer of structures, for his cooperation and assistance with this study. The authors are also indebted to the staff of Fritz Engineering Laboratory, Lehigh University, for their assistance throughout this study. H.T. Sutherland assisted with both the field studies and the fatigue tests, R. Sopko with photography, and R. Dales and C. Hittinger with the laboratory testing.

REFERENCES

1. J. Aston and E.B. Story. Wrought Iron, Its Manufacture Characteristics and Application. A.M. Byers Company, 1939.
2. I.A.S. Elkholy. Estimated Fatigue Damage in the 83'-0 Deck Truss Span of the Muskoka River Bridge, Mile 116.8, Newmarket Subdivision, Huntsville, Ontario, Canada. Technical Report. Canadian National Rail, Montreal, Quebec, Canada, April 1981.
3. R.A.P. Sweeney and I.A.S. Elkholy. Estimated Fatigue Damage in the 206'-3 Through Truss Span of the Ottawa River Bridge, Ste Anne de Bellevue, Quebec, Canada. Technical Report. Canadian National Rail, Montreal, Quebec, Canada, June 1980.
4. R.A.P. Sweeney. The Load Spectrum for the Fraser River Bridge at New Westminster, B.C. Proc., American Railway Engineering Association, Washington, D.C., 1976.

Publication of this paper sponsored by Committee on Dynamics and Field Testing of Bridges.

Evaluation and Field Testing of the Dan Ryan Rapid Transit Structure

ANDREW E. N. OSBORN and MICHAEL J. KOOB

ABSTRACT

The Dan Ryan rapid transit structure is a 40-span, 4,000-ft-long elevated structure that carries Chicago Transit Authority (CTA) rapid transit trains into and out of the Chicago Loop. The structure, which was completed in 1969, consists of welded stringers and is supported by steel box-girder bents. Splices in the stringers are field bolted. The steel stringers carry two sets of track on a ballasted concrete deck. In January 1978 major brittle fractures occurred in three of the steel box-girder bents. Since discovering the bent fractures, CTA inspectors found two long cracks in the bottom of the stringers. These cracks were found to originate at welded lateral gusset-plate connections. Approximately 1,800 lateral gussets are used in the 40-span system to attach lateral bracing. Each gusset plate contains a cutout to accommodate the vertical stiffener of the stringer. This detail creates a short gap between the cutout of the gusset and the vertical stiffener. An extensive investigative study of seven spans of the superstructure was carried out to assess the fatigue sensitivity of the stringers with the lateral gusset-plate connections. The study included a review of details used in the structure, field instrumentation and testing, an analytical review, in-depth examination of gusset-plate connections, examination and testing of samples that contain cracks, and the development of retrofits. The information collected during the study, particularly the field testing data, is reviewed. Reviews are also made of the fractographic examination conducted on a sample that contains a 4-in. crack and the in-depth inspection findings. As part of this study retrofits were developed to either shield the crack origin from stress or to increase the gap between the gusset-plate cutout and the vertical stiffener.

A post-construction investigation of the Dan Ryan elevated rapid transit structure between 17th and 23rd streets in Chicago was conducted for the Chicago Transit Authority (CTA). The purpose of the investigation was to evaluate the sensitivity of welded details in the structure to fatigue.

Field work consisted of in-depth inspection and strain-gauge instrumentation of critical conditions in the structure. This work was carried out between August and November 1982. Office activities included identification of critical details, structural analyses, evaluation of test data, and development of recommendations for retrofitting and ongoing inspection.

DESCRIPTION OF STRUCTURE

The CTA's Lake-Dan Ryan rapid transit line provides direct service between the south and west sectors of Chicago. The structure under investigation consists of 40 spans, with a total length of about 4,000 ft. A plan view of the structure is shown in Figure 1.

The viaduct structure is of welded steel construction and was completed in June 1969. The superstructure consists of continuous and suspended plate girders (stringers) with a cast-in-place, U-shaped concrete deck. Figure 2 shows a typical structural cross section at a hammer-head pier. In addition to single-column supports referred to as pier, the structure includes seven inverted U-shaped supporting structures that have double columns; these are referred to as bents. Three of these bents sustained major fractures in January 1978 (1). Six stringers are used in each of spans 2-16 (double track); four stringers are used in each of spans 1 and 17-34 (double track); and spans 35NB-37NB and 35SB-40SB use two stringers (single track). Stringers are curved in spans with sharp curvature.

The plate girders are provided with vertical stiffeners spaced approximately 4 ft apart and horizontal gusset plates spaced at approximately 8 or 16 ft, depending on location. The gusset plates are located about 4 in. above the bottom flange of the stringers. Deep, channel-shaped diaphragms are bolted to stiffeners along the web of the channel and gusset plates at the channel flange. Lateral bracing members are also bolted to the gusset plates. Lateral bracing consists of angle K bracing to bent 34 and structural tee X bracing beyond bent 34. A plan view of three spans that shows the variation in framing systems is presented in Figure 3. The underside of span 15 is shown in Figure 4; it shows the lateral bracing system typical of spans 2-16.

Lateral gusset plates are welded to the webs of stringers, with the vertical stiffener fitting into a cutout in the gusset plate, as shown in Figures 5 and 6. In spans 1-27 the cutouts are close fitting, and fillet welds were used for the gusset plate to stringer web connection. In spans 28 and above there is an approximate 0.5-in. gap between the cutout edge and the stiffener, and the gusset plates were single-bevel groove welded to the web. Back-up bars were used to make the groove weld connections in spans 35-40. The back-up bars or gusset plates were attached with short intermittent fillet welds for fit-up before completing the groove welds. The termination of all these welds represents conditions that are sensitive to fatigue (2).

In 1978 the CTA found an 8-in.-long crack in span 35 that originated in the gap between the gusset-plate cutout and the vertical stiffener. Holes were drilled at both the top and bottom ends of the crack as a retrofit measure.

In fall 1982 a crack was found in the stringer of span 15. Again the crack originated at the gap between the vertical stiffener and the gusset-plate cutout. The crack had propagated down through the bottom flange and also up about 12 in. into the web. A hole was drilled at the top end of the crack and a cover plate was bolted to the bottom flange across the crack. An exterior view of the crack is shown in

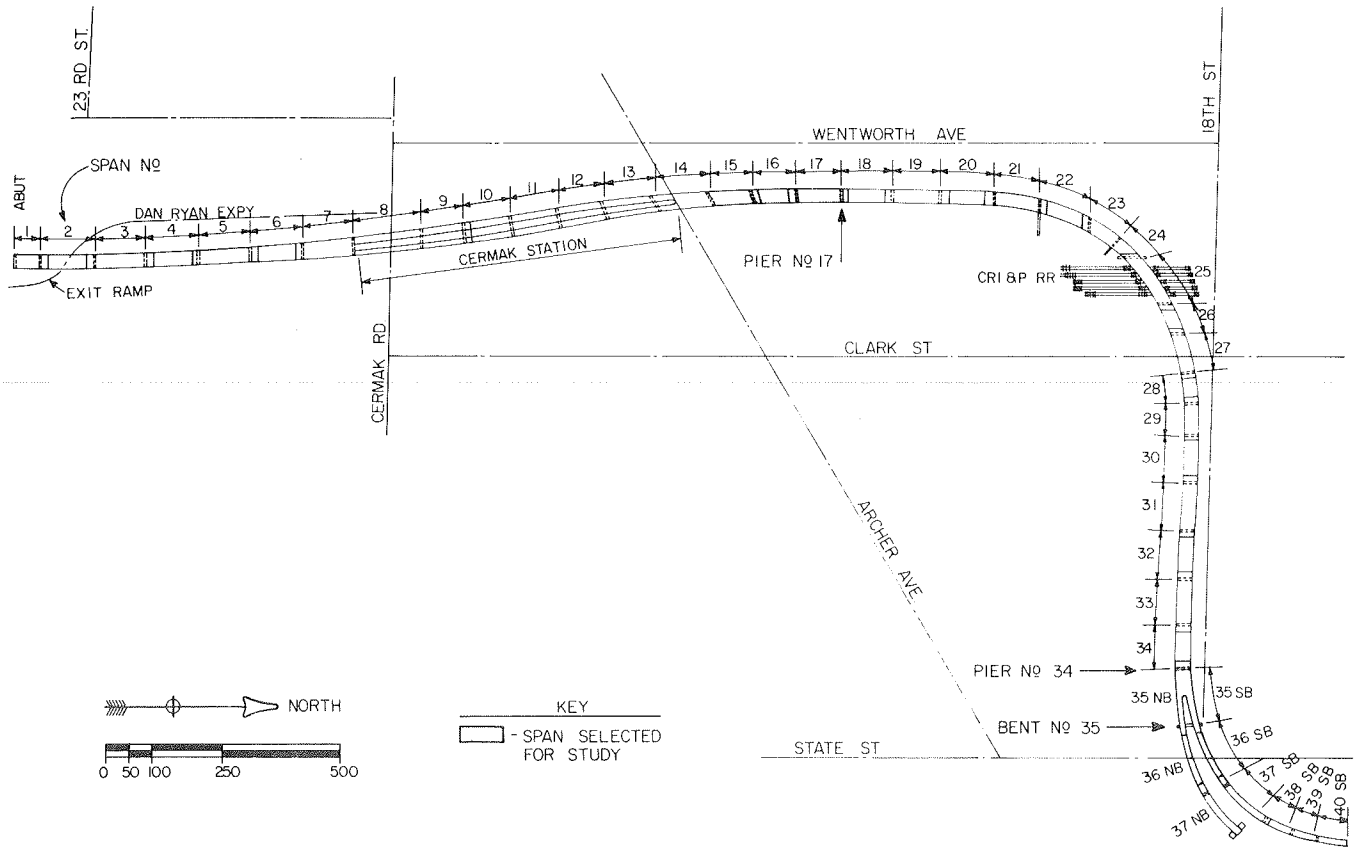

FIGURE 1 Plan of Dan Ryan elevated structure under study.

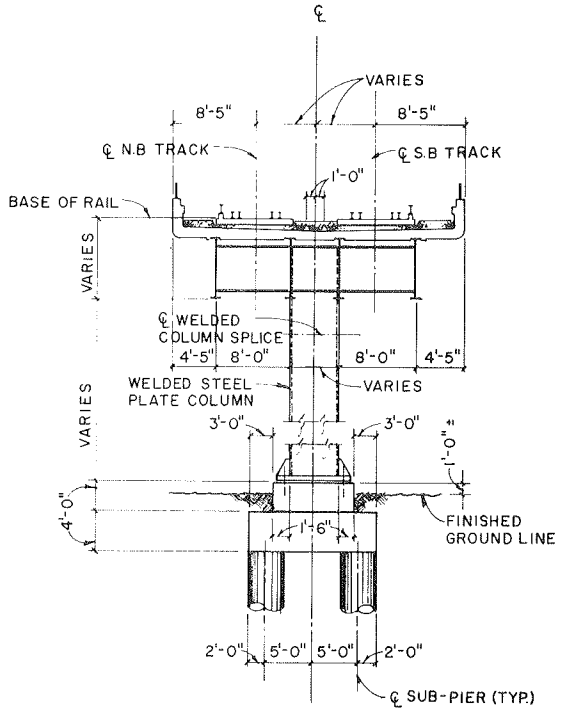

FIGURE 2 Cross section of structure at a hammer-head pier.

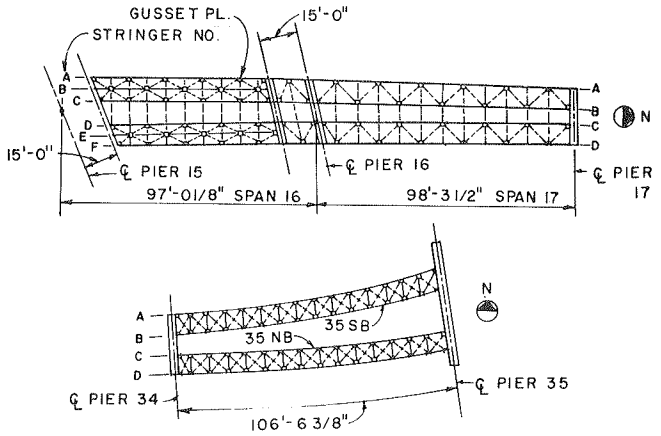

FIGURE 3 Schematic showing the three general types of framing.

Figure 7. Staining in Figure 7 is from the cutting oil used for drilling.

The discovery of these cracks increased concern over the fatigue sensitivity of the lateral gusset-plate connection and precipitated this evaluation study.

DESCRIPTION OF WORK

The study consisted of five tasks, as follows:

1. Conduct a limited structural analysis of the viaduct superstructure to determine theoretical stress ranges at fatigue-sensitive details,
2. Install strain-gauge instrumentation and per-

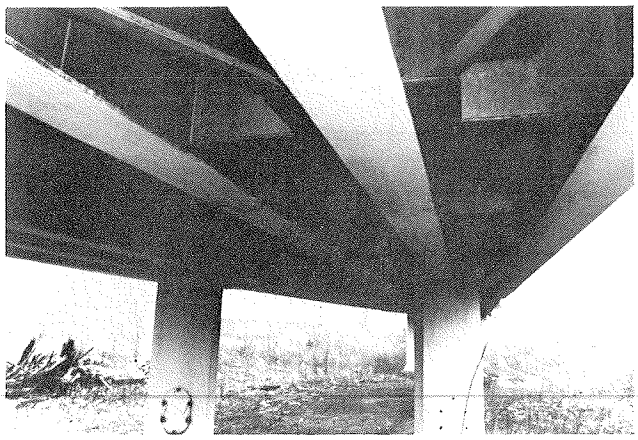

FIGURE 4 View of framing on the underside of span 15.

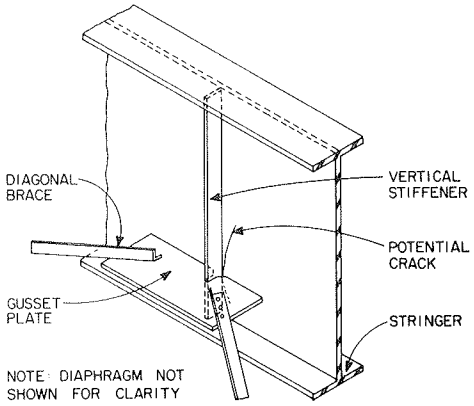

FIGURE 5 Gusset-plate connection: schematic view.

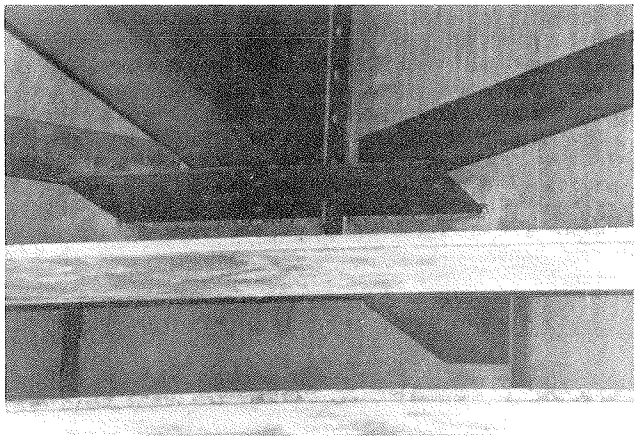

FIGURE 6 Gusset-plate connection: typical detail.

form tests at selected locations in several spans under normal and controlled loadings,

3. Perform a high-quality fatigue crack inspection of gusset-plate welds in the same spans where instrumentation was installed,

4. Remove steel samples for visual and microscopic evaluation, and

5. Develop a structural retrofit for the gusset-plate detail.

FIGURE 7 Appearance of retrofitted crack located in span 15.

Structural Analysis

A structural analysis was performed on a simplified analytical model of the elevated structure. The steel stringers were assumed to act compositely with the concrete deck, and curvature effects were included in the model. The stiffnesses of the box bents included consideration of soil-structure interaction. The lateral rigidity of the U-shaped deck was modeled; however, the torsional rigidity provided by lateral bracing and diaphragms was omitted.

Dead loads were based on information contained in the design drawings. Live load was based on the fatigue and deflection loading criteria of 19.5 kips per axle established by CTA (see Figure 8). These loads are higher than those used when the structure was designed because of the introduction of the heavier 2600 series cars in 1981. An impact factor of 40 percent was added; however, testing discussed later indicated that impact effects were much smaller. Thus the tabulated stresses reported here do not include impact.

The actual train weights were somewhat less than the design loading criteria. Empty train car weights vary from 45 to 54.3 kips for all series of cars used on this structure. The weight of passengers that can occupy the seat and aisle area is expected to be about 26 kips under maximum loading conditions. Normal rider weight during rush-hour traffic, however, is probably closer to 16 kips per car, or 4 kips per axle. Thus normal rush-hour axle loads are probably in the vicinity of 17.5 kips. This estimate has been used to compare theoretical and field-measured results. On a weekday 78 eight-car trains, 131 four-car trains, and 20 two-car trains traverse the line in both directions. On weekends the traffic is lighter. Altogether, about 1,400 trains pass in each direction every week.

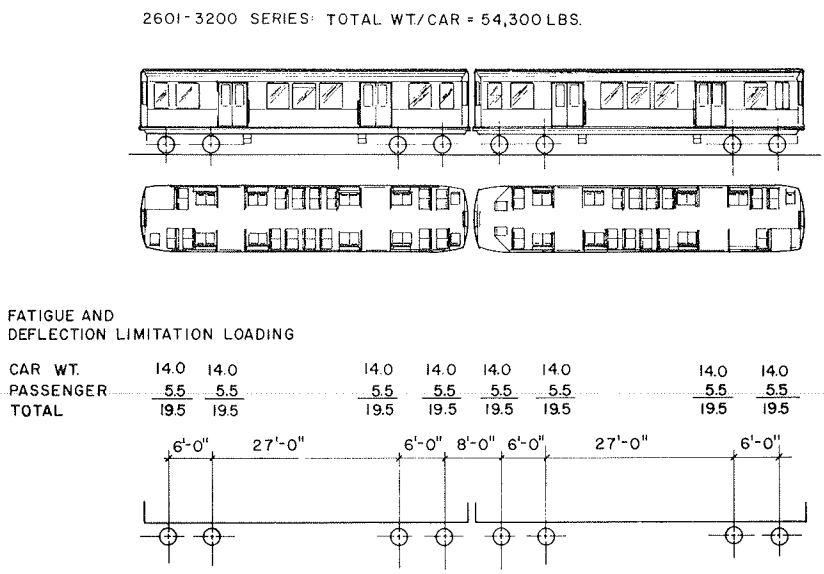

FIGURE 8 Elevation and axle load pertaining to transit car.

TABLE 1 Calculated Midspan Stringer Stresses at Level of Gusset Plate

Span No.	Approximate Dead-Load Stress (ksi)	Live-Load Stress Range (ksi)	
		Two-Car Train	Eight-Car Train
1	3.0	1.4	1.1
2	10.8	2.1	2.1
3	10.3	3.8	3.1
4	10.5	1.9	1.9
5	11.6	1.6	3.1
6	10.8	1.8	1.8
7	10.1	3.2	2.6
8	17.3	3.3	3.0
9	9.0	2.9	2.3
10	15.7	2.0	1.8
11	12.4	2.7	2.4
12	10.4	2.0	1.8
13	10.1	2.4	2.1
14	15.1	3.1	2.9
15	6.2	2.6	2.1
16	8.1	2.5	2.5
17	11.8	4.0	3.4
18	11.7	2.3	2.3
19	8.8	3.6	3.0
20	11.7	2.3	2.3
21	10.5	3.9	3.2
22	9.2	1.7	1.7
23	6.2	2.8	2.2
24	6.1	1.4	1.4
25	15.9	3.8	3.5
26	5.9	1.5	1.5
27	7.4	2.1	1.9
28	3.9	1.0	1.0
29	3.1	1.8	1.4
30	9.6	1.9	1.9
31	9.5	3.9	3.1
32	8.6	1.7	1.7
33	10.1	3.8	3.1
34	9.2	2.0	2.0
35NB	8.5	2.8	2.3
35SB	7.5	2.6	2.1
36NB	12.2	1.9	1.9
36SB	11.6	1.7	1.7
37NB	17.4	2.8	2.7
37SB	10.8	2.9	2.5
38SB	8.1	1.2	1.2
39SB	6.1	1.4	1.2
40SB	6.1	1.3	1.1

Note: Live-load tabulation based on axle load of 19.5 kips. In curved spans the longest storage span was analyzed.

In calculating the total dead-load stresses, noncomposite action was assumed for the weight of the steel stringers, steel bracing, and concrete deck. Composite action was assumed for the remaining dead loads and all live loads. This procedure increased the calculated dead-load stresses by about 30 percent when compared to an analysis based on a fully composite structure. The calculated stresses from the structural analysis are given in Table 1.

Instrumentation

Locations in seven spans and three supports were selected for strain-gauge instrumentation. Altogether, 85 gauges were installed. The instrumented areas included both simple and continuous spans, curved spans, and spans where relatively high levels of stress range were expected.

Strain gauges were installed primarily on webs of stringers adjacent to gusset plates, on stringer flanges, and on cross-bracing members. Figure 9 shows an installation adjacent to a gusset plate. Gauges were also installed on the webs and flanges of box bents and on a hinge link. Details of the strain-gauge layout are shown in Figure 10.

Installation Details

Locations in spans 15-17, 21, 22, 35, and 36, and in bents 17, 34, and 35 were instrumented. Single-element, 0.25-in. foil-type strain gauges were bonded to the steel structure by using long-life epoxy adhesive. Copper lead wires of 18 or 22 gauge were soldered to the strain gauges, and the gauges were waterproofed. The entire installation was intended to be durable so that readings could be taken for several years, if desired. The lead wires were extended to three primary junction areas located in bents 16, 21, and 35 and connected to multiple socket connectors. In this way the strain reading equipment could be moved from bent to bent instead of running all the lead wires to one location.

Data Acquisition

The strains were measured by using a Hewlett-Packard

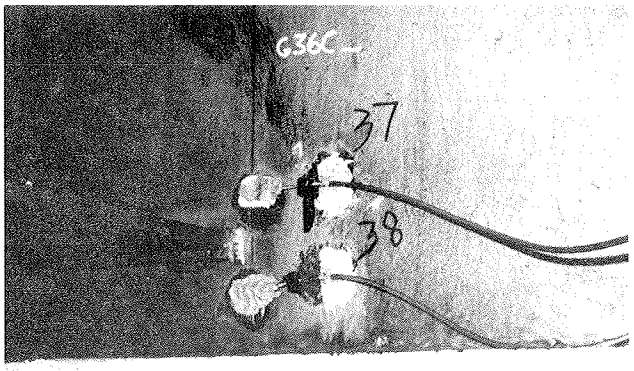

FIGURE 9 Type A gauge installation on web of stringer adjacent to gusset plate.

HP3054 Data Acquisition System coupled to an HP9826 computer. The data logger had the capability of measuring and transmitting approximately 50 channels of voltage data per second. Five gauges were monitored at one time, which permitted about 10 measurements per gauge per second to be recorded for each train. Gauges at comparable locations were generally read together to provide comparisons on the basis of a single train passage.

The accuracy of the data-logging equipment was verified by recording strain data using a strip-chart analog recorder and a peak read digital strain indicator. Both of these instruments gave strain values that were close to those recorded with the digital data-logging equipment. The analog recorder also indicated that there were no high-frequency stress cycles that were being missed because of the sampling rate of the data acquisition system.

Data were recorded dynamically during passages of commuter trains, and both statically and dynamically

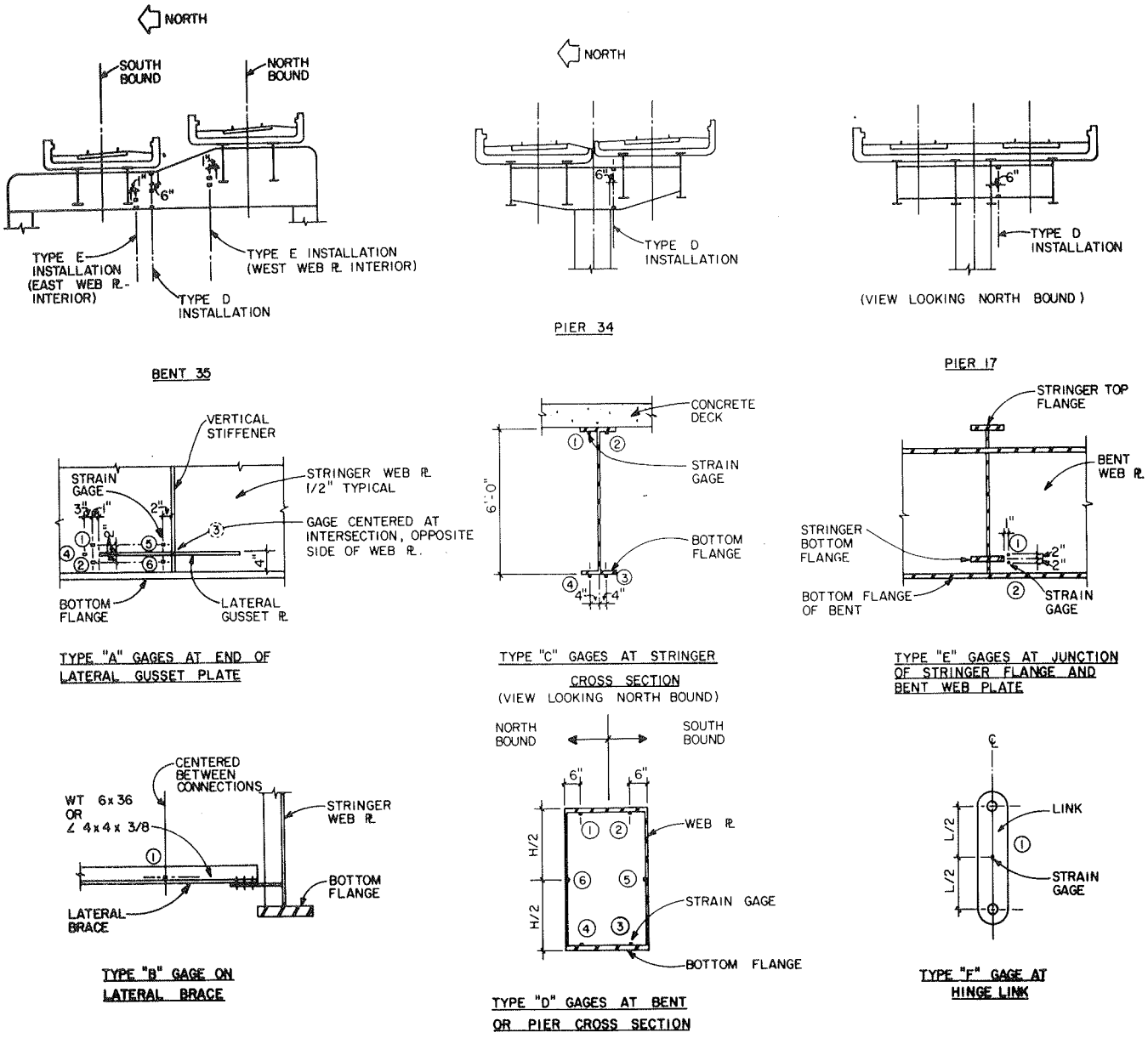

FIGURE 10 Location and designation of strain gauges.

TABLE 2 Comparison of Stress Ranges Measured on Selected Spans

Span No.	Test Train: Two-Car Train Dynamic (ksi)	Test Train: Two-Car Train Static (ksi)	Test Train: Two-Car Train Impact Dynamic[a] (ksi)	Commuter Trains: Four-Car Train Dynamic (ksi)	Commuter Trains: Eight-Car Train Dynamic (ksi)	Test Train: Eight-Car Train Dynamic (ksi)	Test Train: Eight-Car Train Static (ksi)
15SB	1.5	1.6	-	1.4	1.3	1.3	1.3
16SB	1.5	1.4	-	1.6	1.4	1.5	1.5
17NB	1.9	2.0	-	2.0	1.9	1.7	1.8
21SB	2.0[b]	2.0[b]	-	2.0[b]	1.8[b]	1.9[b]	1.9[b]
22SB	1.6	1.5	-	1.7	1.6	1.7	1.6
35NB	2.1	2.0	1.9	1.9	1.8	1.9	1.8
35SB	2.2	2.2	-	1.9	2.1	1.8	1.9
36NB	2.0	1.9	2.0	2.2	2.1	2.2	2.0
36SB	1.7	1.6	-	1.8	2.1	1.9	1.6

[a]These data were obtained by having the two-car train brake suddenly at midspan on 35NB and 36NB only.

[b]Actual measured stresses ranged from ±1.6 to ±2.3 ksi.

by using a CTA test train. Data were obtained from four- and eight-car commuter trains and two- and eight-car test trains.

Commuter Trains

The commuter trains consisted of coupled cars of the 2000, 2200, 2400, or 2600 series. Cars of different series were mixed in a single train. Strain recordings were started as the commuter train approached the point on the structure where it could be expected to have an influence on any of the strain gauges in that region.

Test Trains

Data acquisition involving the test trains was done at night by using 2600 series cars. For the dynamic tests, the motorman was instructed to maintain a constant speed of 25 mph. Data recording was initiated just before the front axle of the train reached the point where it was anticipated to have influence on the strain gauges being monitored. For the static tests, location marks were painted at 10-ft intervals on the rails. For each test, the front wheels of the test train were positioned over a location mark, data were recorded, and the train was advanced 10 ft to the next station. In this way a stress influence line was generated for each gauge. This influence line was compared with those of the dynamic runs to indicate moving train position, speed, and impact factors.

A special dynamic test was also conducted near bent 35 by using a two-car train on the northbound tracks. The train was brought up to speed and then stopped quickly at critical locations by using the emergency brakes. It was expected that this maneuver would result in additional impact loading information for the structure.

Analysis of Data

Type A Gauges Adjacent to Gusset Plate

The stresses measured adjacent to gusset plates agree reasonably well with the theoretical analyses, if a lesser axle load is used in calculations. The measured stress ranges are given in Table 2. Stresses ranged from 1.0 to about 2.5 ksi, with most of the values within 1.5 to 2.0 ksi. The agreement between gauges located adjacent to the same gusset plate was quite satisfactory. The following four observations are based on type A strain-gauge readings.

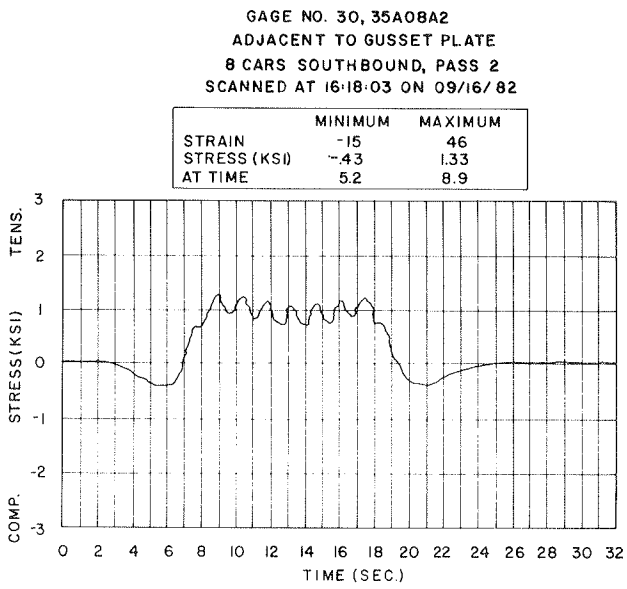

FIGURE 11 Dynamic strain response during the passage of an eight-car train.

1. In all the measured strain responses it was observed that a single train, regardless of length, induces a single large cycle of stress. A typical plot of dynamic strain response during the passage of an eight-car train is shown in Figure 11. In many cases the groupings of four axles at the ends of adjacent cars caused individual cycles to have magnitudes of up to one-third the maximum stress ranges measured. In the most extreme cases the magnitudes of the individual cycles were found to be less than about 400 psi, which is not considered to be significant.

2. Dynamic stresses are a maximum of 10 percent greater than static stresses in simply supported spans, as shown in Figures 12 and 13. In continuous spans the dynamic results are generally equal to the static results (Table 2). These effects are difficult to quantify because the differences are small.

3. As expected, the outside stringer on horizontal curves carries greater loads than the inside stringer. Figure 14 shows comparisons in stress range for geometrically similar gauge locations in adjacent stringers in three different spans. Note that there appears to be a somewhat more equal distribution of load in spans 36NB and 36SB, which are simple spans of only two stringers. The relationship

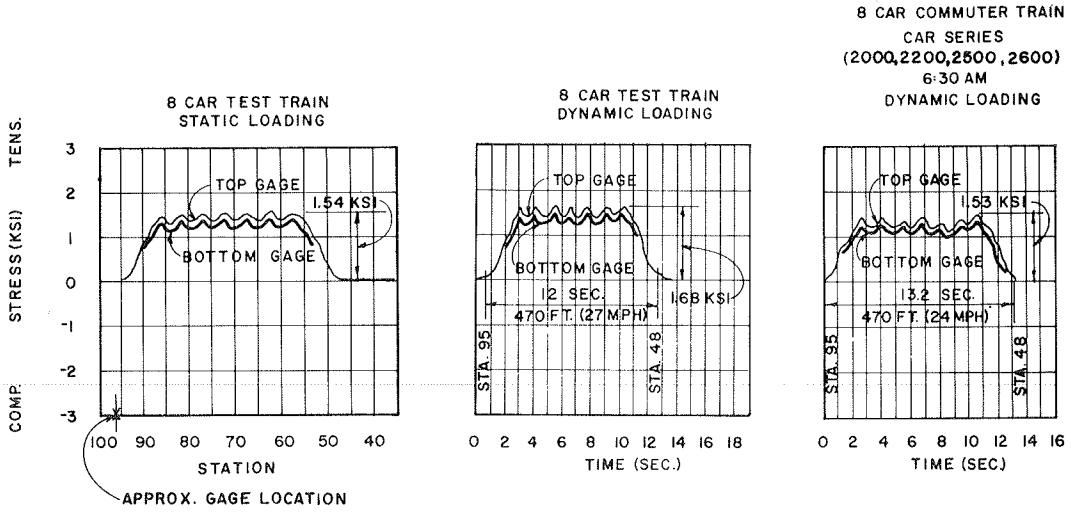

FIGURE 12 Comparison of upper and lower type A gauges in span 22 under different loading conditions.

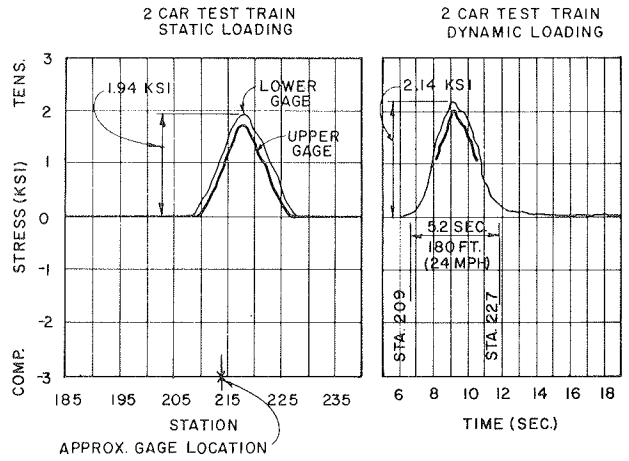

FIGURE 13 Comparison of upper and lower type A gauges in span 36 under different loading conditions.

between the radius of curvature of the stringers and the lateral distribution of loads could not be established with the amount of instrumentation used.

4. Overall, the measured stress ranges adjacent to gusset plates were less than the stress ranges predicted by the analytical studies. The average of measured stress ranges from eight-car commuter trains is 1.7 ksi. The computed value is 2.3 ksi based on 19.5 kips per axle, and 2.1 ksi for 17.5 kips per axle. The maximum measured stress range at any gauge was 2.4 ksi compared with the theoretical values of 4.0 ksi for 19.5 kips per axle or 3.5 ksi for 17.5 kips per axle. Thus measured stress ranges average 60 and 70 percent of the calculated values based on expected and design train loads of 17.5 and 19.5 kips per axle, respectively.

One of the reasons for the difference between theoretical and measured stress levels is shown in Figure 15, which compares stresses from northbound and southbound trains. These gauges are on the exterior stringer under the southbound track in spans 35 and 21. Note that the stresses from northbound trains are 18 and 39 percent of the values from southbound trains, which show the substantial lateral distribution of loads by the concrete deck and steel diaphragms. Smaller lateral stiffnesses for span 35 relative to span 21 are also indicated. Span 35 has a limited lateral bracing system between the northbound and southbound sides of the structure.

Type B Gauges on Lateral Bracing

Readings on type B gauges generally were relatively

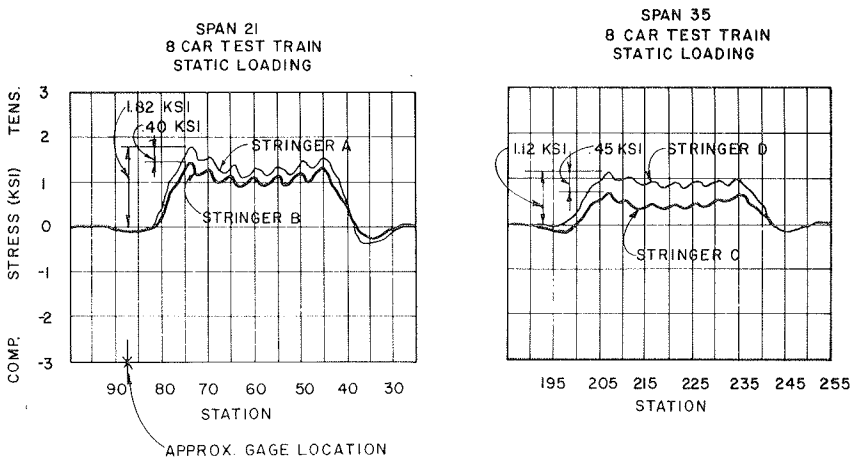

FIGURE 14 Comparison of stresses measured in type A gauges for adjacent stringers.

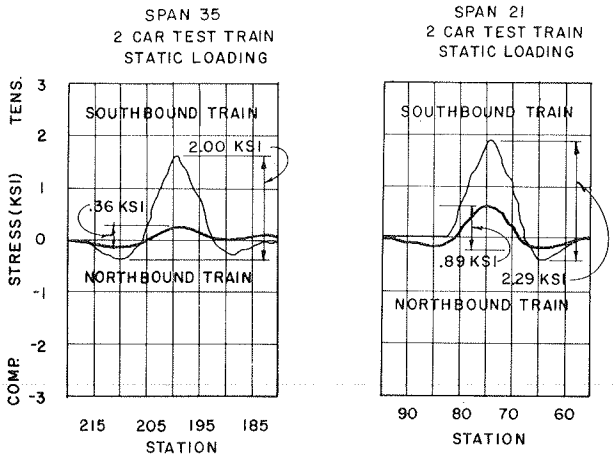

FIGURE 15 Comparison of influence of northbound and southbound trains showing lateral load distribution.

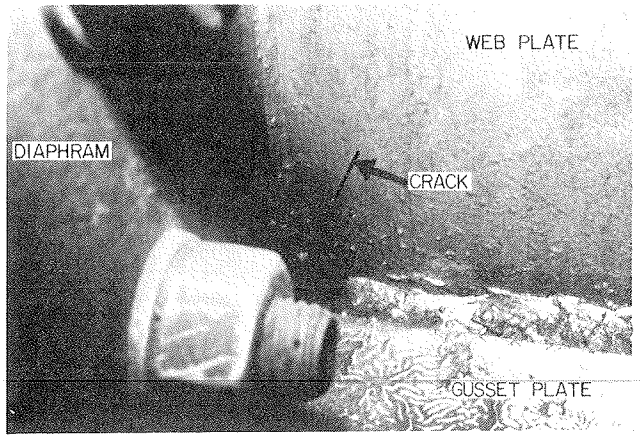

FIGURE 16 Upper segment of 4-in.-long crack found near midspan of span 16.

small, which indicated that axial forces in the bracing were low. This is to be expected, because torsional moments that would generate axial forces in the lateral bracing are generally smaller at midspan than near supports. Maximum force levels of 7 to 10 kips were indicated.

Type C Gauges on Top and Bottom Flange of Stringers

Type C gauges were placed near type A gauges in most spans to yield additional information about the distribution of stress in the stringers. It was found that the bottom flange gauges gave lower strains than type A gauges, which indicates that the gusset plates produced some stress-magnification effects. These gauges indicated strains about 15 percent greater than those measured in type C gauges.

The type C gauges also demonstrated the composite behavior assumed for the analytical model. The position of the neutral axis determined from measured strains agreed within 8 percent of the theoretical position.

Type D Gauges: Cross-Sectional Gauges in Bents and Piers

Strains were measured on the cross sections of one bent box support and two pier box supports. The measurements indicated that the neutral axis was located at approximately the mid-depth of the box section. Maximum dynamic tensile stress ranges are about 1.2, 1.0, and 0.8 ksi at bents 35 and 34 and pier 17, respectively. The dynamic stresses are roughly 20 percent higher than static values, which indicates that impact factors for box bents and piers may be somewhat higher than those measured in the stringers.

Type E Gauges on Bent 35 Web Plate Adjacent to Flange Tips of Stringers

The stresses measured in type E gauges compared well with the stresses measured on the bottom flange of bent 35. The overall indicated stress range is about 0.9 ksi under dynamic loading. Magnification of web plate strains caused by out-of-plane bending was not indicated.

Inspections of Gusset-Plate Welds

Close inspection of gusset plate to stringer web welds was made in the seven instrumented spans. The inspections concentrated on the toes of welds near the cutouts and around the ends of the gusset plates, where fatigue cracks are most likely to initiate.

The inspections were conducted by first thoroughly cleaning the area and examining it with a bright light and a magnifying glass. If any indication of a crack or discontinuity was observed, the weld toe was subjected to additional cleaning and magnetic particle inspection. If the observed discontinuity was located at either end of the gusset plate, the weld toe was lightly ground and the magnetic particle inspection was repeated. This procedure was used to verify and aid in the removal of a small defect. If the crack was located adjacent to the gusset-plate cutout (i.e., adjacent to the vertical stiffener), it was not ground out because the structural configuration at these locations prevented access to the crack origin. Nevertheless, any slight extension of a crack out of the cutout area was detected by using the inspection procedures. Altogether, more than 400 gusset plates were inspected, which represented approximately 23 percent of the total number in the structure. Typically, each gusset represented four separate inspection locations.

During the field examination one major crack and a total of 42 small cracks or cracklike indications were found. The terminology major crack is used because of its significant length (4 in.) and because it penetrated the full thickness of the stringer web. No other observed crack had these characteristics. The major crack was located adjacent to the vertical stiffener near the midspan of span 16 (see Figure 16). For comparison purposes, the crack found in span 15 is shown in Figure 7.

Approximately 20 small cracks or cracklike indications were subjected to grinding. The term cracklike indication is used to define a discontinuity that resembles a crack in a region where crack growth would be expected. All of these indications were eliminated by light grinding.

Removal and Evaluation of Samples

Two steel samples that contained cracks were removed from the webs of stringers at gusset locations in spans 15 and 16 for examination. The examination was performed by John W. Fisher at Lehigh University. It was found that the crack surface of the sample from span 15 was too corroded to yield useful information about the cause of fracture. The crack

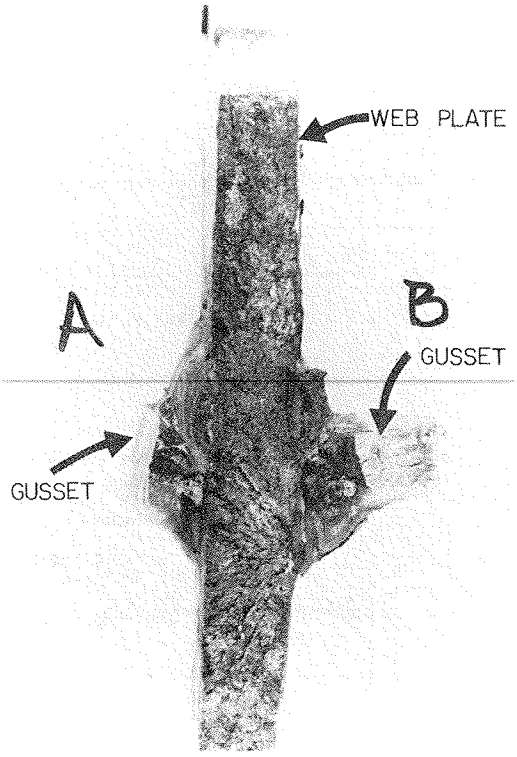

FIGURE 17 Exposed crack surface of specimen from span 16.

surface of the sample from span 16 was found to exhibit fatigue crack growth in the stringer web near the bottom surface of the gusset plate. The web plate fracture surface is shown in Figure 17. The fatigue crack was roughly elliptical in shape, its dimensions were about 0.125 in. deep by 0.375 in. long, and it exhibited fatigue crack growth striations. The striation spacing or crack growth rate was observed to vary between 1.4×10^{-6} and 5×10^{-6} in. per cycle. Figure 18 is a transmission electron microscope photograph that shows the striations. It is estimated, based on these data, that the crack after initiation can propagate to critical size after only 6 months of service.

This evaluation included a fracture mechanics analysis to predict fatigue crack growth, brittle fracture, and crack arrest. The analysis was conducted based on recommendations by Platten et al. (3). Measured stress ranges, however, were considered to be too small to have caused the cracking. Thus it is postulated that out-of-plane bending in the stringer web is occurring, which generates a stress level of 8 to 12 ksi. Unfortunately, the out-of-plane bending of the web was not shown by the strain measurements.

EVALUATION AND DISCUSSION

During this study weld details in the superstructure were carefully reviewed and classified in categories according to current AASHTO and American Railway Engineering Association (AREA) specifications (2). It was determined that the most severe condition currently in the structure is the weld junction of the lateral gusset plate to the stringer web plate. Altogether, about 1,800 lateral gusset plates are used in the 40-span stringer system.

Under current AREA specifications, the structural elements of the Dan Ryan elevated structure would be designed for varying members of constant stress

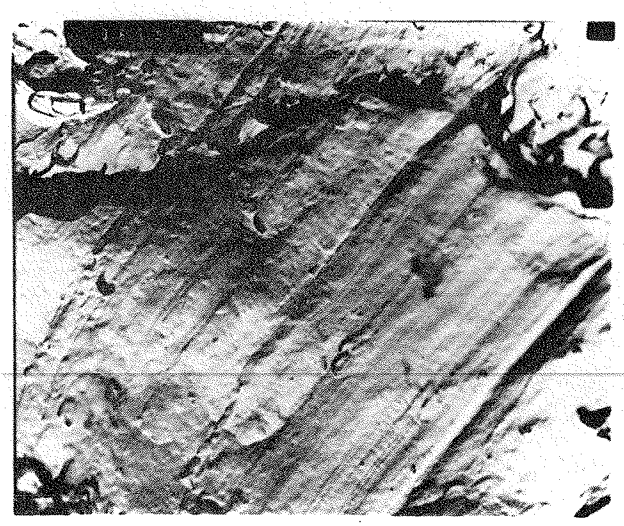

FIGURE 18 Transmission electron microscope photomicrograph: side B at 17,000X showing striation lines.

cycles caused by rail car loading according to member classification. However, the results of the test program indicate that the main consideration for all of the critical conditions is the stress range under high cyclic loading. The allowable range of stress for the various classifications of details in the structure, as defined in Table 1.3.13B of Article 1.3.13 of the AREA specifications, are given in the following table:

Stress Category	Allowable Range of Stress (S_{Rfat}) for More Than 2,000,000 Cycles (ksi)
A	24
B	16
C	12
D	7
E	5

These values are the most stringent requirements for design under AREA specifications. For a category E type detail, an allowable stress range of 5 ksi has been established.

Based on the analytical studies, a maximum stress range of 1.7 to 4 ksi was anticipated at the level of the lateral gusset-plate connection. However, the actual measured range of stress was found to vary between 1 and 2.5 ksi. The measured stresses are lower than the calculated stresses primarily because the actual train weight is lower than that used in the analysis and because of the lateral distribution of wheel loads to adjacent stringers.

The measured stress range values are less than the commonly accepted threshold for crack growth and are less than the allowable design stresses established by AREA. Therefore, typical conditions classified as category E details should exhibit satisfactory performance without fatigue crack extension. Nevertheless, the cutout between the vertical stiffener and the horizontal gusset represents a condition that is more severe than a category E detail. The small gap causes a significant magnification of stresses due apparently to out-of-plane deformation of the stringer web plate. Furthermore, the small gap makes it difficult to fabricate the detail without overlapping or intersecting welds, thus causing an unsatisfactory condition and potential built-in cracks caused by weld shrinkage and restraint. The

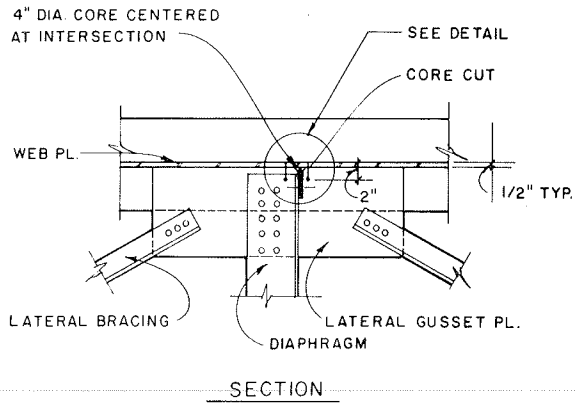

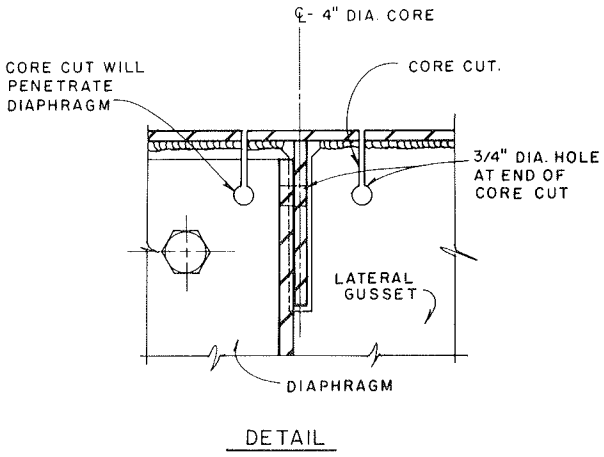

FIGURE 19 Exterior stringer retrofit by coring through web plate.

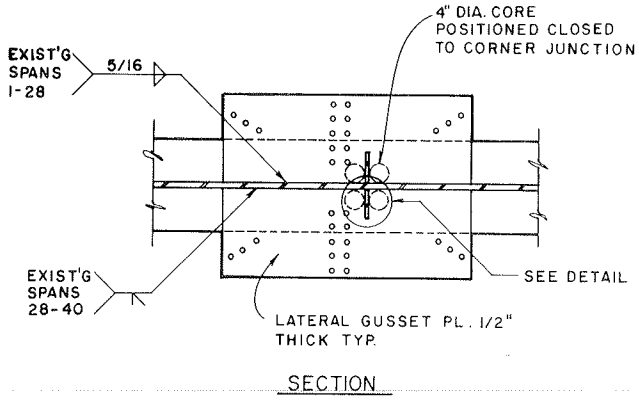

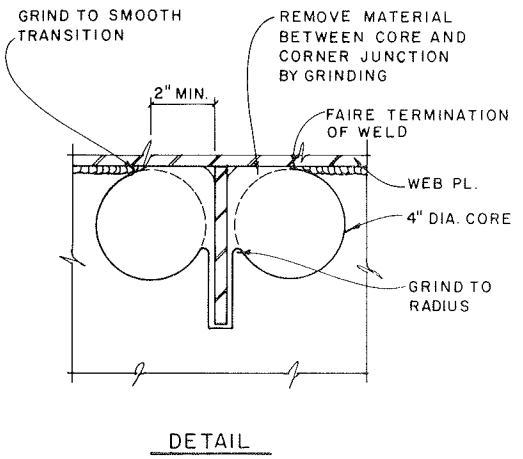

FIGURE 20 Interior stringer retrofit by coring holes through lateral gusset plate.

out-of-plane deformation of the web appears to be partly due to bending of the gusset plate by diaphragm loads and by axial loads in lateral bracing. However, the level of stress required to propagate a fatigue crack was not measured by the instrumentation used.

To date, one crack-related fracture in the stringer web adjacent to termination of a gusset-plate weld has occurred in span 15. Also, two significant cracks have been discovered. The first, in span 35, was found in early 1978 and was retrofitted. The second, in span 16, was found during the inspection of the gusset plate to stringer web welds. These major cracks all originated in the small gap at the connection between the gusset and vertical stiffener.

The crack surface in the sample from span 16 was found to have only a small fatigue portion; most of the crack was propagated by brittle fracture. Given the unsatisfactory access in the small gap, the fatigue portion is considered too small to have been discovered by visual or magnetic particle techniques.

In summary, the applicable codes indicate that fatigue should not be a problem in the structure, given the low levels of stress measured in the primary plate material. However, cracking has occurred and has been attributed to out-of-plane bending of the stringer web. The fatigue portions of cracks cannot be observed because of the confined location of the crack origin. For these reasons, a retrofitting program is essential.

RECOMMENDATIONS

The stringers require limited retrofitting to modify the lateral gusset-plate connections at the small gap. It is believed that the retrofit program may be limited to the middle third of all spans because the greatest bending stresses and differential movements between adjacent stringers occur in this region. All of the observed cracks were located within the middle third of their respective spans.

In addition, it has been recommended that the remaining 33 spans of the structure not included in this study be inspected, concentrating on the weld terminations of the lateral gusset plate to stringer web connections. The inspection of the spans in this study suggests that additional cracks may be found in the uninspected portions of the structure, and this information may alter the scope of the retrofitting program.

Two retrofit details have been developed to improve the small gap condition in the lateral gusset-plate attachment. These details are shown in Figures 19 and 20 and are described as follows.

1. Exterior stringer: This retrofit requires coring a 4-in.-diameter hole into the stringer web, as shown schematically in Figure 19. The core cutter is intended to penetrate the lateral gusset and transverse stiffener by 1.5 in. The purpose of this retrofitting procedure is to shield the fatigue-sensitive detail from stress and increase the gap width. It is intended to be used on exterior or fascia stringers.

2. Interior stringer: This procedure requires coring 4-in.-diameter holes vertically through the lateral gusset plate on both sides of the transverse stiffener. The edge of the hole along the web plate is milled or ground to achieve the profile indicated in Figure 20. The purpose of this retrofit is to increase the gap width between the gusset plate and stiffener. This modification will reduce the stress gradient in the gap region, thereby improving the fatigue life of the detail and providing a condition that will be easier to inspect.

In conjunction with the limited retrofitting program, both routine and in-depth inspections at periodic intervals should be continued. It is recommended that routine inspections be carried out on a 2-year interval, while a 10-year interval is appropriate for the in-depth inspection.

It has been concluded that the small gap condition in the lateral gusset plate has the potential for fatigue cracking and fracture. Assuming that the recommended retrofitting is carried out and a 10-year in-depth inspection program is followed, satisfactory performance of this structure should be assured.

ACKNOWLEDGMENT

This investigative study was carried out by Wiss, Janney, Elstner Associates, Inc., for the CTA. The support provided by Thomas Wolgemuth, Pat McCarthy, and Dennis Penepacker of the CTA was especially appreciated.

REFERENCES

1. The Technical Committee. Final Report on Causes of Fractures in Bent Nos. 24, 25, and 26, Dan Ryan Rapid Transit. Department of Public Works, Chicago, 1979.
2. J.W. Fisher. Bridge Fatigue Guide--Design and Details. American Institute of Steel Construction, Chicago, 1977.
3. D.A. Platten, K.H. Frank, and J.A. Yura. Analytical Study of the Fatigue Behavior of a Longitudinal Transverse Stiffener Intersection. Res. Report 247-1. Center for Transportation Research, University of Texas, Austin, Aug. 1981.

Publication of this paper sponsored by Committee on Dynamics and Field Testing of Bridges.

Post-Construction Evaluation of the Fremont Bridge

MICHAEL J. KOOB, JOHN M. HANSON, and JOHN W. FISHER

ABSTRACT

The Fremont Bridge is a three-span, stiffened-steel tied arch that is 2,159 ft long. During construction a major brittle fracture occurred in one of the box-shaped tie girders near the end of the bridge at the beginning of the arch rib. Since completion in 1973, small cracks and other discontinuities were found in welds in the vicinity of the junction of the tie girders and arch ribs. Cracks were also found in welds that connect wide flange stiffeners to the side plates of the tie girders. A comprehensive post-construction evaluation of the bridge was made to assess the long-range integrity of main load-carrying, nonredundant tensile members and components of the structure. The study included a review of drawings and records of construction, visual inspection of the tie girders, nondestructive examination of welds, field testing, an analytical review, and examination and testing of cores. The information collected during the study, particularly the testing and examination of core samples, is reviewed. Also, the evaluation of the resistance of the bridge to fatigue and fracture is summarized. As part of this study, a surveillance plan was developed that is intended to reveal crack growth in time to take corrective action.

The Fremont Bridge is a three-span, stiffened-steel tied arch that is 2,159 ft long (Figure 1). It was designed in the late 1960s (1) to meet the requirements of the ninth edition (1965) of the AASHO Standard Specifications for Highway Bridges (2). This was before the adoption of new fatigue provisions that appeared in the 1974 AASHTO Interim Specifications (3). Construction of the bridge was completed in 1973.

Under the 1978 AASHTO fracture control plan (4), the tie girders of the Fremont Bridge are classified as main load-carrying, nonredundant tensile members. There are numerous conditions in the tie girders that can be classified as category E or E', according to current AASHTO specifications.

During construction a major brittle fracture occurred in one of the tie girders near the end of the bridge at the beginning of the arch rib. As a result of this fracture, a major modification was made in the structure at this location.

Since completion of the bridge, small cracks and other defects were found in welds in the vicinity of the junction of the tie girders and arch ribs. Cracks were also found in welds that connect wide flange stiffeners to the web plates of the girders.

A comprehensive post-construction evaluation of the Fremont Bridge was made to assess the long-range integrity of main load-carrying, nonredundant tensile members and components of the structure. The study included a review of drawings and records of construction, visual inspection of the tie girders, nondestructive examination of welds, field testing,

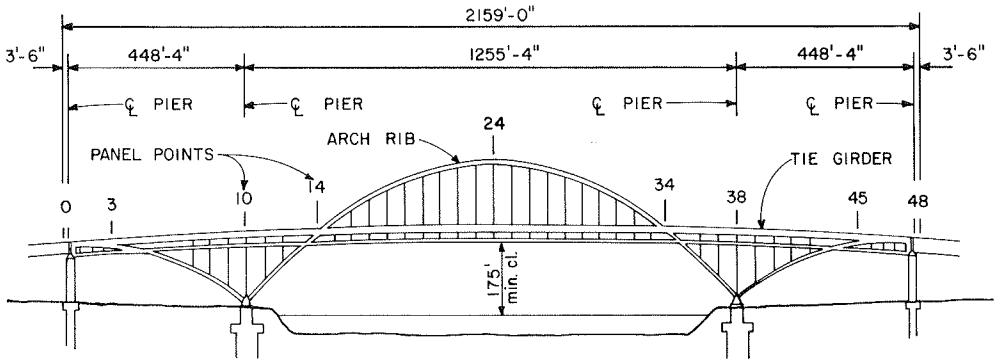

FIGURE 1 Elevation of Fremont Bridge.

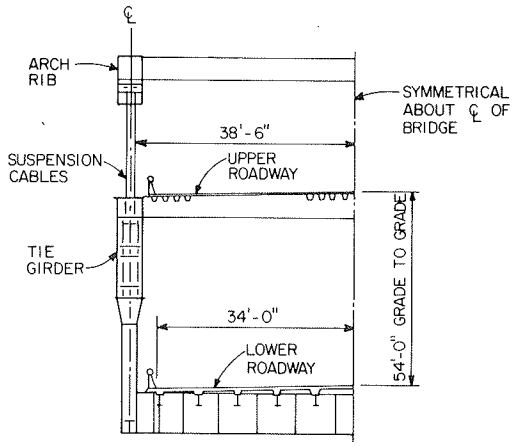

FIGURE 2 Typical section where arch is above roadway.

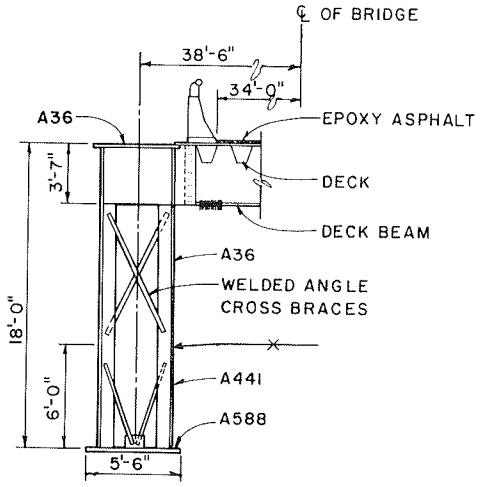

GIRDER SECTION

FIGURE 3 Representative details of tie girder.

an analytical review, and examination and testing of cores.

The information collected from the various tasks, particularly the testing and examination of core samples, is reviewed. This study was limited to the tie girders and the junction of the arch rib and tie girder. Also, the evaluation of the resistance of the bridge to fatigue and fracture is summarized. As part of this study a surveillance plan was developed that is intended to reveal crack growth in time to take corrective action.

DESCRIPTION OF BRIDGE

The main span is divided into 28 panels, and each side span is divided into 10 panels. Each panel has a length of 44 ft, 10 in. Junctions between panels are numbered 0 through 48. In this structure the arch is loaded in compression and the tie girder is loaded in tension to conteract the thrust of the arch, as well as in flexure to resist the live-load bending moments. A detailed description of the bridge and its design is given elsewhere (1).

A typical section through the bridge, in the region where the arch is above the roadway, is shown in Figure 2. The orthotropic steel upper deck, which carries four lanes of westbound traffic, acts integrally with the tie girders. The bottom deck, which carries four lanes of eastbound traffic, is a reinforced-concrete slab supported on stringers and floor beams. In the middle 896 ft of the bridge, where the arch ribs are above the tie girders, the bottom deck is suspended by hangers from the tie girders. Outside of this region the bottom deck is framed into compression struts that extend between the arch ribs and the tie girders.

Representative details of the orthotropic deck and tie girders are shown in Figure 3. The top flange is A36 steel, whereas the bottom flange is A588. The webs are 0.5 in. thick, except at the junctions with the arch ribs and pier columns. Typically, the lower 6 ft are fabricated from a high-strength, low-alloy steel that meets the requirements of ASTM A441, and the upper part is fabricated from A36 steel. This hybrid design reflects the integral action of the orthotropic deck and tie girders, with the neutral axis about 6 ft below the top flange. Welded construction is used throughout the tie girders, except for high-strength bolted field splices.

The arch ribs are box shaped and have a constant width of 4 ft, 0 in. The depth of the web plates is 3 ft, 10 in.; hence the overall depth of the arch ribs varies, depending on the flange plates, which have a maximum thickness of 2.25 in. High-strength, quenched and tempered ASTM A514 steel is used for the arch ribs, which are welded, except for bolted field splices.

At the junctions of the girders and arch ribs located at panel points 14 and 34, the cross section of the arch rib is changed from a box shape to three A514 strap plates, each 3 in. thick and 3 ft, 10 in. deep and oriented vertically. These three straps are stiffened by a welded diaphragm at mid-depth.

The straps extend through slots in the top and bottom flanges of the girder.

The center section of the bridge, from panel point 14-34, was fabricated off site, transported on barges, and erected by hydraulic jacking. A bolted splice connects the center and end sections located within the junction of the tie girder arch rib. Heavy jacking stiffeners are also welded and bolted to the sides of the tie girder in this area.

FATIGUE-SENSITIVE CONDITIONS

Several fatigue-sensitive conditions occur repeatedly in the tie girders. These conditions are shown in Figure 4a--the junction of the longitudinal and transverse stiffeners; Figure 4b--cover plates adjacent to vent openings; Figure 4c--slots in the bottom flange for lower deck hangers; and Figure 4d--the junction of deck beams and side plates. Terminations of fillet welds, which are parallel to the axis of the tie girder in Figures 4a, c, and d, are classified as category E by AASHTO specifications (5,6). Overlapping welds at the junction of longitudinal and transverse stiffeners and the heavy welds of the thick cover plates at the vent openings are particularly severe conditions.

Vent and slot openings in the bottom flange were made by flame cutting. A number of these openings contained severe notches and gouges, as shown in Figure 5. These conditions do not meet the workmanship requirements of the AASHTO Standard Specifications for Welding of Structural Steel Highway Bridges (7).

Ultrasonic testing revealed six groove welds in the A588 bottom flange of the tie girders that are not in compliance with AASHTO requirements.

FIELD TESTING

A testing program was carried out to provide information about the behavior of the bridge under traffic and environmental conditions. Strain-gauge and thermocouple instrumentation was installed at four cross sections in the vicinity of panel point 14 to obtain a measure of overall response of the bridge. Additional instrumentation was installed at locations where conditions were believed to be susceptible to fatigue crack growth. This work is described in detail in a separate paper (8).

Field testing indicated that stress ranges in the tie girders under traffic are generally less than 2 ksi, with infrequent excursions to 3 ksi. The number of cycles varies with location, but it does not exceed the average daily truck traffic. However, the temperature of plates exposed to the sun was up to 50 degrees higher than for plates in the shade, which were always close to the ambient temperature. The nominal stress varied by about 10 ksi as a result of daily thermal effects.

The bridge was also subjected to a controlled

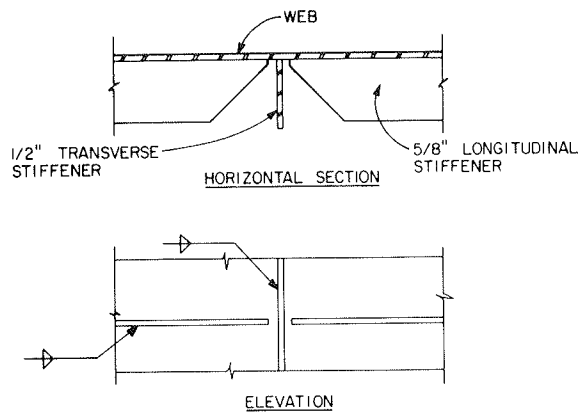

(a) Junction of longitudinal and transverse stiffeners.

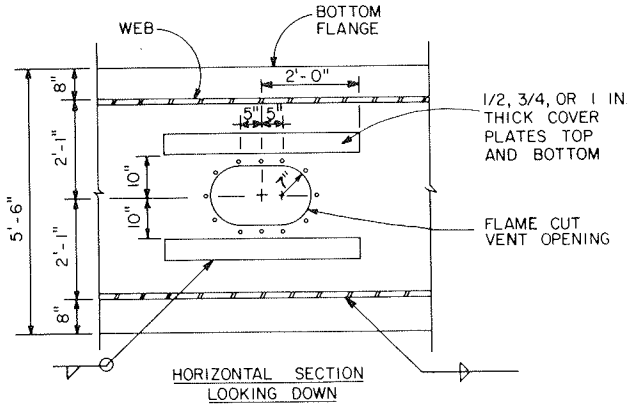

(b) Cover plates at vent opening.

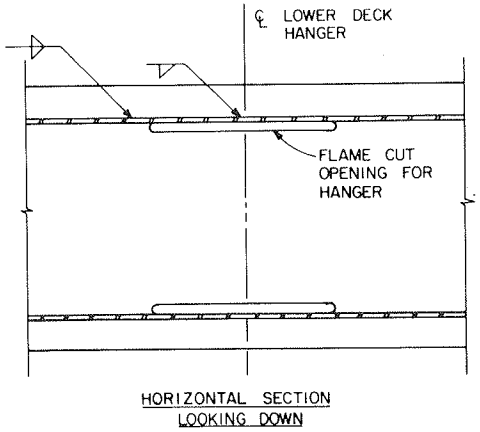

(c) Slots in bottom flange for deck hanger.

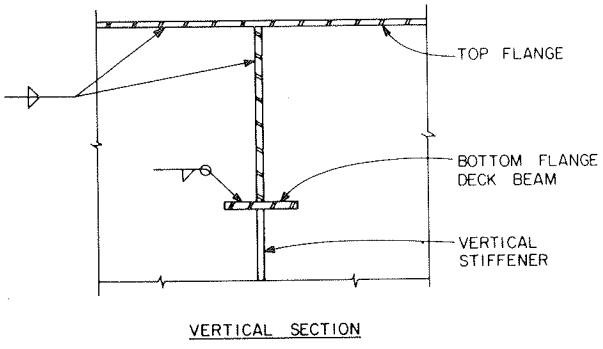

(d) Junction of deck beam and web plate.

FIGURE 4 Fatigue-sensitive conditions in tie girder.

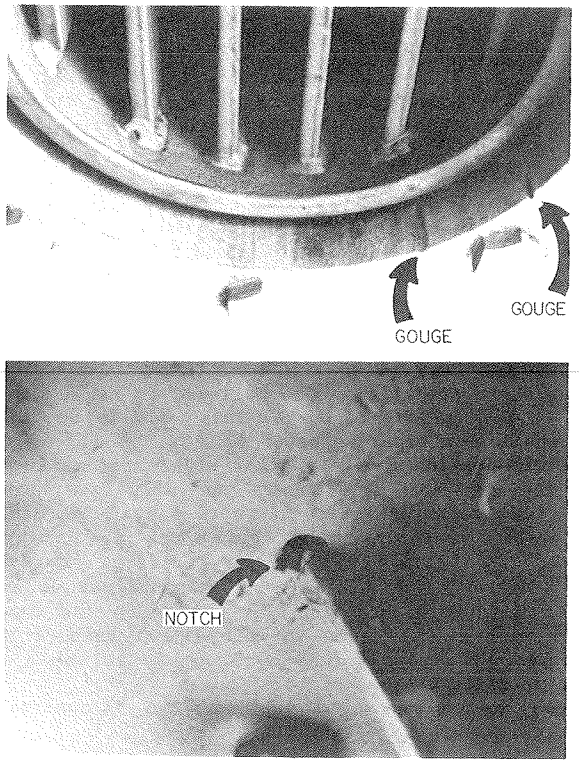

FIGURE 5 Notches and gouges on flame-cut openings: (top) vent opening in bottom flange, and (bottom) end of hanger slot.

loading test by using a group of four trucks weighing a total of 177,100 lb. Static and dynamic tests were conducted. The stress levels recorded during both tests were quite low, with the maximum recorded stress being 2.2 ksi at any instrumented location.

ANALYTICAL STUDIES

An independent design review essentially confirmed the original design and a previous review of that design. The design review was made by using a computer program developed for bridges of this type. The program considered a model of the entire bridge by using linear beam elements. Influence lines were developed for each panel point, and maximum stress ranges were computed for the live-load cases.

The maximum computed tensile stress range from an AASHTO loading on four lanes was 21.2 ksi in the bottom flange and 14.6 ksi in the top flange. For four standard HS20 trucks moving as a group across the bridge, the computed tensile stress range in the bottom flange varied from 4.0 to 5.0 ksi, and for the top flange the variation was from 0.7 to 2.9 ksi. The measured stress range was smaller because the design load condition is not representative of the actual service loads. This is recognized in the fatigue provisions of the AASHTO specifications and is the reason why only 100,000 design cycles are considered.

Following the design reveiw, a state-of-the-art finite-element analysis of the overall region from panel point 13.5 to 14.5 (the junction of the arch rib and tie girder) was carried out. The analysis did not reveal unusual force concentrations in this region.

REVIEW OF INFORMATION FROM MILL REPORTS

A diagram that shows the location of various thicknesses and types of steel plates in the tie girders is presented in Figure 6. From review of the available mill reports and the shop drawings, information was compiled relating to the heat number and the physical and chemical properties of about 90 percent of the steel plates. The mill reports for the ASTM A588 plates in the bottom flange included values of material toughness obtained from Charpy V-notch (CVN) specimens tested at +40°F in accordance with ASTM E23.

The physical and chemical properties met the requirements of the ASTM and AASHTO specifications for A36 (M183), A441 (M188), and A588 (M222) structural steels.

CVN values were obtained from the mill reports for 80 out of a total of 90 A588 bottom flange

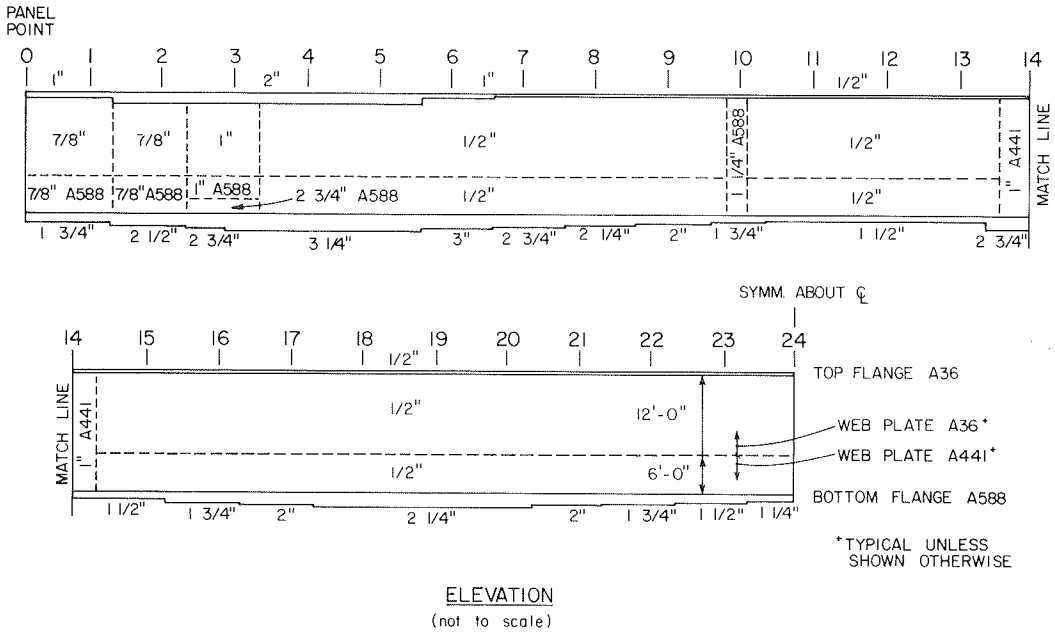

FIGURE 6 Diagram showing location and thickness of plates in tie girder.

plates. There was substantial variation in the toughness values. At three locations the values did not meet the AASHTO Guide Specifications for Fracture Critical Non-Redundant Members (4) requirements of 25 ft-lb, or 30 ft-lb for welded material more than 2 to 4 in. thick, at 40°F for zone 2. Minimum service temperature for zone 2 is from -30° to -1°F. The A588 steel at these locations came from 1.25- and 3-in.-thick material. According to the mill reports, the CVN values of the two 3-in.-thick plates were 18, 16, and 17 ft-lb at 40°F. CVN values for the 1.25-in. plate were 15, 16, and 15 ft-lb.

TESTING OF STEEL SAMPLES

Fifty cores were extracted from the tie girders of the bridge. Thirty-four 4-in.-diameter cores, along with additional plate material recovered from the location of the previous fracture near panel point 3, were used for tests to determine toughness properties. Sixteen 2- or 3-in.-diameter cores were taken from areas suspected of containing cracks or defects for metallographic and fractographic examination. This testing is described more fully in the following section.

The 4-in.-diameter core size was selected because it was adequate, after preparation, for either a special compact tension (CT) test or for machining CVN specimens. In a 0.5-in. plate, two cores were rquired at each sample location to obtain sufficient material for 12 CVN tests. Otherwise, one core sample was sufficient. Two cores were extracted at each desired sample location for a CT test in order to have replication. In general, the samples represented either common material or material that was found to have low toughness properties on the mill reports. In total, the testing program included 168 CVN tests and 20 CT tests. All of the toughness tests were conducted such that the fracture surface of the specimen was perpendicular to the longitudinal axis of the tie girder.

Two CVN specimens from each sample location were tested at each of the following temperatures: -20°, -10°, 0°, 10°, 40°, and 70°F. The results of these tests are given in Table 1. The CVN test results of

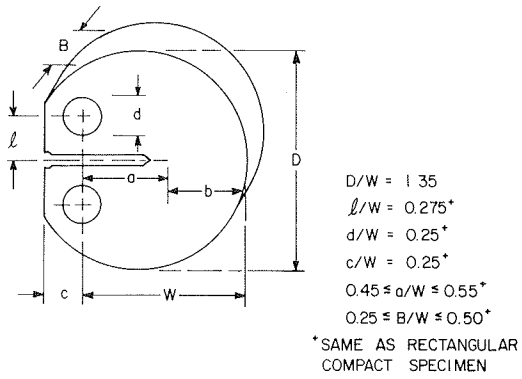

FIGURE 7 Geometry of round compact specimen.

11 and 15 ft-lb at 40°F for sample M19A taken from the 3-in.-thick A588 material confirmed the mill report values.

The 2-in.-thick A36 steel represented by sample M7A was found to have low CVN values of 7 and 8 ft-lb at 40°F. This sample represents four 2-in.-thick plates in the tie girders. It was selected for testing because the yield strength given on the mill reports was unusually high--46,900 psi.

All compact tension tests were run at -10°F, which represented the minimum service temperature for the bridge. The tests were conducted by using a time of 1 sec from zero load to failure, which represented an intermediate strain rate. Compact tension specimens made from the cores were round, as shown in Figure 7. Standard rectangular compact tension specimens were machined from the pieces of an A588 plate taken from the material recovered from panel point 3 of the previous failure, following the requirements of ASTM E399. The results of the compact tension tests are given in Table 2.

EXAMINATION OF DEFECTS

As previously indicated, sixteen 2- or 3-in.-diame-

TABLE 1 CVN Test Results

Steel Designation	Sample No.	Thickness (in.)	CVN Test Results (ft-lb) at Test Temperature (°F)					
			-20°	-10°	0°	10°	40°	70°
A36	M1A and M1B	0.5	5	8	14	21	46	99
			5	10	7	24	46	99
	M2A and M2B	0.5	5	15	26	26	58	54
			5	21	12	47	58	60
	M3A and M3B	0.5	8	8	10	10	48	69
			4	10	15	19	58	83
	M5B	1	5	8	42	54	36	82
			4	7	11	48	82	86
	M7A	2	2	3	3	4	8	13
			3	3	3	7	7	13
A441	M9A and M9B	0.5	21	13	32	44	67	84
			15	17	16	21	27	43
	M11A and M11B	0.5	6	7	21	11	39	71
			9	9	11	26	29	61
	M13A and M13B	1	5	12	13	14	31	48
			6	9	13	19	33	57
A588	M15A	1.25	8	17	16	47	66	76
			15	10	34	17	65	66
	M16A	1.5	8	10	29	23	28	84
			22	13	11	32	57	54
	M17A	1.75	13	4	8	10	37	37
			2	4	11	10	38	10
	M19A	3	11	9	6	11	11	12
			9	15	6	5	15	13
	M20A	2.5	8	6	12	50	85	
			17	26	32	45	61	
	M21A	3.25	11	4	6	19	51	72
			20	20	5	10	28	50

TABLE 2 CT Test Results

Steel Designation	Sample No.	Thickness (in.)	B (in.)	W (in.)	K_Q (ksi$\sqrt{in.}$)	ASTM E399 Validity		Stress Intensity Factor (ksi$\sqrt{in.}$)		
						P_{max}/P_Q	$2.5(K_Q/\sigma_y)^2$	K_{Ic}	K_{max}	K_J
A36	M4A	0.5	0.5	2	43.6	1.83	2.64		80.0	
	M4B	0.5	0.5	2	45.7	1.66	2.90		76.1	
	M6A	1	1	2	50.7	1.33	3.92		67.8	92.7
	M6B	1	1	2	48.8	1.59	3.62		77.6	116
	M8A	2	1.5	3	52.7	1.53	3.16		80.8	104
	M8B	2	1.5	3	55.6	1.66	3.52		92.1	130
A441	M12A	0.5	0.5	2	54.8	1.95	2.18		111	
	M12B	0.5	0.5	2	52.3	2.05	1.98		106	
	M14A	1	1	2	58.4	1.61	>1		93.9	152
	M14B	1	1	2	49.0	1.78	>1		87.3	123
A588	M18A	1.5	1.25	2.5	70.6	1.30	4.04		91.8	110
	M18B	1.5	1.25	2.5	59.2	1.08	2.84			
	M22A	3	1.5	3	57.5	1.00	1.64			
	M22B	3	1.5	3	62.2	1.00	1.92			
	M23A	2.5	2.5	5	72.6	1.25	4.10		91.1	114
	M23B	2.5	2.5	5	83.0	1.22	5.36		101	128
	M24A	3.25	3.1875	6.5		1.00	2.88	59.0[a]		
	M24B	3.25	3.1875	6.5	74.7	1.00	4.63			
	M25A	2.75	2.5	5	74.4	1.00	3.99			
	M25B	2.75	2.5	5	70.1	1.00	3.54			

Note: B = specimen thickness, W = specimen depth, K_{Ic} = critical stress intensity factor, K_Q = critical stress intensity factor (conditional result), K_{max} = critical stress intensity factor (based on P_{max}), and K_J = J integral stress intensity factor.

[a]Test result meets ASTM E399 validity requirement.

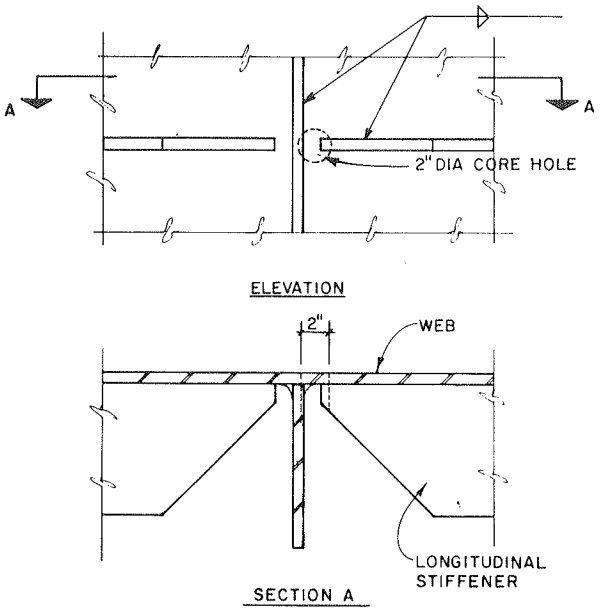

(a) C1 cores at ends of horizontal stiffeners.

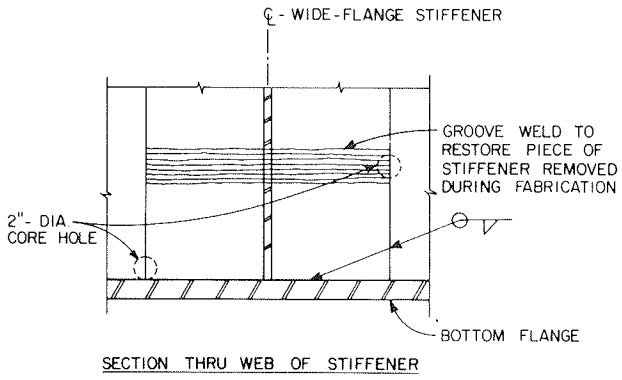

(b) C2 cores at base of wide flange stiffeners.

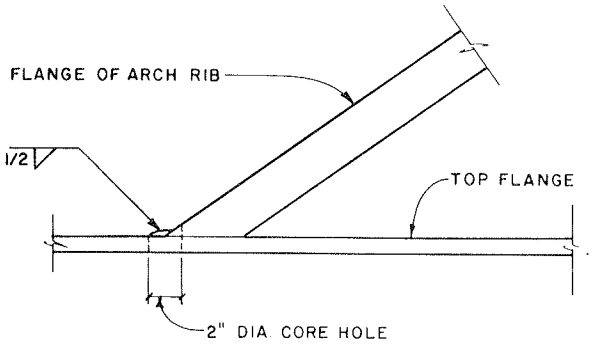

(c) C3 cores through welds at the junction of the arch rib and top and bottom flanges of the tie girder.

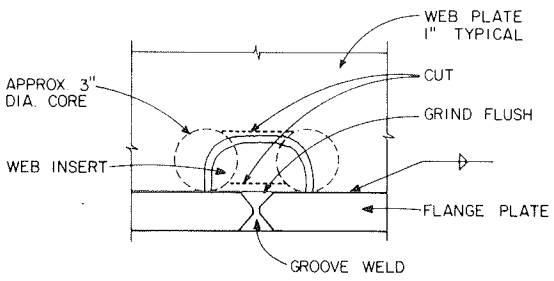

(d) C4 cores through welded inserts in web plate.

FIGURE 8 Regions where cores were extracted for examination.

ter cores were taken from locations representing four different conditions in the bridge (Figure 8) for metallographic and fractographic examinations. These samples were from locations where visual inspection had indicated a possible discontinuity.

Cores From Ends of Longitudinal Stiffeners

Four cores were removed from the junction of longitudinal and transverse stiffeners, cut into segments, and examined. The only significant defect was found at a weld overlap, where there was entrapped slag and a small crack, which may have occurred during fabrication or handling. This condition is shown in Figure 9. No evidence of fatigue crack propagation was detected when the crack was split open for examination.

Cores in Welds of Wide Flange Stiffeners

These cores were also cut into segments. Significant root cracking was present in all four cores, where the fillet welds connected the stiffener flange to the girder web. A typical root crack is visible in Figure 10. This crack originated from the sharp slag pocket at the vertical weld root.

It was evident that cracking at wide flange stiffener connections had developed at the time of fabrication. Two out of the four cores exhibited fatigue crack growth with a striation spacing of about 10^{-6} in. per cycle. This striation spacing indicated that the crack growth rate was near the lower limit detectable by fractographic examination. These cracks were not considered to be significant. Growth was the result of stress passing from the web plate into the stiffener through the vertical fillet

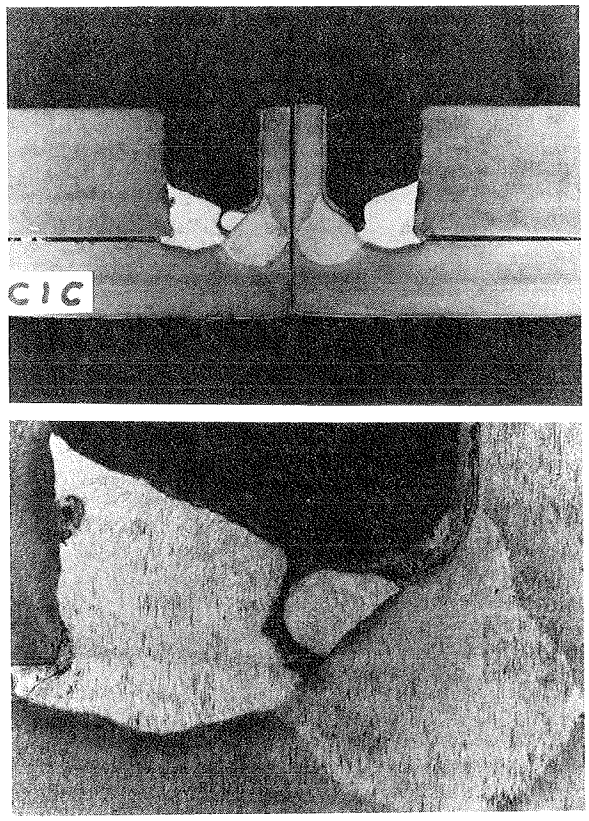

FIGURE 9 Split segments from core C1C: (top) etched cross section showing lack of fusion, and (bottom) close-up showing slag and crack in weld overlap.

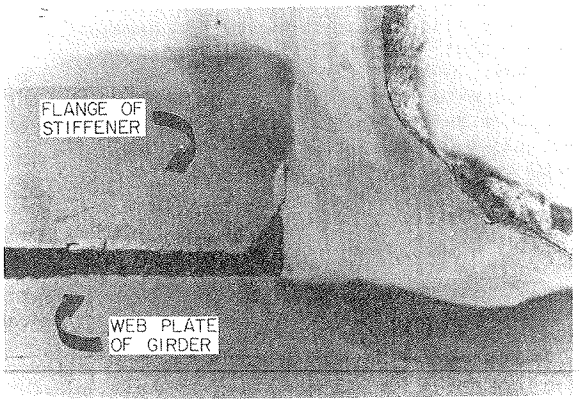

FIGURE 10 Etched surface of split segment of core C2D showing root crack from slag pocket.

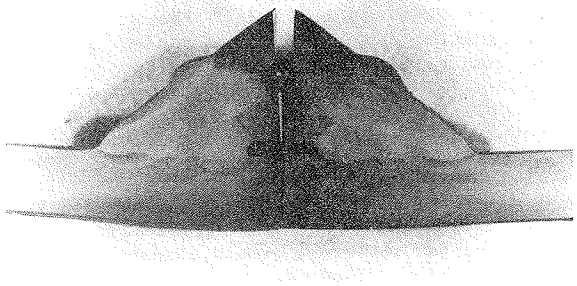

FIGURE 11 Etched sections of sample core C3C showing insert plate and notches at weld roots.

welds, promoted by the existence of extensive weld root cracking. However, the crack propagates along the leg attached to be stiffener, and the lack of fusion gap between the web and stiffener flange prevents it from moving into the girder web and creating a more serious crack condition.

Core Through Welds at Junction of Arch Rib and Flanges of Tie Girders

Four cores were extracted and cut into segments for examination. There was no evidence of cracking in any of the weldments, although it was visually apparent that sharp notch conditions exist at the weld roots. A substantial gap was present in all of the core samples between the flange and the arch rib plates. In one sample a 0.3125-in. plate was found to have been inserted to fill part of the gap between the arch rib and top flange before welding. The weld fused the insert plate and the arch rib and tie girder flanges, as shown in Figure 11. However, sharp notches were found at two locations. Slag was also apparent at the root of the weldments that connect each plate. Although no sign of cracking was detected at the weld root, the distance between the root and the outside surface was only 0.3125 in. in this core. This small ligament may be susceptible to cracking.

Cores From Welded Inserts in Webs

Two pairs of cores were removed from small insert plates welded into cope holes in the web, as illustrated in Figure 8d. These holes were made during

fabrication of the groove welds in the flange. The cores were sliced into segments for examination. It appeared that the welds were intended to be double V-grooves, but the root pass was not back-gouged. There was evidence of some fatigue crack growth from the larger defects. The striation spacing suggested that fatigue crack propagation was near the crack growth threshold.

EVALUATION OF POTENTIAL FOR FRACTURE

In recent years substantial research has been directed toward evaluation of the resistance of welded steel bridges to fatigue and fracture. This research has provided the basis for the current provisions on fatigue and fracture in the AASHTO specifications.

In principle it is possible to establish relationships between flaws or defects in a steel structure and the conditions under which brittle fracture may occur by using fracture mechanics. In practice, however, it must be recognized that there is variability in the properties of steel and difficulties in defining defects, as well as theoretical limitations, on this relatively new technology.

Virtually all welded steel bridges contain discontinuities that are built into the structure during fabrication. Such discontinuities occur from lack of fusion, porosity, toe cracks, or even a weld arc strike. In addition, the geometry of the welded connections also induces stress concentrations.

Discontinuities oriented parallel to the primary stress generally do not cause problems. However, even extremely small discontinuities may induce crack growth if they are oriented perpendicular to the stress flow and the cyclic stress range is large enough to exceed the crack growth threshold.

Under repeated loading, crack propagation may occur at low stress ranges, especially if occasional higher stress ranges also occur. The rate of crack propagation depends on ΔK, the range of stress intensity at the crack tip. The stress intensity range (ΔK) may be computed as follows (9):

$$\Delta K = F(a)\, S_r \sqrt{\pi a} \qquad (1)$$

where S_r is the nominal uniform stress range, and a is the crack length. The parameter F(a) varies, depending on crack size, orientation, and shape, as well as loading conditions.

During the field testing measured peak cyclic stresses from traffic were typically less than 1 ksi and almost always less than 2 ksi for the tie girders. For small initial defects, ΔK computed from Equation 1 is about 2.5 ksi $\sqrt{\text{in.}}$ for a stress range of 10 ksi. A value of ΔK equal to 2.5 ksi $\sqrt{\text{in.}}$ is generally considered to be close to the threshold value for fatigue crack propagation. The examination of the cores supported the position that crack extension was occurring near the threshold value.

Stress intensity factors for simple crack geometries (9) are given in Figure 12. These factors are complex for most other geometries, but solutions are available in the technical literature.

Fatigue cracks that grow from fillet welds usually have a semielliptical-shaped crack front. This condition is shown in Figure 12b, where K_I is the stress intensity factor for mode I behavior. Assuming as an example that a equal to 0.20 in. and a/2c equal to 0.25 represent a small semielliptical surface crack, and taking Q equal to 1.25, K_I is approximately 0.8 S_r, or S_r is approximately 3 ksi for for ΔK equal to 2.5 ksi $\sqrt{\text{in.}}$ Assuming larger and less tolerable defects leads to lower values of S_r. Recognizing that these stress ranges are comparable to the maximum values measured under traffic in the bridge, it is not likely that crack growth will occur from the observed defect conditions that existed in the girders. The only observed crack propagation was at larger cracks, such as shown in Figure 10.

The propagation rate for cracks in ferrite-pearlite steels (10), which includes the A36, A441, and A588 steels in the tie girders, may be computed from

$$da/dN = 3.6 \times 10^{-10} (\Delta K_I)^3 \qquad (2)$$

where ΔK_I is the stress intensity factor range in ksi $\sqrt{\text{in.}}$, and da/dN is the crack growth per cycle. At a small defect and at threshold level conditions, with $\Delta K_I = 2.5$, crack growth would be expected to occur at 56×10^{-10} in. per cycle. Therefore, in 2 million cycles, for example, the crack extension would be

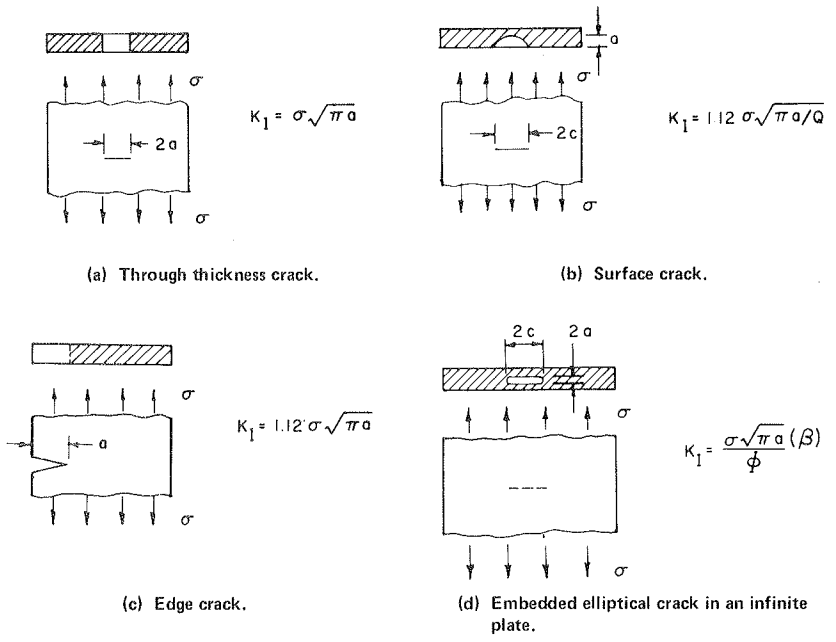

(a) Through thickness crack.

(b) Surface crack.

(c) Edge crack.

(d) Embedded elliptical crack in an infinite plate.

FIGURE 12 Simple intensity factor for simple crack geometries.

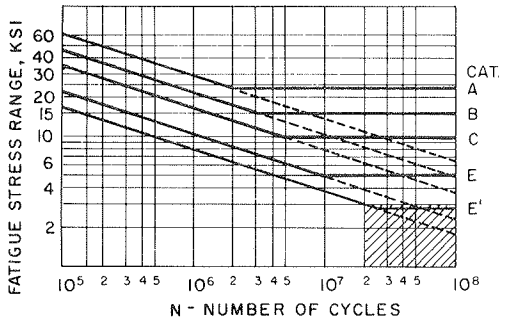

FIGURE 13 Fatigue strength of welded details.

small--about 0.02 in. Larger initial defects would have increased propagation rates.

Although the stress ranges from traffic on the Fremont Bridge are apparently close to and possibly below the threshold levels if the defects are small, a relatively high daily stress cycle caused by temperature is imposed on the traffic stress cycles. According to recent data, these large-magnitude, low-cycle stress ranges may result in crack growth in the low-magnitude, high-cycle stress ranges (11).

Test data on the fatigue strength of various details are presented in Figure 13, where the lines for the various categories are 95 percent confidence limits for 95 percent survival (12). The solid horizontal lines are considered to be a threshold uniform stress range (S_{rth}) for these categories. That is, for stress ranges below S_{rth}, crack growth does not occur and no damage to the structural detail is expected. However, for variable magnitude stress cycles, it is recommended that the dashed extension of the line be used to evaluate fatigue strength when ocassional stress cycles in the variable spectrum exceed S_{rth} (11).

Assuming that the effective stress range is 2 ksi or less, including the daily thermal effect, and that the conditions in the girders are not or can be upgraded to not worse than category E', it appears that 60 million or more cycles would be required to reach the lower bound of fatigue life. This region is cross-hatched in Figure 13.

As a result of the field testing a rough estimate of an effective Miners high-cycle stress range was developed that was expected to occur approximately 3,000 times per day. It was noted that this cycle rate was equal to about 55 percent of the average daily truck traffic. On this basis the Frement Bridge is currently being subjected to approximately 1 million cycles of low-magnitude, high-cycle stress range per year that may be capable of producing crack growth in details with relatively small defects.

As a crack propagates, the stress intensity factor increases until it reaches a critical value (K_{Ic}). At this value the propagation becomes unstable and brittle fracture occurs. The physical testing program that was described previously was intended to provide test results to establish K_{Ic}. However, only one test result reported in Table 2, from sample M24A, met the validity requirements of ASTM E399 for considering K_Q to be equal to K_{Ic}. This sample was obtained from A588 steel recovered from the bottom flange of the girder that sustained the fracture during construction.

The values of K_Q for all of the samples from the A36 and A441 steels were invalid estimates of K_{Ic} because the ratio P_{max}/P_Q was greater than 1.10. This indicates that the steel was tougher than the estimate provided by K_Q.

For the A588 steel, samples M18A, M23A, and M23B failed to meet the requirement that the thickness of the specimen (B) shall be greater than 2.5 $(K_Q/\sigma_y)^2$ as well as the requirement that P_{max}/P_Q shall be less than 1.10. All of the other invalid results on A588 steel failed to meet the requirement for maximum thickness. However, it should be noted that all of the samples failing to meet the requirement, except for M22A and M22B, were tested in full plate thickness; therefore, K_Q should be a satisfactory estimate for K_{Ic}. Further, the thickness of samples M22A and M22B was close to the ratio of 2.5 $(K_Q/\sigma_y)^2$, and the results are probably valid.

Based on review of the test results, K_{Ic} was assumed equal to 80 ksi $\sqrt{in.}$ for the A36 and A441 steels and 60 ksi $\sqrt{in.}$ for the A588 steel in the evaluation of fracture resistance of the tie girders.

Critical crack dimensions for the simple crack geometrics shown in Figure 12 were computed based on K_I equal to 60 or 80 ksi $\sqrt{in.}$ For a crack or defect near a weld, it was assumed that the in situ stress was equal to the yield stress because of the residual shrinkage stress associated with the weld. For defects away from welds, the in situ stress was considered equal to the dead-load stress plus an allowance for thermal effects on the tie girders. Assuming that this allowance for thermal effects is approximately 10 ksi (as measured during the field testing program), the maximum nominal stress for defects not associated with welds was taken to be equal to 0.55 σ_y for all three steels. Critical crack dimensions based on these assumptions are given in Table 3.

TABLE 3 Critical Crack Dimensions

Crack or Defect Geometry	Type of Steel	Critical Crack Dimension[a] (in.) Near Welds[b]	Away From Welds[c]
Through thickness crack (2a)	A36	3.25	10
	A441	1.75	5.25
	A588	1	3
Surface crack with a/2c = 0.1 (a)	A36	1.1	3.6
	A441	0.6	2.0
	A588	0.3	1.1
Edge crack (a)	A36	1.25	4.0
	A441	0.75	2.25
	A588	0.50	1.25
Embedded elliptical crack, a/c = 0.25 (2a)	A36	3.75	11.75
	A441	2.0	6.25
	A558	1.0	3.5

[a] Assuming K_{Ic} = 80 ksi$\sqrt{in.}$ for A36 and A441 steel and K_{Ic} = 60 ksi$\sqrt{in.}$ for A588 steel.
[b] Assuming $\sigma = \sigma_y$.
[c] Assuming $\sigma = 0.55\ \sigma_y$.

CONCLUDING REMARKS

The Fremont Bridge contains low-toughness steel that does not meet current AASHTO specifications. Also, the computed stress ranges under the prescribed loadings of the specifications exceed the allowable design stress range limits. However, the measured stress ranges from traffic are smaller than stress ranges that correspond to the fatigue limit for the worst details. Only the thermal stress cycle was observed to exceed the crack growth threshold. Therefore, the principal conclusion of the evaluation is that a long period of time, on the order of 60 years, is required before there should be any potential for significant fatigue crack propagation within the tie girders, provided there are no existing defects of greater size and sharpness than normally are associated with category E or E' conditions.

Recommendations were made to reduce the severity

of all potentially critical fatigue and fracture conditions, including grinding severe gouges in all of the flame-cut openings and shot-peening weld terminations. The weld around the junction of the arch rib and exterior flange surfaces was to be removed by grinding or milling. The exterior arch rib straps are to be bolted to the webs of the girder to offset the removal of the weld around the junction. An in-depth visual inspection with nondestructive testing was recommended along with work to reduce the severity of the critical conditions.

Future in-depth inspections were also recommended beyond those normally performed in maintaining a bridge. These inspections should be performed at intervals of about 10 years. Because paint would be removed and light grinding would be carried out at critical locations during this work, it appears to be advisable to coordinate these in-depth inspections with repainting of the tie girders.

ACKNOWLEDGMENT

This post-construction evaluation of the Fremont Bridge was carried out by Wiss, Janney, Elstner Associates, Inc. (WJE) for the Oregon State Highway Division. The study was supported by the FHWA. WJE was assisted by John W. Fisher; Ammann and Whitney; Testing Engineers, Inc.; and Materials Research Laboratory, Inc. A technical committee met periodically during the study under the chairmanship of Walter J. Hart, bridge engineer for the state of Oregon.

REFERENCES

1. A. Hedefine and L.G. Silano. Design of the Fremont Bridge. Preprint 1210. Presented at the ASCE National Structural Engineering Meeting, Portland, Oreg., April 1970.
2. Standard Specifications for Highway Bridges, 9th ed. AASHO, Washington, D.C., 1965.
3. Interim Specifications, Bridges. AASHTO, Washington, D.C., 1974.
4. Guide Specifications for Fracture Critical Non-Redundant Steel Bridge Members. AASHTO, Washington, D.C., Sept. 1978.
5. Standard Specifications for Highway Bridges, 12th ed. AASHTO, Washington, D.C., 1977.
6. Interim Specifications for Highway Bridges. AASHTO, Washington, D.C., 1979.
7. Standard Specifications for Welding of Structural Steel Highway Bridges, 2nd ed. AASHTO, Washington, D.C., 1977.
8. M.J. Koob and J.M. Hanson. Field Testing of the Fremont Bridge. In Transportation Research Record 903, TRB, National Research Council, Washington, D.C., 1983, pp. 1-8.
9. R. Roberts, J.M. Barsom, J.W. Fisher, and S.T. Rolfe. Fracture Mechanics for Bridge Design. FHWA, U.S. Department of Transportation, July 1977.
10. S.T. Rolfe and J.M. Barsom. Fatigue and Fracture Control in Structures: Applications of Fracture Mechanics. Prentice-Hall, Englewood Cliffs, N.J., 1977.
11. J.W. Fisher, D.R. Mertz, and A. Zhong. Steel Bridge Members Under Variable Amplitude, Long Life Fatigue Loading. NCHRP Report 267. TRB, National Research Council, Washington, D.C., Dec. 1983, 26 pp.
12. J.W. Fisher. Bridge Fatigue Guide--Design and Details. American Institute of Steel Construction, Chicago, 1977.

Publication of this paper sponsored by Committee on Dynamics and Field Testing of Bridges.

Dynamic Load Testing of Highway Bridges

RETO CANTIENI

ABSTRACT

Between 1958 and 1981 the Swiss Federal Laboratories for Materials Testing and Research (EMPA) performed dynamic load tests on 226 beam and slab-type highway bridges; most of them were concrete structures. Test procedures as well as measurement and data processing techniques are briefly described. As a certain degree of standardization was maintained over the years, it was possible to draw some general conclusions from the summarized test results. In particular, the relationship between fundamental frequency and maximum span is discussed as well as the measured damping values. Additionally it is shown that a highway bridge exhibits a pronounced dynamic response only if (a) its fundamental frequency lies in the same region as one of the two vehicle modes of concern and (b) the vehicle speed and pavement roughness are tuned to each other so that the corresponding vibrations of the vehicle will be excited. As a consequence, it has been proposed to define the dynamic load allowance for highway bridge traffic loads as a function of the bridge's fundamental frequency in the new Swiss Code. Taking advantage of the rapid development in the field of electronics, new data acquisition and processing methods have been introduced at EMPA in the last few years. The synchronous measurement and recording of the test vehicle's dynamic wheel loads and the bridge response is now possible as well as subsequent digital signal analysis.

Load tests on bridges have a long tradition at the Swiss Federal Laboratories for Materials Testing and Research (EMPA). The first publications on such tests still accessible today stem from the work of M. Roš, who held a leading position at EMPA from 1924 until 1949. He described the static and dynamic load tests performed in 1922 on the Kettenbrücke (iron chain suspension bridge) in Aarau (1). His legendary EMPA Report 99 (2) gives the procedures and results of load tests undertaken between 1923 and 1947 on 32 arch and 14 beam-type bridges, including the famous structures of R. Maillart. Nearly all of these structures, most of them highway bridges, were subjected to static as well as dynamic loads.

In 1960 Rösli published some results of dynamic tests on 20 prestressed concrete highway bridges that were performed by EMPA in the years following the Roš era (3). Some of the test reports from that period are still available. They contain the data that were used to form the basis for summarizing results of dynamic tests on 226 highway bridges performed by EMPA since 1958 and presented later.

The question can be asked, how has it been possible, in a small country like Switzerland, to gather a considerable amount of experience in the field of dynamic load testing of highway bridges. A comparison of the various code provisions in force since 1892 shows that dynamic tests were required only between 1892 and 1913 and again since 1970. Therefore, it has been largely due to the energies and competence of the EMPA staff that the majority of static tests on highway bridges, which have been required in Switzerland since 1892, were supplemented by dynamic tests. It has not always been a simple task to convince the respective clients (mainly Cantonal highway administrations) of the advantages of dynamic tests.

There has usually been no reason to question the applicability of the results of static tests. Such tests, for example, allow comparisons of the measured behavior of the structure with the respective calculations. The situation has been somewhat different for dynamic tests. The results of these tests, such as natural frequencies, damping, and dynamic increments (also referred to as impact factor, dynamic load factor, or dynamic coefficient) could neither be compared with calculated values nor with corresponding data from code provisions. Even though the state-of-the-art has advanced considerably during recent years, this statement can be revised only slightly because

- Computing the frequencies of a sufficient number of bridge natural modes is no longer a problem today.
- The great number of attempts undertaken in the last decades to predict damping values or dynamic increments on a theoretical basis have not led, as far as is known to the author, to any generally adopted and easily applicable solutions.
- The qualitative and quantitative comparison of measured dynamic increments with corresponding code provisions is generally still not possible. [The 1979 Ontario Highway Bridge Design Code is an exception (4).]

On the one hand, this is mainly because the loads (to which the dynamic increments are related) used in the load tests are not the same as those in the codes. On the other hand, the question can be asked whether the dynamic effects of moving trucks on the response of a bridge are really predominantly a function of the average bridge span, as assumed, for example, in the present Swiss Code (5).

The dynamic increment, as used in the design of a bridge, is the value of greatest practical interest resulting from dynamic load tests. If straightforward comparison of the measured values with theoretical analyses or code provisions is not feasible, there remains the possibility of comparing the experimental values among each other. This can obviously only be done in a significant way if the procedures of testing, measuring, and data processing are standardized as much as possible. Being aware of this fact, the decision was made by Rösli and Voellmy in the 1950s to standardize the EMPA dynamic load tests on highway bridges. Although EMPA is not the only institution performing such tests in Switzerland, the number of standard tests performed by EMPA since that time is considerable.

Only in the last several years has the client been able to profit from this experience. Now the results of a current load test are related to the results of all previously performed tests. Additionally interpretation of the collected test data has

FIGURE 1 A two-axle vehicle before passing over a contact threshold (speed measurement) and over a 45 mm (1.8 in.) thick plank.

led to a proposal for the definition of the dynamic increment for a future Swiss Loading Code.

STANDARD DYNAMIC LOAD TESTS AS PERFORMED SINCE 1958

Test Procedures

The bridges are tested dynamically through passages of a single, fully loaded, two-axle truck, which is provided by the client. With a normal axle spacing of 4.5 m (15 ft) the gross weight of the vehicle usually lies near the legal limit of 160 kN (35 kips). (In general 280 kN or 62 kips is the maximum legal gross weight limit in Switzerland for any type of vehicle.)

The test vehicle is driven at constant speed, whenever possible, along the longitudinal bridge axis and always in the same direction (Figure 1). The tests are begun with a vehicle speed of 5 km/h (3 mph) which is then increased after every passage in steps of 5 to 10 km/h (3 to 6 mph) up to the maximum achievable speed. Tests on the undisturbed pavement are repeated with a plank placed on the roadway in the main measurement cross section. The plank is approximately 50 mm (2 in.) thick and 300 mm (12 in.) wide.

Data Acquisition

Deflection is measured whenever possible at the characteristic point of the bridge, which is normally at the midpoint of the maximum span (main measurement cross section). In many instances deflection is measured at additional points of the superstructure. This measurement is provided by an invar wire stretched between the measurement point at the structure and a fixed reference point under the bridge. In about 1964 the mechanical vibration recorders (vibrographs) that registered the deflection signal on a rotating cylinder were replaced by electronic measurement setups. These usually consist of an inductive displacement transducer, a signal amplifier, and an ink recorder.

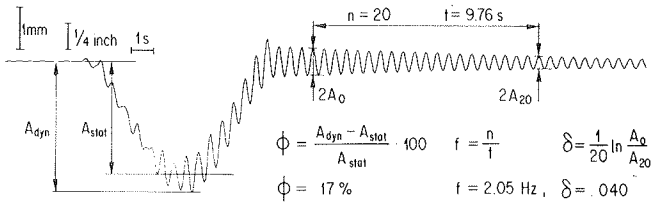

FIGURE 2 Deflection of the midpoint of the Ponte di Campagna Nova, which has one 45-m (148-ft) span, under the passage of a 160 kN (35 kip) vehicle traveling at 25 km/h (16 mph) on the undisturbed pavement (f = fundamental frequency, δ = logarithmic decrement, and ϕ = dynamic increment).

Data Processing

From the dynamic deflection signals, registered on paper strips, the following information can usually be obtained (Figure 2):

1. The frequency of one or more modes of the bridge,
2. Damping of the natural vibration dominant in free decay, and
3. The dynamic increment of one or more measurement signals as a function of the vehicle speed.

Natural frequency and associated damping can be determined by manual signal analysis in the time domain only if the bridge vibrations decay harmonically after the passage of the vehicle. If an accurate time measure has been recorded along with the signal, the natural frequency, Hz, can be established by counting the number of periods in a given portion of the decay process:

$$f = n/t$$

where

n = number of periods, and
t = corresponding time interval in seconds.

Damping, for example the logarithmic decrement δ, can be determined from the same time interval. This requires measurement of the magnitude of the first and last amplitudes having the same phase

$$\delta = 1/n \ (\ln)(A_0/A_n)$$

where

n = number of periods (n+1 amplitudes), and
ln = natural logarithm.

The percentage of critical damping, p, is given by

$$p = (\delta/2\pi) \cdot 100.$$

The dynamic increment is defined as

$$\phi = (A_{dyn} - A_{stat})/A_{stat} \cdot 100$$

where A_{dyn} is the peak value of the bridge response during a passage of the test vehicle and A_{stat} is the peak value of deflection observed under static loading with the same vehicle. Although the readout of A_{dyn} from a paper strip can be performed in a straightforward manner, the determination of A_{stat} may be problematic.

Two basically different methods have been used. In earlier years, A_{stat} was estimated for every passage from the same dynamic trace as the corre-

sponding A_{dyn}. With increasing dynamic response of a bridge, the quality of this estimate for A_{stat} decreases. Therefore, in recent years A_{stat} has been determined from the traces of three very slow passages (crawl tests), and the value thus obtained is subsequently used in the evaluation of all the passages. Comparative tests in 1976 showed that both methods yield the same value for A_{stat} if the driving lane is marked and accurately maintained by the driver.

There is an additional problem in determining the dynamic increment, ϕ. Aside from all the known quantities such as vehicle properties and speed, pavement roughness, and bridge properties, the position of the measurement point in the cross section of the bridge was found, under certain circumstances, to exert a significant influence on the calculated value of the dynamic increment.

This is because the deflection distribution over a bridge cross section under static and dynamic loading is generally not identical. Experience shows that on the one hand, the deflection (A_{stat}) of a statically loaded beam-type bridge will always vary more or less strongly over its cross section, depending on the shape and stiffness of the section. On the other hand, the vertical motional amplitudes (responsible for A_{dyn}) of the same bridge under dynamic loading will remain constant over the cross section, as long as the bridge response consists solely of longitudinal bending modes.

The dynamic increment, ϕ, as a relation between A_{dyn} and A_{stat} therefore will depend on the exact location of the measurement point in the bridge cross section. This dependency is almost negligible for bridges with stiff box-shaped cross sections but may invalidate results gathered from bridges with wide and flexible I-beam cross sections.

RESULTS OF TESTS ON 226 HIGHWAY BRIDGES

In the years from 1958 to 1981 the concrete structures section of EMPA performed load tests on 356 bridges. In the present context, the standardized dynamic part of 226 combined tests on beam and slab-type highway bridges is of interest. The remaining 130 tests concerned tests on other bridge types and purely static tests. Of the 226 bridges, 205 are prestressed concrete, 5 reinforced concrete, 14 composite steel and concrete, and 2 prestressed lightweight concrete structures. The number of spans varies between 1 and 42 with an average of 4 and a value of peak occurrence of 3. The most common structural systems are the continuous beam over more than one span (72 percent) and the simply supported one-span beam (12 percent). Total lengths and lengths of the maximum span can be characterized as follows:

	Total Length	Maximum Span
Minimum	13.0 m (43 ft)	11.0 m (36 ft)
Maximum	3,147.5 m (10,300 ft)	118.8 m (390 ft)
Mean	155.9 m (511 ft)	39.5 m (130 ft)

Of the bridges tested, 109 are straight and without skew, 97 are skewed or curved, and 20 are both skewed and curved. Half of the bridges have a box-shaped cross section, 26 percent a multibeam deck, and 24 percent a solid or hollow-core slab cross section. The cross-sectional width varies between 4.3 m (14 ft) and 30.4 m (100 ft) with a mean value of 12.9 m (42 ft).

The spring constant, defined as gross weight of the test vehicle divided by A_{stat}, was found to lie between 7 kN/mm (40 kip/in.) and 800 kN/mm (4,500 kip/in.) with a mean value of 173 kN/mm (1,000 kip/in.) and a value of maximum occurrence of 75 kN/mm (430 kip/in.).

These data are taken from a computer data bank set up in 1981 in which up to 40 parameters from each of the 226 dynamic load tests are stored. Detailed information on the distributions of these parameters (test conditions as well as results) is given in EMPA Report 211 (6). The most important findings derived from these data are presented in the paragraphs that follow. The number of measured values displayed in the different figures does not equal 226 because (a) it was not possible to meet all the requirements of a standard test as described previously for all tests and (b) the value of concern could not always be determined from the recorded signals.

Fundamental Frequencies

Figure 3 shows the distribution of fundamental frequencies measured on 224 bridges. The result of an attempt to establish a relation between the fundamental frequency of a bridge and the length of its maximum span is shown in Figure 4. The scatter of

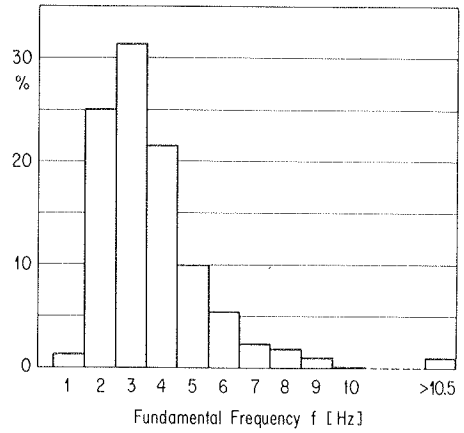

FIGURE 3 Distribution of the fundamental frequencies, f, measured on 224 bridges.

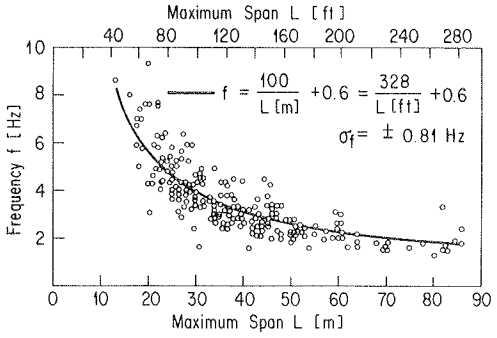

FIGURE 4 Fundamental frequency, f, as a function of the maximum span, L, for 224 bridges (σ_f = standard deviation).

the measured values around a curve determined through nonlinear regression is considerable. This is not surprising in view of the large variations in geometry and stiffness of the bridges tested. To achieve a smaller scatter, the following limitations were introduced:

- Eliminate cantilevered structures,

- Limit the horizontal radius of curvature of the longitudinal bridge axis to ≥900 m (3,000 ft),
- Limit the skew to ≤15 deg.,
- Limit the spring constant, k, to 70 kN/mm ≤ k ≤ 270 kN/mm (400 kip/in. ≤ k ≤ 1,540 kip/in.),
- Eliminate results that were not obtained from measurements on the maximum span.

The regression function calculated from the remaining 100 values is almost identical to the function shown in Figure 4 but the scatter has diminished from $\sigma_f = \pm 0.81$ Hz to $\sigma_f = \pm 0.62$ Hz. As will be shown later, the dynamic increment will probably be defined in a future Swiss Code on bridge loading as a function of the bridge's fundamental frequency. Therefore, the previously mentioned equation to estimate this frequency from the maximum bridge span may be of some practical value in the early design stages.

Damping

The distribution of the logarithmic decrement, δ, determined from the free decay process of 198 concrete bridges is shown in Figure 5. Because the δ-values are scattered over a considerable range, an attempt was made to separate the bridges with relatively strong damping from those with relatively weak damping.

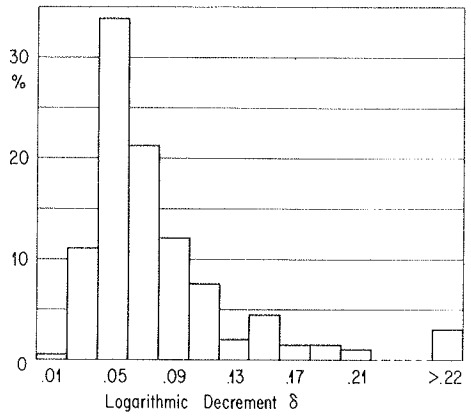

FIGURE 5 Distribution of the logarithmic decrement, δ, measured on 198 concrete bridges (minimum, 0.019; mean, 0.082; maximum, 0.360).

Considering the superstructure of a bridge as a vibrating body, overall damping can be separated into internal or structural damping and external or system damping. Thus, structural damping is due to energy dissipation during all kinds of vibrations of the superstructure; and system damping is due to energy dissipation during relative movements between superstructures and substructures and during all kinds of vibrations of the substructure elements. Because only concrete bridges were taken into account, material damping was not considered. Information was not available on the influence of vibrational amplitude on damping; therefore, the damping relation between this amplitude and the maximum span could not be taken into account. As will be seen later, this influence does not seem to be significant when compared with the factors actually under consideration.

Concerning structural damping it was found that bridges responding predominantly in a longitudinal mode of flexure have on the average a smaller logarithmic decrement than bridges that respond in a superposition of modes of longitudinal flexure, torsion, and transverse flexure. Straight structures with narrow, closed cross sections showed a mean $\delta = 0.063$ ($p = 1$ percent), and curved or skewed bridges with wide cross sections showed a mean $\delta = 0.087$ ($p = 1.38$ percent).

The EMPA data bank does not contain the necessary information to investigate system damping in detail. For example the type of bearing constructions and the relative stiffness of piers are often not given in the test reports. An analysis to confirm the results of Green (7) showed that the total length of a bridge indicates the damping to be expected. Long bridges with a total length of more than 125 m (410 ft) showed a mean $\delta = 0.056$ ($p = 0.89$ percent), and short bridges with a total length of less than 75 m (246 ft) a mean $\delta = 0.098$ ($p = 1.56$ percent). Although the total length of a bridge surely influences the previously mentioned parameters of structural damping, it presumably also reflects influences of system damping. The long structures have an average of 0.26 supports per 100 m (33 ft) of bridge length, the short ones a corresponding value of 0.60.

Figure 6 shows the δ-distributions for two classes of bridges, which were formed by combining the parameters of structural damping and the total length: (a) long, straight bridges with narrow, closed cross sections and (b) short, curved and/or skewed bridges with wide cross sections. These two classes seem to have well separated mean values and distributions of overall damping.

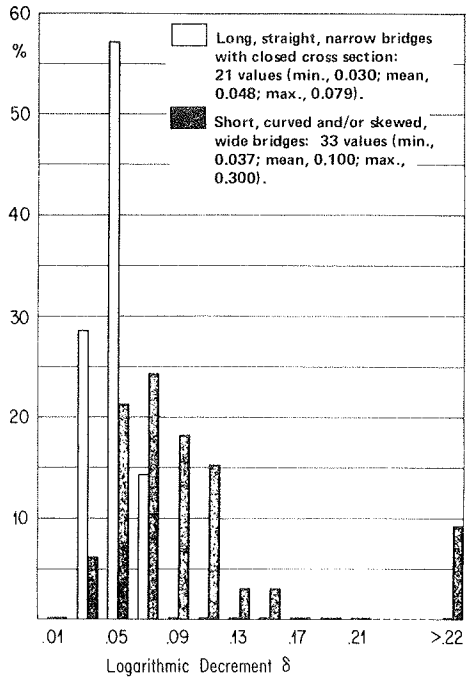

FIGURE 6 Distributions of the δ-values for two classes of concrete bridges.

Dynamic Increments

Where a falsifying influence of the location of the measurement point in the body cross section was to be expected, these values were eliminated before trying to interpret the measured dynamic increments, ϕ. When the measurement point lies outside the region of direct influence of the test vehicle, the resulting ϕ will be too high to a lesser or greater

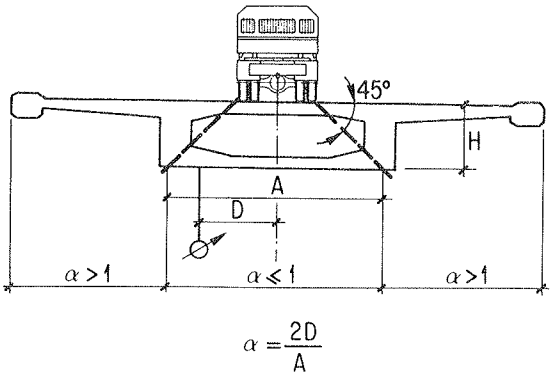

FIGURE 7 Definition of the coefficient, α, describing the location of the measurement point in the bridge cross section relative to the direct influence region of the vehicle.

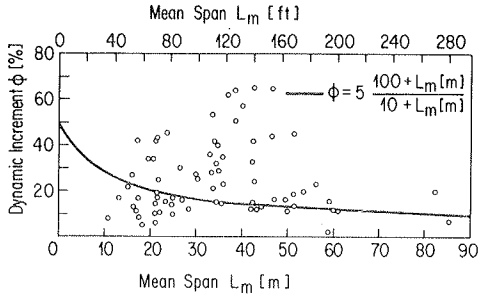

FIGURE 8 Dynamic increments, ϕ, for passages without a plank as a function of the mean span L_m for 73 concrete bridges ($\alpha \leq 0.8$). The solid line indicates the provision in the present Swiss Code (5).

extent depending on the transverse bending stiffness of the bridge. Therefore, only data corresponding to $\alpha \leq 0.8$ (see Figure 7 for the definition of α) were retained.

First the relationship between the dynamic increment and the mean span of the bridge was investigated. It can easily be seen from Figure 8 that this relationship does not correspond to the function implied from the present Swiss Code (5). Each of the measured ϕ-values displayed in Figure 8 represents the peak value of the dynamic increments established from a standard test with the vehicle passing over the undisturbed pavement. As mentioned earlier the comparison between measured values and code provisions can be qualitative only.

Then it was found that the fundamental frequency is an important parameter influencing the response of a bridge to the passage of a test vehicle. A general explanation for this observation is as follows. The bridge as well as the vehicle are mechanical mass/spring/damper systems whose dynamic behavior is determined by natural modes; the bridge response will therefore be influenced by the relationship between the frequencies of these modes. Stated differently, one of the conditions to be fulfilled for a distinct bridge response is a matching of the frequencies of dynamic wheel loads and the natural mode of a bridge.

The natural modes of the EMPA test vehicles were presumably scattered over a relatively narrow frequency band. The vehicles were all fully loaded two-axle tip trucks with leaf springs. Under normal conditions of pavement roughness, the dynamic wheel loads of such vehicles occur mainly in two frequency ranges: (a) in the range of the body bounce frequency between ~2 Hz and ~5 Hz and (b) in the range of the wheel hop frequency between ~10 Hz and ~15 Hz. The body bounce mode of a vehicle is excited by relatively long waves, and the wheel hop mode by relatively short waves of the roadway unevenness. Depending on the vehicle speed, an unevenness of a certain length may be effective in both ranges. As an example of special interest, a plank excites body bounce vibrations for low vehicle speeds and almost pure wheel hop vibrations for speeds above 40 km/h (25 mph).

Figure 9 shows the maximum dynamic increments, ϕ, of test series on the undisturbed pavement as a function of the bridge's fundamental frequency. The curve encompassing the measured values shows a clear peak in the region of 2.5 to 4 Hz (i.e., in the region of the vehicle's body bounce frequency). The statement that the shortwave amplitudes of normal pavements are too small to excite the vehicle's wheel hop mode significantly is based on one single measurement value in the corresponding frequency range.

From the equivalent diagram for the test series with a plank lying on the roadway (Figure 10) it can be seen that a first resonance peak lies in the range of 1.5 to 3 Hz and a second peak at frequencies above 7 Hz. Taking into account that (a) a plank represents a large amplitude of excitation compared with the amplitudes of roughness of a usual pavement and that (b) the natural frequencies of a nonlinear system, such as a leaf-sprung truck, decrease with increasing amplitude of excitation, then the two observed peaks lie in the range of the body bounce and the wheel hop frequencies of the vehicles, respectively.

It can also be seen from Figures 9 and 10 that the dynamic increments do not follow a one- or two-peaked resonance curve. Instead they are scattered below the peaks. Unfortunately the information available is not sufficient to determine the reasons

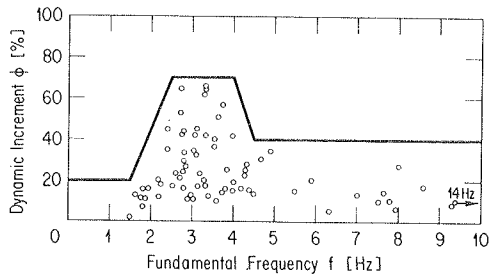

FIGURE 9 Dynamic increments, ϕ, for passages without a plank as a function of the fundamental frequency, f, for 73 concrete bridges ($\alpha \leq 0.8$).

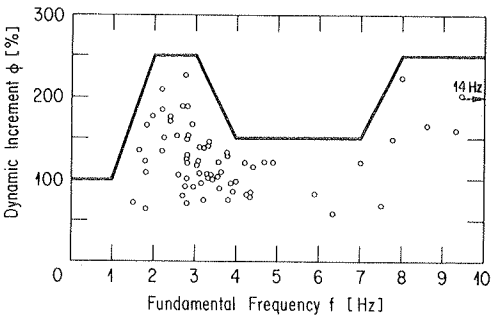

FIGURE 10 Dynamic increments, ϕ, for passages with a plank as a function of the fundamental frequency, f, for 69 concrete bridges ($\alpha \leq 0.8$).

for this scatter in detail. Nevertheless, an attempt was made to evaluate the influence of three parameters available in the EMPA data bank (6). It was found that damping does not appear to exert an important influence on the dynamic increment and that straight, beam-type bridges respond only slightly more strongly than more complicated structures. The investigation also showed that the influence of pavement roughness on dynamic increments for passages without a plank was greater for those bridges with medium or poor pavements than for those with smooth pavements.

Hence, the interpretation of the EMPA test results can be summarized as follows: A highway bridge exhibits a pronounced dynamic response only if (a) its fundamental frequency lies in the same region as one of the two vehicle modes of concern and (b) the vehicle speed and pavement roughness are tuned to each other so the corresponding vibrations of the vehicle will be excited.

The solid curves indicated in Figures 9 and 10 were proposed to be integrated qualitatively into the new version of the Swiss Code on Highway Bridge Loadings. The curve shown in Figure 9 is similar to the curve used in the 1979 Ontario Highway Bridge Design Code (4). However, these two curves were developed independently and were based on two different sets of experimental data.

CURRENT EMPA TESTING METHODS

Scheduled Tests with a Single Vehicle

To reduce variations in the load parameters further, several improvements have been introduced in recent years. Unfortunately EMPA has not been able to obtain its own test vehicle. It is now possible, however, to make use of the same Army vehicle for all the tests. Payload, tires, and tire pressure are always the same, so it can be assumed that the dynamic properties of the vehicle remain approximately constant.

In addition the driving lane is marked with rubber cones or paint (Figure 1) and the vehicle speed is controlled with a special test wheel (Figure 11). Thus it is possible to maintain constant speed

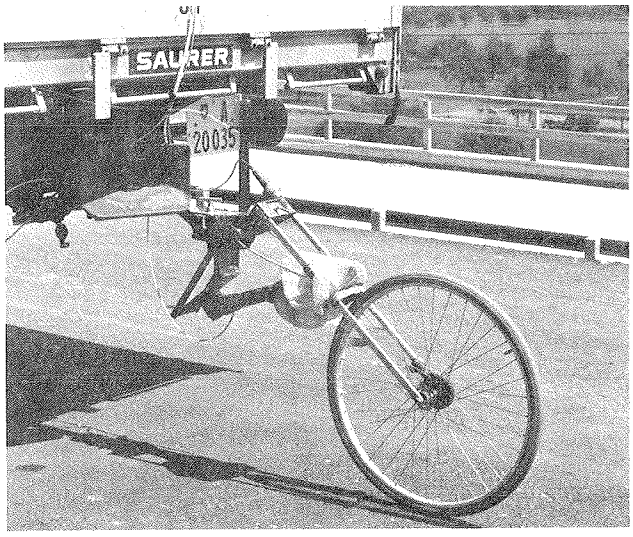

FIGURE 11 With the help of a test wheel, the speed can be accurately measured and controlled during the entire passage.

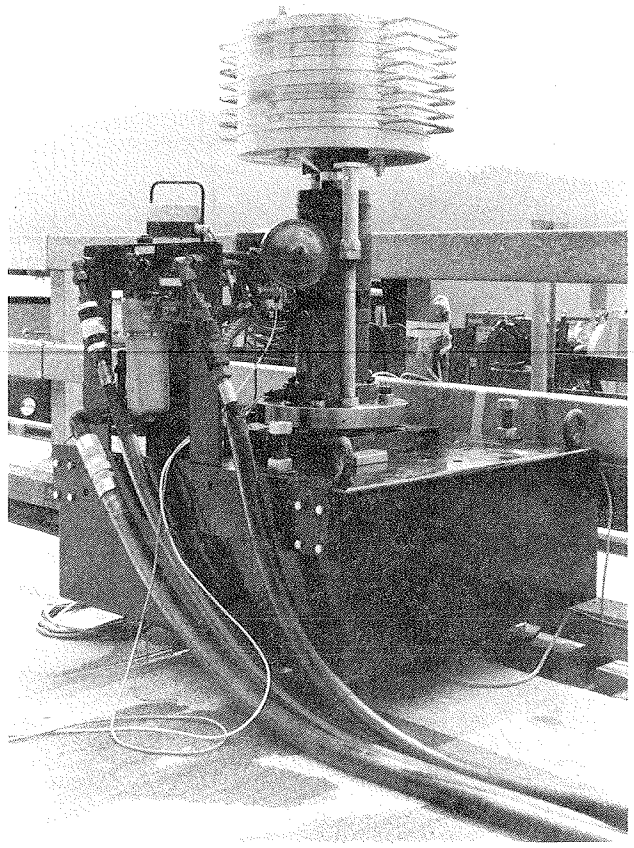

FIGURE 12 Servohydraulic vibration generator (SCHENCK).

within ±0.5 km/h (0.3 mph) from 2 km/h (1.2 mph) up to 100 km/h (62 mph). Furthermore, additional passages are carried out in the range of critical speed, where the bridge response reaches its peak value. In this range, detected by on-line preprocessing of the measurement signals, the speed increment, Δv, is thus reduced to 1 to 3 km/h (0.6 to 1.9 mph).

Excitation with a Servohydraulic Vibration Generator

The natural frequencies of a bridge can be determined very precisely through swept-sine excitation with a vibration generator. In 1977 EMPA purchased the servohydraulic actuator shown in Figure 12. The whole system is mobile and produces a sinusoidal force with a peak value of 5 kN (1.1 kip) in the frequency range between 2.3 Hz and 20 Hz. For frequencies below 2.3 Hz the force decreases with the square of the frequency because the piston stroke is limited to ± 50 mm (± 2 in.). The most important advantage of such a vibration generator is the high frequency resolution that can be achieved. If a suitable function generator is used to produce the drive signal, this resolution may be as high as 0.001 Hz. After looking for the natural frequencies first in a relatively quick sweep, these can later be evaluated in greater detail.

Impulse-Type Excitation

Determination of the natural frequencies or in fact all modal parameters of a structure through impulse-type excitation is common in the investigation of machines, for example, tool machines. The structure to be analyzed is struck with single hammer blows

and the input force and system response (acceleration) are measured to yield the information necessary for the modal analysis. In contrast to a swept-sine excitation as described in the previous paragraph with a long duration input time signal and a very narrow-band frequency spectrum, an impulse-type excitation provides a time signal of very short duration with a correspondingly broad frequency spectrum.

The advantages of the impulse-type excitation are obvious: (a) exciting with a portable hammer is much less expensive than exciting with a complete servo-hydraulic system, and (b) one hammer blow excites all modes simultaneously whereas sweeping through the frequency band of concern may be time consuming.

Disadvantages have to be considered when applying impulse-type excitation to highway bridges. Due to relatively strong damping, the amplitudes of the bridge response may not be significant for a time long enough to allow the determination of a spectrum with a reasonable frequency resolution. This frequency resolution (i.e., the distance between two lines in the spectrum) equals one time window (length of the signal in seconds). Considering a mean logarithmic decrement for bridges of 0.082 (p = 1.3 percent, see Figure 5), and a corresponding fundamental frequency of 3 Hz, the initial amplitude will be damped out to 50 percent after 2.8 sec and to 1 percent after 18.7 sec. Thus, assuming an initial signal-to-noise ratio of at least 40 dB for such a free decay process and transforming one 20 sec time window, a frequency resolution of 0.05 Hz can be achieved. This resolution is considerably lower than that resulting from a swept-sine excitation test.

CURRENT DATA ACQUISITION AND PROCESSING METHODS

Digital Signal Analysis

With measurement signals recorded on paper strips, data processing is possible in the time domain only and has to be performed manually with the help of pencil and ruler. Several problems occurring with this kind of data processing have been mentioned earlier. To solve these problems and above all to allow digital data processing and signal analysis in the frequency domain, a Pulse-Code-Modulation (PCM) system was purchased by EMPA in 1977. Analog signals from up to 32 transducer/amplifier units are digitized by this system with 12-bit resolution and then recorded in digital form with a tape unit. Upon playback, the signals can be transferred directly in digital form to the disk of a computer. With the help of corresponding software, standard time domain analysis can then be performed simultaneously for all signals.

Frequencies of the bridge's natural modes are determined by transforming the time signals into frequencies (i.e., by calculating power spectra, Figure 13). This task is performed by a Fast Fourier Transform (FFT) analyzer, Nicolet 660A, directly linked with the computer. Because the FFT analyzer is able to treat two time signals simultaneously, it is possible to investigate the phase and amplitude relationships between two signals as a function of frequency. Hence, the shapes of all modes contributing to the signals can be determined.

Measurement of Dynamic Wheel Loads

Until sufficient knowledge of the test vehicle's dynamic wheel loads is acquired, no detailed interpretation of the bridge response will be possible. The first successful attempts to solve the problem of continuously measuring dynamic forces between

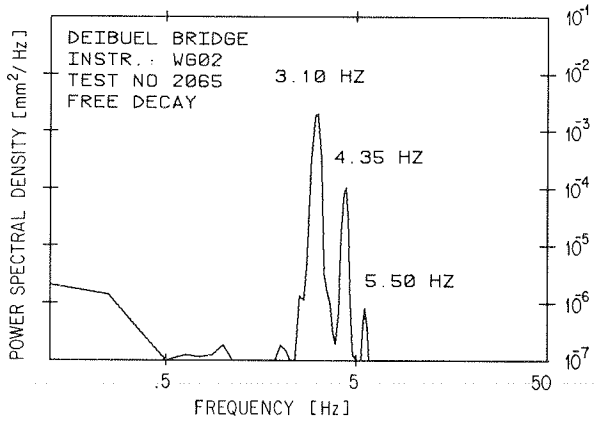

Note: WG 02: Deflection at the midpoint of the largest span. Horizontal axis: Frequency 0-50 Hz, 400 lines, logarithmic scale. Vertical axis: Mean-squared displacement density, full scale = 0.1 mm²/Hz (divide by 645 to convert to sq. in./Hz), logarithmic scale.

FIGURE 13 Power spectral density (PSD) obtained from the free decay of a three-span prestressed concrete bridge, 32 m, 41 m, and 36 m (105 ft, 135 ft, and 120 ft). The frequencies of the first three modes are indicated.

tires and the riding surface were made in the United States and Germany (8,9).

The dynamic wheel loads of a highway vehicle can be measured directly or indirectly. With the direct method the normal wheel hubs are replaced by specially designed and instrumented measurement hubs (force transducers). This method is very accurate but also very expensive (10). With the indirect method, the tire is used as a measurement spring (i.e., the deformation of the tire is measured instead of the force). The necessary calibration curve of the force versus deformation relationship must then be determined in an additional static test. Comparative tests showed that vertical tire deflection reflects the actual wheel load with sufficient accuracy (11).

Therefore, in 1977 EMPA acquired an opto-electronic system that measures the distance between the vehicle's axle and the riding surface (i.e., the vertical tire deformation) with the aid of an infrared beam reflected on the pavement (Figure 14). The main parts of the measurement setup are an infrared emitter, a reception camera, and an electronic control unit. The vertically oriented infrared emitters are located next to the tires; the receivers are slanted at approximately 45 degrees. The infrared light with a wavelength of 930 nm is focused by an objective so as to produce a spot on

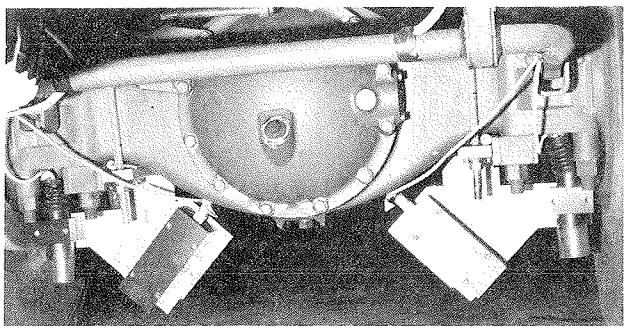

FIGURE 14 Two opto-electronic systems for measuring the dynamic wheel loads mounted on the rear axle of a test vehicle.

the pavement surface of approximately 15 mm (0.6 in.) diameter. The essential component of the camera, which observes the position of the light spot, is a two-dimensional photodetector.

Electric currents that give a measure for the position of the center of the light spot are induced in the photodetector. These currents are transformed to voltages that can be stored on magnetic tape by the PCM-data-acquisition system, which is installed either in the driver's cabin or near the bridge being tested. Signal transfer from the moving vehicle to the stationary PCM-system is performed by a 2.45 GHz telemetry link. Hence, measurement signals stemming from vehicle and bridge are acquired and recorded synchronously. Figure 15 shows an example

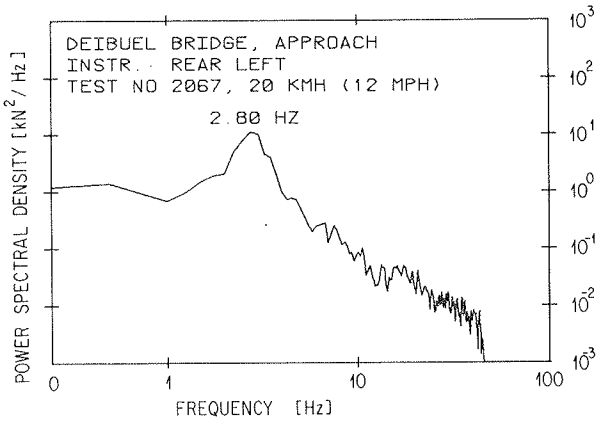

Note: Horizontal axis: Frequency 0-100 Hz, 400 lines, logarithmic scale. Vertical axis: Mean-squared dynamic wheel load density, full scale = 10^3 kN^2/Hz (divide by 20 to convert to sq. kip/Hz), logarithmic scale.

FIGURE 15 Power spectral density (PSD) of a dynamic wheel load signal.

of the power spectral density of a measured dynamic wheel load. The four-channel dynamic wheel load measurement system was extensively used within the framework of a research program but has not yet been introduced to the standard dynamic tests on highway bridges.

REFERENCES

1. M. Roš. Versuche und Erfahrungen an in der Schweiz ausgeführten Stahlbauten 1922-1945. Technische Kommission des Verbandes Schweizerischer Brückenbau- und Stahlhochbau-Unternehmungen, Zurich, 1951.
2. M. Roš. Versuche und Erfahrungen an ausgeführten Eisenbetonbauwerken in der Schweiz 1924-1937. EMPA Report 99, 1937, with supplements for 1939, 1940, 1943, 1945, and 1947.
3. A. Rösli. Ueber das dynamische Verhalten von vorgespannten Brücken, 6. IABSE-Congress, Stockholm, 1960, preliminary report.
4. Ontario Highway Bridge Design Code, 1979. Ontario Ministry of Transportation and Communications, Downsview, Ontario, Canada, Jan. 1979.
5. Schweizerischer Ingenieur- und Architekten-Verein. Normen für die Belastungsannahmen, die Inbetriebnahme und die Ueberwachung der Bauten, Nr. 160, Zurich, May 1, 1970.
6. R. Cantieni. Dynamic Load Tests on Highway Bridges in Switzerland--60 Years Experience of EMPA. EMPA-Report 211, 1983.
7. R. Green. Dynamic Response of Bridge Superstructures, Ontario Observations. Supplementary Report SR-275. Proc., Symposium on Dynamic Behaviour of Bridges, Transport and Road Research Laboratory, Crowthorne, U.K., 1977.
8. A. Mühlfeld. Entwicklung eines hochfrequenztechnischen Verfahrens für Reifen- und Schwingungsmessungen, Diss., TH Braunschweig, 1949.
9. Dynamic Pavement Loads of Heavy Highway Vehicles, NCHRP Report 105. TRB, National Research Council, Washington, D.C., 1970.
10. P. Sweatman. The Dynamic Loading Performance of Heavy Vehicles Suspensions. Proc., Australian Road Research Board, Vol. 9, 1978.
11. V. Gersbach et al. Vergleich von Verfahren zur Messung von Radlastschwankungen, Automobiltechn. Zeitschrift, Vol. 80, 1978.

Publication of this paper sponsored by Committee on Dynamics and Field Testing of Bridges.

Case Histories of Scour Problems at Bridges

STANLEY R. DAVIS

ABSTRACT

Ten case histories of scour problems at bridges are presented to provide a review of the various factors contributing to the problems, corrective actions taken, and the influence of the events on current design practices. Designing bridge foundations to resist scour is still a technical area that requires engineering judgment by experienced bridge and hydraulic engineers, and evidence indicates that additional attention to designing for scour is needed. Analyzing case histories is encouraged as a means of understanding the conditions and events that contribute to bridge scour and ways to avoid or alleviate scour problems.

Scour is an elusive subject because of its complexity. Formulas and mathematical models are still based primarily on theoretical approaches and laboratory tests because of the lack of verifiable field data. Accurate field measurements have been difficult to obtain because of the severe three-dimensional flow patterns that occur at bridges during flooding, and the problems and costs associated with recording instruments or with attempts to get skilled personnel at bridge sites during periods of peak flow.

The stream characteristics, bridge constriction flow pattern, soil and water interaction, and resulting scour will be unique for each bridge crossing as well as for each flood. The evaluation of scour potential at a bridge site, therefore, remains more of an art than a science, requiring a background in river mechanics along with additional inductive skills for making field investigations.

The current approach and emphasis given to evaluating scour varies considerably among highway agencies. Some agencies support highly qualified staffs that make detailed field and office evaluations of scour, whereas others rely on design rules of thumb, with or without the benefit of a field site review.

How much time and effort should be devoted to field and office studies of scour in the design of a bridge? What constitutes a reasonable scour study? What data need to be collected and how should they be analyzed? Engineers tend to respond to these questions with a level of effort commensurate with the perceived risk involved at each bridge crossing. Constraints such as time schedules, budgets, and available personnel may also influence decisions regarding the level of effort that should be applied.

One approach to answering these questions might be: Do bridges perform satisfactorily under design conditions? This may be a tough question to answer because the hydraulic design load is rarely applied. Designers, therefore, often do not have feedback to assess the effectiveness of their designs. This point needs to be emphasized because of the almost unbelievable energy and force of rampaging flood waters.

What should the objective be for accommodating the design hydraulic load? The principles of economic (risk) analysis recognize that bridges and their approaches may be overtopped occasionally without severe damage and that designs that provide for overtopping of the roadway may be economically desirable. These same principles are applied, however, with the assumption that bridges will be well founded and will not suffer major scour damage or settlement from floods well in excess of those anticipated in the bridge design. This approach to foundation design is based on the concept that incremental costs to provide for scour protection for rare events are small in comparison with the consequences of bridge failure.

How well do our nation's bridges compare with this standard? Do they collectively withstand rare floods without damage from scour? Unfortunately data are not collected systematically so that a conclusive answer can be given to this question. The evidence cited in the paragraphs that follow indicates that significant numbers of bridges might be expected to experience distress from scour during future flood events.

A 1973 study for the Federal Highway Administration (FHWA) (2) analyzed 383 bridge failures caused by catastrophic floods and reported that 24 percent of the failures involved pier damage, and 72 percent involved abutment damage. Many of the bridges surveyed, however, were small, single-span structures that failed during Hurricane Agnes in 1973.

A second more extensive study reported by FHWA (1) in 1978 indicated local scour at bridge piers to be a problem about equal to that experienced at abutments. The most common problems included (a) local scour at bridge piers and piled up debris and drift and (b) damage to riprap and erosion of abutment spillthrough slopes with or without the exposure of the pile-supported footings.

FHWA also reported that damage to bridges and highways from major regional floods in 1964 and 1972 amounted to about $100 million per event, and the average loss during this period was estimated at $50 million a year (2). A recent review of FHWA expenditures on emergency relief (ER) projects indicates that flood damage to bridges and highways has been averaging about $75 million annually. This represents only a portion of the total costs to highway systems caused by floods because it includes only highways in the federal-aid system that are involved in declared emergencies. Furthermore, it does not include indirect costs to the public due to temporary closures and detours.

Approximately 85 percent of the 571,000 bridges in the National Bridge Inventory System are built over waterways. The majority of these bridges span rivers and streams that are continually adjusting their beds and banks. Some of these bridges, especially those on the more active streams, can be expected to experience future problems with scour as a result of the natural processes that cause realignment of streams.

CASE HISTORIES

The case histories that follow have been selected to illustrate the types of problems that need to be identified and accounted for in designing bridge abutments and piers. Some of these examples also help to illustrate the difficulty of identifying potential scour problems at the design stage.

State and FHWA bridge and hydraulic engineers have been helpful in supplying information and commentary regarding these case histories. Their assistance is gratefully acknowledged. Continued reporting of future case histories through forums such as TRB is highly desirable to keep designers informed about problems and solutions to scour problems at bridges.

Background

Most transverse flood-plain encroachments involve a combination of highway embankment and bridges and create a constriction in the flood plain for peak flows (Figures 1 and 2). Flow velocities through bridge constrictions are normally greater than the upstream and downstream channel velocities. This difference helps to establish conditions for scour. Scour is commonly classified as (a) general scour or constriction scour (Figures 3 and 4), (b) local scour (Figures 5 and 6) at piers or abutments, and (c) lateral erosion (Figures 7 and 8). Lateral erosion is commonly caused by realignment of the stream and erosion of its banks in the reach of the bridge crossing. The following case histories illustrate the consequences of these types of scour phenomena.

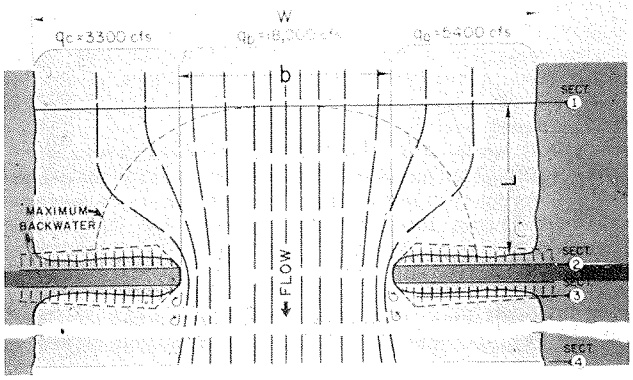

FIGURE 1 Flow lines for a typical stream crossing.

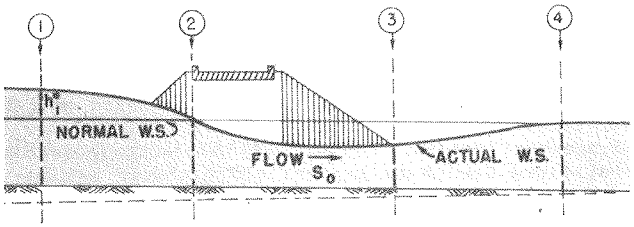

FIGURE 2 Illustration of water surface profile through a bridge constriction.

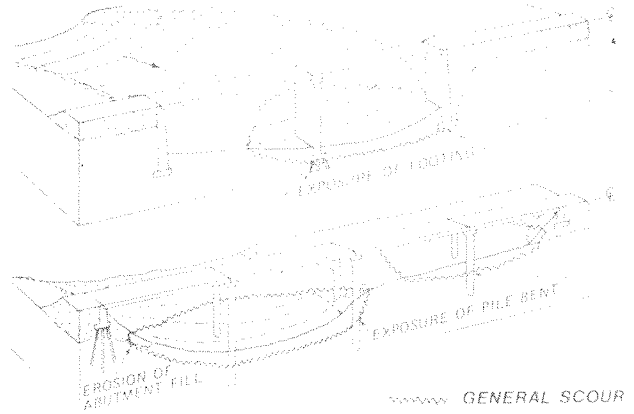

FIGURE 3 Diagram of general scour at a bridge crossing.

I-29 Bridges Over the Big Sioux River Near Sioux City, Iowa

The dual Interstate bridges over the Big Sioux River were five-span, (96, 120, 120, 120, and 96 ft) plate-girder designs 556 ft long supported by rein-

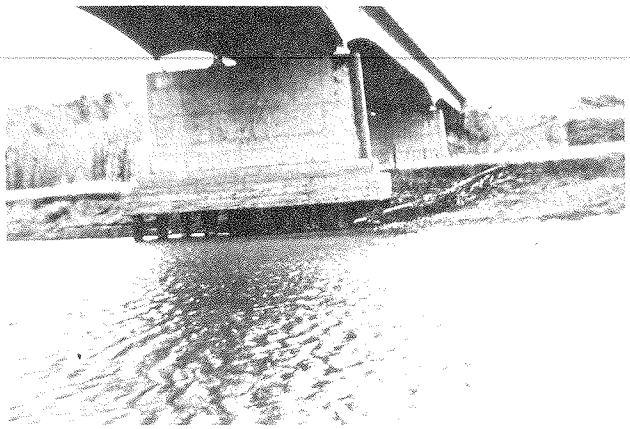

FIGURE 4 Illustration of general scour.

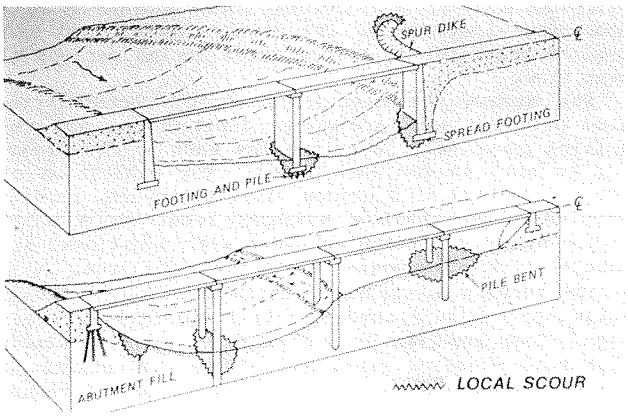

FIGURE 5 Diagram of local scour at bridge piers and abutments.

FIGURE 6 Settlement of bridge pier due to local scour.

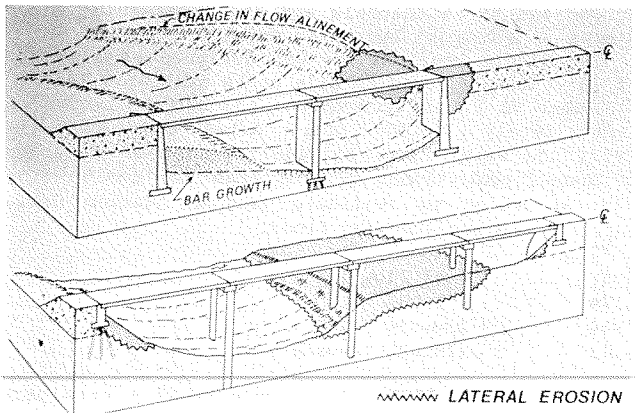

FIGURE 7 Diagram of lateral erosion resulting from realignment of a stream.

FIGURE 8 Illustration of abutment damage caused by lateral movement of stream.

forced concrete piers on continuous footings and timber piles ranging in length from 25 to 34 ft. They were opened to traffic in 1961.

The upstream structure failed during a spring flood on April 1, 1962. Fortunately the bridge was closed immediately after failure so there was no loss of life. Subsequent analysis identified several factors contributing to the failure.

1. Direct cause of failure was due to undermining of pier number 3 by scour.
2. The bridge was located on a bend in the river, and the opening was not normal to the direction of flood flow; instead the flow was at an angle of 25 to 30 degrees to a line normal to the centerline of the crossing. (The design was apparently based on plans for a future channel modification project.)
3. The hydrologic design of the bridge was based on a Q_{50} flow of 42,000 cfs at an elevation of 1,096 ft. The design assumed that the Missouri River, immediately downstream, would also be in flood stage and would create an abnormal stage in the Big Sioux. The 1962 flood was estimated at 54,000 cfs. Flood stage in the Missouri River was about 6 ft lower than the design elevation of 1,096 ft, resulting in a much steeper water surface gradient and a smaller waterway to carry the flows in the Big Sioux River.

This combination of factors resulted in a much smaller waterway to carry the flood flow, a steeper channel gradient and higher velocity, greater flows than anticipated, and finally a bridge with piers skewed adversely to the direction of flood flows.

Corrective Action

All piers of the downstream bridge were underpinned with steel H piles and the scour holes backfilled. The upstream bridge was redesigned and replaced by a three-span structure with single-column round shafts on steel pile supports. Round piers were used to minimize the problem of alignment with the flood flow. This redesigned structure has served satisfactorily and successfully withstood a flow of 81,000 cfs on April 9, 1969.

Significance

Extensive studies were made of the conditions that contributed to the collapse of the Big Sioux River Interstate bridge. A key factor in the success of this effort was the complete cooperation of the state highway agencies of Iowa and South Dakota. The data gathered and conclusions reached from this study were widely disseminated and discussed at that time. The insight gained from the analysis of this failure has been used by many bridge and hydraulic engineers to reinforce the need for careful and reliable hydrologic and hydraulic data in the design of river crossings. These insights include the need to

- Provide a favorable crossing location on a flood plain.
- Align piers with the direction of flood flow and assess the advantages of round piers.
- Carefully coordinate planning for highway projects with channel improvement projects.
- Evaluate performance of a bridge subjected to a range of flows, including flows in excess of the design flow.
- Carefully analyze assumptions for establishing design tailwater conditions and evaluate bridge performance for a possible range of tailwater conditions.
- Evaluate the effect of variable soil conditions in assessing scour.

I-80 N Over the John Day River Near the John Day Dam, Oregon

The main spans of the I-80 N crossing of the John Day River were designed as simple span deck trusses, approximately 200 ft long. The piers in the river were designed to be founded on rock or on piles driven to rock. During construction, the contractor experienced extreme difficulty in excavating the tightly packed or partially cemented gravels in the riverbed. After an evaluation of the problem, including taking borings, the contractor was permitted to place the spread footing on the gravel rather than continue the excavation to rock.

A major factor in this decision was the concurrent construction of the John Day Dam across the Columbia River. Because the I-80 crossing of the John Day River would be located within the pool area behind the dam, it was anticipated that scour would not be a problem once the pool was established. The bridge was completed in September 1963 and the pool behind the dam was expected to be filled within 2 to 3 years. On December 22, 1964, the flood of record occurred on the John Day River before completion of the dam. The river pier foundation experienced serious scour; this resulted in the loss of the pier and two spans.

Corrective Action

A replacement pier, founded on rock, was constructed and the spans replaced at a cost of $880,000. The reconstructed bridge has not experienced any further problems with scour.

Significance

Changes in the field to bridge foundation designs in waterways need to be carefully assessed for the possible consequences of scour. Spread footings placed on alluvial material in a river channel or flood plain are vulnerable to scour. Special design studies to evaluate the scour potential should be made before selection of this type of foundation in a river or flood plain. Rock or pile foundations are normally appropriate for river piers.

Events such as the failure of the John Day Bridge lend credence to the validity of Murphy's Law (if something can go wrong, it will go wrong at the worst possible time). A conservative approach to the design of bridge foundations in waterways is usually warranted.

US-15 Over SR-417 Near Irwins, New York

This highway separation structure was not designed to convey flow because it was at a considerable distance from and above the anticipated flood flows of the Canisteo River. Yet during the Hurricane Agnes flood of 1973 this crossing served as a relief structure for flow in the flood plain. The abutments, which were supported by spread footings, were undermined by the flow through the structure to a depth of 3 to 5 ft and to a maximum lateral distance of about 10 ft under the edge of the spread footing.

Corrective Action

The highway was closed to traffic and temporary timber crib supports were provided for the superstructure. The voids under the spread footing were grouted, the cross section of the local road was restored to its preexisting condition, and the road reopened for normal traffic service. Prompt action by the New York Department of Transportation limited the time Route 15 was out of service to about 4 to 6 weeks. This included the time required to replace the back wall and beam seats of one abutment.

Significance

This case provides an example of the unexpected nature and range of possible problems with structures on flood plains. The damage was unexpected because the highway crossing was not designed as a hydraulic structure and was considered to be above the elevation of anticipated floods. The Hurricane Agnes flood of 1973 was estimated to be greater than the 100-year flood in this region.

New York's decision to restore the preflood condition at the site is viewed as an exercise in risk assessment. That is, the low potential for a recurrence of flooding was not considered to warrant placement of riprap or other special treatment at this bridge.

I-10 Crossing the Pearl River Near Slidell, Louisiana

I-10 crosses the Pearl River flood plain on a series of embankments and bridges; the bridges are designated as the West Pearl bridge, the Middle Pearl bridge, and the East Pearl bridge. The timbered flood plain is several miles wide at the crossing, and the analysis and determination of flood flows across the three channels and the intervening flood plains is a complex hydraulic problem.

The Middle Pearl bridge was designed as a series of 70 ft simple spans on pile bents with pile lengths of about 50 ft to accommodate a flood of record of approximately 125,000 cfs. After completion in 1972, the Pearl River bridges experienced a series of annual peak floods greater than the design flow and, according to available gauging station data, greater than the 100-year flood.

Year	Peak Flow (cfs)
1979	151,000
1980	174,000
1983	225,000 (approx.)

During the 1983 flood, scour undermined a pile bent on the upstream bridge of the Middle Pearl and the bridge settled at this point about 0.5 ft.

Corrective Action

The Middle Pearl bridge was closed and the I-10 traffic was rerouted. A "strong man" or structural frame was placed on the bridge and holes cut in the deck to provide a means of supporting the damaged pier until it could be underpinned.

Additional piles were driven through the holes in the deck and tied in to the existing pile bent. The cost of the emergency repair work was about $81,000. In addition, work on the I-59 bridges about 5 miles upstream of the I-10 crossing will cost on the order of $1.5 million to correct a similar bridge pier scour problem caused by the 1983 flood. Additional studies using a two-dimensional flow model are underway to determine whether additional bridges should be constructed in the Pearl River flood plain.

Significance

The Middle Pearl bridge accommodated flows of the design discharge without damage; however, the bridge was damaged when flood flows greatly in excess of the design occurred. These recent floods have been studied with the conclusion that their occurrence is random in nature and is not accounted for by any identifiable changes in the watershed since the bridge was built. This case illustrates the potential benefits of designing for scour on the basis of an economic analysis that may justify foundation designs for flood flows greater than are used in sizing the waterway of the bridge.

Another interesting aspect of the 1983 flood was its effect on the fendering system for protecting piers from navigational traffic. The fendering system for the West Pearl bridge collected debris and presented an obstacle to the passage of the flood flow. Scour depths at the pier were increased to the point where they became a matter of concern to the state. Increased nationwide attention is now being given to the need for greater protection at bridge piers on navigable waterways. When such systems are provided, they should be carefully evaluated for their influence on local pier scour.

SR-85 Over the Normanskill, Albany County, New York

SR-85 crosses the Normanskill on dual two-span steel bridges; the pier for each bridge is located near the center of the stream and founded on piles. The fine-grained layered silt soils in this region are unstable and slides are common. The Normanskill is a steep fast-rising stream, and the bridges experienced several significant floods; subsequent scour at the center pier reached depths of up to 10 ft.

The scour also undermined the riprap on the south abutment slope and caused sluffing of the backslope in this area.

Corrective Action

Polyfilter woven fabric (70 mesh) was placed on the streambed and banks upstream of and through the SR-85 crossing. Medium stone fill was then placed over the filter cloth to hold it in place and to protect the banks, the spill through abutments, and the piers from the scouring velocities of the Normanskill. A lightweight soil was used to backfill the south abutment slope. This work was done in 1970 at a cost of $70,000 and is considered to be completely successful because no further problems have been experienced at this location. Installing the filter cloth in the bed of the Normanskill was difficult because of the unstable bank and abutment slopes and the fast moving water.

Significance

Selecting the proper type of filter cloth and placing it carefully on the streambed and banks is considered to be a major factor in the success of this repair effort. Also, where feasible, a more desirable alternative to placing a pier near the center of a small, fast-moving stream may be a three-span arrangement that removes the pier obstruction from the center of the channel and facilitates passage of flood waters and debris.

SR-33 Crossing the Homochitto River Near Rosetta, Mississippi

During a period extending from the 1930s to the 1950s, the U.S. Army Corps of Engineers did considerable work on channel modifications to the lower Homochitto River. One reach of the river near Deloroso was reduced from a 20-mile meandering channel to a 9-mile channel with a relatively straight outlet to the Mississippi. The river responded to these changes by degrading its bed (up to 19 ft near Deloroso). At Rosetta the river changed from a slow moving 96-ft wide channel in clay to a 328-ft wide channel in sand, which has meandered over a 3,000-ft flood plain (6). The consequences have been severe to highways and facilities crossing the Homochitto and its tributaries, and damages and bridge replacement costs are approaching $10 million.

Headcutting as a result of channel modification projects is a relatively common problem on streams near the Mississippi River. Similar problems are affecting bridges over the Obion River and its tributaries, the Forked Deer River and its tributaries, and probably other channelized streams in western Tennessee (4).

Corrective Action

In 1974 the SR-33 bridge collapsed and the Mississippi State Highway Department spent $8,000,000 to construct a new 1,500-ft bridge. The new bridge was designed to span a major portion of the flood plain rather than to try to stabilize the existing channel banks, and the north abutment was designed as a pier so the bridge could be lengthened in the future. Attempts to control degradation and meandering of the channel have been generally unsuccessful. The channel moved laterally a distance of 300 ft during the 1974 flood that destroyed the bridge.

Significance

This case provides a graphic illustration of the severe consequences that can result from channel modification projects. When the flow regime of a stream is changed by steepening the stream slope, aggradation and degradation of the streambed and lateral movement of the banks can be expected to occur upstream and downstream over an extended period of time as the stream attempts to readjust to the changed conditions. Many bridges have failed because of headcutting of unstable streams.

It is extremely important that unstable streams like the Homochitto be identified during design so appropriate measures can be incorporated in the design to protect the structure from anticipated scour. Field reviews of proposed bridge crossings are an important element of the design process.

There is, as yet, no final resolution of the problem at this site. The north abutment and approaches may still be vulnerable to attack by the river during future floods.

I-10 Crossing the Gila River, South of Phoenix, Arizona

In October 1983, heavy sustained rains in Arizona and subsequent flooding damaged many highway bridges, including several Interstate structures. The south approaches to the I-10 crossing of the Gila River were breached and several hundred feet of embankment were removed by the floodwaters.

The loss of embankment is attributed primarily to surface mining in the Gila River flood plain just downstream or west of the I-10 crossing. When the floodwaters overflowed the stream banks of the Gila and entered the depressions created by the surface mine, the flow pattern in the river changed abruptly. A significant portion of the floodwaters was diverted to the south, into the mining area, and severe degradation and headcutting began almost immediately. When the headcutting reached the highway, it undermined the embankment and abutment backfill, cutting the highway in two but leaving the abutment undamaged.

Corrective Action

Even before the floodwaters receded, state highway personnel had begun to repair the damage. Traffic was moving across the Gila River in less than 10 days. Quarry stone was brought in and placed to a depth of 6 to 8 ft to bring the embankment above the receding floodwaters and to provide a solid base for the embankment fill. The rest of the fill was then placed and asphaltic concrete pavement used on the approaches up to the bridge abutment. These temporary repairs cost about $700,000 in ER funds. Additional costs for permanent repairs and channel realignment are anticipated over the next few years.

Significance

Sand and gravel mining operations can present a hazard to highway facilities, especially in some of the western states. Existing legislation provides for few controls on surface mining operations, leaving transportation facilities and river control structures vulnerable to the unstable soil conditions created by mining operations. Millions of dollars are being spent to protect or repair highway bridges from the effects of mining, as in the present example, and such efforts often provide only temporary relief.

Lacking effective statewide legislation to control mining operations, state highway agencies may have few options other than to (a) repair and rehabilitate in an attempt to protect against anticipated scour (e.g., drop structures) or (b) buy ease-

ments to protect structures from the unstable soil conditions of surface mining operations. Additional efforts are needed at the state level to develop legislation that provides for reasonable protection of bridges and other public works facilities from surface mining operations.

SR-28 Over Esopus Creek Near Kingston, New York

An inspection in 1982 revealed that a scour hole had formed at pier 1 of this 223 ft, four-span prestressed box beam bridge. The main channel of the stream had shifted to the east about 50 ft so that flows impinged on the pier at an angle of 15 to 20 degrees and a scour hole 5 ft deep had formed.

Corrective Action

The pier foundations are supported by cast-in-place piles 20 to 30 ft long, so the structure was not considered at the time of the inspection to be in immediate danger of settlement or damage due to the developing scour holes. The stream channel was realigned for a distance of about 300 ft upstream to reestablish a smooth flow pattern through the bridge. The scour holes at the piers were filled in with stone. The stream is being carefully monitored by maintenance personnel. If the scour holes recur, consideration will be given to placing heavy stone fill (minimum 150 lb stone) in the scour hole up to the level of the top of the pier footing. The costs of the corrective action to date have been relatively low, consisting primarily of personnel and equipment time for state maintenance forces. Scheduling of corrective work was affected by the need to obtain approval from environmental protection agencies.

Significance

The strict environmental requirements for work in streams, especially good fishing creeks like the Esopus, may present a problem when attempting to correct deficiencies under emergency or near emergency conditions. Highway agencies need to develop special working arrangements with the state and federal regulatory agencies so corrective work can be expedited when a severe scour problem occurs.

In this instance, immediate action was taken to get knowledgeable people from the state central office and regional office to inspect the problem and agree on a solution. A response of this type is most important and deserves special emphasis and recognition. Some bridge failures might have been averted if greater attention had been given to minor scour damage caused by smaller floods before scour damage by the major flood destroyed the bridge.

The National Bridge Inspection Program provides a positive means for identifying incipient scour problems. It is important that bridge inspectors conduct a thorough examination of the waterway piers and abutments during the bridge inspection.

SR-121 Crossing the Mackinaw River Near Peoria, Illinois

During the period 1957 to 1981, following construction of the bridge, a pronounced meander developed upstream, causing the river to move laterally a distance of about 200 ft toward the north abutment. The piers, originally skewed 20 degrees to line up with a straight channel reach, were now receiving flood flows at an adverse angle. One overbank pier experienced severe scour caused by the angle of attack and piled up debris. The scour exposed the pier footing and half the length of support piling.

The development of the meander was attributed to clearing of trees and construction of levees for farming in the vicinity of the bridge. The drainage area of the Mackinaw River is approximately 1,000 square miles at this point. A series of heavy rains in 1980 and 1981 accelerated the bank erosion and lateral movement of the stream toward the north abutment.

Corrective Action

During the winter of 1982, the Illinois Department of Transportation constructed a series of nine stone training dikes or wing dikes of varying lengths along the outside bends of the river for approximately 1000 ft upstream of the bridge. The largest dike, placed near the north abutment, was 140 ft long. Fill was placed behind this dike to restore the cross section near the bridge to the approximate dimensions of the original plan.

The work was designed under emergency conditions to construct the dikes before the spring floods. The biggest problem was obtaining approval of the Section 404 permits for work in the river. The dikes were designed and constructed at a cost of $300,000 using guidance provided by the U.S. Department of Transportation (5). The dikes have been tested by several large floods over the past 2 years and they are performing as planned.

Significance

Early and expeditious action was taken by the state to correct a developing problem. The state chose to spend a significant amount of money ($300,000) to attempt a permanent solution to stopping the development of the meander instead of merely treating the scour at the piers themselves.

Approximately 85 percent of the nation's half-million bridges are over waterways, and it is to be expected that significant numbers of the bridges each year will be subject to potentially severe scour conditions as the streams they cross adjust their bed and banks over time. A careful inspection program and timely corrective action of identified problems are needed to avoid damage to the bridges from scour. Perhaps the most difficult aspects of this problem are the decisions of (a) when to take action and (b) how extensive the repairs need to be.

Debris and ice can have a significant effect on local scour at bridge piers and result in greater scour depths than might be predicted by existing scour formulas.

I-5 Bridge Over the Toutle River Near Castle Rock, Washington

I-5 crosses the Toutle River on a single-span (309 ft) tied-arch steel bridge with vertical abutments. The Toutle River has a steep gradient, flows with high velocities, and carries a tremendous amount of drift and debris from the slopes of Mount St. Helens. In the design of the I-5 bridge, these factors were a consideration in providing a hydraulically efficient opening. The north abutment was founded on piles driven to rock, and the south abutment was founded directly on rock. The construction was completed in 1969.

On May 18, 1980, the Mount St. Helens eruption created a tremendous discharge of mud, water, and debris roughly estimated at three times the previous flood of record. Few bridges were able to survive this event. Two upstream bridges that did remain were the Coal Bank bridge (Route 504) over the Toutle River and the Kidd Valley bridge over the South Fork of the Toutle River. In each case, one

of the road approaches to the bridge was low so that flow-on of the flood plain overtopped the roadway and relieved the pressure on the bridge.

The I-5 and SR-99 bridges both withstood the flood even though almost all the flow had to pass under these bridges. This is attributed to their favorable hydraulic flow characteristics and that both bridges were founded on rock or on piles driven to rock. The I-5 bridge experienced damage to the riprap slope protection at both abutments, some minor pavement damage near the south abutment, and damage to several structural support braces on the superstructure caused by battering from debris.

Corrective Action

Traffic was temporarily detoured to the west for more than 100 miles (one way) until damage to the bridge was evaluated. Because the damage was minor, the bridge was put back into use almost immediately so that I-5 could serve as a major transportation corridor for the recovery efforts following the Mount St. Helens disaster. Heavy rock riprap was replaced around both abutments. The cost of the repairs amounted to approximately $200,000 in ER funds.

Significance

The design features associated with the I-5 crossing of the Toutle River that enabled the bridge to pass a flood of major proportions while suffering only minor damage are

- A hydraulically efficient opening with no piers in the river and generous vertical clearances above the river, offering minimal obstruction to the flood flows and the tremendous volume of debris in the river, and
- Both abutments are solidly tied into or founded on rock.

The only minor bridges on the Toutle River surviving the flood were those with low road approaches. Overtopping of the road approaches relieved the flood pressure on the bridges. This is considered to have been a major factor in their ability to withstand the flood flow. Consideration should be given to designing road approaches for overtopping, wherever practicable, to provide additional protection for the bridge.

GENERAL CONCLUSIONS

1. The interaction between a bridge and a stream is a complex one involving many variables. Although more is being learned about this relationship, no one proven or standard method or approach is available to a designer at this time.
2. Application of the concepts of economic (risk) analysis can be helpful in assessing the extent of scour protection to be provided. It is almost always cost effective to protect foundations from scour for events with greater recurrence intervals than are used in the design of waterway openings. Damage to bridge and highway elements (e.g., spur dikes, riprap, roadway approaches) from rare flood events can usually be repaired and traffic service restored rather quickly as long as the structure itself is not damaged.
3. Information helpful in analyzing the behavior of a river and its probable effects on a bridge can be obtained from field inspections, aerial photography, flood experiences of nearby structures, and other historical data as well as from scour prediction formulas and mathematical models. All available information should be considered.
4. Some structures that failed during the occurrence of a rare flood had suffered distress during previous events of lesser intensity. It is important that personnel involved in inspecting bridges, assessing flood damage, or making repairs know when to get assistance from bridge and hydraulic engineers. Good rapport between designers, bridge inspectors, and maintenance personnel will help to ensure that adequate repair of scour damage is accomplished so as to minimize the vulnerability of the structures to future flood events.

Designing bridge foundations remains a technical area that requires use of sound engineering judgment to (a) evaluate field conditions and (b) apply state-of-the-art knowledge of river mechanics to arrive at a cost-effective foundation design. Both of these aspects should be applied in design on a case-by-case basis to a degree commensurate with the potential risks and consequences of the loss of the bridge from scour. This approach to design should help minimize the future occurrence of the types of problems set forth in this paper.

REFERENCES

1. J.C. Brice, J.C. Blodgett, et al. Countermeasures for Hydraulic Problems at Bridges. Vols. 1 and 2. FHWA, U.S. Department of Transportation, 1978.
2. F.F.M. Chang. A Statistical Summary of the Cause and Cost of Bridge Failures. FHWA, U.S. Department of Transportation, 1973.
3. C. O'Donnell. Highways and the Catastrophic Floods of 1972. In Highway Research Record 479, HRB, National Research Council, Washington, D.C., 1973.
4. C.H. Robbins and A. Simon. Man-Induced Channel Adjustment in Tennessee Streams. Water Resources Investigations Report 82-4098. U.S. Geological Survey, 1983.
5. Highways in the River Environment. FHWA, U.S. Department of Transportation, 1975.
6. K.W. Wilson. Changes in Channel Characteristics, 1938-74, of the Homochitto River and Tributaries, Mississippi. Open File Report 79-554. U.S. Geological Survey, 1979.

Publication of this paper sponsored by Committee on Hydrology, Hydraulics and Water Quality.

An Overview of Factors Affecting River Stability

ROY E. TRENT and SCOTT A. BROWN

ABSTRACT

Anticipating the potential for and recognizing the existence of channel instabilities is a critical aspect of locating and designing highways in river environments. Channel instabilities include oscillations in channel-bed elevation, variations in river orientation and location, and major river migrations or meanders. Factors affecting river stability have been classified as natural or accelerated. Natural instabilities result from changes in hydrometeorology whereas accelerated erosion is usually a result of man's activities within the watershed. Identifying channel instabilities requires an understanding of the geomorphic processes occurring within the watershed in question and an awareness of all activities that affect it. A thorough analysis of the stability of the river system should include consideration of past changes in the system and changes in progress, as well as a geomorphic analysis to predict future changes.

Rivers are dynamic, open systems--dynamic because they are constantly changing and open because they can be significantly influenced or changed by a variety of external forces and factors. They are a complex combination of physical parts working together to form a whole. The dynamic nature of rivers and factors influencing their geometric stability are discussed in this paper.

The amount of water flowing in a river at an instant is variable. Some rivers carry no flow during dry times, but virtually all rivers experience episodes of flooding. The amount of material or sediment transported also fluctuates constantly. Although these changes are usually understood and anticipated in designs, other changes are not. These other changes include oscillations in channel-bed elevation, variations in river orientation and location, and major river migrations or meanders within the valley. Figure 1 illustrates dramatically the changes in channel geometry that can take place. These changes in channel geometry, location, and planform should be of primary interest to the highway engineer designing in river environments.

It is important that engineers designing in river environments recognize and anticipate channel instabilities. A background and approach for recognizing river instabilities are provided in this paper. It starts by discussing geomorphic erosion processes to provide a knowledge of the physical processes involved and to allow for a proper interpretation of channel instabilities. This is followed by discussions of natural and man-induced causes of channel instabilities. Finally methods for identifying channel instabilities are covered. Each of these items is discussed in more detail by Brown (1).

GEOMORPHIC EROSION PROCESSES

The hydraulic geometry of a river system (i.e., its width, depth, and planview form) is a function of the external constraints applied to the particular system. These external constraints include water discharge, sediment discharge, valley slope, and those constraints imposed by the region. During the design life of a typical engineering project, the valley slope and geologic constraints can be assumed to be constant; however, the water discharge and the sediment discharge cannot, because water and sediment discharges will vary with every flow event. Because the hydraulic geometry of a channel is a function of these dynamic elements, a river system will attempt to adjust its geometry in response to these changing conditions to maintain or create a condition of dynamic equilibrium with respect to its own water and sediment load and channel makeup. The geomorphic approach then, looks at channel bank erosion as a natural mechanism of the system to maintain its own equilibrium. The following sections will consider how the flow of water and sediments in alluvial channels affect channel width, depth, and sinuosity.

Functional Relationships

Geomorphic proportionalities that describe functional relationships between the water and sediment load of a channel and the resulting channel size, shape, and sinuosity have been examined by numerous authors. Notable among these are Leopold et al. (2), Lane (3), Schumm (4), and Simons and Senturk (5). More recently a review of these relationships was presented by DeCoursey (6). To demonstrate the effect of changes in flow and sediment load on channel morphology, the geomorphic relationships can be summarized by Equations 1-5.

$$W \sim Q, Q_s \quad (1)$$

$$w/d \sim Q_s \quad (2)$$

$$d \sim Q \quad (3)$$

$$S_c/D_{50} \sim Q_s/Q \quad (4)$$

$$P \sim S_v/Q_s \quad (5)$$

where

W = stream width,
Q = water discharge,
Q_s = sediment discharge,
d = stream depth,
S_c = channel slope,
D_{50} = mean sediment size,
P = sinuosity, and
S_v = valley slope.

These equations are simplified approximations of complete power relationships. In their simplified form, however, they can be used to look qualitatively at changes that can be expected to develop in response to fluctuations in water and sediment load.

Water and sediment discharges are rarely constant, and Equations 1-5 indicate that channels are constantly trying to adjust their width, depth, and planview form. This is true from a morphologic point of view. From a practical engineering standpoint, however, a quasi-equilibrium channel geometry can be defined based on dominant sediment and water discharge conditions. The dominant channel form is that

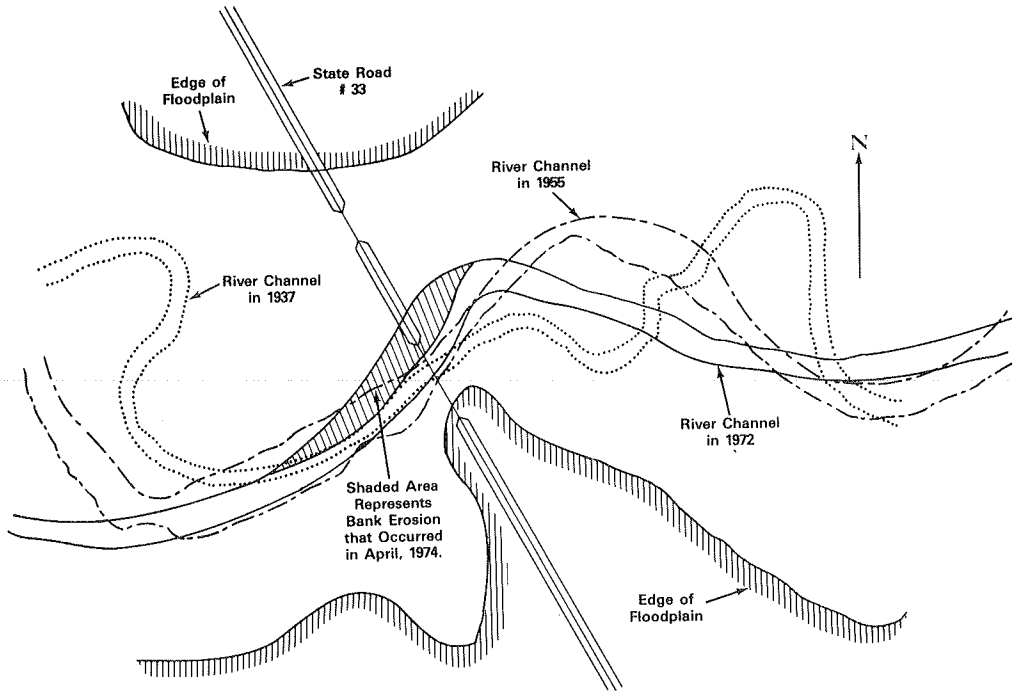

FIGURE 1 Shifts in channel pattern of the Homochitto River at Rosetta, Miss.

which is evident from aerial photography and maps. The stability of this quasi-equilibrium channel form is of primary concern to the engineer designing structures in the vicinity of a river channel.

As mentioned previously, the quasi-equilibrium channel form (that is, its width, depth, and plan view geometry) is a function of dominant sediment and water discharge conditions. The notation of flow frequency plays an important role in defining these dominant conditions. It has been suggested that these dominant conditions be defined as the discharge conditions equaled or exceeded on 0.6 percent of the days of record (or 1 day out of 170 days) (7).

Thus shifts in these dominant conditions (i.e., changes in the frequency distributions) will threaten the stability of a given channel reach in accordance with Equations 1-5 (using dominant values of Q and Q_s as the variable). Equations 1-5 can be used to signal changes in the plan view form or geometry of a channel based on short- or long-term changes in dominant values of Q and Q_s.

To provide a better understanding of the geomorphic proportionalities presented in Equations 1-5, the following section will look at the geomorphic processes described in the equations, consider some of the more common causes of morphologic imbalance, and explain typical system responses to these events.

Geomorphic Response

Three geomorphic responses or processes can result from changes in dominant channel flow and sediment conditions. These are channel widening, channel deepening, and changing plan view form (a change in sinuosity or meander pattern). All of these responses will cause some level of streambank erosion.

Channel widening is evidenced through an increase in channel width, with or without an increase in channel depth. Consideration of Equation 1 indicates that an increase in flow or sediment discharge results in a tendency toward channel widening. When both sediment discharge and flow increase, however, the channel section can be expected to increase its depth as well as its width (see Equations 2 and 3). When only sediment load increases, width increases but the depth may decrease. In this case the channel is said to be aggrading, implying that the channel has filled in because of an excess of sediments.

Channel deepening is a process of channel degradation that increases the depth of the channel. Channel degradation can cause bank instability by producing a steeper bank angle. Whether or not instability actually occurs is a function of the properties of the bank materials and the original bank geometry. Channel deepening results from increased flow without an appreciable increase in sediment discharge (Equation 3). Increased flow rates can result from an overall increase in the volume of water moving through the channel or an increase in channel slope.

Changing plan view form includes changes in channel shape and position as viewed from above. Changes in plan view form are most often exhibited through the downstream migration of meandering bends and changes in the sinuosity of meander bends. Other examples include the shifting of channels and the cutting off of meander bends. Generally these changes are manifested by an adjustment of channel slope to conform with changes in flow or sediment discharge. These changes can be illustrated through an evaluation of Equations 4 and 5.

Equation 4 indicates that either a reduction in sediment discharge or an increase in water discharge will result in a reduction of the channel slope. These slope reductions result in increased channel sinuosity and/or channel-bed degradation; both of which lead to a tendency toward increased bank erosion. Also, Equation 5 indicates that a reduction in sediment discharge will result in an increase in channel sinousity, again, leading to increased bank erosion.

It is important to recognize that the three geomorphic processes just discussed (channel widening, channel deepening, and changing plan view form) are

often interrelated and can occur simultaneously or in sequence. For example, adjustments in channel slope through degradation often are accompanied by increases in channel sinuosity and bank caving or channel widening. Also, the initiation of a given process at a particular site may initiate another process either upstream or downstream. For example, an aggrading channel reach can cause an increase in sinuosity in a downstream reach.

As indicated, shifts in dominant flow conditions cause the geomorphic responses discussed. Shifts in dominant flow conditions can result from either natural or man-induced causes. Recognizing the occurrences that can trigger channel instabilities is a first step in dealing with the problem of channel instability. The more common causes of natural and man-induced or accelerated erosion are discussed in the following sections.

NATURAL EROSION

Natural erosion results from natural occurrences such as normal fluctuations in hydrologic conditions, extended drought or rainy periods, as well as single, extreme storm events. All of these events can cause short-term shifts in the magnitude of the dominant flow conditions, resulting in the adjustments in channel form previously described. For example, extended periods of high flow will cause a temporary shift in dominant discharge levels and possibly a corresponding upward shift in dominant sediment load conditions as well. Previous discussions indicated that these changes result in tendencies toward increased channel widths and depths, as well as a reduction in channel sinuosity. The reduced sinuosity results in a trend to shift meander bends downstream. Each of these responses will increase tendencies toward bank erosion. Similar responses are characteristic of single-flow events as well.

Conversely, consider extended drought periods and the corresponding reductions in flow and sediment transport rates. Equations 1-5 indicate that under these conditions, reductions in channel width and depth and an increase in sinuosity could be expected. Because of the reduced flow conditions, these responses occur within the confines of the dominant channel banks and thus do not pose any significant erosion hazards.

Channel modifications resulting from natural erosion processes include the gradual downstream migration of channel bends and channel avulsions, such as the development of meander cutoffs. When meander cutoffs occur, they can result in extensive reshaping of upstream channel networks. The sudden increase in channel slope that results when a cutoff occurs will result in upstream channel degradation and a tendency toward increased meander activity, both of which will affect channel bank stability.

The extent and rate of change due to the occurrence of a channel cutoff will be relative to the amount of increase in slope produced. If the stream has a relatively flat slope the cutoff would produce a very small increase in stream slope and, therefore, the impact would be lessened. Any changes in response to the new impact(s) would be correspondingly less severe and would occur over longer periods of time.

Natural erosion processes often are difficult to anticipate because they are so dependent on hydrologic events. A seemingly stable river system could suddenly become unstable as a result of a prolonged period of high flow or a single excessive storm event. The uncertain nature of hydrologic events makes it difficult to anticpate such occurrences.

ACCELERATED EROSION

Accelerated erosion can result from some human activity within the watershed that influences flow and sediment transport rates and, thus, morphologic erosion processes. Human activities that influence morphologic erosion processes include agricultural activities, urbanization, construction activities, streambed sand and gravel mining, interbasin water transfers, and reservoir development and operation. Human activities are the most common causes of channel instabilities and, in general, are more widespread and of greater magnitude than natural erosion. Because accelerated erosion is associated with human activities, it often is possible to anticipate any impact on bank stability and provide adequate bank protection in advance. The following discussions will examine the ways that each of the activities mentioned previously affects channel morphology.

Agriculture-related activities include cultivating and harvesting crops, and grazing cattle and other animals. Deforestation and related activities also are included as agricultural activities. The general result of agricultural activity is toward increased peak flows and increased sediment yield. The result will be toward an increase in channel width and a reduction in overall channel sinuosity. Additionally, the grazing of animals along streambanks reduces the vegetative cover, and the continual movement of animals up and down the streambanks can have a significant effect on bank stability.

Stream-channel straightening is another activity that has been associated with agricultural activity in the past. In the early 1900s channel straightening was a common practice in the central and southern agricultural states to make available additional farmlands along the meandering channels of the region. These activities greatly increased the channel slopes of the modified channels. Currently the geomorphic response in these regions is extensive channel-bed degradation and accelerated meander activities. Both of these responses are a result of attempts by the channel to readjust to its previous slopes.

Urbanization normally causes significant increases in the magnitude of runoff events while reducing their duration. Fully developed urban areas are also low sediment producers because of the large percentage of land covered by impervious surfaces. As a result, urbanization reduces the sediment inflow to a river. The combination of the increased peak runoff rates and the reduced sediment loads will result in channel degradation, channel widening, and a reduction in channel sinuosity. Each of these activities will contribute to increased meander activity.

Construction activities are known to increase discharge and sediment loads. The increased discharge (or runoff) results from clearing and grubbing activities that strip away the vegetative cover, which normally acts as a flow retardant. Removal of the vegetative cover (as well as grading and other construction activities) bares and disturbs the soil, accelerating the erosion process and increasing sediment yields to tributary streams. The response of the system to the increased discharge is to increase its width and reduce its meander radius. The response to the increased sediment load is a building up of the channel base level, which when combined with the increased discharge level, will result in accelerating the tendency for channel banks to erode. However, because construction activities usually are temporary, these system responses will be short lived.

Streambed mining is another activity that upsets the natural balance in a river environment. Sand and gravel mining activities affect the sediment movement and supply in a channel system. Excess mining produces both a steeper energy slope in the vicinity of the operation and a reduction in sediment load downstream from the operation. Both of these activities increase the energy available in the water discharge downstream from the mining operation, which increases the potential for bank erosion.

Interbasin transfers of flow are becoming more and more common as the demands on water resources increase. Diverting flow from one basin to another will increase both the magnitude and duration of flows in the receiving channel. Here again, the channel will respond by attempting to increase its dominant width and depth and reducing its sinuosity. These responses will result in a period of channel instability and bank erosion until the new channel regime is established.

Reservoir development and operation for storage and flood control also has an impact on downstream bank stability. Reservoirs trap the incoming sediment load and release clear-water discharges. The clear water released has a higher energy level, because it is not carrying sediment. In an attempt to reduce the energy level, the flow stream will attack the channel bed and banks, producing both degradation and lateral instability. Besides trapping the sediment load, regulating the reservoir also changes the downstream flow characteristics. To satisfy requirements for generating power as well as for irrigation and navigation, reservoir regulation policies encourage higher sustained downstream discharges than was characteristic before regulation. The increased duration of these higher discharges will produce tendencies toward bank erosion. Reservoir operations, particularly for generating hydropower, produce sudden stage fluctuations, which result in saturation and draining cycles on downstream channel banks.

IDENTIFYING CHANNEL INSTABILITY

The goal of any evaluation of stream stability is to detect change and interpret the associated threat to the highway stream crossing or the highway encroachment on the floodplain. The previous discussions indicated some of the more common causes of channel instability. An awareness of the factors that can cause instability is important in identifying channel instabilities. An approach for recognizing river system stability problems includes regional awareness, awareness of natural processes and activities that affect stability, and data collection and analysis procedures. These three topics indicate that the evaluation processes for detecting change have become more sophisticated. Changes that herald instability include long-term and persistent changes in energy gradient, streambed elevation, stream sinuosity, streambed form and material size, stage versus discharge relationships, sediment transport, and similar physical indicators of a variable and troublesome river.

Regional Awareness

Awareness of the region indicates a knowledge of the stability of river systems within the same geomorphic region. It is probably a more useful tool for new highway stream crossings where there is a need to anticipate and recognize the potential for future problems. Problems at an existing structure scheduled for reconstruction or repair are more apparent and will usually be accompanied by a problem history.

Many regions in the United States are prone to gradation problems that, with few exceptions, are caused by streams that flow through valleys or regions composed of fine alluvial material. Most bridge crossings near the lower Mississippi River suffer from some type of gradation problem, and this is also true for western Tennessee and the Missouri River and its tributaries.

A review of local experiences and problems with existing structures and stream crossings can reveal whether a river or the region is prone to channel instabilities. An absence of problems in the past would suggest that none are likely in the future, provided similar design standards are followed. However, the bridge or hydraulic engineer faced with repeated or prolonged lateral and bank erosion, local or general scour, problems with debris, fill, and gradation, must carry the evaluation process further.

Awareness of Activities and Geologic Processes that Affect Stability

As discussed earlier in this paper, there are many activities and geologic processes that affect channel stability. As indicated, human activities within a watershed play a major role, and quite often are the culprit, in cases of channel instability. The importance of these activities on the character, stability, and hydraulic hazards occurring in streams dictates that an attempt be made to identify and consider them during analysis.

Two types of activities affect channel stability: direct instream and watershed characteristics. It is commonly accepted that instream activities have profound effects on stream stability. The principal causes for instability are streambed mining, major channel realignments, and dams. The 110 case histories of problems with stream stability that were analyzed by Keefer et al. (8) illustrate the overriding influence of man's activities. With only two exceptions, the problems presented in the case histories were caused or heavily influenced by attempts to change some aspect of a river's natural morphology.

In addition to examining ongoing processes, it is desirable to communicate with organizations likely to create problems. Government agencies such as the U.S. Army Corps of Engineers plan projects well in advance. Impacts of their activities can be anticipated and accounted for with proper planning. Impacts from the private sector such as gravel mining or changes in land use may be harder to anticipate.

Although instream activities are easier to identify, watershed characteristics can also have immediate and far-reaching effects, and they account for many of the drastic changes that have occurred in streams. Watershed characteristics that affect channel stability include changes in hydrometeorologic conditions and land use. Changes in land use are the most common, and can be related to agriculture or to urbanization and construction activities. Because changes in watershed characteristics usually take more time to develop than instream activities, the subsequent hydraulic hazards develop more gradually. Instability resulting from watershed changes, however, is often more pervasive and more difficult to protect against than instream hazards.

The ever present condition of natural geologic and geomorphic processes must accompany the awareness of problems resulting from human activities. Brice and Blodgett (9) developed a detailed classification scheme oriented primarily toward lateral stability of rivers as summarized in Figure 2, which provides an excellent quick-reference guide to the types of alluvial channels. The indication of sta-

bility for each of the various types of streams (e.g., meandering, braided, incised) shown in the figure are discussed at length in that report and by Brown, McQuivey, and Keefer (10).

Analysis of river system stability must include an examination of the river both at the crossing site and upstream and downstream to determine what processes, conditions, and impacts are likely to cause adverse consequences. Comparing these with recognized problem-producing thresholds and damaging responses of the river system can provide insights into whether problems related to stream stability are present at the site.

Data Collection and Analysis Methods

An awareness of the activities that affect stream stability will provide valuable clues for detecting the presence of stability problems as described previously. Not all engineers, however, will be comfortable with these techniques. In any case, a direct verification of unstable conditions is necessary, and several ways to identify gradation problems and erosion processes are available.

Verification of an unstable river condition is difficult from two standpoints. First, the time span is usually long. Perception of change in riverine conditions is limited by the quality of records or knowledge of prior conditions. The progression of changes to date is the primary indicator of what the future holds. Second, the changes occur in the channel bottom, at remote locations, and often are not persistent. Perennial streams cover the channel bottom and little notice is taken of gradation processes. Natural flow variations and flow regulation vary the depth frequently and only systematic records averaged over long periods will draw attention to the problem. Local scour and contraction scour problems can be obscured by aggradation as the flood flow recedes. Point bars and other fluvial indicators of stability problems may relocate with even minor flows and disarm the uninitiated observer.

Casual observation is not an adequate way to detect problems. Trouble is often not evident until piling supports erode out of the channel bed. Even then the problem may not be detected if the bridge is visited only at high flows or subsurface inspections are not made. Inspection procedures seldom include space or even a checklist for hydraulic and erosion problems, and trouble is often not reported until irreversible damage is sustained.

The data collection and analysis methods used for a particular site will vary with the required level of effort. The level of analysis chosen for a job will be a function of several considerations including instability indicated by awareness, size and character of the river system, cost of the project, availability of requisite data, expertise of persons conducting the analysis, and potential economic and social consequences of damage. An effort to attain balance must guide the level of analysis.

Detection of stability problems requires analysis of either newly compiled or existing data and evidence obtained over periods of several years. It is necessary to determine by some means the change in streambed form, meander patterns, elevation of the channel bottom and/or water surface elevation for a given discharge as a function of time. In some instances knowledge of sediment load or streambed material size may be desirable. A history of each site should be created and evaluated. Techniques for collecting and evaluating data may vary depending on whether interest is in new design or remedial measures. The following is a summary of several analysis techniques that can be used.

Long-Term Observations of Streambed Elevations

Long-term streambed elevation data is extremely valuable for channel stability analysis. Unfortunately streambed elevation data are often scarce or unavailable. Sources of streambed elevation data include

- Data from railroad, pipeline, or old highway bridge surveys;
- Streambed elevation data reported at some gauging stations (these data are updated periodically);
- Historic surveyed channel profiles; and
- Navigation studies.

Another possible source of future streambed elevation data is from periodic bridge inspection reports, many of which are available for the past 30 years. It is highly recommended that measurements be made from bridge decks to streambed as a part of bridge inspections, particularly for streams in regions prone to gradation problems.

Observations of Changes in Stage Versus Discharge Relationships

In many instances, data on the changing bed level may not be available. In these instances analysis of the variation in stage versus discharge relationships at gauging stations is valuable. Long-term data for streamflow are available for many streams of a reasonable size at the gauging stations of the U.S. Geological Survey (USGS) and the U.S. Army Corps of Engineers. Shifts in the rating curves that relate river stage to discharge are often good clues to gradation changes. Changes in the rating curves at gauging stations along the Missouri River as documented by Sayre and Kennedy (11) illustrate the rather dramatic changes that have taken place as a channel degrades. The degradation is primarily due to completion of large reservoirs on the river and efforts to maintain a navigation channel.

Analysis of gauging station stage trends is, again, easily done and yields useful information on long-term trends. On many occasions the USGS and Corps of Engineers have already performed the analysis. Gauging station records are excellent because many cover periods of 30 years or longer.

Observation of Changes in Sediment Load

Another type of useful information available from gauging stations is sediment load. Although only a few stations have continuous sediment data, when available they can provide clues to the presence of gradation problems. By definition, aggradation takes place when sediment inflow to a river exceeds sediment outflow. Degradation occurs when outflow exceeds inflow. Any change in the long-term sediment load signals an imbalance in the stream system. Such imbalances lead to lateral movement, bank sloughing, and gradation problems.

The Missouri River has a number of long-term sediment measuring stations. Data from Sayre and Kennedy (11) illustrate the changes that take place in sediment load when gradation problems occur. A 100-fold change in sediment load (sand, silt, and clay) took place in the early 1950s when the dams above Omaha were closed. This time period coincides with the beginning of major gradation changes along the river.

Streambed Profile Analysis

Another method for verifying the presence of grada-

TABLE 1 Interpretation of Observed Data

OBSERVED CONDITION	CHANNEL RESPONSE			
	STABLE	UNSTABLE	DEGRADING	AGGRADING
Alluvial Fan				
Upstream		√		√
Downstream		√	√	
Dam and Reservoir				
Upstream		√		√
Downstream		√	√	
River Form				
Meandering	√	√	Unknown	Unknown
Straight		√	Unknown	Unknown
Braided		√	Unknown	Unknown
Bank Erosion		√	Unknown	Unknown
Vegetated Banks	√		Unknown	Unknown
Head Cuts		√	√	
Diversion				
Clear water diversion		√		√
Overloaded with Sediment		√	√	
Channel Straightened		√	√	
Deforest Watershed		√		√
Drought Period	√			√
Wet Period		√	√	
Bed Material Size				
Increase		√		√
Decrease		√	Unknown	√

tion changes is stream profile evaluation. The idea is similar to measuring the change in bed elevation from the bridge deck. Instead, a longitudinal profile of the thalweg is surveyed and compared to a historic profile.

Profile analysis requires considerable effort if it is necessary to perform the actual survey. A rough profile analysis can occasionally be performed by plotting as a function of time the elevations of cross sections at pipeline crossings and railroad bridges and obtaining other similar data. This may be required when gauging station records or other more readily available data are lacking. The U.S. Army Corps of Engineers conducts potamology surveys and maintains sediment ranges on many major streams. Data from these sources may be useful in determining bed level changes with time.

Observations of Changes in Stream Classification

River and watershed classification provides insight into typical watershed behavior and response. It also provides information on impacting activities within the watershed. Channel stability can be interpreted from classifications and from field visits. A summary of interpretations taken from Keefer et al. (8) is given in Table 1.

Observations from Maps and Aerial Photographs

A comparison of changes in the channel system with time can be made by using time sequential maps and aerial photographs. This method shows extreme changes in channel alignment and flow habit with time as depicted in Figure 1. These comparisons can signal changes in vertical instability as well as lateral instability because all modes of instability often occur simultaneously. Also, aerial photographs often provide evidence of bank slumping which is indicative of bank undermining caused by streambed degradation. Plotting overlays of meanders and channel movement as a function of time often reveals alarming instabilities. Figure 2 shows an example of the utility of aerial photographs for charting and interpreting channel changes.

Data Sources

Government agencies such as the U.S. Geological Survey, U.S. Army Corps of Engineers, U.S. Soil Conservation Service, and U.S. Forest Service, local river basin commissions, and local watershed districts are valuable sources of data pertinent to analysis of stream stability. Information that these agencies can provide includes historic stream-

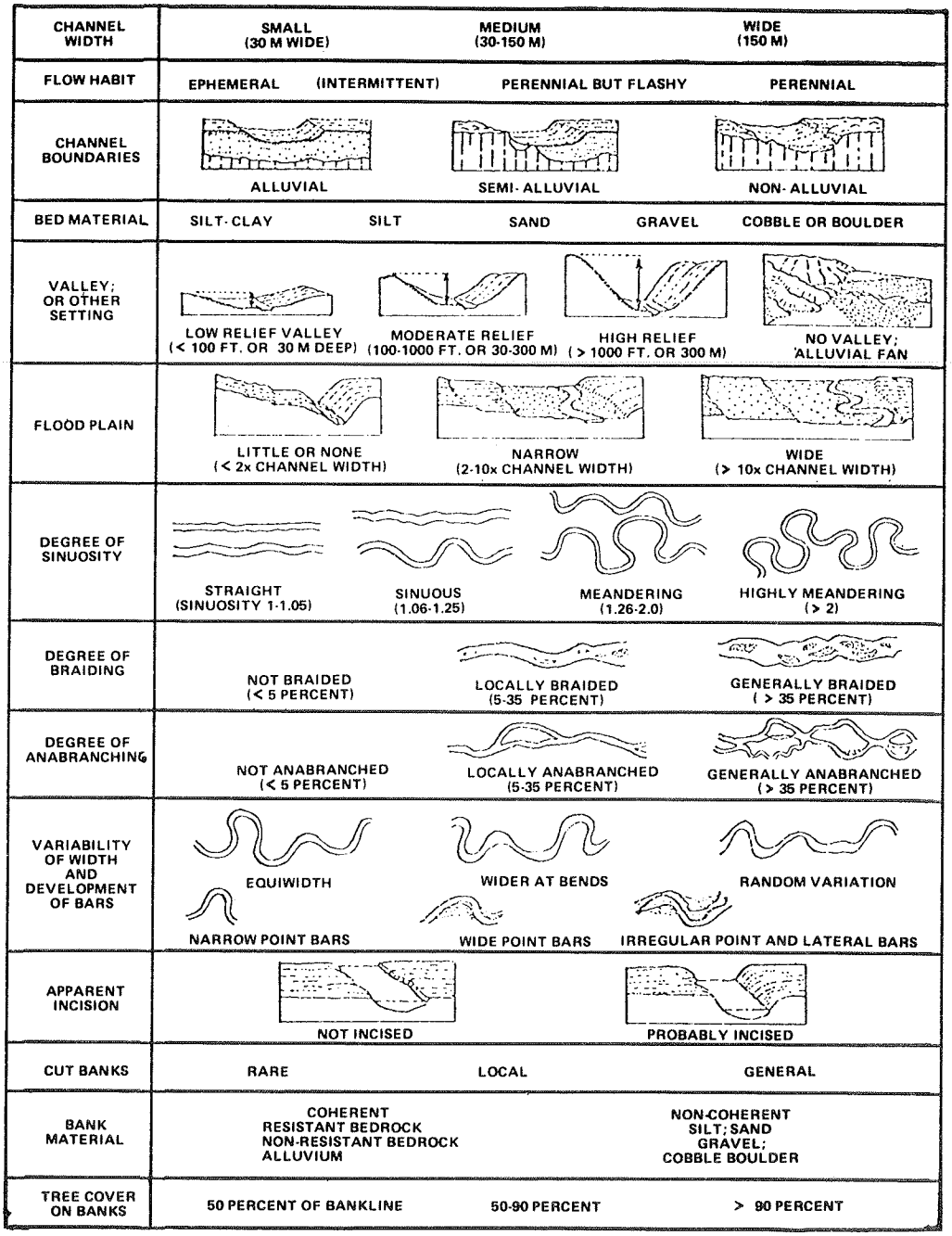

FIGURE 2 Stream properties for classification stability analysis.

bed profiles, stage versus discharge relationships, sediment load characteristics, and very importantly, aerial photographs. These agencies also often have records of past system activities that might have affected stability and might give an indication of future instability characteristics. A checklist of pertinent and peripheral data is so extensive that careful paring of options is essential. The goal of this analysis is to detect and quantify change--the indicator of instability. The engineer should strive to inspect the minimal data set that will result in a conclusion. The checklist of data sources given below demonstrates the possibilities.

Topographic maps
Planimetric maps
Aerial photographs
Transportation maps
Triangulation and benchmarks
Geologic maps
Soil data
Climatological data
Stream flow data
Sedimentation data
Quality of water data
Irrigation and drainage data
Flood control data
Hydro-power data
Basin and project reports
Environmental reports and data
Personal interviews
Paleohydrologic evidence
Diaries and personal records
Field trip and inspection reports

SUMMARY

Recognizing and anticipating channel instabilities is an important part of locating and designing highways in river environments. Channel instabilities include oscillations in channel bed elevation, variations in river orientation and location, and major river migrations or meanders. Factors affecting river stability have been classified as natural or accelerated. Natural instabilities result from changes in hydrometeorology whereas accelerated erosion is usually a result of man's activities within the watershed.

Identifying channel instabilities requires an understanding of the geomorphic processes occurring within the watershed in question and an awareness of all activities that affect stability. A thorough analysis of system stability should include consideration of past system changes and changes in progress, as well as a geomorphic analysis to predict future changes.

REFERENCES

1. S.A. Brown. Streambank Stabilization Measure for Highway Engineers. Final Report, FHWA/RD-83/099. FHWA, U.S. Department of Transportation, 1984.
2. L.B. Leopold. Fluvial Processes in Geomorphology. W.H. Freeman and Company, San Francisco, Calif., and London, England, 1964, 522 pp.
3. E.W. Lane. The Importance of Fluvial Morphology in Hydraulic Engineering. Proc., American Society of Civil Engineering, Vol. 81, No. 745, 1955, 17 pp.
4. S.A. Schumm. The Fluvial System. Wiley, New York, 1977.
5. D.B. Simons and F. Senturk. Sediment Transport Technology. Water Resources Publications, Fort Collins, Colo., 1977, 807 pp.
6. D.G. DeCoursey. Stream Channel Stability, Comprehensive Report. U.S. Army Corps of Engineers, Vicksburg District, Vicksburg, Miss., 1981.
7. F.M. Henderson. Open Channel Flow. Macmillan, New York, 1966.
8. T.N. Keefer, R.S. McQuivey, and D.B. Simons. Stream Channel Degradation and Aggradation: Causes and Consequences to Highways. Interim Report, FHWA/RD-80/038. FHWA, U.S. Department of Transportation, 1980.
9. J.C. Brice and J.C. Blodgett. Countermeasures for Hydraulic Problems at Bridges, Vols. 1 & 2. Final Report, FHWA/RD-78/162. FHWA, U.S. Department of Transportation, 1978.
10. S.A. Brown, T.N. Keefer, and R.S. McQuivey. Stream Channel Degradation and Aggradation: Analysis of Impacts to Highway Crossings. Final Report, FHWA/RD-80/159. FHWA, U.S. Department of Transportation, 1981.
11. W.W. Sayre and J.F. Kennedy. Degradation and Aggradation of the Missouri River. Report 215. Iowa Institute of Hydraulic Research, 1978.

Publication of this paper sponsored by Committee on Hydrology, Hydraulics and Water Quality.

Assessment of Channel Stability at Bridge Sites

JAMES C. BRICE

ABSTRACT

Assessment of channel stability from field study and the comparison of time-sequential aerial photographs provides information that is needed in site selection, bridge design, and countermeasure placement. Channel instability is indicated by bank erosion, progressive degradation (or aggradation) of the streambed, or natural scour and fill of the streambed. Bank erosion rates are related to stream type and are proportional to stream size. Predictions of future rates are based on past rates, as measured on time-sequential photographs or maps, and on the typical behavior of meander loops. Significant degradation of the streambed can usually be detected from indirect field evidence. The sites of greatest potential scour along a channel can be identified from channel configuration. Shift of the thalweg, which is a factor in the alignment of piers, is related to stream type and can be assessed from aerial photographs.

Hydraulic problems at bridges, although less prevalent than structural problems, are nevertheless significant. In the United States the annual damage to bridges and highways from floods has been estimated at $100 million during years of extreme floods (1). Stream-related damage and maintenance problems also occur when there are no floods, but the expense of such damage and problems is difficult to estimate. A study of hydraulic problems at bridges (2) has indicated that damage by streams can be reduced by considering channel stability in site selection, bridge design, and countermeasure placement.

The objective of this paper is to give a brief summary of geomorphic methods used to assess stream channel stability. These methods are presented in greater detail in a research report published by the Federal Highway Administration (3), and a checklist

of geomorphic factors that should be considered in site selection and bridge design are given in an Appendix at the end of this paper.

Many engineers have evidently relied on engineering judgment, based on prior experience and hydraulic analysis of flow (4) to assess scour and other aspects of stream behavior. An assessment of channel stability, from field observations and interpretation of time-sequential aerial photographs, provides additional information to decision makers who select sites and design bridges.

Ideally a stable channel is one that does not change in size, form, or position over time. All alluvial channels change to some extent and therefore have some degree of instability. For engineering purposes, an unstable channel is one in which the rate or magnitude of change is so large that it becomes a significant factor in planning for or maintaining a bridge, highway, or other structure. Changes considered here are (a) lateral bank erosion, (b) degradation or aggradation of the streambed that continues progressively over a period of years, and (c) natural short-term fluctuations of streambed elevation that are usually associated with the passage of a flood (scour and fill).

Applying assessments of channel stability to planning bridges and countermeasures is well stated by Klingeman (5):

> Whereas designers often consider such changes (in bed configuration and channel flow alignment) as a function of stage, it may be more important to recognize the changes that might occur with time . . . best studied from a series of aerial photographs spanning several years. . . . From this assessment of channel stability the designer can expect to make sounder recommendations regarding the best location of the axis of the bridge, the locations of piers in the channel . . . and the likelihood for channel changes and potential maintenance problems during the life of the bridge.

PLANFORM PROPERTIES AND TYPES OF STREAMS

Stream planform properties indicative of channel stability (or instability) are most readily observed in aerial photographs. Unstable streams have wide unvegetated point bars (a and c in Figure 1), cut banks (b in Figure 1), and recent meander cutoffs (d in Figure 1). Stable streams (shown in Figure 2) have a fairly constant stream width, narrow point bars, and well vegetated banks. Major stream types (Figure 3) are characterized by these planform properties and by stability that lies within a fairly well-defined range.

Sinuous Canaliform Streams

The point bars of sinuous canaliform streams (Figures 2 and 3a) are typically covered with permanent vegetation, but narrow crescents of bare sediment may be visible at normal stage. Braiding and lateral bars are rare. If markings are visible on point bars, they tend to be concentric scrolls. Sinuosity tends to be moderate to high, but some reaches are nonsinuous. Banks tend to be well vegetated and cut banks are rare. Natural meander cutoffs are at the necks of meander loops, leaving crescentic oxbow lakes on the floodplain. This is the most laterally stable of all stream types, but meanders gradually migrate. If much vegetation is cleared along the channel, stability may quickly deteriorate; cut banks are an early indication of this. The rate of bedload transport is small in relation to suspended load.

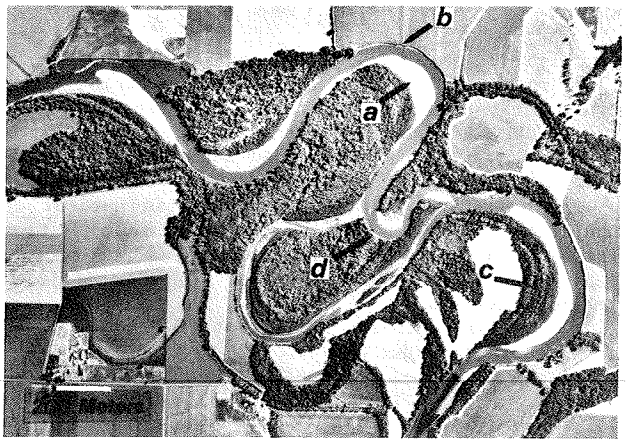

FIGURE 1 Aerial photograph showing typical features of a laterally unstable stream (West Fork White River near Newberry, Ind.).

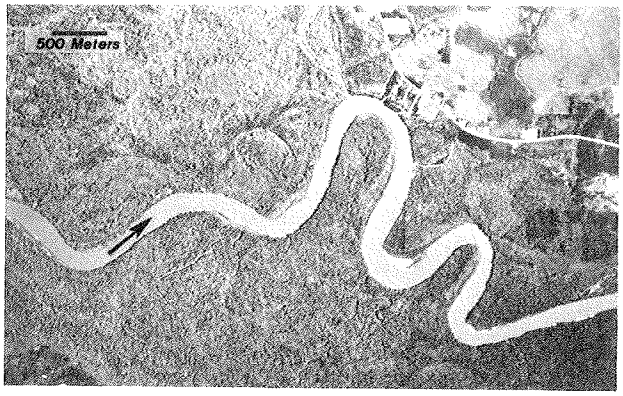

FIGURE 2 Aerial photograph showing typical features of a laterally stable stream (Apalachicola River near Bristol, Fla.).

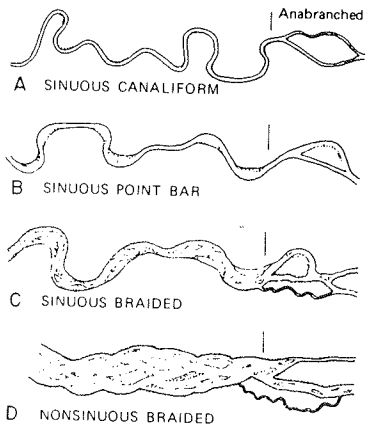

FIGURE 3 Major alluvial stream types.

Sinuous Point-Bar Streams

Bare point bars, clearly visible because of their light tone, tend to be conspicuous on aerial photographs of sinuous point-bar streams (Figures 1 and 3b). Markings on the point bars, if visible, tend

to be concentric (location c in Figure 1). The channel may be locally braided and lateral bars may be present. Sinuosity tends to be moderate, but some reaches are nonsinuous. Cut banks are commonly present on the outside of bends. Both neck cutoffs and chute cutoffs occur, but neck cutoffs are more typical. The rate of bank erosion at bends is potentially high, but nonsinuous reaches may remain stable for decades. Sediment load tends to be moderate, and a significant part of the total load is transported as bed load, either sand or gravel. Most rivers in the United States are of the sinuous point-bar type.

Sinuous Braided Streams

Point bars, lateral bars, and midchannel bars are likely to be present in the channel of sinuous braided streams (Figure 3c). Markings on point bars are irregular or braided. Braiding may be local or general. In contrast with nonsinuous braided streams (Figure 3d), whose thalweg is discontinuous, the thalweg is continuous and likely to be meandering. On some braided point-bar streams, the position of the thalweg is fairly stable; on others, it shifts drastically during floods. The main channel, in contrast with the thalweg, tends to have a low sinuosity. Cut banks are common along the main channel, and natural cutoffs are generally of the chute type.

Sinuous braided streams have a potentially high rate of bank erosion. Rapid shift of the thalweg may cause alignment problems and bypassing of a bridge. Scour depth in the thalweg is potentially great, particularly if the bed material is silt or sand. Sediment load tends to be large and a significant part of total load is transported as bed load (sand, gravel, or cobbles).

Nonsinuous Braided Streams

A typical nonsinuous braided stream (Figure 3d) has a channel bordered by distinct banklines; within these banklines, the channel is divided by unvegetated bars or small vegetated islands. The banklines tend to be irregularly scalloped, with cut banks at indentations. Channel width may change drastically from place to place, but in most places the channel is wide and shallow, requiring a long bridge unless confined by suitable countermeasures. Although the channel is unstable in the sense that braids shift rapidly during floods, the bank erosion rates tend to be low or moderate. Bank erosion occurs where braids shift randomly against the bankline, and hence the point of erosion is unpredictable. Because the banks tend to be erodible, bank protection measures are required in the vicinity of abutments. Braids shift at each high flow, and unexpected depths of scour may occur where braids join to form a deep channel. Much of the load is transported as bed load, either sand, gravel, or cobbles.

Anabranching

Any of the four major stream types may be anabranched (Figure 3). Anabranching differs from braiding in that the flow is divided by islands, or sometimes bars, that are relatively permanent and are large in relation to channel width. The anabranches, or individual channels, are more widely and distinctly separated and more fixed in position than are the braids of a braided stream. A long bridge may be required unless the stream is crossed at a local point where it is not anabranched. If there are two or more anabranches at a crossing site, suitable countermeasures will permit a shorter bridge. If two bridges are used, percentage of total flood flow at each bridge may be difficult to predict. The stability of anabranches differs greatly on different streams, and the stability of each anabranch needs to be assessed as though it were a separate stream.

LATERAL STABILITY

Lateral instability at a bridge site may involve erosion of one or both banks, but commonly only one bank is eroded as the channel migrates laterally and changes its position relative to the bridge (Figure 4). Some degree of lateral migration is to be expected for bridge sites at bends in the channel, but bends may develop at sites where the channel was originally straight. One objective of stability assessment is to anticipate the migration of bends, or the development of new bends. The most common problems associated with lateral migration are the undermining of abutments and the exposure of pile bents that were originally placed on the flood plain.

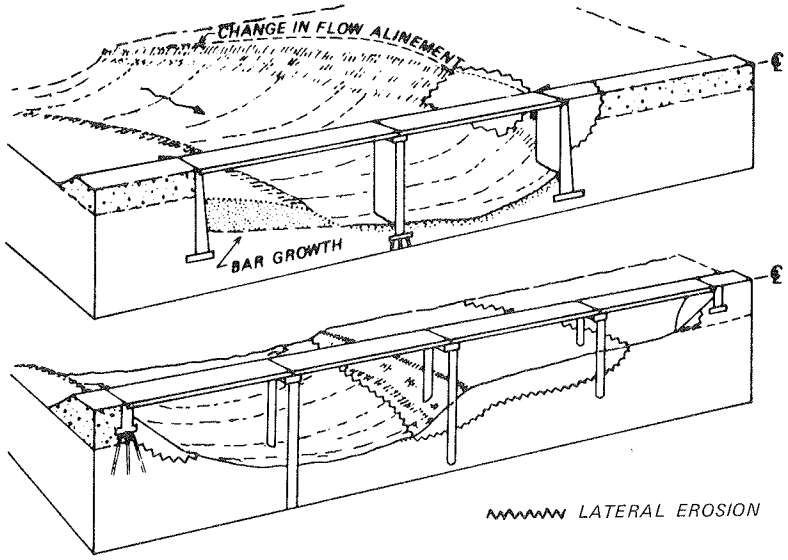

FIGURE 4 Lateral stream erosion and related hydraulic problems at bridges.

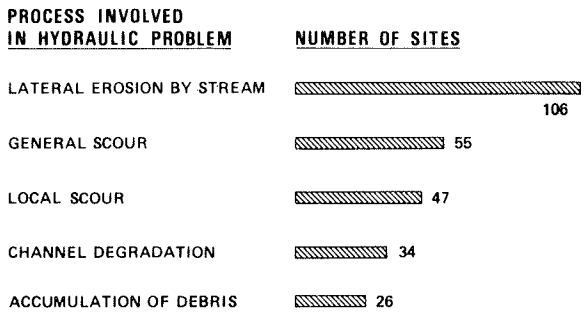

FIGURE 5 Relative importance of different processes in hydraulic problems at bridges.

Lateral erosion is probably more frequently involved in hydraulic problems at bridges than any other stream process. In a study of 224 bridge sites in the United States (2), hydraulic problems were attributed mainly to lateral stream erosion at 106 sites. Other stream processes (general scour, local scour, channel degradation, and accumulation of debris) were less common contributors to problems (Figure 5).

The lateral stability of a channel is measured from records of its position at two or more different times, and the available records are usually maps or aerial photographs. Surveyed cross sections, although useful, are rarely available. For most agricultural regions of the United States, aerial photographs are available for about the last 40 years. Information on the acquisition of time-sequential aerial photographs was given by Brice (3). Maps have the advantage of a longer time span, but time-sequential maps of suitable accuracy are unavailable for large areas of the United States.

Reference Points

Measurement of bank erosion on two time-sequential aerial photographs (or maps) requires the identification of reference points that are common to both. Discernible reference points are either cultural or natural features, which can be identified with much greater confidence by stereoviewing than by examination of a single photograph. If a stereopair is not available, a magnifying lens will assist in identification on a single photograph. In most regions, and particularly on floodplains, cultural features are more likely to maintain recognizable identity over a period of several decades than are natural features.

Cultural features useful as reference points include road and fence corners, buildings, irrigation canals, and bridges. In Figure 6, point 1 is a road corner, point 2 is a fence corner, point 3 is the end of a bridge, and point 4 is a farm building. Points close to the stream have been selected. Because of possible scale variation across the photograph, related to camera tilt, the usefulness of a reference point decreases with increasing distance from the channel. Among the natural features that maintain recognizable identity are rock outcrops and sharp bends in small incised channels. Isolated trees are sometimes useful, as are drainage features on floodplains and lakes of distinctive shape. On some wide, densely forested floodplains, no reliable reference points may be discernible in the vicinity of the channel, and bank erosion distances can only be estimated.

Comparison of Aerial Photographs or Maps

Assessment of lateral stability and the behavior of

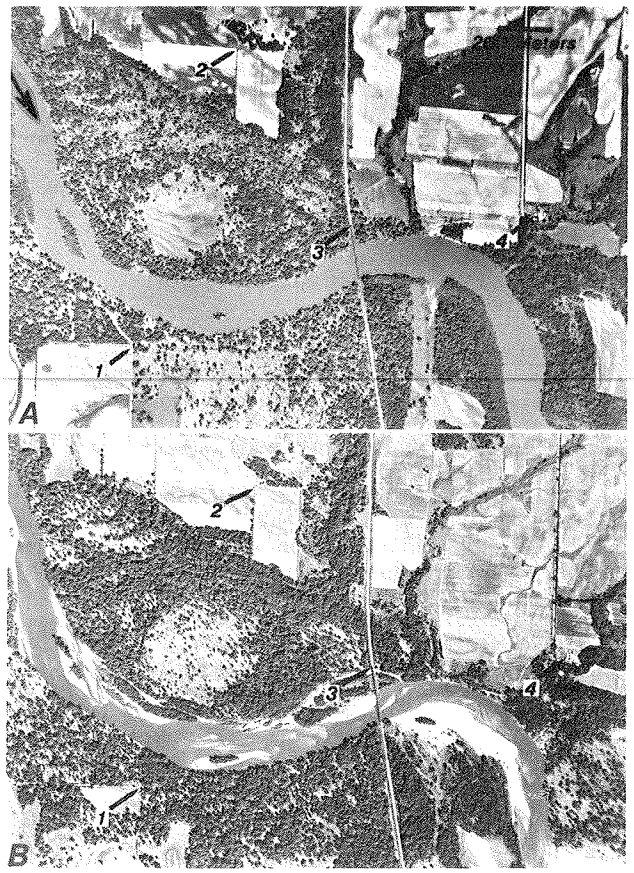

FIGURE 6 Examples of reference points on time-sequential aerial photographs. (A) Points, indicated by numbers, on 1969 photograph of Cedar River, Iowa. (B) Corresponding points on 1937 photograph. (U.S. Dept. of Agriculture photographs).

meanders is greatly facilitated by a drawing which shows the changes with time of banklines and other features of interest (Figure 7). To prepare such a drawing, the aerial photographs (or maps) are matched in scale and the pairs of fixed reference points are placed in register. This involves either (a) bringing the aerial photographs to the same scale by photographic enlargement, or (b) matching scales by projecting the image of one photograph onto another (or a tracing of the other). Projection can be done with a vertical reflecting projector, a graphical data transfer instrument, or an ordinary 35-mm slide projector (3).

Bank Erosion Rates

Bank erosion rates tend to increase with an increase in stream size, as expressed by channel width. In Figure 8, channel width refers to width as measured on aerial photographs, at straight reaches and the inflection points of bends. Median erosion rate was measured on time-sequential bankline diagrams for 36 streams in the United States (3). The dashed curve in Figure 8 is drawn arbitrarily to have a slope of 1 and a position (intercept) to separate most sinuous canaliform streams from most sinuous point-bar and sinuous braided streams. For a given channel width, sinuous canaliform streams tend to have the lowest erosion rates, and sinuous braided streams, the highest. Bank erosion could not be discerned for some sinuous canaliform streams, and an arbitrary rate of 0.01 meter per year was assigned to

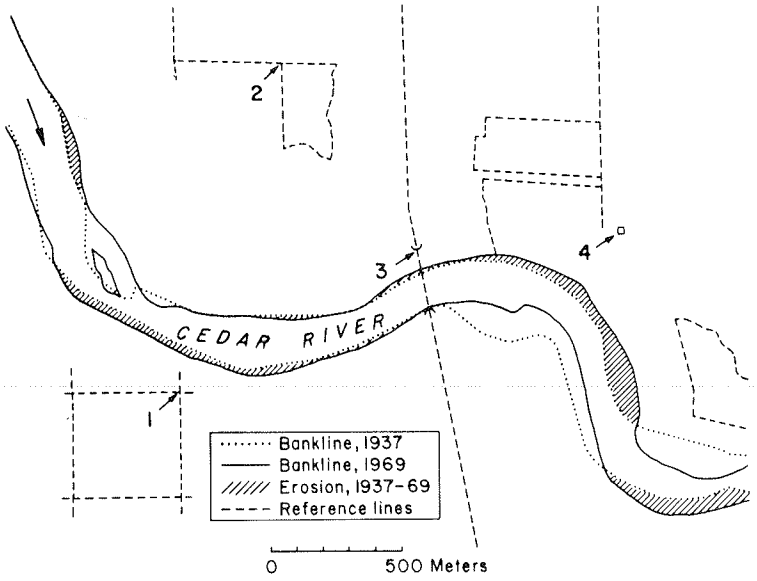

FIGURE 7 Time-sequential banklines for Cedar River, Iowa.

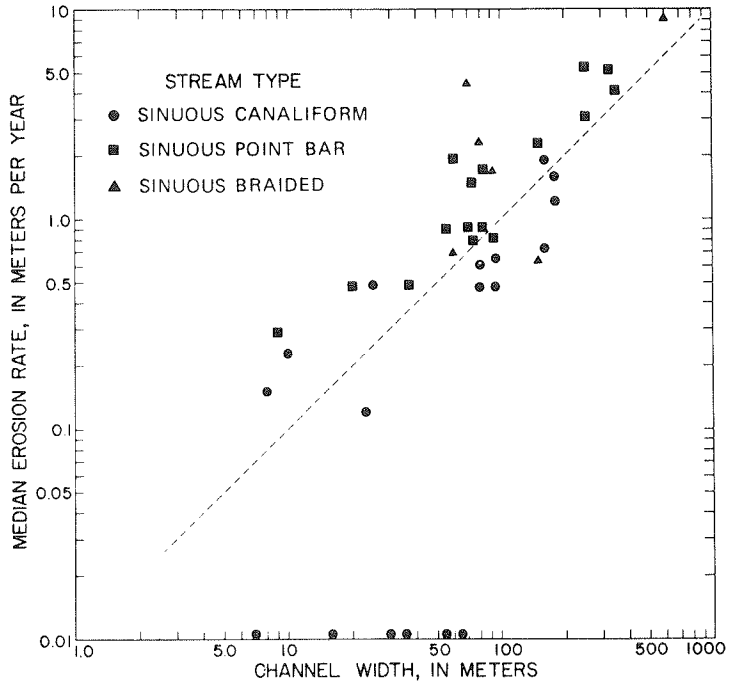

FIGURE 8 Bank erosion in relation to channel size and type.

these. Nonsinuous braided streams, not shown in Figure 8, plot well below the arbitrary curve because their channels are wide relative to their discharges. If nonsinuous braided streams and sinuous braided streams (both uncommon in most parts of the United States) are excluded, the dashed curve in Figure 8 provides a preliminary estimate of erosion rates that may be encountered at a particular site.

The lateral stability of different stream reaches can be compared by means of a dimensionless erosion index (3). The erosion index of a reach is the product of its median bank erosion rate expressed in channel widths per year, multiplied by the percent of reach length along which erosion occurred, multiplied by 1,000. Erosion indexes for 41 stream reaches in the United States are plotted against sinuosity in Figure 9. The length of most of these reaches is 25 to 100 channel widths. The highest erosion index values are for reaches whose sinuosity is 1.2 to 2 and whose type is either sinuous braided or sinuous point bar. An erosion index value of 5 (horizontal dotted line in Figure 9), which separates these types from most sinuous canaliform streams, is suggested as a boundary between stable and unstable reaches. Reaches having erosion index values less than 5 are unlikely to cause lateral erosion problems at bridges. As an example of the use of the erosion index for comparative purposes, the reach of the White River in Figure 2 has an erosion index of about 15, and the reach of the Apalachicola River in Figure 3 has an erosion index of about 4.

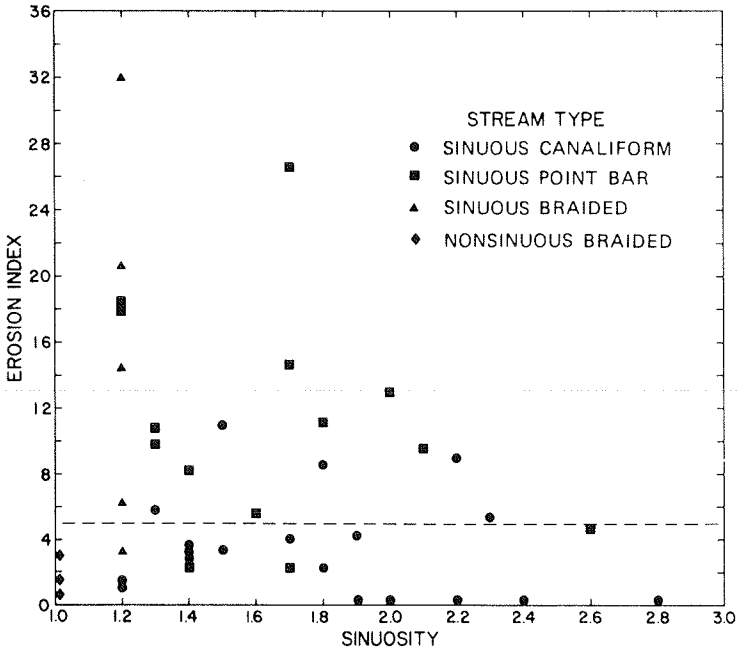

FIGURE 9 Erosion index in relation to sinuosity.

For all stream types, erosion rates are higher at bends than along straight reaches. On the other hand, stream types characterized by the highest sinuosities tend to be the most stable, because some degree of stability is necessary for high sinuosities to be maintained. An unstable stream will not remain highly sinuous for very long, because the sinuosity will be reduced by frequent meander cutoffs.

Prediction of Meander Loop Migration

Most lateral erosion problems at bridges are associated with the migration of meander loops or with the growth of new loops. Prediction of the rate and mode of loop migration may therefore be needed for planning purposes. Some progress is being made on numerical prediction of loop deformation and migration, applying to time intervals significant for engineering purposes (6). At present, however, the best available estimates are based on past rates of lateral migration at a particular reach and on the typical migration behavior of loops. As demonstrated by Nanson et al. (7), erosion rates at a particular loop may fluctuate substantially (and unpredictably) from one period of years to the next. Even so, a rational estimate of erosion at a meander loop, based on the probable distribution and rate of erosion, is better than none.

Erosion at loops involves extension (Figure 10a), translation (Figure 10b), or conversion to a compound loop (Figure 10c). Typically, a loop migrates mainly by translation, with some component of extension. Meanders tend to become compound because they have developed, by growth, a path length that is long in relation to the typical spacing of pools and riffles (or alternate bars) in the channel. Neck cutoffs (Figure 10d) are typical of canaliform and sinuous point-bar streams. As the degree of braiding increases, chute cutoffs (Figure 10e) are more probable. The cutoff of a meander loop, whether by natural or artificial means, tends to increase the bank erosion rate at adjoining loops. However, loop cutoffs are common in nature, and drastic consequences have rarely been observed.

FIGURE 10 Modes of meander loop development and cutoff.

CHANNEL DEGRADATION

Progressive vertical changes in bed elevation (degradation or aggradation) are a common cause of hydraulic problems at bridges in some regions of the United States, and a potential cause in any region where channels are underlain by erodible materials. Degradation occurs more frequently then aggradation, and its consequences are more serious. Of the total number of gradation sites reported by Keefer et al. (8), sites having degradation problems were about three times more numerous than sites having aggradation problems.

Annual rates of degradation that are averaged over a period of time following some man-induced event, such as the closure of a dam or the straightening of a channel, are not a good basis for estimating future rates. According to Simons and Senturk (9), the rate of degradation downstream from a dam is rapid initially and decreases gradually as a new stable profile evolves. Similarly, available evidence suggests that the rate of degradation following channel straightening is likely to be rapid at first and to decrease gradually (10). From a comprehensive study of the effects of channel straightening on streams in western Tennessee, Robbins and Simon (11) were able to describe the channel degradation by an exponential decay function. They concluded that if there were no further disturbance the degradation or aggradation followed a predictable pattern and rate.

Field Assessment of Degradation

If a channel has been recently degrading at a rate

that would significantly affect planning of engineering works, there is likely to be some observable evidence for this along the channel, as seen in the field or by stereoviewing of aerial photographs. Indicators of degradation are listed below in approximate order of reliability:

1. Channel scarps (headcuts, knickpoints). A migrating scarp in the long profile of a channel is unequivocal evidence of degradation, and the rate of degradation is related to the height and migration rate of the scarp. Channel scarps are easy to observe in ephemeral streams or small perennial streams, but are rarely observed in large perennial streams.
2. Gullying of minor side tributaries. As a stream degrades, its tributaries also degrade, and scarps may be present along their profiles.
3. High, steep, unvegetated banks. Some channels have higher banks than others of about the same width. Among the factors that determine bank height are degree of incision and erosional resistance of the banks. Where high banks are also raw and ungraded, recent degradation is suggested.

Other Methods of Assessment

Other methods of assessing channel degradation have been described by Keefer et al. (8). Changes in the elevation of the water surface are determined over a period of years, in relation to a fixed datum. Methods include (a) periodic measurements from bridge deck to streambed, where allowance can be made for local or general scour at the bridge; (b) plotting change in the stage-discharge relation at gauging stations; and (c) repetitive measurement of the longitudinal or cross profile of the stream channel.

NATURAL SCOUR AND FILL

Natural scour and fill has been neglected as a factor in bridge site location, probably because of its complexity and the lack of useful information on it. Bed elevation is difficult to measure during floods, and a reliable analysis of scour and fill requires measurement of several cross sections at about the same time. A continuous longitudinal bed profile along the thalweg is also highly desirable. In a particular cross section, the amount of scour and fill is unevenly distributed, and both the reference bed and the scoured bed are likely to be of irregular shape.

For most streams the magnitude of scour is substantially greater at some places along the channel than at others. According to Neill (12),

> The location of a bridge with respect to the river channel pattern in plan has an important bearing on its liability to bed scour. Bends and narrow sections may be liable to scour at high stages, regardless of the effects of bridge structures . . . . Straight or gently curved reaches with stable banks are to be preferred.

If, however, a crossing must be made on a meandering reach, identification of the segments of least potential scour may be a deciding factor in site location.

Scour below preflood bed elevation probably occurs at most cross sections of an alluvial stream at some time during the passage of a flood, although not at the same time nor to the same degree. At some sections, the scour is due to the migration of bed forms and the mean streambed elevation does not change significantly. In a detailed field study of scour and fill at 11 cross sections on the East Fork River in Wyoming, Andrews (13) measured scour that he considered significant (though less than 0.5 m) during flood crests at 6 of the 11 cross sections, and fill at 5 of the sections. At some time or other during the flood, net scour occurred at all except 2 of the sections.

Natural scour and fill refers to fluctuations of streambed elevation about an equilibrium position, which is commonly taken to be the position at low flow. These fluctuations are associated mainly with floods, and they occur without artificial constriction of the channel and without the presence of artificial obstructions such as bridge piers. The scour induced by a bridge is additive to natural scour. A bed elevation that has been raised or lowered is likely to return to its equilibrium position during the falling stages of the flood; however, the return may require weeks, months, or even years for some streams, particularly those having coarse bed material. Natural scour and fill occurs by three different mechanisms, which may operate jointly or independently: (a) bed form migration, (b) convergence and divergence of flow, and (c) lateral shift of thalweg or braids.

Bed Form Migration

The migration of dunes may result in an amount of scour that is sufficient to warrant consideration in the design of pier foundations. Allowance for scour due to the migration of sand waves is more problematical and would have to be determined from a continuous long profile of the stream at high stage. The maximum scour induced by the migration of a dune is about one-half dune height, and dune height is roughly estimated at one-third the mean flow depth. In sand-bed streams, dune migration can be expected if the quantity of bed load in transport is sufficient for dune formation. Stream type is a reasonably good indication of the bed-load characteristics of a stream. Canaliform streams that have very narrow point bars are likely to be transporting minor amounts of bed load. An increasing transport of bed load is indicated by an increase in degree of braiding.

Most migrating bed forms in gravel-bed streams can be regarded as bars, the height of which is related to flow depth. Migration of a bar through a bridge waterway is mainly of concern because of its deflection and concentration of flow. Bar migration tends to be a random process, and the tendency of bars in a stream to migrate is best determined from time-sequential aerial photographs.

Convergence of Flow

The flow conditions associated with changes in mean bed elevation are summarized by the convergent-divergent flow criterion of Leliavsky (14). Convergent currents in a natural stream are associated with erosion (scour), and divergent currents are associated with deposition (fill).

Persistent pools (Figure 11) in the long profile of an alluvial channel have the strongest convergence of flow and the greatest potential for scour. Such pools are best identified by a continuous bed profile along the thalweg, as sounded at high stage. On a gravel-bed "pool-and-riffle" stream, the water-surface profile at low stage is flattest over the pools and steepest over the intervening riffles. On a sand-bed stream, however, persistent pools may fill at low stage, their position may

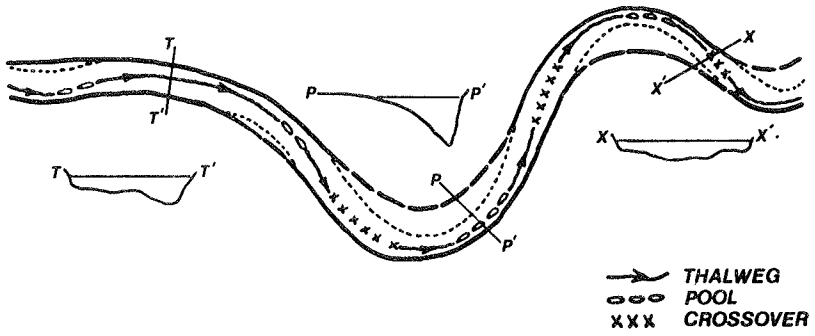

FIGURE 11 Pools, crossovers, and trace of thalweg.

shift to some degree, and they may be difficult to distinguish from random irregularities in the long profile. Pools, as well as riffles and crossovers, tend to be several channel widths in length, which is longer than most random irregularities. As the degree of braiding of a stream increases, the probability of persistent pools in the long profile decreases. Scour holes in braided streams are mostly at the confluence of braids.

For streams having wide point bars, crossovers (Figure 11) can usually be identified on aerial photographs taken at low flow. Pools cannot be observed directly, but they are typically located downstream from the apexes of bends and opposite the point bar. Pools may also occur in straight reaches, where their position is sometimes marked by an alternate bar. At low stage, water-surface width tends to be least at pools, greatest at riffles, and of intermediate value at transitional sites. At bankfull stage, the water-surface width tends to be greater at pools than at crossovers or transitional sections.

As suggested by Neill (15), field measurement of cross sectional area and flow velocity at an incised (straight) reach near bankfull stage provides a good basis for calculation of scour by extrapolation to the design flood. Furthermore, a comparative measurement of this same section at low stage gives the amount of scour from low stage to bankfull stage, which is valuable for confirming results obtained by computational methods. Klingeman (5) recommended that "The lowest undisturbed streambed elevation at or near the bridge crossing (other than a local scour hole) be used as a reference level in setting scour elevations of principal piers at or near the main channel."

Shift of Thalweg

Of the 224 bridge sites studied by Brice and Blodgett (2), hydraulic problems attributed to shift of the thalweg occurred at 6 sites. One of these (site 164, Fort George River, Florida) is at a sand-bed estuary, subject to strong tidal currents. Site 207, Leaf River, Mississippi, and site 170, Red River, Arkansas, are on sinuous point-bar streams having sand beds. At both sites, the thalweg shift was related to a slight curvature of the channel and took place over a period of years rather than during a single flood.

Site 16, Deer Creek, California, and site 186, White River, South Dakota, are at sinuous braided streams in which the thalweg tends to wander. Site 226, Boulder Creek, Washington, is on a steep nonsinuous braided stream having a cobble-boulder bed. The bridge clearance was greatly reduced by aggradation, and the thalweg shifted against an abutment. Although nonsinuous braided streams are commonly regarded as unstable because of the rapid and unpredictable shift of bars and braids, they are readily controlled with suitable countermeasures and are not a particular cause of hydraulic problems.

Instability of the streambed that results from shift to thalweg (or braids) is, like bank instability, related to stream type and can be assessed from study of aerial photographs. On sinuous canaliform streams, shift of the thalweg during flood is minimal. The channel tends to be relatively deep, narrow, and uniform from one place to another. In straight reaches, the alternate bars that indicate meandering of the thalweg are rarely present.

A greater shift of the thalweg, both at bends and in nearly straight reaches, can be expected on sinuous point-bar streams. Flood flow cuts across the ends of the point bars, which are wide and bare at low stage. In straight reaches, alternate bars, visible on aerial photographs taken at low stage, are commonly present. These alternate bars are significant in the planning of bridges and countermeasures, because they indicate the potential for shift of the thalweg and also for bank erosion where the current is deflected against the bankline.

CONCLUSIONS

1. Study of stream morphology on time-sequential aerial photographs provides information that is applicable to site selection and bridge design. By this means, information can be obtained on lateral stream stability, degradation, and natural scour and fill.

2. Lateral stability is related to stream type. Streams that have a uniform width and narrow point bars (canaliform streams) tend to be the most stable. Streams that have wide point bars and cut banks tend to be less stable and, for sinuous streams, stability tends to decrease with the degree of braiding. For a given stream type, median bank erosion rates tend to increase in direct proportion to stream size, as expressed by channel width.

3. Channel degradation is determined by measurement of progressive changes with time of streambed elevation in reference to a fixed datum. For man-induced degradation, the curve of cumulative degradation versus time is more likely to be asymptotic than linear. Equilibrium bed elevation is difficult to predict.

4. Scour by bed form migration is of consequence mainly in sand channels. Gravel bars tend to migrate on braided streams and to remain fixed at riffles on unbraided, pool-and-riffle streams. A migrating gravel bar may concentrate flow at a bridge and cause lateral bank erosion or local scour at piers.

5. Scour by convergence of flow is related to channel configuration and is greatest at persistent

deeps or pools in the channel-long profile, where the water velocity during floods is likely to be greatest. Many cross sections along a stream are transitional between pools and riffles. In general, the scour induced by a bridge will be greater at pools or pool-like cross sections than at riffles or riffle-like cross sections.

6. Shift of the thalweg with increase in stage is a significant factor in bridge design, not only for estimation of the point of maximum bed scour (and bank erosion) but also for alignment of piers with flood flow. Thalweg stability is related to channel stability and to stream type, and can be assessed from aerial photographs.

APPENDIX: CHECKLIST OF GEOMORPHIC FACTORS

Geomorphic factors relevant to site selection and bridge design are listed below in the form of questions. Exact answers to these questions can rarely be obtained, but even probable answers are worth considering.

Selection of Crossing Site

Site on a Nonsinuous Reach

1. Is site at a pool, riffle (crossover), or transition section?
2. Are alternate bars visible at low stream stage?
3. If midchannel bars are present, what would be the effect of their migration through the bridge waterway?
4. Is cutoff imminent at adjacent meanders?

Site at a Meander

1. What has been the rate and mode of migration of the meander?
2. What is its probable future behavior, as based on the past?
3. Is site at pool, riffle (crossover), or transition section?
4. Is cutoff of the meander, or of adjacent meanders, probable during the life span of the bridge?

Design of Bridge

Piers on Flood Plain or Adjacent to Channel

1. Is the channel migration rate sufficient to overtake piers during the life span of the bridge?

Piers in Channel

1. For pier orientation, what is probable position of thalweg at design flood?
2. For scour estimation, what is probable bed form height at design flood?
3. For scour estimation, what is natural mean bed scour at design flood?
4. For scour estimation, what is lowest undisturbed streambed elevation at or near the crossing site?
5. Does the stream have an unstable thalweg that has shifted with time?
6. Is there evidence of recent channel degradation?
7. Are any works of man in prospect that are likely to induce degradation or bank erosion?

ACKNOWLEDGMENT

This paper was prepared under an interagency agreement between the Federal Highway Administration and the U.S. Geological Survey. Much of the information relating to hydraulic problems at specific sites has been obtained through the generous cooperation of engineers in state highway agencies.

REFERENCES

1. F.M. Chang. A Statistical Summary of the Cause and Cost of Bridge Failures. Final Report. FHWA, U.S. Department of Transportation, 1973.
2. J.C. Brice and J.C. Blodgett. Countermeasures for Hydraulic Problems at Bridges. Vol. 1, Analysis and Assessment. Report FHWA-RD-78-162; Vol. 2, Case Histories for Sites 1-283, Report FHWA-RD-78-163. FHWA, U.S. Department of Transportation, 1978.
3. J.C. Brice. Stream Channel Stability Assessment. Report FHWA/RD-82/021. FHWA, U.S. Department of Transportation, 1982.
4. Scour at Bridge Waterways. NCHRP Synthesis of Highway Practice 5, HRB, National Research Council, Washington, D.C., 1970.
5. P.C. Klingeman. Hydrologic Evaluations in Bridge Pier Scour Design. Journal of the Hydraulics Division, Vol. 99, American Society of Civil Engineers, 1973, pp. 2175-2184.
6. G. Parker. Stability of the Channel of the Minnesota River near State Bridge No. 93, Minnesota. Project Report 205, St. Anthony Falls Hydraulic Laboratory, Minneapolis, Minn., 1982.
7. G.C. Nanson and E.J. Hickin. Channel Migration and Incision on the Beatton River. Journal of Hydraulic Engineering, Vol. 109, American Society of Civil Engineers, 1983, pp. 327-337.
8. T.N. Keefer, R.S. McQuivey, and D.B. Simons. Interim Report on Stream Channel Degradation and Aggradation, Causes and Consequences to Highways. Report FHWA/RD-80/038. FHWA, U.S. Department of Transportation, 1980.
9. D.B. Simons and F. Senturk. Sediment Transport Technology. Water Resources Publications, Fort Collins, Colo., 1977, 807 pp.
10. L.W. Yearke. River Erosion due to Channel Relocation. Civil Engineering, Vol. 41, American Society of Civil Engineers, 1971, pp. 39-40.
11. C.H. Robbins and A. Simon. Man-Induced Channel Adjustment in Tennessee Streams. Water Resource Investigation 82-4098. U.S. Geological Survey, 1982, 129 pp.
12. C.R. Neill. River-Bed Scour, A Review for Bridge Engineers. Technical Publication 23, Canadian Good Roads Association, Ottawa, Canada, 1964, 37 pp.
13. E.D. Andrews. Scour and Fill in a Stream Channel, East Fork River, Western Wyoming. Professional Paper 1117. U.S. Geological Survey, 1979, 49 pp.
14. S. Leliavsky. An Introduction to Fluvial Hydraulics. Constable and Company, London, 1955, 257 pp.
15. C.R. Neill. Guide to Bridge Hydraulics. University of Toronto Press, Toronto, Canada, 1973, 191 pp.

Publication of this paper sponsored by Committee on Hydrology, Hydraulics and Water Quality.

Effect of Bridge Piers on Streamflow and Channel Geometry

JAMES C. BLODGETT

ABSTRACT

Piers in the waterway affect the velocity distribution across the channel and may act as barriers to floating debris. In addition, they also affect channel geometry by causing general and local scour in the vicinity of the bridge. The level of hydraulic efficiency of an unobstructed channel may be reduced by several percent if piers are placed in the waterway. Reductions of up to 11 percent were observed at sites used in the study. Field studies of several channels indicate that depths of general scour may be greater than local scour. Maximum depths of general scour usually occur midway between piers. General scour may extend several hundred feet upstream and downstream from the bridge. Large piers in alluvial channels may initiate long-term general scour that may continue for decades. General scour at a bridge has been observed to cause enlargement of the channel by as much as 23 percent to compensate for reduced flow area and flow inefficiency associated with bridge piers. Pier design should consider the probability that the channel alignment and geometry will change with time. To reduce the potential for pier damage by streamflow; pier shape, size, spacing, location in the channel, and footing elevation relative to the lowest point in the channel bed should be considered. Pier size should individually or collectively occupy not more than about 5 percent of the original waterway at bankfull discharge.

Bridges across waterways are usually located in response to alignment and traffic considerations, and the length of the bridge is minimized by extending the approach embankments to reduce costs. The bridge designer needs to be aware that the stream will maintain its capacity for the full range of flows that occur at the site. Site alterations as part of bridge construction can cause stream changes such as channel-bed scour, alignment, bank erosion, backwater, and modified flow distribution. In the process, the stream may damage or destroy the bridge and approach embankment.

The purpose of this paper is to describe the effect of bridge piers on streamflow and channel geometry. Two types of scour occur near a bridge: general scour which is related to the flow constriction caused by the bridge piers, abutments, and approach fill, and local scour which is caused by turbulence around the pier. Most of this paper is concerned with general scour caused by piers and abutments. The analysis is based on a comparison of data for unlined canals; streams with cobble, gravel, or sand beds; and streams with bridges. All the data obtained from streamflow measurements of canals, streams, and bridge sites were assembled as part of the annual data collection program or from site-specific studies done by the U.S. Geological Survey. A discussion of the hydraulic characteristics of bridge piers at 10 sites is presented, followed by suggestions to minimize the impact of bridge abutment and piers on a stream.

VELOCITY DISTRIBUTION ACROSS CHANNELS AND CHANNEL EFFICIENCY

The velocity distribution across an open channel that is unobstructed by piers is related to channel shape, alignment, depth of flow, and boundary roughness. The highest velocities at the cross section normally occur midway between the banks where the influence of the boundaries is minimal. For laminar flow in pipes, it has been determined (1) that the rate of velocity change across one-half of a cross section is nonlinear and is proportional to the inverse of the distance from the boundary (Figure 1). Accordingly, the shape of the (lateral) velocity

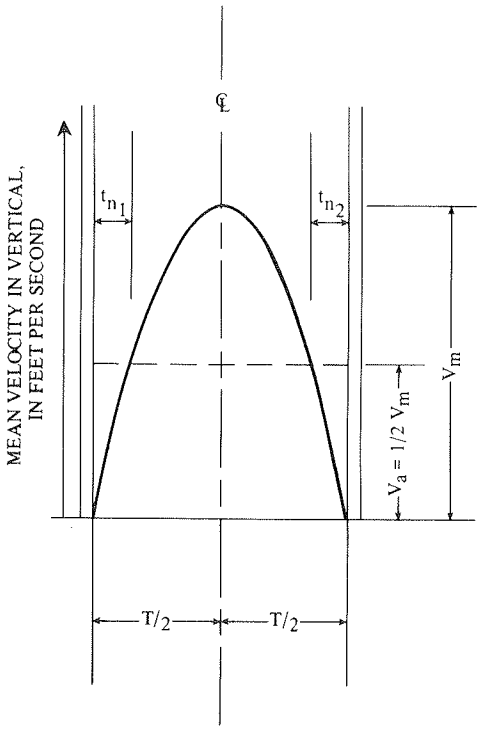

EXPLANATION

t_n = Width of pipe in which the mean velocity is less than mean for cross section

$V_a = \frac{Q}{A}$ = Mean velocity for cross section

V_m = Maximum velocity for cross section

T = Width of pipe

FIGURE 1 Definition sketch of velocity distribution across a pipe.

profile approximates a parabola and the maximum velocity may be estimated as

$$V_m = 2V_a \quad (1)$$

where

V_m = maximum velocity in the cross section, and
V_a = average velocity in the cross section.

The velocity distribution curve in a circular pipe is similar along any diameter, with the maximum velocity (V_m) at the center. In open channels, the velocity distribution is usually considered in the vertical or horizontal direction. The velocity distribution among verticals in the cross section is described in this paper, and point velocities or the distribution within any vertical are not considered.

The velocity distribution on the horizontal is defined by the average velocity in a vertical for several locations in the cross section. The highest average velocity measured in any of the verticals is designated as V_m.

The most efficient velocity pattern in a channel would have a velocity distribution that is uniform throughout the cross section. This implies no boundary friction, and the ratio of the maximum velocity in any given vertical (V_m) to mean velocity in the cross section (V_a) would be 1.0. The velocity distribution does not reach this condition in pipes and open channels because of the effects of boundary roughness. Velocity distributions for canals usually have the highest level of hydraulic efficiency because bank roughness is at a minimum, as shown in Figure 2. The average ratio of V_m/V_a for the canal

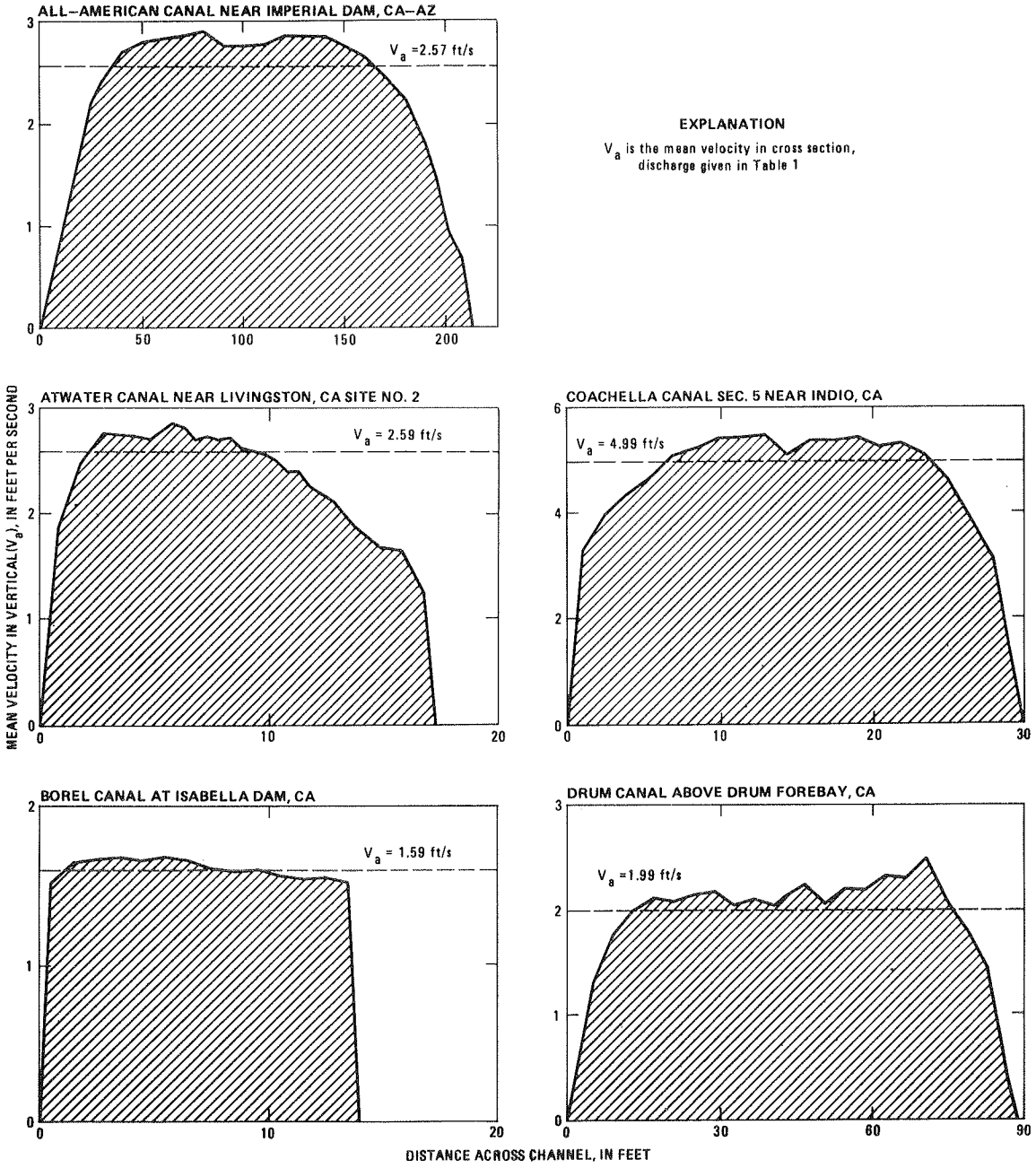

FIGURE 2 Typical velocity distribution across canals.

TABLE 1 Channel and Velocity Properties of Canals

Site	Discharge (ft^3/s)	Mean Depth, d_a (ft)	Mean Velocity, V_a (ft/s)	Ratio of Maximum to Mean: Depth, d_m/d_a	Ratio of Maximum to Mean: Velocity, V_m/V_a	Channel Efficiency, C_e (%)
California						
All-American Canal near Imperial	7,640	13.9	2.57	1.24	1.13	60.5
Arena Canal near Livingston						
Site 1	124	2.7	2.64	1.47	1.08	47.8
Site 2	122	2.6	2.65	1.51	1.15	48.7
Site 3	126	2.7	2.65	1.48	1.12	46.8
Atwater Canal near Atwater						
Site 1	123	2.7	2.66	1.54	1.17	51.4
Site 2	115	2.6	2.61	1.59	1.10	43.1
Site 3	117	2.3	3.12	1.57	1.17	46.8
Site 4	115	2.3	3.11	1.54	1.12	41.4
Borel Canal at Isabella Dam	108	4.9	1.59	1.00	1.05	61.9
Bowman Spaulding Canal at Jordan	292	4.5	4.35	1.25	1.12	47.9
Chicago Park Plume near Dutch Flat	442	4.8	5.10	1.00	1.13	56.9
Coachella Canal near Indio						
Section 1	911	5.2	2.20	1.12	1.13	67.7
Section 2	908	5.3	2.21	1.15	1.10	67.2
Section 3	884	4.7	2.33	1.17	1.20	53.9
Section 4	898	5.1	2.16	1.12	1.12	69.0
Section 5	923	5.2	1.99	1.12	1.25	70.4
Drum Canal at Tunnel Outlet	569	6.5	3.90	1.17	1.07	56.3
Drum Canal above Drum Forebay	669	4.5	4.99	1.14	1.10	58.7
Dutch Flat Flume no. 2	636	6.1	7.45	1.01	1.08	62.9
South San Joaquin Canal	266	3.1	5.87	1.21	1.07	59.2
Indiana						
King Hall Canal near Hagerman	342	4.3	6.42	1.00	1.09	65.2
Salmon River Canal near Rogerson	485	6.1	2.58	1.15	1.29	50.5
Utah						
Westside Canal near Collinston	660	5.9	6.23	1.00	1.09	59.5

sites listed in Table 1 was 1.13. Velocity distributions for selected natural channels, which are usually affected by more bank roughness than canals, are shown in Figure 3. For the natural channels, given in Table 2, the average ratio of V_m/V_a was 1.34. In general, increasing boundary roughness translates to a channel with lesser hydraulic efficiency, and a corresponding increase in the ratio of maximum to mean velocity.

The hydraulic efficiency of a channel can also be measured by the amount of channel width in which the mean velocity in the vertical is less than the mean velocity for the cross section, as illustrated in Figure 1. That part of the channel near the boundary with velocities less than the mean for the cross section is designated t_n. The channel efficiency ratio (C_e), in percent, is computed by the equation

$$C_e = [1 - (\Sigma t_n/T)]\ 100 \quad (2)$$

where

t_n = the width of each flow area (including piers) where the mean velocity in one or more verticals is less than the cross section average, and
T = width of channel.

At bridge sites, the value of T is determined as the gross width between abutments.

The channel efficiency ratio (C_e), which indicates the degree of contraction caused by the bridge, has been developed in preference to the channel contraction ratio (m). The channel contraction ratio (m) as discussed by Matthai (2) is a measure of the proportion of total flow that enters the contraction from upstream of the embankments. The ratio m is based on the geometry of the main channel and flood plain, and may be computed by the equation

$$m \cong [1 - (q/Q_t)] \quad (3)$$

where

q = discharge that could pass through the opening without contraction, and
Q_t = total discharge.

In comparison, the channel efficiency ratio (C_e) is a measure of the impact of the bridge structure on flows by evaluating the reduction in channel efficiency at the bridge opening. Any flow contraction created by the return of overbank flow into the channel at the bridge is incorporated in the estimate of channel efficiency (C_e). Velocity is a measure of the potential for channel scour; therefore, the channel efficiency (C_e) has been selected as an indicator of the impact that a bridge structure has on the channel geometry. At many bridges, problems of scour and bank erosion occur when flows are confined to the main channel and there is no overbank flow.

To develop a comparison of the hydraulic efficiency of various open channels, flow and geometry data were assembled for selected canals (Table 1), natural streams (Table 2), and streams affected by bridge piers and abutments (Table 3). The sites were selected to provide a sample of diverse hydraulic and channel conditions. If the velocity ratio (V_m/V_a) is used as a measure of efficiency, the natural channels that are obstructed by bridge piers or abutments are, on an average, 35 percent less efficient than unobstructed canals (Table 4). For streams with bridges, the mean velocity (V_a) is computed as the mean velocity for the net opening of the bridge. On the other hand, if channel efficiency (C_e) is used, the unobstructed natural channels are 17 percent less efficient than canals (Table 5).

A test of the variation in the means of the two measures (Tables 4 and 5) used to indicate that the hydraulic efficiency of various channels was made by analysis of variance. The test consisted of analyzing for significant differences of the mean velocity ratio (V_m/V_a) and the channel efficiency ratio (C_e).

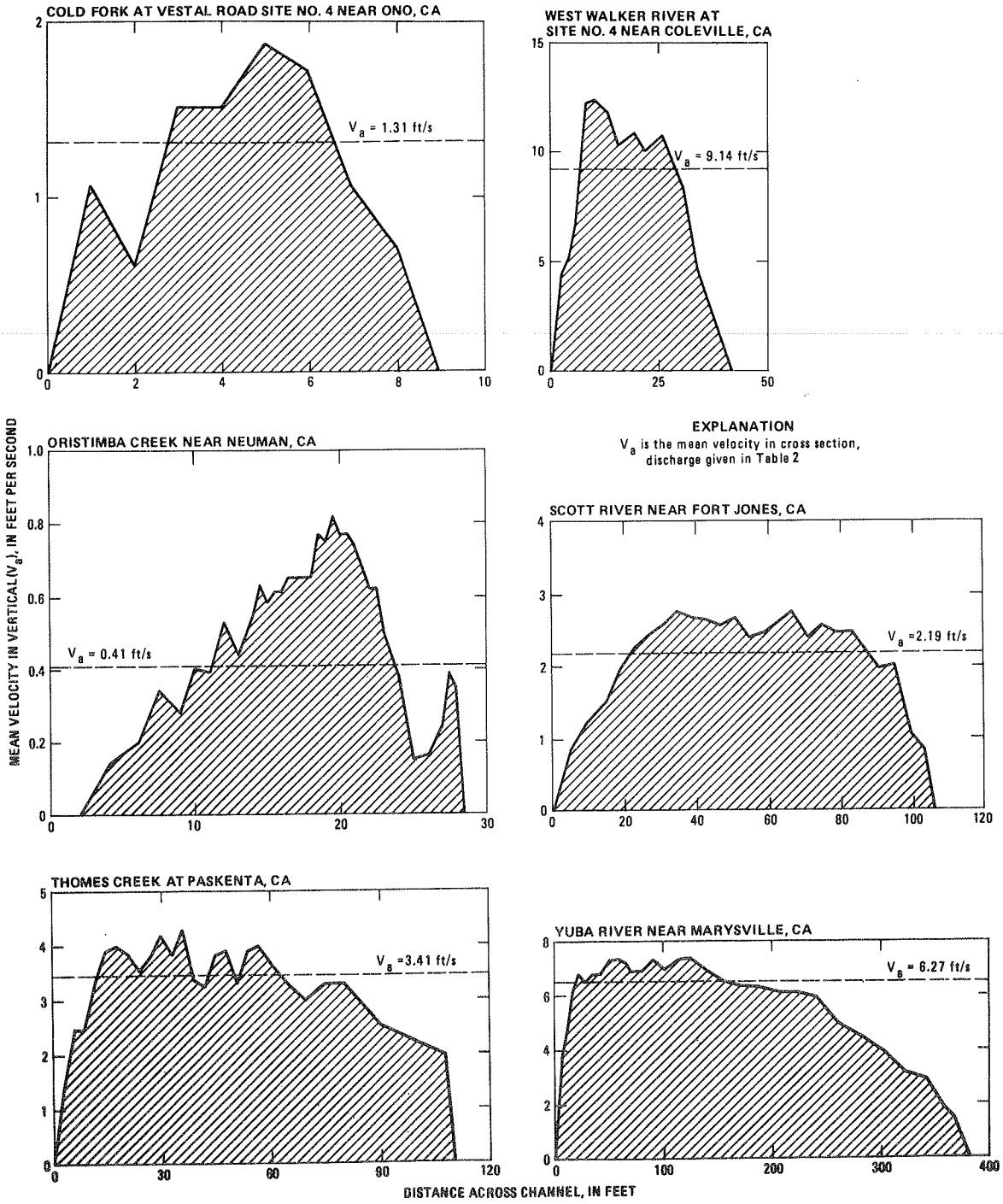

FIGURE 3 Typical velocity distributions across stream channels.

Results of the test indicated that the means of the two measures were significantly different for each of the channel conditions (canals, streams, and streams with bridges). For example, the means 1.13, 1.34, and 1.53 given in Table 4 are statistically different. The probability is less than 1 percent that the observed difference in the means of the velocity ratio or channel efficiency ratio would have occurred by chance.

EFFECT OF PIERS ON STREAMFLOW

Velocity Distribution Across Channels

The placement of piers and abutments in a previously unobstructed channel reduces the flow area in proportion to the size of the piers and footings. The velocity distribution across the channel is now affected by a new set of boundaries imposed by the channel bed, the sides of each pier, and possibly the abutments. Although boundary shear along pier faces may be minimal, piers can cause localized turbulence that may be more significant than the original bank boundary roughness. A definition sketch showing the velocity distribution in a channel with piers is shown in Figure 4.

The effect of piers on streamflow as indicated by the ratio A_p/A_g, where A_p is area of piers and A_g is gross area of cross section, is given in Table 3. For

TABLE 2 Channel and Velocity Properties of Streams

Site	Discharge (ft^3/s)	Mean Depth, d_a (ft)	Mean Velocity, V_a (ft/s)	Ratio of Maximum to Mean: Depth, d_m/d_a	Ratio of Maximum to Mean: Velocity, V_m/V_a	Channel Efficiency, C_e (%)
Arizona						
Hassayampa River at Bos Damsite near Wickenburg	316	0.82	5.02	1.40	1.30	49.8
Santa Cruz River at Nogales	638	0.99	3.69	1.52	1.34	61.0
Santa Maria River near Bagdad	301	0.68	2.26	2.35	1.47	40.7
California						
Cold Fork at Vestal Road near Ono	4.89	0.42	1.31	1.52	1.44	43.7
Klamath River near Seiad Valley	15,100	4.3	7.06	1.29	1.37	47.7
Mokelumne River near Mokelumne Hill	782	3.09	2.53	1.42	1.25	50.0
North Fork Cottonwood Creek near Ono	29.7	0.59	1.21	1.90	1.36	50.0
Oristimba Creek near Newman	12.1	0.99	0.41	1.76	2.00	47.8
Sacramento River above Bend Bridge near Red Bluff	35,200	14.93	5.75	1.15	1.33	54.4
Sacramento River at						
Colusa	45,900	20.54	4.47	1.84	1.30	55.7
Verona	20,800	15.93	2.48	1.31	1.35	62.2
Butte City	12,600	10.61	2.50	1.14	1.22	67.0
Hamilton City	9,680	4.66	3.19	1.18	1.19	55.9
Scott River near Fort Jones	640	2.75	2.19	1.27	1.25	61.6
Thomas Creek at Paskenta	529	1.11	3.41	2.27	1.25	41.2
West Walker River no. 4 near Coleville	1,280	3.33	9.14	1.44	1.37	45.2
Yuba River near Marysville	11,600	4.96	6.27	2.14	1.18	53.3

TABLE 3 Channel and Velocity Properties of Streams with Bridge Piers

Site	Discharge (1000 ft^3/s)	Mean Depth, d_a (ft)	Mean Velocity, V_a (ft/s)	Ratio of Maximum to Mean: Depth, d_m/d_a	Ratio of Maximum to Mean: Velocity, V_m/V_a	Channel Efficiency, C_e (%)	Ratio A_p/A_g (%)
California							
Angel Slough at Ord Ferry Road near Ord Bend	12.4	6.39	5.79	1.49	1.73	41.5	4.6
	3.34	3.77	2.65	1.91	2.00	35.3	4.6
	0.442	3.19	0.92	1.63	2.33	41.0	5.3
Butte Creek at Gridley-Colusa Road near Gridley[a]	3.60	9.41	2.68	2.39	1.39	28.2	1.4
Butte Creek Overflow at SR-162 at Butte City (BR11-26)	1.86	5.00	2.10	1.48	1.36	53.1	5.0
Dry Creek at County Road at Galt	6.11	11.7	3.49	1.50	2.37	43.0	4.1
Honcut Creek at SR-70 near Live Oak							
Bridge 1	0.698	5.18	2.17	1.39	1.43	50.0	3.2
Bridge 2	2.77	5.70	3.24	1.75	1.61	47.1	2.0
Bridge 3	3.85	6.31	2.82	2.57	1.53	54.1	4.5
Sacramento River at							
Delta	12.5	6.60	9.47	1.79	1.34	36.9	7.2
	15.3	7.76	9.62	1.61	1.50	35.9	7.2
SR-32 at Hamilton City	155	27.7	9.74	1.49	1.31	46.6	7.6
	144	24.9	10.02	1.35	1.27	55.2	7.9
	134	25.0	9.35	1.45	1.19	55.1	7.8
	119	24.9	8.32	1.32	1.27	50.9	7.5
	87.7	20.3	7.57	1.29	1.31	52.3	7.5
	78.8	19.1	7.25	1.33	1.17	50.9	7.0
	57.6	16.8	5.91	1.48	1.33	52.9	5.3
	10.1	6.71	2.63	1.82	1.32	50.8	1.1
Ord Ferry Road near Ord Bend	107	22.4	3.79	1.71	2.15	45.2	4.2
SR-162 at Butte City	92.3	30.3	6.18	1.52	1.57	40.2	15.0
County Road at Colusa (Old Br.)	40.2	25.2	4.38	1.67	1.36	40.0	10.5
County Road at Colusa (New Br.)	33.4	24.1	3.83	1.49	1.28	65.1	2.0

[a]Wall-type piers subject to 19 degree angle of flow.

most bridges, the proportion of the waterway occupied by piers is less than 5 percent. Extra bridge maintenance problems associated with general scour and lateral erosion have been observed at sites where bridge piers occupy more than 5 percent of the waterway. In general, the following flow and channel changes will occur after bridge construction:

1. Local increase in flow velocity,
2. General scour in vicinity of bridge,
3. Local scour around piers and abutments,
4. Backwater from flow constriction or debris lodged against the piers, and
5. Increased flow turbulence near boundaries.

The magnitude of these changes is dependent on the occurrence of floods and amount of flow constriction imposed by the bridge.

Measurements of the reduction in channel size and scour caused by the construction of a bridge are

TABLE 4 Comparison of Channel Hydraulics for Different Stream Types on the Basis of Maximum and Mean Velocity

Type of Stream	Sample Size	Ratio of Maximum to Mean Velocity at a Cross Section			Average Increase in Velocity Ratio in Relation to Canals (%)
		Minimum	Maximum	Mean	
Canal	26	1.05	1.29	1.13	0
Stream channels	18	1.17	2.00	1.34	18.6
Channels with bridge piers	23	1.19	2.37	1.53	35.4

TABLE 5 Comparison of Channel Hydraulics for Different Stream Types on the Basis of Channel Efficiency Ratio

Type of Stream	Sample Size	Channel Efficiency Ratio at a Cross Section (%)			Average Decrease in Channel Efficiency in Relation to Canals (%)
		Minimum	Maximum	Mean	
Canals	26	41.4	70.4	55.9	0
Stream channels	18	40.7	67.0	52.8	5.5
Channels with bridge piers	23	28.2	65.1	46.6	16.6

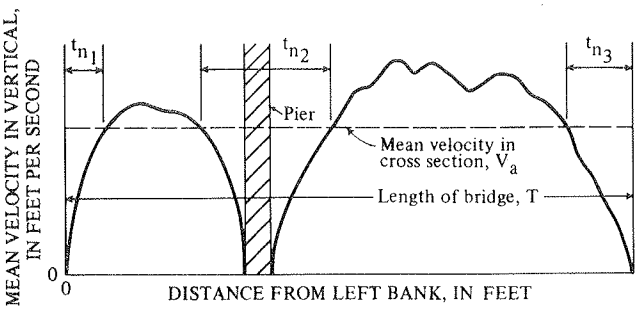

FIGURE 4 Definition sketch of velocity distribution across a channel with bridge piers.

difficult to obtain. Immediately during and after a bridge is constructed, the channel geometry changes in the vicinity of the bridge site. Moreover, most hydraulic data collected at the bridge correspond to postbridge construction conditions.

Assuming no general scour or lateral erosion at the bridge site, the effective flow area is reduced by the flow constriction (vena contracta) between piers and the turbulence associated with overbank flow returning to the opening. The amount of constriction caused by the bridge at the crossing is a function of the pier size, pier shape, number of piers or bents in the waterway, and amount of debris lodged against the pier. If the bridge superstructure is inundated, the wetted perimeter and amount of flow constriction is increased further. The influence of piers on the magnitude and velocity distribution in the bridge opening is shown in Figure 5 for 10 sites. Below each velocity distribution plot, a plan of the bridge showing the location, relative size, and the shape of the piers or bents is shown. In general, bridges with large piers (sites 7a, 7b, 9, and 10a in Figure 5) affect the velocity distribution across the channel much more than bridges with narrow piers (sites 1, 3, and 10b in Figure 5). The size, shape, and placement of the bridge piers also affect the velocity distribution (sites 2, 4, and 5 in Figure 5).

The shape and size of a wall-type pier, described by Brice and Blodgett (3), influences the amount of flow disturbance near a pier, especially at skewed crossings. If the pier is not aligned with the flow, the wall of the pier acts as a barrier and reduces the effective channel flow area. The effect of a wall-type pier on Butte Creek at Gridley-Colusa road near Gridley, California (site 2), is shown in Figure 5. At this site, flow velocities for about 25 ft of the channel width were reduced to zero or negative values, giving a channel efficiency ratio of 28.2 percent (Table 3). This site illustrates the adverse effect of wall-type piers that may occur if they are not situated parallel to the flow.

The variation in velocity distribution is related to the magnitude of velocity at a site. For example, the pile location, size, and spacing for Butte Creek overflow (site 1, Figure 5) and Angel Slough (site 4, Figure 5) are similar, but the amount of velocity distribution disturbance at these sites is very different. Flows are confined for both channels and the effect of vegetation is minimal. The variation in velocity profiles between bents for these bridges is attributed to the low mean velocity (2.1 ft/s) on Butte Creek overflow and the high velocity (5.8 ft/s) on Angel Slough.

The pattern of velocity distribution across an opening is generally the same for different flows, provided no changes in the channel alignment occur. The stability of velocity patterns in a bridge opening is shown for the Sacramento River at Hamilton City (site 7a and 7b, Figure 5). In this case, the shape of the velocity profile for discharges of 10,100 and 155,000 ft^3/s are similar in each opening; only the magnitude of velocity is different for the two measurements.

The change in channel hydraulics that occurs when a new bridge with small streamlined piers is built is indicated by the different velocity distributions for the Sacramento River at Colusa (site 10a and 10b, Figure 5). For the old bridge, the ratio of pier area to gross area (A_p/A_g) was 10.5 (Table 3); the velocity ratio (V_m/V_a) was 1.36; and the channel efficiency (C_e) was 40 percent. The corresponding values for the new, more efficient bridge were 2.0, 1.28, and 65.1 percent.

A review of the data in table 3 and the plots in Figure 5 indicate that some characteristics of flow velocity in relation to bridge piers for the 10 sites may be summarized as follows:

1. The pattern of flow velocity across the opening is consistent, regardless of the discharge, provided the channel alignment is stable (sites 7a and 7b).
2. Differences in mean velocities of over 12 ft/s in the vertical between the middle of the span and pier face (site 7b) have been observed.
3. The alignment or geometry of a channel in the vicinity of the bridge significantly affects the velocity pattern if wall-type piers are not placed parallel to the flow (site 2).
4. The amount of velocity profile disturbance in a cross section is related to the number, width, and shape of the piers (sites 4, 10a, and 10b).
5. The amount of velocity distribution disturbance is apparently related to the mean velocity at the cross section (sites 1 and 4).

Maximum Velocity

The mean ratio of maximum velocity (V_m) to mean velocity (V_a) for natural channels that are unaffected by piers (Table 2) averages about 1.3 and is

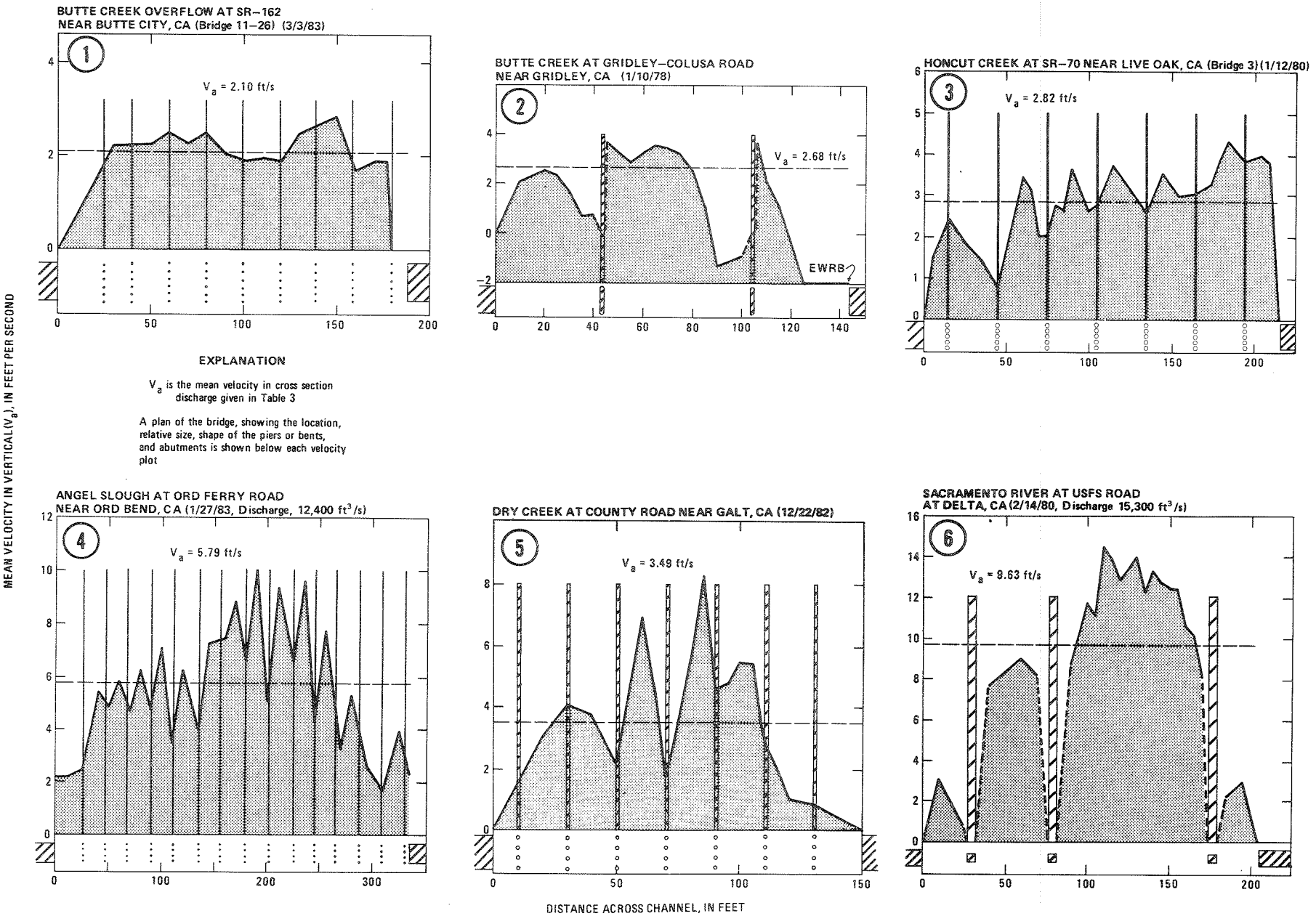

FIGURE 5 Typical velocity distribution across stream channels with bridge piers.

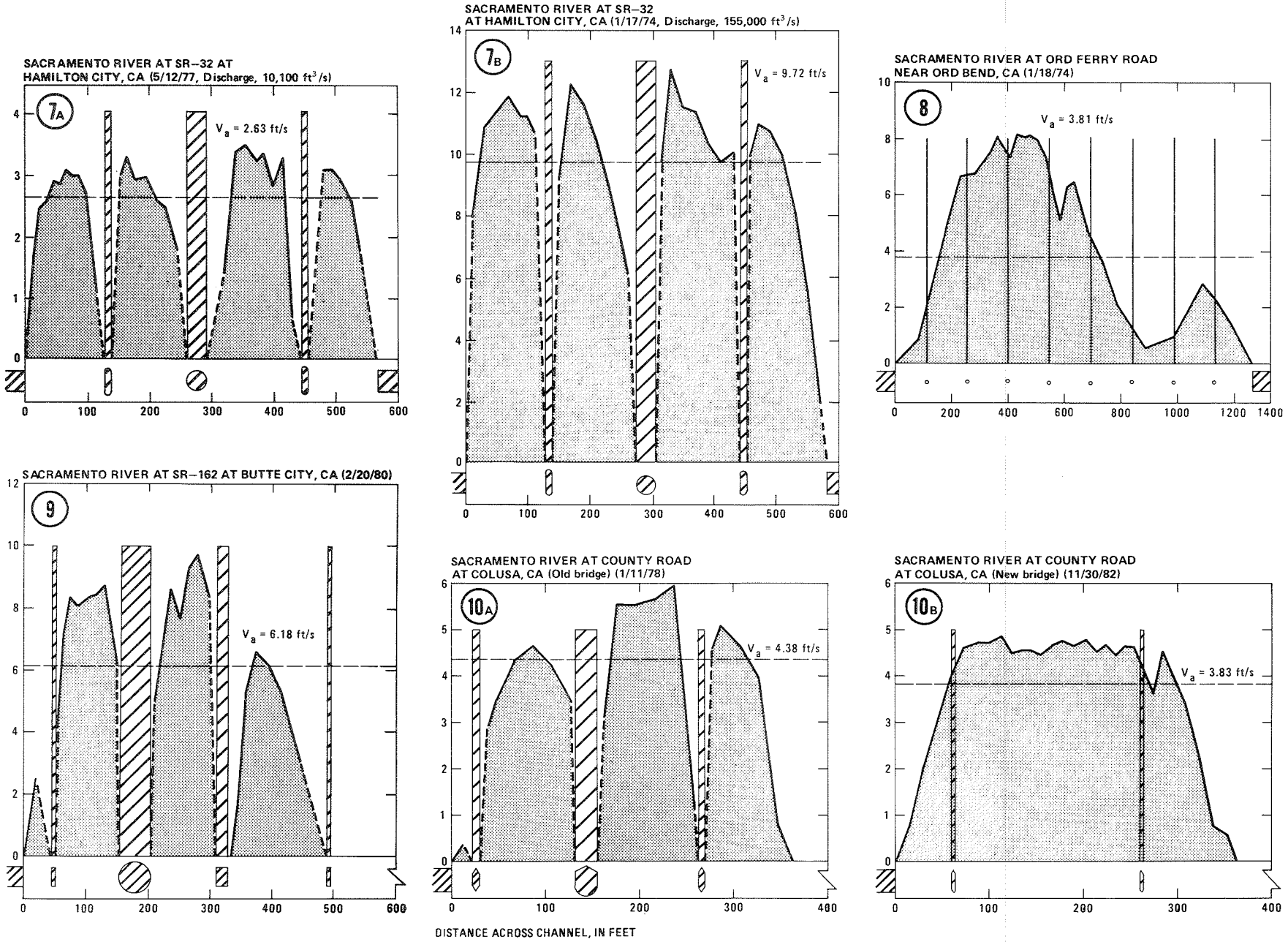

FIGURE 5 (continued)

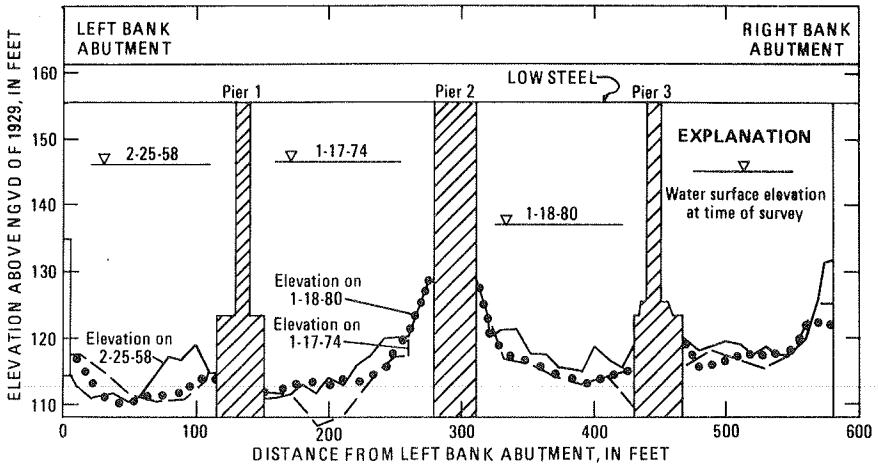

FIGURE 6 Changes in scour between 1958 and 1980 at downstream side of SR-32 bridge, Sacramento River at Hamilton City, California, adapted from Blodgett (4).

nearly constant regardless of discharge or channel size. For channels with piers (Table 3), the mean ratio of V_m/V_a increases to 1.5. The ratio of maximum to mean velocities (V_m/V_a) for the channels with piers is about 14 percent greater than channels without piers. The ratio is affected at low flow by local effects such as piers, boundary roughness, grass, and brush. This is indicated by the increase in the ratio V_m/V_a for decreasing discharges of Angel Slough at Ord Ferry Road near Ord Bend, California (Table 3). These estimates of the relation between maximum and mean velocities are limited to flows in the main channel (less than bankfull).

EFFECT OF PIERS ON CHANNEL GEOMETRY

Depth of Scour

The lateral constriction of flow caused by a bridge usually results in a general lowering of the streambed. This lowering of the streambed is defined as general scour. The depth of general scour is related to the amount of lateral constriction of flow caused by the piers and abutment. Scour is computed as the difference in elevation between the normal and present channel bed at the bridge. In most cases, it was necessary to estimate the normal bed elevation on the basis of the overall channel-bed profile that may extend several hundred feet upstream and downstream from the constriction.

Following bridge construction, the depth and lateral extent of general scour in channels that have sand-and-gravel beds and stable alignment do not change greatly once a state of channel equilibrium is obtained, as illustrated in Figure 6.

Turbulence around piers and abutments causes additional scour defined as local scour (3). The depths and extent of local scour are difficult to measure because soundings near a pier are difficult to obtain.

Both general and local scour may occur at a site. The combined effect of these types of scour may produce unequal depths of scour across the channel. The effects of the piers on depths of scour indicated by the mean ratio d_m/d_a for bridge sites is 1.63 (Table 3). In comparison, the corresponding ratio is 1.57 for natural (unobstructed) streams (Table 2) and 1.23 for canals (Table 1).

The location of maximum scour depths at a bridge site is difficult to determine. In some instances, scour associated with turbulence of flow at the pier may cause depths of local scour greater than general scour. However, the channel-bed profiles in Figure 6 suggest that the location of greatest scour may be midchannel between piers. This observation also is supported by field surveys at other bridge sites. The condition of greater scour depths at midchannel is attributed to higher flow velocities in midchannel, away from the piers (Figure 5). A summary of maximum observed scour depths below the unobstructed channel bed is given in Table 6. The amount of scour may vary during the period of flooding, independent of discharge. Therefore, discharges given in the table may not be related to the depth of scour observed.

Longitudinal Extent of General Scour

The effect of piers on the channel bed may extend several hundred feet upstream and downstream from the bridge. The extent of general scour is related to the magnitude of channel constriction by the bridge, bed-material, size, discharge, and size and shape of the piers. Surveys of channel-bed profiles for the Sacramento River at SR-32 near Hamilton City, California (Figure 7), show that the influence of the piers and the draw rest extends more than 400 ft upstream and downstream from the bridge. The

TABLE 6 Depth of Scour Below Normal Channel-Bed Elevation at Selected Bridge Sites

Location	Date of Survey	Discharge (ft^3/s)	Mean Depth of Flow (ft)	Scour (ft)
California				
Sacramento River at SR-32 at Hamilton City[a]	1-17-74	154,800	27.7	10.7
Sacramento River at SR-162 at Butte City	1-17-70	79,100	26.5	12.1[b]
Sacramento River at County Road at Colusa	1-11-78	40,200	28.2	4.6[b]
Eel River at US-101 near Ferndale[a]	2-?-63[c]	275,000	—	21[c]
Oklahoma				
Canadian River at US-75 near Calvin[a]	10-?-70	94,100	—	13[c]
Canadian River at US-270 near Calvin[a]	10-?-70	130,000	—	20[c]
Mean				13.6

[a] Data adapted from Brice, Blodgett, et al (3).
[b] Unpublished data.
[c] Depths of scour estimated from divers' reports and observation of pier footings at the time of excavation for repair work.

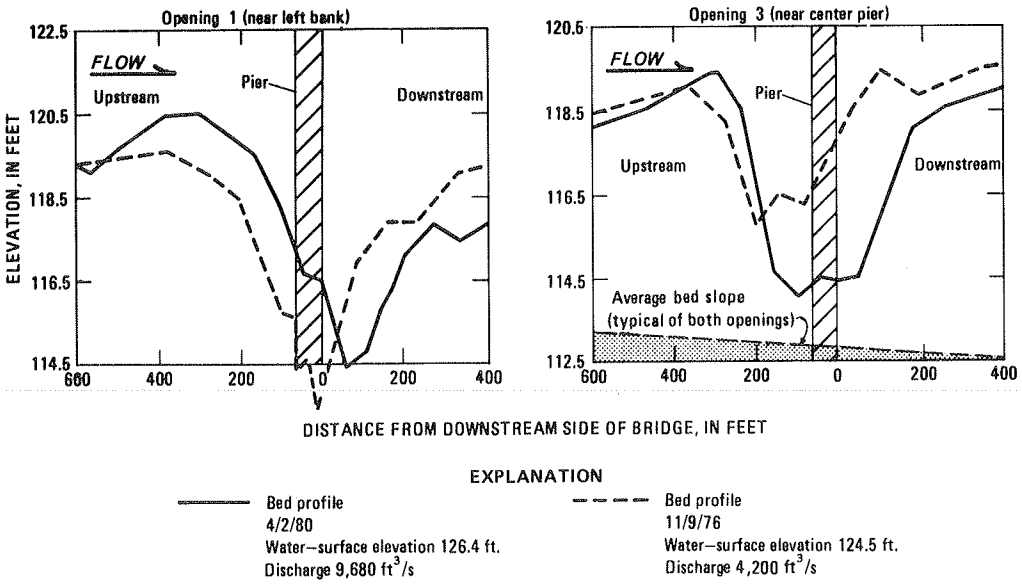

FIGURE 7 Channel-bed profiles through two openings of SR-32 bridge, Sacramento River at Hamilton City, California. (A draw rest at the center pier extends upstream 200 ft.)

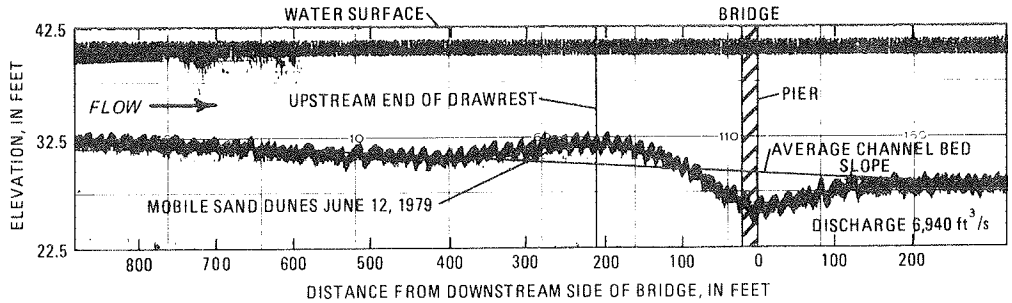

FIGURE 8 Channel-bed profile through right opening of old county bridge showing mobile sand dunes, Sacramento River at Colusa, California.

amount of channel constriction associated with the channel-bed scour, expressed as the ratio of pier area to gross area (A_p/A_g) of the unobstructed channel, is about 8 percent (Table 3). The deepest point of scour may be near either the upstream or downstream side of the pier. The apparent negative slope in the channel-bed profile is caused by levees on both banks upstream from the bridge preventing deposition of material and overbank flow downstream that allows deposition.

The upstream-downstream extent of bed scour in a sand-bed channel is indicated in Figure 8 for a county bridge across the Sacramento River at Colusa, California. Scour extends about 400 ft upstream and 200 ft downstream from the bridge. Maximum scour depths occurred at the downstream side. The amount of flow constriction caused by the piers for the original bridge, expressed as a ratio of pier area to gross area (A_p/A_g) associated with the depth of scour, is about 8 percent (Table 3). Depending on flow conditions, mobile sand dunes cause ripples on the channel bed (Figure 8) that fluctuate in height. The presence of sand dunes on a channel bed tends to increase the boundary roughness. If no dunes are present, which means the channel bed is smooth, the roughness (Manning's coefficient n) would be about 0.015 to 0.020. If dunes are present, and depending on the depth of flow, the roughness coefficient may increase to 0.040 or higher. Estimates of the channel capacity at a bridge site should assume a rough, less efficient channel boundary if changes in the bed form are anticipated. A bridge designed with an inadequate capacity for handling discharge will increase the potential for scour and lateral erosion, in addition to backwater.

Long-Term Trends to Equilibrium Channel Size

Construction of piers in the waterway may cause scour, lateral erosion, and changes in the channel geometry that occur for many years after the bridge is built (3). The following site history for the Sacramento River at SR-160 at Butte City, California, illustrates the effect of large piers on the channel geometry. A swing-span bridge with four large piers (4, 45, 4, and 4 ft wide) was constructed in 1946. The piers required to support the swing span and adjacent approach spans in the main channel occupied about 9 percent of the original channel (measured in 1946) at a bankfull discharge. The channel bed was composed of gravel and cobbles. The primary factor causing scour and lateral erosion at the site was the presence of the large piers, timber draw rest, and pier fenders that cause a lateral constriction of the waterway and induce turbulence of flow.

Beginning in 1943, streamflow data collected at the site were used to determine channel conditions before construction of the bridge. Following bridge construction, the lowest point in the channel bed

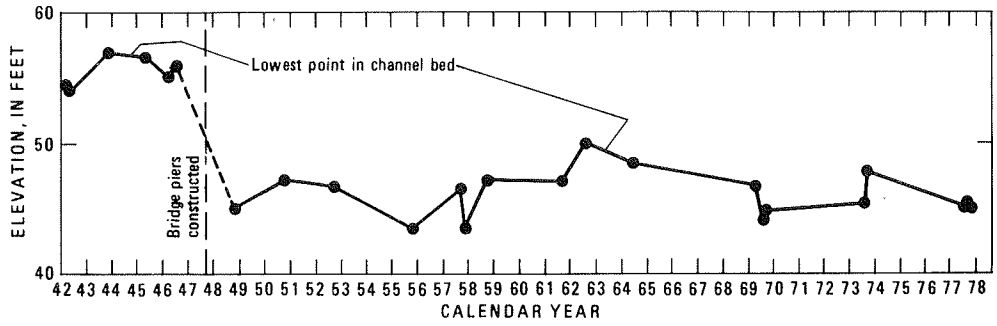

FIGURE 9 Variation in elevation of lowest point in channel bed between 1943 and 1978, Sacramento River at SR-162, Butte City, California.

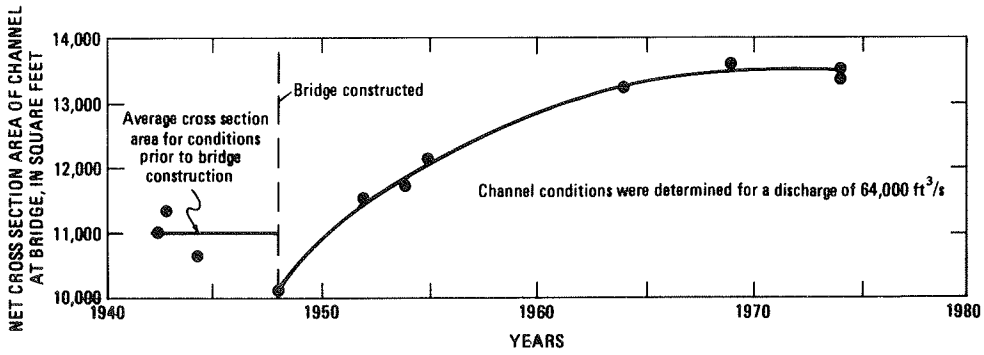

FIGURE 10 Variation in net channel area before and after bridge construction for period 1943 to 1974, Sacramento River at SR-162, Butte City, California, adapted from Brice, Blodgett, et al. (3).

scoured about 10 ft as shown in Figure 9. Floodflows in 1947 and 1948 were smaller than the mean annual flood, so scour at the site was probably continuous between 1946 and 1949. The variation in elevation of the lowest point in the channel bed between 1949 and 1978 indicated no overall trend of increasing scour, but the annual changes in scour and fill are probably dependent on floodflow conditions. For example, the 2 ft of scour observed between 1969 and 1970 is attributed to large floods in January 1969 and January 1970.

Although the low point in the channel bed remained at a relatively stable elevation between 1949 and 1978 and did not show progressive scour, the channel geometry was undergoing a significant long-term change. As shown in Figure 10, the net cross-sectional area at the bridge began to increase shortly after the bridge was built. The channel ultimately enlarged 23 percent to compensate for the flow inefficiency and reduction in area caused by the piers. This increase in flow area apparently reached an equilibrium about 1974, or 28 years after bridge construction.

LATERAL MIGRATION OF LOWEST POINT IN CHANNEL BED

Lateral migration of the lowest point in the channel bed may result in undermining pier footings that were originally placed in shallow water near the margins of the channel. The rate and magnitude of bed shift are substantial for some streams (Table 7).

In the design of foundations and placement of piers, it should be assumed that the lowest point in the channel bed may move laterally to any location within the active channel banks. The potential of lateral migration of the stream is greatest for gravel and sand-bed channels or channels with banks of small-grained material such as sand or silt-loam material.

TABLE 7 Lateral Movement of Lowest Point in Channel Bed Between Bridge Abutments

Location	Year	Distance to Lowest Point in Channel Bed from Left Abutment (ft)	Net Change in Distance Since Initial Date (ft)
Deer Creek near Vina, California	1951	84	0
	1962	127	+43
	1974	297	+213
	1976	308	+224
Snake River near Heise, Indiana	1971	123	0
	1977	247	+124
Canadian River near Sanchez, New Mexico	1928	186	0
	1943	255	+69
	1965	196	+10
	1976	73	-113

Note: Data adapted from Brice, Blodgett, et al. (3).

HYDRAULIC CONSIDERATIONS IN PIER DESIGN

In designing bridges across waterways of the type discussed in this report, several hydraulic factors need to be considered to minimize the impact of the structure on the stream. The effect of bridge piers on streamflow increases if the bridge is constructed so that the abutments constrict the main channel or approach embankments force overbank flow into the opening at the bridge, causing cross-channel flow.

To improve the hydraulic efficiency of bridge piers and reduce the potential for scour, lateral erosion, and bridge damage at a site, the following

hydraulic factors, which are based on data for 10 bridge sites, should be considered in bridge design:

1. As a general guideline, bridge maintenance problems associated with general scour and lateral erosion have been observed at sites where bridge piers occupy more than about 5 percent of the original waterway.
2. Using canals as the most efficient open channel, typical streams are 5 percent less efficient, and streams with bridge piers are 17 percent less efficient. To minimize future bridge maintenance related to scour and lateral erosion, an effort should be made to prevent encroachment by the abutments, minimize the number and size of piers or pile bents in the waterway, and select pier shapes that will provide minimal obstruction to the stream.
3. The effect of piers or pile bents on the velocity distribution across a stream is apparently related to the mean velocity. For a low velocity stream (2 ft/s or less), the effect of piers is very low; at high velocities (6 ft/s or more), the effect of piers on the velocity profile is more pronounced.
4. At sites where flows are not normal to the opening, such as at bends or where the channel alignment is unstable, rounded or cylindrical piers have a lessor effect on the pattern of velocity distribution than wall-type piers. At these sites, the use of wall-type piers or multiple-pile bents (which act as wall-type piers) should be discouraged.
5. The average ratio of the maximum velocity to mean for the cross section, for channels unaffected by piers, is 1.3. For channels with piers, the ratio increases to 1.5.
6. For natural streams the average maximum depth to mean depth ratio (d_m/d_a) is 1.57; for streams with bridge piers the ratio is 1.63.
7. The lowest point in the channel bed attributed to scour may occur in midchannel between the piers, where the velocity of flow is the highest, rather than adjacent to a pier.
8. Near bridge piers, scour depths have been documented that are up to 20 ft below the normal lowest point in the channel bed.
9. General scour of the channel bed has been observed for distances more than 400 ft upstream and downstream from a bridge.
10. During the first 2 or 3 years after construction of a bridge that constricts a channel, scour may lower the channel bed several feet.
11. Scour resulting from flow being constricted by bridge piers may increase the channel area to compensate for the decreased flow efficiency.
12. Abutments and piers that create large amounts of constriction may induce changes that require maintenance to prevent lateral erosion and undermining of piers. The period of instability may continue for decades.
13. When selecting a pier footing elevation, the designer should assume that the location of the stream and the lowest point in the channel bed may move laterally to any location within the active channel banks.

REFERENCES

1. Rouse, Hunter, and J.W. Howe. Basic Mechanics of Fluids. Wiley, New York, 1953, 245 pp.
2. H.F. Matthai. Measurements of Peak Discharge at Width Contractions by Indirect Methods. In Techniques of Water-Resources Investigations, Book 3, Chapter A4, U.S. Geological Survey, 1967, 44 pp.
3. J.C. Brice and J.C. Blodgett. Countermeasures for Hydraulic Problems at Bridges, Vol. 1: Analysis and Assessment. Report FHWA-RD-78-162. FHWA, U.S. Department of Transportation, 1978.
4. J.C. Blodgett. Floodflow Characteristics of the Sacramento River in the Vicinity of Gianella Bridge, Hamilton City, California. Open-File Report 81-328. U.S. Geological Survey, 1981, 33 pp.

Publication of this paper sponsored by Committee on Hydrology, Hydraulics and Water Quality.

Use of Spurs and Guidebanks for Highway Crossings

E.V. RICHARDSON and DARYL B. SIMONS

ABSTRACT

Bridge engineers often need to protect bridge abutments from scour; maintain, stabilize, and improve the alignment of a stream approaching a bridge crossing; protect the bank of a stream along a highway; maintain a stream in a given location; maintain or decrease the width of a stream; protect highway approaches to a bridge crossing across flood plains; and improve the hydraulic characteristics of the bridge opening. Spurs and guidebanks are structures river engineers use to fill this need. Other names for spurs are dikes, jetties, spur dikes, retards, and dyke fields. Spurs and guidebanks are described and design recommendations based on a literature review are given.

A spur is a structure or embankment projected into a stream from the bank at some angle and for a short distance to deflect flowing water away from critical zones, to prevent erosion of the bank, and to establish a more desirable channel alignment or width. By deflecting the current from the bank and causing sediment deposits behind them, a spur or a series of spurs may protect the stream bank more effectively and at less cost than riprapping the bank. Also, by moving the location of any scour away from the bank, failure of the riprap on the spur can often be repaired before damage is done to structures along and across the rivers. Conversely, failure of riprap on the bank may immediately endanger structures.

Spurs are used to protect highway embankments that form the approaches to a bridge crossing. Often these highway embankments cut off the overbank flood flows causing these flows to run parallel to the embankment enroute to the bridge opening. Spurs constructed perpendicular to the highway embankment keep the potentially erosive current away from the embankment thus protecting it. Spurs as used in this report encompass the terms dikes, jetties, groins, and spur dikes that are also used to describe these structures.

Spurs are also used to channelize a wide, poorly defined stream into a well-defined channel that neither aggrades nor degrades, thus maintaining its location from year to year. Spurs on streams with suspended sediment discharge can cause deposition to establish and maintain the new alignment. The use of spurs in this instance may decrease the length necessary for the bridge opening and may make a more suitable, stable channel approach to the bridge. This decreases the cost of the bridge structure.

Guidebanks are a type of spur used at waterway crossings to straighten the flow, increase the discharge through the bridge opening, and to move the location of deep scour away from the abutments of the crossing.

When using spurs and guidebanks, the bridge engineer must understand the characteristics of the river. Some of these river characteristics are river form (e.g., meander or braided); sediment discharge (e.g., quantity, size distribution, and mode of movement--suspended or contact); magnitude and time distribution of floods; size of the bed and bank material; and geometry of the river cross sections. Except for a short description of river form, river characteristics are beyond the scope of this paper. The reader is referred to the literature review for further information (1-12).

STREAM FORM

For spurs used to protect embankments, improve river alignment, and so forth, or for a highway crossing or encroachment, knowledge of the plan and profile of a stream is useful in understanding stream morphology. River forms (i.e., plan view appearance of streams) are many and varied (2,3) and are the result of many interacting variables. Small changes in a variable can change the form and profile of a river, adversely affecting a highway crossing or encroachment. Conversely the highway crossing or encroachment can inadvertently change river form or profile and affect adversely the river environment.

All classifications of river form are subdivisions of two major river forms--braided and meandering. A braided stream consists of multiple and interlacing channels [see Figure 1 (9)]. In general, a braided channel has a steeper slope, a large bed-material load in comparison with its suspended load, and relatively small amounts of silts and clay in the bed and banks. Also a braided stream is difficult to work with because it is unstable, changes the alignment of its channels rapidly, carries large quantities of sediment, is wide and shallow even at flood flow, and is unpredictable. The potential width of a braided river may be much greater than casual observation indicates. Under certain geologic conditions, however, some braided streams may be stable enough for stable islands to form and for the channels that form the braids to shift relatively slowly or only when large floods occur. The shifting of the channels that form the braids of a braided river can change the angle of attack of the flow on bridge piers, abutments, and the stream banks. At high flow the flow often will have zero angle of attack but at low flow, because of channel shifts, have large angles of attack. If river spurs and guidebanks are carefully used, they can improve flow condition at a crossing or encroachment.

A meandering channel consists of alternating S-shaped bends. This is a static definition; in reality the meandering river is subjected to both lateral and longitudinal movement caused by the formation and destruction of bends. Even straight channels have a meandering current (Figure 1) that tends to develop alternate bars that may ultimately lead to the development of a meandering channel. The meandering channel is defined by E.W. Lane (4) as one in which channel alignment consists principally of pronounced bends that have not been shaped predominantly by the varying nature of the terrain through which the channel passes. Mathes (8) stated, "meander is here applied to any letter-S channel pattern, fashioned in alluvial materials, which is free to shift its location and adjust its shape as part of a migratory movement of the channel as a whole down the valley."

A meandering river consists of pools and crossings. The thalweg, or main current of the channel, flows from the pool through the crossing to the next pool forming the typical S-curve. In the pools, the

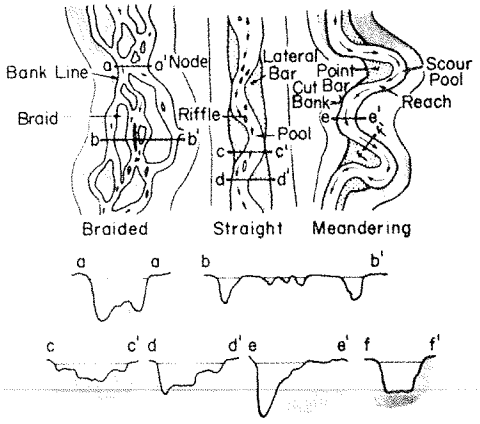

FIGURE 1 River channel patterns (9).

channel cross section is somewhat triangular, and point bars form on the inside of the bends (Figure 1). In the crossings, the channel cross section is more rectangular and depths are shallower. At low flows the local slope is steeper and velocities are higher in the crossing than in the pool. At low stages the thalweg is located close to the outside of the bed. At higher stages the thalweg tends to straighten. More specifically the thalweg to some degree moves away from the outside of the bend encroaching on the point bar. In the extreme case, chute channels develop across the point bar during large flood flows.

Bridges stabilize or fix the river cross section at a given time and place, but the nature of a meandering or braided river is to shift its channel. Bends of a meandering stream move downstream. In some rivers, this movement is slow; in others it is relatively rapid, depending on the magnitude of flow and the nature of the bed and bank material. This movement changes the angle of attack of the flow on the piers and abutments, and can bring the flow against the approach embankment (if one exists) and cut behind the abutments.

SPUR DESIGN CONSIDERATIONS

The physical quantities to consider in designing spurs are form, angle (θ) to the bank, length (L) of spurs, spacing (S) between spurs, materials, spur crest elevation, cross section, and scour. Figure 2 shows a definition sketch for spurs and guidebanks. These design considerations will be described in the following sections.

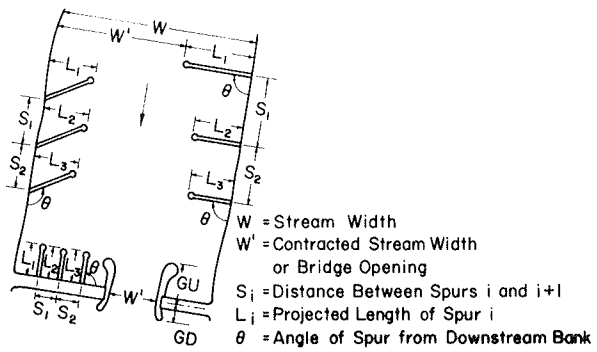

FIGURE 2 Definition sketch for spurs and guidebanks.

Types of Spurs

Types of spurs are shown in Figure 3. The straight spur (13-16) is set at some angle (θ) to the bank and normally has a round nose to provide more volume and area for scour protection at the outer end. The T-head spur (13,14,16-18) is a straight spur with a rectangular guide vane set at the outer ends. The angle (θ) to the bank is normally 90 degrees. The angle (α) varies and is set by the degree of deflection of the current that is desired. However, α that would set the T-head at angles to the flow larger than 10 degrees are not recommended. The length (a) varies, and no particular length was recommended in the literature reviewed.

L-head and wing or trails spurs (14,16,18-21) provide more protection to the bank. The length (a)

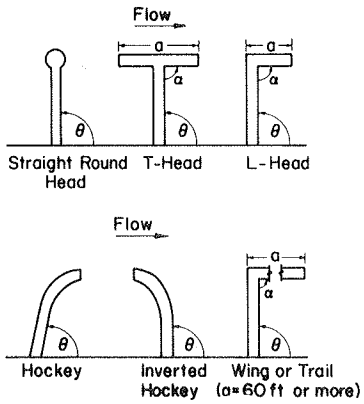

FIGURE 3 Forms of spurs.

should close 45 to 65 percent of the gap between spurs (19,21). As with T-heads the angle α should be set so that the L-head has an angle 10 degrees or less to the stream lines of the flow. L-heads are designed to provide more deposition between spurs and decrease scour around their ends and provide greater protection to the banks. This is rather obvious when their recommended length closes 45 to 65 percent of the opening between spurs. This small opening increases their costs but also makes them more effective in channelization. The straight spur is more cost-effective. Hockey shape and inverted hockey shape (14,19) (also called J-shape and inverted L) do not appear to have any advantage over straight or T-shape, as their scour holes are more extensive in area than the T-shape (19).

The straight spur with a round nose should be used for most bank protection. To protect concave banks at bends, short (30 to 50 ft) straight spurs are effective if the bank between is armored or naturally resists erosion. To channelize and guide the flow, T-head spurs with the head set at a small α to the flow are recommended. They should be less expensive if the head of the T is made relatively long as the spacing can be increased, decreasing the number of shanks. L-head spurs may also be used.

Angle of Spur to the Bank

The angle (θ) of the spur to the bank (internal angle from downstream bank to spur, Figure 2) given

in the literature ranges from 30 to 120 degrees (15-17, 22-24). Spurs with angles larger than 90 degrees are termed repelling spurs and those with angles less than 90 degrees are termed attracting spurs (14,17). There is also an example of a downstream pointing spur that caused bank failure (17). Mamak (23) and Neill (15) state that the best results (deflecting flow and trapping load) are obtained with spurs inclined upstream (θ from 100 to 110 degrees). The angle for T-head spurs is normally 90 degrees and deflection of the current is provided by the angle (α) of the head to the shank. The study by Franco (20) where angles of 60, 90, and 120 degrees were studied showed that for channelization to improve navigation, the normal or downstream angled spurs performed best. But the downstream angled spurs "produced a greater tendency for scouring at their bank end than dikes (spurs) angled upstream."

In general a spur at 90 degrees to the bank is the most economical for bank protection. For channeling or directing, flow angles of 100 to 110 degrees may be more effective. There does not appear to be a significant advantage to streamlining angling a spur downstream. However, the upstream spur in a series might be angled downstream to decrease the scour depth and move the scour hole to a preferred location.

Length of Spur

The length of a spur depends on its location (e.g., straight reach, concave bank of bend, along embankments), amount of contraction of stream width, economics, and purpose of the spur. The length is also closely related to the spacing because spacing is expressed as some multiplier of the projected length. If spurs are too short, the spacing is close and construction is expensive. If they are too long they may contract the flow too much, or the spacing may be so large that a meander loop may form between two spurs. The spurs in the literature reviewed ranged from 60 ft to hundreds of feet long (8,22,24, 25) and no rules were given.

On the Missouri River spurs were used to change a braided shallow stream to a single channel consisting of gentle curves. A fixed width and depth of channel was desired and spurs long enough to establish this width and depth were built. In some cases, spurs 1,000 ft long or more were built. For other streams where only a small shift in channel is required or a bank is to be protected, short spurs (50 ft or less) are built Neill (15) states

> [T]he length of bank protected by each spur appears to be at least twice its projected length perpendicular to the current...whether to choose fewer long spurs or a greater number of short ones depends upon their disturbing effects on the opposite bank and the channel upstream and downstream. For earthwork the longest spur that will not produce excessive erosion and disturbance should be used, since the major cost of this type is in the slope revetment.... In lieu of a series of short spurs, consideration should be given to...riprapping the bank.

For channel control, the length depends on the desired flow and channel considerations. The maximum permissible length can be established by determining the optimum channel width for the bankfull discharge. Optimum channel width is determined by scour, sediment transport, minimum flow disturbance, and maximum allowable velocity.

For protecting banks of straight reaches, long radius bends, and braided channels, the minimum length is 50 ft and the maximum length should be less than 10 to 15 percent of bankfull channel width (W). Maximum length can be greater than 15 percent of W but only after analyzing the effect of this more severe constriction on the flow and the channel. The 50 ft length appears to be the most economical minimum length. With spurs shorter than 50 ft, it is probably cheaper to riprap the bank. With more information, such as costs of spurs versus cost of riprapping the bank, a more realistic length can be determined.

The maximum length is not only limited by stream contraction and economics, but also by spacing. If spur spacing (S) is limited by the meander wave length, it is not economical to establish spur lengths longer than 1/6 to 1/2 S to protect banks.

Number of Spurs

The number of spurs to protect stream banks or to contract the stream should not be less than three. For protection of embankments across the stream one or two spurs may be sufficient.

Spacing Between Spurs

Spacing (S) between spurs is primarily related to the length of the spur, although the velocity of flow, angle of flow streamlines with the spurs, curvature of the bank, and purpose of the spur also affect spur spacing. The literature provides considerable information on spacing distance between spurs in feet or as a function of spur length (9,14, 15-17,19,20,21,23,24,26-29). Actual distances range from 200 to 4,000 ft. The recommended spacing (S) is from 1.5 to 6 L_i where L_i is the upstream projected spur length into the flow, Figure 2. The spacing is, in general, a function of the length of the next upstream spur. Spacing distance (S_i) equal to 1.5 to 2 L is recommended to obtain a well-defined deeper channel for navigation and flood control. If these spacings are used, dredging to keep a deep channel is decreased or eliminated. For protecting banks longer spacings are used (S_i = 2 to 6 L_i). With T-head spurs, the recommended S_i is from 3 to 4 L_i for navigation channels. A 1918 report on practice (24) gives S as a function of channel width. In this case S ranges from 0.75 to 1 W.

To base spacing on length of spur is logical because flume and wind tunnel studies have shown that the separation zone downstream of a vertical barrier in the flow ranges from 7 to 11 times the barrier height. The distance between spurs (S) to protect the banks of straight reaches, long radius bends, or braided channels from erosion may be 3 to 4 times the upstream spur length. To obtain a well-defined channel the spacings should be 1.5 to 2 times the upstream spur length. However, the spacing should not be longer than 0.5 times the meander wave length of the stream.

If spurs are placed on the concave side of bends, spacing may be 4 to 6 spur lengths. Their use here is to move the high velocity flow away from the bank. The spurs must be short (20 to 30 ft) to be effective and not disrupt the flow around the bend. In addition the bank may need riprap, but the spur, by decreasing the velocity, will decrease the size of riprap needed. Spurs placed on embankments across streams may be 6 to 10 times spur length or greater if the velocity along the embankments is low. If the velocity is high the spacing should be from 4 to 6 L.

Elevation of Spur

Height recommendations depend on the purpose of the spur, the amount of contraction of the flow, the magnitude and importance of the overbank flow, and possible ice problems (21,24,27-29). Related to the elevation of the spur is whether it is level, slopes up from a low point on the streamward end to the bank, or is set at the same elevation or stepped up or stepped down in elevation going from the upsteam spur to the downstream spur. In stepped down fields the spurs decrease in elevation in the downstream direction. The sloping crest spur gives a gradually increasing flow area as stage increases. This type of crest reduces high velocities for the higher stages, helps force the flow into its low water alignment more effectively, and does not hold the flow concentrated at one location over a large change in stage. For these reasons, a sloping crest is often preferred (19).

Laboratory studies by the U.S. Army Corps of Engineers (20) indicated that for navigation purposes the best spur system has level individual crests but each downstream spur is at a lower elevation. However, sloping-crest spurs can be designed to be as effective as level-crest spurs. To control the navigation channel, level-crest spurs should be placed normal to the flow or angled downstream, whereas, sloping-crest spurs should be normal or angled upstream.

The elevation of the crests on the lower Mississippi is from 4 to 15 ft above low water elevation (21,24,29). On the Columbia River elevations are from 1 ft below bank level to one-half flood stage elevation (28). These elevations appear adequate to maintain a navigable channel in a meandering river system. When spurs are set at elevations where they are overtopped frequently, the top and downstream slope of the shank have to be riprapped, which increases their cost.

The L-headed spur may be constructed with the head at a lower elevation than the stem. Fenwick (19) states that "it was found...that little benefit was derived from building the L-head above the water surface." This makes them a little less expensive. He also states "L-heads are expensive so that additional testing and experience are needed to show whether their merits are sufficient to recommend their general use in connection with channel contraction."

On braided channels or where side channels are cut off by using spurs, their elevations are set at bankfull stage. Also, when spurs are used for protecting banks their elevation is bankfull stage or slightly higher to prevent the flow from scouring the bank. In these cases the crest may be sloping to increase flow area, particularly at the large discharges.

With aufeis the elevation of the spurs should be higher than the expected elevation of the ice. Otherwise the ice can build up and cause the stream to flow over the top of the spur. The spurs would no longer confine the flow to the channel, and during the spring breakup the water could cut a new channel through the ice. If the spurs were lower than the aufeis elevation, the new channel could be on the flood plain behind the spurs or on top of them. In the first instance the spurs would no longer be effective in maintaining a channel, and in the second the spurs would need riprap on the crown and on both upstream and downstream sides. With aufeis the spur crest could be level or sloping depending on aufeis elevation and bank height. If the outer or streamward end were above the aufeis, the crest could be level or sloping to the bank.

Construction Materials

Materials used to construct spurs may be rock or earth banks covered with rock (9,21,23,29,30,32); timber, steel, or concrete piles (9,18,20-22,24,29-31); trees (30); sand bags (30); automobile bodies (30); brownlow weeds (18); brush (15,23,32); Kelner steel jacks; and so forth. They may be pervious or impervious (18,20,21,25,29,30,31,33). Permeability of spurs is a relative term in that impervious spurs, because of cost, are not made watertight. A study on the Apalachicola River (34) indicated that stone spurs were more effective than pile spurs in river control for navigation. Typical details of the spurs are shown in Figures 4-7.

The size of riprap for spurs of rock can be determined by estimating the velocity of flow along, across, and around the end of the spur. Several methods may be used to determine the appropriate size of stone to resist this velocity (9,28,33,34-42).

Cross Section (Crest Width and Slope)

Typical cross sections of pile and stone spurs are given in Figures 4 and 5. Data on cross sections may be found in numerous publications (17,18,20,21,23,24,28-32,34). Crest widths range from 3 to 20 ft and side slopes from 1:1.15 to 1:5. The top width of rock or rock-covered earth spurs is often controlled by the equipment placing them. A 3-ft width is a minimum and larger widths are used to facilitate hauling and placing. Winkley (21) states that on the lower Mississippi River crown width for stone placed by trucks is from 14 to 20 ft and a minimum 5-ft crown is used for stone placed by barges. Side slopes are slightly less than the angle of repose of the material but can be determined by the method described by Stevens and Simons (39).

Scour

Scour may be the result of constricted flow caused by a bridge or spurs used to channelize the flow or by local acceleration of the flow going around the spur or abutment. The former is called general scour and the latter local scour. Also, a river reach may be subjected to a long-term degradation or aggradation of the bed elevation. This long-term degradation or aggradation at a bridge crossing or

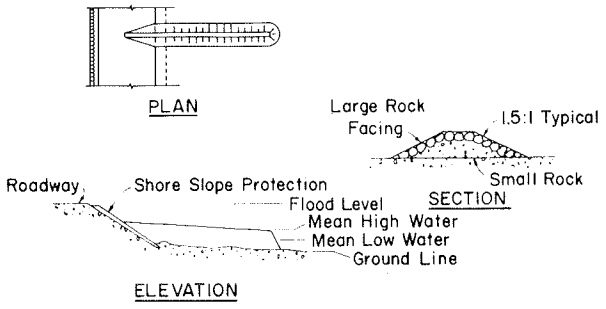

FIGURE 4 Typical stone or earth spur.

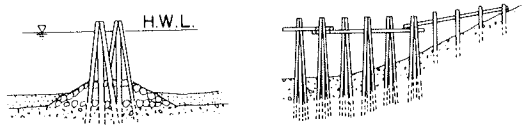

FIGURE 5 Timber pile spur.

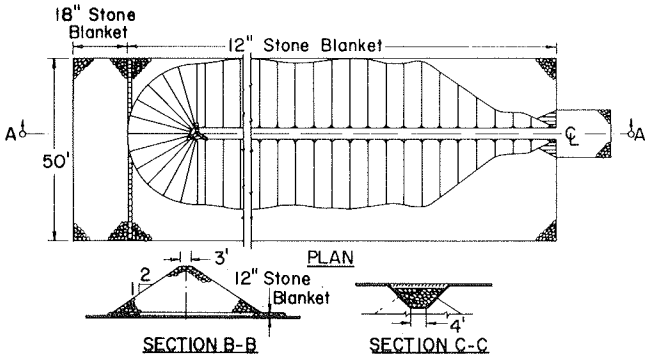

FIGURE 6 Typical stone spur (34).

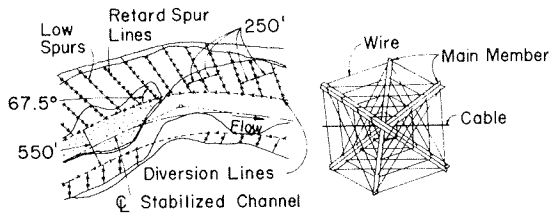

FIGURE 7 Typical spur field layout using Kelner jacks.

highway encroachment must be anticipated by studying the morphology of the river and its morphological changes over time. Otherwise foundation depths of piers, abutments, and spurs may be inadequate if degradation occurs.

General scour at contractions occurs because as the flow area becomes smaller than the normal stream, the average velocity and bed shear stress increase; hence stream power increases locally at the contraction and more bed material is transported through the contracted section than is transported into the section. As the bed level is lowered, the velocity decreases, shear stress decreases, and equilibrium is restored when the transport rate of sediment through the contracted section is equal to the incoming rate.

Laursen (5) developed Equation 1 for general scour at a contraction, where, in addition to channel flow, there is overbank flow into the contracted channel

$$y_2/y_1 = (Q_t^{6/7}/Q_c)[(W_1/W_2)^{6(2+f)/7(3+f)}][(n_2/n_1)^{6f/7(3+f)}] \quad (1)$$

where y_2 is the depth of the constriction and y_1 is the normal upstream (uncontracted) depth, Q_c is the approach channel flow rate and Q_t is the contracted channel flow rate, which is greater than the approach channel flow by the amount of flow on the floodplain. The variable n is the Manning roughness coefficient, W is the channel width, and the exponent f is given below.

V_{*c}/ω	f
<0.5	0.25
1	1
>2	2.25

Here V_{*c} is the shear velocity, $\sqrt{\tau_o/\rho}$, in the approach channel where τ_o is the shear on the bed, ρ is the water density, and ω is the fall velocity of the bed material. When there is no overbank flow $Q_t = Q_c$. There are other equations for general scour at constructions such as Straub's (43).

Local scour occurs in the bed of the channel around embankments because of the actions of the accelerated flows and vortex systems induced by the obstructions to the flow. Local scour occurs in conjunction with or in the absence of general degradation, aggradation, and scour due to contractions.

The basic mechanism causing local scour is the vortex of fluid resulting from the pileup of water on the upstream edge and subsequent acceleration of flow around the nose of the spur. The action of the vortex is to erode bed materials away from the base region. If the transport rate of sediment away from the local region is greater than the transport rate into the region, a scour hole develops. As depth increases, the strength of the vortex decreases, the transport rate decreases, and equilibrium is reestablished and scouring ceases.

The depth of local scour varies with time because the sediment transported into the scour hole from upstream varies, depending upon the presence or absence of dunes. The time required for dune motion is much longer than the time for local scouring action. Thus, even with steady state conditions the depth of scour is likely to fluctuate with time when there are dunes traveling on the channel bed: the larger the dunes, the more variable the depth of the scour hole. When the crest of a dune reaches the local scour area, the scour hole will fill and the scour depth will be decreased temporarily. When a dune trough approaches, there will be less sediment supply and the scour depth will increase. A mean scour depth between these oscillations is referred to as equilibrium scour depth. It is not uncommon (as determined in laboratory tests) to find maximum depths to be 30 percent greater than equilibrium scour depth. The depth that would be reached if no sediment was transported into the scour hole is the "clear water" scour.

Most of the detailed studies of scour around embankments have been made in laboratories. There are few case studies for scour at field installations. According to the studies of Liu et al. (44), the equilibrium scour depth for local scour is determined by

$$d_s/d_1 = 1.1(L/(d)_1)^{0.4}(F_1)^{0.33} \quad (2)$$

where L is the spur length (measured normal to the wall of a flume), d_1 is upstream depth, d_s is depth of scour measured from mean streambed elevation, and F_1 is the upstream Froude number determined as

$$F_1 = V_1/\sqrt{gd_1} \quad (3)$$

The lateral extent of the scour hole can almost always be determined from the depth of scour and the natural angle of repose of the bed material.

Field data for scour at embankments for various size rivers are scarce, but data collected at rock spurs on the Mississippi indicate that

$$d_s/d_1 = (4F_1)^{0.33} \quad (4)$$

determines the equilibrium scour depth. The data are scarce primarily because equilibrium depths were not measured. Dunes as high as 20 to 30 ft move down the Mississippi and their movement is slow compared with the time required to form local scour holes. Nevertheless, it is believed that these data represent the limit in scale for scour depths compared with laboratory data and provide a basis for credible extrapolation of laboratory studies to field installations.

If $L/d_1 > 25$, then scour depth is independent of L/d_1 and depends only on the Froude number and depth of flow. Accordingly, it is recommended that Equation 2 be applied for spurs with $0 < L/d_1 < 25$ and Equation 4 be used for $L/D_1 > 25$. In applying Equation 2 the spur length L is measured from the high water line at the valley bank perpendicular to the end of the spur.

It should be recalled that maximum depth of scour is about 30 percent greater than equilibrium scour depth. The lateral extent of scour can be determined from the angle of repose of the material and scour depth. If the spur is angled downstream, the depth of scour will be reduced because of the streamlining effect. Spurs that are angled upstream will have deeper scour holes. The calculated scour depth should be adjusted in accordance with the curve of Figure 8, which is patterned after Ahmad (9,13).

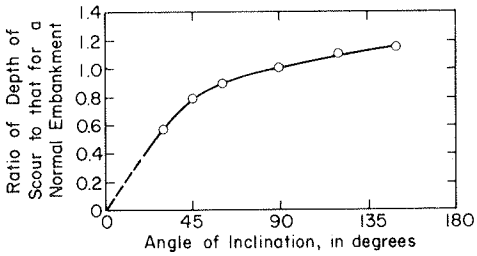

FIGURE 8 Scour reduction due to embankment inclination (9).

Winkley (21) states, "Attempts have been made to predict by analytical means the extent and depth of the scour hole caused by a dike (spur), but there have not yet been a sufficient number of correlations to enable design to be based on such forecasts with confidence. This hole seems to scour to the optimum depth of the river."

The scour depth calculated from the above equations for wide braided rivers with many channels may not be the maximum. The maximum depth of scour at a spur may occur at flows much less than bankfull. For this case, depth of scour should be calculated by determining the depth of flow for the largest expected channel in the braided river. This depth is transposed to the tip of the spur. This depth of scour should be compared with the scour depth calculated from the previous equations and the largest scour depth used.

Scour is controlled by placing a stone blanket around the toe at the outer edge. This blanket must have sufficient rock to armor plate the scour hole after it forms. For scour that occurs when the shank is overtopped, excess stone is put at the downstream toe of the shank to armor plate any scour hole that forms.

It should be noted that most scour prediction equations are for sand bed streams. In gravel bed streams the scour hole will be armored by selective transport of the material forming the bed. Thus, the blanket to control scour on spurs in gravel bed streams need not be as thick or as large as for sand bed streams.

Riprap

The nose of the spur must be riprapped. Also if the shank is set lower than bankfull level, so that overtopping will be frequent, its crest and downstream toe must be riprapped. If the shank is constructed of gravel and cobbles, it may not need to be riprapped to protect it from overtopping by the design flood.

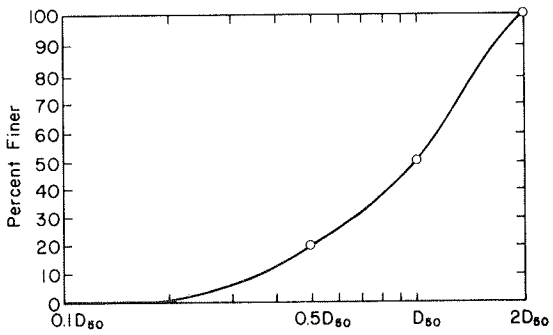

FIGURE 9 Suggested gradation for riprap (5).

Riprap should be placed on the upstream side of the shank if it is made of erodible soil and it is anticipated that flow will occur along it.

Riprap can be designed by using the Bureau of Public Roads (37), U.S. Army Corps of Engineers (36), or Stevens and Simons (9,41) methods. Quantities of riprap should be sufficient to allow for some removal of material. If large-size material is not available, gabions (wire baskets) are used to protect against scour.

Riprap gradation should follow a smooth, size-distribution curve such as that shown in Figure 9. Riprap must be placed on the spur at its outer end to protect it from the high velocity flow around it. This riprap must be carried around the spur nose in both the upstream and downstream direction until the predicted velocities on these side slopes are less than critical for the base material forming the spur. If it is probable that the spur will be overtopped frequently, the top and downstream slope of the spur shank must be riprapped.

The thickness of riprap should be sufficient to accommodate the largest stones in the riprap, and in a well-graded riprap with no voids, that thickness should be adequate. If strong wave action is of concern, however, the thickness should be increased by 50 percent. Filters should be placed under the stone unless the material forming the core of the structure is coarse gravel or of such a mixture that it forms a natural filter. Two types of filters are commonly used: gravel filters and plastic filter cloths.

When gravel filters are used, a layer or blanket of well-graded gravel should be placed over the embankment before placing the riprap. Sizes of gravel in the filter blanket should be from 3/16 in. to an upper limit depending on the gradation of the riprap; maximum sizes would be about 3 to 3.5 in. Thickness of the filter may vary depending on the riprap thickness but should not be less than 6 to 9 in. Filters that are one-half the thickness of the riprap are quite satisfactory. Suggested specifications for gradation are as follows:

$$D_{50}(\text{Filter})/D_{50}(\text{Base}) < 40,$$

$$5 < D_{50}(\text{Filter})/D_{50}(\text{Base}) < 40, \text{ and}$$

$$D_{15}(\text{Filter})/D_{85}(\text{Base}) < 5.$$

Plastic filter cloths are being used with considerable success beneath riprap and other revetment materials such as articulated concrete blocks. The cloths are generally in 100-ft long rolls, 12 to 18 ft wide. The plastic is overlapped 8 to 12 in. with pins at 2 to 3 ft intervals along the seam to pre-

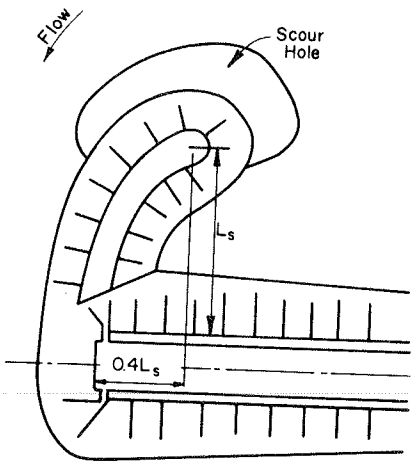

FIGURE 10 Typical guidebank (48).

vent separation. Care must be exercised to prevent damage when placing riprap over the plastic cloth filters. Experiments and results with various cloth filters were reported by Calhoun, Compton, and Strohm (45) in which specific manufacturers and brand names are listed. Stones weighing as much as 3,000 lb have been placed on plastic filter cloths with no apparent damage.

Filters can be placed under water by using steel rods as weights fastened along the edges. Additional intermediate weights assist in sinking the cloth in place. The durability of filter cloths has not yet been established because they have been used only since about 1967. However, inspections of test installations indicate little or no deterioration in the few years that have elapsed.

DESIGN CONSIDERATIONS FOR GUIDEBANKS

Guidebanks have been used in many parts of the world on both sand bed and gravel streams to guide the flow of water through a bridge opening and to move the scour away from the abutments (1,9,15,17,46-48). Guidebanks are placed at the upstream ends of the bridge abutments to guide the stream through the bridge opening. In some situations they are also placed on the downstream side (see Figure 1). Flow disturbances, such as eddies and cross flow, will be eliminated by properly constructed guidebanks and the waterway under the bridge will be more efficient. They are also used to protect highway approach embankments and to reduce or eliminate local scour at abutments and adjacent piers. The effectiveness of spur dikes is a function of river geometry, quantity of flow on the floodplain, and size of bridge opening. A typical guidebank is shown in Figure 10.

The recommended shape of a spur dike is a quarter ellipse with a major to minor axis ratio of 2.5. The major axis should be approximately parallel to the main flow direction. For bridge crossings normal to the river, the major axis would be normal to the highway embankment. However, for skewed crossings, the spur dike should be at an angle to the embankment for the purpose of streamlining the flow through the bridge opening. An illustration of spur dikes for a skewed crossing is shown in Figure 11.

The length of a spur dike, L_s, required depends on quantity of flow on the floodplain, width of bridge opening, and skewness of the highway crossing. Shorter spur dikes may be used where floodplain flow is small or scour potential is minor at piers and embankment ends.

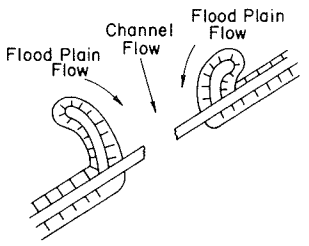

FIGURE 11 Spur dikes at skewed highway crossing.

The principal factors to consider in designing guidebanks are whether they will be convergent or parallel to the opening, plan shape, upstream and downstream length, cross section, crest elevation, scour, and riprap.

Convergent or Parallel

American practice is to give guidebanks an elliptical form convergent to the opening, whereas in Pakistan and India guidebanks are straight and parallel to the opening with a curved section at the upstream and downstream ends. The form of the elliptical guidebank is given in Figure 10, and the design dimensions as determined by Karaki (48) are given in Figure 12. Mahmood (personal communication) stated that parallel guidebanks straighten the flow more effectively than convergent ones. Straight guidebanks probably do a better job of straightening the flow, which could be important if piers are placed in the opening, and of reducing the attack on the abutments. Elliptical guidebanks move the scour hole further upstream and downstream of the bridge opening.

Plan Shape

The plan shape of the guidebanks depends on the type of channel (meander or braided), direction of the streamlines of the flow approaching the opening, and location of the crossing. Neill (15) summarizes the plan shape for guidebanks for bridge openings, Figure 13. In general, the designer should pick the shape that best fits the streamlines of the flow in the channel. If the streamlines are curving, a straight guidebank on the concave side and a curved guidebank on the convex side may be best. For short

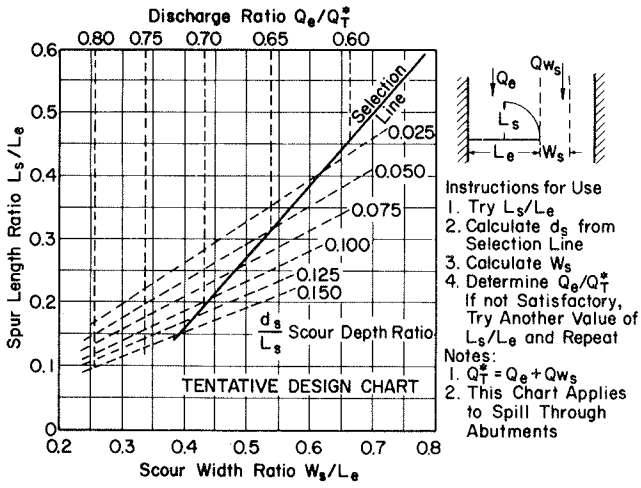

FIGURE 12 Guidebank design procedure (48).

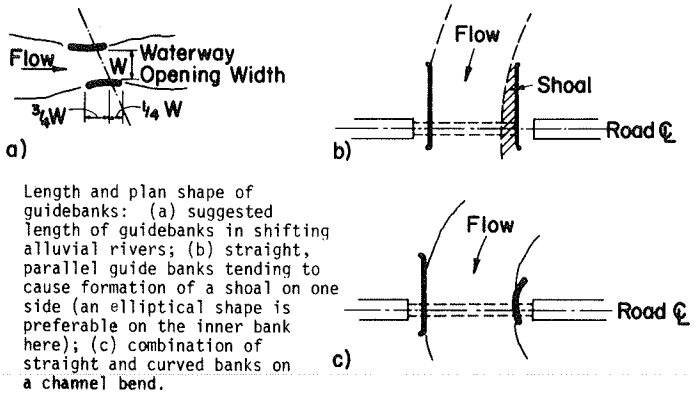

Length and plan shape of guidebanks: (a) suggested length of guidebanks in shifting alluvial rivers; (b) straight, parallel guide banks tending to cause formation of a shoal on one side (an elliptical shape is preferable on the inner bank here); (c) combination of straight and curved banks on a channel bend.

FIGURE 13 Guidebank plan (15).

TABLE 1 Radius of Curvature for the Curved Portion at the Upstream End of Straight Guidebanks

Sand Classification	Probable Maximum Abnormal Scour Below Bed Level (ft)	Radius of Curvature (ft) Fall per Mile of River (in.)[a] 3	6	9	12	18
Very coarse	Under 20	200	250	300	350	400
	Over 20	250	310	375	440	500
Coarse	Under 30	300	360	425	490	550
	Over 30	350	430	510	590	670
Medium	Under 40	400	425	550	625	700
	Over 40	450	550	650	750	850
Fine	Under 50	500	590	675	760	850
	Over 50	600	725	825	925	1,020
Very fine	Under 60	600	700	800	900	1,000
	Over 60	800	900	1,000	1,100	1,200

[a]These are average values; slopes may be much steeper locally.

guidebanks the ellipse of Karaki (48) can be used. The radius of curvature for the curved portion at the upstream end of straight guidebanks is given in Table 1 (17).

Upstream and Downstream Length

The upstream and downstream lengths for straight guidebanks are as follows:

	Reference
GU = 0.75 to 1 W'	2
GD = 0.25 W'	6, 29
GU + GD $\leq$ 150'	32
GU + GD = W'	24
GU = 1 to 1.1 W'	6
GD = 0.1 to 0.2 W'	6
GU = 1.25 to 1.5 W'	6
GU = 0.75 W'	29

In general, the lengths are given as a function of W', the width of the opening. This width is established by determining the desired opening for the design flow taking into account scour. In determining the opening width, local scour caused by a low flow meandering in too large an opening must be considered.

The diagram in Figure 11 can be used to design and select the length for an elliptical guidebank. It is not necessary that both guidebanks on the upstream side be the same length. For some flow conditions a short curved guidebank on one side and a long straight bank on the other may be the best solution.

Other Factors

The remaining factors to consider in designing guidebanks (cross section, crest elevation, scour, and riprap) are similar to those for spurs with two exceptions.

1. The crest elevation should be 1 ft higher than the elevation of the design flood taking into consideration the effect of the contraction of the flow; this is because the design flow should not overtop the guidebank.
2. For elliptical guidebanks, the depth of scour is given in the design procedure shown in Figure 12. For straight guidebanks the design considerations are the same as for spurs.

CONCLUSIONS

1. Spurs and guidebanks are effective methods of protecting bridge abutments from scour, maintaining and improving the alignment of a stream, stabilizing and maintaining a stream in a given location, and improving the hydraulic characteristics of a bridge opening to increase its flow-passing ability and to decrease scour.
2. Spurs can provide a narrow, more consistent channel for braided channels with zero or small angle of attack of the flow on the pier and abutments; this decreases cost. For a meandering channel, spurs can stabilize a longer reach of river and prevent meander loops from moving down and eroding the abutments or approach embankments.
3. Spurs may decrease the cost of protecting banks by eliminating or decreasing the amount of

riprap needed to protect banks on river crossings or encroachments.

4. Guidebanks provide a more efficent (less headloss) flow of water through a bridge opening. They also decrease scour depth and move the scour energy away from the abutments.

5. In the design of spurs and guidebanks, the following must be considered: stream form, angle of the structure to the bank, shape and form, length, spacing between spurs, construction materials, riprap design, crest elevation, top width and cross section, and scour.

REFERENCES

1. T. Blench. Mobile-Bed Fluviology. The University of Alberta Press, Edmonton, Alberta, Canada, 1969.
2. J.S. Price. Stream Channel Stability Assessment. Report FHWA/RD-82/021. FHWA, U.S. Department of Transportation, 1982.
3. D.M. Dulbertson, L.E. Young, and J.C. Brice. Scour and Fill in Alluvial Channels. Open File Report, U.S. Geological Survey, 1967.
4. E.W. Lane. A Study of the Shape of Channels Formed by Natural Streams Flowing in Erodible Material. Sediment Series 9. Missouri River Division, U.S. Army Corps of Engineers, Omaha, Neb., 1957.
5. E.M. Laursen. Scour at Bridge Crossing. Journal of Hydraulics Division, Vol. 86, No. HY2, ASCE, 1960.
6. L.G. Leopold and T. Maddock, Jr. The Hydraulic Geometry of Stream Channels and Some Physiographic Implications. Prof. Paper 252. U.S. Geological Survey, 1953, 57 pp.
7. L.G. Leopold, M.G. Wolman, and J.P. Miller. Fluvial Processes in Geomorphology. W.H. Freeman, San Francisco, Calif., 1964.
8. G.H. Mathes. Basic Aspects of Stream Meanders. Transactions of the American Geophysical Union, 1941.
9. E.V. Richardson, S. Karaki, K. Mahmood, D.B. Simons, and M.A. Stevens. Highways in the River Environment--Hydraulic and Environmental Design Considerations, Training and Design Manual. FHWA, Colorado State University, Fort Collins, 1973.
10. S.A. Schumm. Fluvial Geomorphology--The Historical Perspective. In River Mechanics, H.W. Shen, ed., Colorado State University, Fort Collins, 1971.
11. S.A. Schumm. River Morphology, Benchmark Papers in Geology. Dowden, Hutchinson & Ross, Inc., Stroudsburg, Pa., 1972.
12. B.R. Winkley, D.B. Simons, and S.A. Schumm. Rivers as Dynamic Systems. ASCE Task Committee Paper. Presented at the ASCE National Water Resources Engineering Meeting, Washington, D.C., 1973.
13. M. Admad. Experiments on Design and Behavior of Spur Dikes. Proc., International Association for Hydraulics Research, ASCE Joint Meeting, University of Minnesota, Aug. 1953.
14. M.A. Gill. Discussion on Research for River Regulation Dike Design. Journal of the Waterways and Harbor Division, Vol. 94, No. WW2, ASCE, 1968.
15. C.R. Neill. Guide to Bridge Hydraulics. Roads and Transportation Association of Canada, University of Toronto Press, 1973.
16. S.D. Rao. A Laboratory Study of the Effect of Dikes on Channels. M.S. thesis, Colorado State University, Fort Collins.
17. Manual on River Behavior. Publication 60. Control and Training, Central Board of Irrigation and Power, India, 1956.
18. S.W. Fox. Technical Methods of River Improvement as Developed on the Lower Missouri River by the Federal Government from 1876 to 1903. Transactions of the ASCE, Vol. 54, Paper 995, June 1905, pp. 280-345.
19. G.B. Fenwick, ed. State of Knowledge of Channel Stabilization in Major Alluvial Rivers. Technical Report 7. U.S. Army Corps of Engineers, 1969.
20. J.J. Franco. Research for River Regulation Dike Design. Journal of the Waterways and Harbor Division, Vol. 93, No. WW3, ASCE, Aug. 1967, pp. 71-87.
21. B.R. Winkley. Practical Aspects of River Regulation and Control. In River Mechanics, H.W. Shen, ed., Colorado State University, Fort Collins, 1971.
22. H.F. Cozzens. Steel Rails for Bank Protection on Salinas River, California. Civil Engineering, Vol. 16, No. 3, ASCE, Mar. 1946, pp. 113-115.
23. W. Mamak. River Regulation. U.S. Department of the Interior and the National Science Foundation, Washington, D.C., 1964.
24. B.F. Thomas and D.A. Watt. The Improvement of Rivers, Part I. Wiley, New York, 1918.
25. Aerial Photography and Maps of the Missouri River Front, Sioux City, Iowa to Rulo, Neb. Omaha Chamber of Commerce, Omaha, Neb., 1970.
26. J.R. Freeman. Flood Problems in China. Transactions of the ASCE, Vol. 85, 1922, pp. 1405-1460.
27. R.H. Haas and H.E. Weller. Bank Stabilization by Revetments and Dikes. Transactions of the ASCE, Vol. 118, Paper 2564, 1953.
28. R.E. Hickson. Columbia River Ship Channel Improvement and Maintenance. Journal of the Waterways and Harbor Division, Vol. 87, No. WW3, ASCE, 1961.
29. A.J. Tiefenbrun. Bank Stabilization of Mississippi River Between the Ohio and Missouri Rivers. Misc. Publication 970. Proc., Federal Inter-Agency Sedimentation Conference, Agricultural Research Service, U.S. Department of Agriculture, 1963.
30. E.I. Davis and E.B. Lipscomb. Stabilizing the Lower Mississippi River. Civil Engineering, Vol. 35, No. 11, ASCE, Nov. 1965.
31. Channel Stabilization of Alluvial Rivers. Task Committee Progress Report. Journal of the Waterways and Harbor Division, Vol. 91, No. WW1, ASCE, Feb. 1965, pp. 7-37.
32. Foreshore Protection, Lower Mississippi River. Journal of the Waterways and Harbor Division, Vol. 91, No. WW2, ASCE, May 1965.
33. Bank and Shore Protection in California Highway Practice. Department of Public Works, California Division of Highways, Nov. 1960.
34. Channel Stabilization Studies on the Apalachicola River. Mobile District, U.S. Army Corps of Engineers, Mobile, Ala., 1966.
35. Earth Embankments. Manual EM 1110-2-2300. U.S. Army Corps of Engineers, April 1959, 36 pp.
36. Stone Stability--Velocity vs Stone Diameter. Hydraulic Design Criteria Sheet 712-1. U.S. Army Corps of Engineers, Vicksburg, Miss., 1970.
37. J.K. Searcy. Use of Riprap for Bank Protection. Hydraulic Engineering Circular 11. U.S. Bureau of Public Roads, Washington, D.C., 1967.
38. D.B. Simons and G.L. Lewis. Flood Protection at Bridge Crossings. Publication CER71-72 DBS-GLL 10. Engineering Research Center, Colorado State University, Fort Collins, 1971.

39. D.B. Simons and M.A. Stevens. Stability Analysis for Coarse Granular Material on Slopes. In River Mechanics, H.W. Shen, ed., Colorado State University, Fort Collins, 1971.
40. M.A. Stevens. Scour in Riprap at Culvert Outlets. Ph.D. dissertation. Colorado State University, Fort Collins, 1968.
41. M.A. Stevens and D.B. Simons. Stability Analysis for Coarse Granular Material on Slopes. In River Mechanics, H.W. Shen, ed., Colorado State University, Fort Collins, 1971.
42. M.A. Stevens, D.B. Simons, and G.L. Lewis. Safety Factors for Riprap Protection. Journal of Hydraulics Division, No. HY5, ASCE, 1975.
43. L.G. Straub. Approaches to the Study of Mechanics of Bed Movement. Studies in Engineering Bull. 20. Iowa State University, 1940.
44. M.K. Liu, F.M. Chang, and M.M. Skinner. Effect of Bridge Construction on Scour and Backwater. Report CER60-HKL22. Civil Engineering Department, Colorado State University, Fort Collins, 1961.
45. C.C. Calhoun, Jr., J.R. Compton, and W.E. Strohm, Jr. Performance of Plastic Filter Cloths as a Replacement for Granular Filter Materials. In Highway Research Record 373, HRB, National Research Council, Washington, D.C., 1971.
46. G. Hearn. Stabilization of Alluvial Rivers in India. Engineering News-Record, Vol. 108, Mar. 17, 1932, pp. 393-395.
47. C.C. Inglis. The Behaviour and Control of Rivers and Canals. Research Publication 13. Central Waterpower Irrigation and Navigation Research Station, Poona, India, 1949, 2 Vols.
48. S. Karaki. Hydraulic Model Studies of Spur Dikes for Highway Bridge Openings. Bull. 286, HRB, National Research Council, Washington, D.C., 1959.

Publication of this paper sponsored by Committee on Hydrology, Hydraulics and Water Quality.

Design Guidelines for Spur-Type Flow-Control Structures

SCOTT A. BROWN

ABSTRACT

A study investigating the applicability and design of spur-type flow-control and stream-bank stabilization structures has been conducted to establish design guidelines for the use of spurs. The study was conducted jointly by the Sutron Corporation and the Pennsylvania State University for FHWA. The findings and recommendations are presented, and recommendations for the general application of spur-type flow-control structures are given in relation to the function of the spur, the erosion mechanisms that are countered by spurs, the environmental conditions best suited for the use of spurs, and potential negative impacts produced by spurs. An introduction to the most common types of spurs is given, and design guidelines for establishing spur permeability, the required extent of protection, spur length, spur spacing, spur orientation, and spur height are presented. An example outlining a recommended procedure for establishing the geometric layout of spurs within a spur scheme is presented also.

Spurs are defined as permeable or impermeable linear structures that project into a channel to alter flow direction, induce deposition, or reduce flow velocities along a channel bank. Spurs can be classified as permeable or impermeable; they can be classified further by function as retardance structures, retardance-diverter structures, and diverter structures. Retardance and retardance-diverter structures are permeable; diverter structures are impermeable. Retardance spurs are designed to reduce the flow velocity in the vicinity of the bank as a means of protecting the channel bank. Retardance-diverter structures retard the flow along the channel bank, but they also deflect flow currents away from the bank. Diverter spurs, on the other hand, function by diverting the primary flow currents away from the channel bank. Design guidelines primarily for retardance-diverter and diverter spurs are dealt with in this paper.

In the past, little guidance has been available for the design of spur-type structures. Few design guidelines have been available; those that are available are limited in scope and generally inaccessible to highway design engineers. The design of these structures has been based primarily on the designer's experience and numerous rules of thumb. Although actual field design experience is indispensable when flow-control structures are designed, many highway design engineers have only limited experience in this field, indicating a need for some design guidance. A study was sponsored by FHWA to address this need.

The FHWA study included considerations of the overall applicability of spur-type flow-control and stream-bank stabilization structures, the applicability and attributes of individual spur types, criteria for the selection of a specific spur type, and guidelines for the design of spurs. Guidelines for the actual design of spur systems are covered in

this paper. Guidelines for establishing spur permeability, the required extent or upstream and downstream limits of protection, spur length, spur spacing, spur orientation, spur height, spur crest profile, and spur tip or head shape, and for maintaining channel-bed and bank contact are included. An example outlining the procedure for establishing the geometric layout of spurs within a spur scheme is also included. Applicability and spur-type selection guidelines are covered in a report by FHWA (1).

The design guidelines presented here are based on a thorough literature review, extensive review and evaluation of spur field installations, numerous personal contacts with design engineers actively involved in designing flow-control structures, and a laboratory study designed to evaluate critical spur design parameters (2). The following summary of the major design recommendations presented in the FHWA report is organized by design component for easy reference.

PERMEABILITY

For retardance-diverter structures, a variety of spur permeabilities can be and have been designed. The various levels of spur permeability are typically obtained by using different densities of wood slats or wire mesh attached to the support structures. Sample design details of spurs of various permeabilities are given in the FHWA report (1). As referred to here, spur permeability is defined as the percentage of the spur's surface that is open or unobstructed. In environments where it can be reasonably assumed that the permeable structure will not clog with floating debris or other material, the determination of a particular spur's permeability requires only computation of the unobstructed flow area within the structure. In most environments, however, the spur's effective permeability will be reduced as floating debris clogs the face of the spur. An estimate of the amount of spur clogging that will occur must be considered in the computation of a given spur permeability.

The magnitude of spur permeability appropriate for a given flow-control or channel-bank stabilization application is inversely proportional to the magnitude of flow retardance required, the level of flow control desired, or the channel-bend radius. In all cases, the greater the magnitude of the variable, the lesser the degree of spur permeability. Where it is necessary to provide a significant reduction in flow velocity or a high level of flow control or where the structure is being used on a sharp bend, the spur's permeability should not exceed 35 percent. Where it is necessary to provide a moderate reduction in flow velocity or a moderate level of flow control or where the structure is being used on a mild to moderate channel bend, spurs with permeabilities up to 50 percent can be used. In environments where only a mild reduction in velocity is required, where bank stabilization without a significant amount of flow control is necessary, or where there are mildly curving to straight channel reaches, spurs having effective permeabilities up to 80 percent can be used. However, these high degrees of permeability are not recommended unless experience has shown them to be effective in a particular environment.

Recent laboratory studies (2) have provided additional insight into how various spur permeabilities affect spur behavior. The following is a summary of the findings from the FHWA laboratory investigation relating to spur permeability:

1. The greater the spur permeability, the less severe the scour pattern downstream of the spur tip. As spur permeability increases, the magnitude of scour downstream of the spur decreases slightly in size but more significantly in depth.
2. The vertical structural members of permeable spurs should be round or streamlined to minimize local scour effects.
3. The greater the spur permeability, the lower the magnitude of flow concentration at the spur tip.
4. If minimizing the magnitude of flow deflection and flow concentration at the spur tip is important to a particular spur design, a spur with a permeability greater than 35 percent should be used.
5. The more permeable the spur, the shorter the length of channel bank protected downstream of the spur's riverward tip.
6. Spurs with permeabilities up to approximately 35 percent protect almost the same length of channel bank as do impermeable spurs; spurs having permeabilities greater than approximately 35 percent protect shorter lengths of channel bank, and this length decreases with increasing spur permeability.
7. Because of the increased potential for erosion of the channel bank in the vicinity of the spur root and immediately downstream when the flow stage exceeds the crest of impermeable spurs, it is recommended that impermeable spurs not be used along channel banks composed of highly erodible material unless measures are taken to protect the channel bank in this region.

GEOMETRY

The geometry of a spur system is made up of several components that, when combined, produce the spur system's geometric form. These components include the longitudinal extent of the spur system and the length, spacing, and orientation of individual spurs. The longitudinal extent of the spur system describes the length of channel bank that is to be protected; the length, spacing, and orientation of individual spurs are self-explanatory. In this section, there will be a brief discussion of each component separately and then they will be considered together to provide criteria for delineating an appropriate spur geometry.

Extent of Bank Protection

The extent of channel-bank protection required on a typical eroding channel bend has been investigated by several researchers, including Parsons (3), Apmann (4), and the U.S. Army Corps of Engineers (5). These investigators as well as others have found that a common mistake in streambank protection is to provide protection too far upstream and not far enough downstream.

Criteria for establishing the extent of channel-bank protection have been developed by the U.S. Army Corps of Engineers (5) in a series of model studies. From these studies, it was concluded that the minimum distances for extension of protection are an upstream distance of 1.0 channel width and a downstream distance of 1.5 channel widths from corresponding reference lines as shown in Figure 1. A similar criterion for establishing the upstream limit of protection was found by FHWA (2); however, a downstream limit of 1.1 times the channel width was found. The FHWA study was not, however, as extensive in this respect as that of the Corps of Engineers.

These criteria are based on analysis of flow conditions in symmetric channel bends under ideal laboratory conditions. Real-world conditions are rarely as simple. In actuality, many site-specific factors have a bearing on the actual length of bank

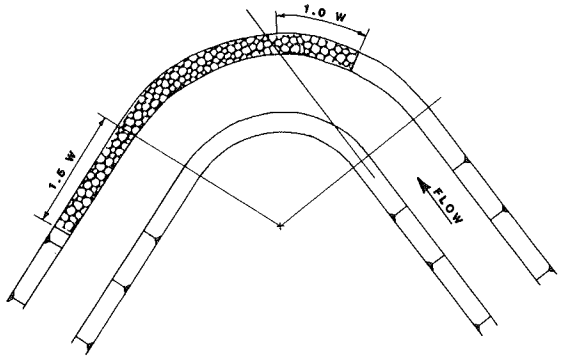

FIGURE 1 Extent of protection required around a channel bend (5).

that should be protected. A designer will find the above criteria difficult to apply on mildly curving bends or on channels having irregular, nonsymmetric bends. Also, other channel controls (such as a bridge abutment) might already be producing a stabilizing effect on the bend so that only a part of the channel bend would need to be stabilized. In addition, the magnitude or nature of the flow event might cause erosion problems only in a localized portion of the bend, again requiring that only a short channel length be stabilized. Therefore, the foregoing criteria should be used only as a starting point. From here, additional analyses of site-specific factors should be conducted, including field reconnaissance, evaluation of flow traces for various flow conditions, and review of flow and erosion forces for various flow-stage conditions. Information from these analyses should then be combined with personal judgment and a knowledge of the flow processes occurring at the local site to establish the appropriate limits of protection.

Spur Length

Spur length as referred to here is the projected length of the spur perpendicular to the main flow direction; it is reported as a percentage of the channel width at bank-full stage. Both the projected spur length and the channel width used in these computations reflect lengths measured from the desired channel-bank line. On channels having smooth, regular bank lines these lengths are measured from the actual bank. When the spurs are being used to shift the channel to a new location or provide a new smooth alignment along channel banks that have been severely eroded, the actual spur projected length and the channel width should be measured from the desired bank line and not the actual bank line. In these cases, the actual spur projected length will be longer than the projected lengths to be recommended here. Actual spur lengths may vary within a spur scheme to provide a smooth flow alignment.

The appropriate length of spurs within a bank-stabilization scheme is dependent on the spur's behavior in the particular environment as well as the desired flow alignment (as discussed earlier). The behavior of specific spur types was investigated during the recent laboratory studies conducted by FHWA (2). The following summary of the findings from the FHWA laboratory studies indicates that as spur length is increased,

1. The scour depth at the spur tip increases,
2. The magnitude of flow concentration at the spur tip increases,
3. The severity of flow deflection increases, and
4. The length of channel bank protected increases.

The following general recommendations are given regarding spur length:

1. The projected length of impermeable spurs should be held to less than 15 percent of the channel width at bank-full stage.
2. The projected length of permeable spurs should be held to less than 25 percent of the channel width. However, this criterion depends on the magnitude of the spur's permeability. Spurs having permeabilities less than 35 percent should be limited to projected lengths not to exceed 15 percent of the channel's flow width. Spurs having permeabilities of 80 percent can have projected lengths up to 25 percent of the channel's bank-full flow width. Between these two limits, a linear relationship between the spur permeability and spur length should be used.

Spur Spacing

Typically, spur spacing has been related to spur length by a spacing factor, which is the ratio of a spur's spacing to its projected length. Based on this criterion, spur spacing is a function of the spur's length only. Based on the FHWA laboratory study (2), however, it was found that spur spacing is also dependent on the spur's orientation, its permeability, the channel bend's degree of curvature, and the direction and orientation of the channel's flow thalweg. Each of these factors is an integral part of a method for establishing spur system geometry, which will be presented later. The spacing criterion presented is based on the projection of a tangent to the flow thalweg off the spur tip.

In addition, the following comments can be made regarding the impact that various spur spacings have on flow patterns in channel bends:

1. Reducing the spacing between individual spurs below the minimum required to prevent bank erosion between the spurs results in a reduction of the magnitude of flow concentration and local scour at the spur tip and
2. Reducing the spacing between spurs in a bank stabilization scheme causes the flow thalweg to stabilize farther from the concave bank toward the center of the channel.

Spur Angle and Orientation

The primary criterion for establishing an appropriate orientation for the spurs within a given spur scheme is to provide a scheme that efficiently and economically guides the flow through the channel bend and at the same time protects the channel bank and minimizes the adverse impacts on the channel system. Meeting these criteria requires consideration of how various spur angles influence flow patterns around individual spurs, flow concentration at the spur tip, scour depths at and just downstream of the spur tip, the length of channel bank protected by individual spurs, and flow deflection.

The following list describes how the foregoing criteria are affected by a spur's orientation:

1. Spurs angled downstream produce a less severe constriction of flows than those angled upstream or normal to the flow.
2. The greater an individual spur's angle in the downstream direction, the less the flow concentra-

tion and local scour at the spur tip. Also, the greater the angle, the less severe the flow deflection toward the opposite channel bank.

3. Impermeable spurs create a greater change in local scour depth and flow concentration over a given range of spur angles than do permeable spurs. This indicates that impermeable spurs are much more sensitive to these parameters than permeable spurs.

4. Spur orientation does not in itself result in a change in the length of channel bank protected for a spur of given projected length. It is the greater spur length parallel to the channel bank associated with spurs oriented at steeper angles that results in the greater length of protection.

5. The smaller the spur angle, the greater the magnitude of flow control as represented by a greater shift of the flow thalweg away from the concave (outside) channel bank.

It is recommended that spurs within a retardance-diverter or diverter spur scheme be set so that the spur that is farthest upstream is approximately 150 degrees to the main flow current at the spur tip and subsequent spurs are at incrementally smaller angles approaching a minimum angle of 90 degrees at the downstream end of the scheme. The method of establishing the spur angle and orientation presented in the geometric design example in the next section should be used to set the orientation of individual spurs within a spur scheme.

Geometric Design Example

A step-by-step approach for establishing the geometric layout of a retardance-diverter or diverter spur scheme follows. This method is designed to provide an optimal geometric layout. Figure 2 shows a meandering channel that has encroached on a bridge abutment. The objective in this situation is to establish the bank line that existed before the erosion shown. Also, because of severity or sharpness of the channel bend and the need for a positive flow deflection, an impermeable spur scheme will be designed. The steps in the procedure are as follows:

Step 1: establish the limits of the flow-control and bank stabilization scheme,

Step 2: set the desired flow alignment and maximum flow constriction,

Step 3: estimate the flow thalwegs through the bend,

Step 4: locate and orient spur 1,

Step 5: locate spur 2,

Step 6: orient spur 2, and

Step 7: locate and orient subsequent spurs.

Setting Limits of Protection

In Figure 3 the procedure used to set the limits of the flow-control scheme is shown. First, the eroded bank area is defined. Delineation of this area can be determined from field surveys. It is important that the design engineer visit the site, not only to establish the limits of the eroded area but also to become familiar with flow conditions at the site.

Next the minimum limits of protection are established. As illustrated, a distance of 1.5 times the channel width is measured downstream of the downstream limit of curvature of the bend to locate the minimum downstream limit of protection. However, because the bridge abutment itself has acted as a channel control, the downstream limit of protection can be set at the upstream side of the abutment.

The upstream limit of flow control or bank protection is set by measuring a distance equal to one channel width upstream of the upstream reference line, which is set by projecting a tangent to the convex channel bank just upstream of the beginning of curvature for the bend. In this case, however, bank erosion was observed upstream of this limit. Therefore, the upstream limit of protection was set upstream of the point of observed erosion.

Setting Maximum Flow Constriction

The object here is to shift the channel-flow alignment to that which existed before the bank erosion. This desired flow alignment was shown in Figure 2. The dashed line in Figure 4 represents a 10 percent constriction of the channel width, which is being used to establish the length of individual spurs. A 10 percent constriction was selected here to minimize local scour and flow concentration at the spur tip. Limiting the flow constriction to 10 percent

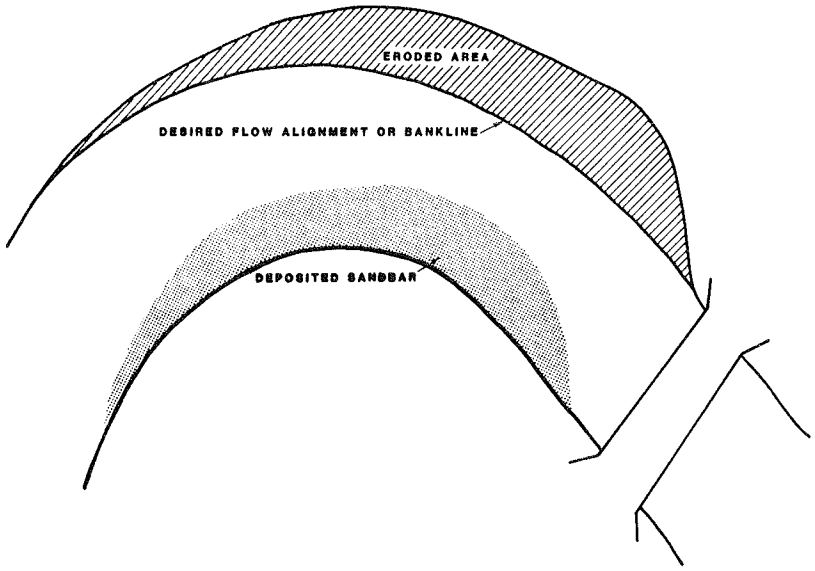

FIGURE 2 Channel bend showing eroded area, desired flow alignment, and deposited sandbar.

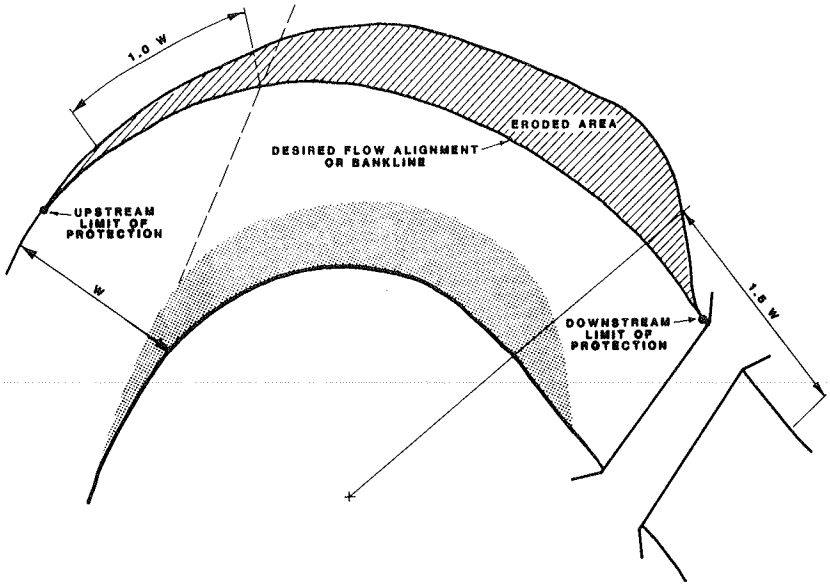

FIGURE 3 Setting the limits of protection.

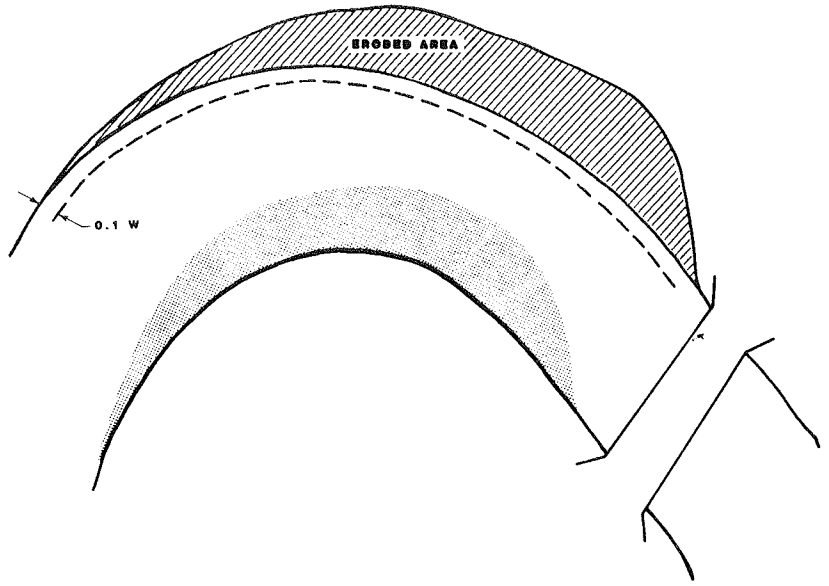

FIGURE 4 Setting maximum flow constriction.

also minimizes the chance that spurs will deflect currents into the opposite channel bank.

Estimating Flow Thalwegs Through Bend

The design criteria for spur spacing and orientation rely on a prediction of the location of the channel flow thalweg for various flow conditions. A general knowledge of flow patterns in channel bends and how these flow patterns change with varying stages of discharge is required to establish appropriate flow thalweg locations. Discussions of this nature are beyond the scope of this paper. Sketching three thalweg locations corresponding to low, medium, and high channel flow conditions will usually provide sufficient definition. Figure 5 shows these three thalweg locations for the sample conditions. A thorough knowledge of flow in natural channel bends is required for accurate estimation of these thalweg locations.

Location and Orientation of Spur 1

Figure 6 shows the procedure used to locate and orient the first spur, the one that is farthest upstream. First the bend radius line R1 is drawn from the center of curvature of the bend through the point limiting the upstream protection as defined in step 1. Next, a flow tangent to the estimated flow stream line at the spur tip is drawn. Typically, the low-flow thalweg location should be used, because it will generally follow the desired flow alignment. Such a flow tangent is shown in Figure 6 as line AA. The flow tangent is then shifted along the radius line R1 until the 10 percent flow constriction line is reached (see line A'A'). The spur angle of 150 degrees is then turned in an upstream direction (clockwise) from line A'A' to establish the line BB, which is parallel to the desired spur orientation through the constricted-width line where it intersects the radius line (R1). The line B'B'

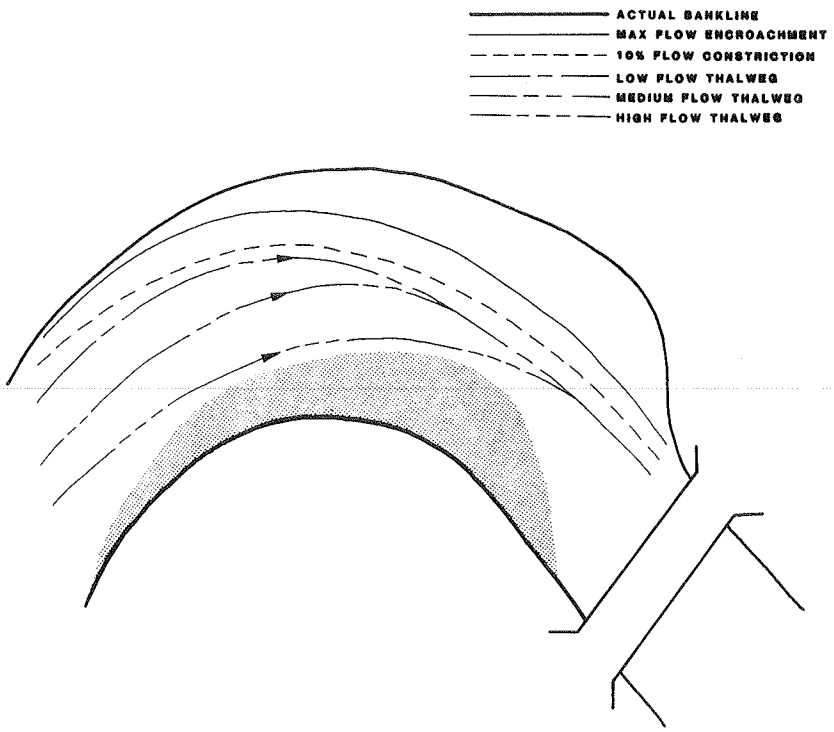

FIGURE 5 Estimates of thalweg locations for various flow conditions.

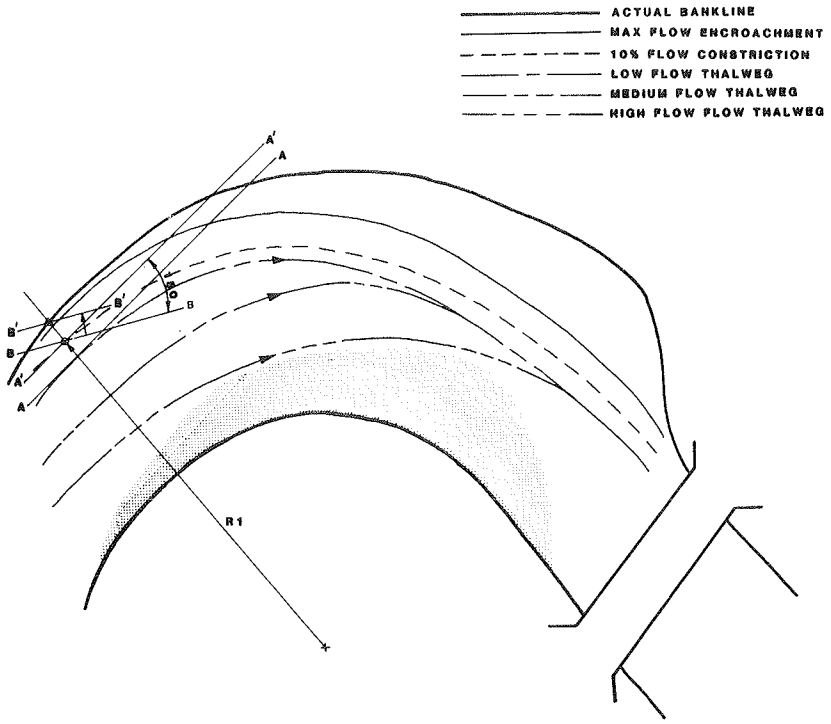

FIGURE 6 Location and orientation of first spur.

is then drawn through the point defining the upstream limit of protection (spur location point) parallel to line BB. This line defines the location of the centerline of the spur. The spur length is then set between the eroded bank line and the 10 percent flow-constriction line.

Location of Spur 2

The approach to locating the second spur is shown in Figure 7. This approach will be used to locate each subsequent spur. First another radius line, R2 in Figure 7, is drawn through the tip of the previous

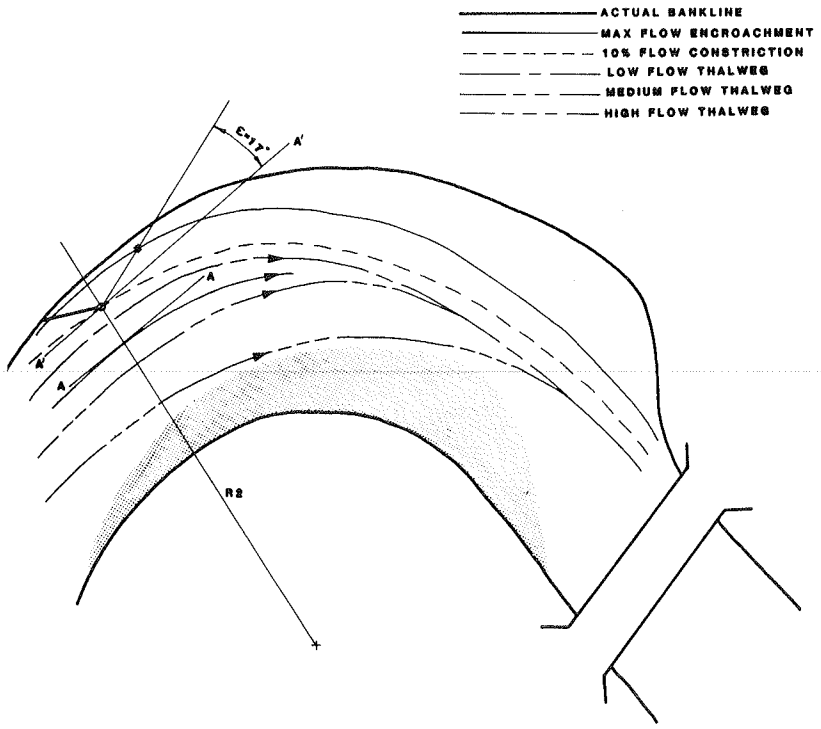

FIGURE 7 Location of second spur.

spur. The location of the next downstream spur depends on the orientation of a tangent to the channel thalweg where it intersects line R2. However, three flow thalweg lines have been sketched representing different flow conditions. The appropriate flow thalweg is that which intersects line R2 at one quarter of the channel width from the flow-constriction line. Line AA in Figure 7 illustrates the tangent drawn to the quarter-point thalweg curvature off the tip of spur 1. Line AA is then slid along line R2 to the tip of spur 1, as indicated by line A'A'. From line A'A', an expansion angle of 17 degrees (as determined for impermeable spurs at 10 percent constriction) is turned toward the concave bank line (counterclockwise). The location of the next downstream spur is defined by the point at which the rotated line intersects the line of maximum flow encroachment. This point is indicated by an asterisk in Figure 7.

Orientation of Spur 2

Setting the orientation of spur 2 and each subsequent spur is the same as the procedure for orienting spur 1. As shown in Figure 8, the first step is to draw a radius line (R3) through the spur location point (asterisk). Next a flow tangent to the estimated flow stream line at the spur tip is drawn (line AA as discussed in step 4). Line AA is shifted along line R3 to the tip of the spur (see line A'A'). The spur angle of 140 degrees is then turned in an upstream direction from line A'A' to establish the line BB. The line B'B' is then drawn through the spur location point. Line B'B' defines the centerline of spur 2. The spur length is then set between the eroded bank line and the 10 percent flow-constriction line.

Location and Orientation of Subsequent Spurs

Steps 5 and 6 are repeated until the downstream limit of protection is reached. Figure 9 shows the final geometry developed in this manner.

Several additional comments can be made about the example just presented. The spur angles used when setting out the sample spur scheme are shown in Figure 9. Note that the spur angles decrease from 150 degrees to 120 degrees and then remain constant. This was done to provide a more efficient flow path through the channel bend. This example documents a relatively sharp bend requiring maximum flow efficiency. For this reason the spurs were not angled more steeply. The magnitude of this limiting spur angle should be set based on conditions particular to each site.

Also, note the dogleg in the next-to-the-last spur. The dogleg was designed into this spur to minimize its total length and thus its cost. This leg of the spur is not affected by channel flows because it is inside the maximum flow encroachment line. Doglegs such as this can be designed where they will provide an economic advantage without affecting the stabilization scheme. It is also interesting to note the relative spacing of the spurs: those on the downstream half of the bend are closer together, which provides a more positive control of flow in this region (1,2).

SPUR HEIGHT

The height to which spurs should be constructed is primarily a function of the height of channel bank to be protected. Factors that influence the appropriate height of bank protection are as follows:

1. The mechanism causing the erosion,
2. The existing channel-bank height,
3. The design flow stage, and
4. The flow stage at which significant debris loads become a problem.

With these factors in mind, the following recommendations are made for establishing the height of spur systems:

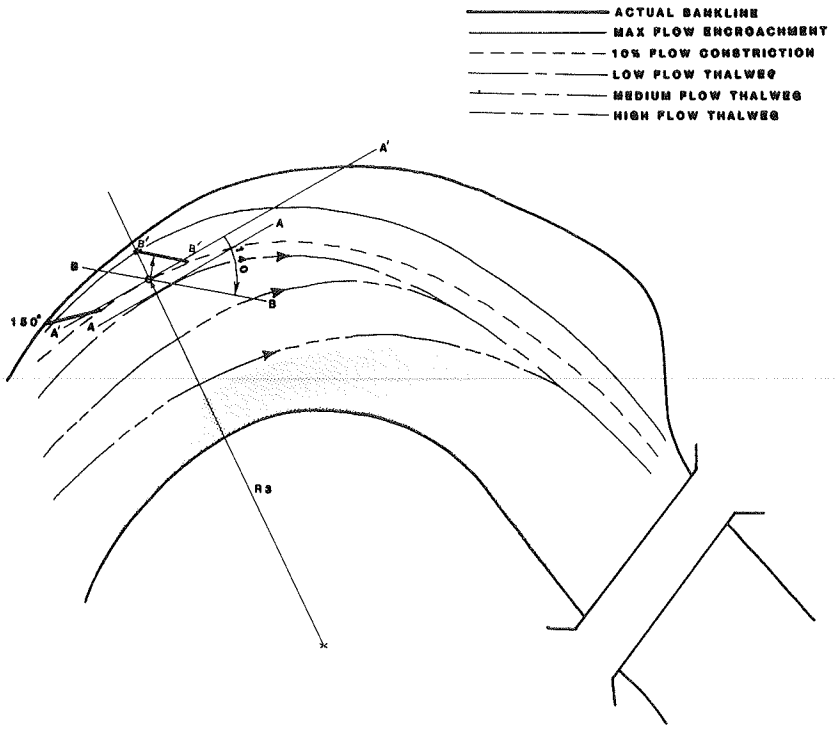

FIGURE 8 Orientation of spur 2.

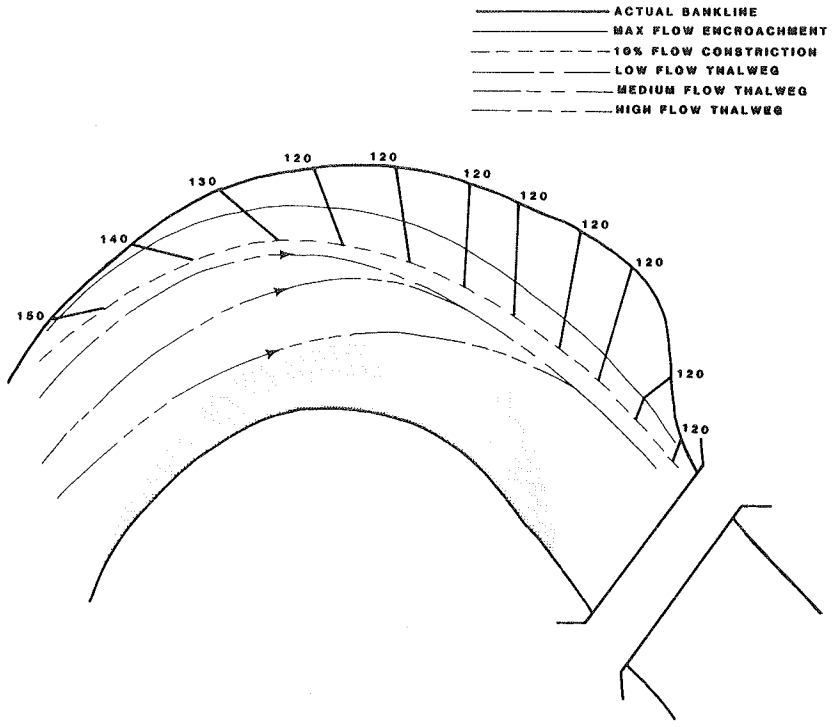

FIGURE 9 Final spur scheme geometry.

1. The spur height should be sufficient to protect the regions of the channel bank affected by the erosion processes active at the particular site.
2. If the design flow stage is lower than the channel-bank height, spurs should be designed to a height no more than 3 ft lower than the design flow stage.
3. If the design flow stage is higher than the channel-bank height, spurs should be designed to bank height.
4. Permeable spurs should be designed to a height that will permit the passage of heavy debris over the spur crest without causing structural damage.
5. When possible, impermeable spurs should be designed to be submerged approximately 3 ft under

their worst design flow condition, thus minimizing the impacts of local scour and flow concentration at the spur tip and the magnitude of flow deflection.

SPUR-CREST PROFILE

The following recommendations are made for spur-crest profile:

1. Permeable spurs should be designed with level crests unless bank height or other special conditions dictate the use of a sloping crest design.
2. Impermeable spurs should be designed with a slight drop toward the spur head, thus allowing different amounts of flow constriction with stage (particularly important in narrow-width channels) and the accommodation of changes in meander trace with stage.

CHANNEL-BED AND CHANNEL-BANK CONTACT

Careful consideration must be given to designing a spur that will maintain contact with the channel bed and channel bank so that it will not be undermined or outflanked. Methods for protecting against structure undermining include

1. Providing a rock toe at the base of the structure,
2. Driving vertical support members to a depth greater than anticipated scour depths,
3. Extending the structure's face material to a depth greater than anticipated scour depths, and
4. Designing the structure so that it can be flexible in the vertical direction and thus maintain bed contact.

To protect against outflanking, the structure should be designed with a root structure that extends for a distance into the channel bank.

SPUR-HEAD FORM

Numerous design shapes have been suggested for the head or riverward tip of the spur: straight, T-head, L-head, wing, hocky, inverted hocky, and so on. However, a simple straight spur-head form is recommended. The only additional recommendation is that the spur tip be as smooth and rounded as possible. Smooth, well-rounded spur tips help minimize local scour and flow velocities at the spur tip.

ACKNOWLEDGMENT

The research on which this paper was based was performed under a contract between FHWA and the Sutron Corporation. The primary purpose of this research contract was to develop guidelines for the design of spur-type flow-control structures.

REFERENCES

1. Design of Spur-Type Streambank Stabilization Structures. Report FHWA/RD(-83/100). FHWA, U.S. Department of Transportation, 1983.
2. Laboratory Investigation of Flow Control Structures for Highway Stream Crossings. FHWA, U.S. Department of Transportation, Aug. 1983.
3. D.A. Parsons. Effect of Flood Flows on Channel Boundaries. Journal of the Hydraulics Division of ASCE, Vol. 86, No. HY4, Proceedings Paper 2443, April 1960.
4. R.P. Apmann. Flow Processes in Open Channel Bends. Journal of the Hydraulics Division of ASCE, Vol. 98, No. HY5, Proceedings Paper 8886, 1972.
5. The Streambank Erosion Control Evaluation and Demonstration Act of 1974, Section 32, Public Law 93-251: Final Report to Congress. U.S. Army Corps of Engineers, 1981.

Publication of this paper sponsored by Committee on Hydrology, Hydraulics and Water Quality.

Comparison of Prediction Equations for Bridge Pier and Abutment Scour

J. STERLING JONES

ABSTRACT

There are at least 10 prediction equations for bridge pier scour, and designers are often at a loss over which one to use. There are only three or four prediction equations for abutment scour, but these have not been highly publicized. The pier scour equations fall into three basic categories: those of the University of Iowa, those of the Colorado State University, and those based on foreign literature. The similarities among the pier scour equations and the range of data on which they are based are shown. FHWA sponsored several studies during the 1970s aimed primarily at comparing field data with the various equations to show which ones best predicted local scour for U.S. streams. These studies were somewhat inconclusive because of the many interrelated variables in the scour process, but they do show which equations are conservative and which are not.

Scour is the term used to describe erosion phenomena that involve unified flow patterns such as those at bridge piers, abutments, and outlet structures. Scour damage to highway structures has been estimated to be as high as $20 million per year (1). Years of research have been devoted to resolving the problem of scour at bridges; yet in spite of the magnitude of the damages attributed to scour, FHWA has never published an engineering circular bringing together the literature and giving guidance on how to account for scour at bridges. Lacking an engineering circular on the subject of bridge scour, there appears to be no better forum than a national conference among leading bridge engineers to reflect the knowledge that has been gained on this pertinent topic.

In a general sense, scour as defined by ASCE in Manuals 43 (2) and 54 (3) is the erosive action of running water in streams that excavates and carries away material from stream beds and banks. Many highway engineers relate to this definition and identify all stream erosion as scour. A preferred definition restricts the term to vertical stream erosion (4,5), thus distinguishing stream-bed erosion from lateral stream migration.

For the purposes of this paper it is useful to look at the components of scour and to focus on those components that are primarily related to bridges. The components are as follows:

1. Local pier scour,
2. Contraction scour,
3. Local abutment scour, and
4. General aggradation and degradation.

Although all these components may occur simultaneously and are probably interrelated in a field situation, they have been studied separately and need to be predicted independently in a design situation.

The two components of primary interest are pier and abutment scour because they are direct consequences of bridge obstructions to water flow and are therefore the primary responsibility of highway agencies. Aggradation and degradation are often the predominant components of scour but usually are site-specific phenomena associated with a stream's reaction to meander cutoffs, effective slope changes, downstream mining, reservoirs, and so on. Aggradation and degradation are probably best predicted by a sediment transport model such as the Corps of Engineers HEC-6 (6,7), the Chang model (7), or the Simons-Li model (7). Contraction scour may occur naturally because of narrowing of the floodplain or may be bridge related because of the encroachment on the floodplain by embankments. Abutment scour is a concentrated part of contraction scour that can be accounted for by empirically distributing the scour in a waterway opening.

NCHRP SYNTHESIS ON SCOUR AT BRIDGE WATERWAYS

In 1969 a synthesis of available literature and practices for dealing with scour at bridge waterways was made by the Highway Research Board. More than 100 organizations, including highway agencies, toll road agencies, consultants, railroad companies, and government agencies, were surveyed.

The synthesis report (5) cited 12 bridge pier scour prediction equations, but in the discussion of the prediction equations it was concluded that it was (5, p. 14) "quite impossible to build a feeling of confidence in any prediction method" because of a lack of field measurements with which to compare the predictions. The only guidance given for selecting the right prediction equation was to check the background of each equation and examine the variables included in each equation.

The synthesis report cited only one abutment scour equation. That was Laursen's equation in an appendix written by Laursen himself.

FHWA FOLLOW-UP STUDIES

FHWA sponsored several studies in the 1970s after the NCHRP synthesis aimed at improving confidence in some of the prediction methods. The West Virginia University study (8) had the objective of developing instrumentation and collecting field data for scour around bridge piers. The researchers found that it was less of a problem to develop instrumentation than to deploy it in a flooding environment so that it would be operational when needed.

Anderson (9) rearranged the equations to make them as similar in format as possible so as to facilitate an analytical comparison. He recommended that some large-scale laboratory studies be conducted to complement the field data, especially for extrapolating equations beyond the range of the original tests. He was able to rearrange the pier scour equations in terms of one or more of three

dimensionless variables--flow depth and effective pier width, Froude number, and shear stress and critical shear stress. In other words, these three variables are the key factors that govern the pier scour process. Following Anderson's recommendation, FHWA sponsored a study at the University of Iowa (10) that had the objective of extending the range of the key factors, especially the Froude number, which includes flow velocity and depth.

PIER SCOUR EQUATIONS

The pier scour equations can be grouped into three basic categories for comparison. One category is the group based on foreign research, primarily in Pakistan and India, where fine bed materials are prevalent. A second category is patterned after the University of Iowa hypothesis that depth of flow is more important than velocity in sediment-transporting pier scour. The third category is patterned after the work at Colorado State University (CSU) and includes velocity (expressed in a Reynolds number or Froude number) as a predominant term.

The equations, identified by primary developer, are shown in the following paragraphs.

Pier Scour Formulas Based on Foreign Research

Ahmad [Pakistan 1962 (11)]

$$d_s/b = y_0/b\,(4.77F^{2/3} - 1) \tag{1}$$

Bruesers [Netherlands 1964 (12)]

$$d_s/b = 1.4 \tag{2}$$

Chitale [India 1962 (13)]

$$d_s/b = y_0/b\,(-5.49F^2 + 6.65F - 0.51) \tag{3}$$

Inglis [India 1949 (14)]

$$d_s/b = 4.05\,(y_0/b)^{3/4}\,[F^{1/2} - (y_0/b)] \tag{4}$$

where

d_s = depth of scour measured from the mean bed elevation,
y_0, y = approach flow depth,
b = projected pier width,
$F = V/gy$ = Froude number, and
V = velocity of approach flow.

Pier Scour Formulas Patterned After University of Iowa Research

Laursen sediment continuity equation [1958 (15)]

$$d/b = 1/\left\{5.5[(1/11.5)\,(d_s/y_0) + 1]^{1.70} - 1\right\} \tag{5a}$$

Laursen [clear-water equation, not used in comparisons that follow (16; unpublished data, 1977)]

$$d/b = (\tau_0/\tau_c)^{1/2}/5.5\,[(1/11.5)\,(d_s/y_0) + 1]^{7/6}\,(\tau_0/\tau_c)^{1/2} \tag{5b}$$

Neil [from Laursen's 1956 design curve (9)]

$$d/b = 1.5\,(y/b)^{0.3} \tag{6}$$

Jain [1979 (10)]

$$d/b = 2.0\,(F - F_c)^{0.25}\,(y/b)^{0.5} \quad \text{for } (F - F_c) \geq 0.20 \tag{7a}$$

$$d/b = 1.84\,(y_0/b)^{0.3}\,F^{0.25} \quad \text{for } F < F_c \tag{7b}$$

where F_c is the critical Froude number when sediment transport is pending. [For $0 \leq (F - F_c) \leq 0.20$ use larger value from both equations.] The procedure for computing F_c is as follows:

1. Estimate the median diameter (d_{50}) for the bed material,
2. Determine τ_c from Figure 2.44 of ASCE Manual 54 (3),
3. Compute $U_{*c} = \tau_c/\rho$,
4. Compute $\delta = 11.6\nu/U_{*c}$ (assume $\nu = 1.08 \times 10^{-5}$ ft²/sec),
5. Compute d_{50}/δ,
6. Select x from Figure 2.97 of ASCE Manual 54 (3),
7. Compute $V = [2.5\,\ln(11.02yx/d_{50})]\,U_{*c}$, and
8. Compute $F_c = V_c/(gy_c)^{1/2}$.

Pier Scour Formulas Patterned After CSU Research

Shen I [1969 (17)]

$$d_s = 0.00073\,Re^{0.619} \tag{8}$$

where Re is the pier Reynolds number, Vb/υ, and υ is the kinematic viscosity.

The Reynolds number is a viscosity parameter dependent on the water temperature, but few designers would be able to predict scour closely enough to account for water temperature, so Anderson reasoned that he could use $\upsilon = 1.2 \times 10^{-5}$ and approximate the exponent 0.619 by 0.66 to get

$$d_s/b = AF^{2/3}\,(y_0/b)^{1/3} \tag{9}$$

Depending on when the exponent is rounded, the coefficient A becomes 3.06 or 4.43. Anderson got 4.43 because he rounded the exponents before he multiplied through by the constants. It is reasonable to use an intermediate value of A = 3.4 and make the Shen I equation identical to the Shen II equation that follows, because both equations are based on the same data. Shen himself considered the equations to be equivalent.

Shen II [1969 (17)]

$$d_s/b = 3.4\,[V/(gb)^{1/2}]^{2/3} \tag{10}$$

which becomes directly

$$d_s/b = 3.4F^{2/3}\,(y_0/b)^{1/3} \tag{11}$$

This will hereafter be referred to as the Shen equation.

CSU [1975 (18)]

$$d_s/b = 2.2\,(y_0/b)^{0.35}F^{0.43} \tag{12}$$

Even without considering the complexities of debris and cohesive materials, a designer is faced with nine equations to make a single computation. One might question why there are so many different equations for the same predictions if each researcher was accurate in his work. Furthermore, one might question whether the differences in the equations are as significant as other environmental factors that could not be included in the model studies used to develop the equations.

The equations are compared graphically in Figures 1 and 2. Because most of the equations are in terms of y/b as well as the Froude number, both figures

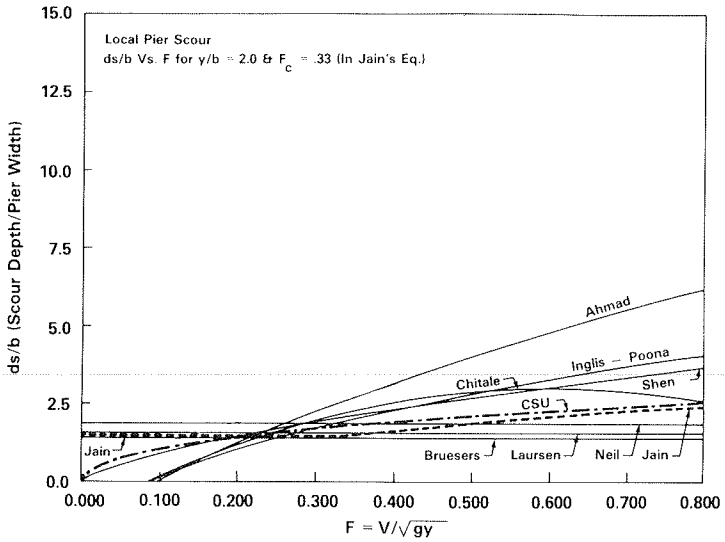

FIGURE 1 Graphical comparison of scour formulas (9) for variable Froude numbers.

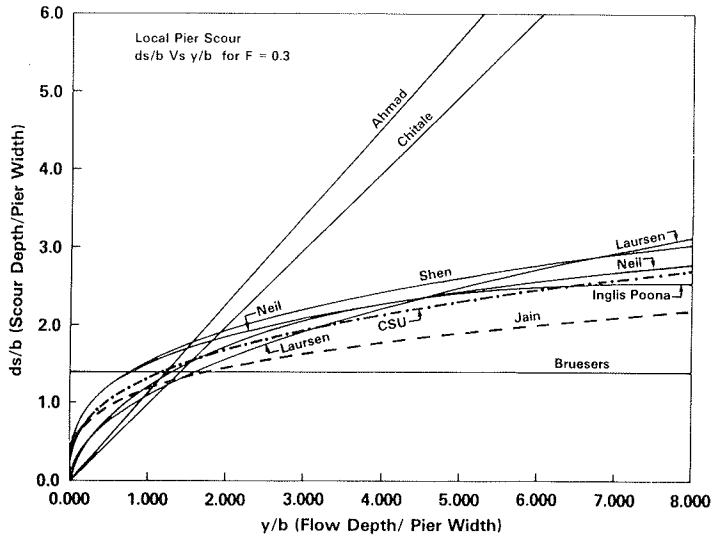

FIGURE 2 Graphical comparison of scour formulas (9) for variable depth ratios (y/b).

are needed to get a graphical comparison of the equations. Figure 1 is for an average depth ratio (y/b) of 2.0; Figure 2 is for an average Froude number of 0.3. The main difference in the equations is not so much in the data as in the way that the curves were fit to the data. All the equations are at least partly empirical and most are reasonably accurate if applied within the range of the empirical data.

SELECTING THE EQUATION FOR DESIGN

According to the NCHRP synthesis report (5), there are two approaches to selecting the most appropriate equation or equations for design. First, the equations should be compared with field data to deter- mine which ones best duplicate field measurements. Second, lacking these data, the conditions under which the equations were derived should be evaluated and the one that best matches the design conditions should be used. Most designers do not have time to review the literature to determine the derivation conditions for all of these equations, so a summary of data is shown in Figure 3 for equations from for- eign literature and in Figure 4 for equations from U.S. literature.

Looking back at Figure 2 where the equations are compared for variable values of y/b, the Ahmad and Chitale equations would not look so extreme if they were not extended beyond the range of experimental data (y/b approximately 3.5).

All of the pier scour equations derived in the literature have been for noncohesive materials with d_{50} ranging from 0.17 to 1.5 mm. The Bruesers equation is based on limited data, but because of its simplicity it serves as a good rule of thumb, which is to anticipate pier scour around 1.5 times the projected pier width. The Neil equation, which is based on the full range of Laursen's data, reduces to scour of 1.5 times the pier width when the flow depth is equal to the pier width. Neil's equa-

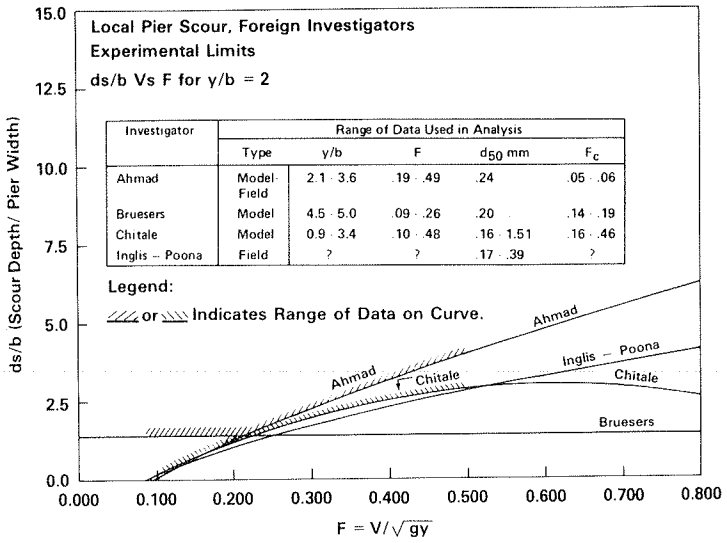

FIGURE 3 Summary of data used to derive pier scour equations: foreign literature.

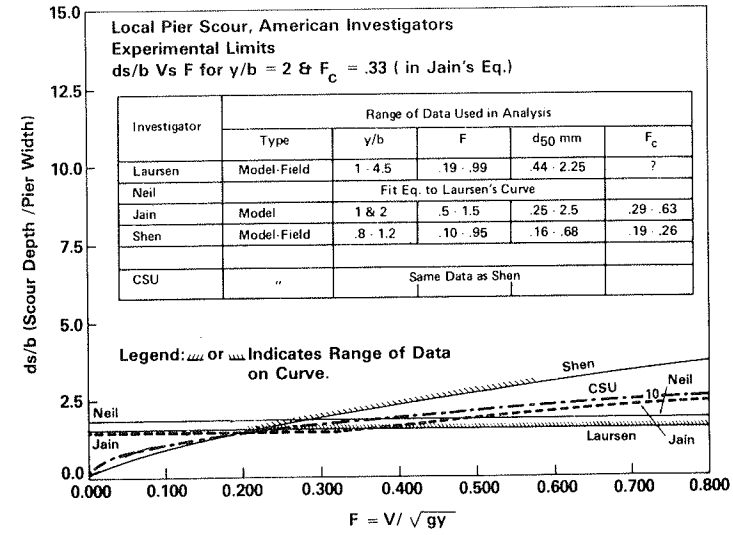

FIGURE 4 Summary of data used to derive pier scour equations: U.S. literature.

tion is just a regression fit to the design curve presented by Laursen in Iowa Bulletin 4 (19). Laursen later published his semitheoretical equations based on continuity of sediment transport, although they also have an empirical factor (Laursen's r-value) to make them fit experimental data. Nevertheless, Laursen's equation probably has the best basis for extrapolation beyond its experimental base. The main criticism of Laursen's equation is that it does not include a Froude number (or velocity term). Although continuity may be satisfied without a velocity term, it seems intuitively that velocity would affect the strength of secondary currents around a pier and therefore would be part of a prediction equation.

Shen's equation is an envelope curve that fits the uppermost scour points for all the available data [Figure 5 (17)]. This equation is appealing from a design standpoint because it is intentionally on the conservative side. The CSU equation is a best fit to much of the same data [Figure 6 (18)].

Jain's equation is somewhat of a compromise between those of Laursen and Shen. It has a Froude number, but the term has a relatively low exponent. Jain introduced the threshold Froude number (F_c) as a way of accounting for relative sediment size. One criticism of Jain's equation is that it is difficult to compute F_c.

FIELD DATA

The most convincing argument for selecting one scour equation rather than another is comparison of predictions with field measurements (8,20,21). Unfortunately, field measurements are scarce, especially under flood conditions, and those measurements that are available must be carefully scrutinized to isolate one component of scour from another.

Figure 7 (8) is a good example of some of the precautions that need to be observed with field measurements. Two floods at the same site are super-

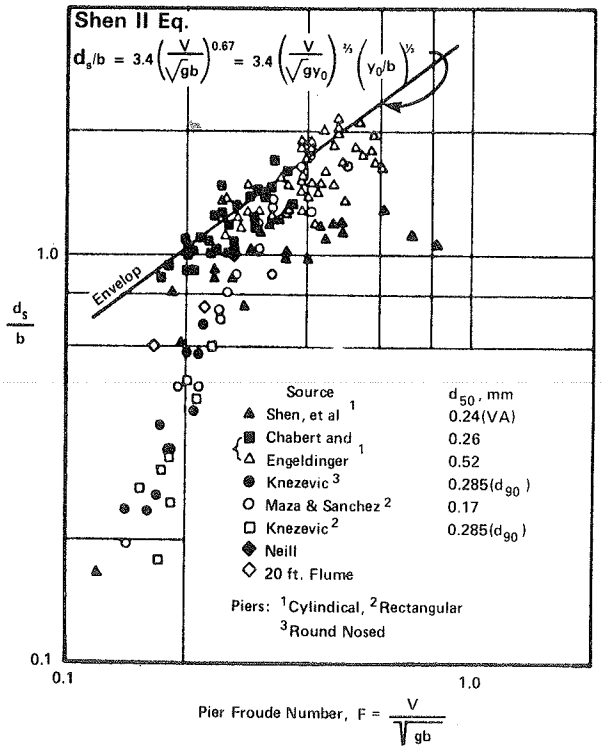

FIGURE 5 Shen's envelope fit to available data (17).

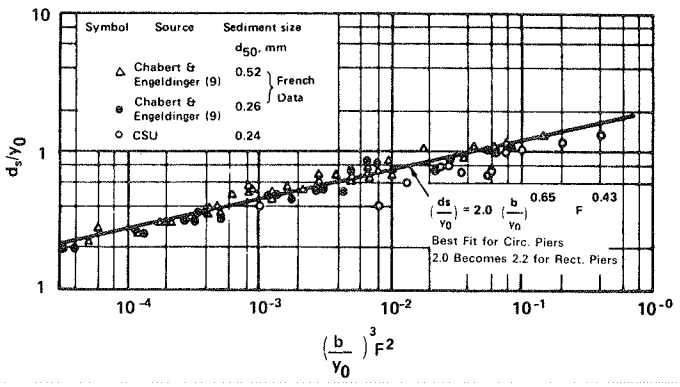

FIGURE 6 CSU fit to pier scour data (18).

imposed. The discharge of one was approximately three times the discharge of the other. The stage increased by 8 ft; the average velocity and Froude number at least doubled but there was apparently a reduction in local scour. How does one explain this discrepancy with the scour formulas?

First, this was not a good site to choose for such a comparison because the bed was already well below the footing (or pile cap); thus, the effective pier was the battered pile group. These conditions are not like any test conditions used to derive the scour formulas. Second, the entire cross section should be measured, not just one point, to even speculate how much local scour occurred. Third, the pier footing, which was approximately 20 ft square, probably served as a scour arrester for the diving currents that were generated by the actual pier at the higher stage, whereas the footing was just below the water surface at the lower stage and tended to generate rather than break up the diving currents at that stage. Data from a site like this give an intuitive feel for the magnitude of scour but they would be a weak argument for validating the scour prediction equations.

The field data gathered from Louisiana files by Chang (20) are summarized in Figure 8. Those sites had good pier configuration and well-defined scour holes, but for two reasons all the data were taken at low Froude numbers. First, the Louisiana streams are low-gradient streams and, second, the data were collected as part of a routine survey of approximately 90 sites by a hydrologic survey team. The surveys were made on a schedule and seldom coincided with floods, which may have generated some higher local velocities.

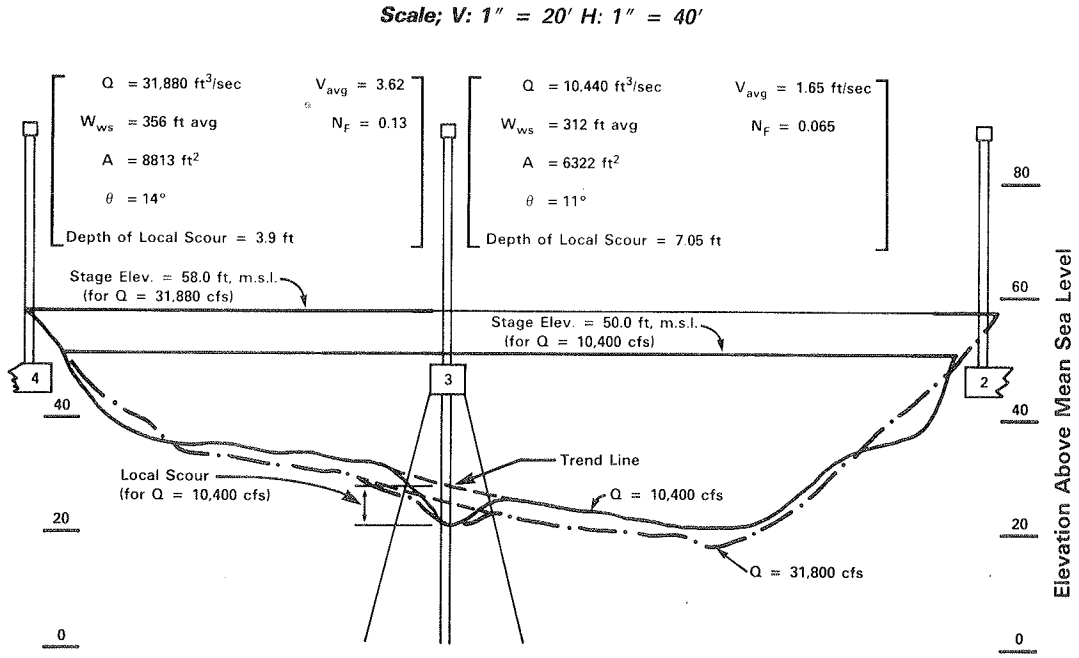

FIGURE 7 Cross section of Brazos River in Texas at bridge crossing (8).

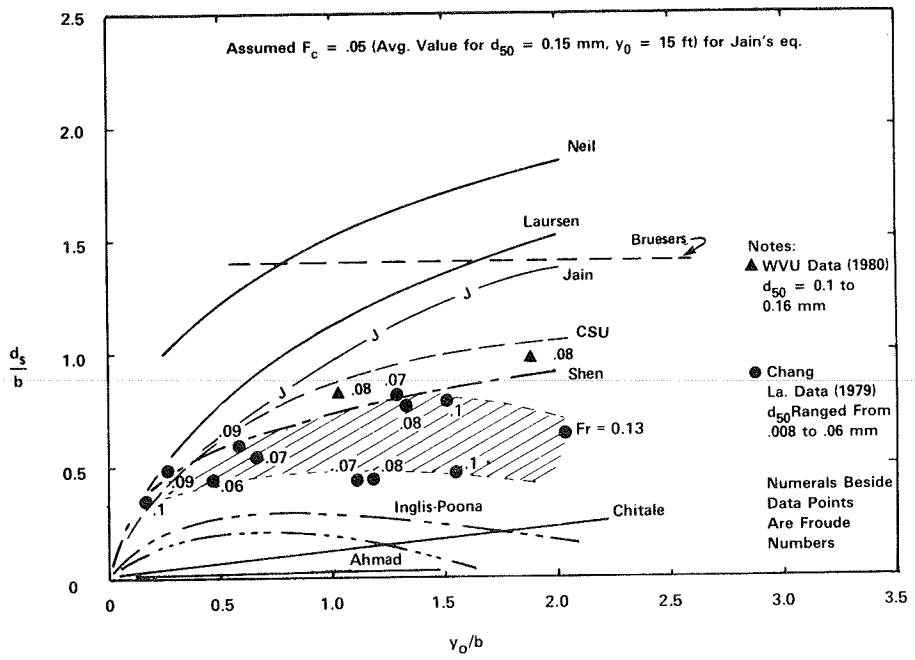

FIGURE 8 Louisiana field measurements compared with prediction equations (20).

EFFECTS OF PIER SHAPE

The pier scour equations presented in the preceding discussion are for rectangular piers. Although there have been investigations (22) of the effects of pier shape, a designer is not likely to be able to take advantage of most of the streamlined shapes because flow directions change as flood levels change. The conservative approach for a designer is to use the projected width of the pier in the direction of flow and to use the rectangular pier equations except for round piers, which scour about 90 percent as much as rectangular piers.

APPLICATION OF PREDICTION EQUATIONS

A consideration that is more important than factors like pier shape and even which equation to use is the manner in which a designer selects design parameters. None of the scour equations is based strictly on field measurements in which the cross section is irregular and flow conditions are nonuniform. Most scour equations are based on uniform, one-dimensional flow conditions. To use an equation effectively, a designer must somehow visualize the field conditions in a manner that resembles the test conditions. The tendency is to use average depths and velocities for an irregular cross section. A more reasonable approach may be to use the depth and velocity in a band of flow just upstream of the pier. Velocity is harder to predict this way, but it can be assumed to follow a logarithmic distribution.

The greatest discrepancy between laboratory conditions and field conditions is in the bed material. Most of the laboratory tests were run with uniform cohesionless soils. General practice in design is to use these equations as a conservative estimate if a soil is considered erodible. If a soil is considered nonerodible, scour is assumed to be zero. The problem is the lack of something in between, but that is a problem that must remain unsolved until someone devises a plan to deal with the effects of different soil properties.

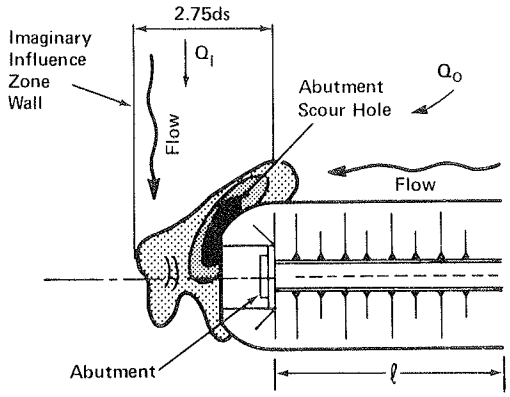

FIGURE 9 Typical scour at an abutment (18).

ABUTMENT SCOUR

Abutment scour occurs when overbank flow reenters the main channel and sets up large vortices in the bridge opening. Laursen reasoned that the continuity equation for sediment flow needed to be satisfied and conceptualized an approach abutment at the symmetrical half of a wide pier. Typically water in the main channel is transporting sediment at capacity, and water in the overbank area is relatively free of sediment (so-called clear water). When these flows mix at the abutment, there is a deficiency of sediment and this deficiency is satisfied with material from the abutment scour hole. Laursen realized that the mixing occurred primarily in the zone of flow near the bank and that it was not reasonable to dilute the overbank flow with the entire channel flow because the computed scour would decrease directly with the width of the bridge opening. He defined an influence zone as shown in Figure 9 and derived the abutment scour equations based on no mixing outside the influence zone. The width of the influence zone is 2.75 times the depth of the abutment scour hole, which means that Laursen's

abutment scour equations must be implicit equations.

For the typical case where the flow in the influence zone (Q_I) transports sediment and flow from the overbank area (Q_0) is clear water, Laursen's sediment continuity equation yields the following:

$$(Q_0/Q_I)\,2.75(d_s/y) = 2.75(d_s/y)\left\{[(1/r)(d_s/y)+1]^{7/6}-1\right\} \quad (13)$$

The recommended value for r in this case is 4.1.

For the special situation in which both the flow in the influence zone and the overbank flow are clear water, which could occur at relief bridges or where the abutments are set back far enough on the floodplain, Laursen's equation yields the following:

$$\ell/y = 2.75\,(d_s/y)\left(\left\{[(1/r)(d_s/y)+1]^{7/6}/(\tau_0/\tau_c)^{1/2}\right\}-1\right) \quad (14)$$

where

ℓ = length of the approach embankment,
$\tau_0/\tau_c = V^2/120d_{50}^{2/3}y^{1/3}$,
r = 4.1 for low velocities, and
r = 11.5 for high velocities.

d_s is the deepest part of the scour hole, which is assumed at the edge of the abutment.

Laursen's r-value essentially distributes the scour in a triangular hole. The larger the r-value, the larger the ratio of the deepest scour depth (d_s) to the average scour depth in the influence zone.

CSU relationships for abutment scour are as follows:

$$d_s/y = 1.1\,(\ell/y)^{0.40}\,F^{0.33} \quad \text{if } \ell/y < 25 \quad (15a)$$

$$d_s/y = 4F^{0.33} \quad \text{if } \ell/y > 25 \quad (15b)$$

There are no field data to compare with the abutment scour equations, but because there are only two equations to consider, it is reasonable to compute with both of them. A designer would have to use the equation that suited his tendency to be more or less conservative.

RECOMMENDATIONS

There is still a need to document field data for both pier scour and abutment scour. Field data should be collected during floods and should as a minimum include a full cross section at several flood stages. Data should be collected by individuals who are knowledgeable about how laboratory tests are conducted and who can document sufficient information to make valid comparisons with predictions.

Although there are a large number of pier scour equations, they can be narrowed down to three or four without much loss in data used in derivations. The recommended equations are those by Laursen, Jain, Shen, and CSU, Equations 5, 7, 11, and 12, respectively.

There are only two equations (13 and 15) to consider for abutment scour if the main channel flow in the zone next to the abutment (the influence zone) is transporting sediment. There is only one equation (14) for abutment scour for relief bridges and large abutment setback where flow in that influence zone is not transporting sediment.

REFERENCES

1. F.M.M. Chang. Statistical Summary of the Cause and Cost of Bridge Failures. Report FHWA-RD-75-97. FHWA, U.S. Department of Transportation, Sept. 1973.
2. Nomenclature for Hydraulics. Manuals and Reports on Engineering Practice 43. ASCE, New York, 1962.
3. Sedimentation Engineering. Manuals and Reports on Engineering Practice 54. ASCE, New York, 1975.
4. J.C. Brice and J.C. Blodgett. Countermeasures for Hydraulic Problems at Bridges, Vol. 1. Report FHWA-RD-78-162. FHWA, U.S. Department of Transportation, Sept. 1978.
5. Scour at Bridge Waterways. NCHRP Synthesis of Highway Practice 5. HRB, National Research Council, Washington, D.C., 1970.
6. Scour and Deposition in Rivers and Reservoirs. Computer Program HEC-6. Hydrologic Engineering Center, U.S. Army Corps of Engineers, Davis, Calif., March 1977.
7. An Evaluation of Flood Level Prediction Using Computer-Based Models of Alluvial Rivers. Committee on Hydrodynamic Computer Models for Flood Insurance Studies, National Research Council, Washington, D.C., 1983.
8. G.R. Hopkins, R.W. Vance, and B. Kasraie. Scour Around Bridge Piers. Report FHWA-RD-79-103. FHWA, U.S. Department of Transportation, 1980.
9. A.G. Anderson. A Report on Scour at Bridge Waterways: A Review. Report FHWA-RD-75-89. FHWA, U.S. Department of Transportation, Nov. 1974.
10. S.C. Jain and E.E. Fischer. Scour Around Circular Bridge Piers at High Froude Numbers. Report FHWA-RD-79-104. FHWA, U.S. Department of Transportation, April 1979.
11. M. Ahmad. Discussion of "Scour at Bridge Crossings," by E.M. Laursen. Transactions of the ASCE, Vol. 127, 1962, pp. 198-206.
12. H.N.C. Bruesers. Scour Around Drilling Platforms. Bulletin Hydraulic Research 1964 and 1965, Vol. 19, p. 276. International Association for Hydraulic Research, Delft, Netherlands, 1965.
13. S.V. Chitale. Discussion of "Scour at Bridge Crossings," by E.M. Laursen. Transactions of the ASCE, Vol. 127, 1962, pp. 191-196.
14. C.C. Inglis. The Behavior and Control of Rivers and Canals. Research Publication 13, Central Power, Irrigation and Navigation Report. Poona Research Station, India, 1949.
15. E.M. Laursen. Scour at Bridge Crossings. Bull. 8. Iowa Highway Research Board, Iowa City, Aug. 1958; Transactions of the ASCE, Vol. 127, 1962.
16. E.M. Laursen. An Analysis of Relief Bridge Scour. Journal of the Hydraulics Division of the ASCE, Vol. 89, No. HY3, May 1969.
17. H.W. Shen, V.R. Schneider, and S.S. Karaki. Local Scour Around Bridge Piers. Journal of the Hydraulics Division of the ASCE, Vol. 89, Nov. 1969.
18. Highways in the River Environment: Hydraulic and Environmental Design Considerations. FHWA Training and Design Manual. Civil Engineering Department, Colorado State University; FHWA, U.S. Department of Transportation, May 1975.
19. E.M. Laursen. Scour Around Bridge Piers and Abutments. Bull. 4. Iowa Highway Research Board, Iowa City, May 1956.

20. F.F.M. Chang. Scour at Bridge Piers: Field Data. Report FHWA-RD-79-105. FHWA, U.S. Department of Transportation, June 1979.

21. E.M. Laursen. Model-Prototype Comparison of Bridge-Pier Scour. HRB Proc., Vol. 34, 1955, pp. 188-193.

22. H.W. Shen and V.R. Schneider. Effect of Bridge Pier Shape on Local Scour. Presented at ASCE National Meeting on Transportation Engineering, Boston, Mass., July 13-17, 1970.

Publication of this paper sponsored by Committee on Hydrology, Hydraulics and Water Quality.

Riprap Stability Analysis

M.A. STEVENS, DARYL B. SIMONS, and E.V. RICHARDSON

ABSTRACT

In the absence of wave and seepage forces, the stability of rock riprap particles on a side slope is a function of the magnitude and direction of the stream velocity next to the particles, the angle of the side slope, and the characteristics of the rock, including the geometry, angularity, and density. A method of designing riprap was developed based on a functional relation among the variables. Rock particles on side slopes tend to roll rather than to slide. Therefore, it is appropriate to consider the stability in terms of moments about a point of rotation. The functional relation has its basis in the balance of moments about a point of rotation at incipient motion between the forces trying to move the particle and the forces resisting movement. A safety factor was developed that is the ratio of the resisting moments to the moments tending to move the particle of riprap. This safety factor takes into consideration the side slope of the bank being protected; the size, density, and angle of repose of the rock; and the lift and drag forces of the following water. The method is described, examples of its use are given, and it is compared with other methods developed by the Bureau of Public Roads, U.S. Army Corps of Engineers, California Division of Highways, Bureau of Reclamation, the ASCE Task Committee on Sedimentation, and others.

Highway crossings or encroachments of rivers usually require some form of protection for the encroaching embankments, bridge abutments, and adjacent riverbanks. Long approach embankments across the floodplain may need protection also. Usually this protection is provided by rock riprap because of its low cost, flexibility, and ease of repair. The important factors in designing rock riprap are durability, size, shape, angularity, angle of repose, and density of the rock; side slope of the bank line being protected; wave action; seepage forces; and flow velocity (both magnitude and direction) close to the rock. The Bureau of Public Roads provided methods of designing riprap or bank protection in Hydraulic Engineering Circular 15. In the 1970s, the problem of riprap design for side-slope protection of banks in contact with flowing water at river crossing encroachments was investigated by Colorado State University for the Wyoming State Highway Department in cooperation with FHWA, U.S. Department of Transportation (1-6). As a result of this investigation a method of riprap design was developed based on a functional relation between the forces moving the particle and those resisting these forces. The method defines a safety factor for the rock riprap, which is defined as the ratio of the moments of the forces resisting rotation of a rock particle and of the riprap to the moments of forces tending to dislodge the particle. The critical condition is the flow for which incipient motion occurs. This critical condition has a safety factor of 1. If the moments of the forces tending to dislodge a particle are larger than the resisting moments, the safety factor is less than 1, rocks are removed from the riprap layer, and failure of the protection may occur. When the safety factor is greater than 1, the riprap is safe from failure.

The equations are developed from theoretical considerations and existing empirical information. The hydrodynamic lift (7,8) and drag forces (9) of the fluid on the rock, the submerged weight and angle of repose of the rock, and the Shields criteria as modified by Gessler (10) for incipient particle motion are considered. The magnitude of the lift force is proportional to the magnitude of the drag force but is perpendicular to the drag force. This is important in analyzing particle stability (11). The theoretical development, a design example, and calculation of the safety factor of several recommended design methods are presented.

THEORETICAL DEVELOPMENT

In the absence of waves and seepage, the stability of rock riprap particles on a side slope is a function of the magnitude and direction of the stream velocity in the vicinity of the particles, the angle of the side slope, and the characteristics of the rock, including the geometry, angularity, and density. In the following development of the safety factor several flow conditions are considered: oblique flow on a side slope, horizontal flow on a

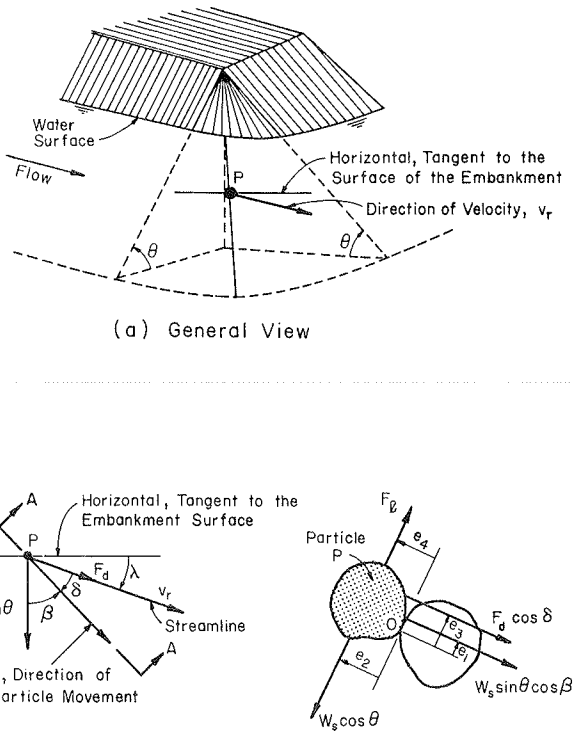

FIGURE 1 Diagrams for the riprap stability conditions.

side slope, flow on a plane sloping bed, and flow on a horizontal bed. The development was previously presented by Stevens et al. (6).

Oblique Flow on a Side Slope

The fluid forces on a rock particle identified as P in Figure 1 result primarily from fluid pressures around the surface of the particles. The lift force (F_ℓ) is defined here as the fluid force normal to the plane of the embankment. The drag force (F_d) is defined as the fluid force acting on the particle in the direction of the velocity field in the vicinity of the particle. Both forces are zero when the fluid velocity is zero.

Gravity acts on the particle and on the fluid surrounding it. The effect of gravity on the particle and fluid is a force equal to the submerged weight of the rock particle (W_s). Forces act at the contact points between particle P and its immediate neighbors. Rotation occurs at one of these points of contact. The forces at the other points of contact are neglected here. The assumption is warranted for mild side slopes, say, 2.5H to IV. At steeper slopes, many particles are subjected to a significant force from particles upslope. This force produces a stabilizing moment on the particle. It is the most prominent force when rocks are hand placed to form a vertical wall.

Rock particles in contact with water tend to roll rather than slide, so it is appropriate to consider the stability of rock particles in terms of moments about a point of rotation. In Figure 1b, the direction of movement is defined by the vector R. The point of contact about which rotation in the R direction occurs is identified as point O in Figure 1c.

The forces F_d and $W_s \sin\theta$ act in the plane of the side slope as shown in Figure 1b. The angle θ is the side-slope angle. The lift force and the component of submerged weight ($W_s \cos\theta$) act normal to the side slope as shown in Figure 1c. There is a balance of moments of these forces about the point of rotation at incipient motion such that

$$e_2 W_s \cos\theta = e_1 W_s \sin\theta \cos\beta + e_3 F_d \cos\delta + e_4 F_\ell \quad (1)$$

The moment arms (e_1, e_2, e_3, and e_4) are defined in Figure 1c; angles and forces are defined in Figure 1b.

The factor of safety (SF) of the particle P against rotation is defined as the ratio of the moments resisting particle rotation to the moments tending to rotate the particle out of the bank, or

$$SF = e_2 W_s \cos\theta / (e_1 W_s \sin\theta \cos\beta + e_3 F_d \cos\delta + e_4 F_\ell) \quad (2)$$

With no flow and a side slope equal to the angle of repose ϕ for the rock particles, SF = 1, $\theta = \phi$, β and $\lambda = 0$ degrees, $\delta = 90 - \lambda - \beta = 90$ degrees (see Figure 1b) and Equation 2 reduces to

$$(e_2 W_s / e_1 W_s) / (\cos\theta / \sin\theta) = 1 \quad (3)$$

or

$$\tan\phi = e_2 / e_1 \quad (4)$$

That is, the ratio of the moment arms (e_2/e_1) is characterized by the natural angle of repose (ϕ). Further, it is assumed that the ratio e_2/e_1 is invariant to the direction of particle motion indicated by the angle β.

If both numerator and denominator are divided by $e_2 W_s$, Equation 2 is transformed into

$$SF = \cos\theta \tan\phi / (\eta' \tan\phi + \sin\theta \cos\beta) \quad (5)$$

in which

$$\eta' = (e_3 F_d / e_2 W_s) \cos\delta + (e_4 F_\ell / e_2 W_s) \quad (6)$$

The variable η' is called the stability number for the particles on the embankment side slope and, as will be shown, is related to the Shields parameter,

$$T = \tau_0 / (S_s - 1)\gamma D \quad (7)$$

where

τ_0 = average tractive force on the side slope in the vicinity of particle P,
S_s = specific weight of the particle,
γ = unit weight of water, and
D = diameter of the rock particles.

The angle λ shown in Figure 1b is the angle between the horizontal and the velocity vector (and drag force) measured in the plane of the side slope. Then

$$\delta = 90 - \lambda - \beta \quad (8)$$

so

$$\cos\delta = \cos(90 - \lambda - \beta) = \sin(\lambda + \beta) \quad (9)$$

Also,

$$\sin\delta = \sin(90 - \lambda - \beta) = \cos\lambda \cos\beta - \sin\lambda \sin\beta \quad (10)$$

It is assumed that the direction of particle motion is along R. This assumption means that the moments of the drag force F_d and the component of submerged weight $W_s \sin\theta$ normal to the path R are balanced. Thus,

$$e_3 F_d \sin\delta = e_1 W_s \sin\theta \sin\beta \quad (11)$$

It follows then from Equations 10 and 11 that

$$\sin\beta = e_3 F_d \sin\delta / e_1 W_s \sin\theta = e_3 F_d (\cos\lambda \cos\beta - \sin\lambda \sin\beta)/e_1 W_s \sin\theta \quad (12)$$

or

$$\tan\beta = \cos\lambda / [(e_1 W_s / e_3 F_d) \sin\theta + \sin\lambda] \quad (13)$$

From Equation 6, the stability number η for particles on a plane bed ($\theta = 0$) with $\delta = 0$ would be

$$\eta = (e_3 F_d / e_2 W_s) + (e_4 F_\ell / e_2 W_s) \quad (14)$$

Equation 5 becomes

$$SF = 1/\eta \quad (15)$$

For incipient-motion conditions for flow over a plane bed, SF = 1.0 by definition, so from Equation 15, $\eta = 1.0$. When the flow along the bed is fully turbulent, the Shields parameter for incipient motion has the value of 0.047 according to Gessler (10). That is, with $\eta = 1.0$,

$$\tau_0 / (S_s - 1)\gamma D = 0.047 \quad (16)$$

For flow conditions other than incipient the stability number is

$$\eta = 21 \tau_0 / (S_s - 1)\gamma D \quad (17)$$

For convenience, let

$$M = e_4 F_\ell / e_2 W_s \quad (18)$$

and

$$N = e_3 F_\ell / e_2 W_s \quad (19)$$

In terms of these new variables, Equation 6 becomes

$$\eta' = M + N \cos\delta \quad (20)$$

and Equation 14 becomes

$$\eta = M + N \quad (21)$$

Thus, η' and η are related by the following expression:

$$\eta'/\eta = [(M/N) + \cos\delta] / [(M/N) + 1] \quad (22)$$

Equation 22 is represented graphically in Figure 2.

The problem is to select the proper value of the ratio M/N so that the stability factor on a side slope (η') can be related to the stability factor on a plane horizontal bed (η), which in turn is related to the Shields parameter. The assumption that the drag force F_d is zero means that M/N is infinite, β is zero, and $\eta' = \eta$. The assumption of zero lift force F_ℓ means that M/N is zero and $\eta'/\eta = \cos\delta$.

In considering incipient motion of riprap particles, the ratios F_ℓ/F_d and e_4/e_3 vary depending on the turbulent conditions of the flow and the interlocking arrangement of the rock particles. In referring to Figure 1c, assume that

$$e_4/e_3 \simeq 2 \quad (23)$$

Then a choice for F_ℓ/F_d is

$$F_\ell/F_d \simeq 1/2 \quad (24)$$

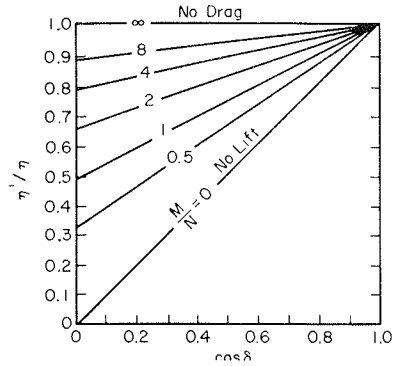

FIGURE 2 Ratio of stability factors.

so that

$$M/N = (e_4/e_3)/(F_\ell/F_d) \simeq 1 \quad (25)$$

With M/N = 1, Equation 22 becomes

$$\eta'/\eta = (1 + \cos\delta)/2 \quad (26)$$

or by using Equation 9,

$$\eta'/\eta = [1 + \sin(\lambda + \beta)]/2 \quad (27)$$

In Equation 13 the term $e_1 W_s / e_3 F_d$ can be written according to Equations 4 and 19 as follows:

$$e_1 W_s / e_3 F_d = (e_2 W_s / e_3 F_d)/(e_1/e_2) = (1/N)(1/\tan\phi) \quad (28)$$

For M/N = 1, Equation 21 becomes

$$N = \eta/2 \quad (29)$$

If we substitute Equations 28 and 29 into Equation 13, the expression for β becomes

$$\tan\beta = \cos\lambda / [(2 \sin\theta/\eta \tan\phi) + \sin\lambda] \quad (30)$$

In summary, SF for rock riprap on side slopes where the flow has a nonhorizontal velocity vector is related to properties of the rock, side slope, and flow by Equation 5, in which

$$\beta = \tan^{-1}\left\{\cos\lambda / [(2 \sin\theta/\eta \tan\phi) + \sin\lambda]\right\} \quad (31)$$

η is given by Equation 17, and

$$\eta' = \eta \left\{[1 + \sin(\lambda + \beta)]/2\right\} \quad (32)$$

Given a representative rock size D of specific weight S_s and angle of repose ϕ and given a velocity field at an angle λ to the horizontal producing a tractive force τ_0 on the side slope of angle θ, the set of four equations (Equations 5, 17, 31, and 32) can be solved to obtain SF. If SF is greater than unity, the riprap is safe from failure; if SF is unity, the rock is at the condition of incipient motion; if SF is less than unity, the riprap will fail.

Horizontal Flow on a Side Slope

In many circumstances, the flow on the side slope is nearly horizontal; i.e., $\lambda \simeq 0$. Then Equations 17 and 31 reduce to

$$\beta = \tan^{-1}(\eta \tan\phi / 2 \sin\theta) \quad (33)$$

and

$$\eta' = \eta\,[(1 + \sin\beta)/2] \tag{34}$$

When Equations 33 and 34 are substituted into Equation 5, the expression for SF for horizontal flow on a side slope is

$$SF = (S_m/2)\,[(\xi^2 + 4)^{1/2} - \xi] \tag{35}$$

in which

$$\xi = S_m\,\eta\sec\theta \tag{36}$$

and

$$S_m = \tan\phi/\tan\theta \tag{37}$$

The term S_m is SF for riprap on a side slope with no flow. Unless the flow is up the slope, SF for the riprap cannot be greater than S_m.

If Equations 35 and 36 are solved for η,

$$\eta = [(S_m^2 - SF^2)/(SF)\,S_m^2]\,\cos\theta \tag{38}$$

Flow on a Plane Sloping Bed

Flow over a plane bed at a slope of α degrees in the downstream direction is equivalent to oblique flow on a side slope with $\theta = \alpha$ and $\lambda = 90$ degrees. Then, according to Equation 31, $\beta = 0$ and from Equation 32

$$\eta' = \eta\left\{[1 + \sin(90^\circ + 0^\circ)]/2\right\} = \eta \tag{39}$$

It follows from Equation 5 that

$$SF = \cos\alpha\,\tan\phi/(\eta\,\tan\phi + \sin\alpha) \tag{40}$$

for flow on a plane bed sloping α degrees to the horizontal. Alternatively solving for η in Equation 40,

$$\eta = \cos\alpha\,[(1/SF) - (\tan\alpha/\tan\phi)] \tag{41}$$

Flow on a Horizontal Bed

For fully developed rough turbulent flow over a plane horizontal bed ($\alpha = 0$) of rock riprap, Equation 40 reduces to

$$SF = 1/\eta \tag{42}$$

If the riprap particles are at the condition of incipient motion, SF = 1, so $\eta = 1$ and the Shields criterion for the initiation of motion is obtained from Equation 16.

Representative Grain Size for Riprap

In using Equations 5, 17, 31, and 32 to determine SF for a given riprap or to design a riprap with a preselected SF, the magnitude of a representative grain size (D) is needed.

In full-scale experiments with rock riprap below culvert outlets, Stevens (5) developed the following expression for a representative grain size for well-graded materials:

$$D = \left(\sum_{i=1}^{10} D_i^3/10\right)^{1/3} \tag{43}$$

in which

$$D_{(1)} = (D_0 + D_{10})/2,$$

$$D_{(2)} = (D_{10} + D_{20})/2 \ldots D_{(10)} = (D_{10} + D_{100})/2$$

The terms D_0, D_{10}, ..., D_{100} are the sieve diameters of the riprap for which 0 percent, 10 percent, ..., 100 percent of the material is finer by weight.

The concept of a representative grain size for riprap is simple. A uniformly graded riprap with a median size (D_{50}) (riprap with a narrow range of sizes) scours to a greater depth than a well-graded mixture with the same median size (Figure 3). Riprap of uniform size scours to a depth at which the velocity is slightly less than that required for the transportation of D_{50} rock. The well-graded riprap, on the other hand, develops an armor plate. That is, some of the finer materials, including sizes up to D_{50} and larger, are transported by the high velocities, leaving a layer of large rock sizes that cannot be transported under the given flow conditions. Thus, the size of rock representative of the stability of the riprap is determined by the larger sizes of rock. The representative grain size (D) given in Equation 43 for riprap is larger than the median rock size (D_{50}). Stevens (5) compared the scour produced in two widely different gradations of riprap (shown in Figure 3) having the same median diameter, D_{50} = 1.2 in.

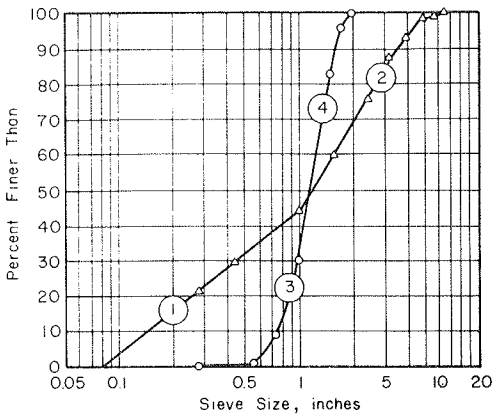

FIGURE 3 Gradation curves.

To illustrate the effect of the larger sizes on the representative grain size, D was computed for four gradations by using Equation 43. The representative grain size (D) and the ratio of representative diameter to median diameter (D/D_{50}) are given as follows for the four gradations (refer to Figure 3):

Curve	D (in.)	D/D_{50}
1-2	2.70	2.25
3-2	2.71	2.26
1-4	1.21	1.01
3-4	1.27	1.06

Inspection of the foregoing values shows that the larger sizes in the gradation have a dominant effect in the determination of the representative grain size. The large sizes of a gradation are the important sizes for stability.

Riprap Gradation and Placement

Riprap gradation should follow a smooth size-distribution curve such as that shown in Figure 4. The ratio of maximum size to median size (D_{50}) should be about 2.0 and the ratio between median size and the 20 percent size should also be about 2.0. This means that the largest stones would be about 6.5

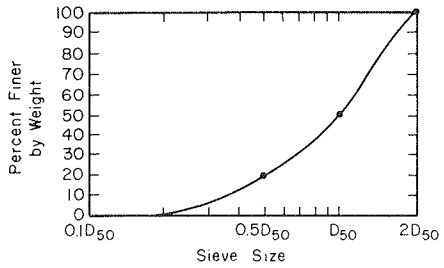

FIGURE 4 Suggested gradation for riprap.

times the weight of the median size and small sizes would range down to gravels. The representative rock size (D) for the gradation shown in Figure 4 is $1.25D_{50}$ (calculated by using Equation 43), which is approximately equal to the D_{67}.

With a distributed size range, the interstices formed by the larger stones are filled with the smaller sizes in an interlocking fashion, preventing formation of open pockets. Riprap consisting of angular stones is more suitable than that consisting of rounded stones. Gradation of the riprap is almost always controlled by visual inspection.

If it is necessary, rock with poor gradation can be employed as riprap provided the proper filter is placed between the riprap and the bank of bed material. Two types of filters are commonly used: gravel filters and plastic filter cloths.

Gravel Filters

A layer or blanket of well-graded gravel should be placed over the embankment or riverbank before riprap placement. Sizes of gravel in the filter blanket should be from 0.187 in. to an upper limit depending on the gradation of the riprap with a maximum size of about 3 to 3.5 in. Thickness of the filter may vary depending on the riprap thickness but should not be less than 6 to 9 in. Filters that are one-half the thickness of the riprap are quite satisfactory. Suggested specifications for gradation are as follows:

1. $D_{50}(\text{filter})/D_{50}(\text{base}) < 40$,
2. $5 < D_{15}(\text{filter})/D_{15}(\text{base}) < 40$, and
3. $D_{15}(\text{filter})/D_{85}(\text{base}) < 5$.

Plastic Filter Cloths

Plastic filter cloths are being used beneath riprap and other revetment materials such as articulated concrete blocks with considerable success. The cloths are generally in rolls 100 ft long and 12 to 18 ft wide. Overlap of 8 to 12 in. is provided with pins at 2- to 3-ft intervals along the seam to prevent separation in the case of settlement of the base material. Some degree of care must be exercised in placing riprap over the plastic cloth filters to prevent damage. Experiments and results with various cloth filters were reported by Calhoun et al. (12), who listed specific manufacturers and brand names. Stones weighing as much as 3,000 lb have been placed on plastic filter cloths with no apparent damage.

Filters can be placed subaqueously by using steel rods as weights fastened along the edges. Additional intermediate weights would assist in sinking the cloth into place. Durability of filter cloths has not yet been established because they have only been in use since around 1967. However, inspections at various installations indicate that little or no deterioration has occurred in the few years that have elapsed for test installations.

Riprap Thickness

If a riprap gradation has a wide range of sizes, the riprap layer must be thick enough to permit the loss of some fines (armorplating) without allowing the protected materials (filter or bank material) to become uncovered. The recommended thickness for the recommended gradation (Figure 4) is D_{100}. For gradations with large gradation coefficients, the thickness must be at least D_{100}. For very large gradation coefficients ($G > 3.0$), the thickness should be increased to $1.5D_{100}$ to provide enough material for armorplating.

Determination of Tractive Force on Riprap

In order to design riprap, it is necessary to be able to determine the tractive force (τ_0) acting on the riprapped bed or bank. This can be done by the relation between the fluid velocity (v) in the vicinity of the riprap and τ_0. For fully turbulent flow, the Prantle-Von Karman relation for the local velocity (v) at a distance (y) above the bed for the hydraulically rough boundary is given by

$$v = 2.5V_* \ln [30.2 (y/D)] \tag{44}$$

in which V_* by definition is the shear velocity:

$$V_* = (\tau_0/\rho)^{1/2} \tag{45}$$

and D is the representative grain size.

If the velocity at a distance y = D above the bed is selected as the reference velocity v_r, then

$$v_r = 2.5V_* \ln 30.2 \qquad v_r = 8.5\ V_* \tag{46}$$

and from Equation 45,

$$\rho v_r^2 = 72\tau_0 \tag{47}$$

This relation is strictly valid only for uniform flow in wide prismatic channels in which the flow is fully turbulent. For the purposes of riprap design, Equation 47 can be employed when the flow is accelerating, for example, on the nose of a spur dike. The equation should not be used where the flow is decelerating or below energy-dissipating structures. In such regions, the shear stress is larger. Also, the equation is not valid for flows with a small y/D ratio.

By substituting Equation 47 into Equation 17, the expression for the stability factor η becomes

$$\eta = 0.30\ v_r^2/(S_s - 1)gD \tag{48}$$

For riprap-size material the depth-averaged velocity in the vertical (V) can be written as follows:

$$V = 2.5V_* \ln [12.3(y_0/D)] \tag{49}$$

in which y_0 is the depth of flow adjacent to the riprap. The ratio of the reference velocity v_r to the depth-averaged velocity is

$$v_r/V = 2.5V_* \ln(30.2)/2.5V_* \ln [12.3\ (y_0/D)] \tag{50}$$

or

$$v_r/V = 3.4/\ln [12.3\ (y_0/D)] \tag{51}$$

Then the expression for the stability factor η can be written in terms of the depth-averaged velocity:

$$\eta = \epsilon V^2/(S_s - 1)gD \quad (52)$$

in which

$$\epsilon = 0.30 \left\{ 3.4/\ln [12.3 (y_0/D)] \right\} \quad (53)$$

The value of ϵ varies from 0.30 for relatively shallow flows to 0.04 for $y_0/D = 1{,}000$ (Figure 5). In Hydraulic Engineering Circular 11 (13) the following expression is used to determine the velocity against the stone:

$$v_s/\bar{V} = 1/[0.958 \log (y_0/D) + 1] \quad (54)$$

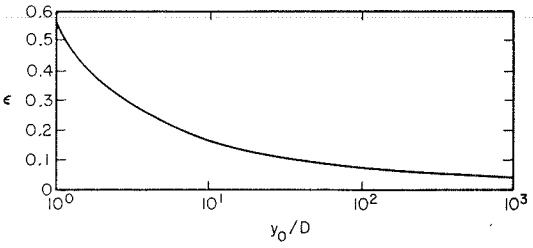

FIGURE 5 Relation between ϵ and y_0/D.

where

v_s = velocity against the stone,
$\bar{V}$ = mean velocity in the channel, and
log = logarithm to the base 10.

In wide channels, the depth-averaged velocity and the mean velocity in the channel are nearly equal; i.e., $\bar{V} \simeq V$. Then the velocity against the stone is related to the reference velocity by the following expression according to the Equations 51 and 54:

$$v_r/v_s = 3.4[0.958 \log (y_0/D) + 1]/\ln [12.3 (y_0/D)] \quad (55)$$

For values of y_0/D between 1×10^0 and 1×10^6, the value of the v_r/v_s is nearly 1.4. By letting $v_r/v_s = 1.4$, the expression for the stability factor η becomes

$$\eta = 0.60\, v_s^2/(S_s - 1)gD \quad (56)$$

In summary, the following expressions for η are employed by definition--Equations 17, 48, 56, and 52--and ϵ is defined in Equation 53.

SAMPLE RIPRAP DESIGN CALCULATIONS

With flow on the nose of an embankment, spur dike, or bridge abutment there can be an appreciable downslope component to the velocity vector. Such a flow is illustrated in Figure 6. If it is assumed that the angle between the horizontal and the velocity vector λ at the point P is 20 degrees, the reference velocity v_r is 6 ft/sec, the embankment side-slope angle θ is 18.4 degrees (3:1 side slope), the specific weight (S_s) is 2.65, the effective rock size (D) is 1.0 ft, and the angle of repose ϕ is approximately 35 degrees, the stability factor is then, from Equation 48, calculated as follows:

$$\eta = 0.30 v_r^2/(S_s - 1)gD = (0.30)(6)^2/[(2.65 - 1)(32.2) \times (1.0)] = 0.203.$$

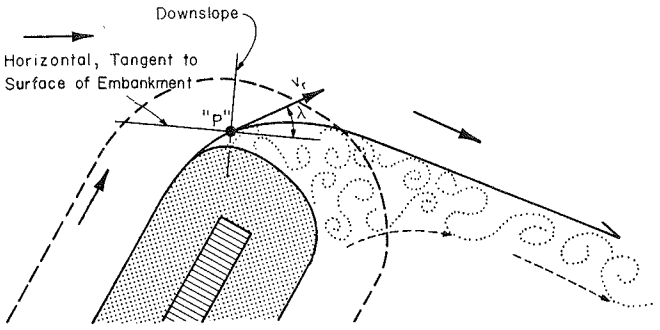

FIGURE 6 Flow around an embankment end.

From Equation 31,

$$\beta = \tan^{-1} \{\cos\lambda/[(2 \sin\theta/\eta \tan\phi) + \sin\lambda]\} = \tan^{-1} \{\cos 20°/[(2 \sin 18.4°/0.203 \tan 35°) + \sin 20°]\} = 11°.$$

From Equation 32,

$$\eta' = \eta \{[1 + \sin (\lambda + \beta)]/2\} = 0.203 \{[1 + \sin (20° + 11°)]/2\} = 0.154.$$

From Equation 5 SF for the rock is calculated as follows:

$$SF = \cos\theta \tan\phi/(\eta' \tan\phi + \sin\theta \cos\beta) = \cos 18.4° \tan 35°/(0.154 \tan 35° + \sin 18.4° \cos 11°) = 1.59.$$

Thus, this rock is more than adequate to withstand the flow velocity.

By repeating the previous calculations for a range of effective rock size D (with $\phi = 35$ degrees), the curve given in Figure 7 is obtained.

Figure 7 shows that the incipient-motion rock size (SF = 1.0) is approximately 0.35 ft and that the maximum SF is less than 2.0 on the 3:1 side slope. The recommended SF for design is 1.0. Thus riprap with a representative size of 0.9 ft is required.

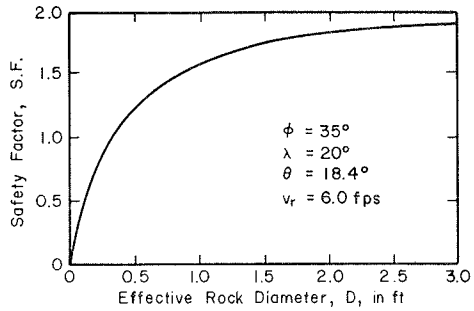

FIGURE 7 SFs for various rock sizes on a side slope.

SF of a particular side-slope riprap design can be increased by decreasing the side-slope angle θ. If the side-slope angle is decreased to zero degrees, Equation 42 is applicable and

$$SF = 1/\eta = 1/0.203 = 4.93.$$

The curve in Figure 8 relates SF and the side-slope angle of the embankment (for $\lambda = 20°$, D = 2.0 ft, and $v_r = 6.0$ ft/sec). The curve is obtained by employing Equations 31, 32, and 5 for various values of θ.

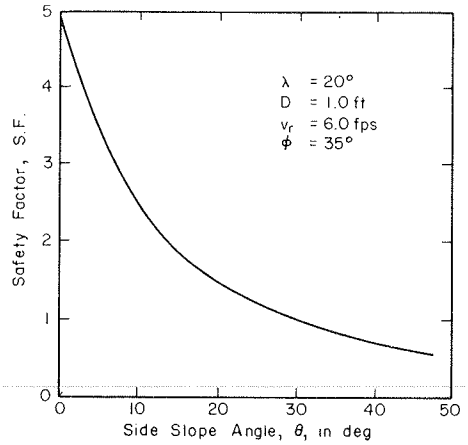

FIGURE 8 SFs for various side slopes.

When the velocity along a side slope has no downslope component (i.e., the velocity vector is along the horizontal), some simple design aids can be developed. Equations 37 and 38 relate SF, stability number, side-slope angle, and angle of repose for this case. The interrelation of the variables in these two equations for the condition indicated is given in Figure 9.

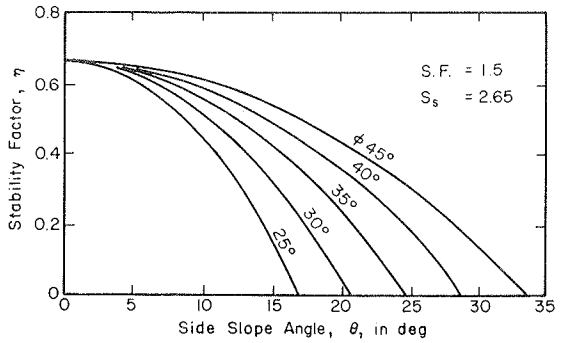

FIGURE 9 Stability factors for an SF of 1.5 for horizontal flow along a side slope θ and angle of repose ϕ.

SAFETY FACTORS FOR EXISTING DESIGN METHODS

In 1976 Stevens et al. (6) compared their riprap stability equations with methods for stability analysis developed by the Bureau of Public Roads (13), Corps of Engineers (14), California Division of Highways (15), ASCE Task Committee on Sedimentation (16), Bureau of Reclamation (17), Lane (9), and Campbell (18). The adequacy of the designs was judged on the basis of the computed values of SF of the riprap size given by the different methods.

In many instances the methods could not be directly compared for all ranges of flow on side slopes. Consequently, the comparisons were made for flow on a plane flat bed. The comparison indicated that in many cases SF for the riprap design was greater than 1. However, in some cases, SFs were less than 1, indicating some loss of material when the riprap was subjected to design flows. The details of the analysis were given by Stevens et al. (6) and are briefly summarized here.

Bureau of Public Roads

Searcy (13) adapted the 1948 ASCE summary on slope production (16). He further recommended riprap gradations patterned after those given by Murphy and Grace (19). These gradations called for an effective diameter of $1.08D_{50}$. The computed SFs for the design curves are less than unity.

U.S. Army Corps of Engineers

It was determined for flow on plane flat beds that the design criteria adopted by the Corps of Engineers (14) have SFs less than unity for relative depths $y_0/D \leq 1.92$ and greater than unity for larger relative depths. SF for flow on side slopes was not analyzed. The Corps no longer uses sheet 712-1 (14) for design. Most highway agencies are now using design procedures based on the laboratory tests of Anderson et al. (20).

California Division of Highways

The California design method (15) gave the same values for SF as those for the Corps of Engineers method for horizontal flow on a plane bed in a wide channel with effective diameter D of $1.2D_{50}$. SF for flow on side slopes could not be directly determined without making many simplifying assumptions.

ASCE Task Committee on Sedimentation

Analysis of this committee's recommendation (16), the design procedure for flow over a horizontal bed in a wide channel, gave an SF 20 percent greater than that for the California Division of Highways' method when the effective diameter of the riprap was $1.2D_{50}$.

Lane's Method

The analysis presented by Stevens et al. (6) determined that Lane's (21,9) design criteria for flow on a plane bed and for horizontal flow along a side slope yield SF less than 1 in most cases.

Campbell's Method

Analysis of Campbell's method (18) indicated that it always gave SFs greater than unity for flow on a plane flat bed. For flow on a side slope no direct comparison was made because his relations are so complex. However, SF for Campbell's sample computation was only 1.015, indicating that his riprap on a 6:1 side slope was at incipient motion.

SUMMARY AND CONCLUSIONS

A method of determining the size of riprap to protect highway embankments along or across rivers is developed. The method takes into consideration the forces tending to move the particle (lift and drag of the fluid and the component of submerged particle weight in the direction of movement) and the resisting force (submerged particle weight in a direction opposing motion). The method involves calculating SF of the riprap, which is defined as the ratio of the moment of the forces resisting motion to the moment of the forces producing movement. It is shown that the maximum safety factor for dumped riprap is $\tan\phi/\tan\theta$, where ϕ is the angle of repose of the riprap and θ is the side slope and this maximum occurs when there is no flow.

Several examples of the design method are given and the method is used to calculate SF of riprap designs given by the Bureau of Public Roads, U.S. Corps of Engineers, California Highway Department, Lane, and others. Because of the differences in the proposed method and these other methods, a direct

calculation of SF often could not be made for all embankment side slopes or flow conditions. Where direct comparisons could be made, SFs in some cases were less than 1, indicating that there could be a loss of riprap under design flow conditions.

REFERENCES

1. G.L. Lewis. Riprap Protection of Bridge Footings. Ph.D. thesis. Colorado State University, Fort Collins, Colo., 1972.
2. D.B. Simons and G.L. Lewis. Flood Protection at Bridge Crossing. Colorado State University, Fort Collins, 1971.
3. D.B. Simons and G.L. Lewis. Flood Protection at Bridge Crossings. Colorado State University, Fort Collins, 1971.
4. D.B. Simons and M.A. Stevens. Stability Analysis for Coarse Granular Material on Slopes. In River Mechanics, Vol. 1 (H.W. Shen, ed.), Water Resources Publications, Denver, Colo., 1971.
5. M.A. Stevens. Scour in Riprap at Culvert Outlets. Ph.D. thesis. Colorado State University, Fort Collins, 1968.
6. M.A. Stevens, D.B. Simons, and G.L. Lewis. Safety Factors for Riprap Protection. Journal of the Hydraulics Division of ASCE, May 1976.
7. E.D.H. Cheng and C.G. Clyde. Instantaneous Hydrodynamic Lift and Drag Forces on Large Roughness Elements in Turbulent Open Channel Flow. In Sedimentation (H.W. Shen, ed.), Water Resources Publications, Denver, Colo., 1972.
8. H.A. Einstein and E.A. Samni. Hydrodynamic Forces on a Rough Wall. Reviews of Modern Physics, Vol. 21, No. 3, 1949, pp. 520-524.
9. E.W. Lane. Design of Stable Channels. Trans. ASCE, Vol. 120, Paper No. 2776, 1955, pp. 1234-1260.
10. J. Gessler. Beginning and Ceasing of Sediment Motion. In River Mechanics, Vol. 1 (H.W. Shen, ed.), Water Resources Publications, Denver, Colo., 1971.
11. B.A. Christensen. Incipient Motion on Cohesionless Channel Banks. In Sedimentation (H.W. Shen, ed.), Water Resources Publications, Denver, Colo., 1972.
12. C.C. Calhoun, Jr., J.R. Compton, and W.E. Strohm, Jr. Performance of Plastic Filter Cloths as a Replacement for Granular Filter Materials. In Highway Research Record 373, HRB, National Research Council, Washington, D.C., 1971, pp. 74-85.
13. J.K. Searcy. Use of Riprap for Bank Protection. Hydraulic Engineering Circular 11. Office of Engineering and Operations, Bureau of Public Roads, FHWA, U.S. Department of Transportation, June 1967.
14. Stone Stability: Velocity Versus Stone Diameter. Sheet 712-1 (revised). Civil Works Investigations, Hydraulic Design Criteria, U.S. Army Corps of Engineers, Waterways Experiment Station, Vicksburg, Miss., Aug. 1970.
15. Bank and Shore Protection in California Highway Practice. Department of Public Works, California Division of Highways, Sacramento, Nov. 1959.
16. ASCE Subcommittee on Slope Protection. Review of Slope Protection Methods. Trans. ASCE, Vol. 74, 1948, pp. 845-866.
17. Hydraulic Design of Stilling Basins and Energy Dissipators. Engineering Monograph 25. Technical Information Branch, Bureau of Reclamation, Denver Federal Center, Denver, Colo., 1958.
18. F.B. Campbell. Hydraulic Design of Rock Riprap. Miscellaneous Paper 2-777. U.S. Army Corps of Engineers, Waterways Experiment Station, Vicksburg, Miss., Feb. 1966.
19. T.E. Murphy and J.L. Grace. Riprap Requirements for Overflow Embankments. In Highway Research Record 30, HRB, National Research Council, Washington, D.C., 1963, pp. 47-55.
20. A.G. Anderson, A.S. Paintal, and J.T. Davenport. Tentative Design Procedure for Riprap-Lined Channels. NCHRP Report 108. HRB, National Research Council, Washington, D.C., 1970.
21. A.C. Carter, E.J. Carlson, and E.W. Lane. Critical Tractive Forces on Channel Side Slopes in Coarse Noncohesive Material. Hydraulic Laboratory Report HYD.-366. Bureau of Reclamation, U.S. Department of the Interior, 1953.

Publication of this paper sponsored by Committee on Hydrology, Hydraulics and Water Quality.

Analysis of Commonly Used Riprap Design Guides Based on Extended Shields Diagram

HSIEH WEN SHEN and SANG-YI WANG

ABSTRACT

River and coastal engineers are often faced with the task of selecting the appropriate riprap size for bank protection. Several empirical formulae based on field and laboratory tests have been suggested for selecting the maximum size and gradation size distribution of the riprap. To facilitate riprap size selection, several commonly used riprap design guides presented by the U.S. Army Corps of Engineers (for shore protection), the U.S. Bureau of Reclamation (for bank protection), and the California Department of Transportation (for both shore and bank protection) as well as guides from projects sponsored by the FHWA (for energy dissipators related to both culverts and channels) are analyzed. It is found that all these design guides are compatible and agree with the extended Shields incipient motion diagram for large sediment sizes.

Several riprap design guides have been presented by various agencies [State of California (1), U.S. Army Engineering Coastal Research Center (2), U.S. Department of Transportation (3-5), U.S. Bureau of Reclamation (6,7)]. The main purpose of this study is to compare these design guides with an extended Shields diagram based on recent Chinese data for large sediment particles.

EXTENDED SHIELDS DIAGRAM FOR LARGE SEDIMENT SIZES

Riprap is used to protect riverbanks and shorelines, and the riprap size should be selected so that it cannot be moved by flows and waves. The Shields diagram (8), shown in Figure 1, has been generally recognized as a valid indication of the incipient motion of sediment particles. In this figure, K* is defined as the ratio between the forces acting on the particles and the resistance force of the particles to be moved:

$$K^* = \tau_c/(\gamma_s - \gamma_f)d \tag{1}$$

where τ_c is the time average shear stress, γ_s and γ_f are the specific weights for the sediments and fluid, respectively, and d is the diameter of the dominant sediment size.

Re_* in Figure 1 is the Reynolds number based on sediment particle sizes. This number is expressed as

$$Re_* = u_* d/\nu \tag{2}$$

where u_* is the shear velocity, d is the diameter of the sediment particle size, and ν is the kinematic viscosity of the fluid. The Reynolds number Re_* can also be treated as the ratio between the diameter of the sediment and the viscous sublayer.

If the riprap is selected so that it cannot be moved by the designed flows and waves, the riprap size should be large enough so that K* is below the Shields curve. The Shields diagram was developed for unidirectional flows only. If one uses the orbital wave velocity as the unidirectional flow velocity, the incipient motion of sediment particles under wave actions can be compared with the Shields diagram. Data and analysis for incipient sediment motion under wave action by Hou (9), Madsen and Grant (10), Bagnold (11), Komar and Miller (12), and Manohar (13) are shown on Figure 1. The averages of all the data points for wave motion seem to agree with the incipient motion curve by Shields for

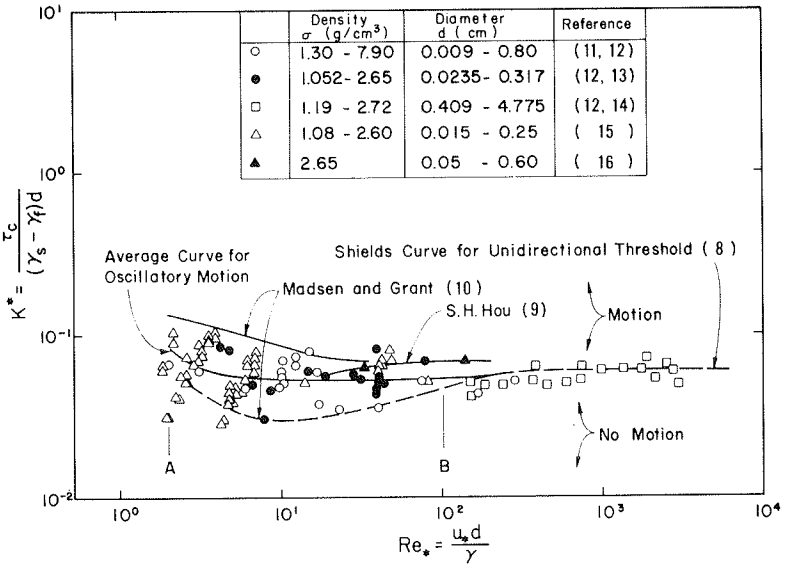

FIGURE 1 Comparison of incipient sediment motion under wave action.

unidirectional flows. The incipient motion for sediment particles under an impinged jet for high turbulent flows by Poreh and Hefez (14) was also plotted on this figure.

To use the Shields diagram to analyze various riprap guides, one must extend the diagram to large sediment sizes because the Re_* numbers for riprap are in the range of 10^4 to 10^7. For large sediment particles (Reynolds numbers 10^4 to 10^5), the drag coefficient decreases sharply. As stated by Schlichting (17):

> The influence of roughness on form drag can be summarized as follows: bodies with sharp edges, such as e.g. a flat plate at right angles to the stream, are quite insensitive to surface roughness, because the point of transition is determined by the edges. On the other hand, the drag of bluff bodies, such as circular cylinders, is very sensitive to roughness. The value of the critical Reynolds number for which the drag shows a sudden drop depends to a marked degree on the roughness . . . (p. 664).

According to this statement, the shape of the riprap should influence the drag coefficient of the sediment particles because the sediment particle shape changes the roughness of the sediment bed.

If the drag coefficient of sediment particles decreases, the drag force acting on the particle by flow will decrease and greater flows will be required to move the sediment particles. Thus the incipient motion curve of sediment particles should be moved upward (critical K* value for incipient motion should increase).

It is difficult to predict the increase in K* associated with an increase in the Reynolds number because the lift and drag forces on a sediment particle are strongly influenced by the orientation and composition of surrounding sediment particles and the intensity of the turbulence.

In China several experiments were conducted in flood channels to investigate the incipient motion of large sediment sizes. Tables 1 and 2 give data collected in Hopei and Chekiang Provinces (18). The limited data shown in Figure 2 indicate that K* increases approximately fourfold from 0.062 to 0.25 as Re_* increases from 10^4 to 10^6. This amount of increase in K* is in the same range as is the decrease in C_D, as shown in Schlichting (17). No data are available to define the dashed line for Re_* between 10^4 and 5×10^5. One may conclude from the Chinese experiments that

$$\text{For } 100 < Re_* < 1 \times 10^5 \quad \tau_c = 0.062(\gamma_s - \gamma_f)d \tag{3}$$

TABLE 1 Incipient Motion of Large Particles According to Wang (19)

Run No.	Data Source	Flow Depth (cm)	Energy Slope	Shear Stress (gm/cm^2)	Specific Particle Weight (gm/cm^3)	Median Particle Size (cm)	K*	Reynolds No.
1	Ku-Long mountain reservoir	108.0	0.014	1.51	2.65	10.7	0.086	0.412
2	Ku-Long mountain reservoir	108.0	0.011	1.19	2.65	10.7	0.067	0.397
3	Bu-Cheng River	95.0	0.009	0.855	2.65	9.65	0.054	0.280
4	Bu-Cheng River	95.0	0.0108	1.03	2.65	9.65	0.065	0.306
5	Bu-Cheng River	95.0	0.0104	0.988	2.65	9.65	0.062	0.300
6	Bu-Cheng River	80.0	0.0102	0.816	2.65	7.37	0.067	0.209
7	Bu-Cheng River	80.0	0.0081	0.648	2.65	7.37	0.0533	0.186
8	Bu-Cheng River	80.0	0.0094	0.752	2.65	7.37	0.062	0.200

TABLE 2 Incipient Motion of Large Particles According to Li (18)

Run No.	Flow Depth (cm)	Energy Slope	Shear Stress (gm/cm^2)	Specific Particle Weight (gm/cm^3)	Median Particle Size (cm)	K*	Reynolds No.
1	370.	0.06	22.2	2.70	40.0	0.326	5.90
2	330.	0.05	16.5	2.70	40.0	0.243	5.09
3	350.	0.05	17.5	2.70	40.0	0.257	5.24
4	300.	0.04	12.0	2.70	40.0	0.176	4.34
5	290.	0.04	11.6	2.70	40.0	0.171	4.27
6	260.	0.04	10.4	2.70	40.0	0.153	4.04

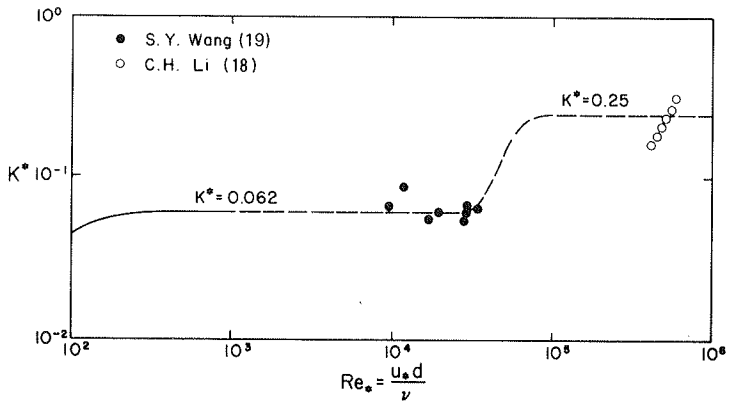

FIGURE 2 Incipient motion of large sediment particles.

and

$$\text{For } Re_* \sim 10^5 \text{ (or perhaps} > 10^5), \tau_c = 0.25\,(\gamma_s - \gamma_f)d \quad (4)$$

INCIPIENT MOTION AND RIPRAP DESIGN

Channel Revetments Under Unidirectional Flow

In the design of channel revetments, the armor stone along the channel slope should be able to withstand anticipated current velocity. The equivalent minimum size of stone diameter, d, may be calculated by the following equation that is based on an equation by the U.S. Army Coastal Engineering Research Center (CERC) (2).

$$v/(2gd)^{1/2} = y\,[(\gamma_s - \gamma_f)/\gamma_f]^{1/2}\,(\cos\theta - \sin\theta)^{1/2} \quad (5)$$

where

v = velocity of water acting directly on stone, expressed as

$$v = 5.75\,u_*\,[\log 12.27\,(h/d)] \quad (6)$$

h = flow depth;
θ = angle of structure slope with the horizontal in the direction of flow; and
y = Isbash constant, 1.20 and 0.86 for embedded and nonembedded stone, respectively.

Combining Equations 5 and 6 for y = 0.86 (nonembedded stone) and for θ = 0°, one obtains

$$K^* = 0.0447/[\log 12.27\,(h/d)]^2 \quad (7)$$

The result for a nonembedded stone condition calculated by Equation 7 is shown in Figure 3 by the solid curves.

The equivalent median stone diameter sizes are given by the U.S. Department of Transportation (U.S. DOT) in graphic form in Hydraulic Engineering Circular No. 14 (4). For a flow depth of between 1 and 3 meters, these U.S. DOT-recommended stone sizes are plotted in Figure 3. For comparison, the U.S. DOT-recommended stone sizes based on Hydraulic Engineering Circular (HEC) No. 11 (3), No. 14 (4), and No. 15 (5) are plotted together in Figure 4. The

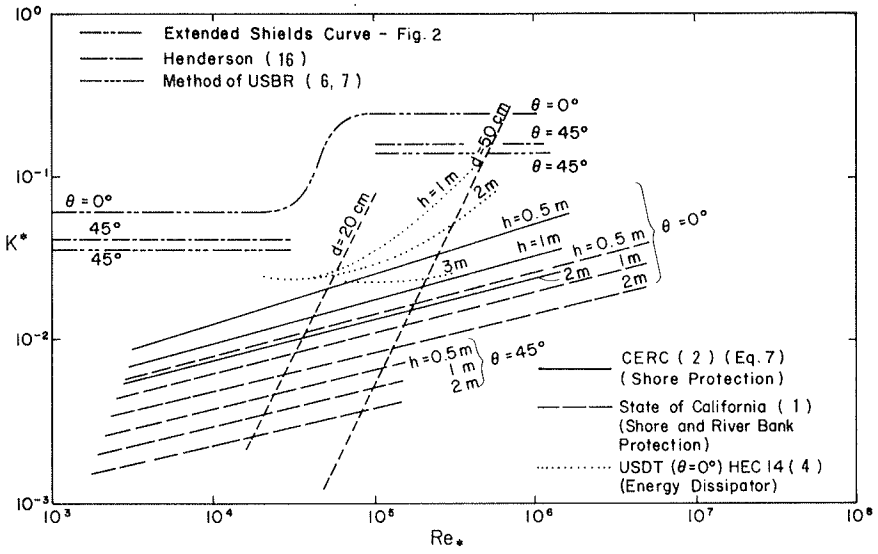

FIGURE 3 Comparison of Shields curve and data for engineering design revetments.

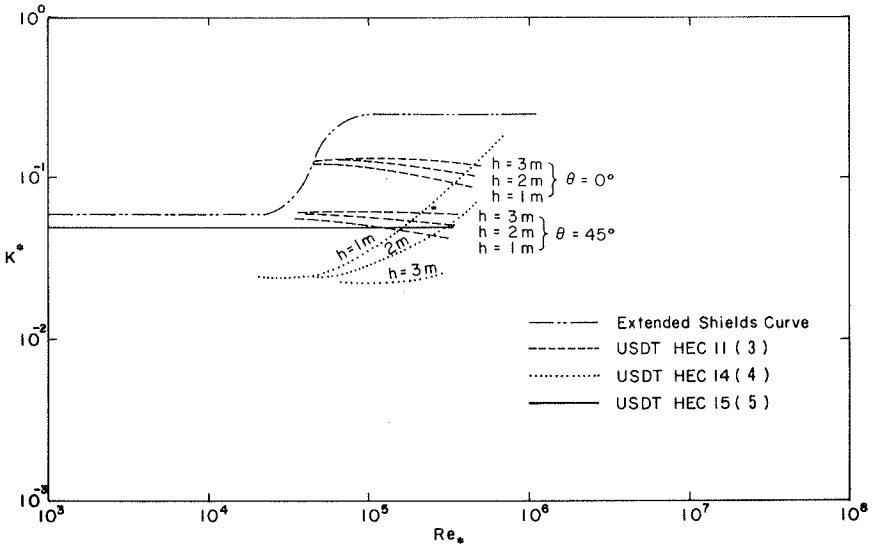

FIGURE 4 Comparison of Shields curve and U.S. DOT data.

curves for HEC No. 11 were obtained by assuming that (a) the hydraulic radius is approximately equal to the flow depth and (b) the Manning n value varies with mean stone size [i.e., $n = 0.0395\ d^{1/6}$ (5)]. Note that if the Manning n value is calculated from Strickler's formula (i.e., $n = 0.0342\ d^{1/6}$) the K* values will be lower.

The California Department of Transportation (Caltrans) presented a formula for the calculation of minimum stone sizes. The Caltrans equation may be reduced to

$$\tau_c = \left\{0.0279/[\log 12.27\,(h/d)]^2\ [\csc(\Phi - \theta)]\right\}(\gamma_s - \gamma_f)d$$
$$= \left\{0.0262/[\log 12.27\,(h/d)]^2\right\}(\gamma_s - \gamma_f)d \qquad (8)$$

where $\Phi = 70$ degrees for randomly placed rubble.

Results from Equation 8 for two different θ values ($\theta = 0$ and $\theta = 45$ degrees) and three different flow depths (h = 0.5 m, 1 m, and 2 m) are plotted as dashed curves in Figure 3.

Riprap sizes of 20 cm and 50 cm are shown as two straight lines in Figure 3. These lines are plotted on the Shields diagram and are independent of any of the riprap size recommendation curves. With a given flow condition, such as u_*, and a flow depth, the minimum riprap size can be selected as the intersection of the flow depth and riprap size for each set of recommendation curves.

For the same flow condition, the differences among the sizes recommended by the three agencies are significant. The U.S. DOT recommends the smallest riprap size. The U.S. Bureau of Reclamation (6,7) and Henderson (16) have suggested the curves shown in Figure 3 for incipient motion at the channel bed ($\theta = 0$ degree) and for incipient motion at the channel banks ($\theta = 45$ degrees).

Rubble Structures in Coastal Engineering

The following equations used to determine the stability of armor units on rubble structures in engineering may be obtained from Hou (9) and CERC (2).

$$d^* = \Phi_* H \qquad (9)$$

where

$$\Phi_* = 0.164\ \csc(\Phi - \theta')/[(\gamma_s - \gamma_f)/\gamma_f] \quad \text{(Caltrans)} \qquad (10)$$

or

$$\Phi_* = 1.24/[(\gamma_s - \gamma_f)/\gamma_f]\ K_D^{1/3}\ \cot^{1/3}\theta' \qquad (11)$$

Here

- d^* = equivalent minimum value of stone diameter,
- H = design wave height at the structure site,
- K_D = stability coefficient (2),
- θ' = angle of structure slope measured from horizontal in degrees, and
- Φ = repose angle of armor units under water surface.

According to wave theory and Equation 9, for the conditions $\gamma_S/\gamma_f = 2.65$; $\Phi = 70$ degrees; and $\theta' = 0$ degree, as derived from Equations 9 and 10, one has the result shown in Figure 5:

$$d^* = 0.106H \qquad (12)$$

From the foregoing analysis it appears that Equation 9 is not completely satisfactory because of the absence of the wave period, T, and wave number, $2\pi H/L$.

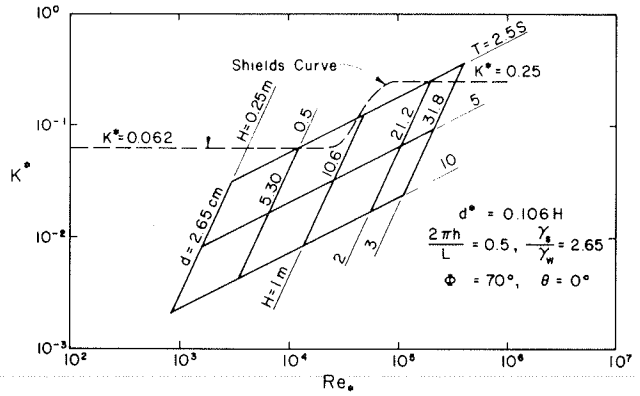

FIGURE 5 Comparison of Shields curve and data for design of rubble structure in coastal engineering.

SUMMARY AND CONCLUSIONS

The Shields diagram for incipient sediment motion has been extended for large particle size and wave environment. An extended Shields diagram is summarized in Figure 6. For Re_* numbers less than 2.0 (point A), the sediment particles are considered to be small. When Re_* numbers are greater than 100 (at point B), the K* value for incipient motion is constant. For Re_* greater than about 4×10^4, the K* value would increase 0.25 because of the decrease of drag coefficient at high Reynolds numbers. This limiting value is indicated as point C in Figure 6. However, the data are rather limited. More data are needed to establish the validity of this increase in K* value.

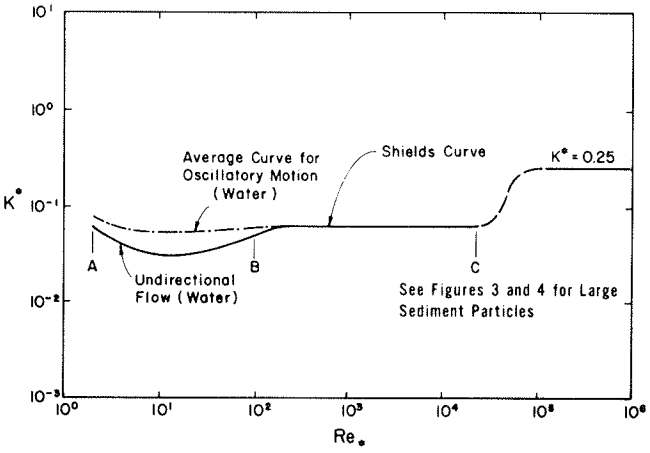

FIGURE 6 Extended Shields diagram.

For wave motion, greater flow shear stress is required to cause incipient motion; this is because of the shorter contact time between maximum orbital velocity and the sediment particle.

Riprap sizes recommended by three government agencies are plotted on the incipient motion diagram. All three agencies recommended minimum particle sizes for the design of riprap. These sizes are all below the criteria indicated by the incipient motion curves. Thus, according to incipient motion criteria, all the recommended sizes should be stable and not be moved by the flow. Caltrans seems to recommend the largest sizes and thus provides the most conservative design. All of the U.S. DOT- and

Caltrans-recommended sizes are smaller than those indicated by the incipient motion criteria. However, one must remember that actual riprap may be subjected to large turbulent fluctuation and thus much larger riprap is needed for shore protection than is indicated by the extended Shields diagram for incipient motion. Some of the riprap will protrude farther into the flow than that tested on a sediment bed under laboratory conditions. This protrusion will also affect the incipient motion of riprap.

The riprap sizes recommended by the U.S. Army Corps of Engineers and Caltrans for a wave environment are also compared with the extended Shields diagram. These recommended sizes are greater than those indicated by the incipient motion diagram. However, in addition to other factors the recommended sizes should also be a function of wave period and wave number. Recommendations for riprap sizes from various agencies are compared and analyzed according to the incipient motion diagram for different ranges of flow conditions. All the recommended riprap sizes are in the nonmotion region according to the extended Shields diagram.

Although the recommended riprap sizes are much greater than those required for incipient motion, it is not safe to use a smaller size without further study of turbulence levels near the riprap in the field and of the effect of particle protrusion into the flow. A comprehensive laboratory test should be conducted to verify the results of this study. A unified riprap design guide can then be developed.

ACKNOWLEDGMENT

The U.S. National Science Foundation sponsored this research under Grant ENG-7825056. We also wish to thank the reviewers for their comments and suggestions.

REFERENCES

1. Bank and Shore Protection in California Highway Practice. Business and Transportation Agency, California Department of Public Works, Division of Highways, 1970, pp. 101-110.
2. Shore Protection Manual, Vol. II. U.S. Army Coastal Engineering Research Center, Washington, D.C., 1973.
3. Use of Riprap for Bank Protection. Hydraulic Engineering Circular No. 11. FHWA, U.S. Department of Transportation, 1967.
4. Hydraulic Design of Energy Dissipators for Culverts and Channels. Hydraulic Engineering Circular No. 14. FHWA, U.S. Department of Transportation, 1975.
5. Design of Stable Channels with Flexible Linings. Hydraulic Engineering Circular No. 15. FHWA, U.S. Department of Transportation, 1975.
6. A.C. Carter. Critical Tractive Forces on Channel Side Slopes. Hydraulic Laboratory Report Hyd-336. U.S. Bureau of Reclamation, Denver, Colo., Feb. 1953.
7. E.W. Lane. Progress Report on Results of Studies on Design of Stable Channels. Hydraulic Laboratory Report Hyd-352. U.S. Bureau of Reclamation, June 1952.
8. A. Shields. Anwendung der Aehnlichkeits-Mechanik und der Turbulenzforschung auf die Geschiebebewegung. Preussische Versuchsanstalt fur Wasserbau und Schiffbau, Berlin, Germany, 1936.
9. S.H. Hou. Study of the Threshold of Sand Movement due to Wave Action. Science Development, Vol. 9, No. 8, 1981, pp. 645-659 (in Chinese).
10. O.S. Madsen and W.D. Grant. Quantitative Description of Sediment Transport by Waves. Proc., 15th Coastal Engineering Conference, ASCE, Vol. 102, No. CE15, July 1976, pp. 1093-1112.
11. R.A. Bagnold. Motion of Waves in Shallow Waters: Interaction Between Wave and Sand Bottom. Proc., Royal Society, London, England, Series A, Vol. 187, 1946, pp. 1-15.
12. P.D. Komar and M.C. Miller. Sediment Threshold Under Oscillatory Waves. Proc., 14th Conference on Coastal Engineering, ASCE, pp. 236-775.
13. M. Manohar. Mechanics of Bottom Sediment Movement due to Wave Action. Technical Memorandum No. 75. Beach Erosion Board, U.S. Army Corps of Engineers, 1955.
14. M. Poreh and E. Hefez. Initial Scour and Sediment Motion due to an Impinging Submerged Jet. Proc., International Association for Hydraulic Research, 1967.
15. J.C. Goddet. L'Etude du début d'entrainement des matériaux mobiles sous l'action de la houle. La Houille Blanche, No. 2, 1960, pp. 126-127.
16. F.M. Henderson. Open Channel Flow. Macmillan, New York, 1966.
17. H. Schlichting. Boundary-Layer Theory, 7th ed. McGraw-Hill, New York, 1979.
18. C.H. Li. The Criteria of Threshold Shearing Stress and Ripple Formation: Experimental Results in Glycerine Flow. Report No. 70. Nanjin Hydraulic Research Institute, Republic of China, 1965 (in Chinese).
19. S.Y. Wang. Stability of Alluvial Rivers. Tianjin University Technical Report. Republic of China, 1975 (in Chinese).

Publication of this paper sponsored by Committee on Hydrology, Hydraulics and Water Quality.

Assessing Vulnerability of Bridges to Floods

EMMETT M. LAURSEN

ABSTRACT

The capacity of both new and old bridges to withstand scour at their foundations and any other flow phenomena that could lead to failure needs to be examined. The problem is somewhat different in the two cases because a new bridge should be designed for the maximum flood to be expected, and there is ample opportunity in the design process to suggest foundations--or even bridge configurations--that may lead to safer, less costly bridges. Making existing bridges less vulnerable is likely to be difficult, awkward, and costly. However, even old bridges can be valuable--as can be discovered after they are lost--but the cost of remedial measures for the maximum expected flood may be more than can be justified. The prediction of scour at bridge foundations is a three-step procedure: (a) the establishment of the flood magnitude-frequency relationship, (b) the conceptualization and analysis of the flow characteristics of floods that might occur during the life of the bridge, and (c) the prediction of scour. The first step needs evidence of the maximum flood that should be expected; the second step is the most difficult as a general rule; the third step is likely to raise questions about scour that have not yet been answered adequately. As a result of the Silver Bridge failure, visual examination of bridges for structural integrity has become routine. Despite occasional spectacular failures like the Interstate bridge in Connecticut, there are probably more bridges lost in floods than from structural inadequacy. The assessment of the vulnerability of existing bridges to floods is also needed and would pay dividends. Recent research, sponsored by the Arizona Department of Transportation and the FHWA, has resulted in relationships for predicting the scour at the toe of a vertical wall and at the toe of a sloping sill. On the basis of the depth of scour, the structural form, and the ease of adding to the sill structure if need be in the future, the sloping sill is the preferred solution. Recent unsponsored student research indicates that the previous solution for sizing riprap was too conservative. Both of these studies are aids to the engineer seeking ways to make existing bridges less vulnerable.

Bridges are expensive. Moreover, bridges are vital links in our transportation system, and our transportation system is a vital part of our economic machine. It would seem obvious, therefore, that we can spend as much to ensure against the possible failure of a bridge as the cost associated with the failure times the probability of the failure. Usually it will be found that the bridge is so expensive, and the added cost of being sure it will not fail is so little, that just saving the bridge is sufficient justification for designing for the maximum flood truly to be expected (1). The magnitude of the maximum, limiting flood used for design purposes depends on the situation. The spillway design flood for a dam located just above a densely populated area will probably be as large as there is any evidence it can be. For a bridge, the maximum can be reduced to be comparable to the largest flood that has happened in the region and that can be expected to happen again.

To say that a bridge should not fail (2) is not to say that traffic will be maintained or that the approach embankments will not fail. These are separate questions. If the economic (or political) cost of traffic delay is not much, perhaps the bridge should be designed as an overflow structure. Highway embankment is comparatively cheap and can be replaced quickly. The acceptable risk of failure for the approach embankments might well be greater than that for the bridge itself.

All too often the risk of failure is evaluated as the probability of an event happening one or more times during the life of the structure; this probability turns out to be equal to unity minus the probability of nonoccurrence (because the sum of the probabilities of nonoccurrence, once-and-only-once, twice-and-only-twice, and so forth is unity). This is correct for a catastrophy after which the bridge is not to be rebuilt. But it is incorrect for recurring loss if the bridge is to be rebuilt. For recurring loss, the risk of failure should be evaluated as the product of the life of the structure times the probability of occurrence of the event in any 1 year. The difference in the two methods is small if that product is 0.1 or less, but becomes quite extreme if one considers designing a culvert, for example, for a 10-year flood if the culvert is supposed to function for 50 years.

This raises the questions of the value of the bridge over its life and the probability of occurrence of a flood of a given magnitude. The answers to both can be off by a factor of two. The optimum of the total expected cost curve (the sum of initial cost and probable loss) is so flat that one solution is not much better or worse than another as shown in Figure 1. Designing more or less conservatively can be justified on the basis of other losses on the one hand, or other societal needs on the other.

Both new bridges and old bridges need to have their vulnerability to floods assessed. The difference between the two cases is found in what can be done about the situation if there is vulnerability. Engineering design is, as a rule, an iterative procedure of assumption, analysis, appraisal, reassumption, reanalysis, and so forth until an acceptable solution is obtained. The hydraulic engineer should

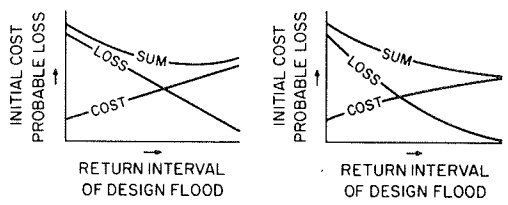

FIGURE 1 Expected cost curves.

be a member of the design team from the beginning to the end. He or she should have a voice in determining the location of the bridge; some locations can be much better than others from a hydraulic viewpoint. The hydraulic engineer should approve the final design as a final assessment of the vulnerability of the bridge. The final solution will not necessarily be the best solution from a hydraulic standpoint, but the hydraulics of the final solution can be important. During the design process, there should be an interplay between the various requirements of function, structure, aesthetics, and hydraulics. For example, if a safety factor is required in the design of a pile foundaton, it would be much better from a scour standpoint to make the piles longer than to require more piles. Or, if debris is anticipated (and it should be), widely spaced columns for a pier would be preferable to closely spaced columns; indeed, a solid pier might be preferable to closely spaced columns.

New bridges can probably always be made safe by making the foundations a little bit deeper. A little bit (comparatively) is enough because the magnitude of the flood that has twice the return interval is not double, the flow depth of a flood of twice the discharge is not double, and the scour depth for twice the depth of flow is not double. A foundation is required for a bridge even if it is not over a river. The added cost of making the bridge safe during the maximum flood to be expected is a small fraction of the cost of the bridge. This is why the best hydraulic solution is not necessarily the best overall solution in the design of a particular bridge and why vulnerable bridges can seldom be justified.

Old bridges present a different problem than do new bridges for several reasons. First of all, there are many more of them; second, their remaining life is limited and their value may be also; and last, decreasing their vulnerability is likely to be more costly if it is feasible at all.

In the aftermath of the failure of the Silver Bridge over the Ohio River, the inspection of bridges for structural integrity and traffic safety and adequacy has become routine. Much can be seen in a visual inspection and, if deemed prudent, measurements can be made and analyses can be performed to evaluate the safety, integrity, and adequacy of the structure. In respect to the vulnerability of the bridge to floods, seeing is only a small part of the assessment procedure required. A hydraulic engineer must predict what scour and what lateral forces could occur and a foundation engineer must predict whether the foundations are adequate for these conditions. If all old bridges over rivers are to be included in an inspection program, more than a few people will be needed. Do all bridges need to be included? An example of a little, old bridge in Arizona is illustrative. This 77-ft bridge was built in 1929 on the highway between Tucson and Nogales. Eventually it was used to carry a frontage road of the Interstate because it, like several other similar bridges, was still serviceable for this purpose. Nothing happened to the bridge until 1968 when one abutment settled about a foot during a 100-year flood. For repair, the bridge was jacked up and concrete was poured for a new bridge seat. Then in 1978 another 100-year flood occurred, and the three piers and four spans went down. One evaluation of the value of this almost-50-year-old bridge would be the cost of the bridge that was built to replace it (several hundred thousand dollars). Old bridges should not necessarily be excluded from a program of re-evaluation.

Certainly not all old bridges, or even all bridges, need to be evaluated. Bridges scheduled for demolition for whatever reason, or which are virtually worthless and are left standing for minor convenience, and bridges whose foundations are on rock or out of the reach of the river and whose superstructures are above floodwaters and debris are not part of the problem. There are still many existing bridges that need to have their vulnerability to floods assessed. As late as 1970 in response to a question about scour predictions, 67 of 97 engineering organizations said that they used engineering judgment, limited the flow velocity, or made no predictions or they did not reply (3). That more bridges do not fall is probably due to the conservatism of foundation engineers in their evaluation of soil properties and soil-structure interaction. However, they are probably as prone to use more piles than they think are really necessary as they are to use longer piles.

Because there are so many bridges, the evaluation of existing bridges needs to be a two-part effort. First, a quick check should be made of all bridges (starting with the most important, the most used, the most expensive) to divide them into three groups: (a) those that might well be vulnerable, (b) those that might not be vulnerable, and (c) those that cannot be categorized because they are too different or special. Then, those bridges that might be vulnerable should be examined carefully, and, if they are vulnerable, some means to make them invulnerable or less vulnerable should be devised. This last is easier said than done. It is easy in the design of a new bridge to specify foundations 5 or 10 feet deeper, and it does not cost very much. Whether one can actually add to the depth of existing foundations is arguable (but to no good purpose); however, a measure such as encircling existing piers and abutments with sheet piling is going to be costly. Any measures to reduce the vulnerability of a bridge are likely to be costly, and the remaining life and value of the bridge may well be less than when built (in constant dollars, of course). Therefore, it may not be economical to build in resistance to the maximum expected flood. However, protection against some level of flooding can probably be justified in most cases--after all, a bridge failure will always represent a sizable monetary loss, not only that of the bridge itself, but also that associated with delay of the traffic that cannot use the bridge.

Eventually all bridges should be examined, even those that were initially included in the group that might not be vulnerable. It will be the third group--those bridges that are special or different--that will give the most trouble. Either the examiner will need a lot of good imagination or there will need to be more research in the laboratory. All geometry and all situations have not been studied adequately, so the examiner who sets out to predict what can happen to existing bridges is going to encounter things unknown and unanswered questions that point to the need for further research.

RESEARCH

There are three things that need to be predicted in assessing the vulnerability of a bridge to floods: (a) the scour at the bridge foundations, (b) the lateral force of the flow on the bridge, and (c) the backwater due to the bridge. Then, of course, it is necessary to go on to predict how the bridge will react to the scour and lateral force and what additional flooding will occur because of the backwater.

The prediction of scour is a three-step process: (a) the establishment of a flood magnitude-frequency relationship including the magnitude of the maximum expected flood, (b) the quantitative description of

the hydraulics of the flood flows including the divination of the future course and degradation of the river, and (c) the prediction of the scour at the bridge foundations.

Hydrology

There are those who believe in the infinite tails of the probability distribution functions used in hydrologic studies; they, as a consequence, also believe in infinite flood magnitudes. In this finite world there are no infinite floods; it is not possible to design for an infinite flood; and therefore those believing in the infinite flood will almost inevitably advise building for the wrong flood--one that is either too big or too small. Because bridges are usually expensive and because of the societal and economic need for the bridge, the flood of primary interest is the maximum expected flood. This is not the maximum flood anybody can conceive of happening, but merely a flood comparable to the largest floods that have happened in the region, or maybe slightly larger if the records are short. For the question of the maximum expected flood, recent work by geomorphologists is very important. Through the examination of slack-water deposits, Kochel et al. (4), have shown that the 1954 flood on the Pecos River was the largest in the past 2,000, perhaps 10,000, years. That, certainly, should qualify the 1954 flood as the maximum expected flood.

Because design for the maximum expected flood is the ultimate, the design process should start with it and then ask how much can be saved by building for a lesser flood and taking a chance on a loss. Will it be worth the risk? Seldom will the answer be "yes," and when it is, it will probably be in a case where traffic can be interrupted by a frequent (2- to 10-year) flood as long as the bridge is not substantially damaged. Presuming that one designs for the optimum (however one operationally finds the optimum), precise return intervals or probabilities for various magnitude floods are not necessary; one design is about as good or bad as another because the optimum is flat, not a cusp. In this writer's opinion, the 100-year flood is a political flood we could better do without, and the money being spent on determining the 100-year flood and its extent could better be spent investigating prehistoric floods to establish maximum expected floods.

Hydraulics

Deciding on the depth of flow, the direction of flow, and the distribution of flow across the full width of flow to predict scour is not easy, even for a river channel and floodplain as they exist. This is not enough. One must describe the character of the flow for the channel and floodplain as they might exist at some time during the life of the bridge. This is the step where divine inspiration would be very helpful but where imagination and some knowledge and experience in the behavior of rivers must suffice.

The description of the flow must be more than the one-dimensional analysis that is commonly employed to describe the flow in the river. Some notion of the two-dimensional pattern of flow in the plan view is absolutely required, and overtones of the third dimension are more than just desirable. The sediment-transport pattern of supply and capacity is needed for the determination of scour and deposition. The depth and direction of flow are needed to predict the scour at piers. The depth of flow and the quantity of flow obstructed by the approach embankment and abutment are needed to predict the scour at the abutment.

For existing bridges, the routine inspection program should be expanded to include observations of the river upstream and downstream (with pictures for the record and for comparison over the years). If the channel is shifting or the streambed is degrading or aggrading, the original design calculations should be referred to in order to check whether what is happening is within the conditions for which the foundations were designed. If not, there should be a determination of whether something should be done. There is always the possibility that in the "big flood," the river will change drastically and suddenly. Insofar as possible, however, this drastic, sudden change should have been anticipated during design. It is known that rivers widen during major hurricane floods (5,6), and the regime equations from India (7) imply widening. A recent dissertation by Silverston (8) gives an analytic basis for this tendency to widen and indicates that for rivers in regions like Arizona the widening tendency is more extreme than would be predicted by the regime equations.

Scour

This writer feels that the prediction of local scour at the piers and abutments is the easier part of the game as long as the geometry of the situation bears some resemblance to the geometries that have been studied in the laboratory. For others, this may not be quite the case. There are a number of relationships that have been proposed for predicting the depth of scour; for most, therefore, the first difficulty is to decide which relationship to use. To use all of them and take an average is to plead an inability to make a crucial decision. This paper is not the place to go into a comprehensive critique of the various scour relationships, but Figure 2 shows the primary difference between some of the scour relationships. The experimental data are from a

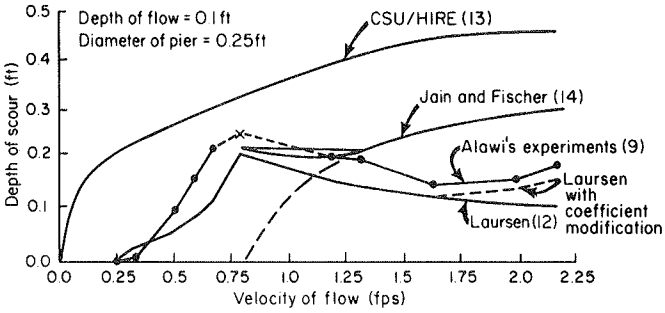

FIGURE 2 Comparison of various scour formulas with experimental data.

thesis by Alawi (9). The Laursen curve includes the clear-water scour case, the good general movement case, and the transition between (10-12). The deepest scour is that predicted by the Colorado State University version of scour, which can be found in a training and design manual prepared for the Federal Highway Administration (13). The Jain and Fischer relationship is from a study, conducted at the Iowa Institute of Hydraulic Research, that achieved supercritical flow (14). The difference in opinion about the effect of velocity (or Froude number) on the depth of scour is shown again but from different points of view in Figures 3 and 4.

How does one "prove" which scour relationship (if any) is correct? By means of field measurements, of course. A few have been made. Most if not all are somewhat flawed and are not entirely satisfying.

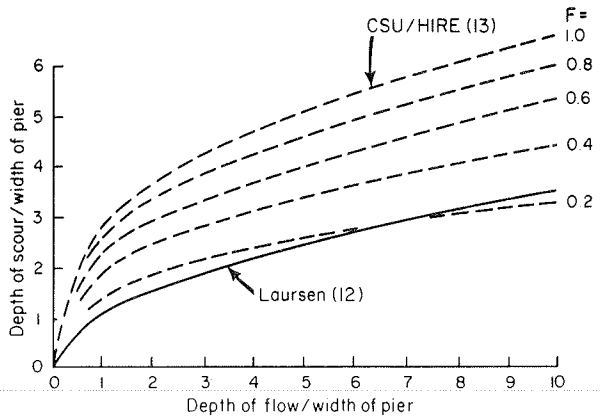

FIGURE 3 Predicted pier scour comparison.

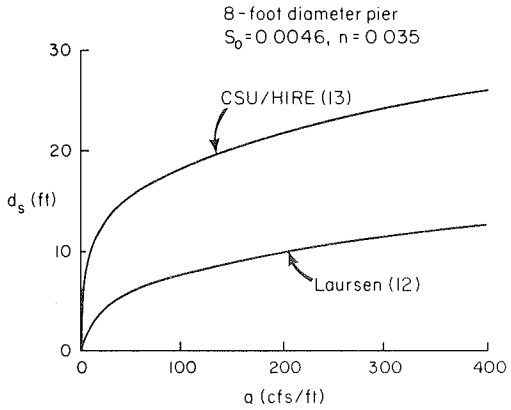

FIGURE 4 Scour predictions for typical Arizona conditions.

Figure 5 is a comparison of some measurements and the Laursen scour predictions, done as honestly and well as possible. Finally, it can be stated with little fear of contradiction that if the CSU/HIRE (13) scour relationship predicted the true state of affairs, there would be very few bridges still standing in Arizona.

This observation is illustrated by the same little, old bridge between Tucson and Nogales mentioned before (15) that had footings only 6 ft below streambed. A reasonable estimate of the flow pattern of the flood of 1968 resulted in a prediction using the Laursen relationships that the one abutment would settle as it did. Another "reasonable" estimate of the flow pattern of the flood of 1978 resulted in the prediction that the piers would fail (some bank-protection work had been done and a borrow pit had been dug during the construction of the Interstate). If a more correct scour prediction had been much less, there was no good reason for the damage and failure that occurred. If a more correct scour prediction had been much more, the bridge should have failed years before in some lesser flood. Therefore, the scour predictions must have been better than just "in the ball park," and predictions twice as large because of a velocity effect could not have been more correct.

Backwater

Highway embankments across the floodplains and a bridge across a river channel are without a doubt obstructions to the flood flow. Therefore, the question of how much backwater is caused by the obstruction is valid and should be asked. Unfortunately, the usual answer is based on some variation of the backwater to be expected for a boundary constriction in a comparatively narrow fixed bed and bank flume. If the valley is wide, and especially if it is heavily vegetated, the backwater may be much different and much greater (16). On the other hand, if there is scour, the backwater may be much less (11). Experiments at Colorado State University (CSU) found that if there was scour the backwater was so small it was sometimes measured as negative (17). It is possible the negative backwater was real and not measurement error because, if the jet issuing from the bridge opening digs itself a long contraction, the overall energy loss can be less than that of the natural flood flow. The backwater with scour found in a small laboratory flume is shown in Figure 6 (18). In Figure 7 that backwater is compared with the backwater predicted by the FHWA procedures without and with scour. The scour used was the measured scour, because the FHWA procedure gave no hint of how to predict scour.

Lateral Force

A solution for the lateral force on a bridge superstructure was published recently by Naudascher (19).

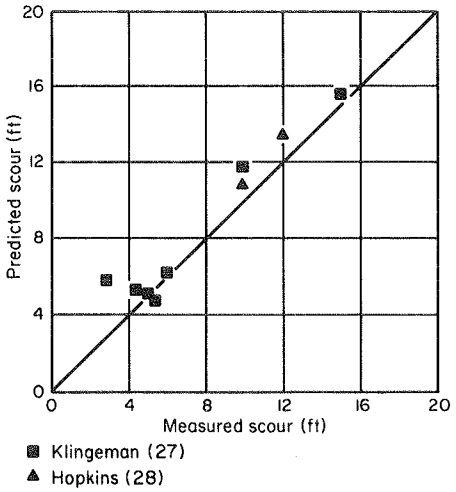

FIGURE 5 Predicted (11) and measured pier scour.

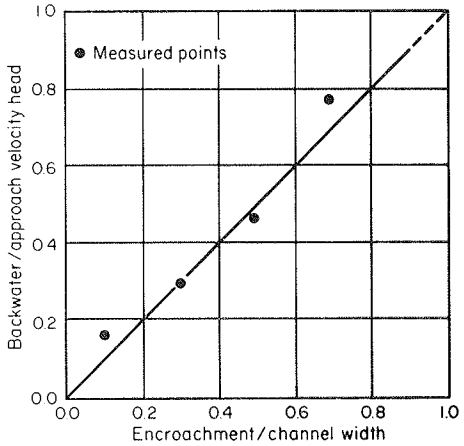

FIGURE 6 Backwater versus encroachment with scour (18).

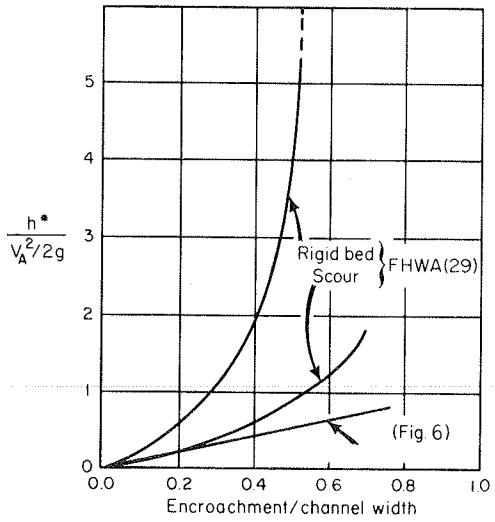

FIGURE 7 Backwater comparisons with scour (18).

This solution does not include the lateral force on the piers, which can be important even if the water level does not get up to the bridge superstructure. More important, this solution does not include the effect of debris. Of course, one must know how much of what kind of debris, and this is a great unknowable. Today one starts to think in terms of mobile homes when one thinks of debris. These could be even worse than the timber and lumber that were plastered against the bridges in northern California in the floods of about 15 years ago.

Naudascher's solution does not consider the effect of scour either. The sluice-gate flow pattern at the water surface would probably result in scour of an erodible bed. The flow, as a whole, would then experience very little contraction. It is difficult to say whether the flow around the superstructure and the pressure distribution around the structual members would be noticeably different with and without scour, but the backwater would be less and the water should not be as high on the superstructure. Experiments need to be repeated with an erodible bed.

INADEQUATELY ANSWERED QUESTIONS

The instant one tries to assess the vulnerability of bridges to floods, one begins to ask questions and finds the anwers are not completely satisfying. The first questions are about hydrology, and quickly one finds that information about the maximum flood to be expected is lacking. Carmody (20), looking at the largest floods in Arizona, found none of the largest floods adequately documented and, upon critical examination, many appeared to be estimated ultraconservatively high. The next questions are about the hydraulics of the flow, and one finds that there is not a satisfactory and convincing method of solving flood flow as a two-dimensional problem.

These questions relate to the preliminary steps in predicting scour. When one comes to predicting the scour itself, more questions will arise. The questions of which scour prediction equation is best, what is the effect of velocity or Froude number, and what is the backwater have been raised already and answers suggested. One is almost bound to run into geometry that has not been tested: Do very short elliptical piers lose all their shape effect? What about very long, thin piers at an angle to the flow and spaced so closely that the piers overlap? Exploratory research indicated that most but not all of the shape effect is lost, even for 2 to 1 and 1.5 to 1 ellipses, and that the overlapping length of the long, thin piers can be ignored (21,22)

REMEDIAL MEASURES

When an existing bridge has been determined to be vulnerable to scour, there are several remedial measures that can be considered and that are not changes to the bridge itself: (a) spur dikes to guide the flow and thereby lessen the scour, (b) riprap to limit the depth of scour, and (c) a sill structure to raise the streambed.

Spur Dikes

Spur dikes can guide the flow, but how long must they be to correct the flow in the center of the channel? A good answer to this question is still lacking. Spur dikes also shift the deepest scour to the end of the spur dike, away from the abutment. This is good, but it means that the spur dike must be long enough so that the tail of the scour hole has about reached bed elevation, as was demonstrated in another exploratory study (23). However, another caution in the use of spur dikes is that they must stay there during the big flood or they will not do their job when most needed. Again, there is really no available information on how the spur dike should be protected or how long it will last during the big flood.

Riprap

The available means of sizing riprap is the result of an analysis of the long contraction of the clear-water case (10) adapted to the pier or abutment in the same manner as the sediment-transporting case. Approximate evaluations for the boundary shear and the critical tractive force, which were reasonable and perhaps slightly conservative for channel flow, were employed in this analysis. A little bit of fragmentary evidence from the CSU tests seemed to be confirmatory. The solution seemed to work fairly well in predicting field measurements from Alaska; however, the size of the self-sorted riprap was not measured there and had to be assumed. Another exploratory investigation at the University of Arizona (24) suggests that the critical tractive force can be taken as 7d instead for 4d (d = riprap size in feet), giving riprap sizes of about half those that would be given by the original solution. Especially in Arizona, that is welcome news because of the high flow velocities of 15 or 20 fps, requiring riprap of 6-foot diameter or more using the 4d criterion. Much more testing needs to be done to be more sure of this preliminary finding.

Sill Structures

A sill downstream from the bridge is often the preferred solution in Arizona for reducing the vulnerability of an existing bridge. One reason is that degradation is a contributing factor; stream slopes are so great that a small percentage flattening of the slope or shortening of the stream can result in many feet of degradation. Combining several parallel washes in one drainage structure is, in effect, a long contraction case with lesser slope. Another reason is that, in much of Arizona, one is not worried about backwater and flooding. In addition, a construction style of H-piles (or old railroad rail), heavy wire fabric, and loose rock (of which there is plenty in Arizona) used by contractors experienced in this construction keeps prices down.

The key question in designing a sill structure is the depth of scour on the downstream side, or toe, of the structure. If the scour can be predicted, various sill geometries for various flows can be designed, and a decision can be made about what to build. Note that most of the possible loss is the bridge. Because no one was able to find the needed scour-predicting formulas, this became the subject of a research project sponsored by the Arizona Department of Transportation. The two geometries studied were the vertical wall and a 1 vertical (V) to 4 horizontal (H) sloping sill.

Experiments with a vertical-wall sill structure resulted in the following equation to predict the scour at the toe (25):

$$D_s/y_c = 8(V_c/w_0)^{3/4} - \left\{[6 + (V_c/w_0)]/[1 + (2\Delta WS/y_c)]^{1/2}\right\} \quad (1)$$

where

D_s = the scour measured from the downstream water surface,
y_c = the critical depth of flow,
V_c = the critical velocity,
w_o = the fall velocity of a quartz sphere of the median sieve diameter, and
ΔWS = the drop in water surface upstream to downstream of the sill.

Figure 8 shows that, except for a few inexplicable runs, the equation predicts the depth of scour

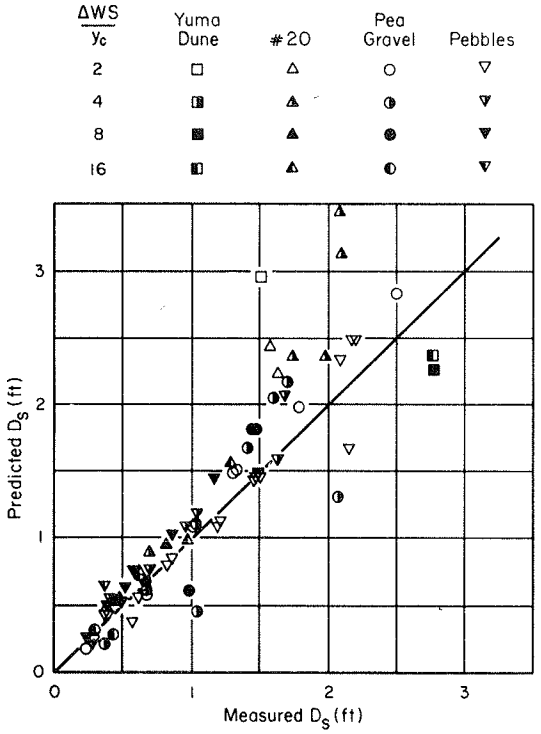

FIGURE 8 Comparison of measured and predicted scour at the toe of a vertical wall (25).

correctly or conservatively. It should be noted that although the flow was supposed to be two dimensional, the resulting scour was not two dimensional. Variation in the scour across the stream is to be expected in real life.

The sediment left the scour hole in suspension in the case of the vertical wall. The next experiments were with a sloping sill with a slope of 1V to 4H (26). In this case, the sediment left the scour as bed load except during the early stages of the development of the scour hole. Another difference was that the drop in water surface was not an important parameter, but that the size of the riprap covering the sill structure was. The scour prediction equation was

$$D_s/y_c = 4(y_c/d)^{0.2} - 3(d_{rr}/y_c)^{0.1} \quad (2)$$

where

D_s = the scour measured from the downstream water surface,
y_c = the critical depth of flow,
d = the diameter of the sediment being scoured out, and
d_{rr} = the diameter of the riprap.

The comparison of measured and predicted scour is shown in Figure 9.

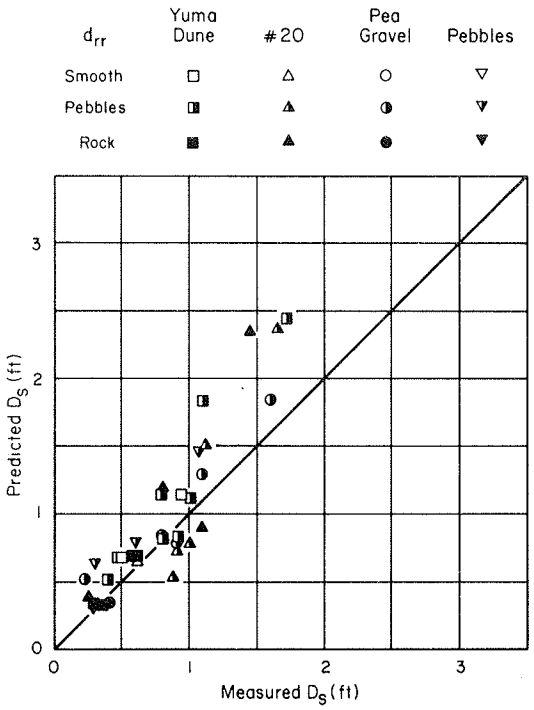

FIGURE 9 Comparison of measured and predicted scour at the toe of a sloping sill (26).

For both sills the scour is less when the flow is transporting sediment, but how much less depends on how much sediment is being transported. If the critical flow at the brink of the sill is transporting the maximum load it can, the scour is about 75 percent of the clear-water scour. A great many runs would be necessary to evaluate the sediment-transporting case adequately, but because the reduction is probably less than 25 percent, the effort does not seem warranted at this time.

The scour can also be less if the scour hole is riprapped, whether by self-sorting or artificially. In the case of the vertical sill, the depth of scour of the riprapped hole needs to be 50 percent more than it would be if the riprap were the sediment being scoured. This is because, at the natural limit, there is still action in the bottom of the scour hole; the surface material is moved about and the underlying material is exposed. Even if new

material is not brought in for riprapping, it is suggested that the best practice would be to excavate a preformed scour hole and cover the bottom of the scour hole with the coarsest fraction of the excavated material. This assumes, of course, that there is coarse material in the native material; otherwise, it will have to be imported. This technique will ensure that all the coarse material will be available for riprap; otherwise, in the initial stages of scour-hole development, much coarse material can be lost.

The sloping sill would seem to be the preferable form for several reasons: The scour depth is less; the basic structure is just an earthen dike (although it needs to be protected by anchored riprap); and it can be added to easily if the tailwater continues to drop because of continued degradation.

SUMMARY

The thesis of this paper is that it is in the public interest that the vulnerability of bridges to floods be lessened. Bridges are expensive; they are vital links in our transportation system; and many of them are vulnerable to an unjustifiable (probably also unknown) degree.

In the design phase of new bridges, hydraulics and scour should be duly considered in planning, site selection, and final design. This is not to say that hydraulics should dictate design, merely that it should be properly considered and any vulnerability should be assessed and justified.

The matter of existing bridges, new and old, is much more difficult to work out. A program is needed to assess the vulnerability of every existing bridge and to contrive remedial measures to lessen the vulnerability of those bridges worth saving. This would be a program comparable to the ongoing bridge inspection program in size, in scope, and in importance. It would differ in that when a bridge has once been assessed for vulnerability to floods, only cursory inspection should be required to be sure hydraulic conditions have not changed.

There would be difficulty in carrying out such a program--partly because of the sheer number of bridges that would be involved; partly because there are questions regarding hydrology, hydraulics, and scour that remain unanswered or not answered adequately and convincingly.

In hydrology the most important and difficult question is the magnitude of the maximum flood to be considered in evaluating designs. In hydraulics the most important and difficult question is the two-dimensional flow pattern in the vicinity of the bridge, including the backwater due to the bridge. For scour the most difficult question is probably which scour-prediction relationship to use.

Further investigations are needed to better answer all these questions. In contriving remedial measures, other studies will be needed. To illustrate this contention, several exploratory studies have been referred to; the most promising of these is the one that indicated that the riprap size needed to arrest scour might be half that previously indicated.

Finally, the results of a laboratory investigation of the scour at the toe of sill structures are given in the form of scour-predicting equations for a vertical wall and for a sloping sill. The need to have this question answered was apparent to the Arizona Department of Transportation as they embarked on a program to re-evaluate the most vulnerable of their bridges and to contrive remedial measures for those too vulnerable.

ACKNOWLEDGMENT

This paper is based, in part, on two research projects. The first was sponsored solely by the Arizona Department of Transportation and was entitled "A Study to Advance the Methodology of Assessing the Vulnerability of Bridges to Floods." The second on scour at sills was sponsored by the Arizona Department of Transportation in cooperation with the FHWA as Research Project HPR-1-19(184).

REFERENCES

1. E.M. Laursen. Bridge Design Considering Scour and Risk. Journal of the Transportation Engineering Division, ASCE, Vol. 96, No. TE2, May 1970.
2. M.L. Corry, J.S. Jones, and P.L. Thompson. The Design of Encroachments on Flood Plains Using Risk Analysis. Hydraulic Engineering Circular 17. FHWA, U.S. Department of Transportation, Oct. 1980.
3. Scour at Bridge Waterways. NCHRP Synthesis of Highway Practice 5. TRB, National Research Council, Washington, D.C., 1970.
4. R.C. Kochel, V.R. Baker, and P.C. Patton. Paleohydrology of Southwestern Texas. Water Resources Research, Vol. 18, No. 4, Aug. 1982.
5. J.E. Costa. Response and Recovery of a Piedmont Watershed From Tropical Storm Agnes, June 1972. Water Resources Research, Vol. 10, No. 1, Feb. 1974.
6. A. Gupta and H. Fox. Effects of High Magnitude Floods on Channel Form: A Case Study in Maryland Piedmont. Water Resources Research, Vol. 10, No. 3, June 1974.
7. T. Blench. Regime Theory for Self-Formed Sediment-Bearing Channels. Transactions, ASCE, Vol. 78, 1952.
8. E. Silverston. The Stable Channel as Shaped to Flow and Sediment. Ph.D. dissertation. University of Arizona, Tucson, 1981.
9. A.J. Alawi. Effect of Velocity on Scour. M.S. thesis. University of Arizona, Tucson, 1981.
10. E.M. Laursen. An Analysis of Relief Bridge Scour. Journal of the Hydraulics Division, ASCE, Vol. 89, No. HY3, May 1963.
11. E.M. Laursen. Scour at Bridge Crossings. Journal of the Hydraulics Division, ASCE, Vol. 89, No. HY2, Feb. 1960.
12. E.M. Laursen. Predicting Scour at Bridge Piers and Abutments. General Report No. 3. A Study to Advance the Methodology of Assessing the Vulnerability of Bridges to Floods, Engineering Experiment Station, University of Arizona, Tucson, Feb. 1980.
13. E.V. Richardson, D. Simons, S. Karaki, K. Mahmood, and M. Stevens. Highways in the River Environment: Hydraulic and Environmental Design Considerations. FHWA, U.S. Department of Transportation, May 1957.
14. S.C. Jain and E.E. Fischer. Scour Around Circular Bridge Piers at High Froude Numbers. Report FHWA-RD-79-104. Iowa Institute of Hydraulic Research, University of Iowa, Iowa City, April 1979.
15. E.M. Laursen and D. Duffy. I-19 West Frontage Road Bridge (Old US 89) at Agua Fria Canyon Wash (North of Nogales). Site Report 1. Engineering Experiment Station, University of Arizona, Tucson, Feb. 1980.
16. E.M. Laursen. Bridge Backwater in Wide Valleys. Journal of the Hydraulics Division, ASCE, Vol. 96, No. HY4, April 1970.
17. H.K. Lui, J.N. Bradley, and E.J. Plate. Backwater Effects of Piers and Abutments. Report

CER57HKL10. Civil Engineering Department, Colorado State University, Fort Collins, 1957.
18. E.M. Laursen and N.J. Antonas. Scour and Backwater and Progressively Encroaching Embankments. Research Report 2. Engineering Experiment Station, University of Arizona, Tucson, Feb. 1980.
19. E. Naudascher and H.J. Medlarz. Hydrodynamic Loading and Backwater Effect of Partially Submerged Bridges. Journal of Hydraulic Research, Vol. 21, No. 3, 1983.
20. T. Carmody. A Critical Examination of the "Largest" Floods in Arizona. General Report No. 1. A Study to Advance the Methodology of Assessing the Vulnerability of Bridges to Floods, Engineering Experiment Station, University of Arizona, Tucson, Feb. 1980.
21. A. Elhasan. The Effect of Pier Shape and Angle of Attack on the Relative Depth of Scour. CE 300 Report. Department of Civil Engineering and Engineering Mechanics, University of Arizona, Tucson, July 1983.
22. E.M. Laursen and N.J. Antonas. Scour at Long, Thin Piers Which Are Closely Spaced. Research Report 1. Engineering Experiment Station, University of Arizona, Tucson, Feb. 1980.
23. E.M. Laursen and N.J. Antonas. Scour As Affected by a Spur Dike. Research Report 3. Engineering Experiment Station, University of Arizona, Tucson, Feb. 1980.
24. K.B. Marcus. Determination of the Size and Depth of Gravel Used in a Riprap Layer Around a Circular Pier. CE 900 Report. Department of Civil Engineering and Engineering Mechanics, University of Arizona, Tucson, Aug. 1983.
25. E.M. Laursen and M.W. Flick. Predicting Scour at Bridges: Questions Not Fully Answered--Scour at the Toe of a Vertical Wall. Report FHWA-AZ/83/184-2. Engineering Experiment Station, University of Arizona, Tucson, Aug. 1983.
26. E.M. Laursen. Predicting Scour at Bridges: Questions Not Fully Answered--Scour at the Toe of a Sloping Sill. Report FHWA-AZ/83/184-2. Engineering Experiment Station, University of Arizona, Tucson, Sept. 1983.
27. P.C. Klingeman. Prediction of Pier Scour in Western Oregon. FHWA, U.S. Department of Transportation, 1971.
28. G.R. Hopkins, R.W. Vance, and B. Kasraie. Scour Around Bridge Piers. Interim Report FHWA-RD-75-56. FHWA, U.S. Department of Transportation, March 1975.
29. J.N. Bradley. Hydraulics of Bridge Waterways. Hydraulic Design Ser. 1. FHWA, U.S. Department of Transportation, 1970.

Publication of this paper sponsored by Committee on Hydrology, Hydraulics and Water Quality.

Computer-Based Prediction of Alluvial Riverbed Changes

F.M. HOLLY, JR., T. NAKATO, and J.F. KENNEDY

ABSTRACT

Recent investigations and research programs at the Iowa Institute of Hydraulic Research have involved both the analysis and development of computer-based simulation techniques for alluvial riverbed evolution. The primary use of such techniques is in the prediction of riverbed aggradation and degradation caused by perturbations in the river's equilibrium geometry and sediment inflow supply over extended reaches. In this paper the mathematical basis of the problem is reviewed and several general numerical approaches and associated difficulties are described. Seven published programs are then described, and their performance when applied to three actual field situations is compared. The conclusions point out a critical dependence on field data and identify the need for further research in understanding physical mechanisms such as sediment sorting, armoring, scour, and deposition.

Mother Nature, in providing the Earth with a system of drainage channels to return surface waters to the sea, has endowed man in general, and river engineers in particular, with both a blessing and a curse. The blessing is that rivers whose channels are formed of loose, noncohesive alluvium are able to adjust their geometry to carry widely varying discharges with only moderate changes in water-surface elevation. The curse is that river engineers have found this self-regulating mechanism extremely difficult to understand and accommodate in their projects.

The sheer complexity of alluvial river response, which involves dozens of relevant variables and even ambiguity as to which are the dependent and independent ones, has defied attempts to formulate a coherent, reliable, "desktop" methodology for alluvial river design. Although field experience and laboratory tests have led to the establishment of fairly reliable procedures for the prediction of local scour around bridge piers, bank stability, and other such local phenomena, no such procedures exist for the analysis of alluvial riverbed and bank changes over long river reaches and extended periods of time.

The design engineer's interest in alluvial river response is generally focused on anticipating how the riverbed and water-surface elevations will change if an existing stable or equilibrium situation is perturbed. This perturbation may be the

occurrence of an unusually large annual flood that temporarily scours the bed and banks to accommodate the higher flow before returning to normal conditions. Or the perturbation may be a permanent change in river discharge patterns and geometry caused by upstream regulation of flows or bank stabilization and channelization. The first type of perturbation is often susceptible to simulation using a physical scale model. Although difficult problems of scaling laws and with the interpretation of results arise, such physical models, in the hands of experienced modelers, can yield valuable information on local scour and deposition around structures. However, the sheer expense and space requirements of physical scale models generally disqualify them for simulation of long-term, large-distance riverbed response to the second type of perturbation. This is where numerical, computer-based models, which can simulate both short- and long-term response, find their natural area of application.

Numerical models of alluvial river response are the natural outgrowth of rigid-boundary, unsteady flood-propagation models that have proven to be so useful in engineering design. These unsteady flow models have succeeded because they are based on mathematical descriptions that incorporate all the important physical processes involved and use reliable, carefully implemented numerical methods to obtain approximate solutions to the appropriate partial-differential equations. However, alluvial river-response models have enjoyed nowhere near the success of their rigid-boundary cousins, precisely because of the weaknesses in our understanding and mathematical formulation of the relevant physical processes. Notwithstanding this fundamental difficulty, design engineers have an immediate need for reliable numerical simulations, and hydraulic research engineers have targeted alluvial river hydraulics as a prime area for continuing fundamental and applied research. Out of this fortunate confluence of interest have arisen a variety of simulation techniques and industrialized software systems, as well as many apparently successful simulations of prototype situations.

The remainder of this paper is devoted to brief descriptions and critical analyses of several of the currently available software systems for alluvial river simulation. All are limited to one-dimensional simulation, in which it is assumed that river response can be described in terms of the average longitudinal flow, without detailed knowledge of secondary currents, backwater eddies, flow patterns in the immediate vicinity of structures, and so forth. At this time (1984), it would appear that engineering use of two- and three-dimensional simulation must await the development of a more complete understanding of the physical processes involved.

MATHEMATICAL REPRESENTATION OF ALLUVIAL RIVERBED EVOLUTION

The most basic one-dimensional description of water and sediment flow in an alluvial river consists of four relations (1):

Conservation of water

$$(\partial h/\partial t) + (\partial q/\partial x) = Q_\ell/B \tag{1}$$

Conservation of water momentum

$$(\partial u/\partial t) + [u(\partial u/\partial x)] + [\underline{g}\,(\partial h/\partial x)] + [\underline{g}\,(\partial z/\partial x)] + \underline{g}S_f = M_\ell/\rho\ Bh \tag{2}$$

Conservation of sediment

$$(1-n)\,[\tilde{B}(\partial z/\partial t)] + (\partial G/\partial x) = G_\ell \tag{3}$$

Sediment-transport law

$$f(G, S_f\, u, h, D_{50}, \ldots) = 0 \tag{4}$$

where

- h = water depth,
- q = water discharge per unit channel width ($q = uh$),
- u = depth-averaged water velocity,
- Q_ℓ = lateral water-inflow rate per unit length,
- B = channel width,
- $\underline{g}$ = gravitational acceleration,
- S_f = energy gradient,
- M_ℓ = contribution to longitudinal momentum from lateral water inflow,
- ρ = water density,
- n = sediment porosity,
- $\tilde{B}$ = channel width affected by sediment transport,
- z = bed elevation,
- G = volumetric sediment-transport rate,
- G_ℓ = lateral sediment-inflow rate per unit length, and
- D_{50}, ...symbolically represents all sediment properties that determine the amount transported and the shear stress at the riverbed.

Solutions to Equations 1 through 4, if they could be obtained for appropriate initial and boundary conditions, would produce the time and one-dimensional space variation of velocity $u(x,t)$, depth $h(x,t)$, bed elevation $z(x,t)$, and sediment transport rate $G(x,t)$. However, any implementation of a conceptual model based on these equations also requires assumptions about how erosion or deposition is distributed across the width of the channel, as well as a quantifiable conceptual model relating the composition (size distribution) of sediment in the bed alluvium to the composition of sediment being transported. Numerical models are more often distinguished one from another by the way they treat such processes than by their solution of the basic equations.

Equations 1 through 4 form a nonlinear partial-differential system that in general cannot be solved analytically. Approximate numerical methods can be used to solve these equations, but such methods are often tedious and expensive, especially when Equation 4 incorporates the interdependence of sediment-transport rate and flow resistance. Consequently, use is often made of the fact that the typical time scale of liquid wave-propagation phenomena is much shorter than the time scale of longitudinal bed-profile modification (1). The propagation time of a flood peak along a 100-km reach may be of the order of 1 or 2 days, whereas it would take several years for a bed-level perturbation to cover such a distance. Whenever this is the case, the system of Equations 1 through 4 can be simplified by assuming that the water flow remains quasi-steady during a certain interval of time; or, in other words, that water-wave propagation effects are of secondary importance for sediment-transport phenomena.

When this quasi-steady water-flow assumption is justified, Equation 2 for unsteady conservation of water momentum reduces to the familiar "backwater equation," an equivalent statement of steady-state momentum or energy conservation:

$$[u(\partial u/\partial x)] + [\underline{g}(\partial h/\partial x)] + [\underline{g}\,(\partial z/\partial x)] + \underline{g}S_f = M_\ell/\rho\ Bh \tag{5}$$

The mathematical problem is then reduced to one of solving just the nonlinear partial-differential

system of Equations 3, 4, and 5 in each time interval over which the water discharge is assumed to be nonvarying in time, be it for several hours during a rising flood hydrograph or several years if the effects of a single dominant discharge are of interest.

There are two general types of sediment-transport and flow-resistance formulae as represented symbolically by Equation 4. In the first type, the energy gradient S_f is taken to be an explicit function of known flow roughness and other parameters, and the sediment-transport rate G is an explicit function, albeit indirect and often complex, of the flow. In the second general type of Equation 4, the effects of bed forms, changing bed-material composition, and bed armoring on both flow resistance and sediment-transport formulae are taken into account in an attempt to represent the known interdependence of flow resistance and sediment transport (2, pp. 114-126).

NUMERICAL SOLUTION OF GOVERNING EQUATIONS

Virtually all published software systems for the solution of the water- and sediment-flow equations use one form or another of the finite-difference method, in which time and space derivatives are approximated by differences of nodal values of grid functions that replace the continuous functions, leading to a system of algebraic equations. Some authors have used the finite-element method, but in one dimension there does not appear to be any strong reason for doing so. In any case, the quality and reliability of numerical models for bed evolution are determined primarily by the sediment-transport formulation and mechanisms adopted for sorting, armoring, and so forth. The particular numerical method used, as long as it is consistent with the partial-differential equations and is stable, has only a secondary effect on simulation quality.

Whether the full unsteady set of Equations 1 through 4 or the quasi-steady set of Equations 3 through 5 is solved numerically, two basic approaches are possible: coupled or uncoupled (1). In the coupled case, a simultaneous solution of both water and sediment equations is sought. This is evidently the physically proper way to proceed, because the water-flow and sediment-transport processes occur simultaneously. However, the simultaneous solution may involve certain computational complications, especially when the sediment-transport flow-resistance equation (4) involves not just an analytic mathematical expression but a whole series of procedures and computations to simulate armoring, sorting, bed forms, and so forth.

The uncoupled procedure has arisen essentially to circumvent the computational difficulties of the coupled approach. The uncoupling of the liquid and solid transport occurs during a short computational time step, Δt. First the water-flow equations are solved to yield new values of depth and velocity throughout the reach of interest, assuming that neither the bed elevation nor the bed-sediment characteristics change during the time step. Then the depths and velocities are taken as constant, known inputs to the sediment continuity and transport equations (3 and 4); these equations then become relatively easy to solve numerically, yielding the new bed elevations. When the overall model includes bed-sediment sorting or armoring, these processes are simulated in a third uncoupled computational phase using new depths, velocities, and bed elevations as known inputs. Although it is difficult to quantify the error associated with this artificial uncoupling of simultaneous, mutually dependent processes, it is intuitively obvious that the uncoupling is justified only if bed elevations and bed-material characteristics change very little during one time step. Experience in the use of uncoupled models, with both the unsteady and quasi-steady water-flow equations, has shown that the uncoupling is not a serious obstacle to successful simulation.

Another hybrid approach involves an iterative application of the uncoupled approach within one time step. The computational practicalities of the uncoupling are retained, but the water and sediment processes are allowed to interact through iterative coupling until the algebraic equivalents of the water- and sediment-flow equations are truly simultaneously satisfied at the end of the time step. Additional computational cost would appear to be the only reason (and a weak one at that) not to iteratively couple the equations.

ARMORING AND SORTING

Another distinguishing feature of numerical bed-evolution models is the representation of sediment sorting and bed-surface armoring. Alluvial sediments are rarely of uniform grain size. A broad range of sizes are represented, from gravels and coarse sands down to fine silt and clay in varying proportions. Finer particles are preferentially entrained into the flow as erosion occurs, so that the material remaining on the bed contains a progressively higher proportion of coarser material. This so-called sorting process tends to increase the mean bed-material size as degradation occurs, thus affecting the sediment-transport rate, river regime (existence of ripples and dunes), and flow resistance through both particle roughness and bed-form effects (3). If the original bed material contains a high enough proportion of large, nonmovable materials (coarse gravel, cobbles, and small boulders), an interlocking armor layer may form on the surface, arresting further degradation. These processes are qualitatively reversed during deposition, but become even more difficult to quantify.

No computer-based models presently available incorporate a general, adequate treatment of sorting and armoring processes. Nevertheless, some models attempt to simulate their effects on bed evolution; others ignore them completely. Thus another important distinguishing feature of computer-based models is the degree to which they incorporate sorting and armoring effects.

PERFORMANCE OF SELECTED MODELS

Numerical modeling of alluvial river flows has become very popular in recent years because of the advancement of digital-computer technology. However, the number of computer-based, alluvial riverbed prediction models that are readily available for application to prototype cases seems to be quite small. Most of the available models have been developed for specific rivers under particular flow and alluvial riverbed conditions, and many of them are, to some extent, well tuned or calibrated for those particular rivers. In this section, attention will be focused only on those models that are related to the investigations conducted at the Iowa Institute of Hydraulic Research (IIHR) in the last few years (4-7).

The assessment of the selected models is made for two different groups: short-term models and long-term models. The short-term models are best suited to compute changes in alluvial riverbed level during a relatively short time period. They are suited for a single-flood event because of the relatively high cost of backwater computation using either unsteady flow equations or a rather complex fixed-bed water-routing model such as HEC-2 (8). On the other hand, the long-term models employ simpler implementations

of steady-state flow equations, and thus are suited for long-term prediction of riverbed level for multiple-flood events over multiple years. However, it should be recognized that the short-term models can also be applied for long-term prediction if variable time steps are employed. In that case a shorter time step is used for highly unsteady flows and a longer time step is used otherwise.

Short-Term Models

HEC2SR (HEC-2 with Sediment Routing)

The known-discharge, uncoupled, water- and sediment-routing model was developed by Simons, Li and Associates (SLA) for simulating watershed sediment yield and the attendant riverbed aggradation and degradation in a river system (9). The model uses the HEC-2 fixed-bed, backwater-computation program developed by the U.S. Army Corps of Engineers (COE), Hydrologic Engineering Center (HEC) (8) for water routing. HEC-2 solves one-dimensional, steady-state, gradually varied flow using the flow-continuity and flow-energy equations (1 and 5). HEC-2 accounts for various kinds of flow encroachments, such as bridge constrictions and multiple channels, and allows for nonuniform distribution of the bed-roughness coefficient across the channel.

Once various hydraulic parameters are determined by the HEC-2 computation, the bed-material and wash-load discharges are estimated for each computational reach. The model uses the Meyer-Peter and Mueller formula (10) for the bed-load discharge computation and the Einstein formula (11) for the suspended-load discharge. The combined bed-material transport rates are further corrected for wash-load effects using Colby's empirical relationships (12). The sediment-volume change determined from the balance between the sediment inflow and outflow of each subreach is distributed uniformly along the reach. Therefore, the sediment-routing model that solves the sediment-continuity equation (3) cannot predict local scour or deposition patterns. However, dredging effects can be incorporated during the computation of the sediment-volume change. The change in cross-sectional profile is determined by a weighting factor based on flow conveyances in adjacent lateral subsections. Armoring effects and changes of bed-material composition are considered during each sediment-routing phase. After the sediment-routing phase, hydraulic and bed-profile data in the HEC-2 data file are updated, and the water- and sediment-routing computation for the next time step begins.

Because of the high cost of backwater computation, the model is not suitable for the long-term prediction of riverbed changes. The model is purely one dimensional and accounts for neither lateral channel migration nor secondary flows.

UUWSR (Uncoupled, Unsteady Water and Sediment Routing)

This model was developed at Colorado State University by Tucci, Chen, and Simons (13) for simulating one-dimensional, gradually varied, unsteady, water and sediment flows in complicated river networks. The model first solves the unsteady flow-continuity and flow-momentum equations (1 and 2) by an unconditionally stable, four-point, implicit, finite-difference scheme assuming a fixed bed during one time step. It is assumed that the bed-roughness coefficient for the unsteady flow is the same as that for a steady flow. Three types of boundary conditions may be used: upstream discharge hydrograph, upstream stage hydrograph, and downstream stage-discharge rating curve. The water-routing model also considers the effects of tributary confluences and dams on water-surface profiles in the study reach.

The computed flow information is used to compute the sediment-transport capacity, G, which is given by

$$G = a u^b h^c \quad (6)$$

where a, b, and c are empirical regression coefficients determined either from field data or by generating data using the Meyer-Peter and Mueller formula and Einstein's bed-load function for bed-load and suspended-load discharges, respectively. Computed sediment discharges are then applied to the sediment-continuity equation (3) to compute the change in the cross-sectional area by means of an explicit finite-difference scheme. Changes in bed-material composition are not taken into account. It should be noted that steady-state conditions are assumed at confluences and dams of the study reach. The model is able to simulate, with minimal computer cost, a complex river-network system in which islands, meander loops, and tributaries are connected to the main channel. The model can also account for effects of hydraulic structures such as dikes, locks, and dams. The flood-wave movement in a long reach can be simulated by this unsteady flow-routing model.

FLUVIAL-11

This uncoupled model was developed at San Diego State University in 1976 by Chang and Hill (14) to simulate one-dimensional, unsteady, gradually varied, water and sediment flows for channels with erodible banks. FLUVIAL-11 first solves the unsteady, flow-continuity and flow-momentum equations (1 and 2) in one time step by neglecting storage effects due to unsteady flow. The model uses an implicit, central-difference, numerical scheme in solving for the two unknown variables of water discharge and cross-sectional area. The flow information is then used to compute the bed-material discharge at each section using either the Graf formula (15) or the Engelund-Hansen formula (16).

The net change in cross-sectional area is next obtained by solving the sediment-continuity equation (3) using a backward-difference scheme for space and a forward-difference scheme for time. The computed cross-sectional area change is then adjusted for the effects of channel width, cross-sectional profile, and lateral channel migration. Width adjustments are made in such a manner that the spatial variation in power expenditure per unit channel length is reduced along the reach by a trial and error technique. Further adjustment of cross-sectional area is made to reduce the spatial variation in power expenditure along the channel. The effect of lateral channel migration is determined by solving the sediment-continuity equation in the transverse direction, which incorporates the effect of radius of curvature of the river bend into the transverse component of the sediment-transport rate. FLUVIAL-11 in unique because of its capability to predict changes in erodible channel width, changes in channel-bed profile, and lateral migration of a channel in bends.

Examples of Short-Term Model Performance

A National Research Council study committee conducted an investigation for the Federal Emergency Management Agency (FEMA) during 1981-1983 to determine whether riverbed degradation during flood passage has an effect on the flood stage that should be incorporated into the calculation of flood-zone limits (4). The study involved application of sev-

eral flow- and sediment-routing models for alluvial streams to study reaches of the San Lorenzo, San Dieguito, and Salt rivers. These rivers were selected because they have historically experienced flash-flood-type events with appreciable riverbed changes and channel migration during floods. In the National Research Council study, the same input data for each river were furnished to the participating modelers and principal computational results were submitted by the modelers to the committee for evaluation. Only two cases of numerical simulation that are pertinent to the topic of this paper are presented in the National Research Council study results.

The first example is for the San Lorenzo River, which is located in Santa Cruz County in northern California and flows into the Pacific Ocean at Monterey Bay. The approximately 4.7-mile-long study reach comprises two different subreaches: the relatively steep upper-half reach and the 2.4-mile-long lower-half reach with a much smaller slope. The input data included hydrographs for the February 16-20, 1980, flood, preflood channel cross-sectional profiles coded in HEC-6 format, suspended-sediment discharge rating curves by particle sizes collected upstream from the upper-reach boundary, and bed-material composition data coded in HEC-6 format. The peak discharge was 12,800 cfs, and the median bed-material size varied between 0.34 mm at the downstream and 0.93 mm at the upstream boundary. The downstream boundary condition reflected tidal effects. The thalweg profiles at the peak discharge computed by HEC2SR, UUWSR, and FLUVIAL-11 are shown in Figure 1 together with the initial thalweg profile. As seen in the figure, UUWSR and FLUVIAL-11 predicted significant changes in thalweg elevation compared with the HEC2SR prediction. The general agreement of predictions of thalweg elevations among the three models is seen to be limited to extremely small portions of the study reach. Longitudinal distributions of the total-load discharge, mean flow velocity, and median bed-material size at peak flow were also found to differ significantly among the three models.

The second example is for the San Dieguito River, which flows through San Diego County in southern California. The 2-mile-long reach was studied for two peak flows of 4,400 cfs and 22,000 cfs. The San Dieguito River channel has a wide, flat cross section with highly erodible banks, and had been disturbed extensively, before the simulated floods, by sand-mining activities and construction of the Via de Santa Fe bridge. The channel bed is composed primarily of sand-range materials. The duration of each flood was approximately 2 days.

Thalweg elevations computed at a peak discharge of 22,000 cfs by HEC2SR, UUWSR, and FLUVIAL-11 are plotted in Figure 2 (no observed profile after 2 days was available). FLUVIAL-11 predicted a generally aggrading thalweg pattern over the entire reach, and the two Colorado State models predicted an aggradation pattern for the upper reach and a degradation pattern for the lower reach. The FLUVIAL-11 prediction of riverbed aggradation is believed to be due to the effect of a channel-widening module in the model. The prediction gap among these models is seen to amount to about 20 feet at a river distance of 3,600 ft at the Via de Santa Fe bridge.

Long-Term Models

KUWASER (Known-Discharge, Uncoupled, Water and Sediment Routing)

The KUWASER model was developed in 1979 at Colorado State University by Simons, Li, and Brown (17). The water discharge is taken as steady during a specified time interval, so that water-flow routing consists of simply solving the backwater equation (5) with an additional term for explicit representation of energy losses other than those caused by bed-shear stress. Equation 3 is solved by first computing the sediment volume to be removed or added to each reach, then allocating 25 percent of this volume to the upstream half of the reach and 75 percent to the downstream half. Cross-sectional changes are computed in a quasi-two-dimensional manner by allocating the volume change across the channel in direct proportion to the local longitudinal hydraulic conveyance factor. Lateral channel boundaries are assumed to be fixed (nonerodible banks); neither hydraulic-sorting nor bed-armoring processes are taken into account explicitly, though their effects may appear indirectly in the regression coefficients a, b, and c, in Equation 6.

KUWASER uses an empirical sediment-transport function. Flow resistance is uncoupled from bed

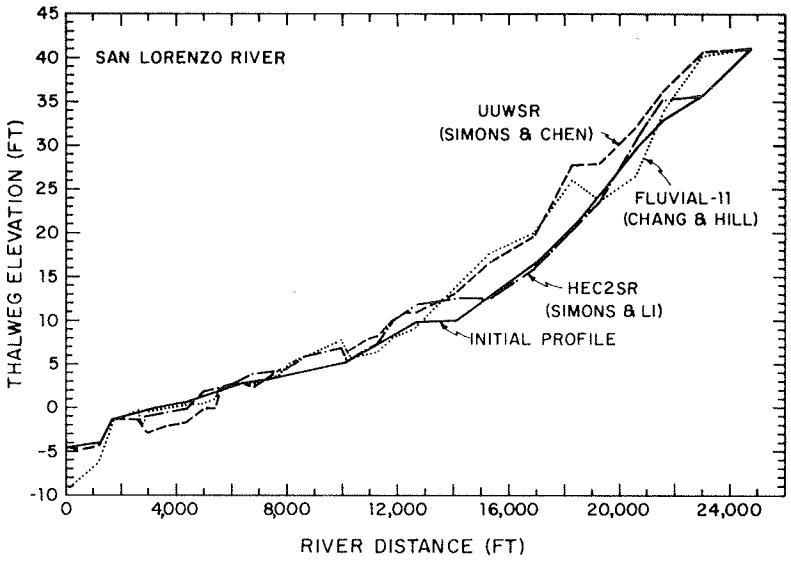

FIGURE 1 Comparison of computed thalweg elevations for the San Lorenzo River.

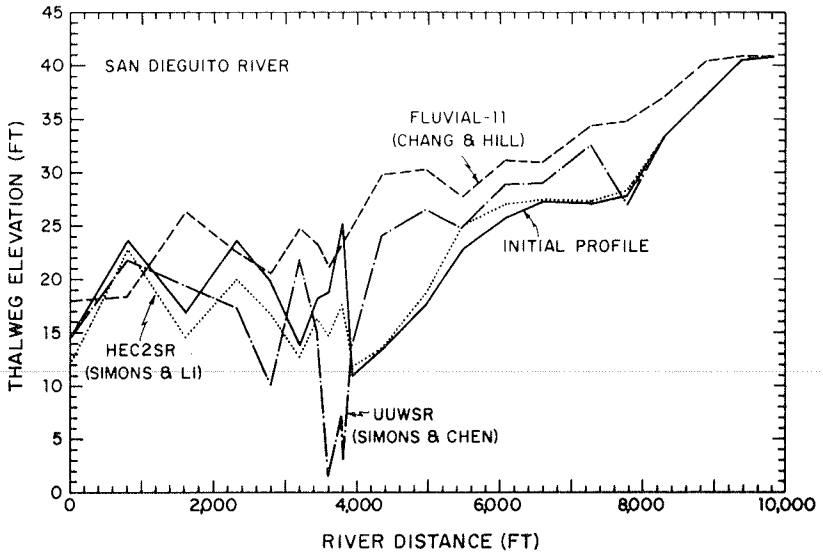

FIGURE 2 Comparison of computed thalweg elevations for the San Dieguito River.

evolution through use of simple Manning-Strickler equations for energy loss.

The use of KUWASER is limited to subcritical flows and channels without extremely irregular grade and geometry. However, it has the capability to model the mainstem and tributaries of a river system and can simulate divided flow associated with bars, islands, or channel breaches.

HEC-6 (Hydrologic Engineering Center)

The HEC-6 program was developed at the Hydrologic Engineering Center of the U.S. Army Corps of Engineers in 1977 (18,19). The quasi-steady backwater equation (5) is used to compute water-flow conditions uncoupled from the sediment-continuity equation, with expansion and contraction losses explicitly taken into account. The Manning-Strickler equation is used to compute energy loss caused by bed and bank roughness; roughness coefficients must be specified as input data, though they can be allowed to vary with discharge or stage.

The sediment-continuity equation (3) is solved using an explicit finite-difference scheme, with sediment-transport capacities determined from water-flow conditions previously determined in the uncoupled backwater computation. The entire movable-bed portion of the channel is assumed to aggrade or degrade uniformly. Sediments are routed by individual size fraction, which makes possible a detailed accounting of hydraulic sorting and development of an armored layer. Bank lines are assumed to be stable and fixed in the HEC-6 computation.

HEC-6 offers a choice of five sediment transport functions in Equation 4: Laursen's relationship, as modified by Madden for large rivers (20); Toffaleti's formula (21); Yang's stream-power formula (22); DuBoys' formula (23); and a special relationship between unit-width sediment-transport capacity and the product of the depth and energy slope developed for the particular river reach under study. In all these relations, it is assumed that sediment-transport capacity can be determined independently of flow conditions; that is, Equation 4 does not explicitly include the coupling of flow resistance and sediment transport through bed-form development.

HEC-6 is strictly a one-dimensional model with no provision for simulating the development of meanders or specifying a lateral distribution of sediment-transport rate across the section. The model is not suitable for rapidly changing flow conditions but can be applied to predict reservoir sedimentation, degradation of the streambed downstream from a dam, and long-term trends of scour or deposition in a stream channel, including the effects of dredging.

CHAR II (Charriage dans les Rivieres)

The CHAR II modeling system was developed by the French consulting engineering firm SOGREAH in the early 1970s (1,24,25). It is a coupled, quasi-steady model, simultaneously solving Equations 3 and 5 using an implicit finite-difference scheme. Energy losses caused by bed roughness are based on the Manning-Strickler equation, with overall section conveyances computed as the sums of individual rectangular sections following Chow's method (26). Localized energy losses and hydraulic works are modeled with the appropriate equations discretized between two adjacent computational points.

CHAR II considers banks to be nonerodible. Degradation and aggradation volumes are assumed to be uniformly distributed across the wetted channel section. No procedures for hydraulic sorting or armoring are included in the methodology, which considers only a single representative size fraction.

Sediment transport in the present version of CHAR II is limited to bed load, computed with either the Meyer-Peter and Mueller, Engelund-Hansen, DuBoys, or Einstein-Brown formulae (2) for Equation 4. Hydraulic roughness and sediment transport are uncoupled in CHAR II; SOGREAH's CHAR IV program, although less industrialized than CHAR II, does take this coupling into account through use of the full Einstein method (11).

CHAR II is designed for simulation of long-term riverbed evolution and sedimentation in reservoirs. A mainstem river and its tributaries can be modeled simultaneously with a variety of hydraulic works. The method is not inherently limited to bed-load transport because users can relatively easily add subroutines to compute total load using methods of their choice.

IALLUVIAL (Iowa ALLUVIAL River Model)

The IALLUVIAL program was developed between 1979 and 1982 by Karim and Kennedy at IIHR (6). It is for-

mally classified as an iteratively coupled, quasi-steady model; in each time step Equation 5 is solved with bed elevations fixed; then Equation 3 is solved, using sediment-transport capacities determined as an integral part of the solution of Equation 5, to compute bed-elevation changes. Hydraulic sorting and armoring are then computed in a third phase. The entire procedure is iteratively repeated in each time step until the finite-difference analogues of Equations 3 and 5 are simultaneously satisfied at the end of the time step, although in most applications a single iteration (uncoupled) is sufficient.

The sediment-continuity equation includes sediment contributions from bank erosion and tributaries, and the effects of bank-line geometry changes can be simulated by explicit introduction of known width changes with time. The effects of dredging, cutoffs, and vertical variations in bed-sediment composition are taken into account in the computation.

IALLUVIAL is based on the total load transport model (TLTM) of Karim and Kennedy (27). This system of nonlinear equations, developed through dimensional reasoning and regression analysis of extensive laboratory and field data, specifically incorporates the coupling between sediment-transport capacity and hydraulic-energy losses; thus Equation 4 becomes an integral part of Equation 5.

Although TLTM computes transport capacity based on a mean sediment size, another empirical relationship (27) is used to allocate the total load among the size fractions present on the bed surface. Thus a detailed accounting of hydraulic sorting and armoring processes is included in the program (3).

IALLUVIAL is best suited for the prediction of long-term bed changes following a perturbation to the mainstem river. It has recently been used for extensive study of Missouri River degradation following upstream regulation and channelization (7).

Examples of Long-Term Model Performance

The first example is the performance of KUWASER, HEC-6, and CHAR II when applied to the pool 20 reach of the Mississippi River (RM 343.2-364.2) between Keokuk, Iowa, and Canton, Missouri (5). Periodic, high-cost maintenance dredging has been necessary to maintain the 9-ft depth along the barge passageway in the vicinities of Fox and Buzzard Islands (RM 355-6 and RM 349-50) of pool 20 because of localized shoaling problems. To understand the basic mechanisms responsible for the shoaling problems, two field studies were conducted to obtain detailed information about the flow and sediment-transport characteristics along the shoaling reaches. On the basis of the field data collected, detailed geometric, hydrologic, and sediment-input data were prepared and the three models, KUWASER, HEC-6, and Char II, were tested at Colorado State University, IIHR, and SOGREAH, respectively.

Simulation runs of these models were made for a 28-month period between May 1976 and August 1978. Figure 3 shows the initial, computed, and measured thalweg elevations. The degree of agreement between the computed and measured values is seen to be of almost the same order for each model. It should be noted that KUWASER used a 5-day time step for a water discharge over 100,000 cfs, a 10-day time step for a discharge between 50,000 cfs and 100,000 cfs, and a 30-day time step for a discharge below 50,000 cfs. HEC-6 used monthly averaged flow quantities, and CHAR II used a temporal computation interval ranging between 6 hr and 5 days.

The second example is the application of the IALLUVIAL model to the Missouri River from Gavin's Point Dam down to Omaha. Extensive channelization of most of this 200-mile reach, and virtual complete shut-off of upstream sediment supply by the closure of Gavin's Point Dam, has resulted in severe bed degradation of up to 8 ft in the period 1957-1977. Bed-surface armoring and bed-material coarsening caused by hydraulic sorting appear to be fundamentally important factors in the river's approach to a new equilibrium. IALLUVIAL's incorporation of these phenomena grew out of its specific development goal of becoming a Missouri River prediction model.

Figure 4 shows a comparison of measured and predicted bed and water-surface elevation changes for the 20-year study period (6). This successful simulation of past results has led to further refinements of the input-data set and a program of prognosis simulations to predict river behavior for the next 20 years under various river-management scenarios (7).

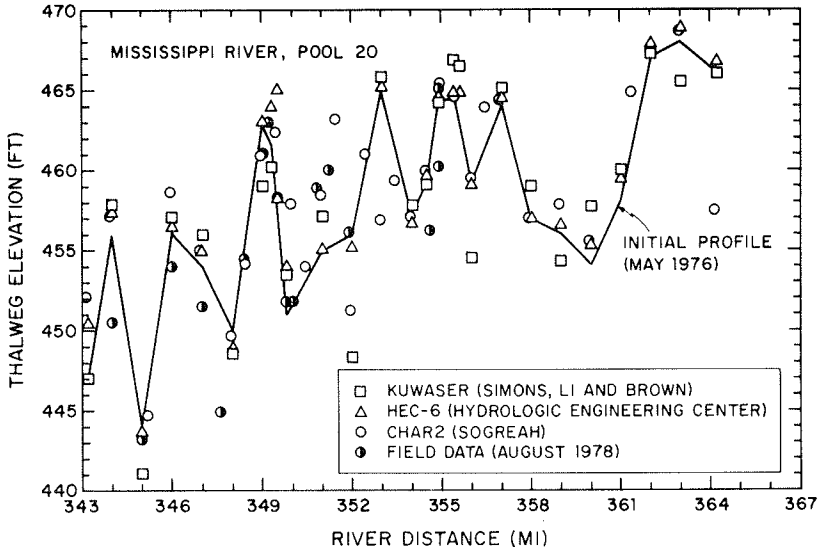

FIGURE 3 Comparison of computed thalweg elevations and several spot measurements for pool 20, Mississippi River.

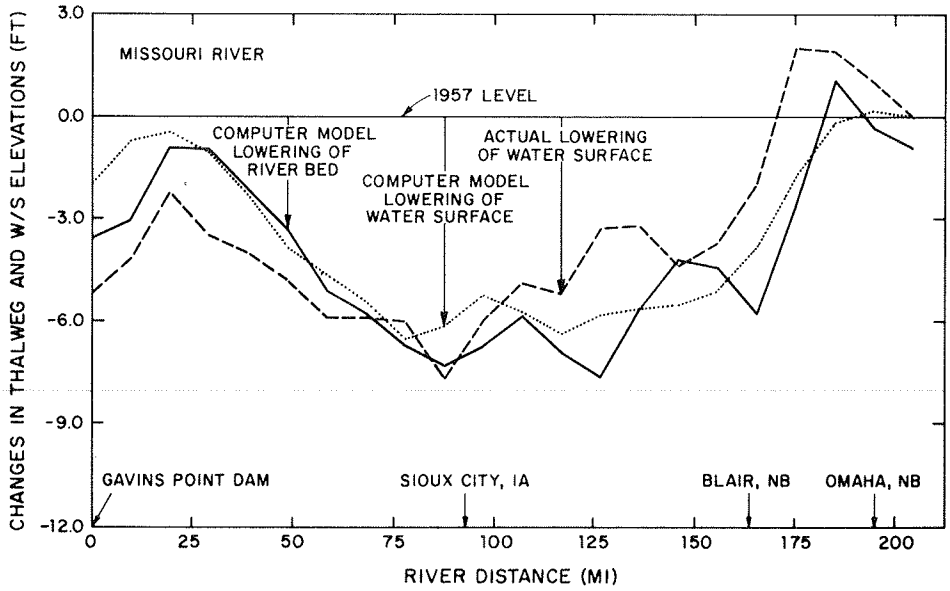

FIGURE 4 Comparison of observed and computed (IALLUVIAL) riverbed degradation and water-surface elevations (36,000 cfs) for the Missouri River.

ASSESSMENT OF STATE-OF-THE-ART ABILITY

Common to all alluvial river-flow models are requirements for the following input information: (a) accurate initial conditions, including a cross-sectional profile and bed-material size distribution at each computational cross section; (b) accurate boundary conditions such as water and sediment inflows along the boundaries, quantitative expressions of bed-load and suspended-load discharges, size distributions of boundary-sediment input, and stage hydrographs at the upstream and downstream boundaries; and (c) bed-roughness characteristics at each computational point. It is clear that a computer simulation would be meaningless without the first and second requirements, and the lack of the third requirement would yield an erroneous estimation of flow characteristics, resulting in erroneous feedback of flow information to the riverbed.

The exclusion of even one of these three requirements may lead to serious errors in computer simulations. However, one can hardly be provided with a complete set of input data in any prototype numerical application. Therefore, a great number of assumptions often have to be made to fill the gap in the input data. Even if adequate data are provided for a study river, there still remains a need to calibrate and verify the model by means of field data. In most natural rivers, only extremely limited field data are available for high flood stages at which major riverbed changes occur, and, consequently, adequate calibration or verification of the models normally cannot be obtained. In this sense, the capability of the alluvial river-flow models can best be assessed according to how accurately they can predict riverbed changes with limited sources of input data. A numerical modeler should be aware of which input information is most important to the final result of predicting riverbed changes.

The National Research Council study (4) pointed out that a principal deficiency of most of the available numerical models described in this paper is their inability to accurately predict channel roughness when calibration data are insufficient. It was in the calculation of sediment-discharge capacities that the various models examined differed most widely. A reliable sediment-transport formula is a prerequisite to reliable estimates of channel-geometry changes because riverbed degradation and aggradation are computed from streamwise gradients in the sediment-transport capacity of streams as the sediment-continuity equation states. The bed-armoring process during channel degradation is also not well understood and has not been adequately formulated. Armoring and the resulting coarsening of the bed-material size have a direct effect on the sediment-transport capacity and the channel-bed roughness or friction factor and thereby impact on the mean velocity, depth, and friction slope of the flow. Bed-degradation processes are generally slowed by bed armoring.

RESEARCH NEEDS

The surprisingly large discrepancies among the computed results described earlier may be taken as symptomatic of inadequate input and calibration data. However, it also may be true that any modeler would be able to simulate observed changes in thalweg elevation exactly by adjusting the model's "tuning knobs" (calibration parameters) if there were fully adequate river data available. At present no alluvial riverbed model seems mature enough to answer the question: What are the input and calibration data required for the model to yield convincing, reliable results? Simple artificial adjustments of the tuning knobs in the numerical simulation, based on the availability of plentiful data, does not appear to be a satisfactory way of predicting riverbed changes.

The most important overall need is for better interpretation of physical processes and their incorporation in the numerical models. Numerical techniques for solution of the governing equations are now adequately developed for accurate prediction of alluvial riverbed profiles if an accurate sediment-transport function and a bed-roughness predictor were available. Improvement in model reliability requires further research in the areas described hereafter.

First, there is a strong need for a very reliable sediment-transport relation because alluvial riverbed changes are the result of a streamwise gradient in the stream's sediment-transport capacity.

Second, the bed-armoring process during channel degradation is not well understood and has not been adequately formulated in a conceptual model. Armoring and coarsening of the bed-material size have a direct effect on the sediment-transport capacity and the bed-friction factor, and consequently affect the velocity, depth, and energy slope of the flow.

Third, there is a need to develop a better friction-factor predictor that depends on flow depth and velocity and sediment discharge.

Fourth, there is a need to incorporate into models the bank-erosion and channel-migration effects of channel widening.

Fifth, it is unlikely that an alluvial riverbed model that is applicable to all types of rivers will be forthcoming in the near future. Instead, each model will be most dependable for rivers of the type for which it was developed. Therefore, there is a need for an effort to classify natural rivers in terms of their hydraulic and geomorphologic characteristics, to guide engineers in the selection and application of a model that uses formulations of sediment discharge, channel roughness, channel widening, and so on that are most appropriate for their study cases.

If there is one important message to be drawn from this catalog of deficiencies, it is the following: Model developers and users must not let their preoccupations with improvements in numerical methods, user friendliness, program generalization, and other pleasant but peripheral concerns cause them to lose sight of the central and often unpleasant need to obtain a better understanding and conceptual formulation of the basic physical processes of alluvial riverbed evolution.

REFERENCES

1. J.A. Cunge, F.M. Holly, Jr., and A. Verwey. Practical Aspects of Computational River Hydraulics. Pitman, New York, 1981.
2. V.A. Vanoni. Sedimentation Engineering. ASCE Manuals and Reports on Engineering Practices No. 54. ASCE, New York, 1975.
3. M.F. Karim, F.M. Holly, Jr., and J.F. Kennedy. Bed Armoring Procedures in IALLUVIAL and Application to the Missouri River. IIHR Report No. 269. Iowa Insitute of Hydraulic Research, University of Iowa, Iowa City, 1983.
4. An Evaluation of Flood-Level Prediction Using Alluvial-River Models. National Research Council, Washington, D.C., 1983.
5. T. Nakato and J.L. Vadnal. Field Study and Tests of Several One-Dimensional Sediment-Transport Computer Models for Pool 20, Mississippi River. IIHR Report No. 237. Iowa Institute of Hydraulic Research, University of Iowa, Iowa City, July 1981.
6. M.F. Karim and J.F. Kennedy. IALLUVIAL: A Computer-Based Flow- and Sediment-Routing Model for Alluvial Streams and its Application to the Missouri River. IIHR Report No. 250. Iowa Institute of Hydraulic Research, University of Iowa, Iowa City, Aug. 1982.
7. F.M. Holly, Jr., and M.F. Karim. Computer Simulation Prognosis for the Degradation of the Missouri River Between Gavins Point Dam and Iowa's Southern Border. IIHR Report No. 267. Iowa Institute of Hydraulic Research, University of Iowa, Iowa City, 1983.
8. HEC-2 Water Surface Profiles, Programmers Manual. Hydrologic Engineering Center, U.S. Army Corps of Engineers, Davis, Calif., Aug. 1981.
9. Simons and Li Associates, Inc. Scour and Sedimentation Analysis of the Proposed Channelization of the Salt River for Protecting the Sky Harbor International Airport in Phoenix, Arizona. Howard, Needles, Tammen, and Bergendoff, Kansas City, Mo., 1980.
10. E. Meyer-Peter and R. Mueller. Formulas of Bed-Load Transport. Report on Second Meeting of International Association for Hydraulic Research, Stockholm, Sweden, 1948, pp. 39-64.
11. H.A. Einstein. The Bed Load Function for Sediment Transportation in Open Channels. Technical Bulletin 1026. Soil Conservation Service, U.S. Department of Agriculture, 1950.
12. B.R. Colby. Relationship of Unmeasured Sediment Discharge to Mean Velocity. Transactions, American Geophysical Union, Vol. 38, No. 5, Oct. 1957.
13. D.B. Simons and Y.H. Chen. A Mathematical Model of the Lower Chippewa River Network System. Report CER78-79-DBS-YHC58. Colorado State University, Fort Collins, June 1979.
14. H.H. Chang and J.C. Hill. Computer Modeling of Erodible Flood Channels and Deltas. Journal of the Hydraulics Division, ASCE, Vol. 102, No. HY10, Oct. 1976.
15. W.H. Graf. Hydraulics of Sediment Transport. McGraw-Hill, New York, 1971.
16. F. Engelund and E. Hansen. A Monograph on Sediment Transport in Alluvial Streams. Teknisk Vorlag, Copenhagen, Denmark, 1967.
17. D.B. Simons, R.M. Li, and G.O. Brown. Sedimentation Study of the Yazoo River Basin--User Manual for Program KUWASER. Report CER79-80DBS-R. Colorado State University, Fort Collins, Aug. 1979.
18. Scour and Deposition in Rivers and Reservoirs. Computer Program HEC-6. Hydrologic Engineering Center, U.S. Army Corps of Engineers, Davis, Calif., March 1977.
19. W.A. Thomas and A.L. Prasuhn. Mathematical Modeling of Scour and Deposition. Journal of the Hydraulics Division, ASCE, Vol. 103, No. HY8, Aug. 1977.
20. E.M. Laursen. The Total Sediment Load of Streams. Journal of the Hydraulics Division, ASCE, Vol. 54, Feb. 1958.
21. F.B. Toffaleti. A Procedure for Computation of the Total River Sand Discharge and Detailed Distribution, Bed to Surface. Technical Report 5. Committee on Channel Stabilization, U.S. Army Corps of Engineers, Vicksburg, Miss., Nov. 1968.
22. C.T. Yang. Incipient Motion and Sediment Transport. Journal of the Hydraulics Division, ASCE, Vol. 99, No. HY10, Oct. 1973.
23. C.B. Brown. Sediment Transportation. In Engineering Hydraulics, H. Rouse, Ed., Wiley, New York, 1950.
24. J.A. Cunge and J.A. Perdreau. Mobile Bed Fluvial Mathematical Models. La Houille Blanche, No. 7, 1973.
25. Modeling of River Longitudinal Profile Evolution Using the CHAR2 System. SOGREAH Consulting Engineers, Grenoble, France, Oct. 1978.
26. V.T. Chow. Open-Channel Hydraulics. McGraw-Hill, New York, 1959.
27. M.F. Karim and J.F. Kennedy. Computer-Based Predictors for Sediment Discharge and Friction Factor of Alluvial Streams. IIHR Report 242. Iowa Institute of Hydraulic Research, University of Iowa, Iowa City, Dec. 1981.

Publication of this paper sponsored by Committee on Hydrology, Hydraulics and Water Quality.

Modeling General Scour at Bridge Crossings

HOWARD H. CHANG

ABSTRACT

Modeling of general scour at bridge crossings using a mathematical model for water and sediment routing is described. For a given bridge configuration, general scour that results from imbalance in sediment supply and transport capacity of the river is evaluated based on river channel evolution reflecting the flow and sediment-transport processes. Two case studies are presented to illustrate the prediction of general scour caused by man-made factors including sand mining and flow constriction by a bridge. Depth of general scour is found to be sensitive to channel width; therefore, width formation of the alluvial river plays an important role in scour development.

River-channel scour may be considered as consisting of local scour and general scour. Local scour that occurs around bridge piers and abutments is caused by local obstructions to flow. General scour refers to the change in river-channel configuration provoked by sediment imbalance, due to natural or man-made causes, between the supply and transport capacity of the river. The bridge structure is one such man-made cause if it interferes with the flow pattern. Because general scour at bridge crossings is related to the flow and sediment-transport processes of the adjacent river as a system, evaluation of such scour requires modeling of the river channel for water and sediment routing.

Bridges are often constructed with the span shorter than the channel width, particularly across broad floodplains in semiarid regions. Therefore, the river flow is often constricted at the bridge crossing, resulting in higher velocities and channel-bed scour. Flow constriction at the bridge crossing varies with the discharge or stage. During high flows, the river channel is wide and thus the constriction effect is more pronounced. In this situation, greater general scour at the bridge crossing can usually be expected. During low flows, the channel width may be less than the bridge opening and thus flow constriction no longer exists. Therefore, general scour caused by the constriction effect during the high flood stage may be refilled to the preflood level during the subsequent low-flow period. Because the riverbed cannot be observed during flood stage because of muddy water, such major scours may occur but not be noticed. However, because the bridge footings are affected by the scour, such scour development should be evaluated for bridge design and restoration.

General scour develops when more sediment is removed from an area than is supplied from upstream. This development is accompanied by changes in bed-material composition caused by hydraulic sorting and by other river-channel changes. These changes provide the mechanisms with which the river seeks to establish equilibrium in sediment transport; that is, equal sediment load along the river reach. Net scour at the bridge crossing ceases when equilibrium is established or when bed armoring forms to prevent further scour.

The mathematical model FLUVIAL-11 (1), which was developed for water- and sediment-routing in alluvial channels, is employed for modeling general scour. For a given river channel and bridge configuration, river-channel changes in channel-bed profile, width, and sediment composition can be evaluated using this model for specified flow conditions. The scour depth is directly measured by the channel-bed elevation. Because channel-bed profile is part of river-channel formation, which also involves channel width, evaluation of the scour depth must also consider width changes.

THE MATHEMATICAL MODEL

The mathematical model, FLUVIAL-11 has five major components: (a) water routing, (b) sediment routing, (c) changes in channel width, (d) changes in channel-bed profile, and (e) lateral migration of the channel as detailed in previous publications (1,2). This model employs a space-time domain in which the space domain is represented by the discrete cross sections along the river reach and the time domain is represented by discrete time steps. In water routing, the time and spatial variations of the discharge, stage, velocity, energy gradient, and so forth along the reach are obtained by an iterative procedure. At each time step, sediment discharge at each cross section is computed; changes in channel width, channel-bed profile, and lateral migration are obtained and applied to each cross section. The bed-material composition is updated at each time step. Because changes in channel geometry and bed-material composition are slow in comparison with water routing, corrections for them are made separately for each time step.

Width changes are related to energy expenditure. Simulation of width variation is based on the concept of minimum stream power. At a time step, width corrections for all cross sections are such that the total stream power (or rate of energy expenditure) for the reach is minimized. These corrections are subject to the physical constraint of rigid banks and limited by the amount of sediment removal or deposition along the banks within the time step. Total stream power of a channel reach is

$$P = \int_L \gamma Q S dx \qquad (1)$$

where

P = total stream power of the reach,
L = length of the reach,
Q = discharge,
S = energy gradient,
γ = specific weight of water and sediment mixture, and
x = distance in the flow direction.

Written in finite-difference form, this equation becomes

$$P = \sum_{i=1}^{N-1} 1/2\,[\gamma(Q_i S_i + Q_{i+1} S_{i+1})\Delta x_i] \qquad (2)$$

where

N = total number of cross sections for the reach,
i = cross-sectional index, and
Δx_i = distance between sections i and i + 1.

Previous studies (2-4) have established that minimum stream power for an alluvial river reach is equivalent to equal power expenditure per unit channel length, that is, constant QS along the reach. A river reach undergoing changes usually has uneven spatial distribution of power expenditure or γQS. Usually the spatial variation in Q is small but that in S is pronounced. Total stream power of a reach decreases with the reduction in spatial variation of QS or S along the reach. Adjustments in channel widths are made in such a way that the spatial variation of QS is minimized subject to the constraints and limitations stated previously. An adjustment in width reflects the river's adjustment in flow resistance, that is, in power expenditure. A reduction in width at a cross section is usually associated with a decrease in energy gradient for the section, whereas an increase in width is accompanied by an increase in energy gradient. Following these guidelines, a technique for width correction has been developed (2).

Width changes in alluvial rivers are characterized by the formation of small widths at degrading reaches and widening widths at aggrading reaches (2-7). Such changes represent adjustment of the river's resistance to equalize power expenditure along its course as described later. A degrading reach usually has a higher channel-bed elevation and energy gradient than do its adjacent sections. Formation of a narrower and deeper channel at the degrading reach decreases its energy gradient because of reduced boundary resistance and lowered elevation. On the other hand, an aggrading reach is usually lower in channel-bed elevation and energy gradient. Widening at the aggrading reach increases its energy gradient because of increased boundary resistance. These adjustments in channel width reduce the spatial variation in energy gradient and total power expenditure of the channel. Because the sediment discharge is proportional to the stream power (8), these adjustments also favor the establishment of channel sediment-load equilibrium.

A river's adjustment in width in relation to power expenditure may also be explained based on the water-surface profile. If the energy gradient is approximated by the water-surface slope, the equal energy gradient is equivalent to the straight water-surface profile. A river reach undergoing changes usually has an uneven water-surface profile, but it constantly seeks to establish a straight profile through adjustments in channel geometry, roughness, and so forth subject to physical constraints such as abutments, rigid banks, and check dams. In this model, the channel geometries are adjusted, subject to the constraints, so that they favor uniformity in the water-surface profile.

SANTA MARGARITA RIVER STUDY

General scour at a bridge crossing caused primarily by the flow-constriction effect may be illustrated by the Santa Margarita River study using the FLUVIAL-11 program. The study reach of the river is near the Basilone Road bridge (Figure 1) at Camp Pendleton, California. Because it is an ephemeral river, the Santa Margarita flows only during floods. The width of flow varies significantly with the discharge. For the 100-year flood, the floodplain is

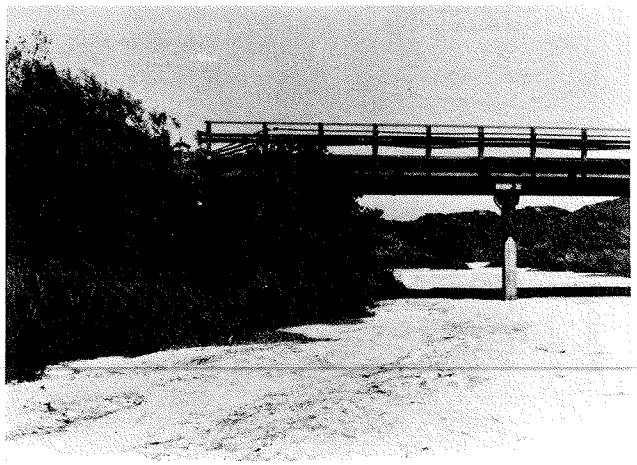

FIGURE 1 Basilone Road bridge on Santa Margarita River.

computed to be about 1,000 feet wide, but the channel during low flows may be 10 to 20 feet wide. The Basilone Road bridge has long approach embankments and a span of 200 ft. Except at very high flood stages when flood waters are overtopping the approach embankments, flood flows are confined to the small bridge opening in the broad floodplain.

A major flood with a magnitude approximately that of a 50-year flood occurred in the winter of 1978. A picture taken after this flood (Figure 1) shows no sign of significant channel-bed scour at the bridge crossing. However, evidence of severe scour at this location during the flood was strong (9). For example, muddy flows of very high velocities through the constriction were observed, and bridge abutments were undermined. Eroded bridge abutments were repaired and reinforced after the flood. During inspection excavation of the bridge footings, which reach about 10 feet below the riverbed, a broken reinforced concrete pile was found; its 40-ft lower section was never found. This could be explained only by the fact that this pile section was washed away during the flood.

A simulation study of the Santa Margarita River near the bridge crossing at Basilone Road was done using the FLUVIAL-11 model. The hydrograph of the 50-year flood used in the study is shown in Figure 2. Simulated results shown in Figure 3 include the spatial variations of water surface, channel invert, and mean velocity at different time intervals. At peak discharge (t = 30 hr), maximum channel-bed scour at the bridge crossing is predicted to reach a minimum elevation of 57.3 ft, which means a scour

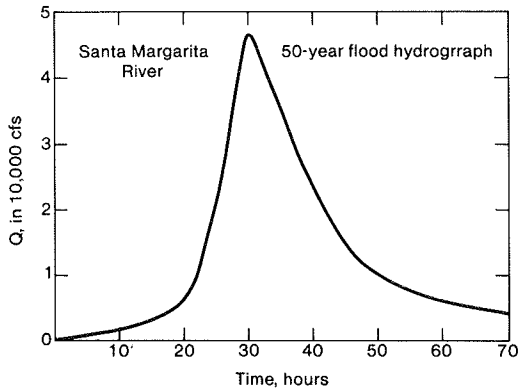

FIGURE 2 Flood hydrograph, Santa Margarita River.

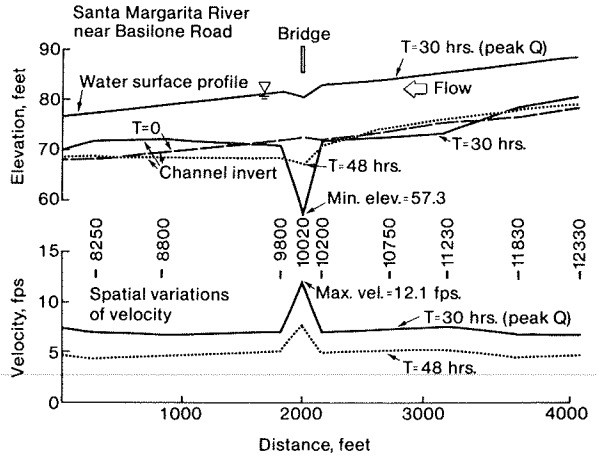

FIGURE 3 Simulated results for 50-year flood.

depth of 15.4 ft from the original bed level. At this discharge, the flood channel has a width about 5 times that of the bridge opening. However, the width of flood flow decreases with discharge during the falling limb of the hydrograph. Thus, as the flow-constriction effect becomes gradually less so does the channel-bed scour at the bridge crossing. In the absence of other factors for general scour, restoration of the channel bed, more or less to its preflood level at the end of the flood, is predicted.

At peak flood, the river reach has an uneven width, primarily because of the small bridge opening. Although at this time the river channel has established a more or less uniform sediment load along the reach, the energy gradient is not constant as indicated by the uneven water-surface profile near the bridge shown in Figure 3. The physical constraint in width at the bridge crossing prevents the formation of a straight water-surface profile through the bridge. This example demonstrates that continuity in sediment transport (i.e., equal sediment load along the reach) does not necessarily mean equal energy gradient or constancy in power expenditure. Therefore, they are independent physical conditions.

SAN DIEGUITO RIVER STUDY

The San Dieguito River at Rancho Santa Fe, California, experienced significant changes in a 2-mile reach (Figure 4) during recent floods. The bridge on Via de Santa Fe Road was damaged (Figure 5) by channel-bed scour and high velocities. Documentation of river-channel changes and flood hydrographs were made by the county of San Diego (10,11); these provide a valuable set of field data for river studies. The study reach is about 4 miles from the ocean and about 5 miles below Lake Hodges Dam. The channel has a wide and flat natural configuration; the natural slope and bed-material size decrease significantly in the downstream direction. Bed material of the study reach varies from coarse sand (d_{50} = 0.85 mm) at the upstream end to fine sand (d_{50} = 0.24 mm) downstream.

The natural channel configuration was changed before recent flood events by man's activities including sand mining and construction of the Via de Santa

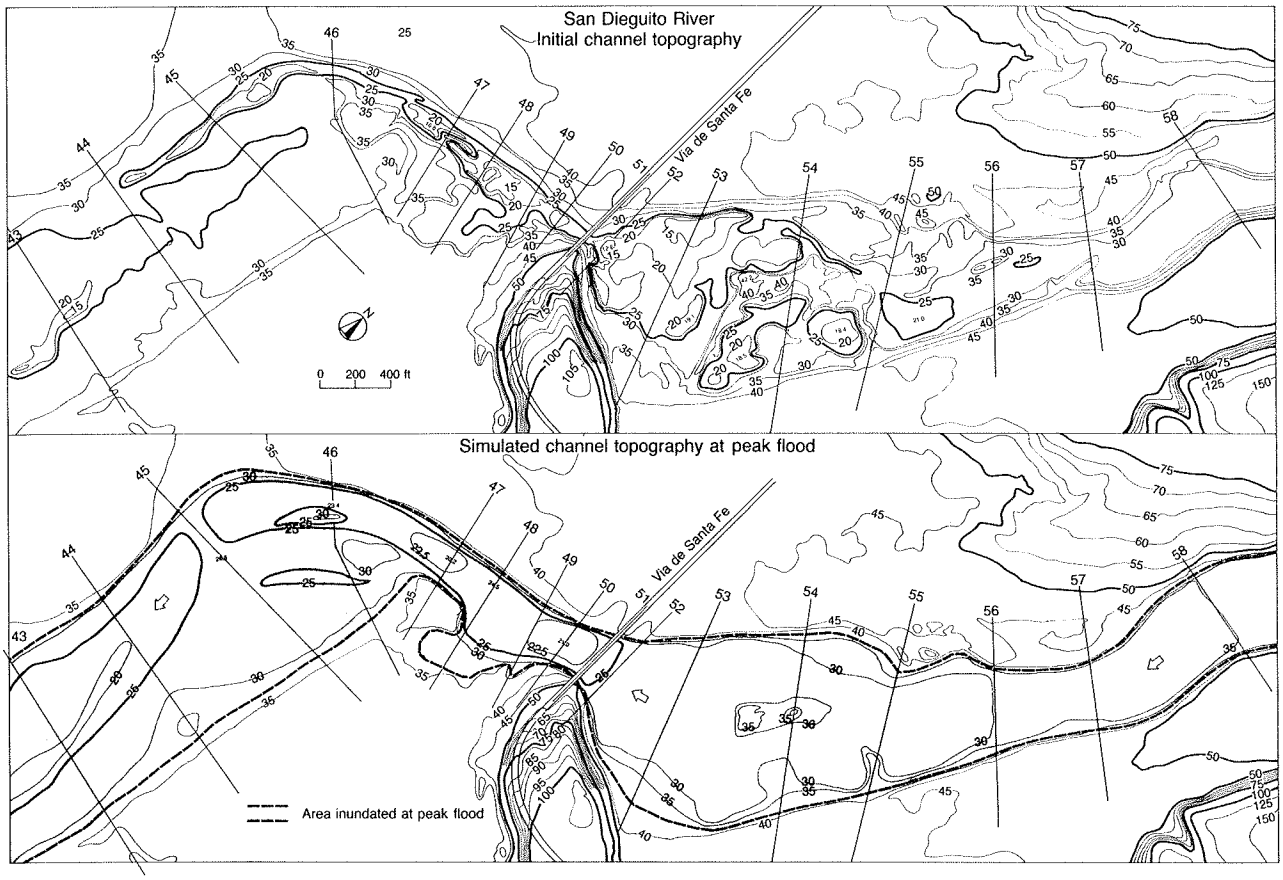

FIGURE 4 Topography and location of cross sections.

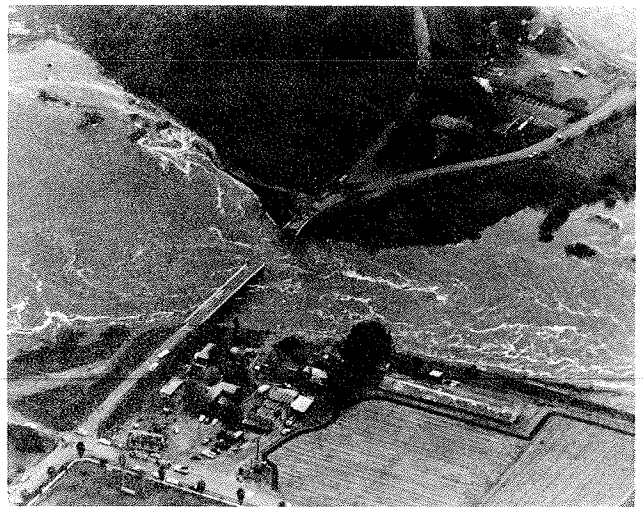

FIGURE 5 Damaged bridge on San Dieguito River.

Fe Road and bridge shown in Figure 4. As a result of sand mining, several large borrow pits, both upstream and downstream of the bridge, with a depth as great as 25 feet were created. The natural wide channel is encroached on by the approach embankment on each side of the bridge (section 51). The river channel has erodible bed and banks; the banks, however, are constrained by the hills at the south bank of section 51 and along the north banks of sections 60 to 63 and by bank protections at the north banks of sections 51 and 58.

Two floods passed through the river in March 1978 (peak flow = 4,400 cfs) and in February 1980 (peak flow = 22,000 cfs) when Lake Hodges spilled. Hydrographs of these floods are shown in Figure 6. Be-

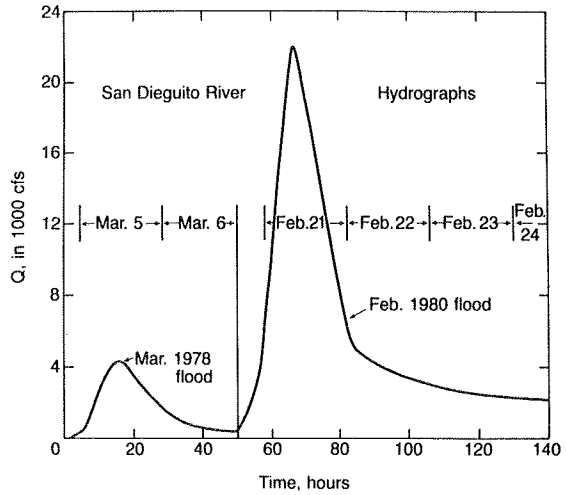

FIGURE 6 Flood hydrographs, San Dieguito River.

fore these events, Lake Hodges had not spilled for 26 years. Significant changes in the river channel were observed after the March 1978 flood. Channel-bed scour occurred near borrow pits and notably at the bridge crossing where measurements were made (Figure 7). Deposition was observed in the borrow pits. Because of limited flood discharge and duration, these borrow pits were only partly refilled. Major changes in the river channel occurred during the greater February 1980 flood. These changes in-

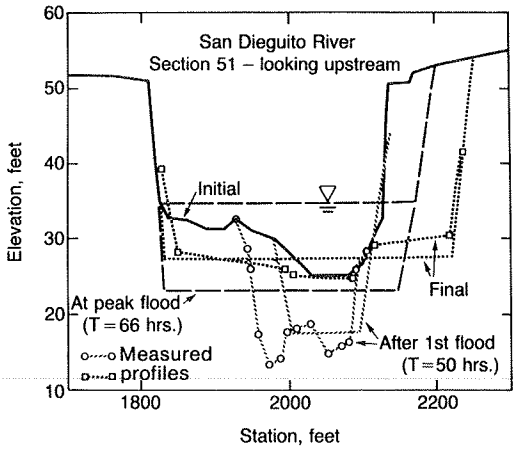

FIGURE 7 Simulated and measured riverbed profiles at bridge crossing.

cluded channel-bed aggradation and degradation, width variation, and lateral migration of the channel (1).

The mathematical model FLUVIAL-11 was used to simulate river-channel changes in the San Dieguito River during the 1978 and 1980 floods. Graf's equation (12) for bed-material load was used in computing sediment movement. Channel roughness in terms of Manning's n was selected to be 0.035 in consideration of channel irregularity and minor vegetation growth; it was estimated to be 0.04 at the bridge crossing. A combined duration of 140 hours for these two floods was computed using 2,000 time steps.

Simulated results are shown in Figures 4, 7, and 8. River-channel changes, including those in channel-bed profile and channel width, as simulated by the computer model, are described herein. Changes in the longitudinal channel-bed profile (Figure 8) are characterized by aggradation in the borrow pits, erosion of higher grounds, and the gradual formation of a more or less smooth channel-bed profile at the end of the flood. In that process, considerable variation in the longitudinal channel-bed elevation through the downstream portion of the river reach is predicted at peak flood as shown in Figures 4 and 8. The higher channel-bed elevations at sections 45, 46, and 48 are associated with large channel widths, and the lower elevations at sections 47 and 50 are due to their smaller widths. Changes in channel width that occur concurrently with variations in channel-bed elevation are simulated. Width changes are characterized by the gradual widening of the initially narrow sections, notably sections 47, 49, 50, 51, 57, 58, and 59 and reductions in width of initially wide sections, notably sections 53 and 54. Simulated channel width at peak flood (shown in Figure 4) is highly uneven in its spatial variation along the river. This variation is gradually reduced during the flood. Widening of a section is caused by bank erosion, and reduction in width is usually caused by sandbar formation along the bank.

That changes in channel width and channel-bed elevation are closely related may be illustrated by the simulated time variation of the cross-sectional profile at the bridge crossing (Figure 7). Initially this section is on a sand ridge with borrow pits on both sides (Figures 4 and 8). Gully erosion through this sand ridge during the first flood is simulated, followed by gradual widening and lessening of the gully depth during the second flood. The maximum scour depth is predicted to occur in the initial gully. The simulated results correlate well with

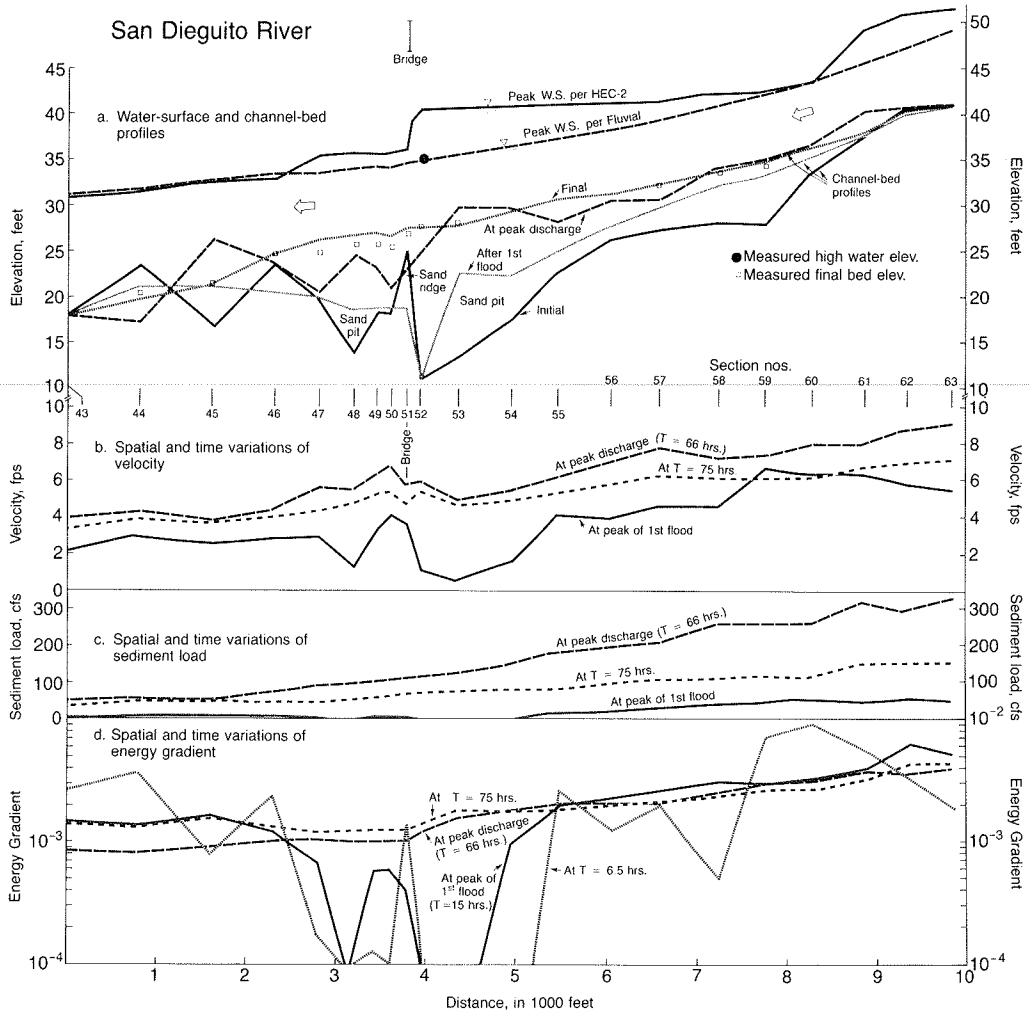

FIGURE 8 Simulated and measured results.

measurements at this section shown in Figure 7, in which the uneven final channel-bed profile as measured is related to the removal of several piers during the flood (Figure 5).

RIVER-CHANNEL CHANGES IN RELATION TO POWER EXPENDITURE

Changes in river-channel configuration are accompanied by changes in flow resistance and hence in the rate of energy (or power) expenditure. The γQS product represents the rate of energy expenditure per unit channel length. Because the spatial variation of Q is small, the spatial variation of γQS may be represented by the spatial variation of the energy gradient S shown in Figure 8. Simulated river-channel changes are associated with the gradual reduction of the spatial variation of energy gradient along the channel subject to the physical constraint of rigid banks. That the adjustment in river-channel configuration is closely related to the change in power expenditure can be illustrated by the sequential changes of cross-sectional profile at the bridge crossing as shown in Figure 7. Because it is initially on a sand ridge, the energy gradient at this section is initially much greater than those of adjacent sections. This pronounced spatial variation in energy gradient is reduced through gully formation in this section and deposition in adjacent sections. The gully, which is small in width and has a low channel-bed elevation, provides the least possible flow resistance and hence the lowest energy gradient at this section; it also reduces the backwater effect on the upstream section and thereby increases its energy gradient. At subsequent time intervals, the energy gradient at this section becomes less than those of adjacent sections. Cross-sectional changes at this section then include channel widening and aggradation in the gully. These changes are accompanied by increases in boundary resistance and energy gradient at this section, favoring the establishment of equal energy gradient along the reach. This pattern of river-channel changes, characterized by the formation of a narrow channel during channel-bed degradation and a wider channel during aggradation, is evident in nature and has been reported elsewhere (3-7, 13).

SUMMARY

General scour represents river-channel changes in response to any change imposed on the river by nature or by men. Because channel-bed evolution at bridge crossings is related to the flow and sediment-transport processes of the river reach as a system, general scour is evaluated using a mathematical model for water and sediment routing. Sample studies are presented to illustrate scour development caused by sand mining in the adjacent river channel and by flow constriction at the bridge open-

ing. Although scour depth is measured by channel-bed elevation, evolution of bed elevation is found to be closely related to variation in channel width. Greater scour depth often occurs in a narrower channel and vice versa. For the ephemeral rivers studied, width changes are generally greater in magnitude than is scour development.

REFERENCES

1. H.H. Chang. Modeling of River Channel Changes. Journal of Hydraulic Engineering, ASCE, Vol. 110, No. 2, Feb. 1984, pp. 157-172.
2. H.H. Chang. Mathematical Model for Erodible Channels. Journal of the Hydraulics Division, ASCE, Vol. 108, No. HY5, May 1982, pp. 678-689.
3. W.B. Langbein and L.B. Leopold. River Meanders, Theory of Minimum Variance. Professional Paper 282-B. U.S. Geological Survey, 1957.
4. L.B. Leopold, M.G. Wolman, and J.P. Miller. Fluvial Processes in Geomorphology. W.H. Freeman, San Francisco, 1964.
5. H.H. Chang and J.C. Hill. Minimum Stream Power for Rivers and Deltas. Journal of the Hydraulics Division, ASCE, Vol. 103, No. HY12, Dec. 1977, pp. 1375-1389.
6. K.J. Gregory, Ed. River Channel Changes. Wiley, New York, 1977.
7. S.A. Schumm. The Fluvial System. Wiley, New York, 1977.
8. R.A. Bagnold. An Approach to Sediment Transport Problem from General Physics. Professional Paper 422-I. U.S. Geological Survey, Washington, D.C., 1966.
9. Graves Engineering. Repair Abutments at Three Bridge Sites, MCB Camp Pendleton, Basis of Design. Western Division, Naval Facilities Engineering Command, San Diego, California, Sept. 1981.
10. Flood Plain Changes During Major Floods. Department of Sanitation and Flood Control, Community Services Agency, County of San Diego, California, 1979.
11. Storm Report, February 1980. San Diego County Flood Control District, San Diego, California, 1980.
12. W.H. Graf. Hydraulics of Sediment Transport. McGraw-Hill, New York, 1971.
13. E.W. Lane. A Study of the Shape of Channels Formed by Natural Streams Flowing in Erodible Material. Missouri River Division Sediment Series No. 9. U.S. Army Engineer Division, Missouri River, Corps of Engineers, Omaha, Nebraska, 1957.

Publication of this paper sponsored by Committee on Hydrology, Hydraulics and Water Quality.

Mathematical Model for Estimating Scour Through Bridge Crossings

DARYL B. SIMONS, RUH-MING LI, and GEORGE K. COTTON

ABSTRACT

Changes in bed level in alluvial channels are an important design consideration for bridge crossings. The general problem of scour at bridge crossings involves degradation, aggradation, and local scour. Three types of interrelated scour phenomena are found at bridges: (a) local scour caused by piers and abutments disturbing the flow, forming vortices and eddies; (b) scour due to contraction of the flow at the crossing, causing increased velocities in the contracted width; and (c) degradation or aggradation of a stream channel over relatively long reaches and over a long time due to bed-level controls, changes in sediment supply, and changes in river form. A model of these scour phenomena has been developed by Simons, Li & Associates using a known-discharge sediment-routing procedure called HEC2SR. The model determines scour in reaches of a river system based on available sediment supply, local hydraulic conditions, and sediment-transport capacity. Hydraulic conditions for the river are determined using the U.S. Army Corps of Engineers HEC-2 computer program. The procedure was designed to take advantage of the bridge hydraulic modeling routines in HEC-2. Output from the modeling procedure includes detailed hydraulic and sediment-transport data as well as cross-sectional information. Application of the model to a complex site is shown. The analysis procedure provides important information pertinent to the design of river-training measures used in conjunction with bridge crossings.

HEC2SR is a sediment-routing procedure developed by Simons, Li & Associates (SLA), Inc., for routing watershed sediment yield and determining the subsequent degradation and aggradation in a mainstem river. The staff of SLA continues to improve and expand the capabilities of HEC2SR as it is applied to new river systems and hydraulic design problems. An area in which it has been applied extensively by SLA is the hydraulic design of bridges. In this paper the use of HEC2SR in modeling riverbed-level changes and how information from the model is incorporated in the hydraulic design of bridges are discussed.

The model HEC2SR was developed to provide detailed information on bed-level changes in natural channels with hydraulic structures. The procedure incrementally computes a series of water-surface profiles for varying discharges in river channels of any cross section or flow state (subcritical or supercritical) using the U.S. Army Corps of Engineers program HEC-2. The effects of natural obstructions to flow and of hydraulic structures can be simulated by HEC-2. Procedures used in program HEC-2 provide an acceptable method for determining the hydraulics of a bridged channel. HEC-2 supplies hydraulic data that is used to calculate the sediment-transport capacity of river reaches. Sediment supply from upstream and tributary watersheds is also calculated as an additional supply input to the mainstem river reach. The procedure can model a variety of hydraulic structures including bridges, culverts, weirs, grade-control structures, channel improvements, embankments, and levees. Hydraulic information summarized from the HEC-2 program during the procedure allows determination of local scour at piers and abutments and determination of sediment-wave movement such as antidunes in upper regime flow.

The principal use of HEC2SR has been in the design of hydraulic structures on very dynamic rivers, which in many cases have been disrupted by development activities. The simulated bed-level changes and related local scour information are used to evaluate the burial depth for piers, abutments, bank protection, and minimum freeboard requirements at hydraulic structures. Although the procedure evaluates only bed-level changes, it can be very useful in identifying critical reaches where lateral migration is likely. When used in conjunction with other methods in fluvial geomorphology and river mechanics (1), the HEC2SR procedure provides additional refinement and detail necessary for complete hydraulic structure design.

HEC2SR WATER- AND SEDIMENT-ROUTING PROCEDURE

Theoretic Basis

The HEC2SR simulates the movement of alluvial sediment in a river channel for the duration of a flood event. This model can be categorized as a known-discharge, uncoupled water- and sediment-routing model. Known discharge means the discharge in the study reach is given by the upstream inflow unless there is a lateral inflow (tributary). The lateral inflows are added to the mainstem and carried to the downstream reaches. The unsteady flood-wave movement is considered secondary in the known-discharge model. Uncoupled routing means that water and sediments are routed separately. For each time step, the backwater profile is determined first and then the sediment routing is performed based on the hydraulic parameters obtained through the backwater computations. As the name implies, HEC2SR utilizes the HEC-2 backwater computation model to determine the backwater profile. The Meyer-Peter and Mueller bed-load equation (2) combined with the Einstein suspended-load computation procedure (3) is adopted in the model to estimate bed-material transport capacities. The actual transport rate for each river reach is determined by considering both soil availability and transport capacity in the reach. The computed bed-material discharges are further corrected for the fine-sediment concentrations based on Colby's empirical relation (4). Sediments are routed by size in this model. Transport rate, armoring effect, and bed-material changes are considered for individual size fractions. The modified Universal Soil Loss Equation (MUSLE) developed by Jimmy Williams and H.D. Berndt (5) is used to com-

pute the wash-load discharges from the upstream and tributary watersheds.

For computational efficiency and stability the main river is subdivided into a series of computational reaches. Each of these subreaches is a section of the main river in which hydraulic and geomorphic characteristics are similar. The sediment inflow to each subreach is from the upstream reach of the main river. Additional sediment and water discharges may enter a subreach from tributary watersheds. The channel degradation or aggradation in each subreach is governed by sediment continuity. If there is more sediment inflow than outflow, aggradation occurs in the reach. If sediment inflow is less than outflow, degradation results. The volume of aggradation or degradation for each reach is uniformly distributed along the length of the reach, but the bed-elevation change for each cross section is weighted according to the flow conveyance across the section.

The cross-sectional data are modified at the end of each time step. Because the HEC2SR procedure is intended for application on fairly dynamic river reaches for a single runoff event, this frequent modification of the channel cross-sectional data is warranted. Elevation changes of less than 0.01 ft are ignored.

The amount of material transported or deposited in a channel reach is the result of the interaction of two processes. The first is the transport capacity of the reach. This is determined in part by the hydraulic conditions that are a direct result of water discharge, channel configuration, and channel resistance. Transport capacity also depends on the sediment sizes present in the riverbed. Smaller particles can be transported at higher rates than larger particles under the same flow conditions. The second process is the supply of sediment entering the reach. This is determined by the characteristics of the watershed and river system upstream of the study reach.

When the sediment supply is less than the sediment transport capacity, channel degradation, or bank erosion, or both occur to reduce the sediment deficit. In some cases degradation can be limited by the development of an armor layer. If the sediment supply is greater than the capacity, the excess sediment will be deposited in the channel, causing aggradation.

In HEC2SR the Meyer-Peter and Mueller equation (2) is used to compute the bed-load transport for each sediment size fraction. The suspended sediment ratio (suspended load to bed load) is estimated by a simplified Einstein procedure. A detailed description of this procedure is presented elsewhere (3). The resulting equations are as follows:

The bed-load formula is

$$q_b = 12.85/(\rho^{1/2})\,\gamma_s\,(\tau_o - \tau_c)^{1.5} \quad (1)$$

where

q_b = bed load (cfs/ft),
ρ = density of water (slugs/ft^3),
γ_s = specific weight of sediment (lb/ft^3),
τ_o = boundary shear stress (psf), and
τ_c = critical tractive force to initiate particle motion (psf).

The critical shear stress τ_c in Equation 1 is

$$\tau_c = 0.047\,(\gamma_s - \gamma)\,d_s \quad (2)$$

where

τ = specific weight of water and
d_s = size of sediment (ft).

The boundary shear stress acting on the grain in Equation 1 is

$$\tau_o = (f_o/8)\,\rho\,V^2 \quad (3)$$

where

f_o = Darcy-Weisbach friction factor (dimensionless) and
V = mean velocity of flow (fps).

The suspended bed-material discharge is based on exchange theory using Einstein's approach, where

$$q_s = (q_b/11.6)\,[G^{w-1}/(1-G)^w]\left\{[(V/U_*) + 2.5]\,I_1 + 2.5\,I_2\right\} \quad (4)$$

and where

q_s = suspended load (cfs/ft),
G = relative thickness of bed layer (dimensionless),
U_* = shear velocity (fps), and
w = dimensionless parameter given by
$w = V_s/\kappa U_*$ where $\kappa = 0.4$

I_1 and I_2 are integrals that cannot be evaluated directly. One must use either tables or numerical techniques. In HEC2SR, these integrals are evaluated using a Newton first-order approximation. Calibration of Equations 1 and 4 to known transport conditions involves adjustment of parameters describing the boundary shear or the relative thickness of the bed-layer zone of sediment transport. The boundary shear stress is adjusted using the Darcy-Weisbach friction factor, f_o, within accepted limits. Adjusting the bed-layer thickness, G, directly influences the suspended sediment concentration. Both parameters are input variables in the HEC2SR procedure.

The bed-material distributions are updated at each time step throughout the entire flood period according to the estimated scour or deposition. The bed-material distributions are allowed to vary; this is an essential capability for simulating an armoring process in a river channel. The presence of coarser particles can significantly influence degradation through channel armoring.

Wash load is estimated based on a modified version of the Universal Soil Loss Equation (5) where

$$C_w = 95\,Q^{0.56}\,V^{-0.44}(K_e)(LS)(CP) \quad (5)$$

and where

C_w = wash-load concentration (ppm),
Q = hydrograph peak (cfs),
V = hydrograph volume (acre-feet),
LS = USLE slope-length factor (dimensionless), and
CP = USLE cover-practice factor (dimensionless).

The wash-load concentration is assumed to be constant for the duration of the storm. The sediment discharge is corrected for the effect of water temperature, wash load, and sediment size using factors developed by Colby. The correction factor is given by

$$K = 1 + (k_1 k_2 - 1)\,0.01 k_3$$

where

K = Colby correction factor (dimensionless),
k_1 = water-temperature correction factor (dimensionless),
k_2 = fine-sediment correction factor (dimensionless), and

k_3 = mean particle-size correction factor (dimensionless).

The correction factors as presented by Colby (4) have been digitized for use in HEC2SR.

Computational Method

Spatially the HEC2SR procedure recognizes two components of the watershed-river system in a distinct fashion. Each tributary and the upstream portion of the main channel contain a watershed. HEC2SR computes a wash-load concentration and bed-material discharge for each of these watershed areas. In the case of the upstream watershed, the user has the option to directly input either sediment load. This allows the modeling to be decomposed at grade controls (i.e., a bedrock outcrop or man-made drop structure) or where relatively stable reaches may exist in the river system. This option can also be used when sediment inputs have been modeled in detail or actual sediment concentrations are known.

The basic geometric unit for description of the river channel is the cross section. In describing the cross-sectional geometry and reach lengths for HEC2SR, the river should be considered in exactly the same manner as it is viewed by program HEC-2. The modeler should understand the capabilities and limitations of one-dimensional backwater-profile calculation in simulating various flow conditions. In fact, the water-surface profile portion of the HEC2SR can be run and checked before executing the full sediment-routing procedure. This is advisable because the sediment-routing portion of the procedure adds significantly to the complexity of the procedure. Several limitations are placed on the HEC-2 input when it is used in conjunction with the model procedure HEC2SR. These limitations are discussed later in this paper and are for the most part minor constraints.

The sediment-routing component of HEC2SR uses river reaches identified by the user. These reaches consist of several channel cross sections and are defined as portions of the river that have similar hydraulic or geomorphic characteristics. Division of the river into reaches is based on a number of considerations. First, HEC-2 water-surface profiles should be run over the range of flows to be considered in the modeling. Plots of depth, top width, velocity, and main-channel discharge versus distance along the channel should be prepared and reviewed. Portions of the channel displaying similar behavior for the range of discharges considered can be combined as a single reach. Maps and aerial photographs should also be consulted in selecting reaches. Portions of the river of special concern in the modeling, such as bridges or grade-control structures, should be handled separately. Suggested approaches for modeling hydraulic structures using HEC2SR are given later in this paper.

Temporally, the HEC2SR procedure uses time steps specified by the user. All inputs are made discrete using these time steps. Time steps that provide a reasonable approximation of the main-channel hydrograph should be selected. The time steps can vary in length depending on the shape of the hydrograph, that is, a rapidly rising portion of the hydrograph may use several short time steps whereas a long recession limb could be adequately described using a few long time steps.

HEC2SR procedure consists of a series of programs linked sequentially by job-control statements. Figure 1 shows a flow chart of the HEC2SR model that exhibits the execution procedure of the programs included in the model. At the beginning of routing, a data set describing the channel geometry is prepared in HEC-2 format and a river and watershed information data set is prepared and stored in a separate data file. The river and watershed data file includes reach delineation, particle size distributions, and hydrographs. This file is then subdivided into several data files in program FLMSB5 for use in subsequent programs. Program STDSB5 expands any condensed information on the HEC-2 file. For example, some cross sections may use the GR cards of the previous cross section (set field 2 of the X1 card equal to zero). The resulting HEC-2 file contains channel geometry for each cross section so that each cross section can be updated independently after water and sediment routing. If the original HEC-2 data are already in the desired format, program STSB5 can be skipped.

As stated previously, the HEC-2 program is used to determine the backwater-surface profile for a given discharge. The hydraulic parameters are extracted from tape 96 in program INFSB5 after running HEC-2. Program RCHSB5 estimates the average hydraulic parameters for each reach to be used in computing sediment discharges.

Program SEDSB5 is the major module for sediment transport and routing. The fine-sediment concentration and the bed-material transport capacities are computed for each reach. The actual transport rate is determined and compared with the sediment inflow. The channel degradation or aggradation volume is computed and stored for later use in modifying the cross-sectional data, and a new surface-sediment layer is computed establishing a new sediment size distribution within the reach.

After the channel aggradation or degradation has been determined, program CHDSB5 updates the HEC-2 data file. The scoured or deposited sediments are distributed uniformly along the defined reach. In this way, each cross section in the reach has the same amount of change in cross-sectional area. The distribution of the aggraded or degraded area across the section (normal to the flow) is weighted according to the flow conveyance of each portion of the flow area. Finally, program CHDSB5 also updates the stage-discharge data in the HEC-2 file to be used in the following time step.

After program CHDSB5 has been run, the model is ready to execute the water and sediment routing for the next time step. Before this, program OUTSB5 outputs all the hydraulic and sediment transport parameters of the study reach for the investigated time step. Program OUTSB5 also writes out the thalweg elevation changes for each cross section. In addition, the updated HEC-2 data file is stored in a separate data file so that the channel geometry for each cross section during flood routing can be retrieved if more detailed study is required.

After program OUTSB5 has been run, the model repeats the procedure for a predetermined number of time intervals that span the flood period. After the last time interval the model exits from the water- and sediment-routing loop. Finally, program ELMIN5 prints out the maximum water-surface elevation and minimum thalweg elevation encountered for each cross section throughout the entire flood period.

Data Requirements

The input data required for HEC2SR are an HEC-2 data file and a river and watershed data file. The HEC-2 data can include all of the encroachment and bridge constriction cards necessary. The condensed format of the X1 card (field 2 is zero or field 9 is not zero) is allowed, but the channel improvement (CI) and additional points for cross section (X4) options should be explicitly expressed and incorporated into

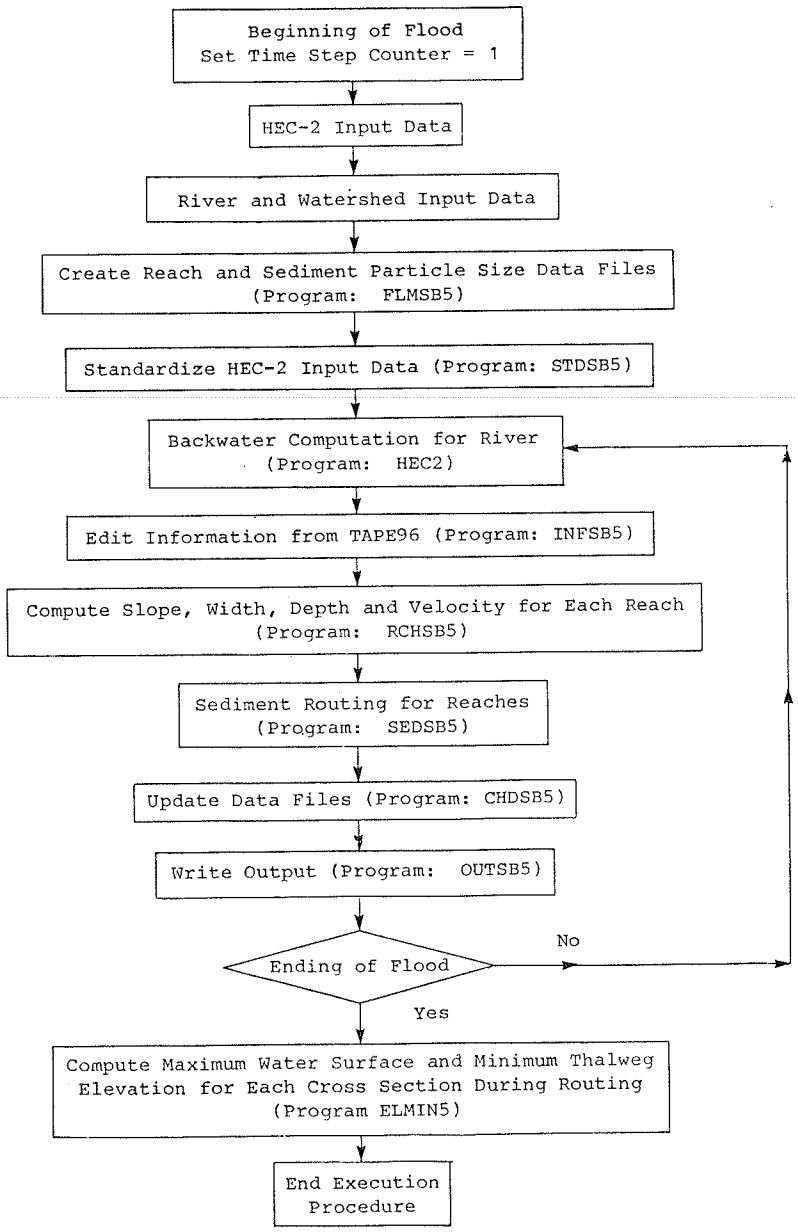

FIGURE 1 Flow chart for model HEC2SR.

the GR cards before running the model. The option to use known water-surface elevations is not applicable (X5) to the procedure and therefore not allowed.

In the river and watershed data file, the river-reach delineation (including the number of cross sections and the extent of each reach) and soil data (sediment size distributions for the subsurface and surface layers and the potential armor depth) are given first. The downstream stage relationship is then given or, if the slope-area or critical-depth method is used, the approximate water-surface elevations. The upstream and lateral-inflow hydrographs are then provided with the time step lengths for the digitized stage and discharge hydrographs. The data to compute the sediment loading (wash load and bed-material load) from the watersheds are also given in this portion of the data if the option of computing sediment yield of the upstream and lateral watersheds is desired.

The additional data collection that is required in developing a complete and accurate data set for the HEC2SR procedure are sediment samples of surface and subsurface material in the channel. The data collected should be sufficient to identify the variation of sediment size along the river system and vertically within a cross section. Geologic mapping should also be reviewed and any geologic controls of the river profile identified. Available sampling data should be reviewed carefully and a preliminary field survey conducted before any new data collection effort is made.

Assumptions and Their Limitations

The major assumptions made in the sediment-routing procedure are that during any time step the flow is steady, gradually varied, and moving predominantly in the downstream direction. Unsteady aspects of flood-wave movement, such as attenuation of the flood peak, are ignored. Routing of the flood is based on conservation of mass alone. If the un-

steady behavior of the flood wave is known, certain adjustments can be made to the original flood hydrograph. This can be accomplished by using artificial tributaries to add or delete water mass from the mainstem of the river and by suppressing the sediment inflow calculations for these tributaries. Depletion hydrographs are allowable in the river and watershed data file, but careful review should be given to the net hydrograph resulting from such tributary inflows and outflows. A net negative hydrograph will terminate program execution. There is no explicit means in the HEC2SR procedure to determine the unsteady behavior of flood-wave movement.

The limitation of the steady-flow assumption regarding the movement of sediment is generally minor. The associated movement of the sediment wave is many times less than that of the flood wave and the refinement of this assumption using full dynamic models is usually unwarranted. The one-dimensional assumption can present more limitations if there are areas of channel that may receive a substantial sediment load due to a lateral flow. Breaching of levees or complex floodplain areas are examples of conditions that can be interpreted as sediment "sinks" that cannot be directly assessed in the HEC2SR procedure.

HEC2SR is limited in its inability to incorporate and predict localized scour or deposition. The model does not account for bank erosion either in the case of an incised channel with severe degradation or in the case of a river that may be altering its meander pattern. Secondary currents and superelevation caused by accelerating flow around a river bend initiate local scour and deposition patterns that will not be recognized by the one-dimensional assumption in this model. The model assumes a uniform aggradation or degradation pattern along each reach as it is defined. In reality the spatial distribution of the deposition or scour is a function of sediment settling distance, local variation in sediment transport rates, and channel geometry.

Despite these limitations, this model has been successfully applied to sand- and gravel-bed rivers for analysis of existing structures and for bridge design. If the discharge, bed-material, and cross-sectional data are properly input, the river reaches appropriately defined and sediment discharge measurements available to validate the employed sediment equations, this model can reasonably predict channel response to floods of various magnitudes. HEC2SR offers the options of inputting sediment inflow directly or internally generating sediment-loading data by considering the sediment-transport capacities in the upstream supply and tributary reaches. The modular structure of this model also enables users to easily understand and modify each individual functional component.

SIMULATION OF BED-LEVEL CHANGES THROUGH BRIDGES

Reach Definition

The analyst has two options for computing bed-level changes through a bridge. The method chosen depends on the degree to which the bridge affects the hydraulics of the channel. In river reaches where the bridge does not constrict the flow, a single reach is sufficient to model the aggradation or degradation process. River reaches with a bridge that severely constricts the flow require two computational reaches to model the aggradation or degradation process.

Figure 2 shows the general layout of cross sections in the vicinity of a bridge. A subcritical profile is assumed and the location of the sections is in keeping with the recommendations made in Appendix IV of the HEC-2 users manual (6). Summarizing these cross-sectional locations in relation to the sediment transport process is done as follows:

Section 4 is located upstream of the bridge at the minimum distance where the flow lines are not distorted by the bridge (approximately equal to the

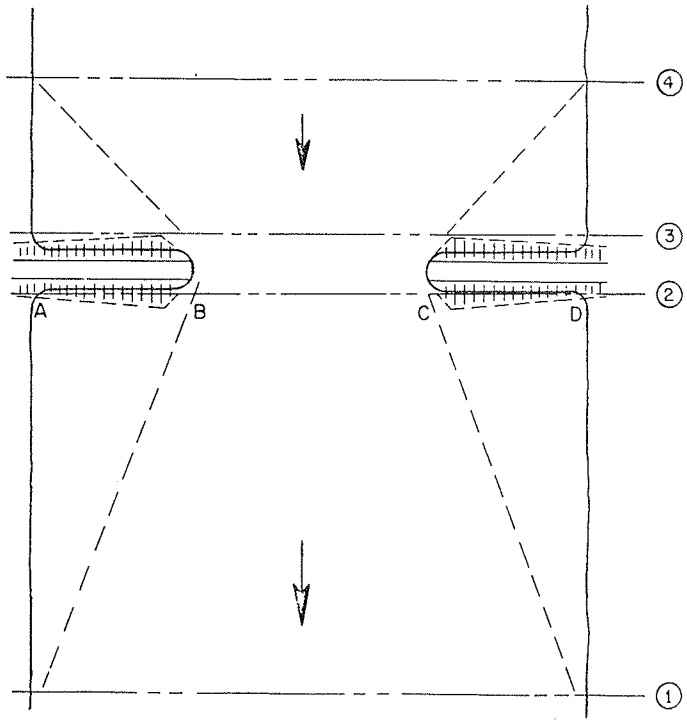

FIGURE 2 Locations of cross sections in the vicinity of bridges.

width of the bridge opening, B-C, or, in the case of wide floodplains with narrow bridge openings, equal to the longer approach, A-B or C-D). The incoming sediment load is conveyed across this section from the upstream reach. This sediment load is derived from upstream watershed and river processes including deposition and scour.

Sections 3 and 2 are located immediately above and below the bridge to represent the effective flow through the bridge. Hydraulic conditions at these points are computed using either the normal bridge method or the more detailed momentum equations of the special bridge method. As a result of these altered hyraulic conditions, the sediment-transport rate is changed as well, leading to scour or deposition as the transport rate adjusts. When the sediment-transport capacity through the bridge waterway is increased, the general scour that occurs is often referred to as contraction scour.

Section 1 is downstream of the bridge at a location where the flow can first be recognized as fully expanded and no longer affected by the bridge (approximately four times the average constriction distance). Sediment-transport capacity will be similar to that of section 4; however, the sediment supply will have been affected by scour or deposition at the bridge constriction.

Two reach definition schemes are used in modeling bridge constrictions using HEC2SR. First, when the flow remains subcritical through the reach (class A flow), it is recommended that all sections be included as one computational reach. The mean hydraulic characteristics of the reach provide a reasonable estimate on which to base sediment-transport capacity. The mean hydraulic characteristics are based on a distance weighting of each parameter and therefore add emphasis to conditions at the bridge site (typically 40 percent or more). Given the uniform nature of the flow under class A conditions, a single reach is adequate to describe sediment-transport characteristics through the bridge.

When the flow passes through critical depth at the bridge (class B flow), hydraulic conditions on each side of the bridge are sufficiently different to warrant a refinement in reach designation. In this case a substantial backwater condition is created upstream of the bridge, followed by a brief supercritical zone, hydraulic jump, and subcritical tailwater. Cross sections 1 and 2 are therefore combined as one reach and cross sections 3 and 4 as another reach. Under class B flow, deposition above the bridge may occur followed by additional scour below the bridge. For a bridge or culvert that substantially constricts the flow, modeling will indicate a sequence of deposition, which may cause plugging and overtopping of the structure, followed by flushing of the deposition during the recession limb of the hydrograph.

Local Scour

For analysis of bed-level changes at a bridge to be complete, several local phenomena that contribute to the total scour at the bridge must also be included. Additional phenomena that can be determined are local scour at piers and sand-wave movement. Solutions of Shen's equation and Neill's equation are generally used to determine scour at piers. Scour at the abutments can also be determined using Liu's equation (1). Kennedy's equation for antidune height is used to determine the effect of sand-wave movement (8). Sand-wave movement contributes to both increased scour and water-surface depth as the sand wave passes through the bridge.

Total scour at a bridge site is therefore the sum of general degradation plus local scour. Low chord elevation will be based on the sum of general aggradation plus the sand-wave height. Low chord elevation should also include consideration of debris passage and superelevation of the water surface.

Other Considerations

River reaches showing large aggradation or degradation adjacent to a bridge reach should be given special consideration. A large profile adjustment will not occur without some effect on channel alignment. HEC2SR provides enough information on profile changes to evaluate their consequences if the nature of fluvial processes is understood. For example, aggradation of a reach with a high sinuosity relative to the river in general may indicate a strong likelihood of channel evulsion, or a reach with a degrading profile may indicate the possibility of significant bank failure. Either condition should alert the designer to the need for other river-training measures to protect the bridge site.

EXAMPLE APPLICATION

The movable-bed characteristics of the Rillito River system were studied extensively by Simons, Li & Associates, Inc. (9), using the HEC2SR sediment-routing procedure. The results for two bridges in this study are presented to illustrate the two different approaches to modeling scour through a bridge crossing.

The first bridge site was located on the Agua Caliente Wash, a tributary of the Rillito River east of Tucson, Arizona. A 6-mile reach of the Agua Caliente was studied assuming existing development conditions would prevail during the 100-year storm event of 10,000 cfs. An existing box culvert (10 ft high, 20 ft wide) at Tanque Verde Road with a capacity of approximately 3,000 cfs was included in this reach. The box culvert was expected to create a significant backwater effect and therefore induce deposition upstream of the culvert. Separate subreaches were used to model the pattern of deposition and scour, with one subreach above the culvert and one below.

Results of the routing analysis show the dynamic process of aggradation and degradation at the site. Figures 3 and 4 show this process over the duration of the 100-year flood hydrograph. The reach above the bridge initially scours. Then, as the hydraulic capacity of the structure is exceeded ($\cong$ 3,000 cfs), a backwater is created that causes significant aggradation. On the recession limb of the hydrograph, scour removes 1.7 ft of sediment. Below the bridge the channel bed responds in the opposite manner with upstream scour causing downstream deposition.

The second bridge site was located on the Rillito River at Alvernon Road within metropolitan Tucson. The reach at Alvernon Road was not constricted by a bridge crossing. The subreach, including the bridge site, was part of an extensive river and watershed system for the Rillito River and Tanque Verde Creek. This system consists of 58 subreaches, three tributaries, and an upstream watershed input. The three major tributaries in the system are Pantano Wash, Sabino Creek, and Agua Caliente Wash. In addition to the tributaries, seven water-discharge nodes were included in the system to account for the variation in discharge due to flood attenuation and floodwater contributions from smaller drainages. Sediment input to the routing procedure occurred at the three tributaries. Upstream sediment supply was assumed to equal the transport capacity of the first upstream subreach.

The results of the sediment routing at the Alvernon Road site show both aggradation and scour

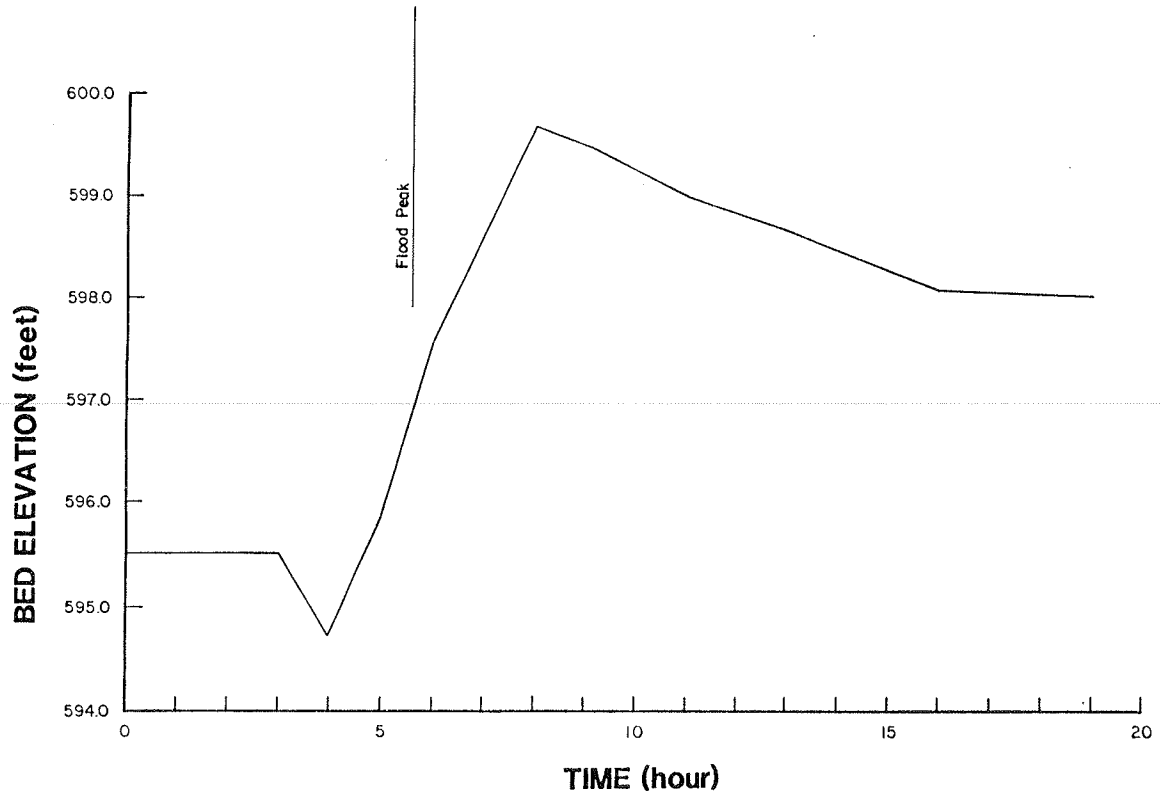

FIGURE 3 Agua Caliente Wash bed-elevation change above Tanque Verde Road, 100-year flood.

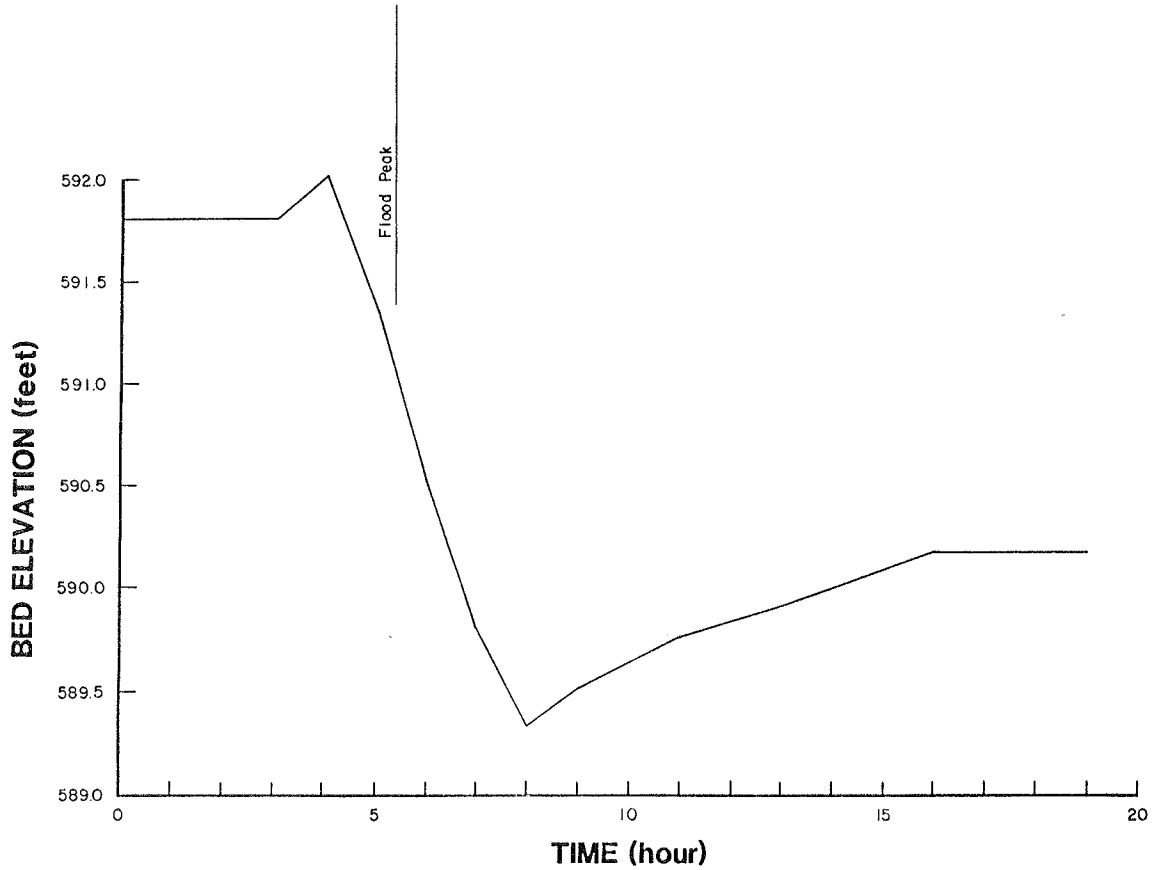

FIGURE 4 Agua Caliente Wash bed-elevation change below Tanque Verde Road, 100-year flood.

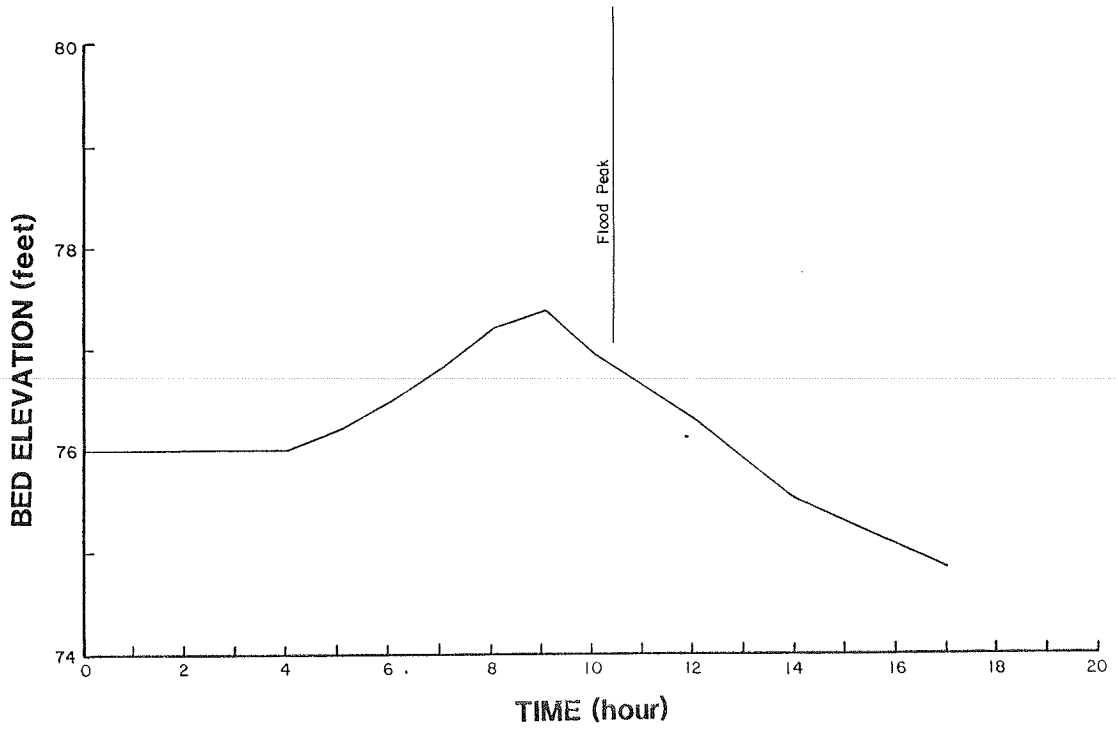

FIGURE 5 Aggradation and degradation of Rillito River at Alvernon Road, 100-year flood.

demonstrating a complex interaction with sediment-transport characteristics in the upper river reaches. Figure 5 shows a period of aggradation on the rising limb of the hydrograph followed by scour during the recession of the flood.

CONCLUSION

HEC2SR provides a useful and complementary addition to a standard water-surface profile analysis using HEC-2. The procedure is essential for analysis of dynamic river reaches where bed-level changes have a significant effect on bridge design. The procedure addresses both general and local scour effects at bridge sites. The analysis also yields important results pertinent to the design of river-training measures used in conjunction with bridge crossings.

REFERENCES

1. R.M. Li and G.K. Cotton. Geomorphic and Hydraulic Design of Bridge Crossings. Proc., Workshop on Bridge Hydraulics, Banff, Alberta, Canada, 1983.
2. E. Meyer-Peter and R. Mueller. Formula for Bed Load Transport. Proc., 3rd Meeting of the International Association for Hydraulic Research, Stockholm, Sweden, 1948, pp. 39-64.
3. H.A. Einstein. The Bed Load Function for Sediment Transportation in Open Channel Flows. Technical Bulletin 1026. U.S. Department of Agriculture, 1950.
4. B.R. Colby. Practical Computations of Bed-Material Discharge. Journal of Hydraulics Division, ASCE, Vol. 90, No. HY2, March 1964.
5. J.R. Williams and H.D. Berndt. Sediment Yield Computed with Universal Equation. Journal of Hydraulics Division, ASCE, Vol. 98, No. HY12, Dec. 1972, pp. 2087-2098.
6. HEC-2 Water Surface Profiles, Users Manual. Hydrology Engineering Center, U.S. Army Corps of Engineers, Davis, Calif., 1982.
7. Scour Around Bridge Piers. FHWA, U.S. Department of Transportation, 1980.
8. D.B. Simons and F. Senturk. Sediment Transport Technology. Water Resources Publications, Fort Collins, Colo., 1977.
9. Sediment Transport Analysis of Rillito River and Tributaries for the Regional Flood Control Element of the Tucson Urban Study. Simons, Li & Associates, Inc., Fort Collins, Colo., 1981.

Publication of this paper sponsored by Committee on Hydrology, Hydraulics and Water Quality.

Role of Calibration in Application of HEC-6

D. MICHAEL GEE

ABSTRACT

Calibration, the process of adjusting model parameters so that model results conform with observed prototype behavior, is an essential ingredient of any modeling effort, be it physical or mathematical. Calibration strategies for movable boundary numerical modeling (i.e., HEC-6) vary widely depending on the type and availability of field data and study scope and objective. The process of calibrating HEC-6 and interpreting field data and model results is described. Examples drawn from past project studies are used to illustrate important points. The theoretical and numerical limitations on extrapolation of model results beyond the calibration range are described. Sensitivity of model results to key input data is discussed. Applicability of HEC-6 to bridge design is addressed. The future research and development program for movable boundary mathematical modeling at the Hydrologic Engineering Center is also presented.

HEC-6 (1) is a one-dimensional movable boundary open channel flow model designed to simulate streambed-profile changes over fairly long periods (typically years). The continuous-flow record is broken into a sequence of steady flows of variable duration. For each flow a backwater profile is calculated that provides energy slope, velocity, and so forth at each cross section. Potential sediment-transport rates are then computed at each section. These rates combined with the duration of the flow make possible a volumetric accounting of sediment for each reach. The amount of scour or deposition at each section is then computed and the shape of the cross section adjusted accordingly. The computations proceed to the next flow in the sequence and the cycle is repeated beginning with the updated geometry. The sediment calculations are performed by grain size fraction thereby allowing for the simulation of hydraulic sorting and armoring. Many options and features are available such as capability to include tributary and distributary flows, automatic channel dredging, gravel mining, and graphical display of simulation results. HEC-6 has been widely distributed and is frequently used by the U.S. Army Corps of Engineers, other government agencies, universities, and the private sector.

Experience has shown that successful application of movable boundary models often requires substantial effort to reproduce field observations; that is, the model must be calibrated. Consequently the focus of this paper is on the process used and variables adjusted during the calibration phase of a study.

The key components of the calibration and verification process for HEC-6 applications, which will be described in this paper, are

1. Comprehending the historical behavior of the stream system.
2. Developing representative geometric, sediment, and hydrologic data.
3. Performing the calibration by (a) selecting calibration measures of changes in bed profile, changes in cross-sectional geometry, changes in volumes of sediment, rating curve shifts, and other characteristics that suit study level and objectives; (b) selecting the calibration time period; (c) identifying acceptable model performance; and (d) adjusting parameters.
4. Verifying the calibration.

In calibrating a complex fluvial hydraulics model such as HEC-6 it is important to distinguish between the following three types of data: (a) run data--the specific input information required to operate the mathematical model; (b) calibration data--prototype measurements used to adjust various model parameters so that model results conform to the observed prototype behavior; and (c) verification data--an independent set of measurements, not used in calibration, that is used to test the validity of the calibrated model.

HISTORICAL BEHAVIOR OF THE STREAM SYSTEM

It is essential for the modeler to comprehend the historical behavior of the stream system early in the study. Development of appropriate representative data and assessment of the model's performance require such an understanding. Historical behavior refers to an engineering time scale rather than the geologic time scale. Contemporary engineering analyses address time frames ranging from single flood events to project life spans.

Selection of the study area requires certain considerations. The area should extend far enough upstream from the problem area so alternatives being evaluated do not produce changes to the streambed profile or sediment load at the upstream boundary of the area being modeled. The study area should also include all major sediment-producing tributaries. Usually the location of stream gauging stations will determine the limits of a study area. Hydraulic structures may also be used as a study boundary; they are more appropriate as a downstream boundary than as an inflow boundary.

To ascertain the historical behavior of the stream system, assemble all information from office files: maps; surveyed cross sections; observed water-surface profiles; aerial photographs; ground photographs; flow hydrographs; stage hydrographs; stage-discharge rating curves; water-temperature records; suspended-sediment loads; total sediment loads; gradation of the suspended and total loads; gradation of the streambed material; the location, date, and size of all impoundments; the location, date, and extent of all bridge construction activities; the location, date, and extent of all construction activities adjacent to the stream channels; the location, date, amount, and material gradation for each dredging activity in the study area; land use and soil types; and prior studies.

The availability of each type of data may be shown on a time line. This is particularly useful for flow data used to determine a base period for calibration. Having organized and inventoried available data, begin a detailed study to accomplish each of the following tasks.

1. Establish a general knowledge of extreme events in the study area and of how the system responded in terms of channel changes and amount of sediment transported;
2. Establish a general awareness of the response time of the stream system in terms of rate of movement of flood hydrographs, rate of response to changes in sediment load, and so forth;
3. Evaluate the impact of recent impoundments on the water-discharge hydrograph and the sediment load;
4. Reach a general understanding of the historical behavior of the stream system--the part of the behavior that would have occurred naturally and the part that may be attributed to man's activities in the study area (land use as well as stream use);
5. Locate anomalies in geometric, hydrologic, hydraulic, and sediment characteristics within the study area;
6. Refine the study objectives, identify possible project alternatives and appropriate analytical approaches; and
7. Identify missing data that can be supplied only by additional field measurements or field reconnaissance.

It is important to view the study area with someone who is intimately familiar with it. Particularly note all locations where scour or deposition occurred and the stream did not return to its original cross section or alignment. Locate and date each bridge crossing, each cut-off (natural or man-made), each encroachment, each levee, each diversion or bifurcation. Note overbank areas that flood first and locate their natural levees.

The streambed and banks must be studied to locate rock outcroppings or other geologic formations that will resist scour and therefore control the vertical movement of the streambed. The grain size of sediment on the point bars should be observed and locations of abrupt changes noted. Of particular interest are locations where the gradual change from coarse to fine particles in the downstream direction is interrupted by a sudden change that persists in the downstream direction.

DEVELOPMENT OF REPRESENTATIVE DATA

Specific input data requirements for the operation of HEC-6 are presented in the users manual (1). The quantity of data necessary to operate HEC-6 for long-term simulations can be quite large. Therefore it is beneficial to have a systematic procedure for storing, manipulating, and displaying those data (2,3). This section addresses the problem of developing representative data. Representative data are not necessarily averages of many samples. For example, representative geometry preserves channel width, depth, and roughness and allows the numerical model to transport sediment with changes in bed elevation that match prototype observations. The representative inflowing sediment load preserves both volume of sediment and rate of sediment inflow at the upstream boundary of the study area. The representative bed-material gradation and gradation of inflowing sediment load allow the model to transport observed sediment discharges while reproducing observed changes to the bed elevation. Representative water discharges include flow rate and, to a lesser extent, flow volume and amount of attenuation of flood hydrographs as they move down the system.

Having flows match the appropriate flow duration relationship is extremely important, (i.e., representative flows for the calibration period are those that occurred during that period, whereas representative flows for the study period are those producing the long-term flow duration curve). Beginning with geometric data, procedures for developing representative data are suggested. These are by no means all-inclusive guidelines, but they stress the most important characteristics of the real physical system that should be preserved.

Geometric Data

Geometric data consist of cross sections, their locations, and boundary roughness (Manning n values). Cross sections should be located at major changes in bed profile, at points where channel or valley width changes, at tributaries, and at all pertinent points where calculated results are required (e.g., stream gauging stations). The geometric model should extend sufficiently far upstream from bridge crossings so that it will be beyond any backwater effects. A portion of each cross section must be specified as movable (Figure 1). This requires good engineering judgment and may require adjustment during calibration.

Avoid locating cross sections too close together. The shorter the distance between sections, the shorter the computation interval has to be in HEC-6. Short computation intervals require more computer time and, therefore, should be avoided in long-period studies. This may prove particularly troublesome because the simulation of scour at a bridge location is a local phenomenon that implies use of a fine-grid analysis. Short time steps (hours or less) may therefore be necessary. It appears that the resulting study would focus on a single-event analysis.

Checking Geometric Data for Errors

Movable streambed calculations are much more sensitive to errors in boundary geometry than are fixed-bed water-surface profile calculations; consequently, more care is required to prepare geometry than is typically required for fixed-bed water-surface profile studies. A cross section that is too wide or too deep will show up as a point of deposition; one that is too narrow or too shallow will exhibit a tendency to scour. Not only will that section be affected, but calculated results will be incorrect at sections upstream and downstream from it. Geometric data errors, therefore, are difficult to locate when HEC-6 is executing in the movable-bed mode. For this reason the first step in debugging and calibrating geometric data is to run the model in fixed-bed mode. This allows calibration of the geometric and hydraulic portions of the study separated from the sediment portions. This is a critical first step because the validity of subsequent sediment computations is dependent on having an accurate hydraulic description of the system as well as representative sediment data.

Selection of n Values

Appropriate values for Manning's n should be determined by running HEC-6 in the fixed-bed mode (i.e., as a step-backwater program). This is necessary to compare calculated water-surface elevations with observed (or calculated, e.g., HEC-2) water-surface profiles or rating curves.

Careful consideration should be given to the selection of n values. Changing n values with distance should be justified by changes in channel appearance or sediment size. Avoid changes where the only reason is to reconstitute an observed stage (4). It is often more logical to approximately reconstitute the stages at several gauge locations over a long reach using a constant n value for a given discharge than it is to change n values at

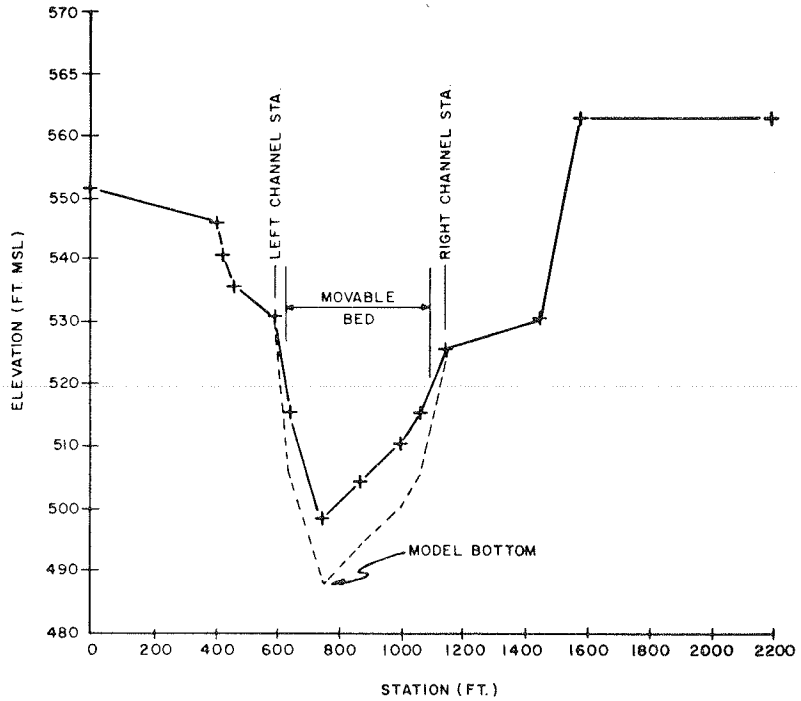

FIGURE 1 Example cross section.

each gauge to exactly match observed stages. Also, n values may vary with discharge, that is, the bed form of alluvial rivers often changes during the passing of a flood event. As yet it is not possible to accurately predict such changes (5-7). Until a theoretical basis is developed one should consider acknowledging such a change by associating n values with water discharge if field data for the particular river support such a variation.

Sediment Data

Preparation of accurate sediment data and development of a representative inflowing sediment load curve are essential. The overall objective in preparing sediment data for river studies is to establish the sediment load that accompanies river flows and determine the proper size distribution and character of the bed material. The most common approach is to plot observed water discharge versus observed sediment load as shown in Figure 2. These plots usually exhibit a log cycle of scatter. The representative load curve produces the proper annual volume of sediment when integrated with the water-discharge hydrograph for the year in question. The total inflowing load, and distribution of grain

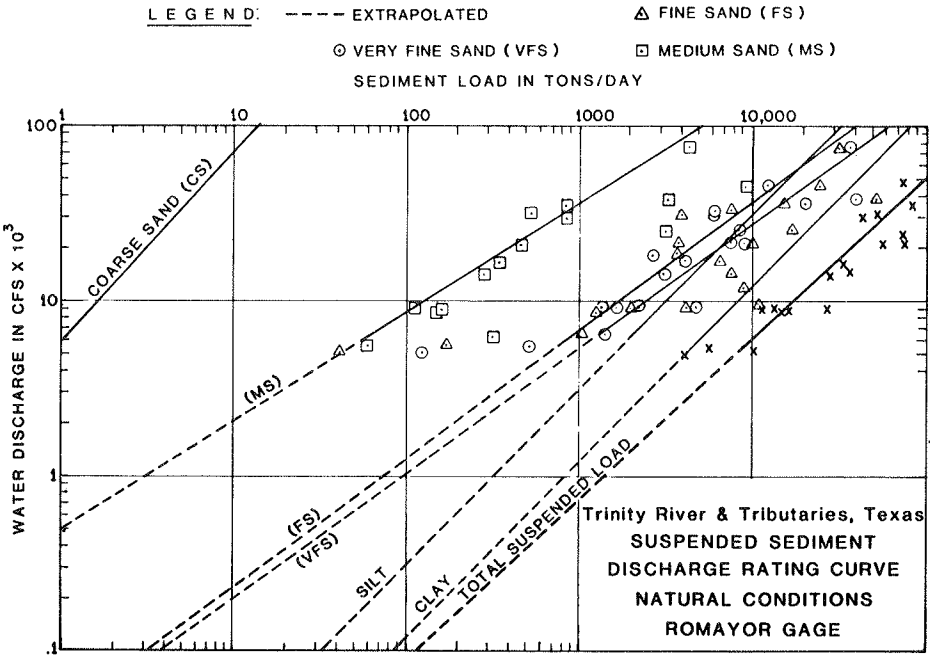

FIGURE 2 Sediment discharge rating curve.

sizes within that load, must be adjusted until a representative curve has been established.

Note that for the purpose of simulating scour at bridge crossings the fine materials (clays and silts) may be irrelevant. These materials are included in suspended load measurements, however, and may, therefore, have to be included in the model input data to reproduce the measured average annual total loads.

Once representative inflowing sediment load curves have been identified for all size classes, bed-material gradation curves must be developed from field samples (see Figure 3). Figure 4 shows an example plot of profiles of grain size gradation versus river mile. Plots such as these assist the modeler in understanding the stream's behavior by illustrating grain size changes along the study reach, which reflect the influences of geologic controls, tributaries, and so forth.

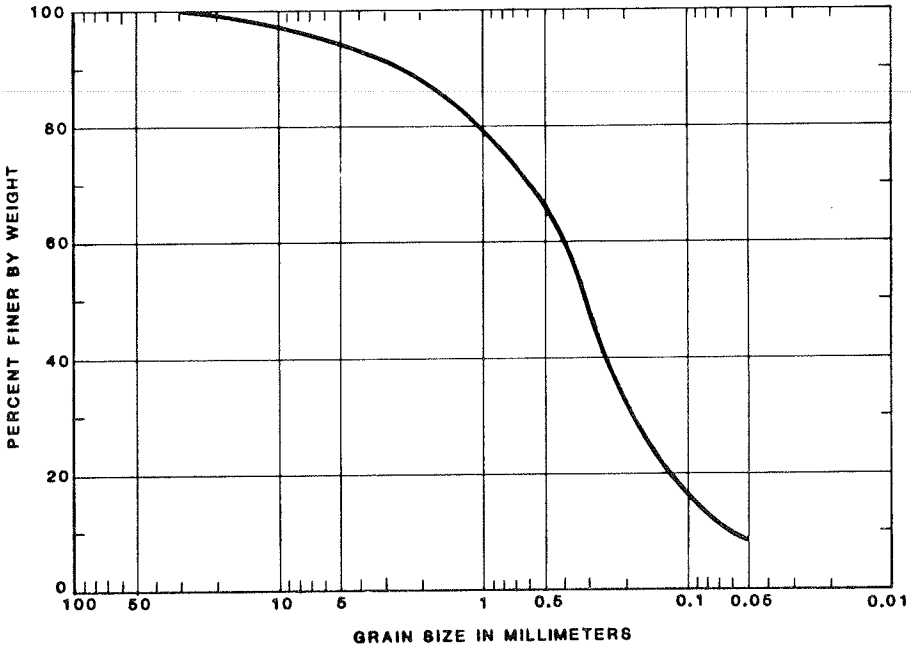

FIGURE 3 Grain size distribution of bed material.

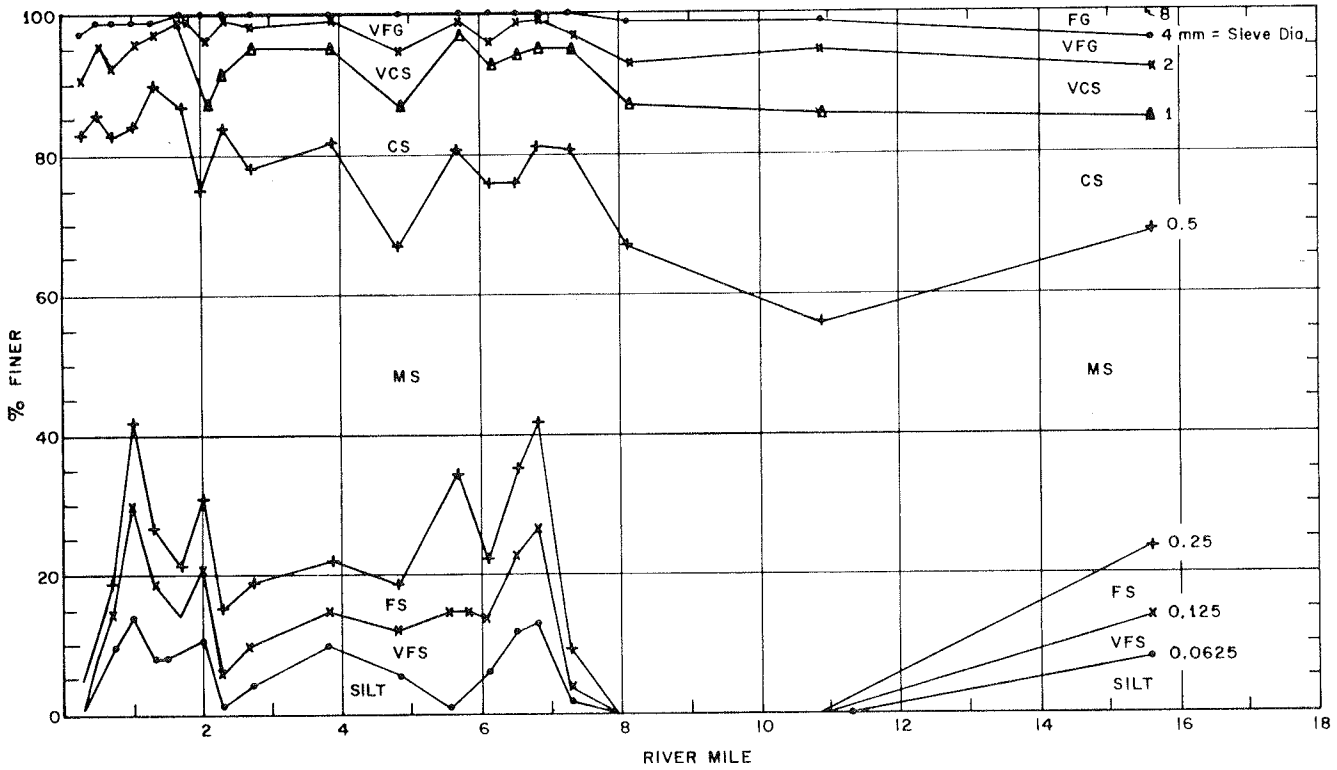

FIGURE 4 Example of profiles of bed sediment size, Big Sandy River, Huntington, West Virginia.

Hydrologic Data

Hydrologic data consist of (a) inflowing water discharges for the mainstem and for all local inflow or outflow points; (b) the stage hydrograph, rating curve, or operating rule giving water-surface elevation at the downstream end of the model; and (c) temperatures for the inflowing water discharges [see (4) for explanation of importance].

ESTABLISHMENT OF COMPUTATION INTERVALS

The computation interval (or time step) used by HEC-6 is usually variable; short time steps must be taken during flood events when large amounts of sediment are moving and the hydrograph is rapidly changing. Longer time steps should be used during low-flow periods (Figure 5). In general the closer

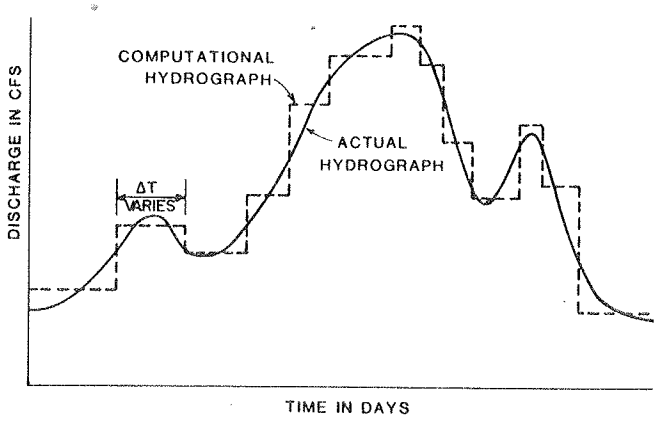

FIGURE 5 Water discharge hydrograph.

the cross sections, the smaller the required time step. The modeler is confronted with the dilemma of wanting to use small time steps for an accurate solution and large time steps for a cheap solution. A procedure for selecting an optimum time step is outlined elsewhere (8). At present, the HEC uses a data preprocessor that automatically develops a variable time step flow record from mean daily flows based on an estimation of the volume of sediment entering the study reach each time step. For a multiyear simulation the time step typically ranges from 1 day to 1 month.

Operation of the model for a test period (perhaps an average year) should be performed as a check on data consistency and reasonableness before calibration runs are attempted. The flow record for an average year can be constructed from the flow-duration relationship. Key items to check at this time are

1. Silt and clay should not deposit in the channel under natural river conditions. Any cross section that exhibits a reduction in silt or clay load passing through that section should be carefully checked. The cross section may be too large or a false channel control may exist downstream.
2. The sand load should approach a steady value, approximately equal to the inflowing load, from section to section rather than an erratic variation. It must be remembered that cross sections used in HEC-6 are representative of reaches; therefore, some smoothing of field data may be required. Sections that have very little transport capacity should be checked for errors in cross-sectional geometry, reach length, n values, limits of movable bed, or perhaps bed-material gradation.

If the model performance simulates in all respects the behavior that would be expected in the prototype, the computation interval and the other parameters have been determined. Otherwise, one must determine what is causing the questionable performance. For example, excessive fill may mean the limits of the movable bed are too narrow or the natural levee is too low. If the prototype is depositing sediment above the overbank elevation, expand the movable-bed limits to include the overbank. If water is spilling onto the overbank in the computer model but that area is not effective for conveyance in the prototype, raise the natural levees. If excessive scour is indicated by the computed results, it may mean that the prototype has an armored, nonerosive, or rocky bottom that is resistant to scour.

PREPARING FLOW RECORDS

The three main points to consider in developing flow records are (a) preserve the total volume of water in the observed hydrograph, (b) preserve the total volume of sediment that was transported during the hydrograph period, and (c) make the computation intervals as long as possible and still preserve computational stability (9).

There is usually a strong correlation between the annual volume of water that passes a gauge and the annual sediment yield of that basin. The rate of sediment movement, called sediment load, is not a function of water volume. It is a function of water discharge (Figure 2) and of the availability of sediment material. In many cases, three-quarters of the annual sediment yield will be transported in less than one-quarter of the year. Therefore, it is necessary that all flow records contain flood peaks.

CALIBRATION MEASURES

Selection of appropriate calibration measures for a movable boundary model such as HEC-6 is not straightforward. Ideally, one would have complete sets of surveyed cross sections and measured sediment-transport rates periodically throughout the calibration period. Such data sets are extremely rare. Consequently, different calibration measures may be used for different studies depending on study objective, data availability, and so forth (8). A useful calibration measure is the observed drift of the rating for a stream gauge. This is a good measure because the rating curve integrates, to a certain extent, behavior of a stream reach rather than a single point or cross section. Care should be taken that the rating-curve drift is being caused by scour or deposition and not roughness changes. The gauge selected for use in calibration should not be within the influence of the downstream boundary. An example reproduction of a rating-curve shift is shown in Figure 6.

Should surveys of cross sections be available over an appropriate time interval, care must be taken to correctly compare model results and field data. Amounts of scour and deposition may not be exactly reproduced at specific locations of cross sections. Regions of scour or deposition should correspond between model and prototype. In some cases it is appropriate to compare volumes of scour and deposition as a calibration measure (10,11).

Before using a numerical model such as HEC-6 for the analysis of projects, the model's performance needs to be evaluated. Evaluation normally consists of two phases: calibration and verification. Calibration is intended to make computed results as accurate as possible. Measured or observed values from the prototype are compared with computed

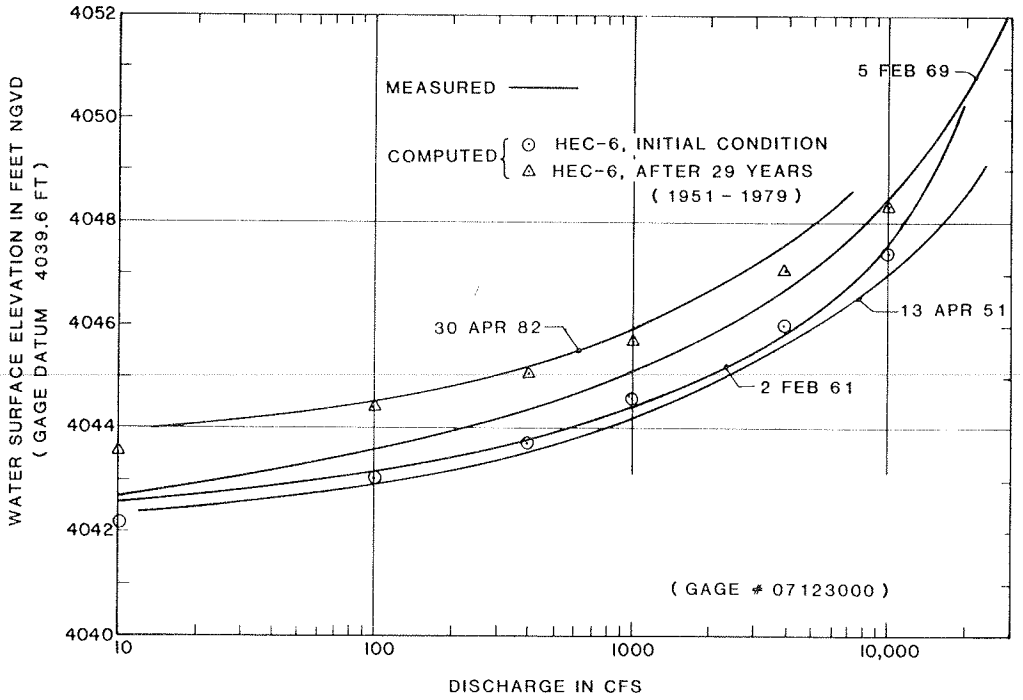

FIGURE 6 Rating curves, Arkansas River at La Junta, Colorado.

results to pinpoint input data deficiencies or physically unrealistic coefficient values. Model parameters are adjusted accordingly to improve the simulation. Calibration, however, does not mean the use of physically unrealistic parameters to force a poorly conceived model to satisfying prototype data. If there is a discrepancy between model results and calibration data, either there is something wrong in the physical realism of the model (a model deficiency as a result of limiting assumptions) or there is something wrong with the measured data or the interpretation of that data for model input (a data deficiency). Therefore, if calibration cannot be accomplished through the use of physically realistic parameter values, the measured prototype data should be checked for possible errors and then the entire model (input data and limiting assumptions) should be examined, data coding should be checked, and boundary specifications should be examined. Experience has shown that the process of rectifying discrepancies between model results and prototype observations can substantially assist the engineer to understand a river's behavior. When it has been calibrated, a model needs to be verified by checking its performance against a situation not used in the calibration.

SENSITIVITY OF SIMULATION RESULTS TO DATA UNCERTAINTIES

The sensitivity of simulated bed-profile changes to various data can best be evaluated in light of the reliability of field measurements of those data. In addition to field data there are various model parameters that cannot be measured directly and must be estimated by the model user and adjusted if necessary during the calibration process. Guidance on selection of model parameters is given elsewhere (8). A qualitative assessment, based on experience gained from many past applications of HEC-6, of the model sensitivity to variations in the various input data is given in Table 1. Note that, in any particular study where uncertainty exists in the value of any particular input item, the model can be run for a range of values of that particular input item to assess the resultant variation in simulation results. This information can then be used to identify what, if any, additional field measurements are necessary to accomplish the study objectives.

APPLICATIONS TO BRIDGE DESIGN

Bridge crossing design must confront both long-term river behavior (particularly lateral migration) and single flood-event response. Applications of HEC-6 to bridge crossing design would probably focus on the latter. This is a relatively new area of use of HEC-6 and many questions remain. Foremost is the stochastic nature of watershed sediment production. The behavior of any river reach is determined not only by local hydraulics, perhaps as modified by bridge construction, but also by the amount and size of sediment transported into the reach from up-

TABLE 1 Sensitivity of Model Results to Field Data

Data Item	Field Measurement Reliability	Model Sensitivity	Remarks
Geometry			
Cross sections	H	H	
Movable bed limits	L	H	Field estimation and calibration
Roughness	M	M	Field estimation and calibration
Sediment			
Bed material gradation	M	H	
Inflowing load	L	H	H locally, M elsewhere
Hydrology			
Flow record	H	M	Developing long-term flow records can be difficult; see (5)
Rating curve	H	L	Local effect
Temperature	H	L	

Note: H = high, M = medium, L = low.

stream. The condition of the watershed at any particular time (e.g., recently burned) is not deterministic (12). Therefore, it is difficult to ascertain, for a given hypothetical flood hydrograph, the appropriate inflowing-load curve.

For single-event bridge scour problems, it may be adequate to assume that the problem is governed by transport of bed material, neglecting wash load. Inflowing load can then be approximated based on equilibrium transport in the reach several stream widths upstream of the bridge site (depending on flood hydrograph duration). HEC-6 applies to this problem providing that local scour phenomena are not coupled with multidimensional hydrodynamic phenomena in the vicinity of the bridge. For two-dimensional, near-bridge problems RMA-2 (13) may be useful.

Another use of HEC-6 in bridge design is prediction of long-term trends in stream-bed profile behavior. Analysis can be made of the impacts of various scenarios regarding upstream and downstream actions (e.g., headcutting) at the bridge site. Note that, for either long-term or single-event studies, HEC-6 is best used to evaluate the relative impacts of different designs (e.g., design A versus base condition, design A versus design B, and so on).

FUTURE RESEARCH AND DEVELOPMENT

The research and development program at the HEC in the area of movable boundary modeling consists of two integrated components. The first component consists of enhancements and improvements to HEC-6; the second, long-range component is the development and implementation of a second-generation movable boundary model.

Several improvements to HEC-6 are under way at this time. The major items are development of a method of allowing the movable bed width to vary with width of the water surface (i.e., water-surface elevation). At present, the scour or deposition at each cross section is applied to a fixed, user-selected portion of that cross section regardless of discharge. Incorporation of an algorithm to automatically identify which portion(s) of the cross section are submerged at each computational time step for scour and deposition calculation will provide a more physically realistic and less user-judgment-dependent solution.

One of the primary features that has contributed to successful application of HEC-6 is its capability to route sediments by grain size fraction. Movement

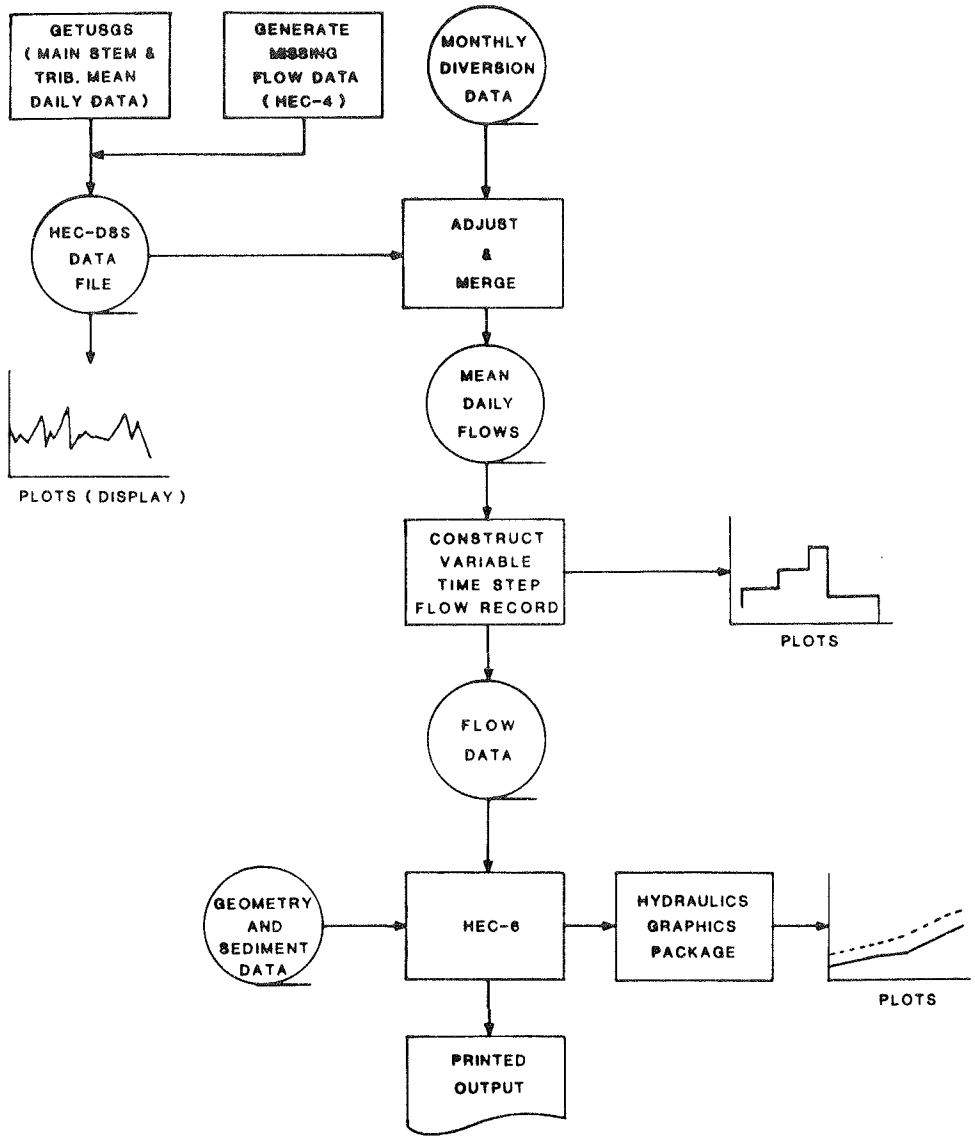

FIGURE 7 HEC-6 data flow and program linkage.

of one clay size, four silt sizes, and ten sizes of sands and gravels can be simulated. This provides the capability to simulate sorting and armoring of the bed material because fines are transported much more rapidly than coarse materials. The algorithm that performs the accounting calculations for all the grain sizes in the bed has evolved over the past 10 years, incorporating the best available theories for the sorting and armoring processes. It has been noticed that a significant amount of computation effort is used by this particular algorithm. It is thought that significant gains in computational efficiency can be achieved by redesigning and simplifying this algorithm. Furthermore, the current algorithm requires the user to specify a (somewhat arbitrary) number of iterations within each computational time step for recalculation of the bed-material gradation. A theoretical investigation has been undertaken to identify a better method of tracking bed-material gradation using a physically based procedure for updating bed-material gradation.

HEC-6 incorporates many of the capabilities and features necessary for a one-dimensional movable boundary river model. An important component not currently available is a method for tracking lateral migration of a river. It appears that viable theories are now becoming available for prediction of meander migration (14). Consideration is being given to incorporating this capability into the next generation of the movable boundary model.

HEC-6 is a widely used model. It has been developed over the past 10 years with features being added as required by various studies. The level of effort necessary to support the model is becoming significant. HEC is, therefore, considering development of a second-generation movable boundary model that would employ the concepts of structured programming and algorithmic modularization. The purpose, use, theoretical basis, and so on would be similar to those of HEC-6. Some new capabilities, such as a lateral movement component, would be added, and obsolete or little-used components discarded. The experience gained with the many applications of HEC-6 provides a valuable basis for the construction of a new model. Development of a new code will emphasize theoretical improvements, computational efficiency, structured programming, user ease, and interfaces with data management systems.

COMPUTATIONAL ASPECTS

Application of a movable boundary model such as HEC-6 can require major computational resources, particularly for long-period studies (50 to 100 years). Operation of the simulation model is only one component of the computational requirements. It is also important to have software available for storage and manipulation of hydrologic data and graphic display of input data and simulation results. The linkage of the various software packages and data files developed for a recent study at the HEC is shown in Figure 7. This support software has become an integral and necessary component of any major movable boundary modeling effort at the HEC. Single-event analyses are less computationally intensive because the study reach is relatively short, the hydrographs are synthetic and of short duration, and the sediment loads can also be synthetically generated. Calibration data are rarely available for single-event analyses.

ACKNOWLEDGMENT

The concepts of calibration of HEC-6 presented herein are those of William A. Thomas, original author of the model. The findings and opinions expressed herein are those of the author and not necessarily those of the U.S. Army Corps of Engineers.

REFERENCES

1. HEC-6 Scour and Deposition in Rivers and Reservoirs, Users Manual. Hydrologic Engineering Center, U.S. Army Corps of Engineers, Davis, Calif., 1977.
2. D.M. Gee. Prediction of the Effects of a Flood Control Project on a Meandering Stream. Rivers '83: A Specialty Conference on River Meandering. ASCE, New Orleans, Oct. 24-26, 1983, proc. in press.
3. The Hydrologic Engineering Center, Data Storage System (HEC-DSS), An Overview. Hydrologic Engineering Center, U.S. Army Corps of Engineers, Davis, Calif., 1982.
4. V.A. Vanoni, Ed. Sedimentation Engineering. Manuals and Reports on Engineering Practice No. 54. ASCE, 1975.
5. H.H. Barnes, Jr. Roughness Characteristics of Natural Channels. Water Supply Paper 1849. U.S. Geological Survey, 1967.
6. H.A. Einstein and N.L. Barbarossa. River Channel Roughness. Transactions, ASCE, Vol. 117, 1952, pp. 1121-1146.
7. D.B. Simons and E.V. Richardson. Resistance to Flow in Alluvial Channels. Professional Paper 422J. U.S. Geological Survey, 1966.
8. Guidelines for the Calibration and Application of HEC-6. Training Document No. 13. Hydrologic Engineering Center, U.S. Army Corps of Engineers, Davis, Calif., 1981.
9. Sediment Transport. IHD Vol. 12. Hydrologic Engineering Center, U.S. Army Corps of Engineers, Davis, Calif., 1977.
10. G.R. Dyhouse. Sediment Analysis for Urbanizing Watersheds. Journal of the Hydraulics Division, ASCE, Vol. 108, No. HY3, March 1982.
11. D.T. Williams. Effects of Dam Removal: An Approach to Sedimentation. Technical Paper No. 50. Hydrologic Engineering Center, U.S. Army Corps of Engineers, Davis, Calif., Oct. 1977.
12. R.C. MacArthur. Evaluation of the Effects of Fire on Sediment Delivery Rates in a Southern California Watershed. In Proc., D.B. Simons Symposium on Erosion and Sedimentation, Fort Collins, Colo., 1983.
13. W.R. Norton and I.P. King. User's Guide and Operating Instructions for the Computer Program RMA-2. Resource Management Associates; Sacramento District, U.S. Army Corps of Engineers, Dec. 1976.
14. Rivers '83: A Specialty Conference on River Meandering. ASCE, New Orleans, Oct. 24-26, 1983, proc. in press.

Publication of this paper sponsored by Committee on Hydrology, Hydraulics and Water Quality.